

©2012

Hiyun Kim

ALL RIGHTS RESERVED

ALLENE-BASED APPROACH TO THE SYNTHESIS OF DE NOVO
ERYTHROMYCINOIDS

by

HIYUN KIM

A Dissertation submitted to the
Graduate School-New Brunswick
Rutgers, The State University of New Jersey
in partial fulfillment of the requirements

for the degree of

Doctor of Philosophy

Graduate Program in Chemistry

written under the direction of

Dr. Lawrence J. Williams Ph.D

and approved by

New Brunswick, New Jersey

January, 2012

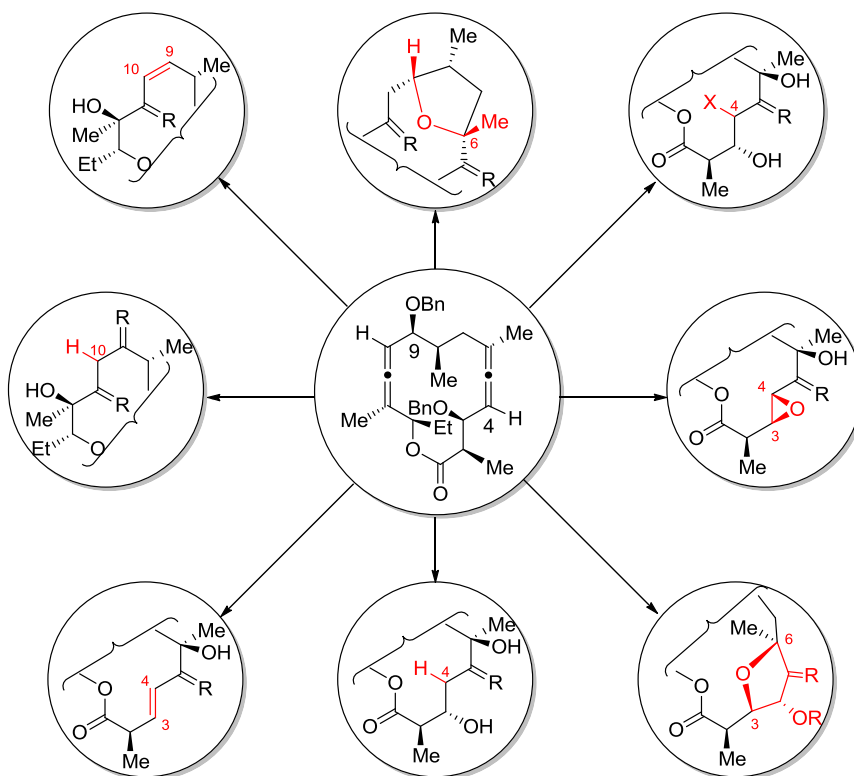
ABSTRACT OF THE DISSERTATION

ALLENE-BASED APPROACH TO THE SYNTHESIS OF DE NOVO ERYTHROMYCINOIDS

By HIYUN KIM

Dissertation Director:

Dr. Lawrence J. Williams Ph.D



We prepared an advanced synthetic module (bis[allene] macrolactone at center) equipped with two allenes embedded in a macrolactone scaffold. The plan was to effect heterogeneous derivatization of the allenes, in tandem or separately. In addition to diversity, this approach is maximally concise and economic, especially in terms of steps. Moreover, immediate derivatives of the macrocyclic bis[allene] can be taken into further steps, thus providing canonical build-up of erythromycin analogs.

To date, our bis[allene] macrolactone has been converted to over 30 novel macrolides. These *de novo* analogs serve to validate the strategy and lay the ground work for further work. Taken together, the allene-based reactions/transformations employed in this study, such as DMDO oxidation/nucleophile addition, allene osmylation/electrophile addition, bromination, allene oxide rearrangement, spirodiepoxide rearrangement, benzylic migration/elimination, mono- and bis-oxidation of bis[allene], chelation-controlled reduction and oxime formation, demonstrate that 8 of the 11 modifiable carbons in this antibiotic can be modified. It is especially noteworthy that each congener was made in less than three steps from the bis[allene] macrolactone.

Acknowledgements

“The mind of man plans his way, But the LORD directs his steps (Proverbs 16:9)”

I would like to note my sincere appreciation to my advisor Prof. Lawrence J. Williams. He has been an excellent teacher, researcher, and writer who possesses “naturally-born” scientific insight and care for the students at the same time. He gave me the second opportunity to pursue a Ph.D. degree at Rutgers. From the first day in his group, everything was new. However, I quickly realized that the novelty which I observed was the extension of creativity, enthusiasm, scientific contribution, and pride in his research. I worked on several very challenging projects, including quite a few different interdisciplinary projects, which were scientifically and experimentally challenging, but fully rewarding at the end. In his group, I have had my eyes opened to science.

The structural assignment of complex compounds reported in this thesis would have been nearly impossible without Dr. Novruz G. Akhmedov. I would like to express my sincere gratitude to Dr. Akhmedov for his continuous scientific and technical guidance on issues of complex NMR analysis.

I greatly appreciate the help of Dr. Joseph R. Cusick, Michael A. Drahl, and Ray Remus for reading and correcting the manuscripts. I also thank them for insightful comments and critiques.

I would like to thank all recent and current post-doctoral and graduate student members of Prof. Williams’s group, particularly Kai Liu, Libing Yu, Rojita Sharma,

Gaojie Hu, Da Xu, Dr. Sipak Joyasawal, Dr. Partha Ghosh, Dr. Robert V. Kolakowski, Dr. Madhuri Manpadi, and Dr. Yue Zhang.

I would like to thank members of my committee; Prof. Longqin Hu, Prof. Kai Carsten Hultsch, and Prof. Ralf Warmuth for their participation.

Lastly, I would like to thank my husband Ozgur Celik, our parents Jin-Seop Kim, Ryoung-Ja Kim, Yasar Celik, and Naciye Celik, and our families. They have always supported and encouraged me in my studies.

Dedication

To My Lord, Jesus Christ, and Orphans in North Korea

Table of Contents

Abstract.....	ii
Acknowledgements.....	iv
Dedication.....	vi
List of Tables.....	xii
List of Schemes.....	xiii
List of Figures.....	xvi
List of Abbreviations.....	xviii

Chapter 1: Erythromycin and Its Derivatives

1.1 Introduction.....	1
1.2. Erythromycin Derivatives.....	2
1.3. Binding Site and Modes of Action	4
1.4. Previous SAR Studies.....	7
1.5. Total Synthetic Approach to Erythromycin Derivatives	9
1.6 Conclusion	10
1.7. References.....	13

Chapter 2: Strategy for the Synthesis of *De Novo* Erythromycinoids

2.1. Introduction.....	14
2.2. Efficient Access to Diverse in Erythromycin Congeners	14
2.3. Synthetic Strategy: Bis[Allene] Macrolactone	15

2.4.	Allene Oxidation: Spirodiepoxide (SDE) Chemistry	16
2.5.	Allene Oxidation: Osmylation	18
2.6.	Model Study: Bis[Allene] Macrolactone	19
2.7.	Convergent Synthesis of Bis[Allene] Macrolactone	20
2.8.	Conclusion	21
2.9.	References.....	23

Chapter 3: Synthesis of the Bis[Allene] Macrolactone

3.1.	Introduction.....	25
3.2.	Synthesis of Coupling Units	25
3.3.	Optimization of the 1st Coupling (Step 6): C1 to C9	29
3.4.	Optimization of the 2nd Coupling: C1 to C14.....	33
3.5.	Synthesis of the Bis[Allene] Seco-acid	35
3.6.	Macrolactonization	36
3.7.	Conclusion: Flexibility of the Synthetic Route	37
3.8.	References.....	38

Chapter 4: Synthesis of Erythromycinoids

4.1.	Introduction.....	39
4.2.	DMDO Oxidation and Nucleophile Addition.....	40
4.3.	DMDO Oxidation and Rearrangement	44
4.4.	Structural Analysis of 4.13 and 4.18	48
4.5.	Structural Analysis of 4.16 and 4.17	49

4.6.	De Novo Glycosylation Strategy	52
4.7.	OsO ₄ Oxidation/Addition/Rearrangement /Application	56
4.8.	Allene Halohydration.....	60
4.9.	Alternative to DMDO Oxidation	62
4.10.	Chelation-Controlled Reduction	65
4.11.	Benzylic Ether Cleavage by DDQ	68
4.12.	Conclusion	69
4.13.	References.....	71

Chapter 5: Allene Osmylation and Multicomponent Coupling

5.1.	Introduction.....	73
5.2.	History of Allene Osmylation.....	73
5.3.	Mechanistic Rationale and Stereochemical Outcome	75
5.4.	Allene osmylation and multi-component coupling.....	77
5.5.	Chiral allene: osmylation and multi-component coupling.....	80
5.6.	Cyclic Allene Osmylation: Model Study	84
5.7.	Cyclic Allene Osmylation.....	89
5.8.	Conclusion	93
5.9.	References.....	94

Chapter 6: The Ligand Design and Synthesis for SiRNA Delivery

6.1.	Introduction.....	95
6.2.	Quantom Dots (QDs)	96

6.3.	Glioblastoma Multiforme (GBM) and the Mutant Epidermal Growth Factors Receptor (EGFRvIII)	97
6.4.	siRNA.....	98
6.5.	Design and Synthesis of the multifunctional QD platform for delivery and tracking of siRNA	100
6.6.	Transfection efficiency & target –specific delivery of siRNA-QDs	102
6.7.	Target–specific delivery of siRNA-QDs	104
6.8.	Knockdown of EGFRvIII as a chemotherapeutic target by siRNA-QDs	104
6.9.	Conclusion.....	106
6.10.	References	108

Chapter 7: Experimental

7.1.	General	110
7.2.	Chapter 3	112
7.3.	Chapter 4	131
7.4.	Chapter 5	146
7.5.	Chapter 6	161
7.6.	References	170

Appendix: Spectral Data..... 171

I.	Chapter 3	172
II.	Chapter 4	212

III.	Chapter 5	521
IV.	Chapter 6	686
CURRICULUM VITAE.....		691

Lists of Tables

Table 3.3-1: Optimization of 1st Coupling Reaction.....	30
Table 5.4-1: Catalytic Allene Oxidation.....	78
Table 5.4-2: Allene Oxidation	79
Table 5.5-1: Chiral Allene Osmylation and Halide Addition	81

List of Schemes

Scheme 1.2-1: Acid Induced Transformation of Erythromycin	2
Scheme 1.5-1 Andrades' Synthesis of 4,8,10-Tridesmethyl Telithromycin.....	9
Scheme 2.5-1: Allene Oxidation.....	18
Scheme 3.2-1: Synthesis of the C6 Alkyne Coupling Partner	27
Scheme 3.2-2: Synthesis of the C5 Aldehyde Coupling Partner	28
Scheme 3.2-3: Synthesis of the C5 Alkyne Coupling Partner	28
Scheme 3.3-1: The 1st Coupling: Chelation-Controlled Alkynylation	30
Scheme 3.3-2: The 1st Coupling: Carreira Asymmetric Alkynylation.....	32
Scheme 3.3-3: Synthesis of Jiang's Modified Carreira Ligand	33
Scheme 3.4-1: Hydrolysis of the Acetal (Step 7)	33
Scheme 3.4-2: The Second Coupling (Step 8).....	34
Scheme 3.5-1: Synthesis of the Bis[Allene] Seco-Acid (Step 10).....	35
Scheme 3.6-1: Synthesis of Bis[Allene] Macrolactone (Step 11)	36
Scheme 4.2-1: Nucleophile Addition to SDE.....	41
Scheme 4.2-2: Dr. Ghosh's Attempt to Add Nucleophile to Bis[SDE].....	42
Scheme 4.2-3: Nucleophile Addition to SDE.....	43
Scheme 4.3-1: DMDO Oxidation and Rearrangement	45
Scheme 4.3-2: Mechanistic Rationale for 4.13 , 4.16 , 4.17 , and 4.18	47
Scheme 4.5-1: Acylation of 4.13 & 4.14 for Structural Proof of Furanone	51
Scheme: 4.5-2: Hydroxyl Protection in 4.16	52
Scheme 4.6-1: Oxime Formation.....	53

Scheme 4.6-2: Glycosylation	54
Scheme 4.6-3: Modified Synthesis of Desosamine Hydrochloric Salt.....	55
Scheme 4.6-4: Addition of Hydroxyl Amine Desosamine	56
Scheme 4.7-1: Desmethyl Erythromycinoids	58
Scheme 4.7-2: Mechanistic Rationale for 6,9-Bicyclolide 4.53	59
Scheme 4.7-3: Formation of C9-C12 α -Hydroxyenone, 4.59	60
Scheme 4.8-1: Electrophilic Bromination.....	60
Scheme 4.8-2: Mechanistic Postulation for 4.60	61
Scheme 4.9-1: Oxymercuration/Demercuration	63
Scheme 4.9-2: <i>m</i> CPBA Oxidation of 4.1	64
Scheme 4.9-3: Mechanistic Rationale for 4.68	65
Scheme 4.10-1: $\text{Zn}(\text{BH}_4)_2$ Reduction on α -Hydroxy Ketone by Paterson	65
Scheme 4.10-2: $\text{Zn}(\text{BH}_4)_2$ Reduction.....	66
Scheme 4.10-3: Key nOe Analysis of Alcohols at C5.....	67
Scheme 4.11-1: Benzylic Ether Cleavage by DDQ	68
Scheme 5.2-1: Asymmetric Dihydroxylation on Allene by Fleming	74
Scheme 5.2-2: Stoichiometric Allene Osmylation on a Steroidal Substrate	74
Scheme 5.2-3: Effect of Sterics on Regioselectivity	75
Scheme 5.2-4: Osmylation on Allenic Ketones	75
Scheme 5.4-1: DCC and DIC Addition	80
Scheme 5.5-1: Halogenated Furanose.....	83
Scheme 5.5-2: In-Situ Cleavage and Cyclization of 5.39	83
Scheme 5.6-1: Cyclic Chiral Allene Osmylation	85

Scheme 5.6-3: Catalytic Osmylation on Macrocyclic Bis[Allene] 2.24	88
Scheme 5.6-4: Polycyclic Ether Formation	88
Scheme 5.7-1: Osmylation of 4.1	89
Scheme 5.7-2: Chlorine Addition to Macrolactone	90
Scheme 5.7-3: Fluorine and Bromine Addition to Macrolactone.....	91
Scheme 5.7-4: Mechanistic Rationale for Stereochemistry of Bis[Fluorine] Addition....	93

List of Figures

Figure 1.1-1: Erythromycin	1
Figure 1.2-1: Commercialized Erythromycin Derivatives.....	3
Figure 1.3-1: Macrolides in Hydrophobic Pocket.....	6
Figure 1.4-1: A <i>Priori</i> SAR Study of Erythromycin	8
Figure 2.2-1: Synthetic Strategy: Bis[Allene] Macrolactone	15
Figure 2.4-1: Allene-Based Chemical Transformation from the Williams Group	17
Figure 2.6-1: Previous Model Study of the Bis [Allene] Macrolactone Strategy.....	20
Figure 2.7-1: Convergent & Recursive Assembly of a Macrocyclic Bis[Allene]	21
Figure 3.2-1: Convergent Synthesis.....	26
Figure 3.7-1: Flexibility of the Synthetic Route	37
Figure 4.1-1: Synthesis of Erythromycinoids	40
Figure 4.2-1: X-ray Crystal Structure of 4.4	42
Figure 4.2-1: Key nOe Analysis for Benzylic Ether Location in 4.12	44
Figure 4.4-1: Key nOe Analysis of 4.13 and 4.18	49
Figure 4.5-1: Structural Analysis of 4.17	50
Figure 4.5-2: Key nOe Analysis of 4.16 and 4.17	51
Figure 4.7-1: X-ray Crystal Structure of 4.54	58
Figure 4.8-1: Key nOe Analysis of 4.60	62
Figure 4.9-1: Key nOe Analysis of 4.68	64
Figure 4.11-1: Key nOe Analysis for Benzylic Ether Location in 4.80	68
Figure 4.11-2: Ground State Minimum Energy Conformation of 4.1	69

Figure 5.3-1: Allene Oxidation	76
Figure 5.5-1: Regiochemistry of 5.39 and 5.40	82
Figure 5.6-1: HMBC Confirmation of Two Central Allenic Carbons	86
Figure 5.6-2: X-ray Crystallography Data of Chlorine Addition, 5.50	87
Figure 5.6-3: Long-Range Correlations Through Oxygens in 5.55	89
Figure 5.7-1: Coupling Constants and nOe Analysis of Cyclic Ether Formation	91
Figure 6.2-1: UV-Vis Absorption Spectra and TEM Image of Quantum Dots	96
Figure 6.4-1: Mechanism of RNA interference	99
Figure 6.5-1: General Diagram of Multifunctional QD Conjugates	101
Figure 6.6-1: Transfection and Knockdown Effect by siRNA-QD Conjugates	103
Figure 6.7-1: Co-cultures of U87-EGFP cells and PC-12	104
Figure 6.8-1: Knockdown of EGFRvIII in U87-EGFvIII	105
Figure 6.8-2: Silencing Effect of EGFRvIII Gene	106

List of Abbreviations

°C	degrees Celsius
Å	Angstroms
Ac	acetyl
Ag ₂ O	silver (I) oxide
Akt	protein kinase B
AZM	azithromycin
Bn	benzyl
Bu ₂ BOTf	dibutylboron trifluoromethanesulfonate
CAM	clarithromycin
CITi(O ^{<i>i</i>} Pr) ₃	chlorotriisopropoxytitanium (IV)
DABCO	diazabicyclo[2.2.2]octane
DCC	<i>N,N'</i> -dicyclohexylcarbodiimide
DCM	dichloromethane
DDQ	2,3-dichloro-5,6-dicyano-1,4-benzoquinone
DIAD	diisopropyl azodicarboxylate
DIC	<i>N,N'</i> -dicycloisopropylcarbodiimide
DMAP	4-(<i>N,N</i> -dimethylamino)pyridine
DMDO	dimethyldioxirane
DMF	<i>N,N</i> -dimethylformamide
DMSO	dimethyl sulfoxide
DTT	dithiothreitol

eGFP	enhanced green fluorescence protein
EGFRvIII	epidermal growth factor receptor variant III
equiv.	equivalents
Et	ethyl
Et ₂ O	diethyl ether
EtOAc	ethyl acetate
FCC	flash column chromatography
GBM	glioblastoma multiforme
Hex	hexane
HFL	heterofunctional linkers
HIV	human immunodeficiency virus
HMBC	heteronuclear multiple-bond correlation spectroscopy
<i>i</i> -Bu	<i>iso</i> -butyl
imid	imidazole
<i>i</i> -Pr	<i>iso</i> -propyl
<i>i</i> -Pr ₂ NEt	diisopropylethylamine
LDA	lithium diisopropylamide
LiCCH-EDA	lithium acetylide-ethylenediamine
<i>m</i> -	meta-
M.S.	molecular sieves
Me	methyl
MLS _B	macrolide-lincosamide- <i>streptogramin</i> B
MsCl	methanesulfonyl chloride

mTOR	mammalian target of Rapamycin
NBS	<i>N</i> -bromosuccinimide
NCS	<i>N</i> -chlorosuccinimide
NMO	<i>N</i> -methylmorpholine <i>N</i> -oxide
nOe	nuclear overhauser effect
<i>o</i> -	ortho-
OsO ₄	osmium (VIII) tetroxide
<i>p</i> -	para-
PBS	phosphate buffered saline
PEG	polyethylene glycol
Ph	phenyl
PhH	benzene
PhMe	toluene
PI13K	phosphatidylinositol 3-kinase
PKS	polyketide synthase
PTEN	protein tyrosine phosphatase
pyr	pyridine
QD	quantum dot
RGD	arginine-glycine-aspartate peptide
RISC	RNA-induced silencing complex
rt	room temperature
RuO ₄	ruthenium (VIII) tetroxide
SAR	structure activity relationship

SDE	spirodiepoxide
siRNA	small interfering RNA
TBDPS	<i>tert</i> -butyldiphenylsilyl
TBS	<i>tert</i> -butyldimethylsilyl
TEA	triethyl amine
TESCl	triethylsilyl chloride
TFA	trifluoroacetic acid
TOPO	tri-octylphosphine oxide
wt%	weight percent

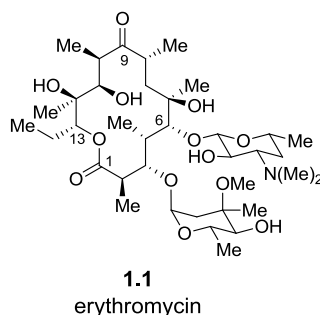
Chapter 1

Erythromycin and Its Derivatives

1.1. Introduction

Erythromycin **1.1**, an archetypal 14-membered macrolide, originally exhibited unique and superior biological properties such as its activity, safety, and mode of action in inhibiting bacterial protein synthesis.¹ Recently, Rubin et al. reported other biological functions such as the selective uptake by macrophages, extracellular kinase activity, and anti-asthmatic functions.²

Figure 1.1-1: Erythromycin



Even though its profuse utility for clinical use in human medicine since 1950, it showed several disadvantages, such as weak activity against gram-negative bacteria, induction of macrolide resistance, a bitter taste, and a tendency to produce gastrointestinal cramp as a consequence of the instability in the acidic medium of the stomach. This acid-instability caused a low and inconsistent bioavailability. These were

the initial major problems which directed the tremendous synthetic efforts to modify erythromycin.^{1, 3, 4}

1.2. Erythromycin Derivatives

It had been recognized that the degradation of erythromycin proceeds via interaction of the 6- and 12-hydroxy, 9-carbonyl and 8-hydrogen groups through intramolecular ketalization (Scheme 1.2-1).⁵ The resulting compound mimics the activity of motilin which causes stomach cramps.⁴ Consequently, significant research was devoted to the modification of these specific positions. The 2nd generation macrolides, clarithromycin **1.3**, azithromycin **1.4**, roxithromycin **1.5**, flurithromycin **1.6** and dirithromycin **1.7** were developed in the 1980s, and eventually commercialized in the 1990s (Figure 1.2-1).

Scheme 1.2-1: Acid Induced Transformation of Erythromycin

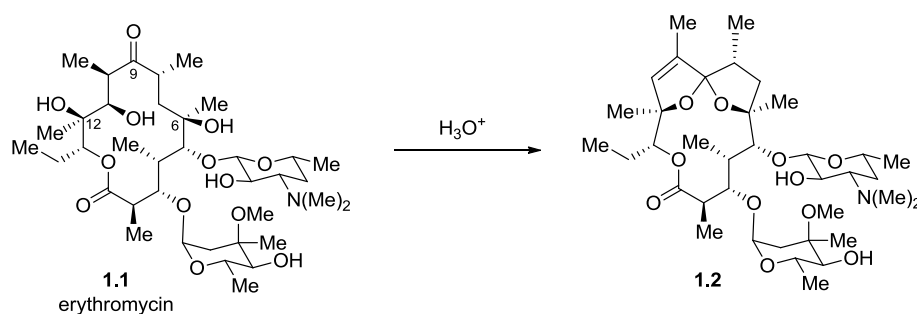
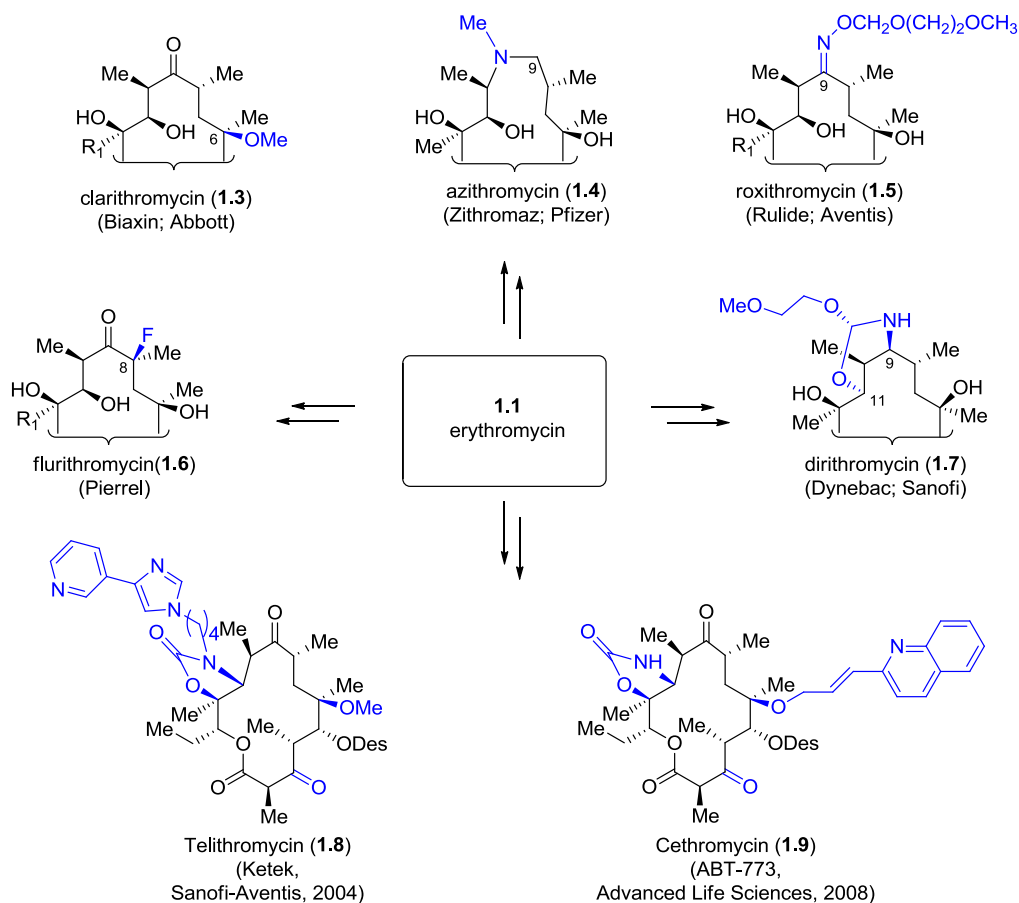


Figure 1.2-1: Commercialized Erythromycin Derivatives

All these drugs, however, present several drawbacks. They are inactive against macrolide, lincosamide, type B streptogramin (MLS_B)-resistant *streptococci* and *Streptococcus pneumoniae* and, with exception of azithromycin, weakly active against *Haemophilus influenzae*.⁴ Furthermore, the resistance of *S. pneumoniae* to erythromycin has increased significantly in recent years.⁶

A 2005 report indicated that ~30% of the *S. pneumoniae* strains in the United States were resistant to macrolides (erythromycin, azithromycin and clarithromycin). Although resistance among *S. pneumoniae* to single agents is problematic, more troublesome is the emergence and dissemination of multidrug-resistant (MDR) strains: MDR phenotypes cross several drugs, including macrolides, β -lactams, sulphonamides and tetracyclines. This emerging drug resistance clearly suggested an exigency for the 3rd generation macrolide and this quest resulted in the development of ketolides, which exhibit increased affinity to the ribosome as well as apparent lower sensitivity to known mechanisms of resistance. These 14-membered ring drugs are characterized by the keto group at the C3 position of the lactone ring, rather than the cladinose sugar found in the macrolides. Among many ketolides, two compounds were commercialized, telithromycin **1.8** and cethromycin **1.9**. Both feature an 11,12-carbamate group (Figure 1.2-1). In addition, telithromycin has an extended alkyl-aryl extending from the 11,12-carbamate group, whereas cethromycin has a quinolylallyl side chain at the C6 position of the lactone ring.

1.3. Binding Site and Modes of Action

The details of the molecular interactions of the various classes of macrolides with the ribosome were determined from X-ray crystallographic structures of the archaeal (*H. marismortui*) and bacterial (*D. radiocurans*) large ribosomal subunits in the laboratories of Tom Steitz^{7, 8} and Ada Yonath^{9, 10} respectively. The X-ray crystallographic structures revealed that the macrolide binding site is located on the large ribosomal subunit inside the nascent peptide exit tunnel near the peptidyl transferase center. Basically, this

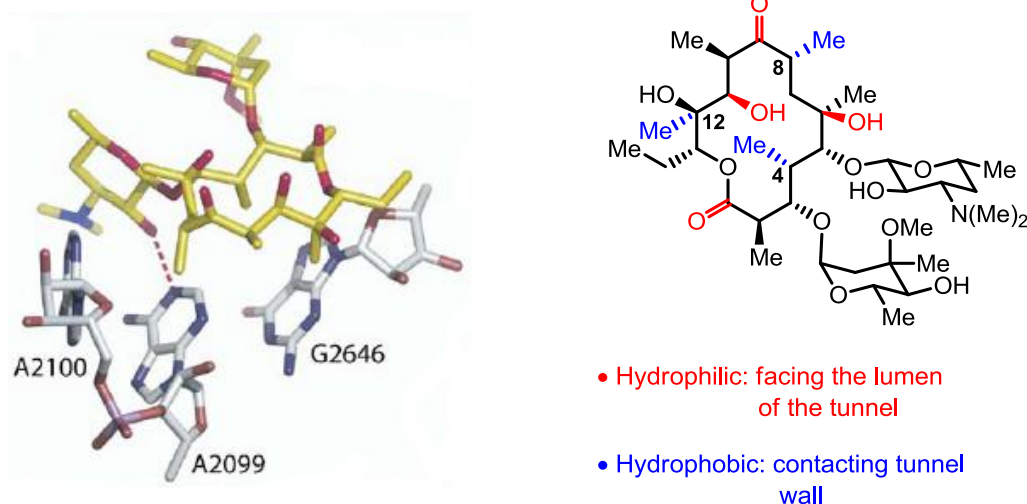
binding blocks the exit tunnel of the ribosome to prevent the departure of the nascent polypeptide, thereby halting protein synthesis. A number of nucleotide residues in domain V of 23S rRNA are involved in bonding with the macrolide molecule. Important contacts are found between the C5 mono- or disaccharide side chains of 14-, 15-, and 16-membered ring macrolides and rRNA. The desosamine sugar of erythromycin and other related 14-membered ring macrolides forms hydrogen bonding with the nitrogen bases of the nucleotide residues A2058, A2059 (*E. coli* numbering). The nucleotide, occupying position 2057, may also be involved in hydrogen bonding with the C5 desosamine of macrolide, or it may be establish hydrophobic interactions with the lactone ring. In addition, the desosamine sugar can potentially interact with the backbone phosphate oxygen of G2505. Hence, certain resistant microorganisms with mutational changes in components of this subunit of the ribosome fail to bind the drug.

Ketolides displayed increased binding to the ribosome as compared to the macrolides of previous generations. Their binding site overlaps the macrolide-binding site of domain V of 23S rRNA. In addition, ketolides bind to domain II. For example, telithromycin¹¹ binds to a specific adenine (A752) on domain II of 23S rRNA via the alkyl-aryl extension from the 11,12-carbamate bridge, whereas the quinolallyl side chain at the C6 position in cethromycin¹² makes a contact with U790 of domain II of 23S rRNA.

Binding affinity is affected not only by hydrogen bonding, but also by the hydrophobic interactions of the lactone ring with the ribosomal subunit. Steitz¹³ illustrated that the side of the lactone ring facing the lumen of the tunnel is hydrophilic, including two axially oriented hydroxyl (C6 & C11) and two axially oriented carbonyl

oxygens (C1 & C9). In contrast, the face of the lactone ring that contacts the tunnel wall is hydrophobic. It contains no hydrogen bond donors or acceptors, only consisting of three methyl groups (C4, C8 & C12) that reside in the hydrophobic pocket formed by the base of A2100 (A2059Ec), the hydrophobic C2 edge of A2099 (A2058Ec), and the base and sugar of G2546 (C2611Ec).

Figure 1.3-1: Macrolides in Hydrophobic Pocket (adapted with permission from ref.¹⁴)

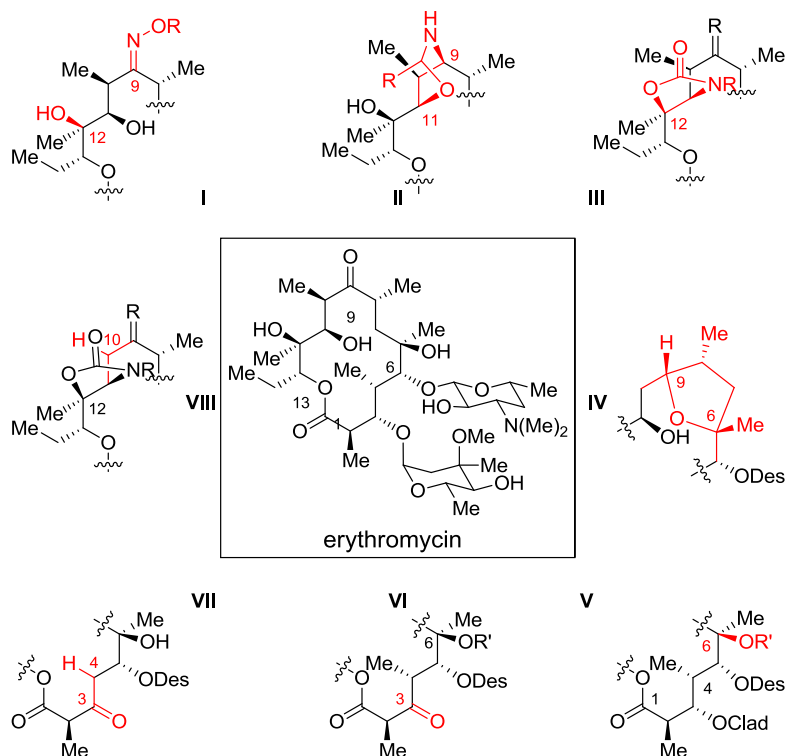


Regardless of the structures, the nucleotide at position 2058Ec was shown to play a major role in the binding of macrolides to the ribosome. As a consequence, it also plays a main role in the resistance to macrolides, often acquired by steric hindrance caused by its methylation or A-to-G mutation.^{15, 16}

1.4. Previous SAR Studies

The combination of low structural processability and high structural complexity of the erythromycins pose serious obstacles to addressing the problem of bacterial resistance. The known structure/activity profile (Figure 1.4-1) for erythromycin represents a tremendous effort.¹⁷⁻¹⁹ Briefly, a *priori* study has shown that: (a) portions of the glycans, especially desosamine, are critical and both the hydrophilic character of the β -face and hydrophobic character of the α -face dictate binding (erythromycin);²⁰ (b) C9 amine or oxime/ether functionality improves pharmacokinetic profiles (**I**);^{17, 19} (c) C9-C11 or C11-C12 heteroannulation can improve binding and appears to provide opportunities to overcome MLS_B resistance (**II**, **III**);^{21, 22} (d) ring formation between C6 and C9 can be beneficial,¹ leading to interesting bioactivities such as gastrointestinal motor stimulant albeit with non-antibiotic function (**IV**);²³ (e) retention of the C6 and C12 heteroatom connectivity is desirable and ether formation at C6 may improve antibiotic activity and suppress other activity (**I**, **V**);^{24, 25} (f) C3 ketone derivatives can improve efflux resistance (**VI**);^{22, 26} and (g) alterations to the hydrophobic face of the macrocycle (e.g. at C4, C8, and C10, **VII** and **VIII**) may overcome resistance.^{14, 27}

Figure 1.4-1: A Priori SAR Study of Erythromycin (adapted with permission from ref.²⁸)



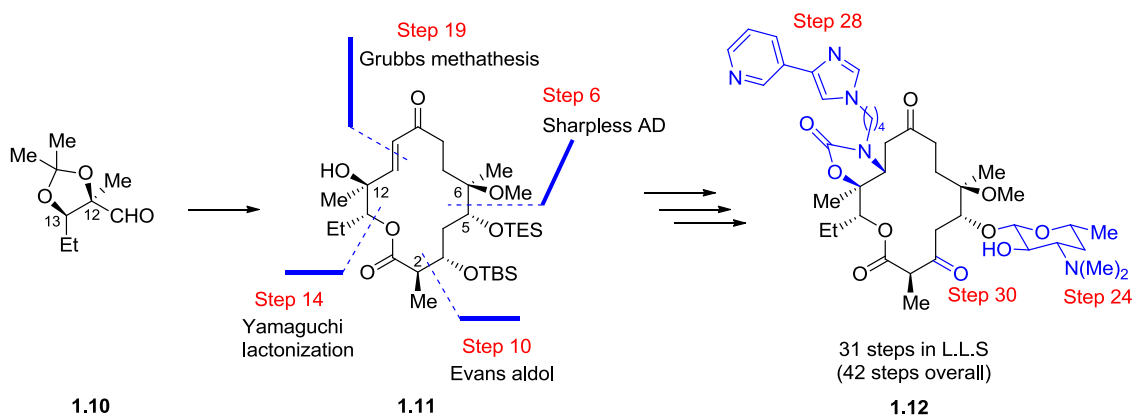
Hence, modification on the C3-C6 and C9-C12 regions offer opportunities to improve drug properties and avoid bacterial resistance.¹⁴ We therefore aimed to directly access diverse modifiable erythromycinoid variants to thereby expedite lead optimization studies.

Conventional medicinal chemistry approaches rely on erythromycin as a starting material (*See* Figure 1.1-2). However, total synthesis represents the only means by which to gain unrestricted access to this structure space. Indeed, *de novo* synthesis of the erythromycins has a rich history, and the knowledge gained from efforts to synthesize these targets is considerable.²⁹

1.5. Total Synthetic Approach to Erythromycin Derivatives

In 2011, Andrade et al. reported the total synthesis of 4,8,10-tridesmethyl telithromycin.¹⁴ As described in Section 1.2, telithromycin is a 3rd generation semisynthetic drug derived from erythromycin and characterized by the 11,12-carbamate side chain and 3-keto group. Their desmethylation strategy is grounded in structural data by Steitz and co-workers.¹³ Bacterial strains resistant to macrolide, lincosamide, type B streptogramin, and ketolide (MLS_BK) antibiotics commonly possess either an N-methyl transferase that methylates the exocyclic N6 amine in A2058Ec in 23S rRNA or a mutated 23S rRNA, often A2058G.¹⁶ Steitz and coworkers postulated the cause of resistance might due to a steric clash of the amino group of guanine 2058 with the C4 methyl of the drug.¹³

Scheme 1.5-1 Andrades' Synthesis of 4,8,10-Tridesmethyl Telithromycin



The synthesis commenced with the known aldehyde **1.10** for the construction of C11-C13 unit. Sharpless asymmetric dihydroxylation established the requisite stereochemistry at C5 and C6 at *step 6*. Construction of C2 and C3 bond was

accomplished via an Evans aldol reaction at *step 10*. After ring-closing methathesis (RCM) at *step 19*, the glycosylation (*step 24*), the elaboration with C11,C12-carbamate (*step 28*) and the oxidation at C3 (*step 30*) were applied. From macrocyclic structure **1.11**, it took additional 12 steps to finish the synthesis. The synthesis was very lengthy (42 steps overall, 31 steps in the longest linear sequence) though **1.12** exhibited antibacterial activity.

Andrades' synthesis demonstrated the advantage of total synthesis over semi-synthesis, namely the ability to modify the carbon skeleton selectively. However, the access to the structural/biological space of erythromycin analogs is far from the reality with single target-oriented synthesis.

1.6. Conclusion

Despite the development of new synthetic methods and strategies toward the erythromycin family, structural complexity and low structural processability are serious obstacles to addressing the problem of bacterial resistance through semi- and/or total synthesis. It is clear that comprehensive knowledge of structure/function space is essential prerequisite for the development of better drugs. Hence, the development of a *de novo* strategy that grants efficient access to diverse structures is imperative in order to conduct a comprehensive SAR study for erythromycin-based antibiotics.

This dissertation focuses on our advances to the efficient generation of erythromycinoids.

Chapter 2: Strategy for the Synthesis of *De Novo* Erythromycinoids

Chapter 3: Synthesis of the Bis[Allene] Macrolactone

Chapter 4: Synthesis of Erythromycinoids

Chapter 5: Allene Osmylation and Multicomponent Coupling

Additionally, a multidisciplinary collaborative project with Prof. Ki-Bum Lee (Department of Chemistry & Chemical Biology, Rutgers) is described in

Chapter 6: The Ligand Design and Synthesis for SiRNA Delivery.

1.7. References

1. *Macrolide antibiotics: chemistry, biology, and practice, 2nd ed.*; Satosh, O., Eds.; Academic Press: Amsterdam; Boston, 2002.
2. Shinkai, M.; Henke, M. O.; Rubin, B. K. *Pharmacology & Therapeutics* **2008**, *117*, 393.
3. Asaka, T.; Manaka, A.; Sugiyama, H. *Current Topics in Medicinal Chemistry* **2003**, *3*, 961.
4. Katz, L.; Ashley, G. W. *Chem. Rev.* **2005**, *105*, 499.
5. Kurath, P.; Jones, P.; Egan, R.; Perun, T. *Cellular and Molecular Life Sciences* **1971**, *27*, 362.
6. Doern, G. V.; Richter, S. S.; Miller, A.; Miller, N.; Rice, C.; Heilmann, K.; Beekmann, S. *Clinical Infectious Diseases* **2005**, *41*, 139.
7. Nenad Ban; Poul Nissen; Jeffrey Hansen; Peter B. Moore; Steitz, T. A. *Science* **2000**, *289*, 905.
8. Hansen, J. L.; Ippolito, J. A.; Ban, N.; Nissen, P.; Moore, P. B.; Steitz, T. A. *Molecular cell* **2002**, *10*, 117.
9. Harms, J.; Schlunzen, F.; Zarivach, R.; Bashan, A.; Gat, S.; Agmon, I.; Bartels, H.; Franceschi, F.; Yonath, A. *Cell* **2001**, *107*, 679.
10. Schlunzen, F.; Zarivach, R.; Harms, J.; Bashan, A.; Tocilj, A.; Albrecht, R.; Yonath, A.; Franceschi, F. *Nature* **2001**, *413*, 814.
11. Hansen, L. H.; Mauvais, P.; Douthwaite, S. *Molecular Microbiology* **1999**, *31*, 623.
12. Schlünzen, F.; Harms, J. M.; Franceschi, F.; Hansen, H. A. S.; Bartels, H.; Zarivach, R.; Yonath, A. *Structure* **2003**, *11*, 329.
13. Tu, D.; Blaha, G.; Moore, P. B.; Steitz, T. A. *Cell* **2005**, *121*, 257.
14. Velvadapu, V.; Paul, T.; Wagh, B.; Klepacki, D.; Guvench, O.; MacKerell, A.; Andrade, R. B. *ACS Med. Chem. Lett.* **2011**, *2*, 68.
15. Douthwaite, S.; Hansen, L. H.; Mauvais, P. *Molecular Microbiology* **2000**, *36*, 183.
16. Weisblum, B. *Antimicrob. Agents Chemother.* **1995**, *39*, 577.

17. Chantot, J.-F.; Bryskier, A.; Gasc, J.-C. *J. Antibiot.* **1986**, *39*, 660.
18. Gouin d'Ambrieres, Solange; Lutz, Andre; Gasc, Jean Claude. (Demande, Fr.). Erythromycin oxime derivatives and their use as drugs. FR Patent 2473525 A1 19810717. Language: French. 1981.
19. Gasc, J.-C.; D'Ambrieres, S. G.; Lutz, A.; Chantot, J.-F. *J. Antibiot.* **1991**, *44*, 313.
20. Mao, J. C. H.; Putterman, M. *J. Mol. Bio.* **1969**, *44*, 347.
21. Counter, F. T.; Ensminger, P. W.; Preston, D. A.; Wu, C. Y.; Greene, J. M.; Felty-Duckworth, A. M.; Paschal, J. W.; Kirst, H. A. *Antimicrob. Agents Chemother.* **1991**, *35*, 1116.
22. Agouridas, C.; Denis, A.; Auger, J.-M.; Benedetti, Y.; Bonnefoy, A.; Bretin, F. o.; Chantot, J.-F. o.; Dussarat, A.; Fromentin, C.; D'AmbriÃ¨res, S. G.; Lachaud, S.; Laurin, P.; Le Martret, O.; Loyau, V. r.; Tessot, N. *J. Med. Chem.* **1998**, *41*, 4080.
23. Omura, S.; Tsuzuki, K.; Sunazuka, T.; Marui, S.; Toyoda, H.; Inatomi, N.; Itoh, Z. *J. Med. Chem.* **1987**, *30*, 1941.
24. Morimoto, S.; Takahashi, Y.; Watanabe, Y.; Omura, S. *J. Antibiot.* **1984**, *37*, 187.
25. Morimoto, S.; Adachi, T.; MisawaI, Y.; Nagate, T.; Watanabe, Y.; Omura, S. *J. Antibiot.* **1990**, *43*, 544.
26. Fernandes, P. B.; Baker, W. R.; Freiberg, L. A.; Hardy, D. J.; McDonald, E. J. *Antimicrob. Agents Chemother.* **1989**, *33*, 78.
27. Dunkle, J. A.; Xiong, L.; Mankin, A. S.; Cate, J. H. D. *P. Natl. Acad. Sci. USA* **2010**, *107*, 17152.
28. Liu, K.; Kim, H.; Ghosh, P.; Akhmedov, N. G.; Williams, L. J. *J. Am. Chem. Soc.* **2011**, *133*, 14968.
29. Peng, Z.-H.; Woerpel, K. A. *J. Am. Chem. Soc.* **2003**, *125*, 6018.

Chapter 2

Strategy for the Synthesis of De Novo

Erythromycinoids: Bis[Allene] Macrolactone

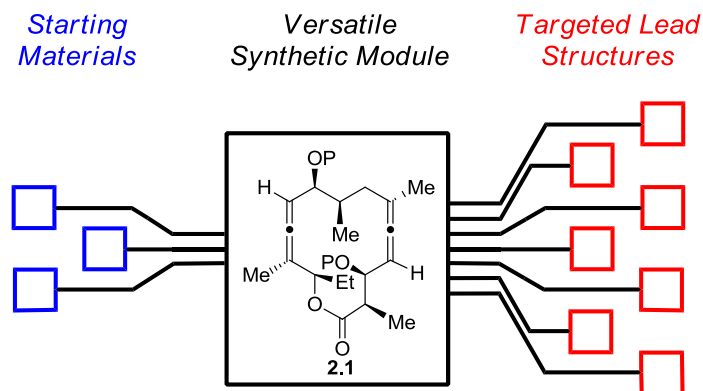
2.1. Introduction

Ideally, unrestricted access to diverse erythromycin analogs, including skeletal and stereochemical modifications, would require a minimal number of manipulations and no dramatic change in the synthetic route. Considering the model study and our extensive experience with and knowledge of allene transformations, we designated the fully functionalized bis[allene] macrolactone as a modular starting point for the construction of new analog scaffolds. Herein, I disclose our bis[allene] macrolactone strategy for the synthesis of *de novo* erythromycinoids.

2.2. Efficient Access to Diverse in Erythromycin Congeners

Our aim is to enable access to the diverse erythromycinoid structure space through efficient synthesis. The synthetic strategy considers: a) the structural space contains skeletal and stereochemical diversity; b) the versatile synthetic module leads to new sets of expandable intermediates, which ultimately constitute sets of targeted lead structure; and c) synthetic maneuvers should be minimal: the routes should be short.

Figure 2.2-1: Synthetic Strategy: Bis[Allene] Macrolactone (adapted with permission from ref.²⁵)



2.3. Synthetic Strategy: Bis[Allene] Macrolactone

To achieve the aim, we developed a bis[allene] macrolactone strategy, which is characterized by the following key points:

- Total synthetic approach
- Late-stage functionalization: allene oxidation
- Macrocyclic stereocontrol
- Convergent synthesis of bis[allene] macrolactone
- Divergent synthesis of erythromycinoids

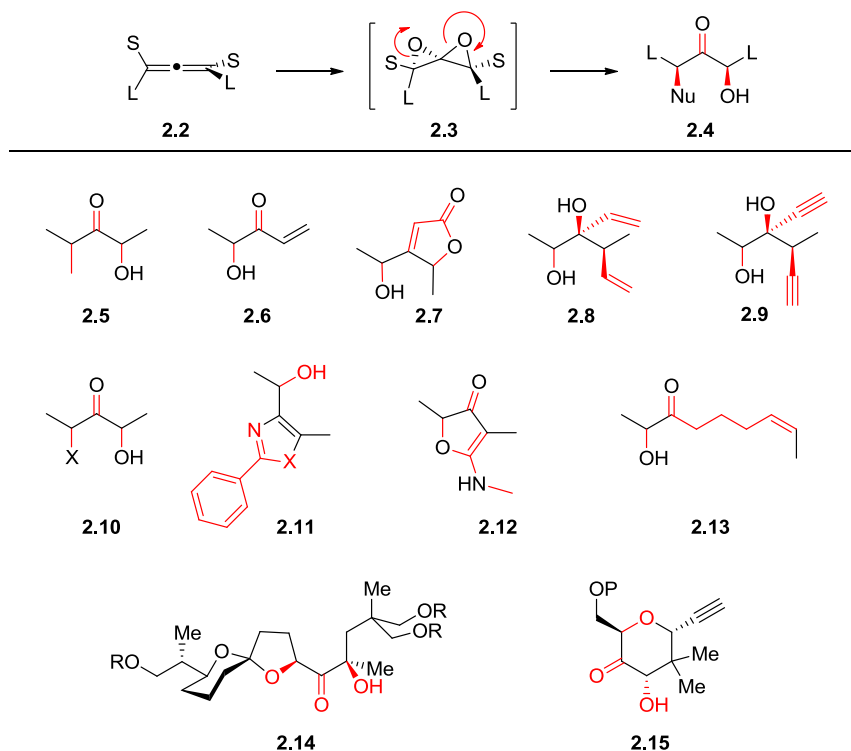
The most common method for erythromycin analog synthesis has been the derivatization of erythromycin itself. This semi-synthetic method has its own benefit from bountiful supply of erythromycin. However, the lack of synthetic flexibility not only requires lengthy synthetic manipulations of erythromycin but also limits the accessibility of potentially useful chemical and biological space.

Total synthesis might be a very lengthy way to generate analogs, but in the context of diversity-oriented synthesis,^{1, 2} it provides an excellent means of modification, especially on the carbon backbone, which is intractable when using the semi-synthetic method. Late-stage introduction of heterofunctionality³ is not considered an ideal strategy for target-oriented synthesis due to the risk of failure at a late stage. However, when it is combined with the versatile synthetic module, it can be greatly appreciated in terms of efficiency and diversity.

2.4. Allene Oxidation: Spirodiepoxide (SDE) Chemistry

As a result of their inherent chirality and high reactivity in such diverse transformations as addition, cyclization/cycloaddition, cycloisomerization, and cross-coupling reactions,^{4, 5} functionalized allenes have been employed in recent years as highly versatile precursors to natural products and other target molecules. Despite their demonstrated utility, allenes are still considered to be an “under-developed” functional group. Prof. Williams’ group has studied the synthesis⁶ and reactivity⁷ of allenes, developing many novel transformations to access diverse motifs (*See* Figure 2.4.-1).

Crandall’s pioneering work⁸⁻¹⁶ demonstrated that upon DMDO oxidation of allenes, the corresponding spirodiepoxides (SDEs) formed and various nucleophiles could be added. However, the synthetic utility of allenes in complex molecule synthesis was realized through the work in the Williams group.

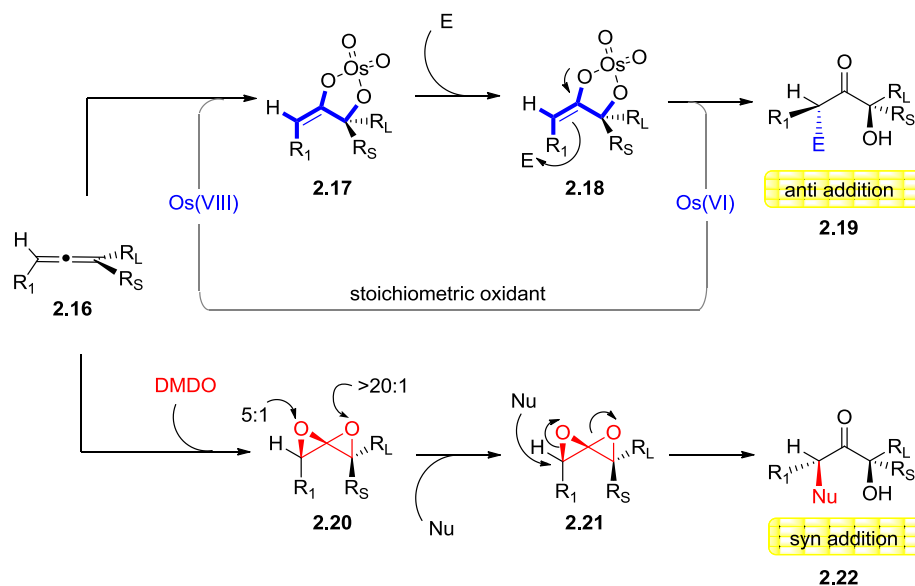
Figure 2.4-1: Allene-Based Chemical Transformation from the Williams Group

Various heteronucleophiles and carbon nucleophiles as well as ambiphilic reagents such as benzamide, thiobenzamide, benamidine, azide, intramolecular oxygen, and organometallic carbon¹⁷ are compatible with SDE chemistry and result in a complex motif such as a vicinal triad composed of hydroxyl, ketone, and syn-substituted nucleophiles,¹⁸ haloketones, α' -hydroxy enone,¹⁹ heterocycles (oxazoles, thiazoles, and imidazoles),²⁰ dihydrofuranone,⁷ butenolides, diendiols, diyndiol, γ -lactones, spiroketals,²¹ and pyrans²² with high regio- and stereoselectivity in a single step. The utility of SDEs was extended in synthetic studies of complex natural products such as epoxomicin,¹⁸ psymberin,²² pectenotoxin 4,²³ and erythromycin.^{24, 25}

2.5. Allene Oxidation: Osmylation

We have recently developed a method of allene osmylation. Osmium tetroxide (OsO_4) readily oxidized simple and complex linear allenes and the hydrolysis of the intermediate osmate ester gave α -hydroxy ketones both under catalytic and stoichiometric conditions (See Chapter 5 for details). When an electrophile is present upon the oxidation, it not only accelerated the hydrolysis of osmate ester **2.18** but also formed a multi-component adduct, giving α -hydroxy- α' -electrophile ketones (**2.16** \rightarrow **2.19**). For now, this OsO_4 -catalyzed multicoupling reaction of allenes is not fully appreciated in complex settings nor has the scope of electrophiles been fully explored. However, studies are ongoing. So far we have found compatible electrophiles are N-bromosuccinimide (NBS), N-chlorosuccinimide (NCS), Selectfluor, Eshenmoser's salt (dimethylmethyldene ammonium chloride), and chloramines-T (N-chloro tosylamide).

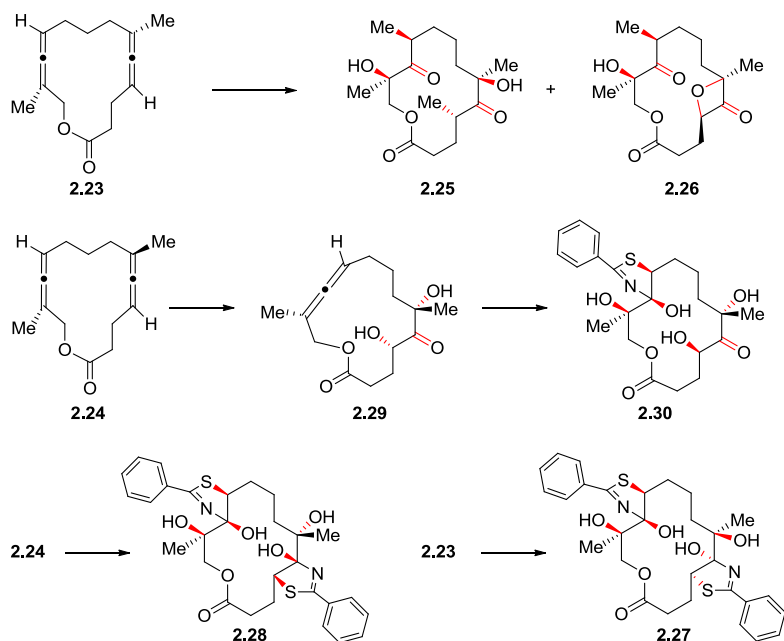
Scheme 2.5-1: Allene Oxidation



When applied on chiral allenes, the stereochemical outcome of the reaction complements our allene spirodiepoxidation/nucleophile capture methodology (**2.16** → **2.22**). Therefore, when applied on the macrocyclic bis[allene], it provides access to stereoisomers, and their unique SAR profiles, without invoking a new asymmetric route. Furthermore, the stereoselectivity is enhanced due the macrocyclic stereocontrol. The use of protecting groups was minimized via late-stage macrocyclic stereocontrol; furthermore, highly stereoselective reactions were achieved due to the conformational preferences of the macrolide intermediates.

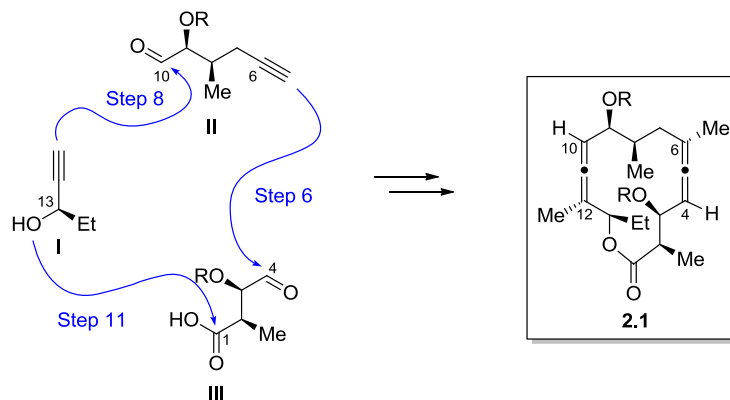
2.6. Model Study: Bis[allene] Macrolactone

Dr. Ghosh and co-workers in Prof. Williams' group demonstrated the macrocyclic bis[allene] strategy²⁴ on a simplified racemic macrocyclic bis[allene] (Figure 2.6-1). The study demonstrated that: (a) heterogeneous derivatization of the bis[allene] by stepwise oxidation; (b) successful addition of an organocuprate (MeCuCNLi) to the SDE, which represented the feasibility of SDE chemistry for polyketide-containing natural product synthesis; (c) complete macrocyclic stereocontrol; and (d) compatibility of SDE/nucleophile addition chemistry in a macrocyclic platform.

Figure 2.6-1: Previous Model Study of the Bis [Allene] Macrolactone Strategy

2.7. Convergent Synthesis of Bis[Allene] Macrolactone

Single-flask allene preparation,⁷ a method recently developed in Prof. Williams' group, helped us envision the synthesis of both allene (C4 to C6, C10 to C12) moieties in **2.1** from propargyl alcohols. The convergent, recursive alkynylation sequence (*step 6* and *step 8*), coordinated allene installation (*step 9*), and lactone formation (*step 11*) produce bis[allene] macrolactone (**2.1**).



2.8. Conclusion

The bis[allene] macrolactone strategy is designed to confer the efficiency and diversity on the structure/function space of erythromycinoids. Diversity will be achieved by late-stage oxidation of the bis[allene], which will undergo selective independent or concurrent modification. We have shown that allene oxidation, depending on the oxidant, can enable multi-component coupling with various nucleophiles and electrophiles in a highly stereoselective manner. This coordinated synthetic maneuver will provide the stereochemical and skeletal diversities, which can easily be expanded into functional group and appendage diversities. The route is designed so as to enable modification on the carbon skeleton where precedent methodologies cannot access.

Hence, the unexplored structure/function space of erythromycin antibiotics can be realistically reached.

In the following chapter, I discuss the synthesis of the bis[allene] macrolactone.

2.9. References

1. Burke, M. D.; Schreiber, S. L. *Angw. Chem. Int. Ed. Engl.* **2004**, *43*, 46.
2. Galloway, W. R. J. D.; Bender, A.; Welch, M.; Spring, D. R. *Chem. Comm.* **2009**, 18, 2446.
3. *The Logic of Chemical Synthesis*; Corey, E. J.; Cheng, X.-M.; John Wiley & Sons, Inc.: New York, 1989.
4. *Modern Allene Chemistry*; Krause, N.; Hashmi, S. K., Eds.; WILEY-VCH: Weinheim, Germany, 2004; Vol. 1 & 2.
5. Kim, H.; Williams, L. J. *Curr. Opin. Drug Discovery Dev.* **2008**, *11*, 870.
6. Kolakowski, R. V.; Manpadi, M.; Zhang, Y.; Emge, T. J.; Williams, L. J. *J. Am. Chem. Soc.* **2009**, *131*, 12910.
7. Sharma, R.; Manpadi, M.; Zhang, Y.; Kim, H.; Ahkmedov, N. G.; Williams, L. J. *Org. Lett.* **2011**, *13*, 3352.
8. Crandall, J. K.; Machleder, W. H. *J. Am. Chem. Soc.* **1968**, *90*, 7292.
9. Crandall, J. K.; Machleder, W. H.; Thomas, M. J. *J. Am. Chem. Soc.* **1968**, *90*, 7346.
10. Crandall, J. K.; Machleder, W. H. *J. Am. Chem. Soc.* **1968**, *90*, 7347.
11. Crandall, J. K.; Paulson, D. R. *J. Org. Chem.* **1968**, *33*, 991.
12. Crandall, J. K.; Conover, W. W.; Komin, J. B.; Machleder, W. H. *J. Org. Chem.* **1974**, *39*, 1723.
13. Crandall, J. K.; Batal, D. J. *J. Org. Chem.* **1988**, *53*, 1338.
14. Crandall, J. K.; Rambo, E. *J. Org. Chem.* **1990**, *55*, 5929.
15. Crandall, J. K.; Batal, D. J.; Sebesta, D. P.; Lin, F. *J. Org. Chem.* **1991**, *56*, 1153.
16. Crandall, J. K.; Machleder, W. H.; Sojka, S. A. *J. Org. Chem.* **1973**, *38*, 1149.
17. Ghosh, P.; Lotesta, S. D.; Williams, L. J. *J. Am. Chem. Soc.* **2007**, *129*, 2438.
18. Katukojyala, S.; Barlett, K. N.; Lotesta, S. D.; Williams, L. J. *J. Am. Chem. Soc.* **2004**, *126*, 15348.

19. Ghosh, P.; Cusick, J. R.; Inghrim, J.; Williams, L. J. *Org. Lett.* **2009**, *11*, 4672.
20. Lotesta, S. D.; Kiren, S.; Sauers, R. R.; Williams, L. J. *Angw. Chem. Int. Ed. Engl.* **2007**, *46*, 7108.
21. Lotesta, S. D.; Hou, Y.; Williams, L. J. *Org. Lett.* **2007**, *9*, 869.
22. Shangguan, N.; Kiren, S.; Williams, L. J. *Org. Lett.* **2007**, *9*, 1093.
23. Joyasawal, S.; Lotesta, S. D.; Akhmedov, N. G.; Williams, L. J. *Org. Lett.* **2010**, *12*, 988.
24. Ghosh, P.; Zhang, Y.; Emge, T. J.; Williams, L. J. *Org. Lett.* **2009**, *11*, 4402.
25. Liu, K.; Kim, H.; Ghosh, P.; Akhmedov, N. G.; Williams, L. J. *J. Am. Chem. Soc.* **2011**, *133*, 14968.

Chapter 3

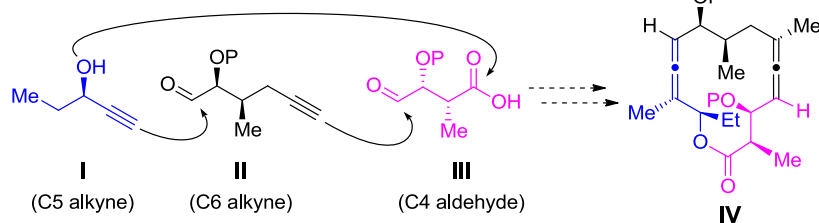
Synthesis of the Bis[Allene] Macrolactone

3.1. Introduction

We have focused on developing a single short route for the chemical synthesis of diverse erythromycinoids. The bis[allene] macrolactone was envisioned as a versatile synthetic module. The first generation of the synthesis was carried out by our former colleague, Dr. Partha Ghosh.¹ Kai Liu and I have since made considerable improvements, especially in terms of reproducibility. This chapter focuses on the experimental details of the synthetic route for the bis[allene] macrolactone.

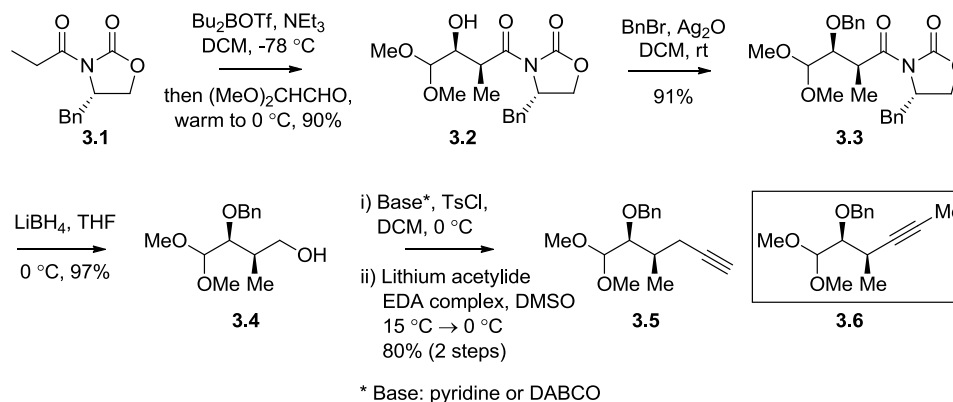
3.2. Synthesis of Coupling Units

Three readily available fragments (**I**, **II**, and **III**) were prepared and combined to provide the bis[allene] macrolactone **IV** (Figure 3.2-1). For the sake of convenience, they are referred to here as the C5 alkyne, C6 alkyne, and C4 aldehyde for **I**, **II**, and **III**, respectively. Two versions of the bis[allene] macrolactone were prepared, one with benzylic ethers and the other with *meta*-fluorobenzyl ethers, masking the hydroxyl groups at C3 and C9.

Figure 3.2-1: Convergent Synthesis

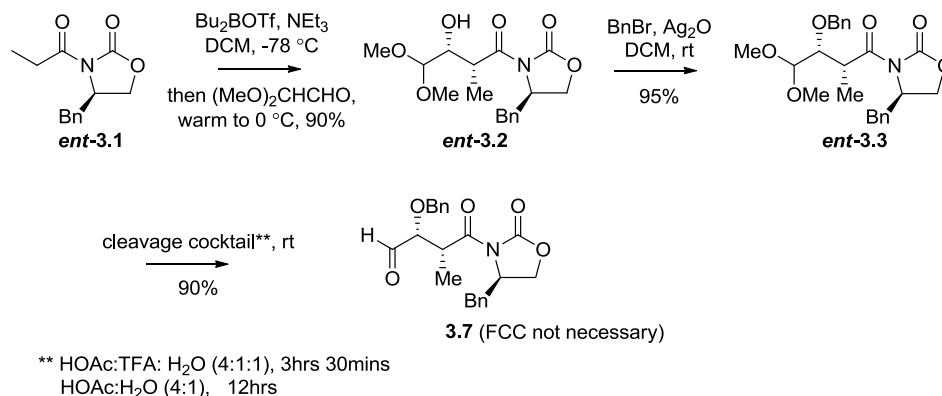
The synthesis of C6 alkyne **3.5** commenced with an Evans asymmetric aldol reaction (Scheme 3.2-1).² The addition of the enolate, derived from oxazolidinone **3.1**, to commercially available dimethoxyacetaldehyde afforded the expected aldol product **3.2** as a single isomer (90%). 1,1-dimethoxyacetaldehyde is commercially available as a solution in H₂O. The anhydrous form of the aldehyde was obtained by extraction with dichloromethane (DCM) and drying over 4Å molecular sieves. Subsequent benzyl etherification was accomplished using benzyl bromide, Ag₂O, and 4Å molecular sieves in anhydrous DCM **3.3** (95%).³ Though the reaction was done cleanly, it was quite slow (2 days). Our former colleague Dr. Ghosh reported that when using conventional NaH and benzyl bromide, the benzylation gave several by-products. He also noted that this is the first example of an Ag₂O mediated benzylation of an Evans aldol product.

Scheme 3.2-1: Synthesis of the C6 Alkyne Coupling Partner



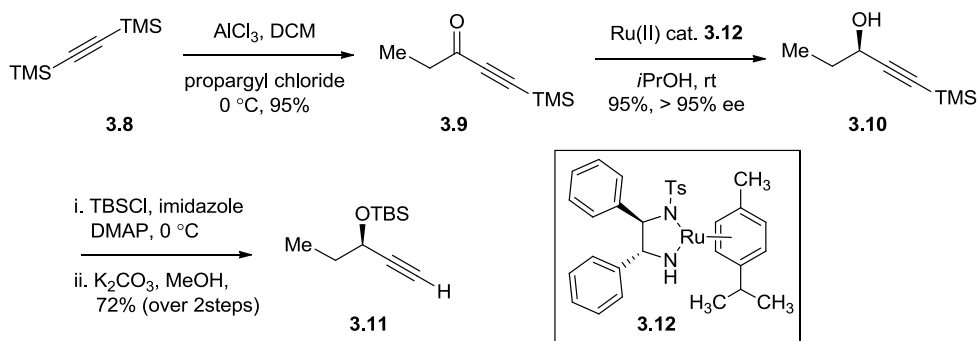
The hydride reduction⁴ provided the desired alcohol **3.4** (97%). It was observed that the yield was reproducible when the temperature was kept at 0 °C, rather than increasing the temperature from 0 °C to room temperature. The tosylation was done within 1 hour when employing 1,4-diazabicyclo[2.2.2]octane (DABCO) as the base.⁵ Dr. Ghosh reported that the tosylation took about 12 hours with pyridine. The primary tosylate was not purified; rather, the crude material was subjected to lithium acetylide to give alkyne **3.5** (80% over two steps).⁶ Upon quenching with saturated aqueous solution of NH₄Cl, the side-product **3.6** formed considerably and was very difficult to separate from **3.5**. Side-product formation was prevented by cooling to 0 °C before quenching.

Scheme 3.2-2: Synthesis of the C5 Aldehyde Coupling Partner



The antipode of **3.3** was prepared from **ent-3.1** using identical procedures (Scheme 3.2-2). For the coupling with alkyne **3.5**, **ent-3.3** was hydrolyzed under acidic conditions. Dr. Ghosh reported that the hydrolysis took 12 hours in 80% aqueous acetic acid, but when trifluoroacetic acid was added into the cleavage cocktail, the hydrolysis went remarkably faster (3.5 hours). It was found that purification of **3.7** by flash column chromatography (FCC) was not necessary for the subsequent alkynylation step. Notably, significant amount of **3.7** decomposed on silica gel.

Scheme 3.2-3: Synthesis of the C5 Alkyne Coupling Partner

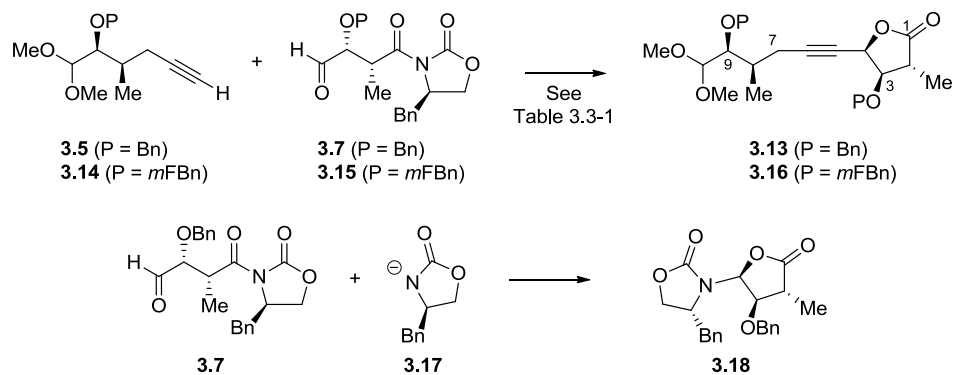


Propargyl alcohol **3.11** was prepared from commercially available bis-TMS acetylene **3.8**, adopting a procedure developed by our former colleague, Dr. Stephen D. Lotesta (Scheme 3.2-3).⁷ AlCl₃-promoted Friedel Crafts-type acylation gave the alkynone **3.9** (95%), which was followed by a Noyori asymmetric reduction of the ketone. The propargyl alcohol was obtained in 90% yield with >95% ee (Mosher ester analysis).⁸ The alcohol was protected as the *tert*-butyldimethylsilyl (TBS) ether, then the trimethylsilyl (TMS) group was cleaved in the same pot (72% yield over two steps).

3.3. Optimization of the 1st Coupling (Step 6): C1 to C9

Two coupling units, aldehyde **3.7** and alkyne **3.5**, were chosen for a chelation-controlled addition to generate propargyl lactone **3.13** (Scheme 3.3-1). Dr. Ghosh reported that the chelation-controlled addition of the zinc alkynylide of alkyne **3.5** to aldehyde **3.7**, followed by spontaneous *in situ* lactonization gave **3.13** in a modest 64% yield as a 8:1 mixture of diastereomers (entry 1, Table 3.3-1). Using the *meta*-fluorobenzyl ether, he also reported **3.16** in a 35 % yield as a 6:1 mixture of diastereomers (entry 4, Table 3.3-1). However, my colleague Kai Liu and I realized that the reaction yield is not reproducible using Dr. Ghosh's condition for both benzylic and *meta*-fluorobenzylic ethers.

Scheme 3.3-1: The 1st Coupling: Chelation-Controlled Alkynylation



In his thesis¹, he argued that the propargylation competes with a side reaction in which the starting aldehyde **3.7** undergoes rearrangement to **3.18**, promoted by the auxiliary anion **3.17**. The amount of anion **3.17** increases as the propargylation proceeds. Consequently, the relative rate of the side reaction increase, relative to the rate of formation of the desired product.⁹ Minimizing this side reaction by adjusting temperature proved difficult as the propargylation only takes place within a narrow temperature range. The reaction is sluggish below -10 °C, but proceeds rapidly at 0 °C.

Table 3.3-1: Optimization of 1st Coupling Reaction

Entry	Equivalents			Addition temp. (°C)		Addition Rate	Yield
	Alkyne	Aldehyde	Base (metal) ^b	ZnBr ₂	Aldehyde		
1 ^a (P=Bn)	1	1	1	-40 → -10	-10	1 hr	57% (8:1)
2 (P=Bn)	2.3	1	2.3	-40 → -10	10	1 hr	58% (6:1)
3 (P=Bn)	2.3	1	2.3 (3.3)	-40 → -10	10	1 hr	63% (8:1)
4 ^a (P= <i>m</i> FBn)	1.3	1	1.3	-78	-10	2 hrs	35% (6:1)

5 (P= <i>m</i> FBn)	3.5	1	3.5	-78	-10	30min	30% (5:1)
6 (P= <i>m</i> FBn)	2.5	1	2	-78 (Et ₂ AlCl)	-10	30min	63% (1:2)

a) Reaction done by Dr. Ghosh and reported in his Ph.D thesis and not reproducible.¹ b) Indicated when the equivalence of metal is different from that of base.

This reaction was optimized by altering several variables such as the equivalents of alkyne and base, the equivalents of chelation metal, the addition temperature of aldehyde, the chelation metal, and the rate of aldehyde addition (Table 3.3-1).

For the benzylic ether, the reaction yield and selectivity were reproducible when using a large excess of alkyne (entry 2), and the diastereoselectivity was better when the equivalents of chelation metal was the sum of the equivalents of alkyne and aldehyde (entry 3). To avoid the side reaction, the temperature was kept at 10 °C for 8 hours after the addition of aldehyde.

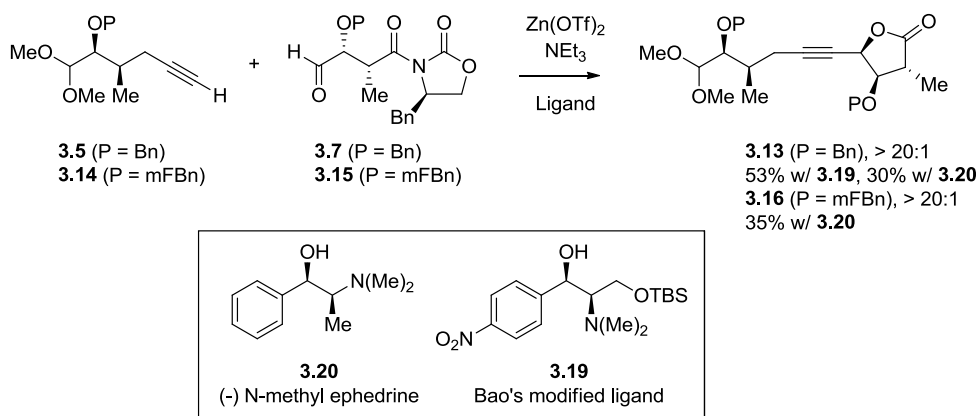
After thorough optimization, reproducible conditions were found and the reaction was scaled up to a maximum of 3.5 g (C4 aldehyde). The highest obtained yield of **3.13** was 63% (entry 3). Based on recovered alkyne **3.5**, however, the yield is an excellent 95%.

Optimization studies using the *meta*-fluorobenzylic ether resulted in a highest yield of 35%. From all the data that was collected, it was concluded that zinc may not be an effective metal in the case of the *meta*-fluorobenzylic ether. The electron-withdrawing nature of the *meta*-fluorobenzyl group may be reducing the ability of the aldehyde oxygen to chelate with the metal. Therefore, we explored alternative metals. Using diethylaluminum chloride as a Lewis acid, we achieved a higher combined yield of

the product, but the selectivity was poor. The undesired diastereomer was preferred under these conditions, giving a 2:1 ratio of undesired/desired diastereomers.

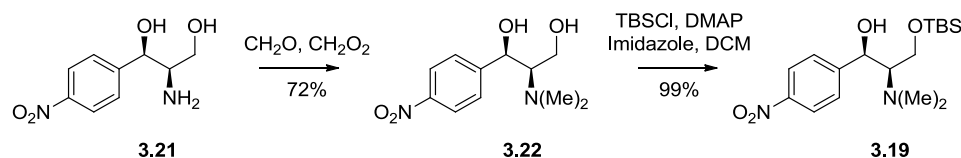
Chelation-controlled addition of zinc alkynilides to α -alkoxy aldehydes is known to proceed with high *syn* selectivity.¹⁰ Although the expected stereochemistry was confirmed later by X-ray crystallography data of erythromycinoids (*See* Chapter 4), it was not clear at this moment if the desired diastereoselection was achieved. The *syn* selectivity in the major diastereomer of **3.13** was rationalized a number of ways such that: *a*) the coupling constant of the propargylic proton in ¹H NMR appeared (1H, td, 2.0 Hz, 6.5 Hz) in the major isomer and (1H, td, 2.0 Hz, 5.0 Hz) in the minor isomer. Although this difference is small, the trend is the same as that for similar substrates reported in the literature;¹¹ *b*) Carreira's asymmetric alkynylation gave the desired product **3.13** as the sole product.¹² When (-)-*N*-methylephedrine **3.20** was used, the reaction yield was 30% with complete diastereoselection. Jiang et al. reported the modified ligand **3.19** for the Carreira reaction.¹³

Scheme 3.3-2: The 1st Coupling: Carreira Asymmetric Alkynylation



3.19 was synthesized in two steps according to Jiang et al. (Scheme 3.3-3).¹⁴ For both protecting groups, it gave complete diastereoselection with moderate yields, but a large excess of alkyne was required (4 equivalents). Since among the three coupling units the synthesis of alkyne **3.5** is the longest linear sequence, it makes ZnBr₂-mediated chelation-controlled alkynylation the most practical approach to pushing material forward.

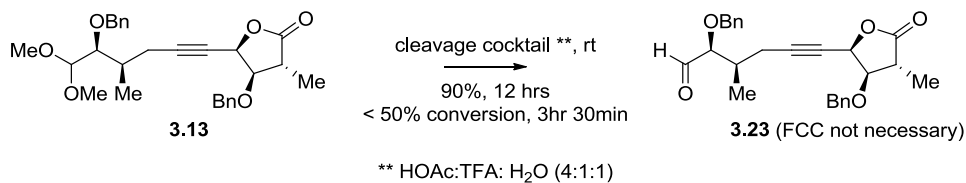
Scheme 3.3-3: Synthesis of Jiang's Modified Carreira Ligand¹⁴



3.4. Optimization of the 2nd Coupling: C1 to C14

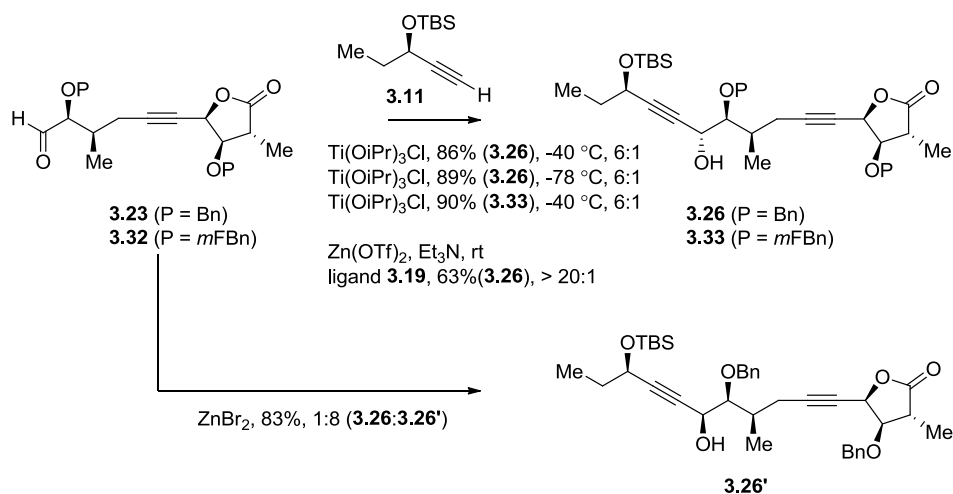
When propargyl lactone **3.13** was subjected to the cleavage cocktail (HOAc:TFA:H₂O = 4:1:1), less than 50% was converted to the desired aldehyde **3.23** in 3.5 hours. This was in sharp contrast to the conversion of *ent*-**3.3** → **3.7** in 90% yield under the same conditions (Scheme 3.4-1).

Scheme 3.4-1: Hydrolysis of the Acetal (Step 7)



Nonetheless, subjecting the acetal **3.13** to a 4:1:1 mixture of HOAc, TFA and H₂O afforded the aldehyde **3.23** in 90% yield after 12 hours of stirring at room temperature. The aldehyde **3.23** turned out to be somewhat unstable to silica gel chromatography. Therefore, it was quickly advanced to the next reaction without chromatography.

Scheme 3.4-2: The Second Coupling (Step 8)



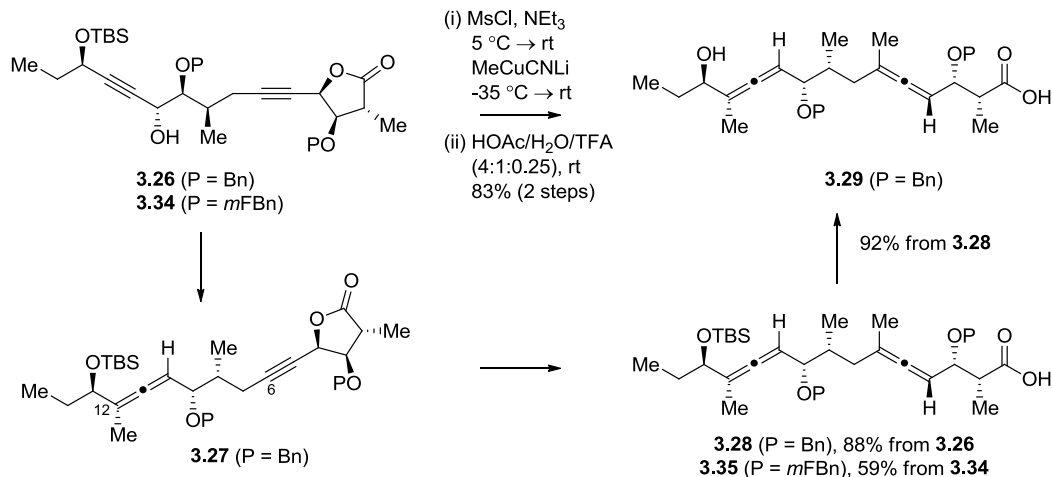
Non-chelation controlled additions of titanium triisopropoxy alkynilides to α -alkoxy aldehydes are known to give products with high *anti* selectivity.¹⁵ The alkynylide derived from **3.11** was combined with **3.23** in the presence of titanium triisopropoxide chloride. These addition products were also readily separable and the major product (**3.26**) was taken forward (89%, dr 6:1). The stereochemistry was postulated at this stage of the synthesis by the comparison of a major product from chelation controlled zinc alkynylide, using ZnBr_2 instead of $\text{Ti}(\text{OiPr})_3\text{Cl}$ and Carreira asymmetric alkynylation. Using ZnBr_2 as the chelation metal, Dr. Ghosh reported that the product **3.27** was obtained in 83% yield, which strongly supported the structural assignment. Carreira's

asymmetric alkynylation with the modified ligand **3.19** gave the desired product with complete diastereoselection in 63% yield.

3.5. Synthesis of the Bis[allene] Seco-acid

A single-flask conversion of the hydroxyl unit of **3.26** to bis[allene] **3.28** was accomplished by converting **3.26** to the mesylate followed by addition of excess lower order methyl cyanocuprate (Scheme 3.5-1). Deprotection of the TBS group under acidic conditions gave the bis[allene] seco-acid **3.29** in 92% yield. It was found that crude **3.28** could also be converted to **3.29** without flash column chromatography (83% over two steps).

Scheme 3.5-1: Synthesis of the Bis[Allene] Seco-Acid (Step 10)



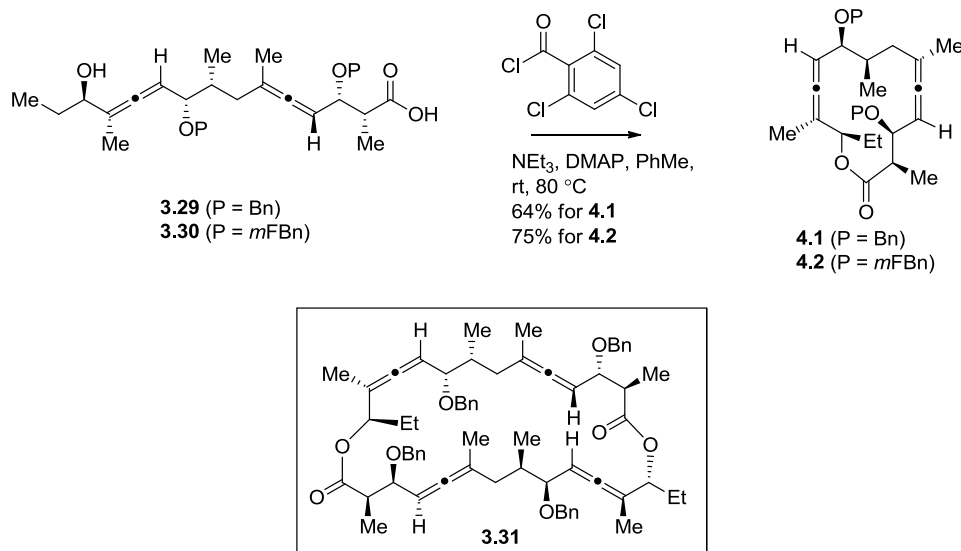
When the temperature was kept below -20 °C after the addition of lower order methyl cyanocuprate to *in situ* mesylate, the major product was mono[allene] **3.27**. Although the single-flask conversion to the bis[allene] is very convenient, mono[allene]

3.27 is a useful intermediate that offers the flexibility to generate heterogeneous functionalities on C6 and C12.

3.6. Macrolactonization

Yamaguchi macrolactonization of seco-acids **3.29** and **3.30** provided bis[allene] macrolactones **4.1** and **4.2** in 64% and 75% yield, respectively. It is well preceded that the addition of sp^2 centers on the periphery of the ring decreases the transannular ring strain, thereby it facilitates the ring closure.¹⁶ The major byproduct of these lactonizations is the dimer **3.31** derived from the seco-acids. Four methyl groups on allenes as doublet of doublet in 1H NMR confirm the dimer formation.

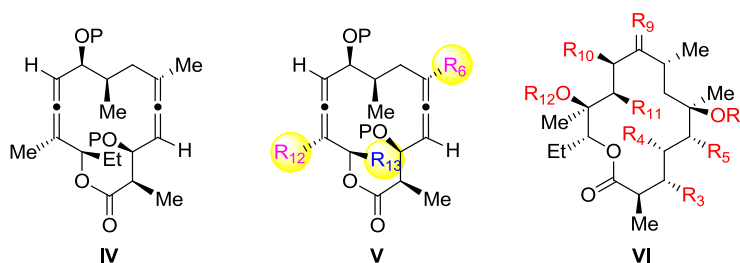
Scheme 3.6-1: Synthesis of Bis[Allene] Macrolactone (Step 11)



3.7. Conclusion: Flexibility of the Synthetic Route

The bis[allene]macrolactone was prepared in a longest linear sequence of 11 steps (overall yield ~ 18%) by two consecutive alkynations (*steps 6 & 8*), single-flask bis[allene] synthesis (*step 9*) and macrocyclization (*step 11*). Considering the relatively late-stage elaboration of the carbon backbone (C6, C12, and C13) and adjustable methodologies, the flexibility of the current synthetic route can be easily envisioned for incorporation of hetero-functionalities at C6, C12, and C13 (**V**, Figure 3.7-1).

Figure 3.7-1: Flexibility of the Synthetic Route



In Chapter 4, I will discuss the synthesis of erythromycinoids (**IV** → **VI**).

3.8. References

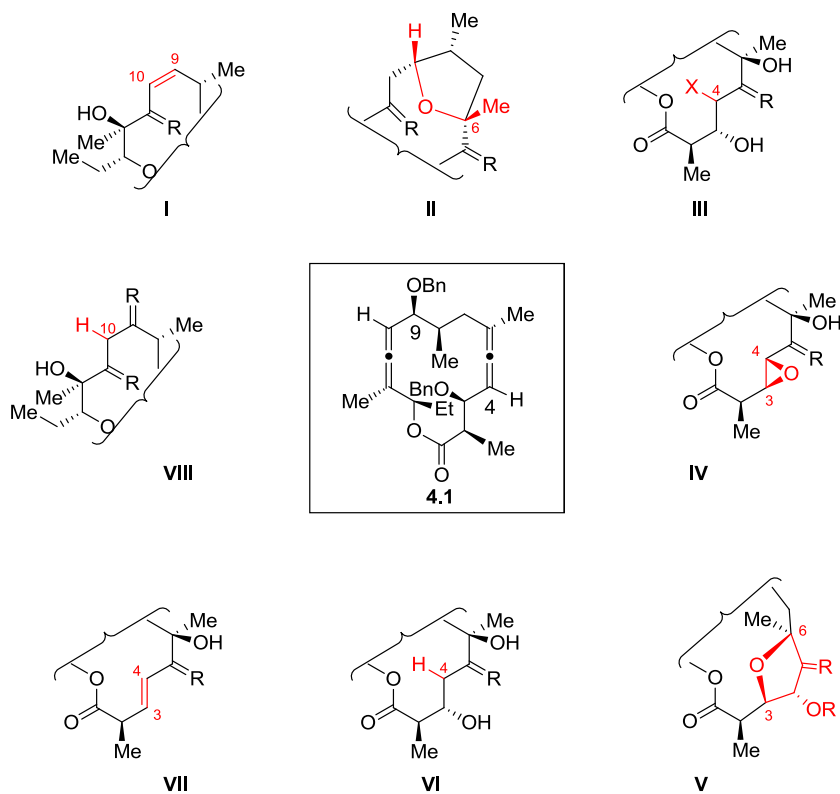
1. Ghosh, P. New methods and strategies towards total synthesis of (9S)-dihydroerythronolide A. Ph.D. Thesis, Rutgers, The State University of New Jersey, New Brunswick, 2008.
2. Evans, D. A.; Bartroli, J.; Shih, T. L. *J. Am. Chem. Soc.* **1981**, *103*, 2127.
3. Vlahov, I. R.; Vlahova, P. I.; Schmidt, R. R. *Tet. Lett.* **1991**, *32*, 7025.
4. Evans, D. A.; Ratz, A. M.; Huff, B. E.; Sheppard, G. S. *J. Am. Chem. Soc.* **1995**, *117*, 3448.
5. Hartung, J.; Hunig, S.; Kneuer, R.; Schwarz, M.; Wenner, H. *Synthesis* **1997**, 1433.
6. Maleczka, R. E.; Terrell, L. R.; Geng, F.; Ward, J. S. *Org. Lett.* **2002**, *4*, 2841.
7. Ghosh, P.; Lotesta, S. D.; Williams, L. J. *J. Am. Chem. Soc.* **2007**, *129*, 2438.
8. Matsumura, K.; Hashiguchi, S.; Ikariya, T.; Noyori, R. *J. Am. Chem. Soc.* **1997**, *119*, 8738.
9. Wu, Y.; Li, L.; Sun, Y.-P. *Synlett* **2004**, *1*, 125.
10. Mead, K. T. *Tet. Lett.* **1987**, *28*, 1019.
11. Rej, R.; Nguyen, D.; Go, B.; Fortin, S.; Lavallo, J.-F. *J. Org. Chem.* **1996**, *61*, 6289.
12. Frantz, D. E.; Fässler, R.; Carreira, E. M. *J. Am. Chem. Soc.* **2000**, *122*, 1806.
13. Jiang, B.; Chen, Z.; Xiong, W. *Chem. Comm.* **2002**, *14*, 1524.
14. Jiang, B.; Chen, Z.; Tang, X. *Org. Lett.* **2002**, *4*, 3451.
15. Shimizu, M.; Kawamoto, M.; Niwa, Y. *Chem. Comm.* **1999**, *12*, 1151.
16. Mulzer, J. *Angw. Chem. Int. Ed. Engl.* **1991**, *30*, 1452.
17. Corey, E. J.; Brunelle, D. J. *Tet. Lett.* **1976**, *17*, 3409.
18. Corey, E. J.; Nicolaou, K. C. *J. Am. Chem. Soc.* **1974**, *96*, 5614.

Chapter 4

The Synthesis of De Novo Erythromycinoids

4.1. Introduction

To date, bis[allene] macrolactone **4.1** has been converted to over 30 novel macrolides (Figure 4.1-1). These de novo analogs serve to validate the strategy and lay the foundation for further work. Taken together, the allene-based transformations employed in this study, such as DMDO oxidation/nucleophile addition, allene osmylation/electrophile addition, halohydrin formation, allene oxide rearrangement, spirodiepoxide (SDE) rearrangement, benzylic migration/elimination, mono- and bis-oxidation of bis[allene], chelation-controlled reduction, and oxime formation, demonstrate that 9 of 11 carbons in ring core of erythromycin can be modified. It is especially noteworthy that each congener was made in less than three steps from a bis[allene] macrolactone of type **4.1**. The congeners contain a variety of functional groups including enone, epoxy ketone, furanone, α' -halo ketone (fluoro-, chloro-, bromo-), vinyl bromide, and furan. These variations of the macrolactone core skeleton are novel, particularly in comparison to conventional analogs, inaccessible from the natural product, and, most importantly, represent further opportunities to create new derivatives. Herein is presented the detailed reaction conditions, mechanistic rationales, and synthetic significance of each compound synthesized to date.

Figure 4.1-1: Synthesis of Erythromycinoids

4.2. DMDO Oxidation and Nucleophile Addition

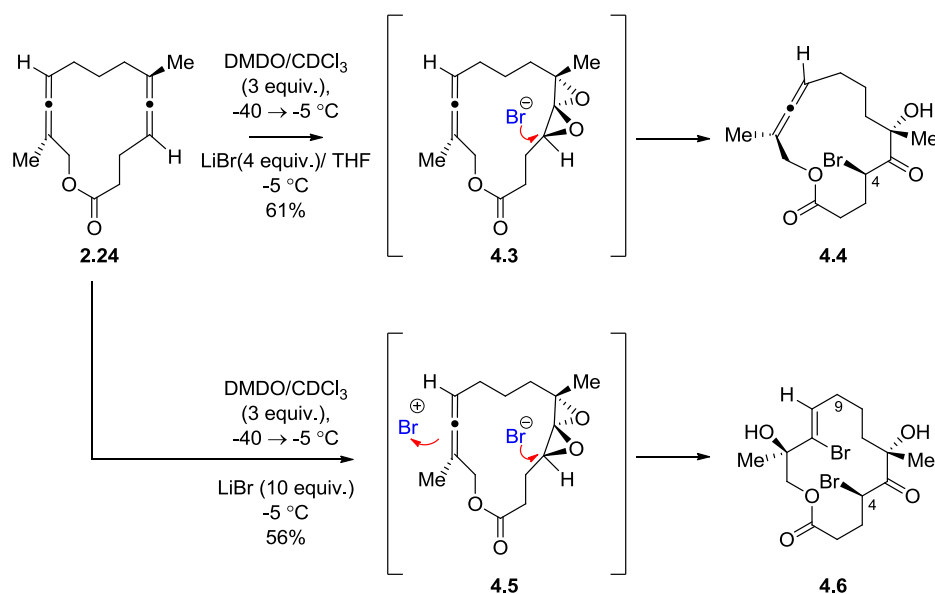
A recent disclosure¹ from our group demonstrated that lithium halide salts are better nucleophiles than tetraalkylammonium salts for addition reactions to SDEs. The former reacts rapidly and reliably to give haloketones in excellent yield upon addition to SDEs, derived from simple trisubstituted allenes.

The model macrolactone, **2.24**, was treated with DMDO (3 equiv.). Scheme 4.2-1 outlines the epoxidation/bromide addition reactions of model macrolactone **2.24**. Addition of LiBr to crude SDE **4.3** gave α -bromo ketone **4.4**. X-ray crystallographic

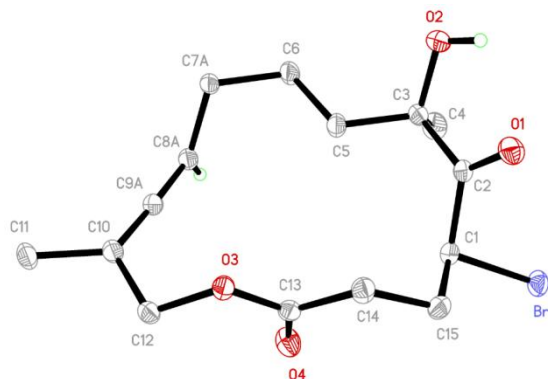
analysis (Figure 4.2-1) confirmed the bromide addition at C4 which is anti to the hydroxy at C6 as expected.²

However, the addition of large excess LiBr (10 equiv.) to the SDE, without removing excess DMDO, resulted in bromine addition to the central carbon (C11) of the unreacted allene (**4.5** → **4.6**). Bromine isotope effect (⁷⁹Br and ⁸¹Br) in HRMS confirmed the presence of two bromines ([M+]:[M+2]:[M+4] = 51:100:47) in **4.6**.

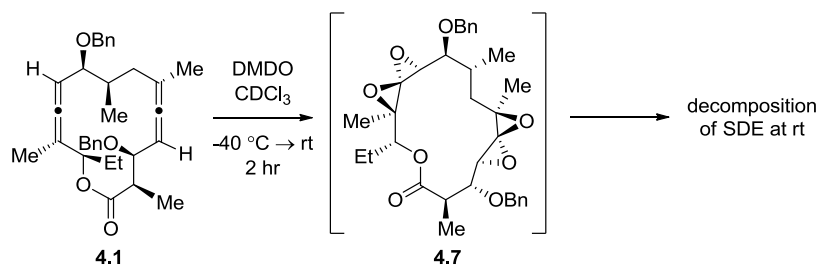
Scheme 4.2-1: Nucleophile Addition to SDE



¹H NMR spectrum of **4.6** revealed the presence of a single vinyl proton resonance (6.03 ppm, CDCl₃). The vinyl proton resonance was coupled to both methylene protons of C9 (2.37 ppm and 2.31 ppm, CDCl₃) as determined by HMBC spectroscopy. A strong nOe was observed between the vinyl proton and the methyl protons at C12, confirming Z-vinyl bromide/β-C12 alcohol in **4.6**.

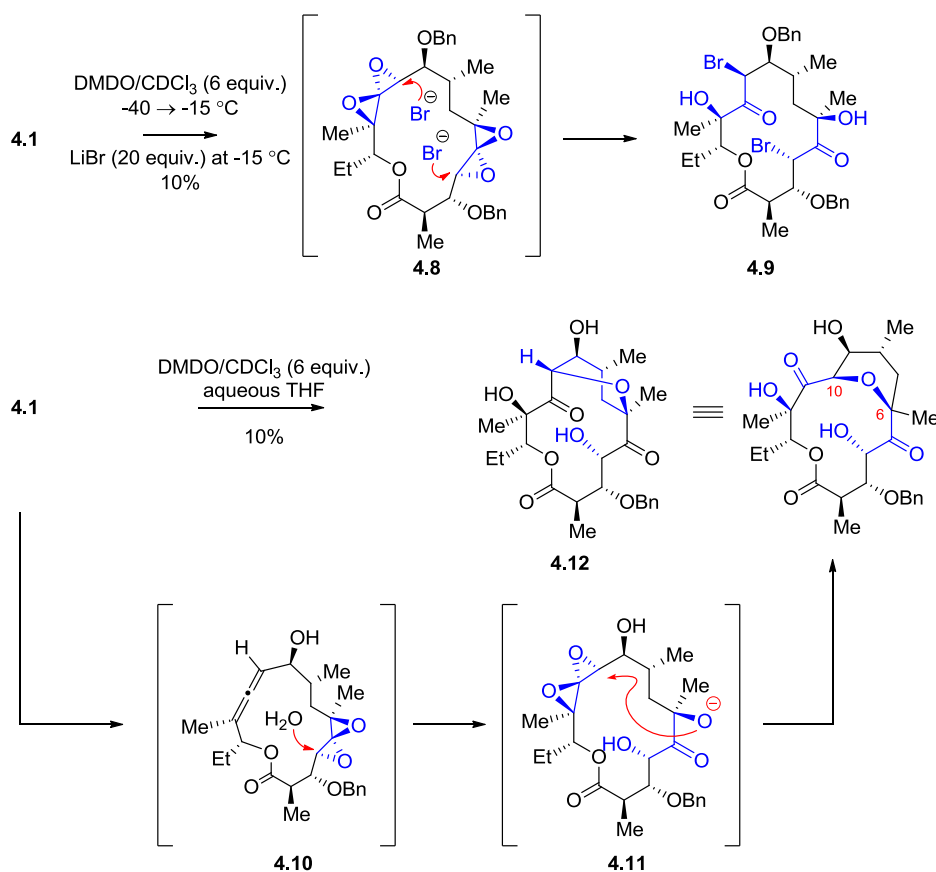
Figure 4.2-1: X-ray Crystal Structure of 4.4

The same strategy was applied to fully functionalized bis[allene] macrolactone **4.1**. Treatment of **4.1** with DMDO (6 equiv.) in CDCl_3 gave bis[SDE] **4.7** (Scheme 4.2-2). Similar to the model study,³ one allene underwent oxidation to SDE below 0 °C while the other allene persisted. After 15 minutes at room temperature, the unreacted allene was completely oxidized to give the second SDE. However, at room temperature, significant cleavage of the benzyl ether was observed (~ 25% by ^1H NMR).⁴ Use of CHCl_3 as solvent instead of CDCl_3 resulted in the recovery of more benzyl cleaved product.

Scheme 4.2-2: Dr. Ghosh's Attempt to Add Nucleophile to Bis[SDE]⁴

Due to the instability of SDEs, LiBr was added at -15 °C to bis[SDE]s (**4.1** \rightarrow **4.8**, Scheme 4.2-3). Albeit in low yield (10%), we isolated the first nucleophile adduct **4.9** to the corresponding SDEs from fully functionalized macrocyclic bis[allene] **4.1**. Remarkably, the reaction installed two ketones, two halides, and four stereocenters in a single flask transformation. The well-known versatility of haloketones⁵ also gives more importance on the utility of SDE chemistry.

Scheme 4.2-3: Nucleophile Addition to SDE

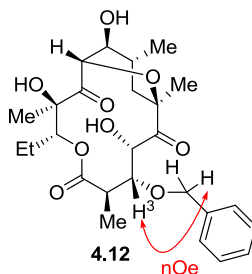


Crandall et al. reported the formation of α,α' -dihydroxy ketones upon the

oxidation of acyclic trisubstituted allenes by DMDO in aqueous THF.⁶ Under the same conditions, we have also observed hydroxyl addition to SDEs **4.12**, however the tertiary C6 alkoxide subsequently added into the C10 SDE terminus **4.11**. It was not a surprising outcome when considering the reactivity of the hydroxyl at C6 to form 6,9-hemiketal in erythromycin.⁷ Excess DMDO was not removed in either reaction in light of the instability of the macrocyclic SDE and its tendency to give complex mixtures upon DMDO removal at room temperature.

As per the previous observation of Dr. Partha Ghosh,⁴ there was benzylic ether cleavage. This type of oxidative cleavage is known and presumed to proceed via insertion of oxygen from DMDO into the benzylic C-H bond to give a hemiacetal which collapses into the alcohol and benzaldehyde.⁸ HRMS confirmed the cleavage of one benzylic group and nOe between the benzylic protons and H3 confirmed the location of cleavage is at C3 (See Figure 4.2-2).

Figure 4.2-2: Key nOe Analysis for Benzylic Ether Location in 4.12



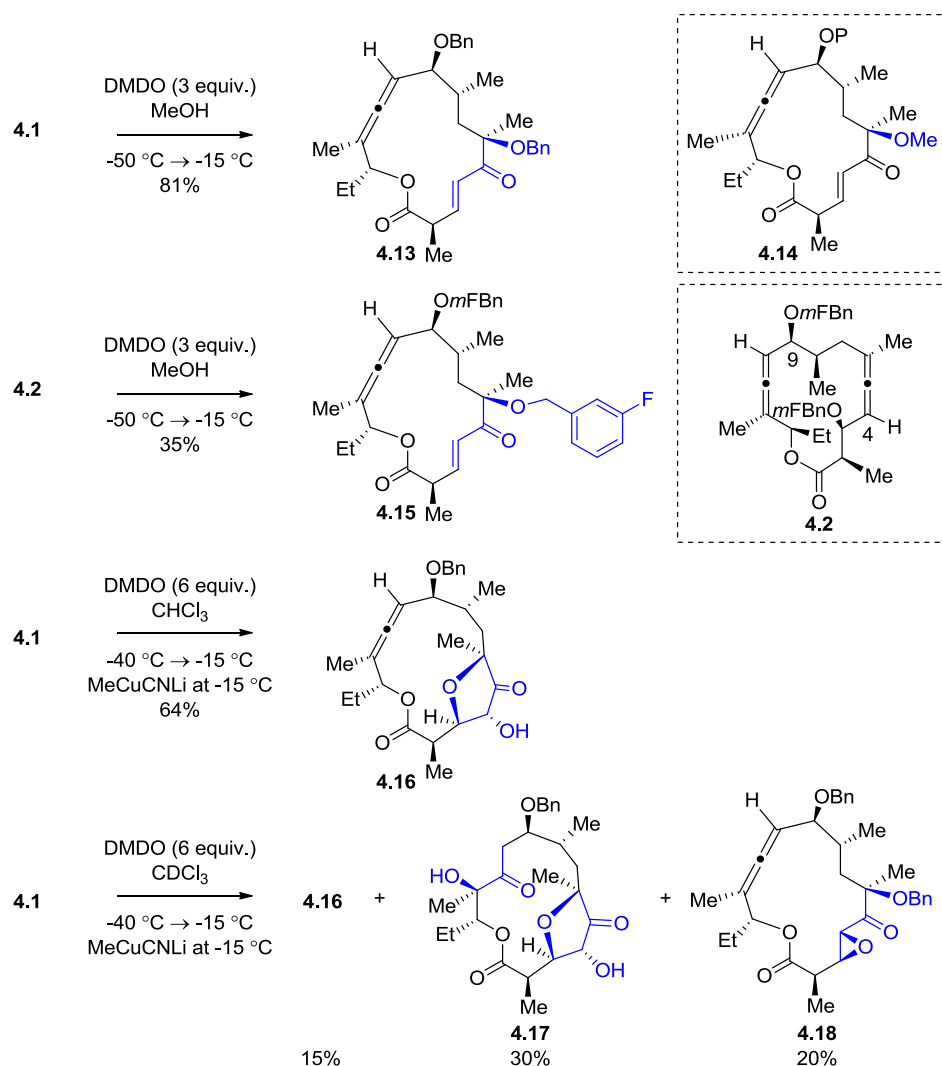
4.3. DMDO Oxidation and Rearrangement

Scheme 4.3-1 shows products derived from epoxidation of **4.1** and **4.2** by DMDO. Upon the exposure of **4.1** to DMDO in methanol, the reaction smoothly delivered α -

benzyloxymethyl ketone **4.13**. However, epoxidation with DMDO in chloroform, followed by treatment with Lewis acid,¹ delivered dihydrofuranone **4.16**. Remarkably, lower order lithium methyl-cyanocuprate efficiently promoted this reaction giving **4.16** in 64% yield.

Benzylic migration product **4.13** is presumably due to hydrogen-bond donation^{9, 10} by methanol to the highly reactive allene oxide intermediate leading to opening of the strained heterocycle faster than a 2nd epoxidation event.

Scheme 4.3-1: DMDO Oxidation and Rearrangement



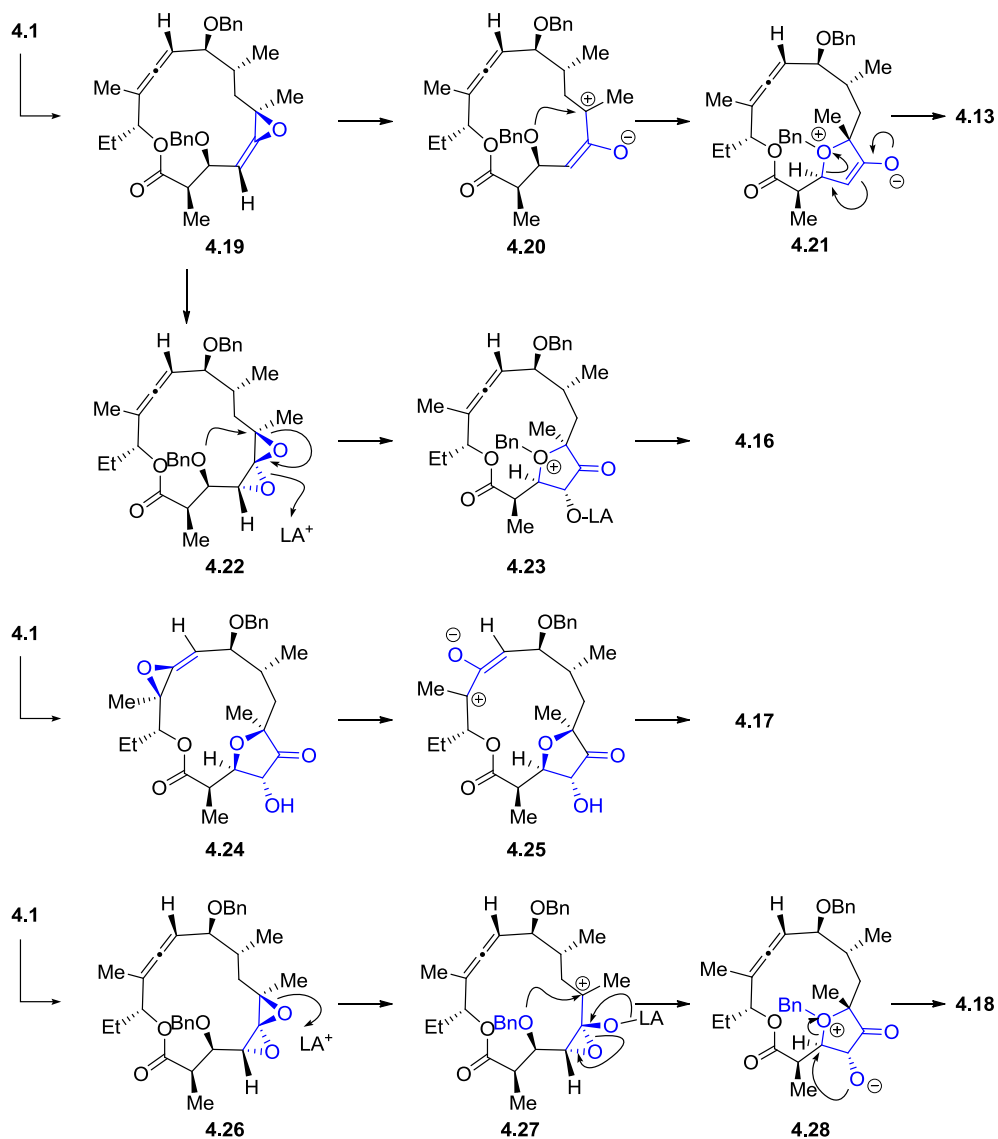
When the less electron-rich *meta*-fluorobenzyl group is used for the protection of the C3 and C9 hydroxyls (**4.2**), I observed the same pattern of migration from C3 \rightarrow C6 as shown in **4.13** giving **4.15**. This suggests that it might be a good methodology for the installation of methoxy group at C6 (**4.14**), which is essential to avoid 8,9-anhydro-6,9-hemi-ketal formation from erythromycin.⁷ Crandall et al. reported the addition of alcohols (e.g., *n*-PrOH, *i*-PrOH) to SDEs in the presence of base (i.e., K₂CO₃, NaH),⁶ however no methanol addition product was observed in reaction of **4.1** and **4.2**.

Upon the oxidation of allene **4.1** using DMDO, SDE formation occurred readily at the C4-C6 allene at low temperature (-20 °C). The nearby electron withdrawing ester functionality retarded oxidation at the C10 to C12 allene. When 6 equivalents of DMDO were used, the mixture of products was obtained including mono-oxidized product **4.16**, bis-oxidized product **4.17**, containing dihydrofuranone and 10-desmethyl α -hydroxy ketone functionalities, and epoxy ketone **4.18**.

Interestingly in the cases where benzylic migration occurred (**4.13** and **4.18**), the stereochemistry at C6 is retained. However, when the benzylic ether is lost (**4.16** and **4.17**), an inversion of configuration at C6 is observed. We postulate that formation of **4.13**, **4.16**, **4.17**, and **4.18** are closely related and involve either allene oxide opening (**4.19** \rightarrow **4.20**) or SDE opening (**4.22** \rightarrow **4.23**) at C6 and subsequent capture of the C3 benzyloxy group (Scheme 4.3-2). The retained stereochemistry at C6 in **4.13** may reflect the comparatively high stability of oxyallyl zwitterions **4.20**, which could explain benzyloxy capture with overall retention of configuration. In the case of **4.16**, two factors such as the comparatively low stability of a cation derived from SDE and the proximity of the C3 benzyl ether to C6 could lead to **4.23** directly with inversion of

configuration at C6. This mechanistic framework is also consistent with the reaction conditions used for these transformations though further studies are needed to evaluate the hypothesis.

Scheme 4.3-2: Mechanistic Rationale for 4.13, 4.16, 4.17, and 4.18



Analogous to **4.20**, subsequent bis-oxidized product **4.17** may involve the formation of oxyallyl zwitterion **4.25** and subsequent water addition from the more accessible top face accounts for retention of configuration at C12 (Scheme 4.3-2). The instability of SDEs in the presence of Lewis acid could form a transient carbocation **4.26**. If the carbocation was captured by C3 benzyloxy group and concurrent (or subsequent) second epoxide opening **4.27** could lead to oxonium **4.28**. The cyclic oxonium ion can then be opened up by closure of the oxygen anion onto C3 furnishing benzyloxy migrated epoxy ketone **4.18**.

4.4. Structural Analysis of 4.13 and 4.18

Analysis of the spectral evidence (^1H NMR, ^{13}C NMR IR) presented below established the structure of compounds **4.13** and **4.18**.

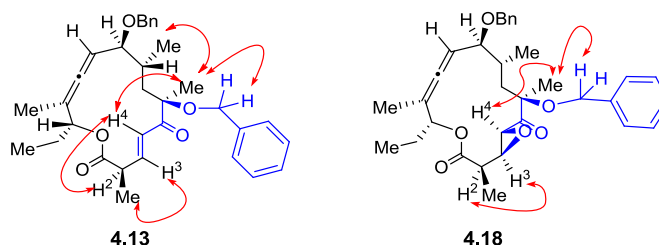
The NMR-spectra of **4.13** revealed the presence of olefin protons (6.73 and 7.05 ppm, CDCl_3). A *trans* configuration was established by the large vicinal couplings constants (ca. 15.7 Hz) observed (Figure 4.4-1). A coupling constant of 1.1 Hz corresponding to allylic coupling of H4 with H2 was observed as well as vicinal coupling of H2 with H3 (8.2 Hz). This firmly established the structure of this portion of the molecule.

The NMR-spectra of **4.18** revealed the presence of epoxide protons (3.37 and 3.97 ppm, CDCl_3) as well as the corresponding ^{13}C NMR signals (59.4 and 52.4 ppm, CDCl_3). The epoxide protons were split by vicinal couplings (ca. 1.8 Hz) and the magnitude of these couplings established the epoxide geometry as *trans*, which was expected as per our mechanistic rationale.

Benzylic migration from C3 to C6 is unambiguously shown by nOes observed between the benzylic protons and the C6 methyl protons in **4.13** and **4.18**. Extensive 2D nOe analysis revealed that the stereochemistry at C6 of **4.13** and **4.18** is retained in comparison to **4.1** (See Figure 4.4-1).

Observation of a signal at 1653cm^{-1} in the infrared spectrum, characteristic of the carbonyl at enones, confirmed the presence of an enone moiety in **4.13**.

Figure 4.4-1: Key nOe Analysis of 4.13 and 4.18

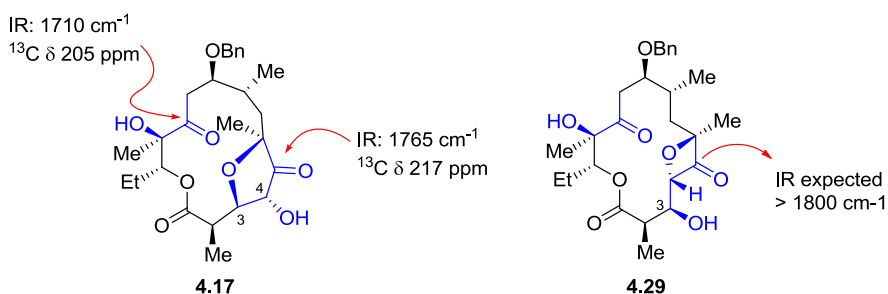


4.5. Structural Analysis of 4.16 and 4.17

Due to their structural complexity, it is very hard to elucidate the structural assignment of **4.16** and **4.17** unambiguously. For compounds **4.16** & **4.17**, the initial concern was whether the newly formed ring was dihydrofuranone or oxetanone. It was initially considered to be an oxetanone (**4.29**, Figure 4.5-1) because the ^{13}C NMR signal at 217 ppm was in close agreement with literature values for other compounds containing oxetanone functionality ($\delta \approx 215$ ppm). Additionally, previous studies on model macrocyclic bis[allene] in which oxetanone was formed encouraged us to favor structure **4.29**.³ However, FTIR analysis showed a carbonyl absorption frequency at 1765 cm^{-1} ,

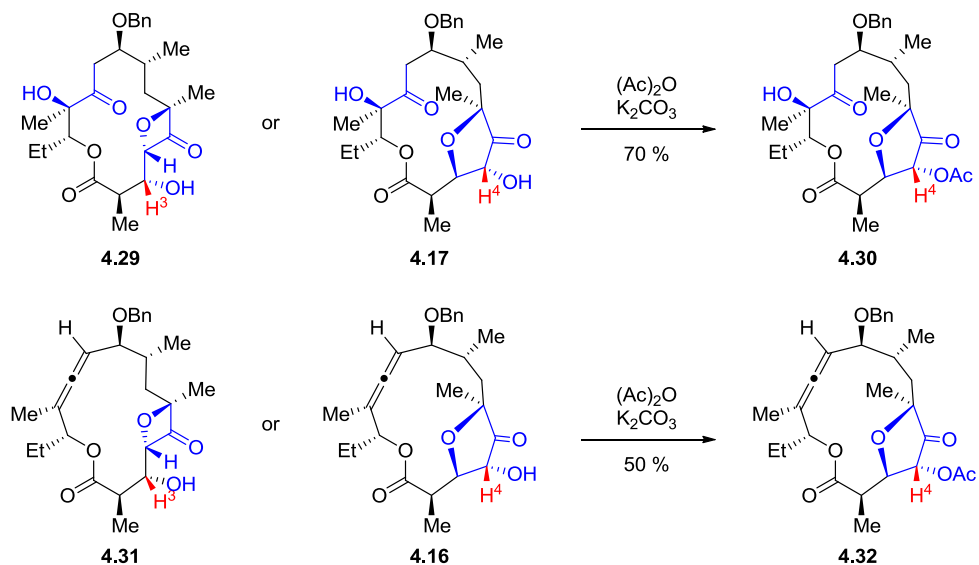
which is consistent with furanone.¹¹ Literature precedent for oxetanone containing molecules showed that an IR signal at 1802-1800 cm^{-1} corresponded to the oxetanone carbonyl.¹²

Figure 4.5-1: Structural Analysis of 4.17



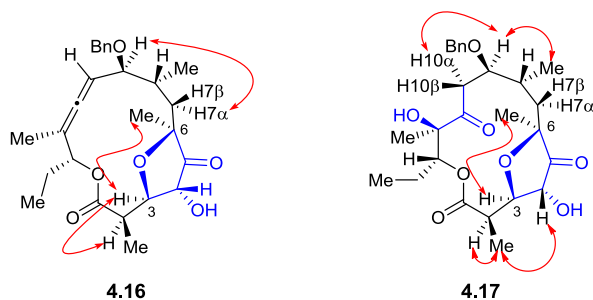
To further verify ring size and, by extension, the location of the hydroxyl (C4 in **4.17**, C3 in **4.29**), the material was acylated using acetic anhydride (Scheme 4.5-1). Upon acylation, the H4 proton in **4.30** shifted 1 ppm downfield in the ^1H NMR spectrum, but the H3 proton did not show the shift. The same acylation strategy was used for mono-oxidized compound and returned similar data confirming the structure of **4.32**.

Scheme 4.5-1: Acylation of 4.13 & 4.14 for Structural Proof of Furanone



Strong nOe between the C6 methyl protons and the H3 proton revealed that the stereochemistry at C6 of **4.16** and **4.17** is reversed in comparison to **4.1** (Figure 4.5-2).

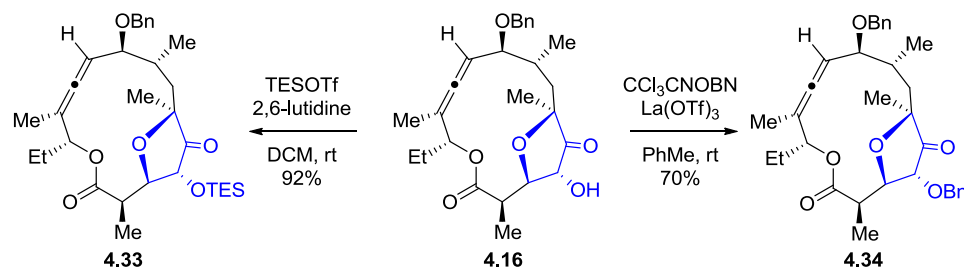
Figure 4.5-2: Key nOe Analysis of 4.16 and 4.17



Mono-oxidation products such as **4.13**, **4.16**, and **4.18** provide the unique opportunities to enhance the heterogeneity among the erythromycinoids. The reactive

secondary hydroxyl in **4.16** was protected either with TES or benzylic ether for further derivatization of the second allene.

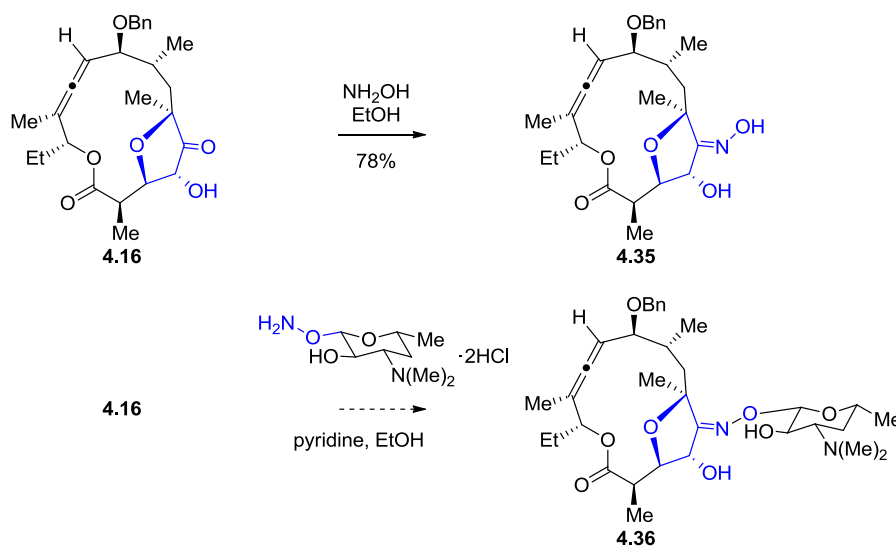
Scheme: 4.5-2: Hydroxyl Protection in 4.16



4.6. De Novo Glycosylation Strategy

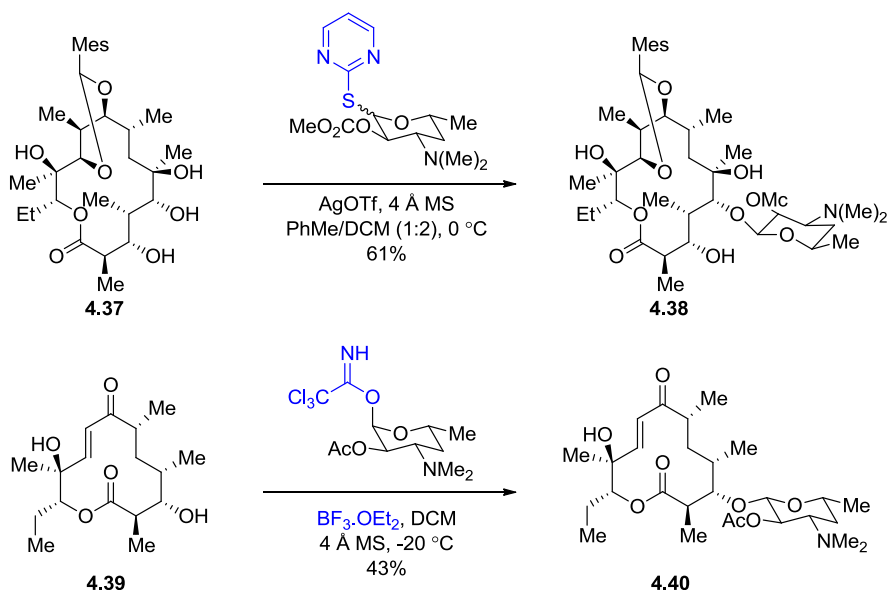
The first reported oxime formation¹³ at C9 in the erythromycin macrolide family lead to invention of 2nd and 3rd generation erythromycins. When **4.16** was treated with hydroxylamine, oxime formation at C5 proceeded smoothly to give **4.35** in 78% yield (Scheme 4.6-1). This clean oxime formation suggested the possibility of adding the C5 sugar as a nucleophile (**4.16** → **4.36**) in contrast to the conventional methodologies.

Scheme 4.6-1: Oxime Formation



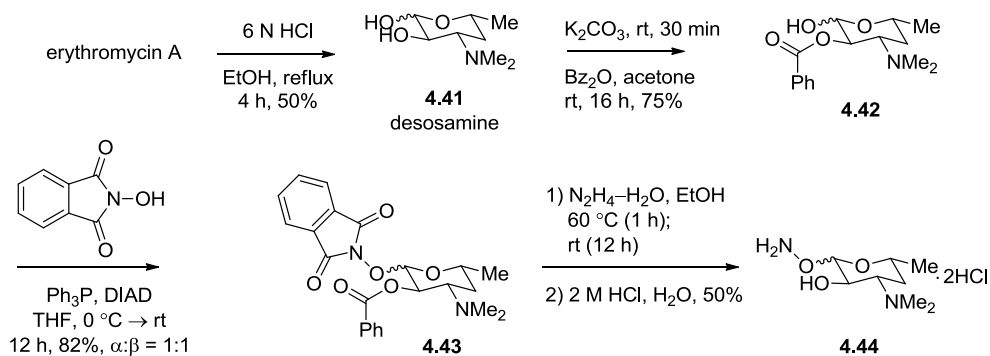
For example, in Martin's synthesis of erythromycin B, a sugar bearing a pyrimidyl thioglycoside at the anomeric position can be added via the intermediate oxocarbenium ion (Section 4.6-2).¹⁴ Woodward and Toshima employed similar methods to glycosylate erythromycin A.^{15,16} These strategies require the 2'-OH on the desosamine sugar to be masked. An alternative method for glycosylation with desosamine is to prepare the corresponding acetimidate as in the synthesis of Methymycin by Kang et al.¹⁷ Though the reaction proceeded regio- and stereoselectively to afford the desired C5-glycosylated β -glycoside as the sole anomer, the reaction requires rigorously anhydrous conditions and low yields are not uncommon.

Scheme 4.6-2: Glycosylation



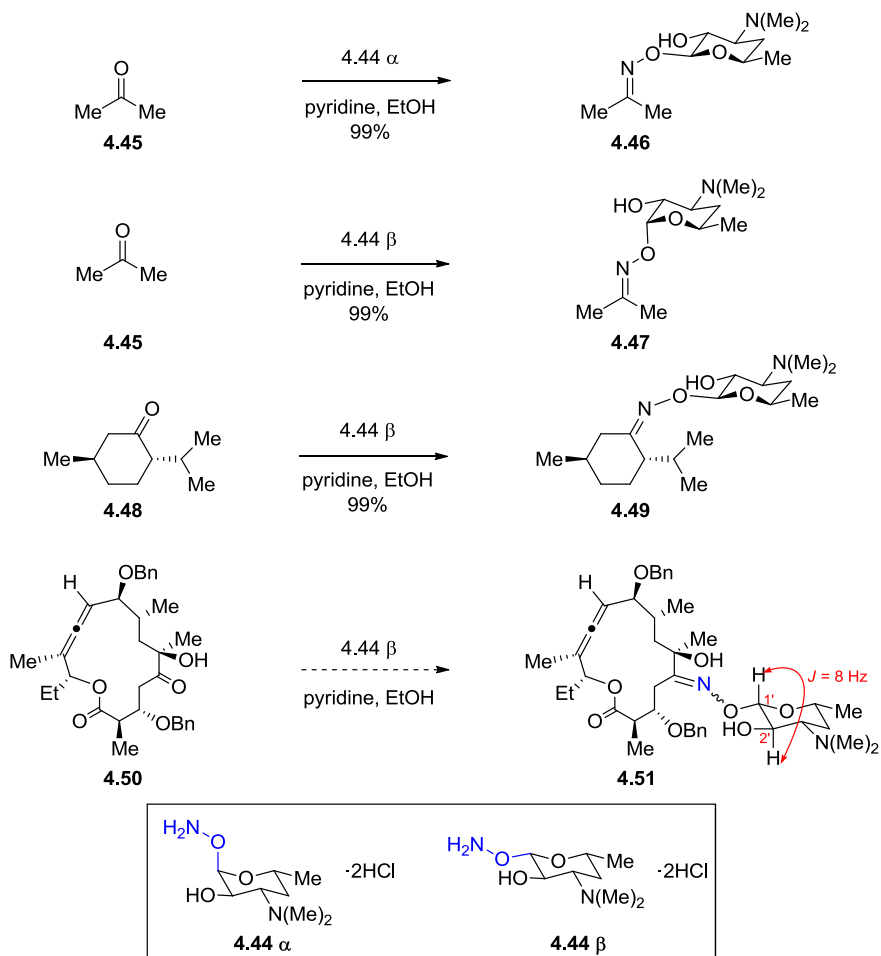
In contrast, the aminooxydesosamine hydrochloride salt will react in aqueous conditions. The aminooxydesosamine hydrochloride salt¹⁸ was prepared in 4 steps (Scheme 4.6-3) by my colleague, Libing Yu, and the hypothesis was tested on simple ketones and macrolide **4.50** (Scheme 4.6-4). The desosamine was isolated from the degradation of erythromycin. Benzoyl protection of the 2'-OH gave **4.42**. Mitsunobo reaction of the anomeric alcohol with *N*-hydroxyphthalimide provided **4.43** as a 1:1 mixture of α : β anomers. Oxyphthalimide **4.43** was then reduced by hydrazine followed by the removal of benzoyl ether to give hydrochloride salt **4.44** in a single flask transformation.

Scheme 4.6-3: Modified Synthesis of Desosamine Hydrochloric Salt



Yu coupled both α and β glycosidic aminohydroxyl desosamine salts with simple ketones (i.e., acetone and menthone) to obtain oxime in 99% yield in all cases (Scheme 4.6-4). When macrolactone **4.50** was treated with **4.44 β** , ^{13}C NMR data showed the appearance of the characteristic oxime signal ($\delta = 168$ ppm in **4.51**) and the absence of the ketone signal of **4.50** ($\delta = 212$ ppm). The stereochemistry of the glycoside bond was confirmed by ^1H NMR coupling constant analysis ($J_{1',2'} = 8.0$ Hz).

Scheme 4.6-4: Addition of Hydroxyl Amine Desosamine



4.7. *OsO₄ Oxidation/Addition/Rearrangement /Application*

According to the outcome of osmylation on linear allenes (*See* Chapter 5 for more detail), we hypothesized that the osmylation of macrocyclic bis[allene] **4.1** in the absence of an electrophile would give 4,10-desmethyl erythromycinoid **4.52** (Scheme 4.7-1). Desmethyl erythromycinoid **4.52** was targeted because Steitz and coworkers demonstrated the cause of resistance might be due to a steric clash of the amino group of guanine 2058 of the large ribosomal subunit with C4 methyl of the drug.¹⁹

Upon oxidation of **4.1** with 2 equivalents of OsO₄, Kai Liu isolated (9*S*)-dihydro-6,9-anhydro derivative **4.53** (46%). Initially, we thought that the bis-oxidized product was **4.52**. However, long-range coupling between the proton at C9 and the methyl carbon at C6 suggested the formation of 6,9-furan. Furthermore, the tertiary hydroxyl at C12 was protected with a TES group and the product was recrystallized to unambiguously determine the structure to be **4.54** by X-ray crystallographic analysis (Figure 4.7-1). It is well preceded that 6,9-linked analogs, so called “motilide”, display biological activity as motilin acceptors, thus promoting gastrointestinal prokinetic activities.^{20, 21}

Scheme 4.7-1: Desmethyl Erythromycinoids

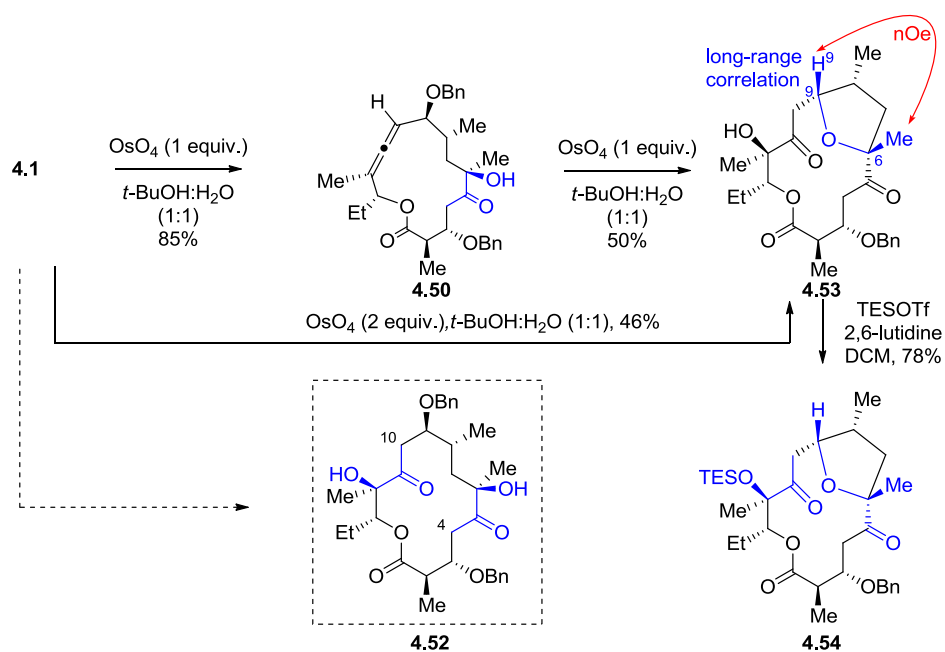
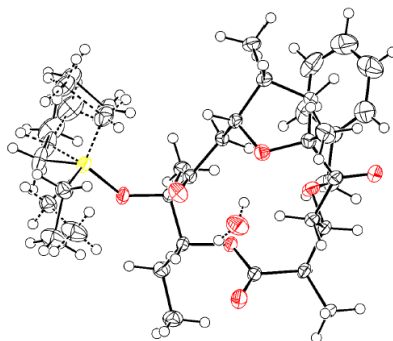


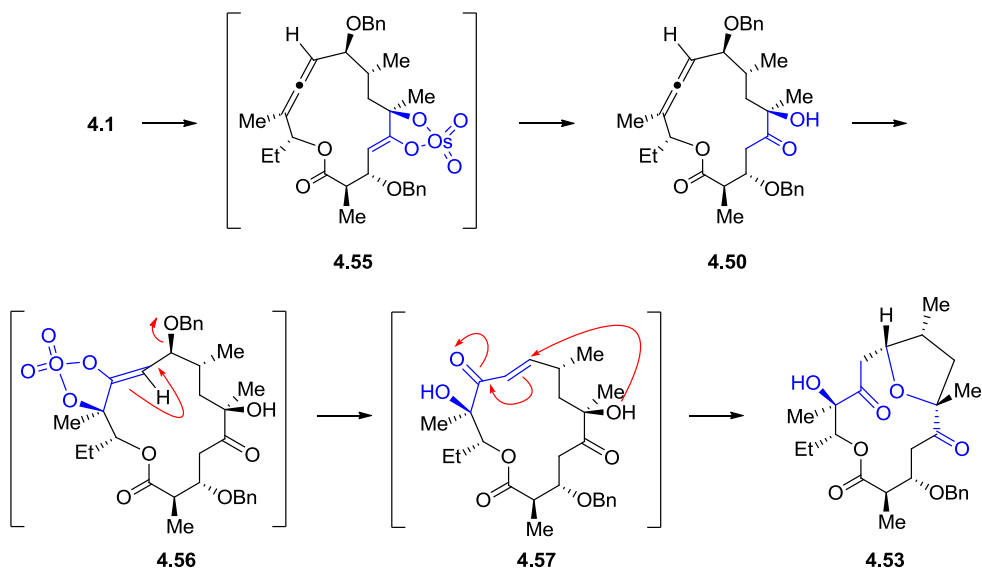
Figure 4.7-1: X-ray Crystal Structure of 4.54



In considering the different reactivity of the two allenes in macrocyclic bis[allene] **4.1**, it was realized that we could oxidize them in a stepwise manner. Thereby, the 2nd allene can be modified heterogeneously. In an attempt to affect stepwise oxidation, macrocyclic bis[allene] **4.1** was treated with 1 equivalent of OsO₄ to give mono-oxidized 4-desmethyl macrolide **4.50** (85%). Addition of a 2nd equivalent of OsO₄ oxidized the second allene to **4.53** (50%).

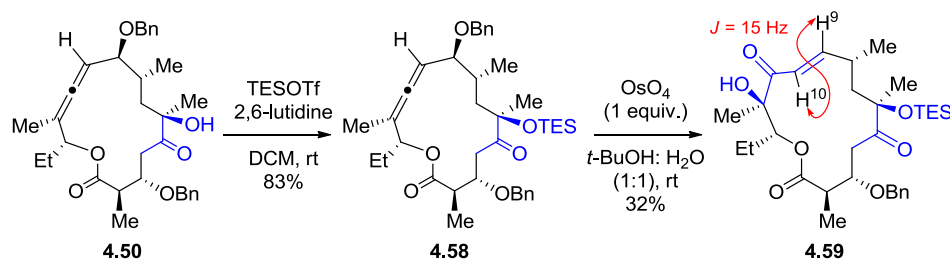
Although the precise structures of the intermediates are a matter of speculation, the osmium adducts formed and were subsequently hydrolyzed (i.e., **4.55** → **4.50**, **4.56** → **4.57**, Scheme 4.7-2). Considering that these intermediates are also enolates,²² unlike simple alkene-derived osmate esters, β-elimination (**4.56** → **4.57**) and subsequent intramolecular conjugate addition (**4.57** → **4.53**) is reasonable and suggestive of other possible transformations. Interestingly, the C3 benzyloxy group is retained whereas the C9 group is eliminated, a phenomenon most likely traceable to the orientation of this group relative to the osmate ester.

Scheme 4.7-2: Mechanistic Rationale for 6,9-Bicyclolide 4.53



C9-C12 α -hydroxyenone **4.59** was isolated when hydroxyl ketone **4.50** was protected with a TES group (**4.51** \rightarrow **4.58**), followed by a second osmylation (**4.58** \rightarrow **4.59**, Scheme 4.7-3). α -Hydroxyenone **4.59** adopts a *trans* configuration, as confirmed by vicinal coupling constants ($^3J_{\text{H9, H10}} = 15.5$ Hz). Considering the synthetic versatility of enones, this functionality in **4.59** and **4.13** provides enormous opportunity to derivatize C3, C4, C6, C9, C10 and C11 to include diverse functional arrays.

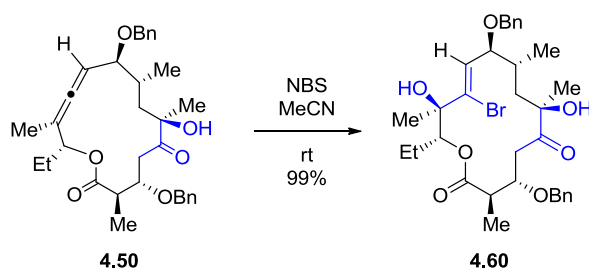
Scheme 4.7-3: Formation of C9-C12 α -Hydroxyenone, 4.59



4.8. Allene Halohydration

Ionic addition to simple acyclic allenes is known,²³ but has never been applied in asymmetric synthesis. We hypothesized that an NBS addition/hydrolysis reaction will be highly stereoselective due to macrocyclic stereocontrol in allene **4.50**. Herein, I described the combination of allene osmylation and electrophilic bromination (Scheme 4.8-1).

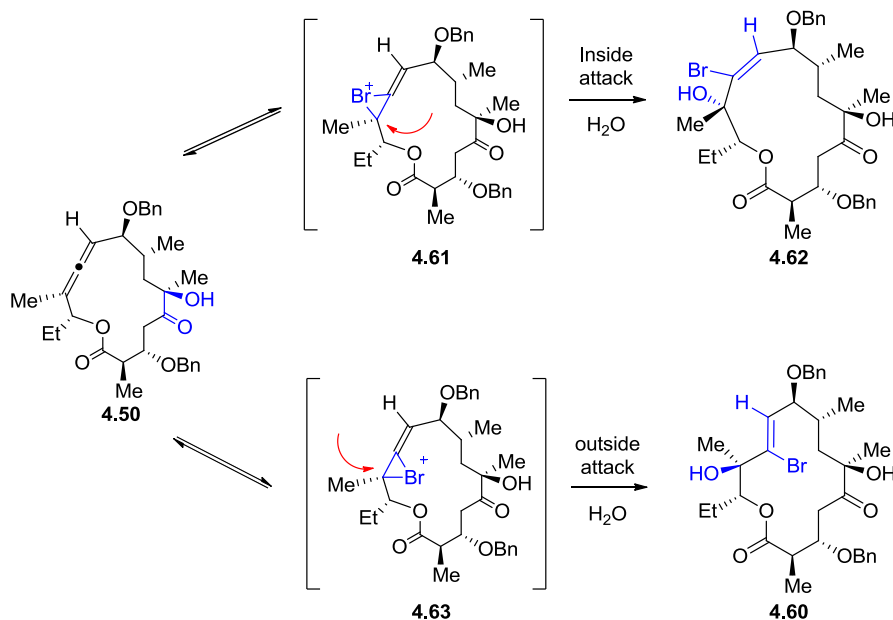
Scheme 4.8-1: Electrophilic Bromination



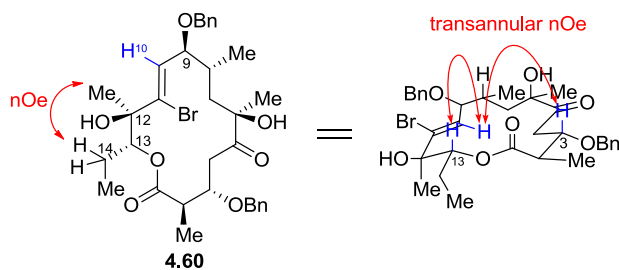
Following osmylation of **4.1**, the resultant ketoalcohol **4.50** was treated with NBS in acetonitrile.²⁴ The C10-C11 Z-vinyl bromide/ β -C12 hydroxyl **4.60** was isolated in excellent yield.

Although there are 2 possible faces of approach for the electrophilic bromination ion to the allene of **4.50** (**4.61** and **4.63**, Scheme 4.8-2), approach of the nucleophile is expected to occur from outside of the macrocycle. This would lead to Z-bromide **4.60** at a significantly faster rate than **4.62**.

Scheme 4.8-2: Mechanistic Postulation for 4.60

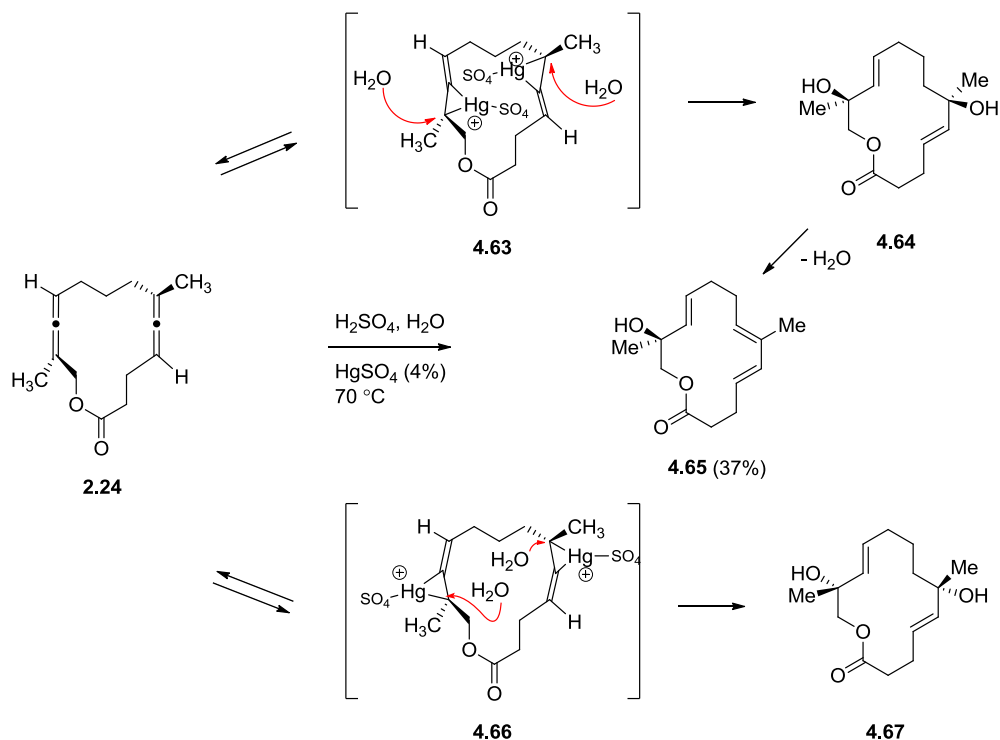


The NMR-spectra revealed the presence of a single olefin proton (6.14 ppm in **4.60**). The olefin proton was split by vicinal coupling ($^3J_{H_{10}, H_9} = 8.4$ Hz in **4.60**). The transannular nOe of H10 with H13 and H3 unambiguously set Z-vinylbromide configuration of **4.60** (See Figure 4.8-1). The absence of an nOe for H10 with the C12 methyl group set the stereochemistry of the C12 hydroxyl as β as well as the nOe between the C12 methyl with the C14 methylene protons in **4.60**.

Figure 4.8-1: Key nOe Analysis of 4.60

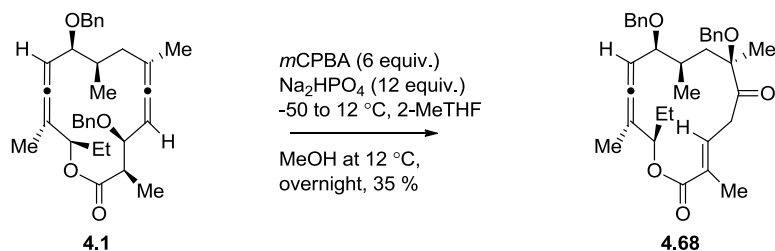
4.9. Alternative to DMDO Oxidation

Oxymercuration/demercuration^{25, 26} of allenes has been well studied, however it has never been applied in the context of macrocyclic allene systems. The stereochemical outcome of product formation in oxymercuration/demercuration is analogous to that of halohydration. Upon exposure of the allene to mercuric sulfate, the formation of the purported mercurium bridge inside the ring would allow for facile attack by a nucleophile from outside the macrocycle (**2.24** → **4.63**) in comparison to formation of the mercurium bridge outside the ring and attack of the nucleophile from inside the macrocycle (**2.24** → **4.66**). The former would lead to *trans* allylic alcohol **4.64**. However, the demercuration step (reflux at 70 °C in sulfuric acid and water) lead to the elimination product **4.65**.

Scheme 4.9-1: Oxymercuration/Demercuration


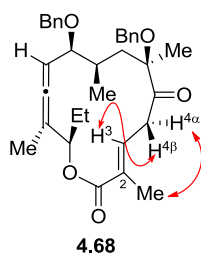
Oxidative cleavage^{8, 27, 28} of benzylic ethers and arenes is known and accounts for the instability of SDEs prepared from macrocycle **4.1** upon reaching ambient temperature. In contrast to DMDO oxidation, exposure of arene-containing allenes to *m*CPBA seems to give SDEs.²⁹ Hence, bis[allene] macrolactone **4.1** was oxidized with *m*CPBA (6 equiv.) in methanol. Instead of the methanol addition adduct, **4.68** was isolated containing a C2 olefin forms. This product was similar to **4.13**, though differed by the position of the olefin.

Scheme 4.9-2: *m*CPBA Oxidation of 4.1

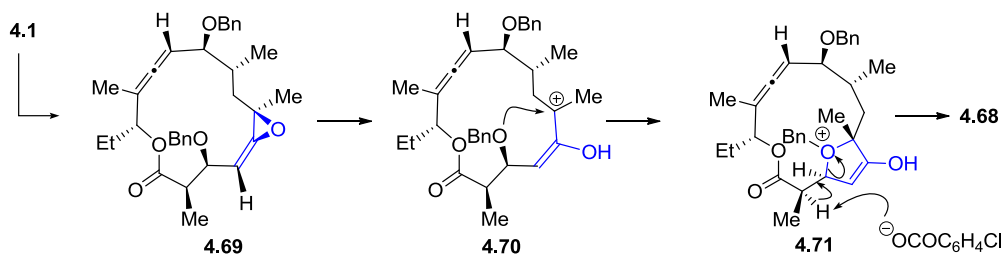


A *trans* configuration of the olefin at C2-C3 in **4.68** was confirmed by nOe analysis. The C3 proton shows an nOe with H4 β only, however in contrast, the C2-methyl protons shows an nOe with H4 α only (Figure 4.9-1). In the *cis* olefin configuration, an nOe between H4 α and the C2-methyl protons is unlikely. The mechanism is analogous to the formation of **4.13**. The highly reactive allene oxide intermediate **4.69** opens up before the second epoxidation event due to hydrogen bond donation. The nearby benzyloxy added to the carbocation of intermediate **4.70** followed by removal of a proton by base promoted by the benzyloxonium ion in **4.71** (Scheme 4.9-3).

Figure 4.9-1: Key nOe Analysis of 4.68



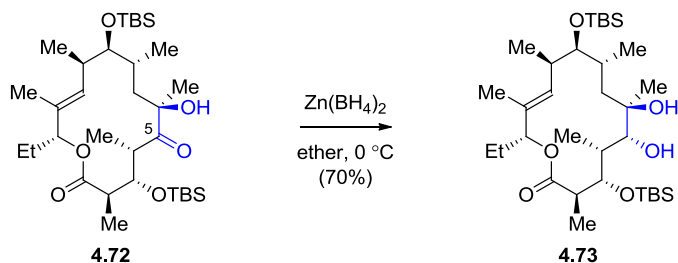
Scheme 4.9-3: Mechanistic Rationale for 4.68



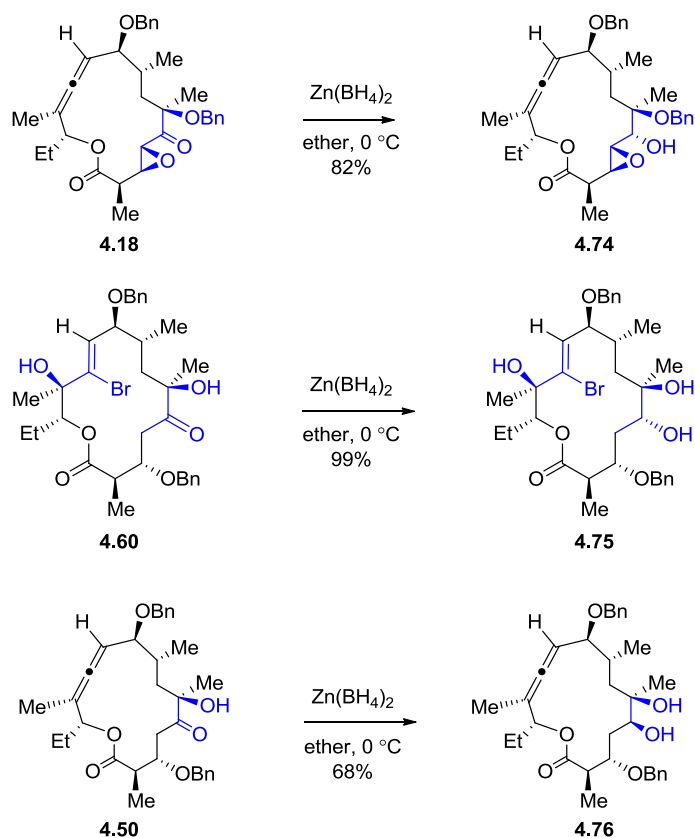
4.10. Chelation-Controlled Reduction

Zn(BH₄)₂ reduction of optically active α,β -epoxy ketones³⁰ and α -hydroxy ketones³¹ in linear systems was reported to afford optically active *erythro* isomers with high selectivity. However, for macrocyclic systems, the stereochemical outcome is different from what is expected in linear systems. It depends on the topographical bias of the macrocycle. Contrary to the stereochemical prediction for linear systems, Paterson showed *threo* reduction at C5 by Zn(BH₄)₂ (4.72 \rightarrow 4.73, Scheme 4.10-1).³²

Scheme 4.10-1: Zn(BH₄)₂ Reduction on α -Hydroxy Ketone by Paterson³²



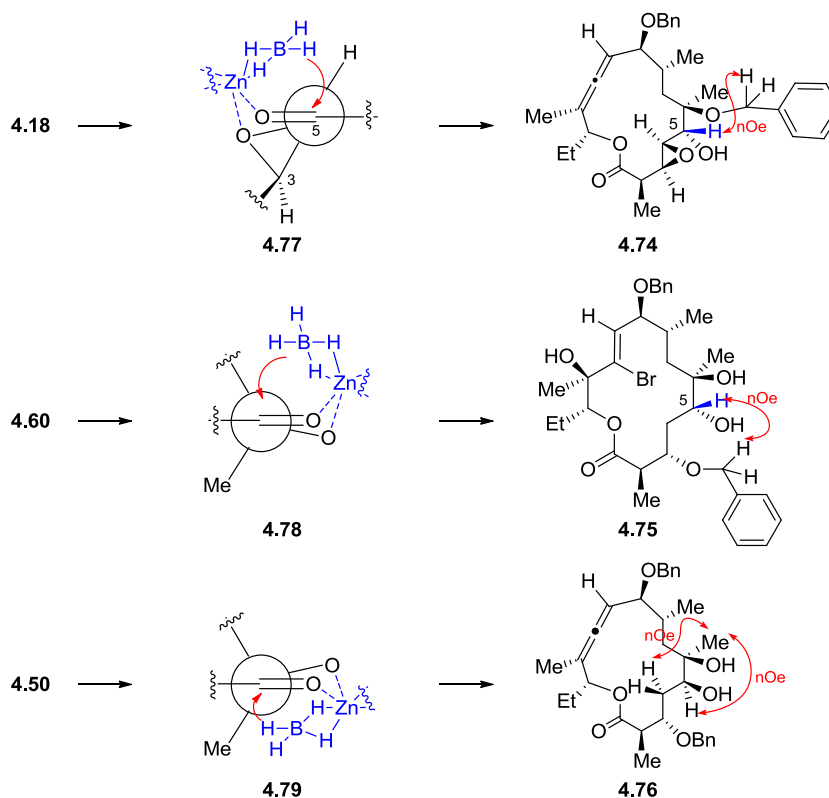
Scheme 4.10-2: $\text{Zn}(\text{BH}_4)_2$ Reduction



Upon reduction with $\text{Zn}(\text{BH}_4)_2$, the macrolactones with epoxy ketone **4.18**, keto alcohol with vinyl bromide **4.60**, and keto alcohol **4.50** show the complete diastereoselection with moderate to good yield (Scheme 4.10-2). The careful and extensive NMR analysis established the structure of the reduction products.

In case of **4.18**, the hydride attack would be more accessible from the opposite side of the epoxide **4.77**, which account for α -hydroxy at C5 in **4.74**. The stereochemistry was confirmed by nOe between H5 and benzylic protons at C6 in **4.74**.

Scheme 4.10-3: Key nOe Analysis of Alcohols at C5

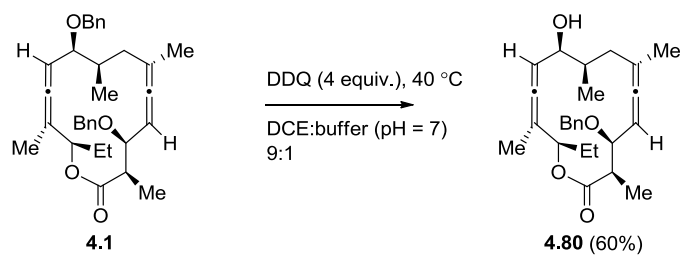


For keto alcohols **4.60** and **4.50**, hydride attack on the ketone at C5 from the top face was predicted to be unlikely due to steric hindrance. **4.75** showed a very strong transannular nOe among H10, H3, and H13 and this led us to assume that the benzylic protons at C3 were positioned at the top face of the compound. The same benzylic protons showed an nOe with H5. This confirmed hydride attack at C5 from the top face as shown **4.78**. However $\text{Zn}(\text{BH}_4)_2$ reduction of **4.50** gave β -hydroxy formation at C5 as a single diastereomer (**4.76**). The nOe between the C6-methyl and C5- α -hydroxy confirmed the assigned stereochemistry in **4.76**.

4.11. Benzylic Ether Cleavage by DDQ

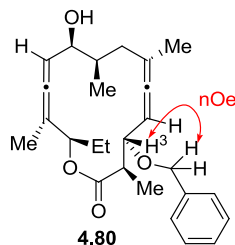
As shown in this chapter, the presence of benzylic ether resulted in a very interesting rearrangement due to its reactivity under the employed oxidation conditions. However, more stable protecting groups such as silyl ethers were also advised.

Scheme 4.11-1: Benzylic Ether Cleavage by DDQ



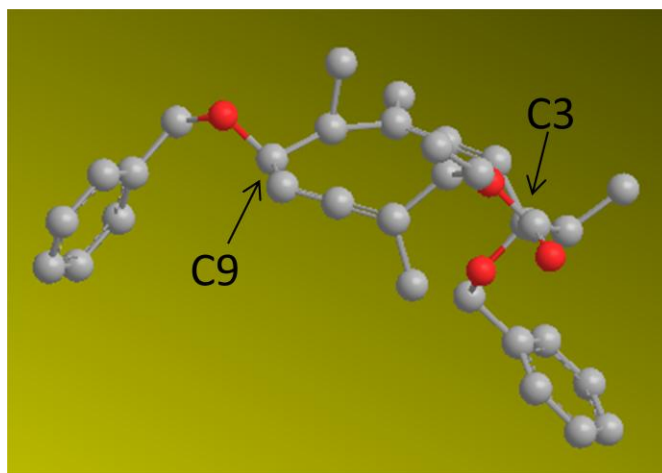
Instead of incorporating the different protecting group at the beginning of the synthesis, if we can manipulate the protecting groups at a later stage of the synthesis, this will ease the synthetic maneuver. Often times, benzylic ethers are cleaved by palladium catalyzed hydrogenolysis, however due to allene reactivity, we affected the cleavage with DDQ. The cleavage occurred stepwise leading to cleavage of the C9 benzyl ether before the C3 benzyl ether.

Figure 4.11-1: Key nOe Analysis for Benzylic Ether Location in 4.80



Computational analysis performed at the MM2 level suggests that the ground state of the bis[allene] macrolactone **4.1** populates a favorable conformation in which the benzylic ether at C9 is more open in space whereas the benzylic ether at C3 is tucked into the ring. This conformation is also consistent with nOe analysis.

Figure 4.11-2: Ground State Minimum Energy Conformation of 4.1



4.12. Conclusion

In summary, the four sites of unsaturation in a bis[allene] macrolactone were transformed with apparently complete selectivity. The observed order of reactivity is C5-C6 > C4-C5 > C11-C12 and then C10-C11. In all of the reactions, the products were isolated as single stereoisomers. The observed stereochemical outcomes reflect the cooperative effects of intrinsic allene stereoselectivity, macrocyclic stereocontrol,³³ and (for the intramolecular transformations) proximity of the reacting partners. Bis[allene] macrolactone has proven to be a processable intermediate and all compounds were

prepared from this species in 3 steps or less. 9 out of 11 modifiable carbons were synthetically manipulated and the new functional moieties included enone, epoxy ketone, furanone, α' -halo ketone (fluoro-, chloro-, bromo-), halohydrin, and furan. Most importantly, this new class of erythromycinoids would allow us to systematically vary the point of interest on the macrolactone carbon backbone to shed light on the complete survey of structure/function space and the mechanisms by which these compounds work.

Taken all together, the bis[allene] macrolactone is a structurally processable intermediate that integrates the routes to targets that intersect with underexplored erythromycinoid structure space. As part of our program to develop *de novo* strategies for the synthesis of erythromycinoids, we have been interested in improving methods to oxidize an allene to synthesize erythromycinoids. Allene osmylation and multicomponent coupling is discussed in more detail in chapter 5.

4.13. References

1. Sharma, R.; Manpadi, M.; Zhang, Y.; Kim, H.; Ahkmedov, N. G.; Williams, L. J. *Org. Lett.* **2011**, *13*, 3352.
2. Ghosh, P.; Lotesta, S. D.; Williams, L. J. *J. Am. Chem. Soc.* **2007**, *129*, 2438.
3. Ghosh, P.; Zhang, Y.; Emge, T. J.; Williams, L. J. *Org. Lett.* **2009**, *11*, 4402.
4. Ghosh, P. New methods and strategies towards total synthesis of (9S)-dihydroerythronolide A. Ph.D. Thesis, Rutgers, The State University of New Jersey, New Brunswick, 2008.
5. Malosh, C. F.; Ready, J. M. *J. Am. Chem. Soc.* **2004**, *126*, 10240.
6. Crandall, J. K.; Batal, D. J.; Sebesta, D. P.; Lin, F. *J. Org. Chem.* **1991**, *56*, 1153.
7. Katz, L.; Ashley, G. W. *Chem. Rev.* **2005**, *105*, 499.
8. Csuk, R.; Dörr, P. *Tetrahedron* **1994**, *50*, 9983.
9. Lotesta, S. D.; Hou, Y.; Williams, L. J. *Org. Lett.* **2007**, *9*, 869.
10. Shangguan, N.; Kiren, S.; Williams, L. J. *Org. Lett.* **2007**, *9*, 1093.
11. Smith, A. B.; Levenberg, P. A.; Jerris, P. J.; Scarborough, R. M.; Wovkulich, P. M. *J. Am. Chem. Soc.* **1981**, *103*, 1501.
12. Dejaegher, Y.; Kuz'menok, N. M.; Zvonok, A. M.; De Kimpe, N. *Chem. Rev.* **2001**, *102*, 29.
13. Djokic, S.; Tamburasev, Z. *Tet. Lett.* **1967**, *8*, 1645.
14. Martin, S. F.; Hida, T.; Kym, P. R.; Loft, M.; Hodgson, A. *J. Am. Chem. Soc.* **1997**, *119*, 3193.
15. Woodward, R. B.; Logusch, E.; Nambiar, K. P.; Sakan, K.; Ward, D. E.; Au-Yeung, B. W.; Balaram, P.; Browne, L. J.; Card, P. J.; Chen, C. H. *J. Am. Chem. Soc.* **1981**, *103*, 3215.
16. Toshima, K.; Nozaki, Y.; Mukaiyama, S.; Tamai, T.; Nakata, M.; Tatsuta, K.; Kinoshita, M. *J. Am. Chem. Soc.* **1995**, *117*, 3717.
17. Oh, H.-S.; Xuan, R.; Kang, H.-Y. *Org. Biomol. Chem.* **2009**, *7*, 4458.

18. Farmer, J. J.; Ashoke, B.; Chen, Y.; Sutcliffe, J. A., Preparation of macrocyclic azithromycin compounds as antibacterial, anti-proliferative, and antiinflammatory agents, US Patent WO 2005085266 (A2), 2005.
19. Tu, D.; Blaha, G.; Moore, P. B.; Steitz, T. A. *Cell* **2005**, *121*, 257.
20. Tsuzuki, K.; Sunazuka, T.; Marui, S.; Toyoda, H.; Omura, S.; Inatomi, N.; Itoh, Z. *Chem. Pharm. Bull.* **1989**, *37*, 2687.
21. Faghieh, R.; Lartey, P. A.; Nellans, H. N.; Seif, L.; Burnell-Curty, C.; Klein, L. L.; Thomas, P.; Petersen, A.; Borre, A.; Pagano, T.; Kim, K. H.; Heindel, M.; Bennani, Y. L.; Plattner, J. J. *J. Med. Chem.* **1998**, *41*, 3402.
22. Azam, K. A.; Deeming, A. J.; Rothwell, I. P. *J. Chem. Soc., Dalton Trans.* **1981**, *1*, 91.
23. *Modern Allene Chemistry*; Krause, N.; Hashmi, S. K., Eds.; WILEY-VCH: Weinheim, Germany, 2004; Vol. 1 & 2.
24. Li, J.; Kong, W.; Yu, Y.; Fu, C.; Ma, S. *J. Org. Chem.* **2009**, *74*, 8733.
25. Waters, W. L.; Kiefer, E. F. *J. Am. Chem. Soc.* **1967**, *89*, 6261.
26. Waters, W. L.; Linn, W. S.; Caserio, M. C. *J. Am. Chem. Soc.* **1968**, *90*, 6741.
27. Murray, R. W. *Chem. Rev.* **1989**, *89*, 1187.
28. Marples, B. A.; Muxworthy, J. P.; Baggaley, K. H. *Synlett* **1992**, *8*, 646.
29. Wang, Z.; Shangguan, N.; Cusick, J. R.; Williams, L. J. *Synlett* **2008**, *2*, 213.
30. Nakata, T.; Tanaka, T.; Oishi, T. *Tet. Lett.* **1981**, *22*, 4723.
31. Nakata, T.; Tanaka, T.; Oishi, T. *Tet. Lett.* **1983**, *24*, 2653.
32. Paterson, I.; Rawson, D. J. *Tet. Lett.* **1989**, *30*, 7463.
33. Still, W. C.; Galynker, I. *Tetrahedron* **1981**, *37*, 3981.

Chapter 5

Allene Osmylation and Multi-component Coupling

5.1. Introduction

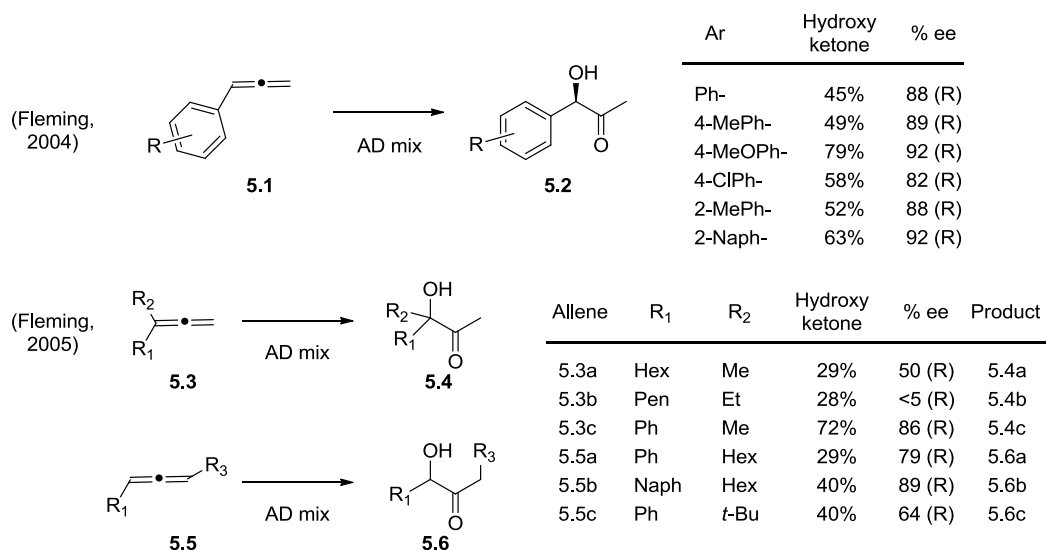
A mechanistic rationale that reconciles earlier methodological shortcomings of allene osmylation is advanced and tested. These insights provide the basis for new efficient methods of catalytic allene osmylation and stereoselective multi-component allene hydroxylation/electrophile capture reactions. These methods constitute a powerful complement to allene spirodiepoxidation/nucleophile capture methods. Simple and complex substrates are used to demonstrate the generality of these new methods.

5.2. History of Allene Osmylation

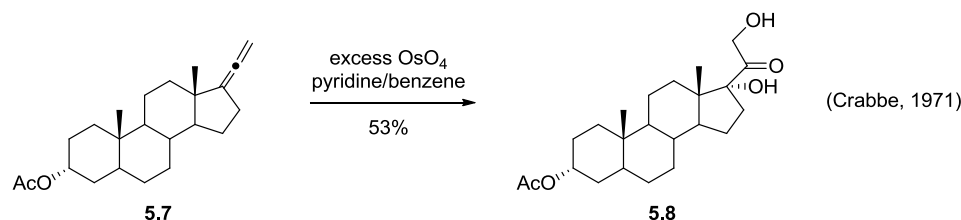
In contrast to the extensive studies of alkene osmylation in the literature, we have found few studies on allene osmylation. These reports detail allene osmylation as sluggish and low yielding reactions with significant byproduct formation that is extremely limited in substrate scope. Fleming reported the asymmetric dihydroxylation of mono-substituted aryl allenes of type **5.1** using AD-mix (Scheme 5.2-1).¹ The reaction gave chiral α -hydroxy ketones with complete regioselectivity and a high degree of stereoselectivity, however the yields were only moderate (45 – 63%) with the exception of the *para*-methoxy substituted allene (79%). In the case of non-aryl 1,1-disubstituted allenes of type **5.3**, the yield and enantioselectivity were poor.² Crabbe disclosed the

stoichiometric osmium tetroxide (OsO_4)-mediated oxidation of steroid **5.7** gave dihydroxy-keto steroid **5.8** (Scheme 5.2-2).³

Scheme 5.2-1: Asymmetric Dihydroxylation on Allene by Fleming



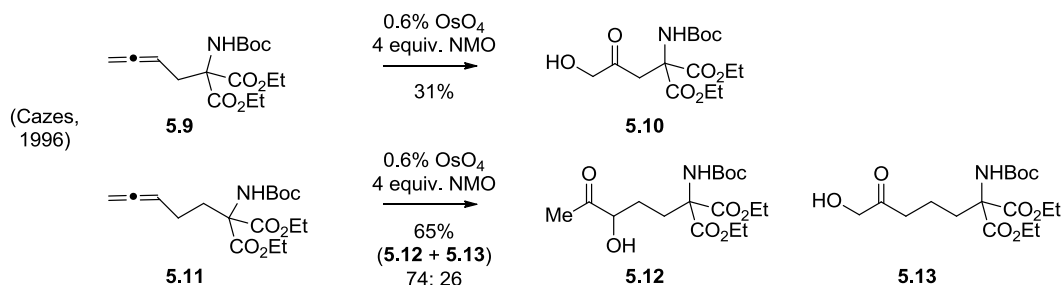
Scheme 5.2-2: Stoichiometric Allene Osmylation on a Steroidal Substrate



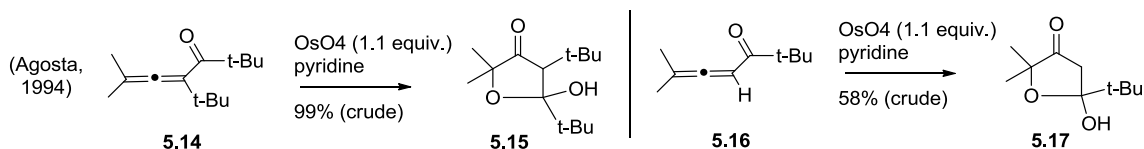
Previous allene osmylations showed that oxidation occurs at the more electron-rich terminus. However Cazes demonstrated a steric effect, that led unexpectedly to unique α -hydroxyketone **5.10** from *N*-Boc aminomalonate **5.9** while osmylation of homolog **5.11** resulted in reversed regioselectivity giving regiomers **5.12** and **5.13** in a

74:26 ratio (Scheme 5.2-3).⁴ OsO₄ was also shown by Agosta to oxidize allenic ketones to cyclic hemiketals (**5.14** → **5.15**, **5.16** → **5.17**, Scheme 5.2-4).⁵

Scheme 5.2-3: Effect of Sterics on Regioselectivity



Scheme 5.2-4: Osmylation on Allenic Ketones



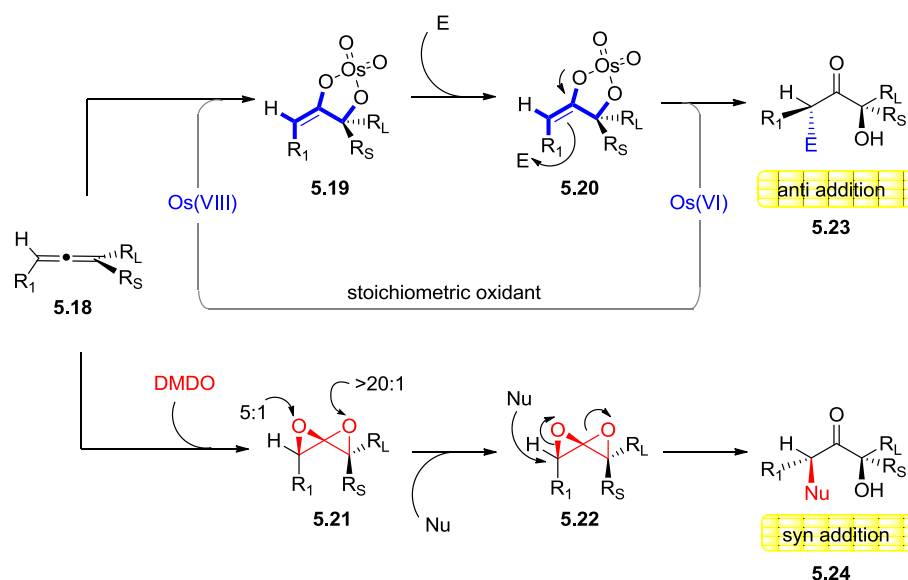
5.3. Mechanistic Rationale and Stereochemical Outcome

The Sharpless group has reported their findings on “ligand-accelerated catalysis” systems in which the addition of a specific ligand increases the reaction rate of an already existing catalytic transformation.^{6, 7} The nature of the ligands bound to a metal center or complex always affects the selectivity and rate of the organic transformations catalyzed by such a species. If the reaction rate is increased upon ligand binding, the stereoselective pathway can dominate over the nonselective one.

Along similar lines, we hypothesized that the addition of an electrophile to an allene osmylation reaction would accelerate decomposition of the relatively stable osmate

enol ester intermediate (**5.20** \rightarrow **5.23**, Figure 5.3-1), thereby increasing reaction rate and selectivity. Allenes are oxidized at the most electron-rich terminus and subsequent decomposition of the osmate ester captures the electrophile syn-facial to the smaller substituent (R_S , **5.20**). This provides regio- and stereoselective allene hydroxylation/electrophile addition anti-adduct. The stereochemical outcome of the reaction is complementary to allene spirodiepoxidation/nucleophile addition syn-adduct **5.24**.

Figure 5.3-1: Allene Oxidation



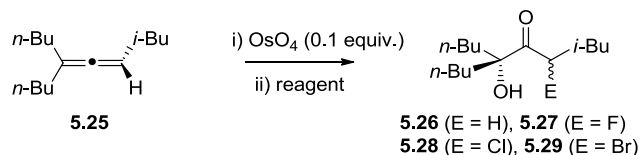
In the DMDO oxidation of acyclic allenes, the first epoxidation will also occur at the most electron-rich terminus with excellent stereoselectivity ($> 20:1$), favoring the less sterically hindered side (H vs. R_1 on **5.21**). The second epoxidation is less selective, but still favors the smaller substituent (R_S). Nucleophile addition then occurs at the least

sterically hindered SDE terminus on the face of the larger substituent (R_L), providing the syn-addition product (**5.24**).

5.4. *Allene osmylation and multi-component coupling*

These hypotheses were tested on achiral tri-substituted allene **5.25** as a model system (Table 5.4-1). All reactions were carried out under catalytic conditions (0.1 equiv. OsO_4) with a specific stoichiometric oxidant. The typical experimental procedure is as follows: to the allene in a *t*-BuOH:pH 7.4 phosphate buffer (1:1) solution was added an electrophile (Selectfluor, NCS, or NBS at room temperature). The mixture was stirred for 20 minutes, then 4% aqueous OsO_4 solution (0.1 equiv.) was added slowly followed by stoichiometric oxidant. After the complete disappearance of allene by TLC observation, the reaction mixture was quenched with a saturated sodium sulfite solution. Purification by flash column chromatography on silica gel following aqueous workup afforded the corresponding α -hydroxy- α' -halo ketone. Under anhydrous conditions (entry 5), a solution of allene in dichloromethane (DCM) was added to a solution of OsO_4 (0.1 equiv.), NMO (1.2 equiv.), acetic acid (4 equiv.) and phenylboronic acid (1.2 equiv.) in DCM. The workup and purification process was identical to that of the above aqueous conditions and afforded the corresponding α -hydroxy ketone.

In all cases, the reaction proceeds with complete regioselectivity. As expected, allene **5.25** is oxidized at the more substituted (electron-rich) terminus and decomposition of the osmate enol ester captures the electrophile at the less substituted terminus. In the presence of a halide electrophile, the reaction provides an α -hydroxy- α' -halo ketone and the rate of the reaction increases (cf. entries 1, 9, 12, and 13) with NMO as the stoichiometric oxidant in a *t*-BuOH:pH 7.4 phosphate buffer (1:1) solution.

Table 5.4-1: Catalytic Allene Oxidation

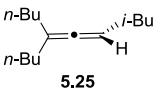
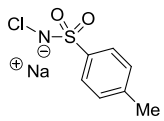
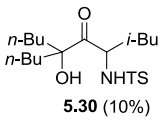
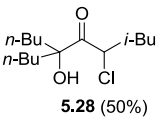
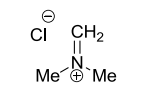
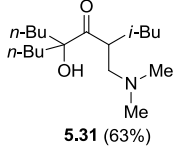
Entry	Stoichiometric oxidant (equiv.)	Additive (equiv)	E	Solvent	Time	Yield
1	NMO (2)	-	-	<i>t</i> -BuOH: H ₂ O (1:1)	48 hr	trace
2	AD-mix (1.4g/mmol)	MeSO ₂ NH ₂ (0.2)	-	<i>t</i> -BuOH: H ₂ O (1:1)	48 hr	56 %
3	K ₃ Fe(CN) ₆ (3)	K ₂ CO ₃ (0.2)	-	<i>t</i> -BuOH: H ₂ O (1:1)	12 hr	65 %
4	NMO (2)	DABCO (0.1)	-	<i>t</i> -BuOH: H ₂ O (1:1)	12 hr	68 %
5	NMO (1.2)	AcOH w/ PhB(OH) ₂	-	DCM	2 hr	65 %
6	NMO (2)	AcOH	-	<i>t</i> -BuOH: H ₂ O (1:1)	4 hr	70 %
7	NMO (2)		NCS	<i>t</i> -BuOH: H ₂ O (1:1)	12 hr	10 %
8	NMO (2)		NCS	acetone: H ₂ O (1:1)	3 hr	34 %
9	NMO (2)		NCS	<i>t</i> -BuOH: buffer (1:1)	24 hr	67 %
10	NMO (2)		NCS	acetone: buffer (1:1)	24 hr	68 %
11	NMO (2)		NBS	acetone: buffer (1:1)	2 d	31 %
12	NMO (2)		NBS	<i>t</i> -BuOH: buffer (1:1)	5 hr	68 %
13	NMO (2)		Selectfluor	<i>t</i> -BuOH: buffer (1:1)	12 hr	40 %

AD-mix with methanesulfonamide also accelerates the rate of the reaction (entry 2). Sharpless et al.⁸ demonstrated that hydrolysis of the osmium (VI) glycolate product can be accelerated considerably by methanesulfonamide.⁴ Potassium cyanoferrate (K₃Fe(CN)₆) in the presence of K₂CO₃, was also evaluated and found to react smoothly in the osmylation of **5.25** (entry 3). Sharpless argued that using K₃Fe(CN)₆, instead of NMO, eliminates the second catalytic cycle because there is no oxidant other than OsO₄

in the organic layer due to biphasic conditions with $\text{K}_3\text{Fe}(\text{CN})_6$.⁵ Thereby, the reported ee under $\text{K}_3\text{Fe}(\text{CN})_6/\text{K}_2\text{CO}_3$ is better than ones using NMO. The tertiary amine, DABCO, is also capable of accelerating the reaction (entry 4).

The reaction can be conducted in organic solvent alone (entry 5). For the dihydroxylation of olefins, aqueous conditions are usually employed to hydrolyze the osmate ester. However, this not only makes it difficult to isolate water soluble polyol derivatives but many electrophiles also react fast with water. Iwasawa, Kato, and Narasaka reported that the use of phenylboronic acid as a diol captor prevents over-oxidation and also enables the reaction to be performed in organic solvent alone.⁹

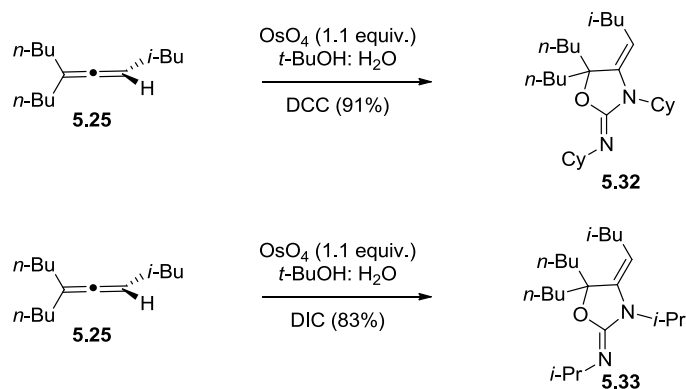
Table 5.4-2: Allene Oxidation

allene	electrophile	solvent	products
 5.25		<i>t</i> -BuOH: H ₂ O	 5.30 (10%)  5.28 (50%)
5.25		DCM	 5.31 (63%)

Other than halide electrophiles, we also tried C-N and C-C bond forming reactions. The addition of Chloramine-T was performed under stoichiometric conditions (1.1 equiv. OsO_4) to give **5.30** (10% yield, Table 5.4-2). The majority of the product was chlorine addition **5.28** (50% yield). The addition of Eshenmoser salt (dimethylmethylenediammonium chloride) was carried out under catalytic conditions

with NMO as the co-oxidant in anhydrous DCM giving **5.31** in good yield (63% yield). When DCC or DIC were added, heterocycles **5.32** and **5.33** were isolated in good yield (Scheme 5.4-1).

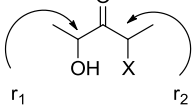
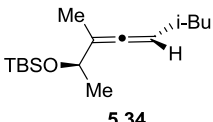
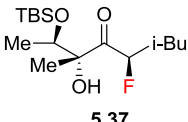
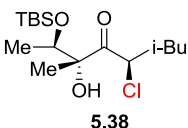
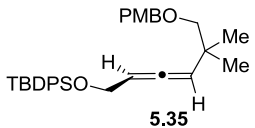
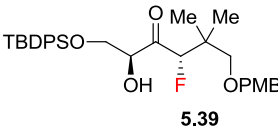
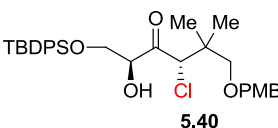
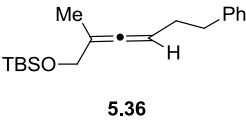
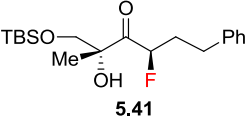
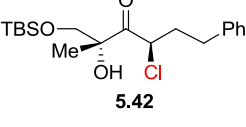
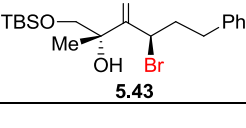
Scheme 5.4-1: DCC and DIC Addition



5.5. Chiral allene: osmylation and multi-component coupling

The osmylation reaction was also performed on chiral di- and tri-substituted allenes (Table 5.5-1). Optically active allenes **5.34** and **5.35** were prepared according to known procedures,^{10, 11} however the racemate of **5.36** was used. Three electrophilic halide sources (Selectfluor, NCS, and NBS) were tested for both the catalytic and stoichiometric conditions. The reaction conditions for the catalytic and stoichiometric processes were the same as described in section 5.4.

Table 5.5-1: Chiral Allene Osmylation and Halide Addition

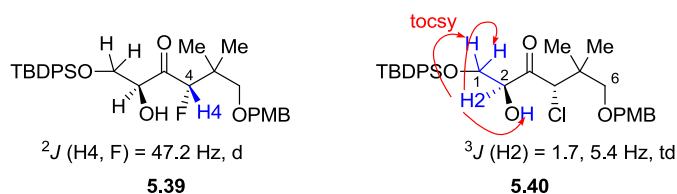
entry ^A	allene	product ^B	<div style="text-align: center;"> selectivity^C  </div>		yield ^D (%)
1	 5.34	 5.37	> 20:1	5.9 : 1	68
2	5.34	 5.38	> 20:1	5.3 : 1	78
3	 5.35	 5.39	> 20:1 (> 20:1)	> 20:1 (> 20:1)	64 (62)
4	5.35	 5.40	> 20:1 (> 20:1)	3.2 : 1 (1.5:1)	68 (79)
5	 5.36	 5.41	(> 20:1)	(7: 1)	74
6	5.36	 5.42	(> 20:1)	(2: 1)	50
7	5.36	 5.43	(> 20:1)	(1.7: 1)	60

A) stoichiometric reactions employed 1.1 equiv. of OsO₄ w/ electrophile (2 or 5 equiv.) at rt. catalytic reactions employed 0.1 equiv of OsO₄ w/ NMO (2 equiv.) & electrophile (2 or 5 equiv.) at rt. B) only anti product is shown: C) black = selectivity in stoichiometric condition, blue = selectivity in catalytic condition: D) combined yield of anti and syn products

In all cases, we observed complete regioselectivity. In tri-substitued allenes (entries 1, 2, 5, 6, and 7), the osmate enol ester formed at the more substituted terminus as expected, leading to carbon-halide bond formation at the less substituted terminus. In

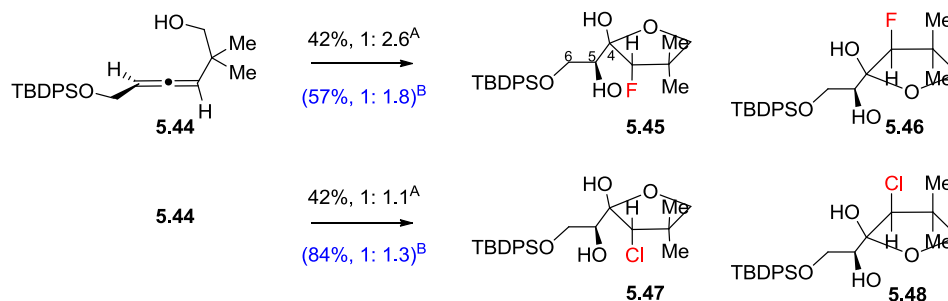
1,3-disubstituted allenes (entries 3 and 4), the steric effect, induced by gem-dimethyl substituents, overrides the electronic effect of the electron withdrawing TBDPS group. The site of fluorine addition (**5.35** \rightarrow **5.39**) was confirmed by observation of H4 geminal splitting by fluorine which appeared as a doublet with a characteristic strong splitting constant (Figure 5.5-1, $J = 47.2$ Hz) while the regioselectivity of **5.40** was confirmed by TOCSY and vicinal splitting of H2, which appeared as a triplet of doublets (Figure 5.5-1).

Figure 5.5-1: Regiochemistry of 5.39 and 5.40



The stereoselectivity is particularly good with bulky Selectfluor in comparison to NCS and NBS. It is likely that the asymmetric bias is enhanced due to the bulkiness of SelectFlour.¹² In all cases, the stoichiometric reaction gave better selectivity than catalytic reactions. For the addition of bromine, NBS had to be pre-solvated in *t*-BuOH:buffer mixture, then added to the mixture of OsO₄, NMO, and allene slowly over at least 1 hour. If these requirements are not met, the allene will react with NBS faster than osmylation can occur.

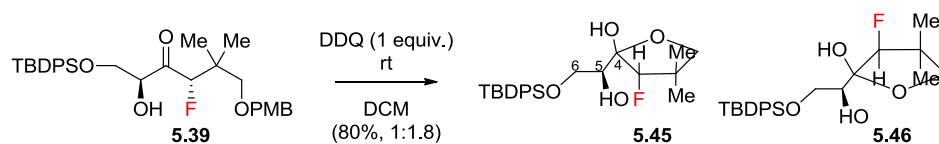
Scheme 5.5-1: Halogenated Furanose



A) Reactions employed 1.1 equiv. of OsO_4 w/ electrophile (2 or 5 equiv.) at rt.
 B) Reactions employed 0.1 equiv. of OsO_4 w/ NMO (2 equiv.) & electrophile (2 or 5 equiv.) at rt.

When the substrate without the para-methoxy benzyl (PMB) group **5.44** is oxidized in the presence of electrophiles, the osmylation reaction gave halo-substituted furanose (Scheme 5.5-1). Unlike the osmylation on the substrate with PMB group **5.35**, I found the mixture of two diastereomers for fluorine adducts (Scheme 5.5-1). Upon the cleavage of PMB group in **5.39** by DDQ (Scheme 5.5-2), the reaction generated the same products **5.45** and **5.46** in the same ratio (1:1.8). This experiment indicated that the diastereoselectivity on fluorine addition is >20:1.

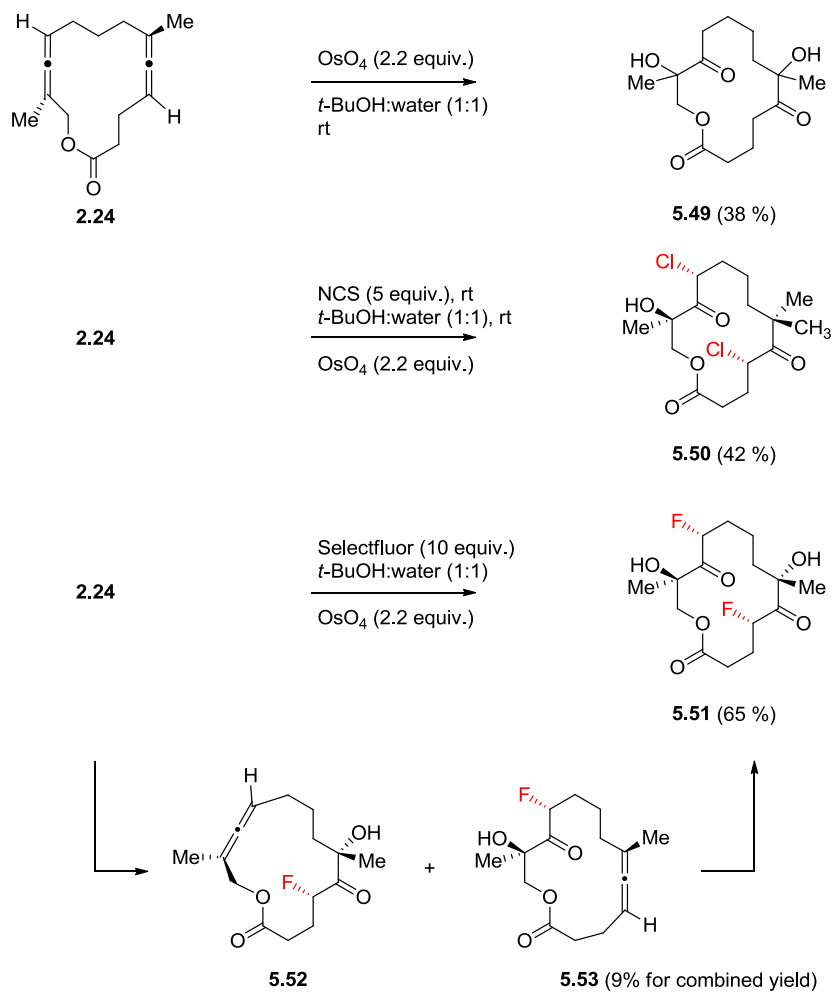
Scheme 5.5-2: In-Situ Cleavage and Cyclization of 5.39



5.6. *Cyclic Allene Osmylation: Model Study*

Macrocyclic bis[allene] **2.24** and compounds of this type provide a unique platform for diversity oriented synthesis due to the reactivity of allenes in various chemical transformations, the heterogeneous manipulation of bis[allene] and enhanced macrocyclic stereocontrol.^{13, 14} Since acyclic allenes show complete regioselectivity and moderate stereoselectivity, the successful application of allene osmylation/electrophile addition methodology for cyclic bis[allene]s of type **2.24** will further prove the utility of the methodology.

Scheme 5.6-1: Cyclic Chiral Allene Osmylation

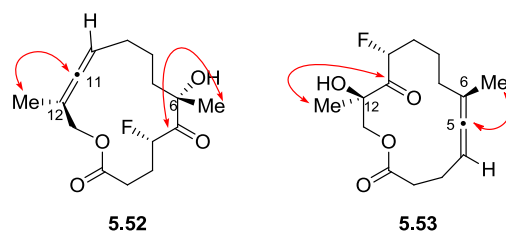


All reactions (Scheme 5.6-1) were carried out under stoichiometric conditions (2.2 equiv. OsO_4). The typical experimental procedure is as follows: to the allene in a $t\text{-BuOH}:\text{water}$ (1:1) solution was added an electrophile (SelectFluor, NCS) at room temperature. The mixture was stirred for 20 minutes, then 4% aqueous OsO_4 solution was added dropwise. After the complete disappearance of allene by TLC observation, the reaction mixture was quenched with a saturated sodium sulfite solution.

In the absence of an electrophile, bis[keto] alcohol **5.49** was isolated as expected. Both NCS and Selectfluor proved to be the compatible electrophiles for macrocyclic bis[allene] **2.24** under the above reaction conditions giving the desired products (**2.24** → **5.50**, **2.24** → **5.51**) in moderate yields. Under the reaction conditions, the conversion from mono-oxidized products of types **5.52** and **5.53** to bis-oxidized product **5.51** is easily monitored by TLC over 1 or 2 hours. Interestingly, the oxidation rate of the two allenes of the macrocyclic lactone (**2.24**) did not show much difference, which could be confirmed by the isolation of a 1:1 mixture of **5.52** and **5.53**. This observation is contrary to the bis[allene] macrolactone oxidation of **2.24** by DMDO (*See* Chapter 4).

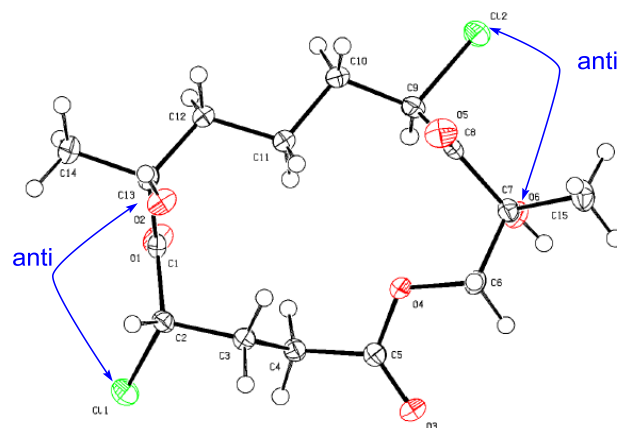
HMBC spectroscopy shows that the central allenic carbon resonances (C11 in **5.52**, C5 in **5.53**) was coupled to methyl protons at C12 in **5.52** and C6 in **5.53** while the tertiary methyl proton resonances at C6 in **5.52** and C12 in **5.53** was coupled carbonyl carbon resonances (C5 in **5.52**, C11 in **5.53**).

Figure 5.6-1: HMBC Confirmation of Two Central Allenic Carbons



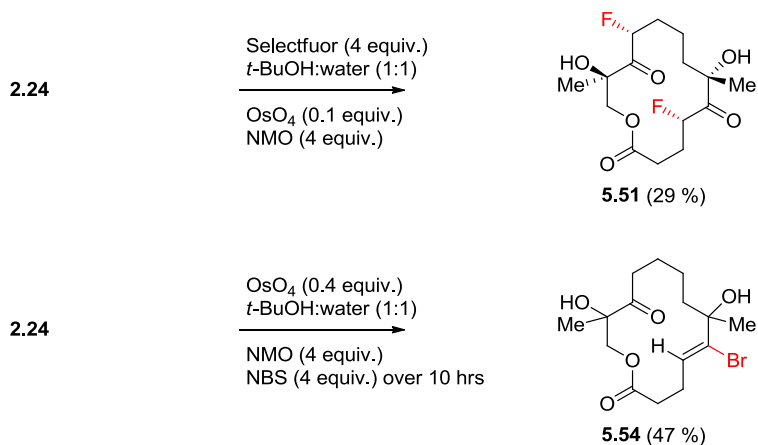
The bis[allene] hydroxylation/electrophile addition showed complete diastereoselection in the products. Kai Liu successfully recrystallized chlorine addition product **5.50** and was therefore able to establish the stereochemistry at C4 and C10 unambiguously (Figure 5.6-1).

Figure 5.6-2: X-ray Crystallography Data of Chlorine Addition, 5.50



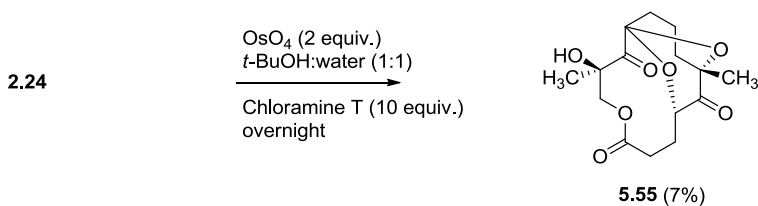
Catalytic conditions with NMO as co-oxidant were also tried for fluorine and bromine additions (Scheme 5.6-2). With Selectfluor, bis-fluorine addition product **5.51** was isolated in 29% yield. Since NBS is able to react with allenes independently, NBS was premixed in *t*-BuOH:water and added over 10 hours into the mixture of allene, OsO₄, and NMO in *t*-BuOH:water. However, the isolated halohydrin (**5.54**) showed NBS addition to the central carbon.

Scheme 5.6-2: Catalytic Osmylation on Macrocyclic Bis[Allene] 2.24



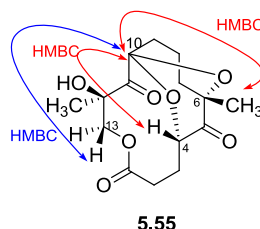
Stoichiometric conditions with OsO₄ in the presence of Chloramine-T led to the formation of polycyclic ether **5.55**. The detailed mechanism for the formation of **5.55** was not clear, but one can presume that the over-oxidation product must be involved as an intermediate.

Scheme 5.6-3: Polycyclic Ether Formation



Long-range correlations through oxygens between the C6 methyl protons and C10 carbon (C6-CH₃ ↔ C10) as well as the C4 protons and C10 carbon (C4-H ↔ C10) confirmed the formation of cyclic ethers. The position of C10 was confirmed by long-range correlation between the C13 protons and C10 carbon (C13-H ↔ C10).

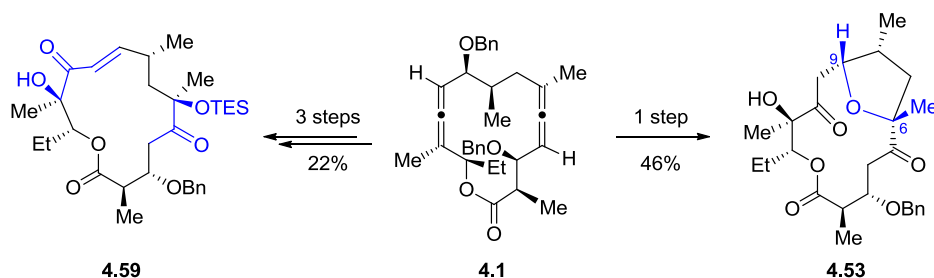
Figure 5.6-3: Long-Range Correlations Through Oxygens in 5.55



5.7. Cyclic Allene Osmylation

In chapter 4, we showed that treatment of macrocyclic bis[allene] **4.1** with OsO_4 can give 6,9-bicyclomacrolide **4.53** or C9-C12 hydroxyenone **4.59** if the osmylation was done stepwise and the hydroxyl group at C6 was masked before subsequent oxidation.

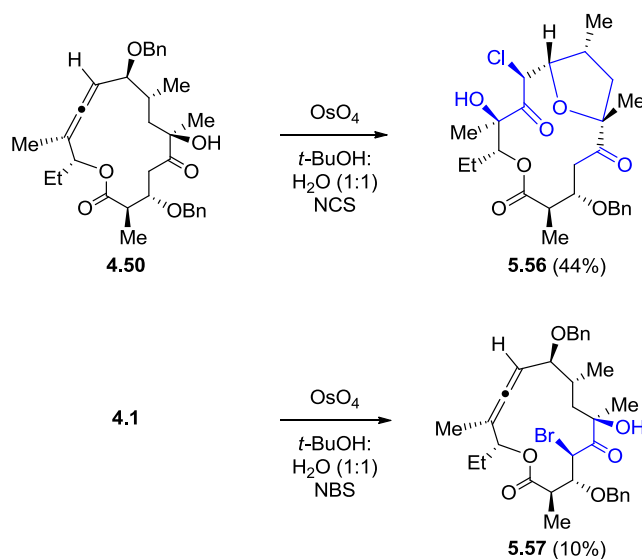
Scheme 5.7-1: Osmylation of 4.1



Model macrolactone of type **2.24** demonstrated that hydrolysis of the osmate ester in the presence of an electrophile will lead to the electrophile-captured adduct even in bis[allene] macrocyclic platform. We can easily envision the synthetic utility of halogenated macrolide. Hence, Kai Liu reacted mono-osmylated adduct **4.50** with OsO_4 (1.1 equiv.) in *t*-BuOH:H₂O. NCS in *t*-BuOH and H₂O solution was slowly added to the

osmate enol ester in solution for 3 hours. The product showed chlorine addition **5.56** at C10 (Scheme 5.7-2). In the analogous way, NBS in *t*-BuOH and H₂O solution was added to the osmate enol ester from bis[allene] macrolactone **4.1**. Due to the reactivity of NBS with allenes, the complex mixture of products was observed on TLC and they were very hard to separate from flash column chromatography. After exhaustive chromatography, we could isolate mono bromine adduct **5.57** adduct in 10% yield.

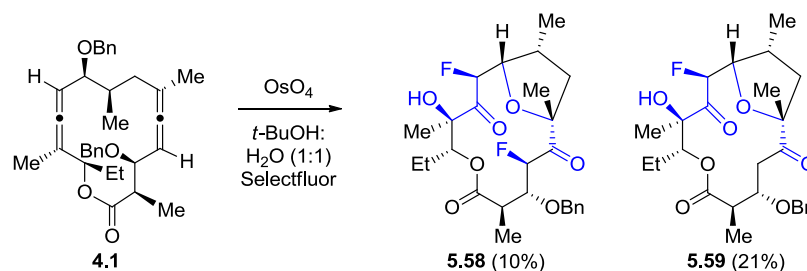
Scheme 5.7-2: Chlorine Addition to Macrolactone



Since chlorine and bromine atoms possess similar Van der Waals radii to a methyl group ($\text{Cl} = 1.80 \text{ \AA}$, $\text{Br} = 1.95 \text{ \AA}$, $\text{Me} = 2.00 \text{ \AA}$), they could be possible candidates for methyl group bioisostere in erythromycin analogs.¹⁵ Especially, the chlorine atom is viewed not only to be isosteric but also isolipophilic with the methyl group and its replacement showed the alternation in drug metabolism.¹⁵

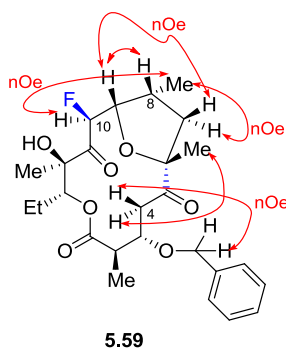
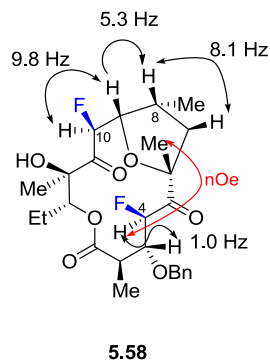
In modern medicinal chemistry, fluorinated compounds are synthesized on a routine basis.¹⁶ Owing to its chemical stability and small size, fluorine is often regarded as a hydrogen bioisostere and has become an important tool in modern drug discovery to fine-tune biological effects and for studies of binding affinity in protein-ligand complexes.¹⁷

Scheme 5.7-3: Fluorine and Bromine Addition to Macrolactone



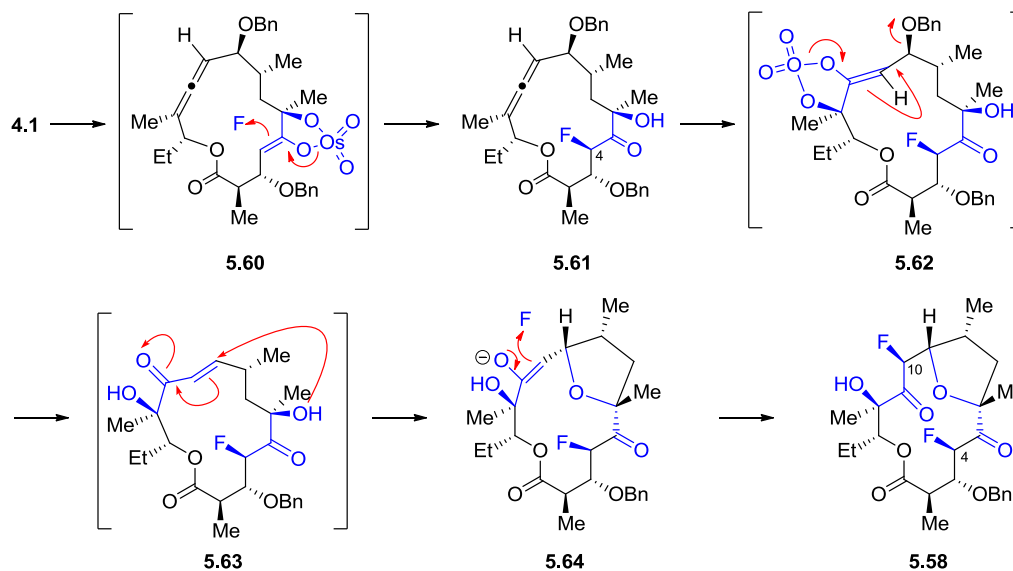
To incorporate fluorine, bis[allene] macrolactone **4.1** was treated with OsO_4 followed by a solution of Selectfluor in $t\text{-BuOH}:\text{H}_2\text{O}$ (1:1) (Scheme 5.7-3). This reaction was not optimized. The isolated products (**5.58** and **5.59**) showed fluorine addition. The syn addition of fluorine at C10 was confirmed by observation of a strong nOe between H10 and the C8 methyl group. Contrary to this, fluorine addition at C4 showed anti addition as expected.

Figure 5.7-1: Coupling Constants and nOe Analysis of Cyclic Ether Formation



Although the precise structures of the intermediates are a matter of speculation, the osmate enol ester intermediate **5.60** formed and subsequent decomposition of the osmate enol ester captured the electrophile at C4 syn-facial to the smaller substituent (methyl vs. osmate ester at C6). However, the osmylation at the C10-C12 allene resulted in β -elimination (**5.62** \rightarrow **5.63**) and subsequent intramolecular conjugate addition formed enolate (**5.63** \rightarrow **5.64**). Considering the relative ground state minimum energies, z-enolate is preferred and the sterics in z-enolate preferred the top face access of electrophile. The same mechanistic rationale could be applied for the stereochemistry of chlorine and bromine adducts (**5.56** and **5.57**).

Scheme 5.7-4: Mechanistic Rationale for Stereochemistry of Bis[Fluorine] Addition



5.8. Conclusion

We discovered that *a*) the catalytic amount of OsO₄ with co-oxidants can be utilized to oxidize the chiral allenes with high regio- and stereoselective manner; *b*) the presence of electrophiles not only accelerates the rate of the reaction but also provides the multicomponent allene hydroxylation/electrophile capture adduct; *c*) when applied on the cyclic allene system, the reaction showed the complete stereoselection; *d*) the compatible electrophiles are Selectfluor, NCS, NBS, Chloramine-T, and Eshenmoser's salt; *e*) taken together these advances have led to one general procedure which is applicable to a wide range of allenic substrates.

5.9. References

1. Fleming, S. A.; Carroll, S. M.; Hirschi, J.; Liu, R.; Lee Pace, J.; Ty Redd, J. *Tet. Lett.* **2004**, *45*, 3341.
2. Fleming, S. A.; Liu, R.; Redd, J. T. *Tet. Lett.* **2005**, *46*, 8095.
3. Biollaz, M.; Haefliger, W.; Velarde, E.; Crabbe, P.; Fried, J. H. *J. Chem. Soc. D: Chem. Comm.* **1971**, *21*, 1322.
4. David, K.; Arient, C.; Greiner, A.; Goré, J.; Cazes, B. *Tet. Lett.* **1996**, *37*, 3335.
5. Wolff, S.; Agosta, W. C. *Can. J. Chem.* **1984**, *62*, 2429.
6. Berrisford, D. J.; Bolm, C.; Sharpless, K. B. *Angw. Chem. Int. Ed. Engl.* **1995**, *34*, 1059.
7. Jacobsen, E. N.; Marko, I.; Mungall, W. S.; Schroeder, G.; Sharpless, K. B. *J. Am. Chem. Soc.* **1988**, *110*, 1968.
8. Sharpless, K. B.; Amberg, W.; Bennani, Y. L.; Crispino, G. A.; Hartung, J.; Jeong, K. S.; Kwong, H. L.; Morikawa, K.; Wang, Z. M. *J. Org. Chem.* **1992**, *57*, 2768.
9. Iwasawa, N.; Kato, T.; Narasaka, K. *Chem. Lett.* **1988**, *17*, 1721.
10. Zhang, Y.; Cusick, J. R.; Ghosh, P.; Shangguan, N.; Katukojvala, S.; Inghrim, J.; Emge, T. J.; Williams, L. J. *J. Org. Chem.* **2009**, *74*, 7707.
11. Shangguan, N.; Kiren, S.; Williams, L. J. *Org. Lett.* **2007**, *9*, 1093.
12. Nyffeler, P. T.; Durón, S. G.; Burkart, M. D.; Vincent, S. P.; Wong, C.-H. *Angw. Chem. Int. Ed. Engl.* **2005**, *44*, 192.
13. Ghosh, P.; Zhang, Y.; Emge, T. J.; Williams, L. J. *Org. Lett.* **2009**, *11*, 4402.
14. Liu, K.; Kim, H.; Ghosh, P.; Akhmedov, N. G.; Williams, L. J. *J. Am. Chem. Soc.* **2011**, *133*, 14968.
15. Patani, G. A.; LaVoie, E. J. *Chem. Rev.* **1996**, *96*, 3147.
16. Böhm, H.-J.; Banner, D.; Bendels, S.; Kansy, M.; Kuhn, B.; Müller, K.; Obst-Sander, U.; Stahl, M. *ChemBioChem* **2004**, *5*, 637.
17. Meanwell, N. A. *J. Med. Chem.* **2011**, *54*, 2529.

Chapter 6

The Ligand Design and Synthesis for siRNA

Delivery

6.1. Introduction

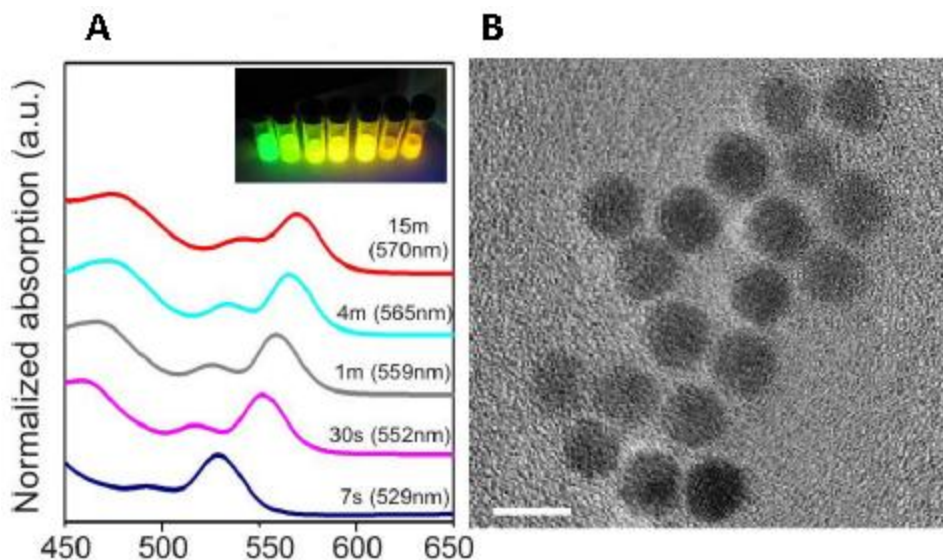
Nanoscience refers to the study of manipulating matter on an atomic and molecular scale of approximately 1~1000 nm and their applications in various fields such as solar cells, electronic devices, drug/gene delivery, regenerative medicine, tissue engineering, and biological diagnosis.^{1, 2} This field has been rapidly growing in the past two decades, and its biological application has been especially widely demonstrated as a proof-of-principle. However, a practical application to clinical medicine is required to solve many key problems concerning cancer biology for therapy as well as regenerative medicine using stem cells.

In this study, I focused on the design and synthesis of target specific quantum dot-based platforms to induce the apoptosis of brain cancer cells and to show their capacity to be extended to in vivo systems for the further clinical purpose of using them as theragnostics which combines therapy and diagnosis.³ This work in chapter 6 was all done in collaboration with Prof. Ki-Bum Lee's group at Rutgers.

6.2. Quantum Dots (QDs)

QDs have been regarded as a representative nanosystem because it shows novel quantum physical properties such as quantum confinement effect and quantum size effect beyond classical mechanics.^{4,5} According to their sizes, QDs emit photons with different wavelengths due to different band gap energies between the conduction and valence bands: smaller sizes emit in the short wavelength range and larger size emits longer wavelength photons, which means the emission wavelength is readily tunable.

Figure 6.2-1: UV-Vis Absorption Spectra and TEM Image of Quantum Dots
(adapted with permission from ref. ³)



(A) Normalized absorption spectra of CdS core while these were growing; (B) TEM image of DHLA-PEG8-amine coated CdSe/CdS/ZnS coreshell QDs (scale bar = 10 nm)

Moreover, they have broad absorption ranges and narrow emission peaks, which enable multicolor detection with a single light source. Most of all, high quantum yields

and extinction coefficients generate about fifty times higher brightness than conventional organic dyes. Their enhanced photostability makes them ideal candidates for the substitution of organic dyes in the fields of single molecule biophysics and cell biology. In addition, QDs are especially suitable in biological applications since they provide high surface area which is ideal for a delivery agent and high quantum yield makes them the ideal tool for tracking agent.

However, despite of its advantages as described above, several drawbacks exist and need to be addressed for practical application, especially on cell biology. Its toxicity to cells is a major issue. Often times, the coating of quantum dots is done with mercaptoacetic acid, which is cytotoxic.⁶ Even though the coating of the quantum dots is compromised, the metallic core (i.e., cadmium or selenium ions) or the dissolution of the core can be toxic. Quantum dot metabolism and degradation within the body is still unknown and several studies have shown the accumulation of the quantum dots in the kidney, spleen, and liver.⁷ In addition, the bioconjugation with different molecules will increase the size of the dots making delivery into cells more difficult.

6.3. Glioblastoma Multiforme (GBM) and the Mutant Epidermal Growth Factors Receptor (EGFRvIII)

Glioblastoma multiforme (GBM) originating from glial cells is known to be the most malignant, invasive, fast-progressive, and difficult-to-treat brain tumor with just 10-12 months of the mean survival rate after cancer treatment.⁸⁻¹⁰ Therefore, it is necessary to develop novel early diagnostic tools and therapeutic strategies and nanotechnology can be a promising tool.

About 40% of glioblastoma show overexpression and amplification of the epidermal growth factor receptor (EGFR) gene locus and about half of these tumors express a mutant receptor (EGFRvIII) which lacks amino acids from 6 to 273 in the extracellular domain and is always activated without ligand binding.¹¹

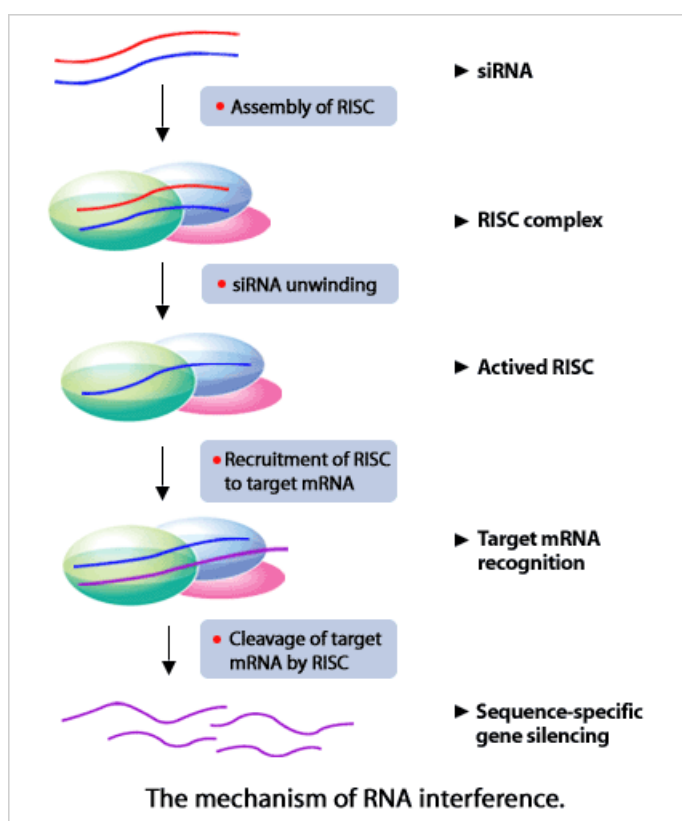
We targeted EGFRvIII, since it is known that knockdown of this gene is one of the most effective ways to down-regulate the PI3K/Akt signaling pathway.^{12, 13} The PI3K/Akt signaling pathway plays a critical role in cell proliferation and apoptosis. Therefore, several drug molecules were developed to inhibit the function of the proteins in this pathway (i.e., Erlotinib/Gefinib for EGFR, and Rapamycin for mTOR). EGFR forms a dimeric complex upon the ligand binding on the extracellular domain. The kinase domain in cytoplasm region of each monomer is close together and subsequently phosphorylates the tyrosine residue on the long and flexible tail. This complex sends the proliferation triggering signal to following proteins in the downstream such as Akt, mTOR, and S6.

6.4. *siRNA*

RNA interference (RNAi) is a system within living cells that is responsible for controlling which genes are active and how active they are. Two types of small RNA molecules; microRNA (miRNA) and small interfering RNA (siRNA), are central to RNA interference pathway. RNAs are the direct products of genes. These small RNAs can bind to target messenger RNA (mRNA) and either increase or decrease their activity. This usually results in translational repression or target degradation and gene silencing. RNAi-based approach can sequence-specifically inhibit the expression of targeted

oncogenes. Therefore, it enables modulation of signaling pathways and regulates the behavior of malignant tumor cells.^{14, 15}

Figure 6.4-1: Mechanism of RNA interference¹⁶



However, in order to harness the full potential of this approach, the prime requirements are to deliver the siRNA molecules with high selectivity and efficiency into tumor cells and to monitor both siRNA delivery and the resulting knock-down effects at the single cell level.

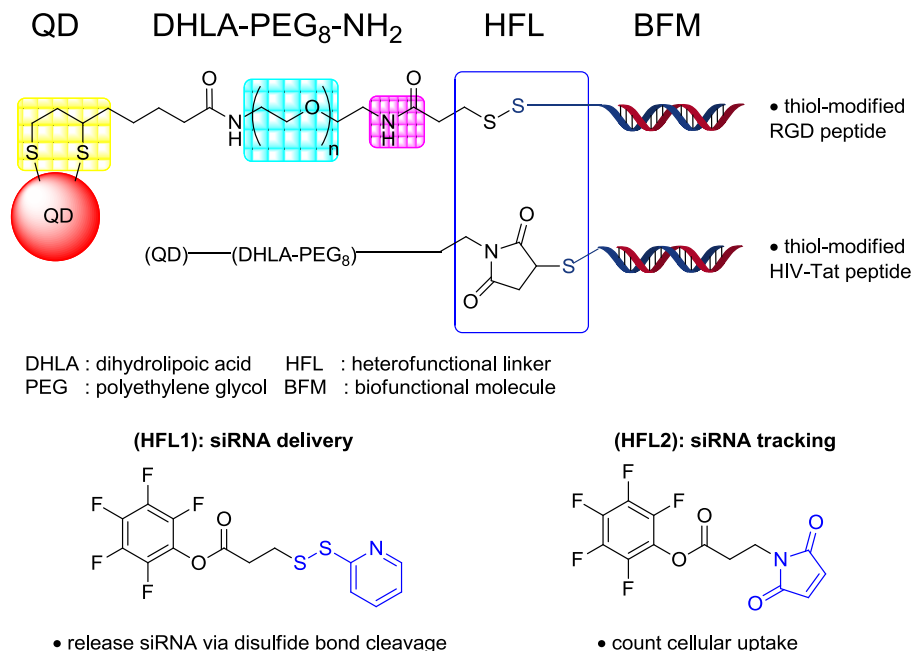
Herein, we describe the synthesis and target-specific delivery of multifunctional siRNA-QD constructs for selectively inhibiting the expression of EGFRvIII in target

human U87 glioblastoma cells, and subsequently monitor the resulting down-regulated signaling pathway with high efficiency.

6.5. Design and Synthesis of the multifunctional QD platform for delivery and tracking of siRNA

We synthesized two types of siRNA-QD conjugates, one for siRNA delivery and the other for siRNA tracking (Figure 6.5-1). My former colleague Dr. Jongjin Jung prepared CdSe/CdS/ZnS core-shell QDs^{17, 18} with a diameter of 7 nm and coated with either trioctylphosphine oxide (TOPO) or hexadecylamine (HDA). In order to make the QD constructs water-soluble and suitable for conjugating with siRNA, we replaced these hydrophobic ligands with a dihydrolipoic acid (DHLLA) derivatized with an amine-terminated polyethylene glycol (PEG) spacers.

Figure 6.5-1: General Diagram of Multifunctional QD Conjugates (adapted with permission from ref. ³)



We hypothesized that since the dithiol moiety would provide strong coordination to the QD surface and increase stability in aqueous media, the PEG space would increase water solubility and reduce nonspecific binding, and the amine group would enable conjugation to the siRNA element.

Two heterofunctional linkers (HFL) were synthesized and evaluated for siRNA conjugation. The linker **HFL1** was designed to release siRNA upon entering the cell by cleavage of the disulfide linkage, through enzymatic reduction or ligand exchange (e.g. glutathione).¹⁹ The second linker **HFL2** was designed to be more robust, thereby enabling evaluation of cellular uptake and localization of the siRNA construct within the cellular compartments.²⁰

The final design component was the combination of three biofunctional molecules, siRNA, thiol-modified RGD (Arginine-Glycine-Aspartic Acid) peptide and thiol-modified HIV-Tat derived peptide.

Since brain tumor cells (U87 and U87-EGFRvIII) overexpress the integrin receptor protein $\alpha_v\beta_3$, they strongly bind to the RGD binding domain.²¹ Thereby, RGD-functionalized siRNA-QDs selectively accumulate in brain tumor cells in vitro, and can be tracked by fluorescence microscopy. In addition, the HIV-Tat peptide promotes efficient transfection of siRNA-QDs in cells when it is directly attached to the QD surface.²²

6.6. Transfection efficiency & target –specific delivery of siRNA-QDs

Prior to targeting EGFRvIII, the transfection efficiency was evaluated with EGFP (Enhanced Green Fluorescent Protein). Three different **siRNA-QD** constructs were prepared as follows.

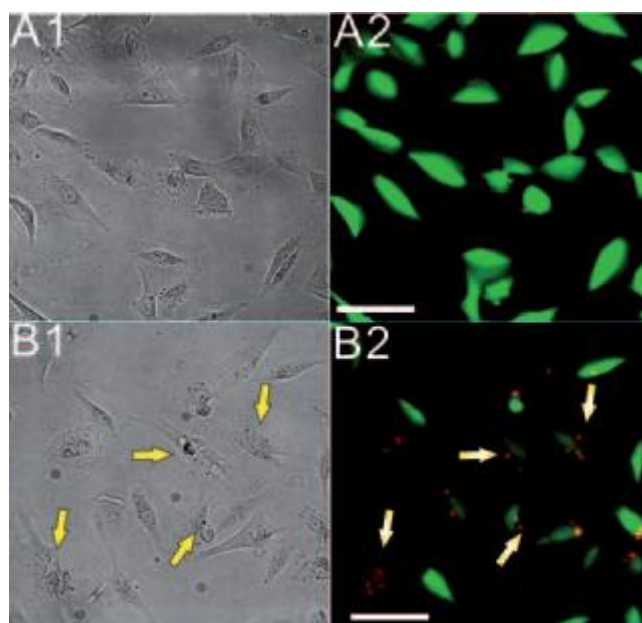
- Construct modified with the RGD peptide only (**siRNA-QD-RDG**)
- Construct with HIV-Tat peptide only (**siRNA-QD-HIV-Tat**)
- Construct with both HIV-Tat and RGD peptide (**siRNA-QD-RGD-HIV-Tat**)

Among three, **siRNA-QD-RGD-HIV-Tat**, (the ratio of siRNA/RGD/HIV-Tat being 1:1:10 per QD) showed the maximum internalization within U87-EGFP cells. Therefore, this optimal condition was used for subsequent experiments.

The U87-EGFP cell line was then treated with siRNA-QD, modified with HIV-Tat and RGD, then simultaneously imaged by fluorescent microscopy.

Figure 6.6-1: Transfection and Knockdown Effect by siRNA-QD Conjugates

(adapted with permission from ref. ³)



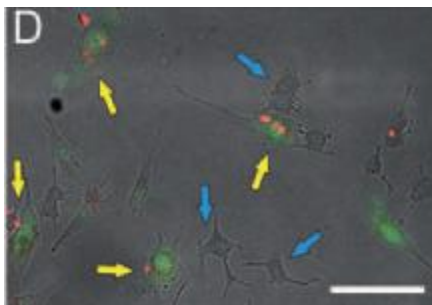
(A) Control U87 cells without siRNA-QDs; (B) U87 cells with siRNA-QDs: A1, B1 = phase-contrast image, A2, B2 = fluorescence image. Scale bar: 100 μ m.

In comparison to control U87-EGFP cells without siRNA-QD conjugates (A1 and A2, Figure 6.6-1), U87-EGFP cells with siRNA-QD conjugates (B1 and B2, Figure 6.6-1) clearly indicate the significant internalization of siRNA-QDs into the cells, which were easily distinguishable from the control cells owing to the bright fluorescence (red dots) of the QDs. Yellow arrows (B1 and B2, Figure 6.6-1) also indicate knockdown of EGFP in U87 cells as expected.

6.7. *Target-specific delivery of siRNA-QDs*

To further demonstrate the target-specific delivery of the siRNA-QDs, we incubated the siRNA-QDs, modified with HIV-Tat and RGD peptides, in co-cultures of the U87-EGFP cell line with PC-12 cell lines which are less-tumorigenic and have less integrin receptors. We hypothesized that the malignant U87 cells have higher cellular uptake of siRNA-QDs than the less tumorigenic PC-12 because the presence of RGD peptide on the surface of siRNA-QD led to specific binding with integrin receptors which over-expressed in the malignant U87 cells. As expected, the U87-EGFP cells showed selective accumulation of the QDs demonstrating the target-specific delivery of the siRNA-QDs (Figure 6.7-1).

Figure 6.7-1: Co-cultures of U87-EGFP cells and PC-12 (adapted with permission from ref. ³)



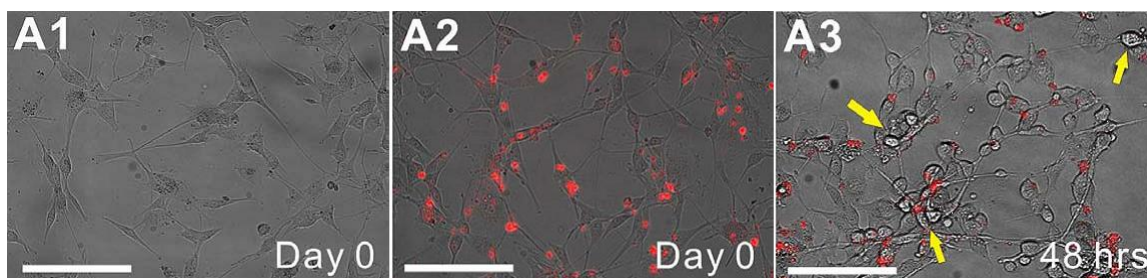
EGFP cells (yellow arrow) and PC12 (blue arrow), Scale bar: 100 μ m

6.8. *Knockdown of EGFRvIII as a chemotherapeutic target by siRNA-QDs*

The successful demonstration of the selective manipulation of the U87-EGFP cell line led us to the examination of siRNA-QD constructs with EGFRvIII. U87-EGFRvIII cells were genetically modified to overexpress EGFRvIII, which only expressed within

cancer cells. This cell type was incubated with our siRNA-QDs, modified with Tat and RGD peptides. The cells were simultaneously imaged for the internalization of siRNA-QDs using fluorescence microscopy. Relative to the control (U87-EGFRvIII without siRNA-QDs), significant cell death was observed in the wells loaded with siRNA-QDs against EGFRvIII after 48 hours (A3, Figure 6.8-1). After 48 hours, the cells have clearly shrunk and appear to have collapsed (yellow arrow, A3, Figure 6.8-1).

Figure 6.8-1: Knockdown of EGFRvIII in U87-EGFvIII (adapted with permission from ref. ³)

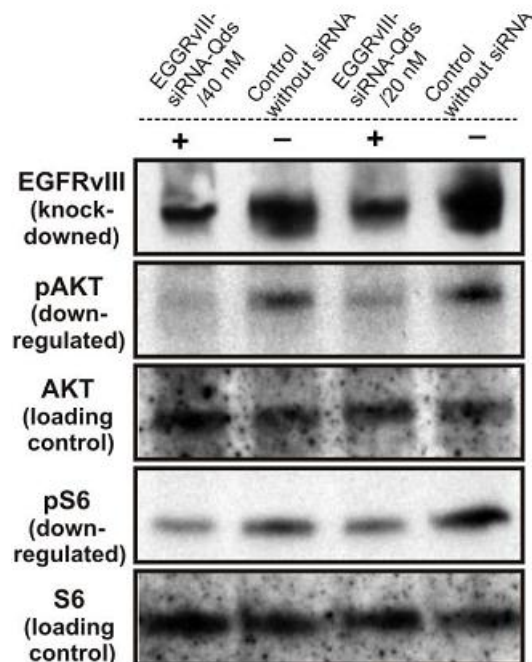


Morphology of (a) U87-EGFRvIII cells before incubation with siRNA-QDs on Day 0; (b) U87-EGFRvIII cells after incubation with siRNA-QDs on Day 0; (c) U87-EGFRvIII cells 48 hrs after incubation with siRNA-QDs, Scale Bar: 100 μ m.

Western immunoblotting (Figure 6.8-2) showed the considerable decrease in the expression of EGFRvIII, and down-regulation of phosphor-Akt and phospho-S6 relative to control.

Figure 6.8-2: Silencing Effect of EGFRvIII Gene (adapted with permission from ref.

³⁾



Taken all together, these results demonstrate the specificity of the siRNA against EGFRvIII, the inherent noncytotoxicity of the QDs, and the facile evaluation and manipulation of cancer cell proliferation with multifunctional QD constructs.

6.9. Conclusion

The small interfering RNA (siRNA) enables manipulation of key oncogenes that modulate signaling pathways and thereby regulate the behavior of malignant tumor cells. In collaboration with Prof. Lee's group at Rutgers, we demonstrated as follows; (a) the synthesis and target-specific delivery of multifunctional siRNA-QD constructs; (b) the selective inhibition of the expression of epidermal growth factor receptor variant III

(EGFRvIII) in target human U87 glioblastoma cells; (c) the subsequent down-regulated signaling pathway with high efficiency was monitored.

6.10. References

1. Tallury, P.; Payton, K.; Santra, S. *Nanomedicine* **2008**, *3*, 579.
2. Petros, R. A.; DeSimone, J. M. *Nat. Rev. Drug Discov.* **2010**, *9*, 615.
3. Jung, J.; Solanki, A.; Memoli, K. A.; Kamei, K.-i.; Kim, H.; Drahl, M. A.; Williams, L. J.; Tseng, H.-R.; Lee, K. *Angw. Chem. Int. Ed. Engl.* **2010**, *49*, 103.
4. Murray, C. B.; Kagan, C. R.; Bawendi, M. G. *Annu. Rev. Mater. Sci.* **2000**, *30*, 545.
5. Kühnemuth, R.; Seidel, C. A. M. *Single Molecules* **2001**, *2*, 251.
6. Alivisatos, A. P. *Science* **1996**, *271*, 933.
7. Hardman, R. *Environ. Health Perspect.* **2006**, *114*, 165.
8. Yamanaka, R.; Saya, H. *Annals of Neurology* **2009**, *66*, 717.
9. Cully, M.; You, H.; Levine, A. J.; Mak, T. W. *Nat. Rev. Cancer* **2006**, *6*, 184.
10. Fan, Q.-W.; Weiss, W. A. *Oncogene* **2004**, *24*, 829.
11. Mellingerhoff, I. K.; Cloughesy, T. F.; Mischel, P. S. *Clinical Cancer Research* **2007**, *13*, 378.
12. Engelman, J. A. *Nat. Rev. Cancer* **2009**, *9*, 550.
13. Liu, P.; Cheng, H.; Roberts, T. M.; Zhao, J. J. *Nat. Rev. Drug. Discov.* **2009**, *8*, 627.
14. Medarova, Z.; Pham, W.; Farrar, C.; Petkova, V.; Moore, A. *Nat. Med.* **2007**, *13*, 372.
15. Dykxhoorn, D. M.; Palliser, D.; Lieberman, J. *Gene. Ther.* **2006**, *13*, 541.
16. Broad RNAi Portfolio from Bioneer.
<http://us.bioneer.com/products/rnai/rnaitechnical.aspx> (accessed 12/10/11).
17. Li, J. J.; Wang, Y. A.; Guo, W.; Keay, J. C.; Mishima, T. D.; Johnson, M. B.; Peng, X. *J. Am. Chem. Soc.* **2003**, *125*, 12567.
18. Xie, R.; Kolb, U.; Li, J.; Basche, T.; Mews, A. *J. Am. Chem. Soc.* **2005**, *127*, 7480.

19. Bauhuber, S.; Hozsa, C.; Breunig, M.; Göpferich, A. *Advanced Materials* **2009**, *21*, 3286.
20. Chiu, Y.-L.; Ali, A.; Chu, C-Y.; Cao, H.; Rana, T. M. *Chemistry & Biology* **2004**, *11*, 1165.
21. Xie, J.; Chen, K.; Lee, H.-Y.; Xu, C.; Hsu, A. R.; Peng, S.; Chen, X.; Sun, S. *J. Am. Chem. Soc.* **2008**, *130*, 7542.
22. Ruan, G.; Agrawal, A.; Marcus, A. I.; Nie, S. *J. Am. Chem. Soc.* **2007**, *129*, 14759.

Chapter 7

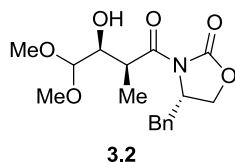
Experimental

7.1. General

All the commercial available starting materials, reagents and solvents were purchased from the suppliers (Aldrich–Sigma, Acros, Strem, TCI America, Fischer Scientific and Ochem.) and used without purification unless otherwise stated. Anhydrous solvent such as tetrahydrofuran (THF), diethyl ether (Et₂O), dichloromethane (DCM), toluene (PhMe) were purchased from Sigma–Aldrich, and then passed over a solvent purification system containing alumina based columns and dried by activated 4 Å molecular sieves for 1 hour before use. Anhydrous THF was further distilled from calcium hydride before use. All the glassware used for anhydrous reaction was flame–dried under vacuum. All the reactions were conducted under the atmosphere of high purity argon gas. The progress of all reactions were monitored by silica gel thin layer chromatography (TLC, Dynamic Absorbents Inc.), visualized under UV and/or stained using different stains such as anisaldehyde, vanillin, cerium ammonium molybdate, KMnO₄. Crude products were purified by flash column chromatography (FCC) on 120–400 mesh silica gel if necessary. Proton nuclear magnetic resonance spectra (¹H NMR) were obtained from either a Varian–300 instrument (300 MHz), Varian–400 instrument (400 MHz), Varian–500 instrument (500 MHz) or Inova–600 instrument (600 MHz). Chemical shifts are reported in ppm with tetramethylsilane (TMS) being the internal standard. Data is reported as follows: chemical shift (multiplicity: s=singlet, d=doublet, t=triplet, q=quartet, br=broad, m=multiplet, coupling constants in Hz and integration).

Carbon nuclear magnetic resonance spectra (^{13}C NMR) were obtained from either a Varian-400 instrument (100 MHz), Varian-500 instrument (125 MHz) or Inova-600 instrument (150 MHz). Chemical shifts are reported in ppm with tetramethylsilane (TMS) being the internal standard. Optical rotations were recorded at 25 °C using the sodium D line (589 nm), using Perkin-Elmer 241 polarimeter. Mass spectra were recorded on a Finnigan LCQ-DUO mass spectrometer (ESIMS) or Finnigan high resolution mass spectrometer (HRMS). Infrared (FTIR) spectra were recorded on ATI Mattson Genesis Series FT-Infrared spectrophotometer.

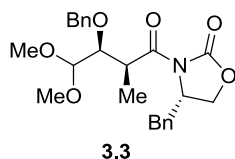
7.2. Chapter 3



The 4(S)-benzyl *N*-propionyl oxazolidinone **3.1** (20.3 g, 87.0 mmol) was dissolved in anhydrous DCM (607 mL). To this solution was added di-*n*butylboron triflate (96.0 mL, 96.0 mmol) and TEA (10.6 g, 104 mmol) dropwise at $-78\text{ }^{\circ}\text{C}$. The reaction mixture was then warmed to $0\text{ }^{\circ}\text{C}$ and stirred for 1 hour at $0\text{ }^{\circ}\text{C}$, and then cooled back to $-78\text{ }^{\circ}\text{C}$. Anhydrous DCM solution of 1,1-dimethoxy acetaldehyde (87.0 mL, 148 mmol, 0.18 g/mL) was added to the reaction mixture slowly at $-78\text{ }^{\circ}\text{C}$, then the resulting solution was slowly warmed to $0\text{ }^{\circ}\text{C}$ over 1 hour and stirred for 1 hour at $0\text{ }^{\circ}\text{C}$. The reaction was quenched with 100 mL solution of methanol and phosphate buffer (pH = 7.4) in 1:3 ratio at $0\text{ }^{\circ}\text{C}$, followed by the addition of 100 mL solution of 30% H_2O_2 and methanol (1:2 ratio). The reaction was stirred for 10 minutes at $0\text{ }^{\circ}\text{C}$, diluted with 200 mL DCM, washed with cold water (2 x 100 mL). Organic layer was separated and dried over anhydrous Na_2SO_4 . The solvent was removed *in vacuo*. Silica gel column chromatography using 40% EtOAc in hexane gave aldol product **3.2** as white solid (26.4 g, 78.3 mmol, 90% yield).

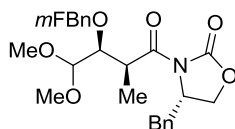
^1H NMR (500 MHz, CDCl_3) δ 7.35 – 7.25 (m, 3H), 7.21 (d, $J = 7.0$ Hz, 2H), 4.72 – 4.65 (m, 1H), 4.33 (d, $J = 6.0$ Hz, 1H), 4.23 – 4.15 (m, 2H), 4.05 – 3.96 (m, 1H), 3.42 (s, 3H), 3.38 (s, 3H), 3.26 (dd, $J = 13.5, 3.5$ Hz, 1H), 2.78 (dd, $J = 13.5, 10$ Hz, 1H), 2.68 – 2.60 (bs, 1H), 1.32 (d, $J = 7.0$ Hz, 3H); ^{13}C NMR (125 MHz, CDCl_3) δ 176.1, 153.2, 135.4, 129.6 (2), 129.1 (2), 127.5, 104.9, 71.4, 66.3, 55.4, 54.9, 54.4, 39.2, 38.1, 12.8; m/z

(ESIMS) calculated for $[C_{17}H_{23}NO_6+Na]^+$: 360.2, found: 360.2; $[\alpha]^{25}_D = 51.5$ ($c = 0.01$, $CHCl_3$); IR $\nu_{max}(neat)/cm^{-1}$ 3485, 2937, 1778, 1696, 1386.



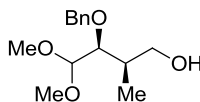
Aldol product **3.2** (17.6 g, 52.2 mmol), 4 Å powdered molecular sieve (20.0 g) and Ag_2O (33.0 g, 142 mmol) were mixed in anhydrous DCM (332 mL). Stirred for 10 minutes at room temperature, and then BnBr (24.4 g, 143 mmol) was added. The reaction mixture was then stirred thoroughly for 2 days under argon in the darkness at room temperature, and then filtered over a short column of celite. The solid residue was rinsed with DCM (3 x 100 mL). The solvent was removed *in vacuo*, silica gel column chromatography using 20% EtOAc in hexane gave compound **3.3** as colorless oil (20.3 g, 47.5 mmol, 91% yield).

1H NMR (500 MHz, $CDCl_3$) δ 7.39 – 7.23 (m, 8H), 7.19 (d, $J = 7.0$ Hz, 2H), 4.81 (d, $J = 11.5$ Hz, 1H), 4.64 (d, $J = 11.5$ Hz, 1H), 4.59 – 4.53 (m, 1H), 4.34 (d, $J = 6.0$ Hz, 1H), 4.14 – 4.03 (m, 3H), 3.84 (dd, $J = 7.5, 6.5$ Hz, 1H), 3.43 (s, 3H), 3.34 (s, 3H), 3.24 (dd, $J = 13.5, 3.5$ Hz, 1H), 2.75 (dd, $J = 13.5, 9.5$ Hz, 1H), 1.31 (d, $J = 7.0$ Hz, 3H); ^{13}C NMR (125 MHz, $CDCl_3$) δ 175.2, 153.3, 138.6, 135.5, 129.6 (2), 129.0 (2), 128.4 (2), 128.2 (2), 127.8, 127.4, 107.0, 79.8, 74.4, 66.1, 55.5, 55.4, 55.2, 39.5, 38.1, 13.8; m/z (ESIMS) calculated for $[C_{24}H_{29}NO_6Na]^+$: 450.2, found: 450.2; $[\alpha]^{25}_D = 22.0$ ($c = 0.01$, $CHCl_3$); IR $\nu_{max}(neat)/cm^{-1}$ 2934, 1778, 1698, 1383, 1107.

**3.32**

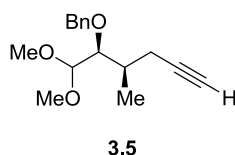
Aldol product **3.2** (8.25 g, 24.5 mmol), Ag₂O (17.0 g, 73.4 mmol) and 4 Å powdered molecular sieve (12.0 g) were mixed together and to that dry DCM (156 mL) was added. After stirring for 10 minutes at room temperature, 3-fluorobenzyl bromide (6.00 mL, 48.9 mmol) was added to the reaction. The reaction was then stirred thoroughly for 5 days under nitrogen at room temperature. The reaction was then filtered through celite and the solid residue was rinsed with DCM (3 x 100 mL). Evaporation of the organic filtrate gave the crude product, which upon further purification by silica gel column chromatography using 20% EtOAc in hexane gave **3.32** as colorless oil (10.3 g, 23.1 mmol, 94% yield).

¹H NMR (500 MHz, CDCl₃) δ 7.35 – 7.27 (m, 4H), 7.23 – 7.19 (m, 2H), 7.14 – 7.08 (m, 2H), 6.99 – 6.93 (m, 1H), 4.80 (d, *J* = 11.7 Hz, 1H), 4.64 (d, *J* = 11.5 Hz, 1H), 4.64 – 4.60 (m, 1H), 4.35 (d, *J* = 6.4 Hz, 1H), 4.15 – 4.08 (m, 2H), 4.10 (d, *J* = 7.1 Hz, 1H), 3.82 (dd, *J* = 7.6, 6.1 Hz, 1H), 3.43 (s, 3H), 3.35 (s, 3H), 3.42 (dd, *J* = 13.5, 3.3 Hz, 1H), 2.76 (dd, *J* = 13.5, 2.8 Hz, 1H), 1.30 (d, *J* = 6.9 Hz, 3H); ¹³C NMR (125 MHz, CDCl₃) δ 175.0, 163.8, 153.2, 141.1, 135.3, 129.8, 129.4, 128.9, 127.3, 123.2, 114.7, 114.4, 114.3, 106.7, 79.9, 73.4, 66.0, 55.3, 55.2, 55.0, 39.3, 38.0, 15.3.

**3.4**

Compound **3.3** (17.1 g, 40.0 mmol) was dissolved in Et₂O (370 mL), and then 11.0 mL methanol was added. The reaction mixture was cooled to 0 °C and then added a solution of LiBH₄ (35.2 mL, 77.4 mmol, 2.20 M solution in THF) slowly. Stirred at 0 °C for 2 hours, and then quenched with aqueous NH₄Cl (50 mL), extracted with EtOAc (3 x 200 mL). Organic layer combined, dried over anhydrous Na₂SO₄. The solvent was removed *in vacuo*. Silica gel column chromatography using 15% EtOAc in hexane gave **3.4** as colorless oil (9.90 g, 38.9 mmol, 97% yield).

¹H NMR (500 MHz, CDCl₃) δ 7.38 – 7.32 (m, 4H), 7.30 – 7.25 (m, 2H), 4.82(d, *J* = 11.5 Hz, 1H), 4.58 (d, *J* = 11.5 Hz, 1H), 4.39 (d, *J* = 6.5 Hz, 1H), 3.59 (dd, *J* = 6.0, 3.5 Hz, 1H), 3.59 – 3.46 (m, 2H), 3.49 (s, 3H), 3.41 (s, 3H), 2.02 – 1.96 (m, 1H), 1.90 (bs, 1H), 0.94 (d, *J* = 7.0 Hz, 3H); ¹³C NMR (125 MHz, CDCl₃) δ 138.9, 128.5 (2), 128.2 (2), 127.8, 106.5, 79.6, 74.1, 65.8, 56.2, 54.6, 36.9, 11.4; *m/z* (ESIMS) calculated for [C₁₄H₂₂O₄Na]⁺: 277.2, found: 277.2; IR ν_{max}(neat)/cm⁻¹ 3431, 2934, 1454, 1071.

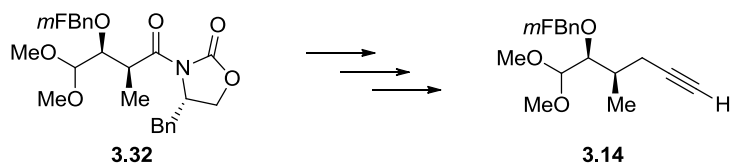


Primary alcohol **3.4** (6.00 g, 23.7 mmol) was dissolved in anhydrous DCM (184 mL), and then added diazabicyclo[2.2.2]octane (DABCO) (3.66 g, 32.6 mmol). The reaction mixture was cooled down to 0 °C and tosyl chloride (4.97 g, 26.1 mmol) was added. The reaction mixture was warmed up to room temperature and stirred for 1 hour. The reaction was then diluted with 150 mL of DCM, washed with aqueous NH₄Cl (3 x 50 mL), water (50 mL). Organic layer combined and dried over anhydrous Na₂SO₄, and then

concentrated down to dryness to give the crude tosylate, which could be used for the next step immediately without further purification.

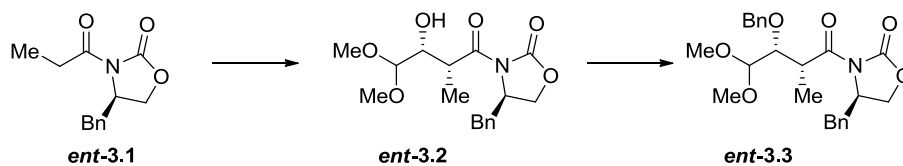
The crude tosylate was azeotroped in toluene, and then dissolved in anhydrous DMSO (50 mL). To this, lithium acetylide–ethylenediamine (4.37 g, 47.4 mmol) solution in 100 mL DMSO was added at 0 °C slowly for 10 minutes. The reaction was stirred for 4 hours at room temperature. Upon the complete consumption of the tosylate, the reaction mixture was cooled down to 0 °C, and then quenched carefully with aqueous NH₄Cl (50 mL). The organic layer was extracted with EtOAc (300 mL), washed with water (3 x 100 mL), and then dried over anhydrous Na₂SO₄. The solvent was removed *in vacuo*. Silica gel column chromatography using 5% EtOAc in hexane gave **3.5** as colorless oil (4.90 g, 18.7 mmol, 80% yield).

¹H NMR (500 MHz, CDCl₃) δ 7.38 – 7.30 (m, 4H), 7.28 – 7.22 (m, 1H), 4.68 (d, *J* = 11.5 Hz, 1H), 4.56 (d, *J* = 11.5 Hz, 1H), 4.36 (d, *J* = 7.0 Hz, 1H), 3.65 (dd, *J* = 7.0, 3.0 Hz, 1H), 3.47 (s, 3H), 3.38 (s, 3H), 2.23 – 2.12 (m, 2H), 2.10 – 2.00 (m, 1H), 1.96 (t, *J* = 7.5 Hz, 1H), 0.98 (d, *J* = 7.0 Hz, 3H); ¹³C NMR (125 MHz, CDCl₃) δ 139.3, 128.4 (2), 127.9 (2), 127.6, 106.4, 83.7, 80.3, 74.8, 69.6, 56.0, 53.8, 34.4, 23.5, 14.0; *m/z* (ESIMS) calculated for [C₁₆H₂₂O₃Na]⁺: 285.1, found: 285.2; IR ν_{max}(neat)/cm⁻¹ 3295, 2935, 2116, 1096.

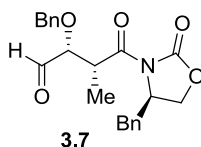


The alkyne **3.14** was prepared from **3.32** in 3 steps using same procedure used for the synthesis of alkyne **3.5**.

^1H NMR (500 MHz, CDCl_3) δ (7.34 – 7.23 (1H, m), 7.14 – 7.03 (2H, m), 6.97 – 6.91 (1H, m), 4.86 (1H, d, $J = 12.0$ Hz), 4.56 (1H, d, $J = 12.0$ Hz), 4.37 (1H, d, $J = 7.0$ Hz), 3.66 (1H, dd, $J = 7.0, 2.5$ Hz), 3.47 (3H, s), 3.39 (3H, s), 2.32 – 2.12 (2H, m), 2.10 – 2.00 (1H, m), 1.97 (1H, t, $J = 2.5$ Hz), 0.99 (3H, d, $J = 7.0$ Hz); ^{13}C NMR (125 MHz, CDCl_3) δ 164.0, 162.1, 142.0 (d, $J = 69$ Hz), 129.9 (d, $J = 66$ Hz), 123.1 (d, $J = 29$ Hz), 114.6, 114.4, 114.4, 114.2, 106.3, 83.5, 80.4, 73.9 (d, $J = 7.5$ Hz), 69.7, 56.0, 53.8, 34.4, 23.4, 14.0; m/z (ESIMS) calculated for $[\text{C}_{16}\text{H}_{21}\text{FO}_3\text{Na}]^+$: 303.2, found: 303.2; IR $\nu_{\text{max}}(\text{neat})/\text{cm}^{-1}$ 3306, 2936, 2117, 1789, 1592.



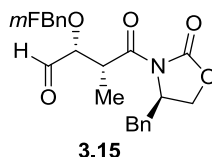
Compound **ent-3.2** and **ent-3.3** could be synthesized by using the same procedure used for the synthesis of compound **3.2** and **3.3**, respectively. The values for the observed optical rotation ($[\alpha]^{25}_{\text{D}}$) are -50.0 ($c = 0.01$, CHCl_3) for the compound **ent-3.2** and -21.0 ($c = 0.01$, CHCl_3) for the compound **ent-3.3**.



Benzyl protected aldol product **ent-3.3** (3.90 g, 9.22 mmol) was dissolved in 46 mL of water: acetic acid: trifluoroacetic acid = 1:4:1 mixed solution at room temperature

for 3hrs 30 minutes. The acidic solution was azeotroped with toluene (5 x 20 mL) and resulting crude product was taken into the next step immediately without further purification. It could also be further purified by silica gel column chromatography using 15% EtOAc in hexane gave **3.7** as colorless viscous oil (3.16 g, 8.30 mmol, 90% yield).

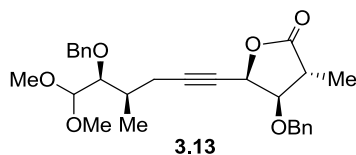
^1H NMR (500 MHz, CDCl_3) δ 9.81 (s, 1H), 7.38 – 7.22 (m, 8H), 7.17 (d, J = 7.0 Hz, 2H), 4.75 (d, J = 12.5 Hz, 1H), 4.64 – 4.54 (m, 1H), 4.59 (d, J = 12.5 Hz, 1H), 4.32 – 4.24 (m, 1H), 4.16 – 4.06 (m, 2H), 3.92 (d, J = 6.0 Hz, 1H), 3.20 (dd, J = 13.5, 3.5 Hz, 1H), 2.76 (dd, J = 13.5, 10 Hz, 1H), 1.33 (d, J = 7.0 Hz, 3H); ^{13}C NMR (125MHz, CDCl_3) δ 202.0, 173.8, 153.1, 137.2, 135.1, 129.6 (2), 129.1 (2), 128.7 (2), 128.4, 128.3 (2), 127.5, 83.3, 73.1, 66.4, 55.4, 41.5, 37.8, 13.4; m/z (ESIMS) calculated for $[\text{C}_{22}\text{H}_{23}\text{NO}_5\text{Na}]^+$: 404.2, found: 404.2; IR ν_{max} (neat)/ cm^{-1} 1778, 1730, 1693, 1390, 1212.



3-fluorobenzyl protected aldol product *ent*-**3.32** (1.23 g, 2.77 mmol) was dissolved in water: acetic acid: trifluoroacetic acid = 1:4:1 mixed solution (13.7 mL) and stirred for 2 hours at room temperature. The mixture was azeotroped with toluene (3 x 50 mL) and resulting crude product upon further purification by silica gel column chromatography using 15% EtOAc in hexane gave **3.15** as colorless viscous oil (1.05 g, 2.63 mmol, 95% yield).

^1H NMR (500 MHz, CDCl_3) δ 9.82 (s, 1H), 7.34 – 7.24 (m, 4H), 7.19 – 6.95 (m, 4H), 4.73 (d, J = 12.5 Hz, 1H), 4.71 – 4.63 (m, 2H), 4.57 (d, J = 12.5 Hz, 1H), 4.34 – 4.26 (m, 1H), 4.16 – 4.13 (m, 1H), 4.12 (quartet, J = 7.0, 1H), 3.92 (dd, J = 6.5, 1.2 Hz,

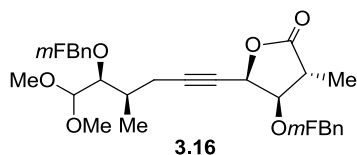
1H), 3.24 (dd, $J = 13.3, 3.1$ Hz, 1H), 2.78 (dd, $J = 13.3, 9.4$ Hz, 1H), 1.33 (d, $J = 7.4$ Hz, 3H), 1.25 (d, $J = 7.0$ Hz, 3H).



Alkyne **3.5** (3.44 g, 13.1 mmol) was dissolved in Et₂O (130 mL) then cooled to -78 °C. To that mixture was added *n*-BuLi (8.2 mL, 13 mmol) slowly. The reaction mixture was stirred at -78 °C for 1 hour and added a solution of ZnBr₂ (4.13 g, 18.4 mmol) in Et₂O (35.9 mL). The reaction flask was moved to 0 °C bath. At 10 °C, the solution of aldehyde **3.7** (2.00 g, 5.24 mmol) in Et₂O (12.5 mL) was added dropwise over 1 hour via syringe pump. The reaction was stirred overnight. The reaction was quenched with aqueous NH₄Cl (50 mL) at 0 °C, and then extracted with EtOAc (200 mL). The organic layer was washed with water (2 x 50 mL), and then dried over Na₂SO₄. The organic layer was concentrated down to dryness to give the crude product (8:1 ratio by ¹H NMR). Silica gel column chromatography using 10% EtOAc in hexane gave major isomer **3.13** as colorless oil (1.53 g, 3.29 mmol, 63% yield).

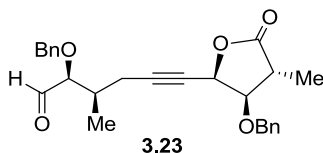
¹H NMR (500 MHz, CDCl₃) δ 7.38 – 7.24 (m, 10H), 5.12 (td, $J = 2.0$ Hz, 6.5 Hz, 1H), 4.82 (d, $J = 11.5$ Hz, 1H), 4.72 (d, $J = 12.0$ Hz, 1H), 4.53 (d, $J = 11.5$ Hz, 1H), 4.51 (d, $J = 11.5$ Hz, 1H), 3.88 (dd, $J = 9.5, 6.5$ Hz, 1H), 3.57 (dd, $J = 10.0, 7.0$ Hz, 1H), 3.47 (s, 3H), 3.37 (s, 3H), 2.86 – 2.76 (m, 1H), 2.38 – 2.20 (m, 2H), 2.10 – 2.00 (m, 1H), 1.25 (d, $J = 7.0$ Hz, 3H), 0.99 (d, $J = 7.0$ Hz, 3H); ¹³C NMR (125 MHz, CDCl₃) δ 176.0, 139.1, 137.1, 128.8 (2), 128.5 (2), 128.4, 128.1 (2), 127.9 (2), 127.7, 106.4, 90.5, 81.0, 80.5, 74.7, 73.9, 72.4, 70.5, 56.1, 54.1, 39.4, 34.4, 24.0, 14.0, 12.7; m/z (ESIMS)

calculated for $[\text{C}_{28}\text{H}_{34}\text{O}_6\text{Na}]^+$: 489.3, found: 489.2; IR $\nu_{\text{max}}(\text{neat})/\text{cm}^{-1}$ 2935, 2238, 1786, 1454.



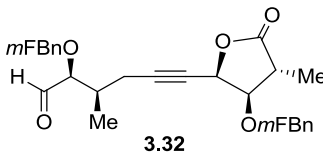
Alkyne **3.14** (54.9 mg, 196 μmol) was dissolved in Et_2O (2 mL) then cooled to -78°C . To that mixture was added $n\text{-BuLi}$ (78 μL , 0.20 mmol) slowly. The reaction mixture was stirred at -78°C for 1 hour and added a solution of ZnBr_2 (44.1 mg, 196 μmol) in Et_2O (0.4 mL). The reaction flask was moved to 0°C bath. At 10°C , the solution of aldehyde **3.15** (60.2 mg, 151 μmol) in Et_2O (0.4 mL) was added dropwise over 1 hour via syringe pump. The reaction was stirred overnight. The reaction was quenched with aqueous NH_4Cl (50 mL) at 0°C , and then extracted with EtOAc (20 mL). The organic layer was washed with water (2 x 5 mL), and then dried over Na_2SO_4 . The organic layer was concentrated down to dryness to give the crude product (8:1 ratio by ^1H NMR). Silica gel column chromatography using 10% EtOAc in hexane gave major isomer **3.16** as colorless oil (26.6 mg, 52.9 μmol , 35% yield).

^1H NMR (500 MHz, CDCl_3) δ 7.40 – 7.25 (m, 3H), 7.09 – 6.93 (m, 5H), 4.88 – 4.82 (m, 2H), 4.75 (d, $J = 12.0$ Hz, 1H), 4.64 (d, $J = 12.0$ Hz, 1H), 4.54 (d, $J = 11.7$ Hz, 1H), 4.36 (d, $J = 6.8$ Hz, 1H), 3.89 (dd, $J = 7.1, 5.6$ Hz, 1H), 3.54 (dd, $J = 7.0, 2.9$ Hz, 1H), 3.48 (s, 3H), 3.39 (s, 3H), 2.68 (quartet, $J = 7.3$ Hz, 1H), 2.37 – 2.19 (m, 2H), 2.13 – 2.01 (m, 1H), 1.36 (d, $J = 7.3$ Hz, 3H), 1.09 (d, $J = 6.8$ Hz, 3H).



Acetal **3.13** (1.90 g, 4.10 mmol) was dissolved in 42.5 mL mixed solution of acetic acid, trifluoroacetic acid and water (4:1:1) at room temperature and stirred for 12 hours. The solvent was azeotroped with toluene (5 x 100 mL) to give a crude product which could be used for the next step without further purification. It could also be further purified by silica gel column chromatography using 12% EtOAc in hexane gave **3.23** as colorless viscous oil (1.50 g, 3.57 mmol, 90% yield).

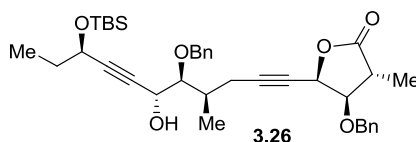
^1H NMR (500 MHz, CDCl_3) δ 9.65 (s, 1H), 7.44 – 7.25 (m, 10H), 5.11 (d, J = 6.0 Hz, 1H), 4.67 (d, J = 13.0 Hz, 2H), 4.54 (d, J = 11.5 Hz, 1H), 4.46 (d, J = 12.0 Hz, 1H), 3.95 – 3.85 (m, 2H), 2.85 – 2.75 (m, 1H), 2.48 – 2.26 (m, 2H), 2.26 – 2.16 (m, 1H), 1.27 (d, J = 7.0 Hz, 3H), 1.01 (d, J = 6.5 Hz, 3H); ^{13}C NMR (125 MHz, CDCl_3) δ 204.3, 175.9, 137.6, 137.1, 128.8 (2), 128.7 (2), 128.5, 128.3, 128.2 (2), 128.0 (2), 89.2, 85.1, 81.0, 74.9, 73.4, 72.4, 70.4, 39.4, 35.2, 23.1, 14.5, 12.7; m/z (ESIMS) calculated for $[\text{C}_{26}\text{H}_{28}\text{O}_5\text{Na}]^+$: 443.2, found: 443.2; IR ν_{max} (neat)/ cm^{-1} 2935, 2240, 1786, 1730, 1455.



Acetal **3.16** (36.3 mg, 72.0 μmol) was dissolved in 0.75 mL mixed solution of acetic acid, trifluoroacetic acid and water (4:1:1) at room temperature and stirred for 12 hours. The solvent was azeotroped with toluene (5 x 100 mL) to give a crude product which could be used for the next step without further purification. It could also be further

purified by silica gel column chromatography using 12% EtOAc in hexane gave **3.32** as colorless viscous oil (31.3 mg, 69.0 μ mol, 95% yield).

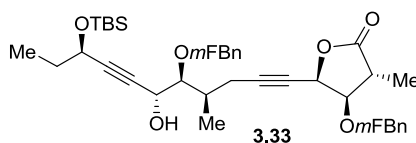
^1H NMR (500 MHz, CDCl_3) δ 9.67 (s, 1H), 7.44 – 6.92 (m, 8H), 5.21– 5.11 (m, 1H), 4.71 (d, J = 12.0 Hz, 2H), 4.68 (d, J = 11.7 Hz, 1H), 4.64 (d, J = 11.7 Hz, 1H), 4.42 (d, J = 12.0 Hz, 1H), 3.96 – 3.84 (m, 2H), 2.90 – 2.78 (m, 1H), 2.50 – 2.19 (m, 2H), 1.29 (d, J = 7.3 Hz, 3H), 1.01 (d, J = 6.7 Hz, 3H).



A solution of alkyne **3.11** (1.38 g, 7.00 mmol) in THF (33 mL) was cooled to -78 $^{\circ}\text{C}$. To that was added MeLi (3.70 mL, 5.87 mmol) slowly. The reaction mixture was stirred for 30 minutes and to that mixture was added the hexane solution of chlorotriisopropoxytitanium (IV) (5.87 mL, 5.87 mmol). The reaction was stirred for 1 hour and to that a solution of aldehyde **3.23** (1.50 g, 3.70 mmol) in THF (15 mL) was added slowly at -78 $^{\circ}\text{C}$. The reaction was then warmed slowly to -30 $^{\circ}\text{C}$ over 1 hour. The reaction was quenched with aqueous NH_4Cl , extracted with Et_2O . The organic layer was dried over anhydrous Na_2SO_4 . Evaporation of the organic filtrate gave the crude product (6:1 ratio by ^1H NMR) which upon further purification by silica gel column chromatography using 10% EtOAc in hexane gave major isomer of **3.26** as colorless oil (2.00 g, 3.23 mmol, 89% combined yield for both diastereomers).

^1H NMR (300 MHz, CDCl_3) δ 7.16 – 7.44 (m, 10H), 5.11 (td, J = 2.1 Hz, 6.0 Hz, 1H), 4.76 (d, J = 12.0 Hz, 1H), 4.72 (d, J = 12.0 Hz, 1H), 4.58 (d, J = 12.0 Hz, 1H), 4.53 (d, J = 12.0 Hz, 1H), 4.43 – 4.54 (m, 1H), 4.32 (t, J = 6.6 Hz, 1H), 3.87 (dd, J = 9.6, 6.6

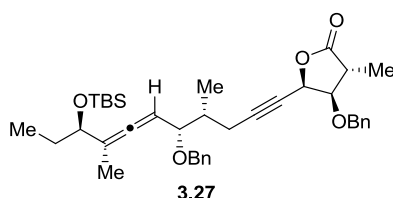
Hz, 1H), 3.58 (dd, $J = 5.4, 5.4$ Hz, 1H), 2.88 – 2.76 (m, 1H), 2.46 – 2.13 (m, 1H), 1.75 – 1.60 (m, 1H), 1.24 (d, $J = 7.2$ Hz, 3H), 1.06 (d, $J = 6.9$ Hz, 3H), 0.87 (s, 9H), 0.08 (s, 3H), 0.10 (s, 3H); ^{13}C NMR (125 MHz, CDCl_3) δ 175.9, 138.4, 137.0, 128.8, 128.6, 128.5, 128.0, 127.9, 127.9, 89.7, 88.4, 83.5, 82.6, 80.9, 77.4, 77.2, 76.9, 74.6, 74.3, 72.3, 70.4, 64.4, 63.5, 39.4, 34.6, 31.9, 26.0, 23.8, 18.4, 14.9, 12.6, 9.8, 0.2, –4.2, –4.8; m/z (ESIMS) calculated for $[\text{C}_{37}\text{H}_{50}\text{O}_6\text{SiNa}]^+$: 641.3, found: 641.3.



A solution of alkyne **3.11** (26.8 mg, 135 μmol) in THF (640 μL) was cooled to –78 °C. To that was added MeLi (75 μL , 0.12 mmol) slowly. The reaction mixture was stirred for 30 minutes and to that mixture was added the hexane solution of chlorotriisopropoxytitanium (IV) (120 μL , 120 μmol). The reaction was stirred for 1 hour and to that a solution of aldehyde **3.32** (36.3 mg, 80.0 μmol) in THF (320 μL) was added slowly at –78 °C. The reaction was then warmed slowly to –30 °C over 1 hour. The reaction was quenched with aqueous NH_4Cl , extracted with Et_2O . The organic layer was dried over anhydrous Na_2SO_4 . Evaporation of the organic filtrate gave the crude product (6:1 ratio by ^1H NMR) which upon further purification by silica gel column chromatography using 10% EtOAc in hexane gave major isomer of **3.33** as colorless oil (46.9 mg, 72.0 μmol , 90% combined yield for both diastereomers).

^1H NMR (300 MHz, CDCl_3) δ 7.37 – 7.24 (m, 3H), 7.15 – 6.93 (m, 3H), 5.18 (td, $J = 2.1$ Hz, 6.2 Hz, 1H), 4.78 (d, $J = 12.0$ Hz, 1H), 4.70 (d, $J = 12.0$ Hz, 1H), 4.58 (d, $J = 5.3$ Hz, 1H), 4.54 (d, $J = 5.3$ Hz, 1H), 4.50 (dd, $J = 11.7, 5.6$ Hz, 1H), 4.32 (td, $J = 6.5,$

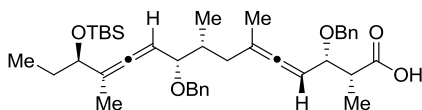
1.5 Hz, 1H), 3.90 (dd, $J = 9.4, 6.2$ Hz, 1H), 3.58 (dd, $J = 5.6, 4.4$ Hz, 1H), 2.89 – 2.79 (m, 1H), 2.43 – 2.16 (m, 4H), 1.71 – 1.61 (m, 2H), 1.30 (d, $J = 7.3$ Hz, 3H), 1.09 (d, $J = 6.8$ Hz, 3H), 0.95 (t, $J = 7.3$ Hz, 3H) 0.89 (s, 9H), 0.14 (s, 3H), 0.07 (s, 3H).



To a solution of **3.26** (0.25 g, 0.40 mmol) in 8 mL of Et₂O was added TEA (60.7 mg, 0.600 mmol) and methanesulfonyl chloride (68.7 mg, 0.606 mmol) respectively at 5 °C. The reaction mixture was warmed to room temperature and stirred for 1 hr 20 minutes at room temperature. The mesylate solution was added a solution of methyl cyanocuprate, prepared from CuCN (0.21 g, 2.4 mmol) and MeLi (1.5 mL, 2.4 mmol) in 12 mL of Et₂O at –35 °C. The temperature was kept below –20 °C for 1 hour. The reaction was then quenched with aqueous NH₄Cl (5 mL), and then extracted in Et₂O (3 x 10 mL). The organic layer was washed with water (10 mL) and dried over anhydrous MgSO₄. After removing the solvent under reduced pressure, the crude material was subject to silica gel column chromatography giving **3.27** (0.12g, 0.020 mmol) in 50% yield.

Data of **3.27**: ¹H NMR (500 MHz, CDCl₃) δ 7.89 – 7.26 (m, 10H), 5.17 – 5.12 (m, 1H), 5.00 – 4.93 (m, 1H), 4.72 (d, $J = 11.7$ Hz, 1H), 4.68 (d, $J = 12.2$ Hz, 1H), 4.64 (d, $J = 11.7$ Hz, 1H), 4.30 (d, $J = 12.0$ Hz, 1H), 4.01 (t, $J = 6.1$ Hz, 1H), 3.89 (t, $J = 6.4$ Hz, 1H), 3.71 (dd, $J = 8.8, 5.4$ Hz, 1H), 2.86 – 2.80 (m, 1H), 2.68 – 2.62 (m, 1H), 2.19 (dd, $J = 9.5, 2.0$ Hz, 1H), 1.73 (d, $J = 2.9$ Hz, 3H), 1.64 (d, $J = 3.0$ Hz, 1H), 1.63 – 1.37 (m, 2H), 1.27

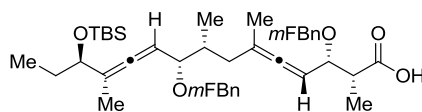
(d, $J = 7.1$ Hz, 3H), 1.10 (d, $J = 6.6$ Hz, 3H), 0.91 (s, 9H), 0.88 (t, $J = 7.3$ Hz, 3H), 0.04 (s, 3H), 0.03 (s, 3H) ; ^{13}C NMR (125 MHz, CDCl_3) δ 202.5, 175.7, 138.5, 136.9, 128.5 (2), 128.2 (2), 127.8(4), 127.5, 127.4, 102.7, 90.3, 89.4, 80.8, 80.7, 75.3, 73.4, 72.0, 70.3, 69.9, 39.1, 38.2, 29.2(3), 25.8, 18.2, 15.1, 13.8, 12.4, 10.0, -4.6, -5.0.

**3.28**

To a solution of **3.26** (1.24 g, 2.00 mmol) in 40 mL of Et_2O was added TEA (0.30 g, 3.0 mmol) and methanesulfonyl chloride (0.34 g, 3.0 mmol) respectively at 5 °C. The reaction mixture was warmed to room temperature and stirred for 1 hr 20 minutes at room temperature. The mesylate solution was added a solution of methyl cyanocuprate, prepared from CuCN (1.07 g, 12.0 mmol) and MeLi (7.49 mL, 12.0 mmol) in 60 mL of Et_2O at - 35 °C. The reaction mixture was then warmed to room temperature and stirred for 1h. The reaction was then quenched with aqueous NH_4Cl (50 mL) and extracted in Et_2O (3 x 100 mL). The organic layer was washed with water (100 mL), and then dried over anhydrous MgSO_4 . Evaporation of solvent gave the crude product **3.28** (1.27 g) and it is subjected to the next step without silica gel column chromatography.

^1H NMR (500 MHz, CDCl_3) δ 7.36 – 7.26 (m, 10H), 5.05 – 4.90 (m, 2H), 4.70 (d, $J = 11.5$ Hz, 1H), 4.69 (d, $J = 11.5$ Hz, 1H), 4.43 (d, $J = 11.5$ Hz, 1H), 4.39 (d, $J = 12.0$ Hz, 1H), 4.03 (dd, $J = 8.0$ Hz, 6.0 Hz, 1H), 4.00 (t, $J = 6.0$ Hz, 1H), 3.66 (dd, $J = 9.5, 5.5$ Hz, 1H), 2.84 – 2.72 (m, 1H), 2.42 – 2.32 (m, 1H), 1.95 – 1.85 (m, 1H), 1.72 (d, $J = 3.0$ Hz, 1H), 1.65 (d, $J = 3.0$ Hz, 3H), 1.60 – 1.50 (m, 2H), 1.24 (d, $J = 7.0$ Hz, 3H), 0.98 (d, $J = 6.5$ Hz, 3H), 0.88 (s, 9H), 0.85 (t, $J = 7.5$ Hz, 3H), 0.02 (s, 3H), 0.00 (s, 3H) ; ^{13}C

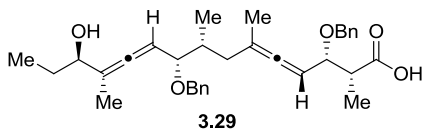
NMR (125 MHz, CDCl_3) δ 203.9, 202.9, 177.0, 138.9, 137.8, 128.6 (2), 128.5 (2), 128.0 (4), 127.8, 127.6, 102.5, 100.0, 89.7, 87.7, 82.2, 79.8, 75.8, 70.7, 70.2, 37.7, 36.7, 29.5, 26.1 (3), 19.0, 18.4, 15.7, 13.8, 12.9, 10.3, -4.3, -4.8; m/z (ESIMS) calculated for $[\text{C}_{39}\text{H}_{56}\text{O}_5\text{SiNa}]^+$: 655.4, found: 655.4; $[\alpha]_D^{25} = 47$ ($c = 0.01$, CHCl_3); IR $\nu_{\text{max}}(\text{neat})/\text{cm}^{-1}$ 2929, 1965, 1710, 1456, 1066.

**3.35**

To a solution of **3.33** (10.5 mg, 16.0 μmol) in 320 μL of Et_2O was added TEA (4.9 mg, 48 μmol) and methanesulfonyl chloride (5.5 mg, 48 μmol) respectively at 5 $^\circ\text{C}$. The reaction mixture was warmed to room temperature and stirred for 1 hr 20 minutes at room temperature. The mesylate solution was added a solution of methyl cyanocuprate, prepared from CuCN (14.4 mg, 160 μmol) and MeLi (100 μL , 160 μmol) in 800 μL of Et_2O at -35 $^\circ\text{C}$. The reaction mixture was then warmed to room temperature and stirred for 1h. The reaction was then quenched with aqueous NH_4Cl (5 mL) and extracted in Et_2O (3 x 10 mL). The organic layer was washed with water (10 mL), and then dried over anhydrous MgSO_4 . Evaporation of solvent gave the crude product is subjected to silica gel column chromatography, giving **3.35** (9.2 mg, 14 μmol) in 86% yield.

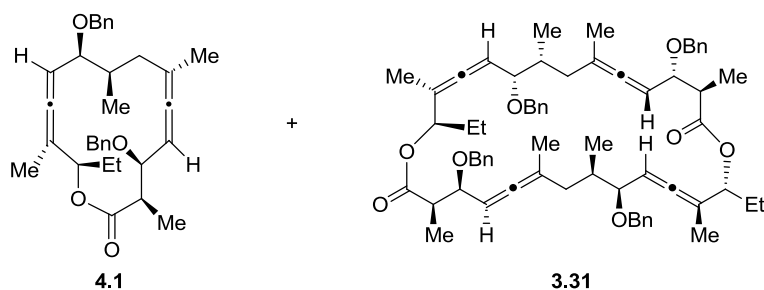
^1H NMR (500 MHz, CDCl_3) δ 7.34 – 7.23 (m, 3H), 7.12 – 6.89 (m, 5H), 6.13 – 6.00 (m, 1H), 5.63 – 5.52 (m, 1H), 5.63 – 5.52 (m, 1H), 4.64 (d, $J = 12.3$ Hz, 1H), 4.36 (d, $J = 12.6$ Hz, 1H), 3.99 (t, $J = 6.2$ Hz, 1H), 3.73 (dd, $J = 8.5$ Hz, 5.3 Hz, 1H), 2.59 – 2.49 (m, 1H), 2.25 – 2.15 (m, 2H), 1.96 – 1.86 (m, 2H), 1.70 (d, $J = 2.6$ Hz, 3H), 1.65 –

1.49 (m, 2H), 1.29 (d, $J = 6.8$ Hz, 3H), 1.08 (d, $J = 6.8$ Hz, 3H), 0.92 (s, 9H), 0.79 (t, $J = 7.5$ Hz, 3H), 0.02 (s, 3H), 0.00 (s, 3H).



The crude Bis[allene] **3.28** was dissolved in 60 mL of acetic acid, water, and trifluoroacetic acid mixture (4:1:0.25 ratio) and stirred for 1 hour at rt. The solvent was azeotroped with toluene (3 x 50 mL) and resulting crude product upon further purification by silica gel column chromatography using 30% EtOAc in hexane gave **3.29** as colorless oil (860 mg, 1.66 mmol, 83% yield over 2 steps, **3.26** \rightarrow **3.29**).

^1H NMR (500 MHz, CDCl_3) δ 7.36 – 7.27 (m, 10H), 5.18 – 5.10 (m, 1H), 5.08 – 5.02 (m, 1H), 4.70 (d, $J = 11.5$ Hz, 1H), 4.68 (d, $J = 12.0$ Hz, 1H), 4.45 (d, $J = 11.5$ Hz, 1H), 4.41 (d, $J = 12.0$ Hz, 1H), 4.04 (t, $J = 6.4$, 1H), 3.99 (t, $J = 6.8$ Hz, 1H), 3.69 (dd, $J = 8.5$, 5 Hz, 1H), 2.84 – 2.76 (m, 1H), 2.38 – 2.32 (m, 1H), 1.94 – 1.84 (m, 1H), 1.75 (d, $J = 3$ Hz, 3H), 1.67 (d, $J = 2.5$ Hz, 3H), 1.66 – 1.50 (m, 2H), 1.23 (d, $J = 7$ Hz, 3H), 0.98 (d, $J = 6.5$ Hz, 3H), 0.90 (t, $J = 7$ Hz, 3H); ^{13}C NMR (125 MHz, CDCl_3) δ 203.6, 201.7, 175.7, 138.9, 137.7, 128.7 (2), 128.5 (2), 128.1, 128.1 (2), 127.8 (2), 127.7, 103.4, 100.6, 92.5, 88.0, 82.1, 79.3, 74.2, 70.7, 70.4, 44.4, 37.6, 37.0, 27.9, 19.4, 15.4, 15.1, 13.3, 9.8; m/z (ESIMS) calculated for $[\text{C}_{33}\text{H}_{42}\text{O}_5\text{Na}]^+$: 541.3, found: 541.3; $[\alpha]_D^{25} = 45.0$ ($c = 0.01$, CHCl_3); IR ν_{max} (neat)/ cm^{-1} 3388, 2933, 1965, 1710, 1454.

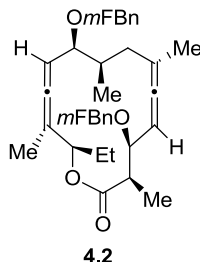


The seco acid **3.29** (195 mg, 0.380 mmol) was azeotroped with toluene (3 x 10 mL) and then dissolved in 20 mL toluene. TEA (0.19 mg, 1.9 mmol) and 2,4,6-trichlorobenzoyl chloride (0.46 g, 1.9 mmol) was added to this solution slowly at room temperature, and then stirred for 6 hours at room temperature. The resulting active ester was then added dropwise over 2 hours to a solution of 4-(*N,N*-dimethylamino)pyridine (DMAP) (0.46 g, 3.5 mmol) in toluene (163 mL) at 80 °C. The mixture was then cooled back to room temperature and quenched with aqueous NH₄Cl (100 mL). The organic layer was washed with water (2 x 100 mL) and dried over Na₂SO₄. The organic layer was concentrated down to dryness under reduced pressure. Silica gel column chromatography using 5% EtOAc in hexanes gave the bis[allene] macrolactone **4.1** (121 mg, 0.240 mmol, 64% yield) and **3.31** (19 mg, 19 μmol, 5% yield) as a colorless oil.

For detailed NMR analysis of **4.1**, see page 204; *m/z* (ESIMS) calculated for [C₃₃H₄₀O₄Na]⁺: 523.3, found: 523.3; [α]_D²⁵ = 50.0 (*c* = 0.01, CHCl₃); IR ν_{max}(neat)/cm⁻¹ 2969, 2934, 1960, 1731, 1454, 1369, 1248, 1065.

Data of **3.31**; ¹H NMR (500 MHz, CDCl₃) δ 7.36 – 7.16 (m, 20H), 5.12 – 5.02 (m, 4H), 4.98 – 4.90 (m, 2H), 4.65 – 4.58 (m, 4H), 4.37 – 4.28 (m, 4H), 3.97 – 3.94 (t, *J* = 7.8 Hz, 2H), 3.71 – 3.67 (m, 2H), 2.73 – 2.60 (m, 3H), 2.36 – 2.28 (m, 2H), 1.95 – 1.78 (m, 5H), 1.74 – 1.60 (m, 12H), 1.24 – 1.23 (m, 8H), 1.03 – 0.97 (m, 6H), 0.89 – 0.81 (m, 6H); ¹³C NMR (125 MHz, CDCl₃) δ 203.6, 202.6, 173.3, 138.9, 138.6, 128.2, 128.1, 127.5,

127.3, 99.1, 98.8, 92.2, 88.2, 81.3, 79.9, 76.1, 70.4, 70.3, 45.9, 38.5, 36.6, 31.9, 29.7, 29.6, 29.4, 25.8, 22.7, 18.3, 14.7, 14.6, 14.1, 13.6, 15.1, 9.7; m/z (ESIMS) calculated for $[C_{66}H_{80}O_8Na]^+$: 1023.3, found: 1023.3; IR ν_{max} (neat)/ cm^{-1} 2922, 1968, 1735, 1453, 1377, 1068.

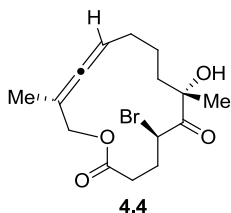


The seco acid **3.30** (280 mg, 0.510 mmol) was azeotroped with toluene (3 x 10 mL) and then dissolved in 15 mL toluene. TEA (260 mg, 2.52 mmol) and 2,4,6-trichlorobenzoyl chloride (617 mg, 2.52 mmol) was added to this solution slowly at room temperature, and then stirred for 6 hours at room temperature. The resulting active ester was then added dropwise over 2 hours to a solution of 4-(*N,N*-dimethylamino)pyridine (DMAP) (610 mg, 5.00 mmol) in toluene (250 mL) at 80 °C. The mixture was then cooled back to room temperature and quenched with aqueous NH_4Cl (100 mL). The organic layer was washed with water (2 x 100 mL) and dried over Na_2SO_4 . The organic layer was concentrated down to dryness under reduced pressure. Silica gel column chromatography using 5% EtOAc in hexanes gave the bis[allene] macrolactone **4.2** (202 mg, 0.380 mmol, 75% yield) as a colorless oil.

1H NMR (500 MHz, $CDCl_3$) δ 7.29 – 7.22 (2H, m), 7.11 – 7.01 (4H, m), 6.97 – 6.89 (2H, m), 5.38 – 5.30 (1H, m), 5.28 (1H, t, J = 6.5 Hz), 5.16 – 5.08 (1H, m), 4.64 (1H, d, J = 12.5 Hz), 4.52 (1H, d, J = 12.5 Hz), 4.48 (1H, d, J = 12.5 Hz), 4.31 (1H, d, J =

12.0 Hz), 3.96 (1H, dd, $J = 8.0, 4.0$ Hz), 3.77 (1H, dd, $J = 7.0, 7.0$ Hz), 2.86 – 2.76 (1H, m), 2.20 – 2.14 (1H, m), 2.04 – 1.94 (1H, m), 1.71 (3H, d, $J = 3.0$ Hz), 1.70 (3H, d, $J = 3.0$ Hz), 1.72 – 1.62 (2H, m), 1.26 (3H, d, $J = 7.0$ Hz), 1.05 (3H, d, $J = 7.0$ Hz), 0.90 (3H, t, $J = 7.5$ Hz); ^{13}C NMR (125 MHz, CDCl_3) δ 203.8, 201.3, 173.8, 164.1 (d, $J = 84$ Hz), 162.1 (d, $J = 89$ Hz), 142.1 (d, $J = 75$ Hz), 141.6 (d, $J = 69$ Hz), 129.9 (d, $J = 46$ Hz), 129.8 (d, $J = 79$ Hz), 123.1 (d, $J = 27$ Hz), 122.9 (d, $J = 27$ Hz), 114.6 – 114.3 (4C, m), 102.6, 99.3, 91.6, 90.5, 81.7, 77.9, 75.8, 70.0 (d, $J = 17$ Hz), 68.1 (d, $J = 19$ Hz), 44.9, 37.7, 35.9, 25.1, 20.5, 17.5, 15.3, 14.0, 9.9; $[\alpha]_{\text{D}}^{25} = -3.0$ ($c = 0.01$, CHCl_3); m/z (ESIMS) calculated for $[\text{C}_{33}\text{H}_{38}\text{F}_2\text{O}_4\text{Na}]^+$: 559.3, found: 559.3; IR $\nu_{\text{max}}(\text{neat})/\text{cm}^{-1}$ 2971, 2935, 1968, 1732, 1617, 1592, 1174.

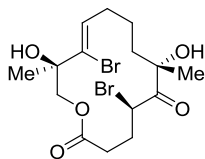
7.3. Chapter 4



To a solution of bis[allene] macrolactone **2.24** (26.6 mg, 115 μmol) in CHCl_3 (1 mL) was added a solution of DMDO in CDCl_3 (1.1 mL, 0.30 mmol) dropwise at -40°C . The reaction was stirred under nitrogen and let it to warm to -5°C over 1 hr 30 minutes. After the consumption of **2.24**, excess DMDO was removed under reduced pressure and the crude mixture was azeotroped with toluene. To the crude mixture was added a solution of LiBr (39.8 mg, 0.450 mmol) in THF (1 mL) via syringe pump for 1 hour at -5°C . After the consumption of SDE, the reaction mixture was diluted with water and then extracted with DCM. The combined organic phase was dried over anhydrous Na_2SO_4 . Evaporation of solvent and silica gel column chromatography using 15% EtOAc in hexanes gave **4.4** (24.2 mg, 69.9 μmol , 61%) of as white solid. The product was recrystallized in 20% EtOAc in hexane.

For detailed X-ray crystallography, see page 214; ^1H NMR (300 MHz, CDCl_3) δ 5.27 – 5.17 (m, 1H), 4.94 (dd, $J = 12.4, 2.9$ Hz, 1H), 4.70 (t, $J = 7.0$ Hz, 1H), 4.11 (dd, $J = 12.5, 1.8$ Hz, 1H), 3.72 (s, 1H), 2.69 – 2.54 (m, 1H), 2.52 – 2.30 (m, 3H), 2.06 – 1.97 (m, 2H), 1.73 (d, $J = 2.93$ Hz, 3H), 1.59 – 1.57 (m, 2H), 1.55 (s, 3H), 1.39 – 1.24 (m, 1H), 0.96 – 0.80 (m, 1H); ^{13}C NMR (101 MHz, CDCl_3) δ 208.9, 203.2, 171.7, 95.8, 92.0, 79.1, 65.8, 41.7, 37.9, 31.8, 29.7, 28.4, 26.8, 22.7, 17.6; m/z (HRMS) calculated for

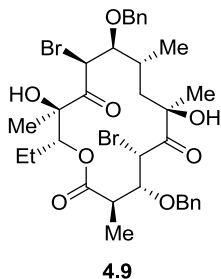
$[\text{C}_{15}\text{H}_{21}\text{BrO}_4\text{Na}]^+$: 369.1, found: 369.1; IR ν_{max} (neat)/ cm^{-1} 3502, 2954, 2924, 2854, 1969, 1736, 1712, 1454, 1376, 1236, 1200, 1154.



4.6

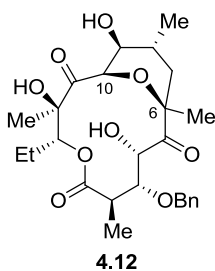
To a solution of bis[allene] macrolactone **2.24** (47.0 mg, 202 μmol) in CDCl_3 (1 mL) was added a solution of DMDO in CDCl_3 (2.0 mL, 0.60 mmol) dropwise at -40°C . The reaction was stirred under nitrogen and let to warm to -5°C over 1 hr 30 minutes. To the reaction mixture was added LiBr (52.8 mg, 0.610 mmol) at -5°C . TLC showed the unreacted SDE. To the reaction mixture was added LiBr (123 mg, 1.42 mmol). After the complete consumption of SDE, the reaction was then diluted with water and extracted with DCM. The combined organic phase was dried over anhydrous Na_2SO_4 . Evaporation of solvent and silica gel column chromatography using 20% EtOAc in hexanes gave **4.6** as colorless oil (50.0 mg, 113 μmol , 56% yield).

For detailed NMR analysis, see page 222; m/z (HRMS) calculated for $[\text{C}_{15}\text{H}_{21}\text{Br}_2\text{O}_5\text{H}]^+$: 441.9, found: 422.9, 424.9, 426.9 $[\text{C}_{15}\text{H}_{21}\text{Br}_2\text{O}_5\text{H}-\text{H}_2\text{O}]$; IR ν_{max} (neat)/ cm^{-1} 3495, 2920, 2860, 1740, 1721, 1454, 1372, 1241, 1143, 1002.



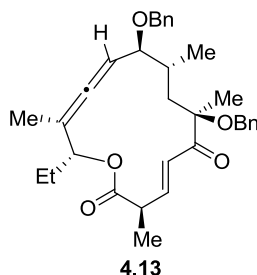
To a solution of bis[allene] macrolactone **4.1** (15.0 mg, 30.0 μmol) in CDCl_3 (1 mL) was added a solution of DMDO in CDCl_3 (0.4 mL, 0.2 mmol) dropwise at $-40\text{ }^\circ\text{C}$. The reaction was stirred under nitrogen and let to warm to $-15\text{ }^\circ\text{C}$ over 30 minutes. To the reaction mixture was added LiBr (53.2 mg, 0.610 mmol) at $-15\text{ }^\circ\text{C}$. After the complete consumption of SDE, the reaction was diluted with water and extracted with DCM. The combined organic phase was dried over anhydrous Na_2SO_4 . Evaporation of solvent and silica gel column chromatography using 15% EtOAc in hexanes gave **4.9** as colorless oil (2.0 mg, 3.1 μmol , 11% yield).

For detailed NMR analysis, see page 235; ^1H NMR (600 MHz, CDCl_3) δ 7.42 – 7.33 (m, 10H), 6.00 (d, $J = 8.51\text{ Hz}$, 1H), 5.17 (dd, $J = 2.64, 10.56\text{ Hz}$, 2H), 4.55 (d, $J = 7.92\text{ Hz}$, 1H), 3.86 (d, $J = 9.39\text{ Hz}$, 1H), 3.83 (dd, $J = 3.82, 9.69\text{ Hz}$, 1H), 3.17 (t, $J = 6.45\text{ Hz}$, 1H), 1.50 (s, 3H), 1.36 (d, $J = 7.34$, 3H), 1.21 (s, 3H), 1.05 (d, $J = 6.75$, 3H), 0.99 – 0.91 (m, 3H); IR ν_{max} (neat)/ cm^{-1} 3435, 2955, 2922, 2851, 1726, 1460, 1377, 1161, 1072.



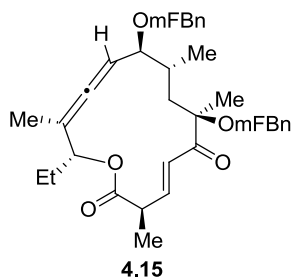
The solution of freshly prepared DMDO in CHCl_3 (0.5 mL, 0.2 M, 0.1 mmol) was added to bis[allene] macrolactone **4.1** (18.0 mg, 36.0 μmol), dissolved in THF/water (1:1, total 1 mL) dropwise at 5 °C. Upon the consumption of allene, the reaction mixture was removed under reduced pressure. The crude was chromatographed with 20% EtOAc in hexane through silica gel and the product was obtained in **4.12** (1.3 mg, 2.6 μmol , 7%).

For detailed NMR analysis, see page 237; m/z (HRMS) calculated for $[\text{C}_{26}\text{H}_{36}\text{O}_9\text{H}]^+$: 493.3, found 493.3.



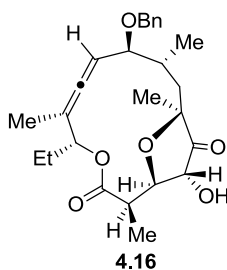
To a solution of bis[allene] macrolactone **4.1** (12.0 mg, 23.9 μmol) in methanol (3 mL) was added a solution of DMDO (0.38 mL, 0.14 mmol) dropwise at -50 °C. The reaction was stirred under nitrogen and let to warm to -15 °C over 1 hr 30minutes. Evaporation of solvent and silica gel column chromatography using 5% EtOAc in hexanes gave **4.13** (10.0 mg, 19.4 μmol , 80%) as colorless oil.

For detailed NMR analysis, see page 247; m/z (HRMS) calculated for $[\text{C}_{33}\text{H}_{40}\text{O}_5\text{Na}]^+$: 539.3, found: 539.3; $[\alpha]_{25}^D = 3.3^\circ$ ($c = 0.005$, CHCl_3); IR ν_{max} (neat)/ cm^{-1} 3065, 2919, 2849, 1966, 1723, 1653, 1455, 1376, 1175, 1066.



To a solution of bis[allene] macrolactone **4.2** (32.9 mg, 65.5 μmol) in methanol (2 mL) was added a solution of DMDO (1.15 mL, 180 μmol) dropwise at $-20\text{ }^{\circ}\text{C}$. The temperature was kept at $-20\text{ }^{\circ}\text{C}$ for 5 hours. Evaporation of solvent and silica gel column chromatography using 5% EtOAc in hexanes gave **4.15** (10.0 mg, 18.1 μmol , 30%) of as colorless oil.

For detailed NMR analysis, see page 272; m/z (HRMS) calculated for $[\text{C}_{33}\text{H}_{38}\text{F}_2\text{O}_5\text{Na}]^+$: 575.3, found: 575.3; $[\alpha]_{25}^{\text{D}} = -85.9^{\circ}$ ($c = 0.005$, CHCl_3); IR ν_{max} (neat)/ cm^{-1} 3066, 2972, 2933, 2876, 1964, 1738, 1696, 1624, 1450, 1379, 1177, 1086.



To a solution of macrolactone **4.1** (17.7 mg, 35.4 μmol) in CDCl_3 (0.5 mL) was added a solution of DMDO (0.56 mL, 0.21 mmol, 0.38 M in CDCl_3) dropwise at $-40\text{ }^{\circ}\text{C}$, warmed up to $-15\text{ }^{\circ}\text{C}$ over 30 minutes, then lower order methyl cyanocuprate (MeCuCNLi , 0.71 mmol) was added, prepared by addition of MeLi (0.44 mL, 0.71 mmol) to a slurry of CuCN (63.3 mg, 0.710 mmol) in 2-methyl THF (6 mL) at $-78\text{ }^{\circ}\text{C}$.

4.17

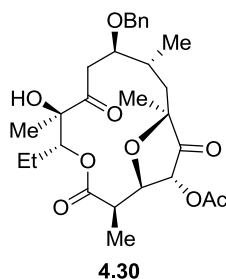
4.18

To the neat bis[allene] macrolactone **4.1** (25.3 mg, 50.6 μmol) was added a solution of DMDO (800 μL , 303 μmol , 0.380 M in CDCl_3) dropwise at $-40\text{ }^\circ\text{C}$. The temperature was increased to $-15\text{ }^\circ\text{C}$ over 1 hr. In another flask, lower order methyl cyanocuprate was prepared by addition of MeLi (632 μL , 1.01 mmol) to a slurry of CuCN (91.0 mg, 1.01 mmol) in Et_2O (10 mL) at $-78\text{ }^\circ\text{C}$ and then warming to $-15\text{ }^\circ\text{C}$. SDE solution was added to the cuprate solution at a $-15\text{ }^\circ\text{C}$. After the complete consumption of SDE, the reaction was then quenched with water and extracted with Et_2O . The combined organic phase was dried over anhydrous Na_2SO_4 . Evaporation of solvent and silica gel column chromatography using 15% EtOAc in hexanes gave a

mixture of **4.16** (3.3 mg, 7.5 μmol , 15% yield), **4.17** (7.3 mg, 15 μmol , 30% yield) and **4.18** (5.4 mg, 10 μmol , 20% yield) as colorless oil.

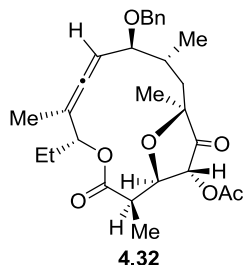
Data of **4.17**: For detailed NMR analysis, see page 311; m/z (HRMS) calculated for $[\text{C}_{26}\text{H}_{36}\text{O}_8\text{H}]^+$: 477.5, found: 477.2; IR ν_{max} (neat)/ cm^{-1} 3427, 3063, 2968, 2934, 2878, 1764, 1734, 1454, 1375, 1164, 1068.

Data of **4.18**: For detailed NMR analysis, see page 329; m/z (HRMS) calculated for $[\text{C}_{33}\text{H}_{40}\text{O}_6\text{Na}]^+$: 555.3, found: 555.3; $[\alpha]_{25}^{\text{D}} = 11.1^\circ$ ($c = 0.005$, CHCl_3); IR ν_{max} (neat)/ cm^{-1} 3436, 3063, 3031, 2969, 2933, 2876, 1966, 1729, 1454, 1376, 1270, 1179, 1065.



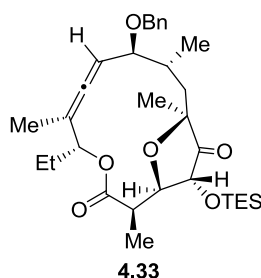
To a solution of alcohol **4.17** (7.4 mg, 16 μmol) in acetone (500 μl) was added grinded K_2CO_3 (4.3 mg, 31 μmol) and stirred for 30 minutes at room temperature. To the mixture was added acetic anhydride (6 μl , 0.07 mmol) at room temperature and stirred for overnight. The reaction mixture was diluted in DCM and the organic layer was washed with water. The combined organic phase was dried over anhydrous Na_2SO_4 . Evaporation of solvent and silica gel column chromatography using 7% EtOAc in hexanes gave **4.30** (5.6 mg, 11 μmol , 70% yield) as colorless oil.

For detailed NMR analysis of **4.30**, see page 345; m/z (HRMS) found: 541.2, calculated for $[\text{C}_{28}\text{H}_{38}\text{O}_9\text{Na}]^+$: 541.2.



To a solution of alcohol **4.16** (3.1 mg, 7.0 μmol) in acetone (500 μl) was added grinded K_2CO_3 (9.6 mg, 70 μmol) and stirred for 30 minutes at room temperature. To the mixture was added acetic anhydride (6 μl , 0.07 mmol) at room temperature and stirred for overnight. The reaction mixture was diluted in DCM and the organic layer was washed with water. The combined organic phase was dried over anhydrous Na_2SO_4 . Evaporation of solvent and silica gel column chromatography using 7% EtOAc in hexanes gave **4.32** (1.7 mg, 3.5 μmol , 50% yield) as colorless oil.

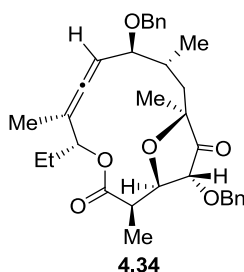
For detailed NMR analysis of **4.32**, see page 347; m/z (HRMS) calculated for $[\text{C}_{28}\text{H}_{36}\text{O}_7\text{Na}]^+$: 507.2, found: 507.2.



To the solution of **4.16** (6.2 mg, 14 μmol) in 1 mL of anhydrous DCM was added imidazole (2.9 mg, 40 μmol) and DMAP (0.5 mg, 4 μmol). After stirring for 5 minutes at room temperature, triethylsilyl chloride (12.6 mg, 83.6 μmol) was added to the mixture at room temperature. Upon the completion of the reaction, the mixture was quenched with

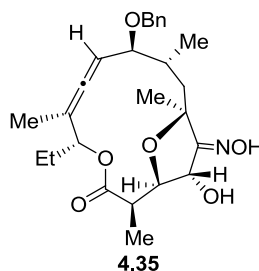
aqueous NH_4Cl and the organic layer was extracted with DCM, dried over Na_2SO_4 . The crude was chromatographed with 3% EtOAc in hexane through silica gel, giving **4.33** (7.2 mg, 13 μmol , 92% yield).

For detailed NMR analysis of **4.33**, see page 353; m/z (HRMS) calculated for $[\text{C}_{32}\text{H}_{48}\text{O}_6\text{SiH}]^+$: 557.3, found: 557.3; IR ν_{max} (neat)/ cm^{-1} 3439, 2957, 2931, 2987, 2897, 2858, 1723, 1471, 1376, 1195, 1103, 837.



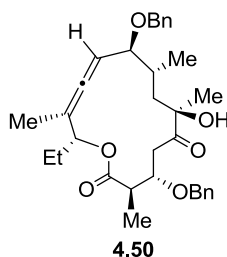
To a stirred solution of macrolactone **4.16** (10.0 mg, 22.6 μmol) in toluene (155 μL) was added benzyl trichloroacetimidate (8.0 mg, 32 μmol) and lanthanum triflate (1.2 mg, 2.2 μmol). Then the mixture was stirred at room temperature for 30 minutes. The reaction mixture was concentrated under vacuum and the residue was subjected to purification by silica gel column chromatography yielding **4.34** (8.4 mg, 16 μmol , 70%).

For detailed NMR analysis, see page 367; m/z (HRMS) calculated for $[\text{C}_{33}\text{H}_{40}\text{O}_6\text{Na}]^+$: 557.3, found: 555.3; IR ν_{max} (neat)/ cm^{-1} 3400, 2965, 2923, 2877, 2851, 1900, 1759, 1725, 1453, 1374, 1186, 1079.



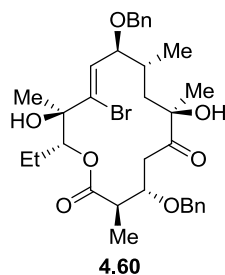
To a solution of **4.16** (3.4 mg, 7.7 μ mol) in ethanol (1 mL) was added hydroxylamine hydrochloride (16.0 mg, 0.230 mmol). The reaction mixture was stirred for 2hrs, then KOH (12.9 mg, 0.230 mmol) was added at room temperature. The reaction was diluted with water and extracted with Et₂O. The combined organic phase was dried over anhydrous Na₂SO₄. Evaporation of solvent and silica gel column chromatography using 15% EtOAc in hexanes gave **4.35** (2.7 mg, 6.0 μ mol, 78% yield) as colorless oil.

¹H NMR (500 MHz, CDCl₃) δ 7.35 – 7.31 (m, 5H), 5.83 (d, J = 6.60 Hz, 1H), 5.57 (dd, J = 8.80, 5.58 Hz, 1H), 5.07 – 5.03 (m, 1H), 4.61 (d, J = 11.74 Hz, 1H), 4.34 (d, J = 11.99 Hz, 1H), 3.93 (dd, J = 6.36 Hz, 4.40, 1H), 3.79 (dd, J = 9.05 Hz, 1.46, 1H), 3.09 (s, 1H), 2.98 – 2.91 (m, 1H), 2.03 – 1.96 (m, 1H), 1.76 (d, J = 2.69 Hz, 3H), 1.73 – 1.60 (m, 4H), 1.31 (d, J = 8.56 Hz, 3H), 0.93 (d, J = 7.33 Hz, 3H), 0.91 (s, 3H), 0.90 – 0.84 (m, 3H); ¹³C NMR (125 MHz, CDCl₃) δ 206.3, 174.3, 167.1, 139.2, 128.2, 127.5, 127.2, 98.6, 90.4, 83.2, 82.3, 76.7, 75.4, 70.5, 67.8, 42.5, 39.9, 34.1, 24.2, 22.7, 14.8, 14.0, 13.6, 10.1; m/z (HRMS) calculated for [C₂₆H₃₅NO₆Na]⁺: 480.2, found: 480.2; [α]_D²⁵ = 6.3° (c = 0.005, CHCl₃); IR ν_{max} (neat)/cm⁻¹ 3309, 2917, 2849, 1959, 1729, 1709, 1458, 1375, 1156, 1070.



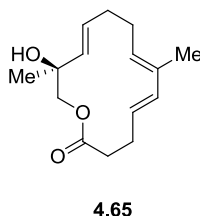
The macrolactone **4.1** (26.0 mg, 52.0 μmol) was dissolved in the mixture of *t*-BuOH and water (1:1 ratio, total 2 mL). To the solution was added 4% aqueous OsO_4 solution (495 μL , 62.2 μmol) at room temperature, and then stirred for 45 minutes. After the complete consumption of **4.1**, the reaction was quenched by 20 mL saturated Na_2SO_3 solution, and then extracted with Et_2O (2 x 20 mL). The solvent was removed *in vacuo*. Silica gel column chromatography using 10% EtOAc in hexane gave the macrolactone **4.50** as light yellowish oil (23.0 mg, 43.0 μmol , 83% yield).

^1H NMR (500 MHz, CDCl_3) δ 7.48 – 7.17 (m, 8H), 5.15 (t, $J = 6.0$ Hz, 2H), 4.94 (dd, $J = 6.8, 3.1$ Hz, 1H), 4.73 (dd, $J = 13.4, 8.4$ Hz, 1H), 4.58 (dd, $J = 21.0, 11.6$ Hz, 2H), 4.35 (d, $J = 12.2$ Hz, 1H), 4.15 (ddd, $J = 8.7, 6.9, 4.0$ Hz, 1H), 3.83 (s, 1H), 3.44 (dd, $J = 8.0, 6.9$ Hz, 1H), 2.95 (qd, $J = 17.8, 5.4$ Hz, 2H), 2.58 (dt, $J = 15.5, 6.8$ Hz, 1H), 1.90 (dd, $J = 15.0, 3.1$ Hz, 1H), 1.79 (d, $J = 2.9$ Hz, 2H), 1.76 – 1.64 (m, 2H), 1.57 – 1.46 (m, 2H), 1.42 – 1.28 (m, 4H), 1.28 – 1.15 (m, 2H), 1.07 (t, $J = 13.0$ Hz, 2H), 0.99 – 0.69 (m, 6H); ^{13}C NMR (126 MHz, CDCl_3) δ 216.5, 208.4, 178.2, 143.0, 142.8, 133.2, 132.9, 132.9, 132.5, 132.5, 132.3, 132.3, 132.1, 131.6, 104.1, 96.1, 86.7, 83.3, 81.9, 81.6, 81.4, 80.8, 80.4, 78.2, 74.4, 50.0, 47.3, 47.0, 38.6, 34.3, 31.8, 29.6, 23.0, 19.9, 18.1, 14.0; m/z (HRMS) calculated for $[\text{C}_{33}\text{H}_{42}\text{O}_6\text{Na}]^+$: 557.3, found: 557.3; IR $\nu_{\text{max}}(\text{neat})/\text{cm}^{-1}$ 3475, 3065, 2930, 2919, 2872, 2849, 1963, 1727, 1453, 1375, 1172, 1069.



To a stirred solution of macrolactone **4.50** (7.8 mg, 15 μ mol) in 1 mL of acetonitrile was added *N*-Bromosuccinimide (34.0 mg, 191 μ mol) at room temperature. Starting material was consumed right away. The reaction mixture was quenched with 1 mL of saturated aqueous solution of $\text{Na}_2\text{S}_2\text{O}_3$, and then extracted with Et_2O . The solvent was removed *in vacuo*, and the residue was subjected to purification by silica gel column chromatography (14% EtOAc in hexane) yielding **4.60** (9.1 mg, 15 μ mol, 99% yield).

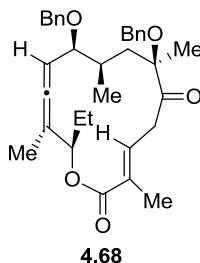
For detailed NMR analysis, see page 372; m/z (ESIMS) calculated for $[\text{C}_{33}\text{H}_{43}\text{BrO}_7\text{Na}]^+$: 653.3, 655.3, found: 653.2, 655.2; $[\alpha]_D^{25} = 7.6^\circ$ ($c = 0.005$, CHCl_3); IR ν_{max} (neat)/ cm^{-1} 3442, 3062, 2956, 2922, 2850, 1728, 1711, 1454, 1376, 1165, 1070.



To a solution of bis[allene] macrolactone **2.24** (36.6 mg, 158 μ mol) in THF (2 mL) was added sulfuric acid (15.5 mg, 0.160 mmol), water (13 μ L, 0.71 mmol), mercuric sulfate (1.9 mg, 6.3 μ mol) sequentially. The reaction mixture was heated under reflux at 70 $^\circ\text{C}$ for 5 hours. After the complete consumption of bis[allene] macrolactone, the reaction was cooled down to room temperature and diluted with water. The organic

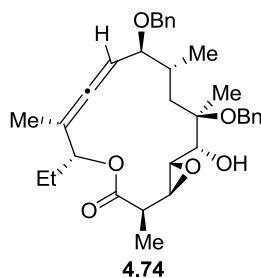
phase was extracted with EtOAc and dried over anhydrous Na_2SO_4 . The solvent was removed *in vacuo*, and silica gel column chromatography using 20% EtOAc in hexanes gave **4.65** (15.9 mg, 63.6 μmol , 40%) as colorless oil.

For detailed NMR analysis, see page 393; m/z (HRMS) calculated for $[\text{C}_{15}\text{H}_{22}\text{O}_3\text{Na}]^+$: 273.1, found: 273.1.



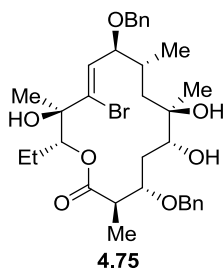
To a solution of bis[allene] macrolactone **4.1** (15.0 mg, 30.0 μmol) in 2-methyl THF (3 mL) was added Na_2HPO_4 (51.0 mg, 0.360 mmol) and *m*CPBA (31.0 mg, 0.180 mmol) sequentially at $-50\text{ }^\circ\text{C}$. The temperature was slowly increased to $12\text{ }^\circ\text{C}$ over 5 hr 30 minute. To the reaction mixture was methanol (4 mL) and stirred overnight. The reaction was quenched with aqueous NaHCO_3 and extracted with EtOAc. The combined organic phase was dried over anhydrous Na_2SO_4 . The solvent was removed *in vacuo*, and silica gel column chromatography using 15% EtOAc in hexanes gave **4.68** as colorless oil (7.0 mg, 14 μmol , 45% yield).

For detailed NMR analysis, see page 419; m/z (ESIMS) calculated for $[\text{C}_{33}\text{H}_{40}\text{O}_5+\text{Na}]^+$: 539.6, found: 539.1.



To epoxy ketone **4.18** (1.7 mg, 3.2 μmol) in Et_2O (1 mL) was added $\text{Zn}(\text{BH}_4)_2$ (46 μl , 14 μmol , 0.30 M in Et_2O) dropwise at 0 $^\circ\text{C}$, then $\text{Zn}(\text{BH}_4)_2$ (115 μl , 35.0 μmol , 0.300 M in Et_2O) twice at room temperature. After the complete consumption of **4.18**, the reaction was quenched with aqueous NH_4Cl and extracted with Et_2O . The combined organic phase was dried over anhydrous Na_2SO_4 . The solvent was removed *in vacuo*, and silica gel column chromatography using 15% EtOAc in hexanes gave **4.74** (1.4 mg, 2.6 μmol , 82% yield) as colorless oil.

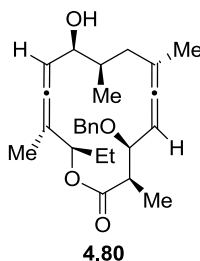
For detailed NMR analysis, see page 442; m/z (HRMS) calculated for $[\text{C}_{33}\text{H}_{42}\text{O}_6\text{H}]^+$: 535.3, found: 535.3.



To a stirred solution of macrolactone **4.60** (5.0 mg, 7.9 μmol) in 1 mL of anhydrous Et_2O was $\text{Zn}(\text{BH}_4)_2$ solution in Et_2O (91 μl , 12 μmol) at 0 $^\circ\text{C}$. The mixture was stirred for 30 minutes at 0 $^\circ\text{C}$. The reaction mixture was quenched with 1 mL of aqueous NH_4Cl , and then extracted with Et_2O . The crude was subjected to purification

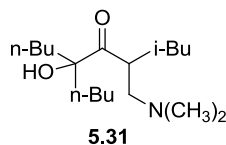
by silica gel column chromatography (20% EtOAc in hexane) yielding **4.75** (4.9 mg, 7.9 μmol , 99% yield).

For detailed NMR analysis, see page 463; m/z (HRMS) calculated for $[\text{C}_{33}\text{H}_{45}\text{BrO}_7\text{Na}]^+$: 655.2, 657.2, found: 655.2, 657.2; $[\alpha]_D^{25} = 5.8^\circ$ ($c = 0.005$, CHCl_3); IR ν_{max} (neat)/ cm^{-1} 3433, 2925, 2851, 1729, 1454, 1375, 1164, 1068.



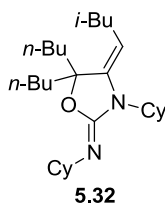
To a solution of bis[allene] macrolactone **4.1** (21.5 mg, 43.0 μmol) in 1,2-dichloroethane (3.6 mL) and phosphate buffer (0.4 mL, pH = 7) was added DDQ (39.0 mg, 172 μmol) and stirred for 15 minutes at room temperature. Then, raise the temperature to 40 $^\circ\text{C}$ until the complete disappearance of **4.1**. The aqueous NaHCO_3 (3 mL) was added and the resulting dark solution was stirred vigorously for 1 hr. The crude mixture was extracted with DCM and the excess solvent was removed under reduced pressure. The crude mixture was chromatographed, yielding **4.80** (10.5 mg, 25.6 μmol , 60%) as colorless oil.

For detailed NMR analysis, see page 500; m/z (HRMS) calculated for $[\text{C}_{26}\text{H}_{34}\text{O}_4\text{Na}]^+$: 433.2, found: 433.2; $[\alpha]_D^{25} = 15.1^\circ$ ($c = 0.005$, CHCl_3); IR ν_{max} (neat)/ cm^{-1} 3435, 2968, 2917, 2848, 1963, 1729, 1453, 1376, 1177, 1069.



To the solution of allene (30.0 mg, 0.140 mmol) **5.25** in anhydrous DCM (3 mL), dimethylmethylenediammonium chloride (70.0 mg, 0.700 mmol), and OsO₄ solution (3.0 mL, 0.15 mmol, 0.050 M in DCM), and NMO (20.0 mg, 0.150 mmol) were added at room temperature. The mixture was stirred for 1 hour, and then quenched by saturated solution of Na₂SO₃. The organic layer was extracted in DCM. The crude was purified by silica gel column chromatography, yielding **5.31** (27.3 mg, 63% yield).

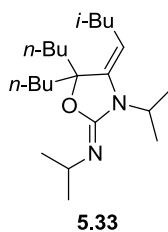
Data of **5.31**: ¹H NMR (500 MHz, CDCl₃) 3.92 (1H, s), 3.50 – 3.38 (1H, m), 2.46 (2H, t, *J* = 7.6), 2.30 (6H, s), 1.76 – 1.00 (15H, m), 0.96 – 0.84 (12H, m); ¹³C NMR (125 MHz, CDCl₃) δ 219.7, 81.2, 64.4, 45.6, 42.3, 39.0, 38.7, 37.4, 26.3, 25.6, 25.5, 23.2, 23.1, 23.0, 22.7, 14.1, 13.9; *m/z* (HRMS) calculated for [C₁₈H₃₇NO₂H]⁺: 300.3, found: 300.3.



To the solution of allene (10.0 mg, 48.0 μmol) **5.25** in *t*-BuOH (900 μL) and water (150 μL) was added *N,N'*-dicyclohexylcarbodiimide (76.5 mg, 371 μmol) at room temperature. The mixture was stirred for 20 minutes, and then 4% aqueous OsO₄ solution (415 μL, 53.0 μmol) was added slowly. After the complete disappearance of

allene on TLC, the reaction mixture was quenched by saturated solution of Na₂SO₃ and the organic layer was extracted in DCM. The crude was purified by silica gel column chromatography, yielding **5.32** (16.4 mg, 79% yield).

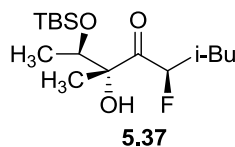
For detailed NMR analysis, see page 528; ¹H NMR (500 MHz, CDCl₃) δ 5.24 (1H, t, *J* = 7.8 Hz), 4.21 – 4.30 (2H, tt, *J* = 4.1 Hz), 2.04 – 2.08 (1H, m), 1.87 – 1.91 (2H, m), 1.7 (1H, m), 0.96 (3H, s), 0.95 (3H, s), 1.15 – 2.20 (20H, m); ¹³C NMR (125 MHz, CDCl₃) δ 182.6, 166.8, 100.5, 94.6, 59.8, 59.2, 41.3, 39.8, 33.9, 32.2, 32.0, 31.9, 31.8, 29.5, 25.9, 25.8, 25.7, 25.6(2), 25.5(2), 23.1, 22.6, 22.5, 22.5, 13.9(2)



To the solution of allene (9.4 mg, 45 μmol) **5.25** in *t*-BuOH (900 μL) and water (150 μL) was added *N,N'*-diisopropylcarbodiimide (114 mg, 902 μmol) at room temperature. The mixture was stirred for 20 minutes, and then 4% aqueous OsO₄ solution (390 μL, 50.0 μmol) was added slowly. After the complete disappearance of allene on TLC, the reaction mixture was quenched by saturated solution of Na₂SO₃ and the organic layer was extracted in DCM. The crude was purified by silica gel column chromatography, yielding **5.33** (8.8 mg, 56% yield).

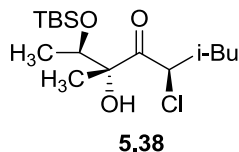
¹H NMR (500 MHz, CDCl₃) δ 7.79 – 7.68 (2H, m), 7.30 – 7.23 (2H, m), 5.31 (1H, d, *J* = 9.5 Hz), 4.51 (1H, dd, *J* = 2.7, 9.5 Hz), 2.39 (3H, s), 1.98 (3H, s), 1.91 – 1.82 (1H, m), 1.66 – 1.00 (14H, m), 0.99 – 0.80 (12H, m); ¹³C NMR (125 MHz, CDCl₃) δ

212.9, 143.4, 137.3, 129.6, 82.3, 55.6, 41.6, 38.1, 37.4, 22.5, 24.7, 24.4, 23.5, 22.9, 22.8, 20.8, 13.8, 13.8.



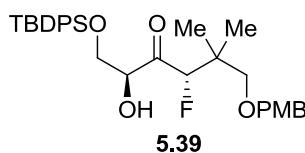
To the solution of allene (17.5 mg, 65.2 μ mol) **5.34** in *t*-BuOH (1 mL), phosphate buffer (0.50 mL, pH= 7.4), and acetone (0.5 mL) was added Selectfluor (115 mg, 326 μ mol) at room temperature. The mixture was stirred for 20 minutes, then 4% aqueous OsO₄ solution (0.51 mL, 65 μ mol) was added slowly. After the complete disappearance of allene on TLC, the reaction mixture was quenched by saturated solution of Na₂SO₃ and the organic layer was extracted in EtOAc. The crude was purified by silica gel column chromatography, yielding the mixture of **5.37** (13.4 mg, 41.8 μ mol, 64% combined yield for anti and syn in 5.9:1 ratio)

Data of **5.37** (anti): ¹H NMR (500 MHz, CDCl₃) δ 5.48 (1H, dddd, *J* = 2.20, 10.27, 51.35 Hz), 4.05 (1H, q, *J* = 6.11 Hz), 2.83 (1H, s), 1.96 – 1.88 (1H, m), 1.81 – 1.68 (2H, m), 1.35 (3H, s), 1.08 (3H, d, *J* = 6.36 Hz), 1.01 (3H, d, *J* = 6.85 Hz), 0.98 (6H, d, *J* = 6.26 Hz), 0.90 (9H, s), 0.86 (3H, s); ¹³C NMR (125 MHz, CDCl₃) δ 210.4 (*J*_{CF} = 16.75), 92.2, 82.1, 72.4, 39.7, 25.8 (3), 25.7, 24.7, 23.3, 21.2, 18.6, 18.0, –4.3, –4.9; *m/z* (HRMS) calculated for [C₁₆H₃₃FO₃SiNa]⁺: 343.2, found: 343.2; [α]_D²⁵ = –46.5° (*c* = 0.01, CHCl₃); IR ν_{max} (neat)/cm^{–1} 3546, 2958, 2931, 2858, 1733, 1464, 1374, 1256, 1159, 1120, 1037, 982, 836.



To the solution of allene (17.5 mg, 65.2 μmol) **5.34** in *t*-BuOH (1 mL) and water (0.5 mL) was added NCS (43.5 mg, 326 μmol) at room temperature. The mixture was stirred for 20 minutes, then 4% aqueous OsO_4 solution (0.51 mL, 65 μmol) was added slowly. After the complete disappearance of allene on TLC, the reaction mixture was quenched by saturated solution of Na_2SO_3 and the organic layer was extracted in EtOAc. The crude was purified by silica gel column chromatography, yielding **5.38** (17.1 mg, 50.9 μmol , 78% combined yield for anti and syn in 5.3:1 ratio).

Data of **5.38** (anti): ^1H NMR (500 MHz, CDCl_3) δ 5.02 (1H, dd, $J = 4.7, 10.2$ Hz), 3.97 (1H, q, $J = 6.3$ Hz), 2.77 (1H, s), 1.90 – 1.82 (1H, m), 1.71 – 1.66 (2H, m), 1.42 (3H, s), 1.04 (3H, d, $J = 6.3$ Hz), 0.97 (3H, d, $J = 6.7$ Hz), 0.93 (3H, d, $J = 6.3$ Hz), 0.91 (3H, s), 0.90 (9H, s), 0.88 (3H, s); ^{13}C NMR (125 MHz, CDCl_3) δ 208.2, 82.1, 73.3, 55.7, 40.9, 25.8 (3), 25.7, 24.8, 23.1, 21.1, 18.4, 18.0, -4.26, -4.81; m/z (HRMS) calculated for $[\text{C}_{16}\text{H}_{33}\text{ClO}_3\text{SiNa}]^+$: 359.2, found: 359.2; $[\alpha]_D^{25} = 24.8^\circ$ ($c = 0.01$, CHCl_3); IR ν_{max} (neat)/ cm^{-1} 3544, 2958, 2931, 2858, 1723, 1464, 1375, 1257, 1169, 1104, 1029, 1008, 837.

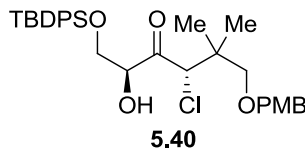


Stoichiometric condition is as follows; to the solution of allene (24.6 mg, 49.2 μmol) **5.35** in *t*-BuOH (1 mL), phosphate buffer (0.60 mL, pH = 7.4), and acetone (0.5

mL) was added Selectfluor (87.0 mg, 246 μmol) at room temperature. The mixture was stirred for 20 minutes, then 4% aqueous OsO_4 solution (0.39 mL, 49 μmol) was added slowly. After the complete disappearance of allene on TLC, the reaction mixture was quenched by saturated solution of Na_2SO_3 and the organic layer was extracted in EtOAc. The crude was purified by silica gel column chromatography, yielding **5.39** (17.4 mg, 31.5 μmol , 64% yield, single diastereomer).

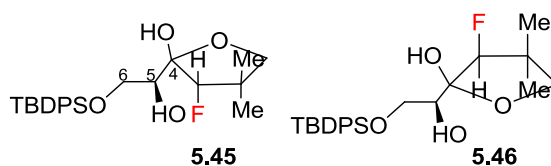
Catalytic condition is as follows; to the solution of allene (35.0 mg, 70.0 μmol) **5.35**, and Selectfluor (124 mg, 349 μmol) in *t*-BuOH (1 mL), phosphate buffer (1.0 mL, pH = 7.4), and acetone (1 mL) was added 4% aqueous OsO_4 solution (55 μL , 7.0 μmol) was added slowly. Then, NMO (16.4 mg, 140 μmol) was added. After the complete disappearance of allene on TLC, the reaction mixture was quenched by saturated solution of Na_2SO_3 and the organic layer was extracted in EtOAc. The crude was purified by silica gel column chromatography, yielding **5.39** (23.8 mg, 43.1 μmol , 62% yield, single diastereomer).

Data of **5.39** (anti): ^1H NMR (500 MHz, CDCl_3) δ 7.67 – 7.63 (4H, m), 7.45 – 7.36 (6H, m), 7.21 – 7.18 (2H, m), 6.87 – 6.84 (2H, m), 5.16 (1H, d, J = 47.2 Hz), 4.49 – 4.46 (1H, m), 4.37 (2H, s), 3.96 (1H, ddd, J = 1.0, 3.4, 10.8 Hz), 3.89 (1H, ddd, J = 1.0, 4.4, 10.8 Hz), 3.80 (3H, s), 3.53 (1H, dd, J = 6.9 Hz), 3.19 (1H, dd, J = 9.3 Hz), 1.02 (9H, s), 1.00 (6H, s); ^{13}C NMR (125 MHz, CDCl_3) δ 208.0, 207.8, 159.2, 135.7, 135.6, 132.9, 132.6, 129.8, 129.1, 127.7, 113.7, 97.0, 95.5, 76.5, 75.0, 72.8, 65.2, 55.2, 40.2, 40.1, 26.7, 20.9, 19.2; m/z (HRMS) calculated for $[\text{C}_{32}\text{H}_{41}\text{FO}_5\text{SiNa}]^+$: 575.3, found: 575.3; $[\alpha]_D^{25}$ = 18.4° (c = 0.01, CHCl_3); IR ν_{max} (neat)/ cm^{-1} 3071, 3048, 2957, 2931, 2857, 1725, 1427, 1362, 1247, 1173, 1112, 1035, 1008, 736, 702.



Stoichiometric condition is as follows; to the solution of allene (24.6 mg, 49.2 μmol) **5.35** in *t*-BuOH (1 mL), phosphate buffer (0.60 mL, pH = 7.4), acetone (0.5 mL) was added NCS (32.8 mg, 246 μmol) at room temperature. The mixture was stirred for 20 minutes, then 4% aqueous OsO_4 solution (0.39 mL, 49 μmol) was added slowly. After the complete disappearance of allene on TLC, the reaction mixture was quenched by saturated solution of Na_2SO_3 and the organic layer was extracted in EtOAc. The crude was purified by silica gel column chromatography, yielding the mixture of **5.40** (19.2 mg, 33.8 μmol , 69% yield for anti and syn in 3.2:1 ratio).

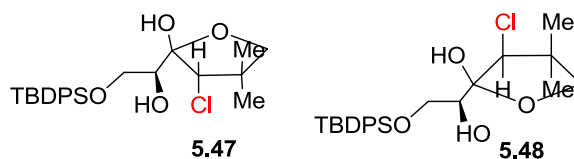
Catalytic condition is as follows; to the solution of allene (18.2 mg, 36.4 μmol) **5.35** in *t*-BuOH (1 mL), phosphate buffer (1.0 mL, pH = 7.4), and acetone (0.5 mL) were added *N*-Methylmorpholine *N*-oxide (NMO) (8.5 mg, 73 μmol) and 4% aqueous OsO_4 solution (28 μL , 3.6 μmol). Then, NCS (24.3 mg, 182 μmol), dissolved in *t*-BuOH (0.5 mL), phosphate buffer (0.50 mL, pH = 7.4), and acetone (0.5 mL), was added dropwise over 3 hours via syringe pump at room temperature. After the complete disappearance of allene on TLC, the reaction mixture was quenched by saturated solution of Na_2SO_3 and the organic layer was extracted in EtOAc. The crude was purified by silica gel column chromatography, yielding the mixture of **5.40** (16.3 mg, 28.2 μmol , 77% yield for anti and syn in 1.5:1 ratio).



Catalytic condition is as follows; to the solution of allene (30.0 mg, 78.9 μmol)

5.44, Selectfluor (140 mg, 394 μmol), and NMO (18.5 mg, 158 μmol) in *t*-BuOH (1

For detailed NMR analysis, see page 549; m/z (HRMS) calculated for $[\text{C}_{24}\text{H}_{33}\text{FO}_4\text{SiNa}]^+$: 455.2; IR ν_{max} (neat)/ cm^{-1} 3427, 3071, 3049, 2957, 2929, 2890, 2856, 1471, 1427, 1392, 1113, 907, 731, 702.

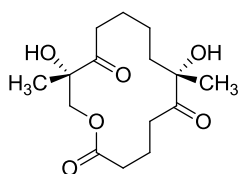


Stoichiometric condition is as follows; to the solution of allene (30.2 mg, 79.4 μmol) **5.44** in *t*-BuOH (1 mL), phosphate buffer (0.37 mL, pH = 7.4), and acetone (0.5 mL) was added NCS (53.0 mg, 397 μmol) at room temperature. The mixture was stirred for 20 minutes, then 4% aqueous OsO₄ solution (0.62 mL, 79 μmol) was added slowly. After the complete disappearance of allene on TLC, the reaction mixture was quenched by saturated solution of Na₂SO₃ and the organic layer was extracted in EtOAc. The crude was purified by silica gel column chromatography, yielding the mixture (17.4 mg, 38.8 μmol , 49% yield for **5.47** and **5.48** in 1: 1.1 ratio).

Catalytic condition is as follows; to the solution of allene (30.0 mg, 78.9 μmol) **5.44**, NCS (52.6 mg, 394 μmol), and NMO (18.5 mg, 158 μmol) in *t*-BuOH (1 mL),

phosphate buffer (1.0 mL, pH = 7.4), and acetone (1 mL) was added 4% aqueous OsO₄ solution (62 μ L, 7.9 μ mol) slowly. After the complete disappearance of allene on TLC, the reaction mixture was quenched by saturated solution of Na₂SO₃ and the organic layer was extracted in EtOAc. The crude was purified by silica gel column chromatography, yielding the mixture (29.7 mg, 84% yield for **5.47** and **5.48** in 1:1.3 ratio).

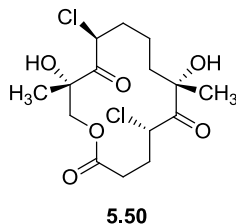
For detailed NMR analysis, see page 556; m/z (HRMS) calculated for [C₂₄H₃₃ClO₄SiNa]⁺: 471.2, 473.2 found: 471.2, 473.2; IR ν_{\max} (neat)/cm⁻¹ 3421, 3071, 3049, 2957, 2928, 2856, 1428, 1417, 1374, 1112, 1070, 916, 737, 702.



5.49

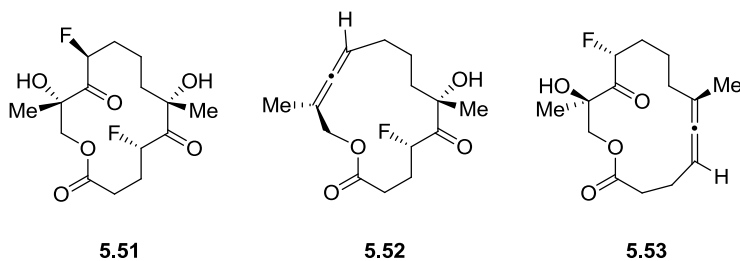
To the solution of allene (9.4 mg, 40 μ mol) **2.24** in *t*-BuOH (400 μ L) and water (50 μ L) was added 4% aqueous OsO₄ solution (0.64 mL, 81 μ mol) slowly. After the complete disappearance of allene on TLC, the reaction mixture was quenched by saturated solution of Na₂SO₃ and the organic layer was extracted in EtOAc. The crude was purified by silica gel column chromatography, yielding **5.49** (4.6 mg, 38% yield).

For detailed NMR analysis of **5.49**, see page 573; m/z (HRMS) calculated for [C₁₅H₂₄O₆Na]⁺: 323.2, found: 323.2; IR ν_{\max} (neat)/cm⁻¹ 3479, 2923, 2851, 1713, 1458, 1374, 1133.



To the solution of allene (10.5 mg, 45.0 μmol) **2.24** in *t*-BuOH (400 μL) and water (50 μL) was added NCS (30.2 mg, 226 μmol) at room temperature. The mixture was stirred for 20 minutes, then 4% aqueous OsO_4 solution (0.70 mL, 90 μmol) was added slowly. After the complete disappearance of allene on TLC, the reaction mixture was quenched by saturated solution of Na_2SO_3 and the organic layer was extracted in EtOAc. The crude was purified by silica gel column chromatography, yielding **5.50** (10.0 mg, 65% yield).

For detailed NMR analysis of **5.50**, see page 585; m/z (HRMS) calculated for $[\text{C}_{15}\text{H}_{22}\text{Cl}_2\text{O}_6\text{H}]^+$: 367.1, 369.1, 372.1, found: 367.1, 369.1, 372.1; IR ν_{max} (neat)/ cm^{-1} 3433, 2920, 2850, 1739, 1462, 1375, 1241, 1157.

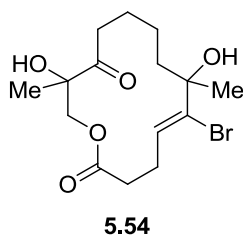


To the solution of allene (10.4 mg, 45.0 μmol) **2.24** in *t*-BuOH (2 mL) and water (1.3 mL) was added Selectfluor (109 mg, 448 μmol) at room temperature. The mixture was stirred for 7 minutes, then 4% aqueous OsO_4 solution (0.70 mL, 90 μmol) was added slowly. After the complete disappearance of allene on TLC, the reaction mixture was quenched by saturated solution of Na_2SO_3 and the organic layer was extracted in EtOAc.

The crude was purified by silica gel column chromatography, yielding **5.51** (6.3 mg, 42% yield) and the mixture of **5.52** and **5.53** (1.2 mg, 9% combined yield).

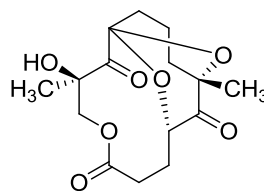
For detailed NMR analysis of **5.51**, see page 603; m/z (HRMS) calculated for $[C_{15}H_{22}F_2O_6Na]^+$: 359.1, found: 359.1; IR ν_{\max} (neat)/ cm^{-1} 3479, 2927, 2853, 1727, 1455, 1372, 1162.

For detailed NMR analysis of **5.52** and **5.53**, see page 618; m/z (HRMS) calculated for $[C_{15}H_{21}FO_4Na]^+$: 307.1, found: 307.1; IR ν_{\max} (neat)/ cm^{-1} 3492, 2929, 1723, 1461, 1371, 1155.



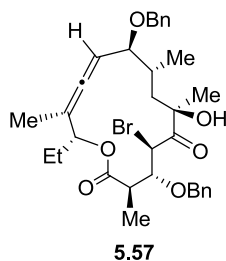
To a solution of bis[allene] macrolactone **2.24** (10.0 mg, 43.0 μ mol) in *t*-BuOH and water mixture (1:1, total 2 mL) was added NMO (20.2 mg, 0.170 mmol) and 4% aqueous OsO₄ solution (135 μ L, 17.0 μ mol) sequentially. NBS (23.0 mg, 129 μ mol) in *t*-BuOH (0.5 mL), phosphate buffer (0.5 mL, pH = 7) and acetone (0.5 mL) was added slowly over 10 hours. After the complete disappearance of SM, the reaction was quenched saturated solution of Na₂SO₃ and the organic layer was extracted with EtOAc. The organic phase was dried with Na₂SO₄ and the excess solvent was removed under reduced pressure. The crude material was chromatographed in silica gel, yielding **5.54** (6.0 mg, 47% yield).

For detailed NMR analysis, see page 631; IR ν_{\max} (neat)/ cm^{-1} 3459, 2923, 2850, 1735, 1712, 1459, 1370, 1163.

**5.55**

To the solution of allene (24.5 mg, 0.110 mmol) **2.24** in *t*-BuOH (2 mL) and water (1.3 mL) was added Chloramine T-trihydrate (259 mg, 1.05 mmol) at room temperature. The mixture was stirred for 1 minute, then 4% aqueous OsO₄ solution (1.66 mL, 0.210 mmol) was added slowly. After the complete disappearance of allene on TLC, the reaction mixture was quenched by saturated solution of Na₂SO₃ and the organic layer was extracted in EtOAc. The crude was purified by silica gel column chromatography, yielding **5.55** (2.3 mg, 7% yield).

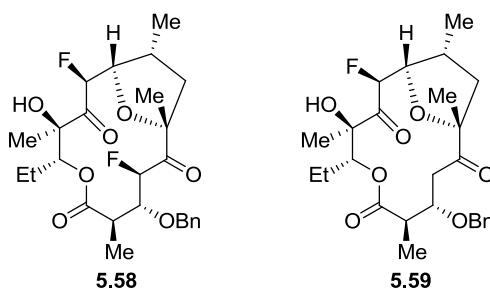
For detailed NMR analysis, see page 638; *m/z* (HRMS) calculated for [C₁₅H₂₀O₇Na]⁺: 335.1, found: 335.1; IR *v*_{max} (neat)/cm⁻¹ 3498, 2921, 2850, 1730, 1446, 1357.

**5.57**

To the solution of allene (20.7 mg, 41.0 μmol) **4.1** in *t*-BuOH (1 mL), phosphate buffer (0.29 mL, pH = 7.4), and acetone (0.50 mL) was added 4% aqueous OsO₄ solution (0.71 mL, 91 μmol) slowly. To the mixture was added NBS (14.7 mg, 83.0 μmol), dissolved in *t*-BuOH (0.5 mL), phosphate buffer (0.50 mL, pH = 7.4), and acetone (0.5 mL). After the complete disappearance of allene on TLC, the reaction mixture was

quenched by saturated solution of Na_2SO_3 and the organic layer was extracted in EtOAc. The organic phase was dried with Na_2SO_4 and the excess solvent was removed under reduced pressure. The crude was purified by silica gel column chromatography, yielding **5.57** (2.5 mg, 10% yield).

For detailed NMR analysis of **5.57**, see page 651; m/z (HRMS) calculated for $[\text{C}_{33}\text{H}_{41}\text{BrO}_6\text{Na}]^+$: 635.2, 637.2, found: 635.2, 637.2; IR ν_{max} (neat)/ cm^{-1} 3452, 3030, 2924, 2852, 1959, 1736, 1454, 1371, 1179, 1068, 697.



To the solution of allene (25.0 mg, 45.0 μmol) **4.1** in *t*-BuOH (1 mL), water (0.27 mL), and acetone (2 mL) was added Selectfluor (177 mg, 499 μmol) at room temperature. The mixture was stirred for 5 minutes, then 4% aqueous OsO_4 solution (1.18 mL, 90.0 μmol) was added slowly. After the complete disappearance of allene on TLC, the reaction mixture was quenched by saturated solution of Na_2SO_3 and the organic layer was extracted in EtOAc. The crude was purified by silica gel column chromatography, yielding **5.58** (2.6 mg, 10% yield) and **5.59** (5.0 mg, 21% yield).

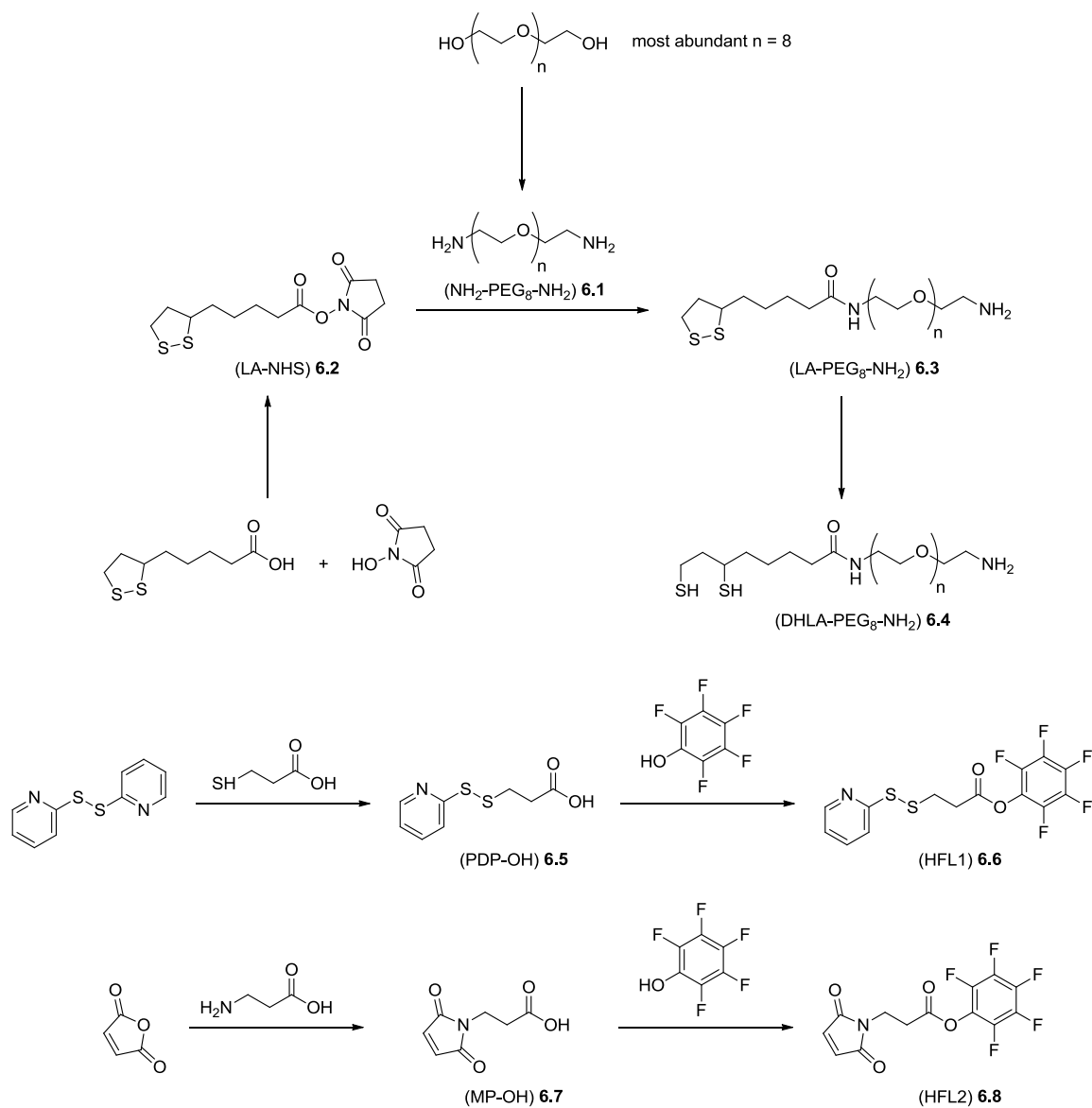
For detailed NMR analysis of **5.58**, see page 653; m/z (HRMS) calculated for $[\text{C}_{26}\text{H}_{34}\text{F}_2\text{O}_7\text{Na}]^+$: 519.2, found: 519.2; $[\alpha]_D^{25} = 7.3^\circ$ ($c = 0.005$, CHCl_3); IR ν_{max} (neat)/ cm^{-1} 3452, 2952, 2922, 2851, 1737, 1456, 1377, 1174, 1068.

For detailed NMR analysis of **5.59**, see page 671; m/z (HRMS) calculated for $[\text{C}_{26}\text{H}_{35}\text{FO}_7\text{Na}]^+$: 501.2, found: 501.2; $[\alpha]_{\text{D}}^{25} = 1.3^\circ$ ($c = 0.005$, CHCl_3); IR ν_{max} (neat)/ cm^{-1} 3500, 2918, 2849, 1736, 1455, 1375, 1169, 1069, 1011.

7.5. Chapter 6

Synthetic Routes to DHLA-PEG-NH₂ and Heterofunctional Linkers:

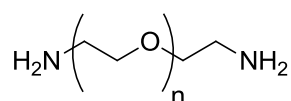
(adapted with permission from ref.¹¹)



Synthesis of the Core-Shell Quantum Dots: CdSe/CdS/ZnS core-shell QDs

were synthesized using well established protocols.^{1, 2} The QDs were then characterized

for size and its distribution using a transmission electron microscope (TEM); See Figure 6.2-1. The spectroscopic properties of the QDs were obtained using a fluorometer (FluoroMax-3, HORIBA Scientific).



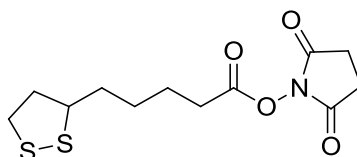
Diamino-PEG (NH₂-PEG₈-NH₂) (**6.1**)

This procedure from the literature³ was modified. Neat PEG₈ (20.0 g, 50.0 mmol, average MW 400 g/mol) was dried at 100 °C for 4 hours with stirring to remove all traces of water. The flask was cooled on an ice bath before thionyl chloride (10.5 mL, 145 mmol) was added dropwise. The solution was warmed to room temperature and stirred for 22 hours. After 22 hours, TLC indicated complete conversion to the bis-chloride; TLC (R_f 0.75, 90% DCM/MeOH, plate dried under vacuum prior to running) and ESI-MS (*m/z* 517.4 [M+H]⁺). The crude product was diluted with DMF (20 mL) and the solvent removed under reduced pressure. After repeating this three times, the flask was left under high vacuum overnight to remove all traces of thionyl chloride. To the crude dark yellow product was added a solution of sodium azide (9.40 g, 145 mmol) in 250 mL of DMF. The resulting dark-orange solution was stirred for 16 hours at 85 °C, indicating complete conversion to the diazide by TLC (R_f 0.6, 90% DCM/MeOH) and ESI-MS (*m/z* 531.4 [M+H]⁺). The solvent was removed under reduced pressure, and diluted with 200 mL of DCM. The precipitate was removed by vacuum filtration through Celite[®] and the solvent removed under high vacuum overnight to yield the intermediate diazide as brown oil. The sample was dissolved in 300 mL of THF, and triphenylphosphine (27.8 g, 106

mmol) was added to the mixture. The dark orange solution was stirred at room temperature for 24 hours, showing complete consumption of the diazide by ESI-MS and formation of the iminophosphorane intermediate by TLC (R_f 0.4, 90% DCM/MeOH). To the crude mixture, 4 mL of water was added and the dark brown mixture was stirred for 24 hours, showing complete reduction to the bis-amine **6.1** by TLC (R_f 0.1, 90% DCM/MeOH) and ESI-MS (m/z 457.4 $[M+H]^+$). THF was removed *in vacuo*, yielding a crude orange solid. 100 mL of water was added, and the precipitate was removed by vacuum filtration through a Büchner funnel. The filtrate was washed with toluene (3 x 50 mL). The water was removed *in vacuo* to give a dark orange oil. The crude product was purified by alumina column chromatography (DCM/MeOH, 95:5), giving **6.1** as a light yellow oil (19.8 g, 99%). Spectroscopic data matched those previously reported.³ Traces of triphenylphosphine oxide were detected by 1H NMR.

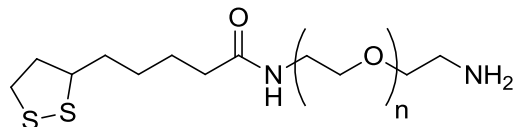
The previously reported protocols^{3, 4} for the synthesis of **6.1** required multiple steps; therefore, we applied a Mitsunobu reaction⁵ to acquire the bis-amine in a single step: PEG₈ (10.0 g, 25.0 mmol), previously dried over 3Å molecular sieves, triphenylphosphine (13.1 g, 2.0 equiv.), and phthalimide (7.4 g, 2.0 equiv.) were mixed in 150 mL of DCM and cooled to 0 °C under nitrogen. To this solution was added 95% diisopropylazodicarboxylate (DIAD, 10.4 mL, 2.0 equiv.) dropwise. The temperature being kept at or below 20 °C. After the addition was complete, the reaction was allowed to warm to room temperature and was stirred for the additional 1 hour. To the mixture was then added 55% hydrazine (3.6 mL, 2.5 equiv.) and the reaction was refluxed overnight under nitrogen. It was then cooled to room temperature and filtered. The

filtrate was stirred with 15 g of Amberlyst[®] 15 cation exchange resin for 5 hours. The resin was then filtered and washed with DCM (3 x 50 mL). It was then added to a solution of 2.9 g of NaOH in 100 mL of anhydrous EtOH and mechanically stirred overnight. The resin was filtered and washed with 95% EtOH (3 x 50 mL). The filtrate was concentrated *in vacuo* to give **6.1** as an amber oil (9.2 g, 93%). Spectroscopic data matched those previously reported.³



Lipoic Acid *N*-Hydroxysuccinimide-Ester (LA-NHS) (**6.2**)

The literature procedure³ was modified. To a solution of lipoic acid (5.00 g, 24.2 mmol) and *N*-hydroxysuccinimide (3.35 g, 29.1 mmol) in 150 mL of THF at 4 °C was added slowly a solution of dicyclohexylcarbodiimide (DCC, 6.00 g, 29.1 mmol) in 10 mL of THF. The mixture was warmed to room temperature and stirred for 8 hours, then showing complete conversion to the coupling product **6.2** by TLC (R_f 0.7, 90% DCM/MeOH). The precipitate was removed by vacuum filtration through Celite[®] and the solvent was evaporated *in vacuo*, giving a yellow solid. The crude product was redissolved in EtOAc and filtered again. This filtrate was concentrated *in vacuo*, giving pale-yellow oil. Recrystallization from a solution of hot ethyl acetate/hexane (1:1 v/v) afforded pure dithiane **6.2** a pale-yellow solid (3.47 g, 47%). The mother liquor was concentrated down and saved for future recrystallizations. Spectroscopic data matched those previously reported.³

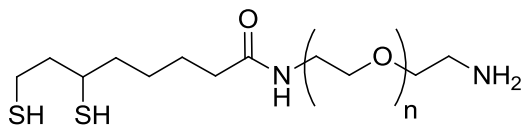


Lipoic Acid-PEG-Amine (LA-PEG₈-NH₂) (**6.3**)

This procedure from the literature³ was modified. To a yellow solution of **6.1** (13.0 g, 32.8 mmol) and sodium bicarbonate (2.75 g, 32.8 mmol) in DMF/water (100 mL, 50:50 v/v) at 4 °C was added dropwise a solution of recrystallized pure **6.2** (1.80 g, 5.90 mmol) in 10 mL of DMF over 1 hour, turning the reaction mixture a lighter yellow. The solution was warmed to room temperature and stirred for additional 16 hours, showing complete conversion to the amide **6.3** by TLC (R_f 0.15, 90% DCM/MeOH) and ESI-MS (m/z 601.3 $[M+H]^+$, see page 686, adapted with permission from ref.¹¹). The crude product mixture was extracted with chloroform (3 x 30 mL). The combined organic extracts were washed with water (3 x 30 mL), dried over Na₂SO₄ and filtered. After removing the solvent under reduced pressure, the crude product was purified by alumina column (DCM/MeOH, 95:5), yielding **6.3** as a yellow oil (1.93 g, 58%). The remainder of the product was contaminated with traces of **6.1**. This material was recycled along with excess **6.1** which recovered from the aqueous layer. Spectroscopic data matched those previously reported.³

The published procedure³ for the synthesis of **6.3** required excessive extractions from the DMF/water layer; therefore, we developed the following procedure: **6.1** (7.8 g, 5.0 equiv.) was dissolved in 50 mL of DCM. To this solution was added a solution of **6.2** in 50 mL of DCM, dropwise with stirring, over 1 hour. After another 30 minutes, the solvent was removed *in vacuo* and the residue was subject to silica gel chromatograph

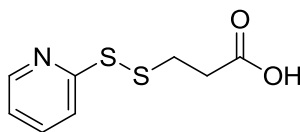
(1% NH_4OH /10% MeOH/DCM). The compound **6.3** was obtained as an amber oil (2.6 g, 96% yield). Spectroscopic data matched those previously reported.³



Dihydrolipoic Acid-PEG-Amine (DHLA-PEG₈-NH₂) (**6.4**)

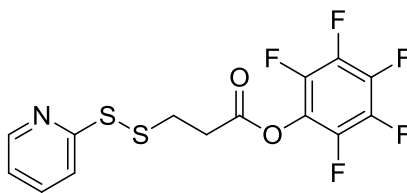
This procedure from the literature³ was modified. To a yellow solution of **6.1** (0.20 g, 0.33 mmol) in 4:1 water/ethanol (3 mL) at 4 °C was slowly added 4 equiv. of sodium borohydride (50.0 mg, 1.33 mmol) over 30 minutes. The bubbling solution was stirred for 4 hours at 4 °C, showing only 67% conversion to the reduction product **6.4** by ESI-MS (m/z 603.3 $[\text{M}+\text{H}]^+$, see page 688, adapted with permission from ref.¹¹). The product and starting material were not distinguishable due to overlapping TLC spots (R_f 0.15, 90% DCM/MeOH). The reaction mixture was left stirring overnight at room temperature. No further conversion was observed, so a total of 8 more equiv. of sodium borohydride was added over 48 hours, driving the reaction to completion in 72 hours. The crude reaction mixture was acidified to pH 2 with 1 M HCl , and extracted with chloroform (3 x 15 mL). The combined organic layer was dried over magnesium sulfate and filtered. The solvent was removed *in vacuo* to furnish the dithiol **6.4** as yellow oil (0.196 g, 98% yield). Spectroscopic data matched those previously reported.³ Traces of triphenylphosphine oxide were detected by ^1H NMR. A stability study was conducted on the dithiol. A 6 mg of **6.4** in CDCl_3 was kept under argon in a capped NMR tube for 48 hours, and no change was observed in the ^1H NMR spectrum. The sample was then

exposed to the atmosphere in an uncapped NMR tube for 48 hours, again showing no change by ^1H NMR. This product appeared to be air-stable.



3-(2-Pyridyl)-dithiopropionic acid (PDP-OH) (**6.5**)

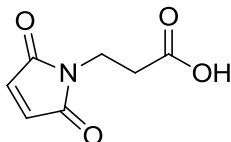
This procedure from the literature⁶ was modified. Pyridyl disulfide (3.11 g, 14.1 mmol) was dissolved in 30 mL of anhydrous EtOH and cooled to $-10\text{ }^{\circ}\text{C}$. Mercaptopropionic acid (MPA, 1.0 g, 9.4 mmol) in 20 mL of anhydrous EtOH was added dropwise over 30 minutes at $-10\text{ }^{\circ}\text{C}$. The reaction mixture was allowed to warm to room temperature. After 24 hours, the solvent was removed *in vacuo* and the residue was chromatographed (15% EtOAc/hexane). The compound **6.5** was isolated as a pale yellow solid (1.3 g, 64%). Spectroscopic data matched those previously reported.⁶



3-(2-Pyridyl)-dithiopropionic acid pentafluorophenyl ester (HFL1) (**6.6**)

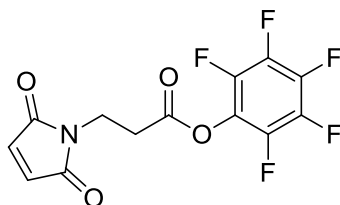
This procedure was modified from the literature.⁷ **6.5** (1.3 g, 6.0 mmol), pentafluorophenol (PFP, 1.1 g, 1 equiv.), and DCC (1.25 g, 1 equiv.) were dissolved in 30 mL of DCM and the reaction mixture was stirred at room temperature under nitrogen. After 48 hours, another 100 mg of both PFP and DCC were added to drive the coupling to completion within 3 hours. The solvent was removed *in vacuo*, and the residue was

purified by silica gel column chromatography (5% EtOAc/hexane). **6.6** was obtained as a yellow oil (1.88 g, 82% yield). Spectroscopic data matched those previously reported.⁸ Traces of DCC were detected by ¹H NMR.



3-Maleimidopropionic acid (MP-OH) (**6.7**)

According to the literature,⁹ MP-OH was synthesized. **6.7** was obtained as a white solid (43% yield). Spectroscopic data matched those previously reported.⁹



3-Maleimidopropionic acid pentafluorophenyl ester (HFL2) (**6.8**)

HFL2 was synthesized according to the literature.⁷ **6.8** was acquired as a white solid (74% yield). ¹H-NMR (CDCl₃) δ: 6.72 (2H, s, maleimide), 3.95 (2H, t, -CH₂^α-), 3.04 (2H, t, -CH₂^β-). Our spectrum agreed with that of the reported hexanoic analogue.⁷

Synthesis of Quantum Dot Conjugates with siRNA: The siRNA molecules for eGFP and EGFRvIII containing 5' thiol group were purchased from Dharmacon, Invitrogen. The siRNA for eGFP was designed as follows: sense sequence was 5'-thiol-GGCUACGUCCAGGAGCGCACC and antisense sequence was 5'-phosphate-

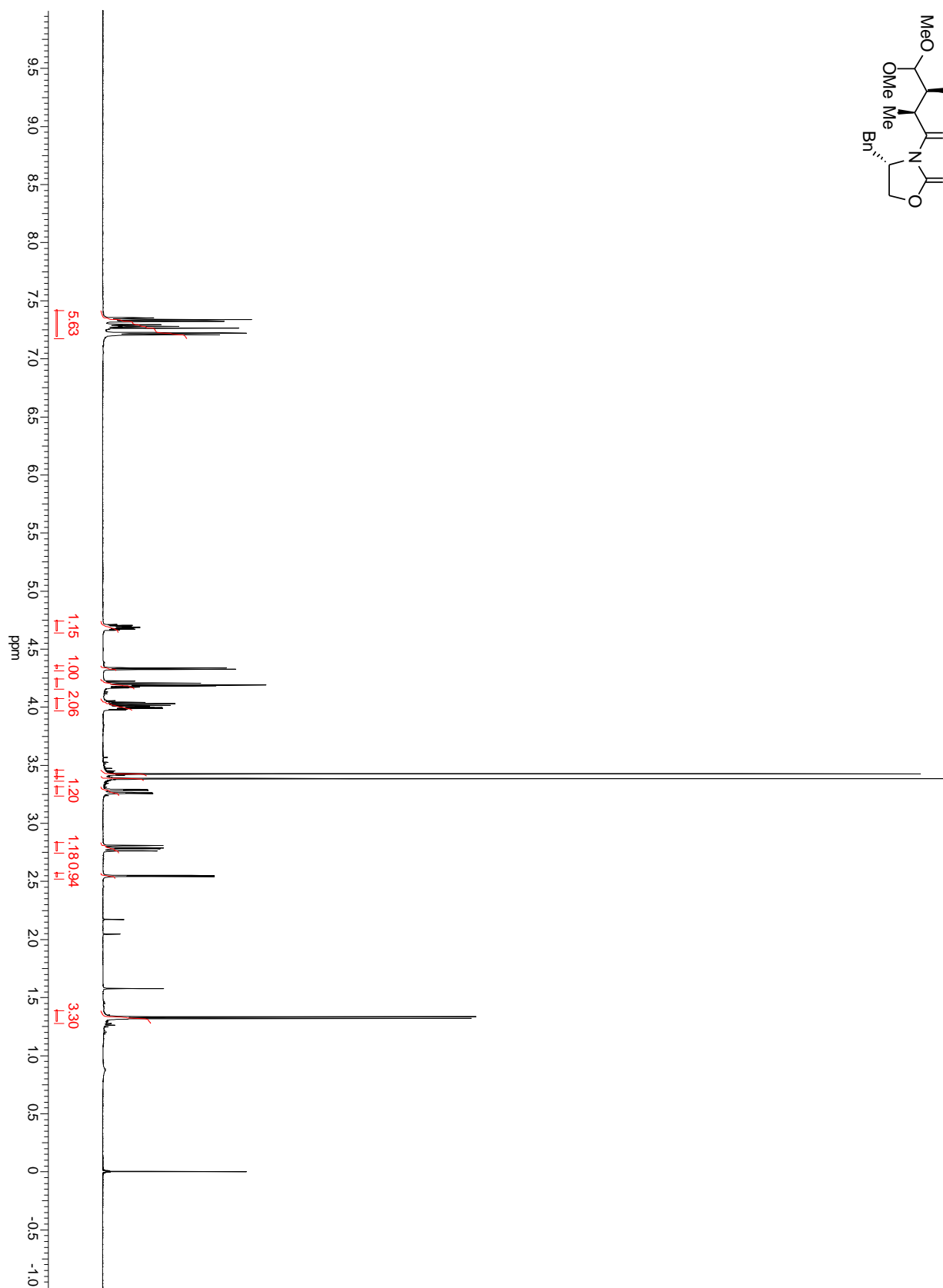
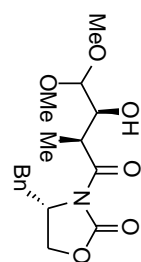
UGCGCUCCUGGACGUAGCCUU. For the knockdown of EGFRvIII, sense sequence was 5'-thiol-GAAAGGUAAUUAUGUGGUGdTdT and antisense sequence was 5'-phosphate-CACCACAUAUUUACCUUUCdTdT. QDs in the PBS were mixed with a 1000-fold excess of the cross linker, **6.6** and **6.8**, for 1 hour. After removing the unreacted linkers by ultracentrifugation, siRNA molecules were coupled to the QDs by mixing them together for 1 hour. After the conjugation, free siRNA was removed using ultracentrifugation.

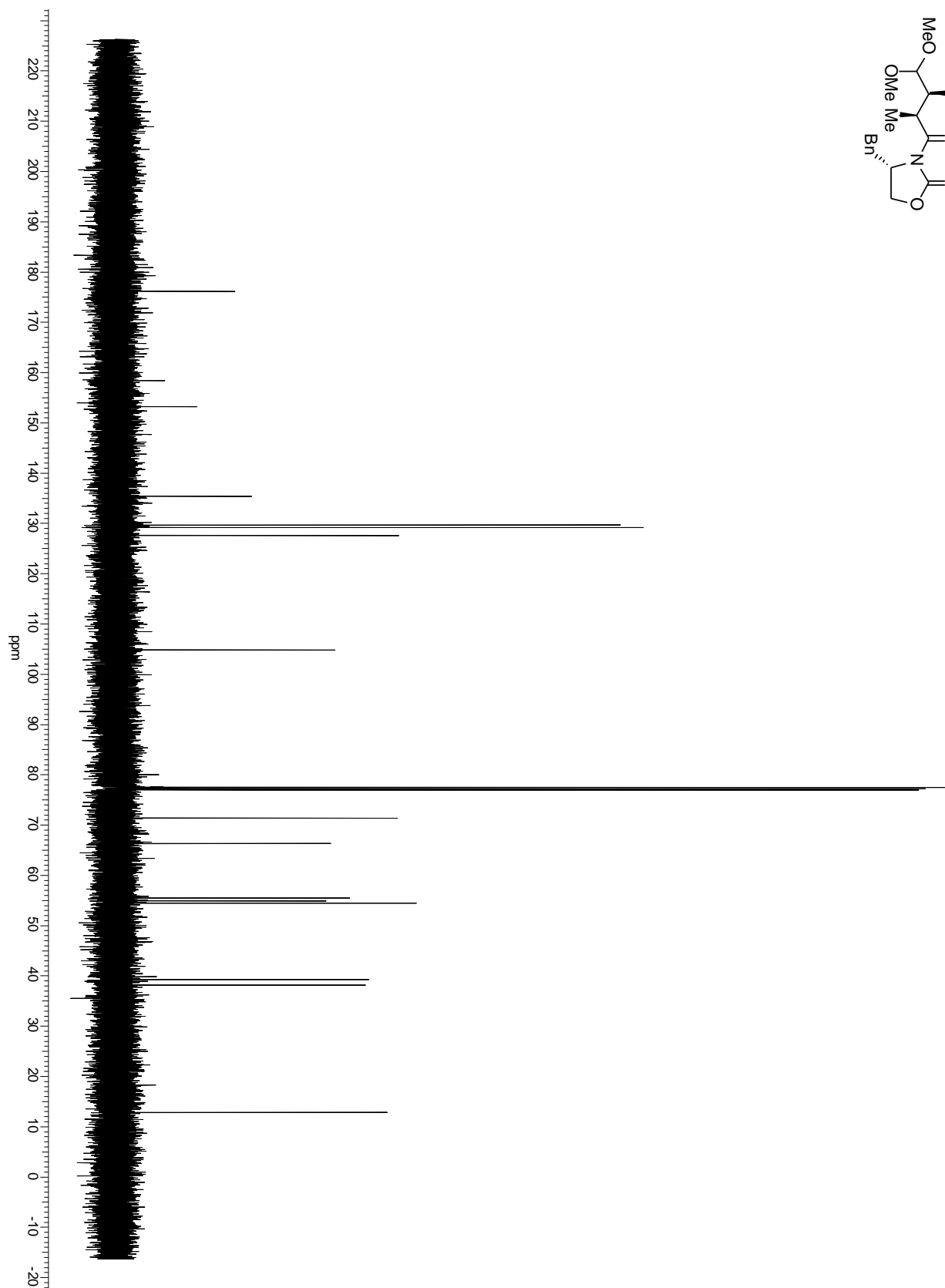
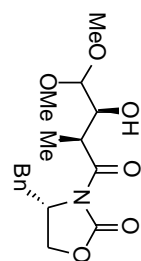
To quantify the ratio of siRNA molecules per QD, the siRNA linked to QDs via **6.6** (disulfide bond) were treated with DTT for 1 hour. After centrifugation, the supernatant was analyzed under UV at 260 nm to quantify the amount of siRNA detached from QDs. By determining the concentration of QDs in the same volume at the first absorption peak,¹⁰ the number of siRNA molecules per QD was estimated. For the conjugation of HIV-Tat(CYGRKKRRQRRR) and RGD(RGDC) to siRNA-QD, the same method as that used to conjugate siRNA to QDs was used to determine the ratio of 1:10:10 (siRNA:RGD:HIV-Tat).

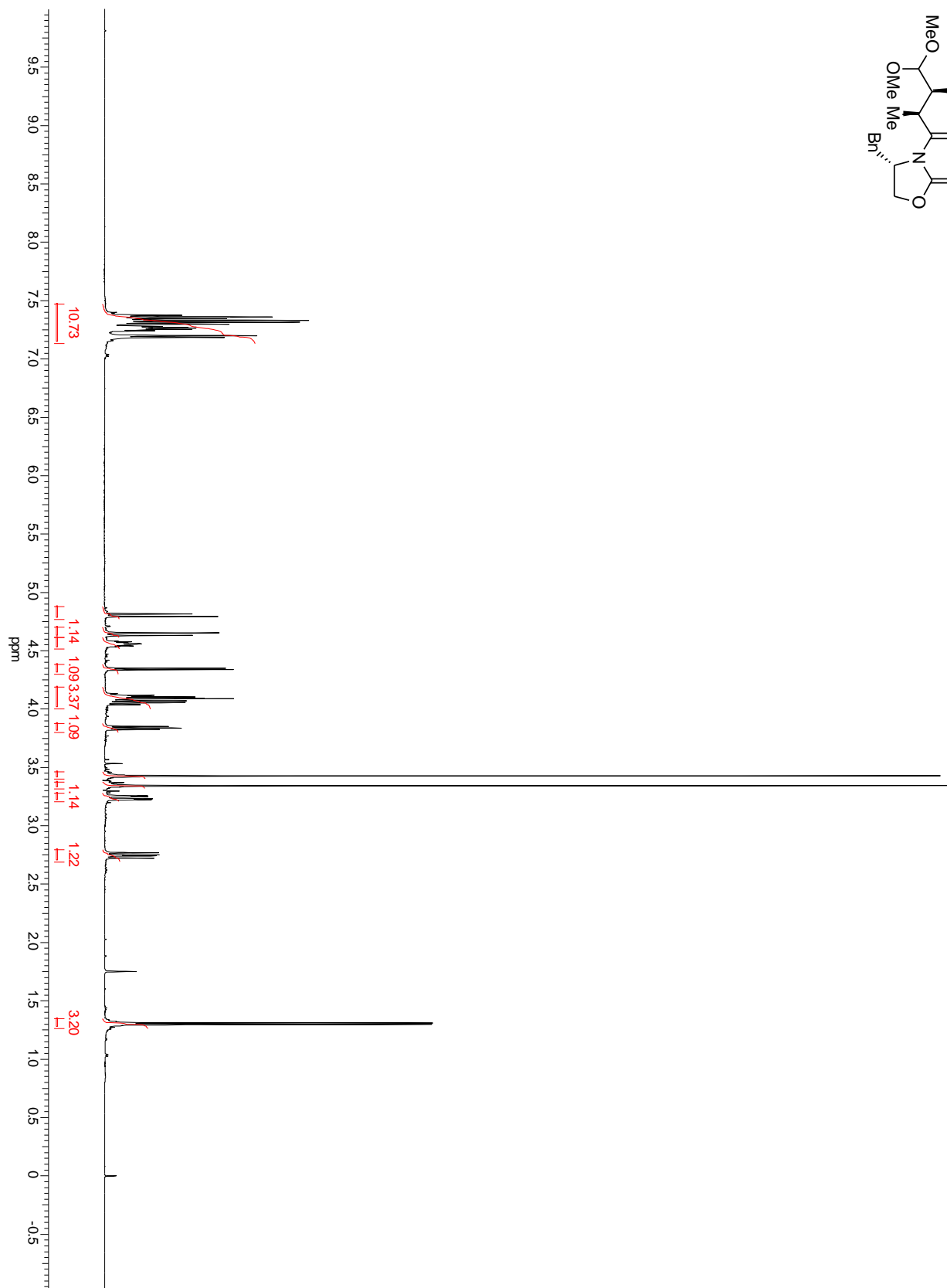
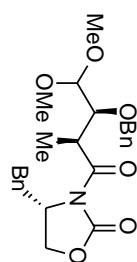
7.6. References

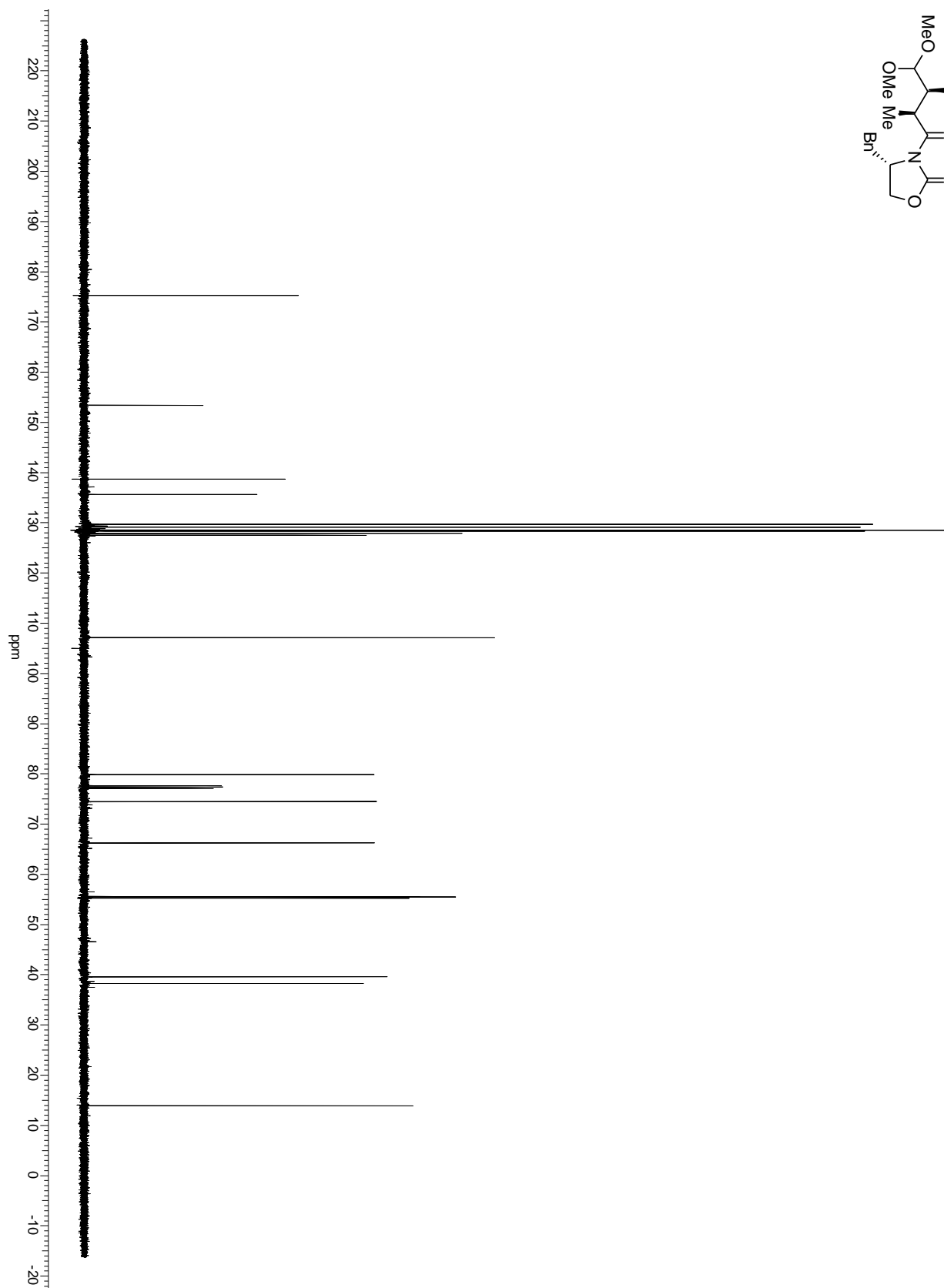
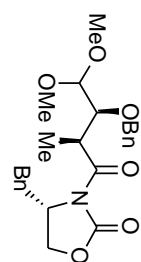
1. Li, J. J.; Wang, Y. A.; Guo, W.; Keay, J. C.; Mishima, T. D.; Johnson, M. B.; Peng, X. *J. Am. Chem. Soc.* **2003**, *125*, 12567.
2. Xie, R.; Kolb, U.; Li, J.; Basch, T.; Mews, A. *J. Am. Chem. Soc.* **2005**, *127*, 7480.
3. Liu, W.; Howarth, M.; Greytak, A. B.; Zheng, Y.; Nocera, D. G.; Ting, A. Y.; Bawendi, M. G. *J. Am. Chem. Soc.* **2008**, *130*, 1274.
4. Susumu, K.; Uyeda, H. T.; Medintz, I. L.; Pons, T.; Delehanty, J. B.; Mattoussi, H. *J. Am. Chem. Soc.* **2007**, *129*, 13987.
5. Chirakul, P.; Prez-Luna, V. H.; Owen, H.; Lapez, G. P.; Hampton, P. D. *Langmuir* **2002**, *18*, 4324.
6. Kamruzzahan, A. S. M.; Ebner, A.; Wildling, L.; Kienberger, F.; Riener, C. K.; Hahn, C. D.; Pollheimer, P. D.; Winklehner, P.; Hzl, M.; Lackner, B.; Schrk, D. M.; Hinterdorfer, P.; Gruber, H. *J. Bioconjugate Chemistry* **2006**, *17*, 1473.
7. Kida, S.; Maeda, M.; Hojo, K.; Eto, Y.; Nakagawa, S.; Kawasakia, K. *Chemical & Pharmaceutical Bulletin* **2007**, *55*, 685.
8. Bell, I. M.; Abell, C.; Leeper, F. J. *J. Chem. Soc., Perkin Trans 1* **1994**, *14*, 1997.
9. Mantovani, G.; Lecolley, F. o.; Tao, L.; Haddleton, D. M.; Clerx, J.; Cornelissen, J. J. L. M.; Velonia, K. *J. Am. Chem. Soc.* **2005**, *127*, 2966.
10. Yu, W. W.; Qu, L.; Guo, W.; Peng, X. *Chem. Mat.* **2003**, *15*, 2854.
11. Jung, J.; Solanki, A.; Memoli, K. A.; Kamei, K.-i.; Kim, H.; Drahl, M. A.; Williams, L. J.; Tseng, H.-R.; Lee, K. *Angw. Chem. Int. Ed. Engl.* **2010**, *49*, 103.

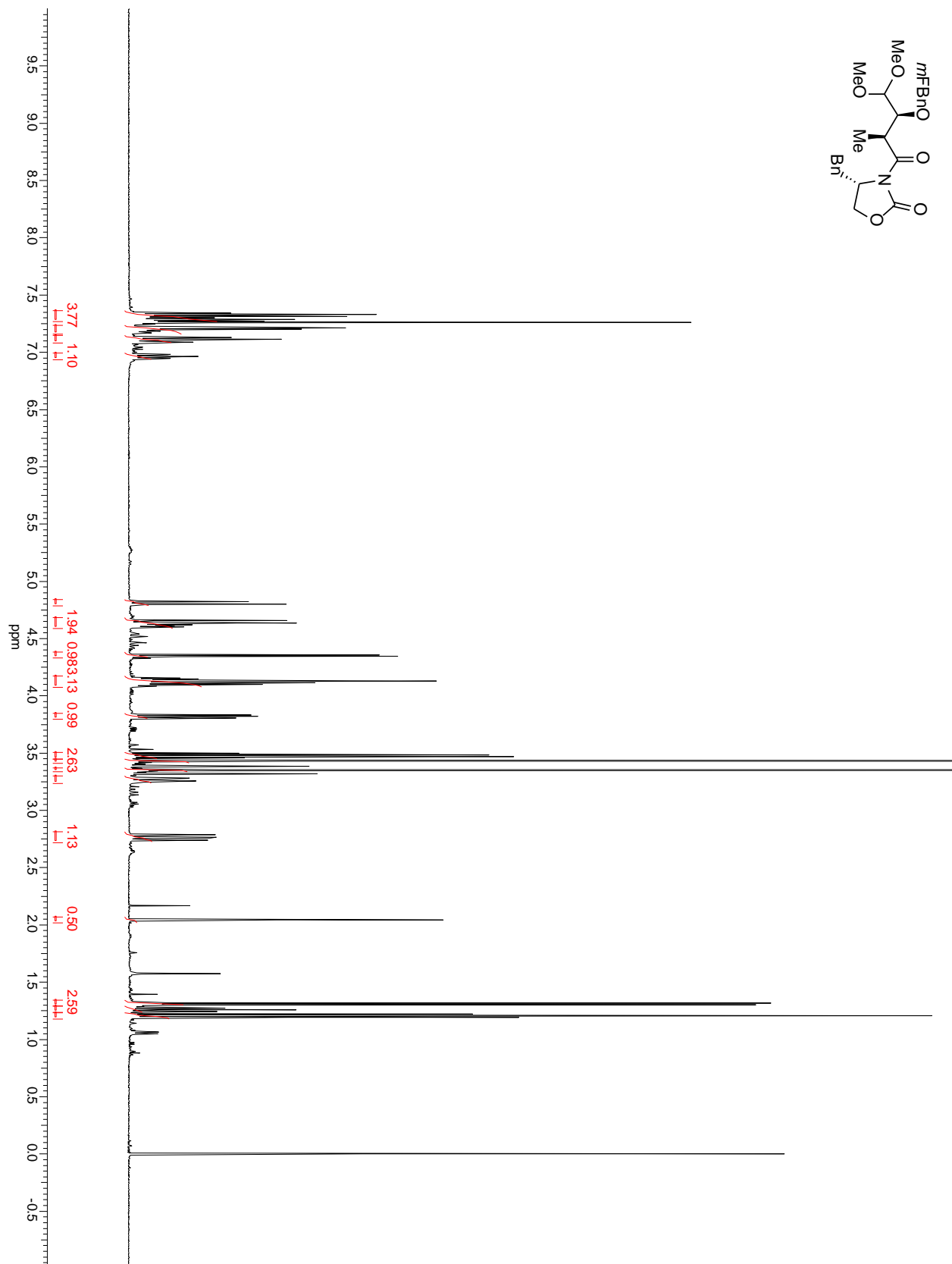
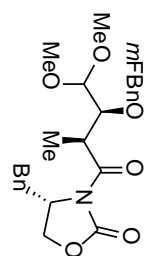
Appendix: Spectral Data

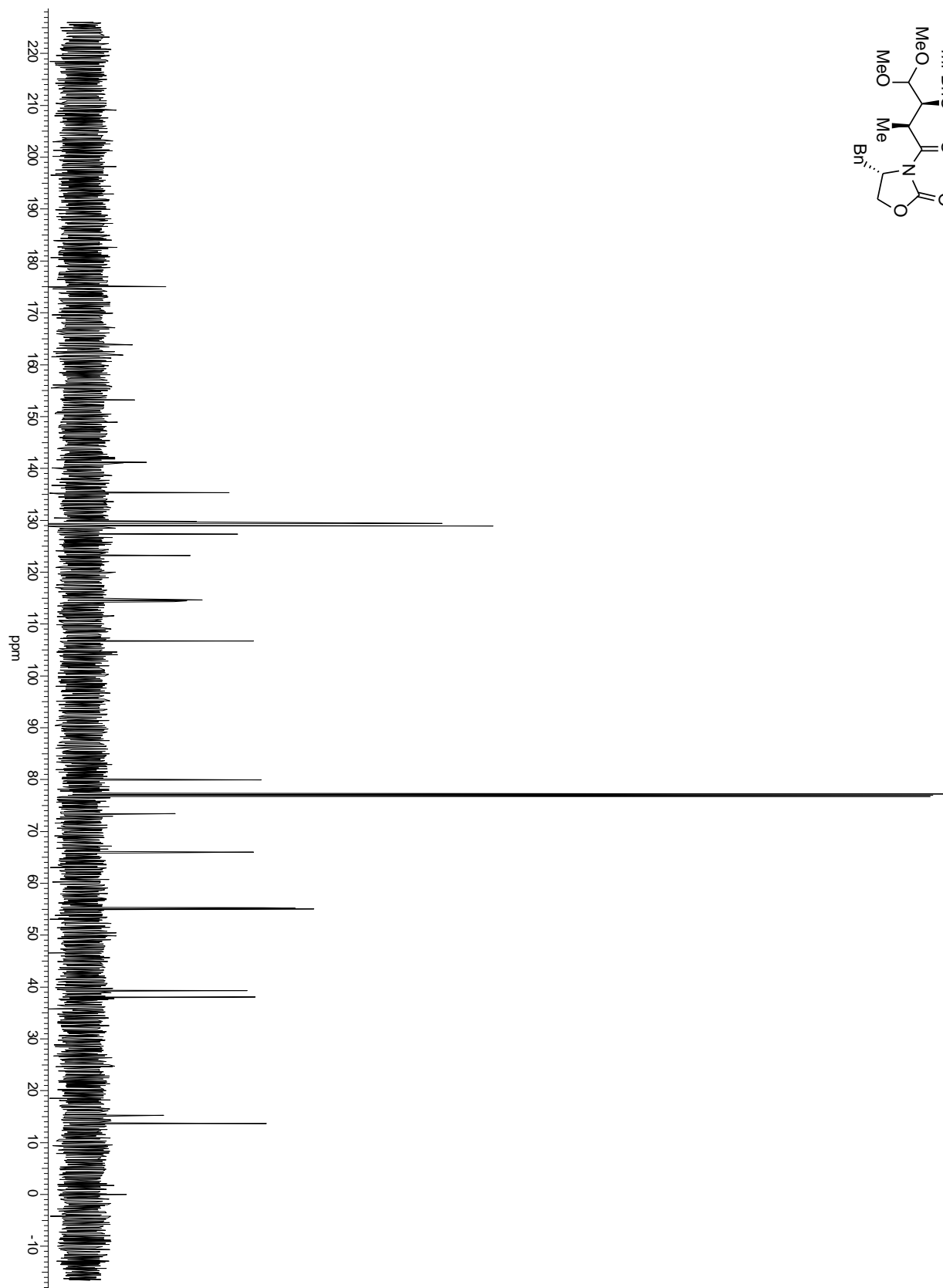
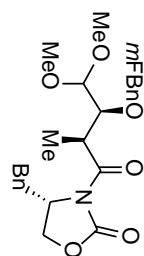


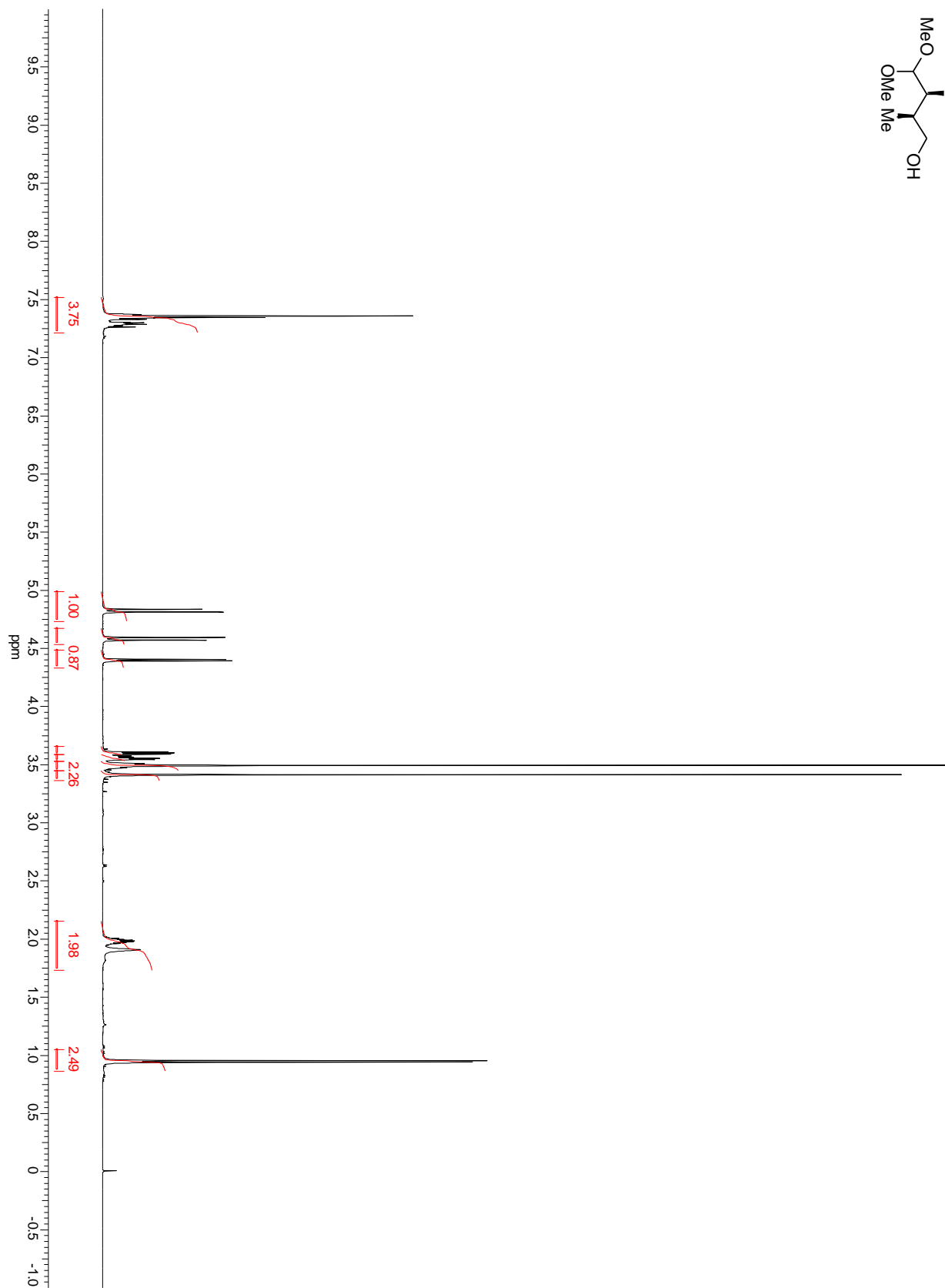
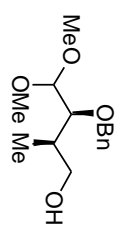


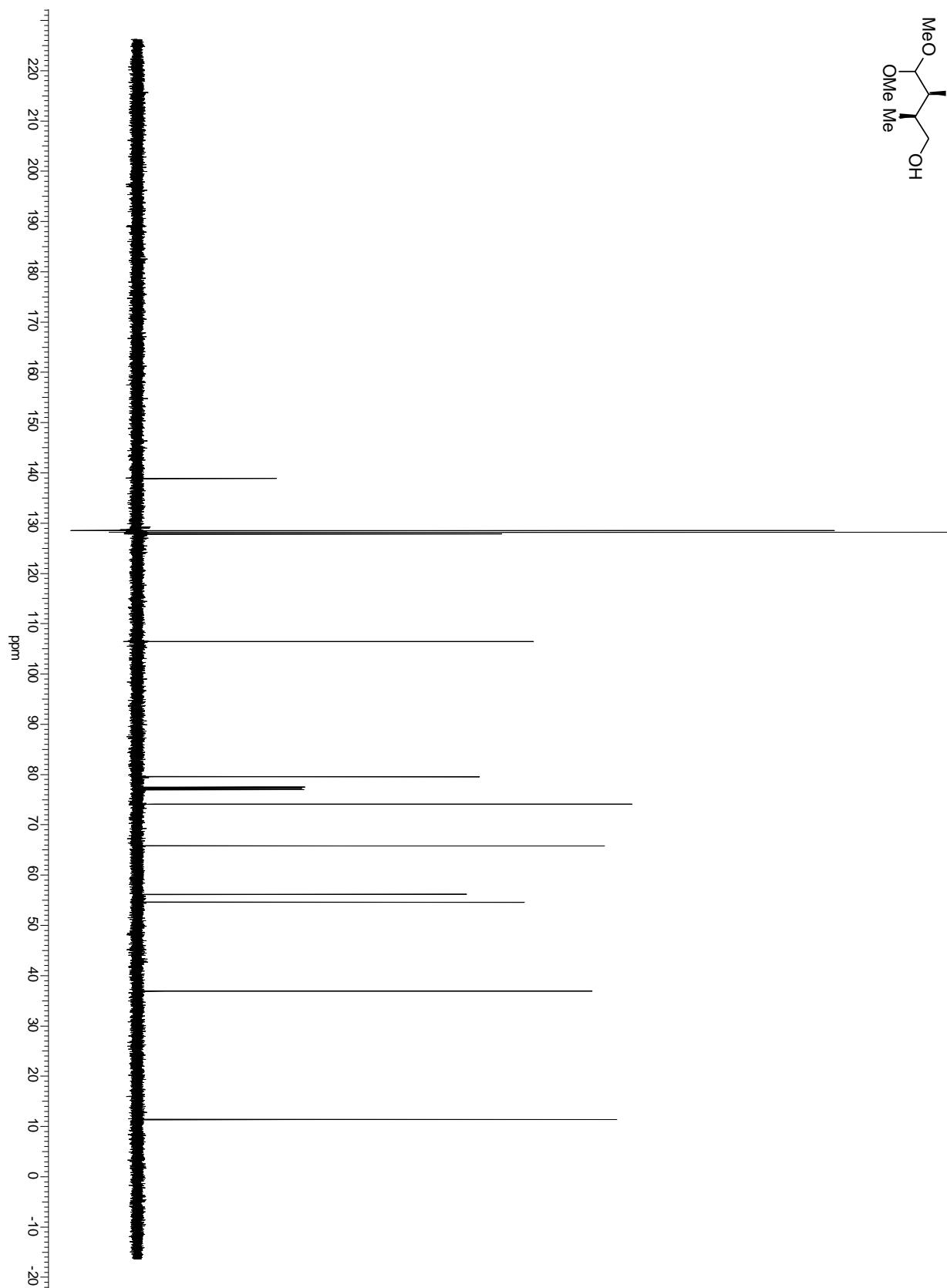
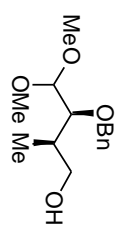


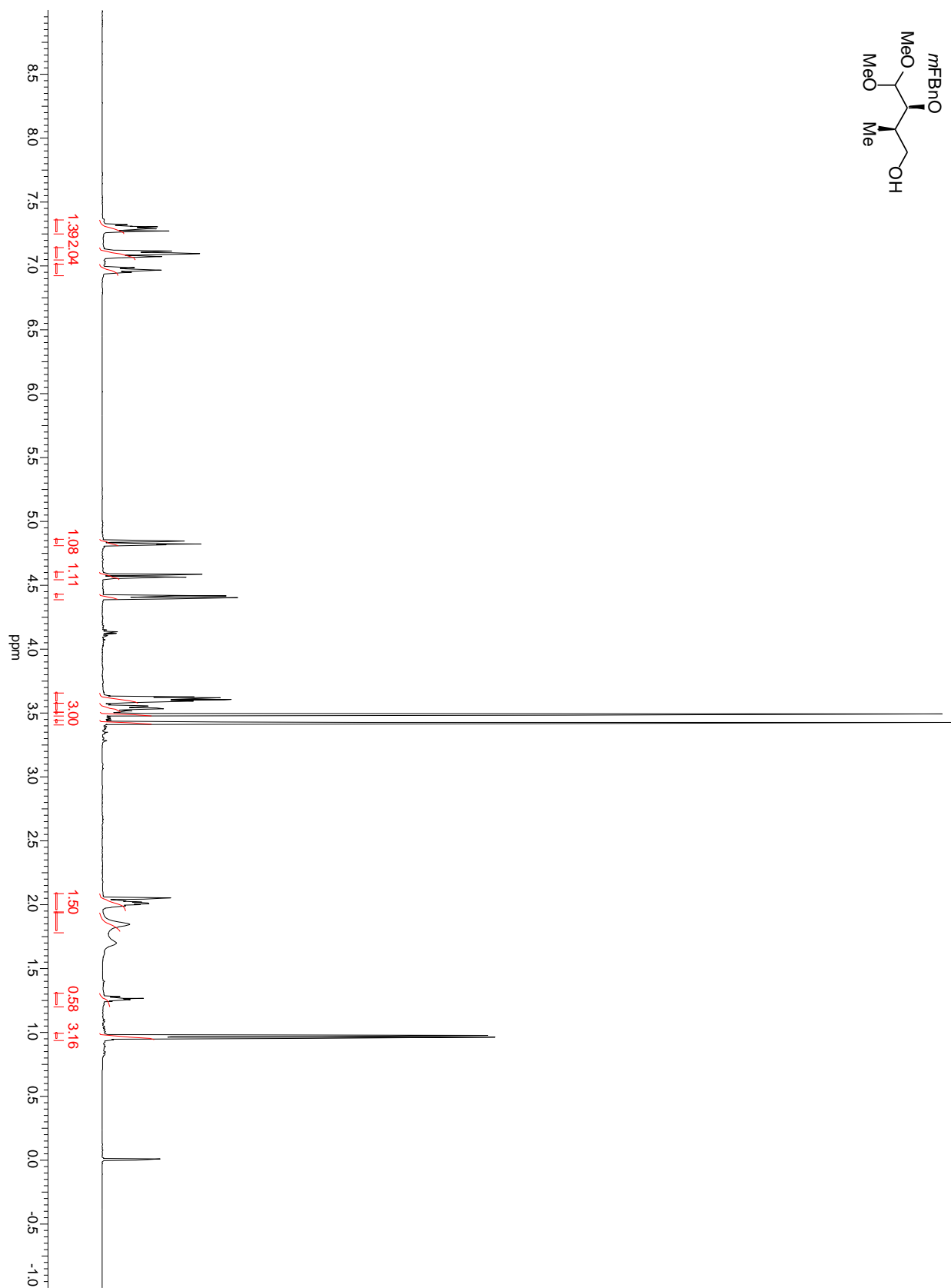
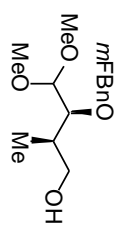


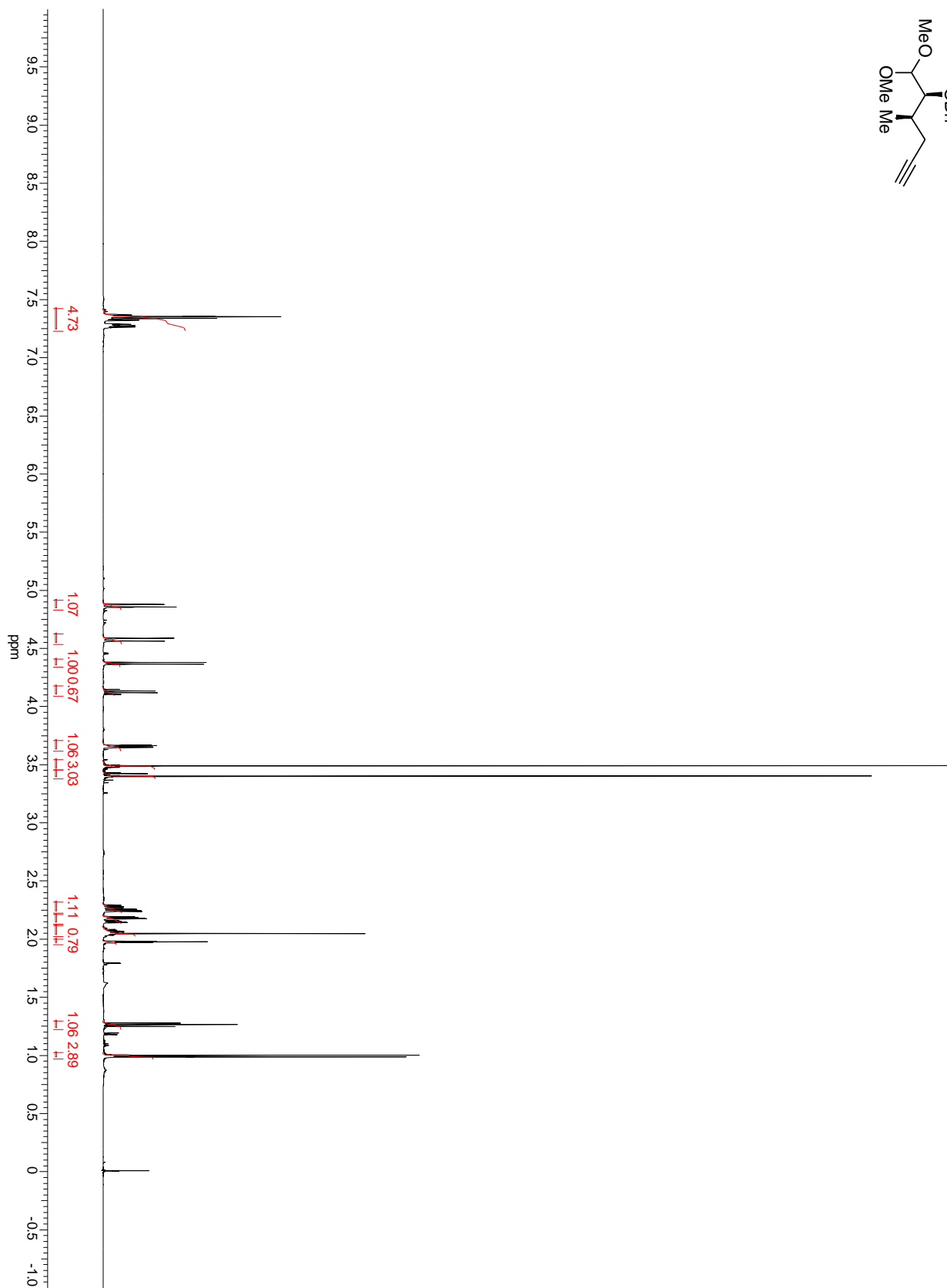
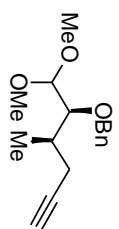


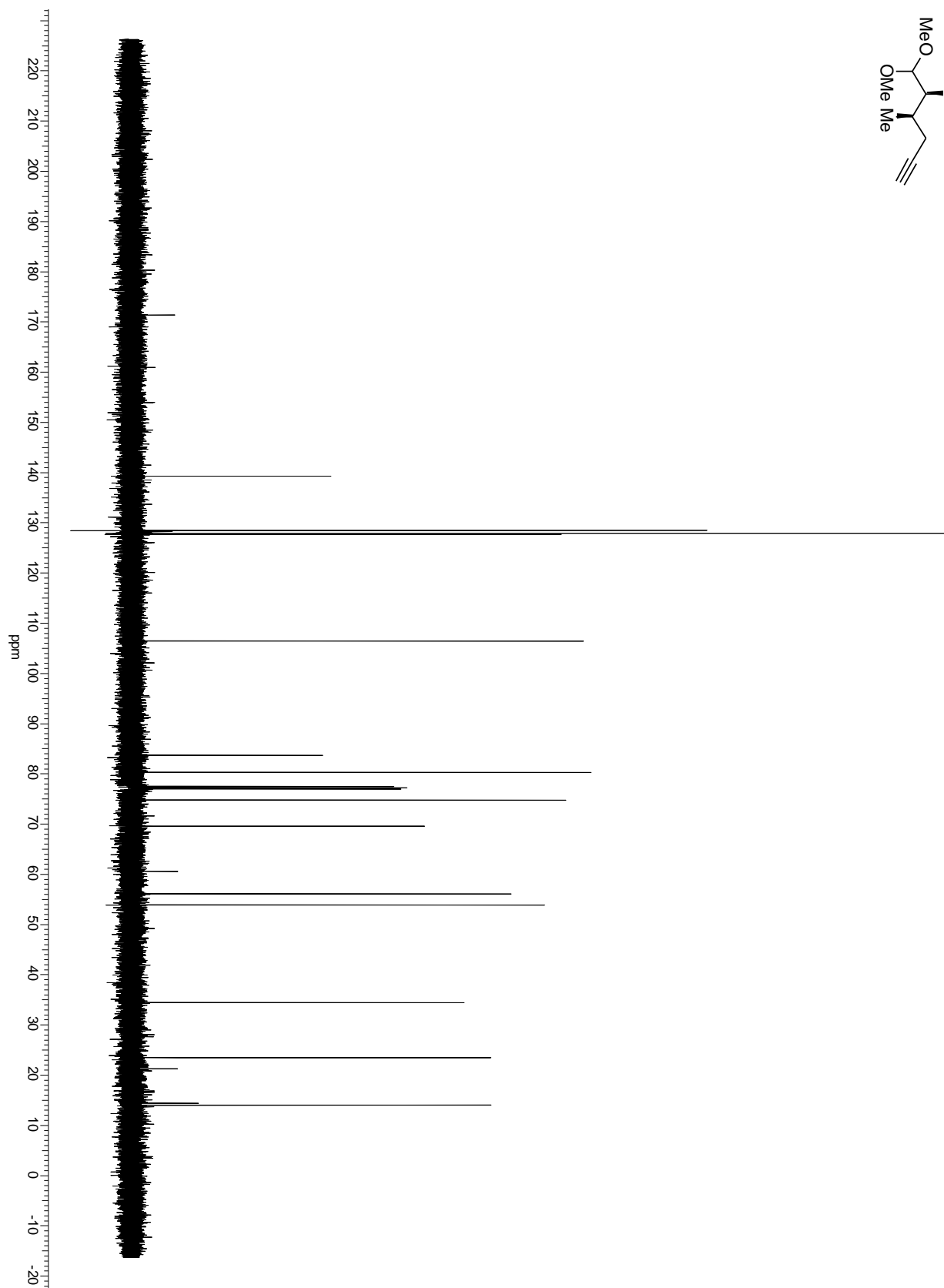


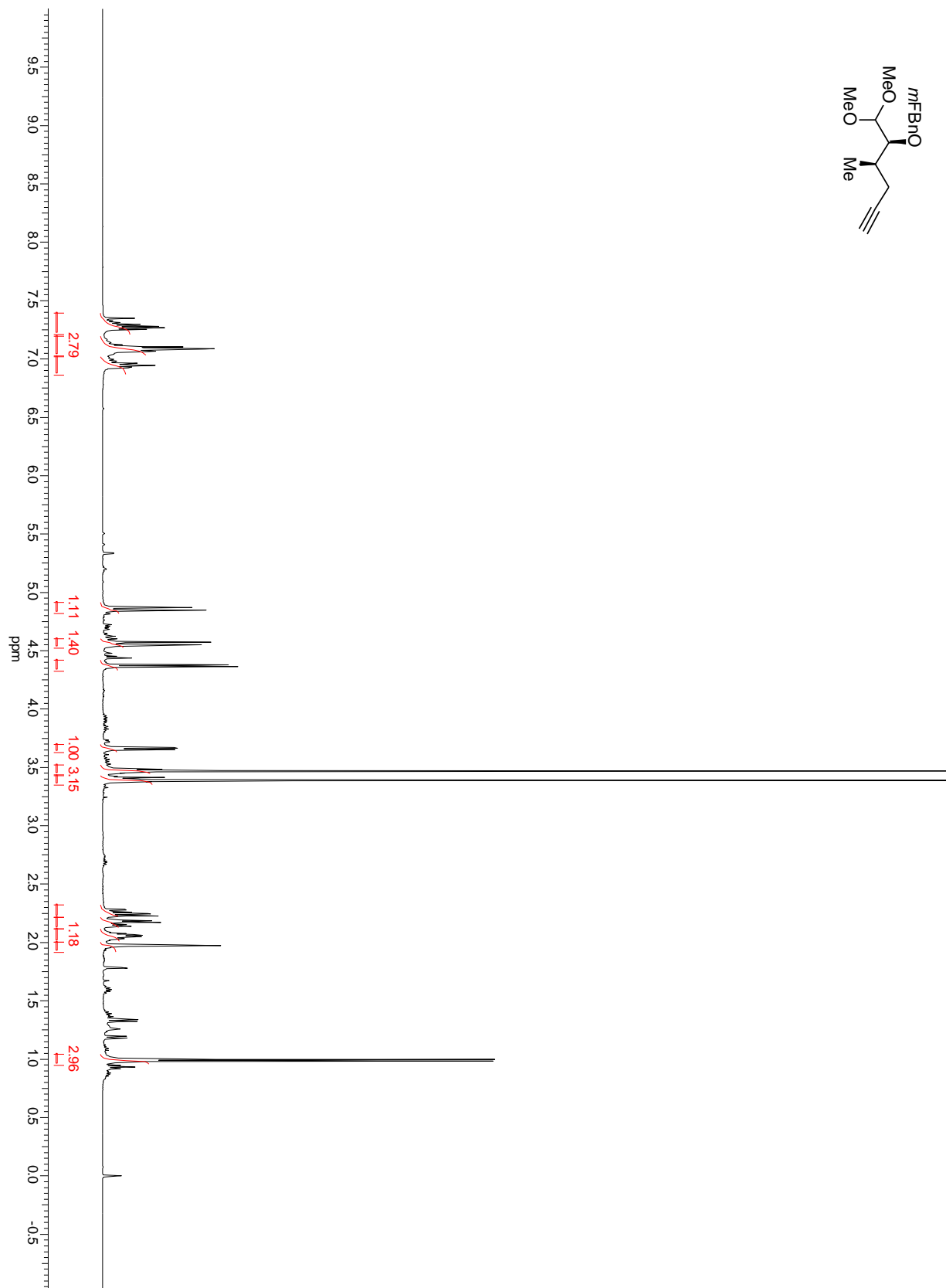
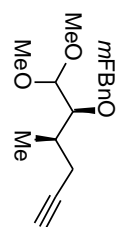


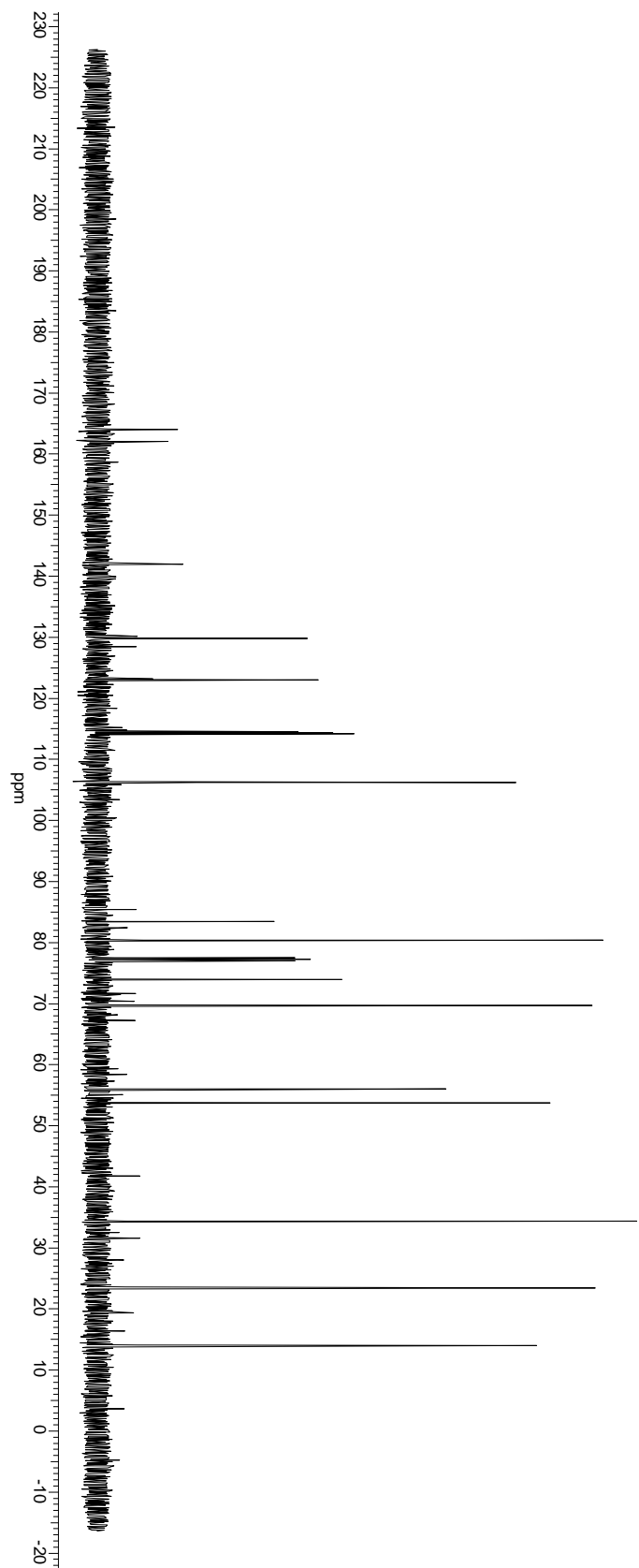
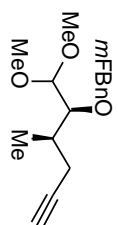


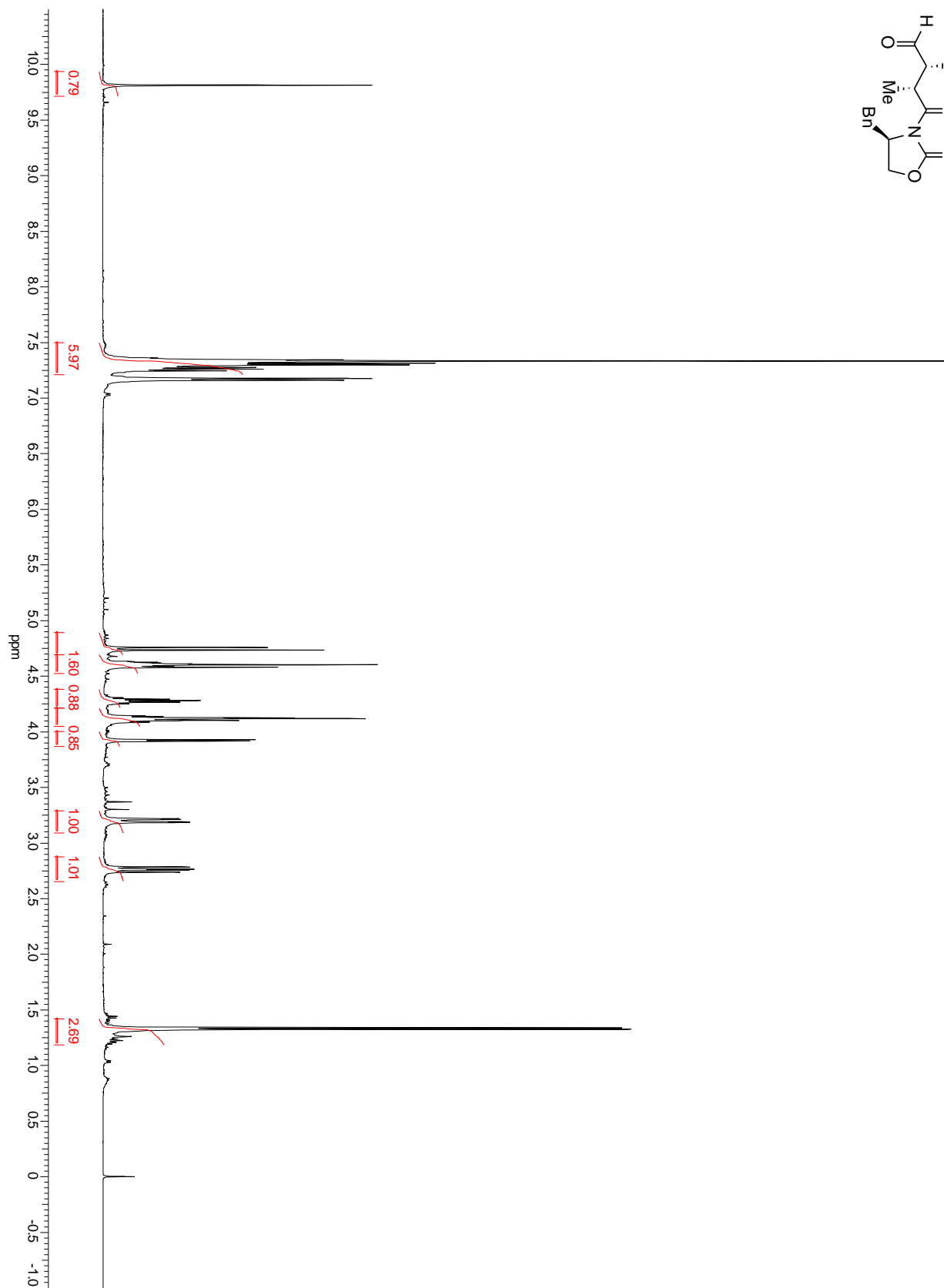
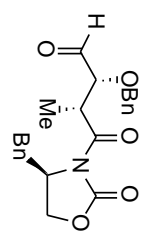


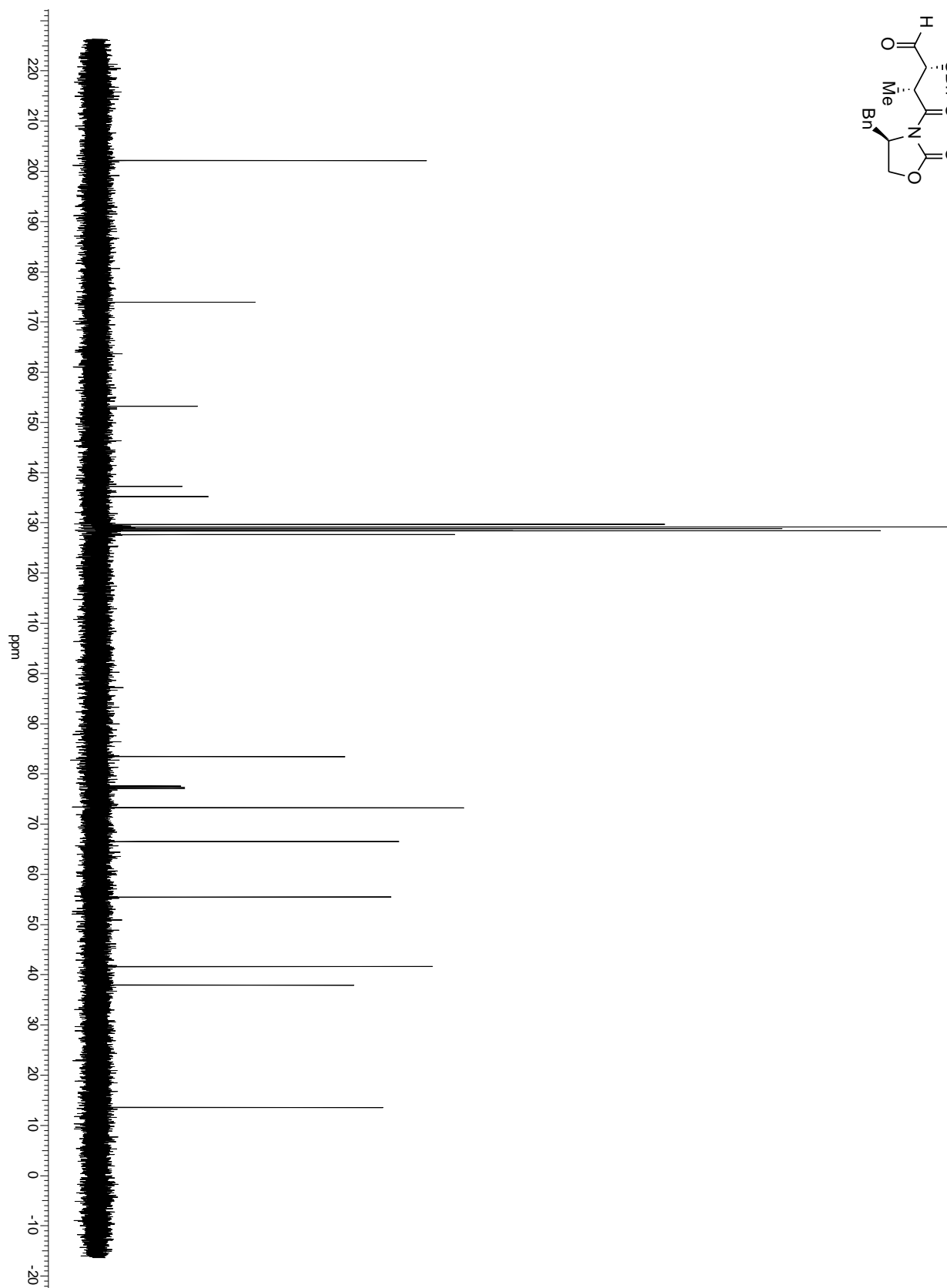
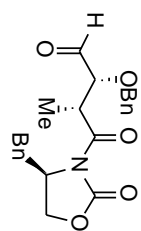


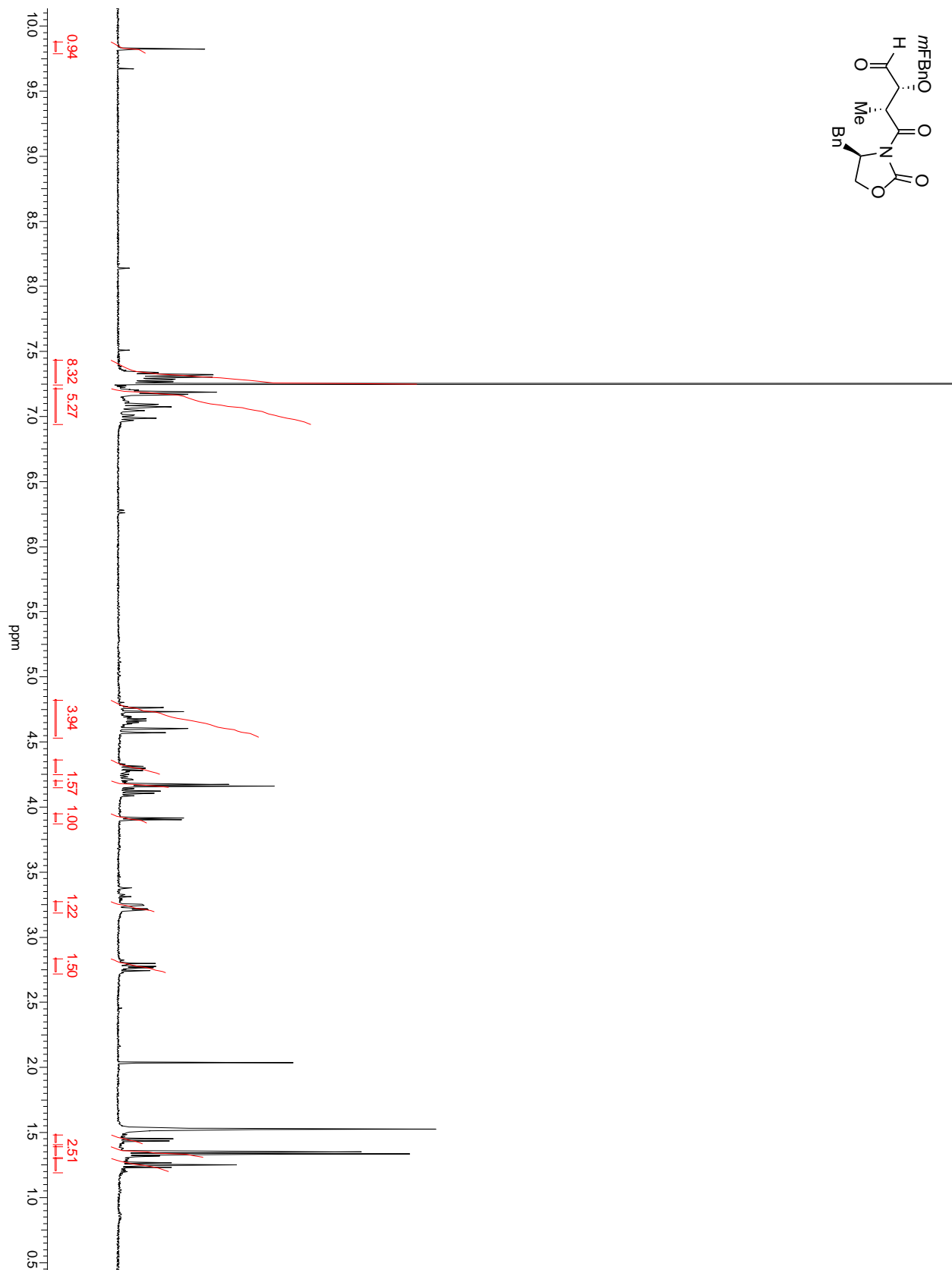
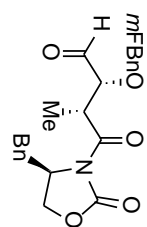


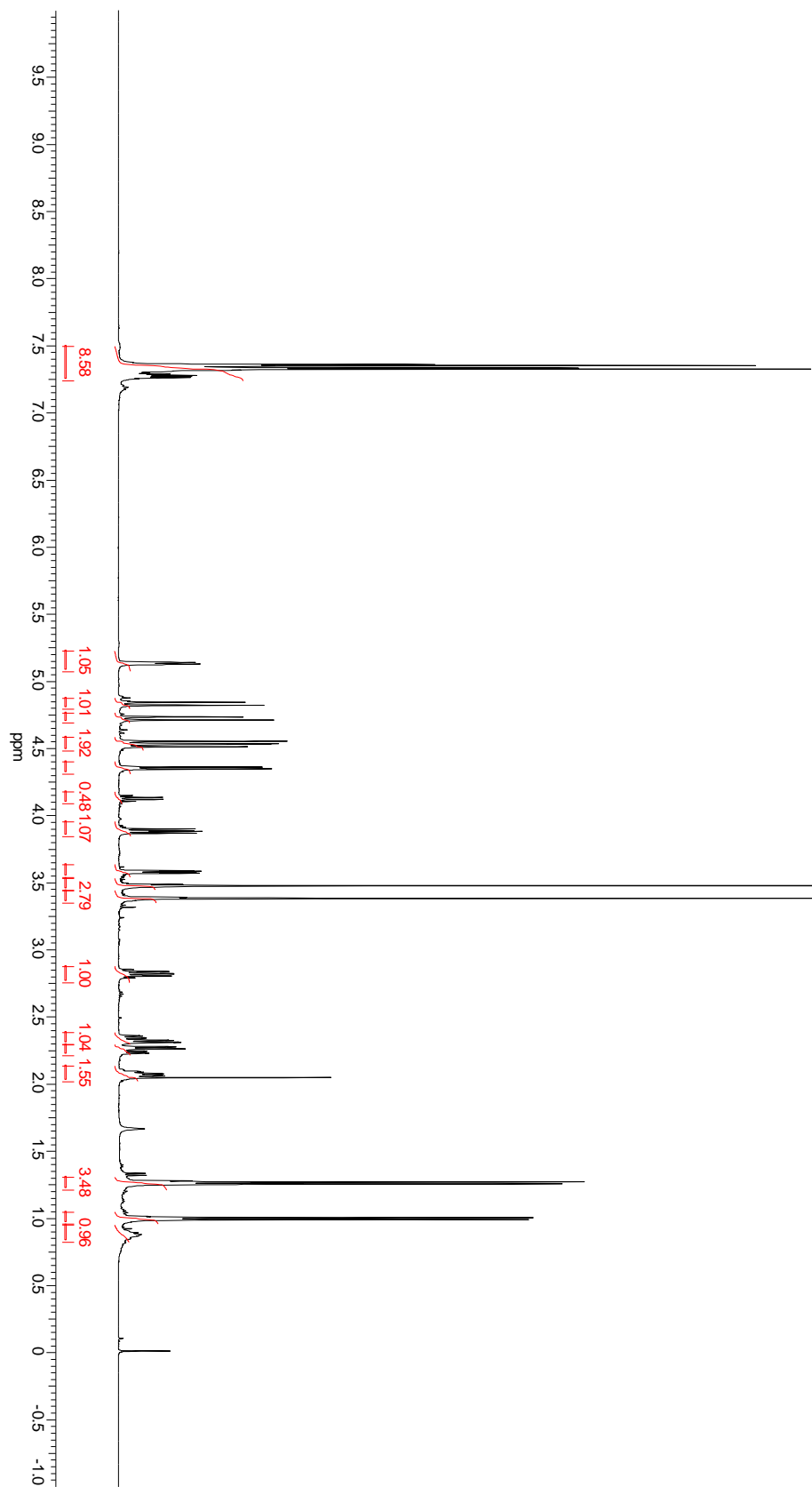
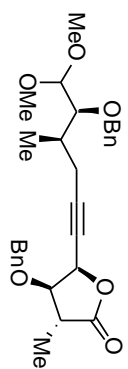


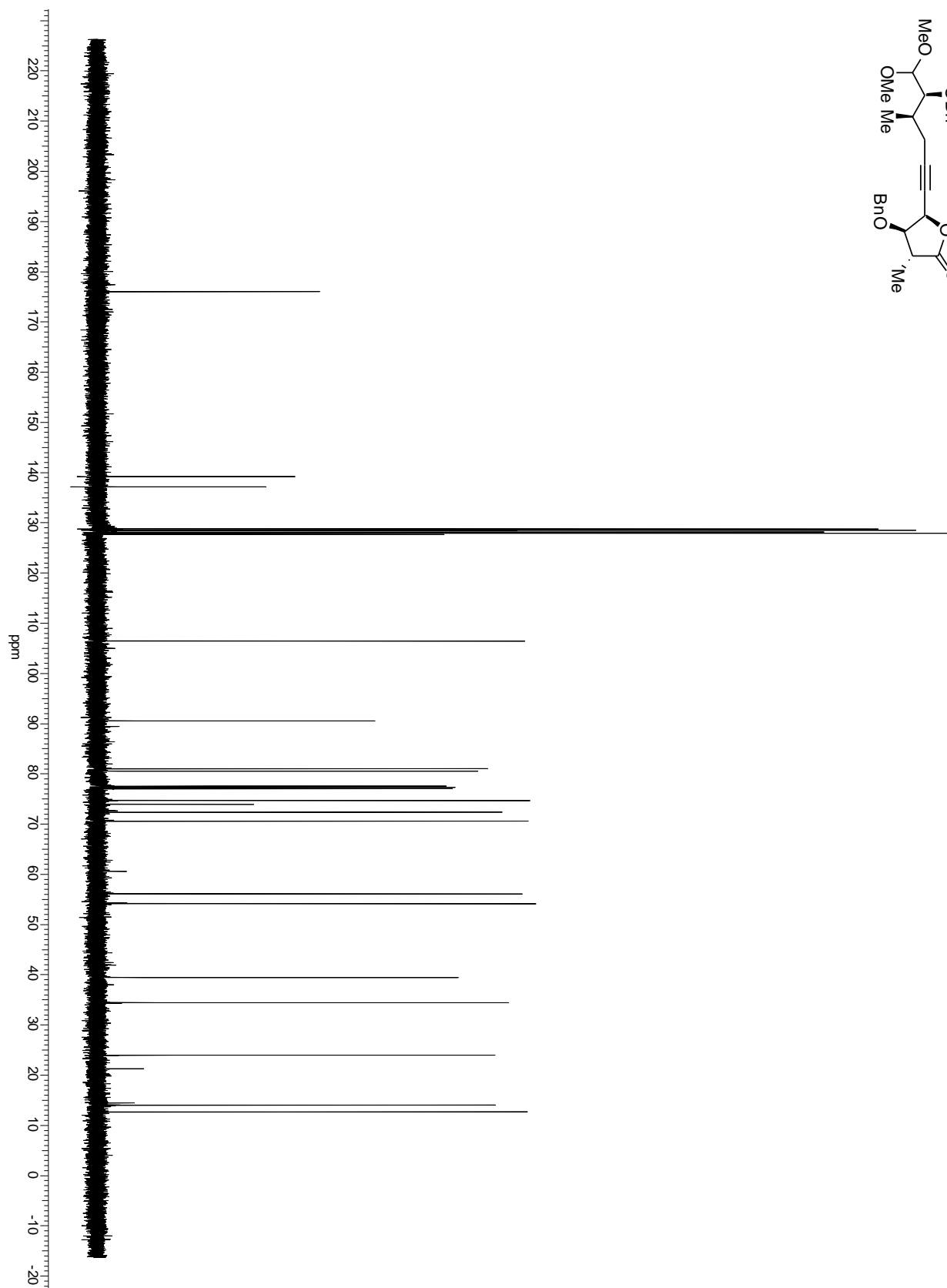
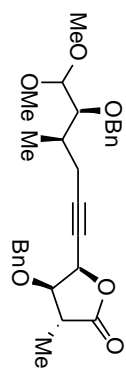


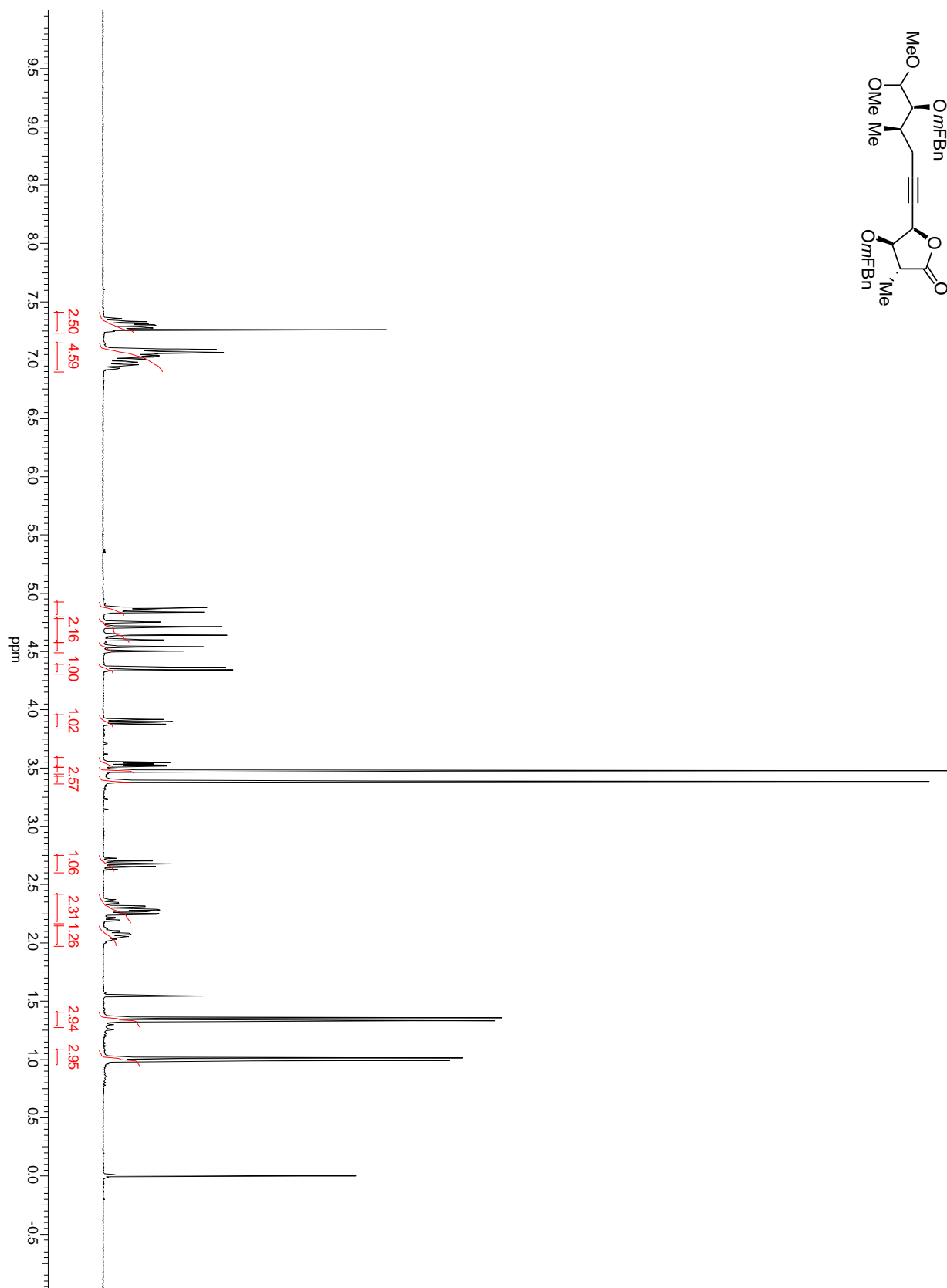
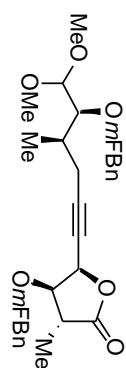


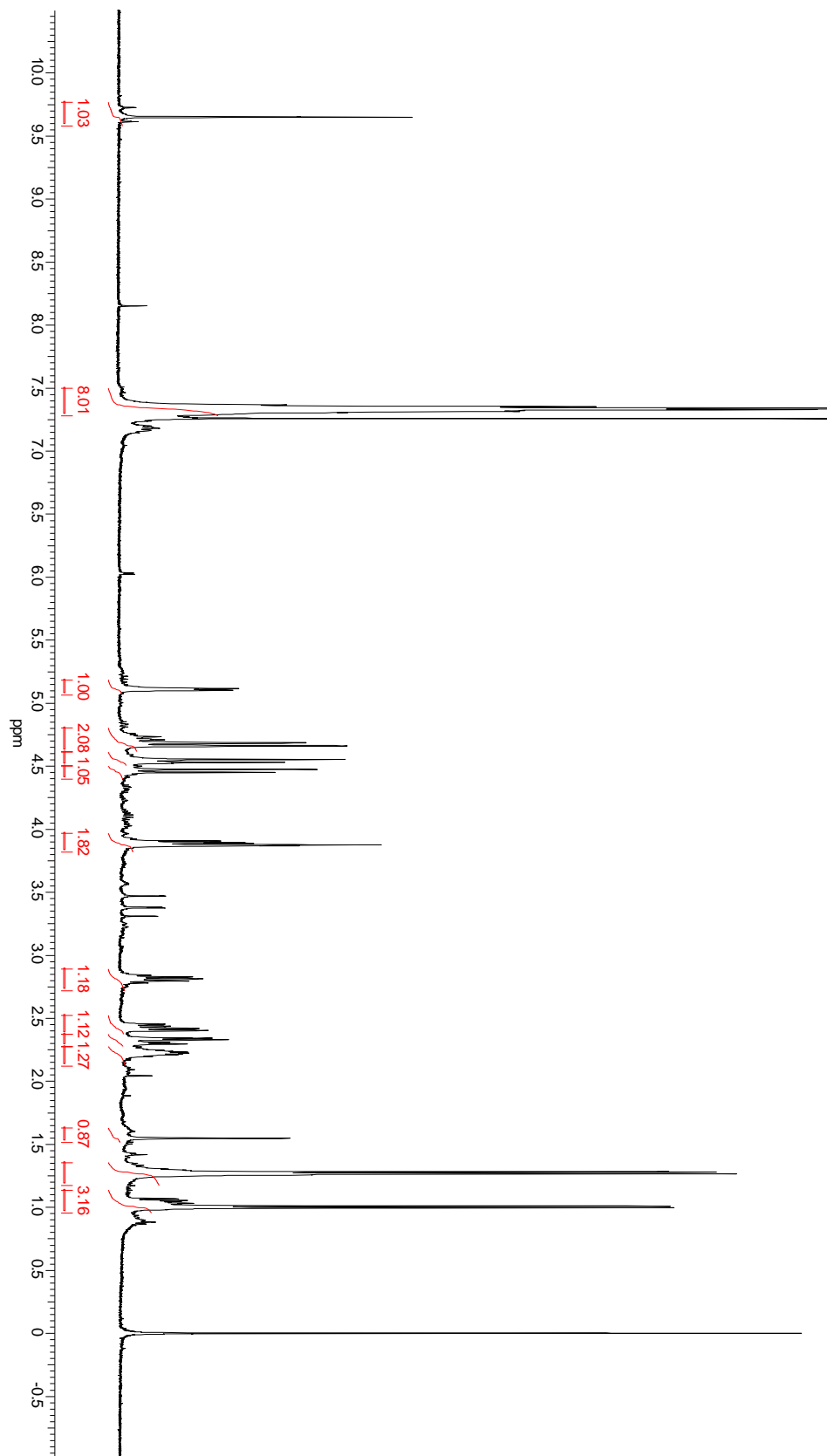
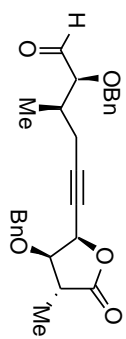


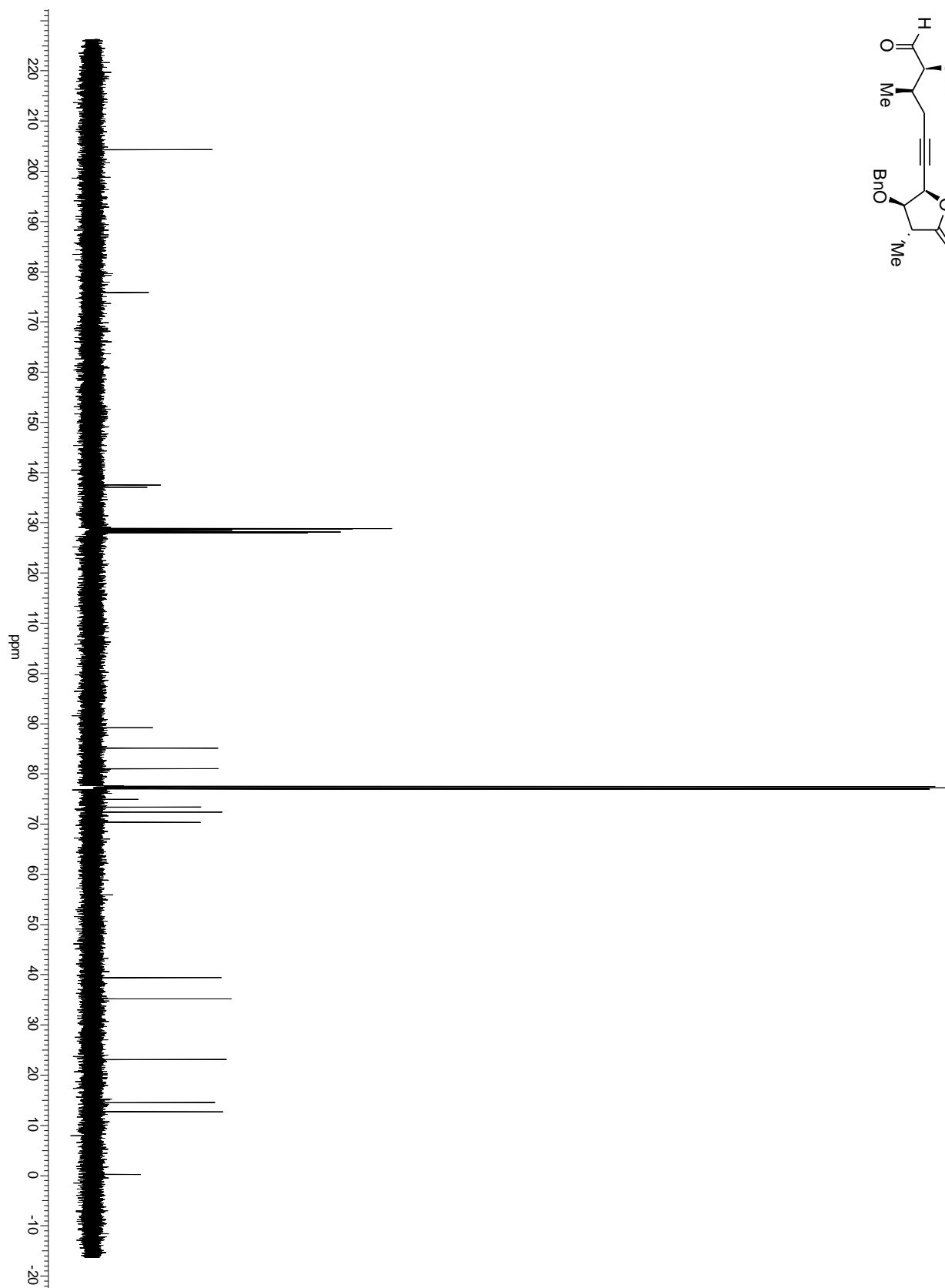
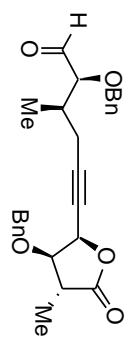


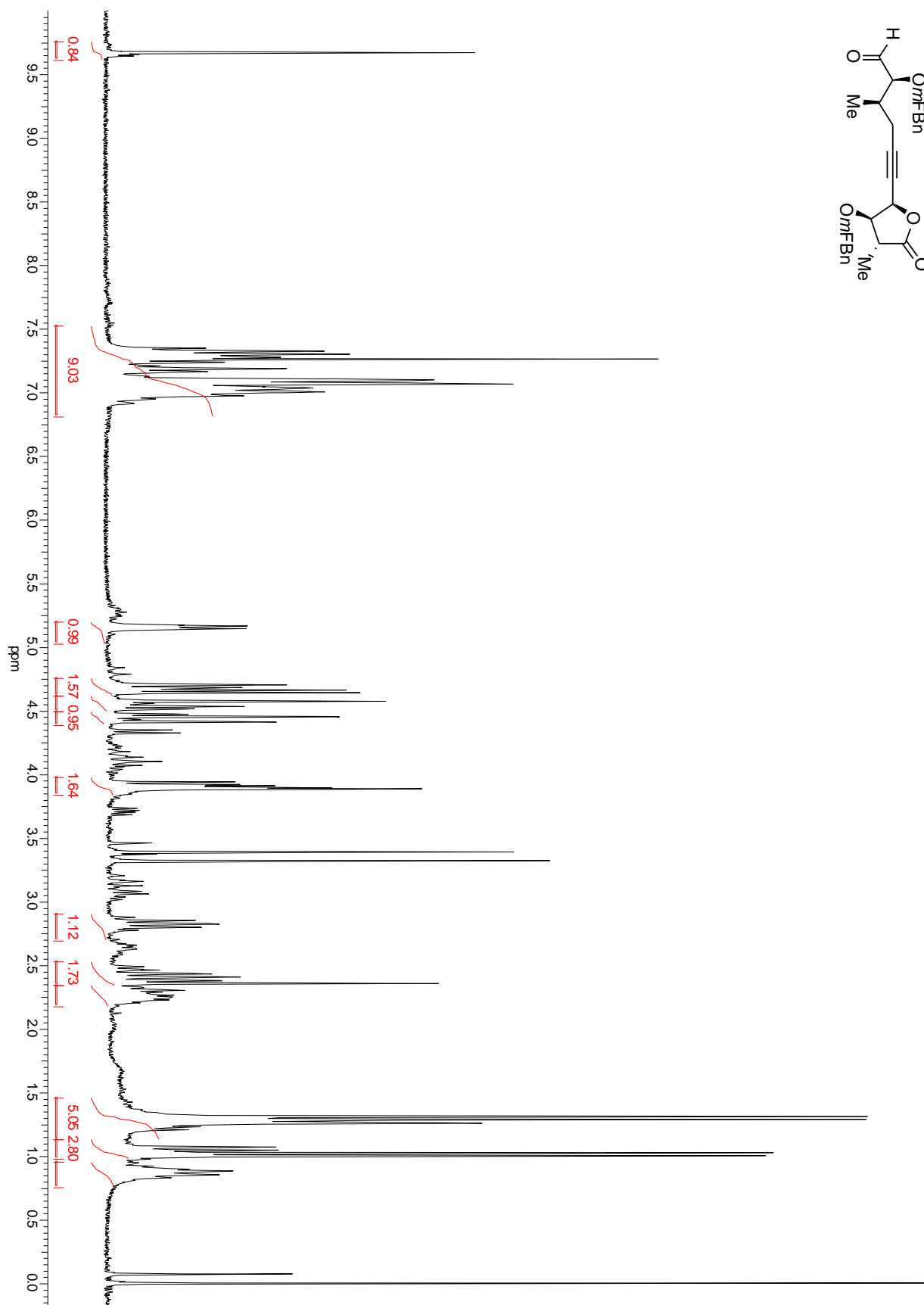
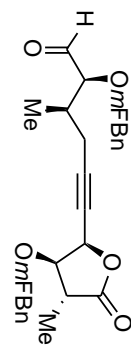


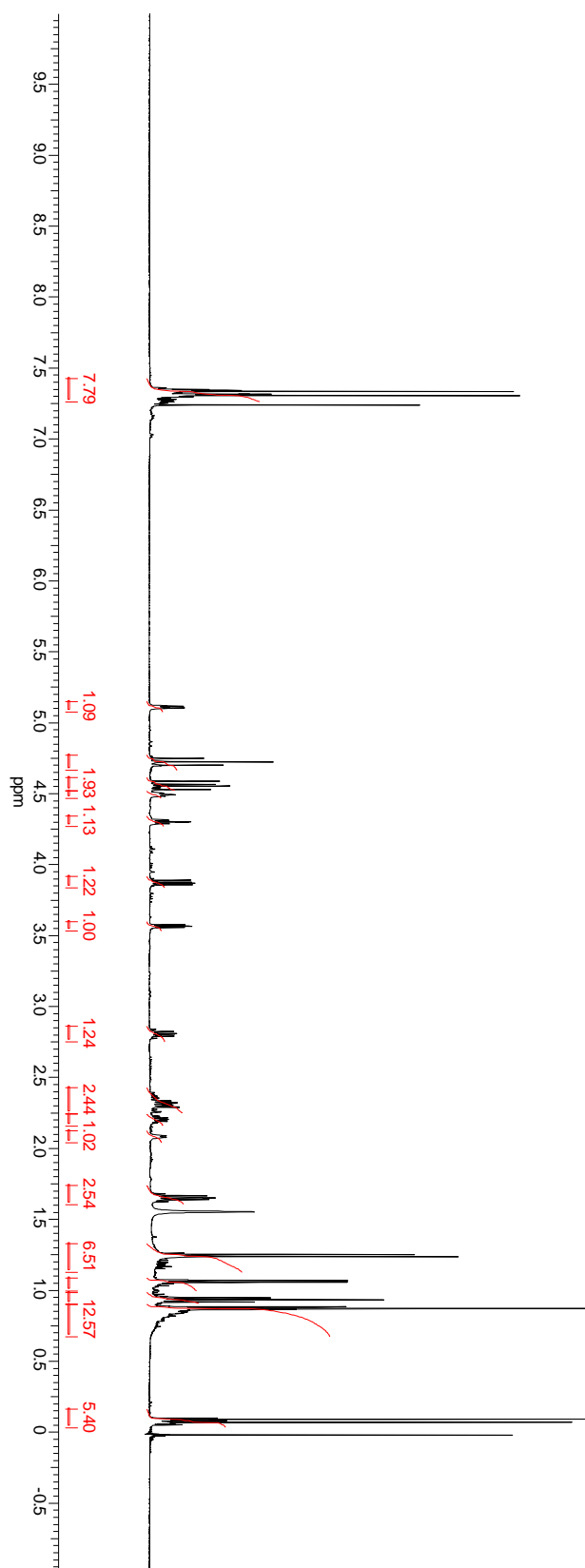
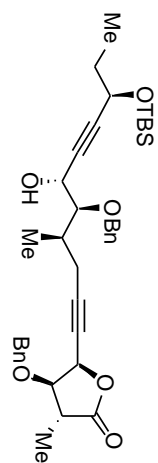


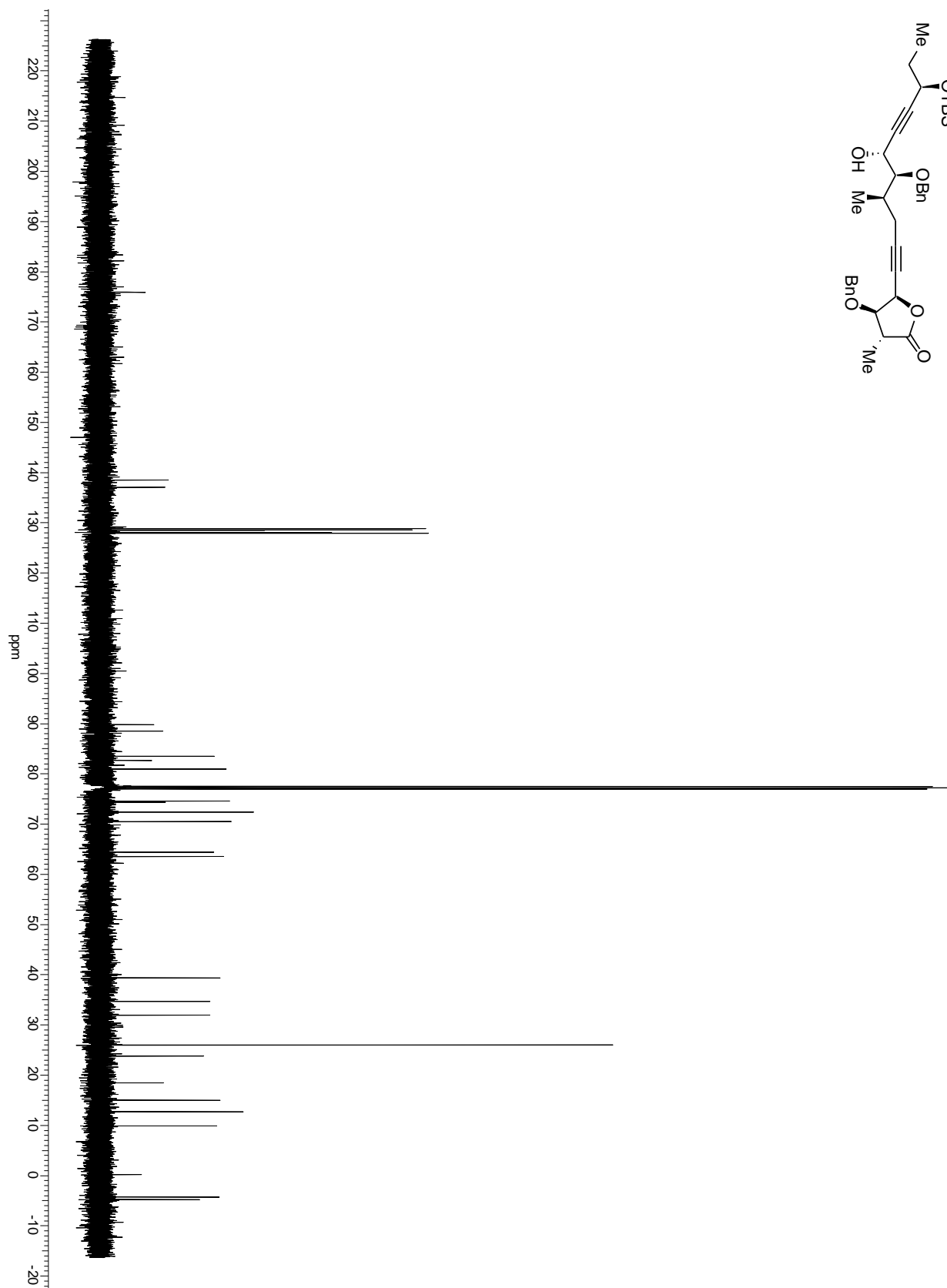
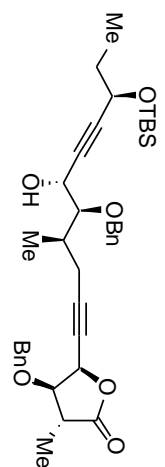


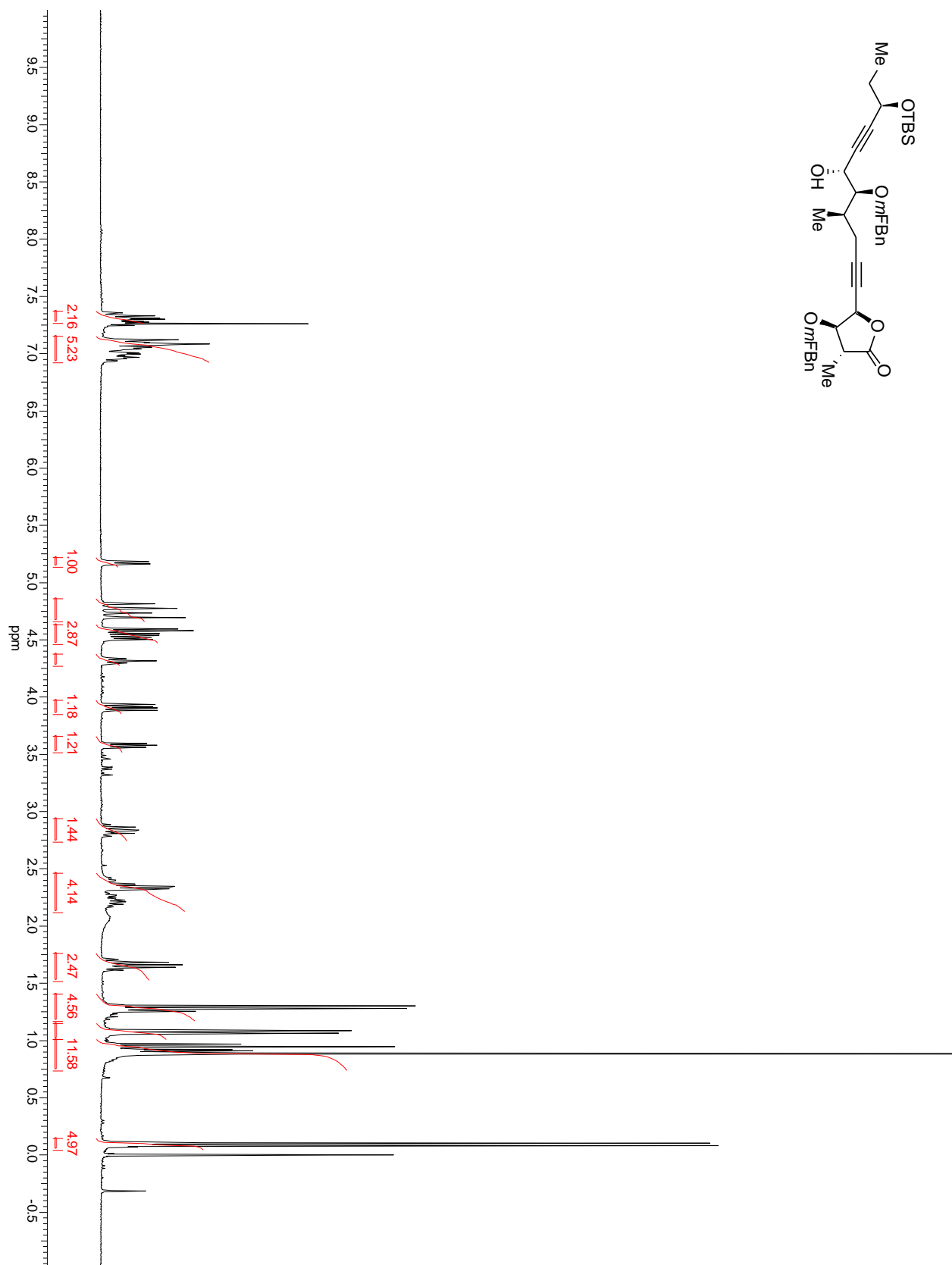
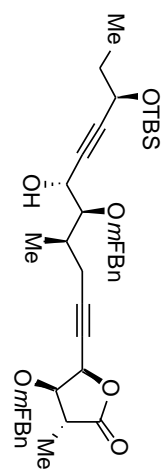


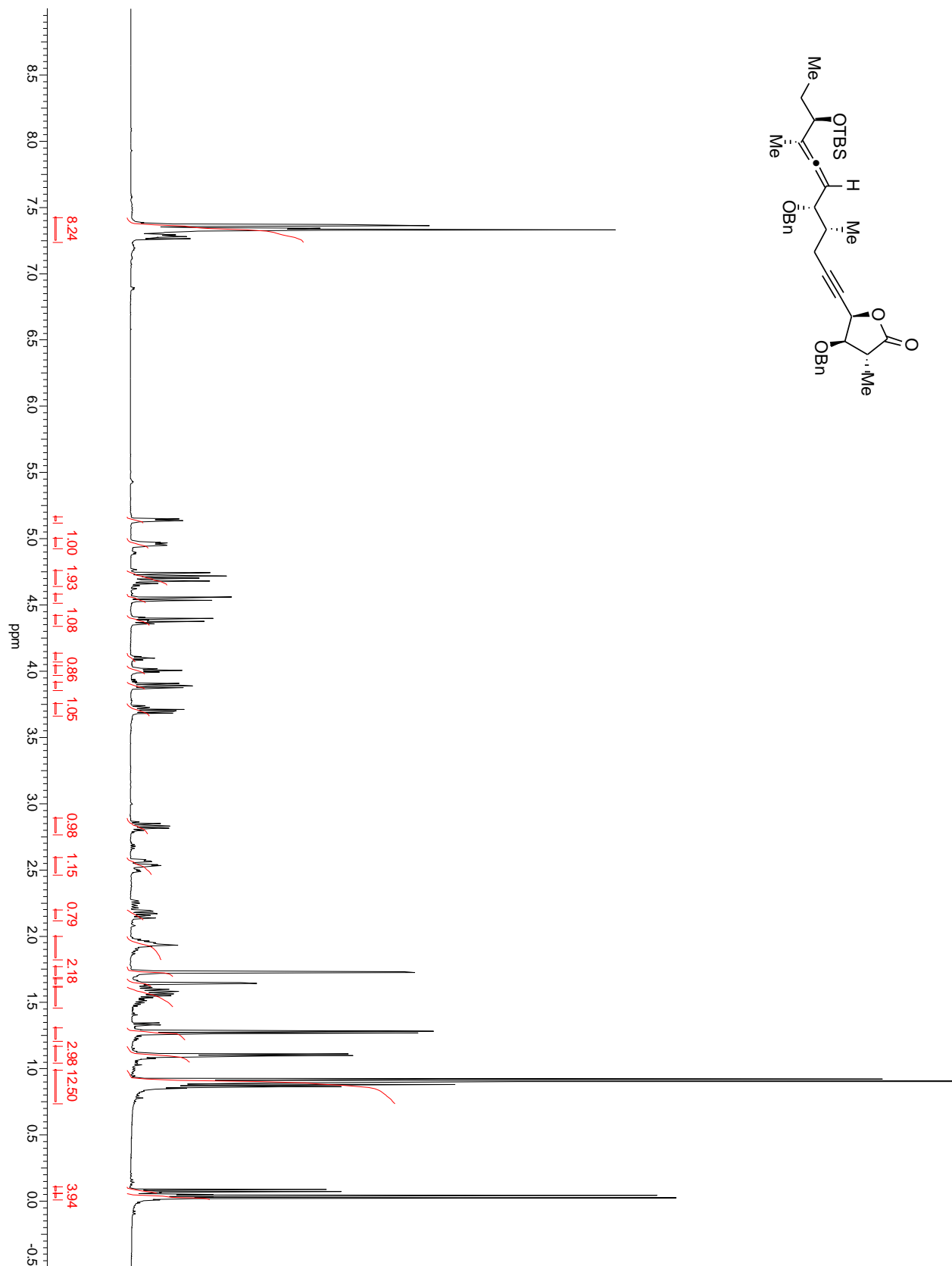
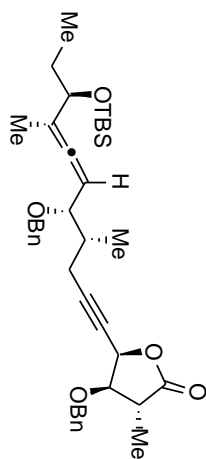


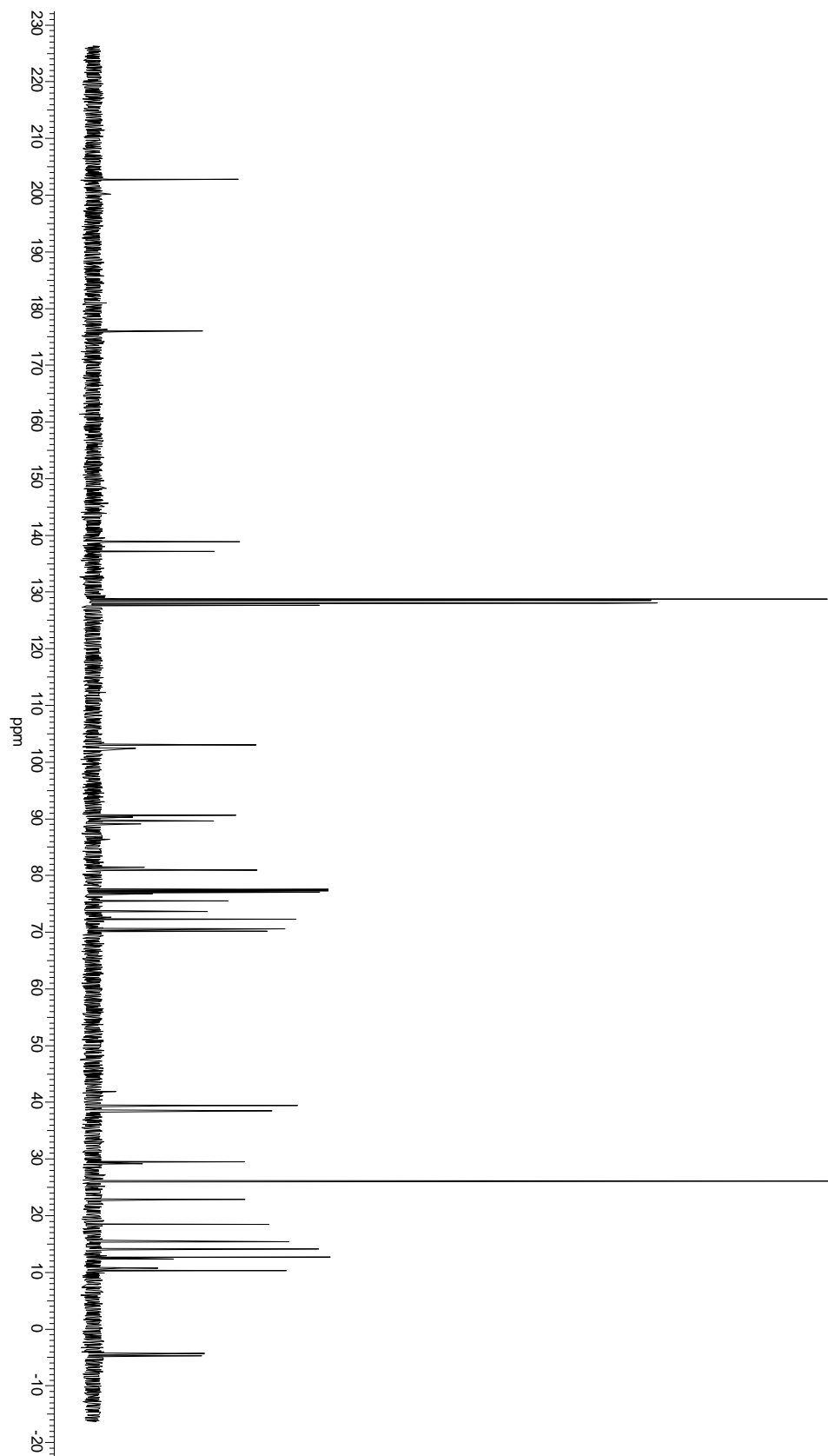
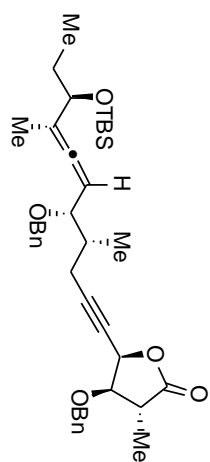


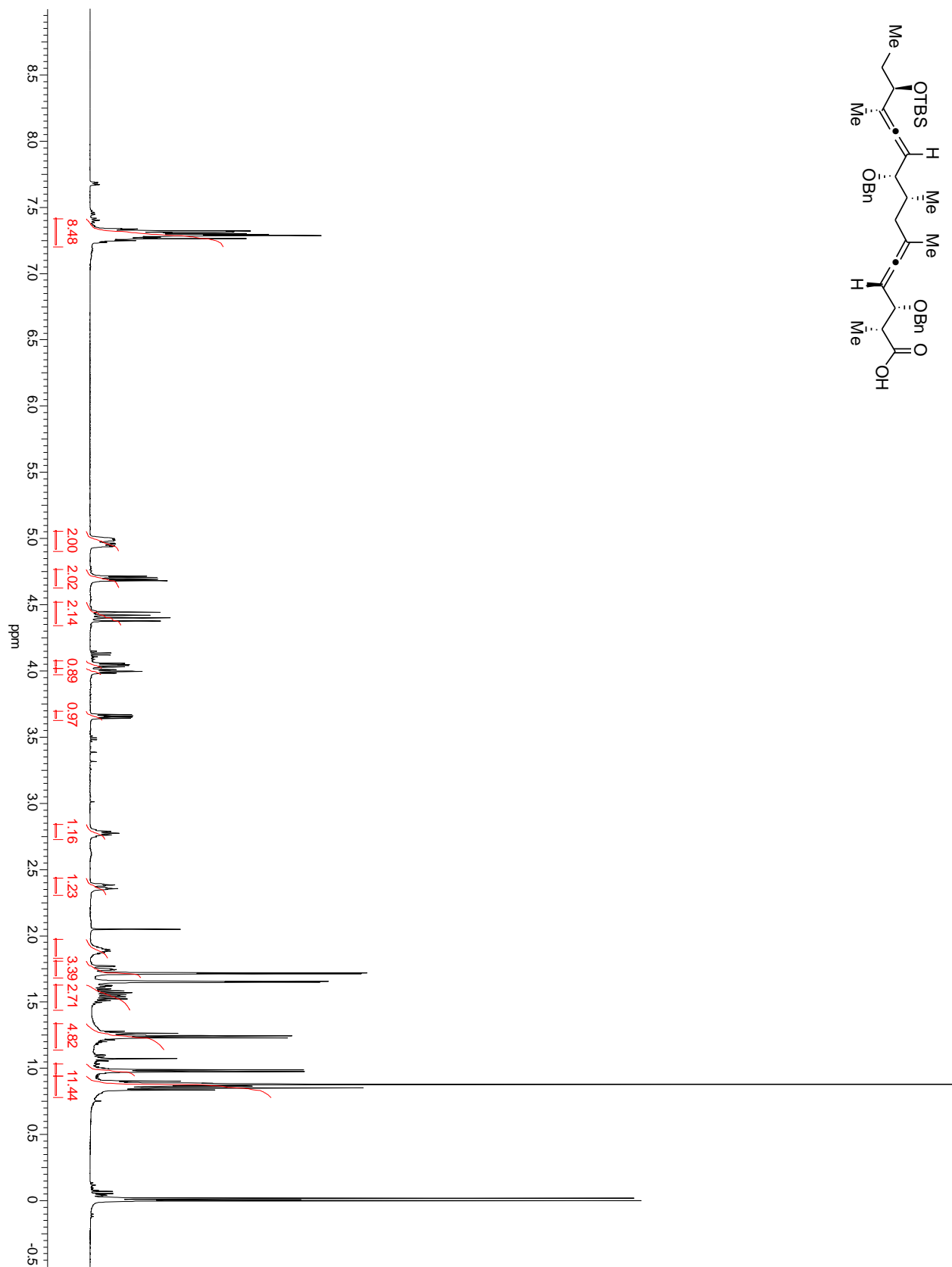
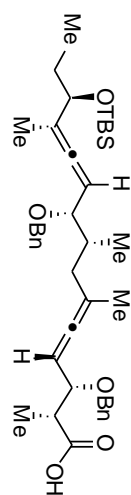


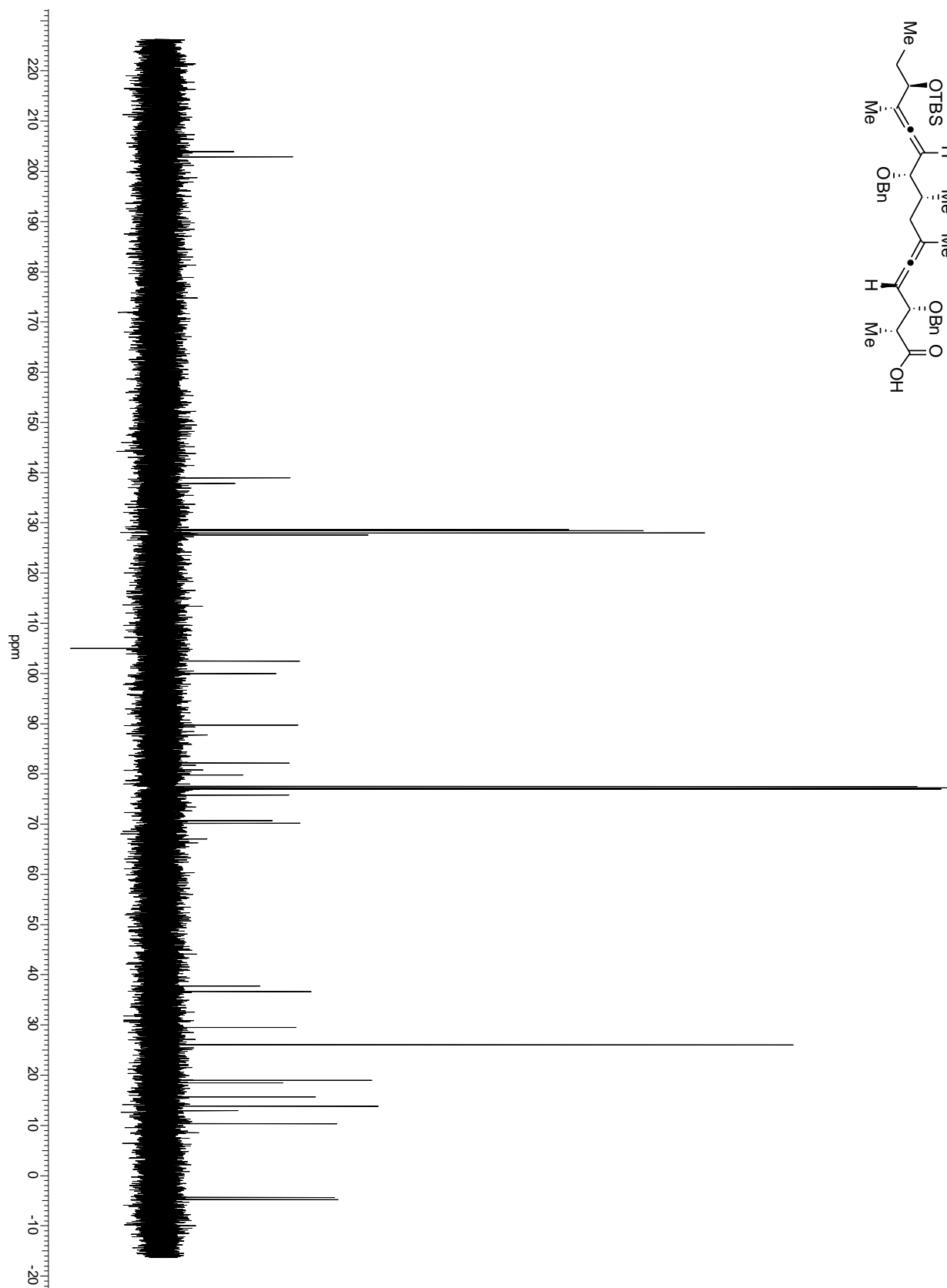
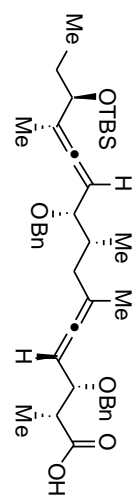


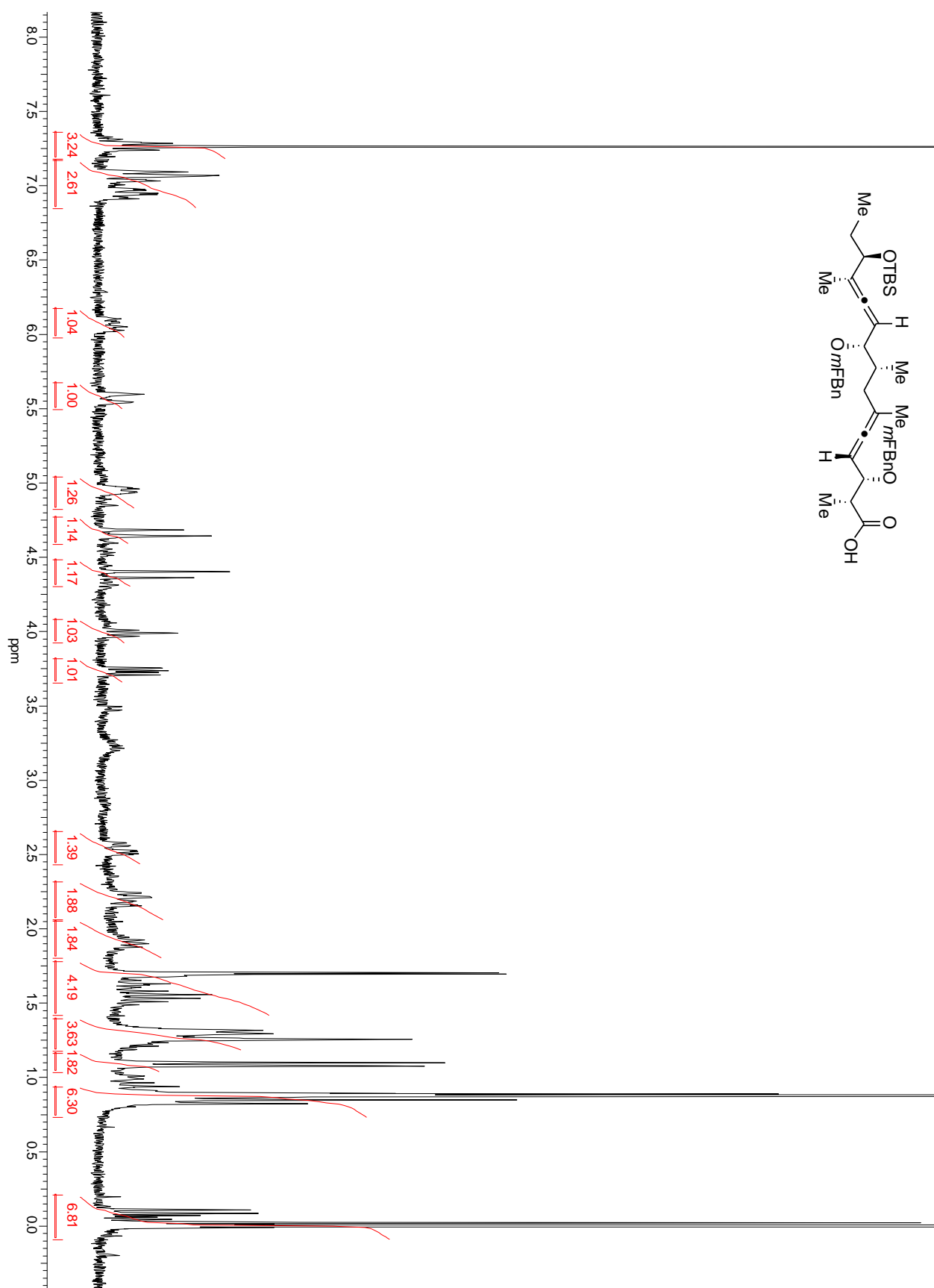
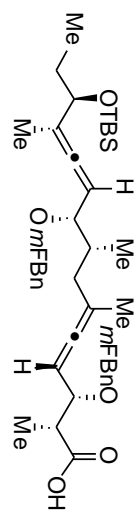


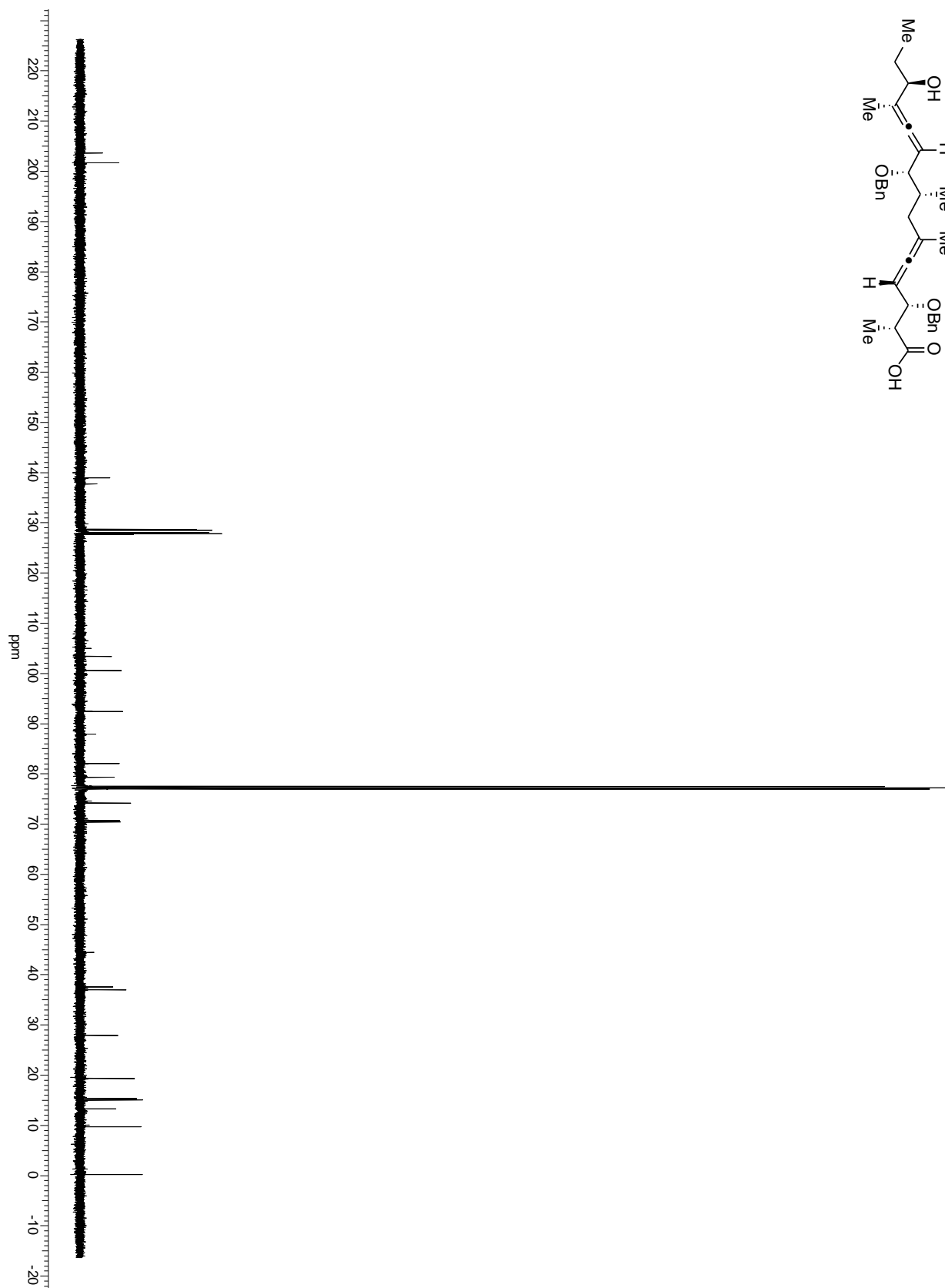
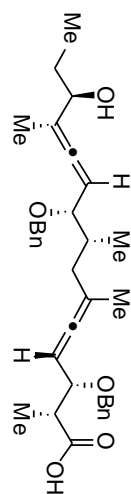


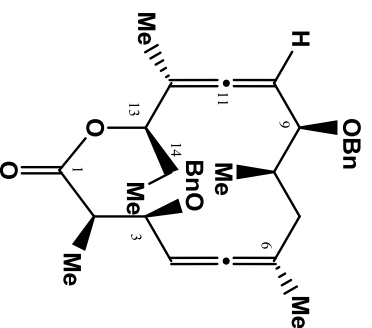




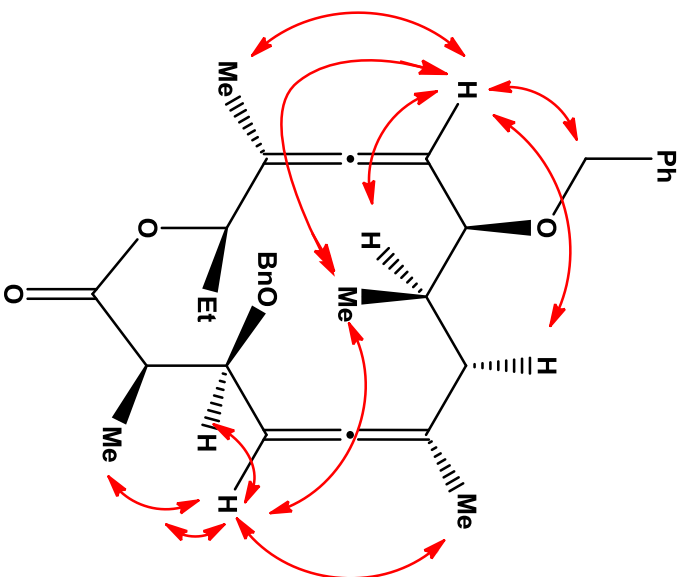
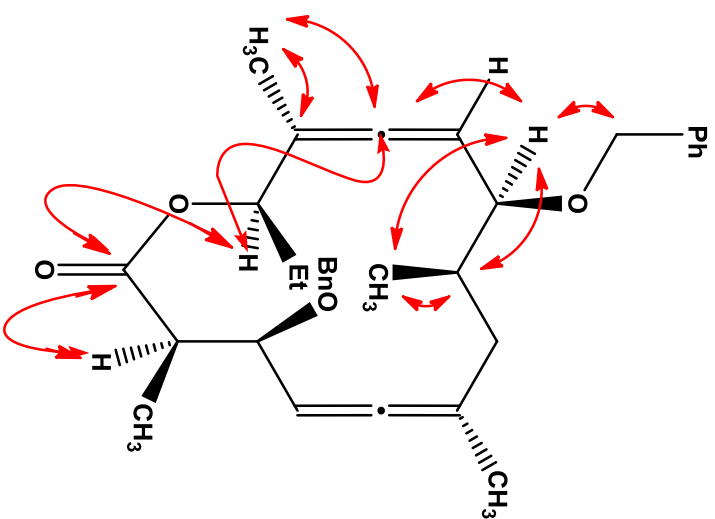
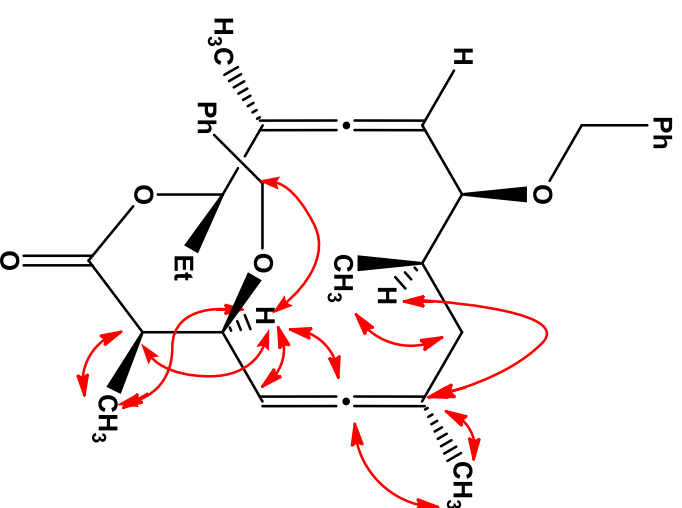


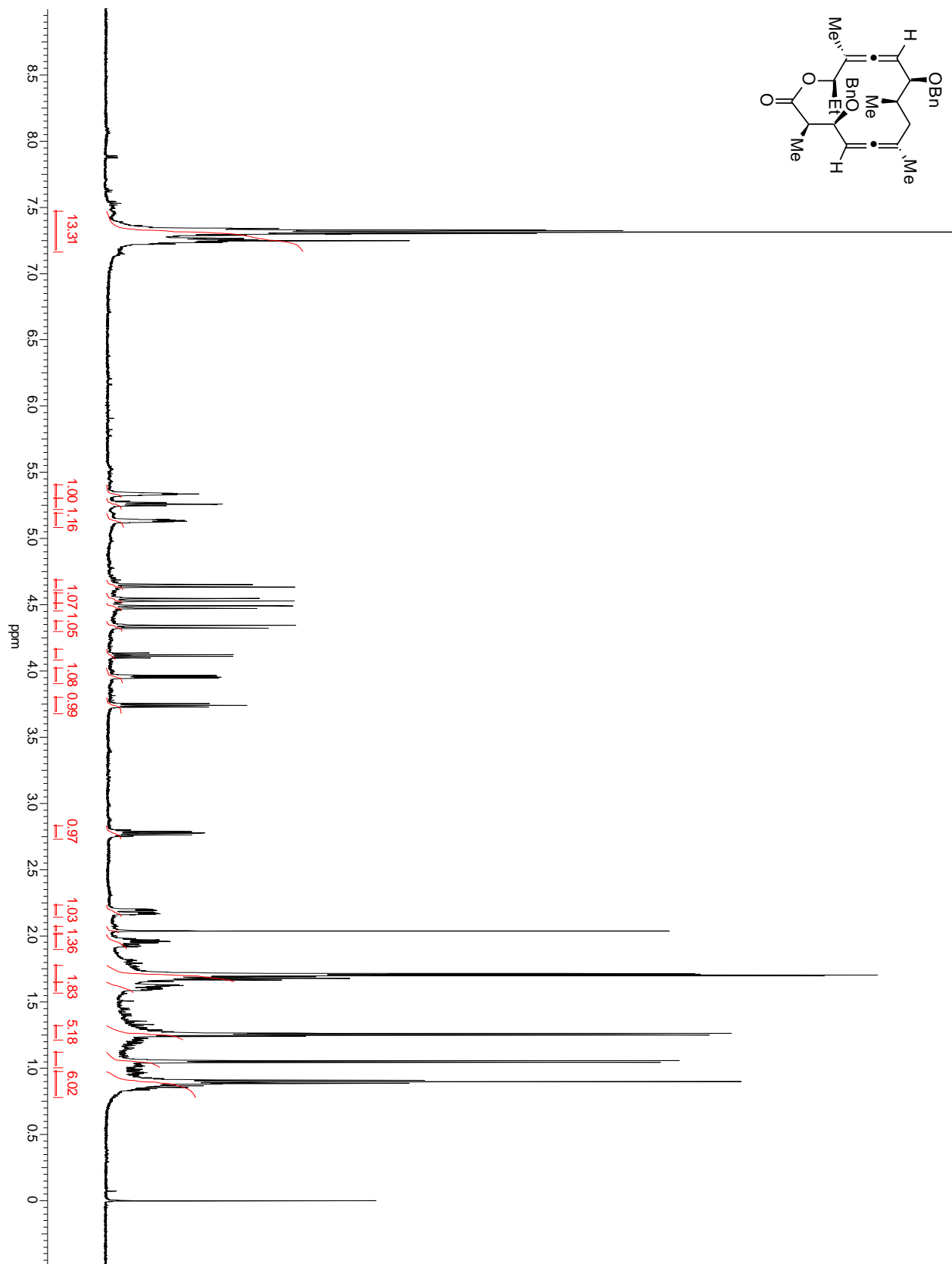
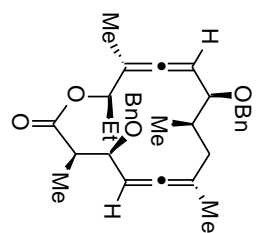


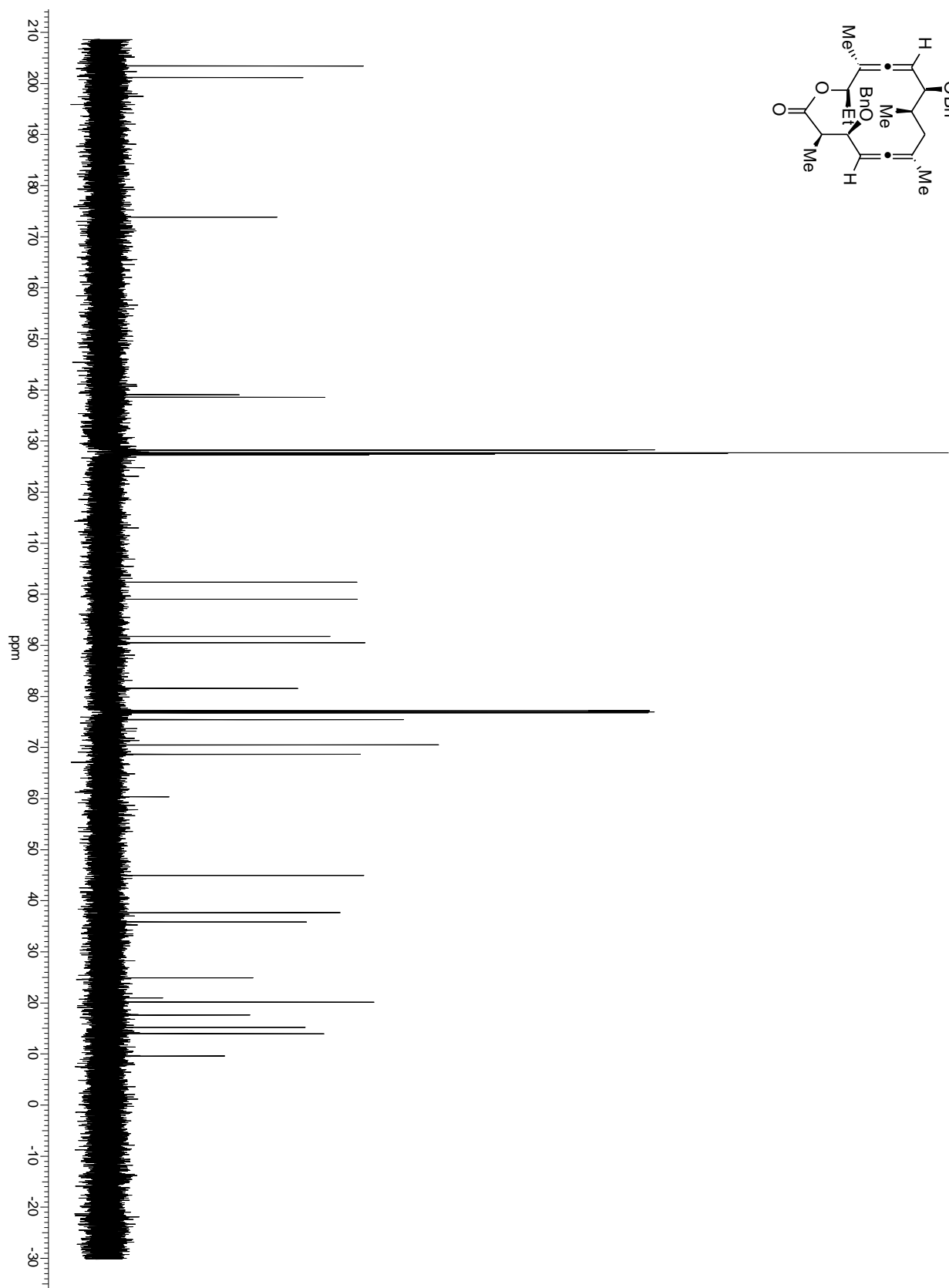
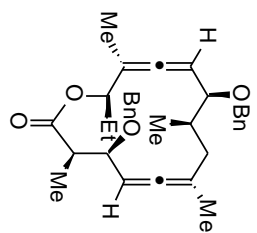


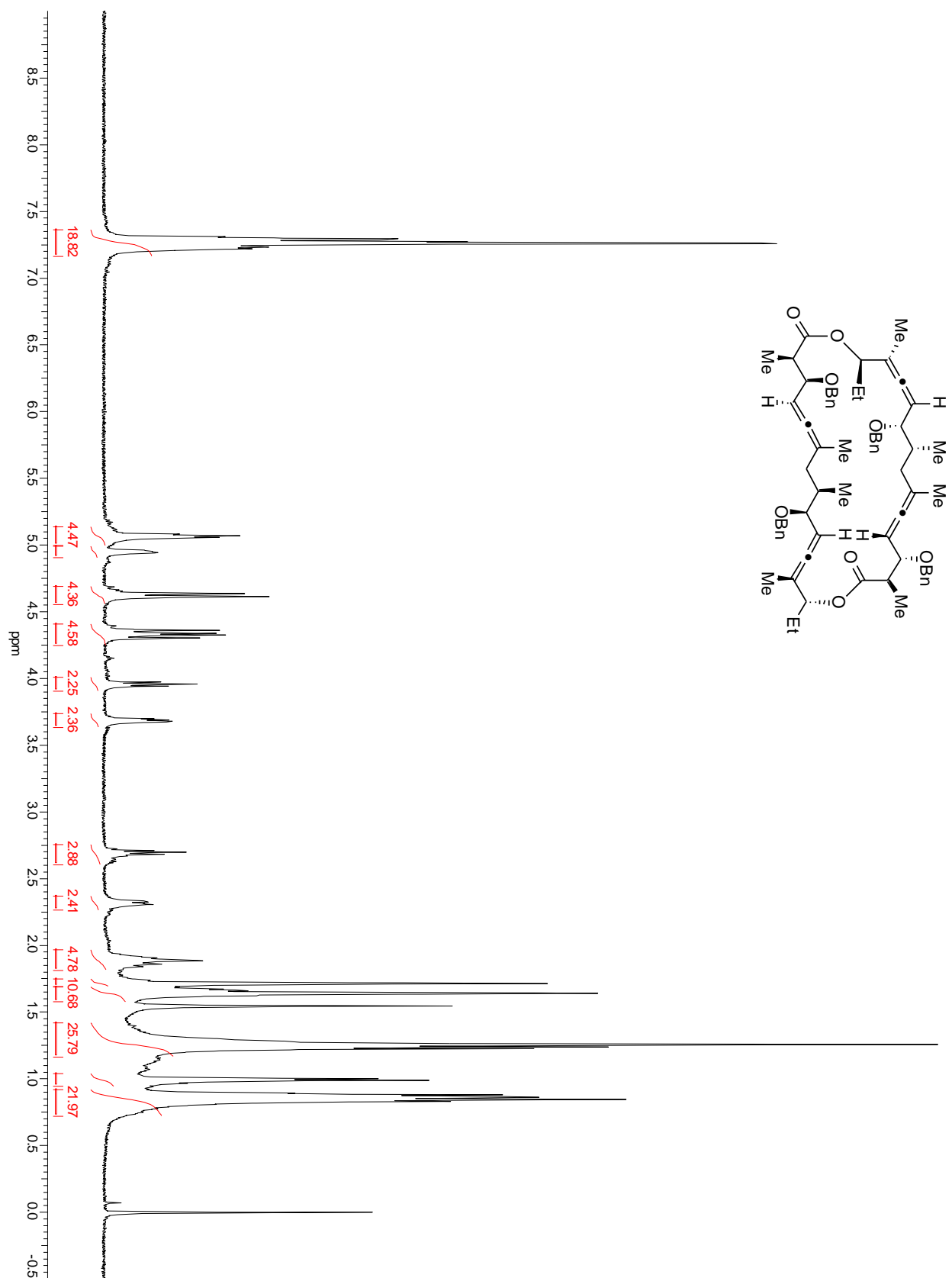


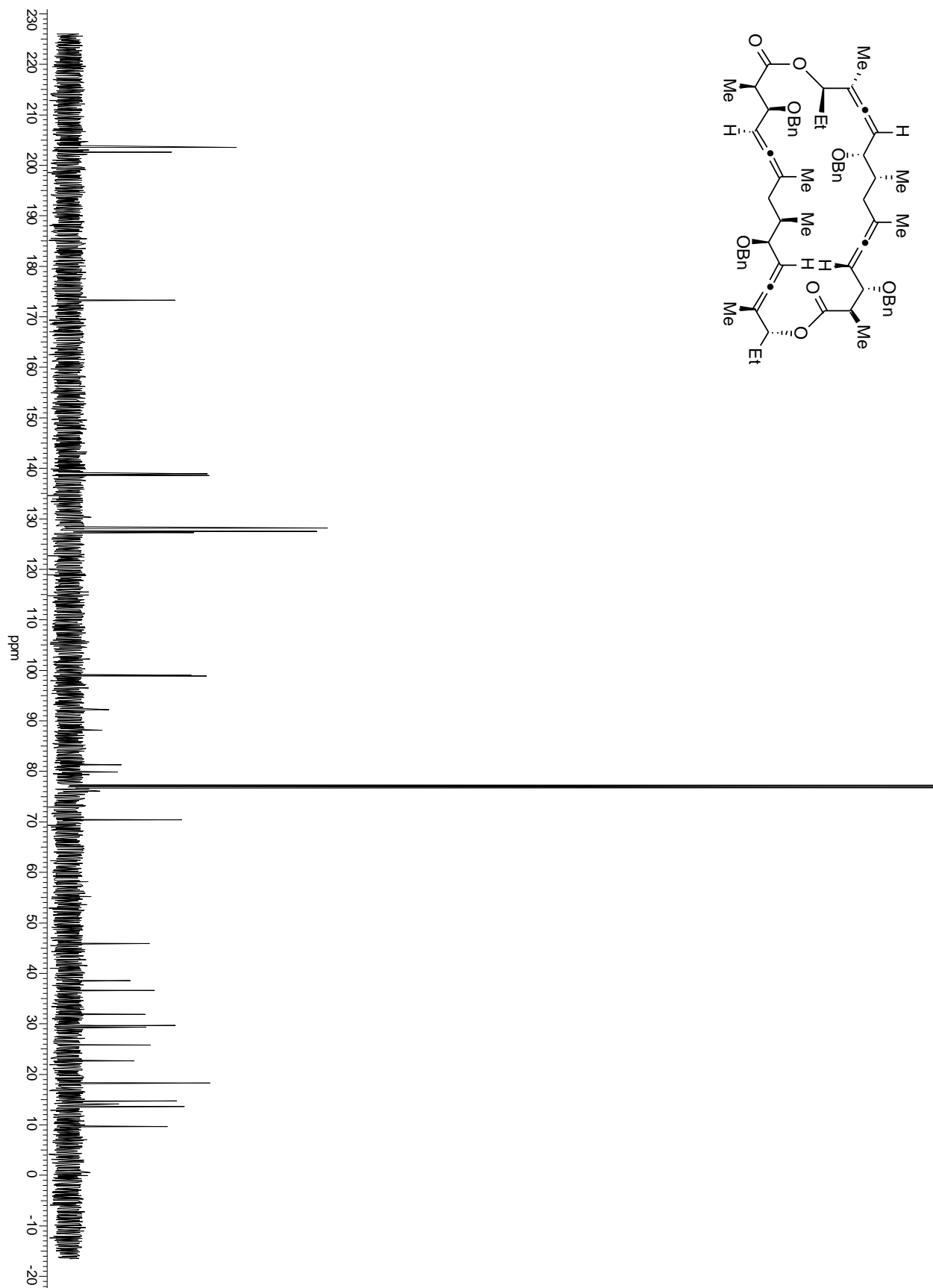
¹H NMR chemical shifts (δ/ppm) with coupling constant (J/Hz)	¹³C NMR chemical shift (δ/ppm)
2.78 (dq, J_{H2, H3} = 8.4Hz, J_{H2, 2-CH3} = 7.1Hz, H2)	173.8 — C1
1.26 (d, J_{2-CH3, H2} = 7.1Hz, 2-CH₃)	44.5 — C2
3.95 (dd, J_{H3, H2} = 8.4Hz, J_{H3, H4} = 4.0Hz, H3)	77.2 — C3
5.33 (m, J_{H4, H3} = 4.0Hz, J_{H4, 6-CH3} = 2.9Hz, J_{H4, H7α} = 2.7Hz, J_{H4, H7β} = 3.4Hz, H4)	90.5 — C4
1.70 (d, 6-CH₃)	201.2 — C5
1.61 (m, J_{H7β, H8} = 5.4Hz, J_{H7β, H7α} = 15.4Hz, J_{H4, H7β} = 3.4Hz, H7β)	102.4 — C6
2.18 (m, J_{H7α, H8} = 5.7Hz, J_{H7α, H7β} = 15.4Hz, J_{H4, H7α} = 2.7Hz, H7α)	37.7 — C7
1.96 (m, J_{H7α, H8} = 5.7Hz, J_{H7β, H8} = 5.4Hz, J_{H8, 8-CH3} = 6.7Hz, J_{H8, H9} = 7.2Hz, H8)	35.9 — C8
1.05 (d, J_{8-CH3, H8} = 6.7Hz, 8-CH₃)	81.6 — C9
3.74 (dd, J_{H9, H8} = 7.2Hz, J_{H9, H10} = 7.8Hz, H9)	91.7 — C10
5.13 (m, J_{H9, H10} = 7.8Hz, J_{H10, 12-CH3} = 2.9Hz, J_{H10, H13} = 1.1Hz, H10)	203.4 — C11
1.71 (d, J_{H10, 12-CH3} = 2.9Hz, 12-CH₃)	99.0 — C12
5.26 (dt, J_{H10, H13} = 1.1Hz, J_{H13, H14} = 6.8Hz, H13)	75.5 — C13
1.69, 1.67 (m, 14-CH₂)	24.9 — C14
0.90 (t, J_{14-CH3, H14} = 7.5Hz, 14-CH₃)	15.2 — 2-CH ₃
4.64 (d, J = 11.7Hz, 3-Bn-CH₂a)	20.2 — 6-CH ₃
4.48 (d, J = 11.7Hz, 3-Bn-CH₂b)	17.6 — 8-CH ₃
4.54 (d, J = 11.9Hz, 9-Bn-CH₂a)	14.0 — 12-CH ₃
4.34 (d, J = 11.9Hz, 9-Bn-CH₂b)	9.6 — 14-CH ₃
7.22-7.35 (two phenyl)	

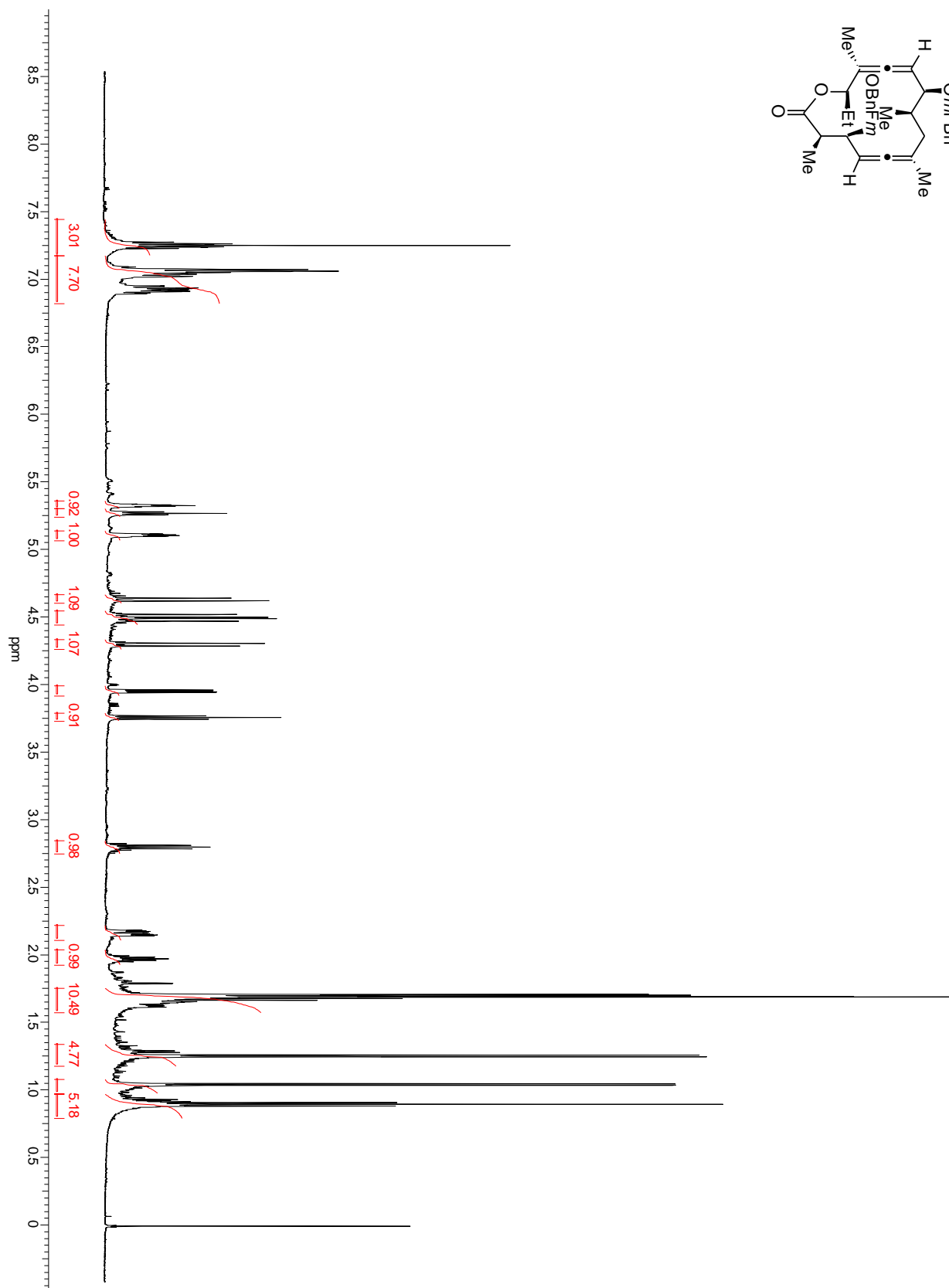
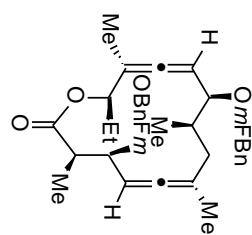
NOESY**HMBC****HMBC**

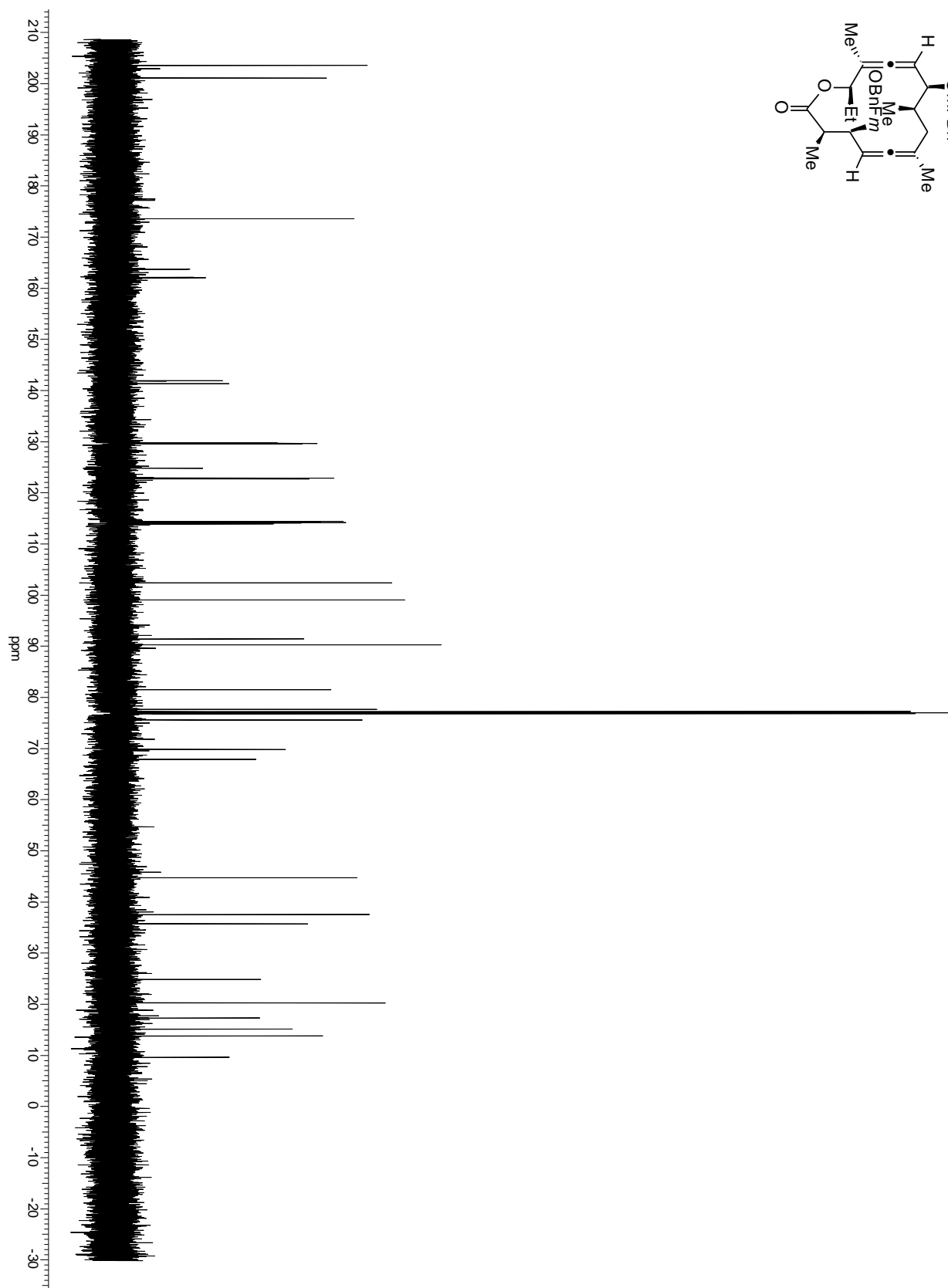
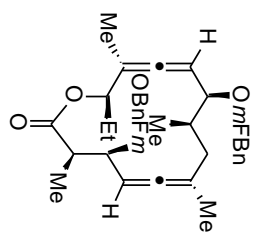


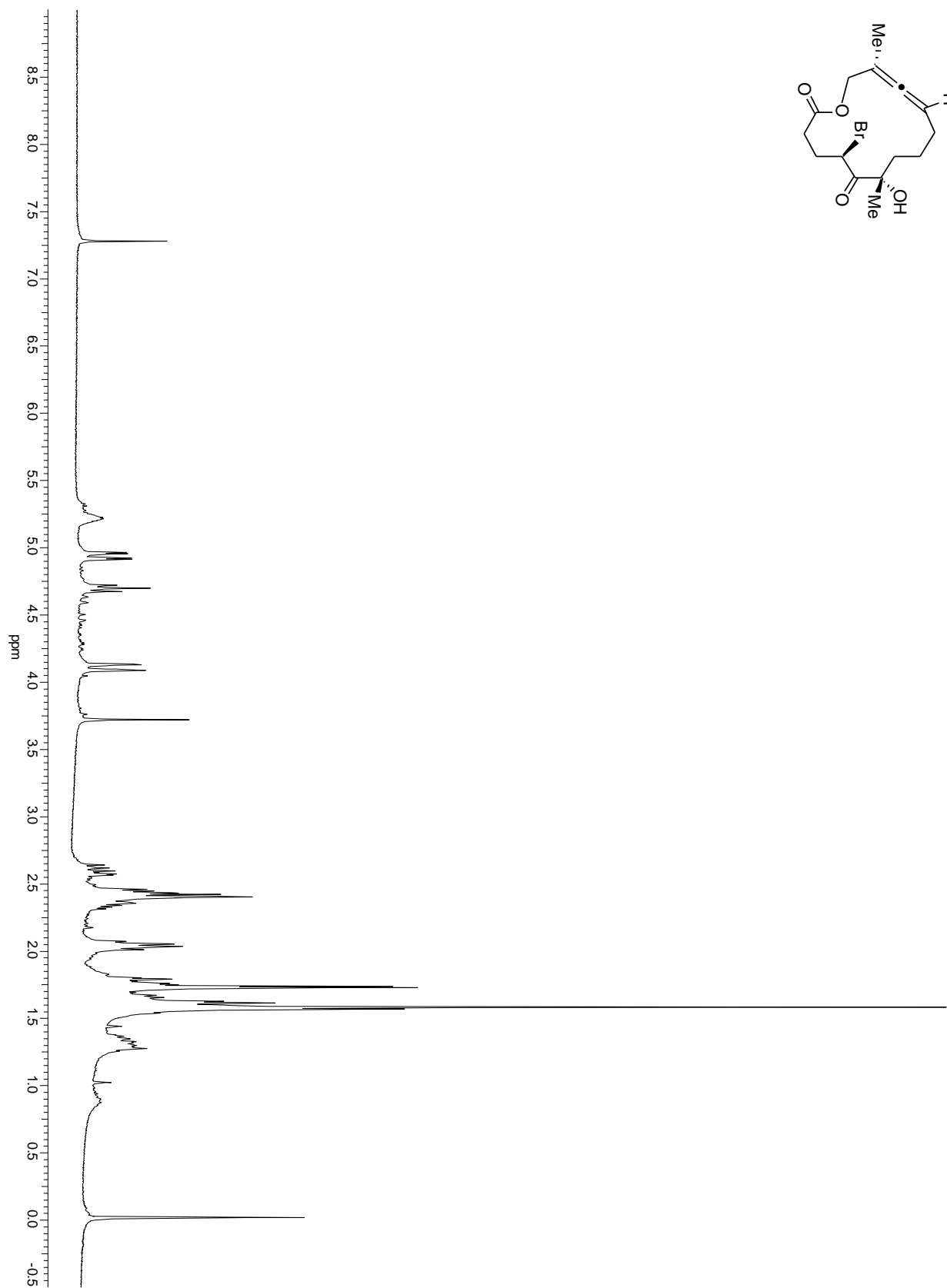
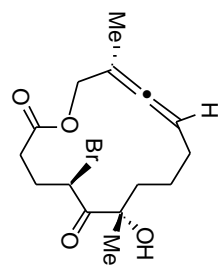


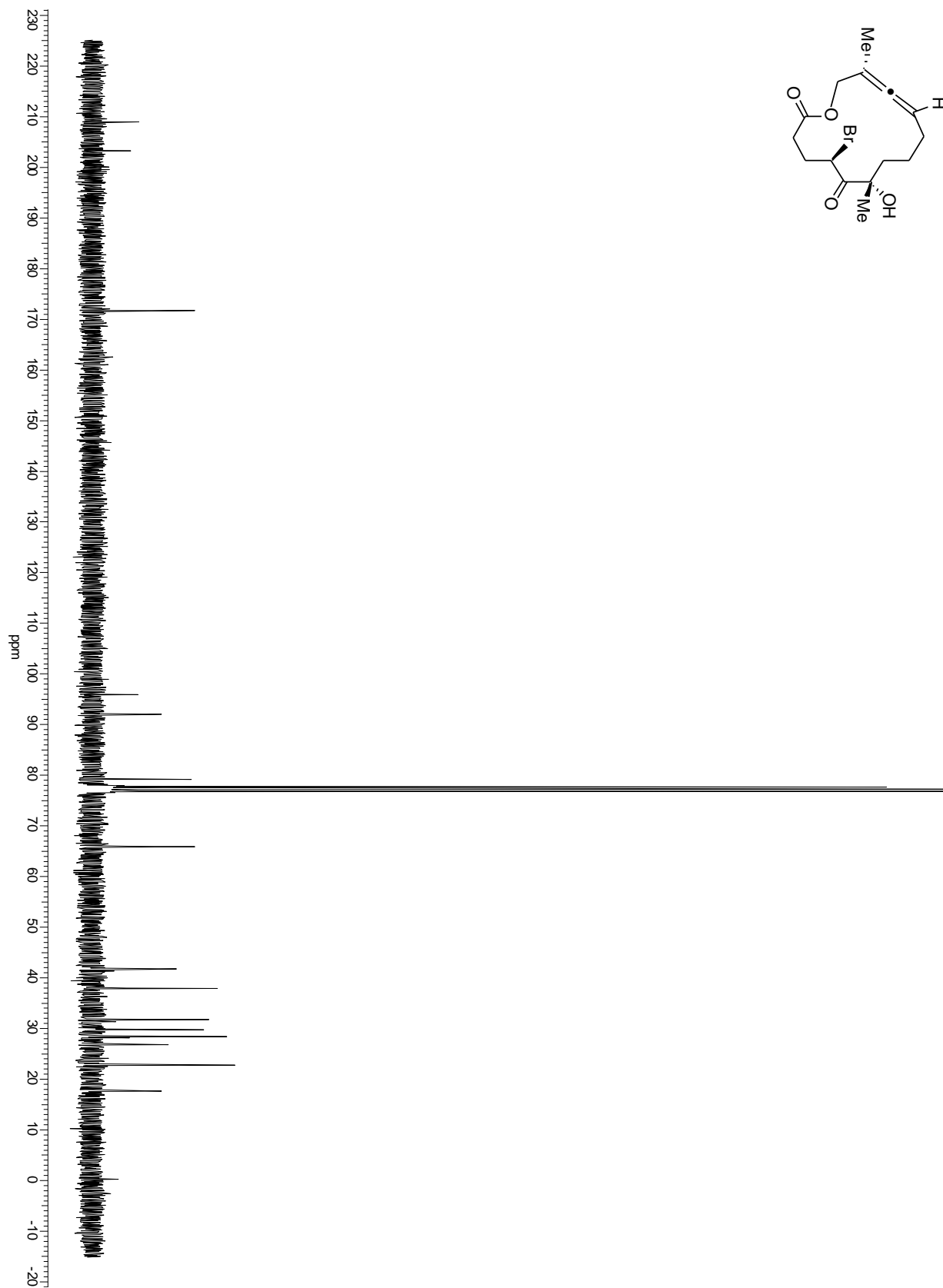
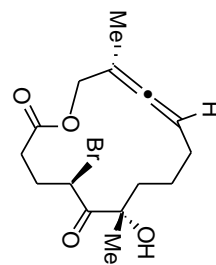












X-ray structure of 4.4

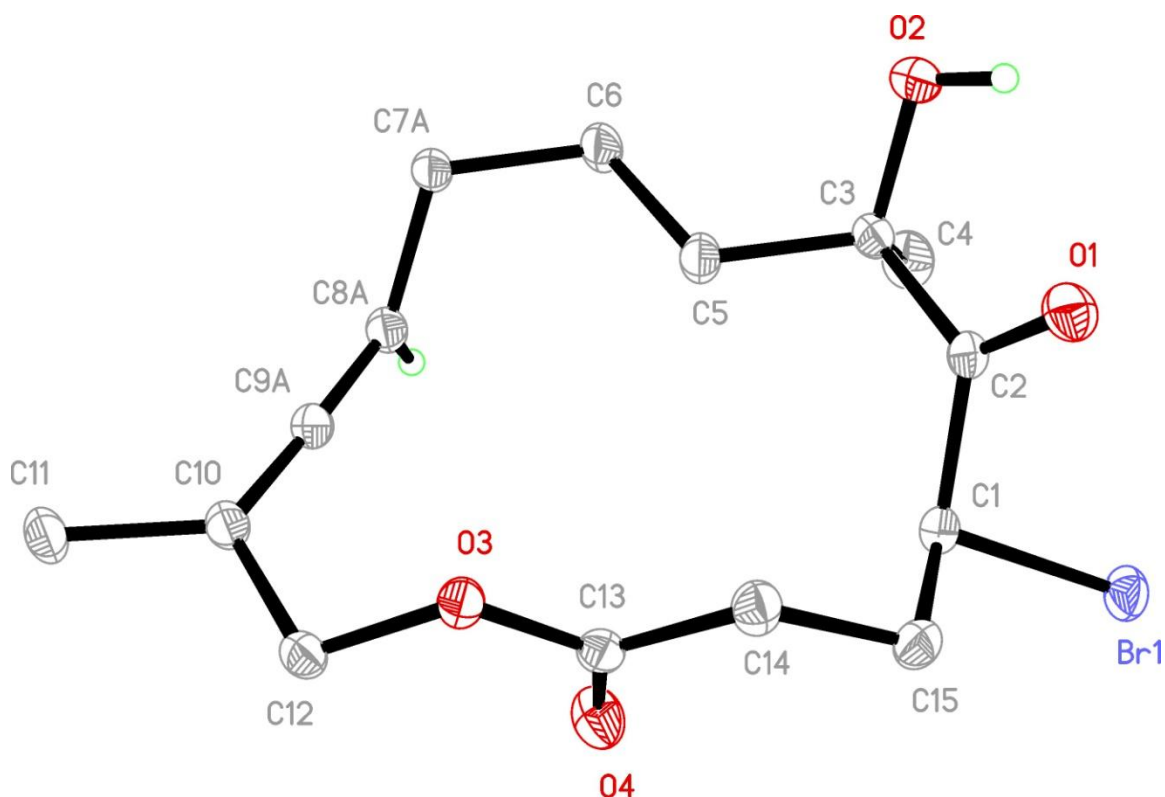


Table 1. Crystal data and structure refinement for brlact.

Identification code	brlact	
Empirical formula	C ₁₅ H ₂₁ Br O ₄	
Formula weight	345.23	
Temperature	100(2) K	
Wavelength	0.71073 Å	
Crystal system	Triclinic	
Space group	P-1	
Unit cell dimensions	a = 8.3053(4) Å	α = 107.384(1)°.
	b = 9.5418(5) Å	β = 100.426(1)°.
	c = 10.3999(5) Å	γ = 98.038(1)°.
Volume	756.85(7) Å ³	
Z	2	
Density (calculated)	1.515 Mg/m ³	
Absorption coefficient	2.726 mm ⁻¹	
F(000)	356	
Crystal size	0.18 x 0.12 x 0.07 mm ³	

Theta range for data collection	2.11 to 30.55°.
Index ranges	-11<=h<=11, -13<=k<=13, -14<=l<=14
Reflections collected	9028
Independent reflections	4557 [R(int) = 0.0119]
Completeness to theta = 30.55°	98.4 %
Absorption correction	Semi-empirical from equivalents
Max. and min. transmission	0.746 and 0.646
Refinement method	Full-matrix least-squares on F ²
Data / restraints / parameters	4557 / 125 / 212
Goodness-of-fit on F ²	1.001
Final R indices [I>2sigma(I)]	R1 = 0.0246, wR2 = 0.0612
R indices (all data)	R1 = 0.0264, wR2 = 0.0621
Largest diff. peak and hole	0.612 and -0.236 e.Å ⁻³

Table 2. Atomic coordinates ($\times 10^4$) and equivalent isotropic displacement parameters ($\text{\AA}^2 \times 10^3$)

for brlact. U(eq) is defined as one third of the trace of the orthogonalized U^{ij} tensor.

	x	y	z	U(eq)
Br(1)	3264(1)	2412(1)	122(1)	21(1)
O(1)	1630(1)	-303(1)	1048(1)	22(1)
O(2)	-501(1)	516(1)	2581(1)	26(1)
O(3)	6668(1)	1709(1)	5678(1)	16(1)
O(4)	6845(1)	3468(1)	4632(1)	24(1)
C(1)	3667(2)	1987(1)	1875(1)	16(1)
C(2)	2034(2)	984(1)	1828(1)	16(1)
C(3)	937(2)	1632(2)	2793(1)	18(1)
C(4)	404(2)	2989(2)	2475(2)	25(1)
C(5)	1941(2)	2013(2)	4290(1)	20(1)
C(6)	977(2)	2614(2)	5385(1)	22(1)
C(7A)	2032(2)	2893(2)	6848(1)	17(1)
C(8A)	3664(2)	3980(2)	7151(1)	17(1)
C(9A)	5142(2)	3708(2)	7538(1)	17(1)

C(7B)	2299(18)	3904(17)	6797(17)	11(2)
C(8B)	3221(16)	2817(16)	7232(17)	13(2)
C(9B)	4857(17)	3010(20)	7556(18)	13(2)
C(10)	6606(2)	3433(1)	7972(1)	17(1)
C(11)	7441(2)	3855(2)	9485(1)	21(1)
C(12)	7643(2)	2752(1)	6993(1)	17(1)
C(13)	6425(2)	2186(1)	4572(1)	16(1)
C(14)	5633(2)	856(1)	3282(1)	18(1)
C(15)	5162(2)	1228(2)	1952(1)	20(1)

Table 3. Bond lengths [Å] and angles [°] for brlact.

Br(1)-C(1)	1.9646(12)	C(7A)-C(8A)	1.5072(18)
O(1)-C(2)	1.2121(15)	C(7A)-H(7A)	0.9700
O(2)-C(3)	1.4210(15)	C(7A)-H(7B)	0.9700
O(2)-H(2)	0.8200	C(8A)-C(9A)	1.3069(18)
O(3)-C(13)	1.3514(15)	C(8A)-H(8A)	0.9300
O(3)-C(12)	1.4414(15)	C(9A)-C(10)	1.3090(17)
O(4)-C(13)	1.2037(16)	C(7B)-C(8B)	1.498(9)
C(1)-C(15)	1.5238(17)	C(7B)-H(7B1)	0.9700
C(1)-C(2)	1.5311(17)	C(7B)-H(7B2)	0.9700
C(1)-H(1)	0.9800	C(8B)-C(9B)	1.312(9)
C(2)-C(3)	1.5284(17)	C(8B)-H(8B)	0.9300
C(3)-C(4)	1.5309(19)	C(9B)-C(10)	1.402(14)
C(3)-C(5)	1.5356(17)	C(10)-C(11)	1.5058(17)
C(4)-H(4A)	0.9600	C(10)-C(12)	1.5089(17)
C(4)-H(4B)	0.9600	C(11)-H(11A)	0.9600
C(4)-H(4C)	0.9600	C(11)-H(11B)	0.9600
C(5)-C(6)	1.5282(18)	C(11)-H(11C)	0.9600
C(5)-H(5A)	0.9700	C(12)-H(12A)	0.9700
C(5)-H(5B)	0.9700	C(12)-H(12B)	0.9700
C(6)-C(7A)	1.5375(18)	C(13)-C(14)	1.5069(18)
C(6)-C(7B)	1.684(16)	C(14)-C(15)	1.5261(18)
C(6)-H(6A)	0.9700	C(14)-H(14A)	0.9700
C(6)-H(6B)	0.9700	C(14)-H(14B)	0.9700

C(15)-H(15A)	0.9700	C(15)-H(15B)	0.9700
C(3)-O(2)-H(2)	109.5	C(7B)-C(6)-H(6A)	135.4
C(13)-O(3)-C(12)	118.64(10)	C(5)-C(6)-H(6B)	109.5
C(15)-C(1)-C(2)	113.30(10)	C(7A)-C(6)-H(6B)	109.5
C(15)-C(1)-Br(1)	108.49(8)	C(7B)-C(6)-H(6B)	77.7
C(2)-C(1)-Br(1)	105.02(8)	H(6A)-C(6)-H(6B)	108.1
C(15)-C(1)-H(1)	110.0	C(8A)-C(7A)-C(6)	111.40(11)
C(2)-C(1)-H(1)	110.0	C(8A)-C(7A)-H(7A)	109.3
Br(1)-C(1)-H(1)	110.0	C(6)-C(7A)-H(7A)	109.3
O(1)-C(2)-C(3)	120.88(11)	C(8A)-C(7A)-H(7B)	109.3
O(1)-C(2)-C(1)	120.43(11)	C(6)-C(7A)-H(7B)	109.3
C(3)-C(2)-C(1)	118.69(10)	H(7A)-C(7A)-H(7B)	108.0
O(2)-C(3)-C(2)	109.26(10)	C(9A)-C(8A)-C(7A)	124.78(13)
O(2)-C(3)-C(4)	109.77(11)	C(9A)-C(8A)-H(8A)	117.6
C(2)-C(3)-C(4)	109.37(11)	C(7A)-C(8A)-H(8A)	117.6
O(2)-C(3)-C(5)	107.37(11)	C(8A)-C(9A)-C(10)	177.73(14)
C(2)-C(3)-C(5)	107.62(10)	C(8B)-C(7B)-C(6)	95.7(10)
C(4)-C(3)-C(5)	113.36(11)	C(8B)-C(7B)-H(7B1)	112.6
C(3)-C(4)-H(4A)	109.5	C(6)-C(7B)-H(7B1)	112.6
C(3)-C(4)-H(4B)	109.5	C(8B)-C(7B)-H(7B2)	112.6
H(4A)-C(4)-H(4B)	109.5	C(6)-C(7B)-H(7B2)	112.6
C(3)-C(4)-H(4C)	109.5	H(7B1)-C(7B)-H(7B2)	110.1
H(4A)-C(4)-H(4C)	109.5	C(9B)-C(8B)-C(7B)	124.0(13)
H(4B)-C(4)-H(4C)	109.5	C(9B)-C(8B)-H(8B)	118.0
C(6)-C(5)-C(3)	113.94(10)	C(7B)-C(8B)-H(8B)	118.0
C(6)-C(5)-H(5A)	108.8	C(8B)-C(9B)-C(10)	172.0(18)
C(3)-C(5)-H(5A)	108.8	C(9A)-C(10)-C(9B)	28.9(8)
C(6)-C(5)-H(5B)	108.8	C(9A)-C(10)-C(11)	122.87(12)
C(3)-C(5)-H(5B)	108.8	C(9B)-C(10)-C(11)	118.9(7)
H(5A)-C(5)-H(5B)	107.7	C(9A)-C(10)-C(12)	122.57(11)
C(5)-C(6)-C(7A)	110.75(10)	C(9B)-C(10)-C(12)	119.4(7)
C(5)-C(6)-C(7B)	109.6(5)	C(11)-C(10)-C(12)	114.46(10)
C(7A)-C(6)-C(7B)	35.0(5)	C(10)-C(11)-H(11A)	109.5
C(5)-C(6)-H(6A)	109.5	C(10)-C(11)-H(11B)	109.5
C(7A)-C(6)-H(6A)	109.5	H(11A)-C(11)-H(11B)	109.5

C(10)-C(11)-H(11C)	109.5	C(13)-C(14)-C(15)	115.32(11)
H(11A)-C(11)-H(11C)	109.5	C(13)-C(14)-H(14A)	108.4
H(11B)-C(11)-H(11C)	109.5	C(15)-C(14)-H(14A)	108.4
O(3)-C(12)-C(10)	113.95(10)	C(13)-C(14)-H(14B)	108.4
O(3)-C(12)-H(12A)	108.8	C(15)-C(14)-H(14B)	108.4
C(10)-C(12)-H(12A)	108.8	H(14A)-C(14)-H(14B)	107.5
O(3)-C(12)-H(12B)	108.8	C(1)-C(15)-C(14)	113.99(10)
C(10)-C(12)-H(12B)	108.8	C(1)-C(15)-H(15A)	108.8
H(12A)-C(12)-H(12B)	107.7	C(14)-C(15)-H(15A)	108.8
O(4)-C(13)-O(3)	124.17(12)	C(1)-C(15)-H(15B)	108.8
O(4)-C(13)-C(14)	126.73(12)	C(14)-C(15)-H(15B)	108.8
O(3)-C(13)-C(14)	109.04(10)	H(15A)-C(15)-H(15B)	107.6

Table 4. Anisotropic displacement parameters ($\text{\AA}^2 \times 10^3$) for brlact. The anisotropic displacement factor exponent takes the form: $-2\pi^2 [h^2 a^{*2} U^{11} + \dots + 2 h k a^* b^* U^{12}]$

	U ¹¹	U ²²	U ³³	U ²³	U ¹³	U ¹²
Br(1)	26(1)	22(1)	15(1)	8(1)	2(1)	0(1)
O(1)	24(1)	17(1)	22(1)	2(1)	5(1)	1(1)
O(2)	19(1)	33(1)	20(1)	2(1)	6(1)	-5(1)
O(3)	17(1)	17(1)	14(1)	5(1)	4(1)	3(1)
O(4)	26(1)	20(1)	23(1)	10(1)	0(1)	2(1)
C(1)	17(1)	18(1)	12(1)	4(1)	3(1)	2(1)
C(2)	16(1)	18(1)	12(1)	5(1)	2(1)	3(1)
C(3)	13(1)	22(1)	14(1)	3(1)	2(1)	2(1)
C(4)	23(1)	29(1)	24(1)	8(1)	4(1)	12(1)
C(5)	15(1)	30(1)	13(1)	4(1)	3(1)	7(1)
C(6)	13(1)	35(1)	14(1)	4(1)	3(1)	7(1)
C(7A)	12(1)	25(1)	14(1)	5(1)	3(1)	4(1)
C(8A)	15(1)	20(1)	14(1)	4(1)	3(1)	4(1)
C(9A)	16(1)	18(1)	13(1)	3(1)	3(1)	2(1)

C(7B)	11(2)	12(2)	11(2)	4(1)	3(1)	2(1)
C(8B)	13(2)	13(2)	12(2)	4(1)	3(1)	3(1)
C(9B)	13(2)	14(2)	13(2)	4(1)	3(1)	3(1)
C(10)	15(1)	20(1)	14(1)	4(1)	2(1)	4(1)
C(11)	18(1)	27(1)	16(1)	5(1)	0(1)	6(1)
C(12)	13(1)	20(1)	16(1)	5(1)	2(1)	4(1)
C(13)	13(1)	21(1)	16(1)	7(1)	4(1)	6(1)
C(14)	18(1)	20(1)	17(1)	4(1)	4(1)	7(1)
C(15)	18(1)	26(1)	16(1)	6(1)	6(1)	6(1)

Table 5. Hydrogen coordinates ($\times 10^4$) and isotropic displacement parameters ($\text{\AA}^2 \times 10^3$) for brlact.

	x	y	z	U(eq)
H(2)	-649	-130	1821	40
H(1)	3899	2923	2660	20
H(4A)	-375	3336	3014	37
H(4B)	-117	2704	1507	37
H(4C)	1371	3778	2707	37
H(5A)	2284	1117	4401	24
H(5B)	2945	2757	4450	24
H(6A)	-53	1896	5214	26
H(6B)	687	3545	5321	26
H(7A)	1405	3290	7526	21
H(7B)	2256	1948	6929	21
H(8A)	3617	4913	7055	20
H(7B1)	3014	4643	6568	13
H(7B2)	1725	4401	7480	13
H(8B)	2595	1952	7275	15
H(11A)	7647	2970	9690	32
H(11B)	6726	4314	10037	32

H(11C)	8483	4549	9692	32
H(12A)	8343	3553	6829	20
H(12B)	8376	2236	7435	20
H(14A)	4632	329	3427	22
H(14B)	6402	177	3156	22
H(15A)	6119	1881	1874	24
H(15B)	4912	307	1167	24

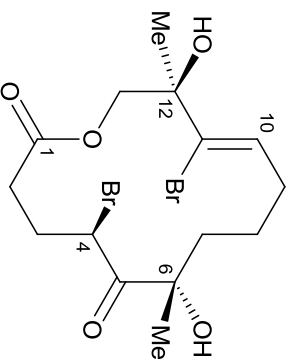
Table 6. Torsion angles [°] for brlact.

C(15)-C(1)-C(2)-O(1)	-46.99(15)	C(8A)-C(9A)-C(10)-C(12)	156(4)
Br(1)-C(1)-C(2)-O(1)	71.25(13)	C(8B)-C(9B)-C(10)-C(9A)	-28(11)
C(15)-C(1)-C(2)-C(3)	132.43(11)	C(8B)-C(9B)-C(10)-C(11)	78(12)
Br(1)-C(1)-C(2)-C(3)	-109.33(10)	C(8B)-C(9B)-C(10)-C(12)	-133(12)
O(1)-C(2)-C(3)-O(2)	-0.42(16)	C(13)-O(3)-C(12)-C(10)	100.16(12)
C(1)-C(2)-C(3)-O(2)	-179.84(10)	C(9A)-C(10)-C(12)-O(3)	-32.96(18)
O(1)-C(2)-C(3)-C(4)	-120.59(13)	C(9B)-C(10)-C(12)-O(3)	0.6(10)
C(1)-C(2)-C(3)-C(4)	59.99(14)	C(11)-C(10)-C(12)-O(3)	150.63(11)
O(1)-C(2)-C(3)-C(5)	115.86(13)	C(12)-O(3)-C(13)-O(4)	-6.90(17)
C(1)-C(2)-C(3)-C(5)	-63.56(14)	C(12)-O(3)-C(13)-C(14)	170.61(9)
O(2)-C(3)-C(5)-C(6)	-59.93(15)	O(4)-C(13)-C(14)-C(15)	-6.82(18)
C(2)-C(3)-C(5)-C(6)	-177.44(11)	O(3)-C(13)-C(14)-C(15)	175.75(10)
C(4)-C(3)-C(5)-C(6)	61.48(15)	C(2)-C(1)-C(15)-C(14)	-64.76(14)
C(3)-C(5)-C(6)-C(7A)	177.15(12)	Br(1)-C(1)-C(15)-C(14)	179.04(9)
C(3)-C(5)-C(6)-C(7B)	-145.5(5)	C(13)-C(14)-C(15)-C(1)	-71.60(14)
C(5)-C(6)-C(7A)-C(8A)	57.99(15)		
C(7B)-C(6)-C(7A)-C(8A)	-36.9(9)		
C(6)-C(7A)-C(8A)-C(9A)	-124.53(14)		
C(7A)-C(8A)-C(9A)-C(10)	-65(4)		
C(5)-C(6)-C(7B)-C(8B)	-69.2(10)		
C(7A)-C(6)-C(7B)-C(8B)	29.2(6)		
C(6)-C(7B)-C(8B)-C(9B)	131.0(17)		
C(7B)-C(8B)-C(9B)-C(10)	32(13)		
C(8A)-C(9A)-C(10)-C(9B)	63(4)		
C(8A)-C(9A)-C(10)-C(11)	-28(4)		

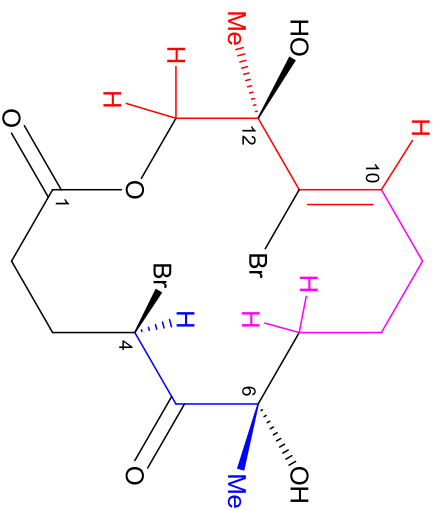
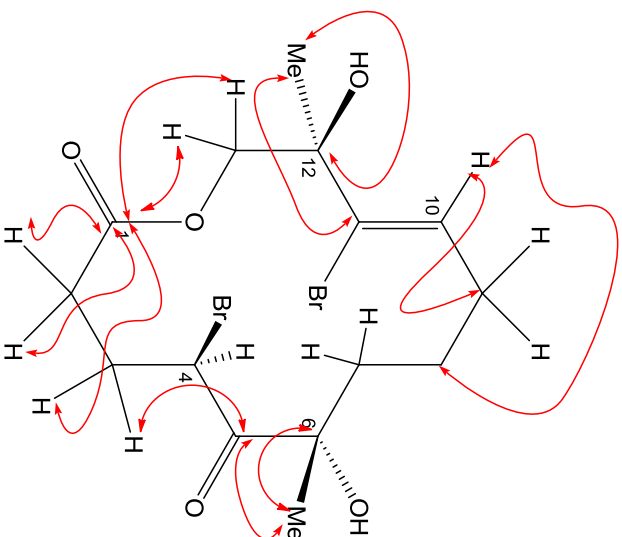
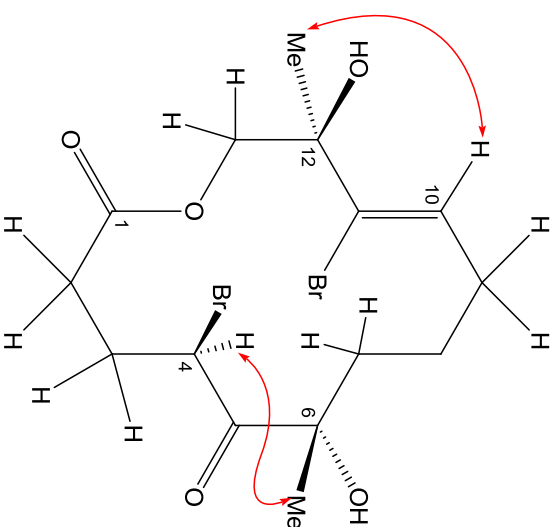
Table 7. Hydrogen bonds for brlact [\AA and $^\circ$].

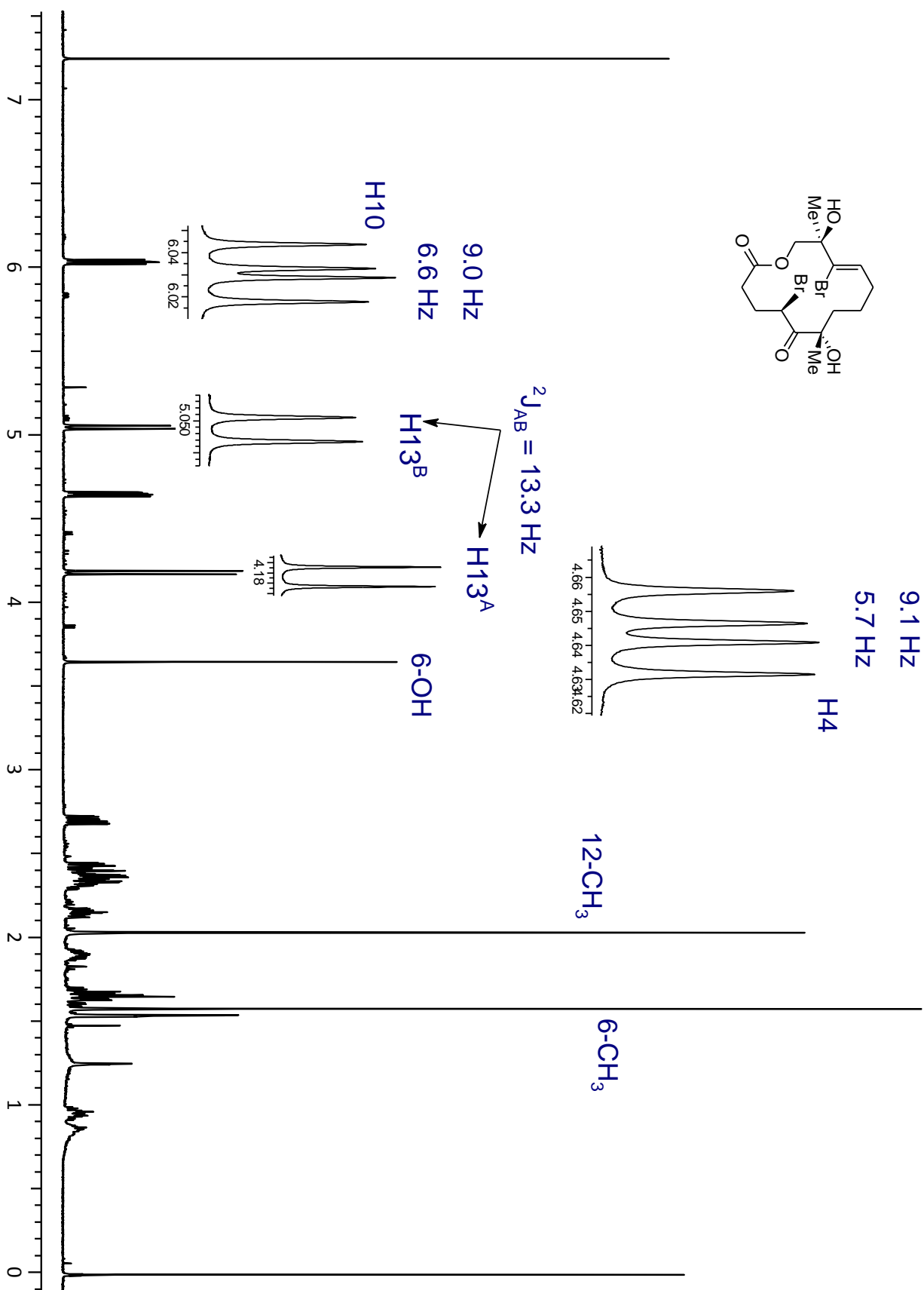
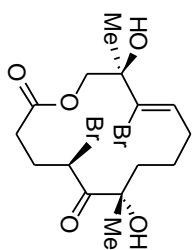
D-H...A	d(D-H)	d(H...A)	d(D...A)	$\angle(\text{DHA})$
O(2)-H(2)...O(1)	0.82	2.19	2.6364(14)	113.9
O(2)-H(2)...Br(1)#1	0.82	2.83	3.4865(10)	138.6

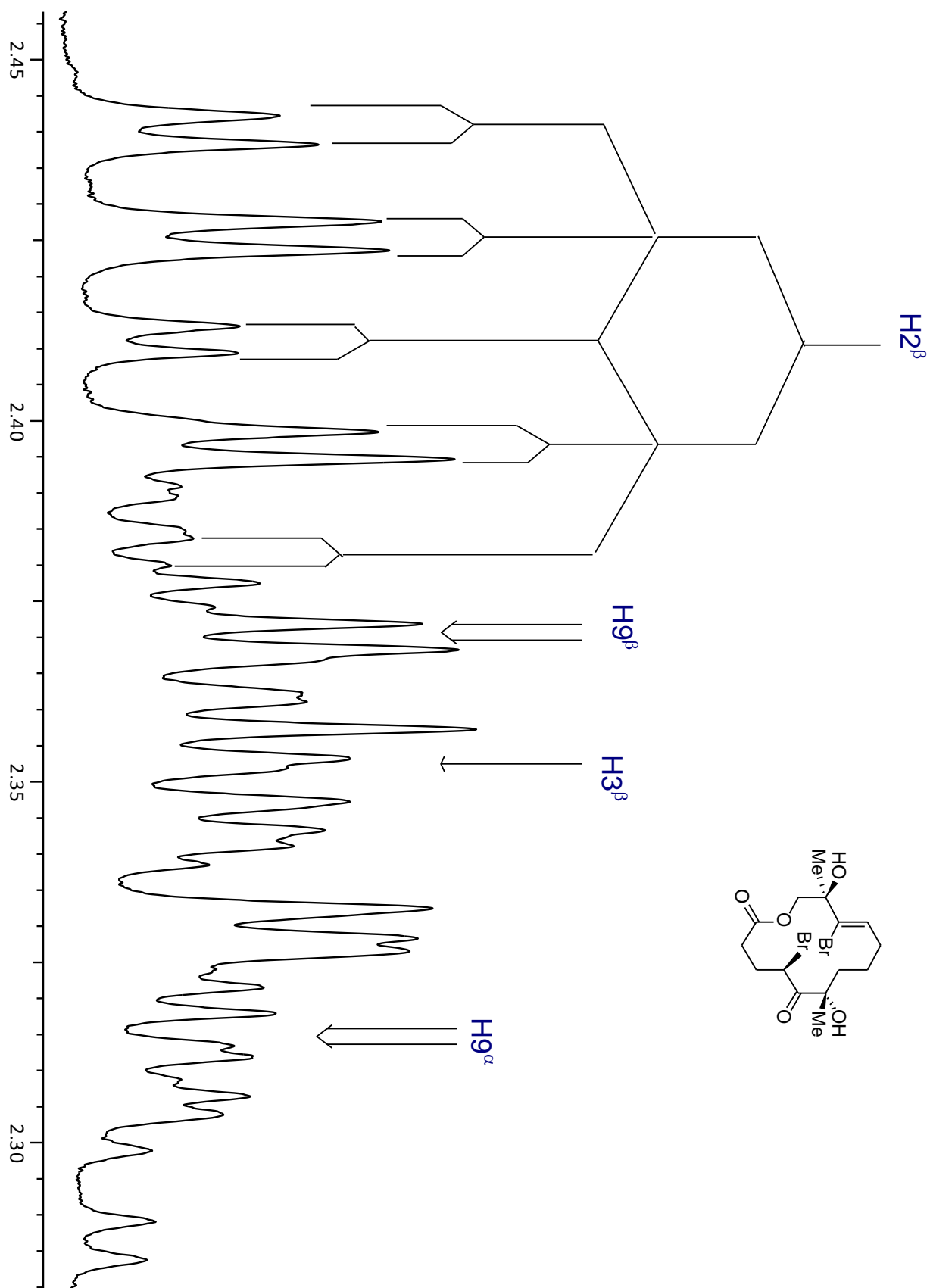
Symmetry transformations used to generate equivalent atoms: #1 -x,-y,-z

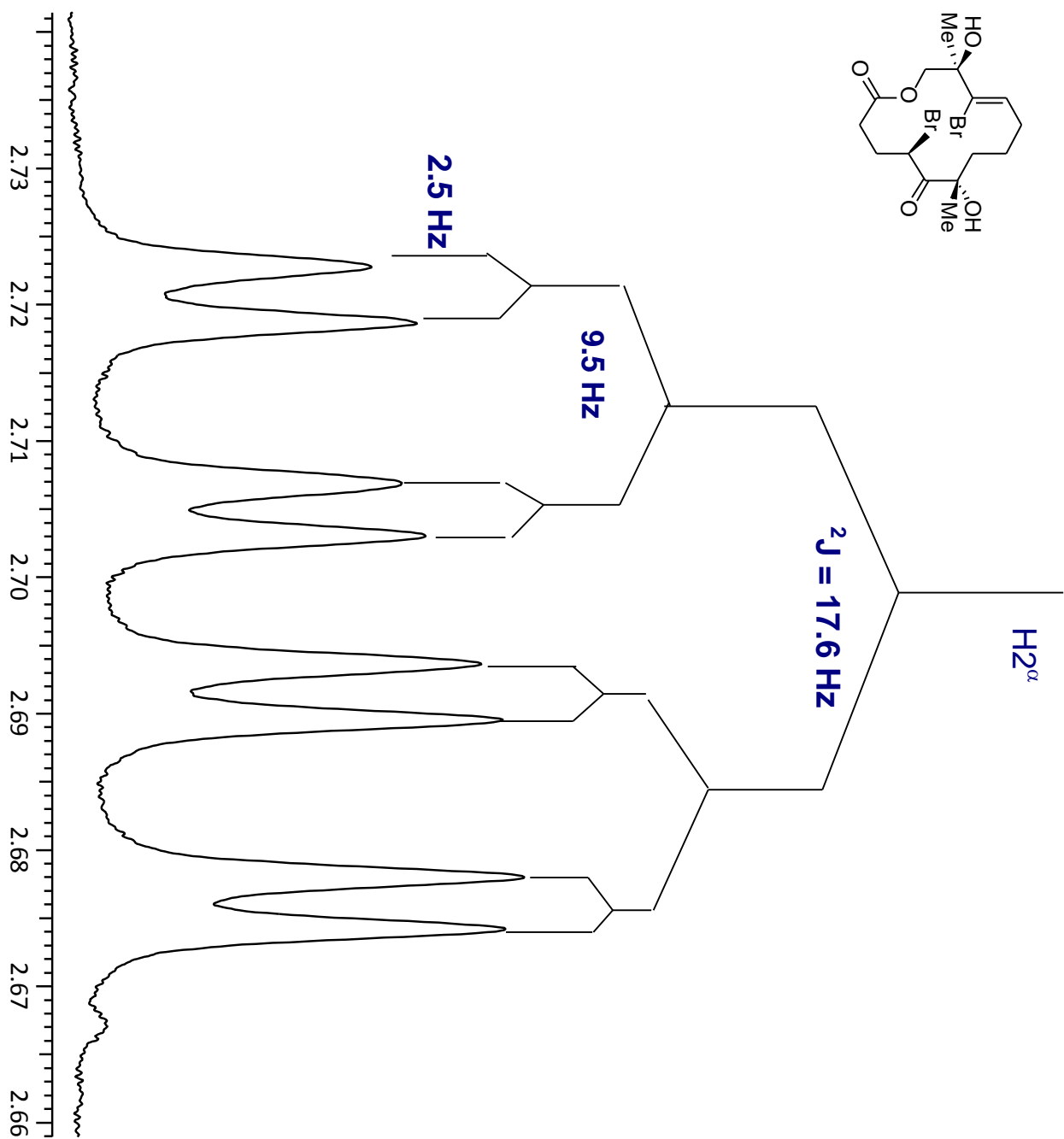
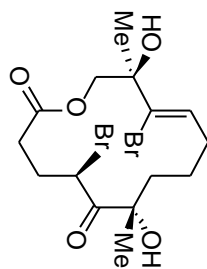


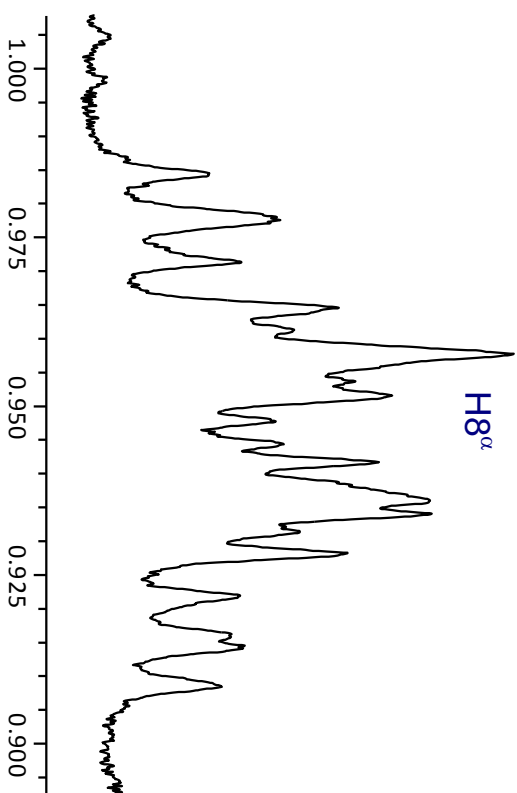
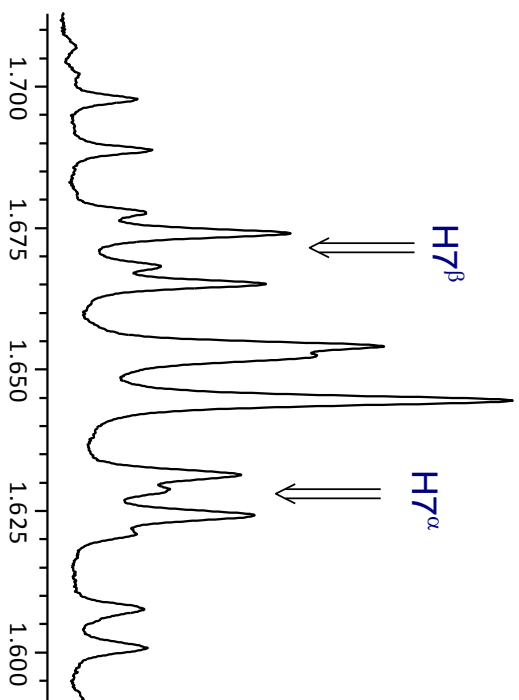
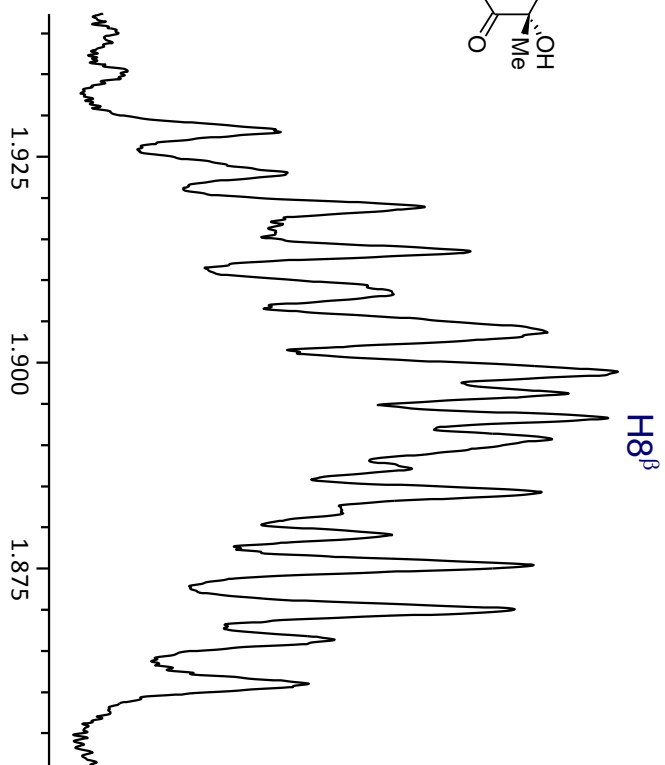
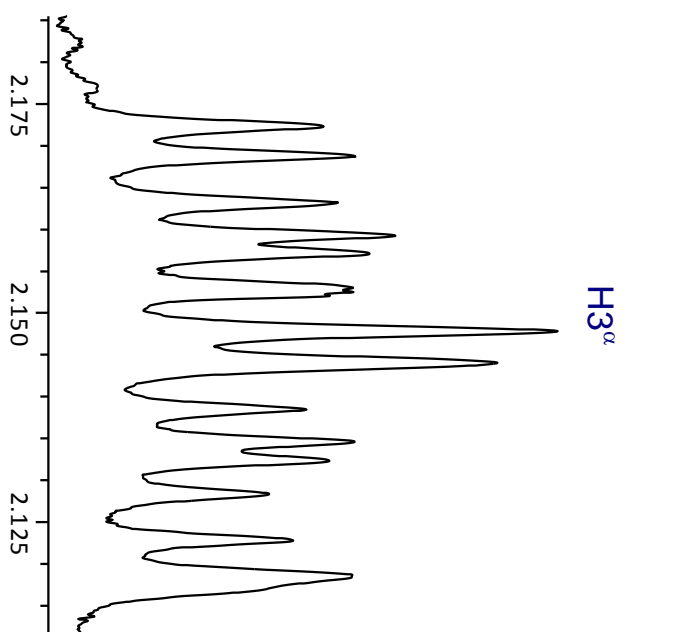
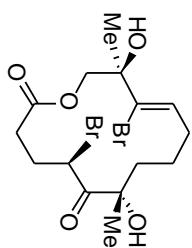
¹H NMR chemical shifts (δ/ppm) & coupling constant (J/Hz)	¹³C NMR chemical shift (δ/ppm)
2.70 (dddd, ² J = 17.6Hz, ³ J _{H2, H3} = 9.5Hz, 2.5Hz, H2)	169.9 ---- C1
2.41 (dddd, ² J = 17.6Hz, ³ J _{H2, H3} = 9.5Hz, 2.5Hz, H2)	31.3 ---- C2
2.35 (m, H3)	28.7 ---- C3
2.17 - 2.12 (m, H3)	42.1 ---- C4
4.64 (dd, J _{H4, H3} = 9.1Hz, J _{H4, H3} = 5.7Hz, H4)	208.1 ---- C5
1.57 (s, 6-CH₃)	78.9 ---- C6
3.70 (s, 6-OH)	36.6 ---- C7
1.70 - 1.60 (m, H7β, H7α)	22.0 ---- C8
1.93 - 1.85 (m, H8)	30.1 ---- C9
0.98 - 0.90 (m, H8)	132.1 ---- C10
2.37 (H9)	131.7 ---- C11
2.31 (H9)	64.5 ---- C12
6.04 (dd, J = 9.0, 6.6Hz, H10)	69.7 ---- C13
2.03 (s, 12-CH₃)	26.9 ---- 6-CH ₃
5.05 (d, ² J = 13.3 Hz, H13)	28.6 ---- 12-CH ₃
4.18 (d, ² J = 13.3 Hz, H13)	

¹d TOCSY**HMBC****NOESY**

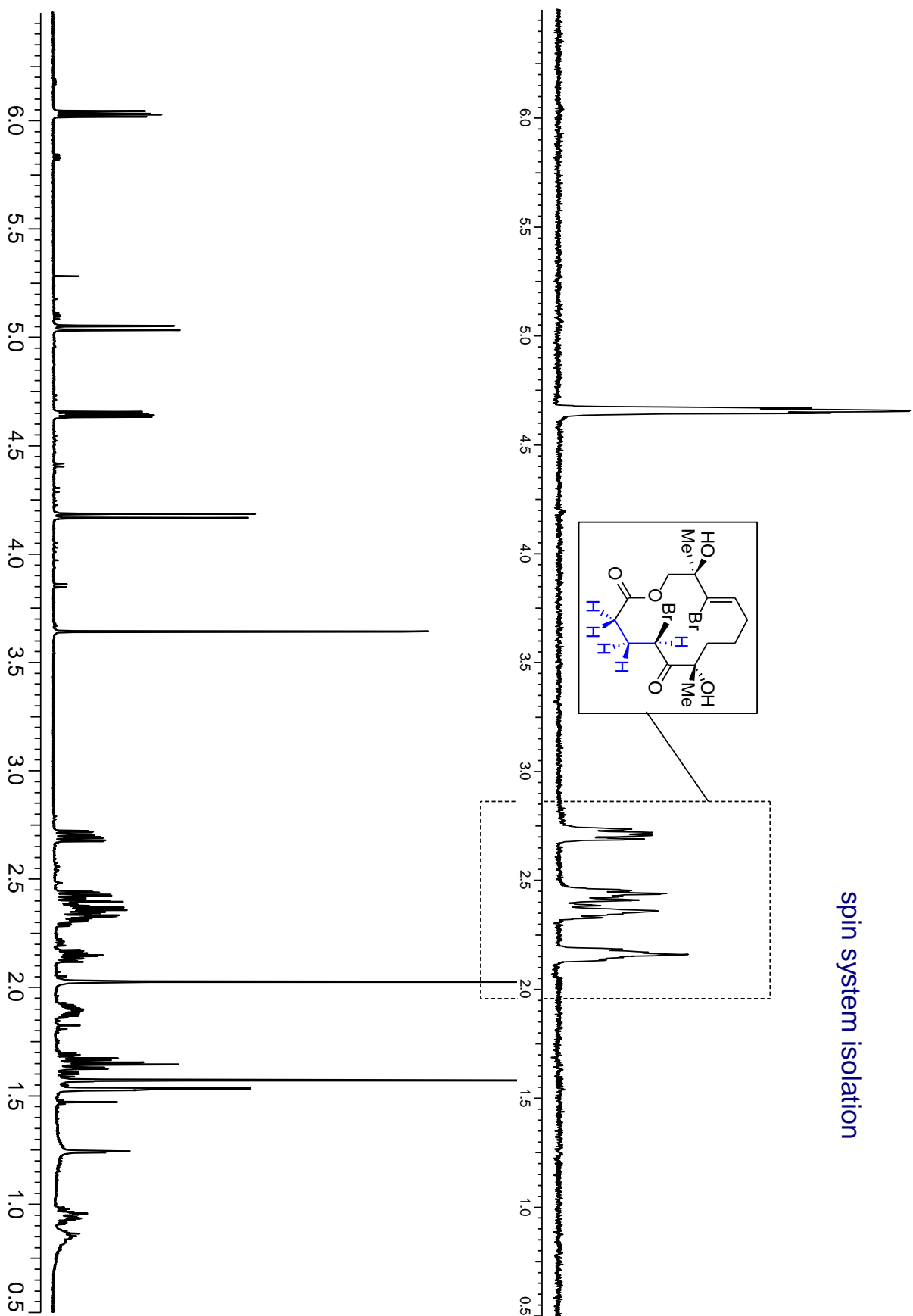




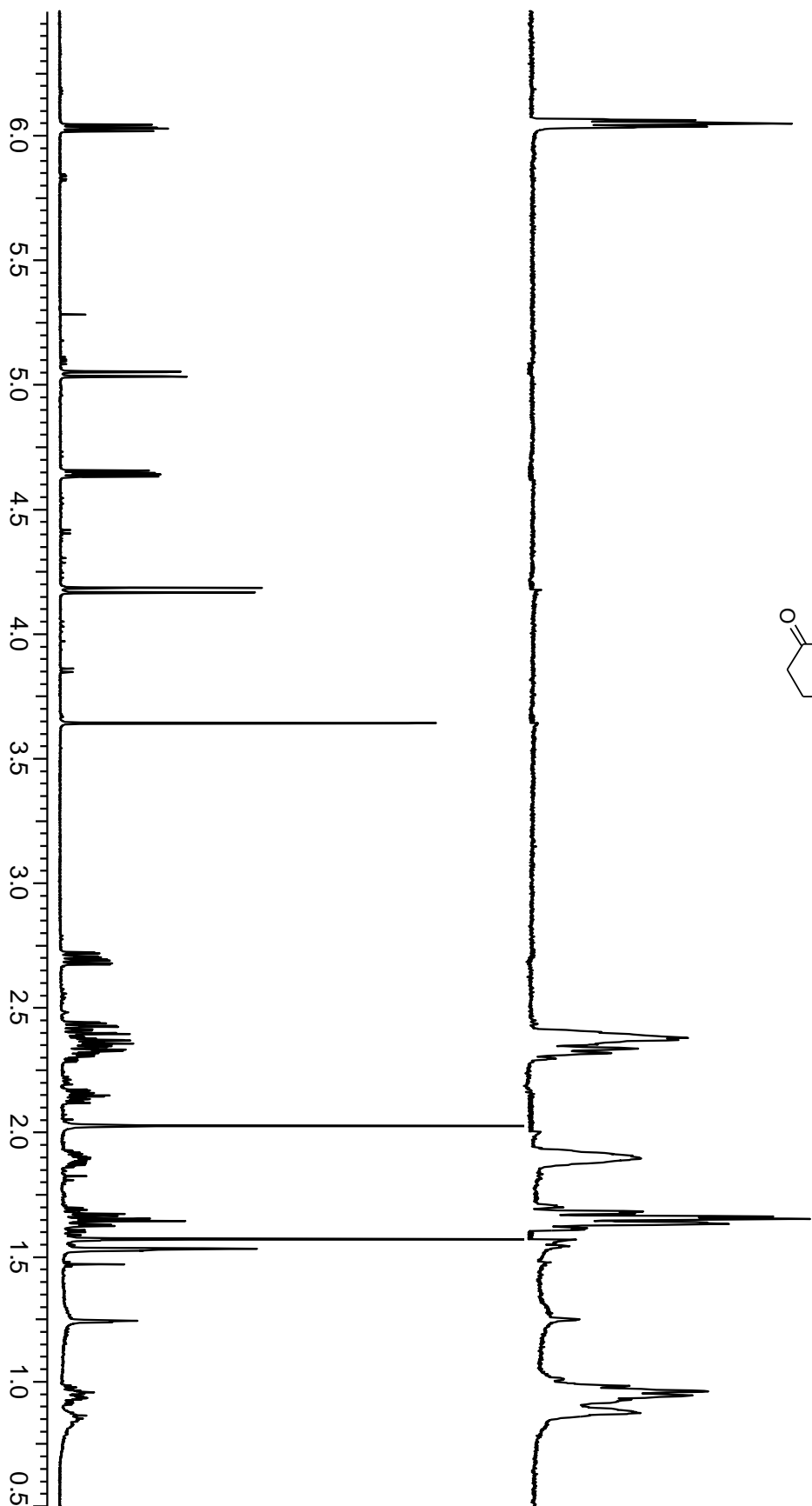
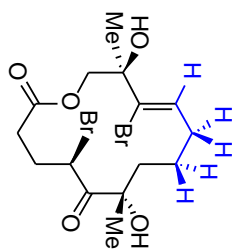


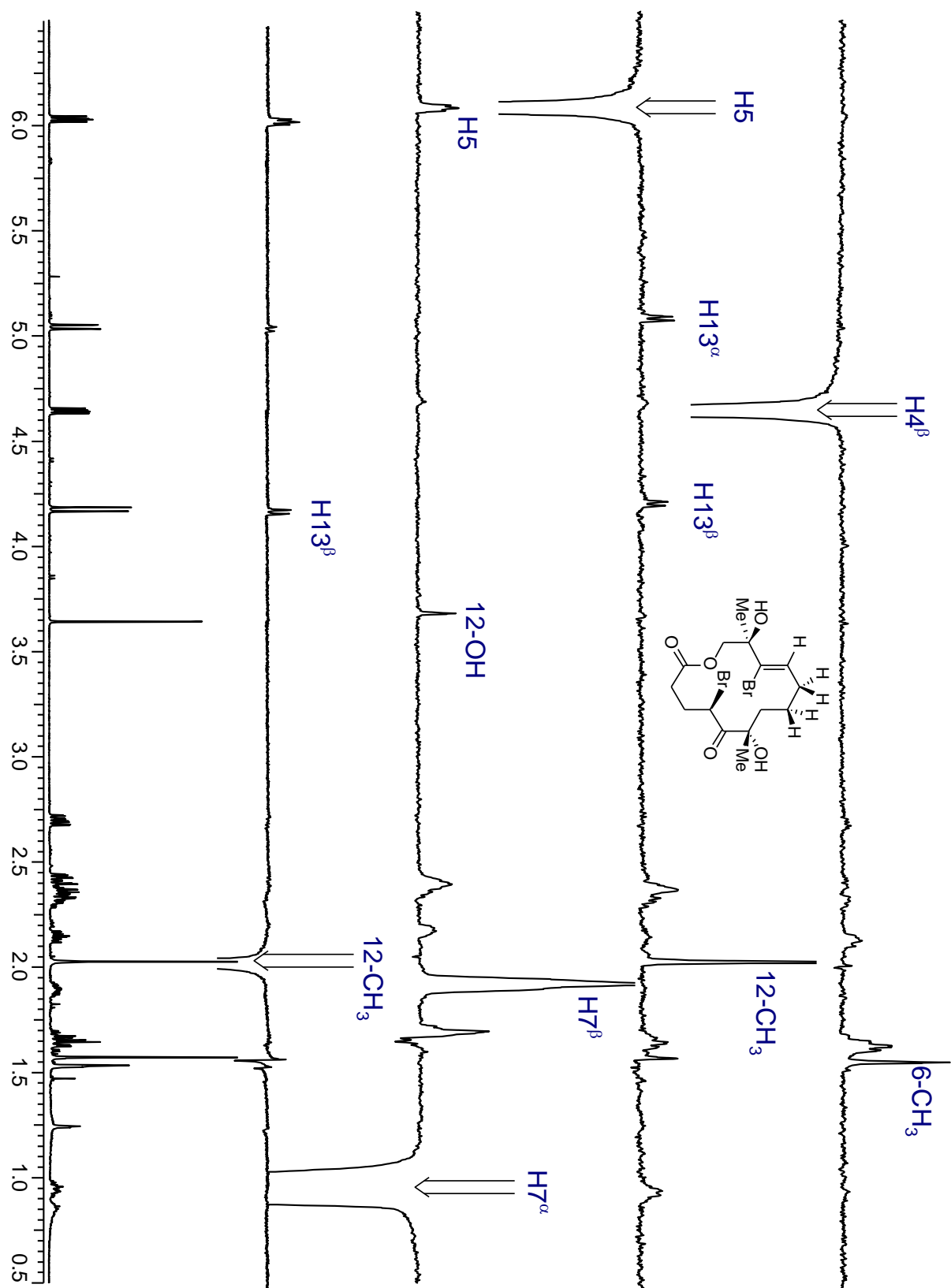


spin system isolation

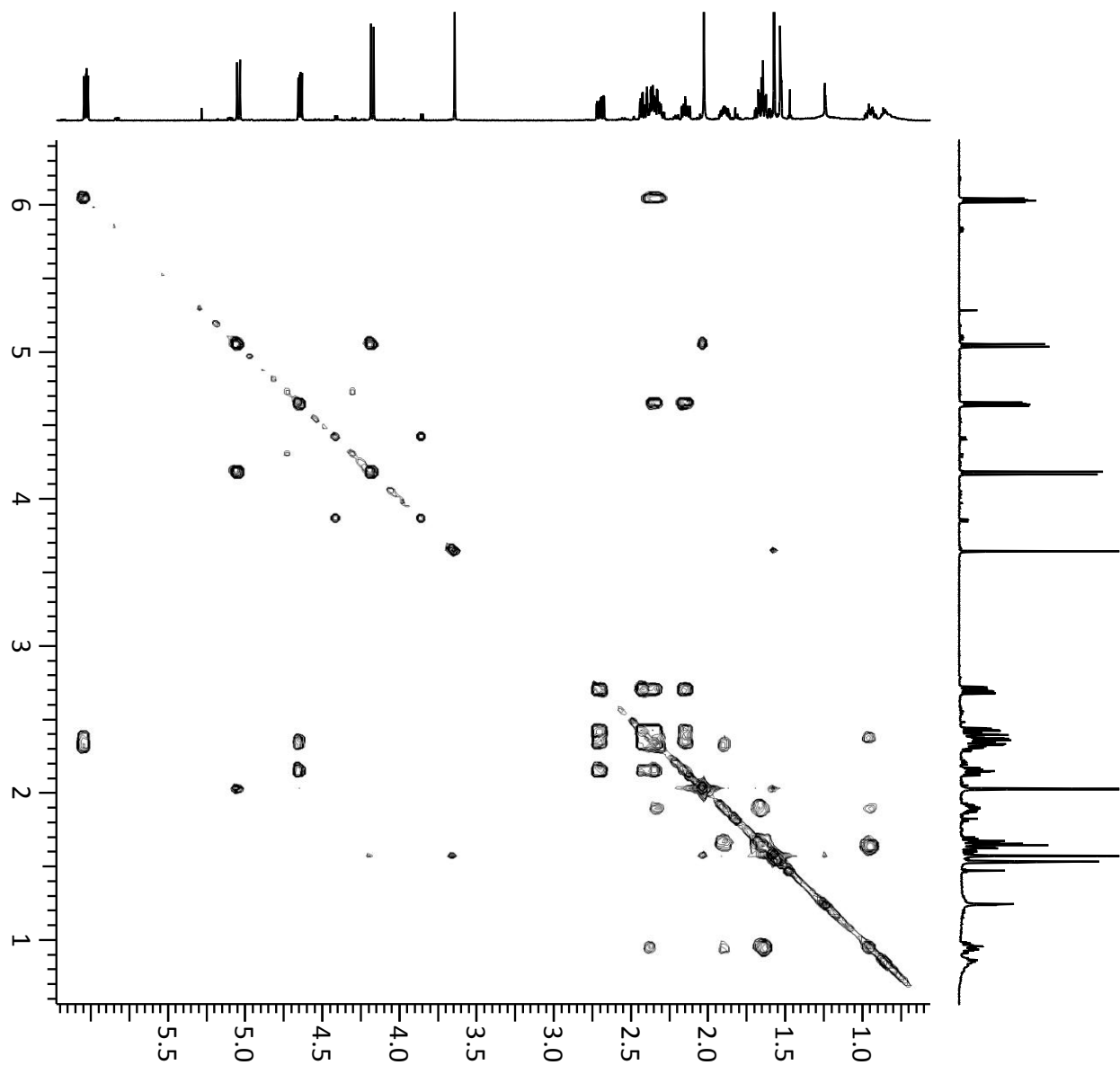


spin system isolation

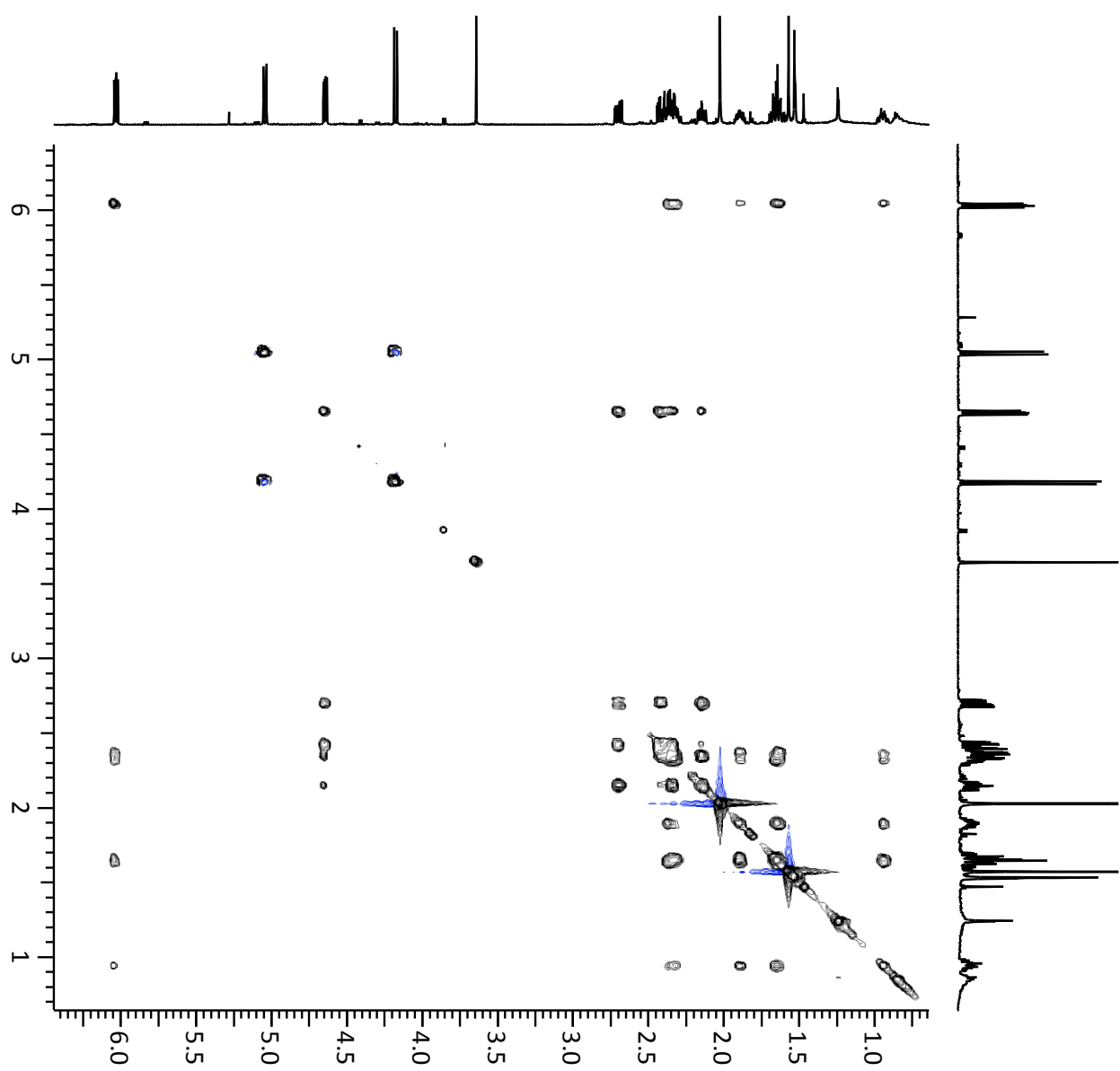




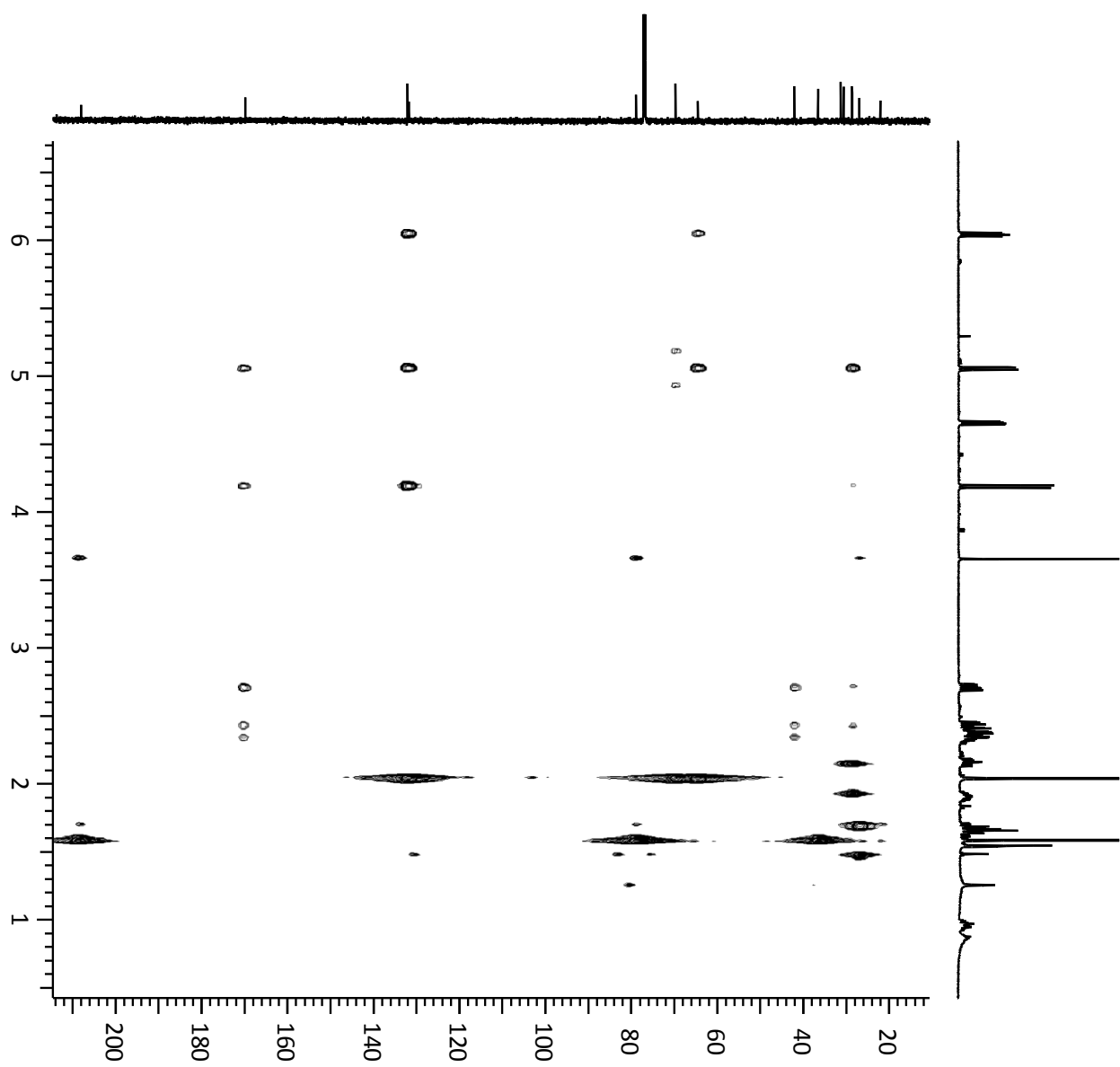
gCOSY

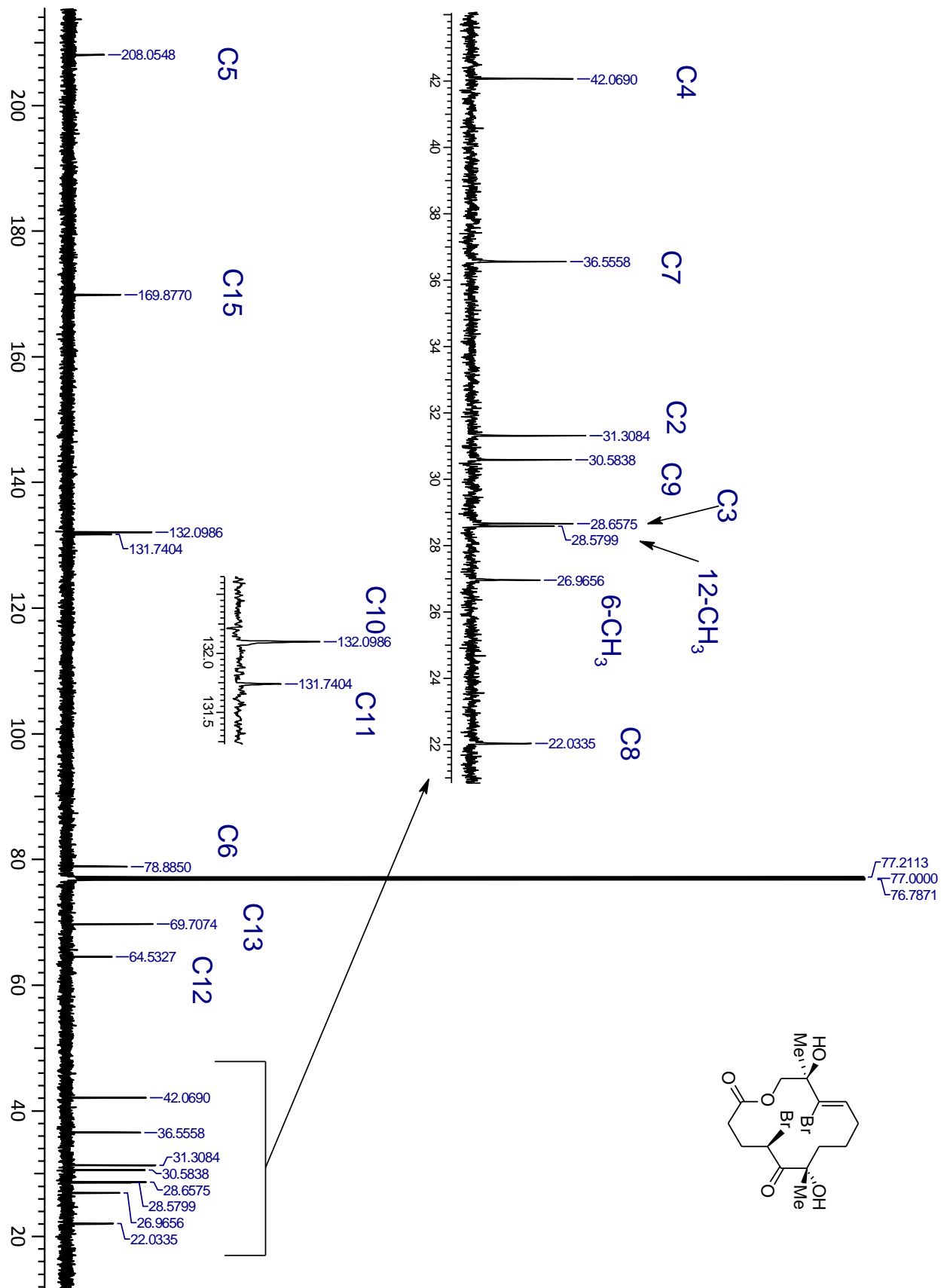


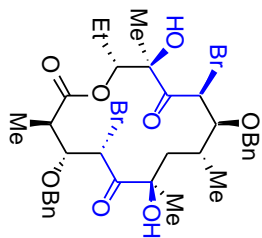
NOESY



HMBC







1D TOCSY spectra

H13

13-CH₂ CH₃

2-CH₃

H4

H3

H2

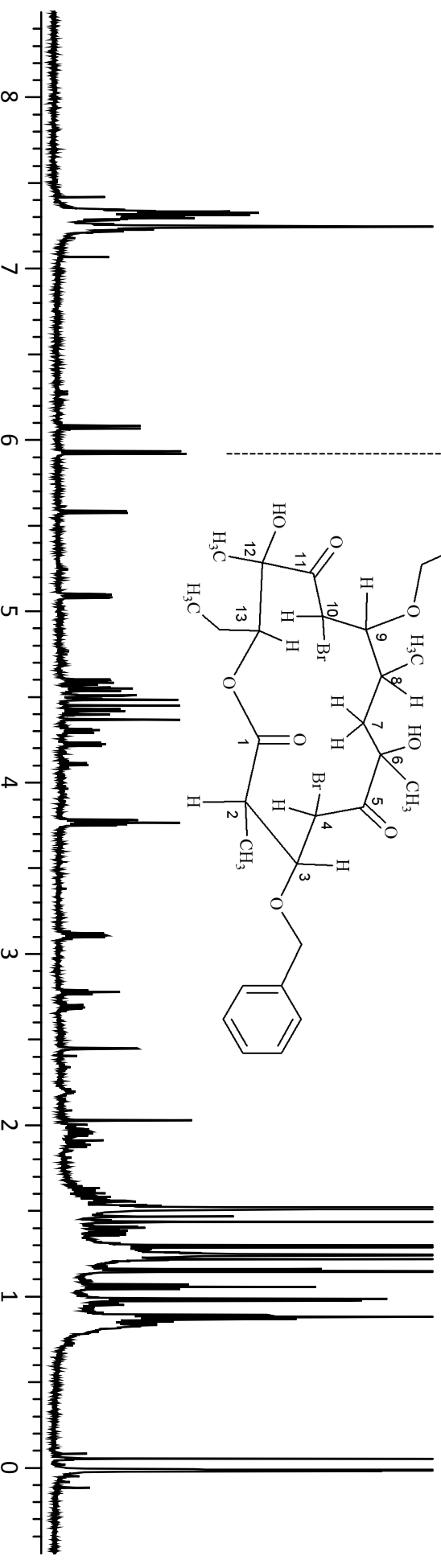
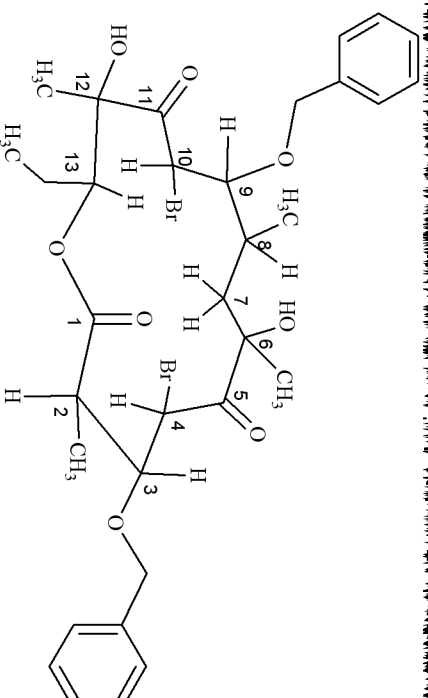
7-CH₂

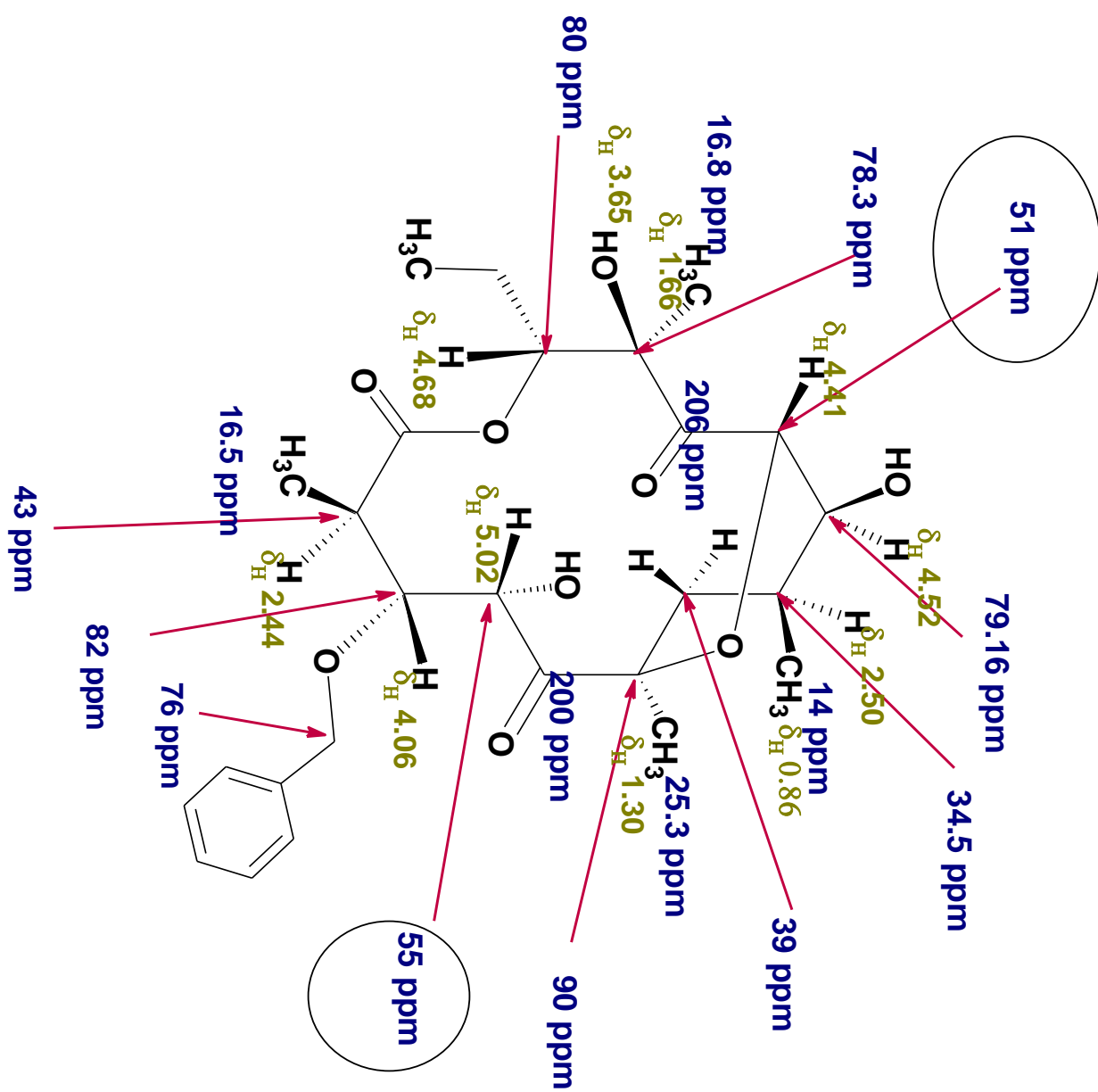
8-CH₃

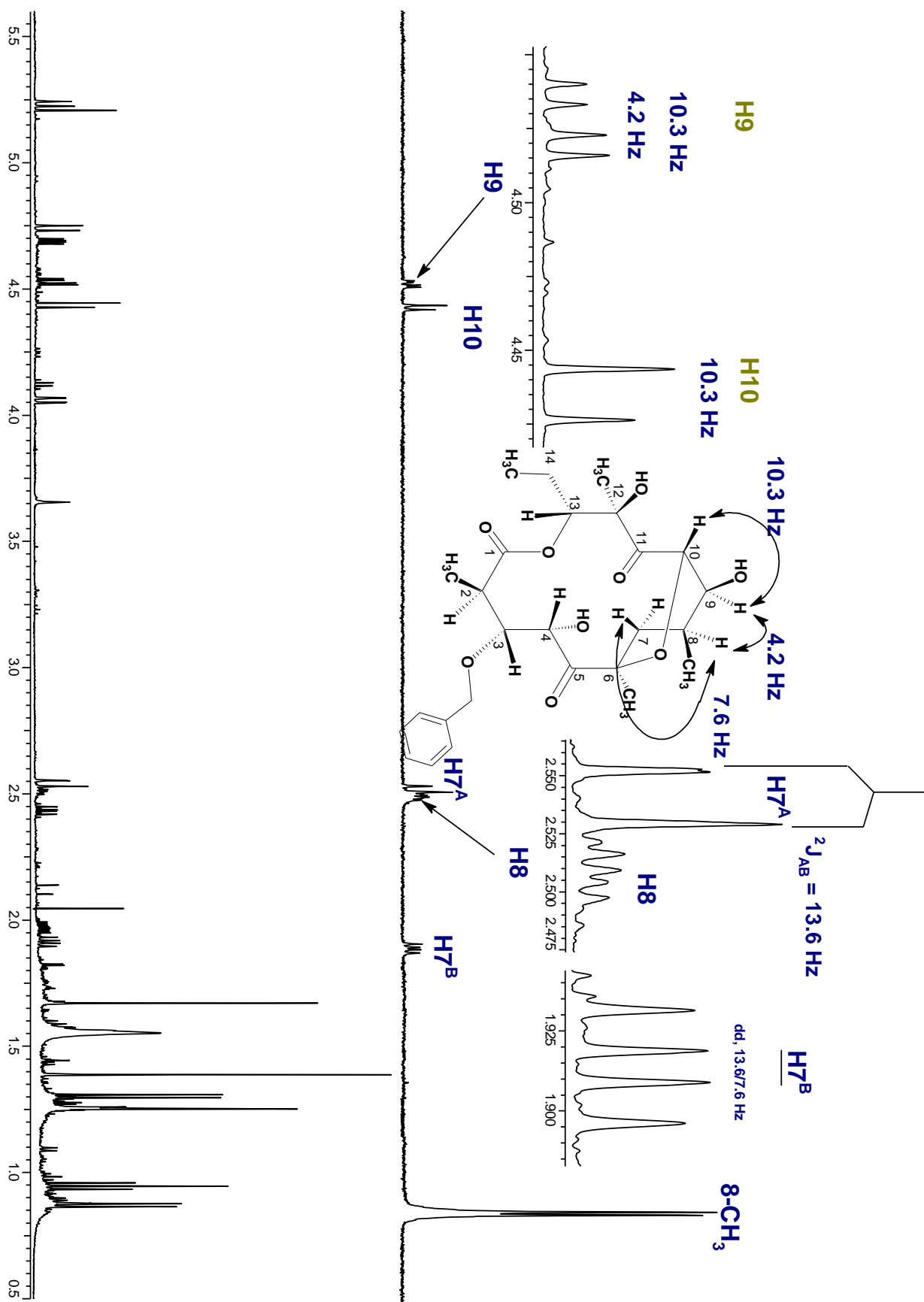
H10

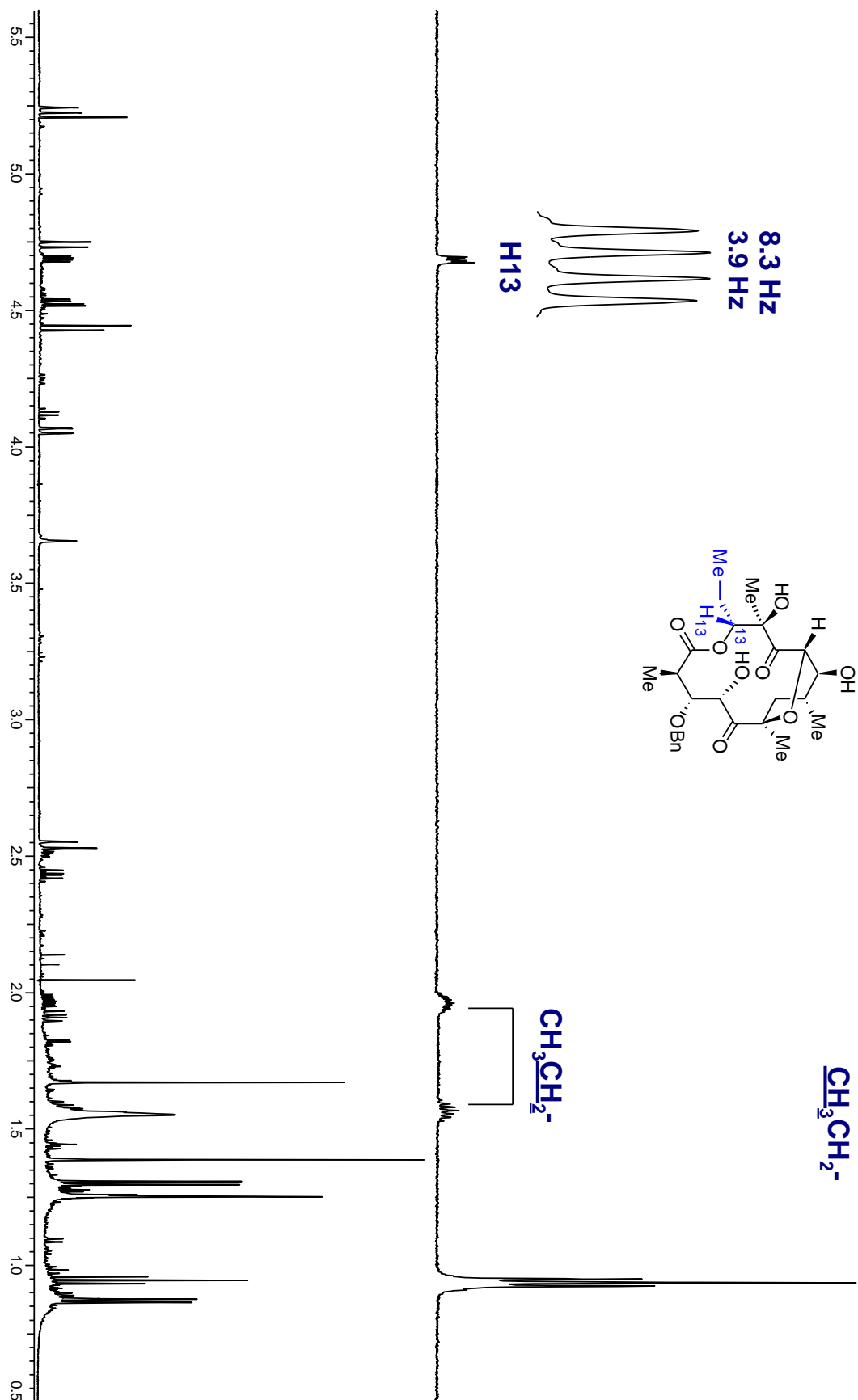
H9

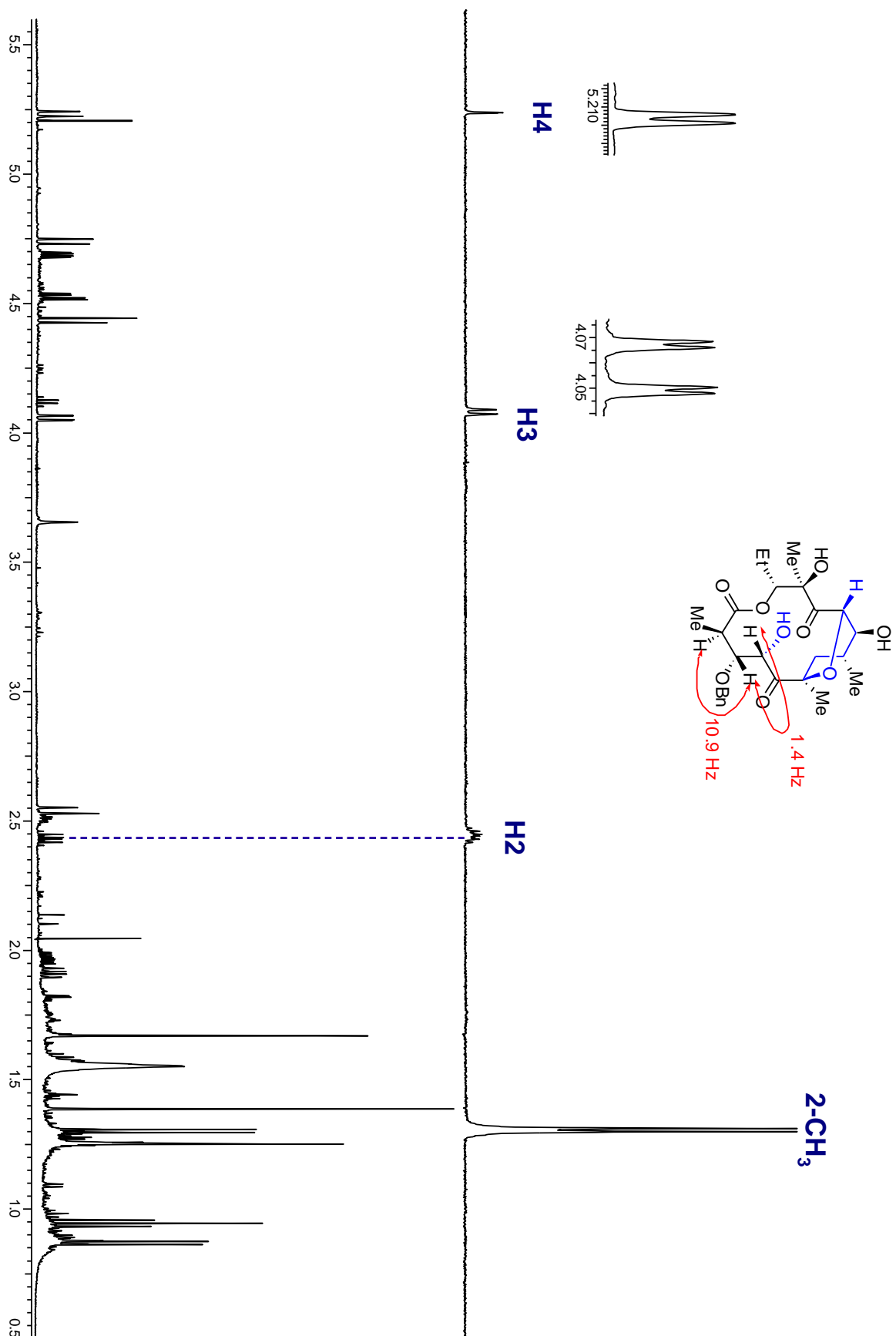
H8



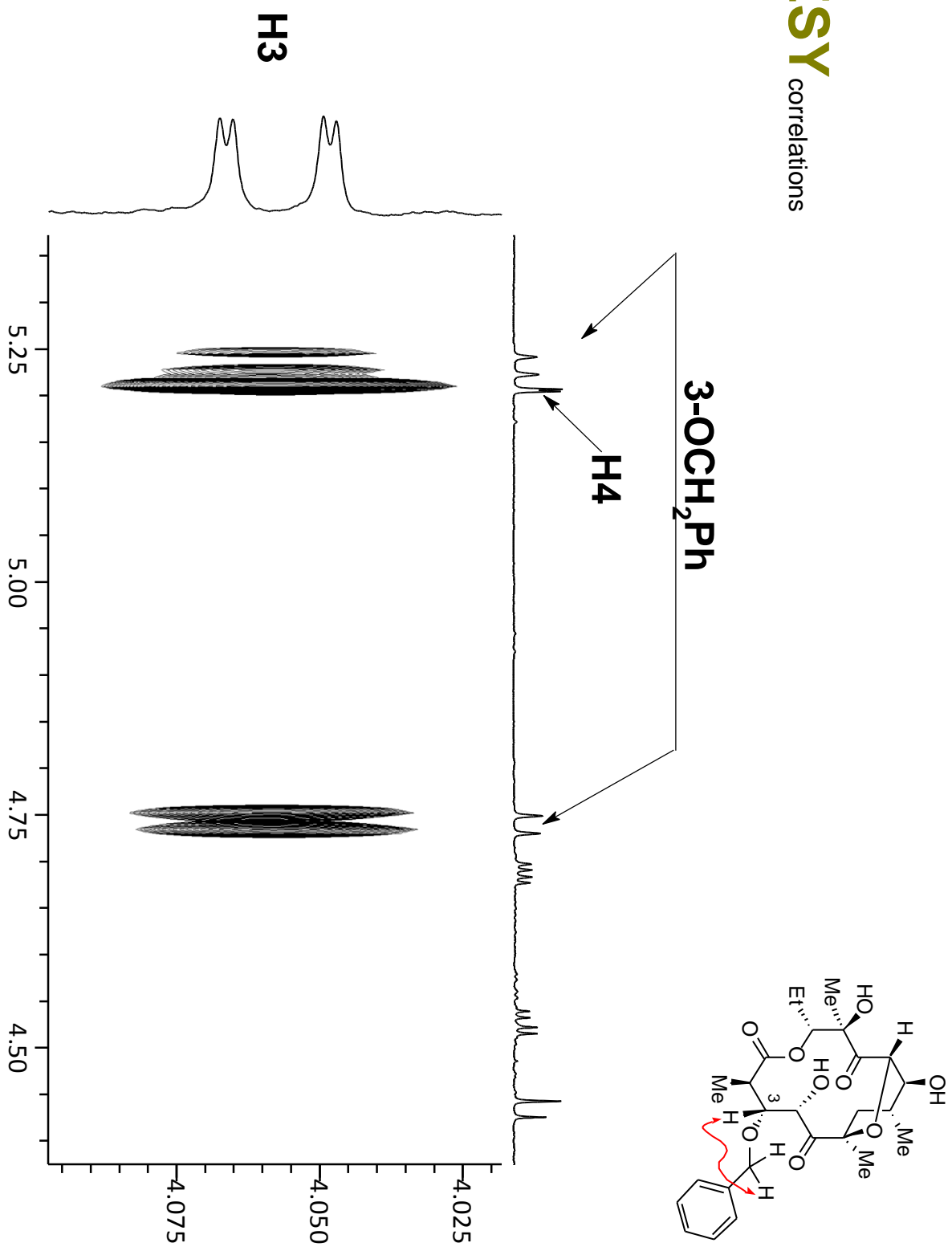






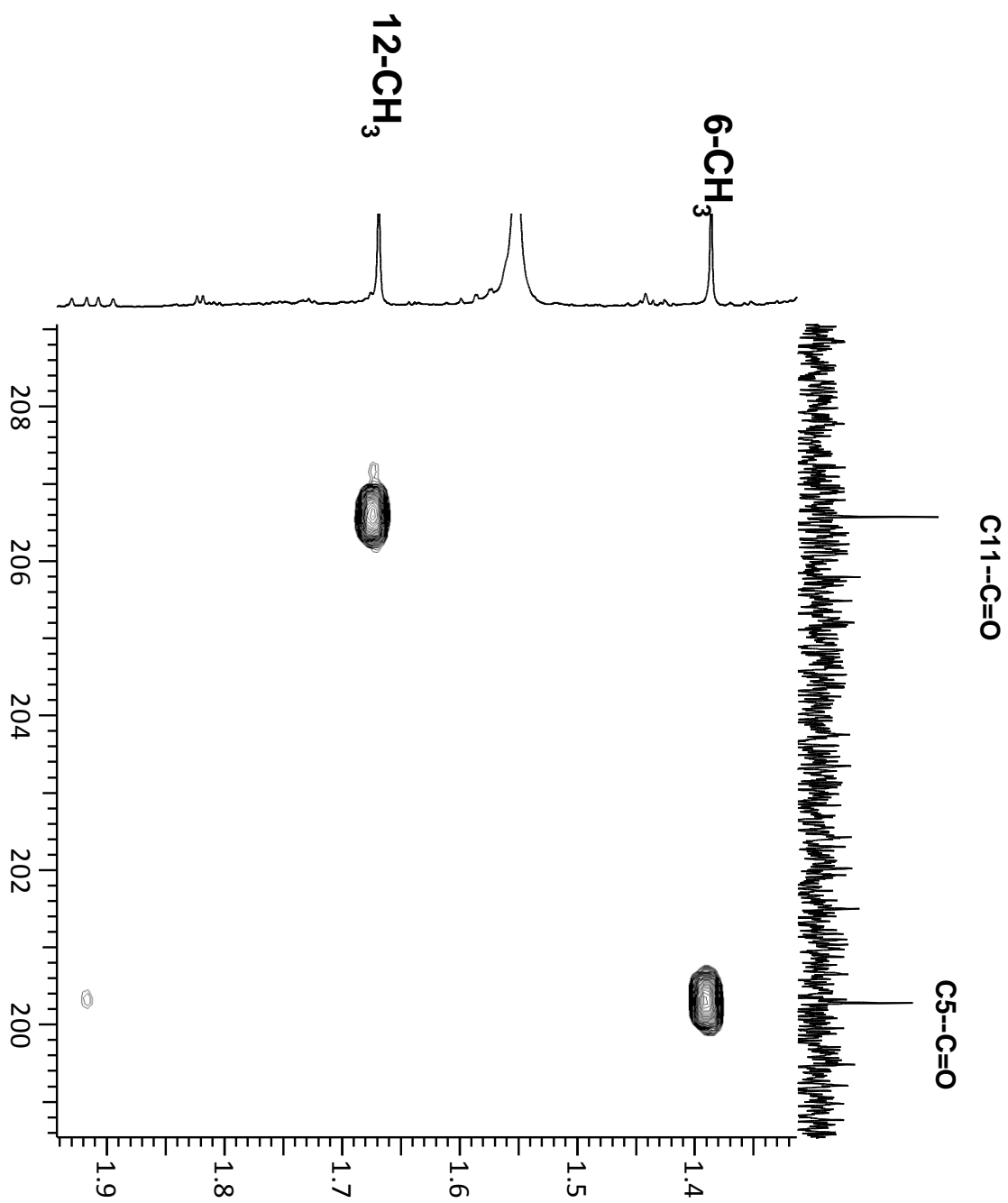


NOESY correlations



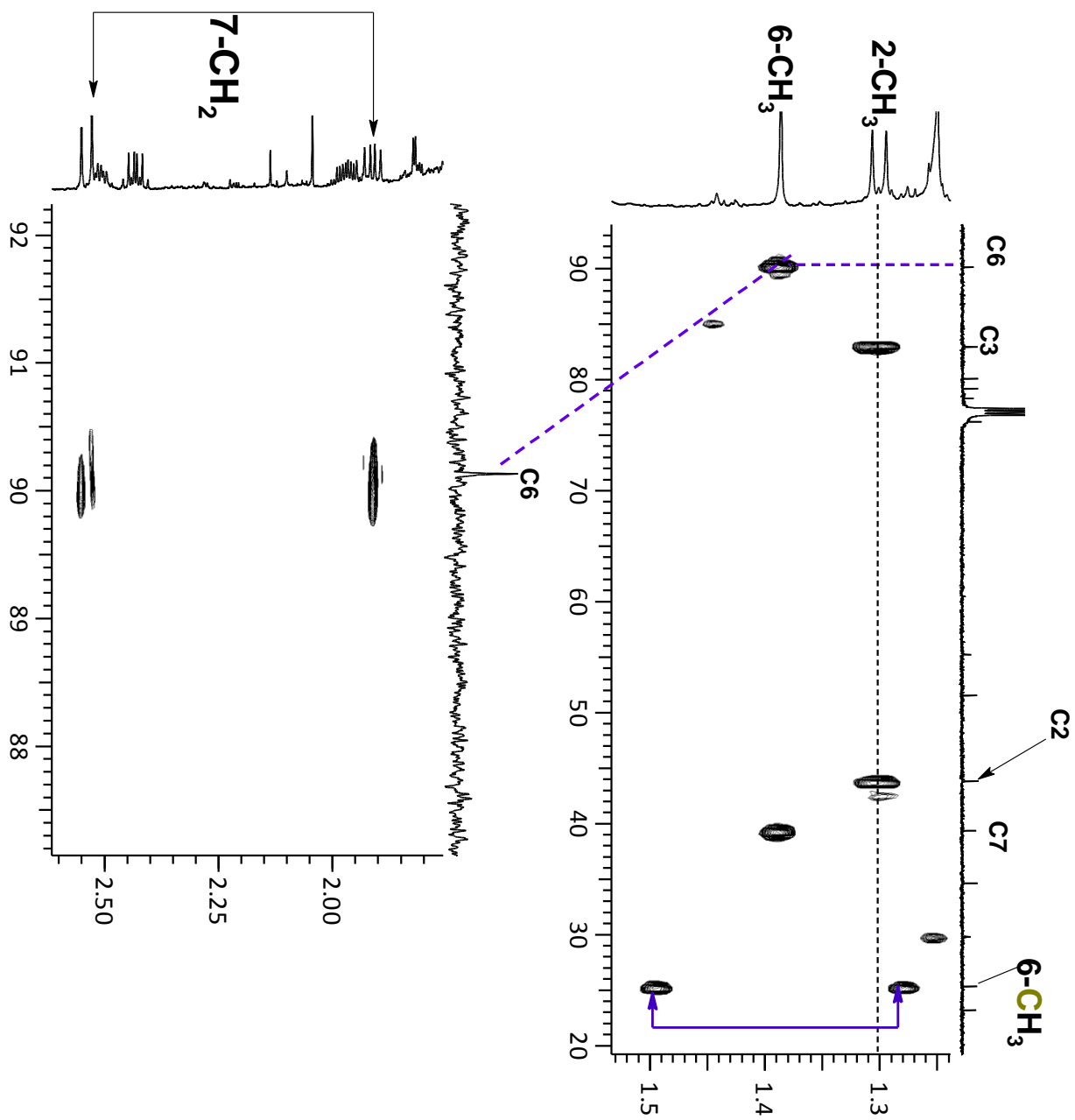
gHMBc

correlations



gHMBC

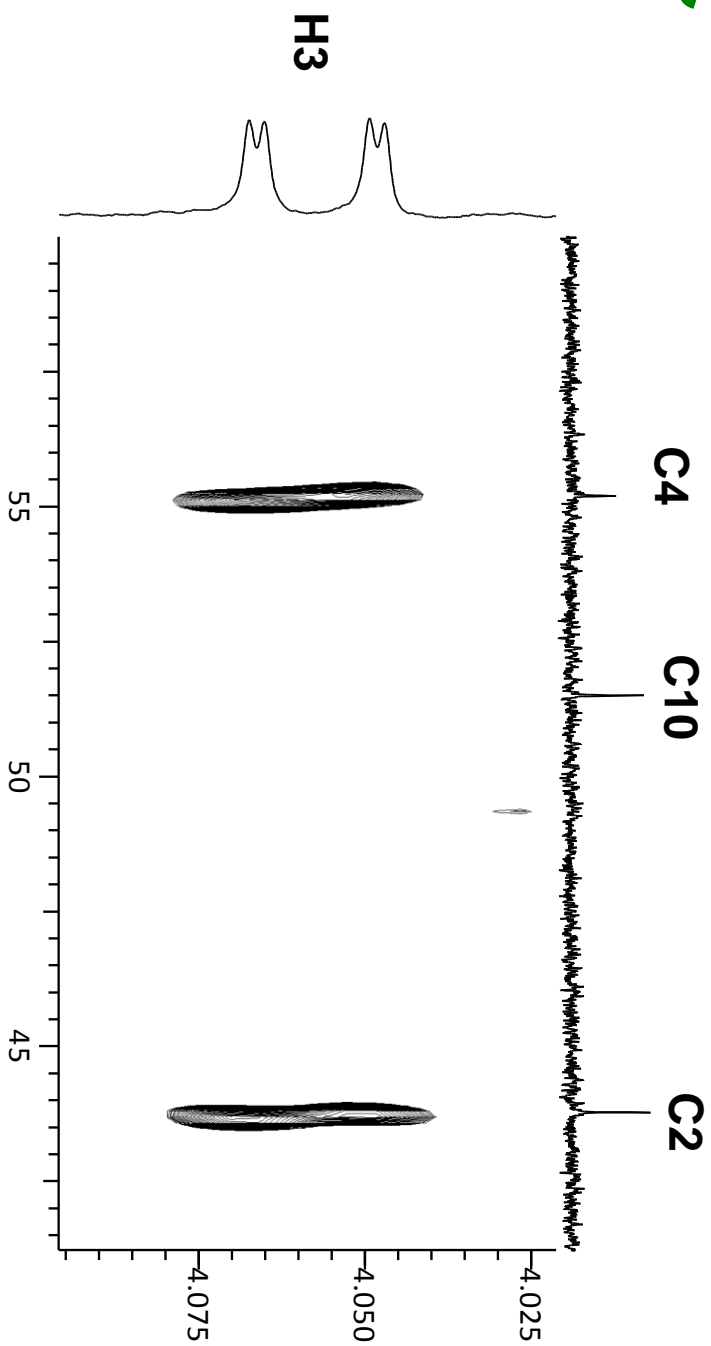
correlations



gHMBC

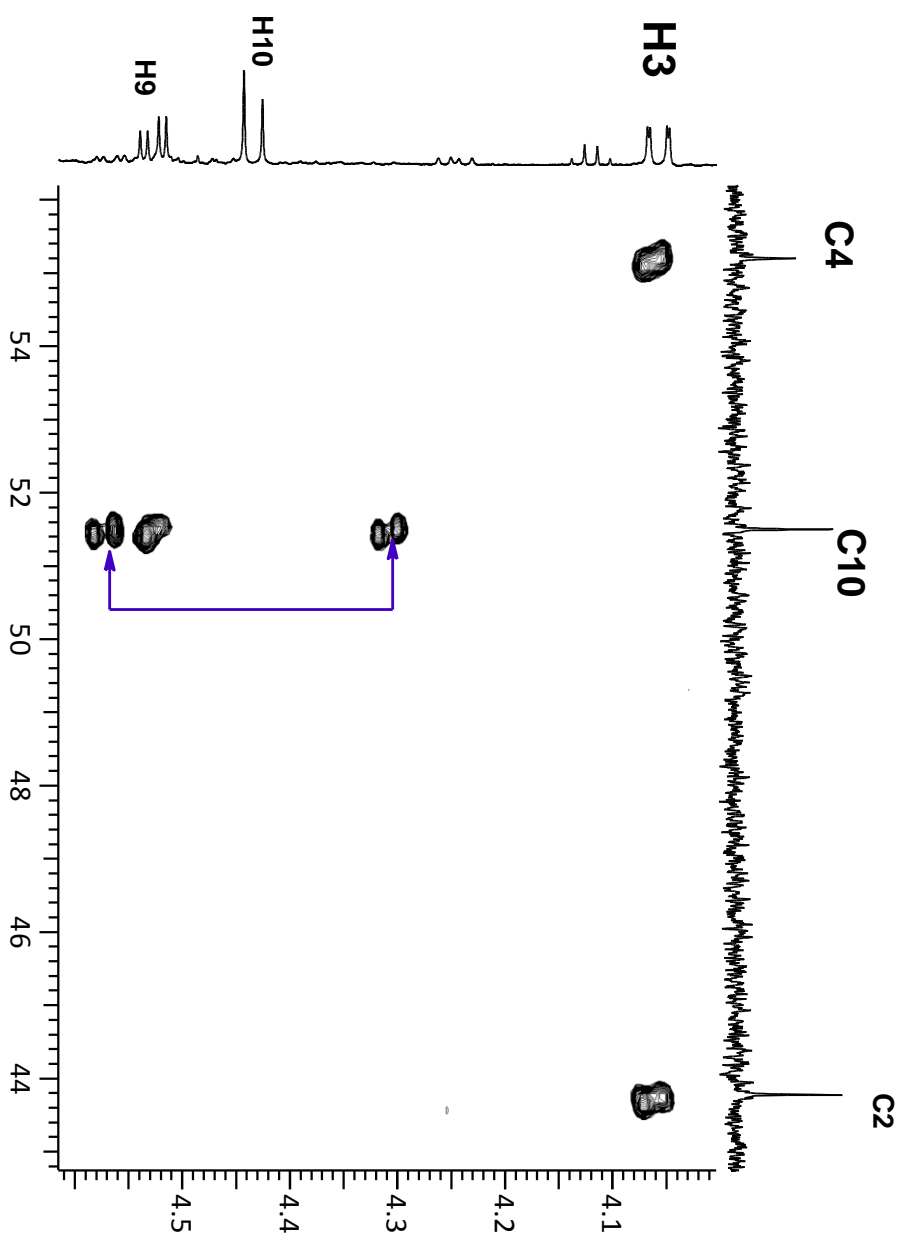
correlations

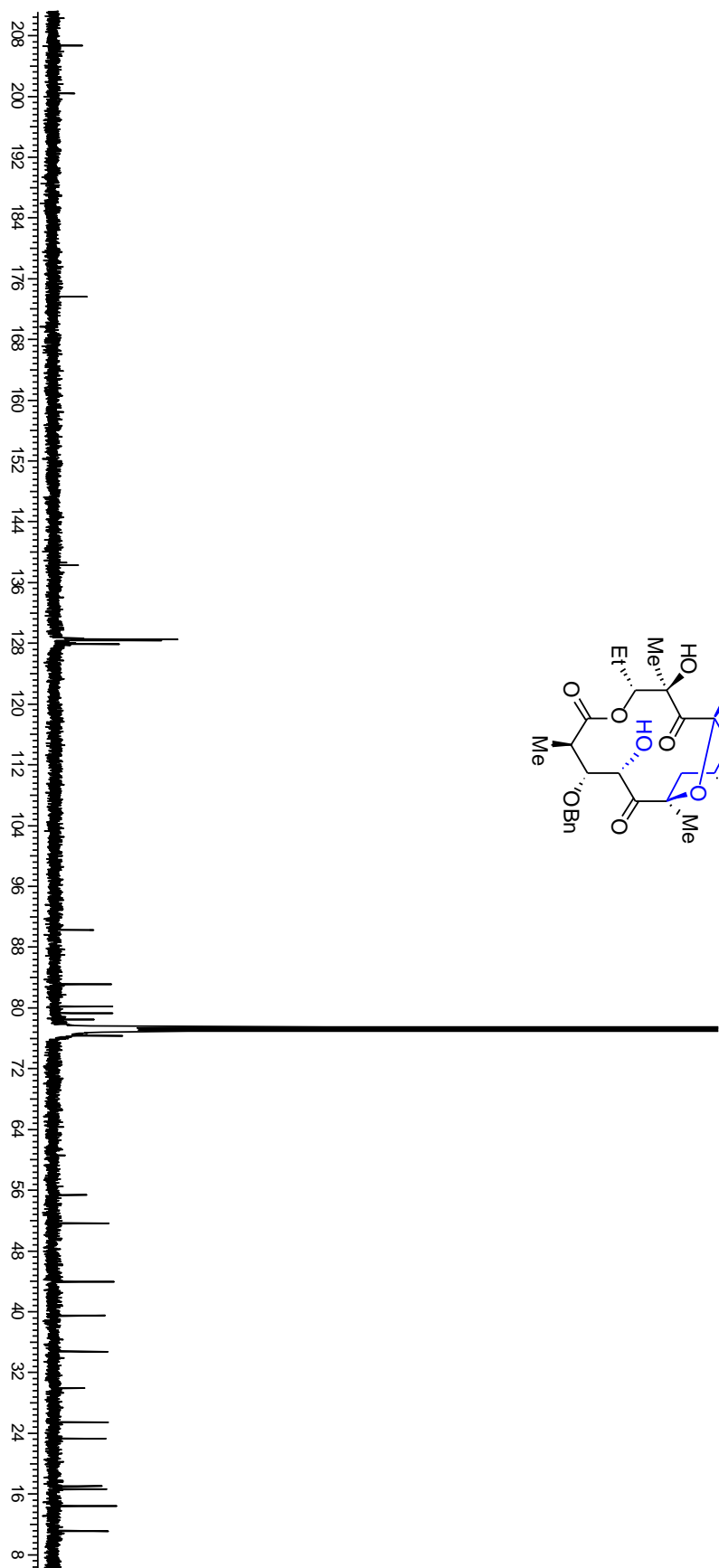
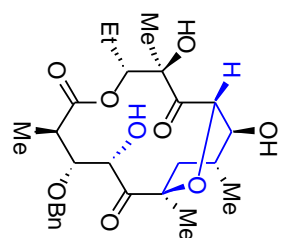
there is no more long range correlation to 55pm! only one between H3 and 55ppm)

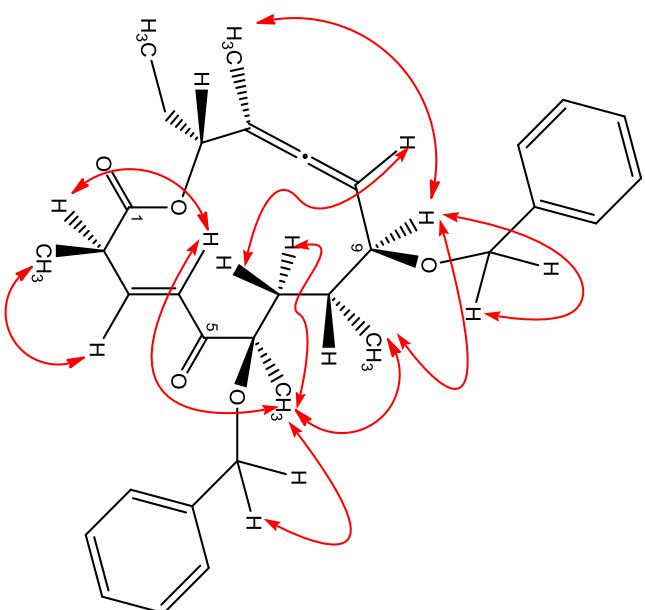
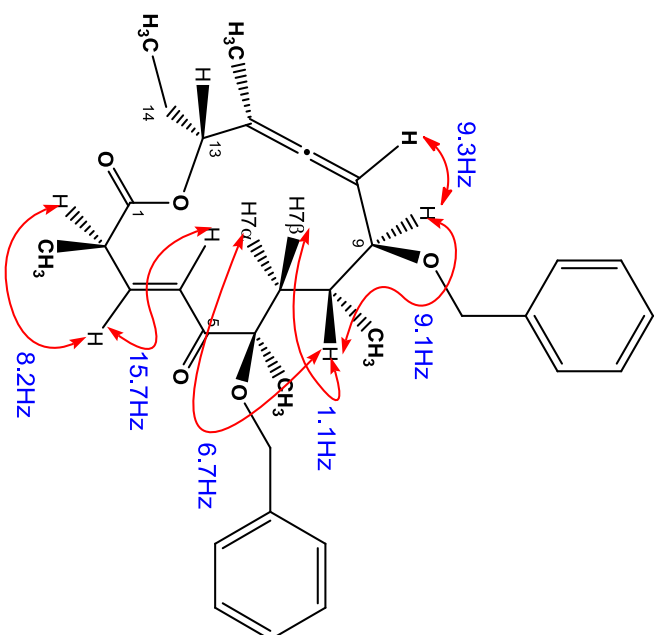
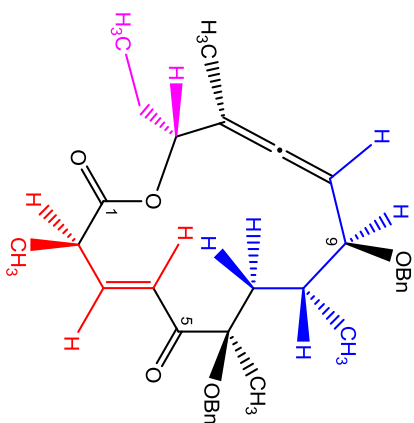


gHMBC

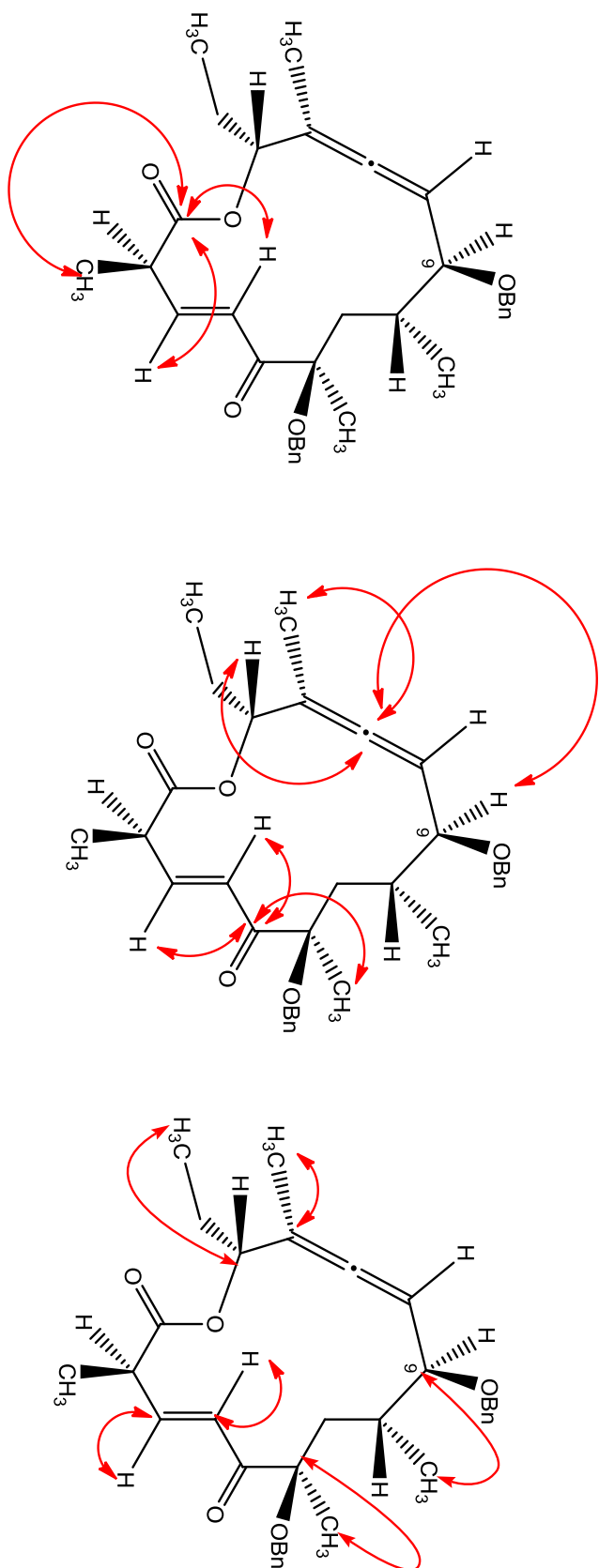
correlations

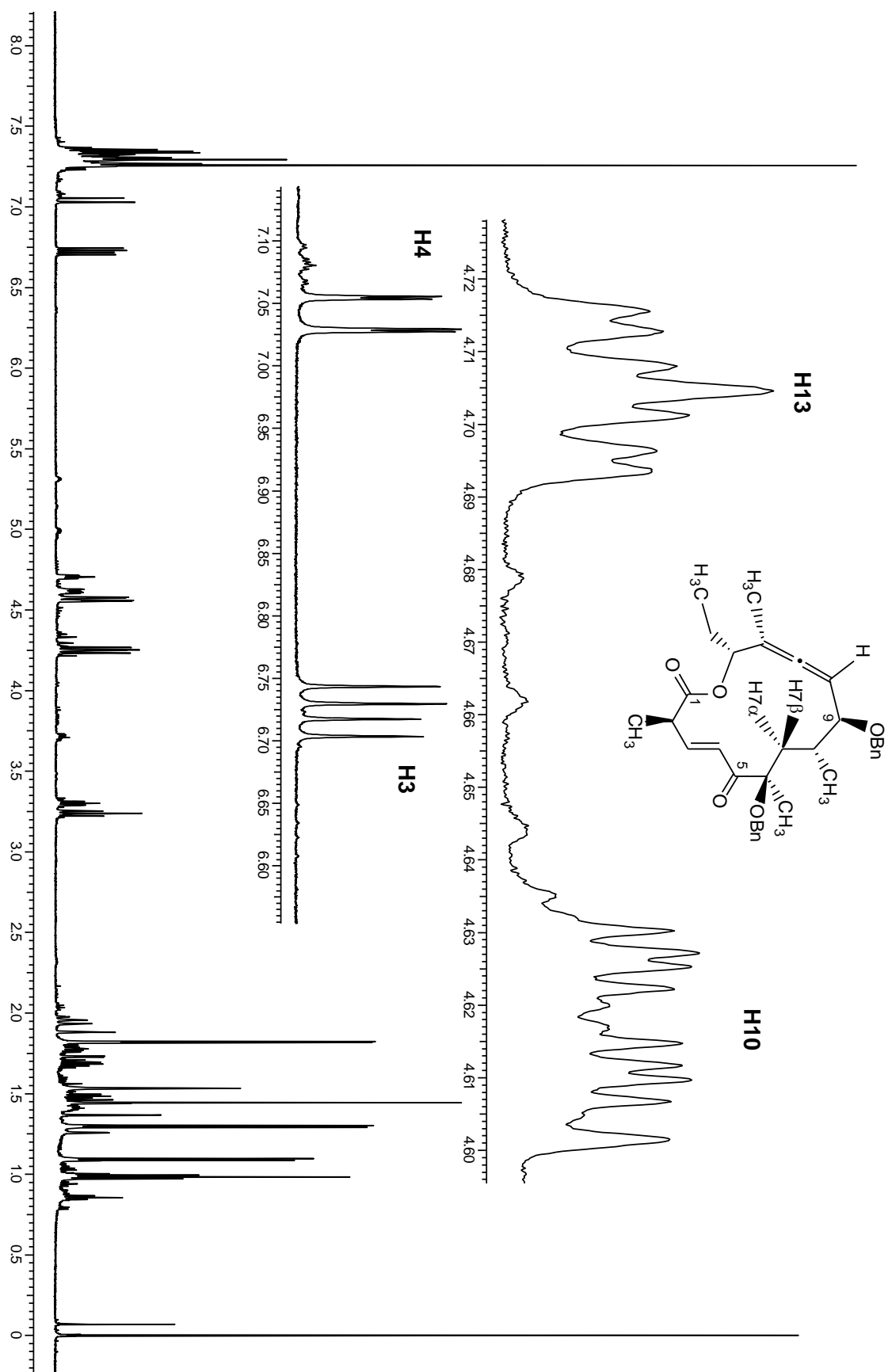


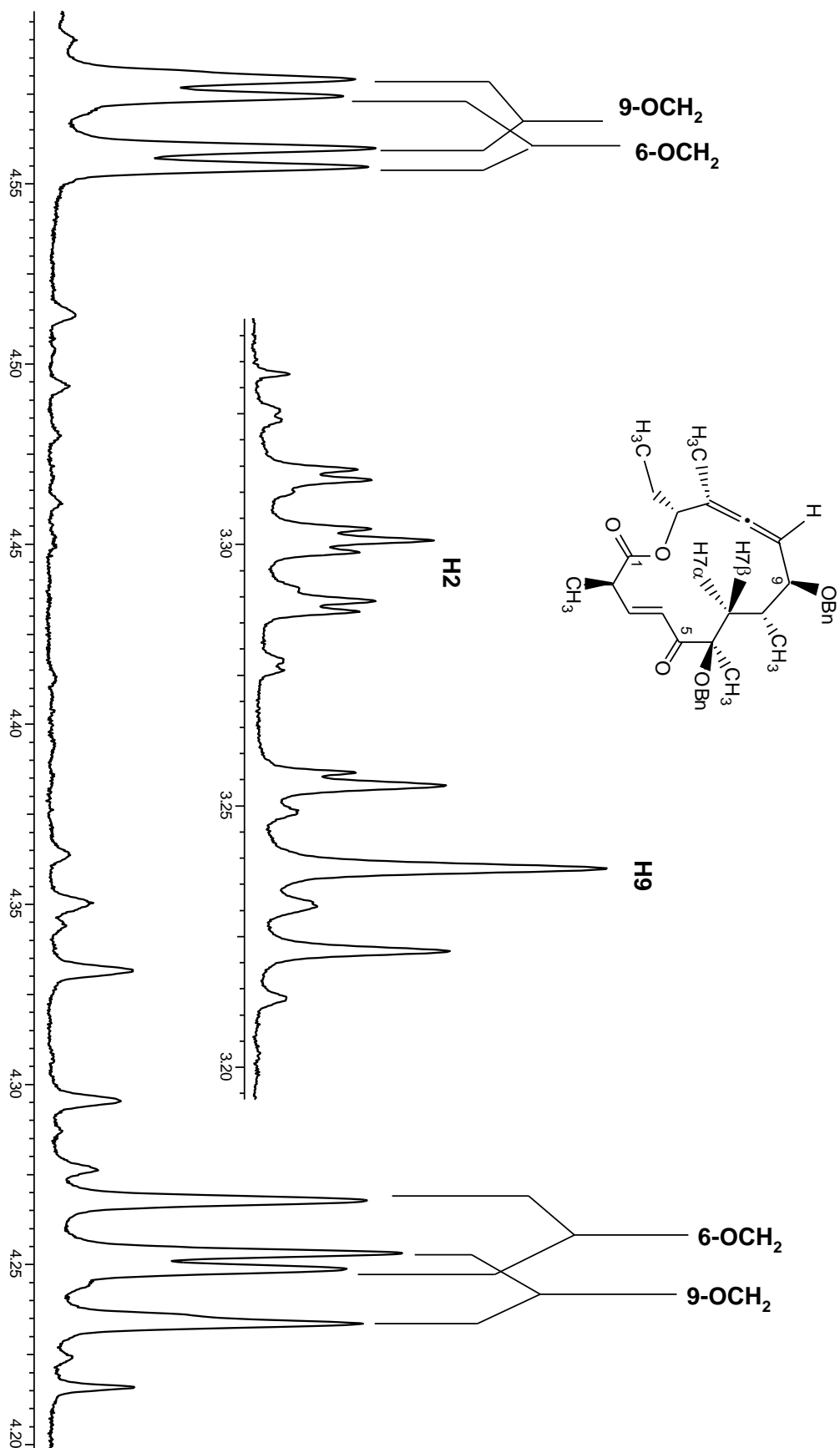


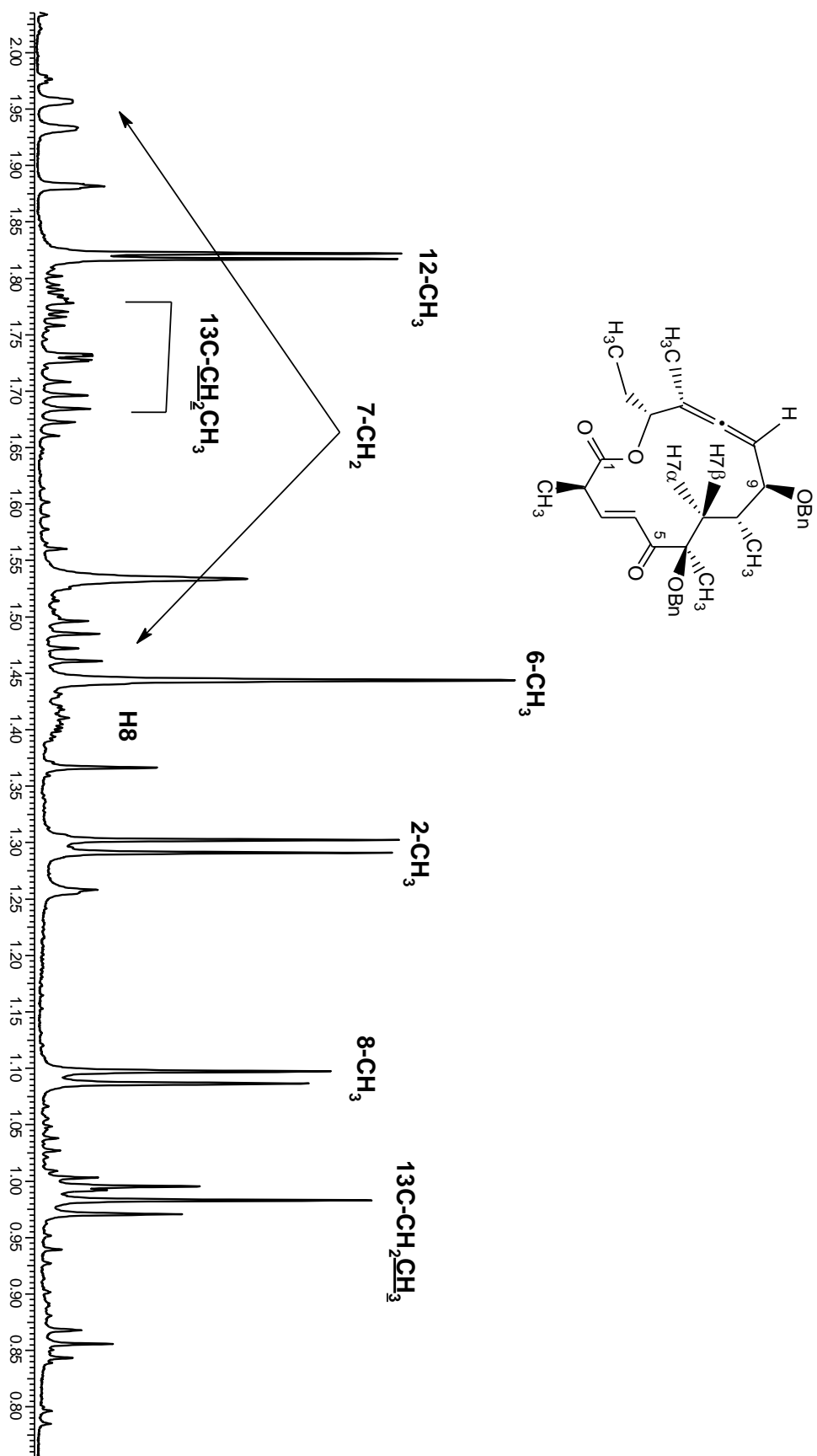
1d TOCSY**Coupling constant (J_{HH})****NOESY**

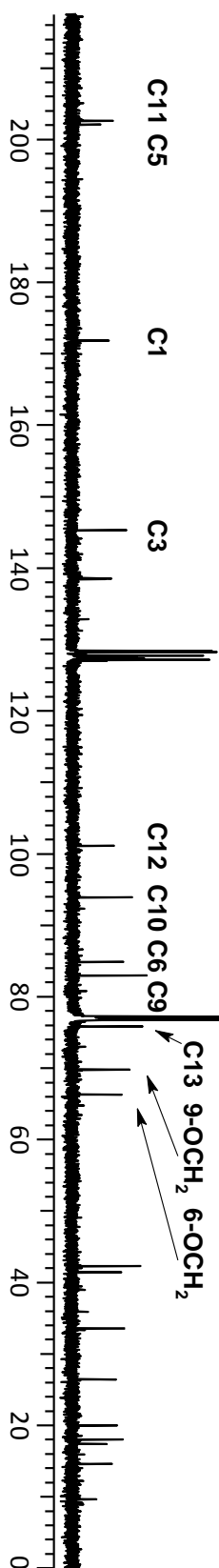
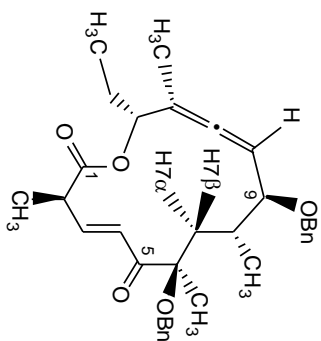
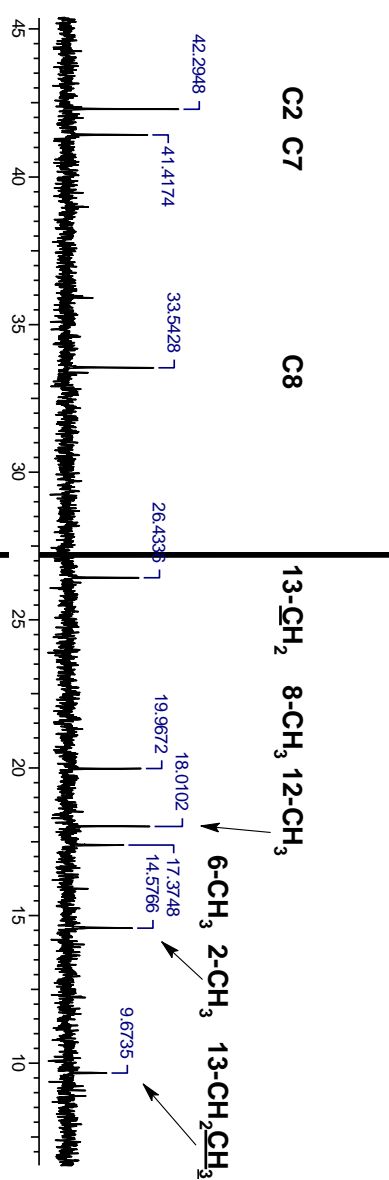
HMBC

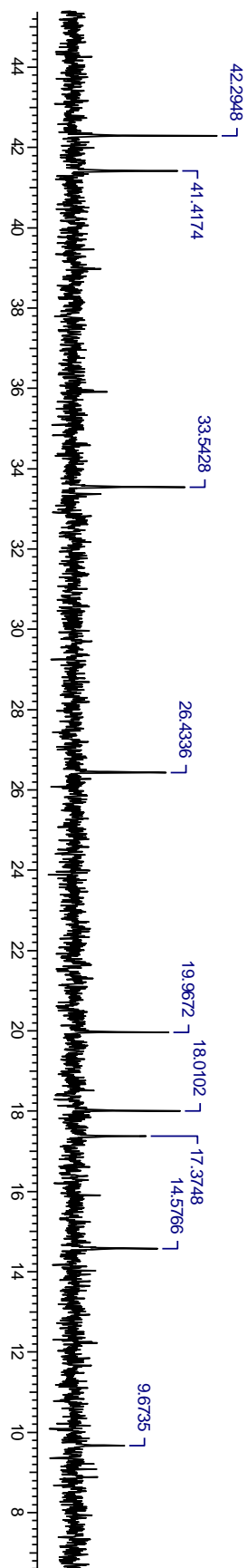
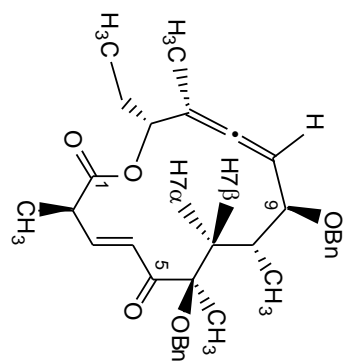


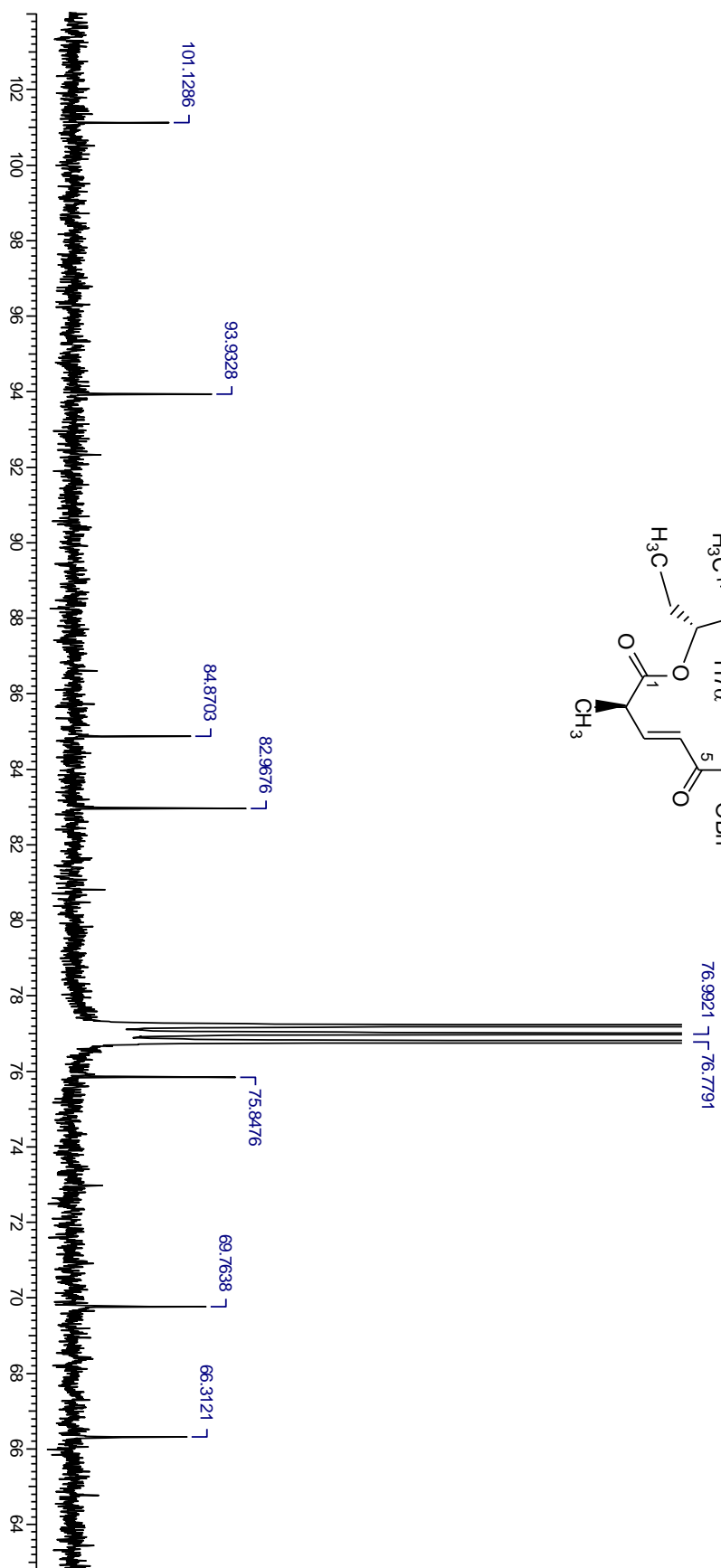
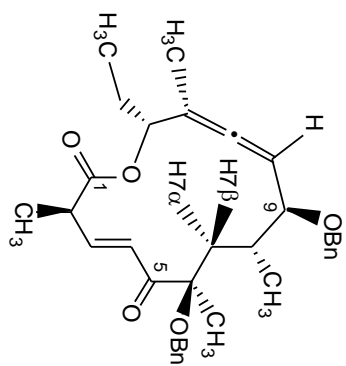


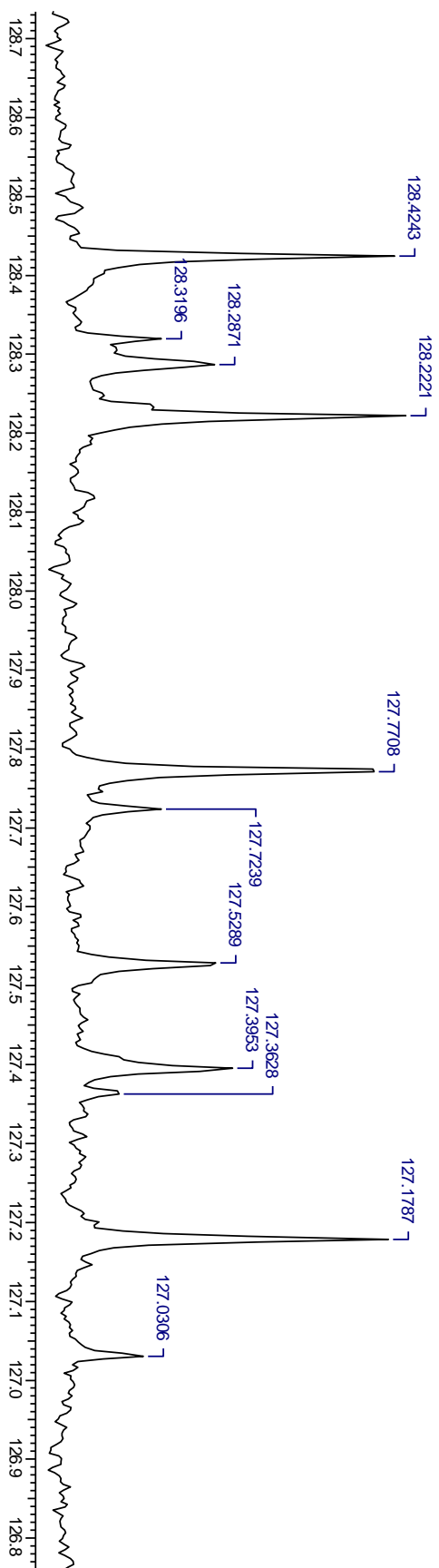
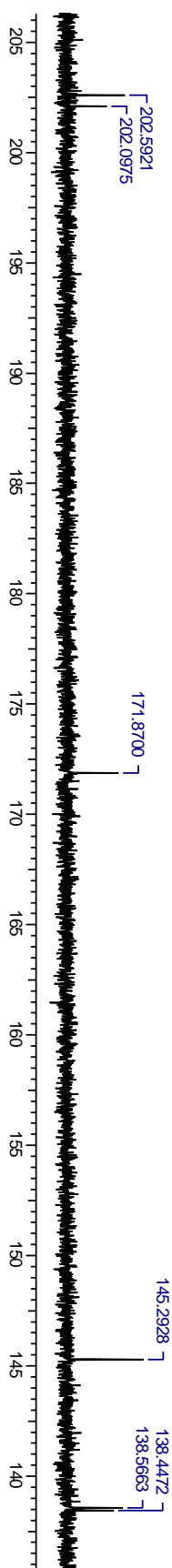
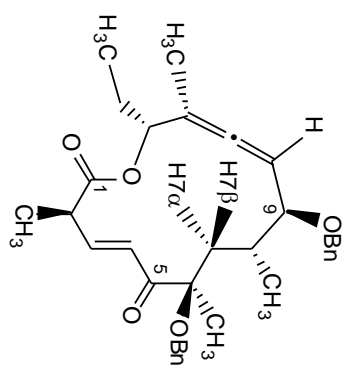




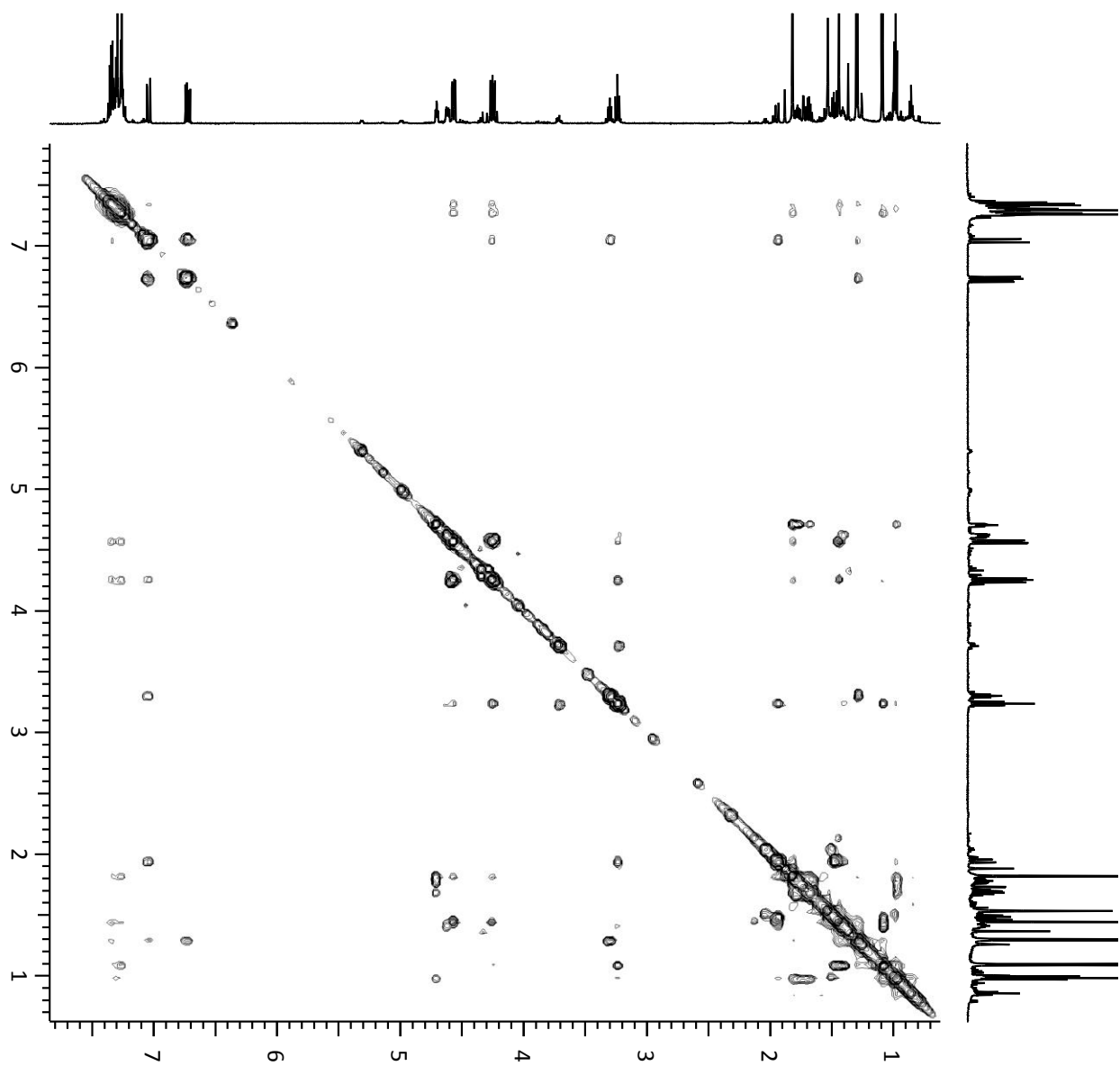


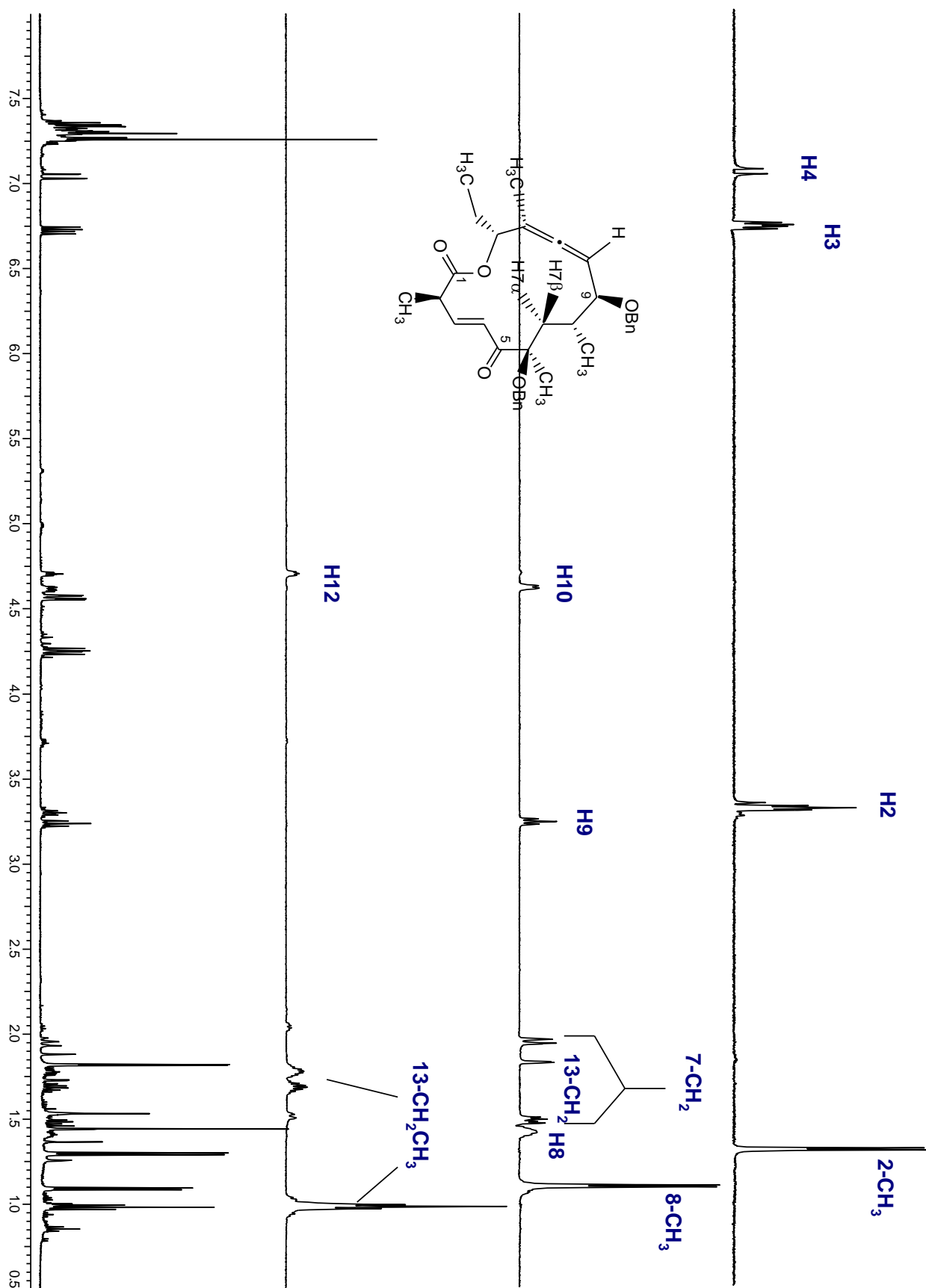




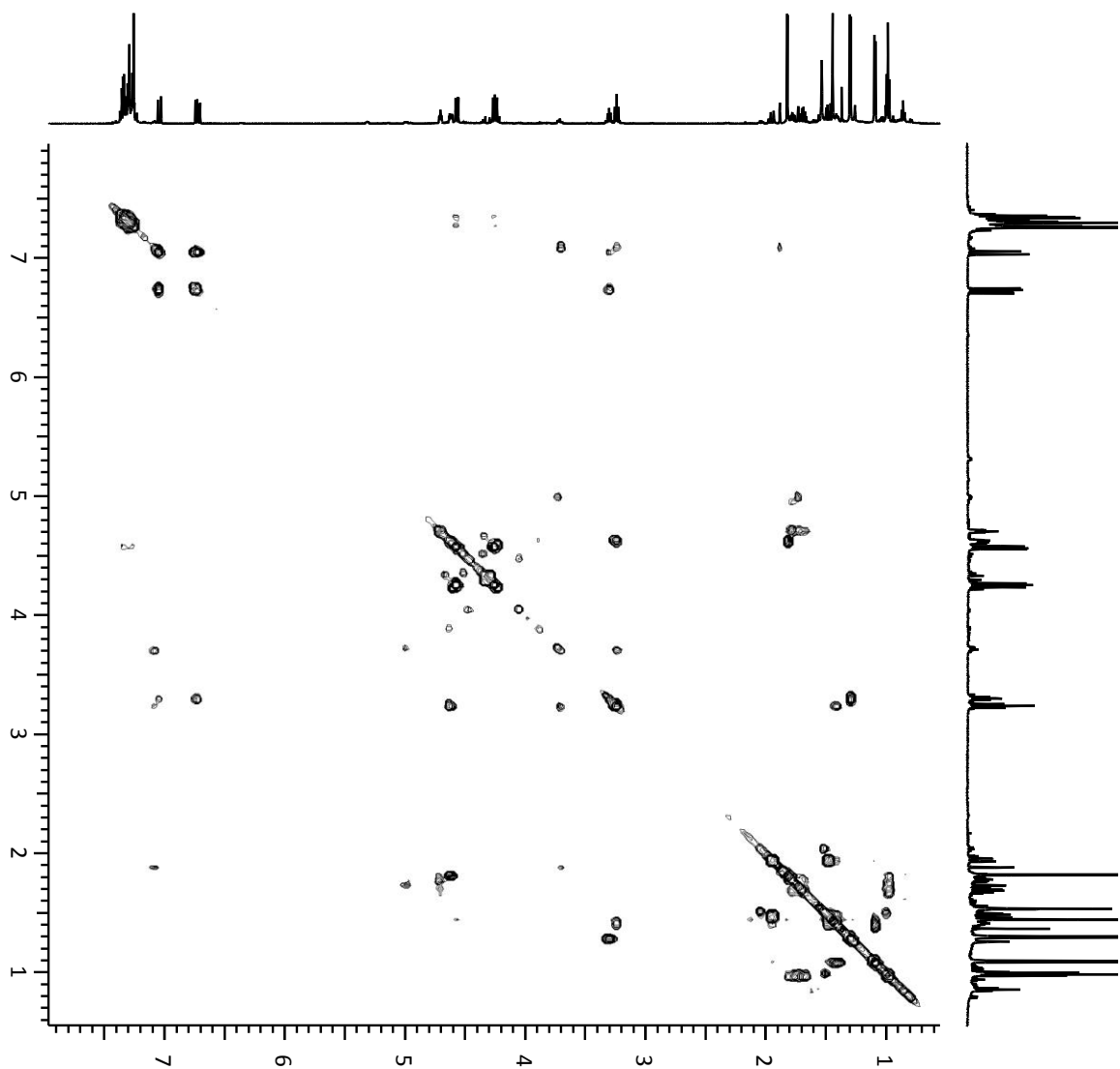


NOESY



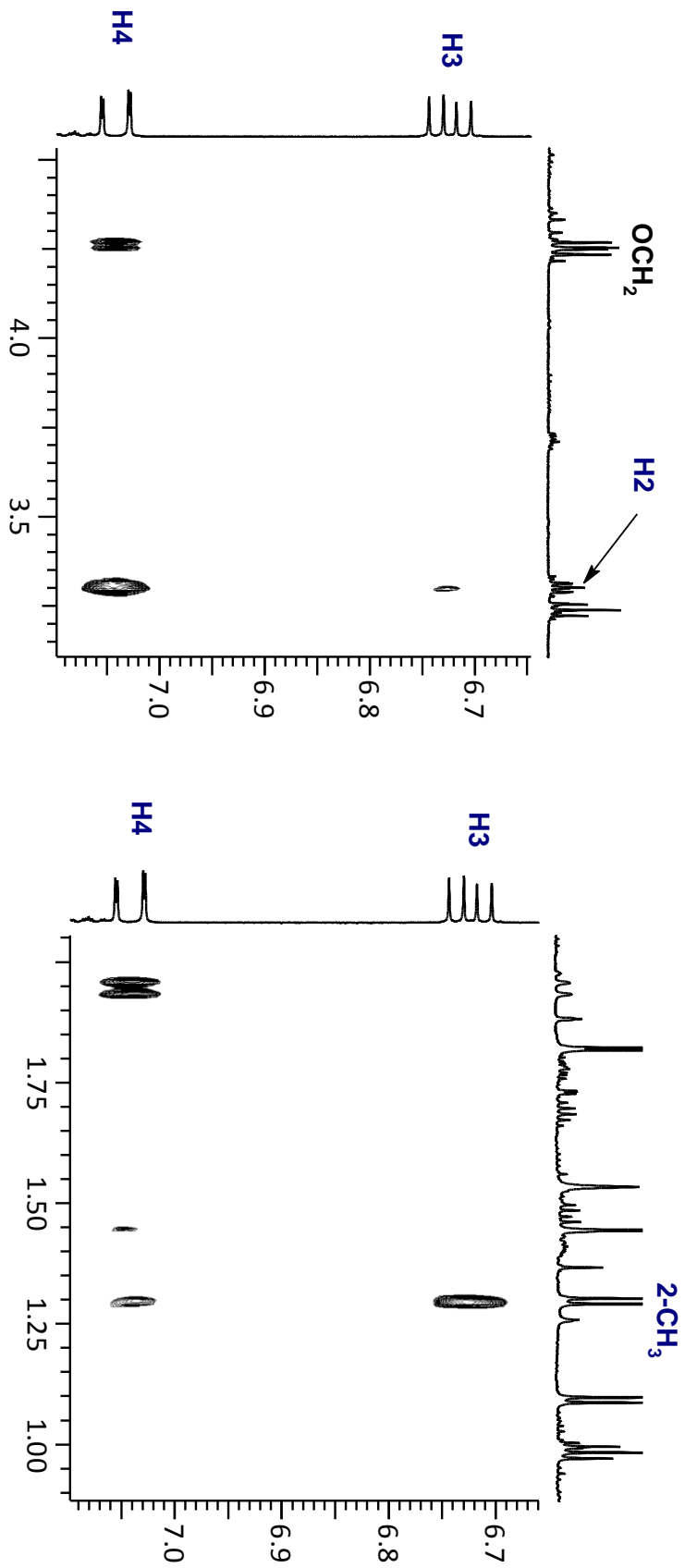
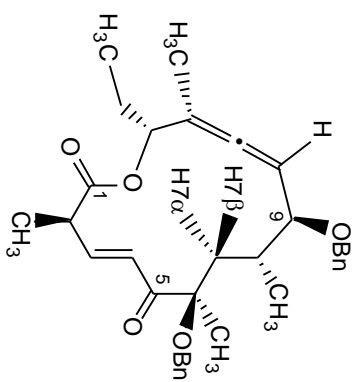


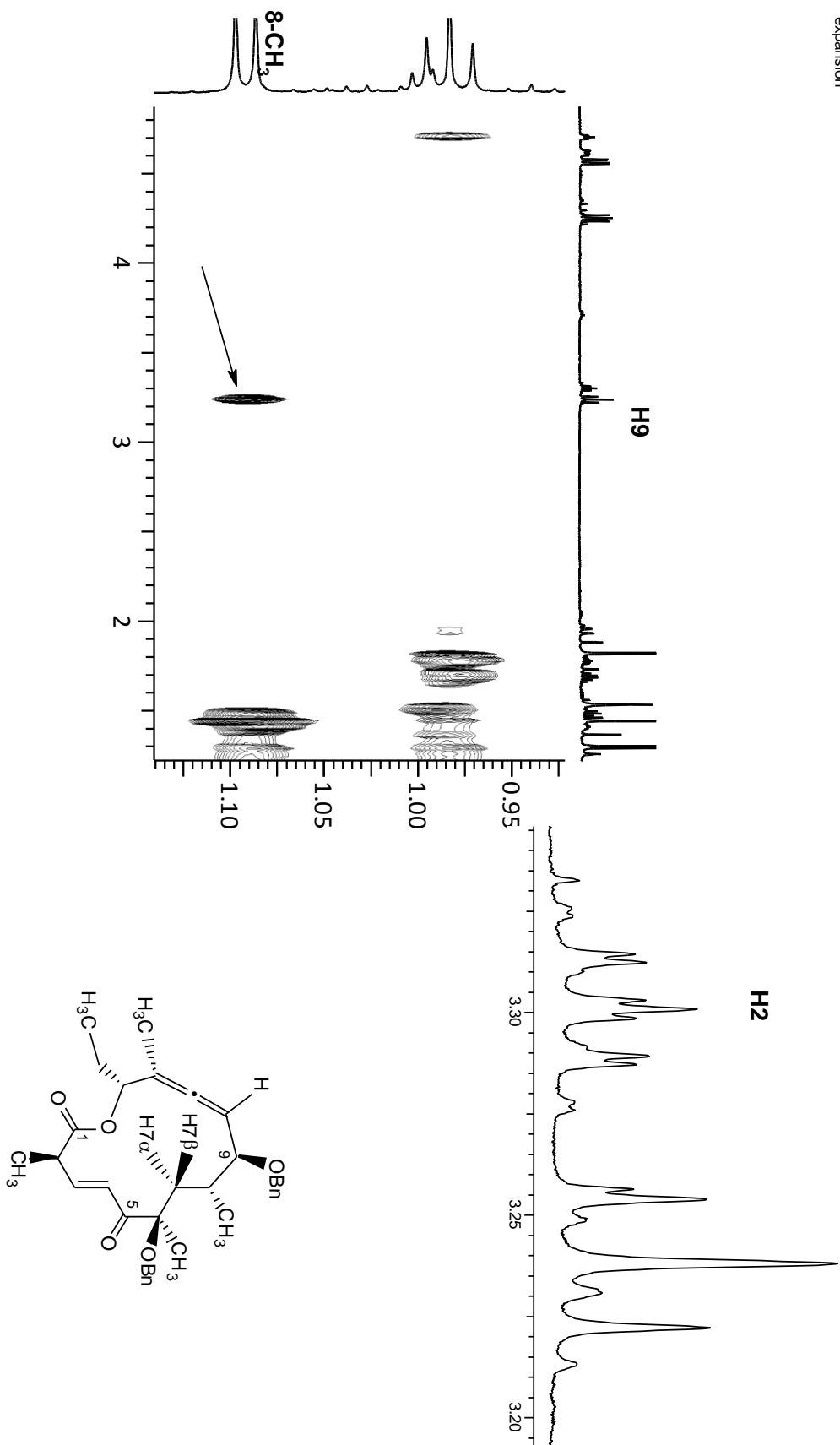
gCOSTY



NOESY

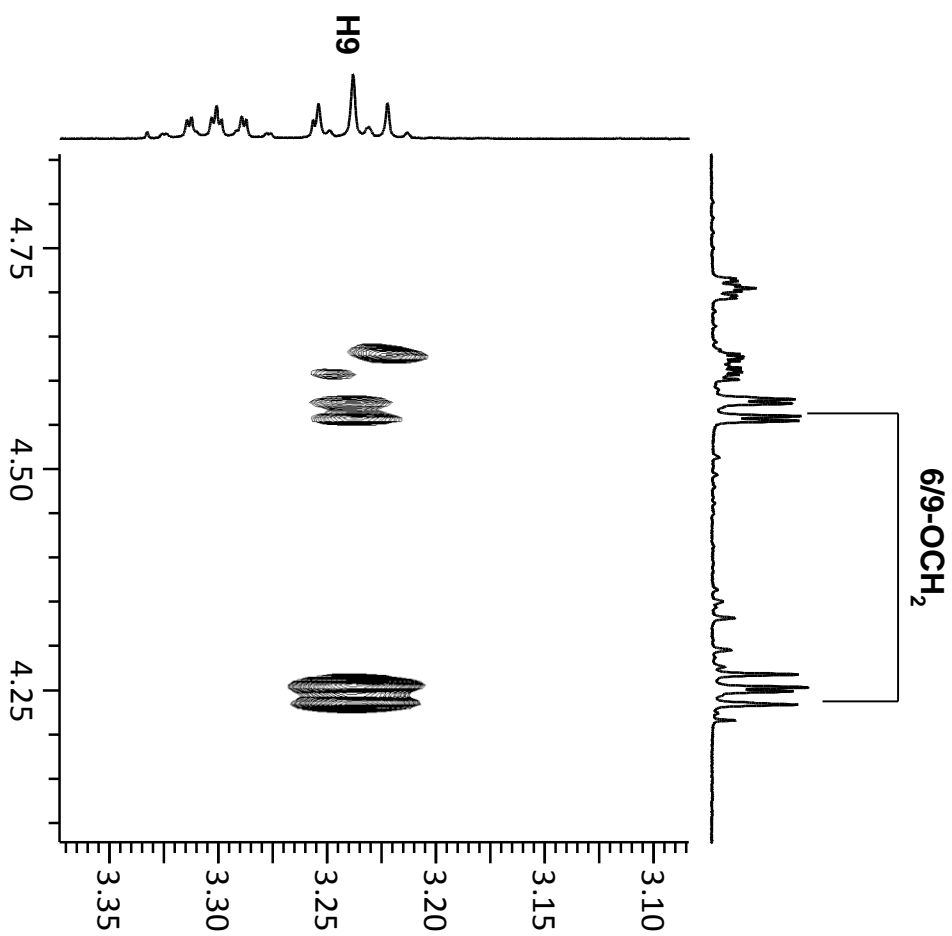
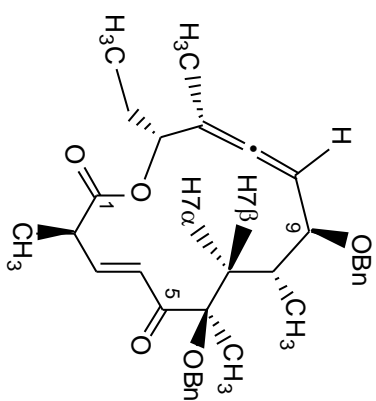
expansions





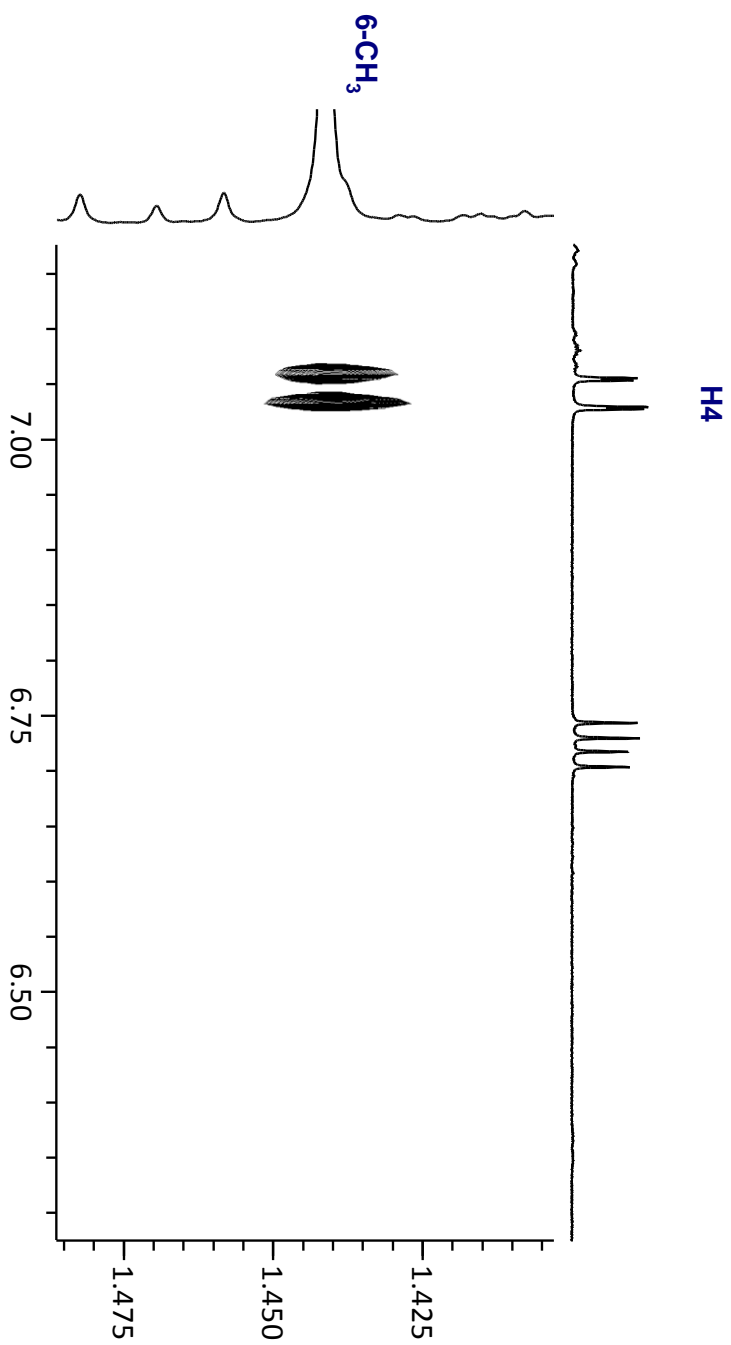
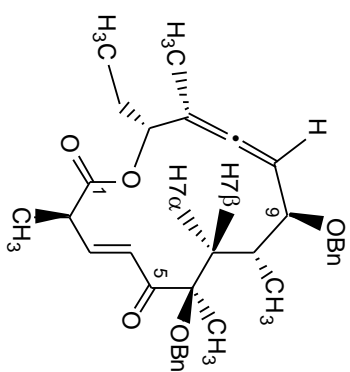
NOESY

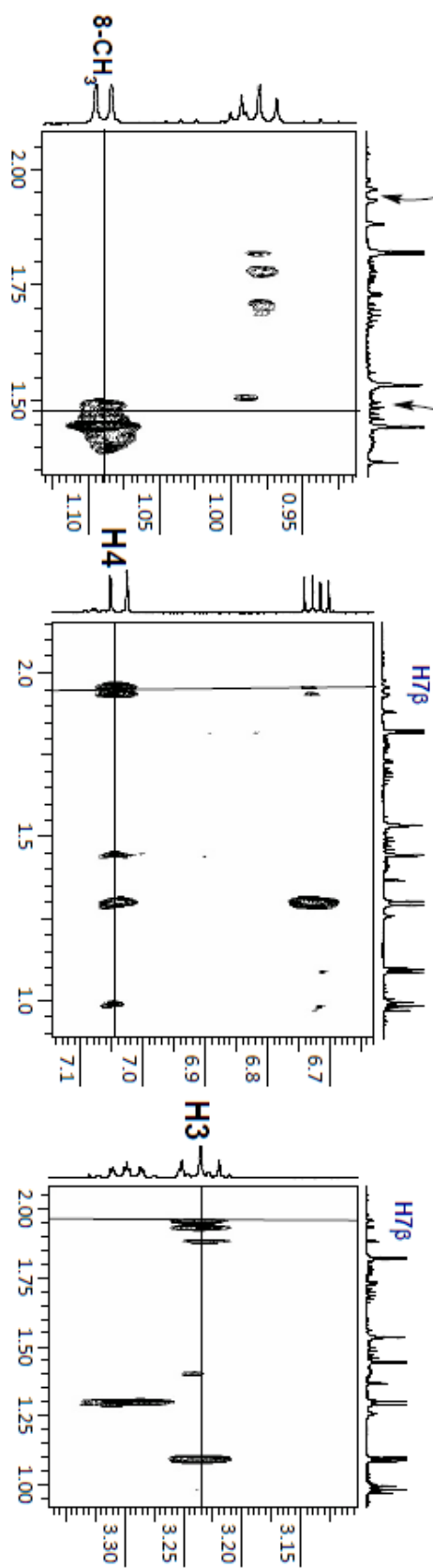
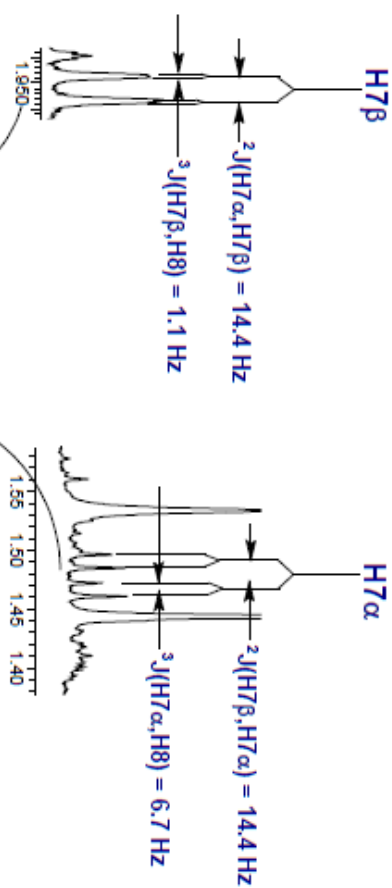
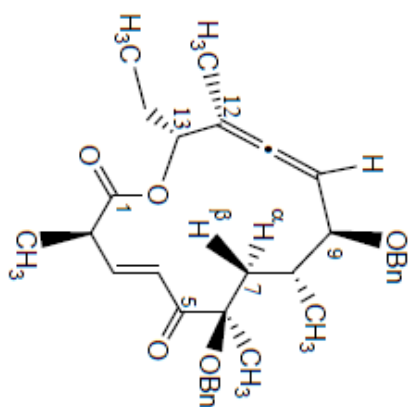
expansion

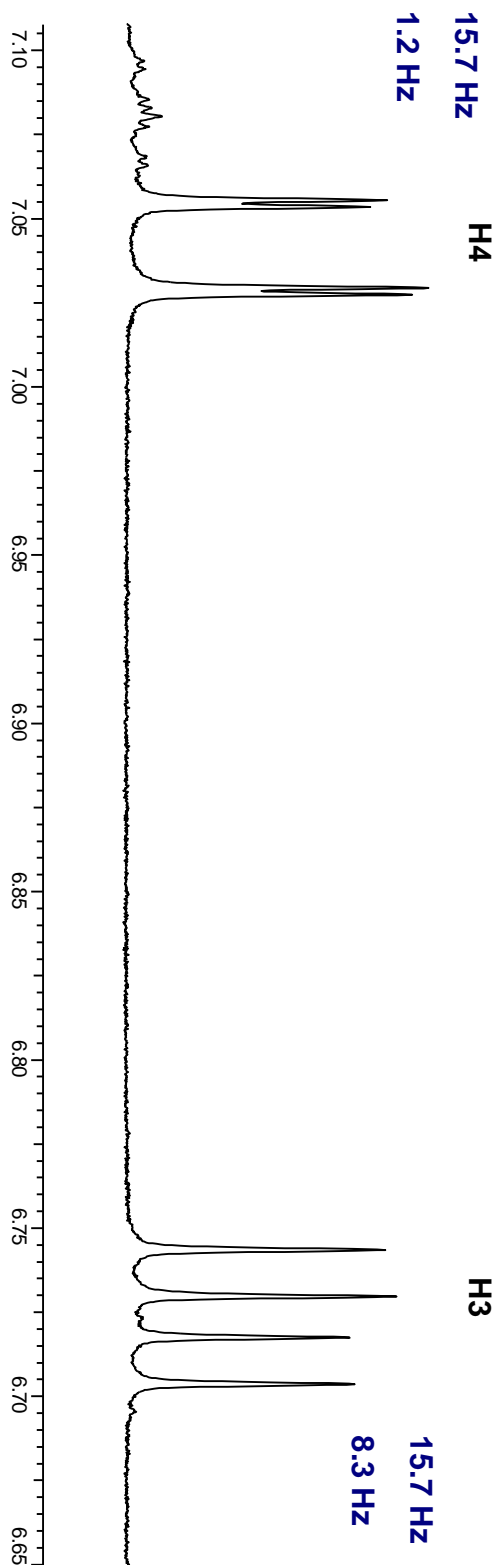
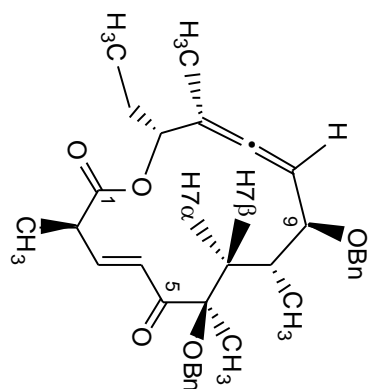


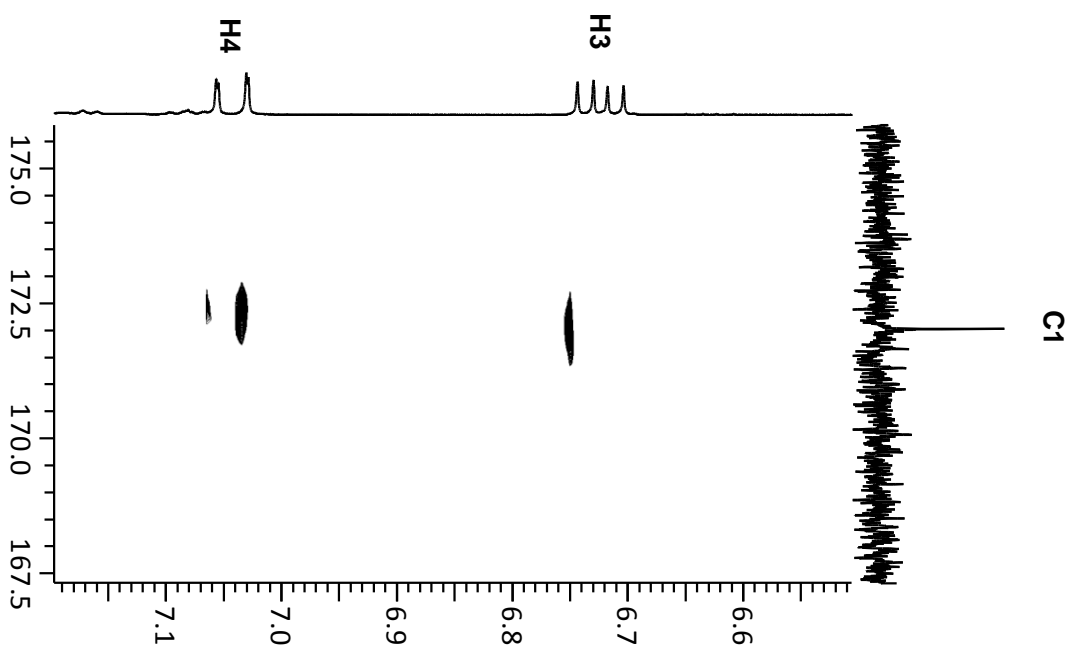
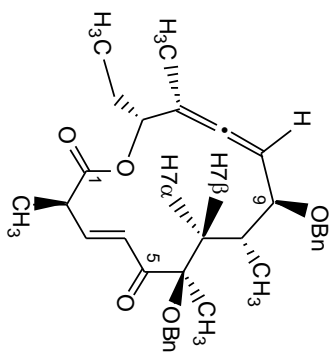
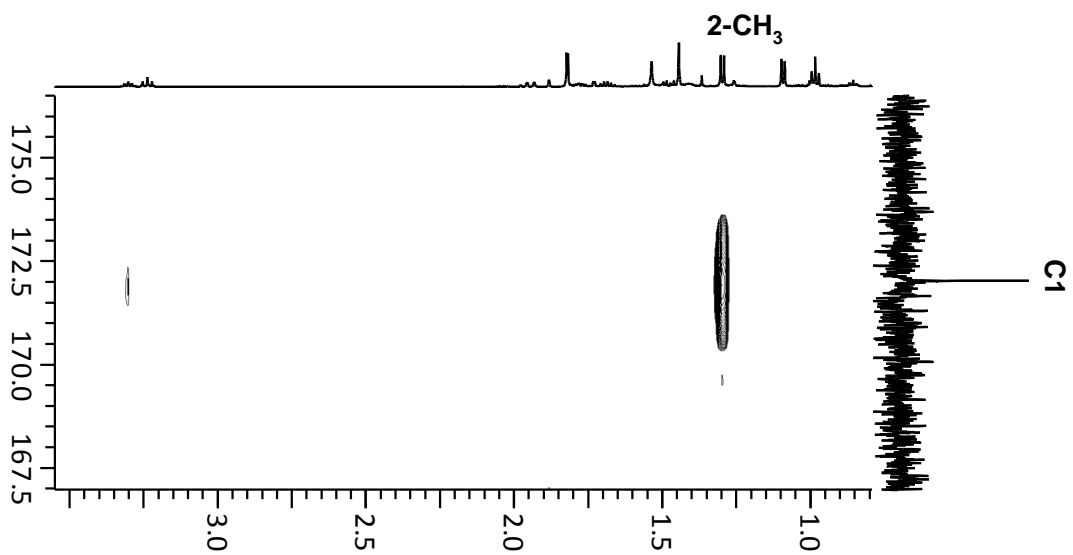
NOESY

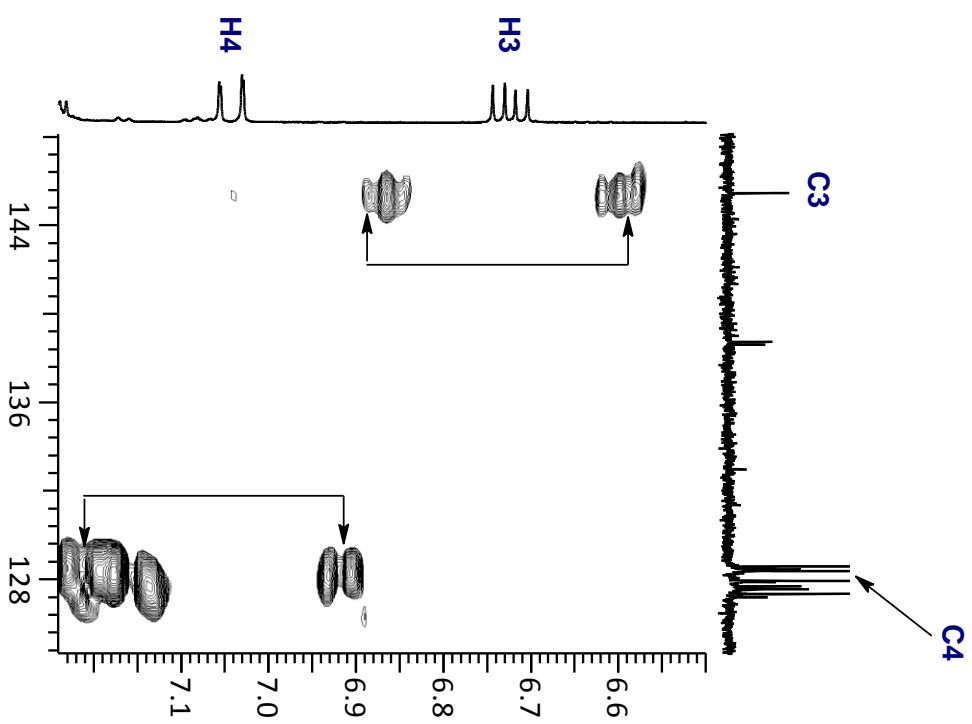
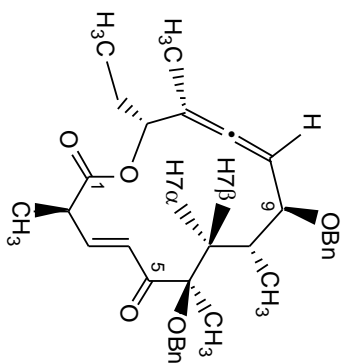
expansion





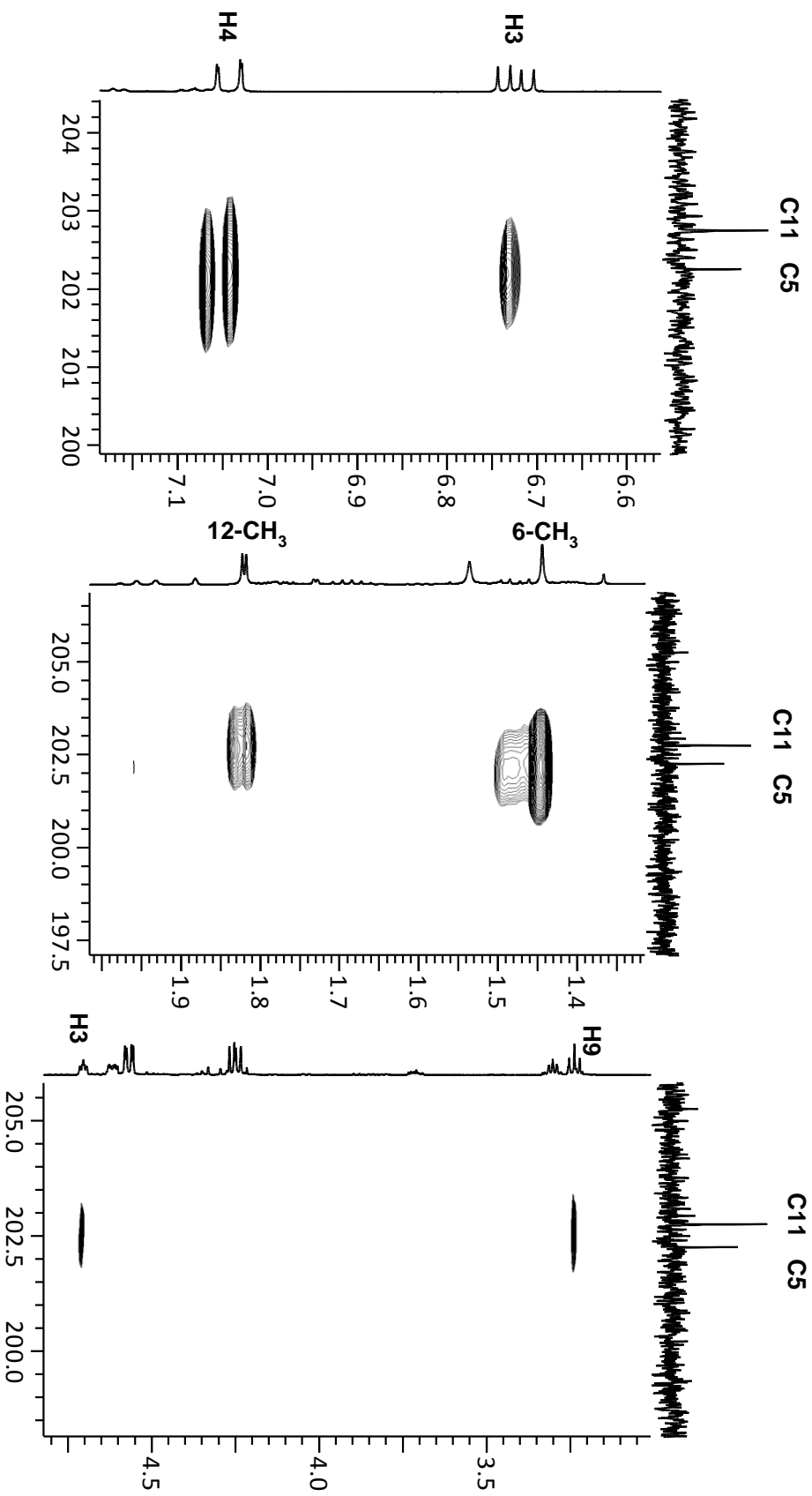


gHMBC
correlations

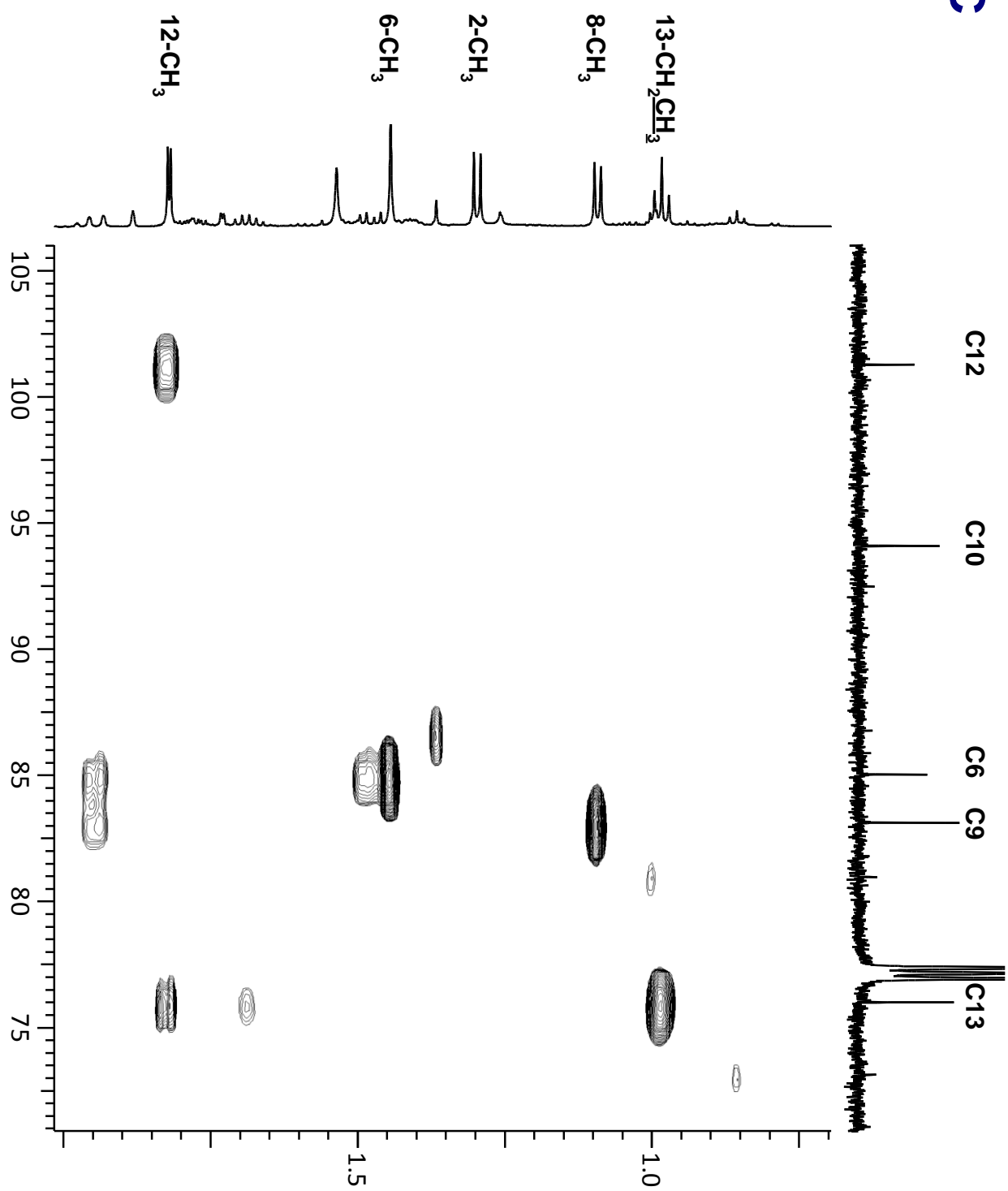


gHMBC
expansions

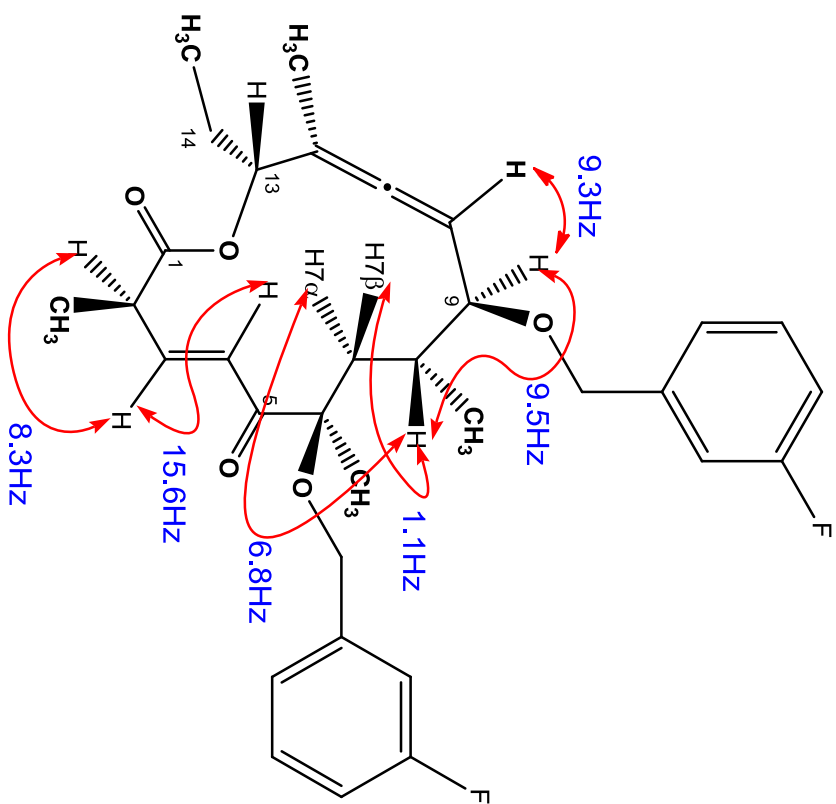
Assignments of CO groups

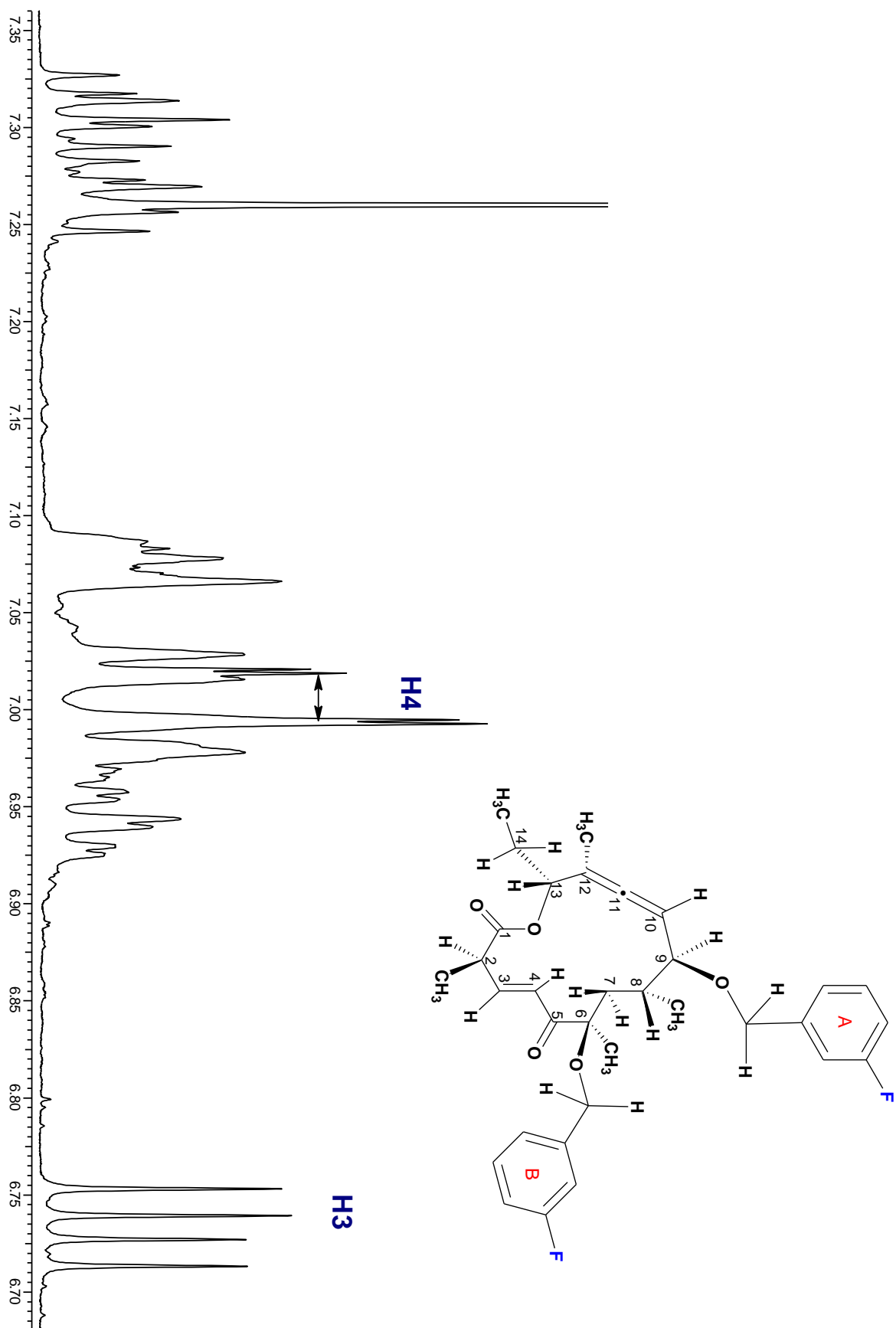


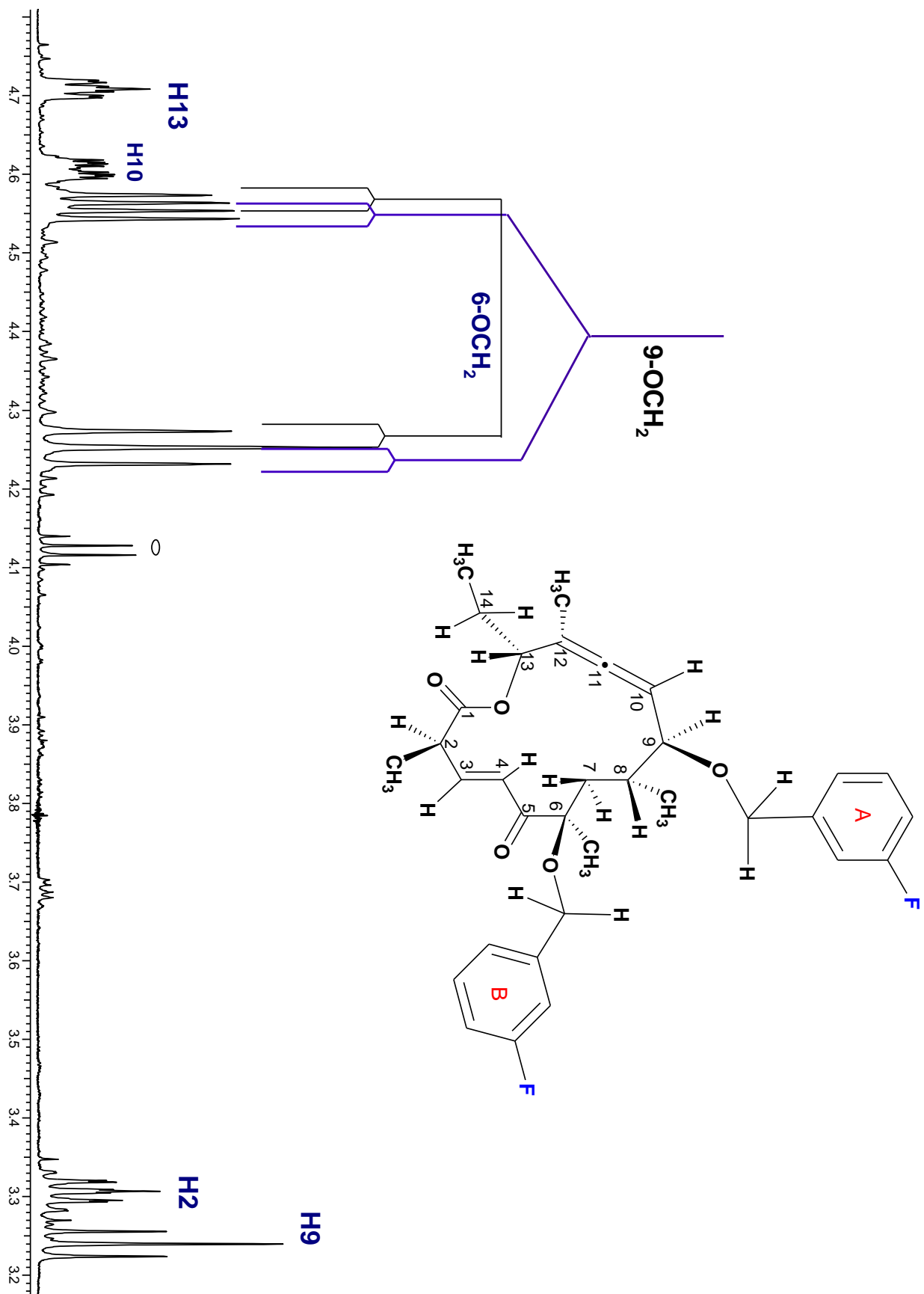
gHMBBC
expansion

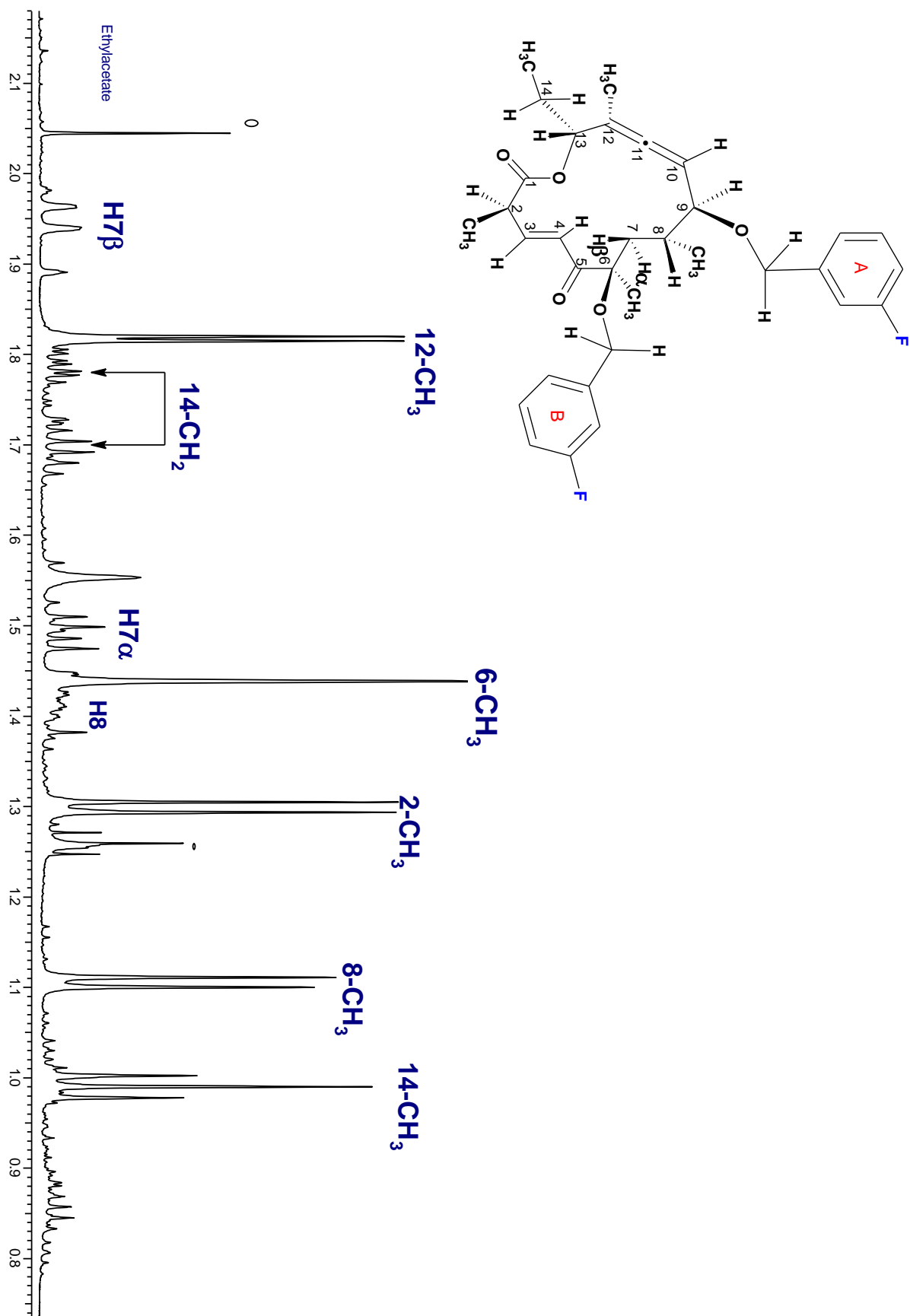


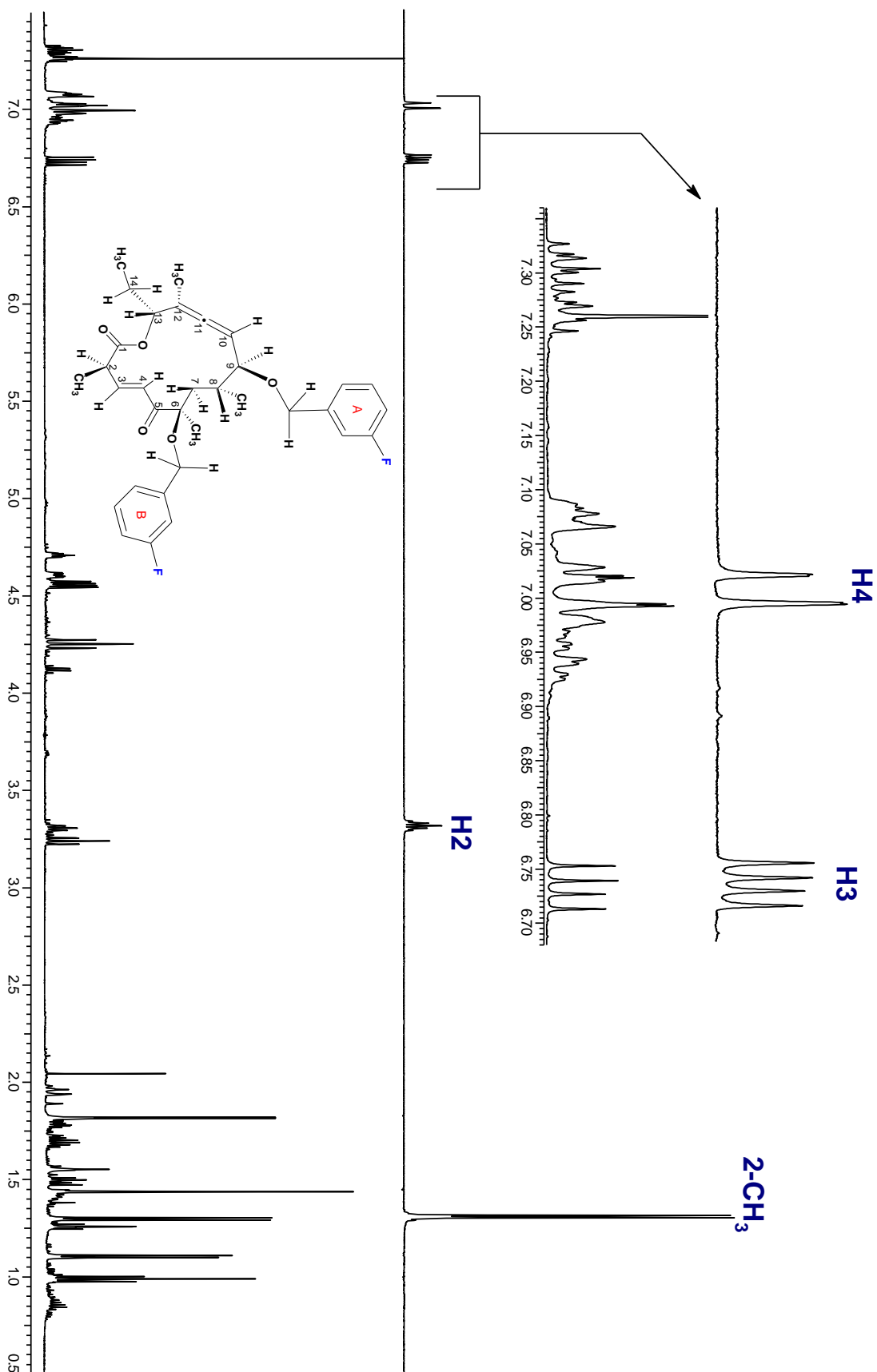
Coupling constant (J_{HH})

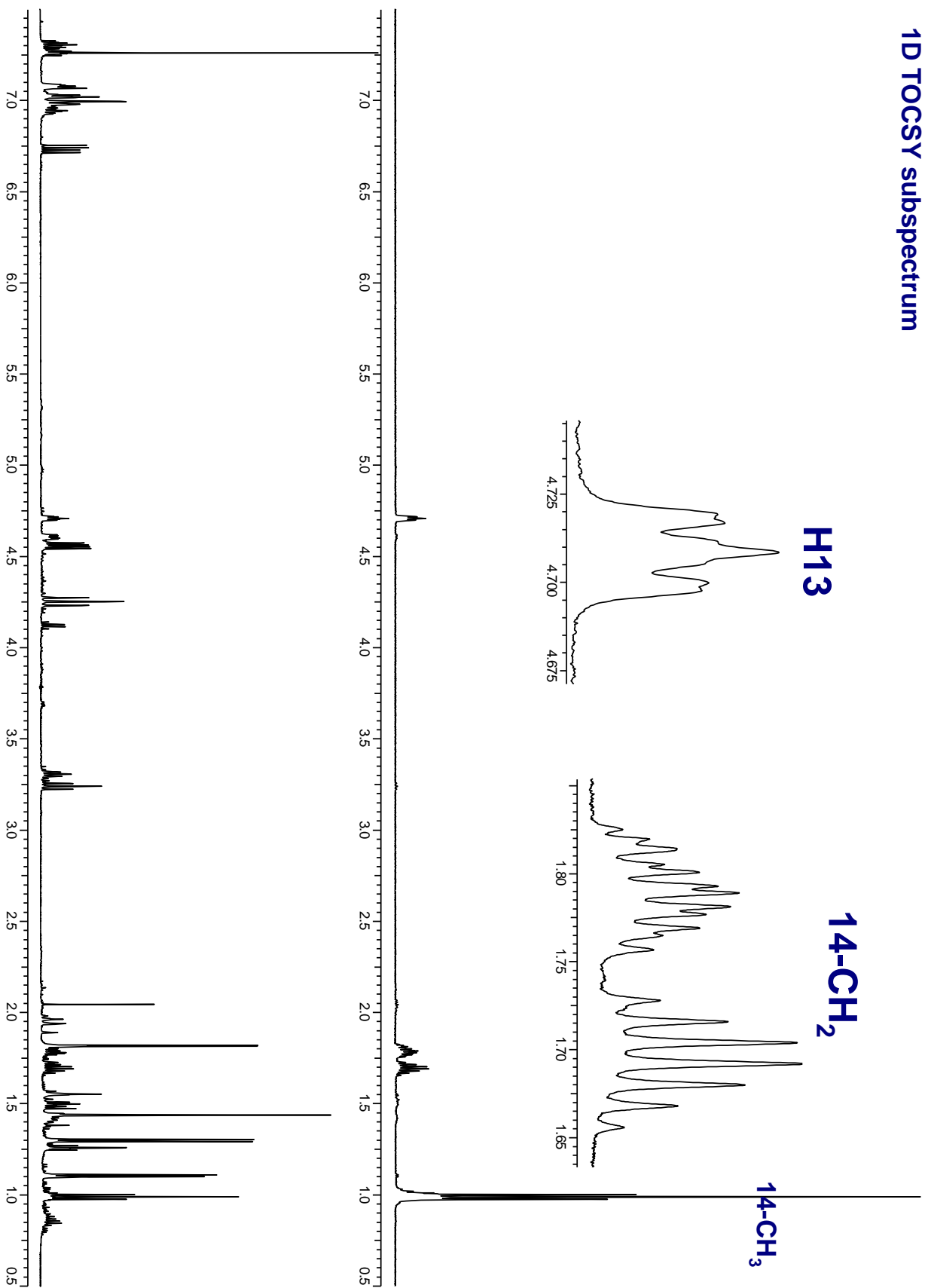




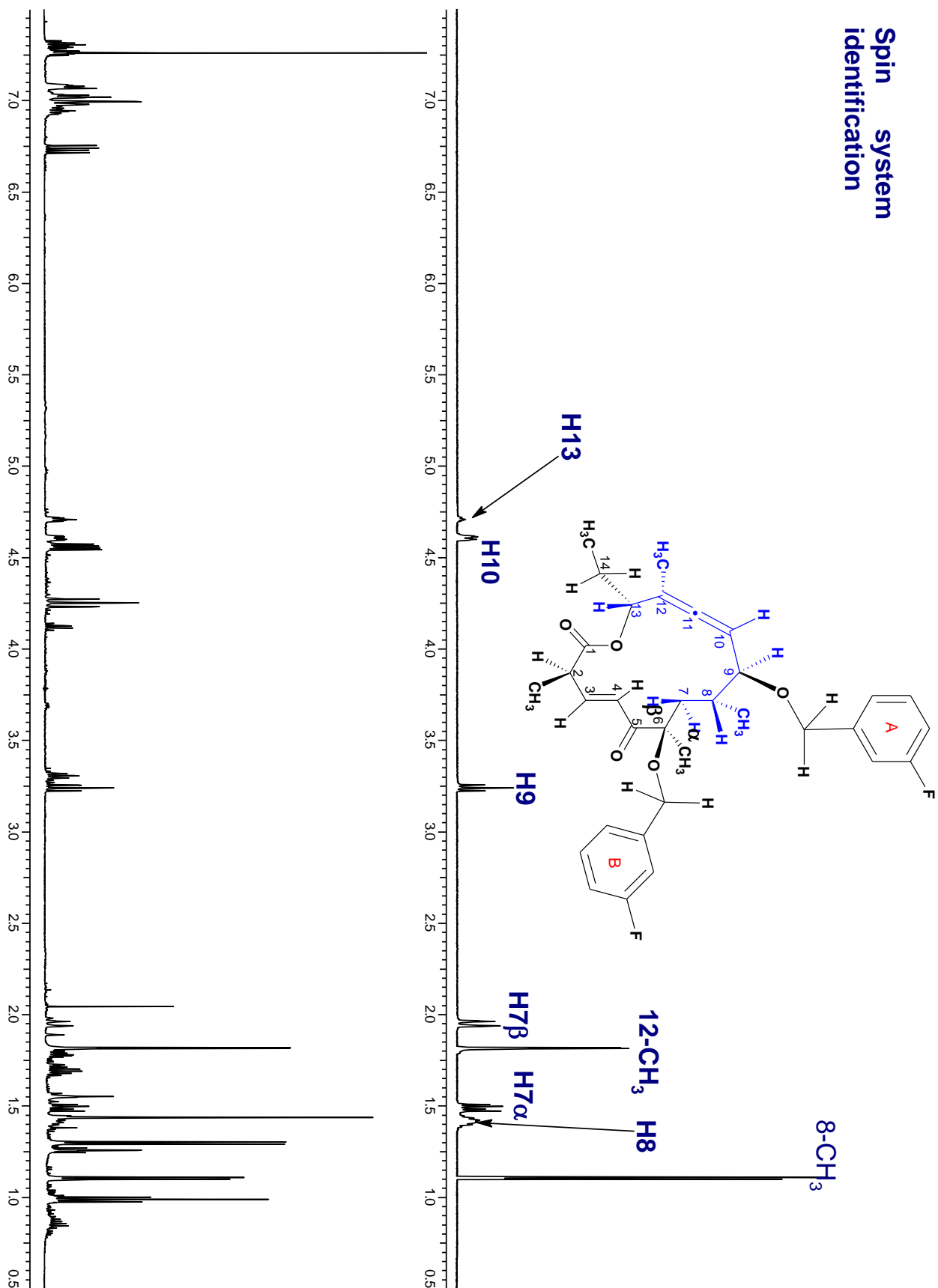


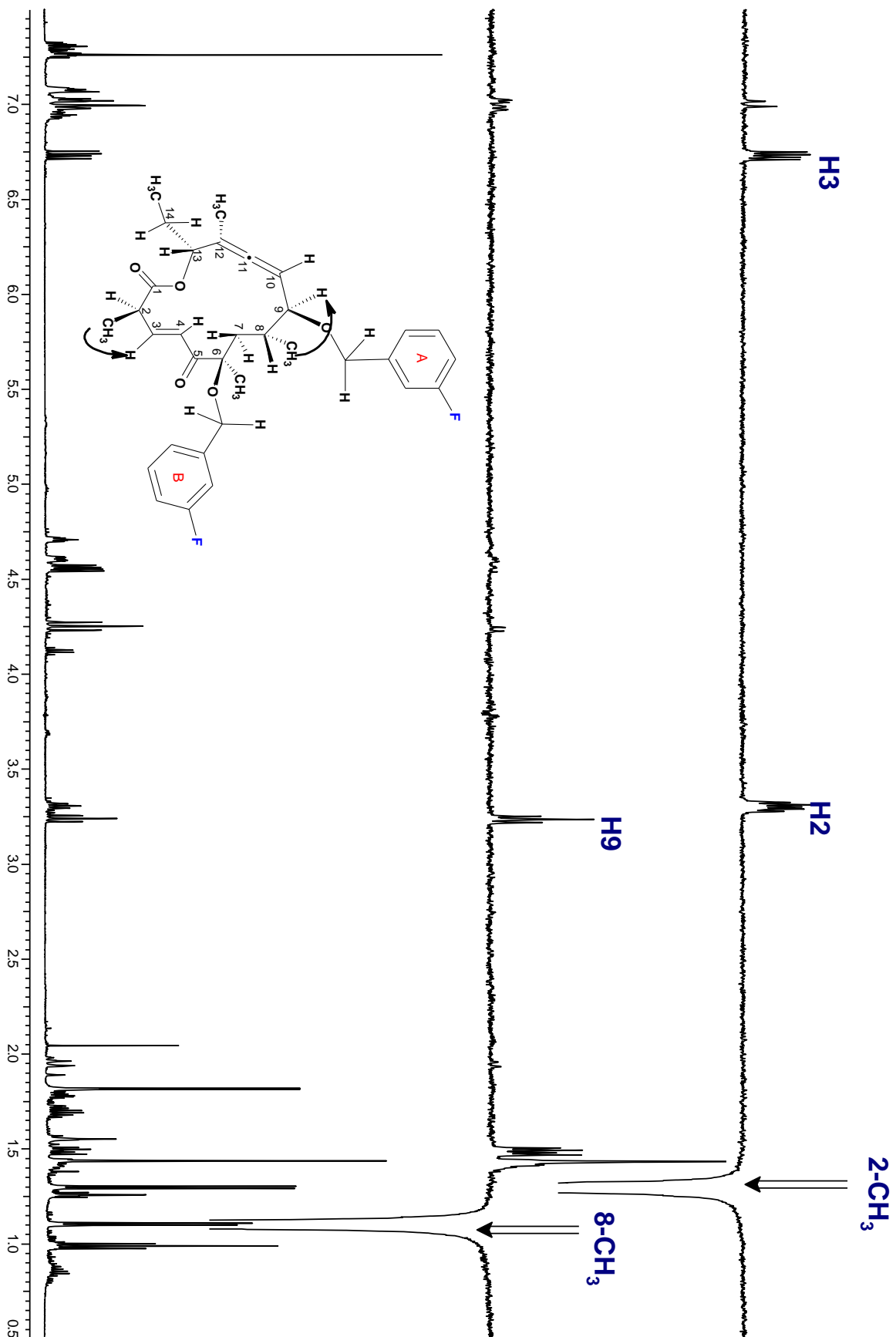


1D TOCSY subspectrum

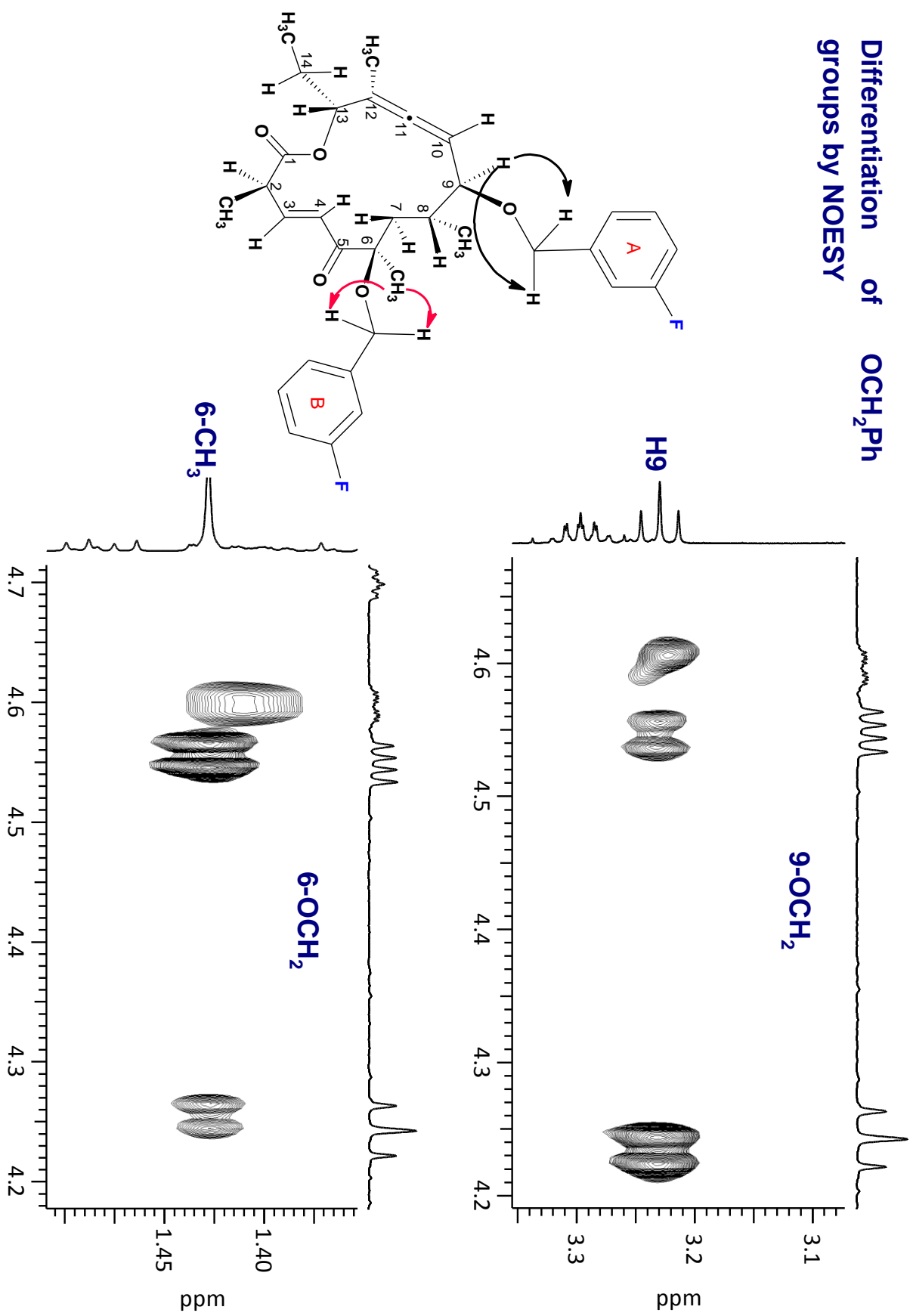
^1D TOCSY subspectrum

Spin system identification

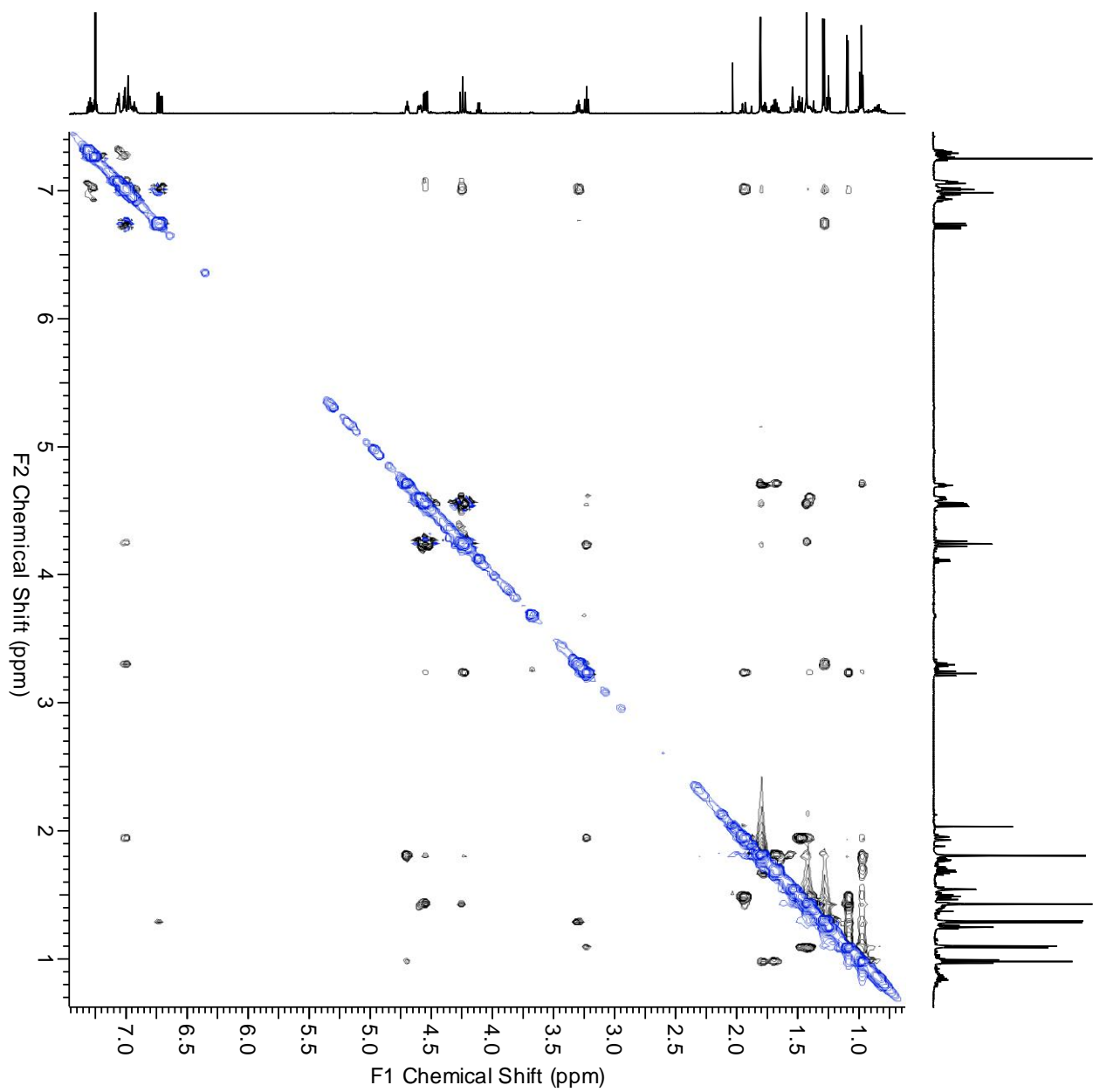


DPFGSENOE
experimental subspectra

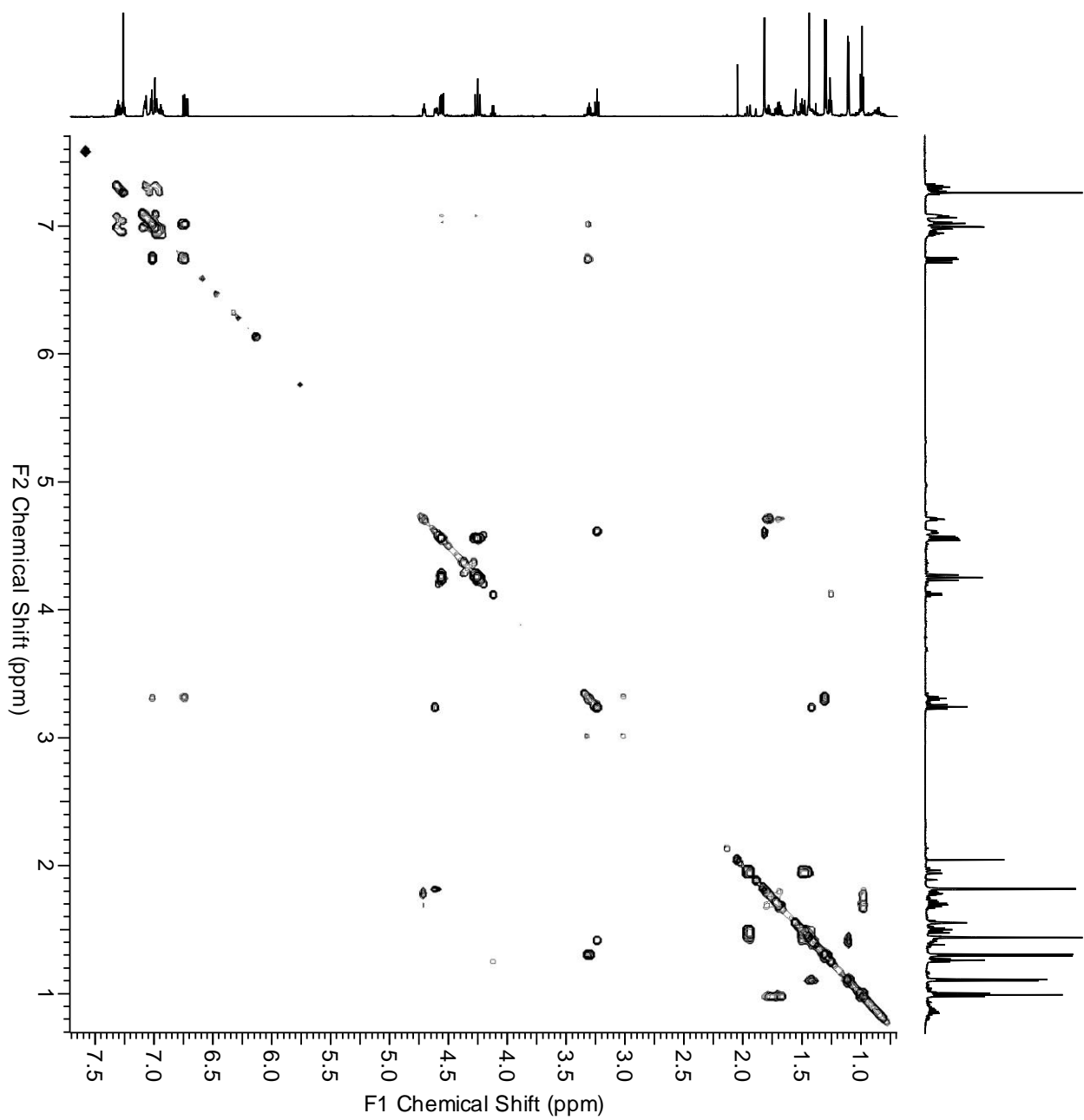
Differentiation of OCH_2Ph groups by NOESY



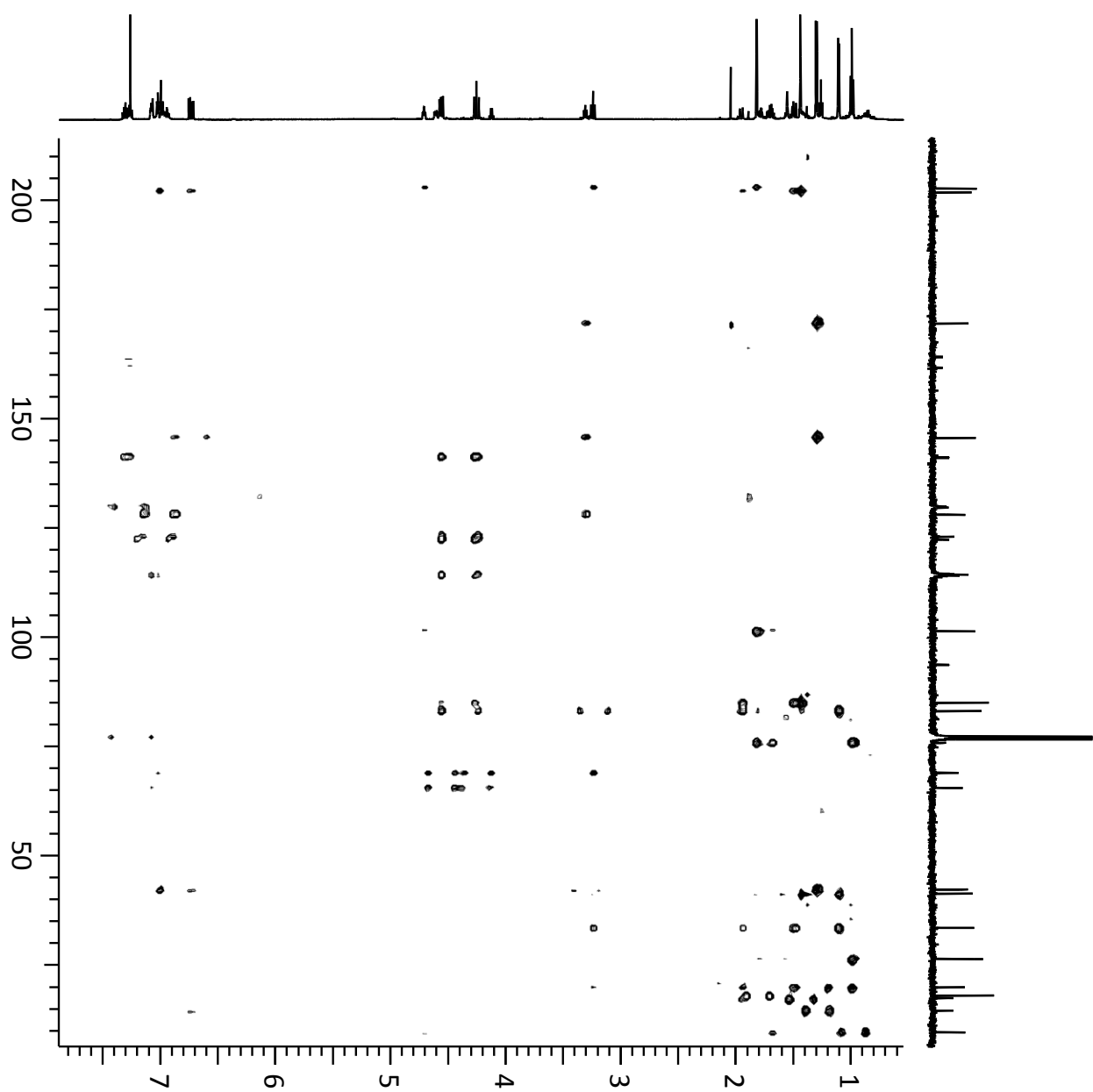
NOESY



gCOSY

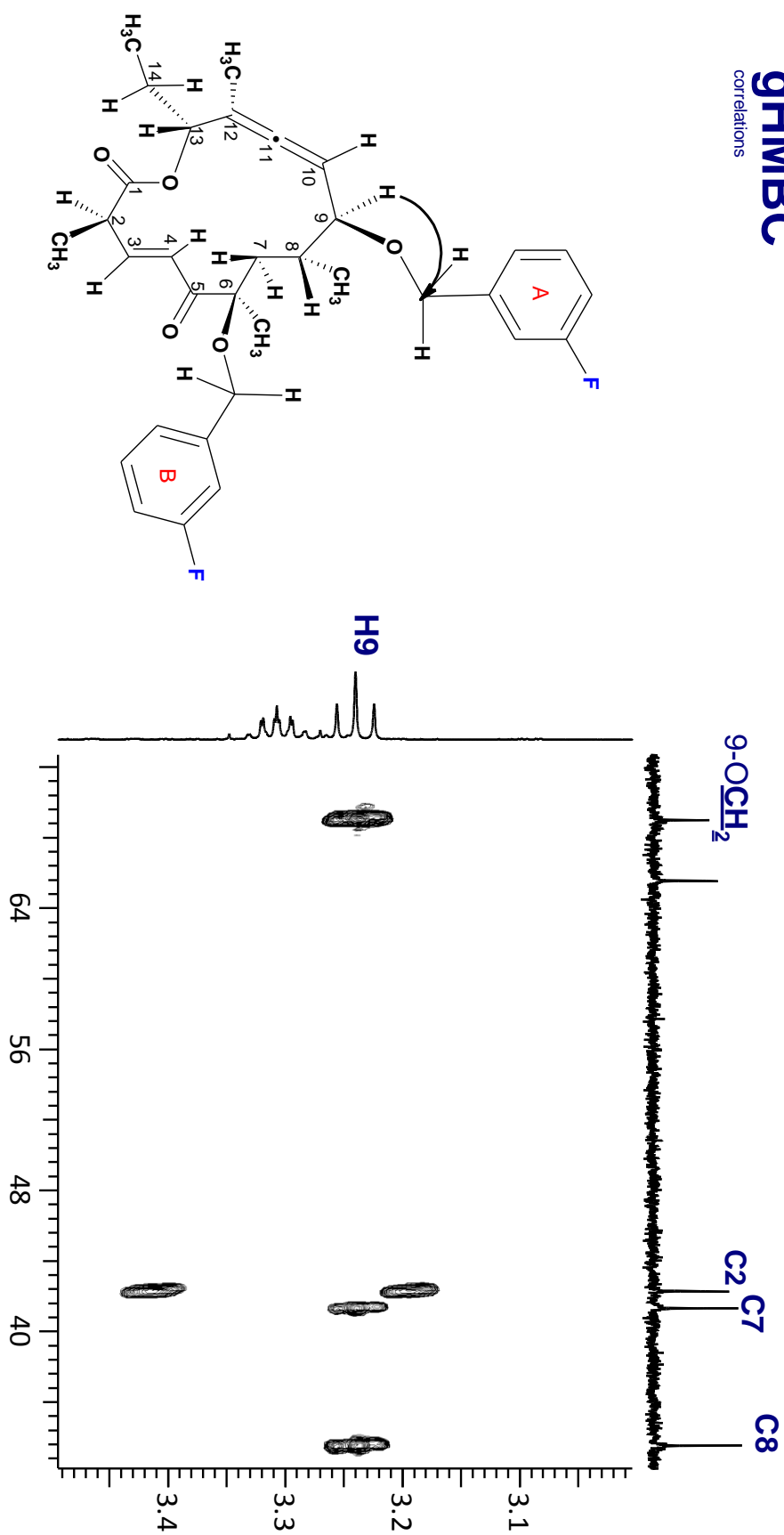


gHMBC



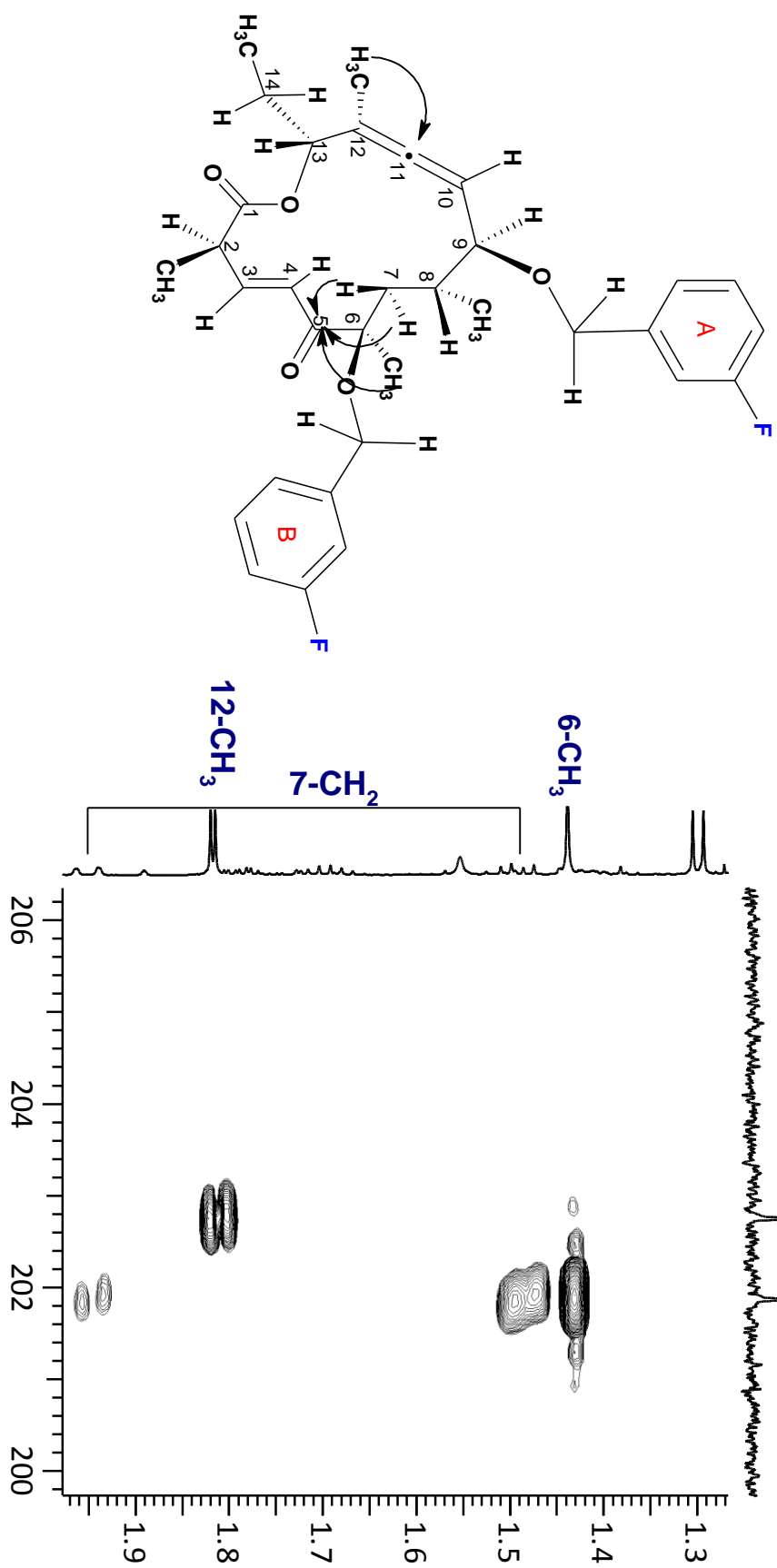
gHMBC

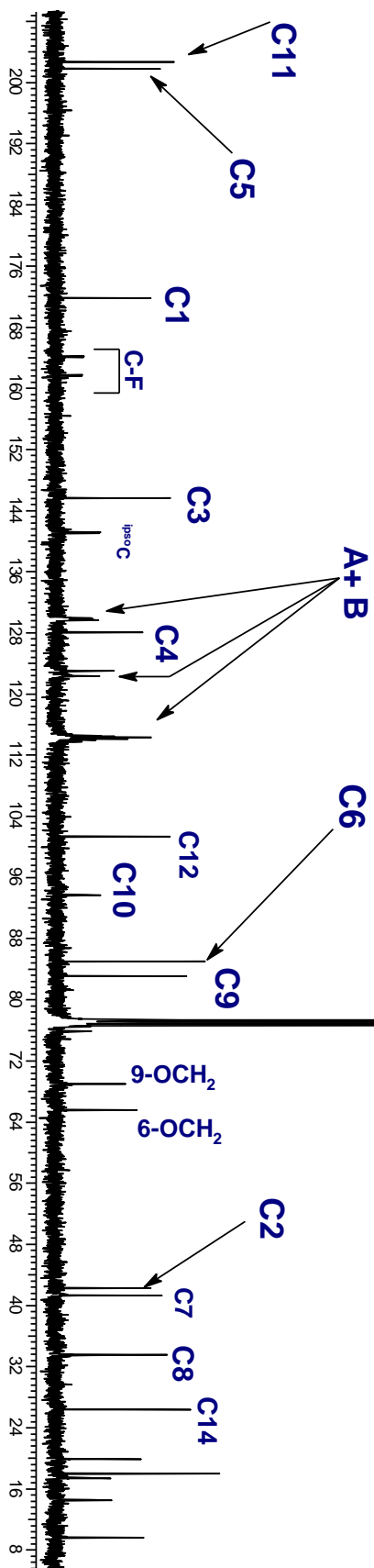
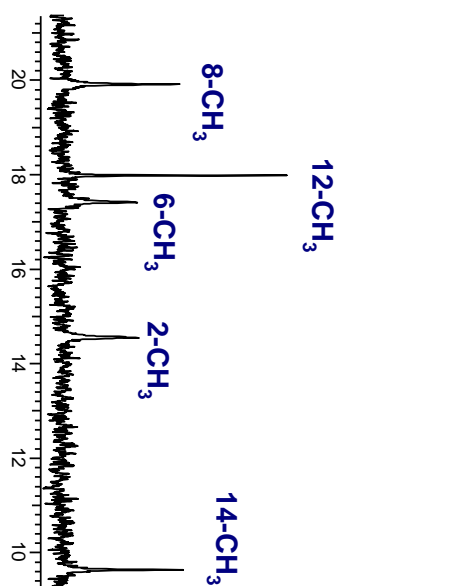
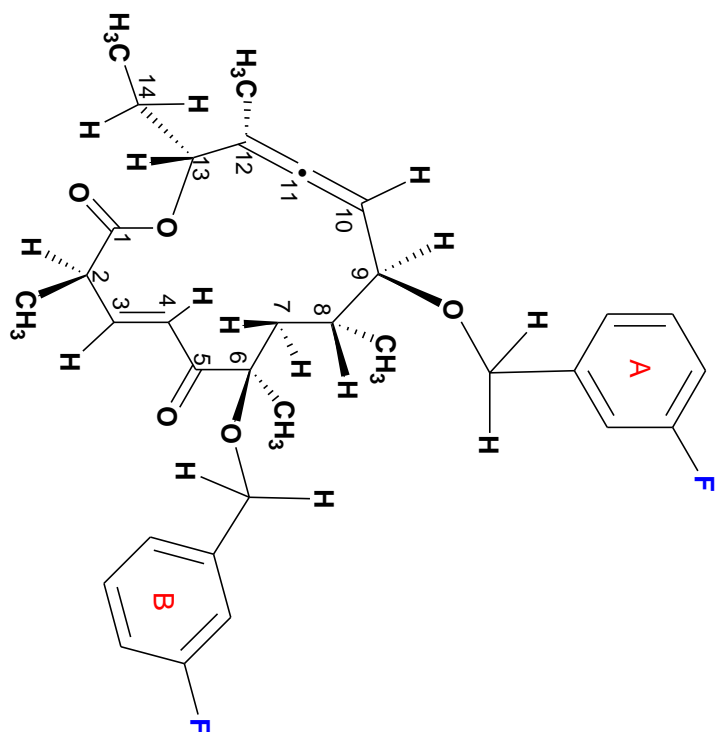
correlations

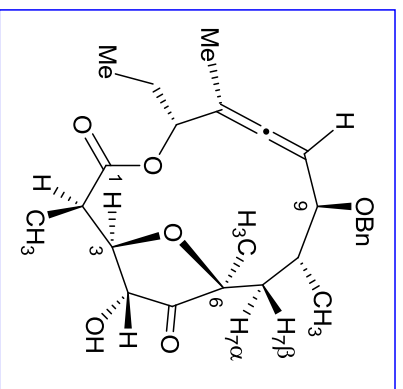


gHMBC

correlations

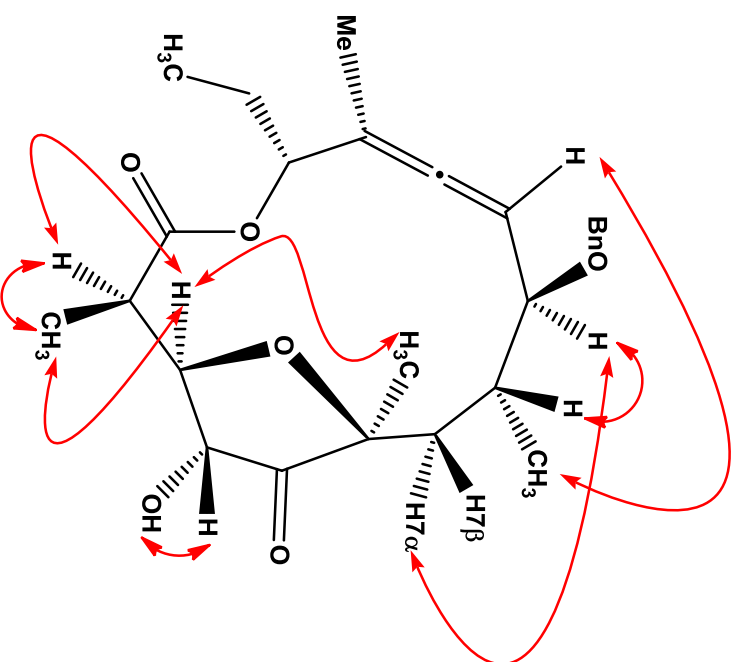


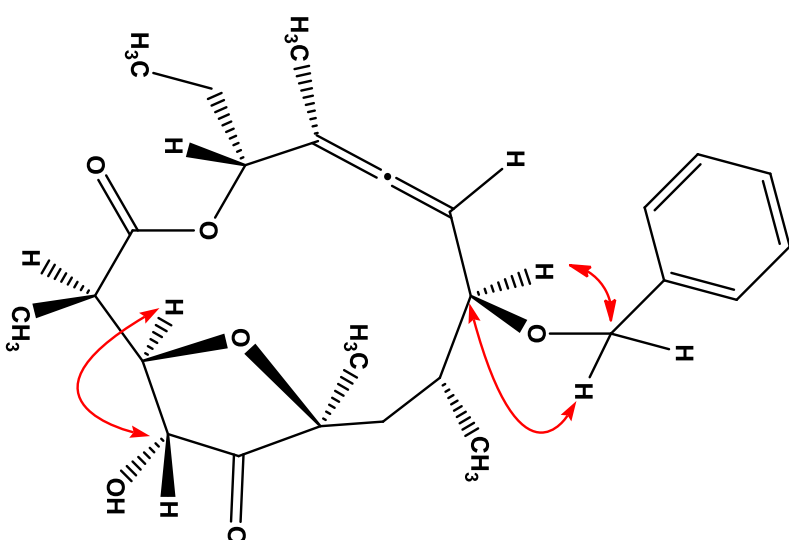




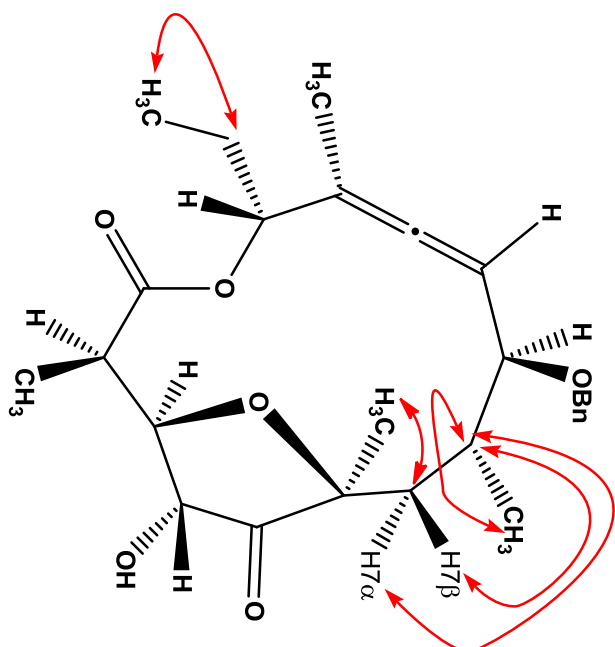
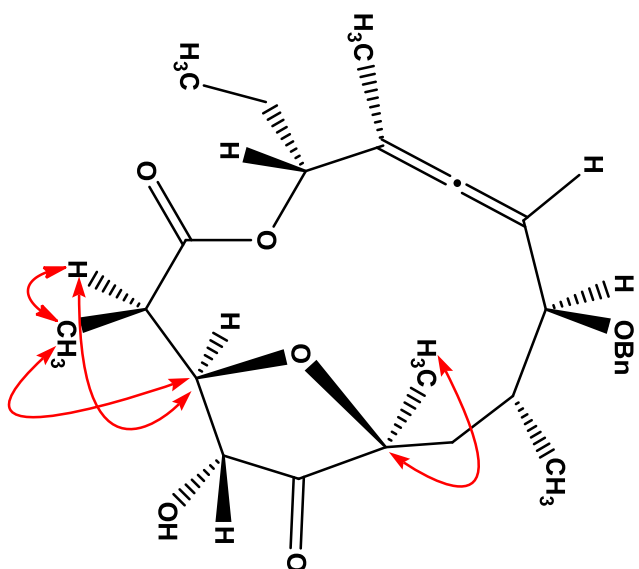
¹H NMR chemical shifts (δ/ppm) & coupling constant (J/Hz)	
3.06 dq, J _{H2, H3} = 4.4Hz, J _{H2, 2-CH3} = 7.4Hz, H2)	
1.35 (d, J _{2-CH3, H2} = 7.4Hz, 2-CH₃)	
3.90 (dd, J _{H3, H2} = 4.4Hz, J _{H3, H4} = 8.7Hz, H3)	
5.07 (d, J _{H4, H3} = 8.7Hz, H4)	
1.14 (s, 6-CH₃)	
1.65 (dd, J _{H7β, H8} = 3.9 Hz, J _{H7β, H7α} = 15.0Hz, H7β)	
1.87 (dd, J _{H7α, H8} = 5.8 Hz, J _{H7α, H7β} = 15.0Hz, H7α)	
1.70 (m, H8)	
0.88 (d, J _{8-CH3, H8} = 7.0Hz, 8-CH₃)	
3.83 (dd, J _{H9, H8} = 2.6Hz, J _{H9, H10} = 8.1Hz, H9)	
4.62, 4.36 (d, J _{AB} = 12.1Hz, 9-OCH₂)	
5.07 (qd, H10)	
1.80 (d, 12-CH₃)	
5.60 (dd, J _{H13, H14} = 6.3, 8.1Hz, H13)	
1.65, 1.70 (m, 14-CH₂)	
0.93 (t, J _{14-CH3, H14} = 7.6Hz, 14-CH₃)	

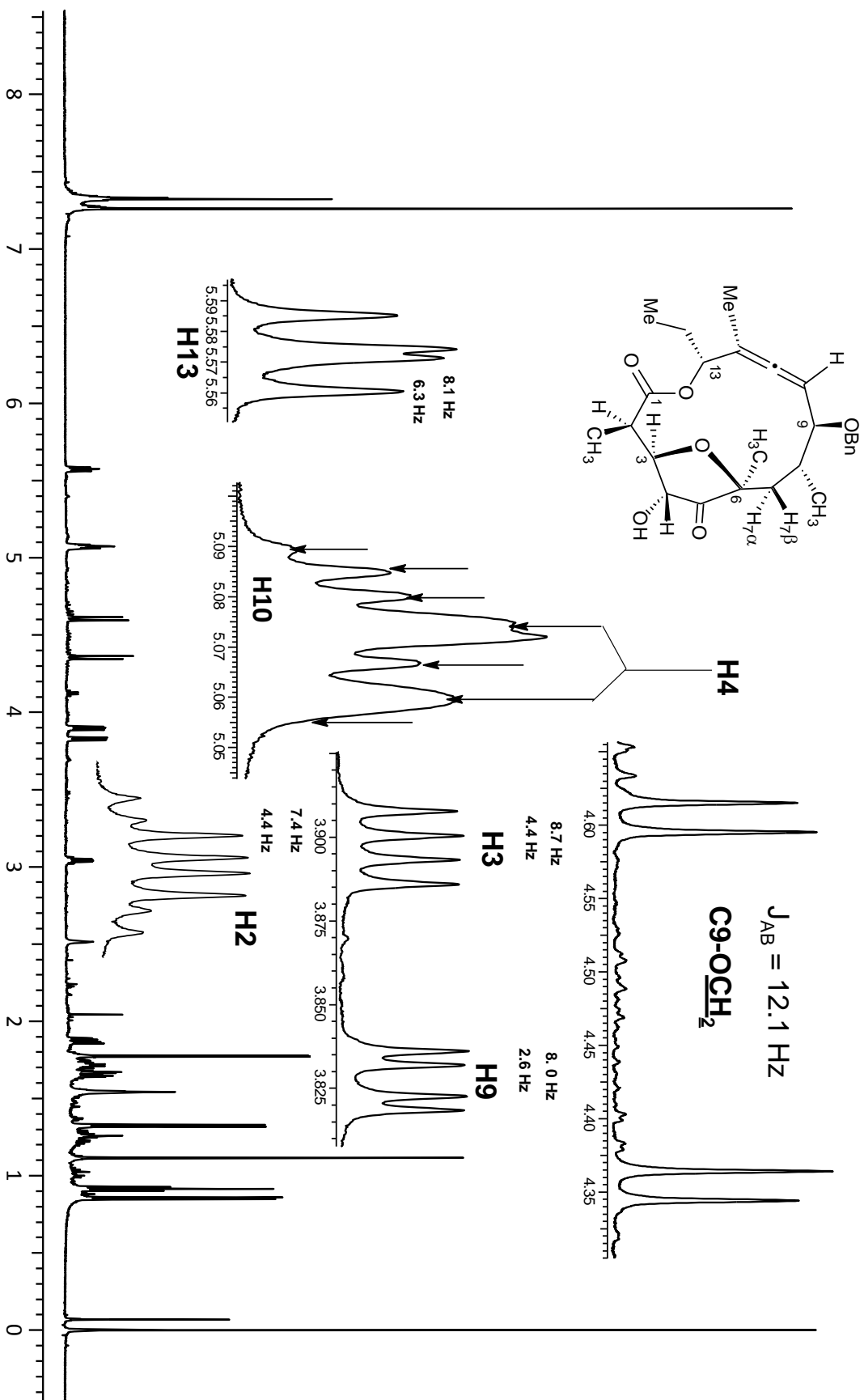
¹³C NMR chemical shift (δ/ppm)	
171.0 — C1	
40.2 — C2	
79.7 — C3	
72.5 — C4	
218.9 — C5	
83.4 — C6	
42.9 — C7	
34.0 — C8	
82.3 — C9	
90.7 — C10	
206.6 — C11	
99.0 — C12	
76.6 — C13	
24.3 — C14	
13.8 — 2-CH ₃	
22.8 — 6-CH ₃	
14.5 — 8-CH ₃	
13.6 — 12-CH ₃	
10.0 — 14-CH ₃	
70.2 — 9-OCH ₃	

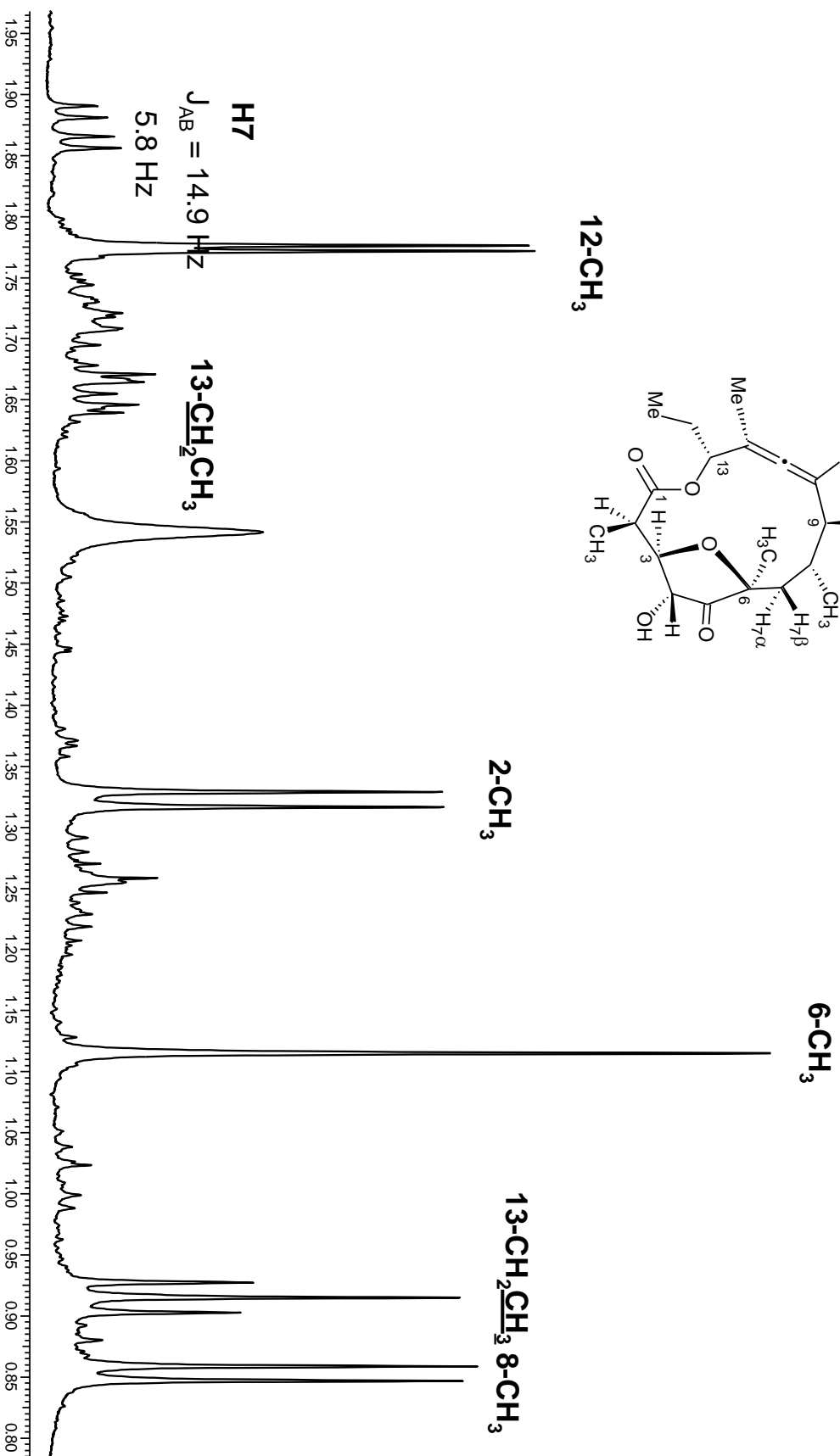
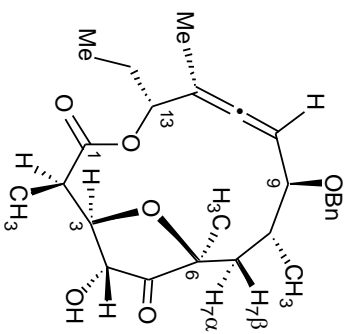




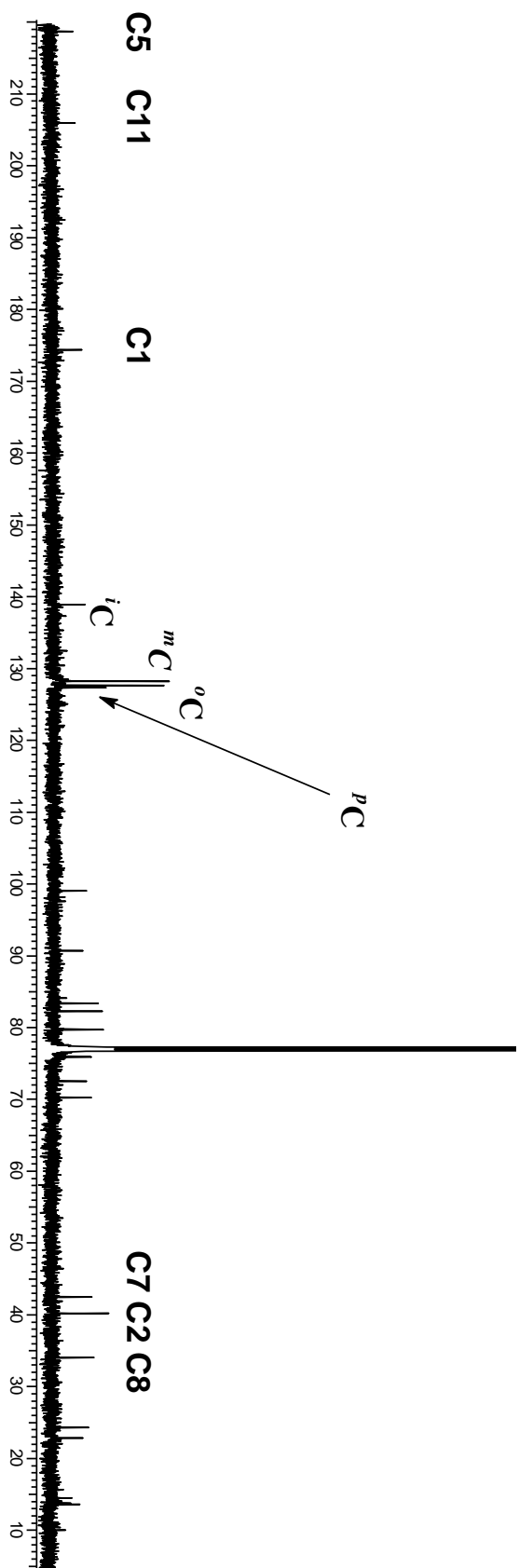
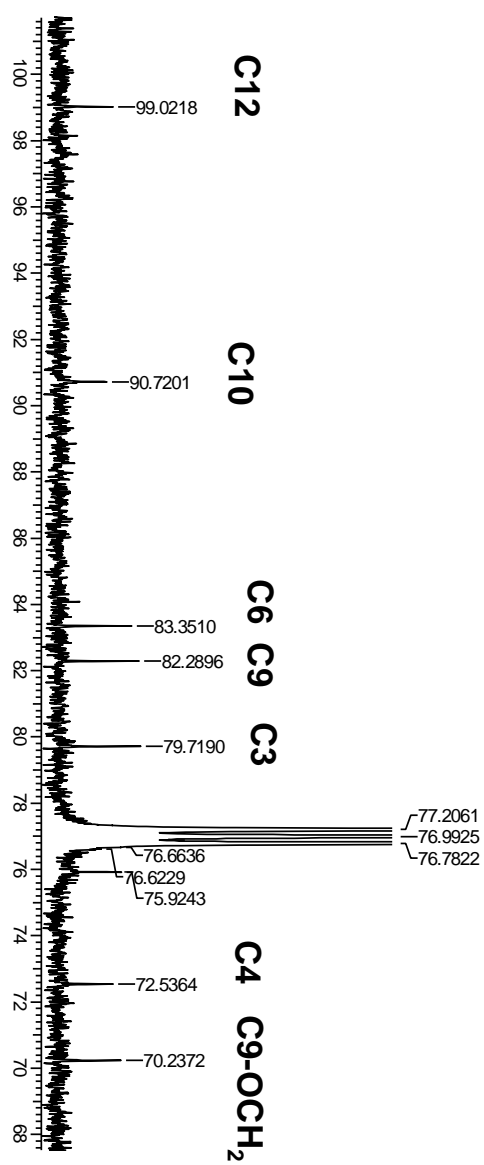
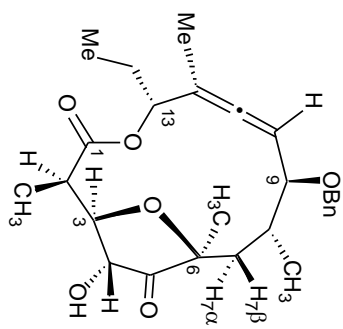
HMBC

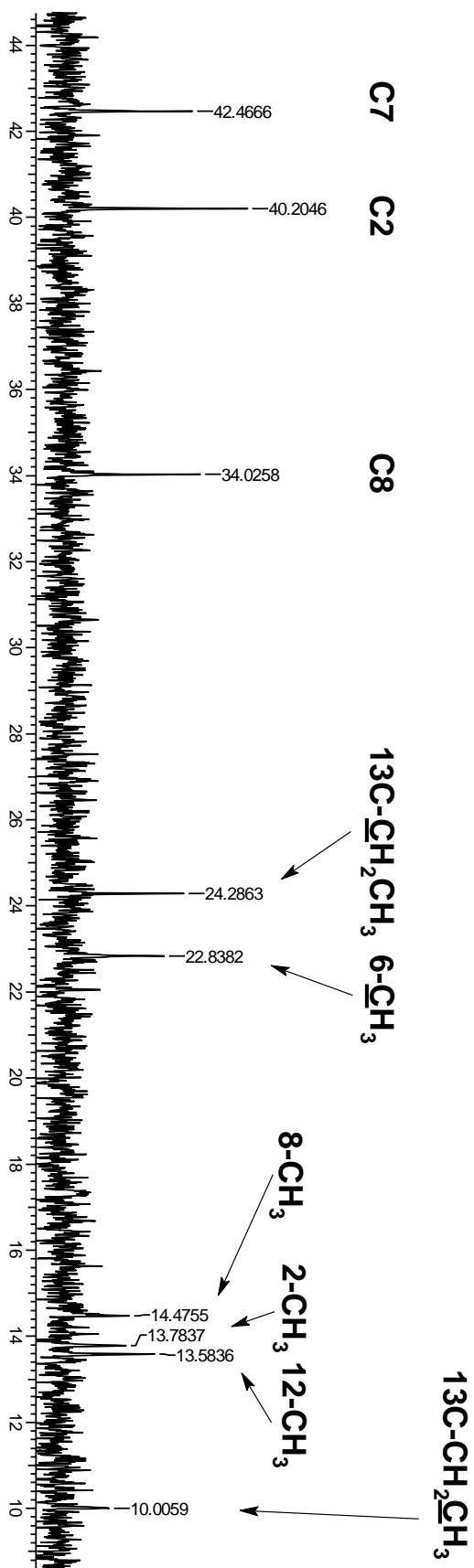
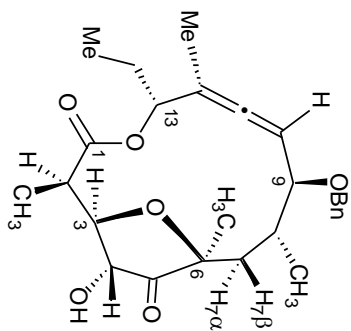


^1H NMR spectrum in CDCl_3 

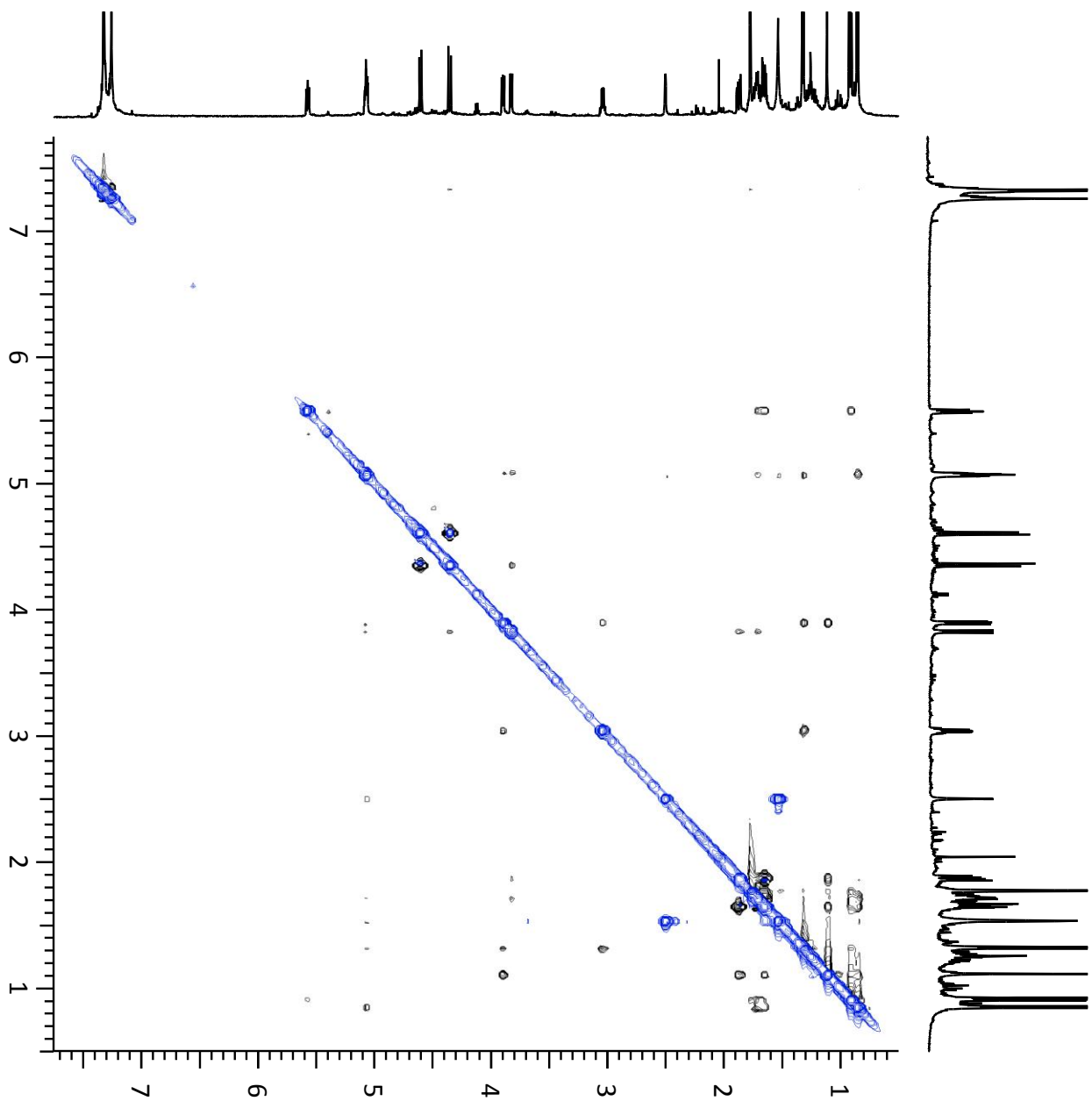
^1H NMR spectrum in CDCl_3 

^{13}C NMR spectrum in CDCl_3

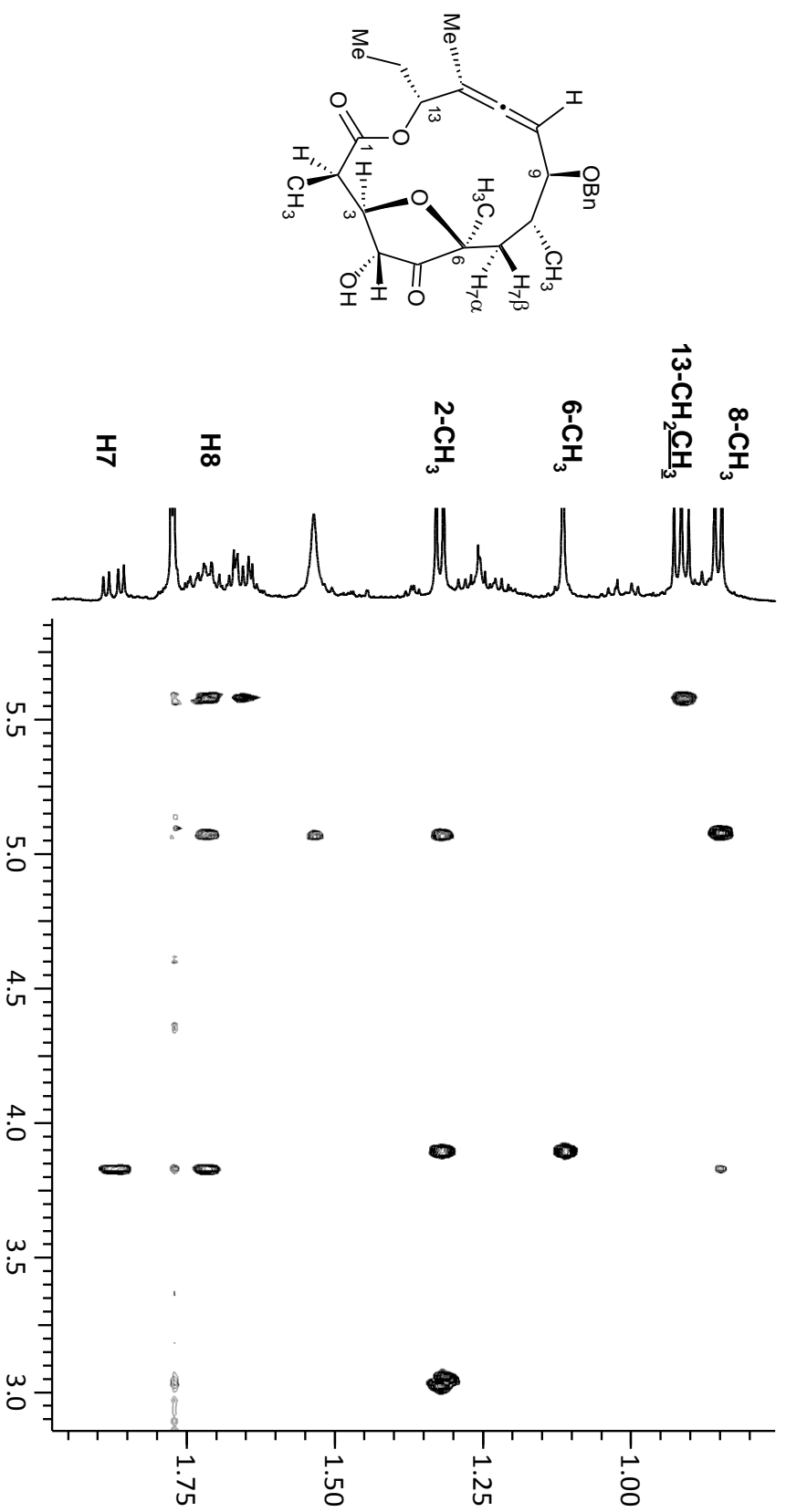


^{13}C NMR spectrum in CDCl_3 

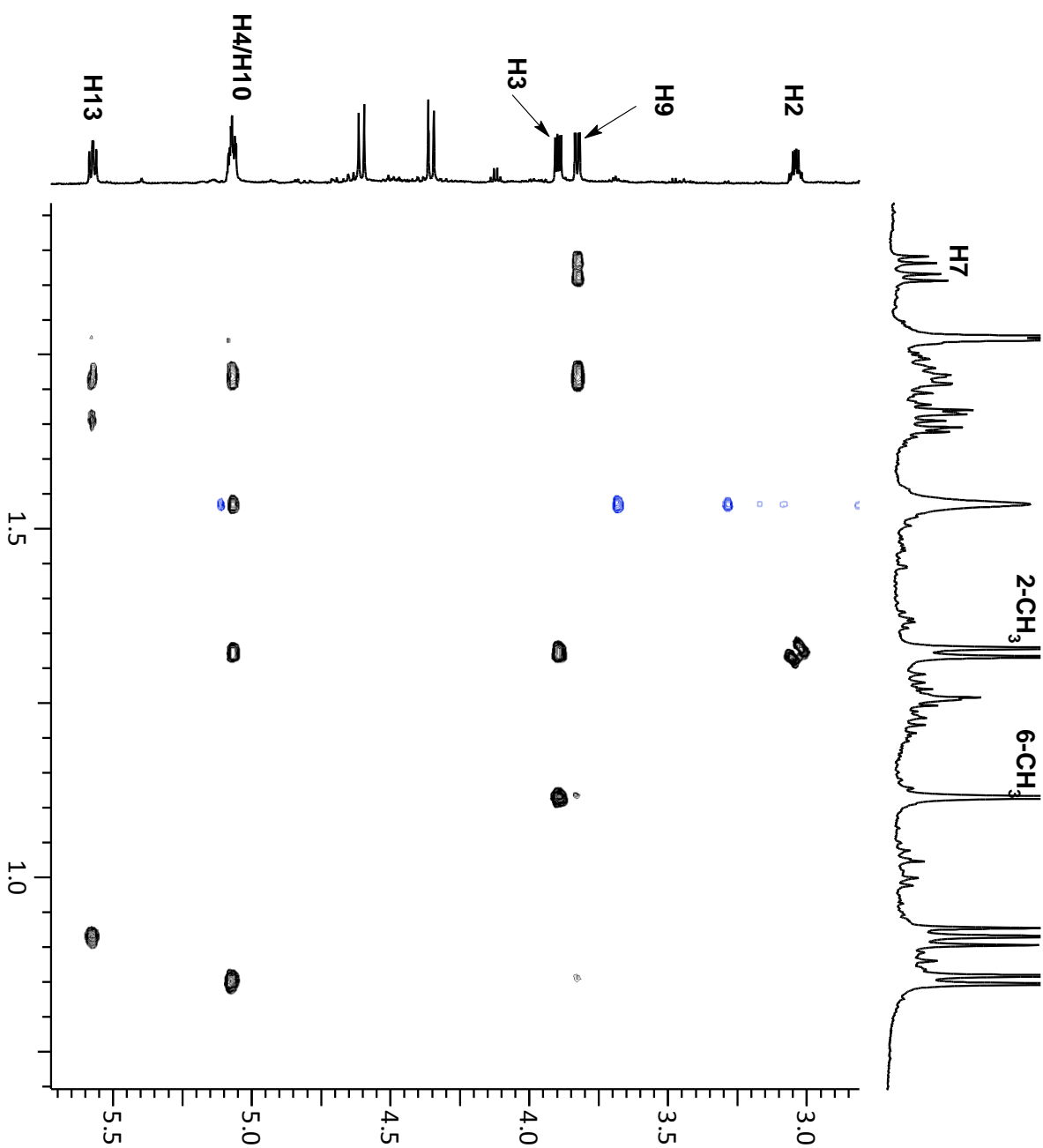
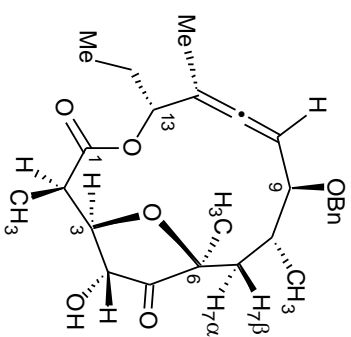
NOESY



expansion

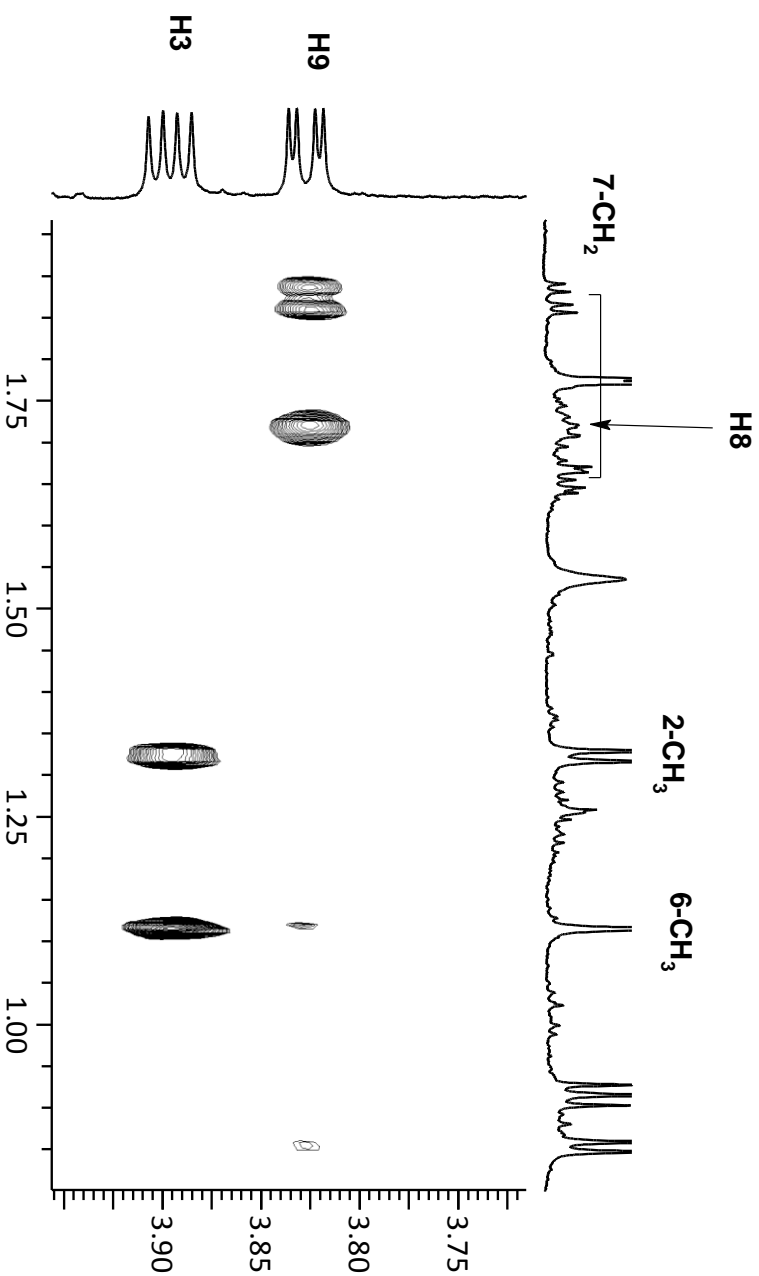
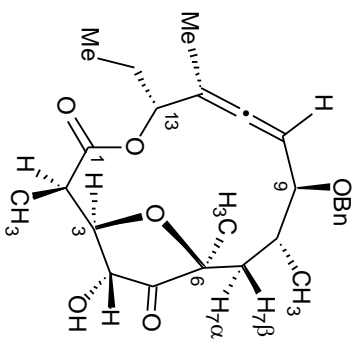


expansion



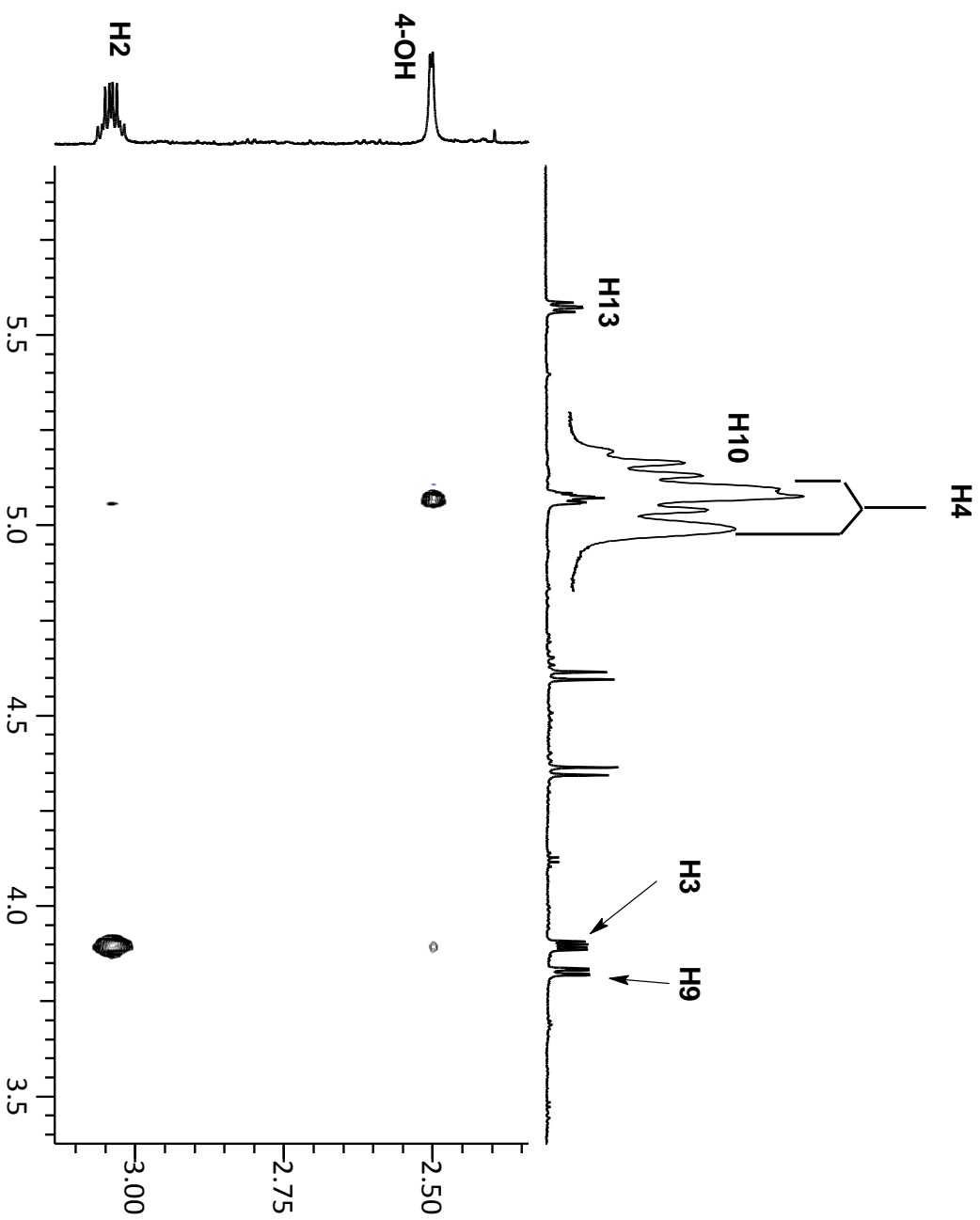
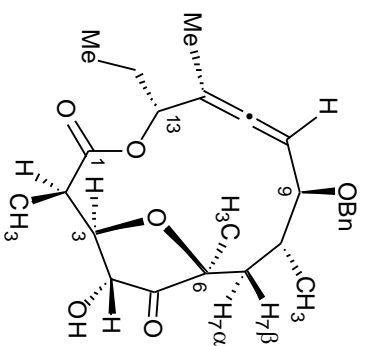
NOESY

expansion



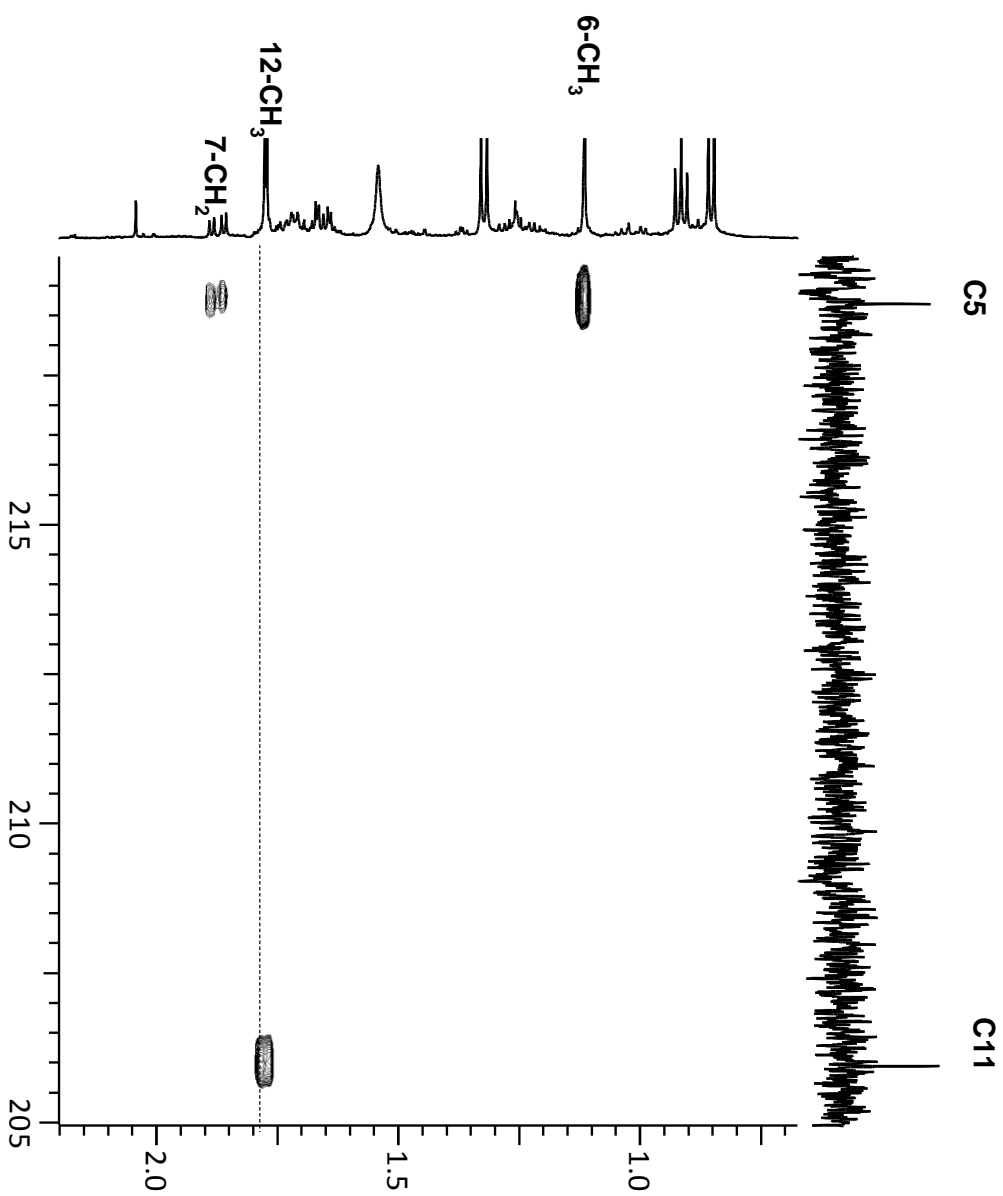
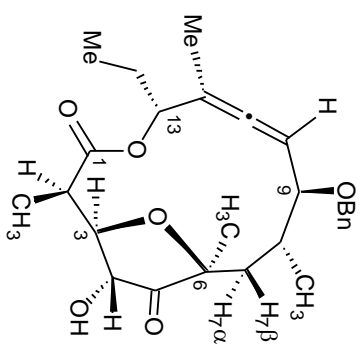
NOESY

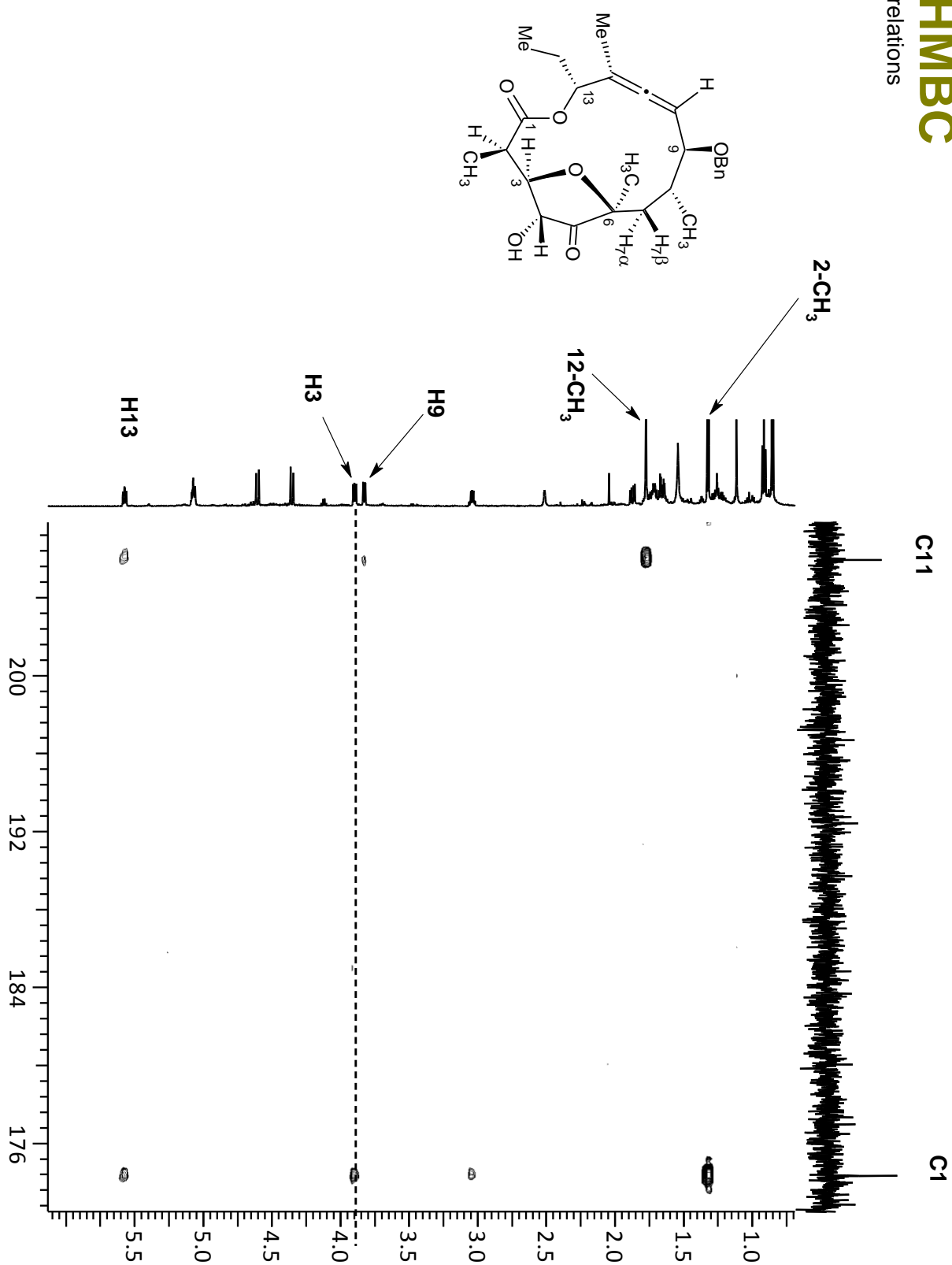
expansion



gHMBC

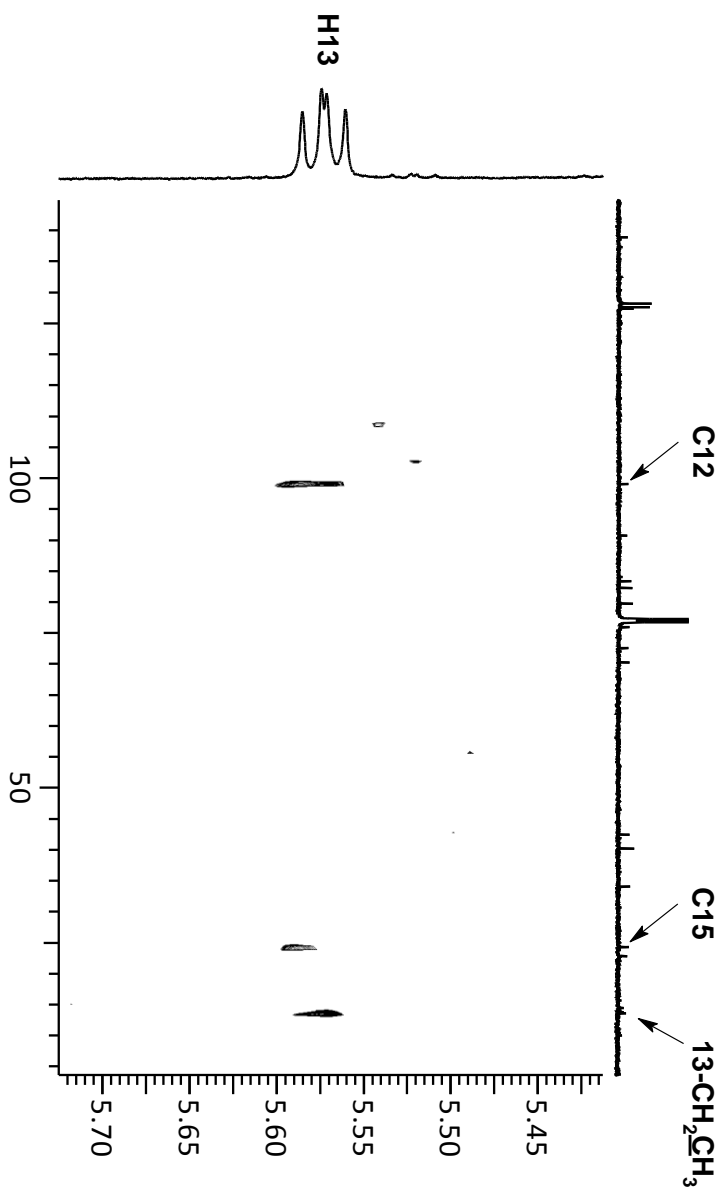
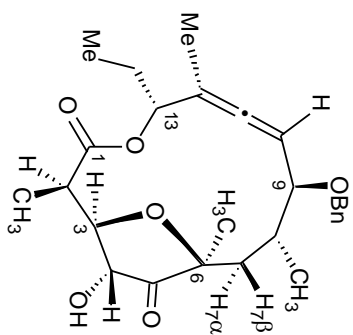
correlations





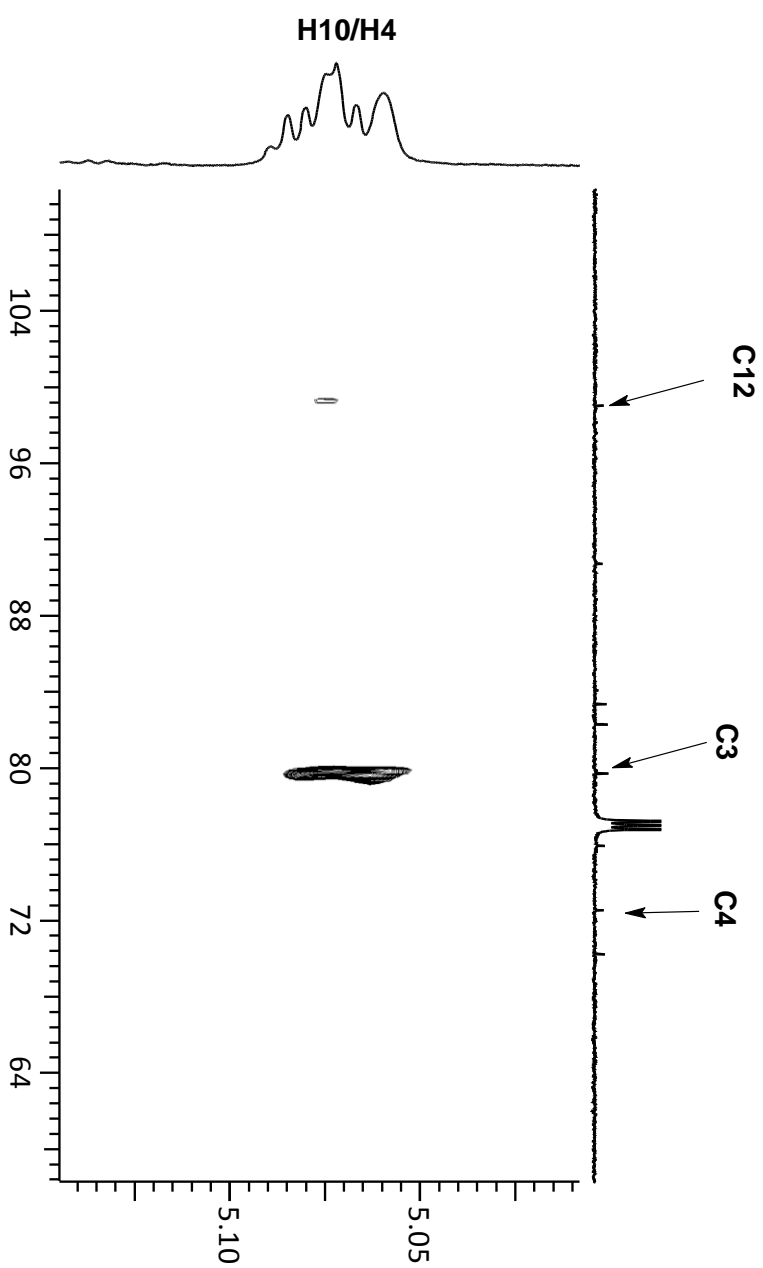
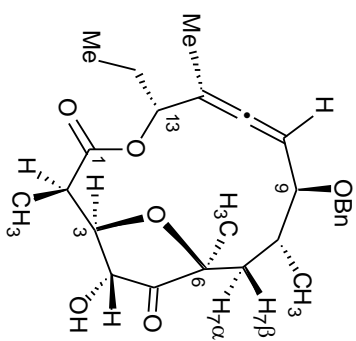
gHMBC

correlations



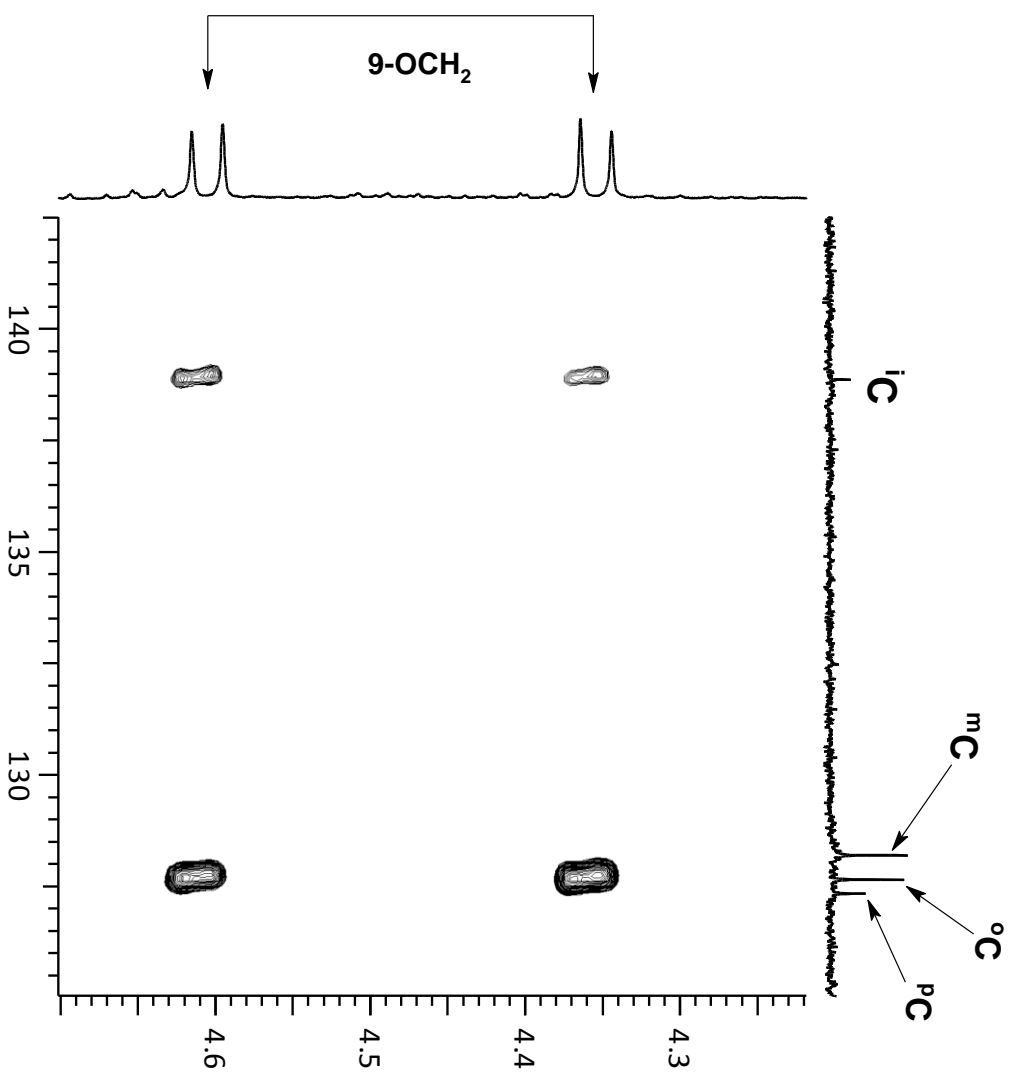
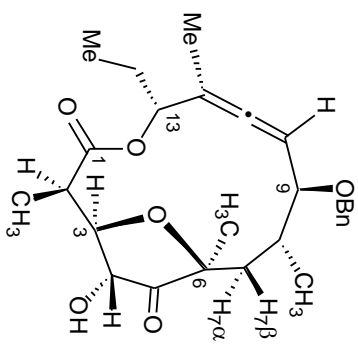
gHMBC

correlations



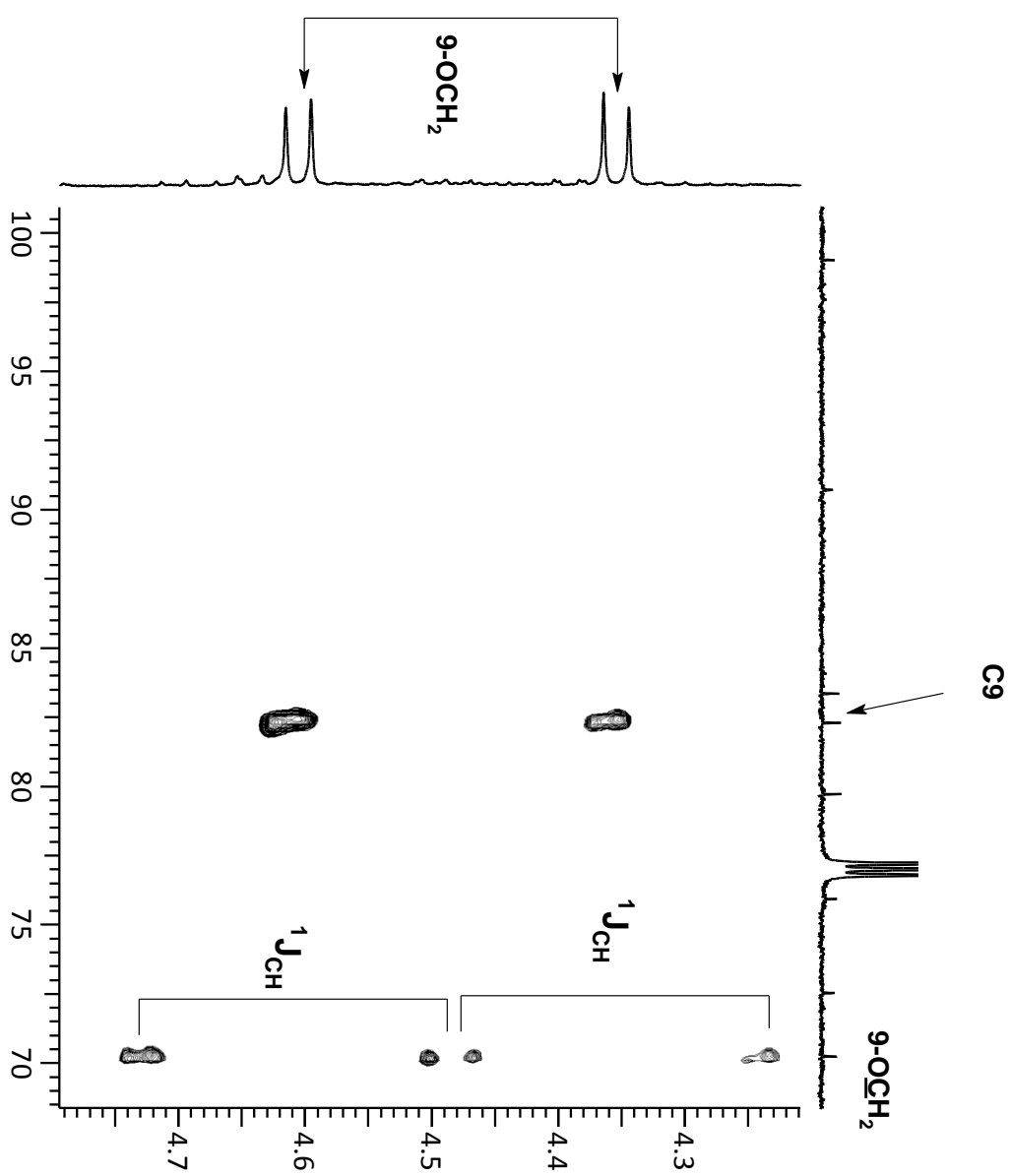
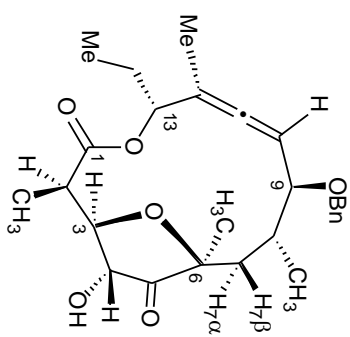
gHMBC

correlations



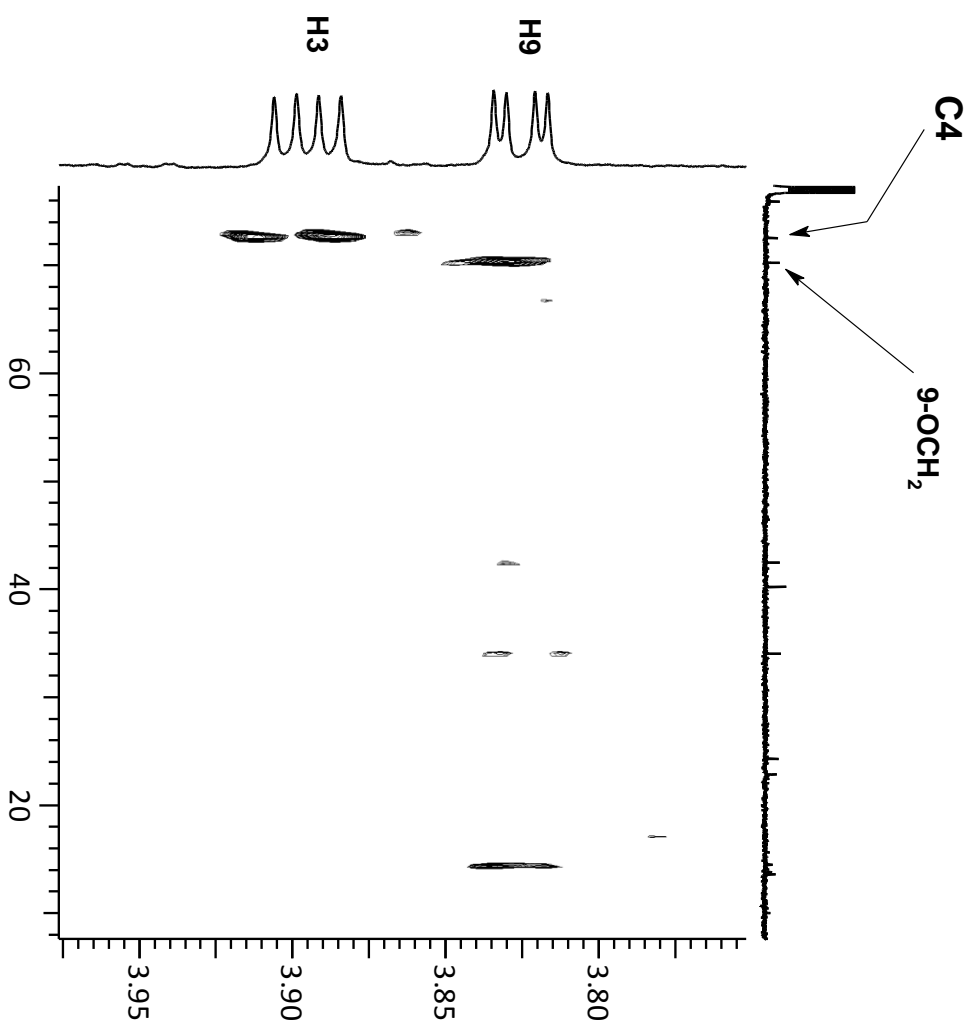
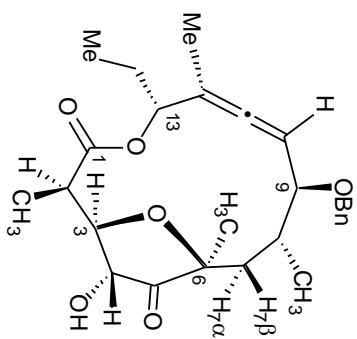
gHMBC

correlations



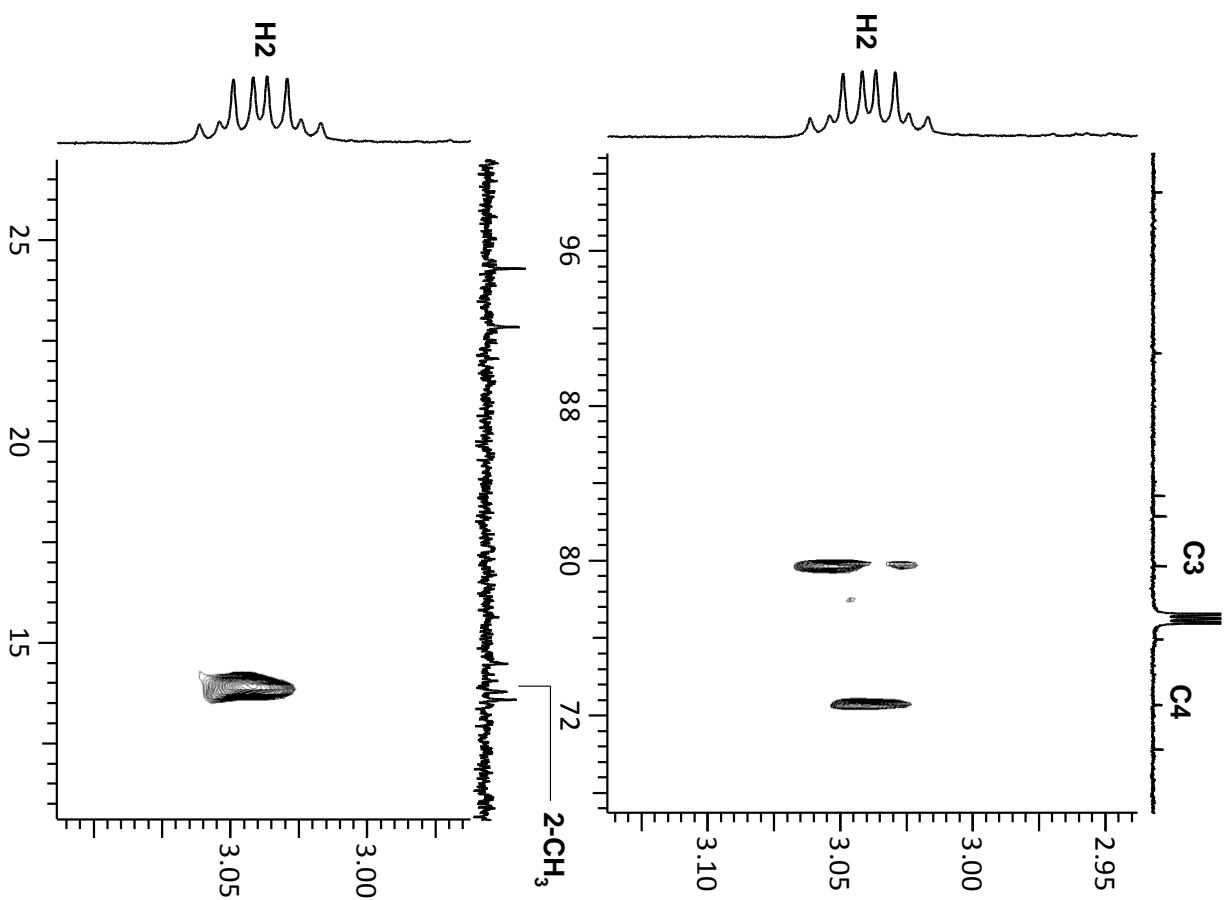
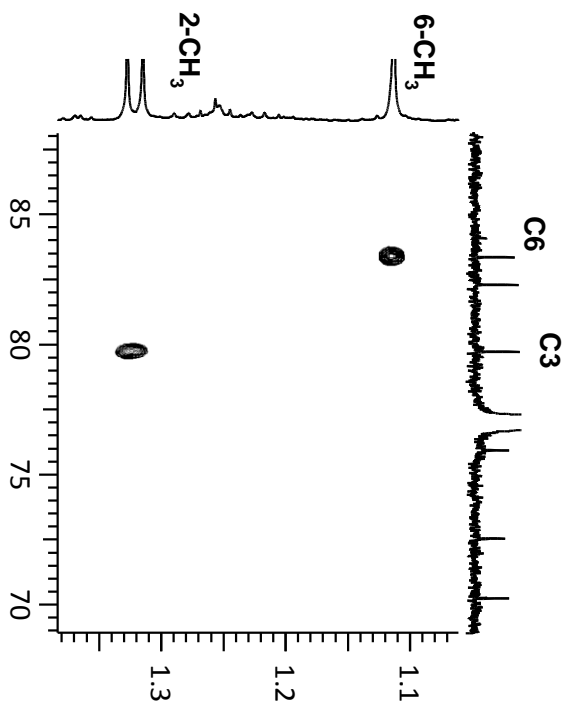
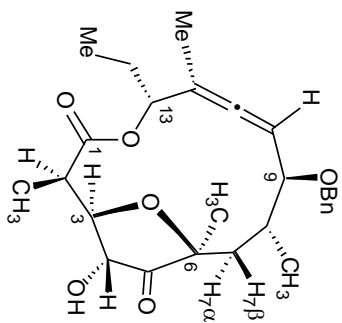
gHMBC

correlations



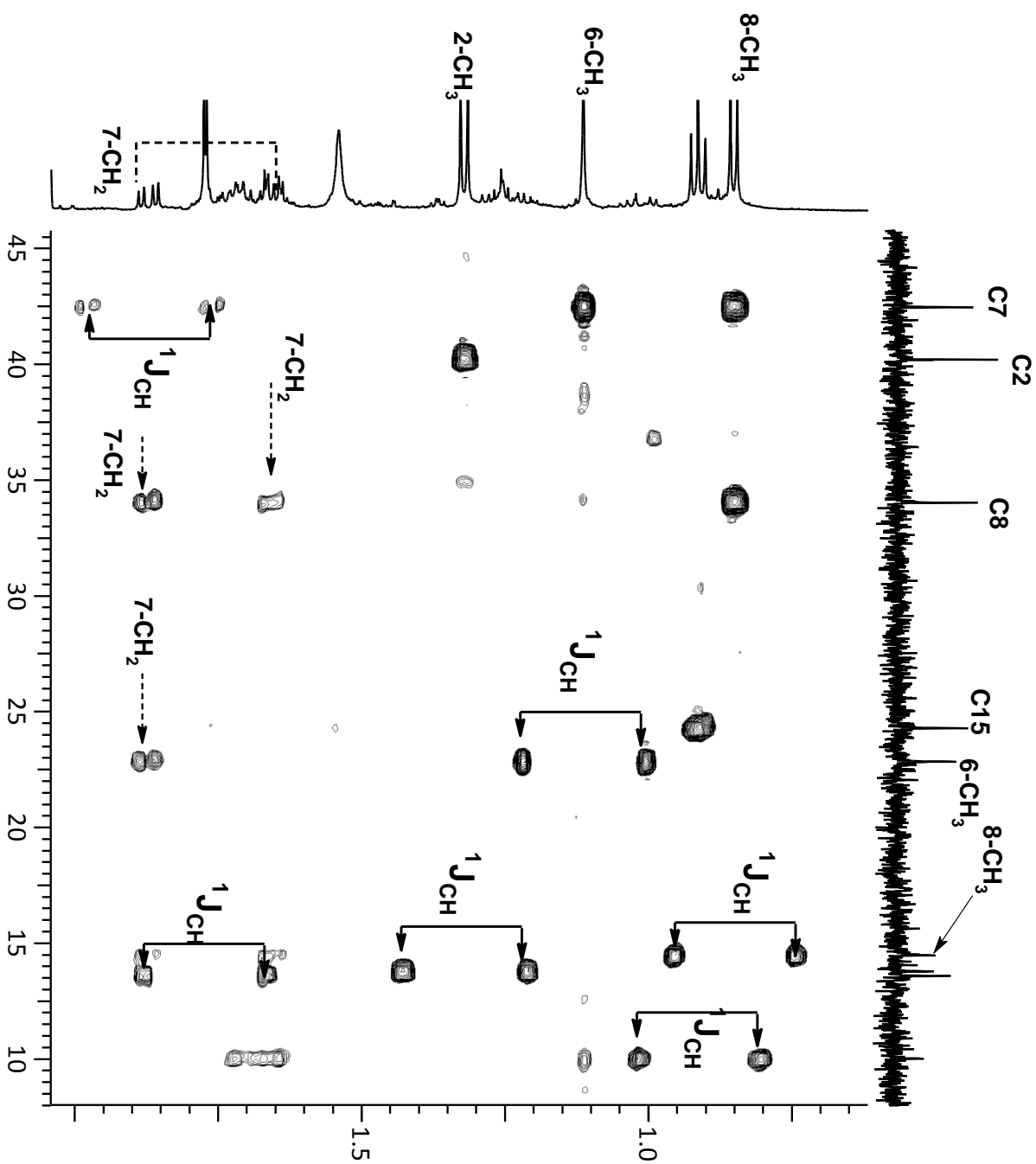
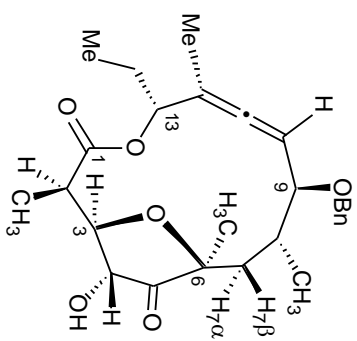
gHMBC

correlations



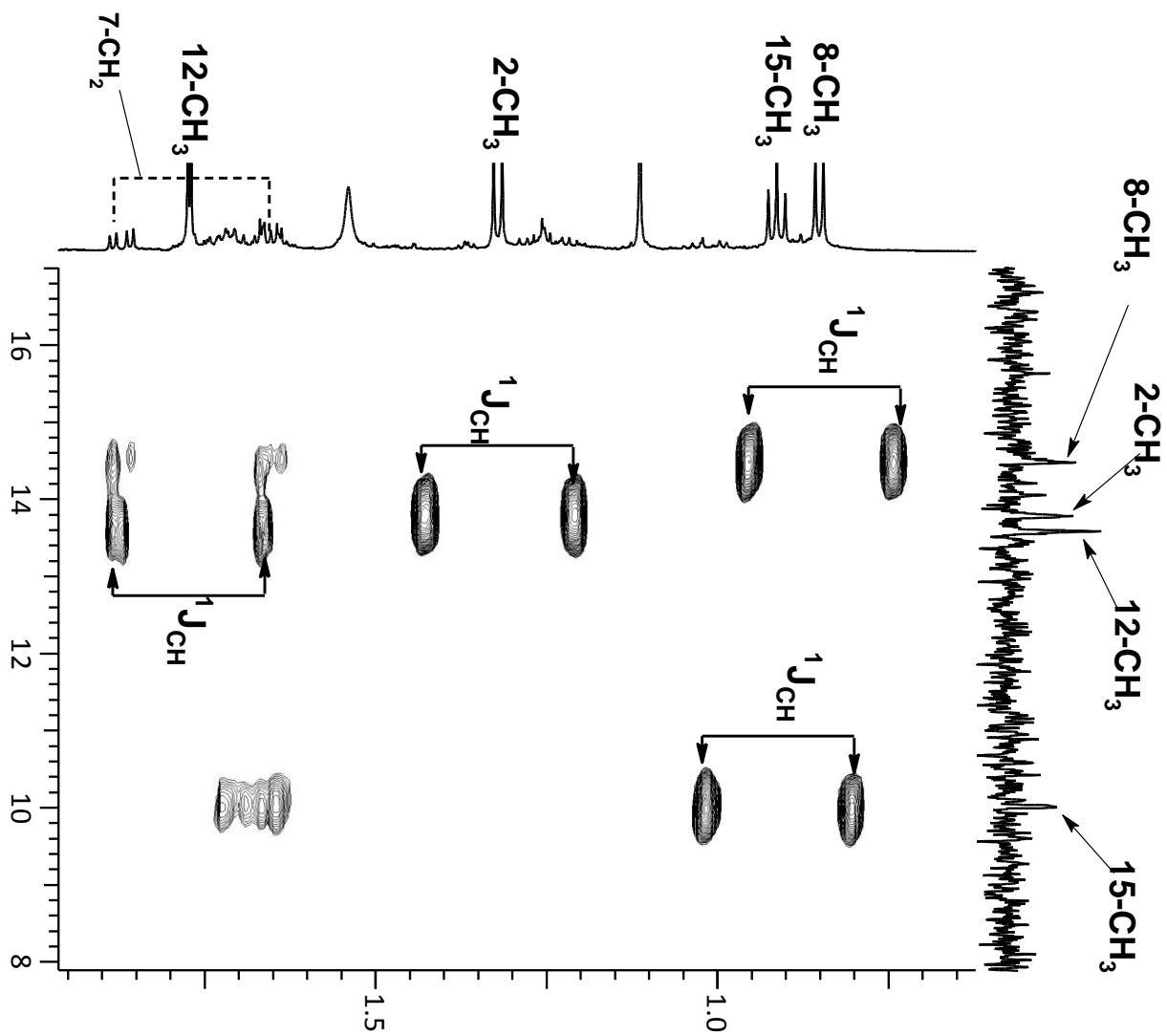
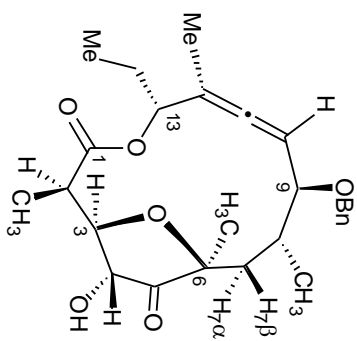
gHMBC

correlations



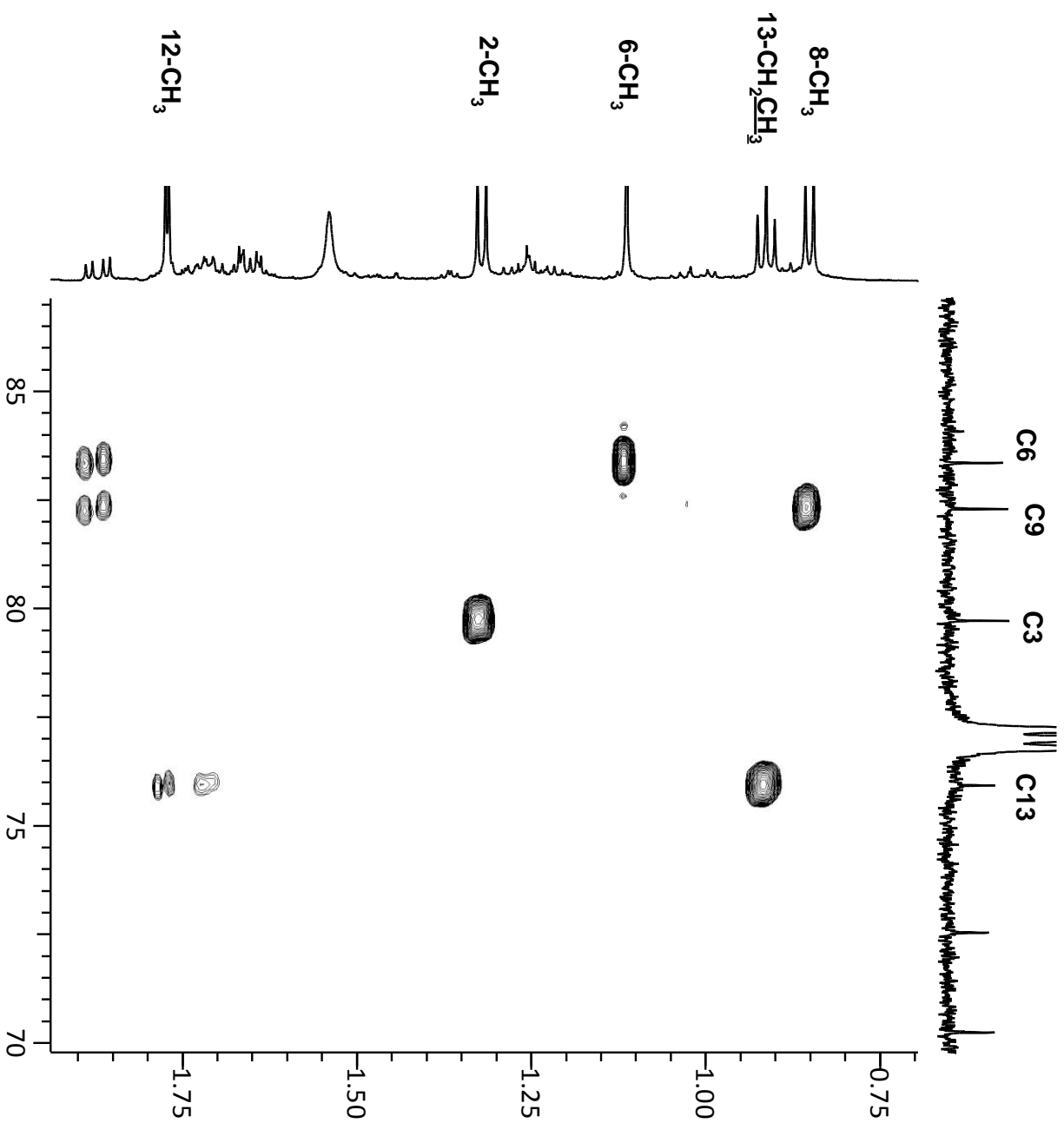
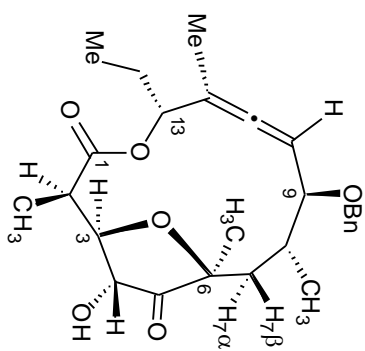
gHMBC

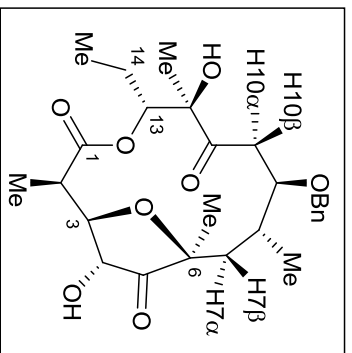
correlations



gHMBC

correlations

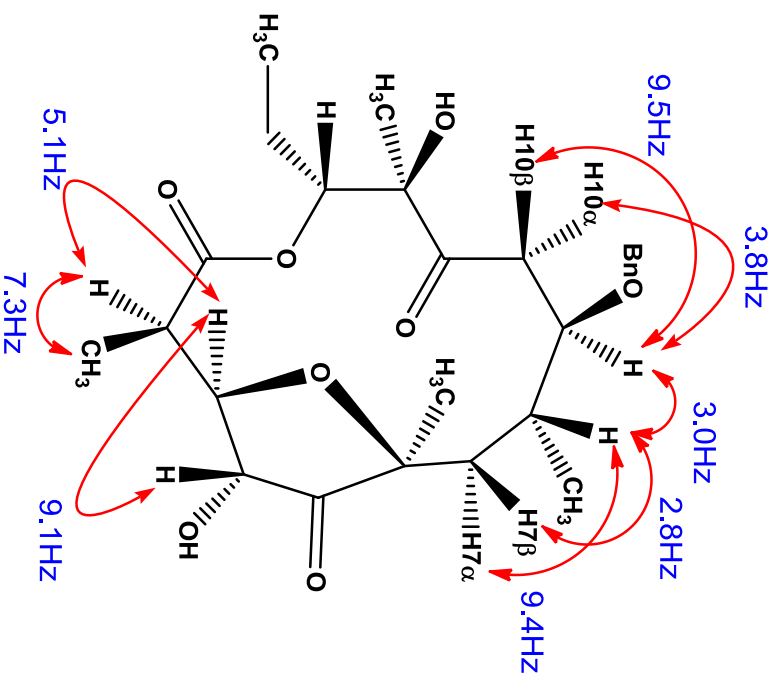
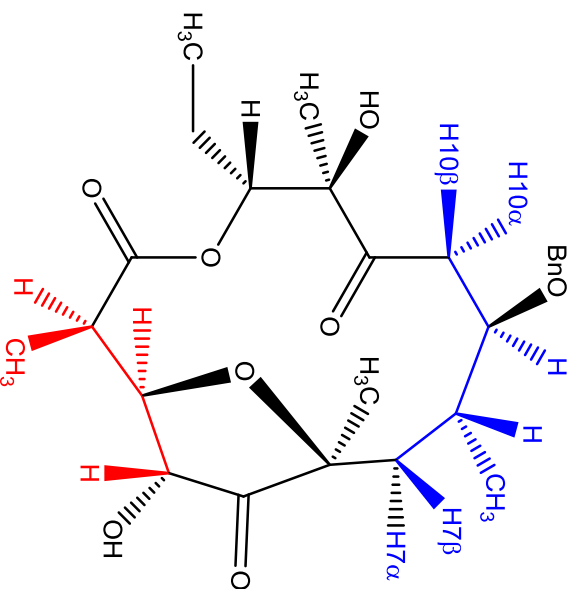




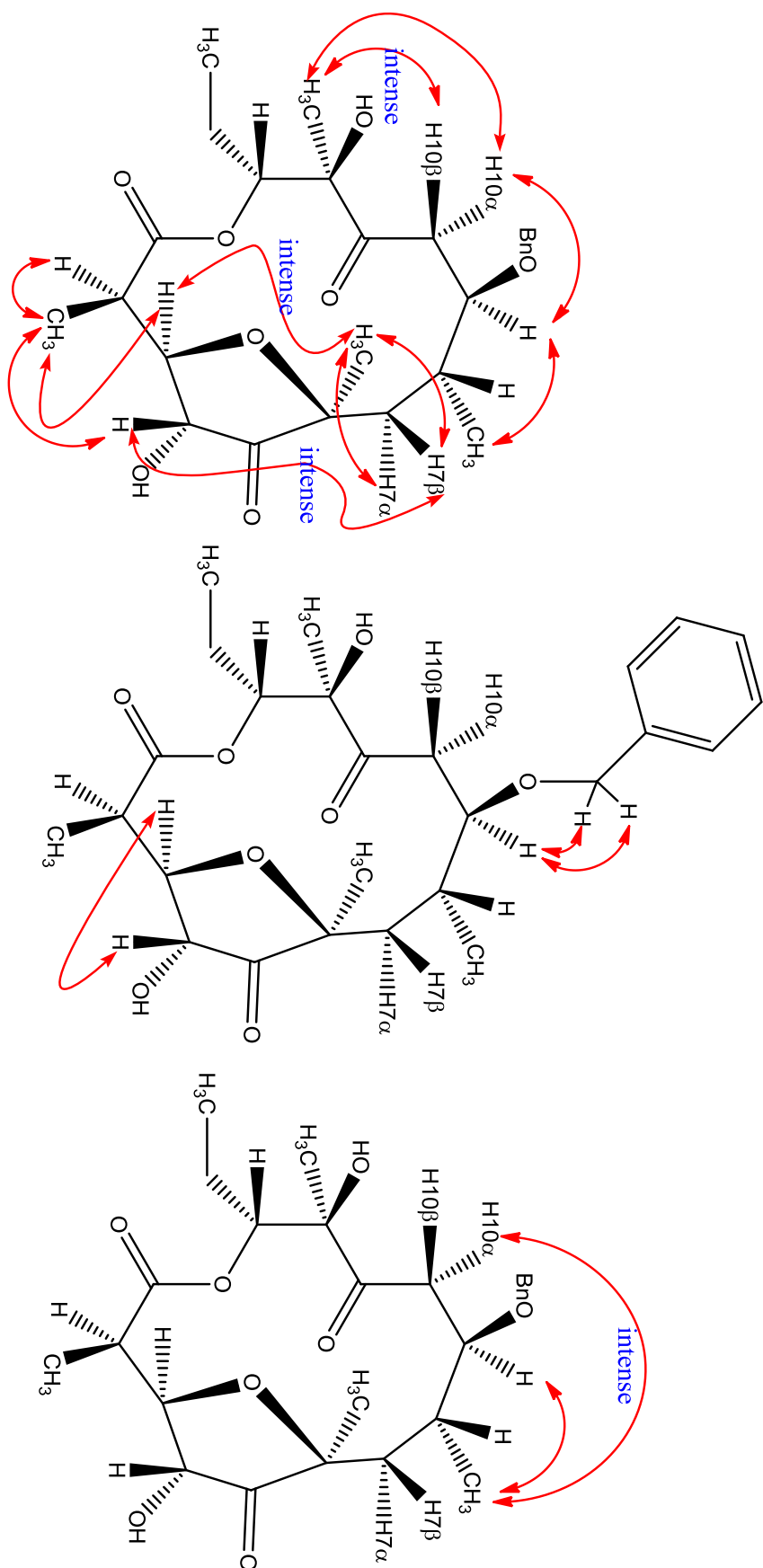
¹ H NMR chemical shifts (δ/ppm) w/ coupling constant (J/Hz)	¹³ C NMR chemical shift (δ/ppm)
3.29 (dq, J _{H2} , H ₃ = 5.5Hz, J _{H2} , 2-CH ₃ = 7.4Hz, H2)	174.5 — C1
1.30 (d, J _{2-CH3} , H ₂ = 7.3Hz, 2-CH₃)	42.0 — C2
3.96 (dd, J _{H3} , H ₂ = 5.1Hz, J _{H3} , H ₄ = 9.1Hz, H3)	73.1 — C3
4.58 (d, J _{H4} , H ₃ = 9.1Hz, H4)	79.8 — C4
1.20 (s, 6-CH₃)	217.1 — C5
1.63 (dd, J _{H7β} , H ₈ = 2.8Hz, J _{H7β} , H _{7α} = 15.0Hz, H7β)	83.9 — C6
1.75 (dd, J _{H7α} , H ₈ = 9.4Hz, J _{H7α} , H _{7β} = 15.0Hz, H7α)	41.2 — C7
1.65 (m, J _{H8} , 8-CH ₃ = 6.9Hz, H8)	35.9 — C8
0.86 (d, J _{8-CH3} , H ₈ = 6.9Hz, 8-CH₃)	78.1 — C9
4.14 (dt, J _{H9} , H ₈ = 3.0Hz, J _{H9} , H _{10α} = 3.8Hz, J _{H9} , H _{10β} = 9.5Hz, H9)	42.6 — C10
4.32, 4.49 (d, J _{AB} = 10.9Hz, 9-OCH₂)	208.1 — C11
2.51 (d, J _{H10α} , H ₉ = 3.8Hz, H10α)	93.2 — C12
3.41 (d, J _{H10β} , H ₉ = 9.5Hz, H10β)	76.2 — C13
1.47 (s, 12-CH₃)	24.9 — C14
4.04 (dd, J _{H13} , H ₁₄ = 2.1, 10.4Hz, H13)	13.1 — 2-CH ₃
1.26, 1.64 (m, 14-CH₂)	23.5 — 6-CH ₃
1.05 (t, J _{14-CH3} , H ₁₄ = 7.4Hz, 14-CH₃)	17.6 — 8-CH ₃
	21.0 — 12-CH ₃
	11.3 — 14-CH ₃
	73.2 — 9-OCH ₃
	137.9 — ipsoC
	129.0 — orthoC
	128.3 — metaC
	128.0 — paraC

$1d$ TOCSY

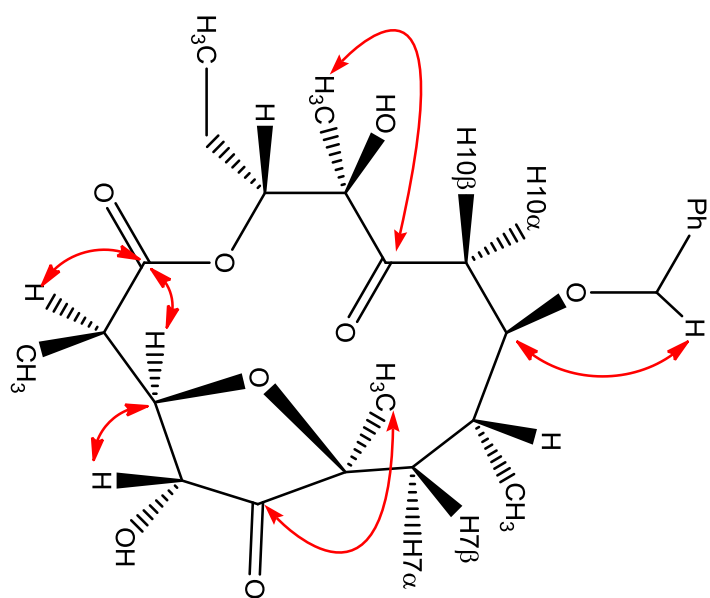
Coupling constant (J_{HH})

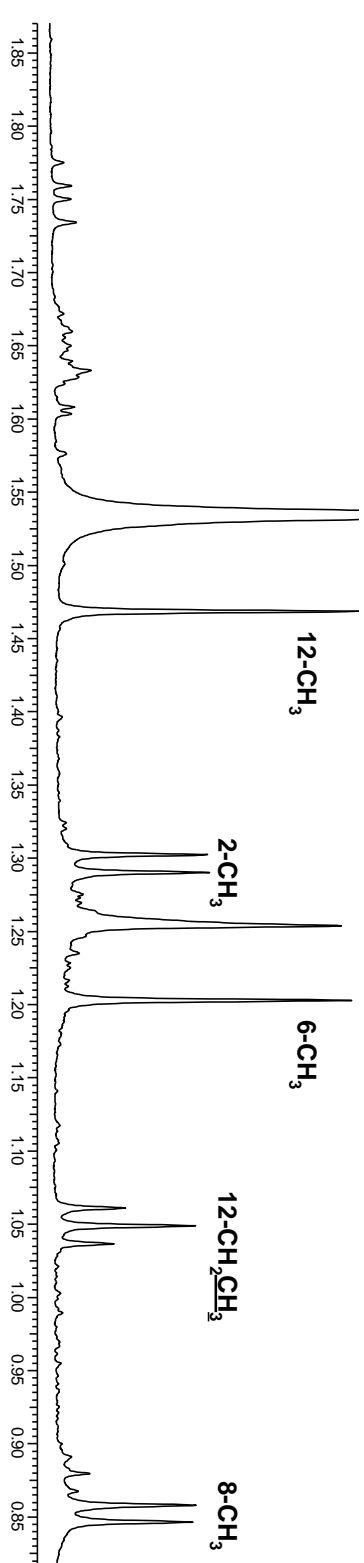
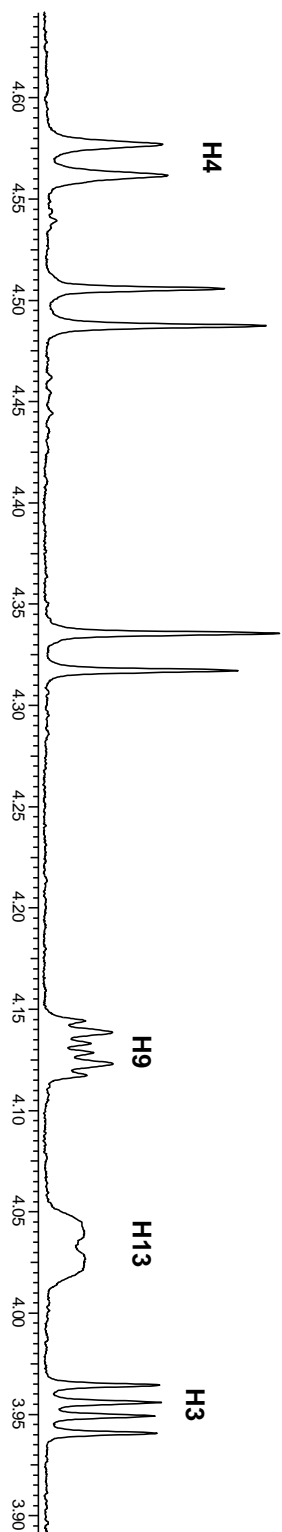
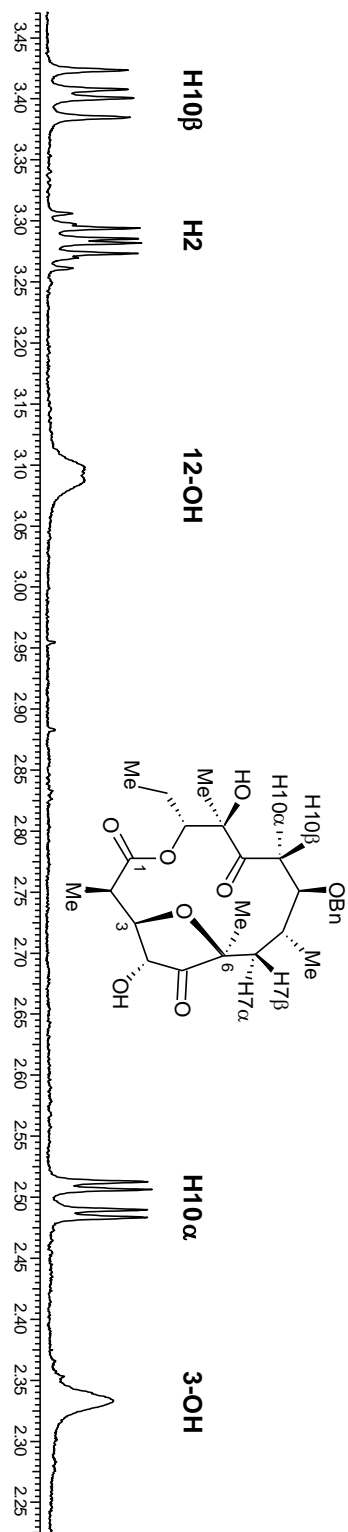


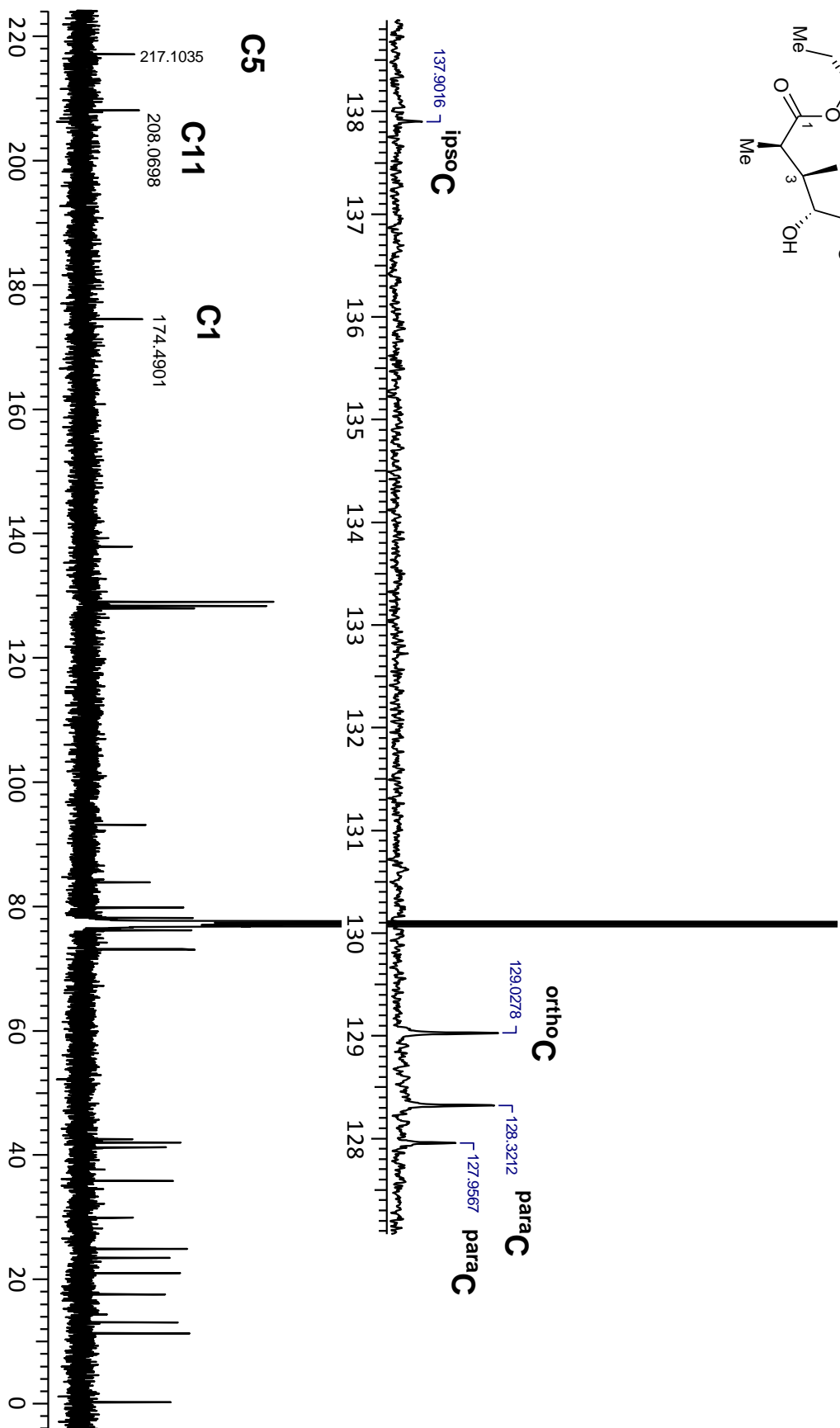
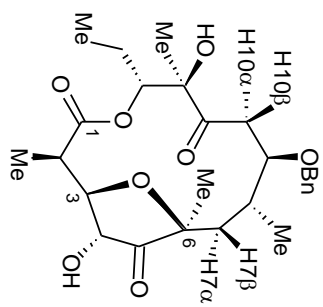
NOESY

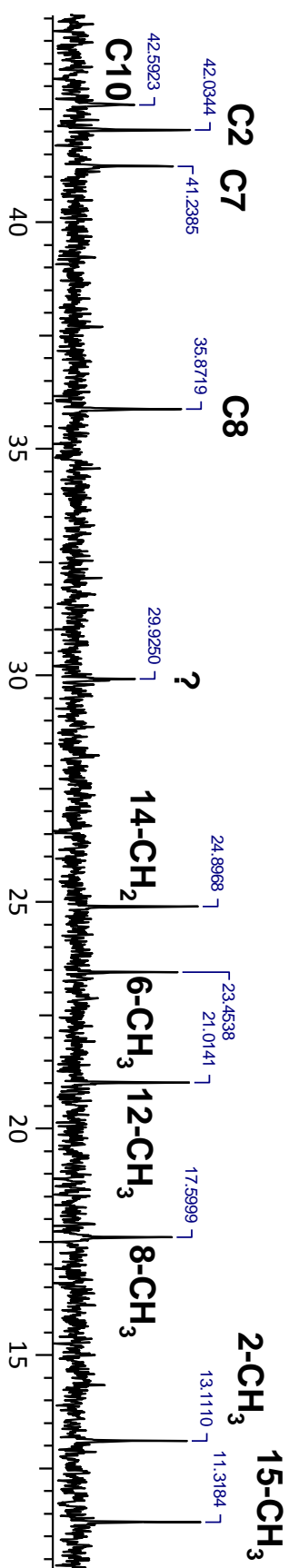
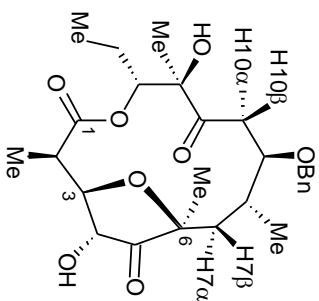


HMBC

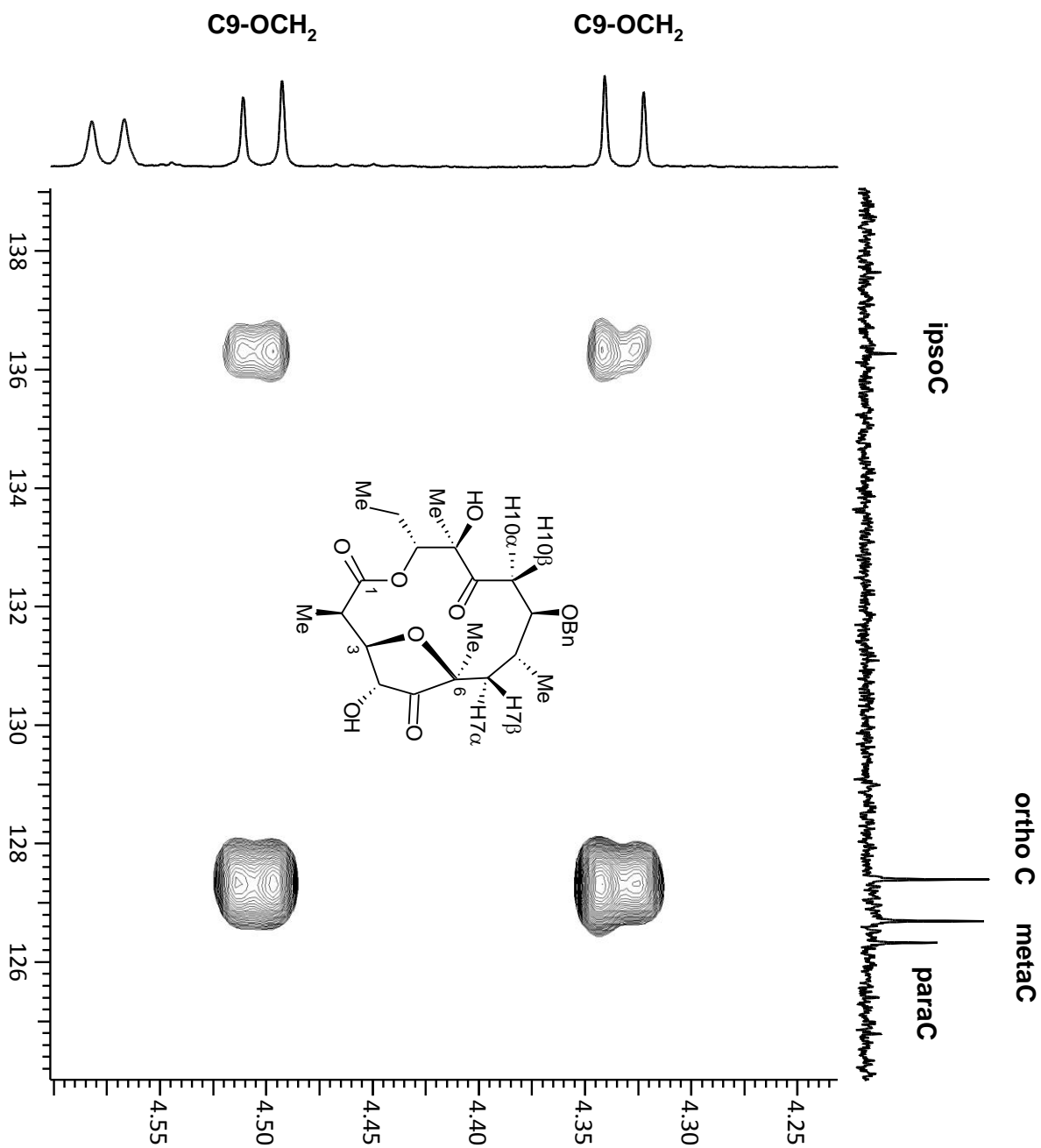


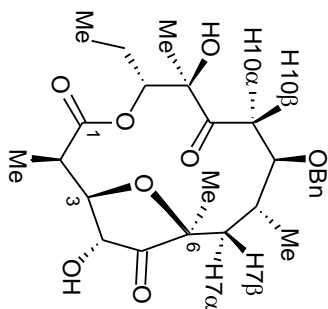


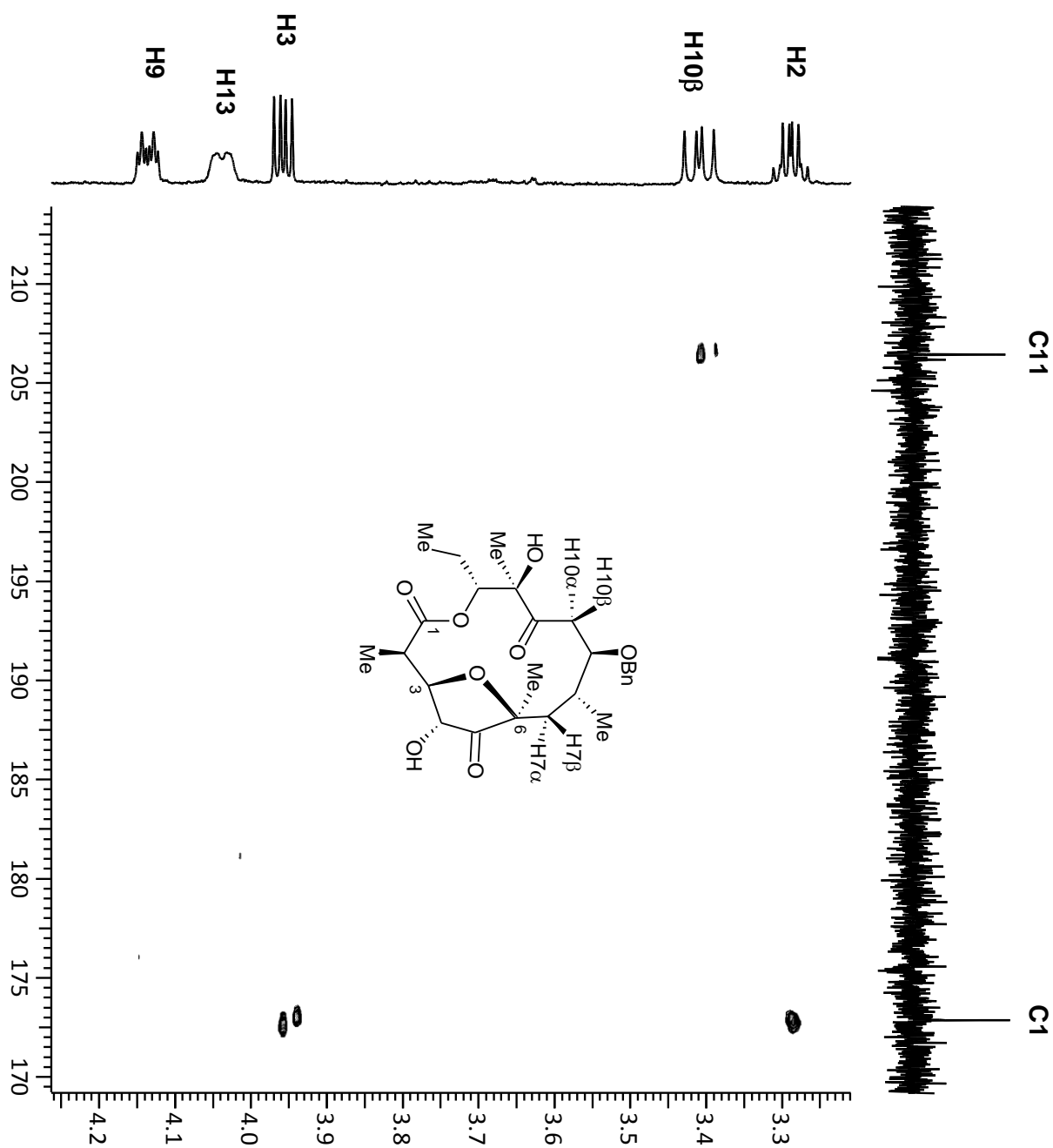


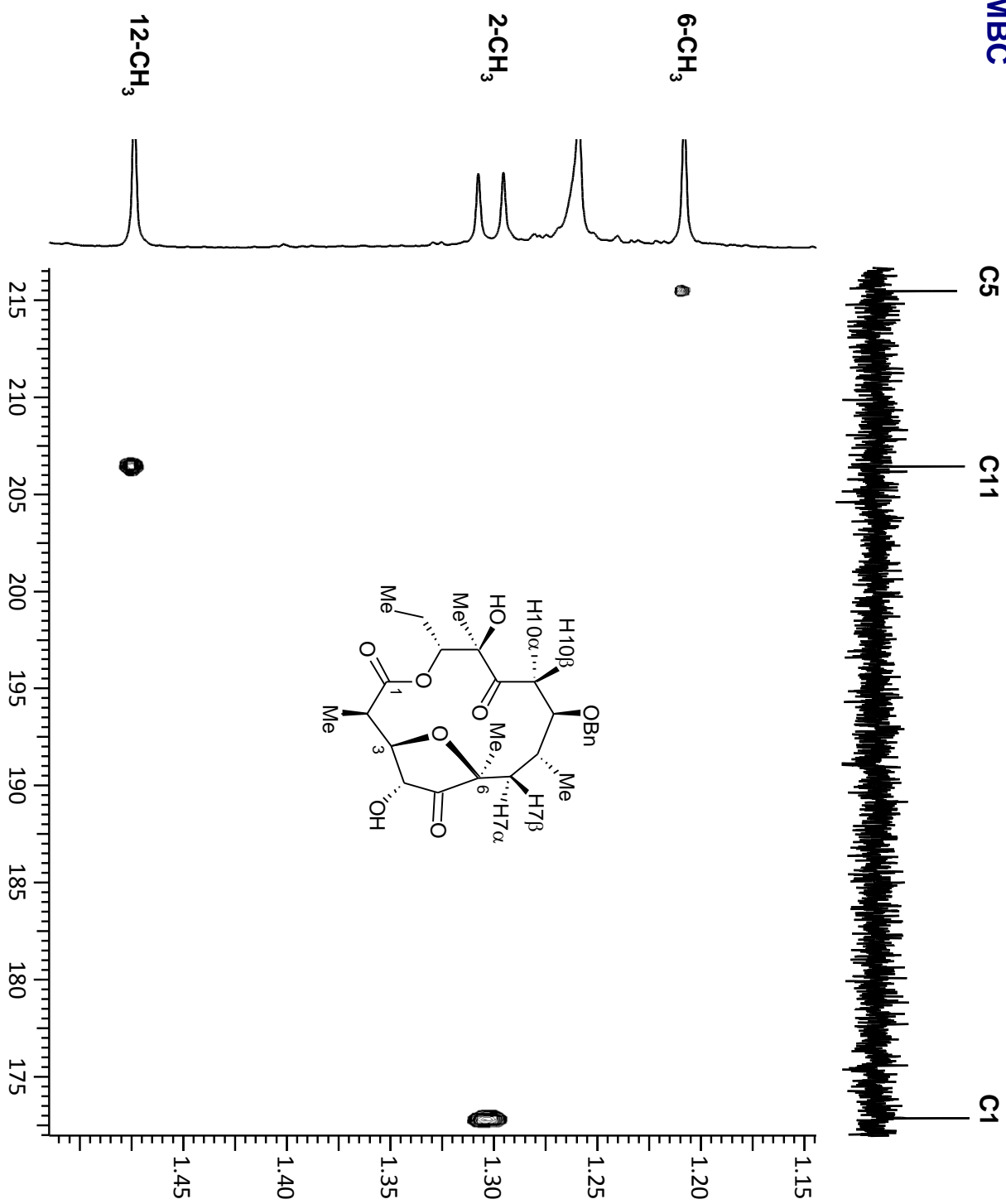


gHMBC

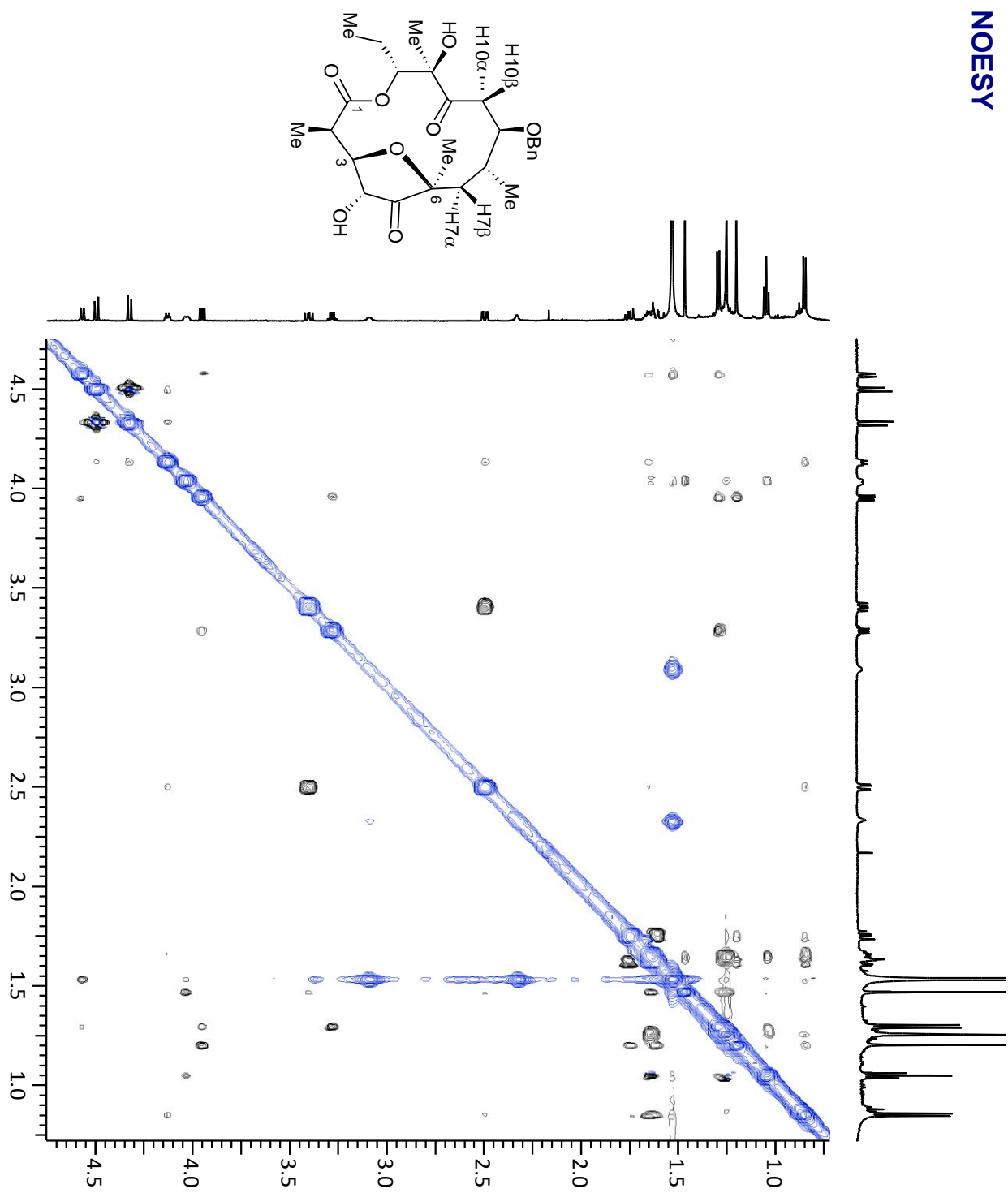




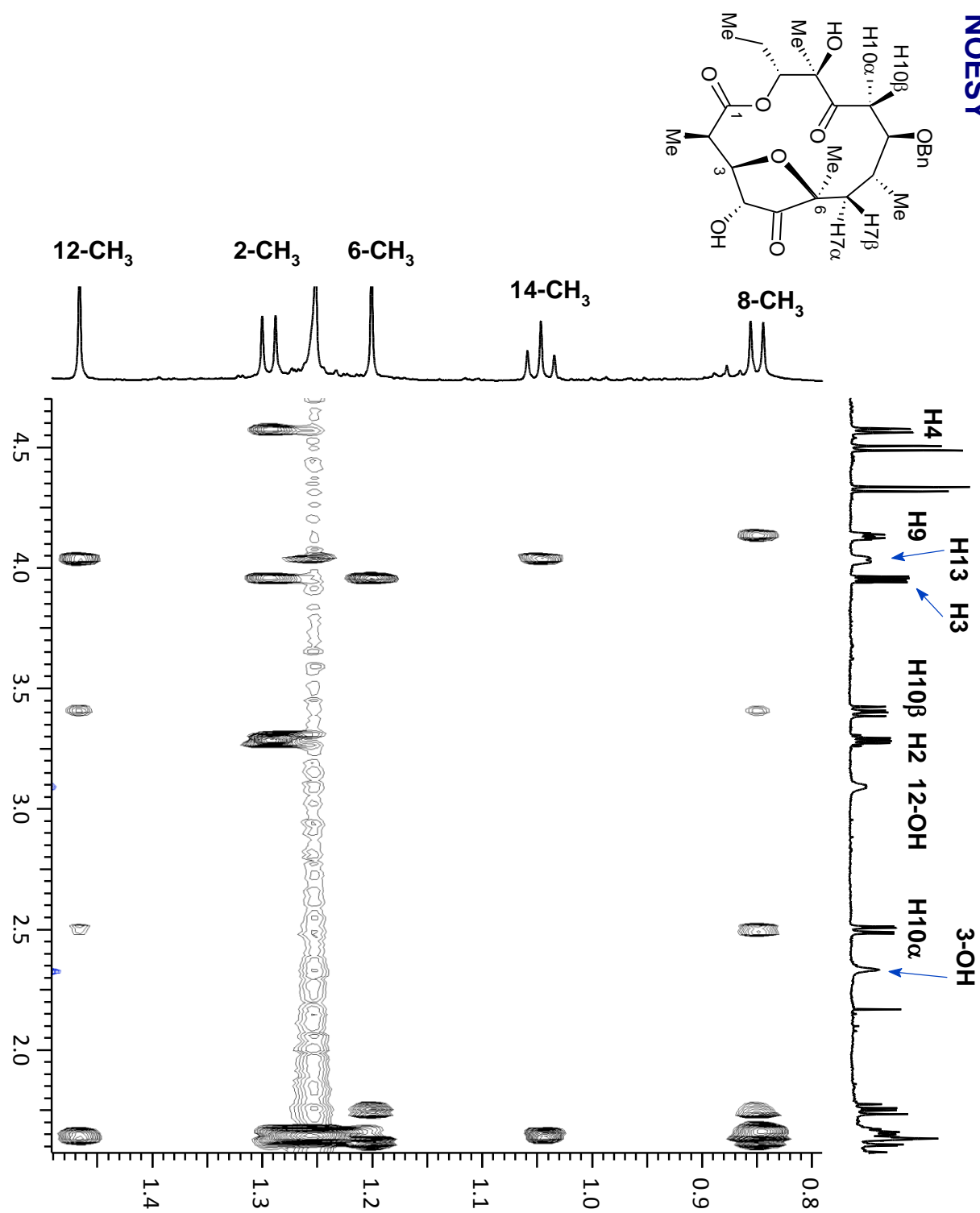




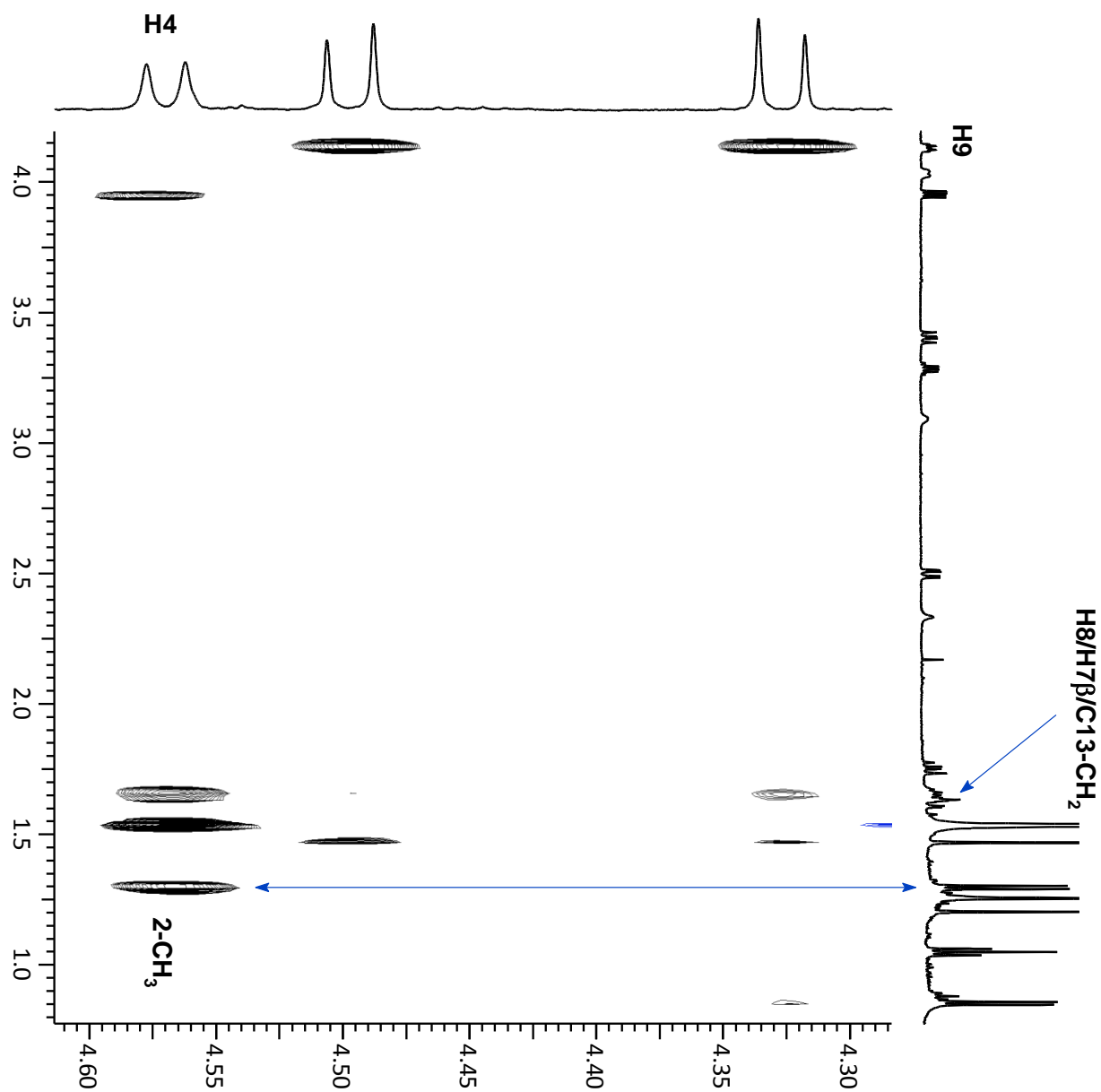
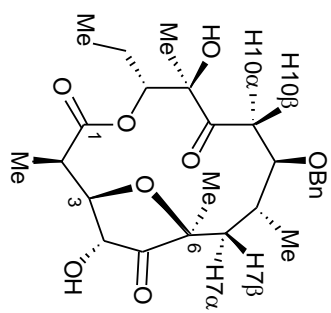
NOESY

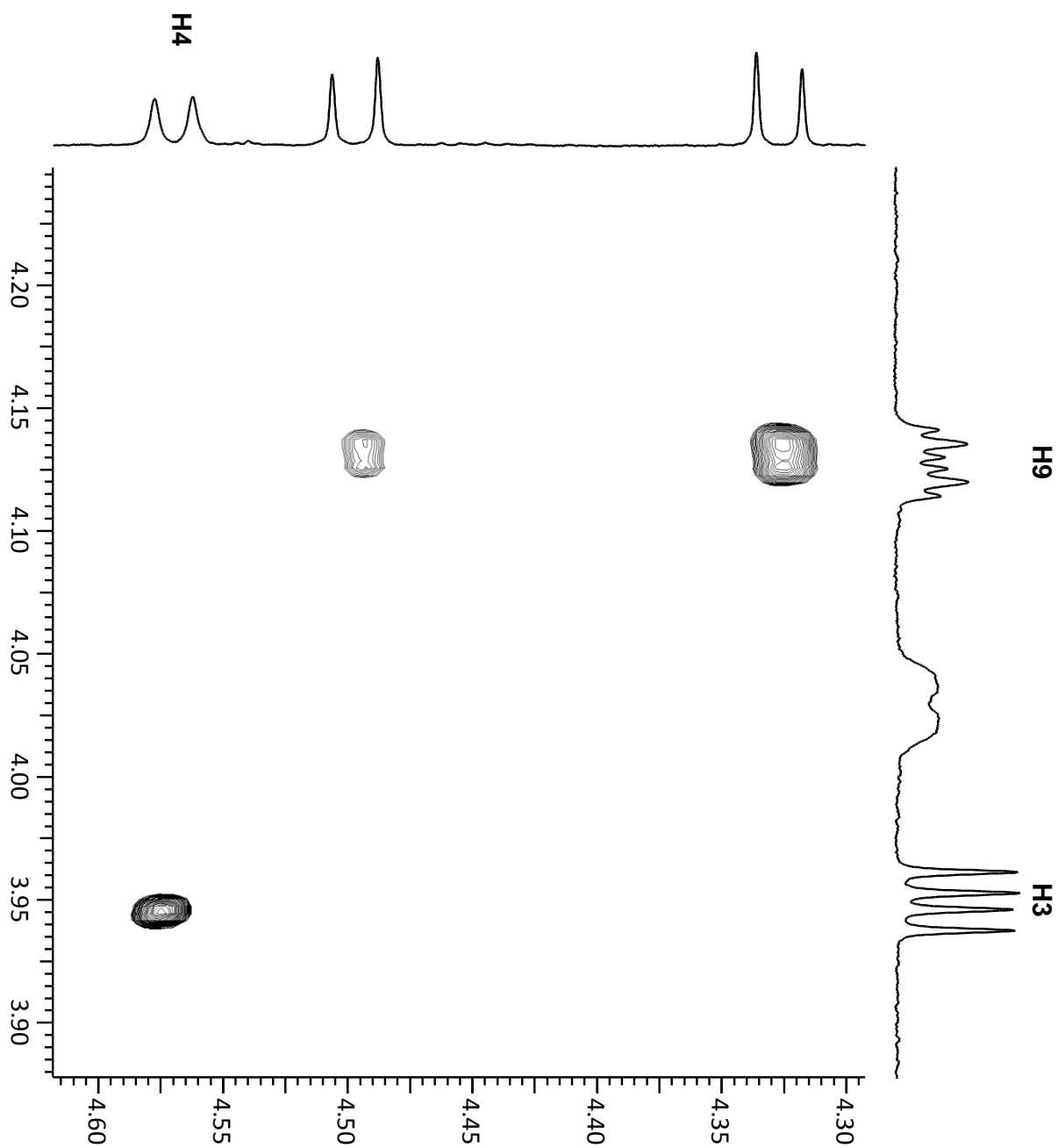
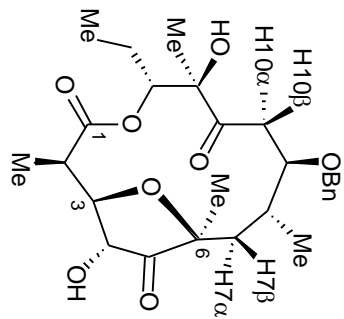


NOESY

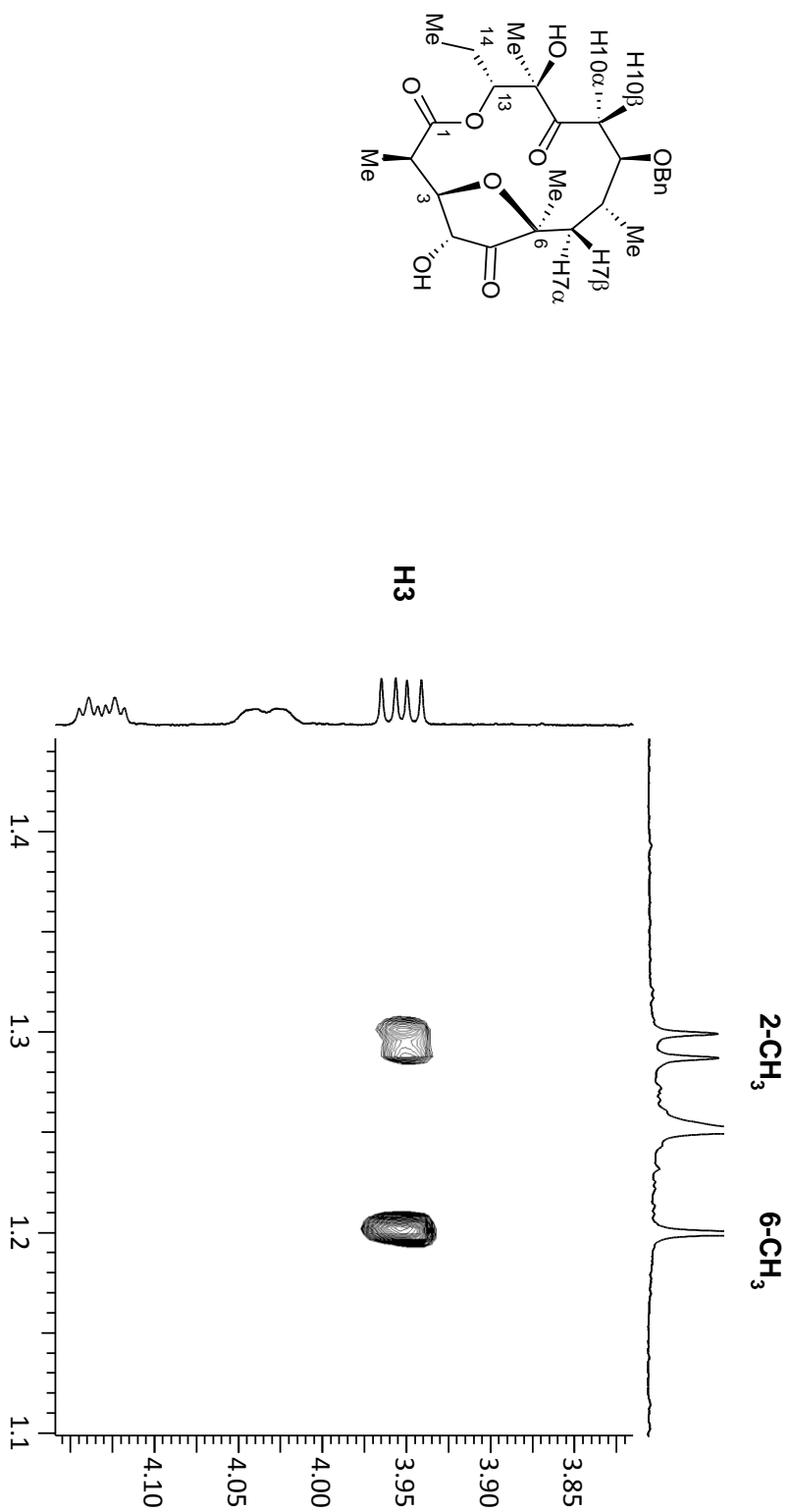


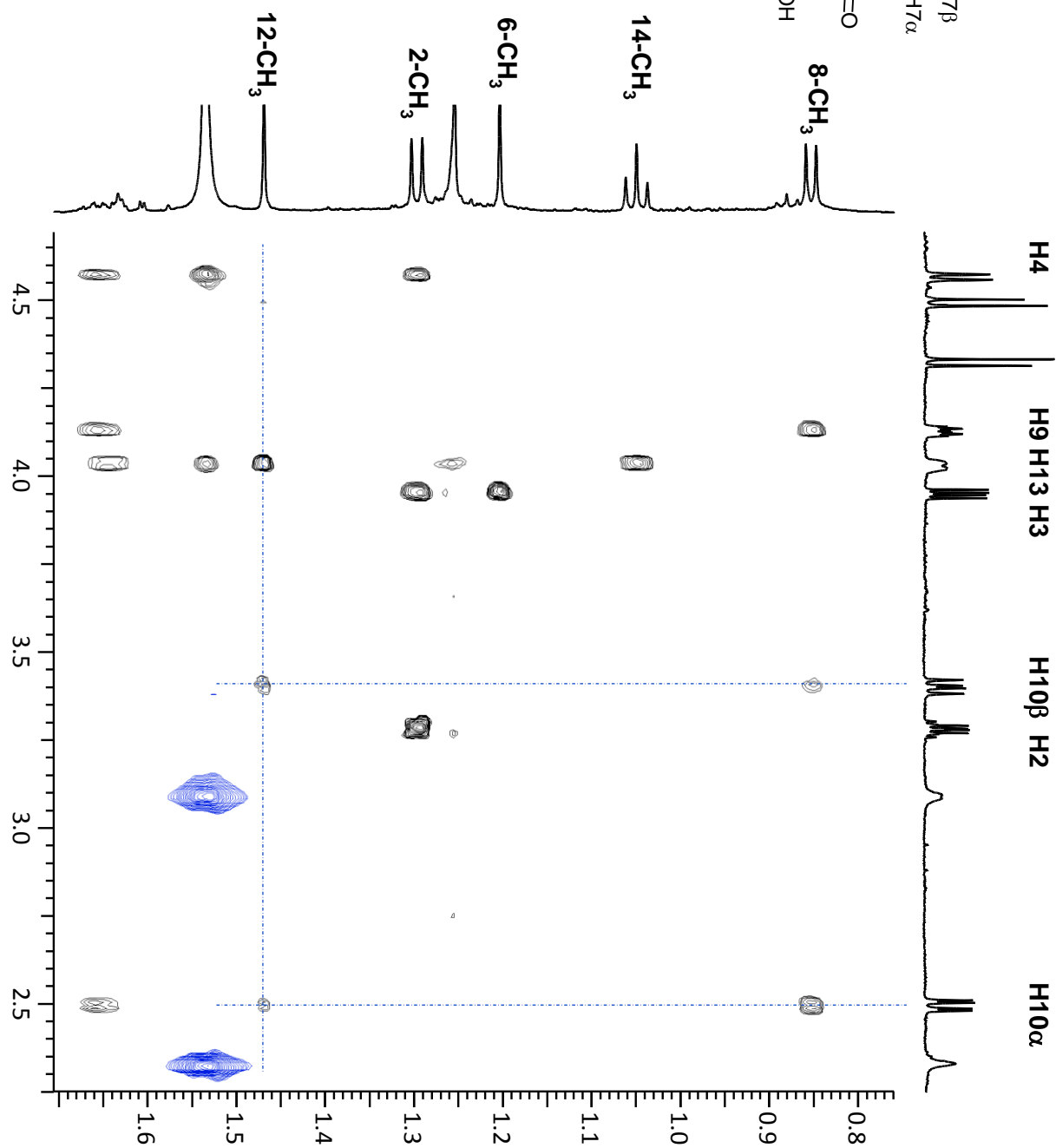
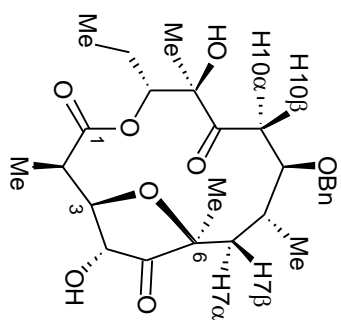
NOESY

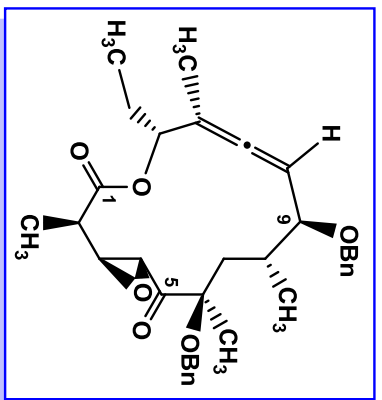


NOESY

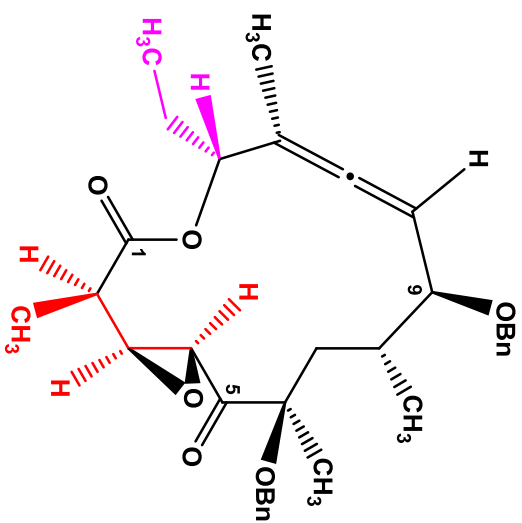
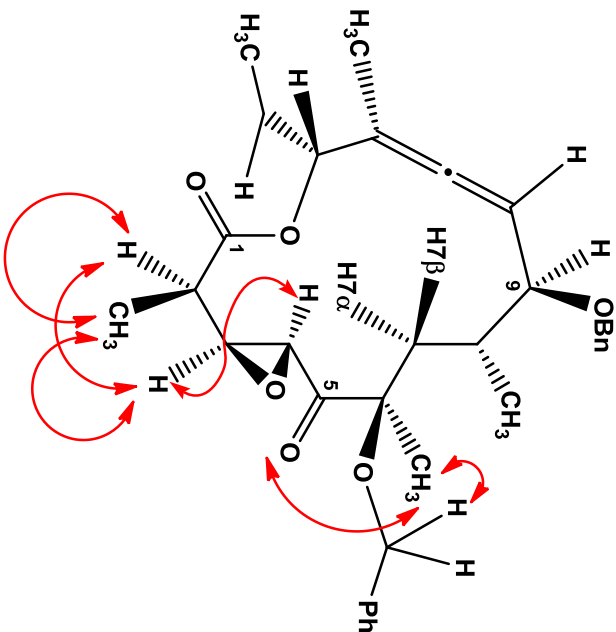
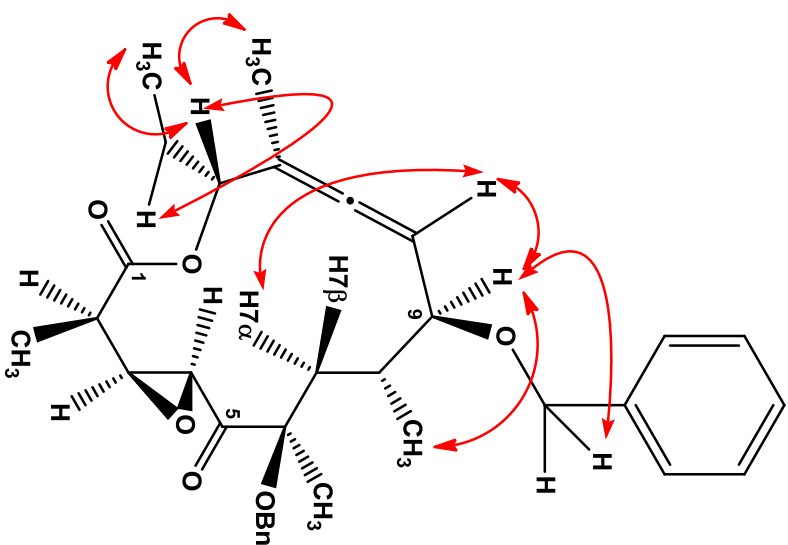
Observed NOESY cross peaks between H3 and 2-CH₃/6-CH₃



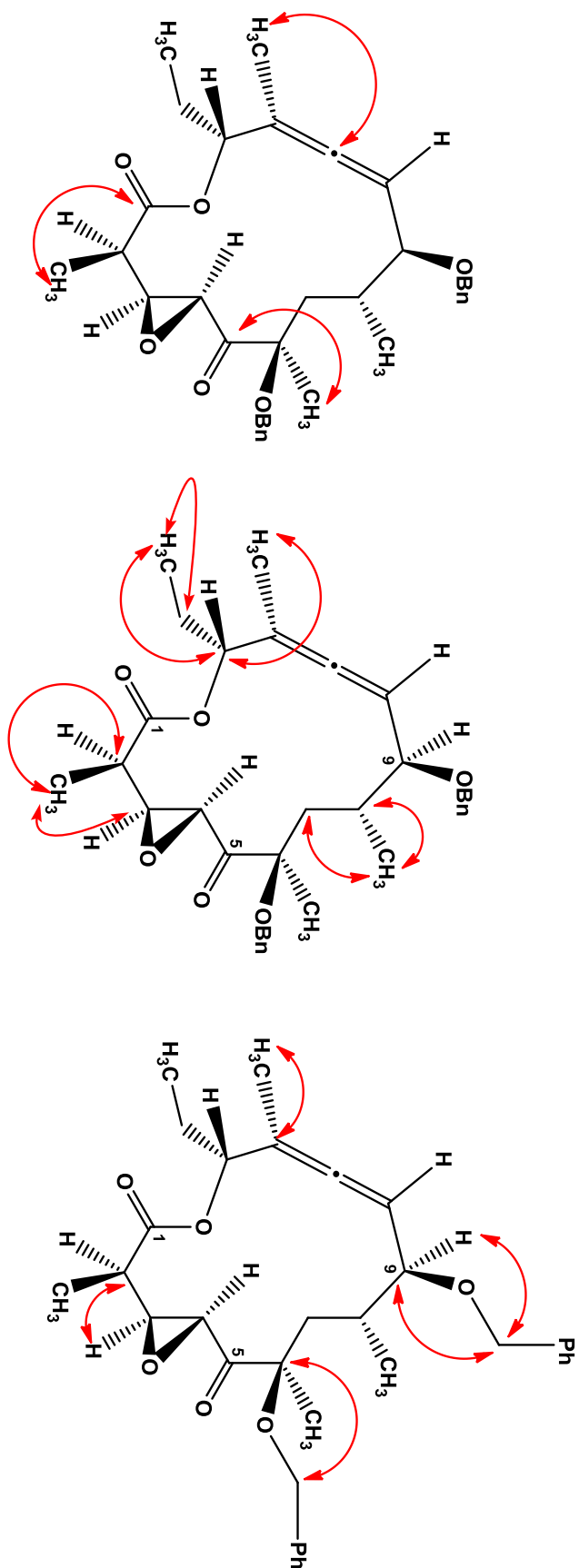
NOESY

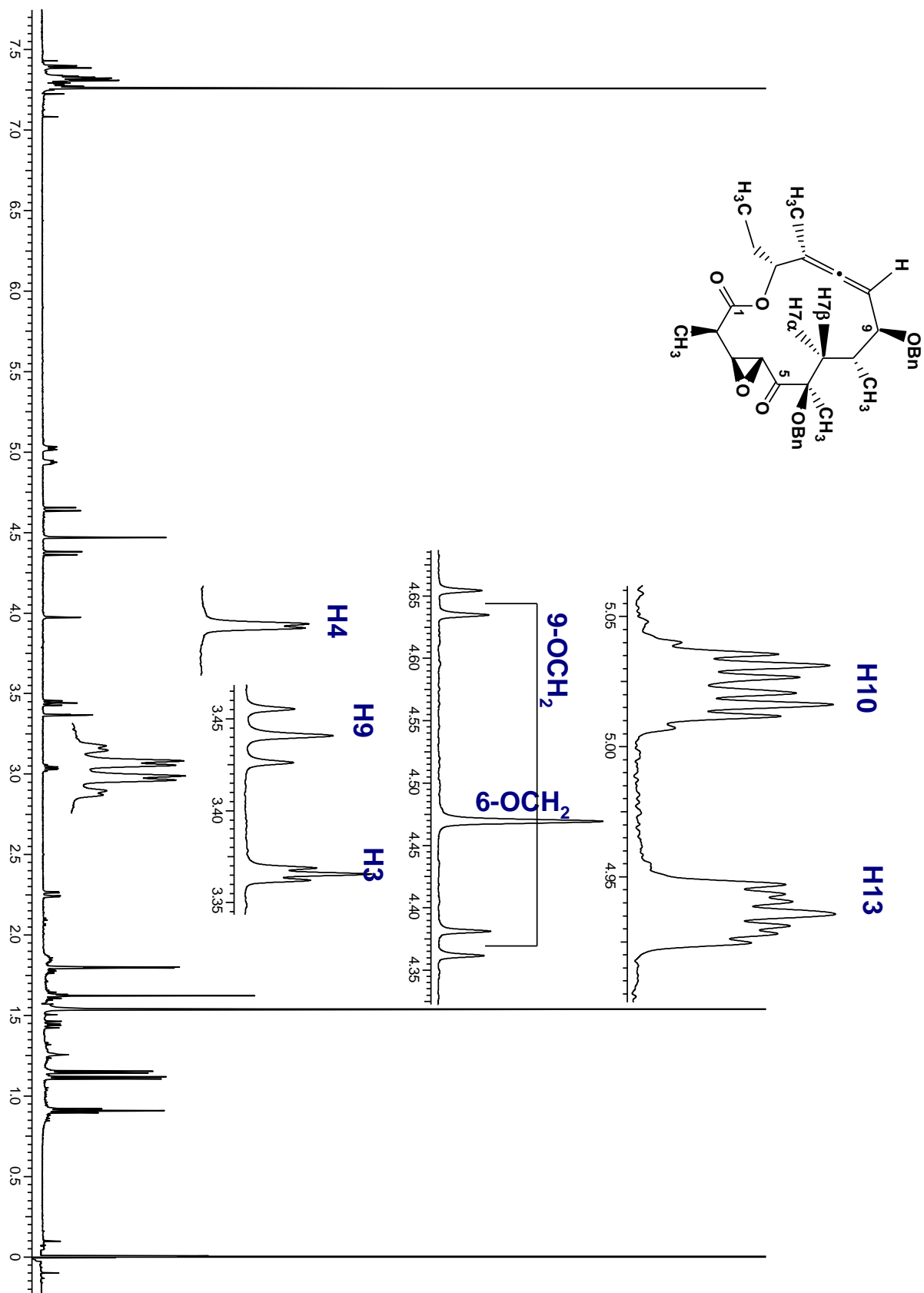


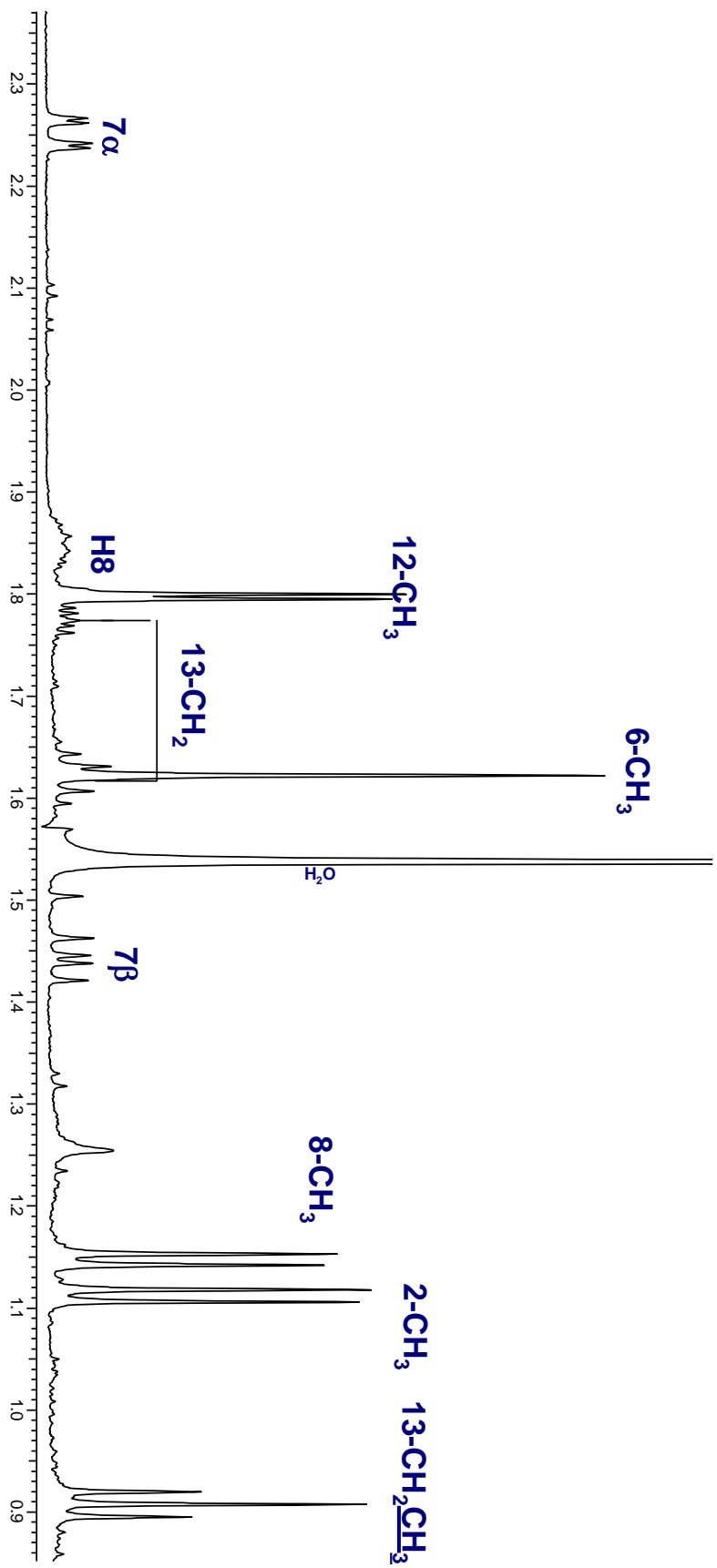
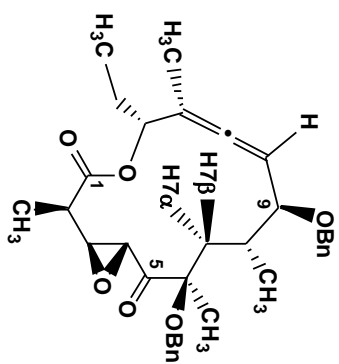
¹ H NMR chemical shifts (δ/ppm) & coupling constant (J/Hz)	¹³ C NMR chemical shift (δ/ppm)
3.03 (qd, J _{H2} , H3 = 2.1Hz, J _{H2} , 2-CH3 = 6.7Hz, H2)	170.4 ---- C1
1.10 (d, J _{2-CH3} , H2 = 7.1Hz, 2-CH3)	39.5 ---- C2
3.37 (t, J _{H3} , H2 = 2.1Hz, H3)	59.4 ---- C3
3.97 (d, J _{H4} , H3 = 1.8Hz, H4)	52.4 ---- C4
1.62 (s, 6-CH3)	206.2 ---- C5
4.47 (s, 6-OCH2)	83.8 ---- C6
1.83 (dd, J _{H7β} , H8 = 10.2 Hz, J _{H7β} , H7α = 14.9Hz, H7β)	34.7 ---- C7
2.25 (dq, J _{H7α} , H8 = 2.7Hz, J _{H7α} , H7β = 14.6Hz, H7α)	40.1 ---- C8
1.85 (m, H8)	83.8 ---- C9
1.14 (d, J _{8-CH3} , H8 = 6.5Hz, 8-CH3)	94.3 ---- C10
3.44 (t, J _{H9} , H8 = 8.8Hz, H9)	202.1 ---- C11
4.37 (d, J _{AB} = 11.7Hz, 9-OCH2)	100.8 ---- C12
4.64 (d, J _{AB} = 11.7Hz, 9-OCH2)	76.8 ---- C13
5.02 (dt, J ₁₀ , 12-CH3 = 2.6, J _{H10} , H9 = 9.1Hz, H10)	26.3 ---- C14
1.81 (d, J _{12-CH3} , H10 = 2.9Hz, 12-CH3)	11.4 ---- 2-CH3
4.94 (ddd, J _{H13} , H = ? Hz, J _{H13} , 12-CH3 = ? Hz, H13)	19.6 ---- 6-CH3
1.80 - 1.77, 1.65 - 1.58 (m, 14-CH2)	17.9 ---- 8-CH3
0.91 (t, J _{14-CH3} , 13-CH2 = 7.3Hz, 14-CH3)	17.1 ---- 12-CH3
7.48 - 7.17 (m, 10H, Ph)	9.8 ---- 14-CH3
	66.6 ---- 6-OCH3
	70.8 ---- 9-OCH3

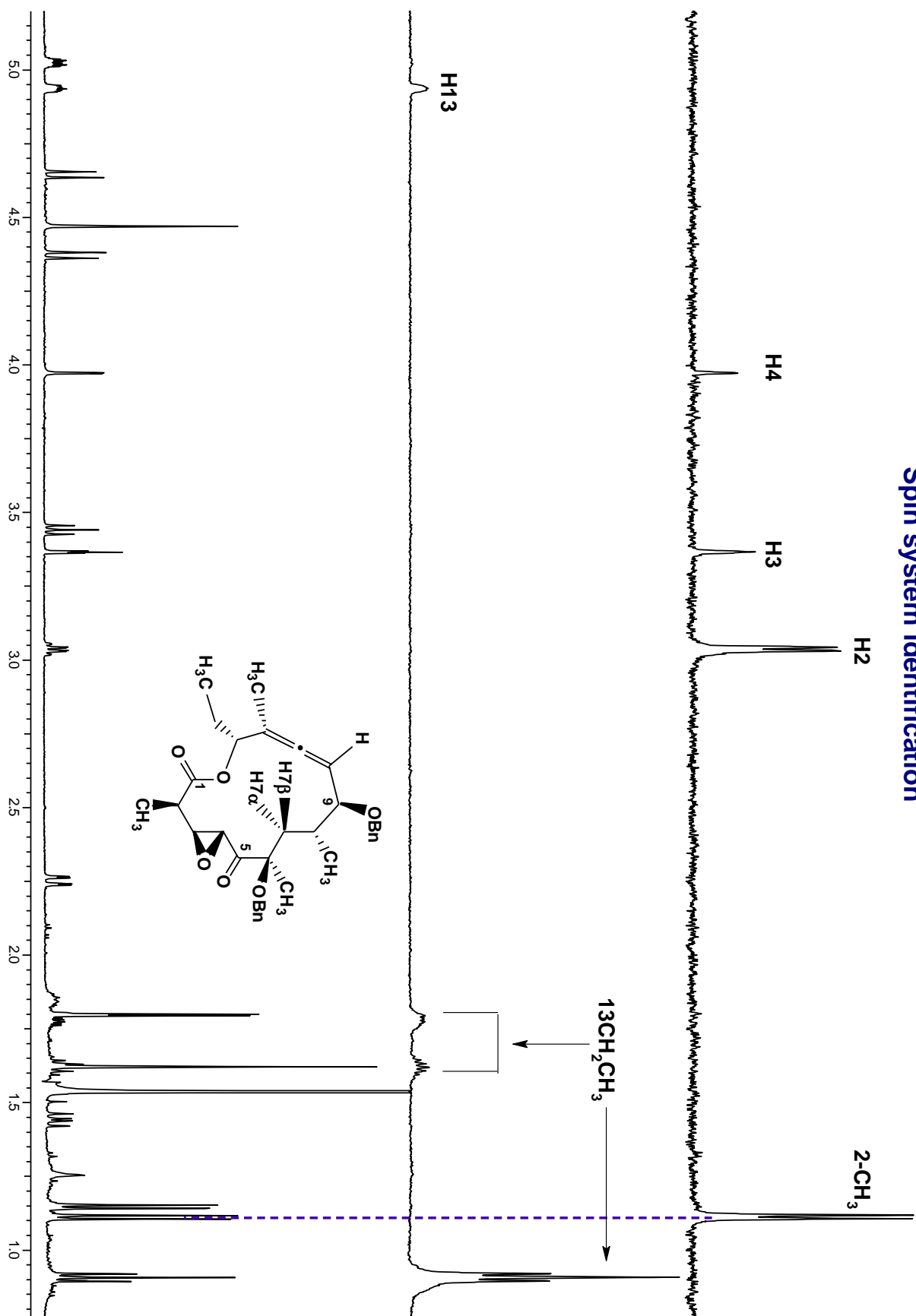
1d TOCSY**NOESY****NOESY**

HMBC

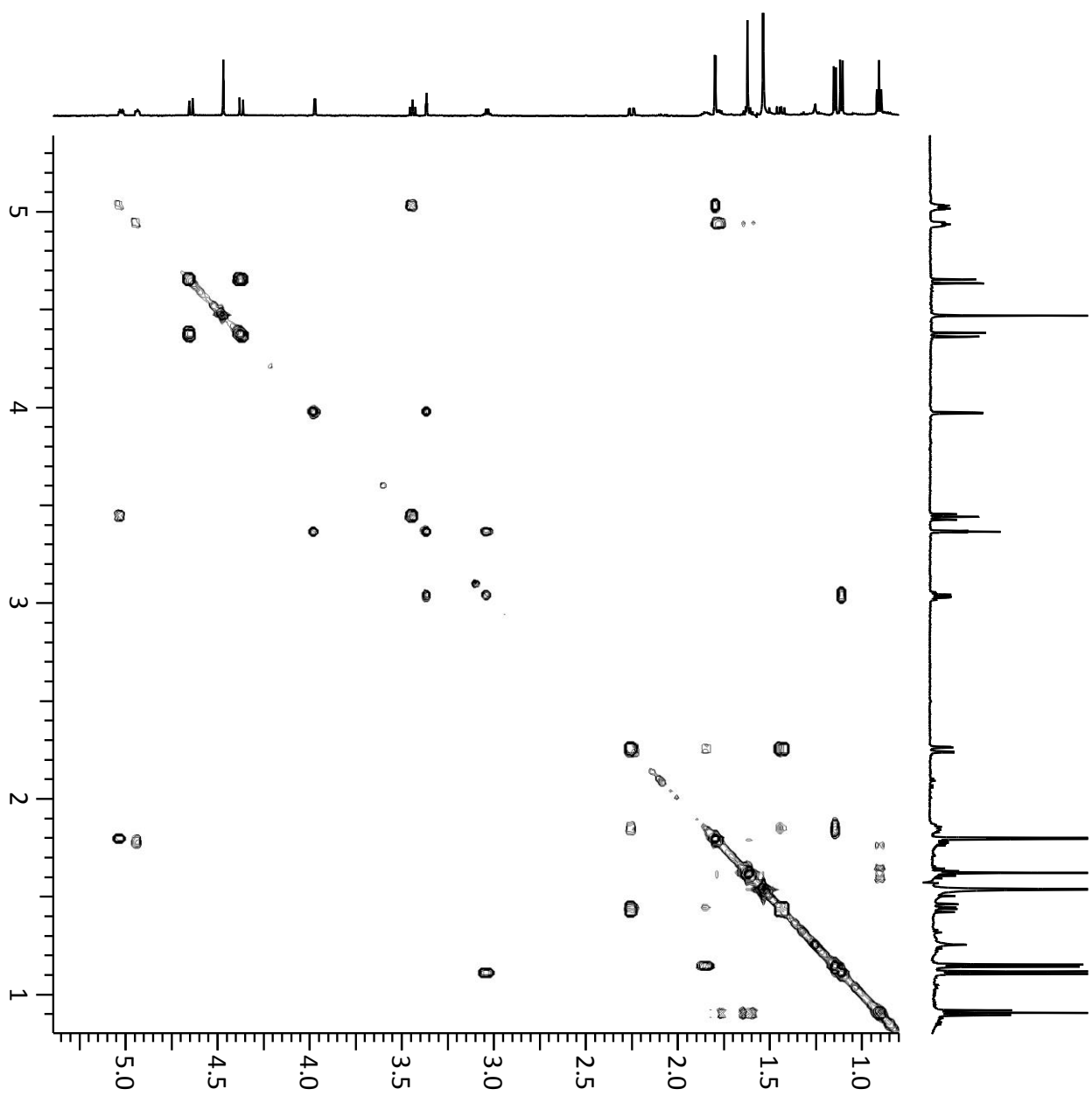




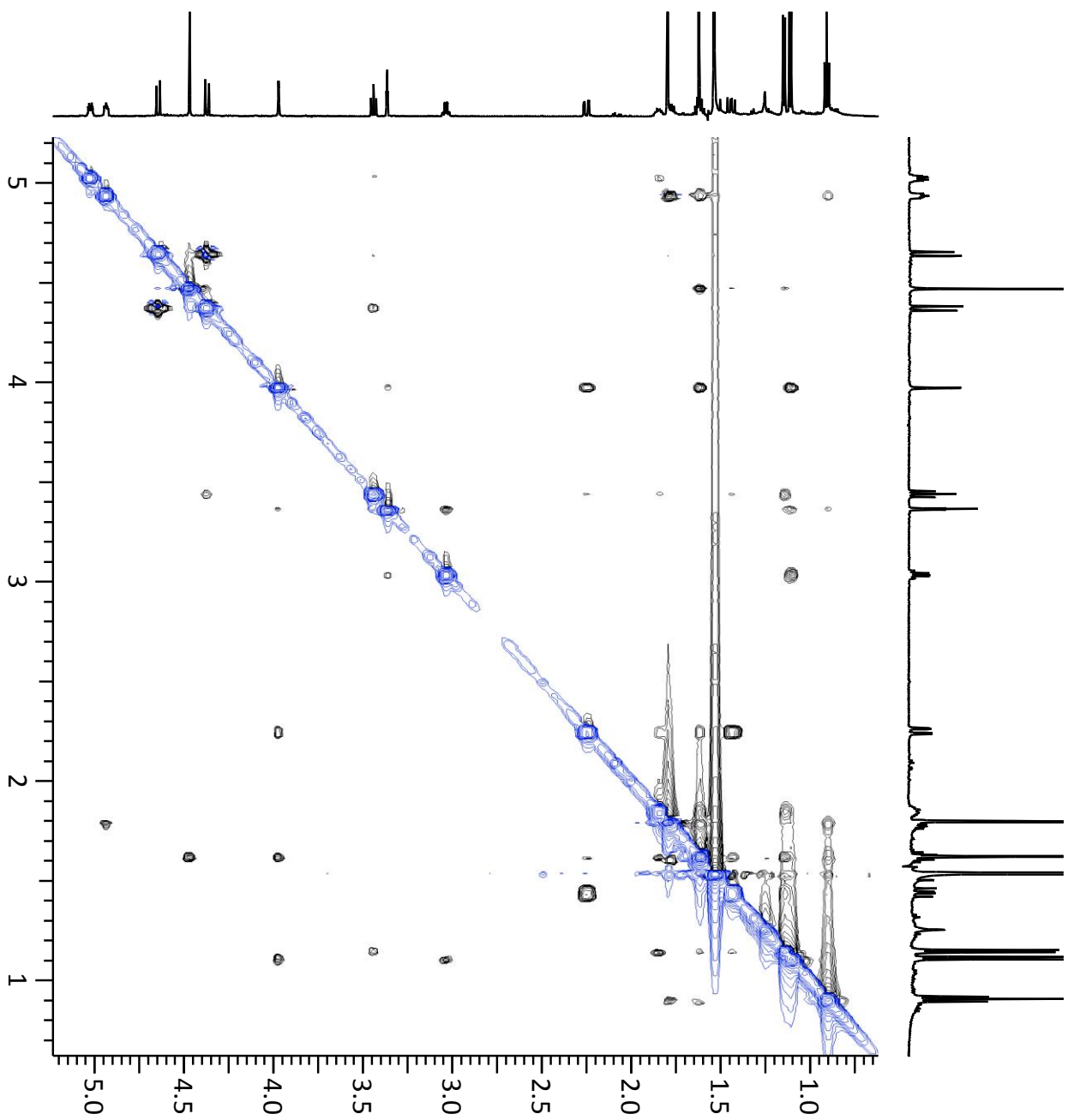




gCOSTY

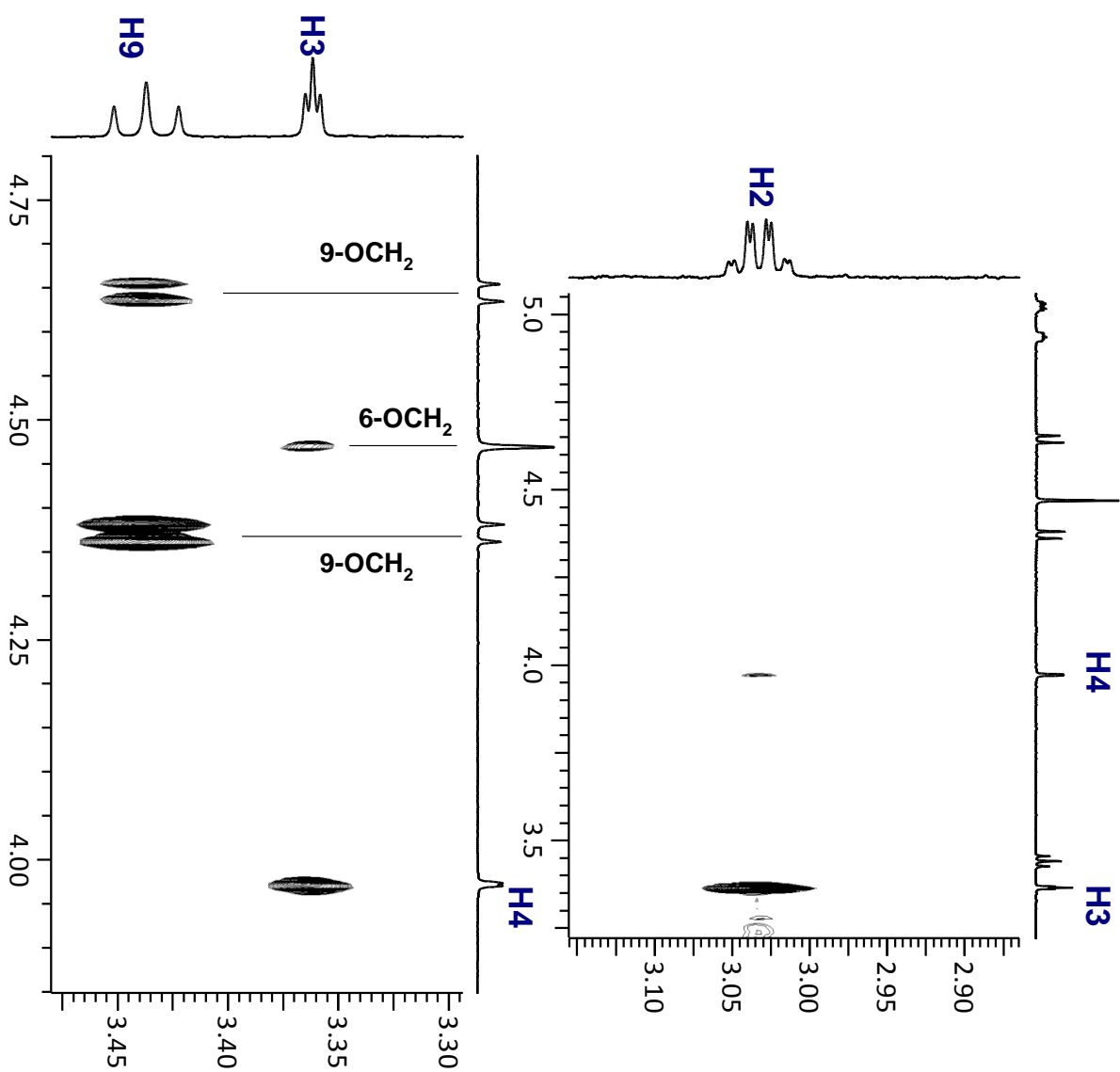
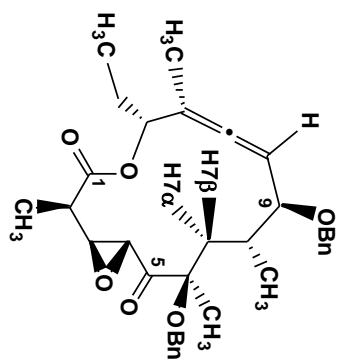


NOESY



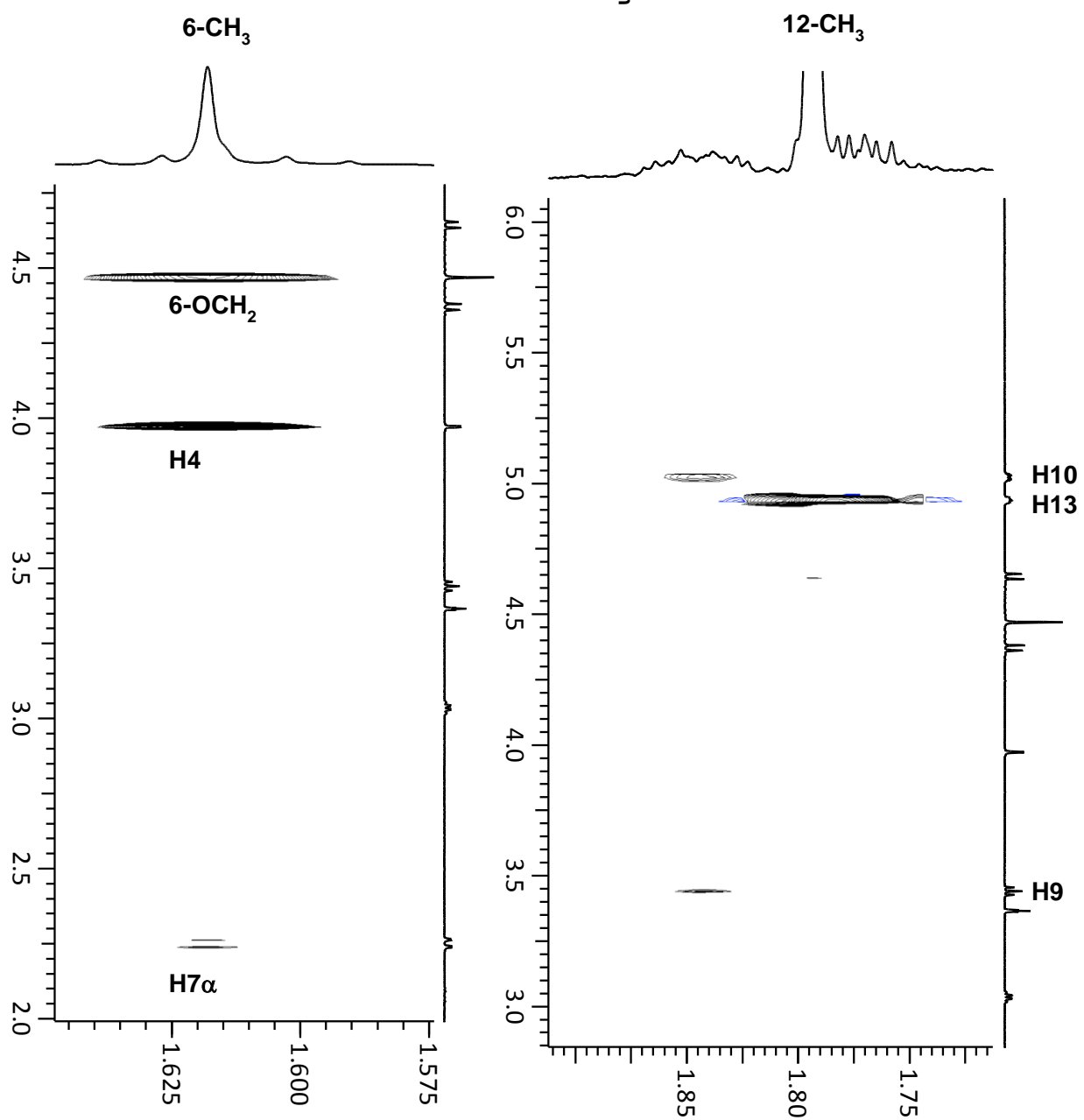
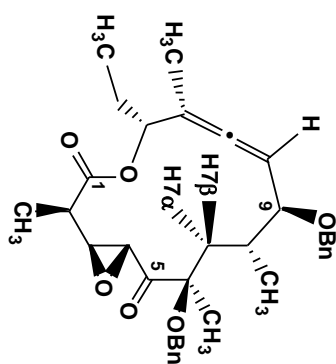
NOESY

correlations



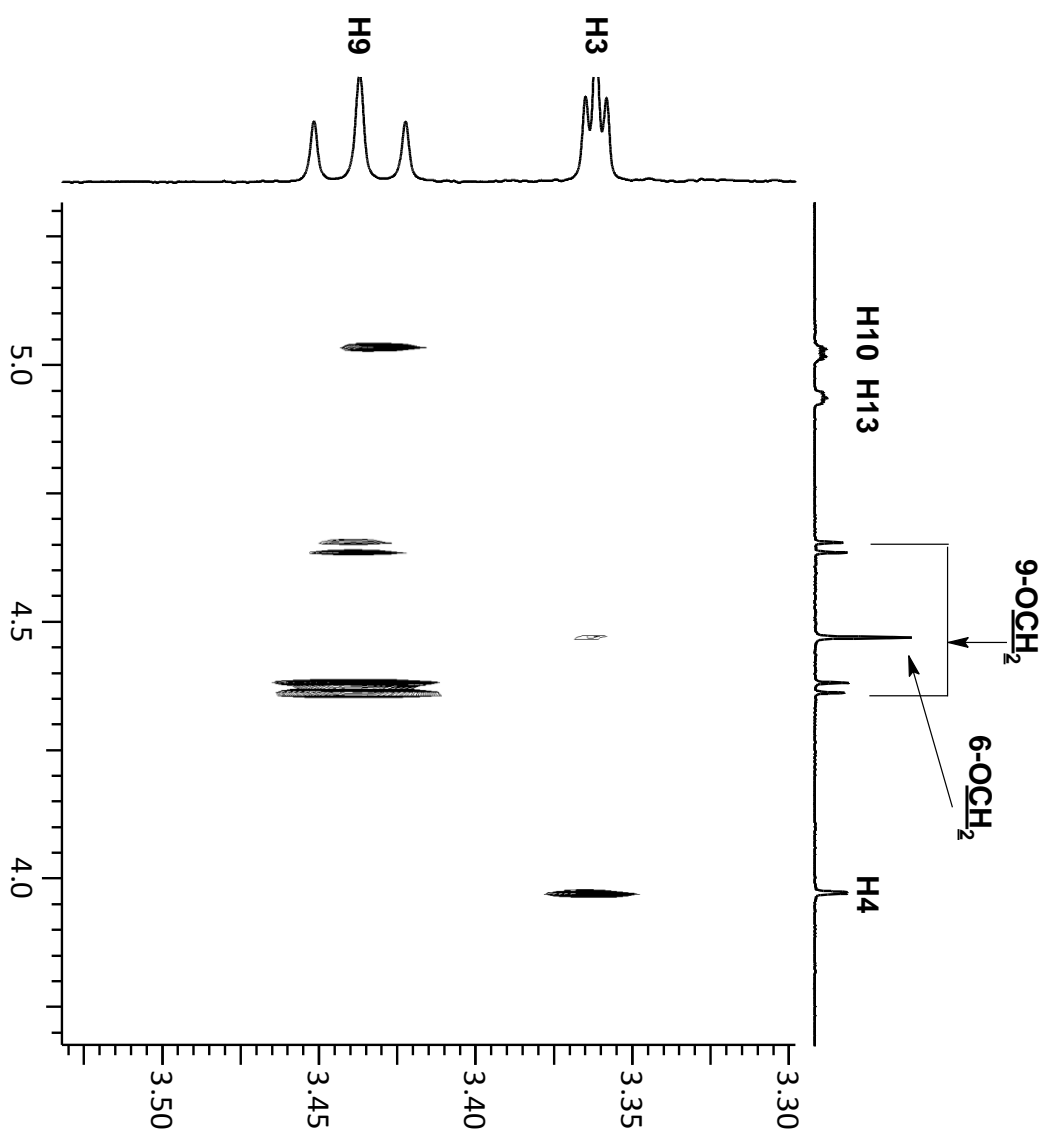
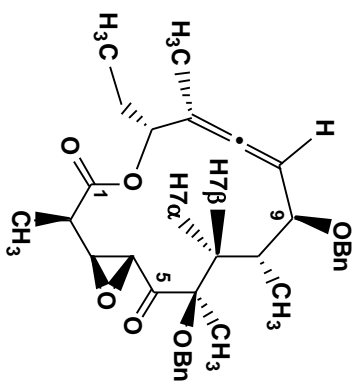
NOESY

correlations



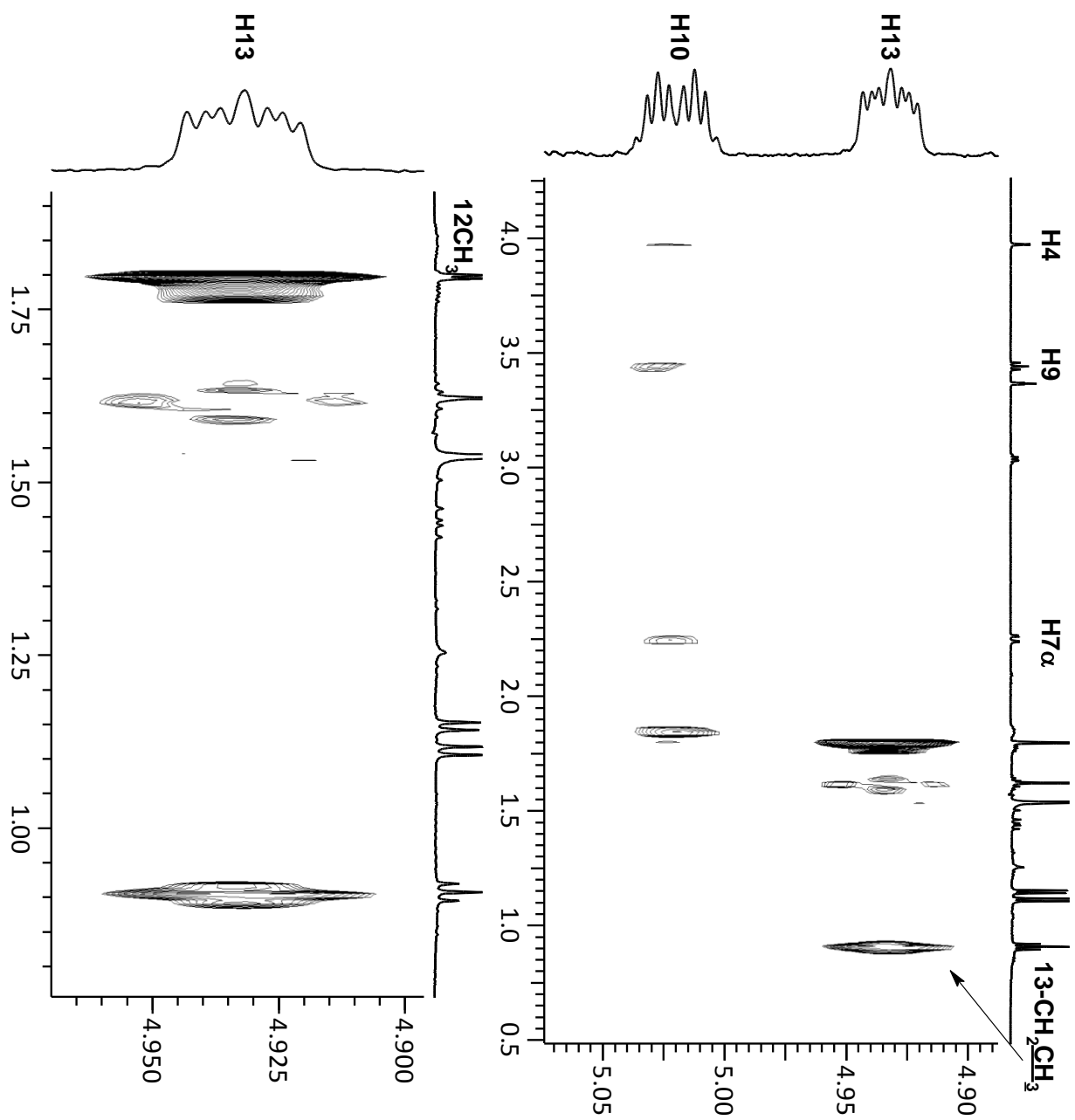
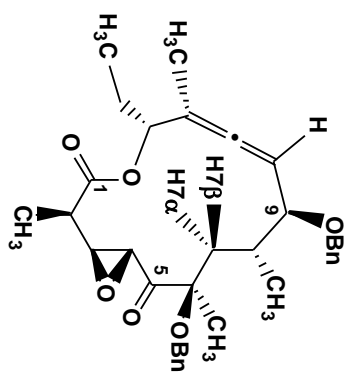
NOESY

correlations



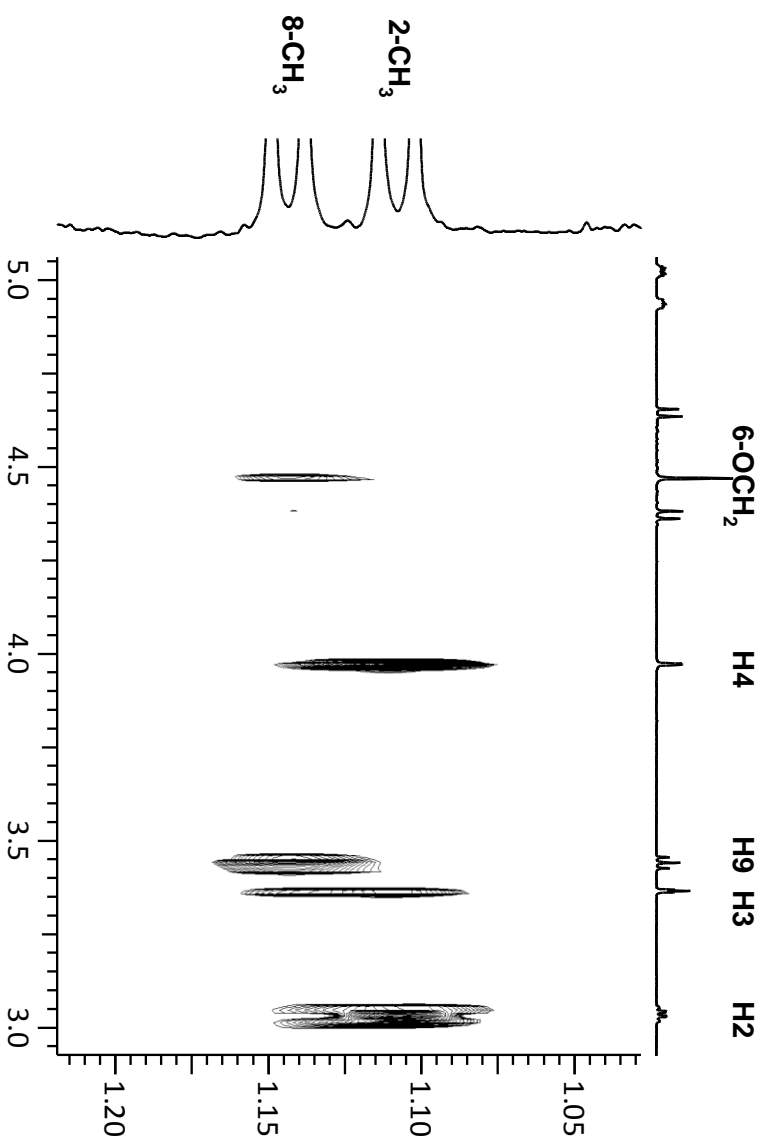
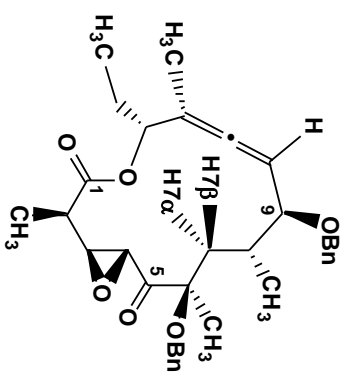
NOESY

correlations



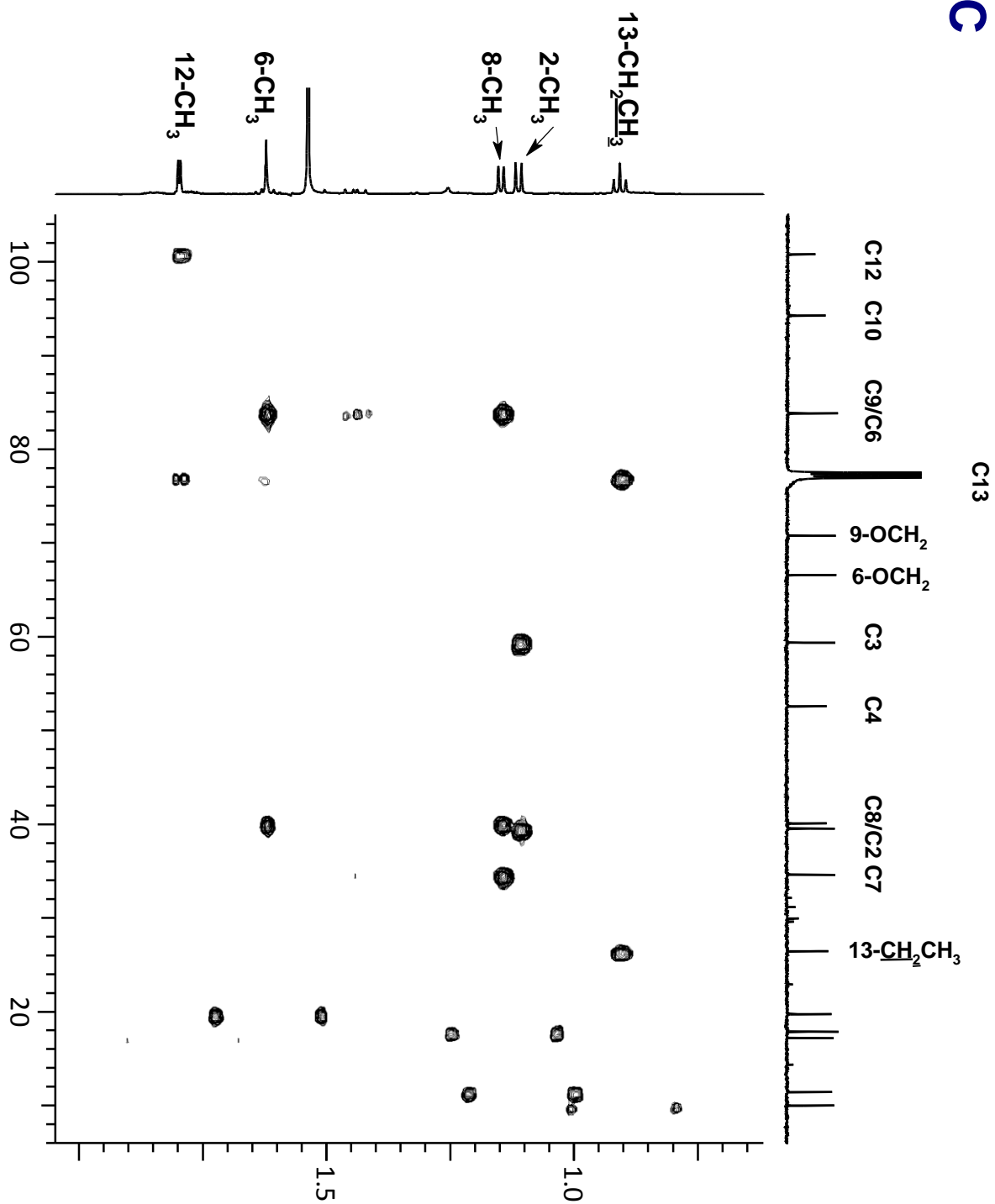
NOESY

correlations



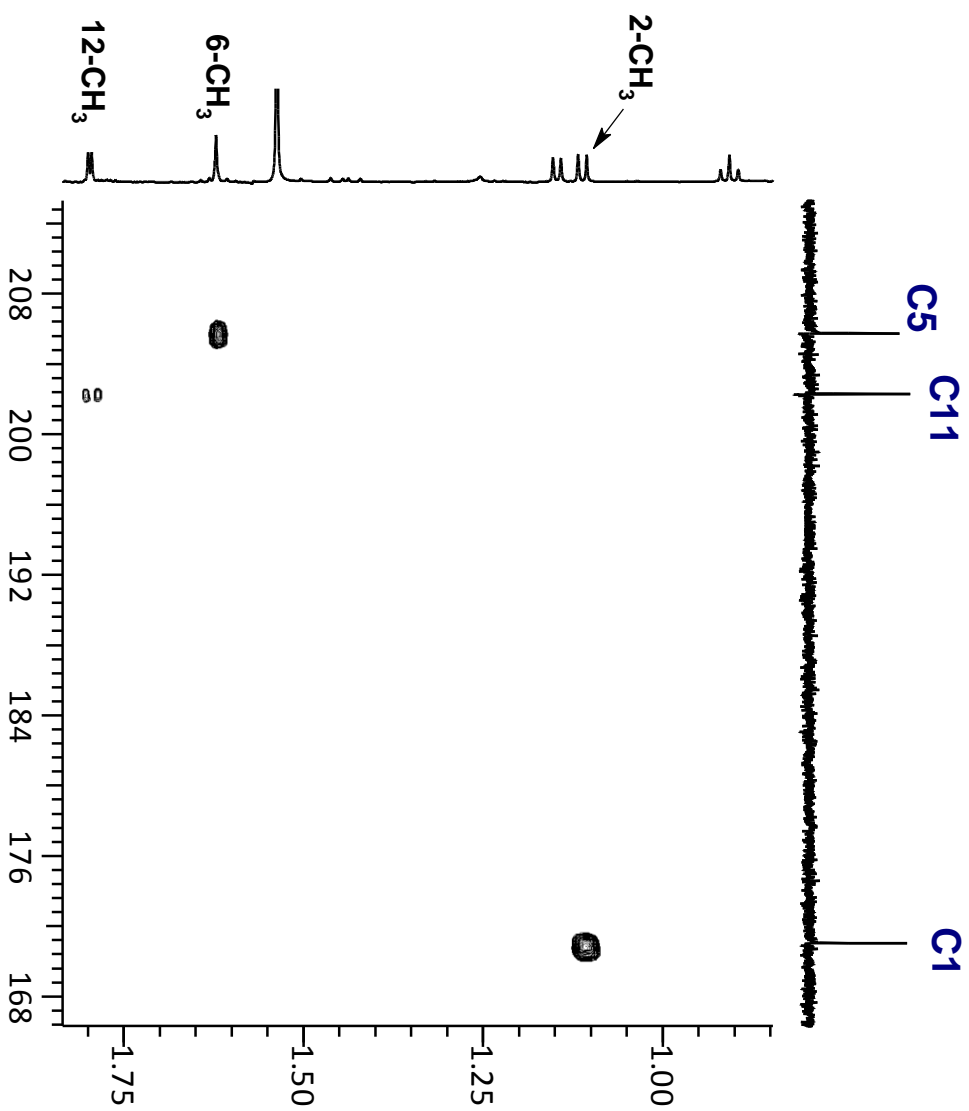
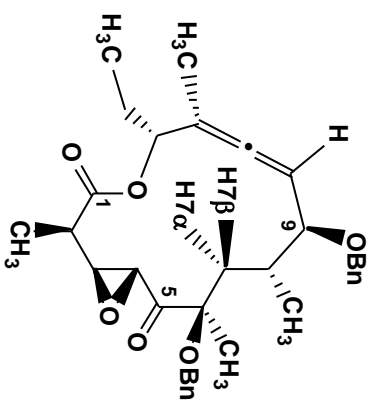
gHMBC

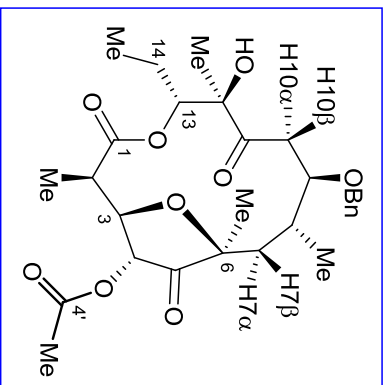
correlations



gHMBC

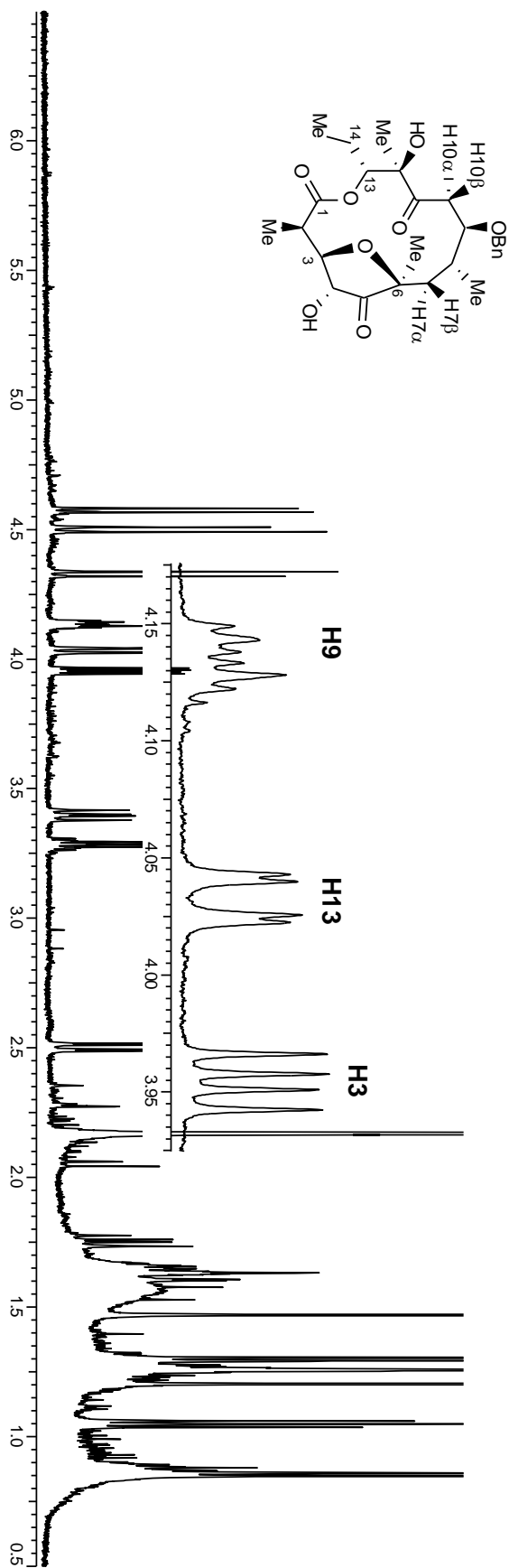
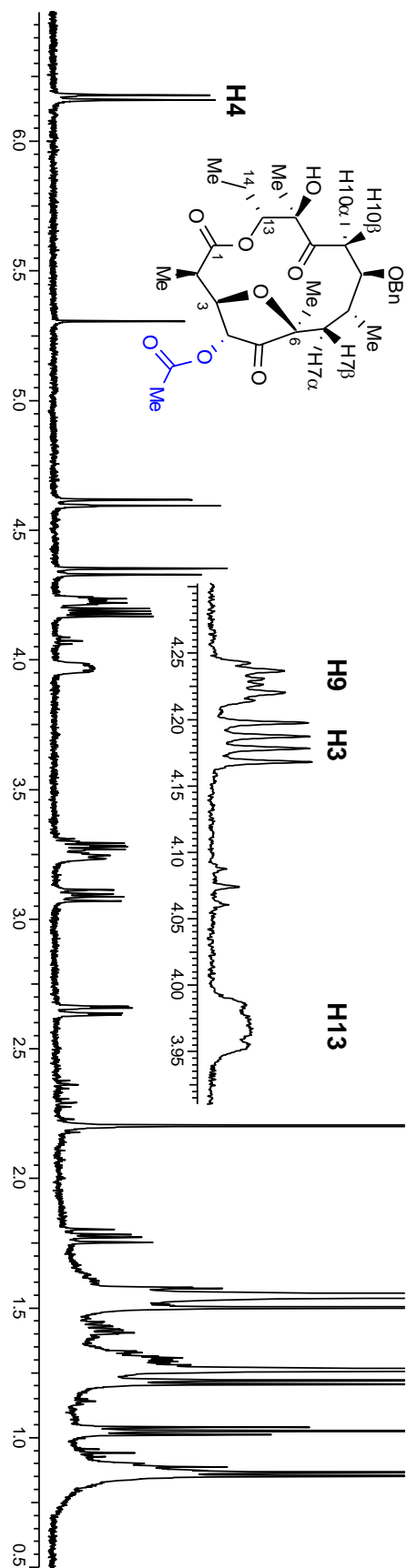
correlations

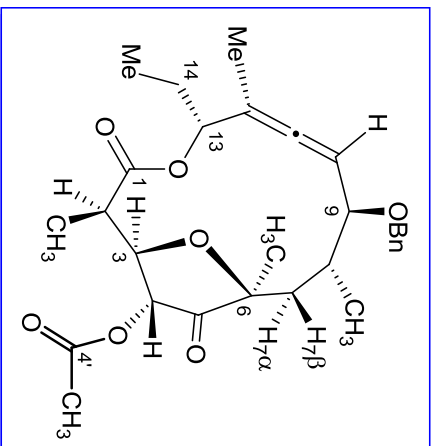




¹H NMR chemical shifts (δ/ppm)
w/ coupling constant (J/Hz)

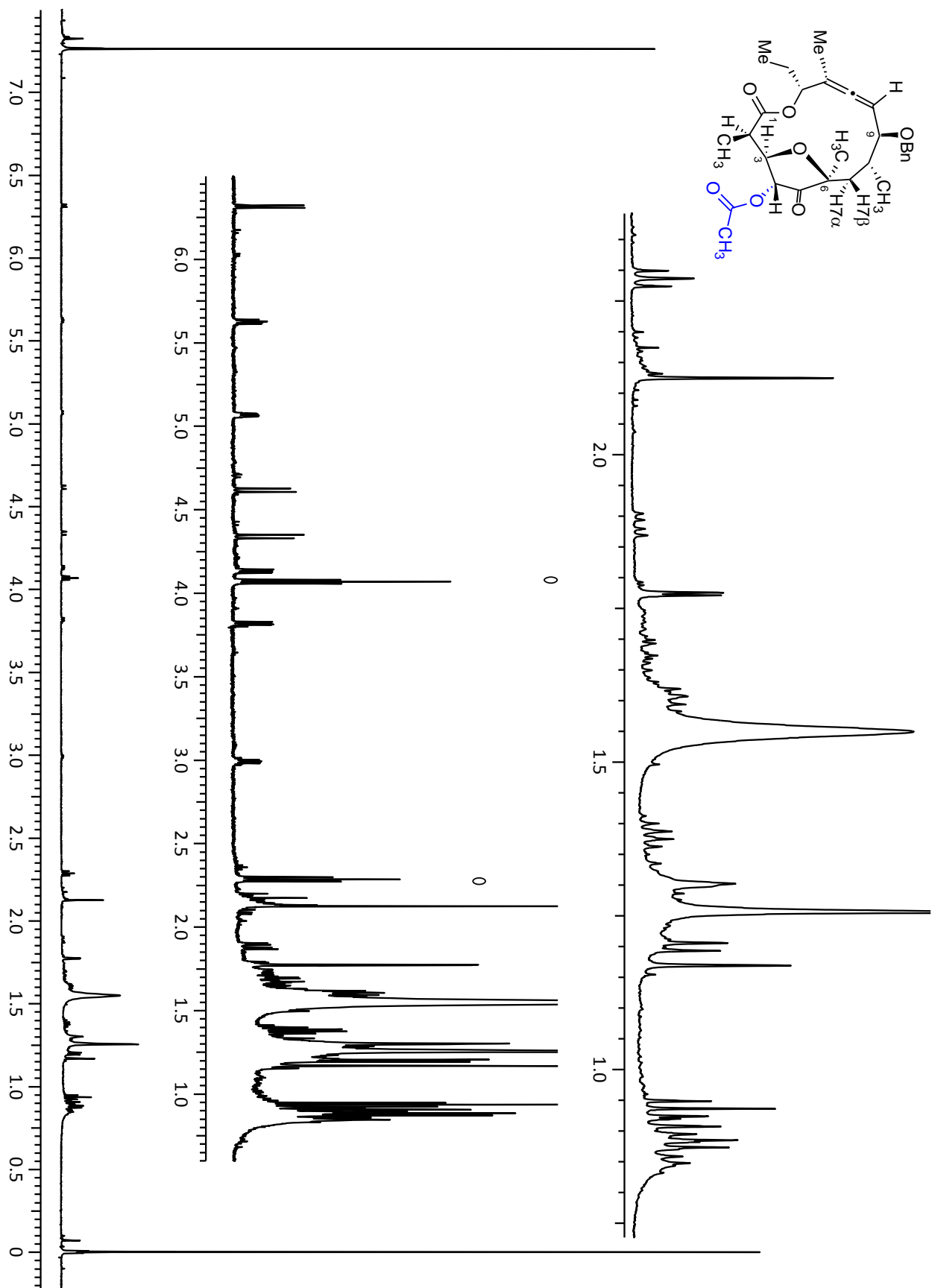
- 3.29** (dd, J_{H2, H3} = 5.1Hz, J_{H2, 2-CH3} = 7.3Hz, **H2**)
1.20 (d, J_{2-CH3, H2} = 7.3Hz, **2-CH₃**)
4.18 (dd, J_{H3, H2} = 5.1Hz, J_{H3, H4} = 9.6Hz, **H3**)
6.18 (d, J_{H4, H3} = 9.5Hz, **H4**)
2.20 (s, **4'-CH₃**)
1.26 (s, **6-CH₃**)
1.54 (dd, J_{H7β, H8} = 2.2Hz, J_{H7β, H7α} = 15.2Hz, **H7β**)
1.75 (dd, J_{H7α, H8} = 9.9Hz, J_{H7α, H7β} = 15.2Hz, **H7α**)
1.52 (m, **H8**)
0.85 (d, J_{8-CH3, H8} = 6.8Hz, **8-CH₃**)
4.23 (dt, J_{H9, H10α} = 3.2Hz, J_{H9, H10β} = 8.3Hz, **H9**)
4.33, 4.59 (d, J_{AB} = 11.5Hz, **9-OCH₂**)
2.63 (dd, J_{H10α, H9} = 3.2Hz, J_{H10α, H10β} = 13.5Hz, **H10α**)
3.07 (dd, J_{H10β, H9} = 8.3Hz, J_{H10β, H10α} = 13.5Hz, **H10β**)
1.60 (s, **12-CH₃**)
3.96 (dd, J_{H13, H14} = 2.1, 10.0Hz, **H13**)
1.45 - 1.29 (m, **14-CH₂**)
1.02 (t, J_{14-CH3, H14} = 7.1Hz, **14-CH₃**)





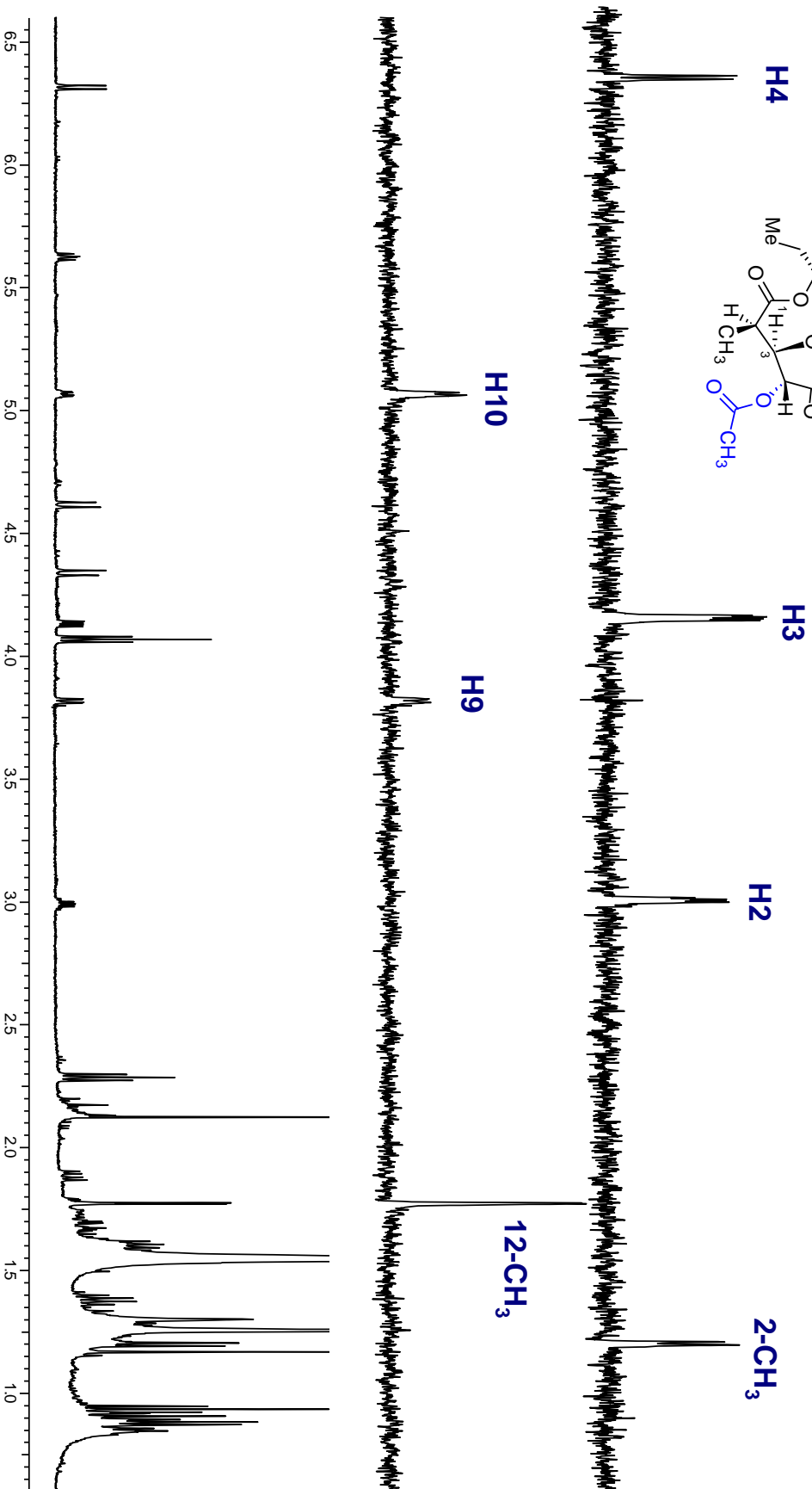
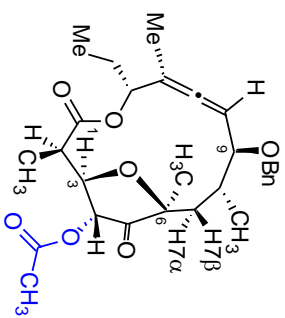
¹H NMR chemical shifts (δ/ppm) & coupling constant (J/Hz)

- 3.00** (dd, $J_{H_2, H_3} = 2.2\text{Hz}$, $J_{H_2, 2\text{-CH}_3} = 8.3\text{Hz}$, **H2**)
1.21 (d, $J_{2\text{-CH}_3, H_2} = 7.4\text{Hz}$, **2-CH₃**)
4.13 (dd, $J_{H_3, H_2} = 4.2\text{Hz}$, $J_{H_3, H_4} = 8.6\text{Hz}$, **H3**)
6.31 (d, $J_{H_4, H_3} = 8.6\text{Hz}$, **H4**)
2.13 (s, **4'-CH₃**)
1.17 (s, **6-CH₃**)
1.65 (m, **H7β**)
1.85 (m, **H7α**)
1.70 (m, **H8**)
0.88 (d, $J_{8\text{-CH}_3, H_8} = 7.1\text{Hz}$, **8-CH₃**)
4.07 (dd, $J_{H_9, H_8} = 6.6\text{Hz}$, $J_{H_9, H_{10}} = 2.0\text{Hz}$, **H9**)
4.61, 4.33 (d, $J_{AB} = 11.7\text{Hz}$, **9-OCH₂**)
5.08 - 5.05 (m, **H10**)
1.77 (d, $J = 2.7\text{Hz}$, **12-CH₃**)
5.63 (t, $J_{H_{13}, H_{14}} = 9.0\text{Hz}$, **H13**)
1.70 - 1.60 (m, **14-CH₂**)
0.93 (t, $J_{14\text{-CH}_3, H_{14}} = 7.3\text{Hz}$, **14-CH₃**)



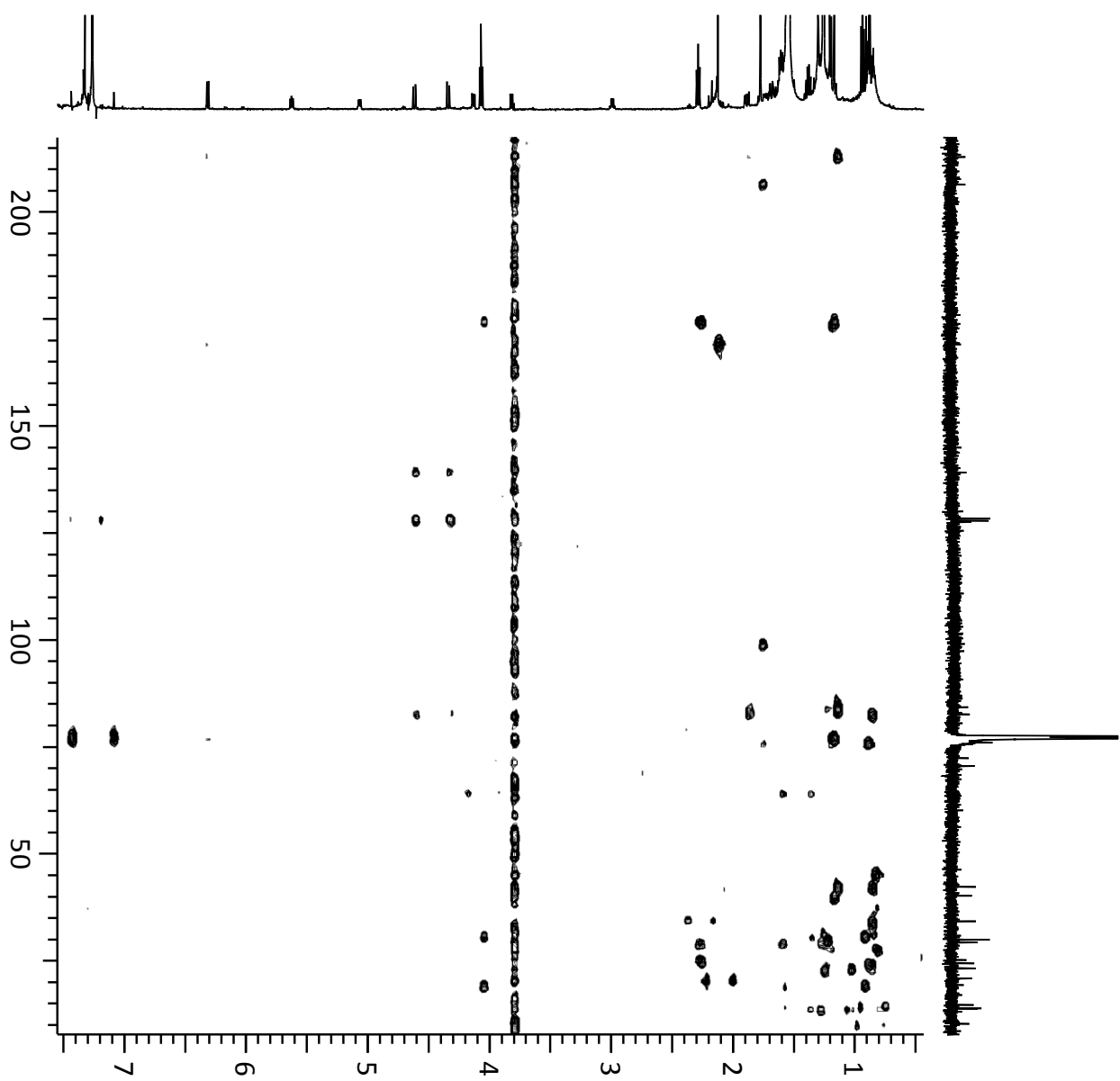
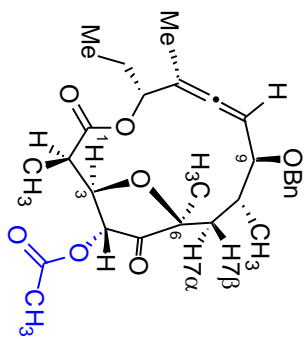
spin systems

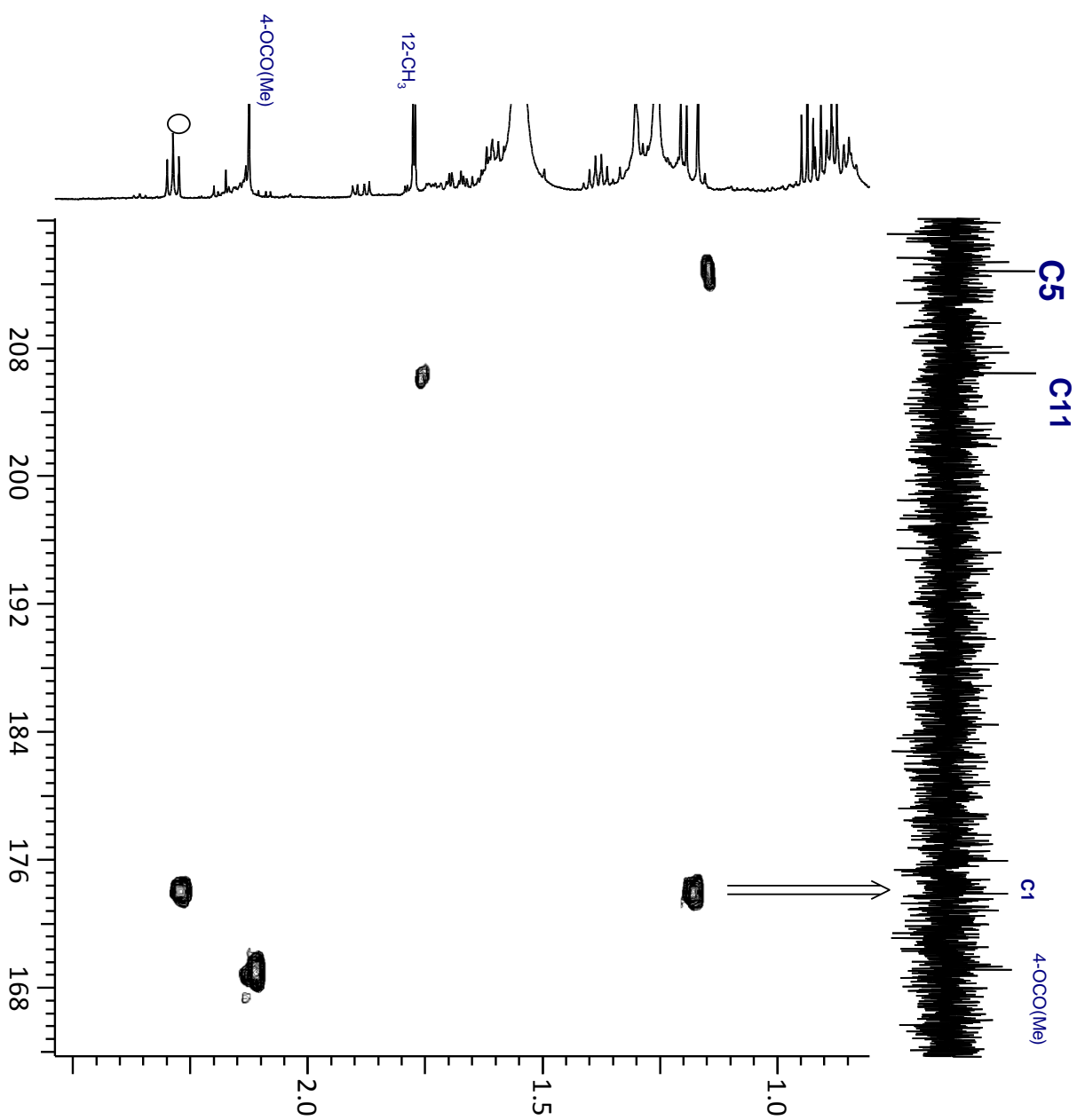
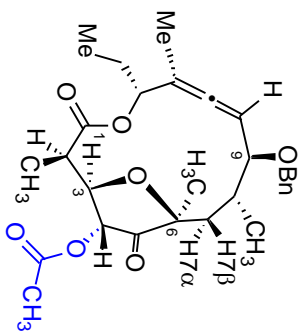
identification



HMBC

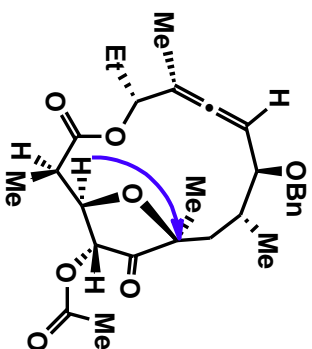
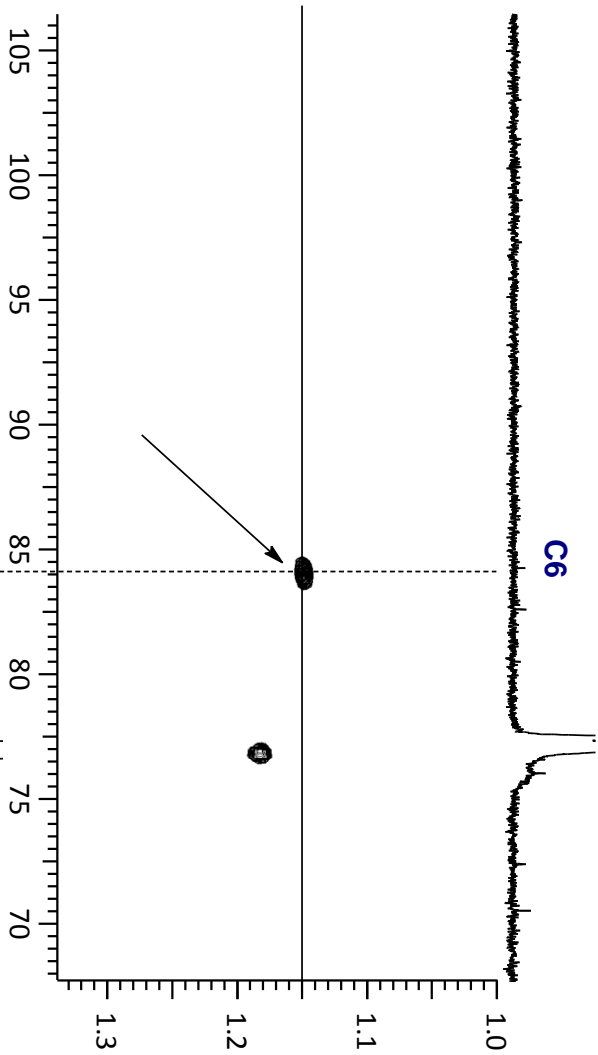
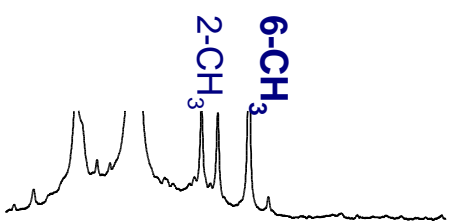
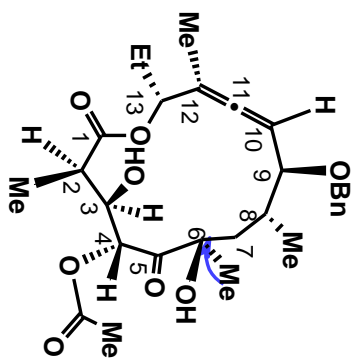
correlations



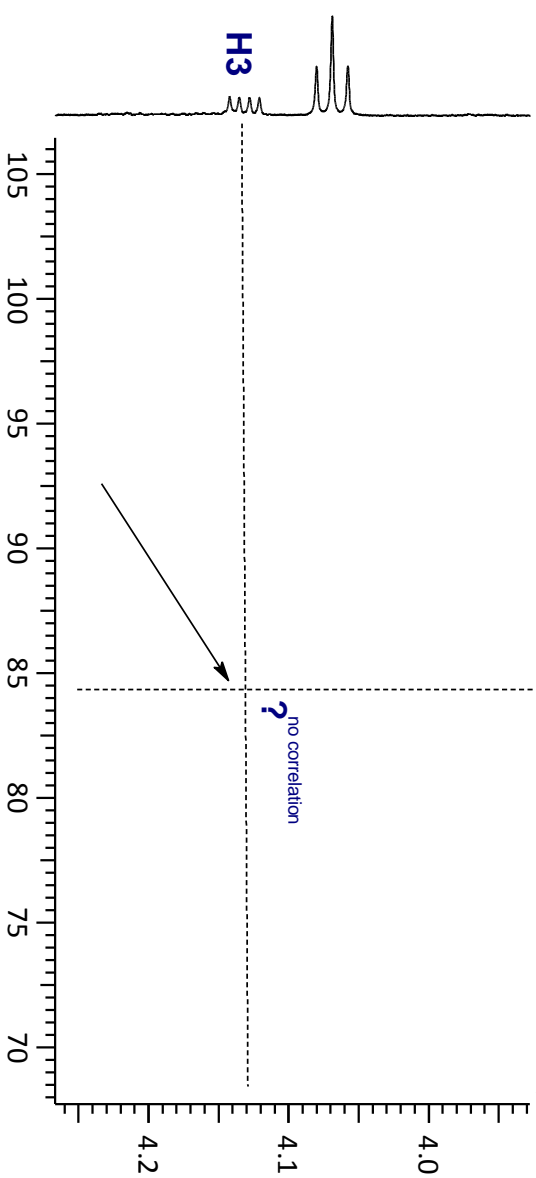


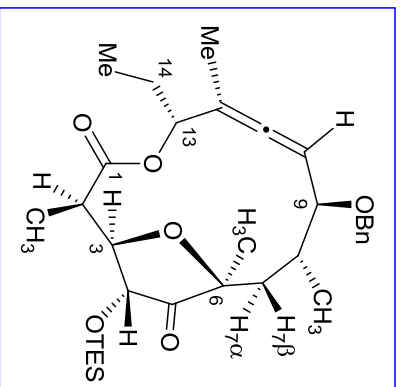
HMBC

correlations



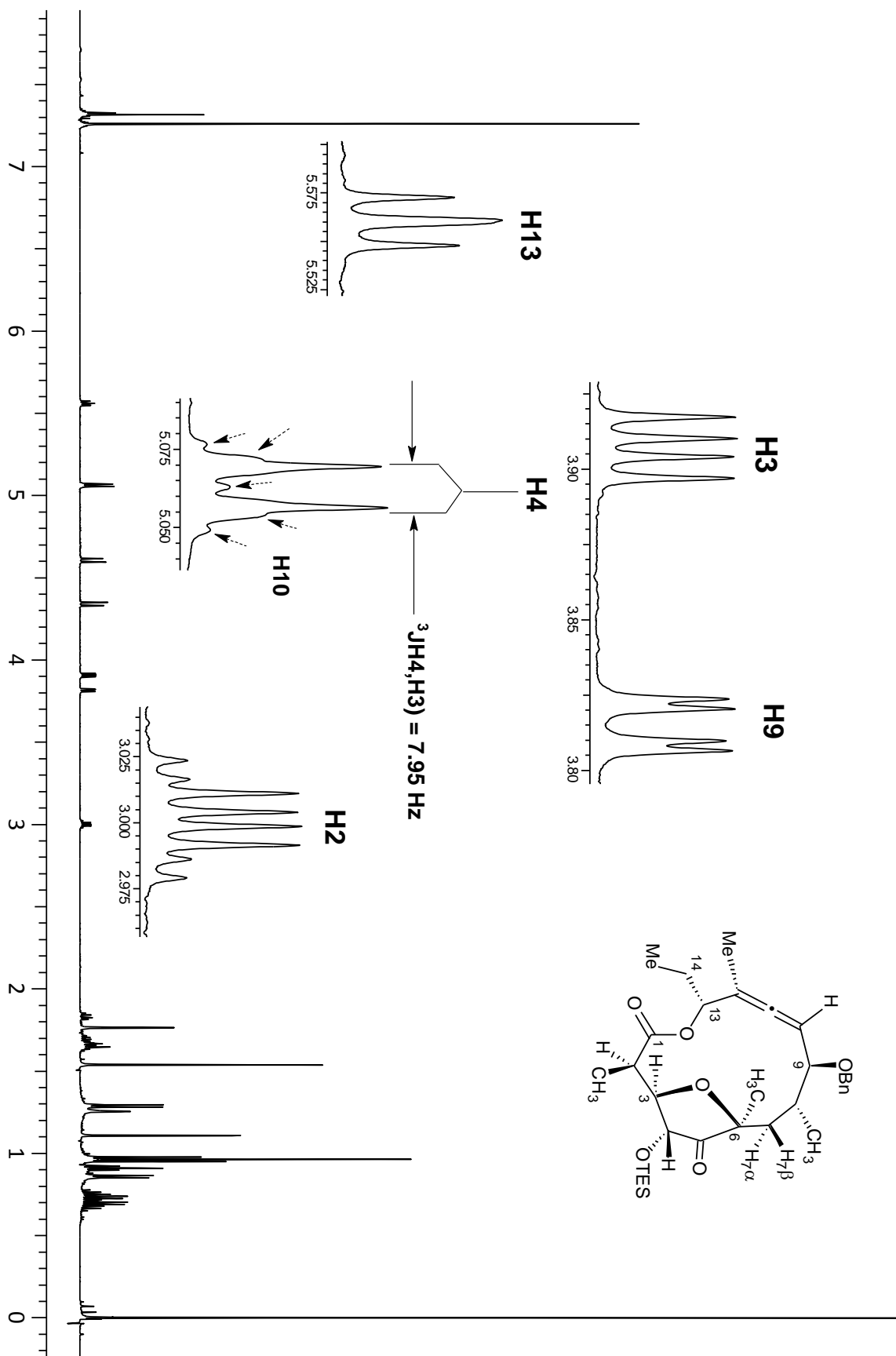
Expected correlation

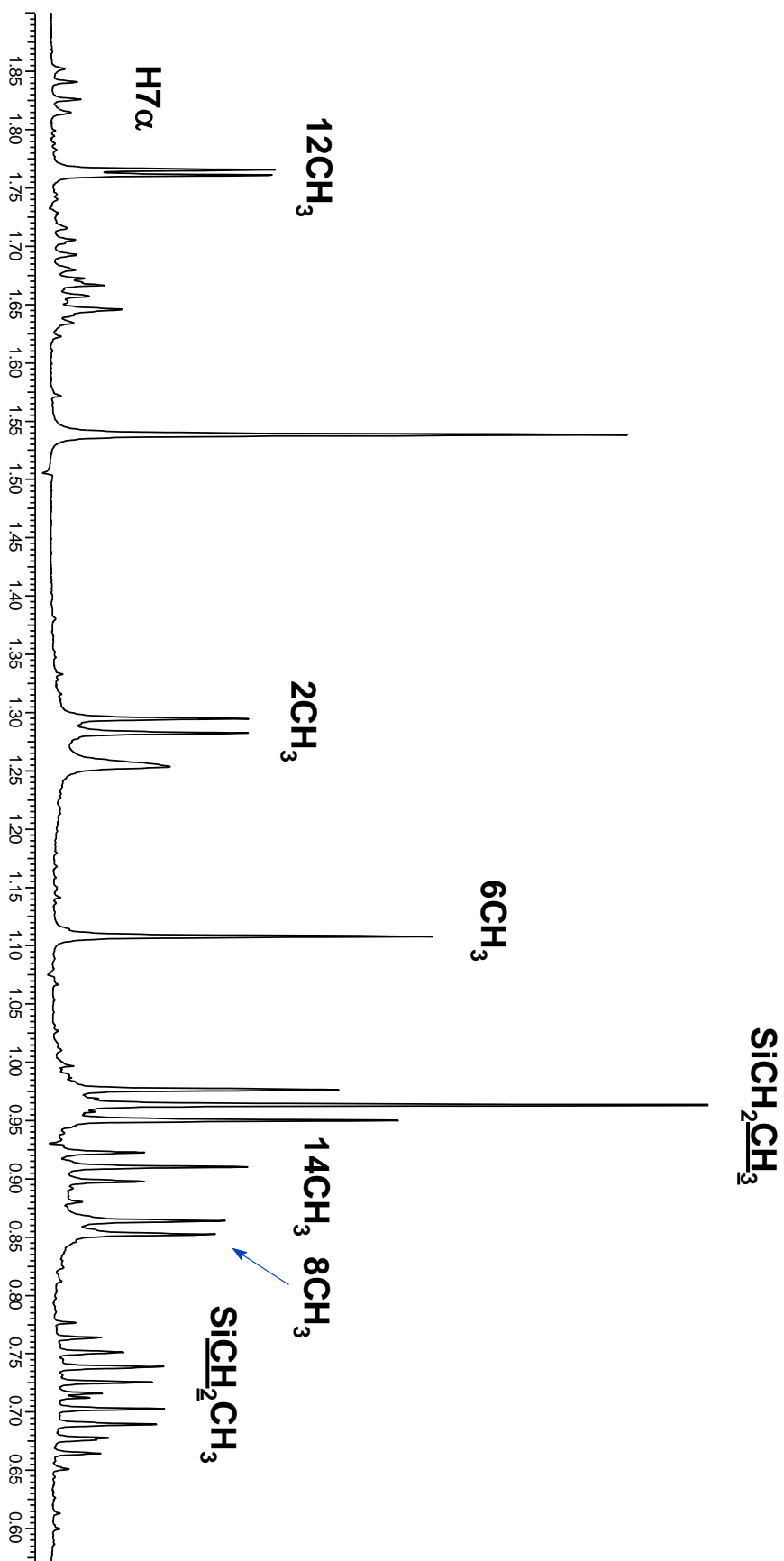




¹H NMR chemical shifts (δ/ppm) & coupling constant (J/Hz)	
3.00 (dd, J _{H2, H3} = 4.2Hz, J _{H2, 2-CH3} = 7.3Hz, H2)	
1.30 (d, J _{2-CH3, H2} = 7.3Hz, 2-CH₃)	
3.90 (dd, J _{H3, H2} = 4.2Hz, J _{H3, H4} = 8.0Hz, H3)	
5.07 (d, J _{H4, H3} = 8.0Hz, H4)	
1.10 (s, 6-CH₃)	
1.65 (m, H7β)	
1.85 (m, H7α)	
1.70 (m, H8)	
0.85 (d, J _{8-CH3, H8} = 7.0Hz, 8-CH₃)	
3.83 (dd, J _{H9, H8} = 8.3Hz, J _{H9, H10} = 2.0Hz, H9)	
4.60, 4.35 (d, J _{AB} = 12.0Hz, 9-OCH₂)	
5.07 - 5.05 (m, H10)	
1.75 (d, J = 2.9Hz, 12-CH₃)	
5.55 (t, J _{H13, H14} = 8.1Hz, H13)	
1.70 - 1.60 (m, 14-CH₂)	
0.90 (t, J _{14-CH3, H14} = 7.6Hz, 14-CH₃)	

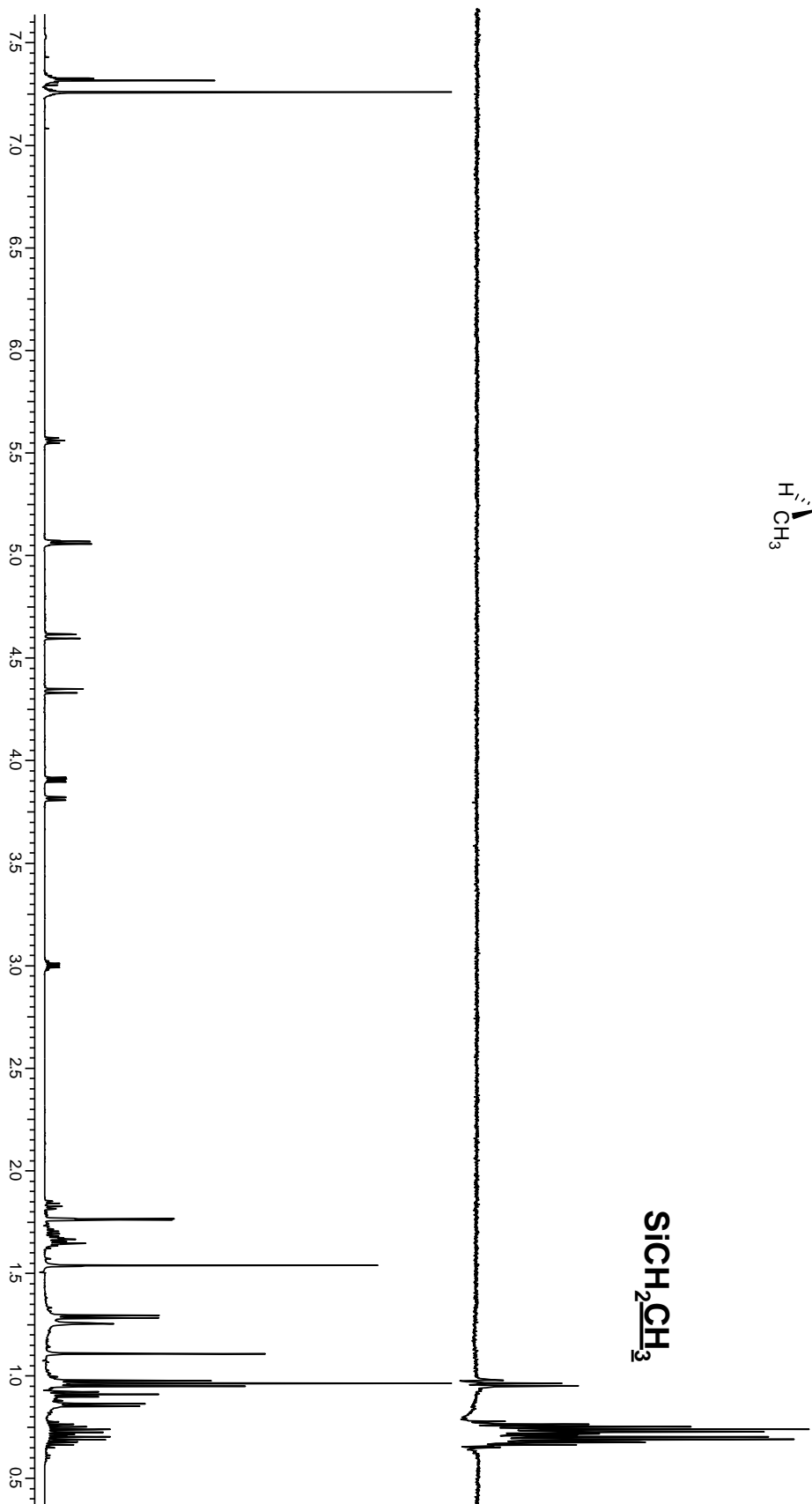
¹³C NMR chemical shift (δ/ppm)	
174.5	C1
40.5	C2
80.6	C3
72.7	C4
217.1	C5
83.3	C6
42.1	C7
34.3	C8
82.7	C9
90.8	C10
206.0	C11
98.9	C12
75.7	C13
24.2	C14
14.1	2-CH ₃
22.5	6-CH ₃
14.4	8-CH ₃
13.6	12-CH ₃
10.0	14-CH ₃
70.4	9-OCH ₃
6.8	SiCH ₂ CH ₃
5.2	SiCH ₂ CH ₃



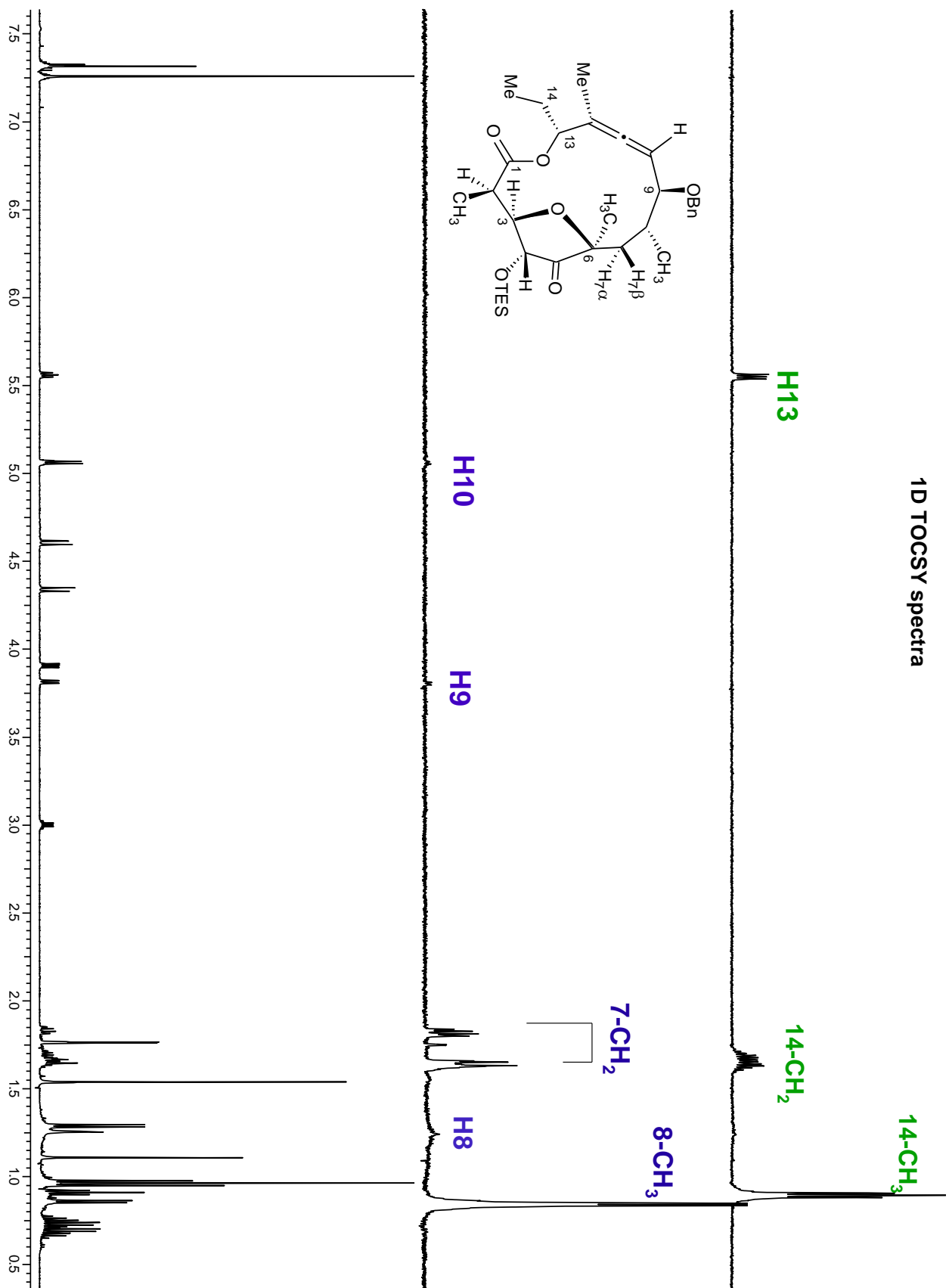




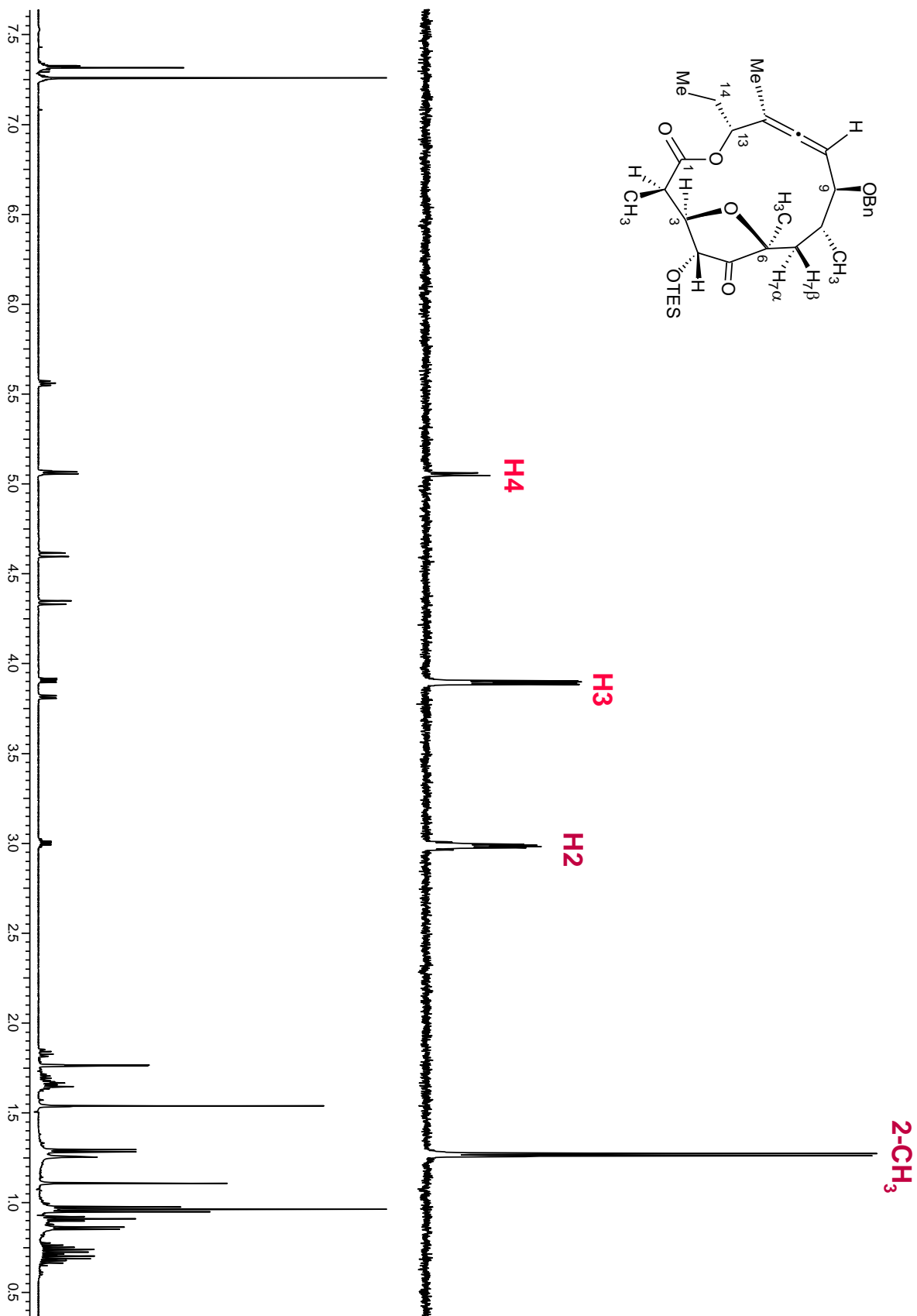
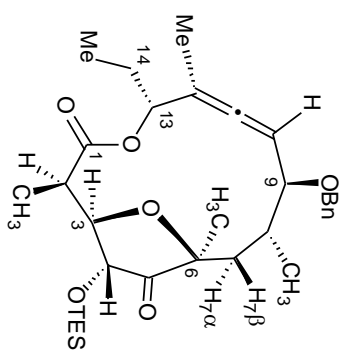
Sich₂CH₃



1D TOCSY spectra

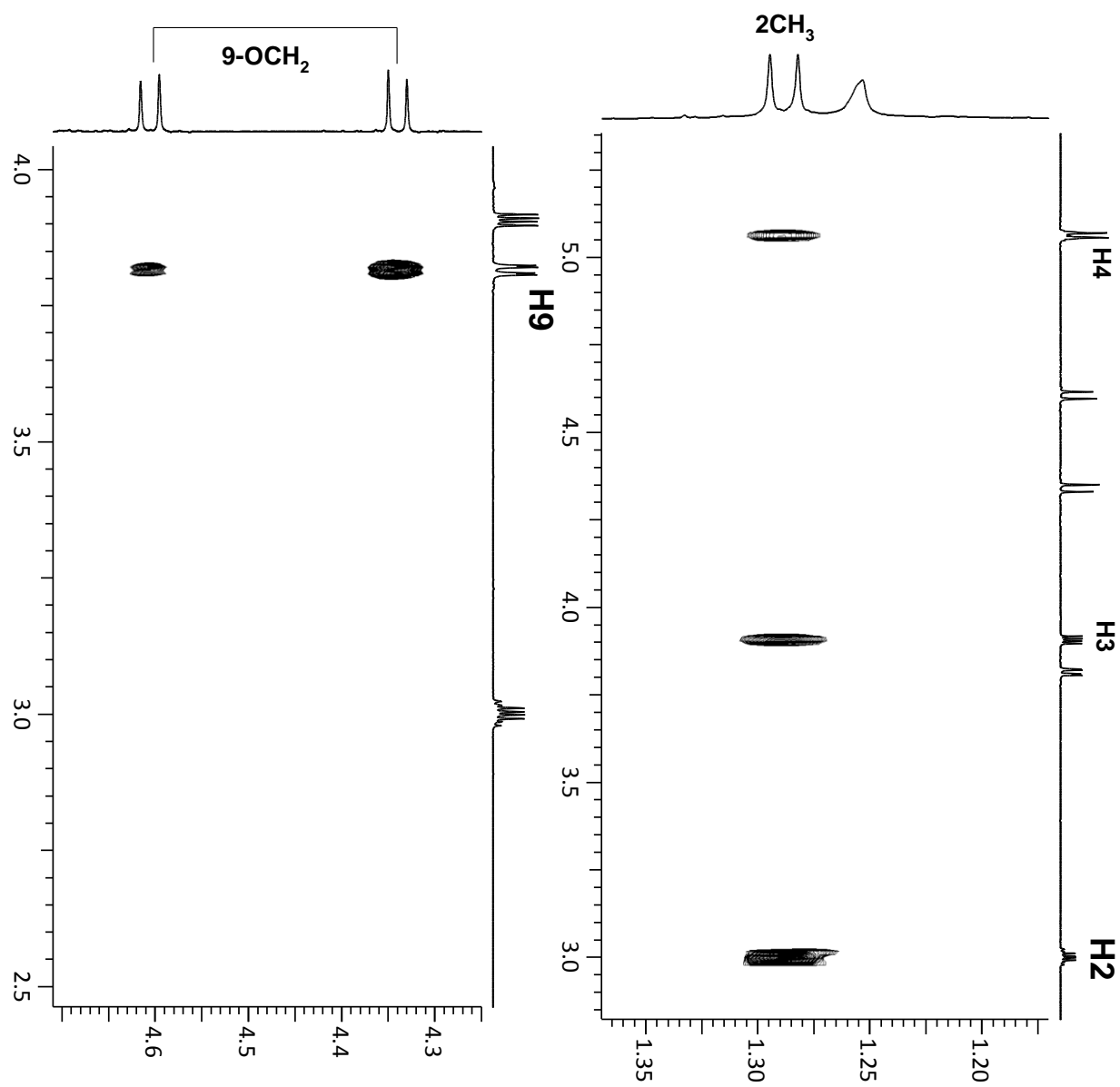
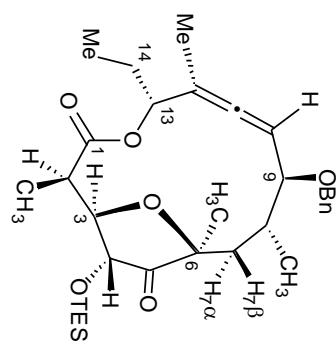


1D TOCSY spectra

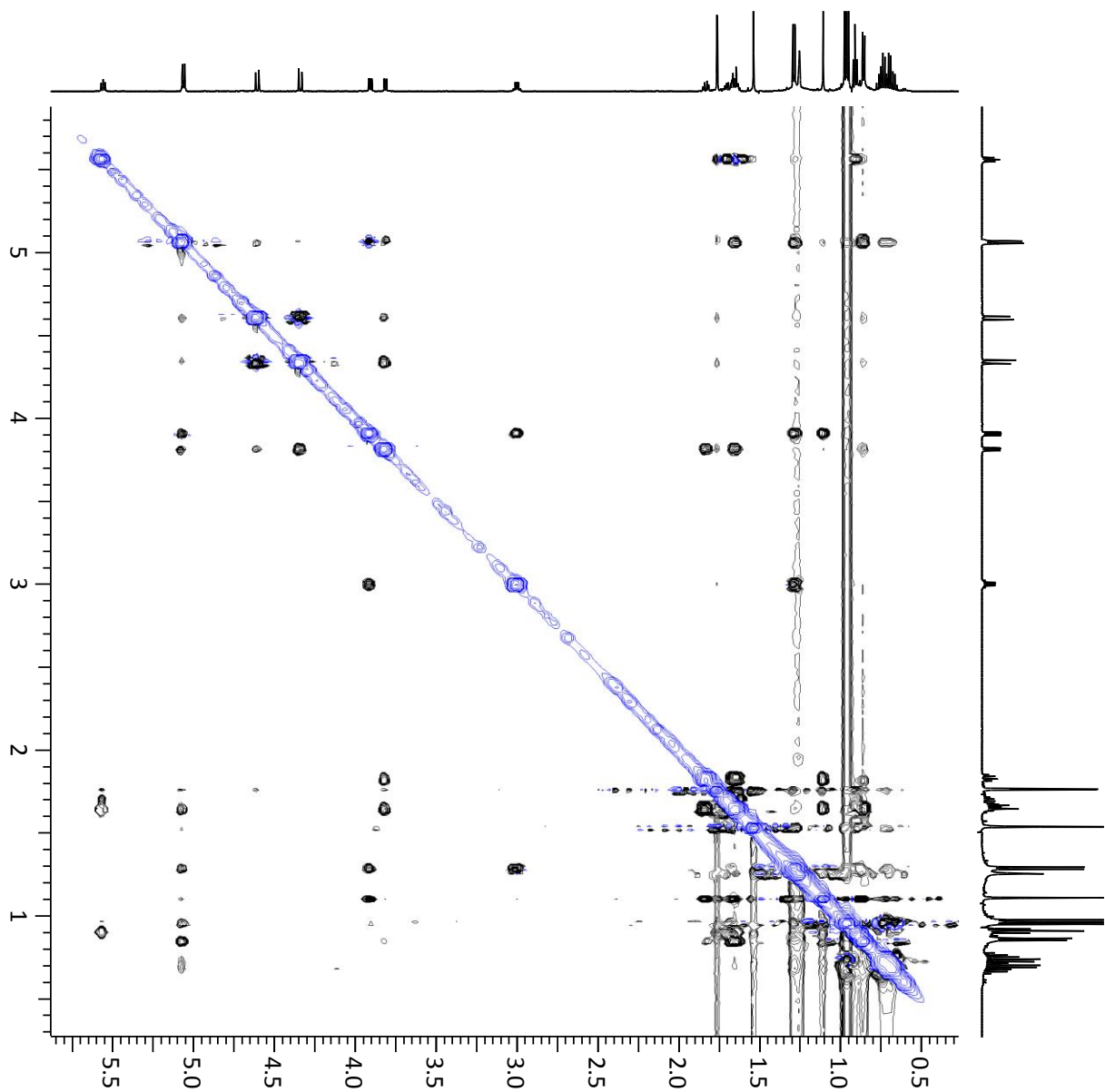
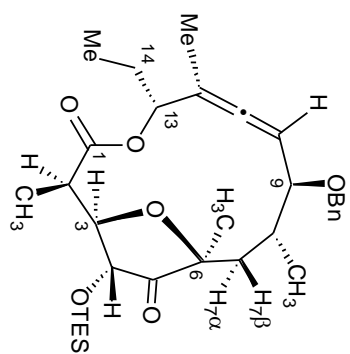


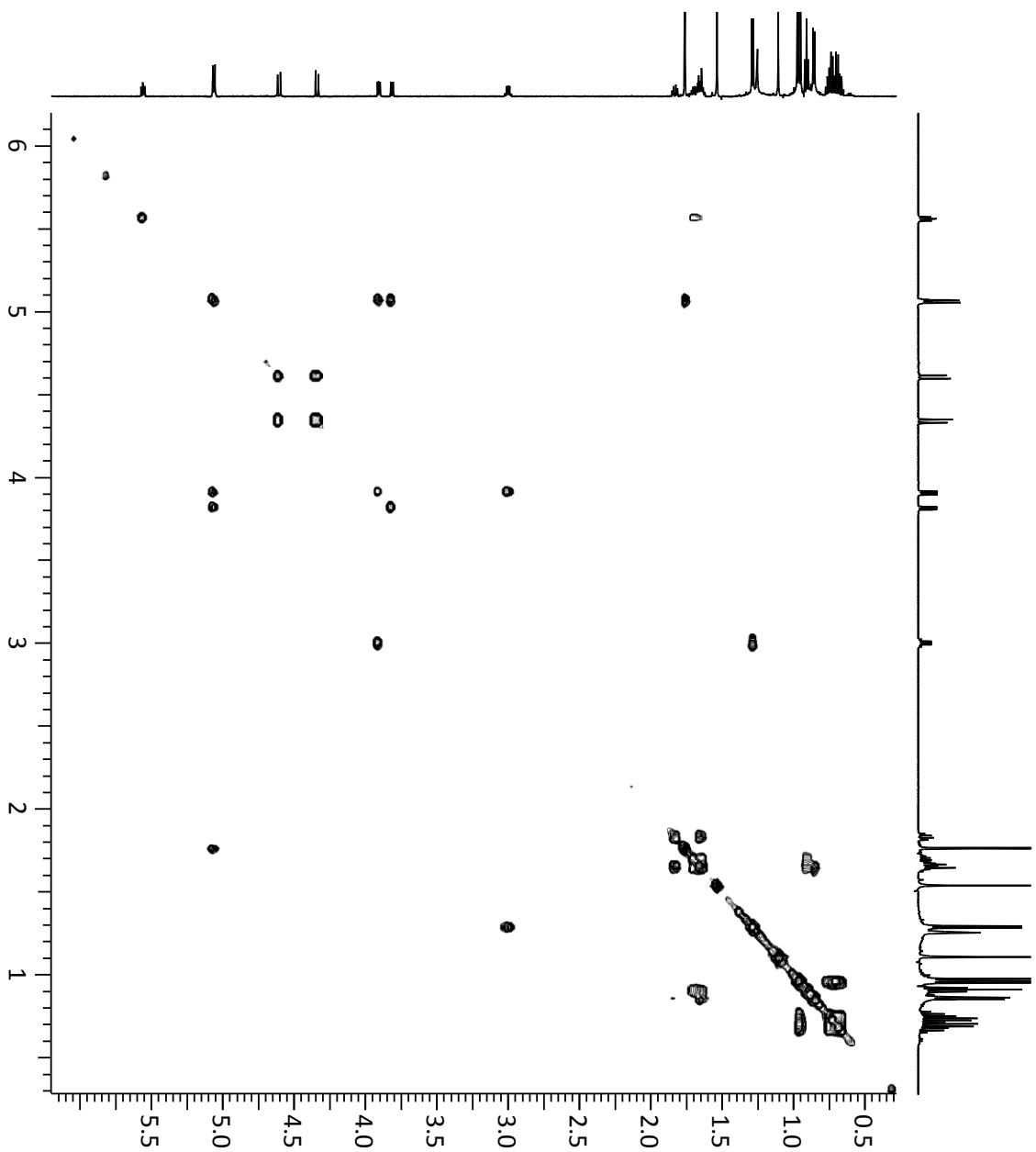
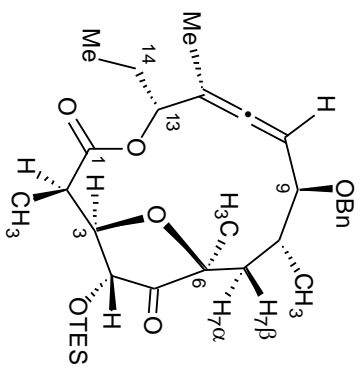
NOESY

expansions

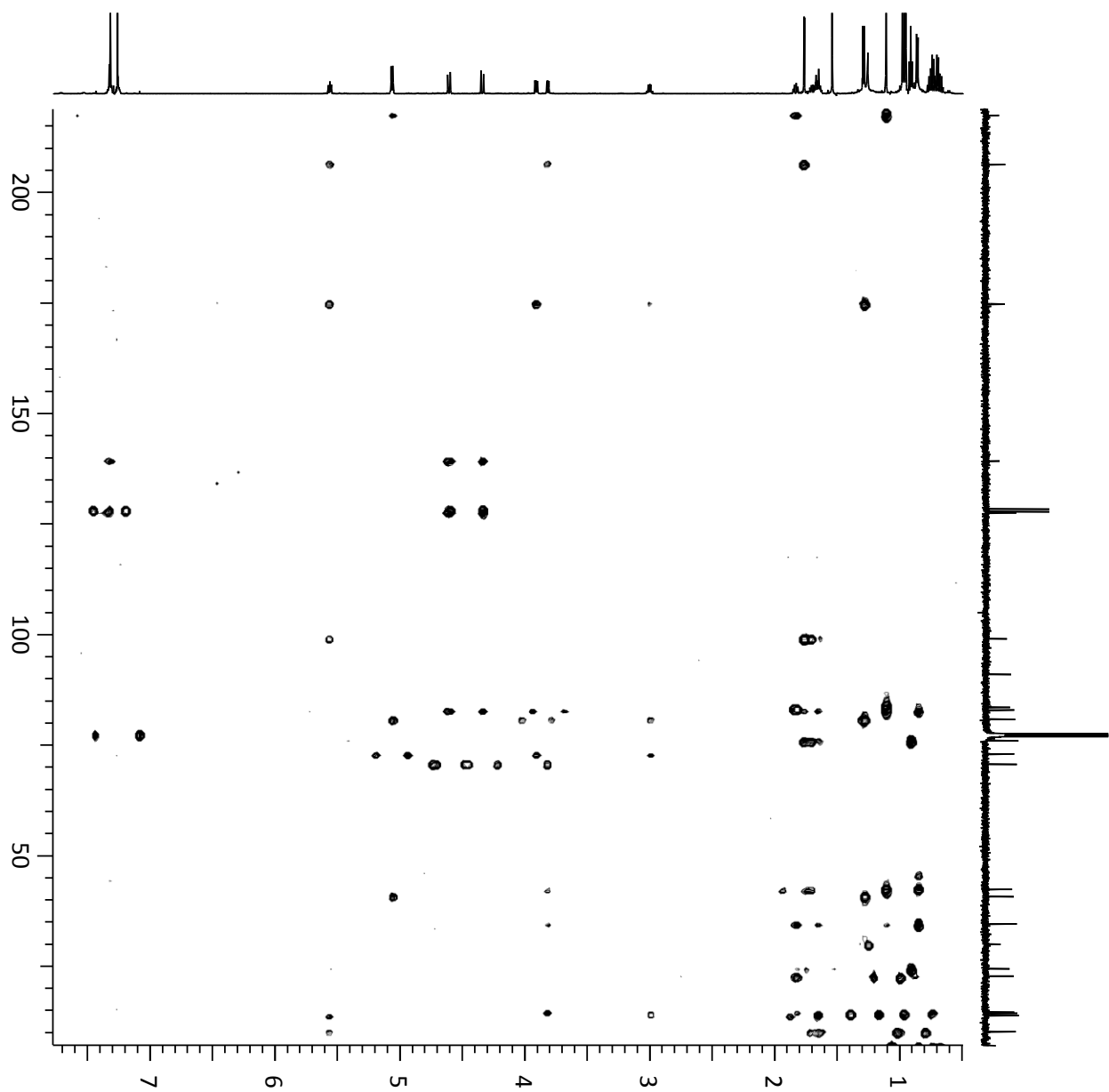
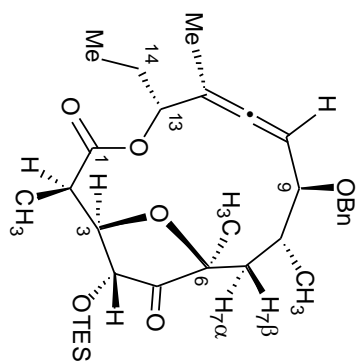


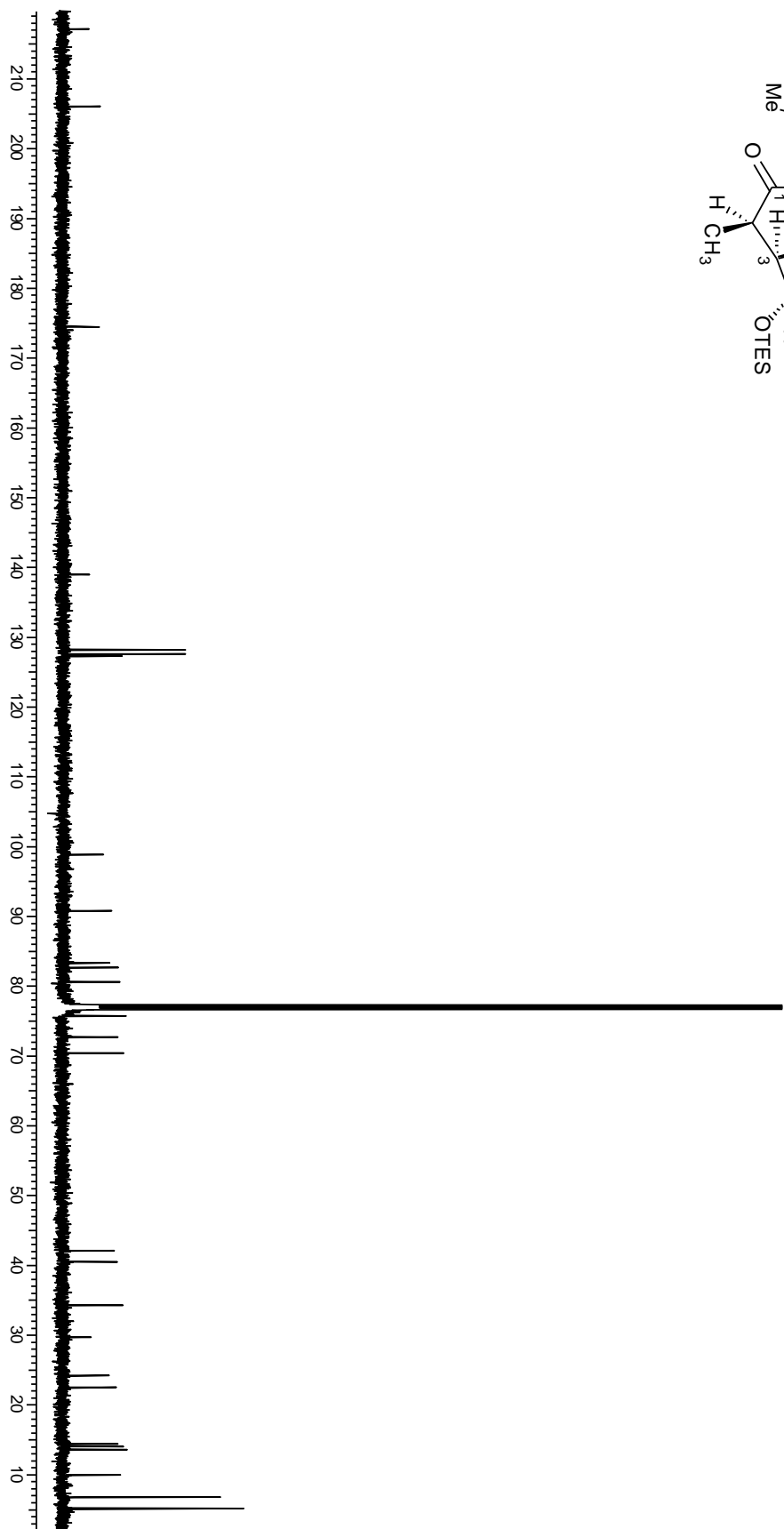
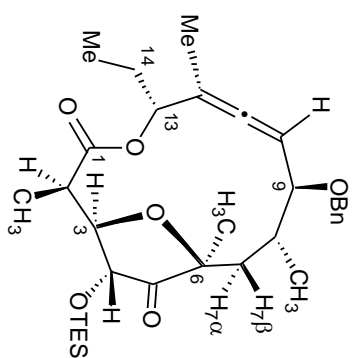
NOESY

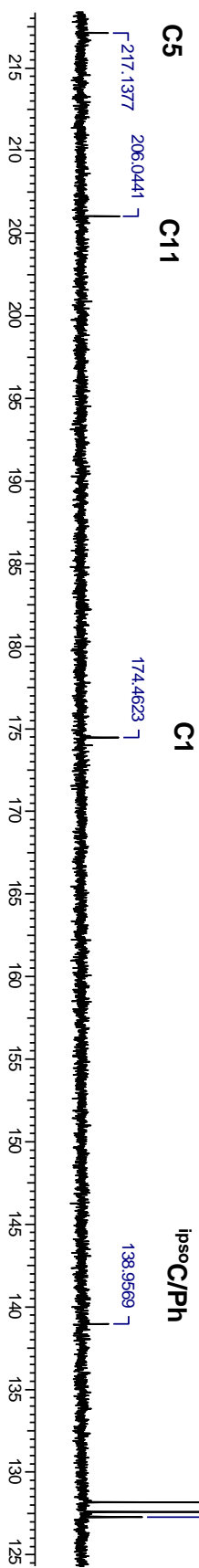
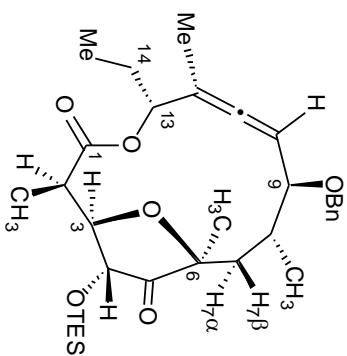
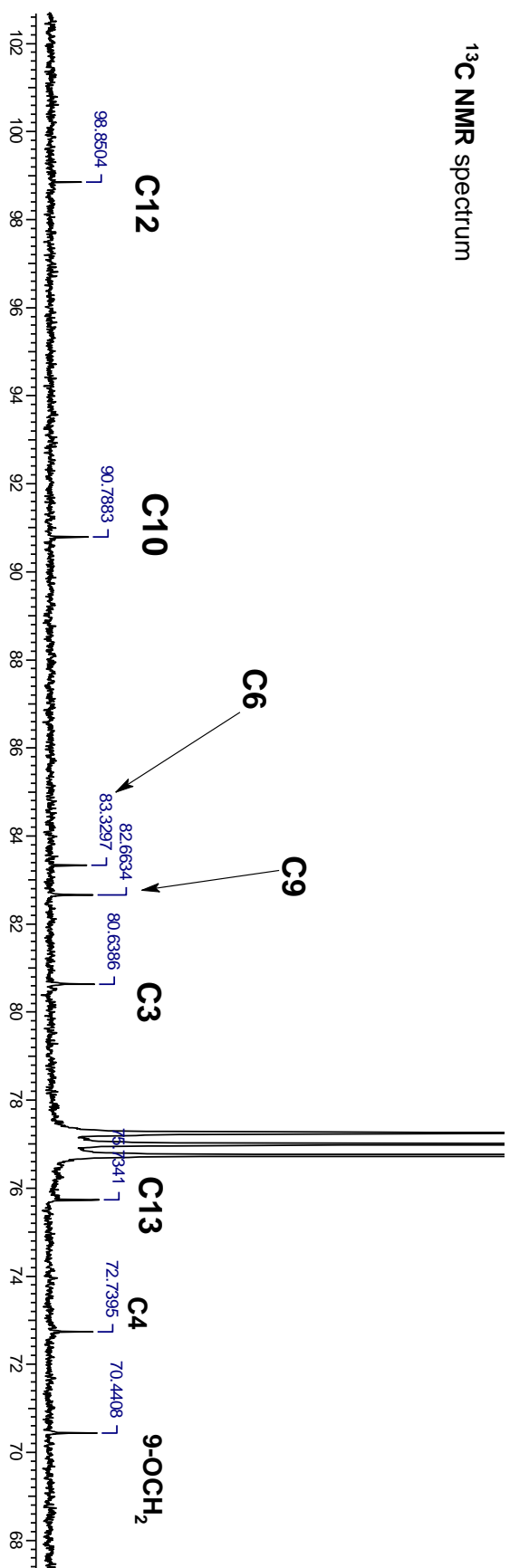


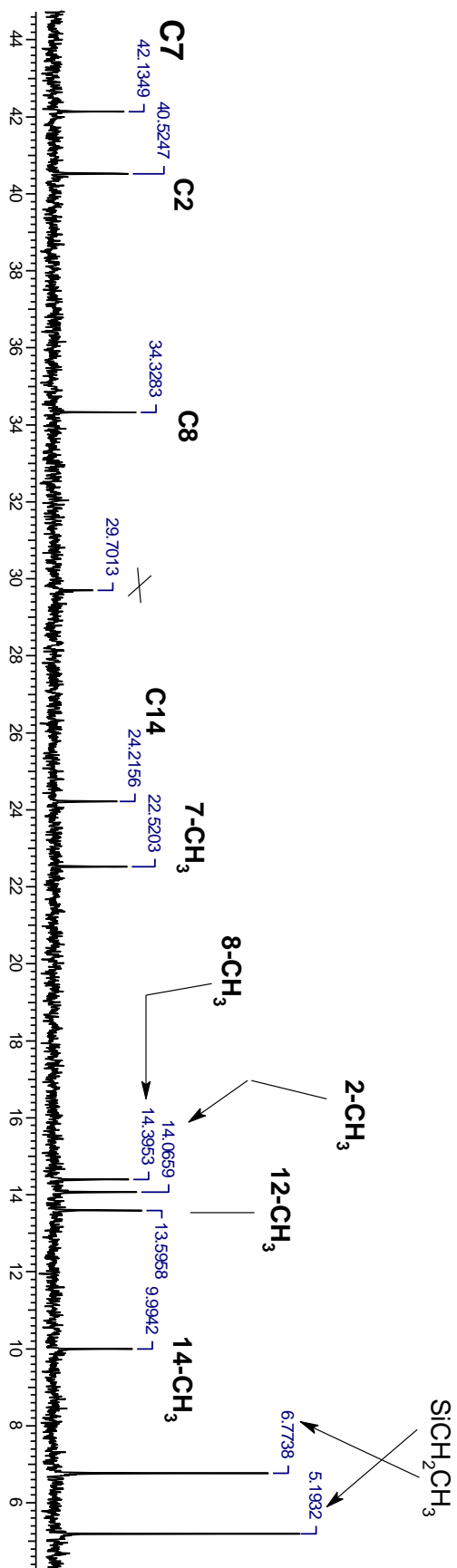
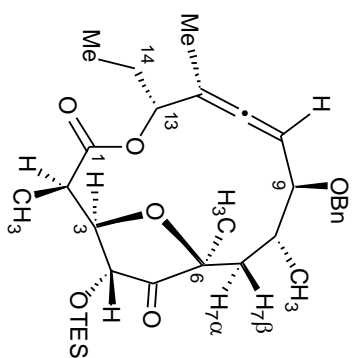
gcOSY

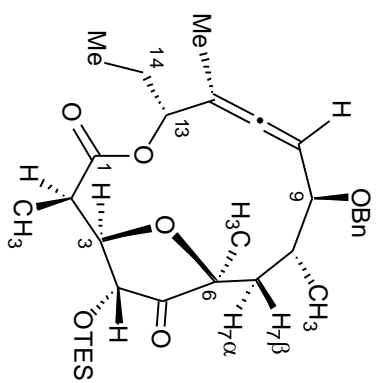
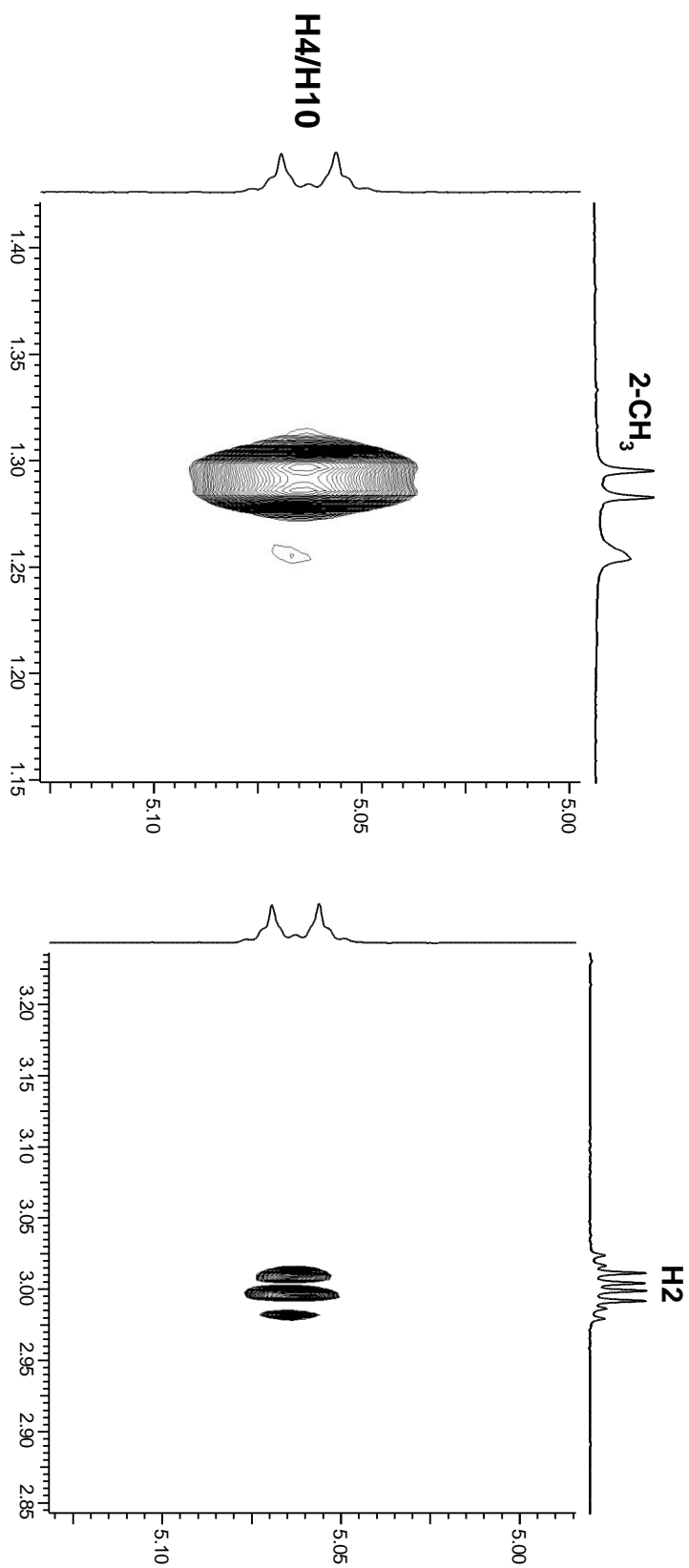
gHMBC

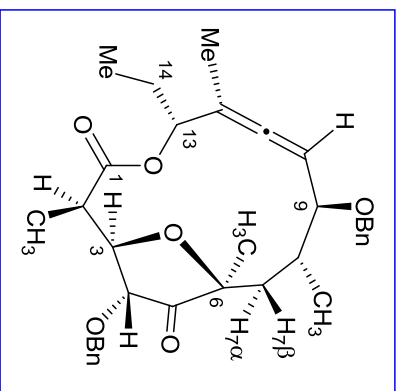


^{13}C NMR spectrum

¹³C NMR spectrum

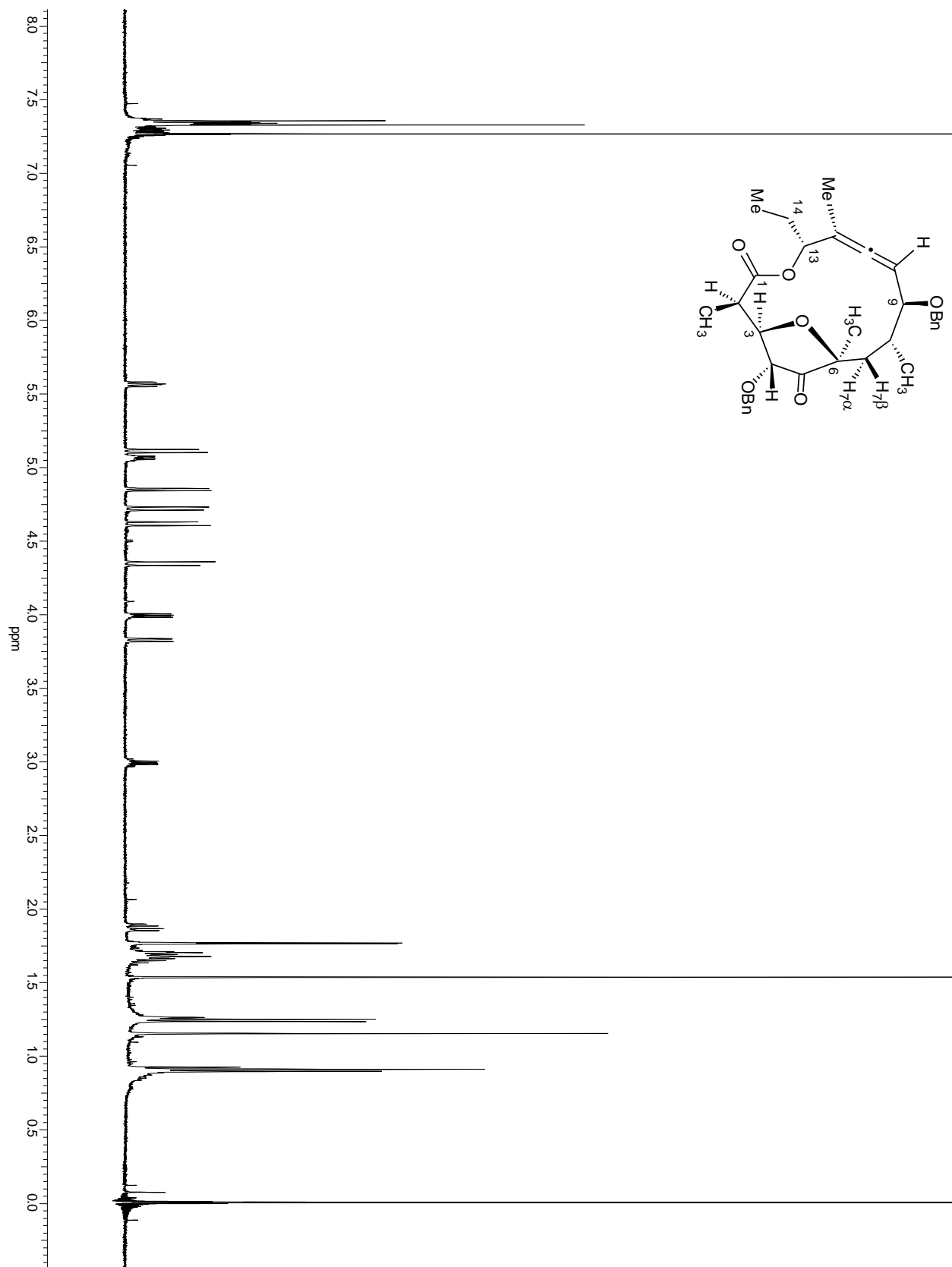
¹³C NMR spectrum

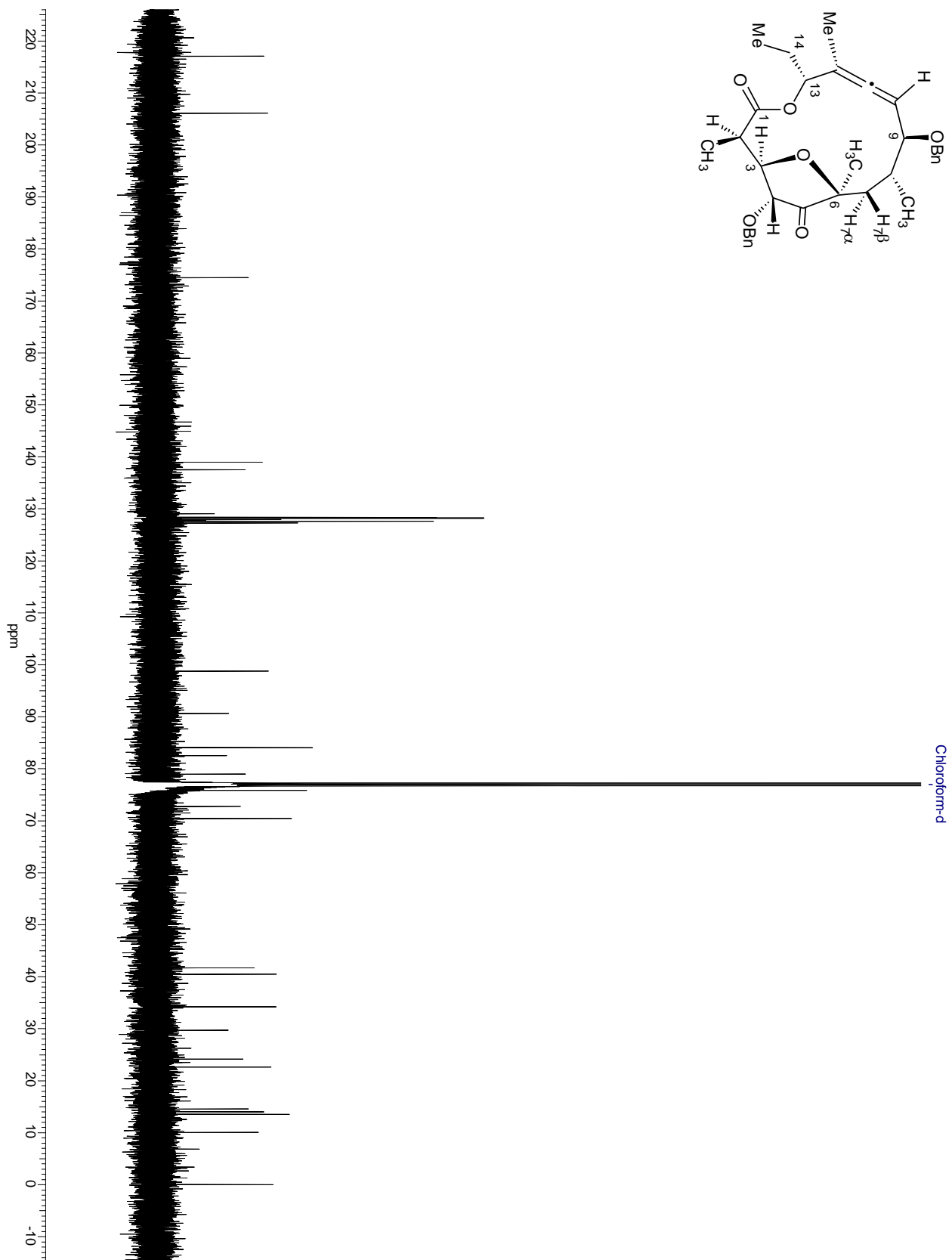
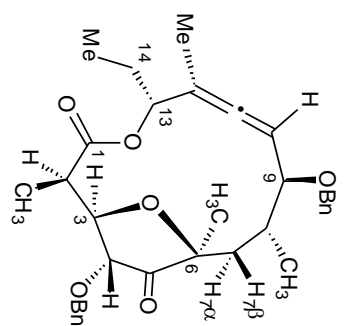


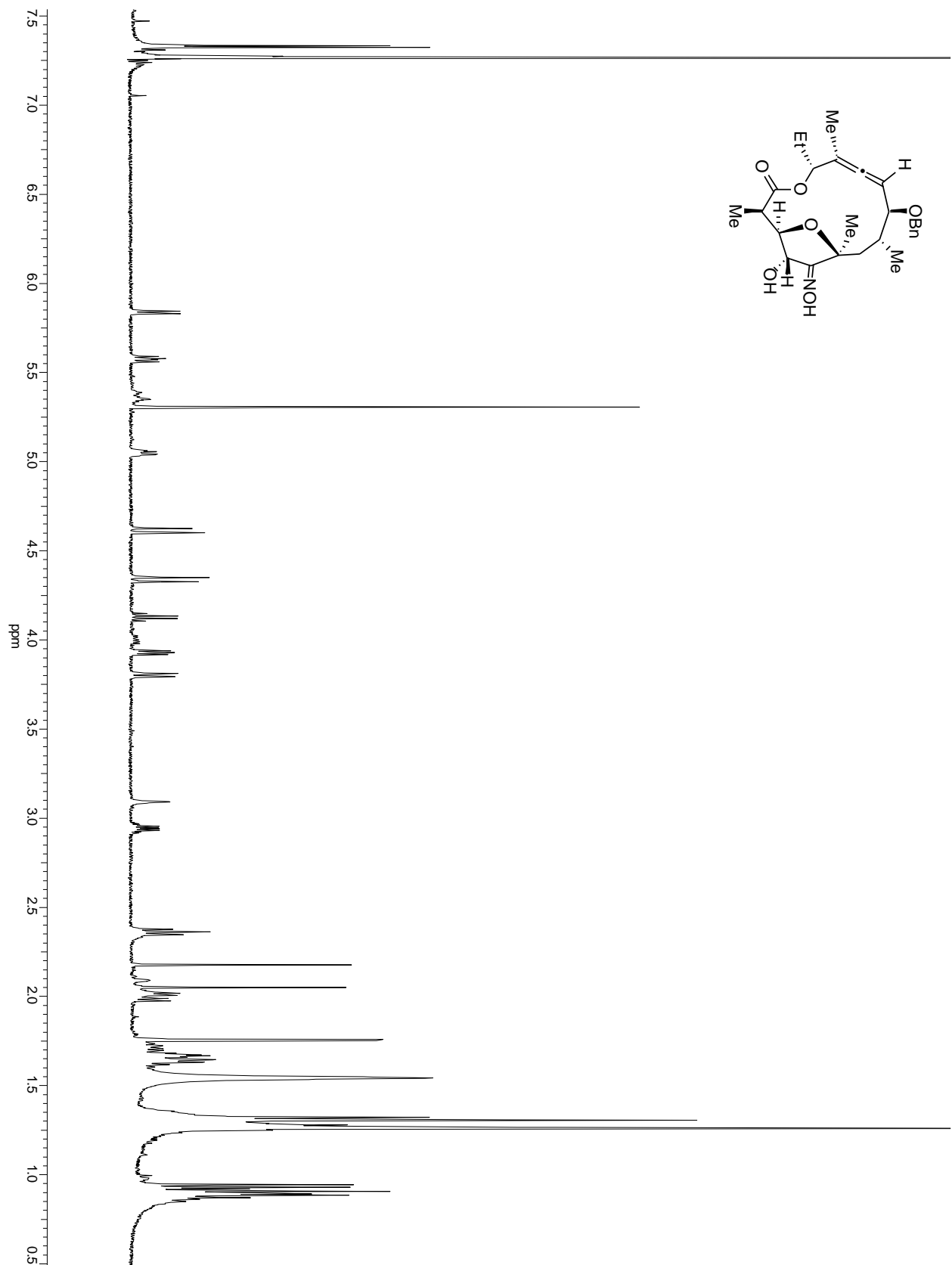
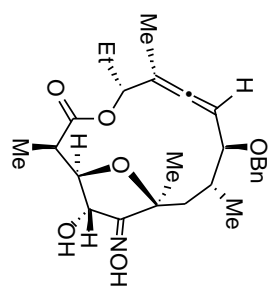


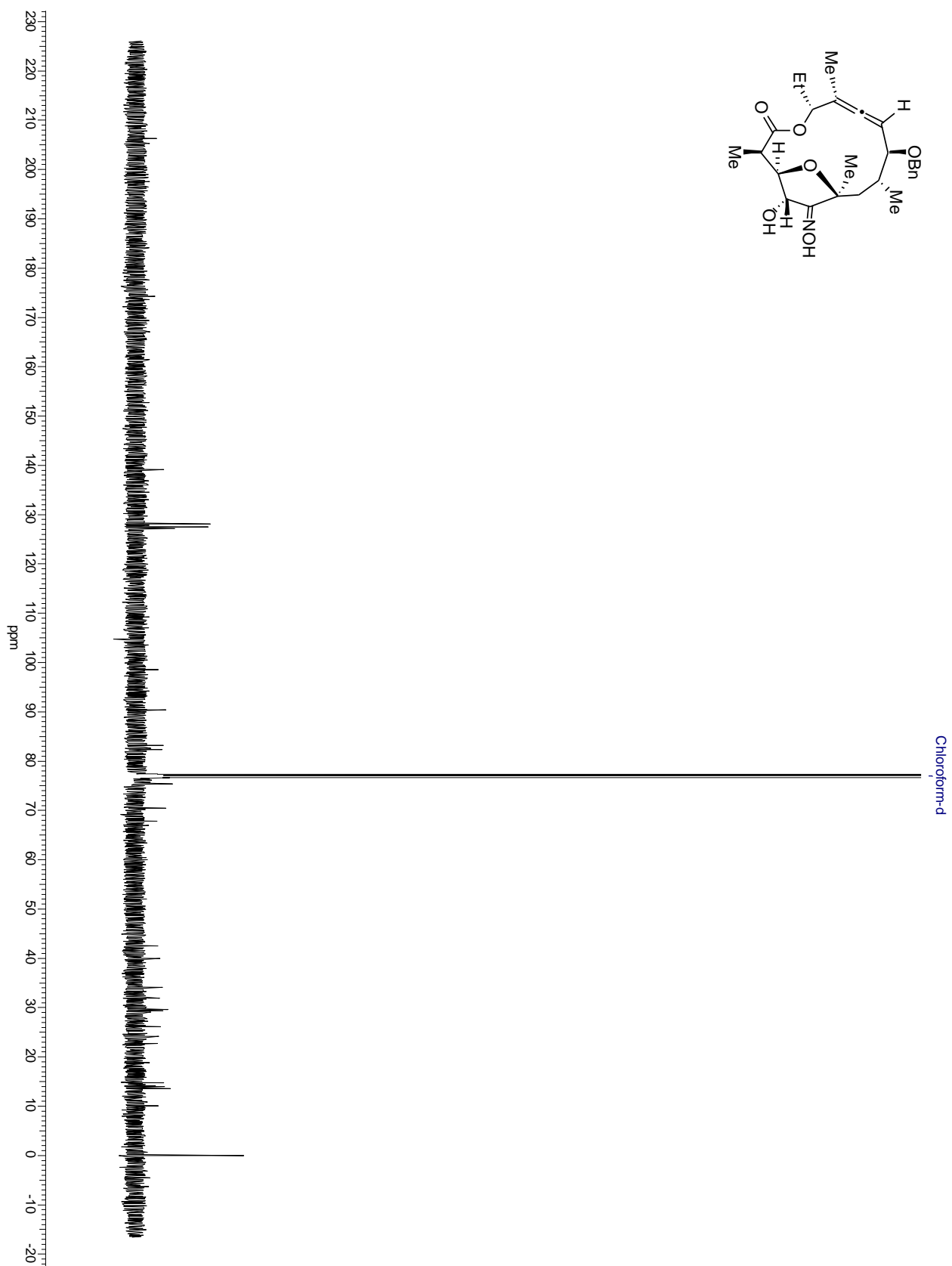
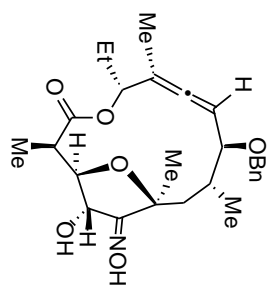
¹H NMR chemical shifts (δ/ppm) & coupling constant (J/Hz)	
2.99 (dd, J _{H2, H3} = 4.4Hz, J _{H2, 2-CH3} = 7.6Hz, H2)	
0.91 (d, J _{2-CH3, H2} = 7.6Hz, 2-CH₃)	
4.00 (dd, J _{H3, H2} = 4.4Hz, J _{H3, H4} = 7.6Hz, H3)	
4.86 (d, J _{H4, H3} = 7.6Hz, H4)	
1.15 (s, 6-CH₃)	
1.65 (m, H7β)	
1.89 (dd, J _{H7α, H8} = 6.8, J _{H7α, H7β} = 15.7Hz, H7α)	
1.72 - 1.62 (m, H8)	
1.25 (d, J _{8-CH3, H8} = 7.6Hz, 8-CH₃)	
3.83 (dd, J _{H9, H8} = 8.6Hz, J _{H9, H10} = 2.0Hz, H9)	
5.12, 4.73, 4.63, 4.36 (d, J _{AB} = 11.0, 12.0 Hz, 4-OCH₂, 9-OCH₂)	
5.07 (m, H10)	
1.77 (d, J = 2.7Hz, 12-CH₃)	
5.56 (dd, J _{H13, H14} = 6.4, 9.0Hz, H13)	
1.72 - 1.62 (m, 14-CH₂)	
0.91 (t, J _{14-CH3, H14} = 7.1Hz, 14-CH₃)	

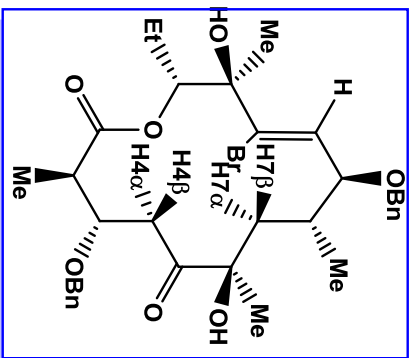
¹³C NMR chemical shift (δ/ppm)	
174.4	C1
40.5	C2
79.0	C3
72.9	C4
217.1	C5
84.1	C6
41.7	C7
34.2	C8
82.5	C9
90.6	C10
206.1	C11
98.8	C12
75.9	C13
24.2	C14
14.0	2-CH ₃
22.6	6-CH ₃
14.5	8-CH ₃
13.6	12-CH ₃
10.0	14-CH ₃
70.4	9-OCH ₃









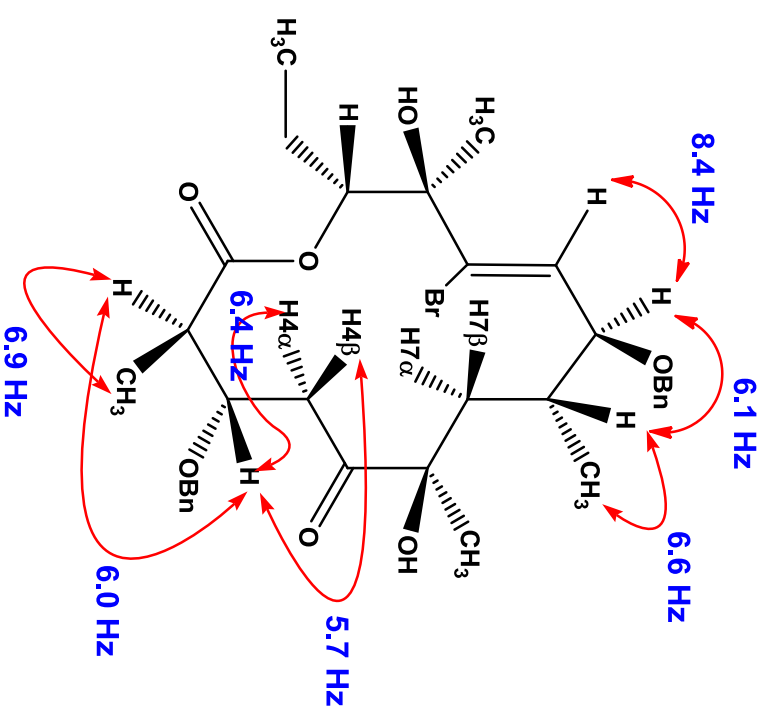
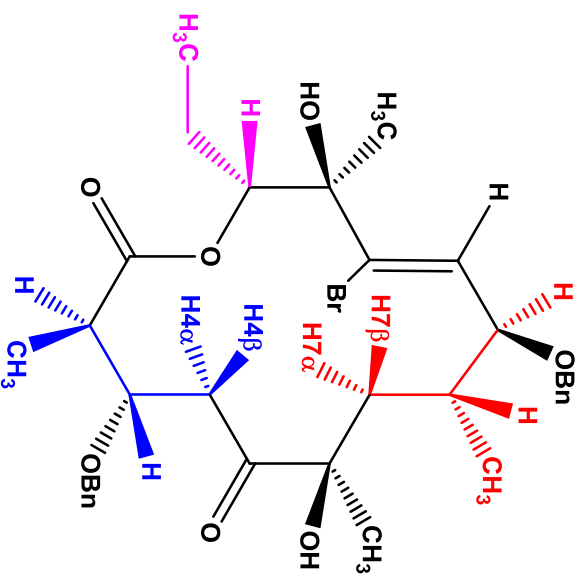


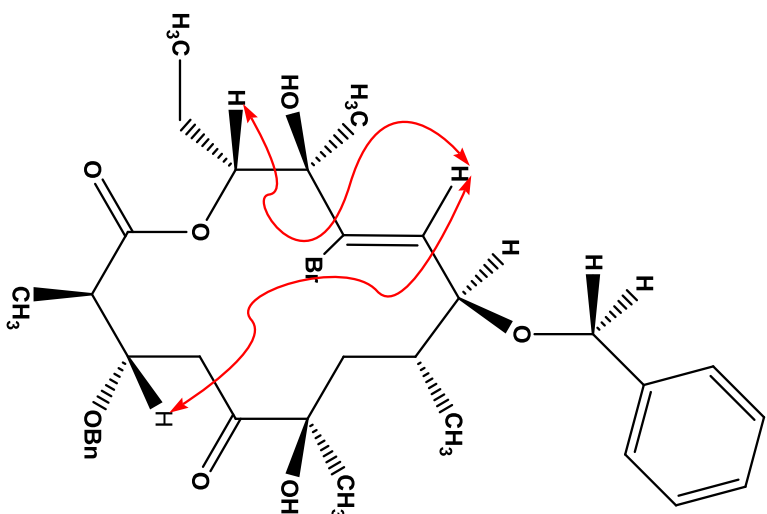
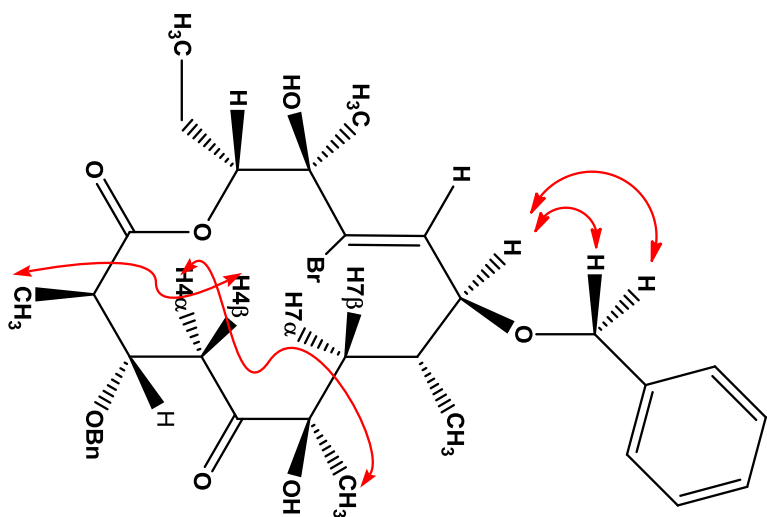
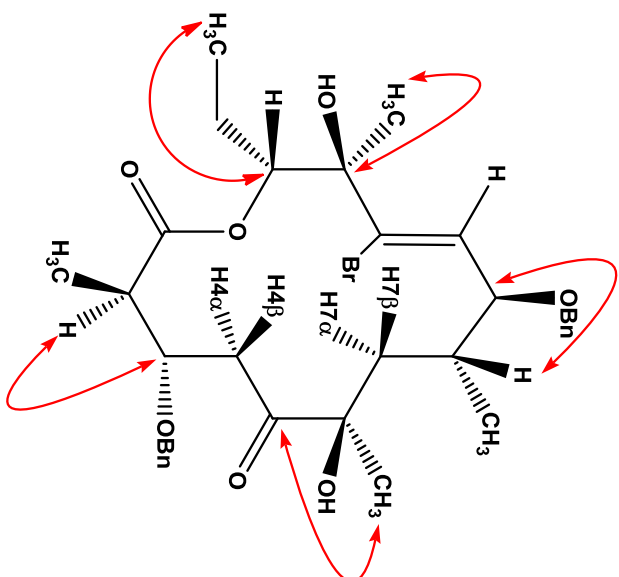
¹ H NMR chemical shifts (δ/ppm) & coupling constant (J/Hz)	
2.56 (quintet, J _{H2, 2-CH3} = 6.9Hz, H2)	
1.20 (d, J _{2-CH3, H2} = 6.9Hz, 2-CH₃)	
4.34 (m, H3)	
4.64, 4.52 (d, J _{AB} = 11.1Hz, C3-OCH₂)	
3.11 (dd, J _{H4α, H4β} = 15.6Hz, J _{H4α, H3} = 6.4Hz, H4α)	
2.47 (dd, J _{H4β, H4α} = 15.6Hz, J _{H4β, H3} = 5.7Hz, H4β)	
1.23 (s, 6-CH₃)	
1.79 (dd, J _{H7β, H7α} = 14.4Hz, H7β)	
1.45 (J _{H7α, H8} = 5.90 Hz, J _{H7α, H7β} = 14.4Hz, H7α)	
1.70-1.85 (m, H8)	
1.05 (d, J _{8-CH3, H8} = 6.6Hz, 8-CH₃)	
4.00 (dd, J _{H9, H10} = 8.3Hz, J _{H9, H8} = 6.1Hz, H9)	
4.52, 4.40 (d, J _{AB} = 12.3Hz, 9-OCH₂)	
6.14 (d, J = 8.4Hz, H10)	
1.44 (s, 12-CH₃)	
4.89 (dd, J _{H13, H14} = 2.4, 10.9Hz, H13)	
1.75-1.82, 1.47-1.55 (m, 14-CH₂)	
0.80 (t, J _{14-CH3, H14} = 7.4Hz, 14-CH₃)	

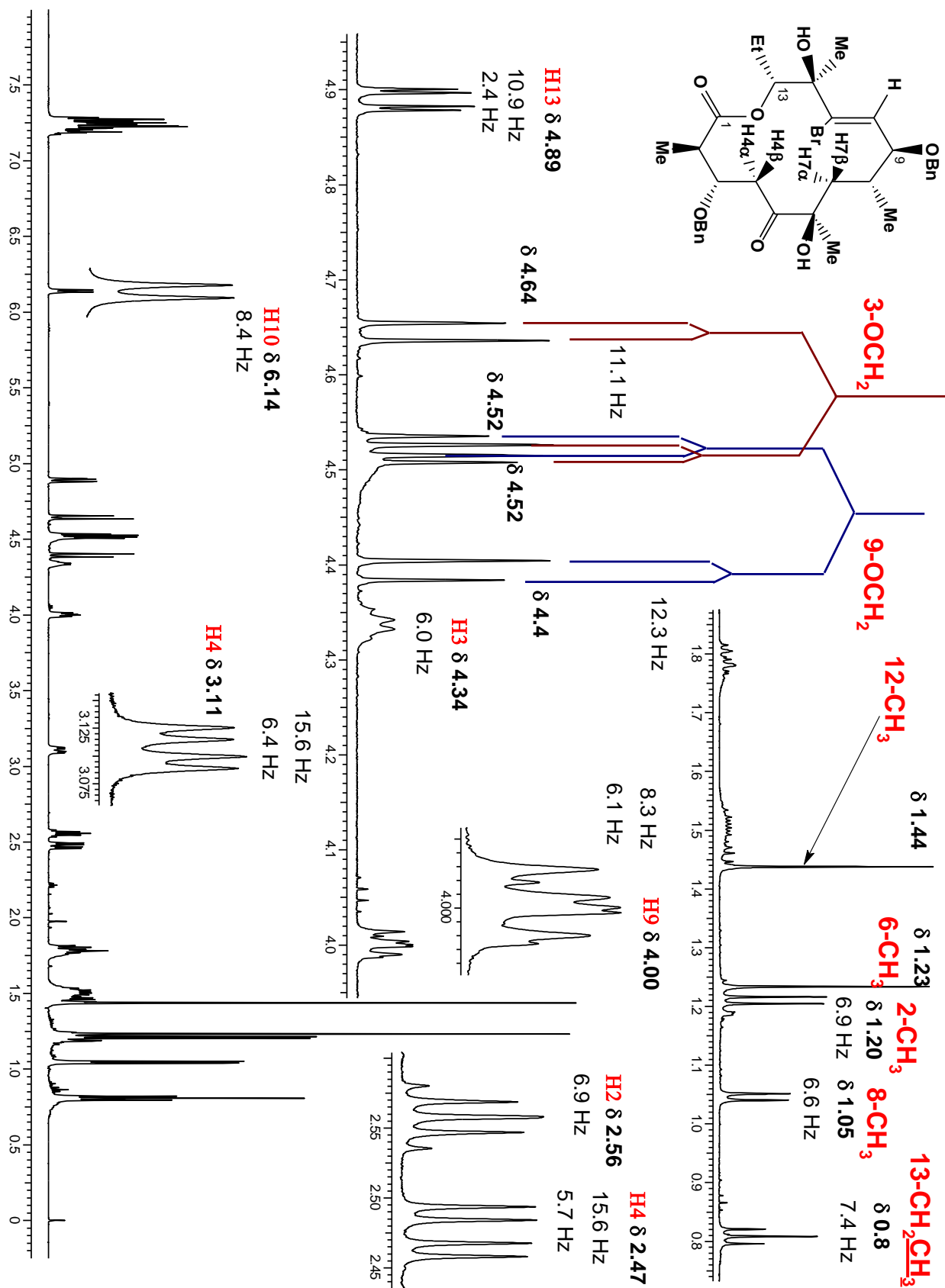
¹³ C NMR chemical shift (δ/ppm)	
174.6 — C1	
42.5 — C2	
76.1 — C3	
44.8 — C4	
212.7 — C5	
79.4 — C6	
41.3 — C7	
35.0 — C8	
84.0 — C9	
131.2 — C10	
134.2 — C11	
77.1 — C12	
79.3 — C13	
24.4 — C14	
12.6 — 2-CH ₃	
26.8 — 6-CH ₃	
19.6 — 8-CH ₃	
25.1 — 12-CH ₃	
11.1 — 14-CH ₃	
73.3 — 6-OCH ₃	
72.2 — 9-OCH ₃	

$1d$ TOCSY

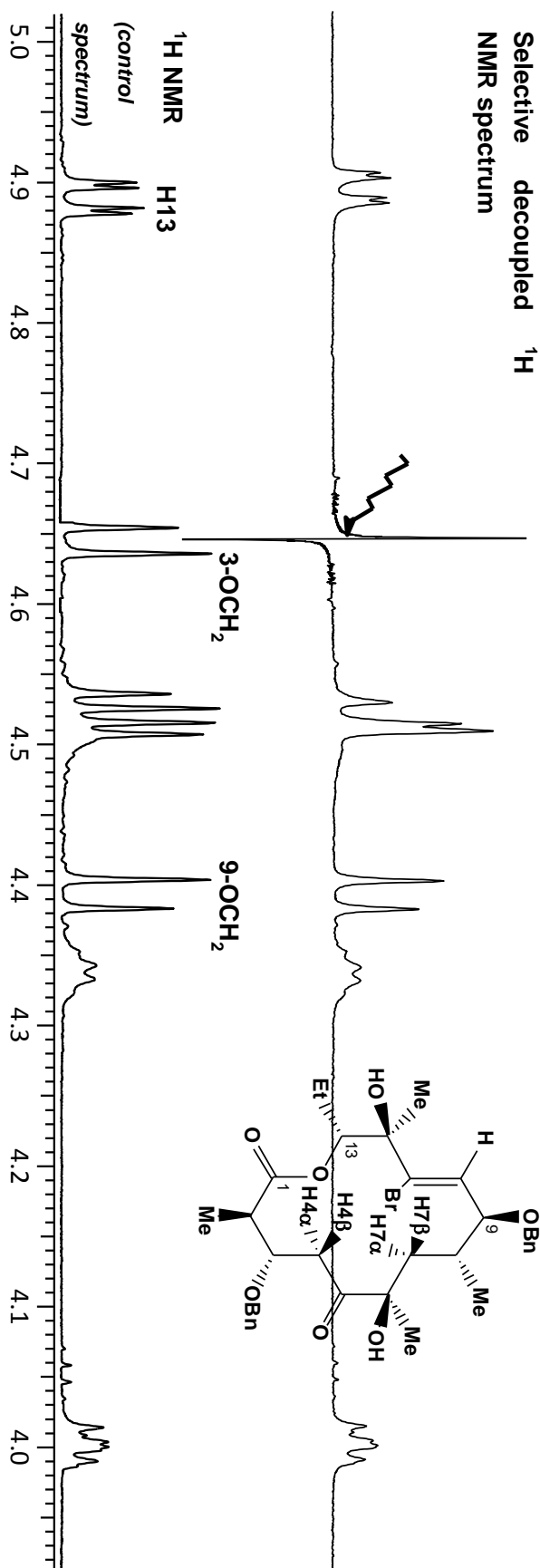
Coupling constant (J_{HH})



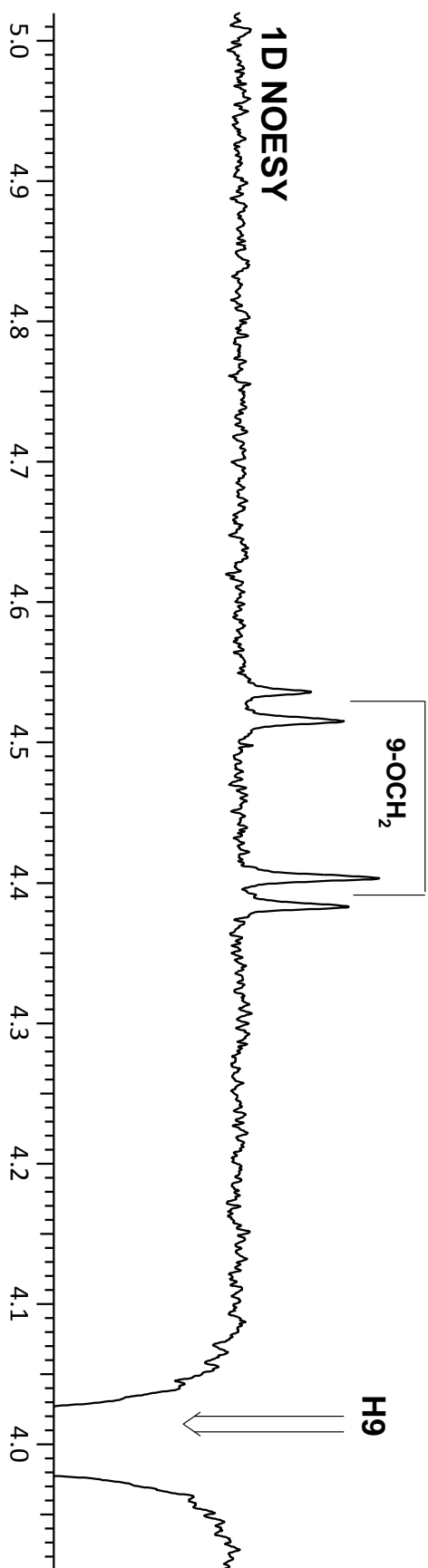
NOE**NOE****HMBC**



Selective decoupled ^1H
NMR spectrum

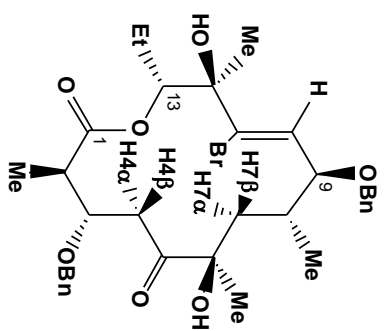


1D NOESY



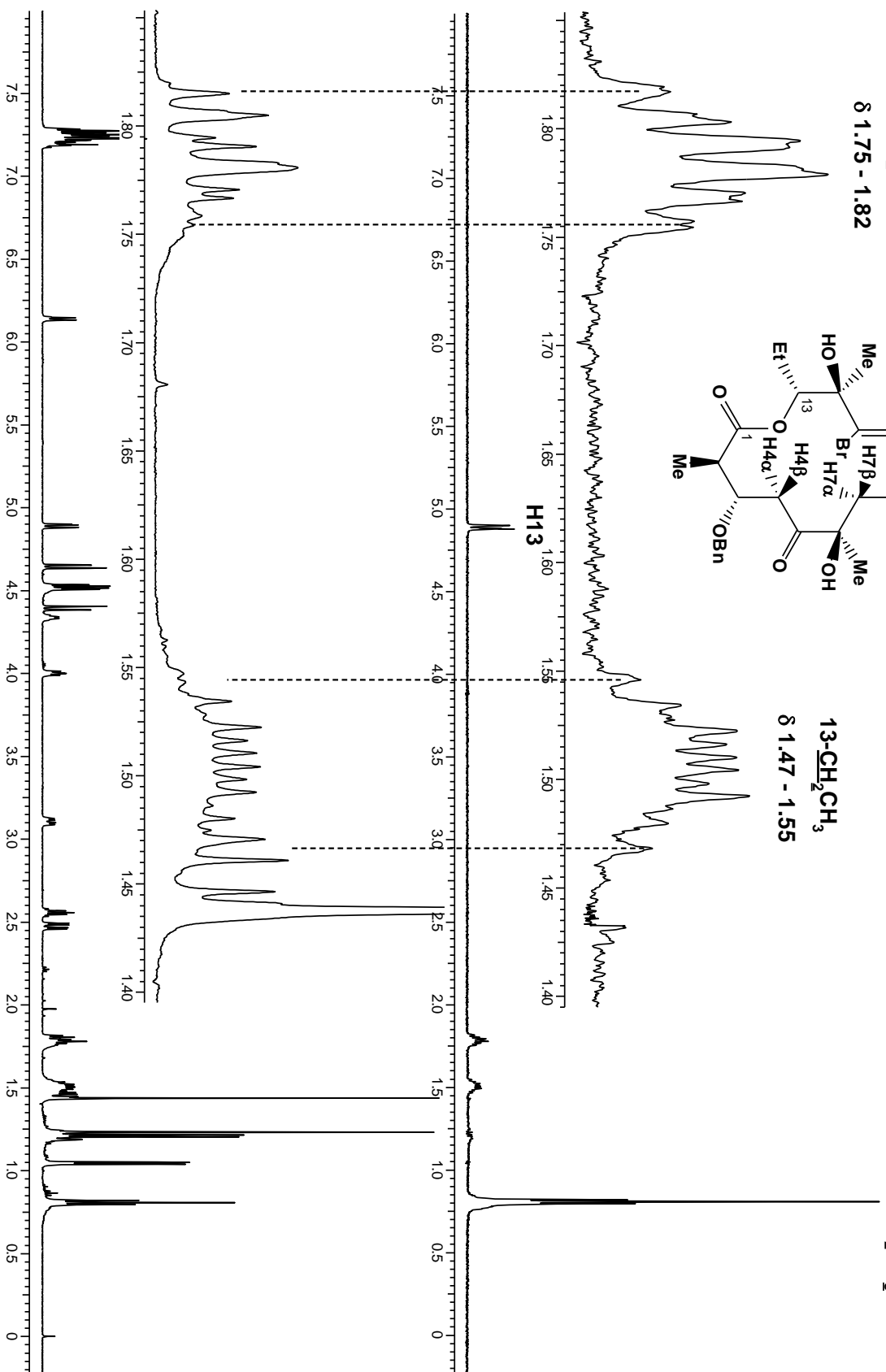
1D TOCSY

$^{13}\text{-CH}_2\text{CH}_3$
 δ 1.75 - 1.82

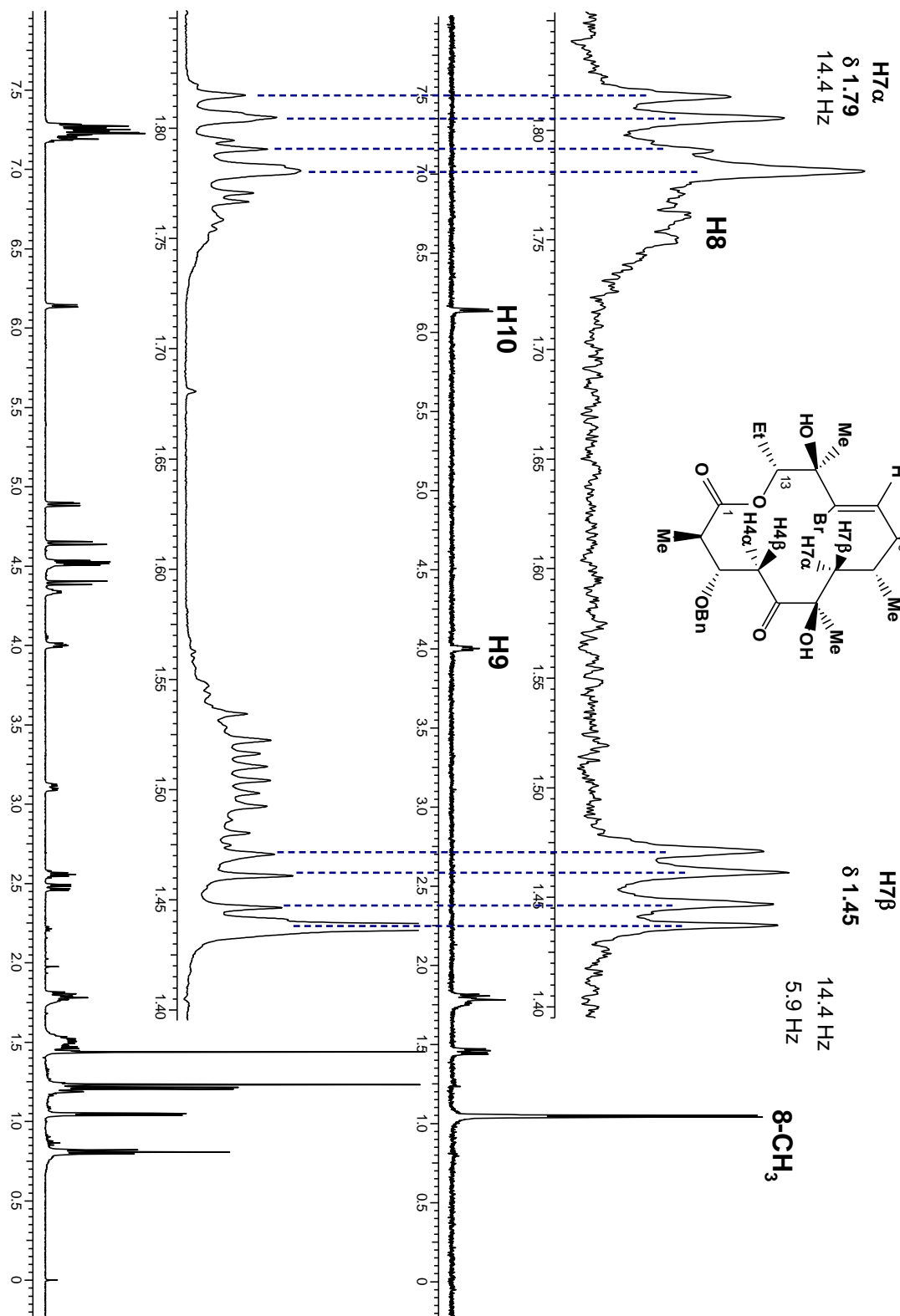


$^{13}\text{-CH}_2\text{CH}_3$
 δ 1.47 - 1.55

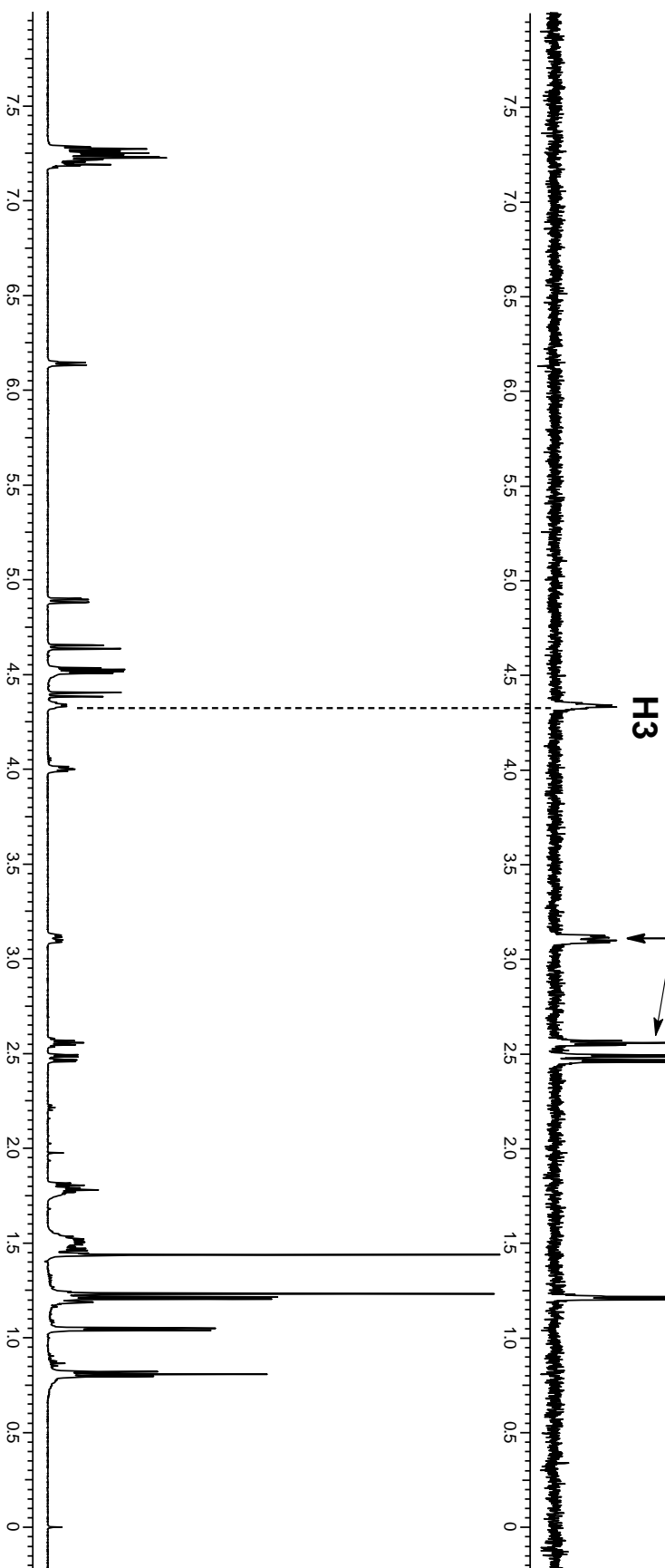
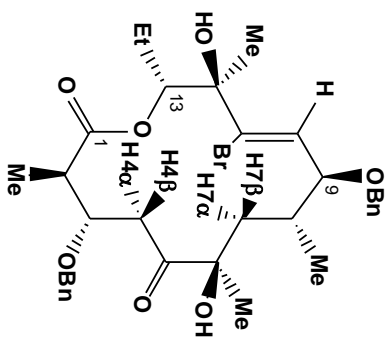
$^{13}\text{-CH}_2\text{CH}_3$

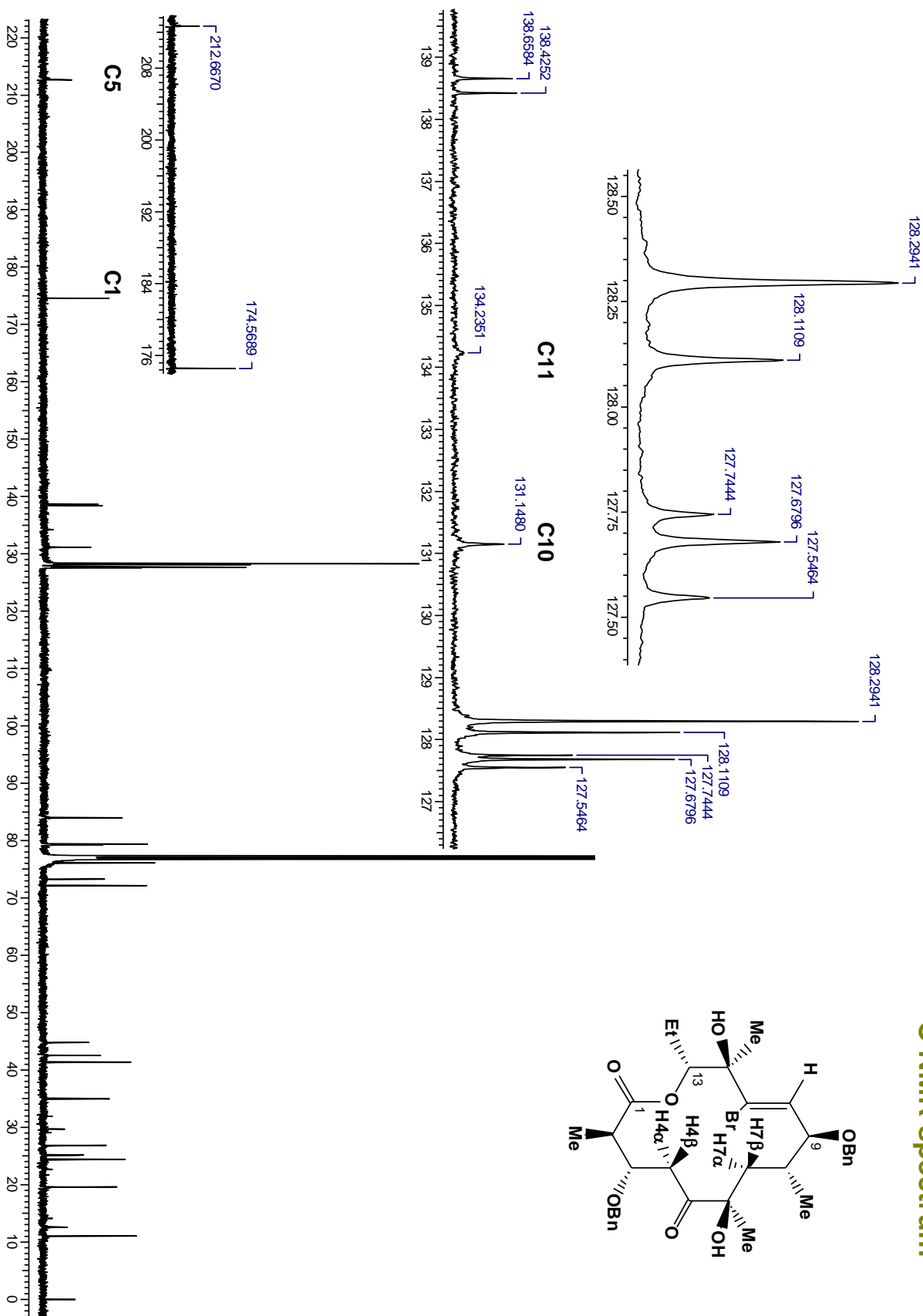


1D TOCSY

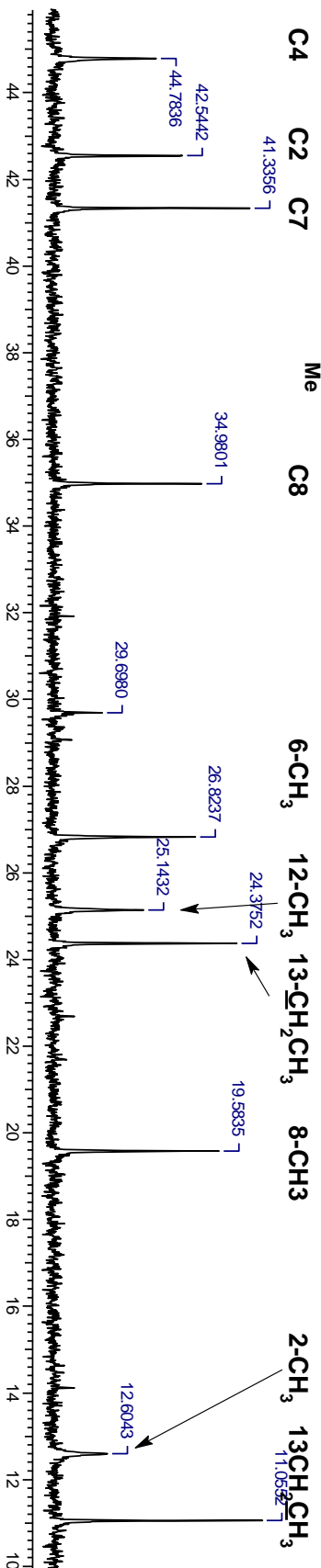
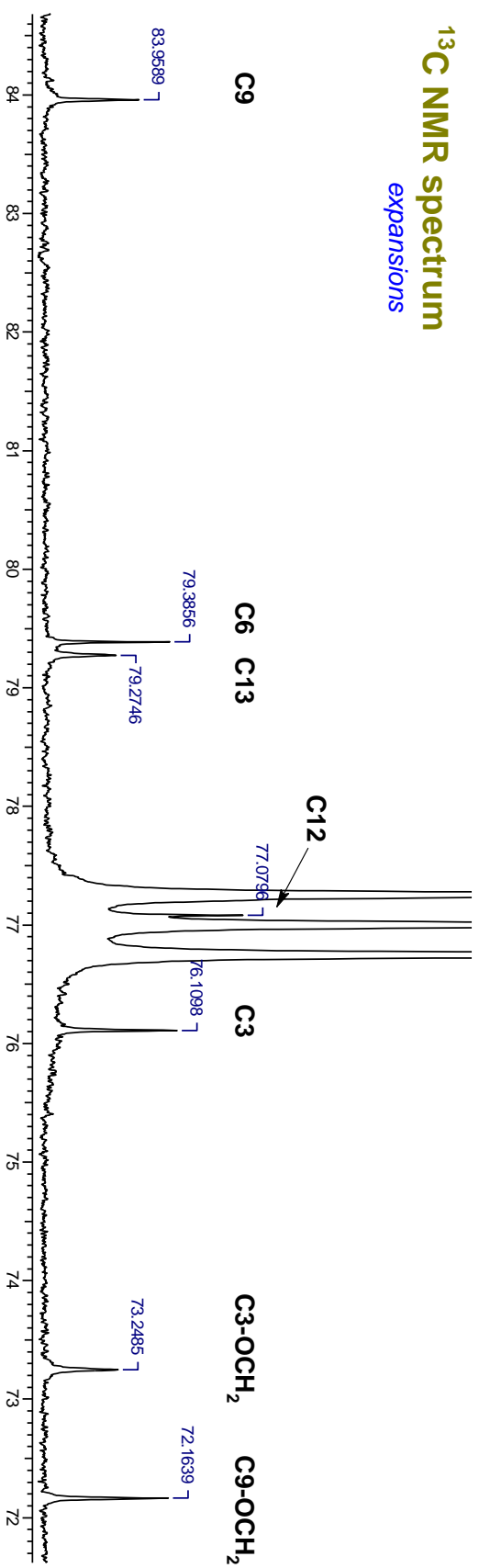


1D TOCSY

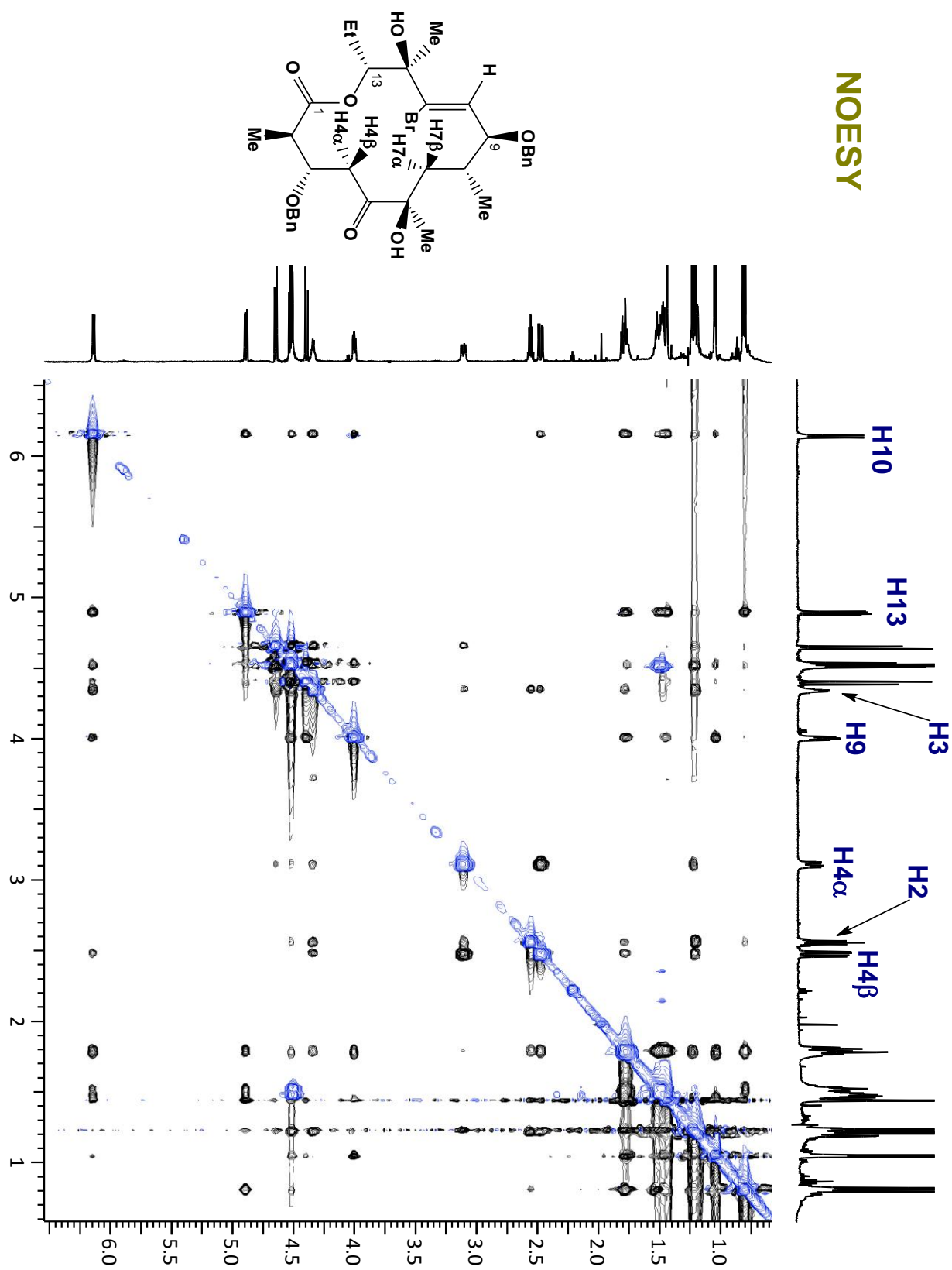


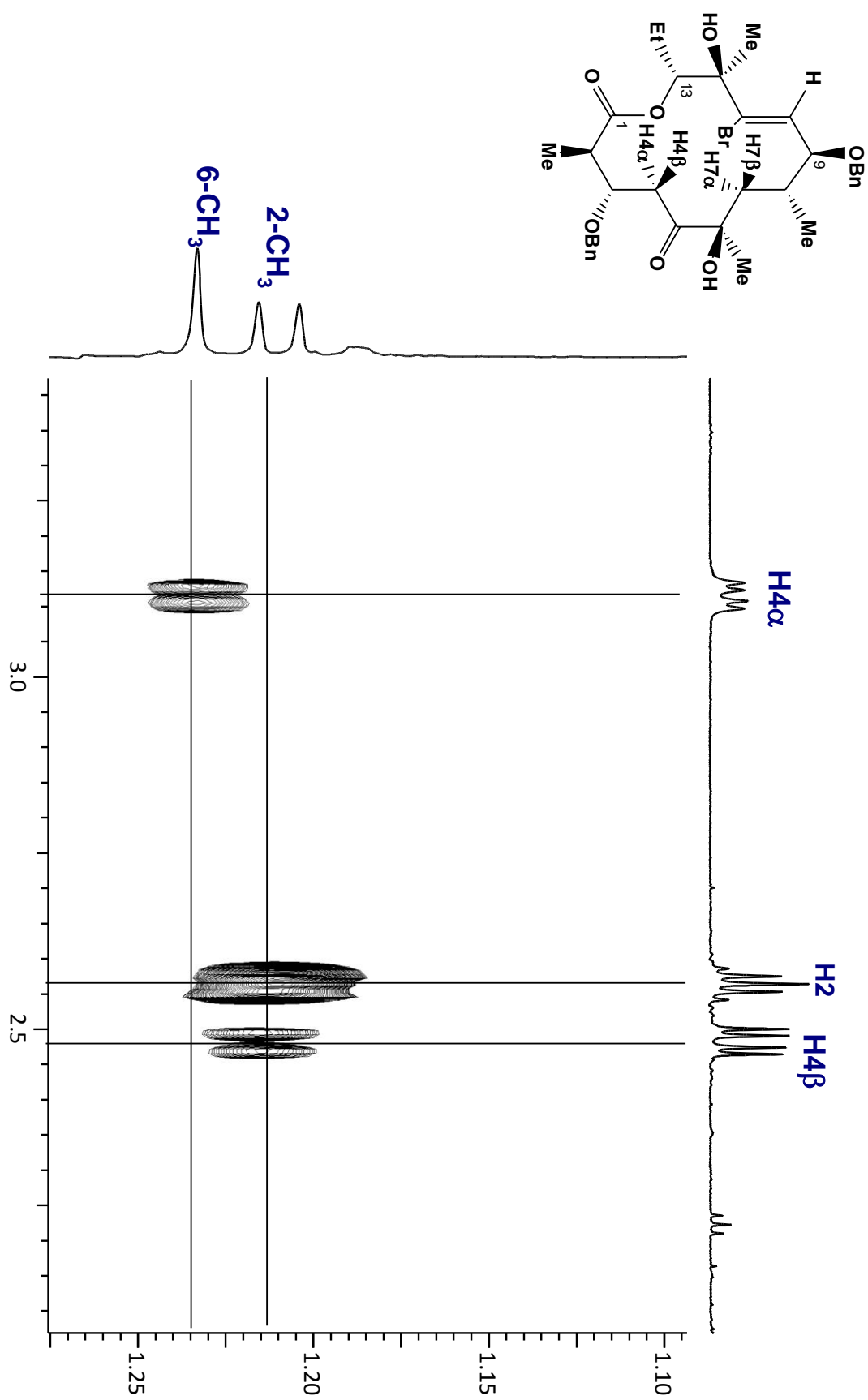
^{13}C NMR spectrum

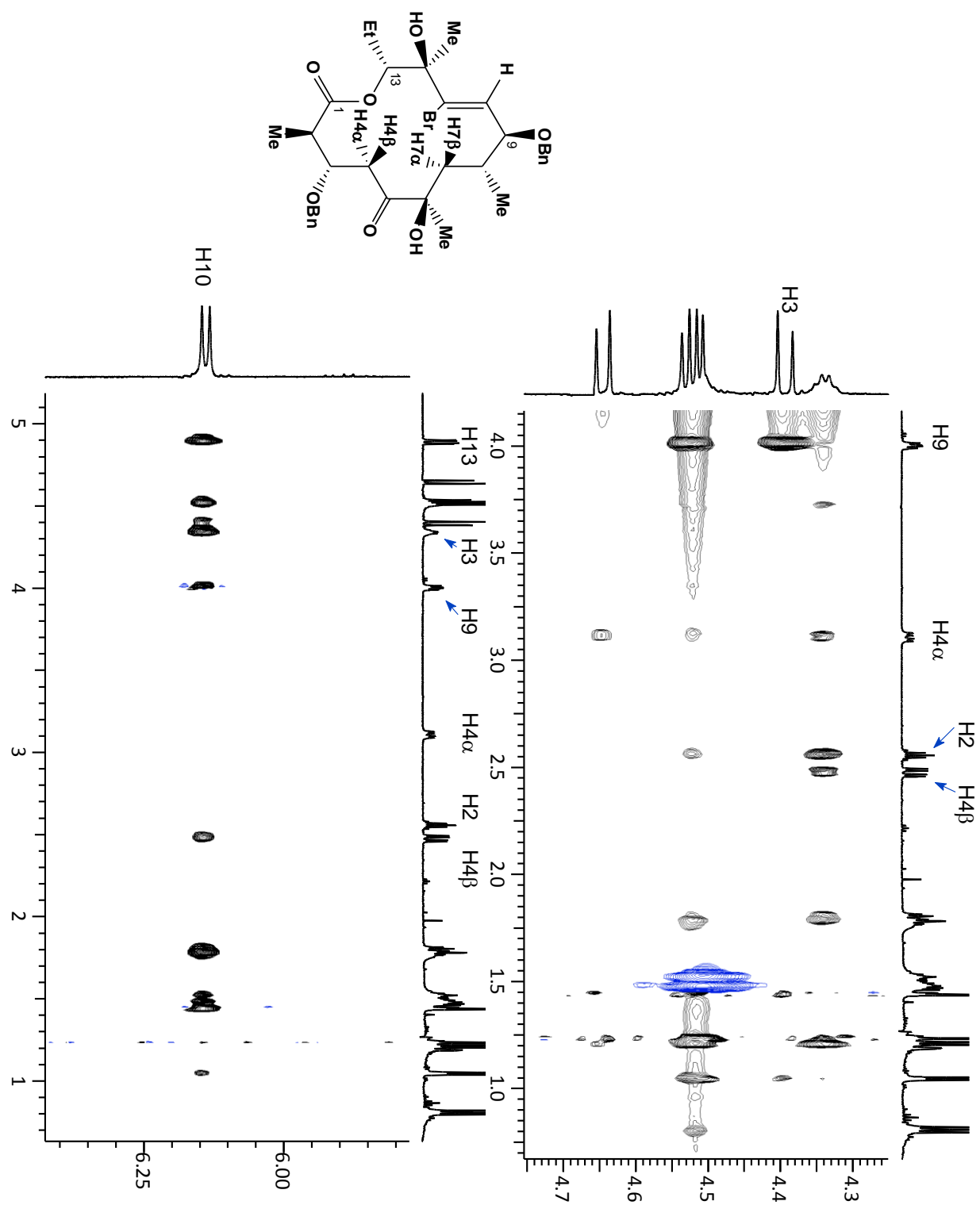
^{13}C NMR spectrum
expansions

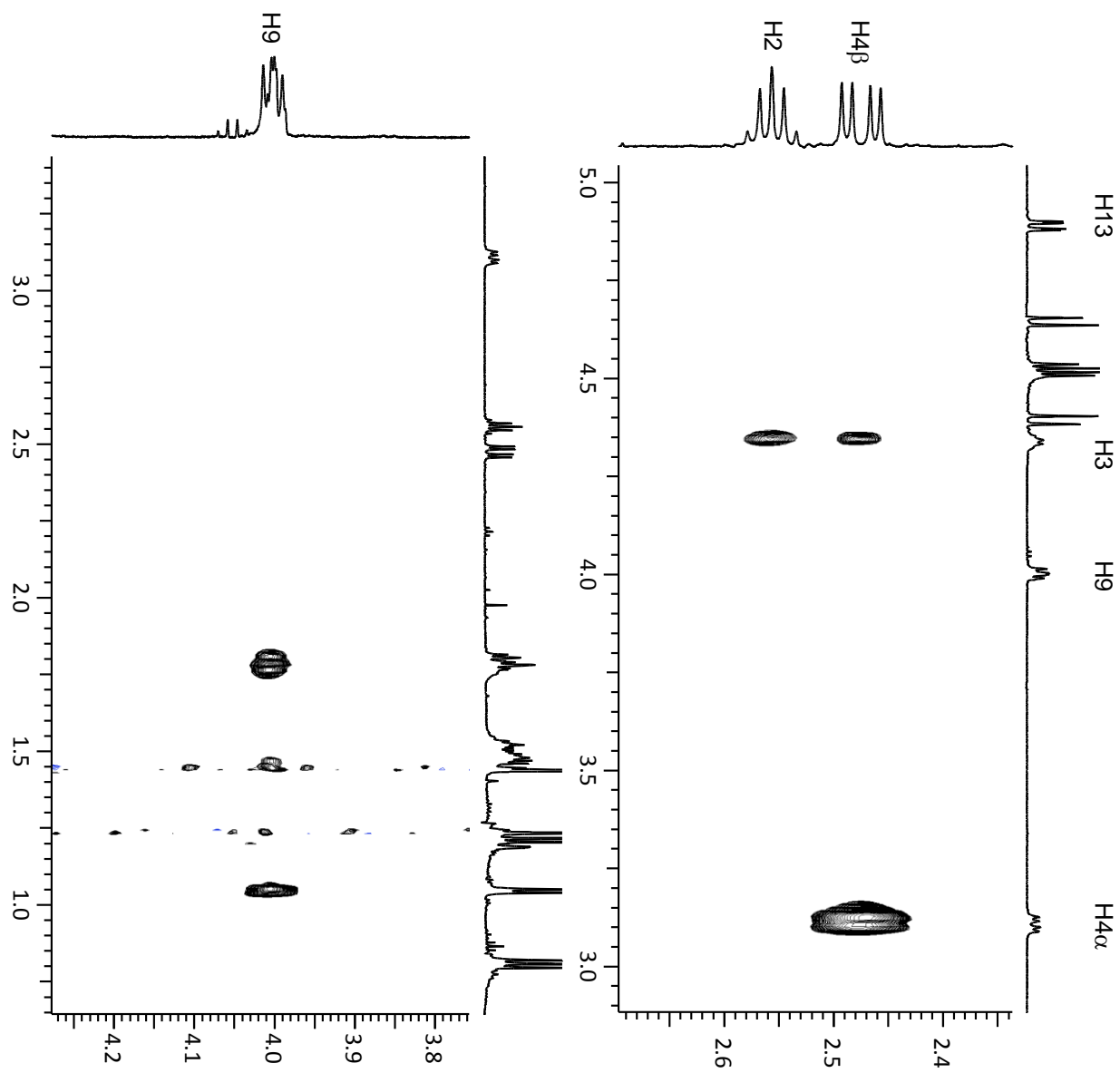
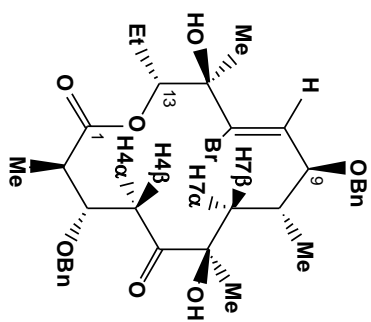


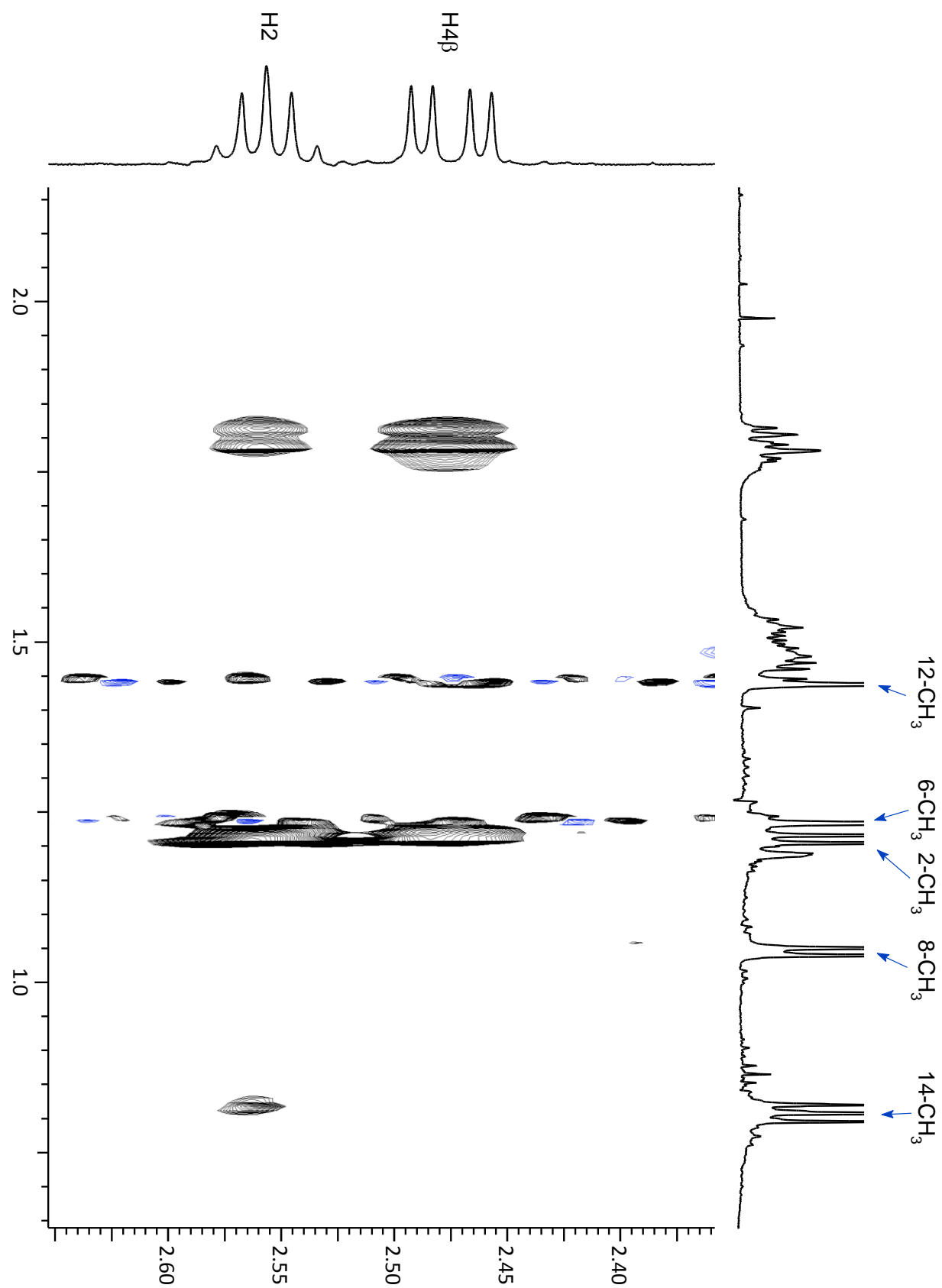
NOESY

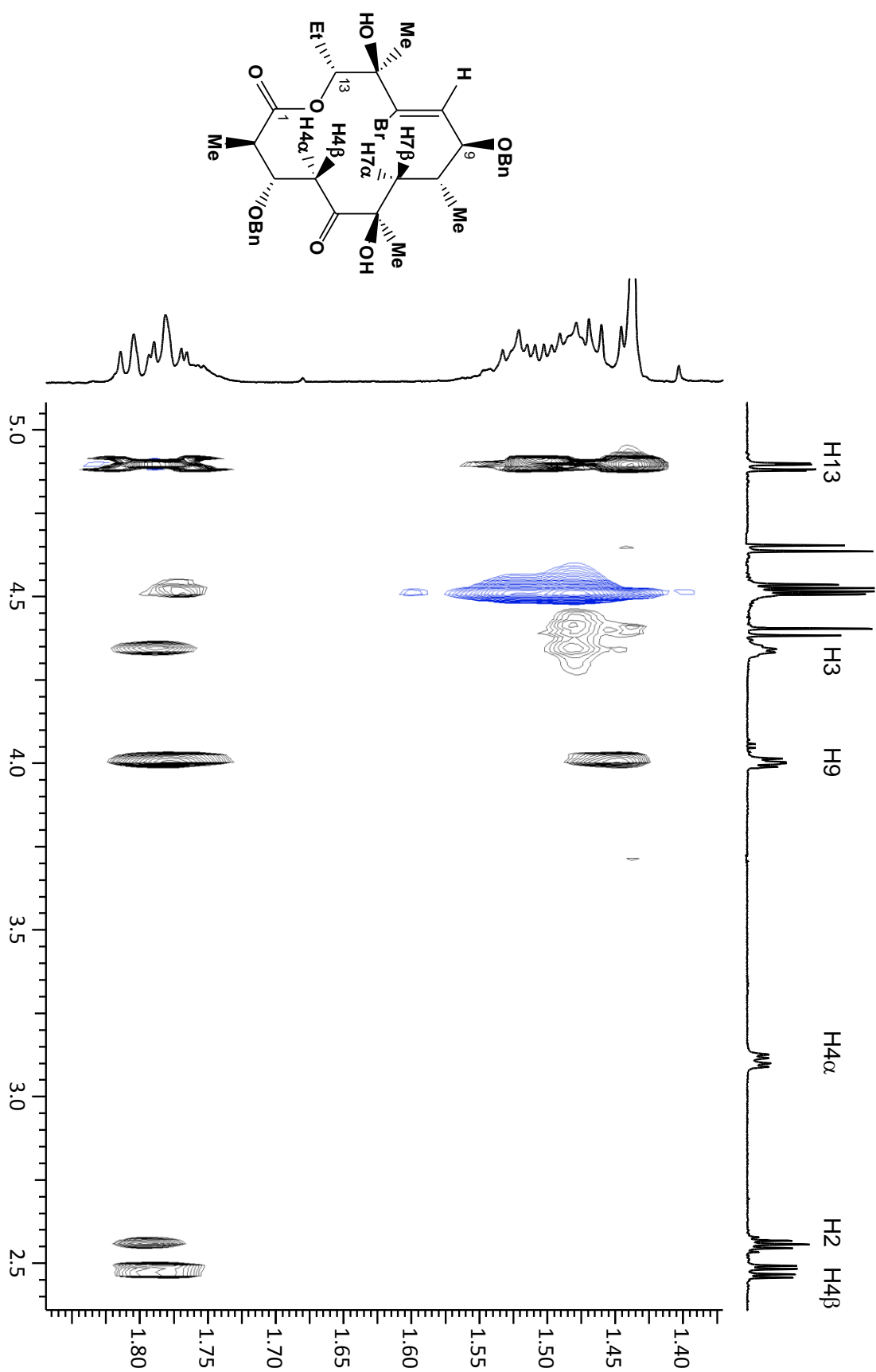


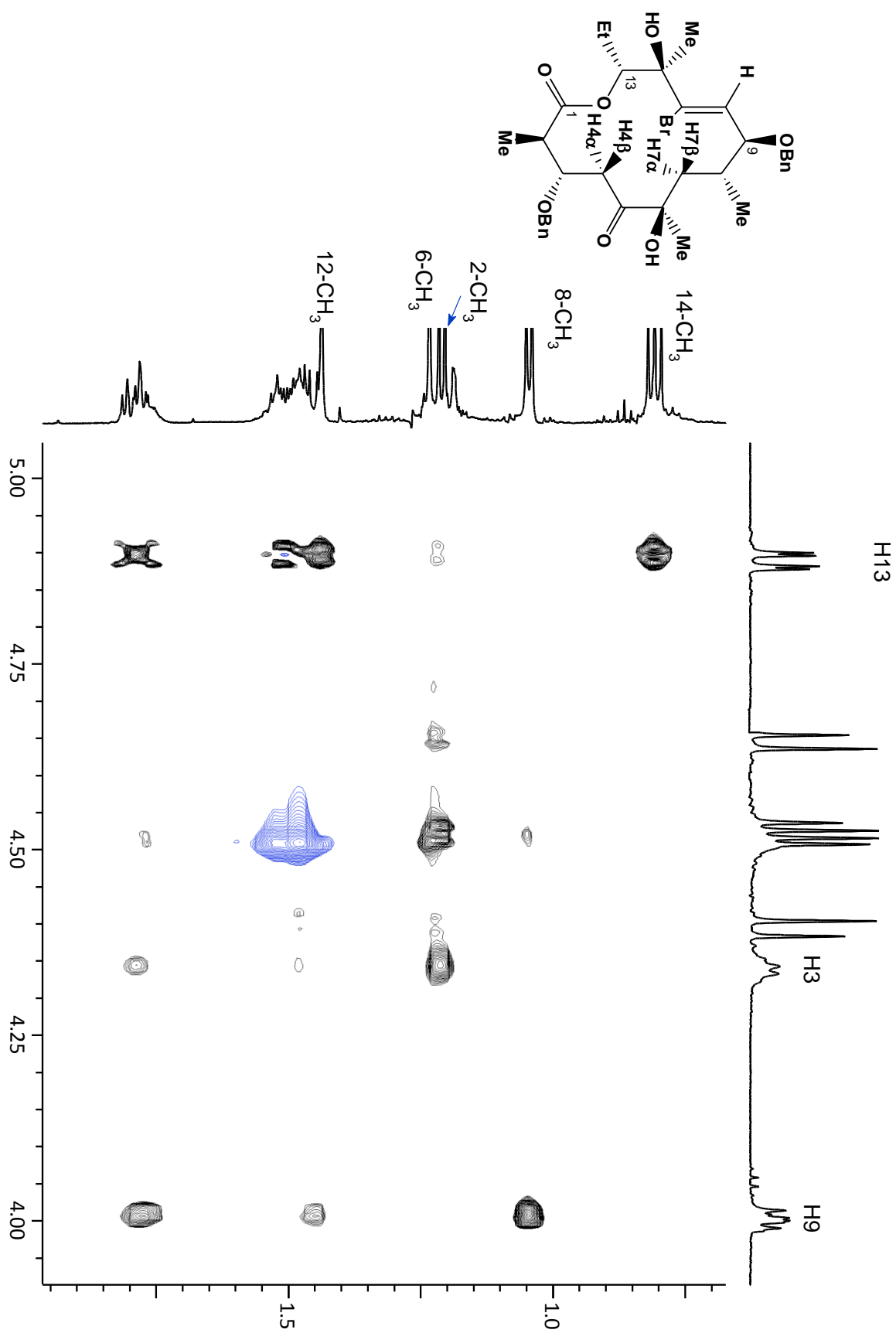


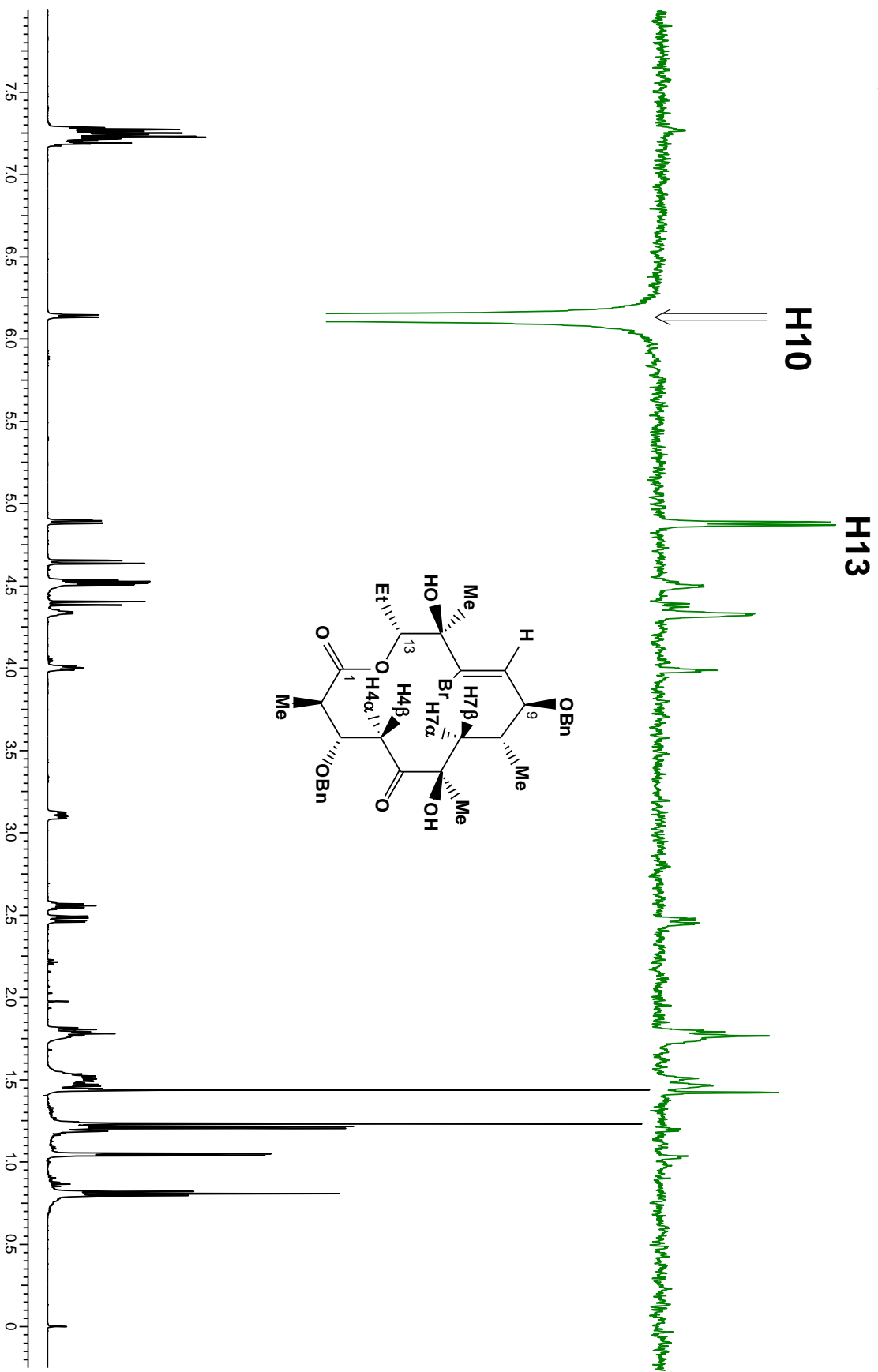




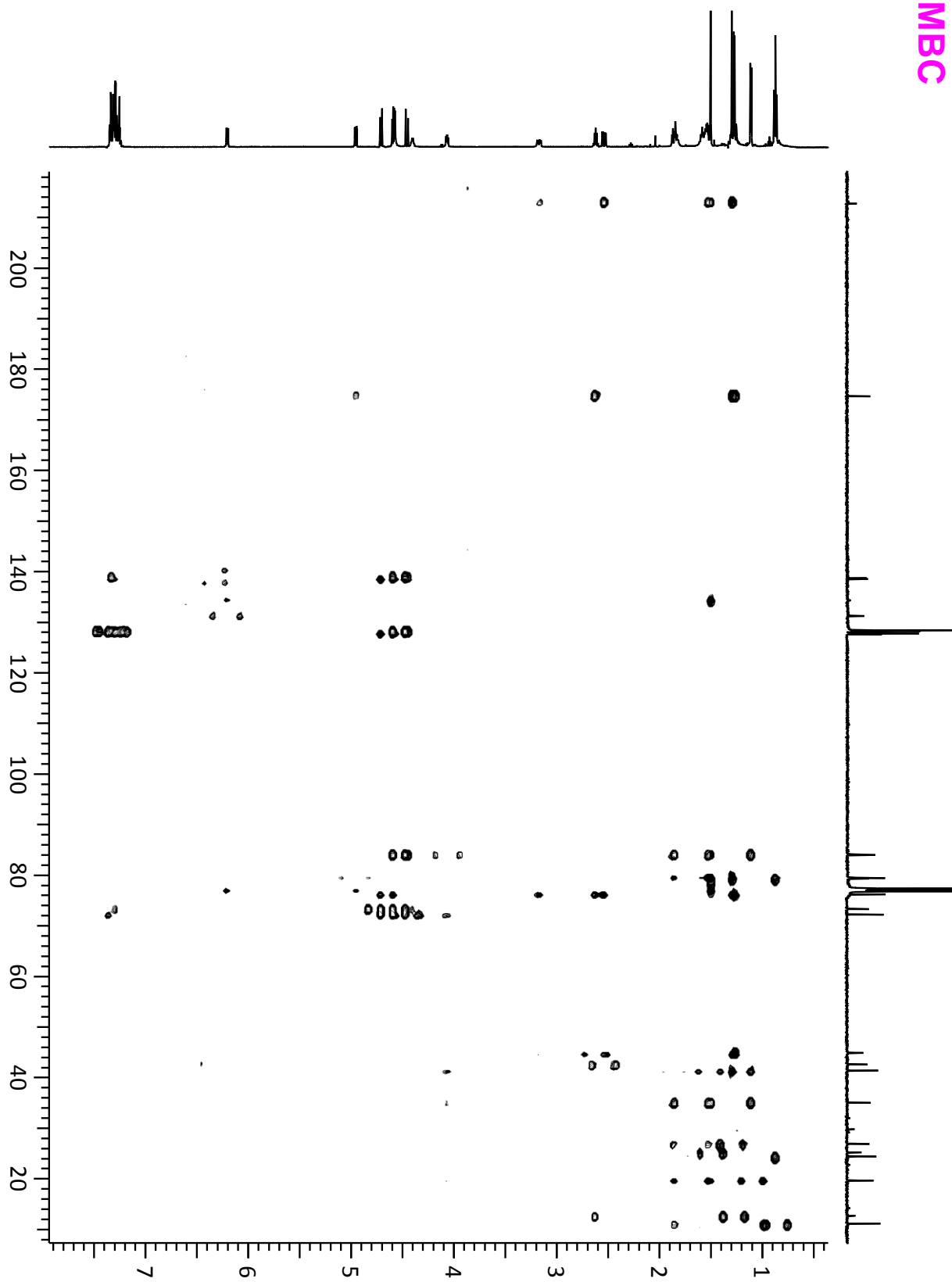


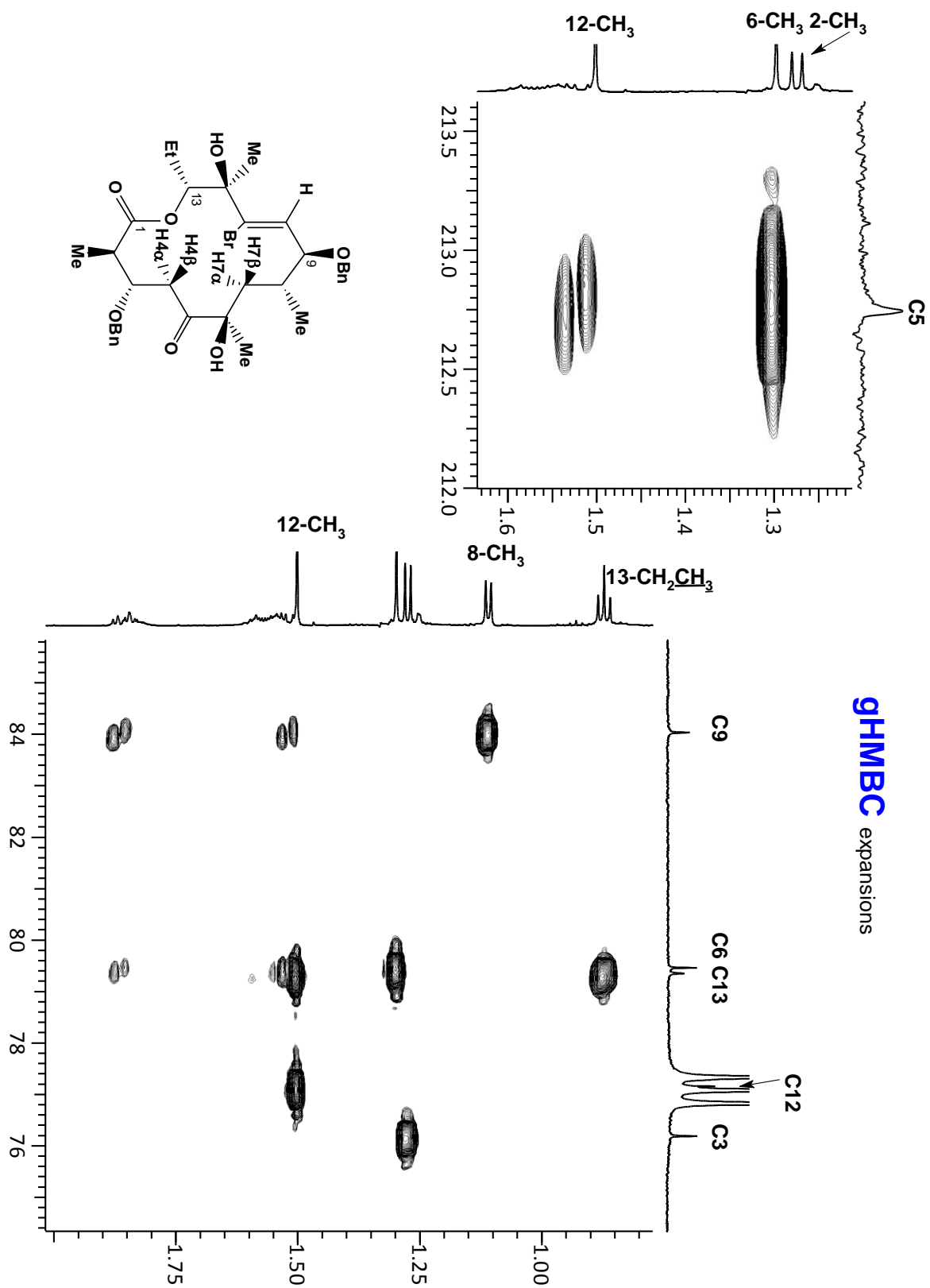


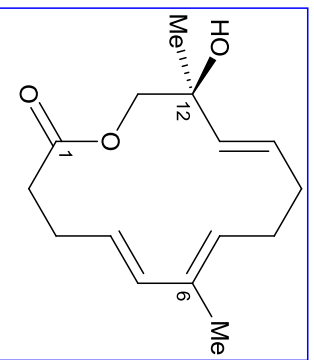




gHMBC

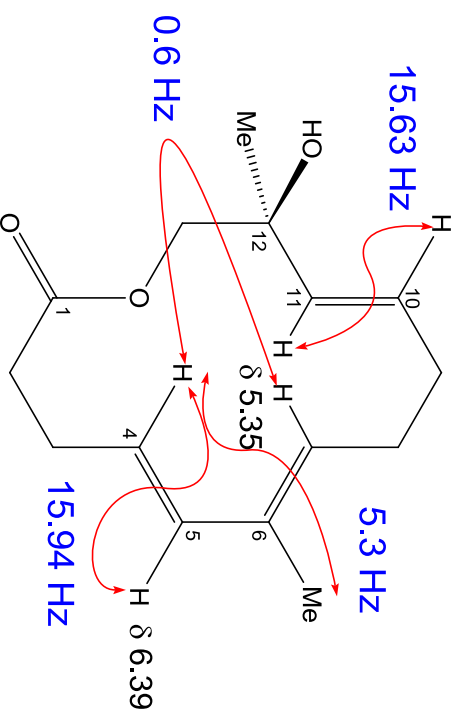




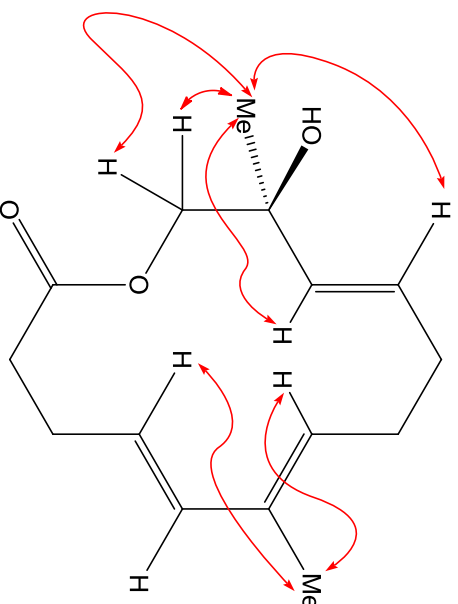


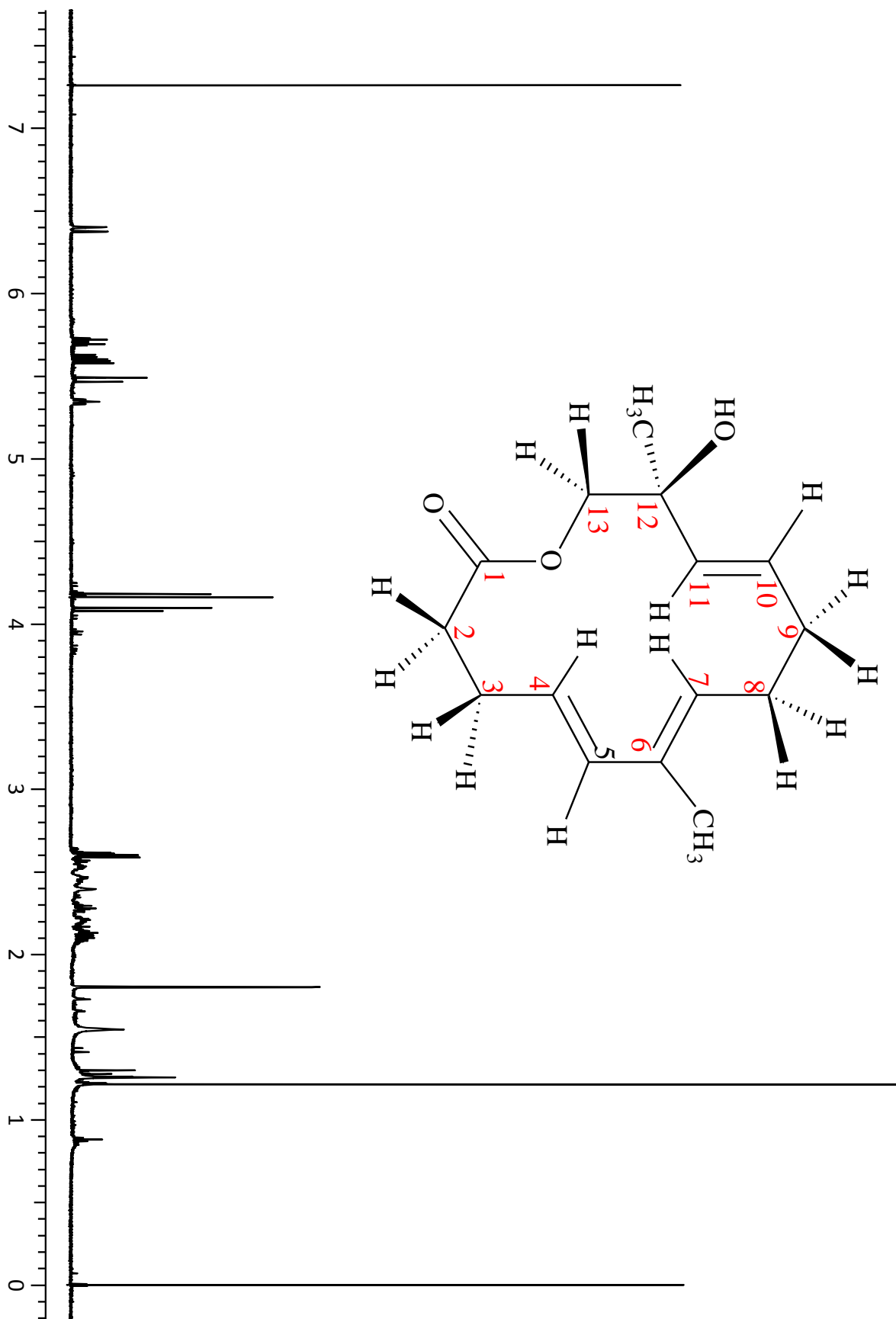
¹H NMR chemical shifts (δ/ppm) & coupling constant (J/Hz)	¹³C NMR chemical shift (δ/ppm)
2.64 - 2.55 (m, H2)	173.45 ---- C1
2.55 - 2.41 (m, H3)	32.33 ---- C2
5.69 (dtd, J_{H4, H5} = 15.94Hz, J_{H4, 3-CH2} = 5.3Hz, J_{H4, H7} = 0.6Hz, H4)	26.96 ---- C3
6.39 (d = J_{H5, H4} = 15.94Hz, H5)	126.70 ---- C4
1.80 (s, 6-CH₃)	127.62 ---- C5
5.35 (t, J_{H7, H8} = 8.64Hz, H7)	133.28 ---- C6
2.33 - 2.17 (m, H8)	127.40 ---- C7
2.17 - 2.04 (m, H9)	27.62 ---- C8
5.59 (ddd, J_{H10, H11} = 15.63Hz, J_{H10, H9} = 7.03Hz, H10)	31.77 ---- C9
1.21 (s, 12-CH₃)	129.37 ---- C10
4.16 (d, ²J = 11.3 Hz, H13)	134.02 ---- C11
4.08 (d, ²J = 11.3 Hz, H13)	25.59 ---- C12
	70.76 ---- C13
	20.34 ---- 6-CH ₃
	25.59 ---- 12-CH ₃

Coupling constant



NOESY





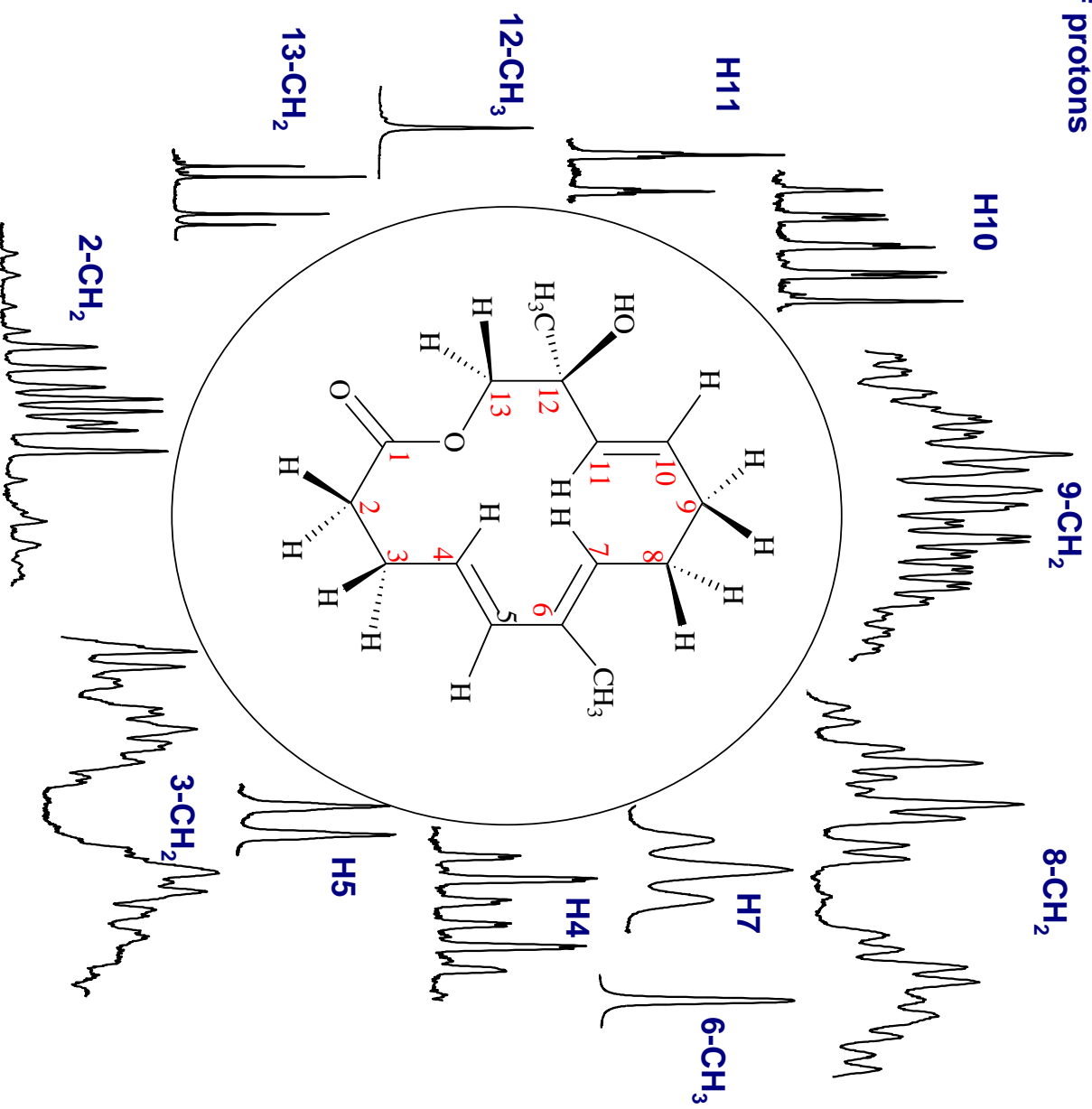
Multiplicity patterns of protons

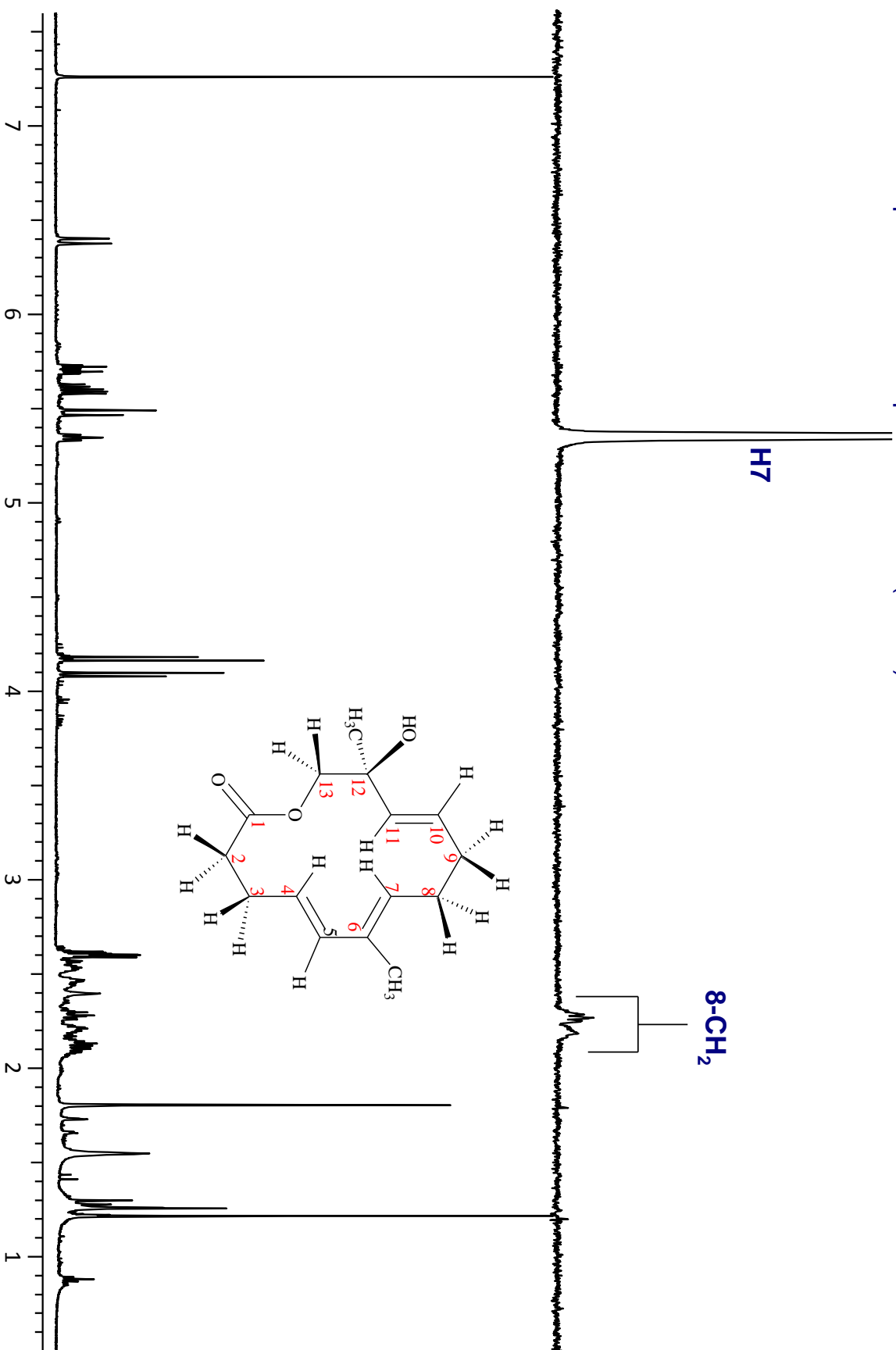
$$^3J(\text{H}_4, \text{H}_5) = 15.94 \text{ Hz}$$

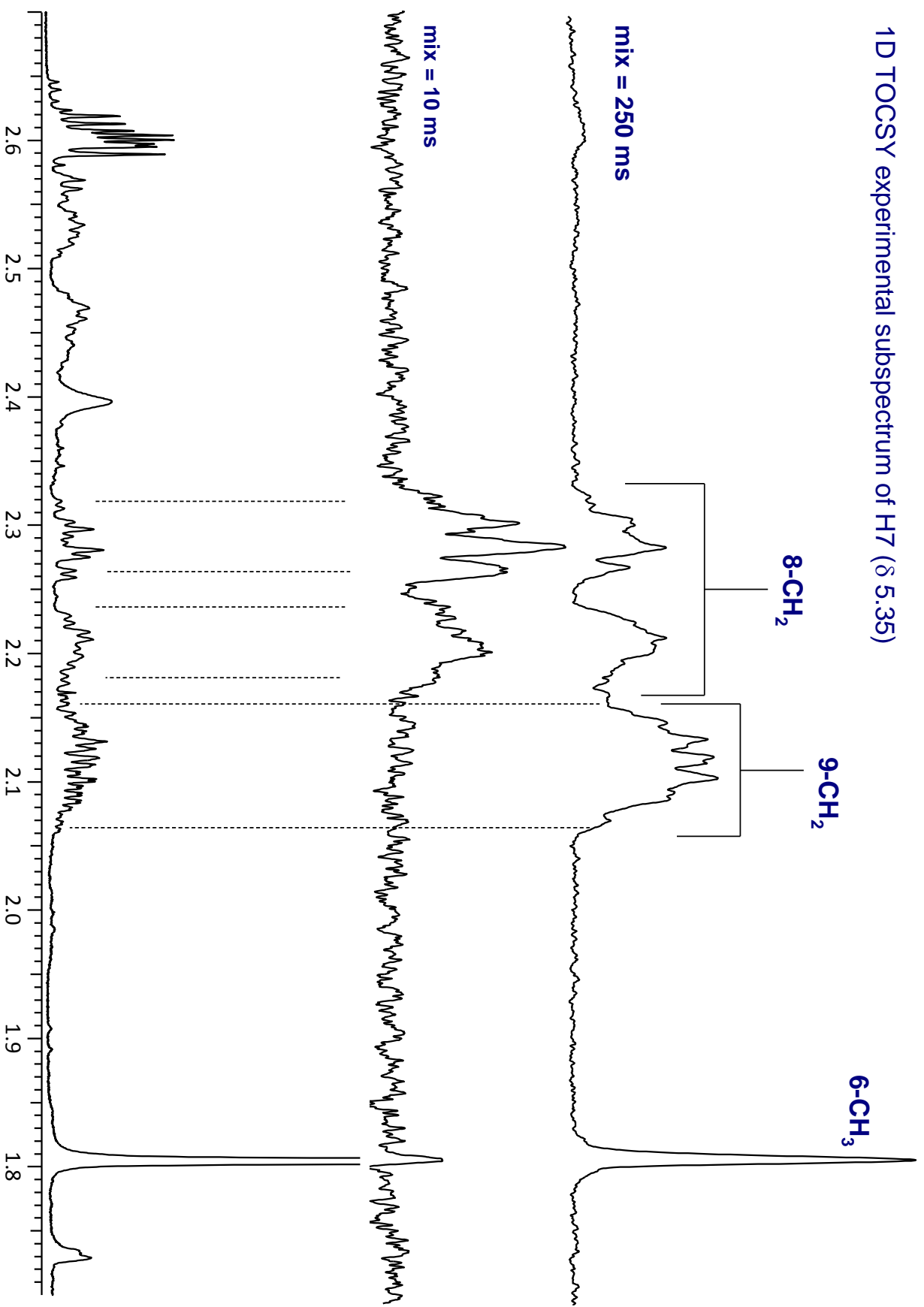
$$^3J(\text{H}_4, 3\text{-CH}_2) = 5.3 \text{ Hz}$$

$$^5J(\text{H}_4, \text{H}_7) = 0.6 \text{ Hz}$$

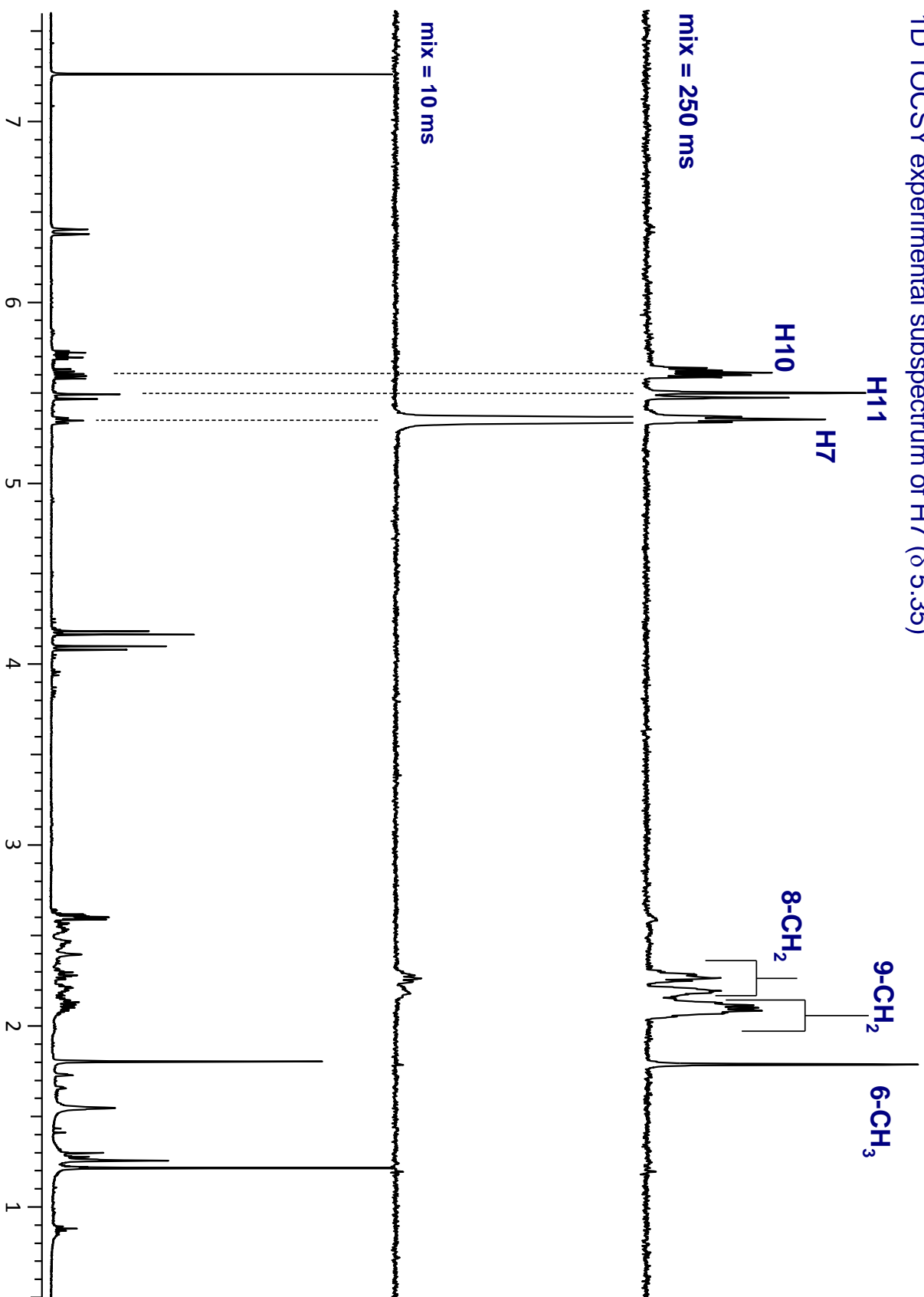
$$^3J(\text{H}_{10}, \text{H}_{11}) = 15.63 \text{ Hz}$$



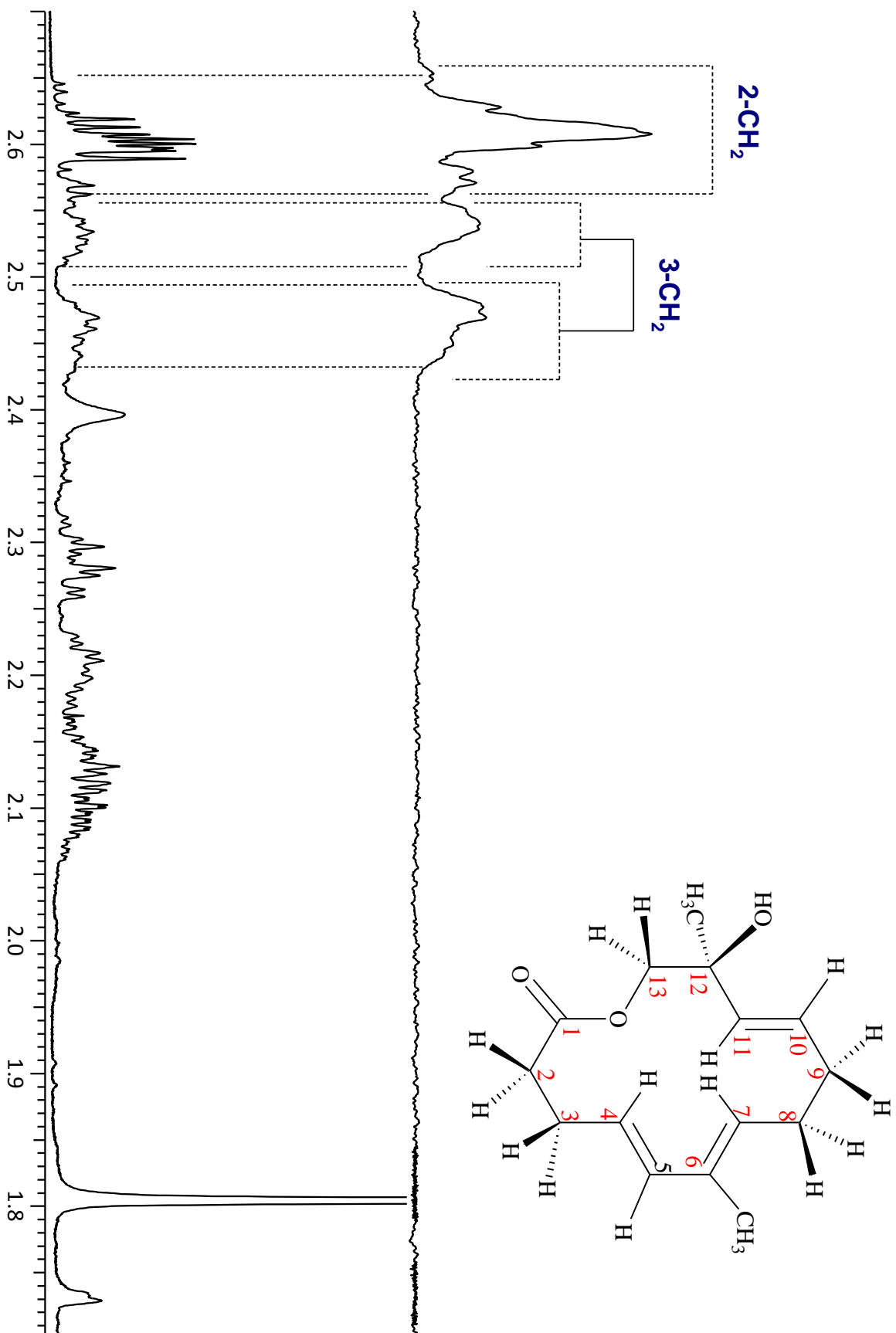


1D TOCSY experimental subspectrum of H7 (δ 5.35)

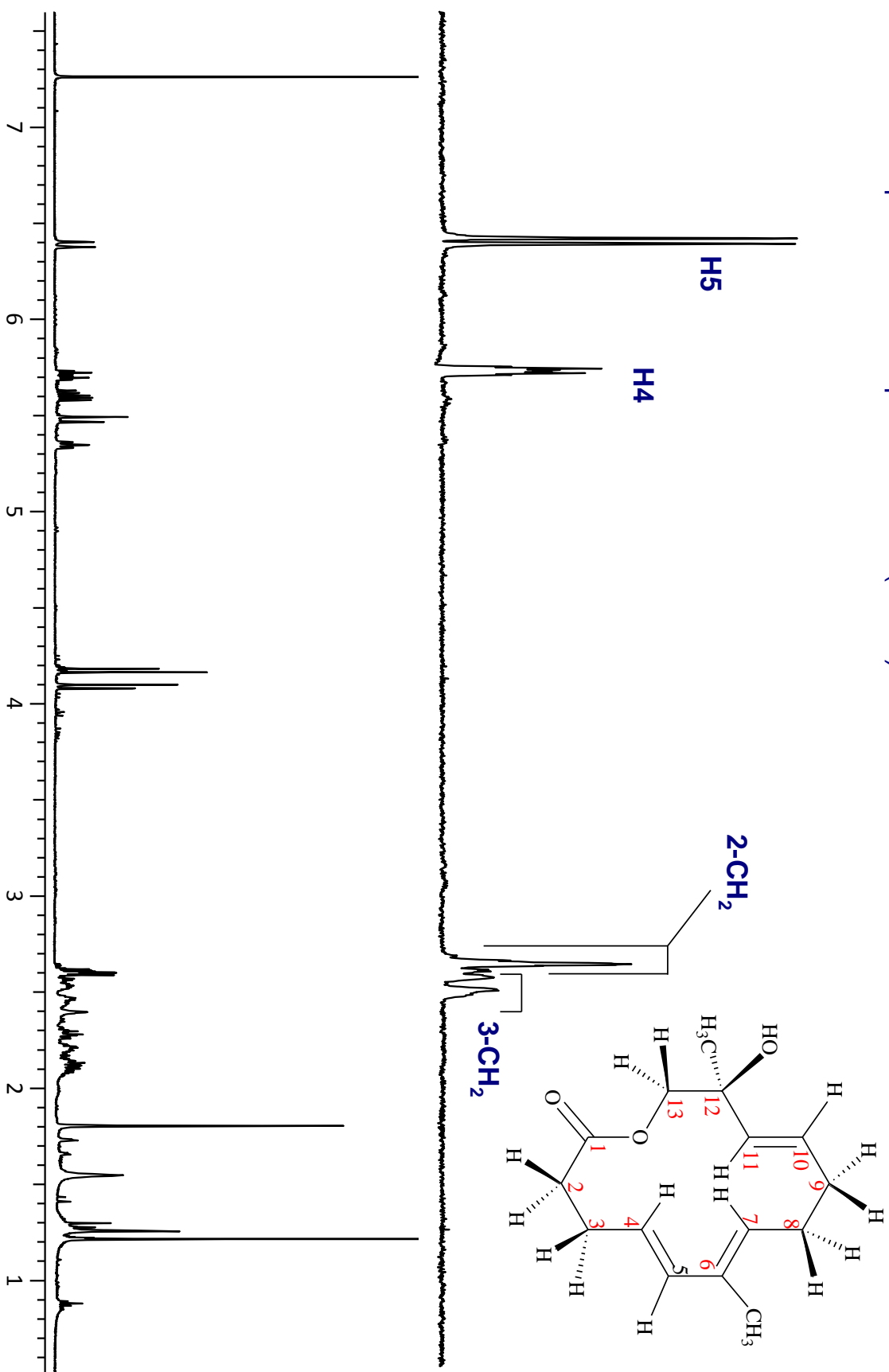
1D TOCSY experimental subspectrum of H7 (δ 5.35)

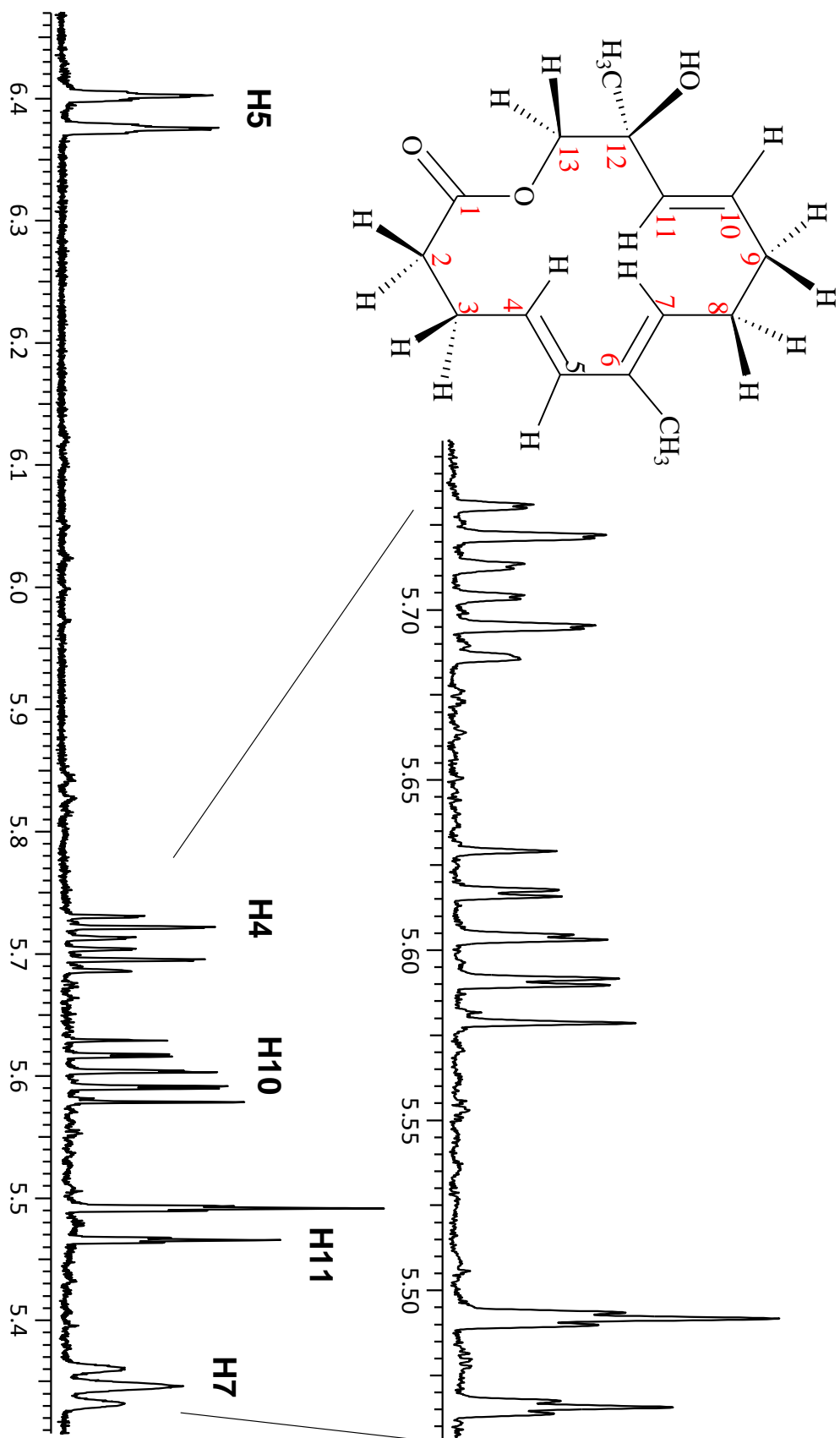


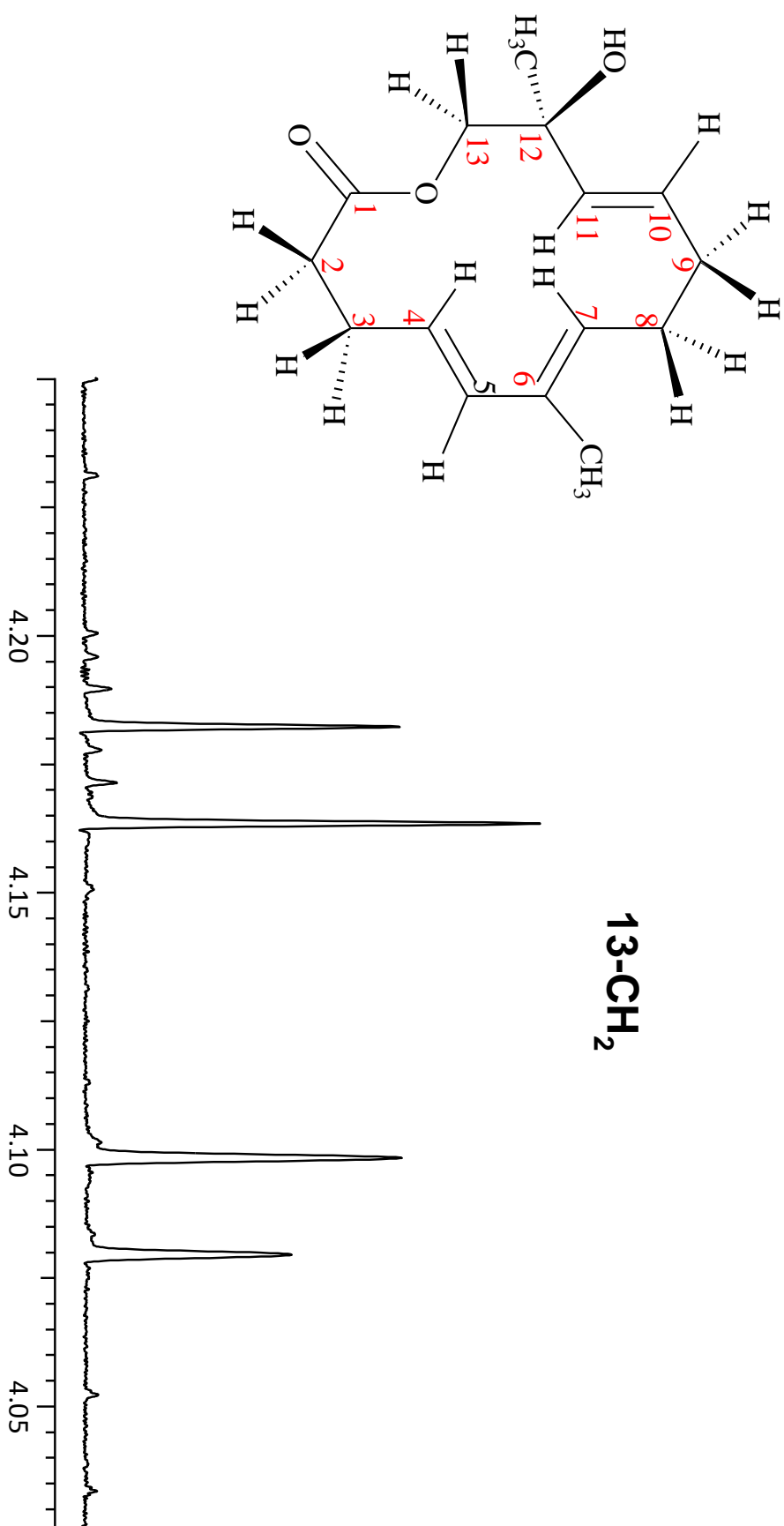
$1D$ TOCSY experimental subspectrum of H5 (δ 6.39)

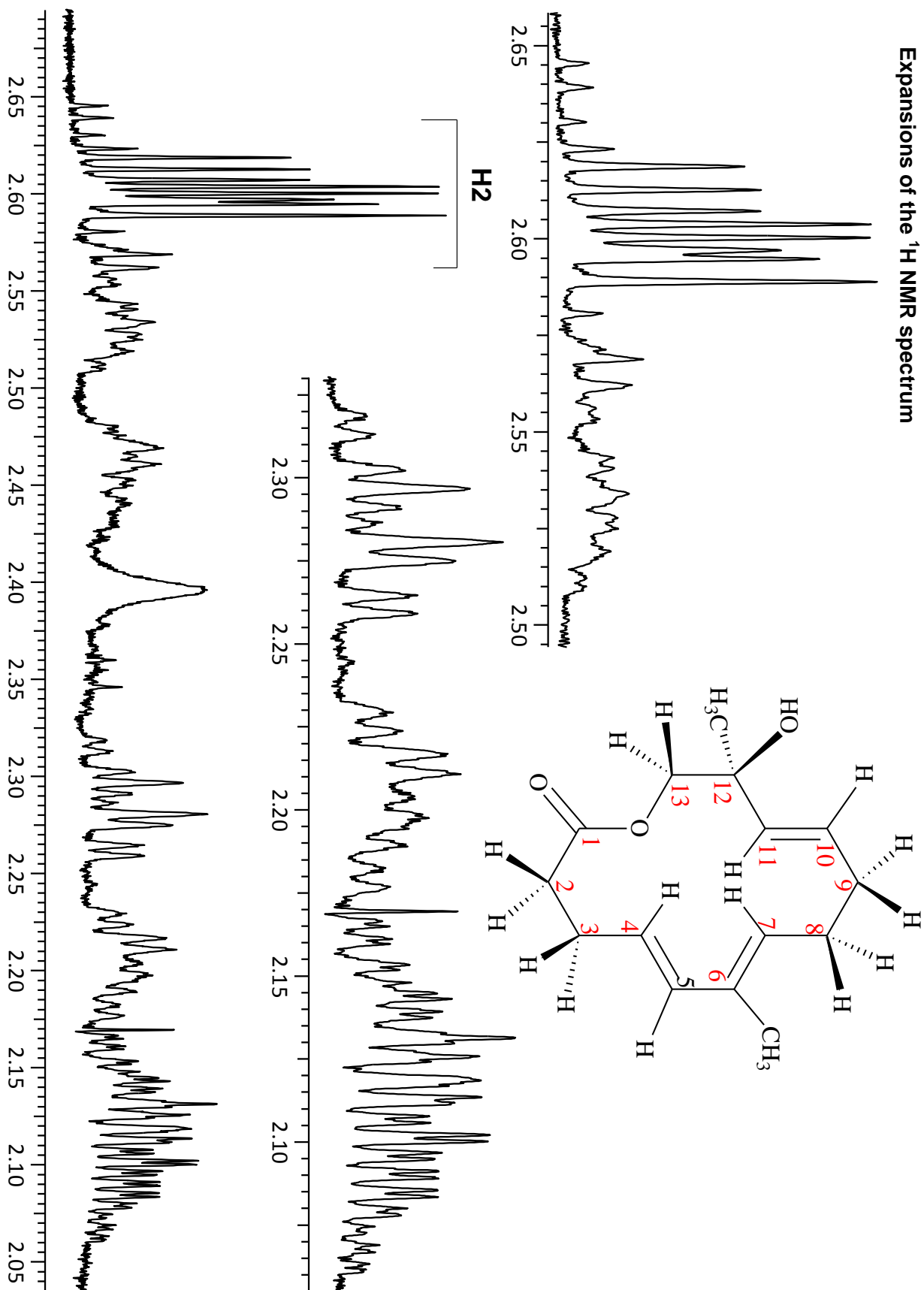


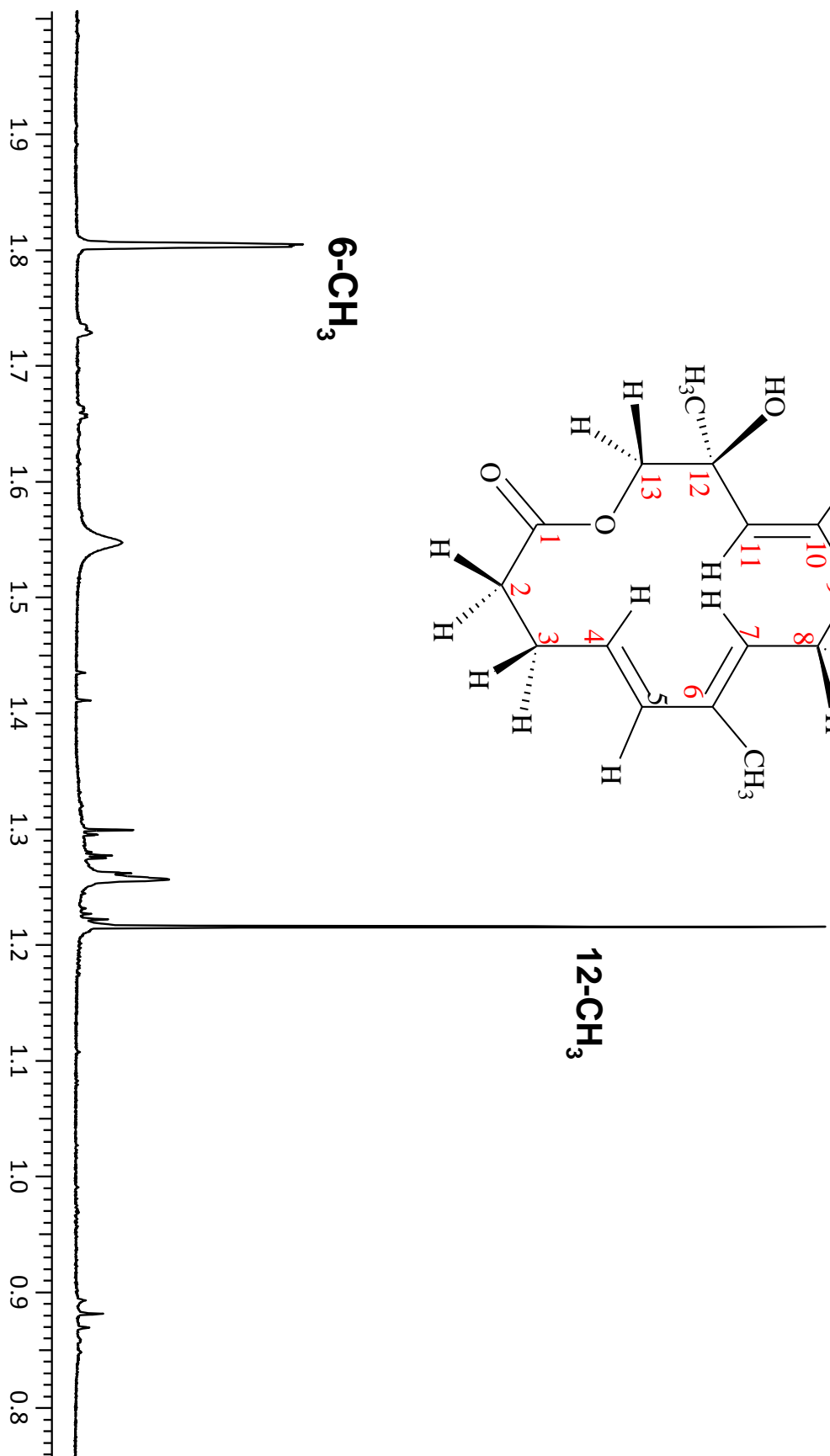
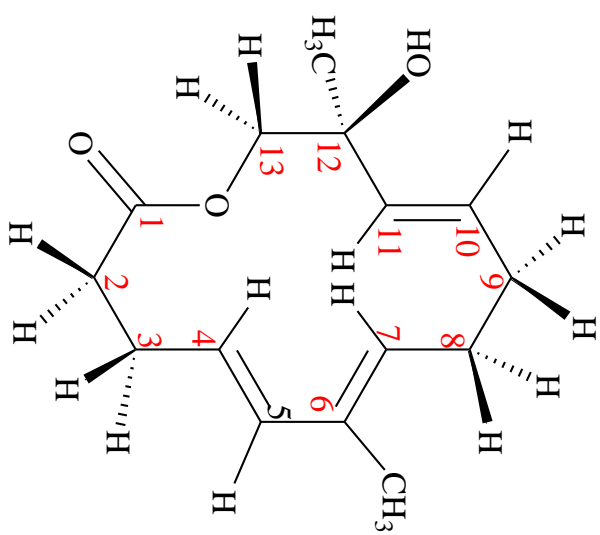
¹D TOCSY experimental subspectrum of H5 (δ 6.39)



Resolution enhanced ^1H NMR spectrum

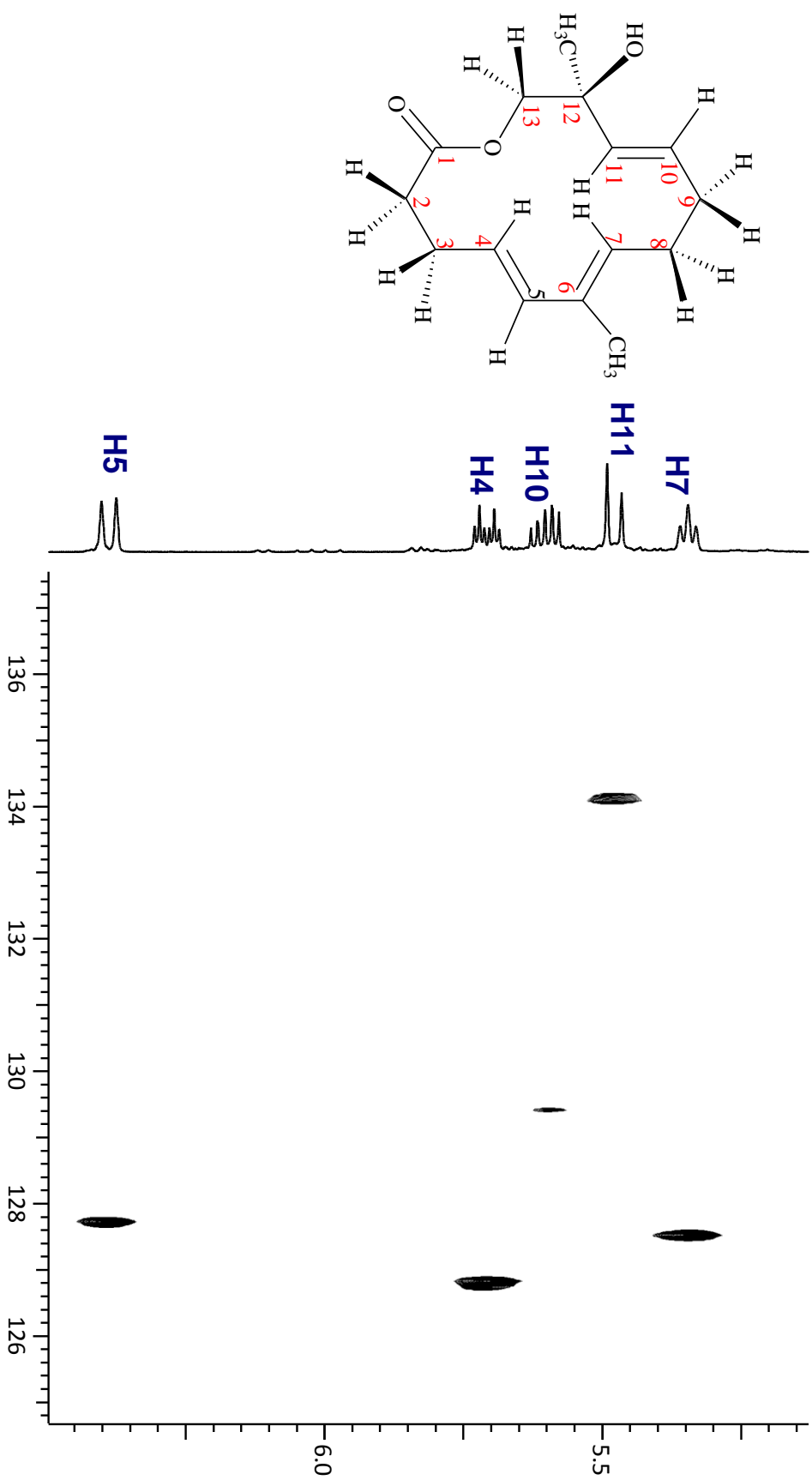


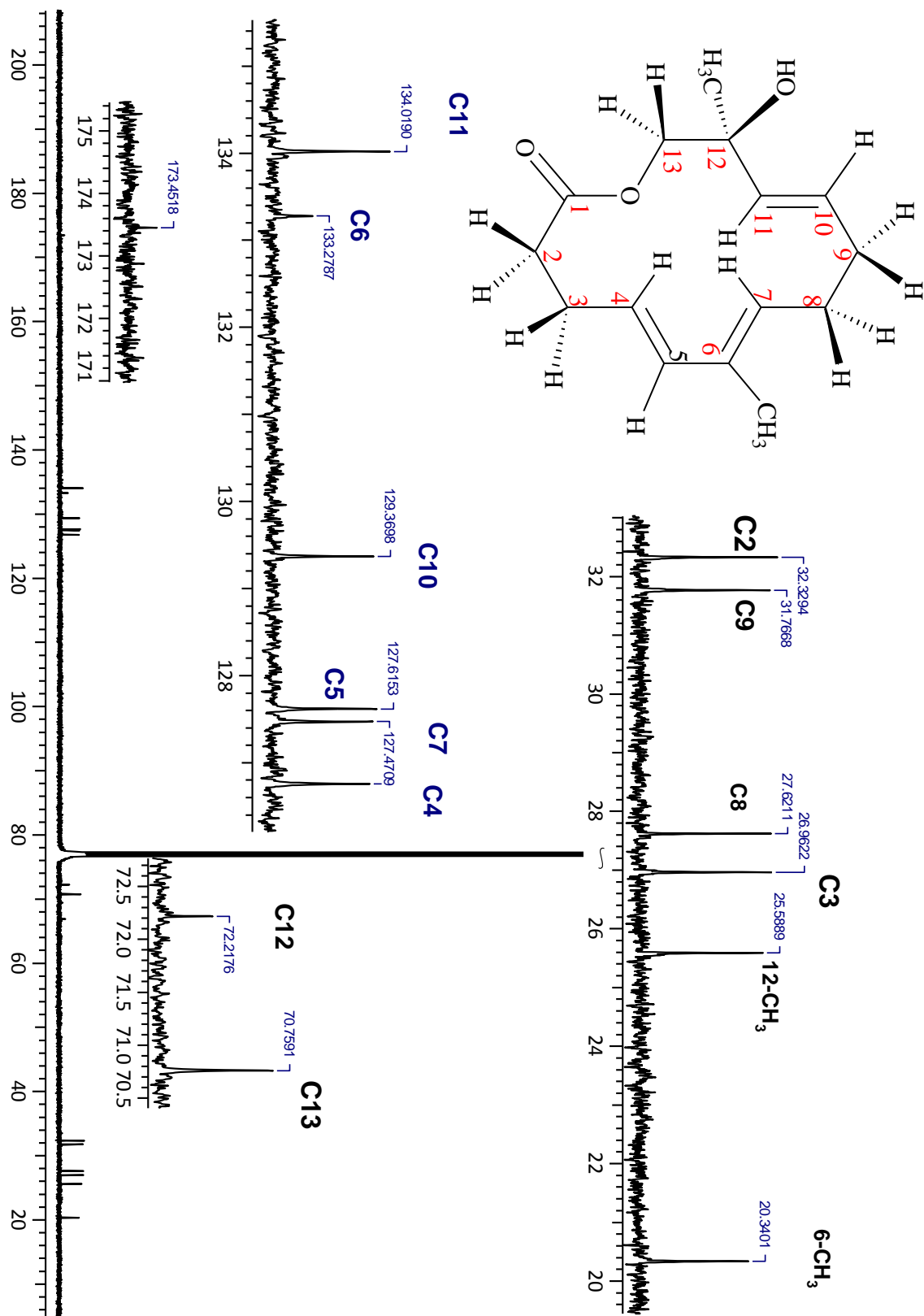
Expansions of the ^1H NMR spectrum



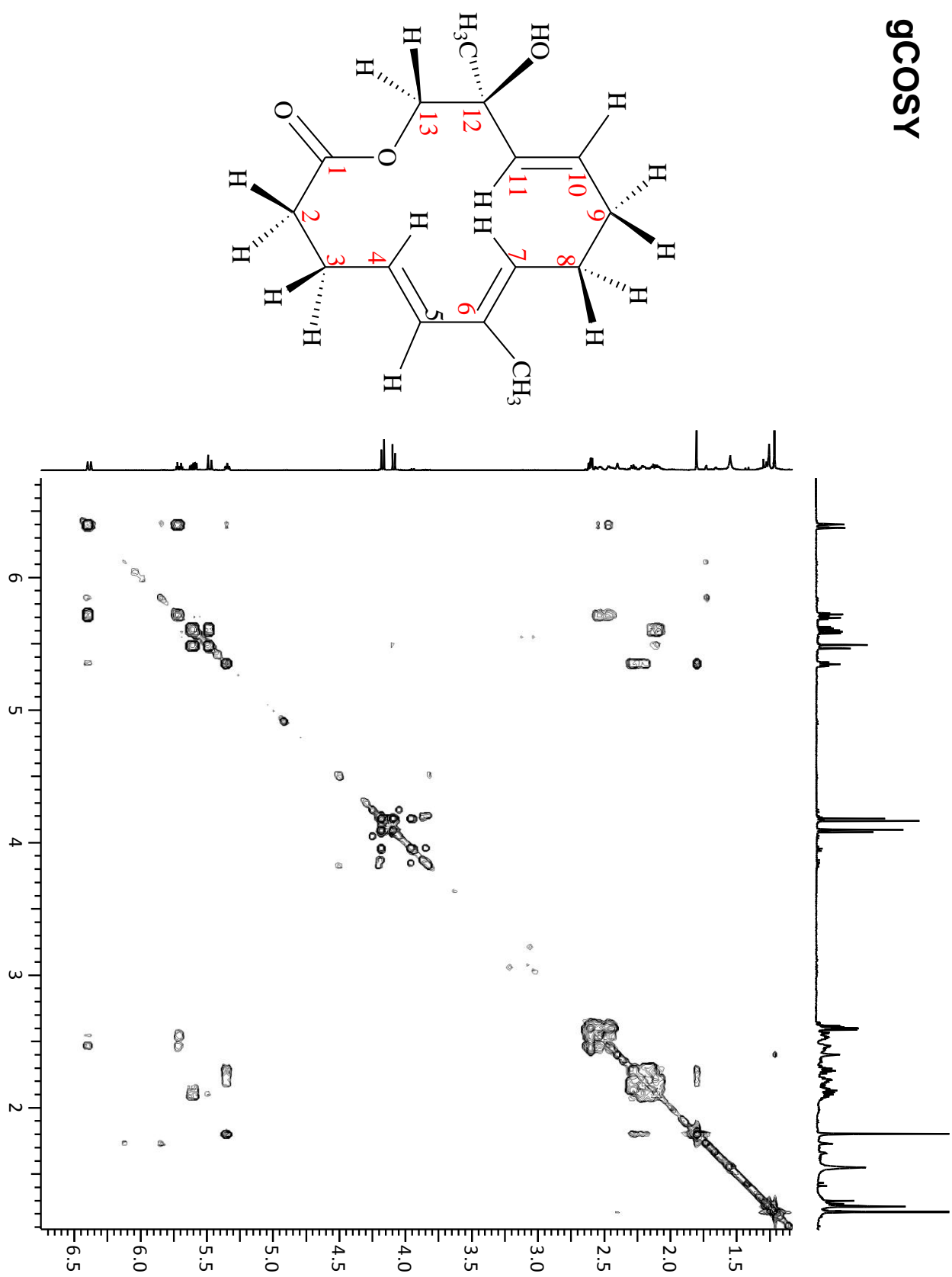
HETCOR

(aromatic region)

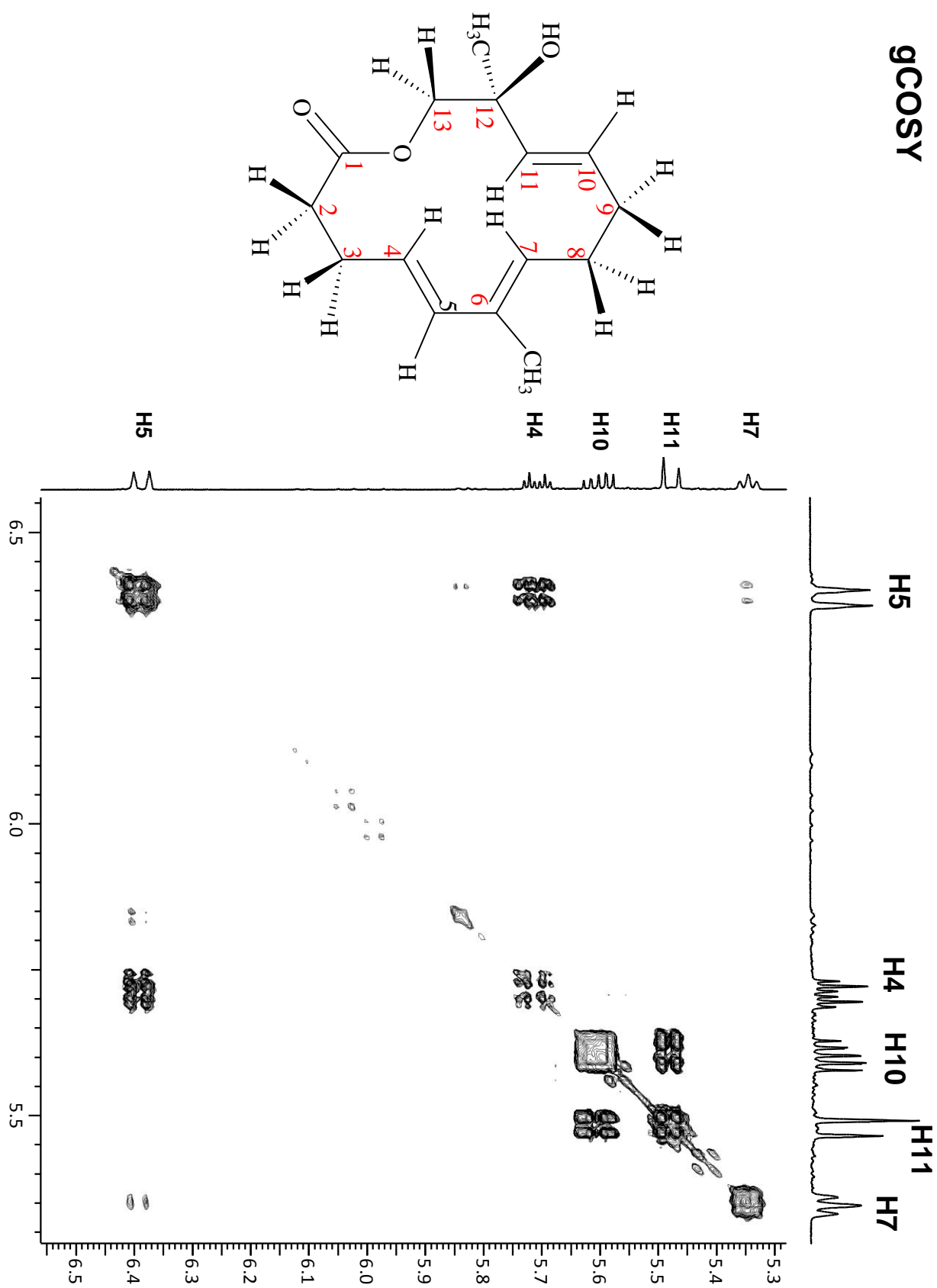




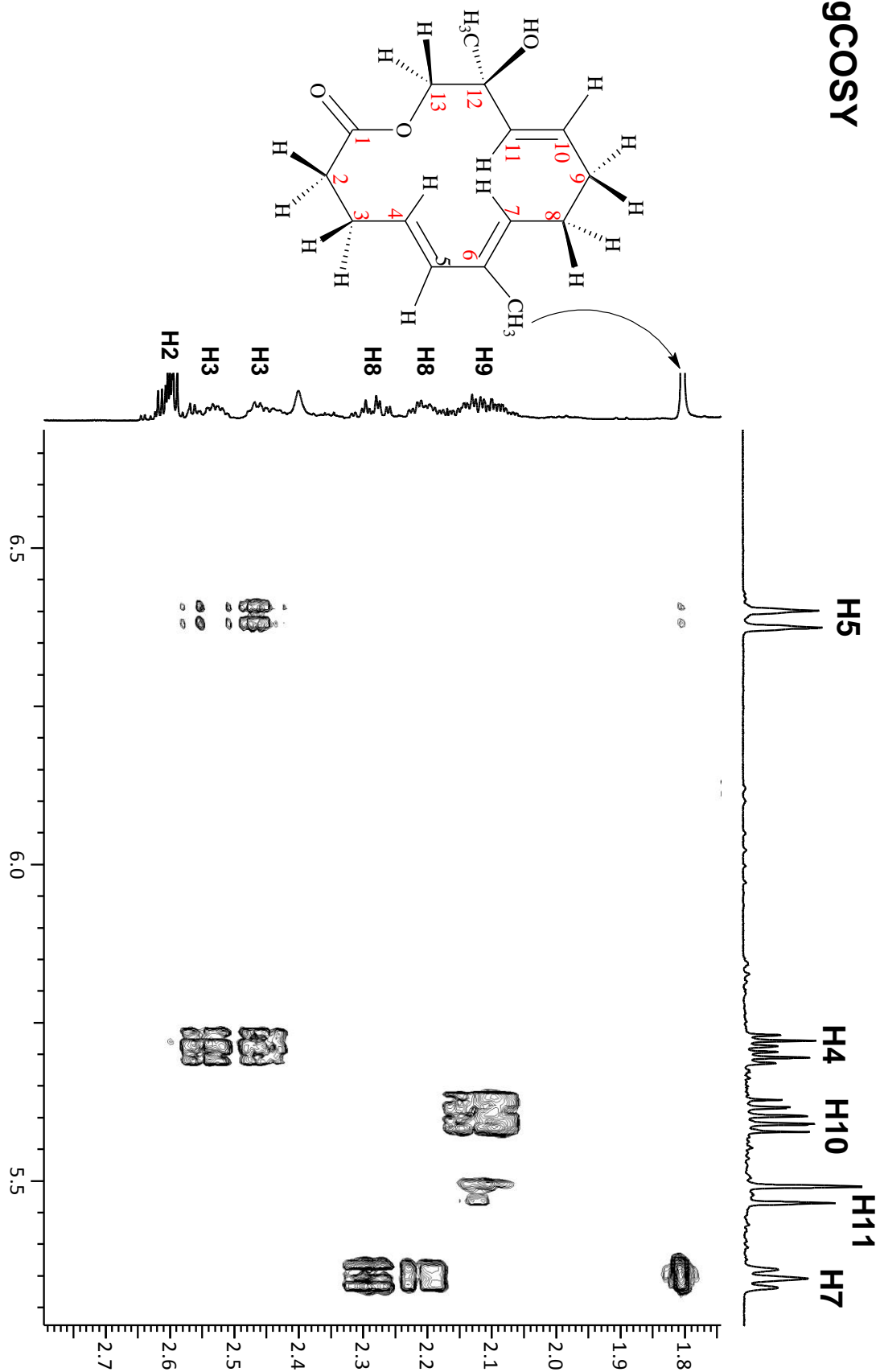
gCOSY



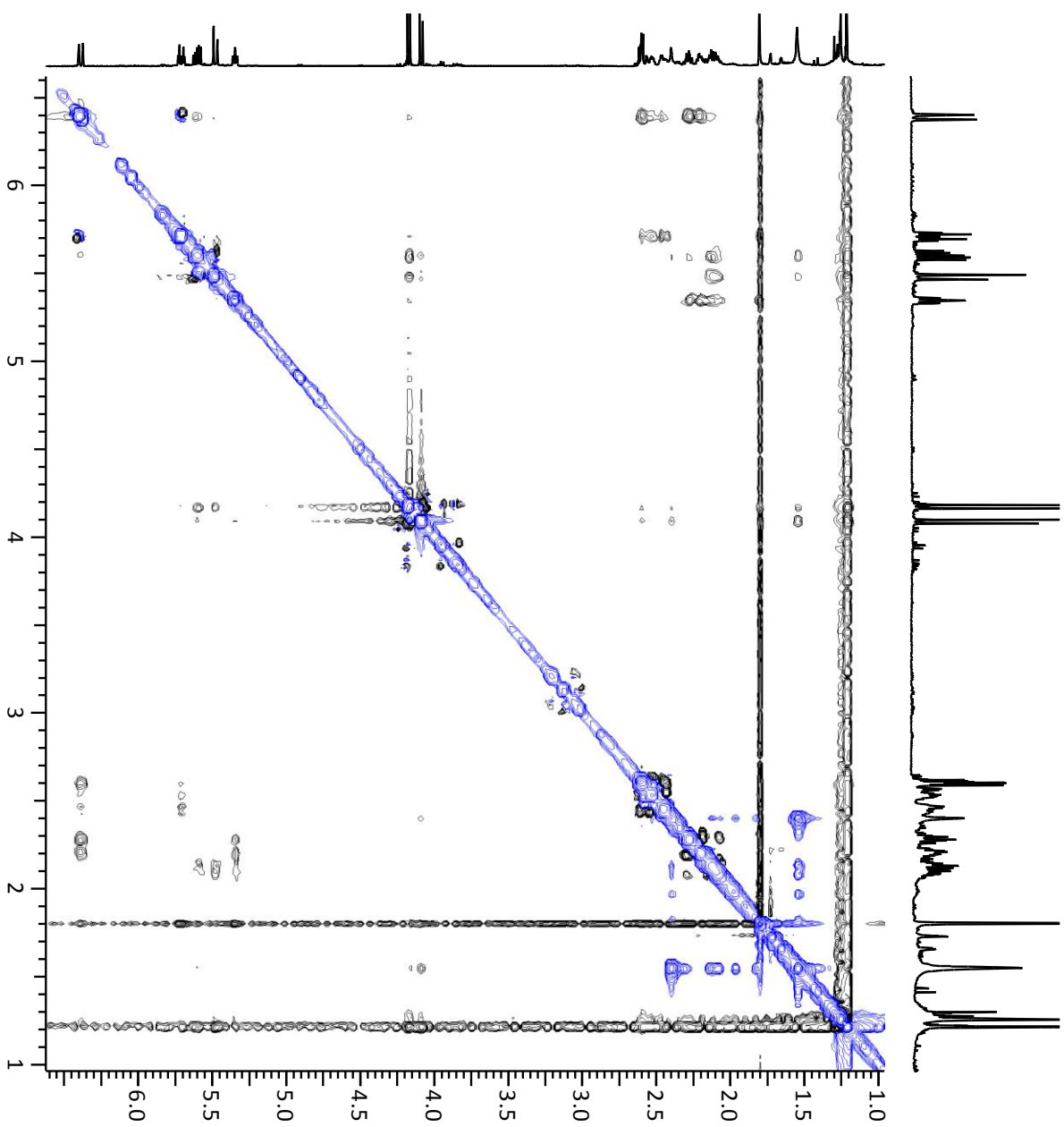
gCOSY



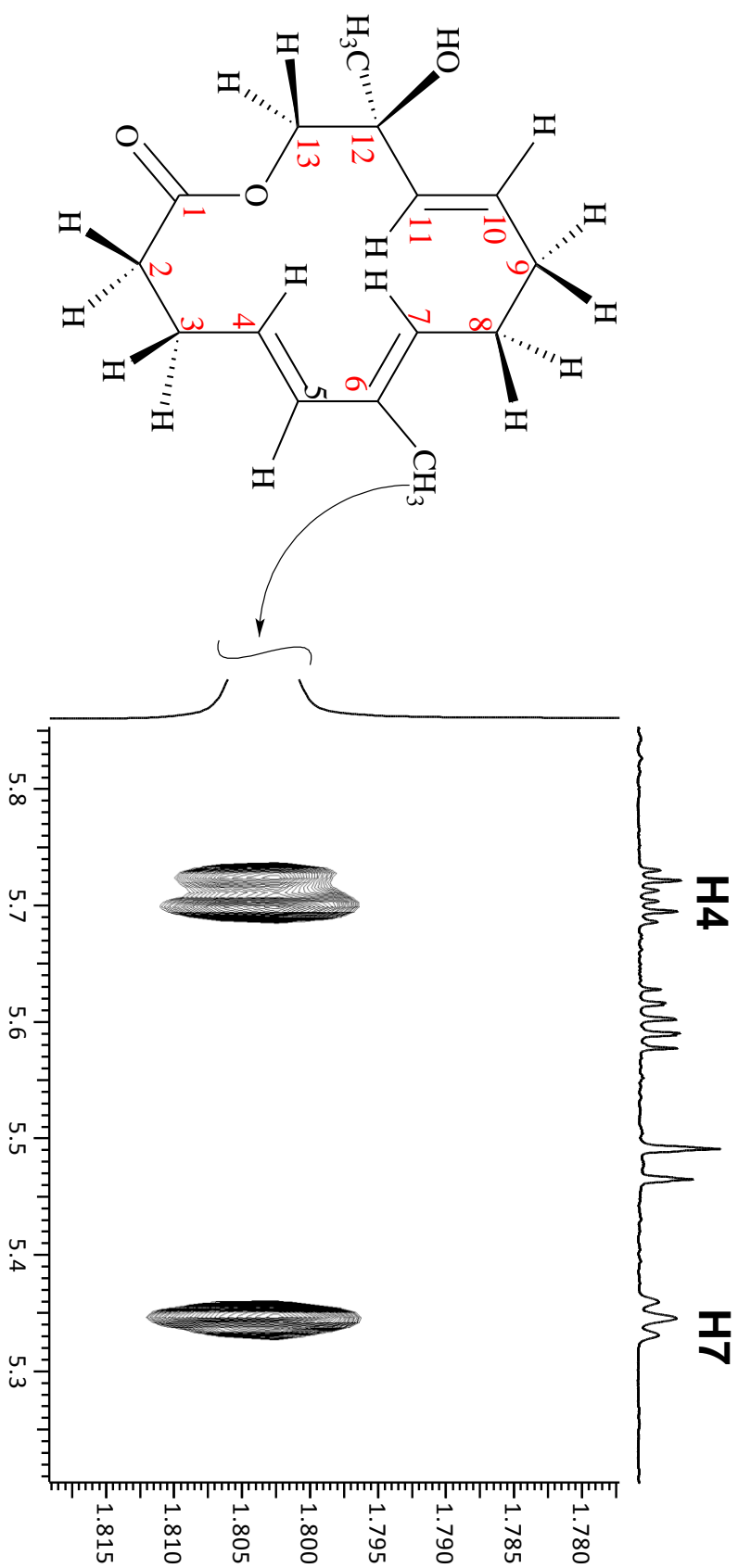
gcOSY



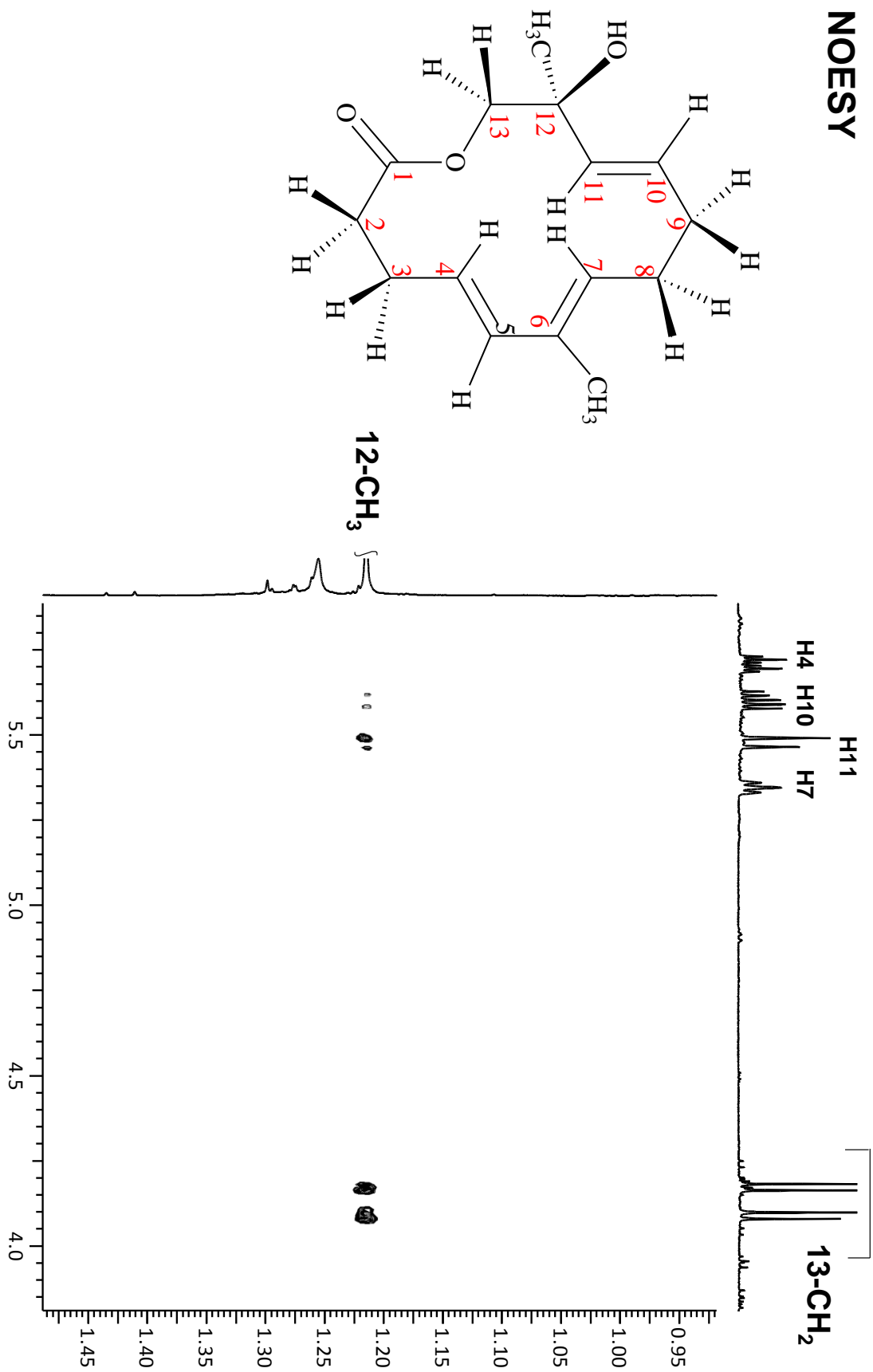
NOESY



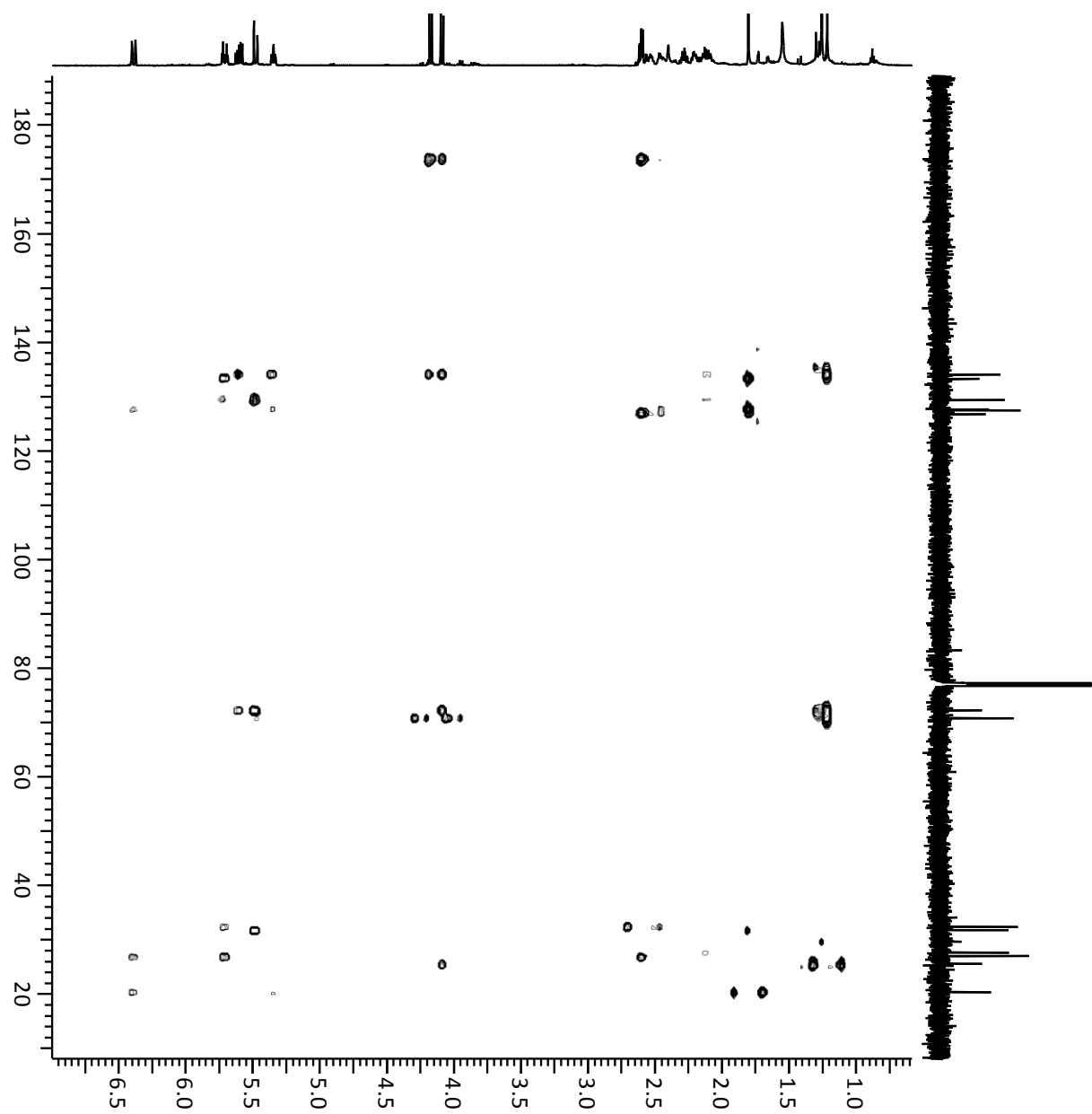
NOESY



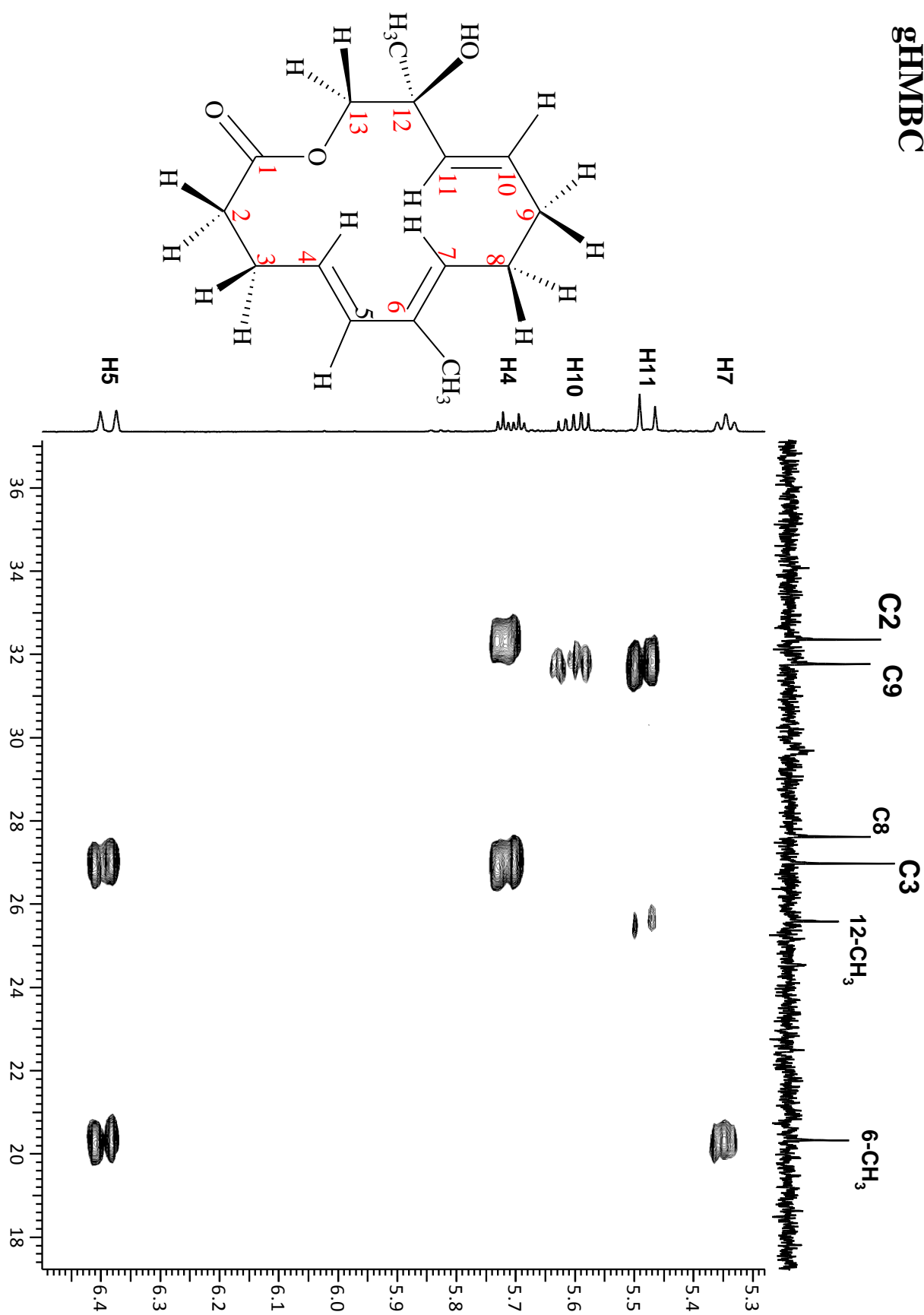
NOESY



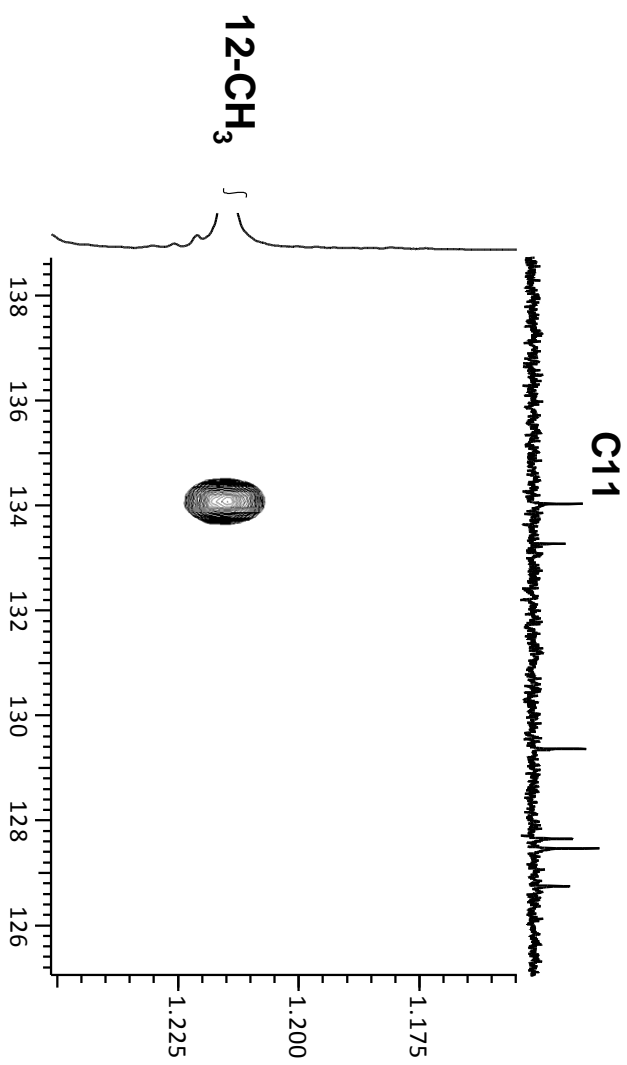
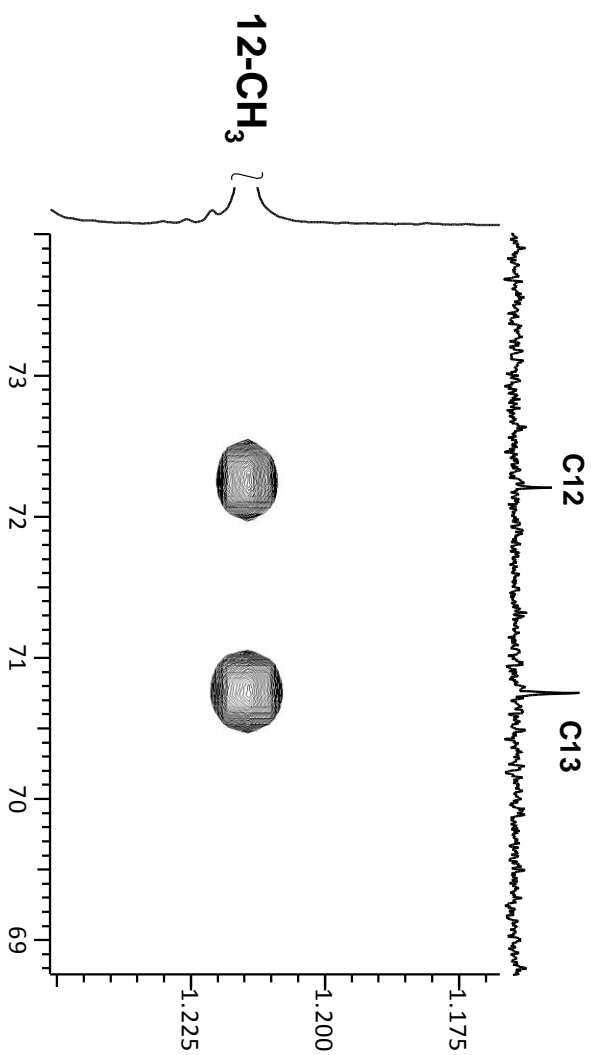
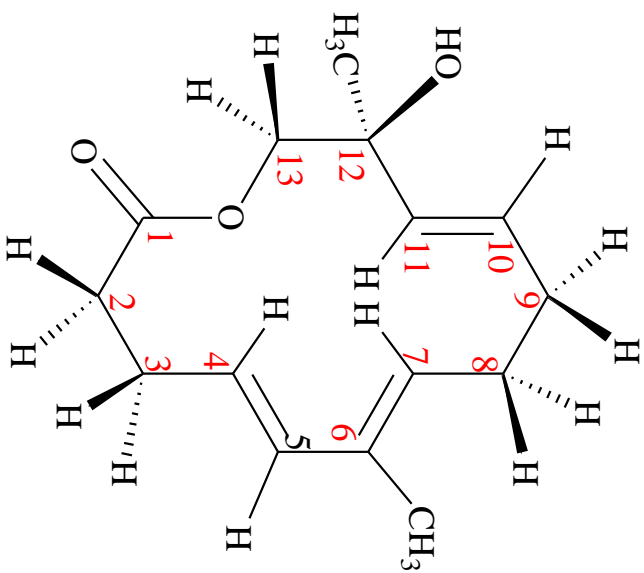
gHMBc

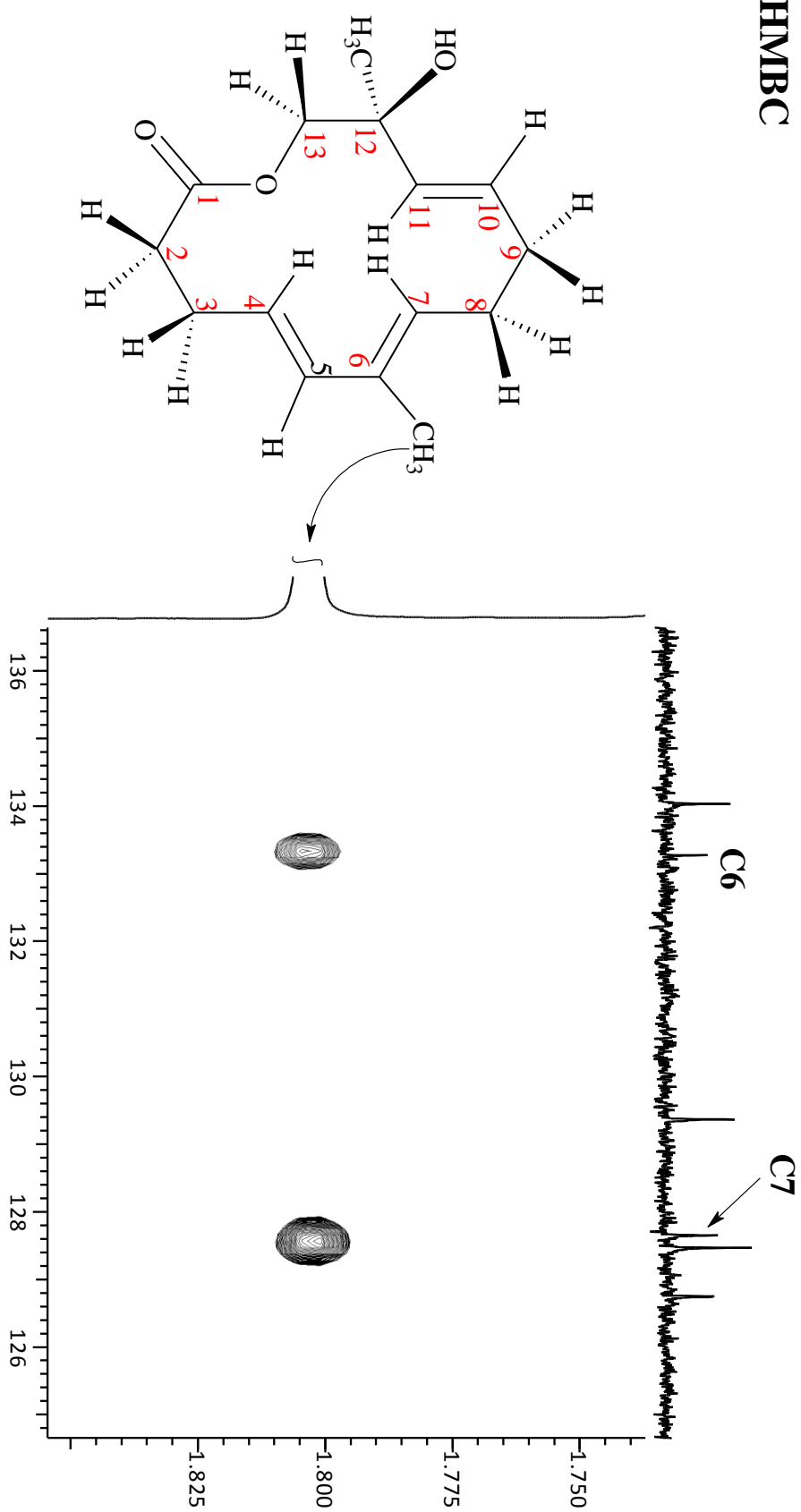


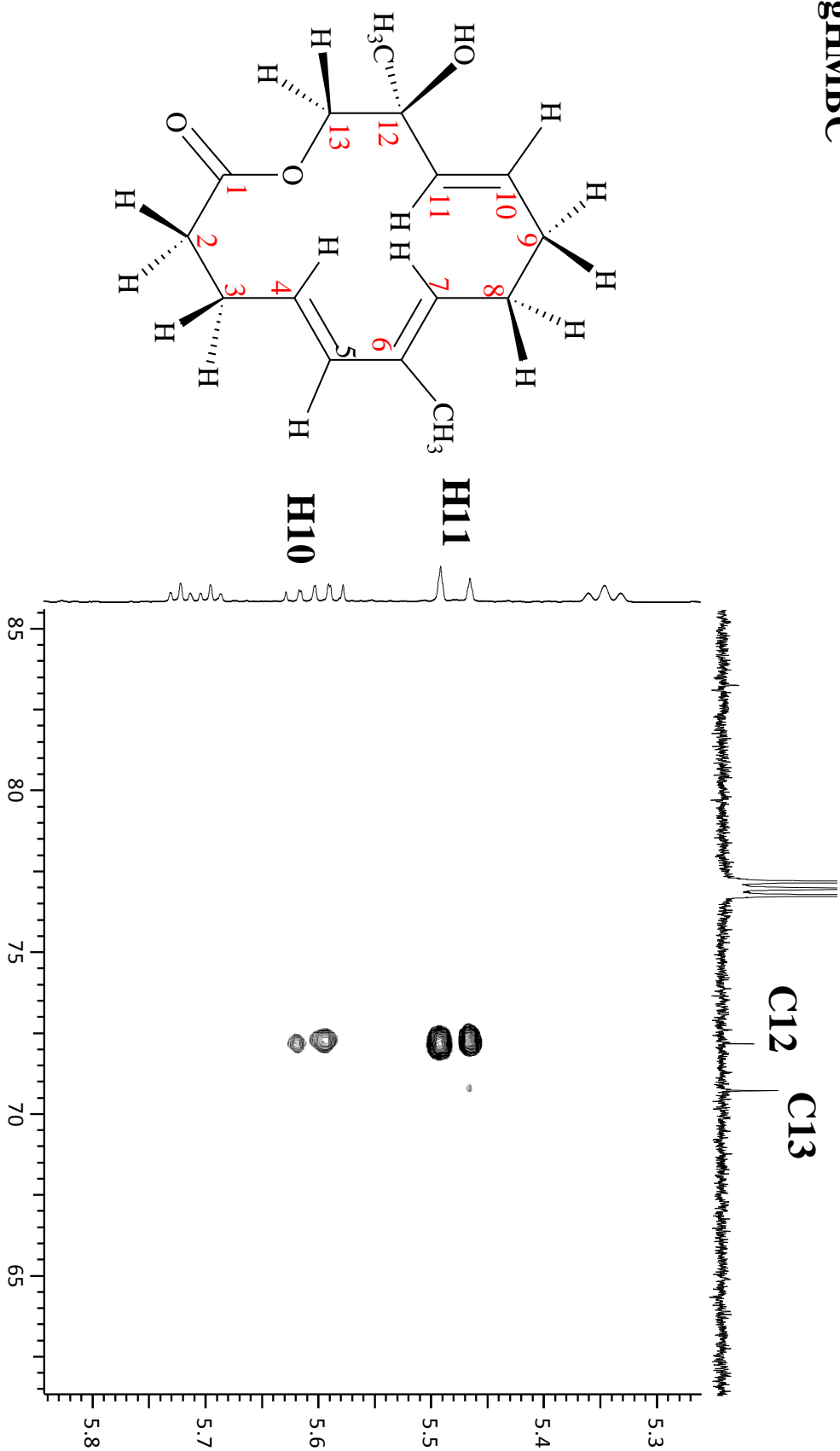
gHMBC

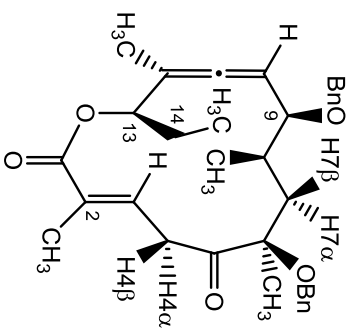


gHMBC

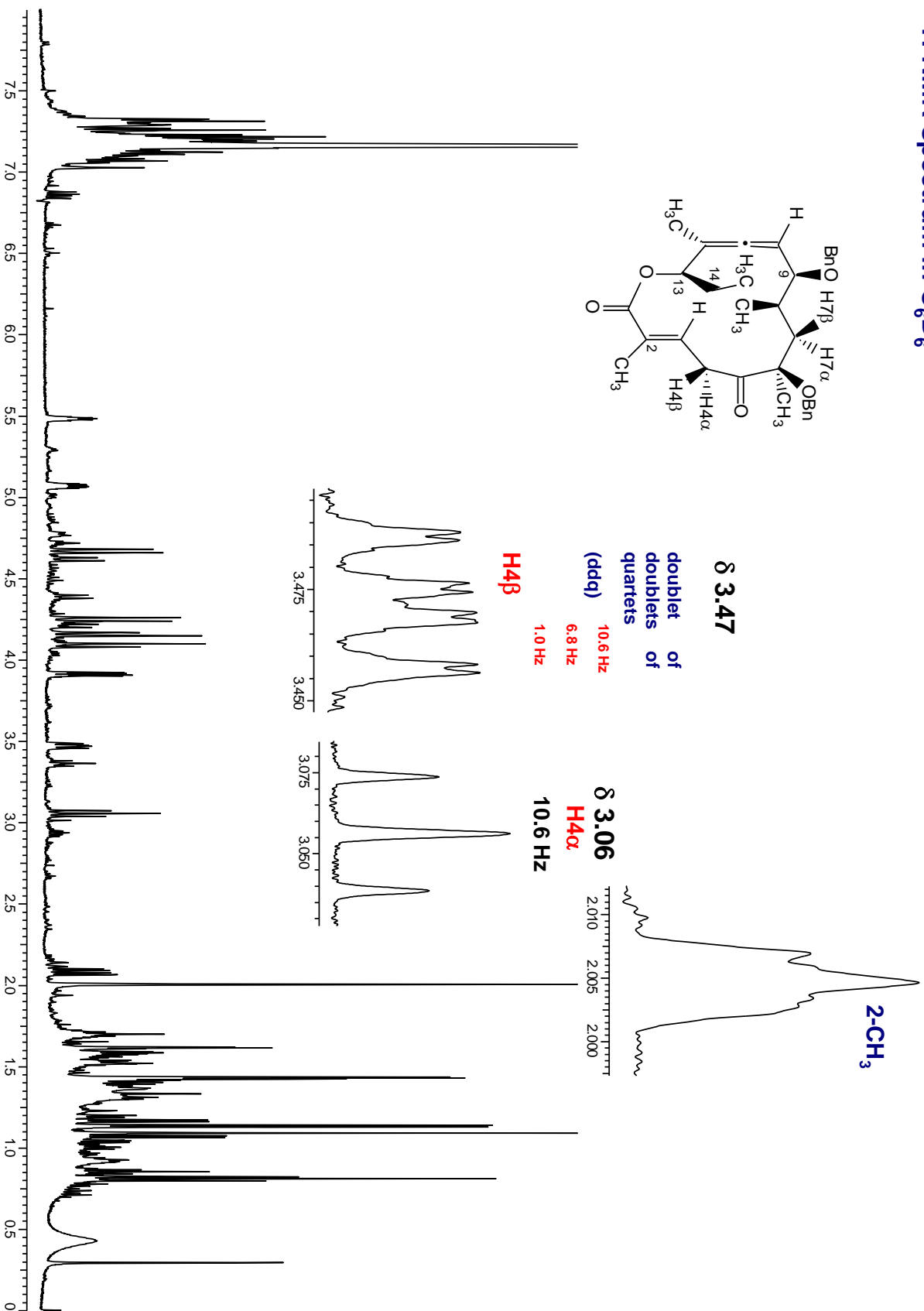


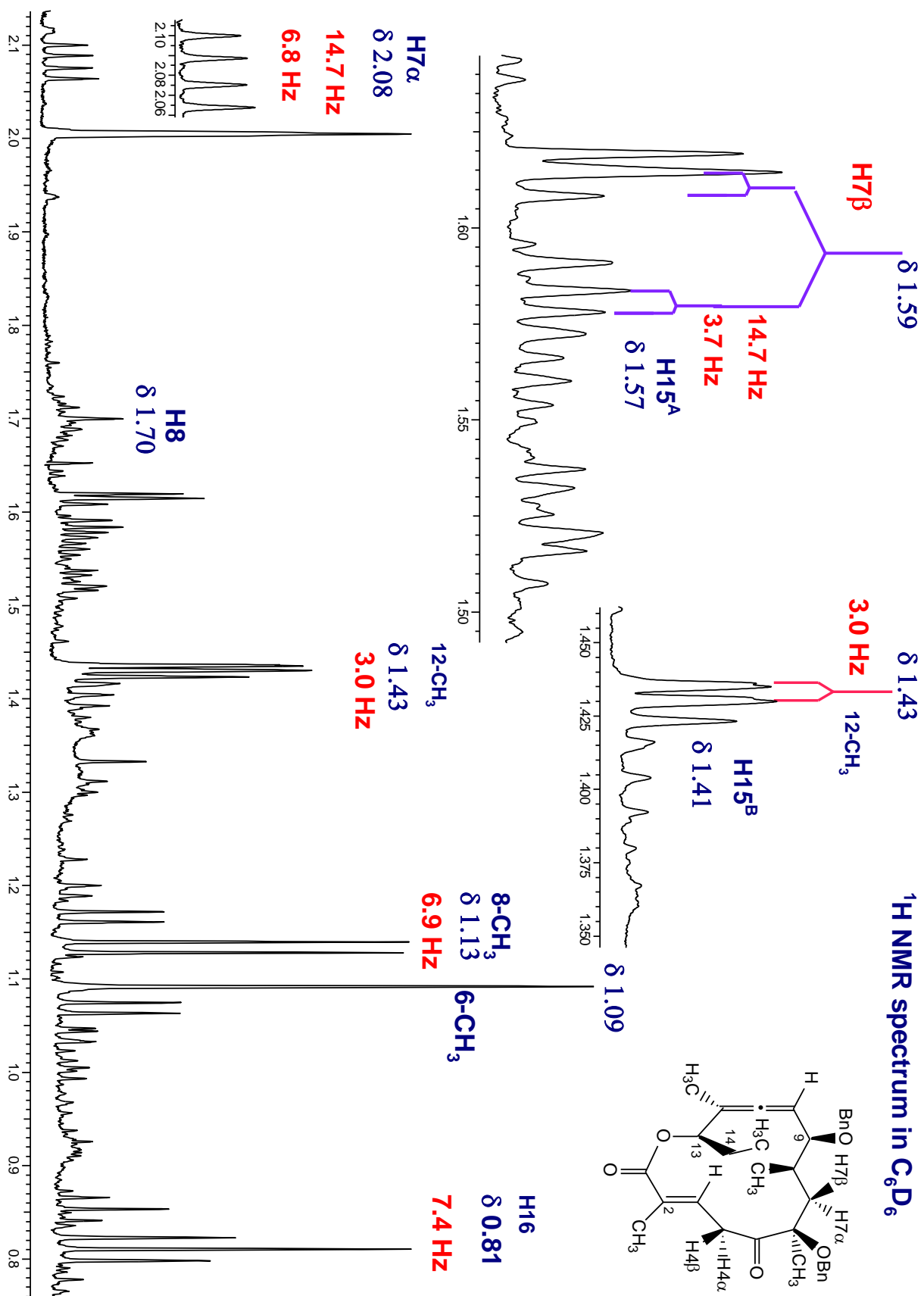
gHMBC

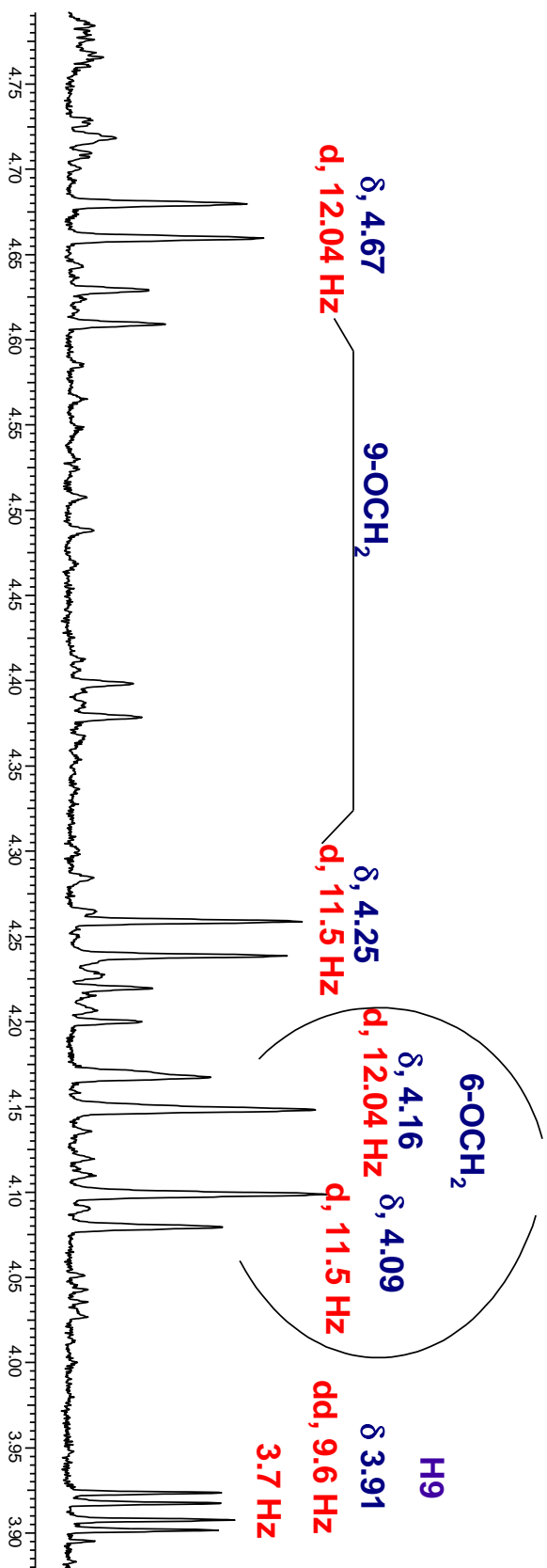
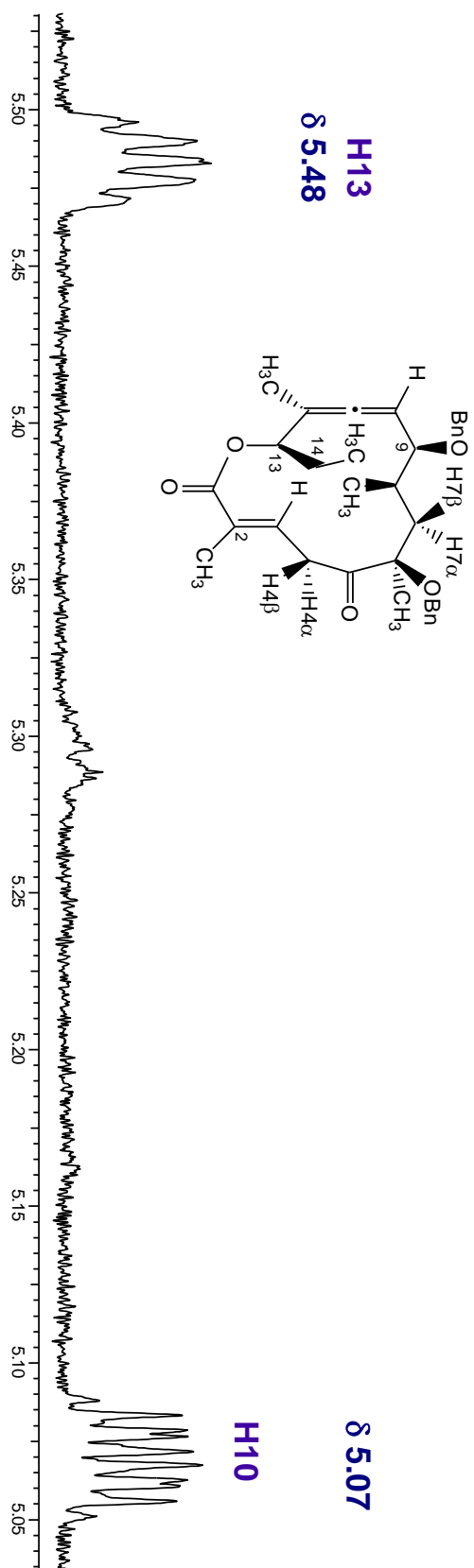
gHMBC



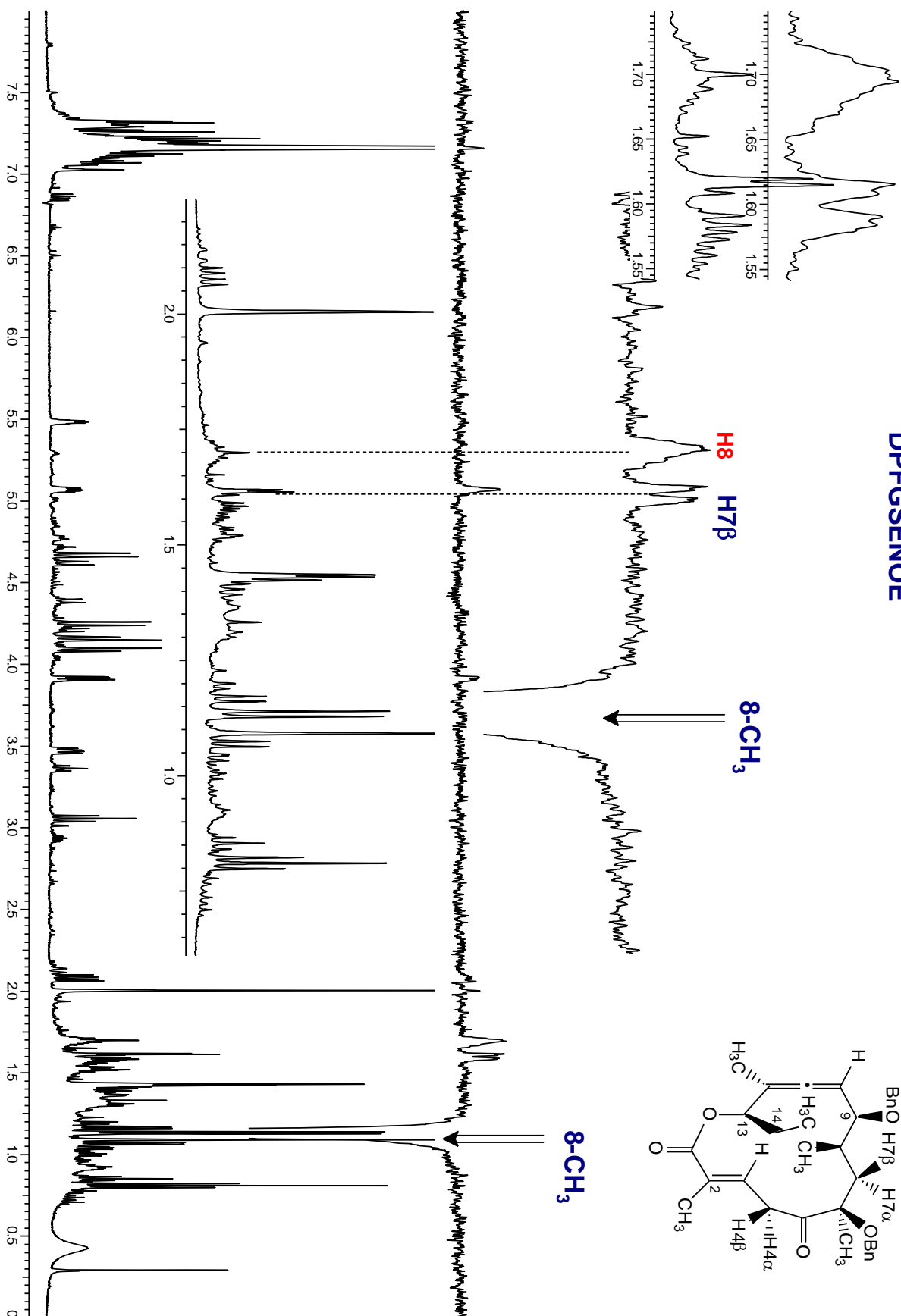
¹ H NMR chemical shifts (δ/ppm) & coupling constant (J/Hz), C ₆ D ₆	¹³ C NMR chemical shift (δ/ppm), CDCl ₃
2.00 (dt, J(2-CH ₃ , H3) = 1 Hz, J(2-CH ₃ -4-CH ₂) = ~0.7 Hz, 2-CH₃)	171.36 — C1
7.22 (ddq, H3)	165.89 — C2
3.06 (t, J _{H4α, H4β} = 10.6 Hz, H4α)	127.28 — C3
3.47 (ddq, J _{H4β, H4α} = 10.6 Hz, J _{H4β, H3} = 6.8 Hz J _{H4β, 2-CH3} = 1.0 Hz, H4β)	41.98 — C4
1.09 (s, 6-CH₃)	208.77 — C5
4.09 (d, J _{AB} = 11.6 Hz, 6-OCH₂)	86.88 — C6
4.16 (d, J _{AB} = 11.6 Hz, 6-OCH₂)	39.01 — C7
1.59 (dd, J _{H7α, H8} = 3.7 Hz, J _{H7α, H7β} = 14.7 Hz, H7α)	36.50 — C8
2.08 (dd, J _{H7β, H8} = 6.8 Hz, J _{H7α, H7β} = 14.7 Hz, H7β)	80.83 — C9
1.70 (dddd, H8)	99.84 — C10
1.13 (d, J _{8-CH3, H8} = 6.9 Hz, 8-CH₃)	203.36 — C11
3.91 (dd, J _{H9, H8} = 9.6 Hz, J _{H9, H10} = 3.7 Hz, H9)	92.62 — C12
4.25 (d, J _{AB} = 12.2 Hz, 9-OCH₂)	72.78 — C13
4.67 (d, J _{AB} = 12.2 Hz, 9-OCH₂)	24.86 — C14
5.05 - 5.07 (m, H10)	12.44 — 2-CH ₃
1.43 (d, J _{12-CH3, H10} = 3.0 Hz, 12-CH₃)	21.94 — 6-CH ₃
5.47 - 5.50 (m, H13)	16.35 — 8-CH ₃
1.55 - 1.60, 1.37 - 1.42 (m, 14-CH₂)	15.67 — 12-CH ₃
0.81 (t, J _{14-CH3, 13-CH2} = 7.4 Hz, 14-CH₃)	9.14 — 14-CH ₃
7.48 - 7.10 (m, 10H, Ph)	64.76 — 6-OCH ₂
	69.88 — 9-OCH ₂

^1H NMR spectrum in C_6D_6 

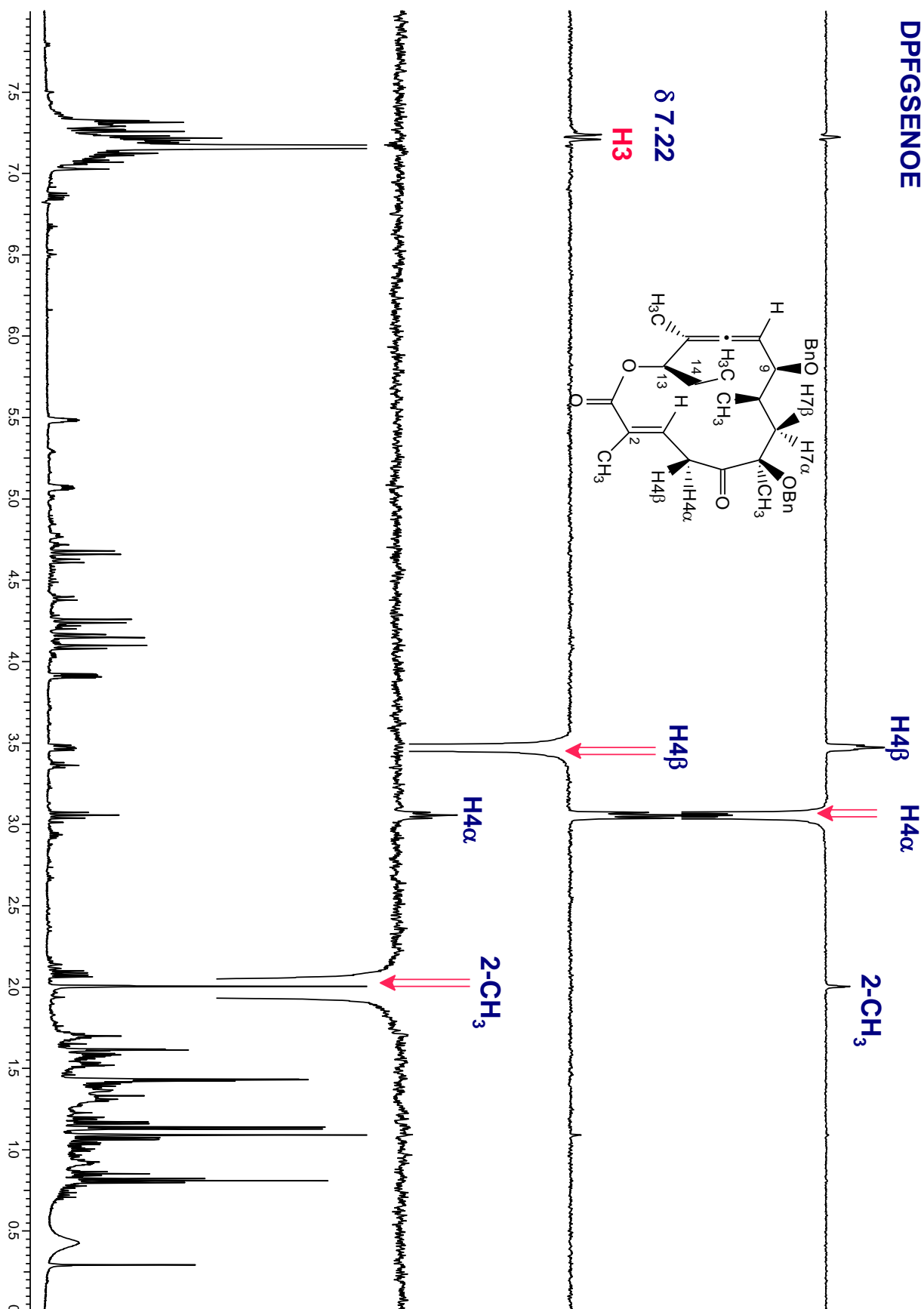
¹H NMR spectrum in C₆D₆



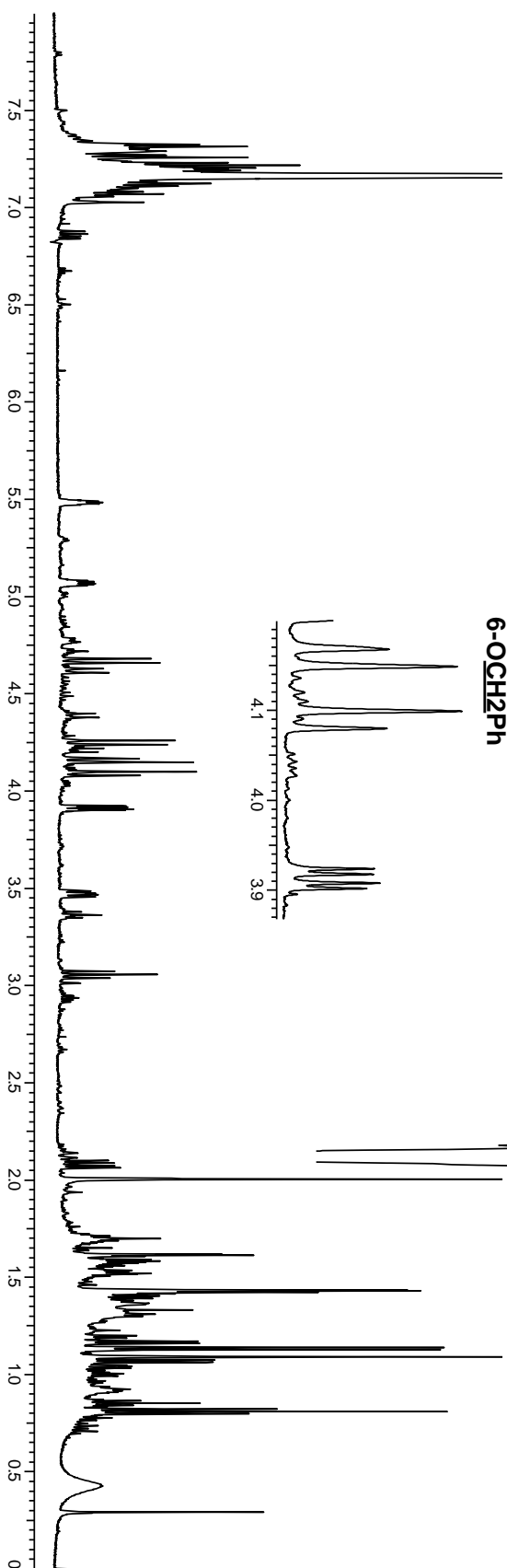
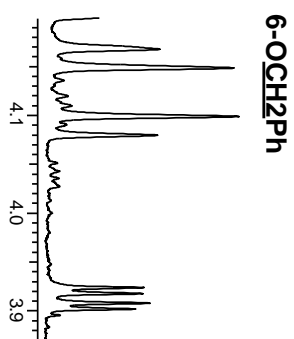
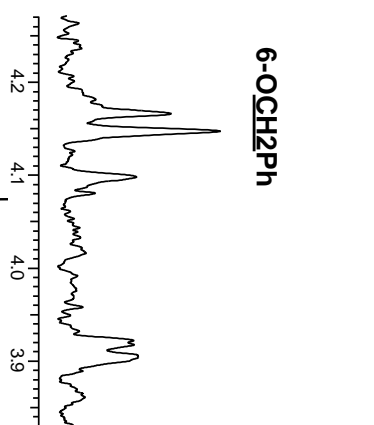
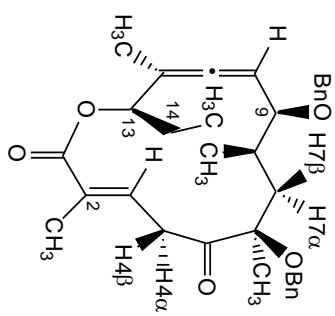
DPFGSENOE



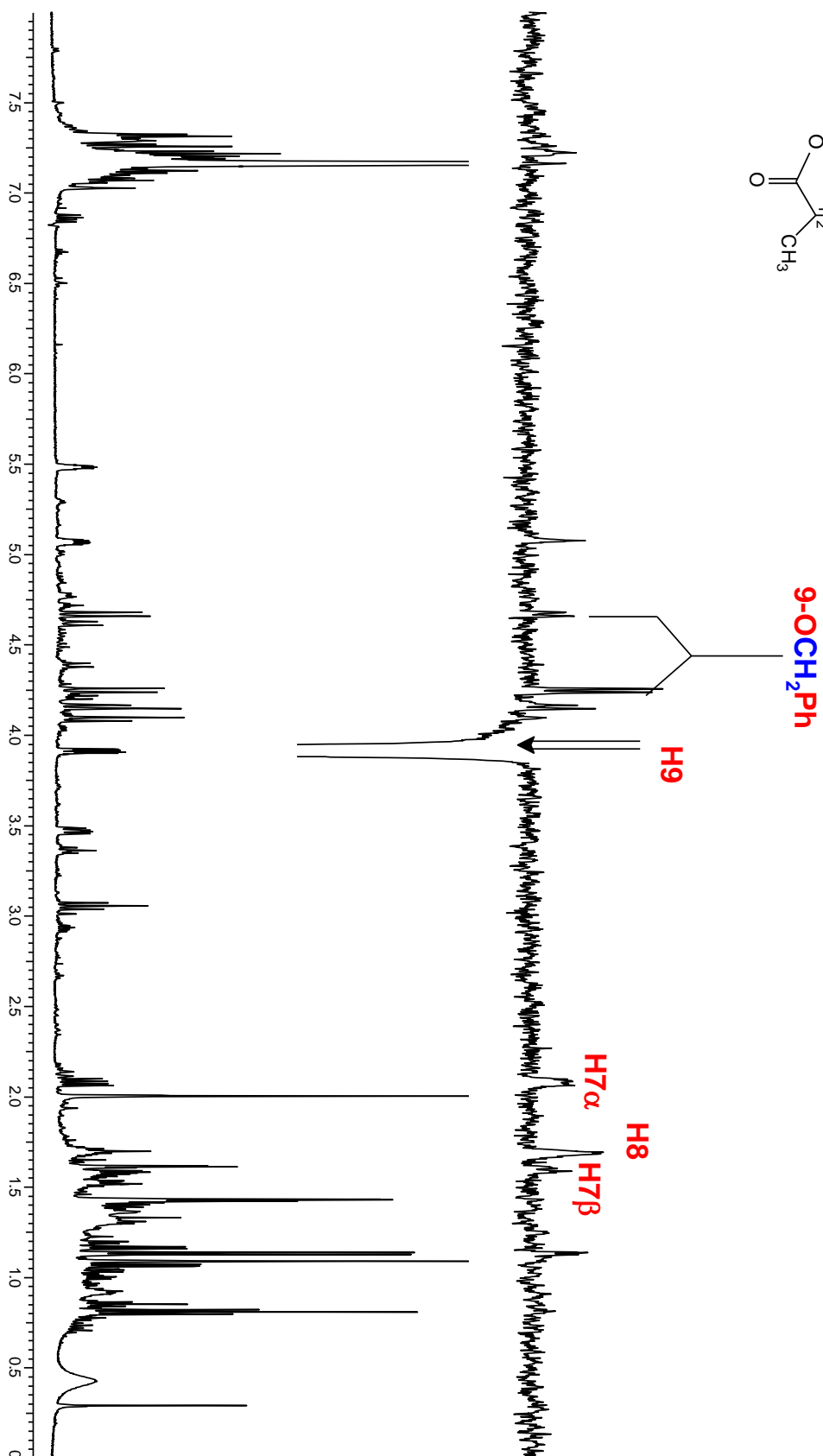
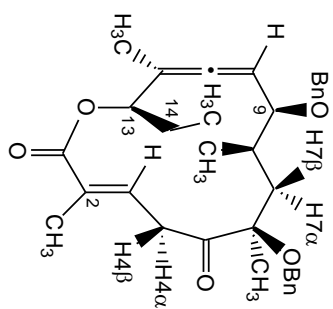
DPFGSENOE



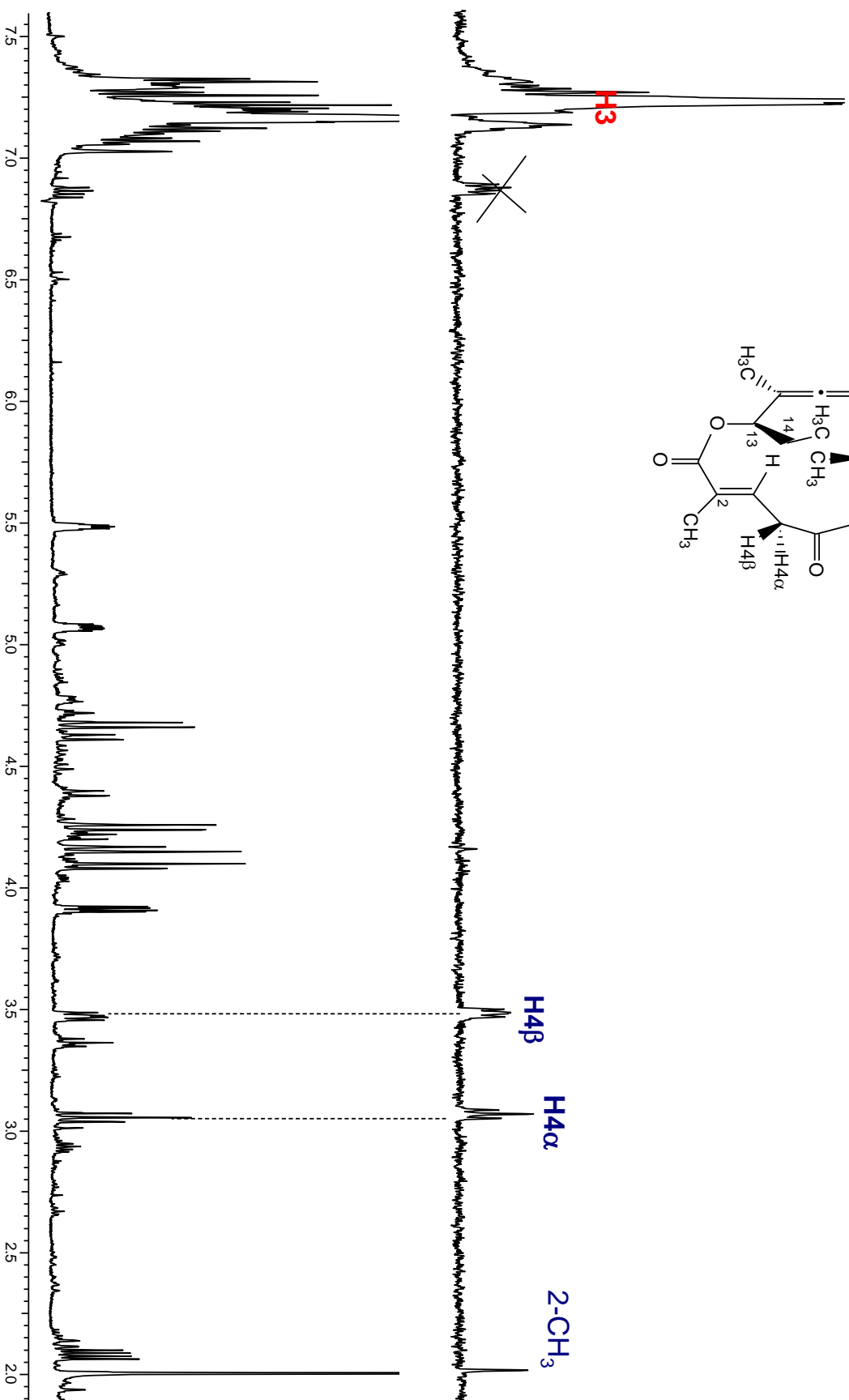
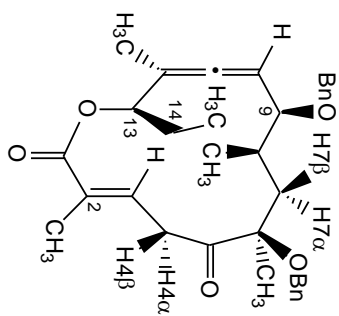
DPFGSENOE



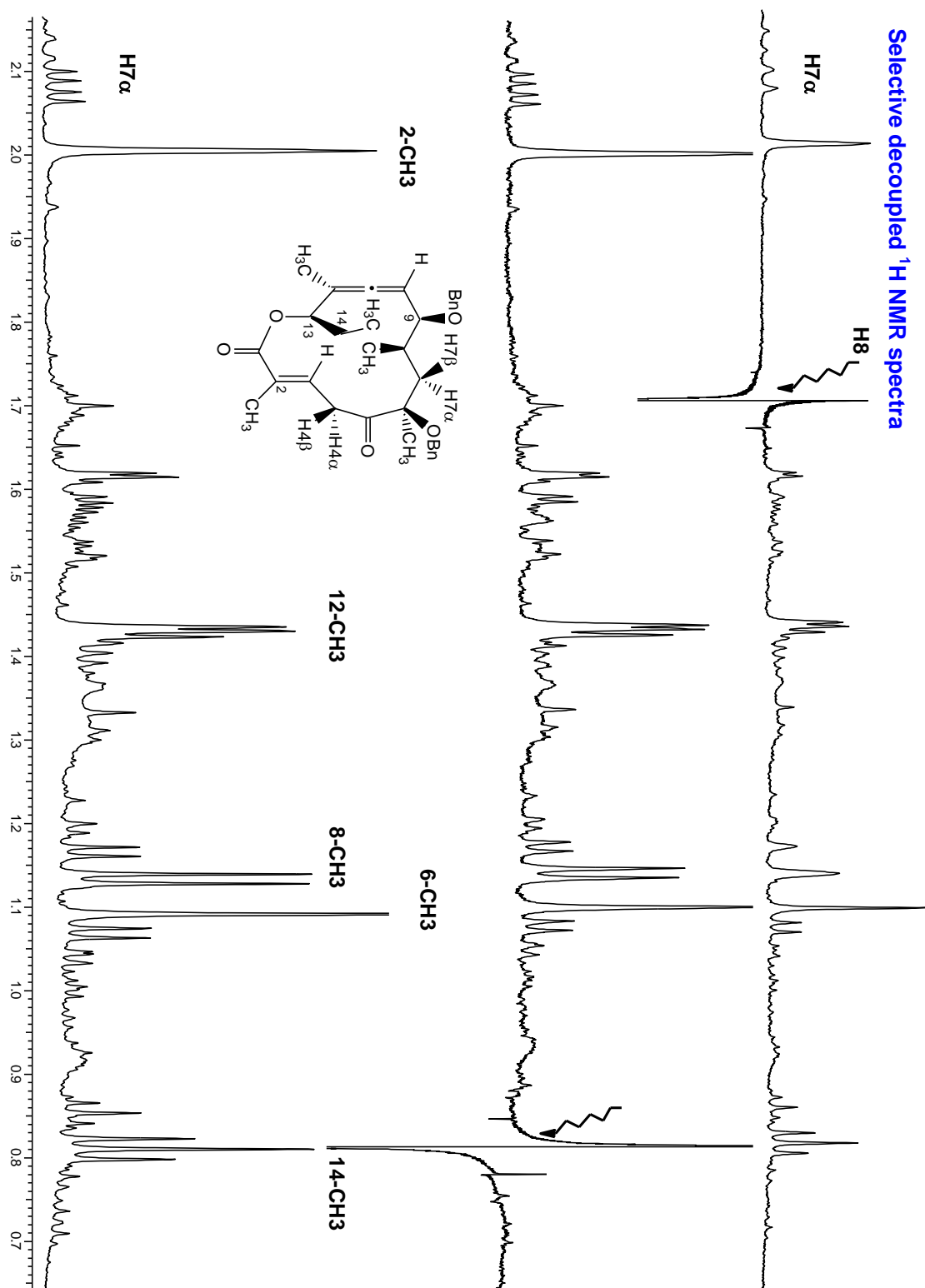
DPFGSENOE

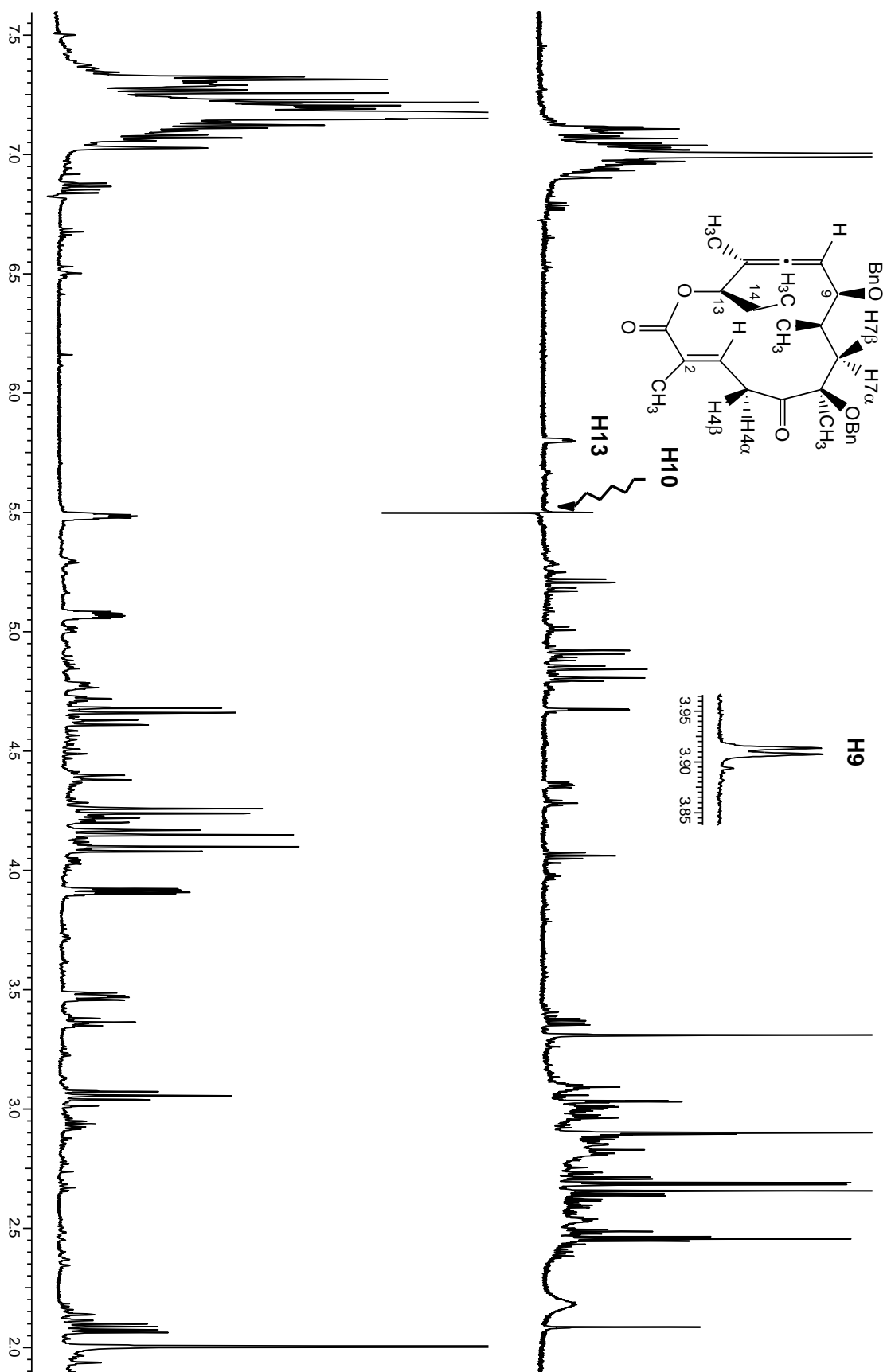


selective
excitation of H3
at 7.22 ppm

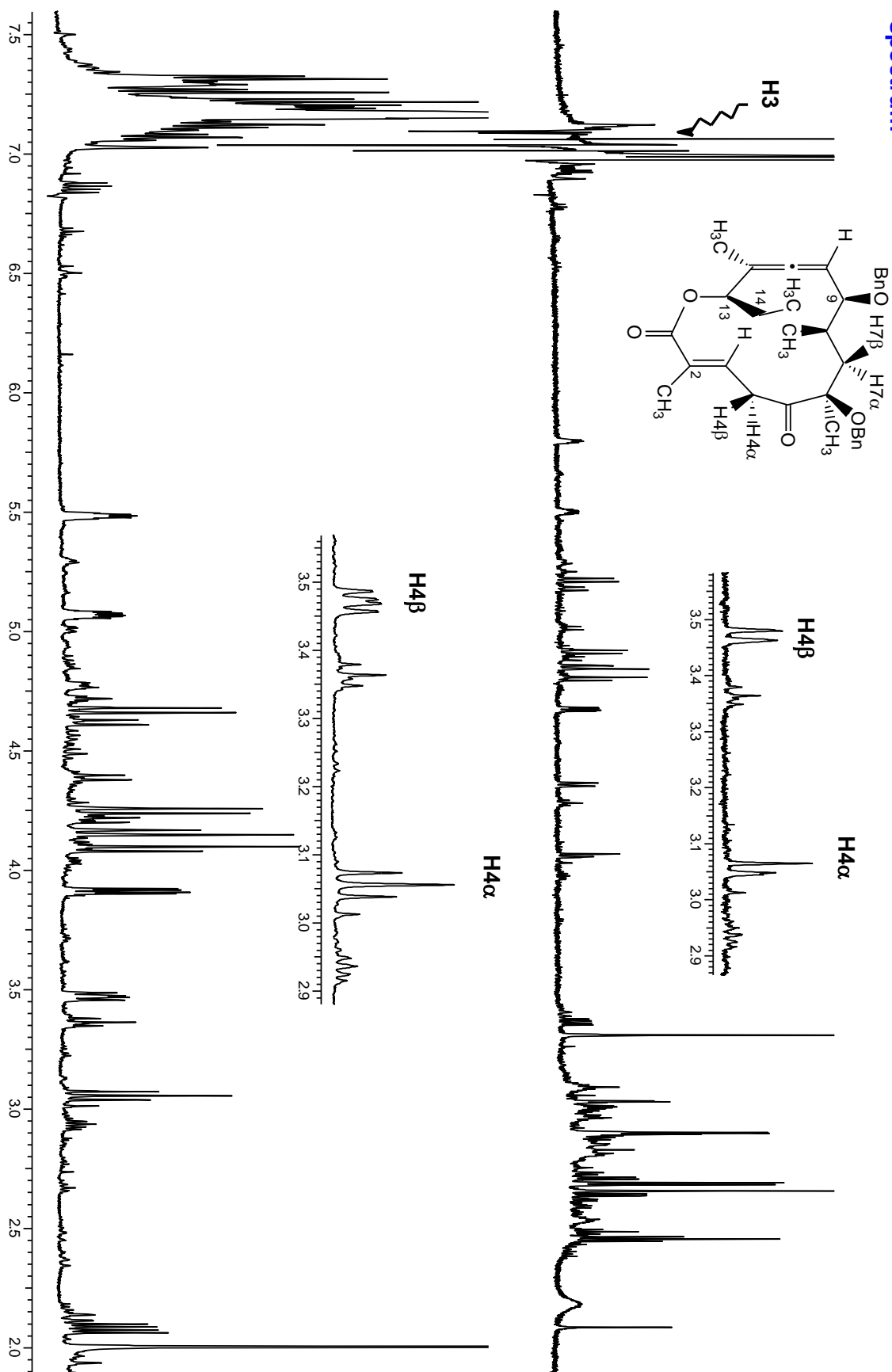


Selective decoupled ^1H NMR spectra

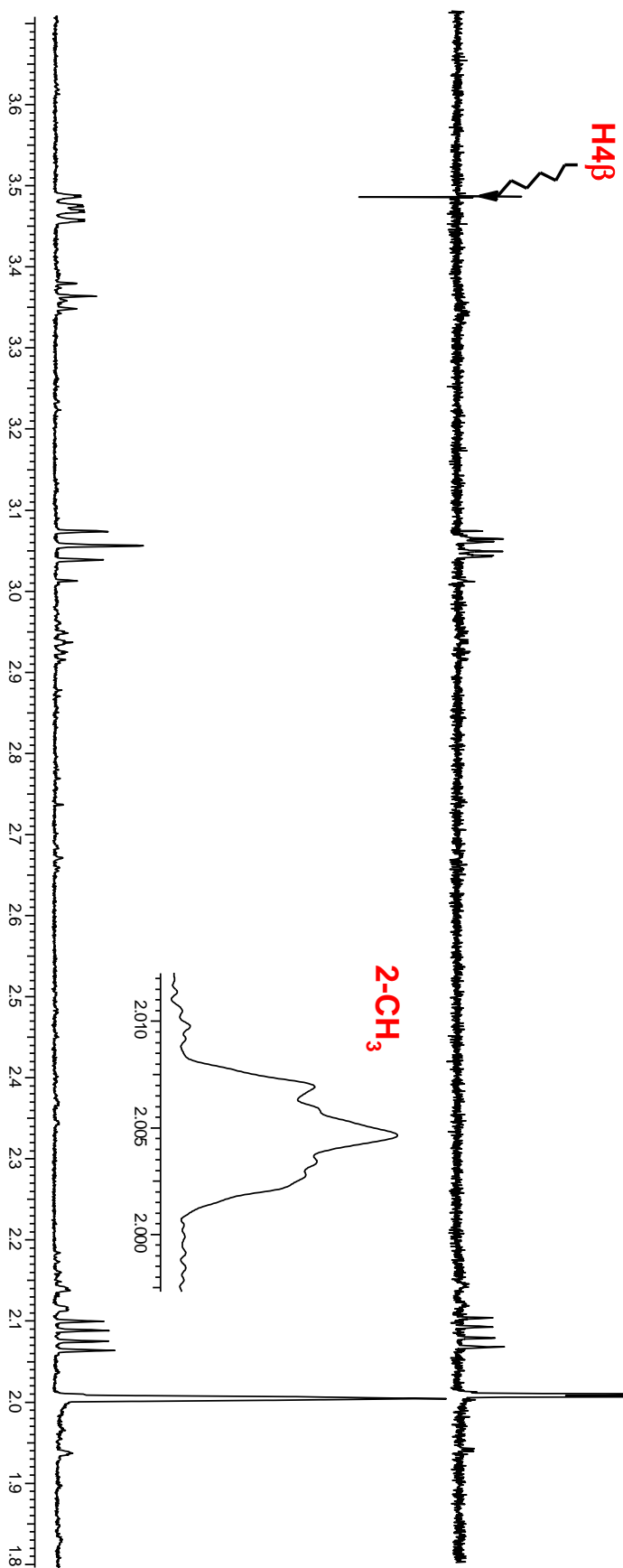
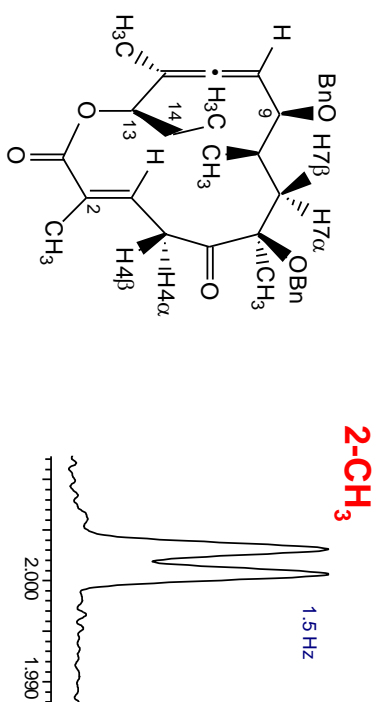


Selective decoupled ^1H NMR spectrum

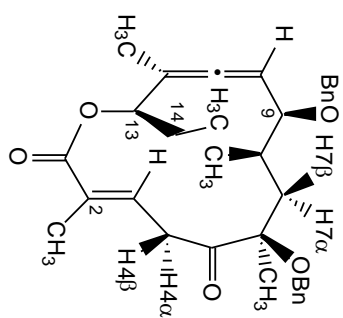
Selective decoupled ^1H NMR spectrum



Selective decoupled ^1H NMR spectrum



Selective decoupled ^1H NMR spectrum



1.4 Hz
1.0 Hz

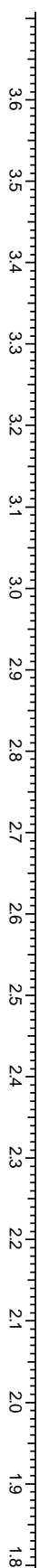
2-CH_3

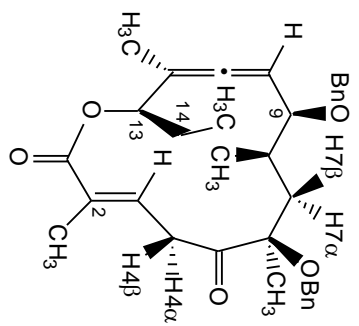
2.010 2.005 2.000 1.995 1.990

$\text{H}_4\alpha$

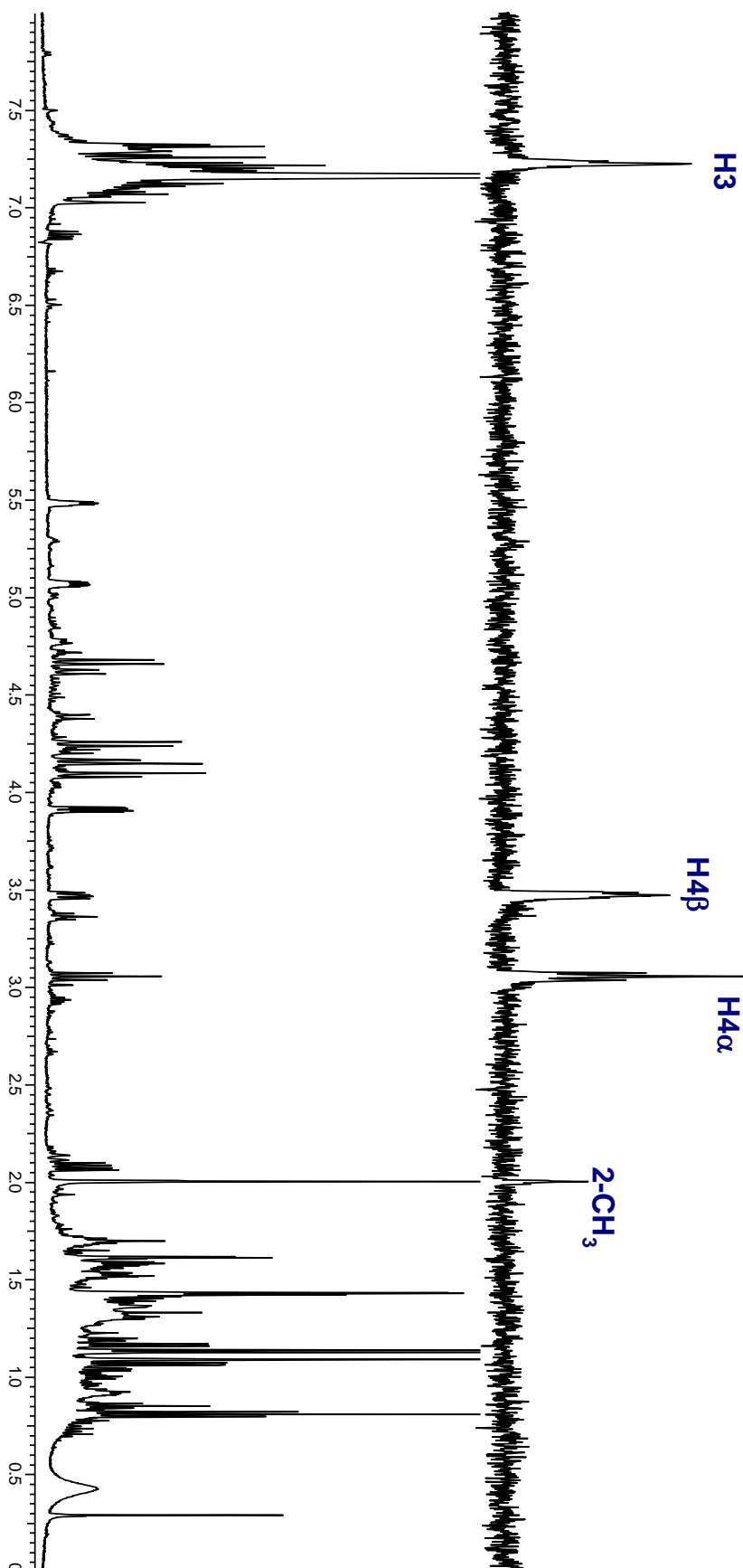
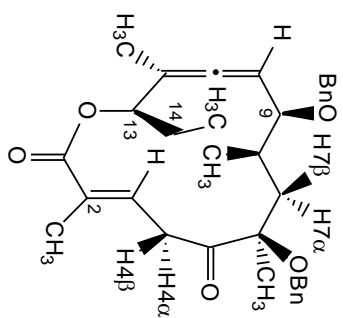
2-CH_3

2.010 2.005 2.000

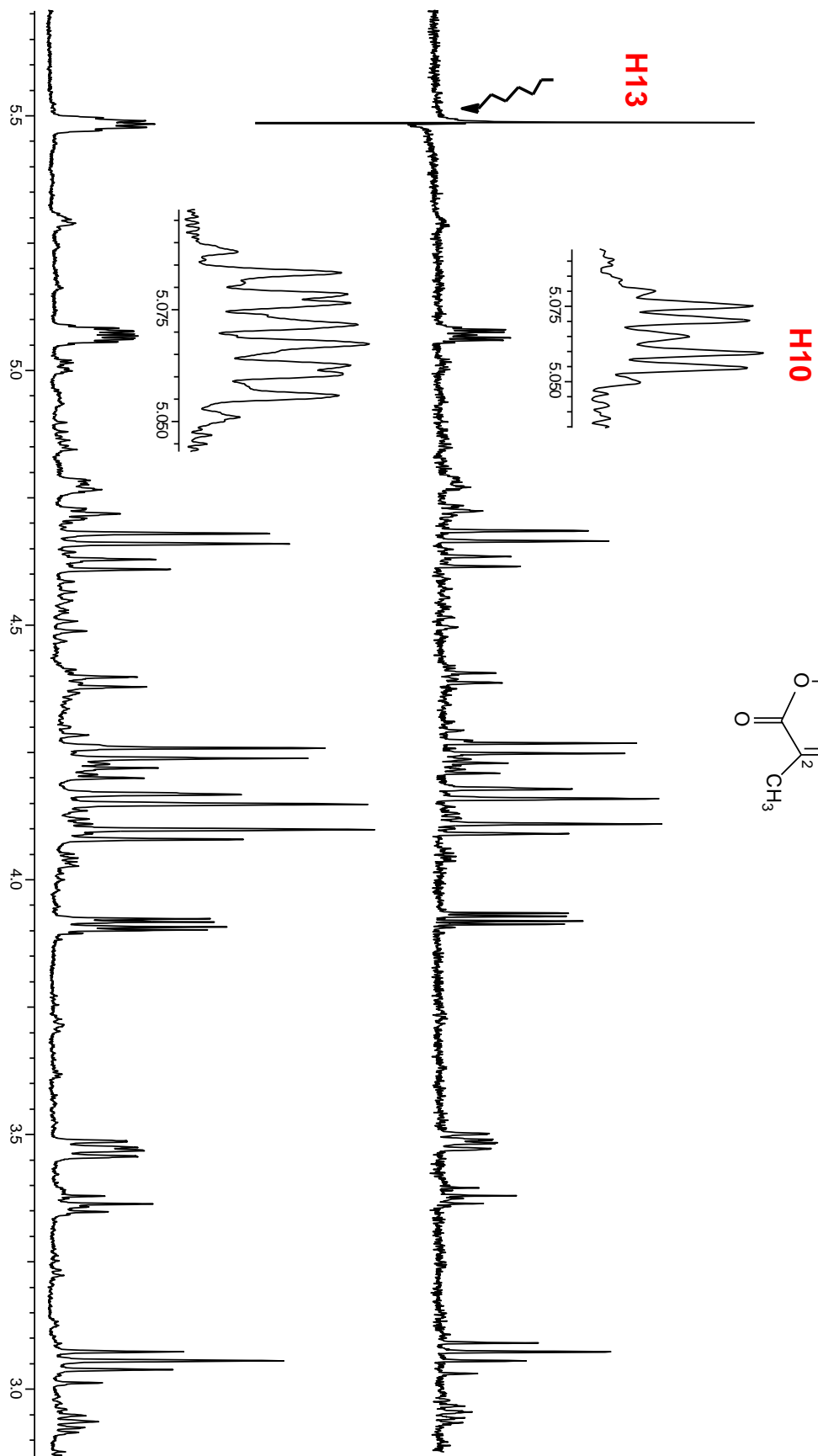
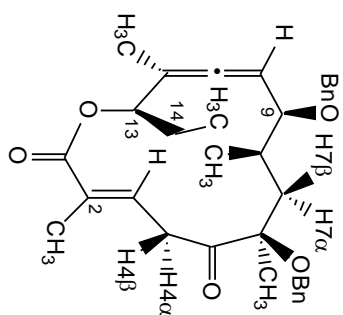




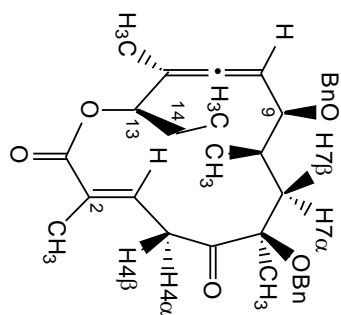
1D TOCSY



Selective decoupled ^1H NMR spectrum

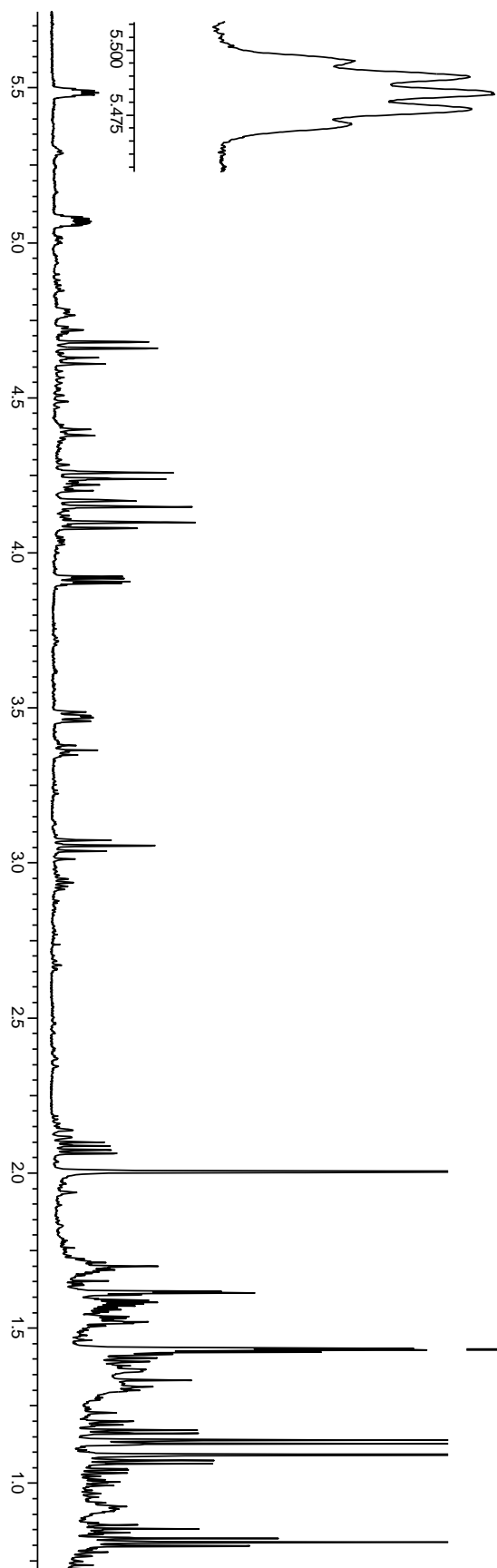


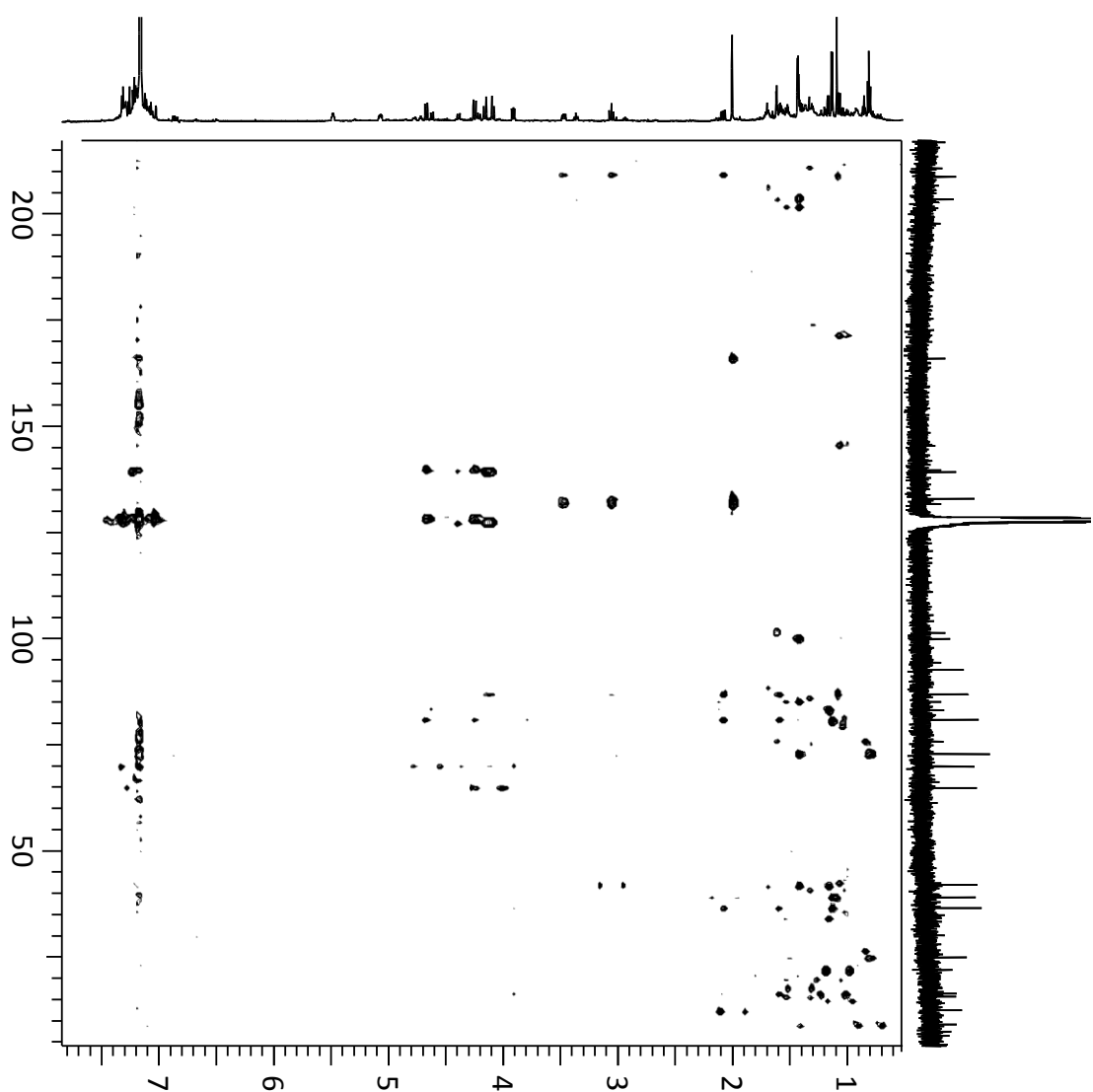
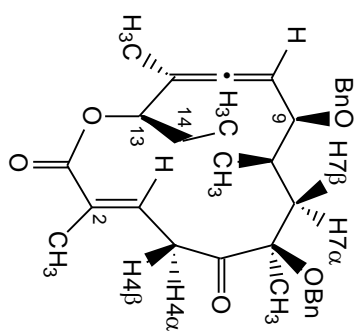
Selective decoupled ^1H NMR spectrum

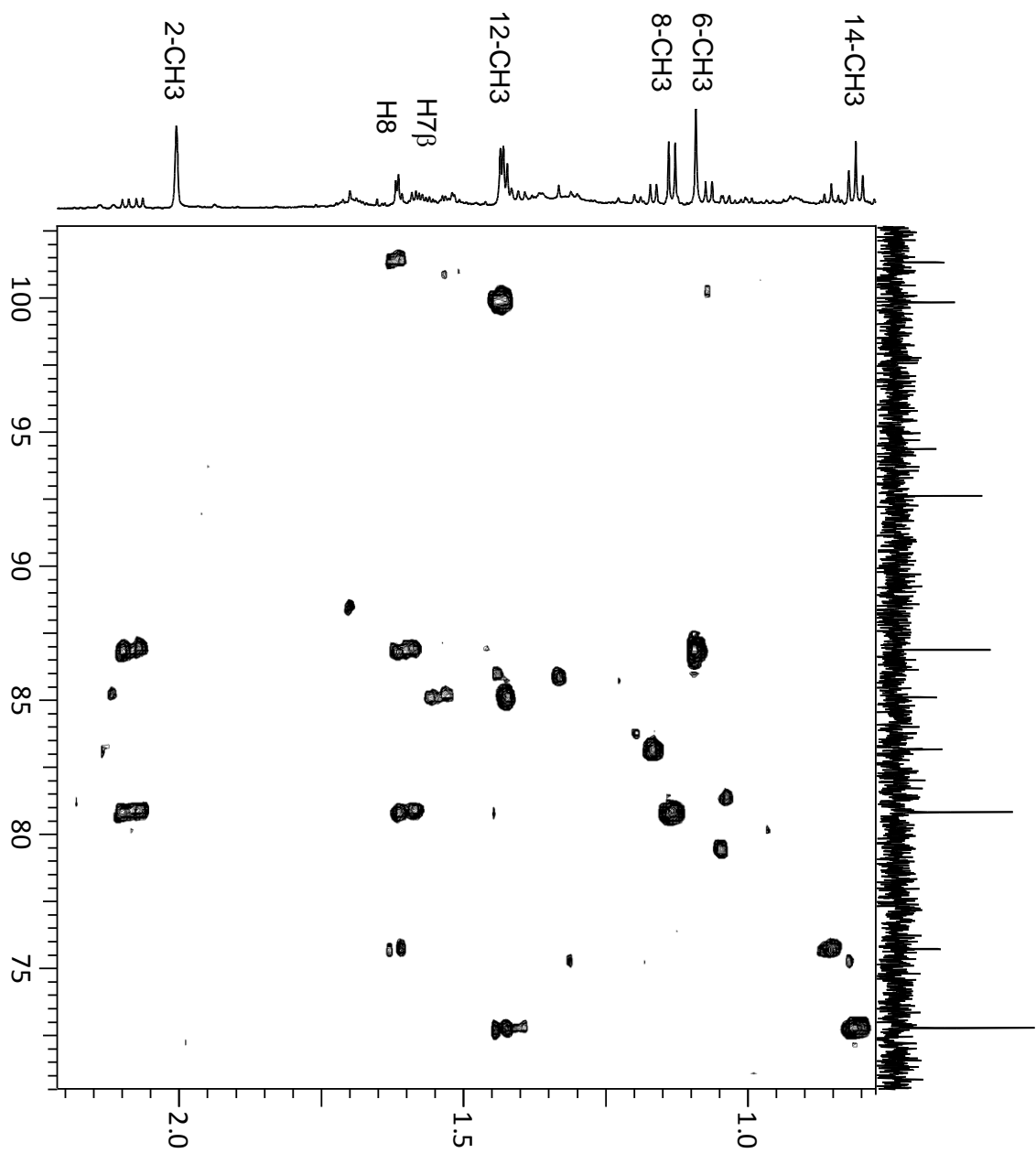
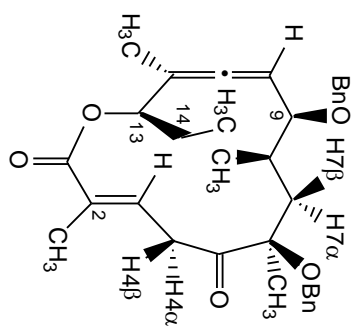


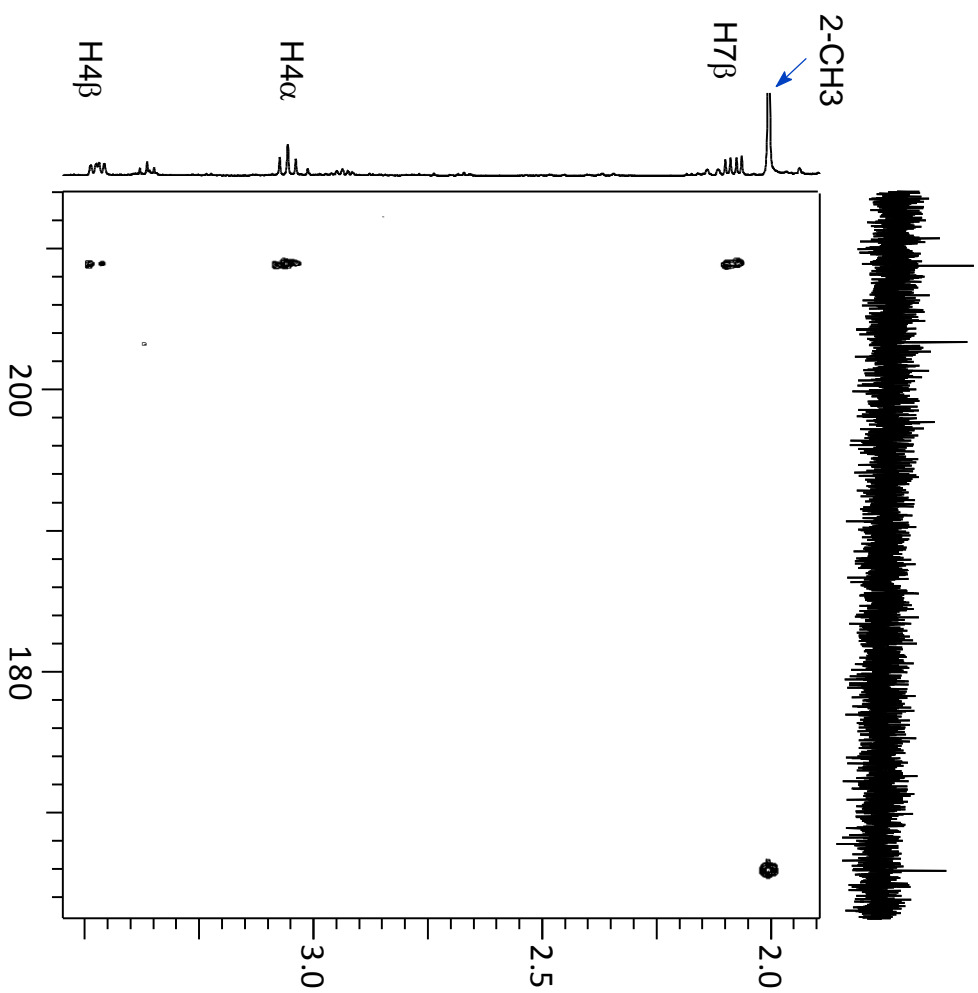
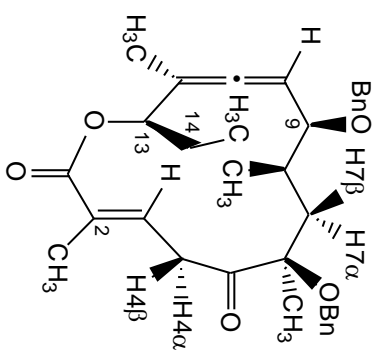
12-CH₃

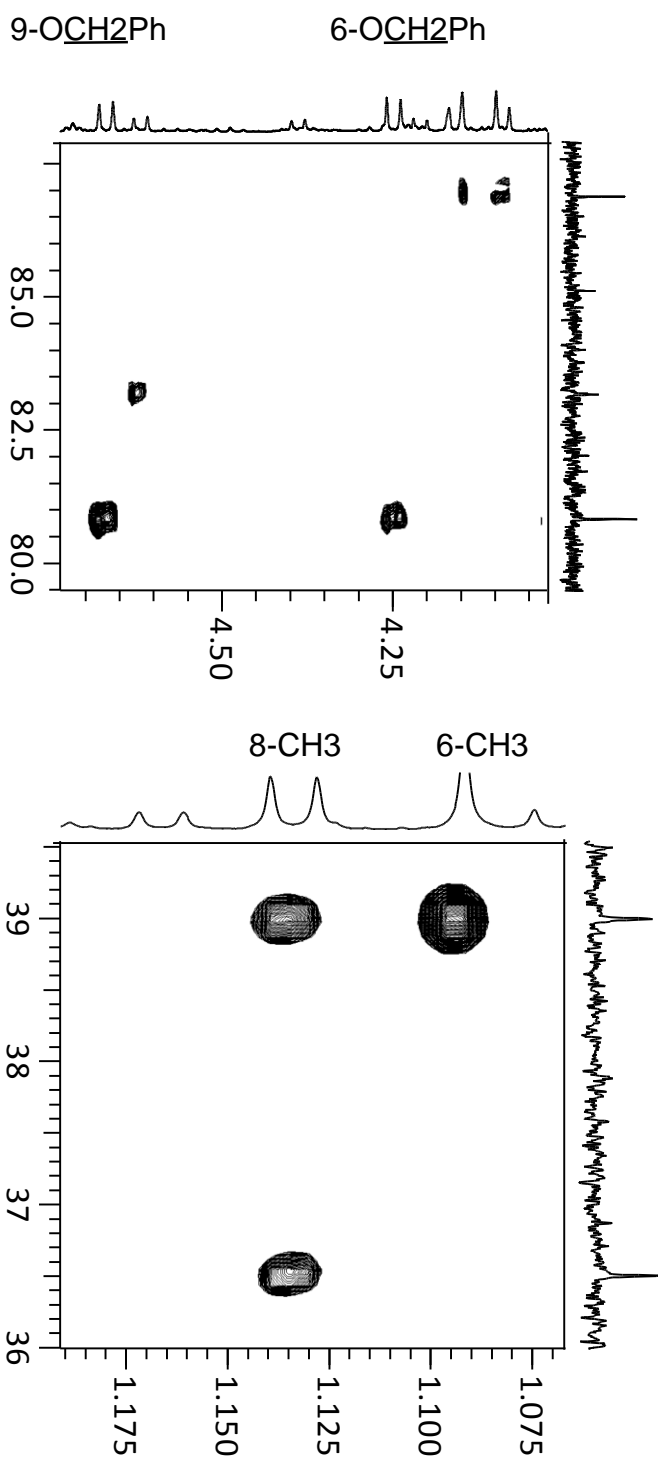
H13

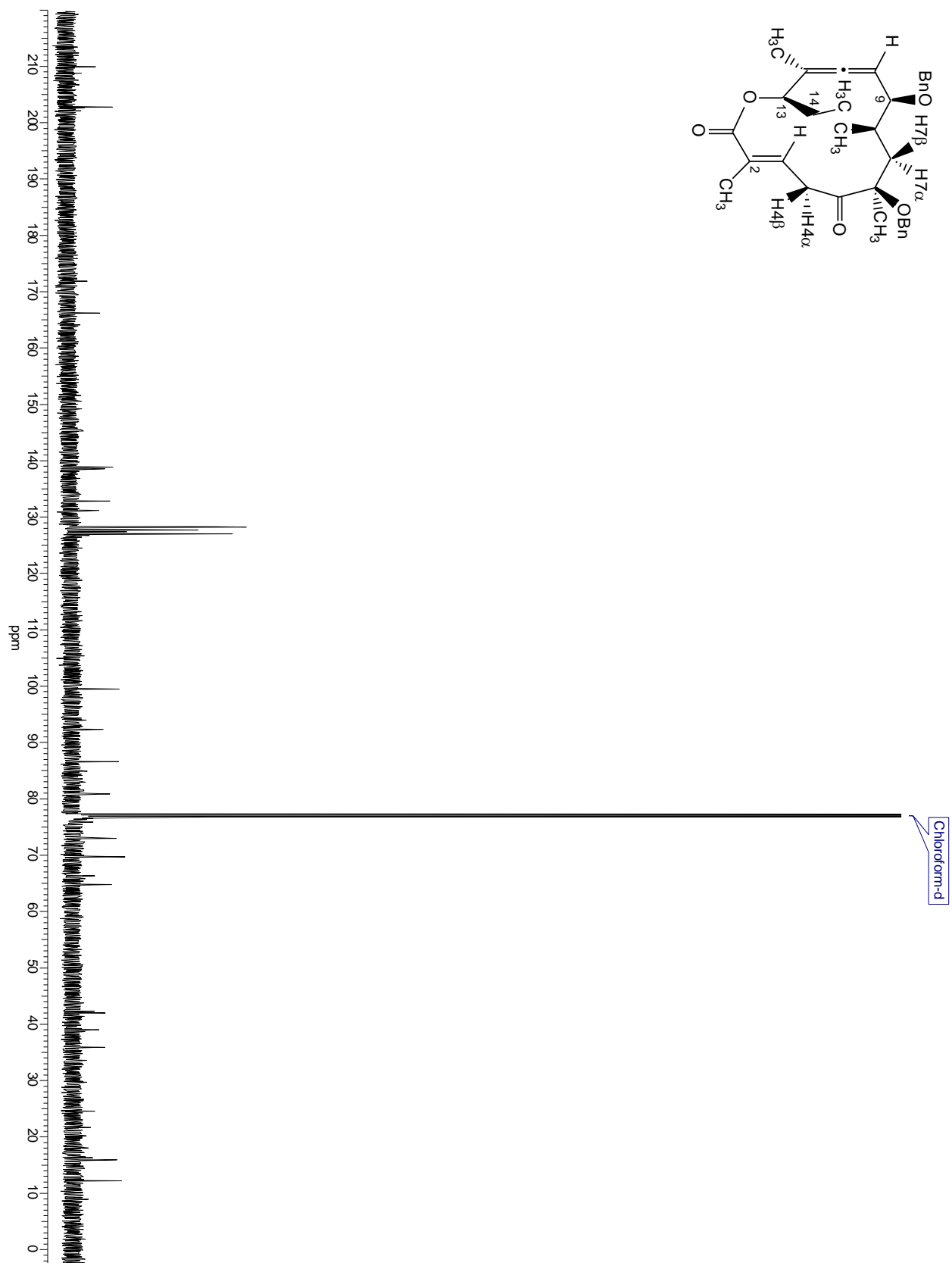
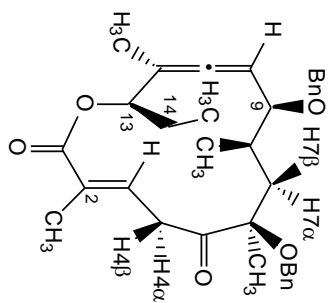


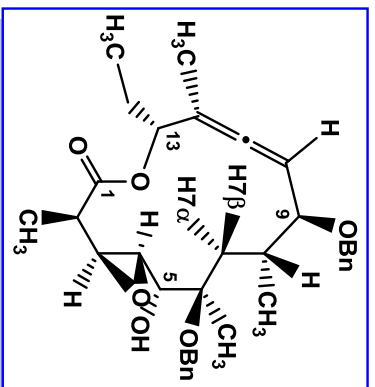
GHMBC

GHMBC

GHMBC

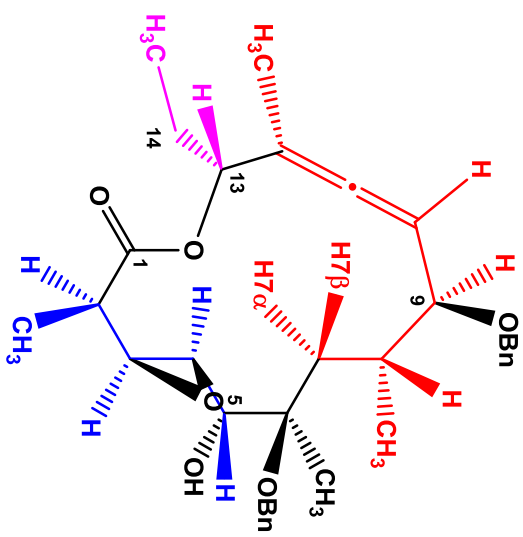




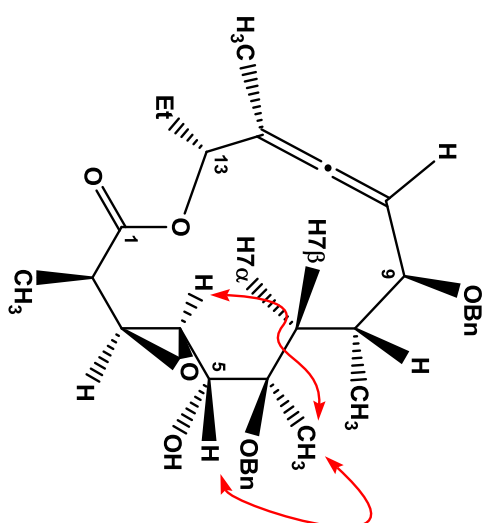
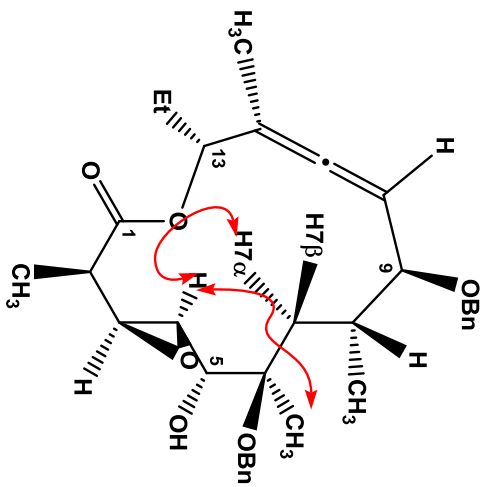
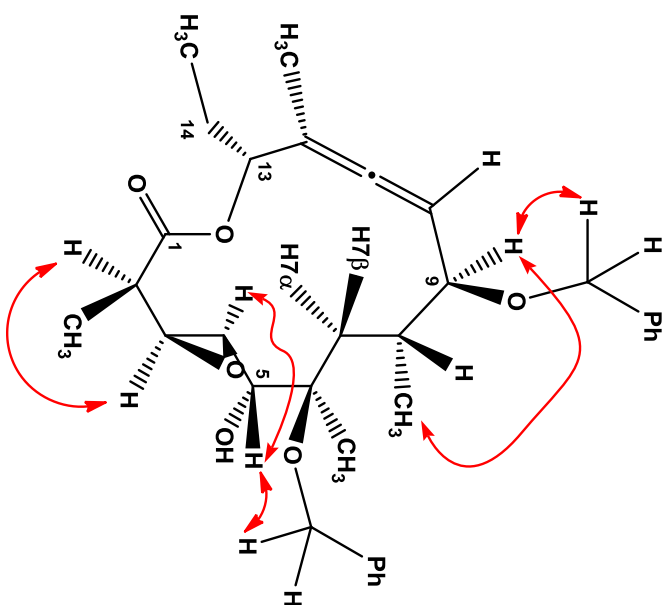


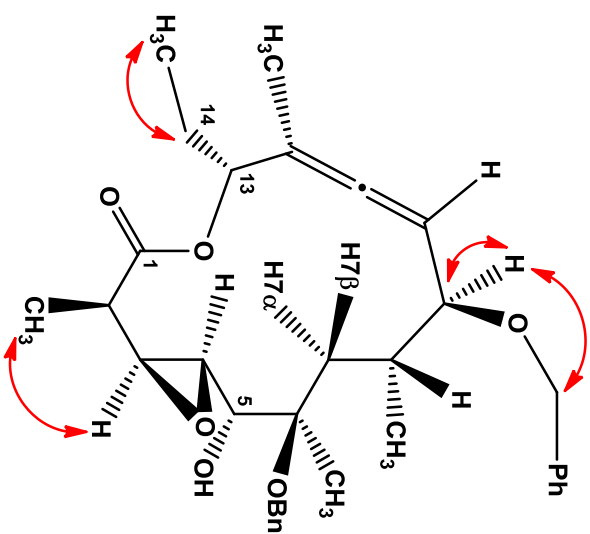
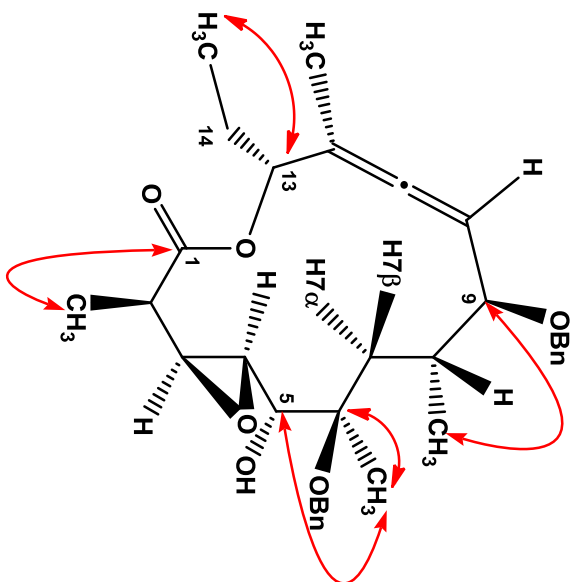
¹ H NMR chemical shifts (δ/ppm) coupling constant (J/Hz)	¹³ C NMR chemical shift (δ/ppm)
3.09 (dd, J _{H2, H3} = 2.0Hz, J _{H2, 2-CH3} = 7.3Hz, H2)	171.9 ---- C1
1.05 (d, J _{2-CH3, H2} = 7.3Hz, 2-CH3)	34.9 ---- C2
3.86 (dd, J _{H3, H2} = 2.0Hz, H3)	55.3 ---- C3
3.05 (dd, J _{H4, H3} = 1.9Hz, H4)	53.7 ---- C4
4.26 (s, H5)	71.5 ---- C5
4.52 (d, J _{AB} = 11.0Hz, 6-OCH₂)	79.3 ---- C6
4.45 (d, J _{AB} = 11.0Hz, 6-OCH₂)	39.2 ---- C7
1.41 (s, 6-CH₃)	18.3 ---- C8
1.45 (dd, J _{H7β, H8} = 1.9 Hz, J _{H7β, H7α} = 14.8Hz, H7β)	85.1 ---- C9
1.68 (dd, J _{H7α, H8} = 11.2Hz, J _{H7α, H7β} = 14.8Hz, H7α)	95.5 ---- C10
1.87 - 1.78 (m, H8)	202.5 ---- C11
1.18 (d, J _{8-CH3, H8} = 6.4Hz, 8-CH₃)	101.3 ---- C12
3.29 (t, J _{H9, H10} = 9.5Hz, H9)	77.4 ---- C13
4.68 (d, J _{AB} = 11.7Hz, 9-OCH₂)	25.6 ---- C14
4.38 (d, J _{AB} = 11.7Hz, 9-OCH₂)	12.0 ---- 2-CH ₃
4.92 (td, J _{10, 12-CH3} = 2.9, J _{H10, H9} = 9.5Hz, H10)	19.7 ---- 6-CH ₃
1.80 (d, J _{12-CH3, H10} = 2.7Hz, 12-CH₃)	18.3 ---- 8-CH ₃
4.96 (td, J _{H13, H10} = 2.7 Hz, H13)	17.0 ---- 12-CH ₃
1.71 - 1.6 (m, 14-CH₂)	9.1 ---- 14-CH ₃
0.92 (t, J _{14-CH3, 14-CH2} = 7.3Hz, 14-CH₃)	64.0 ---- 6-OCH ₂
7.40 - 7.28 (m, 10H, Ph)	70.6 ---- 9-OCH ₂
	136.7 ---- ipsoC
	128.7 ---- orthoC
	128.3 ---- metaC
	127.8 ---- paraC

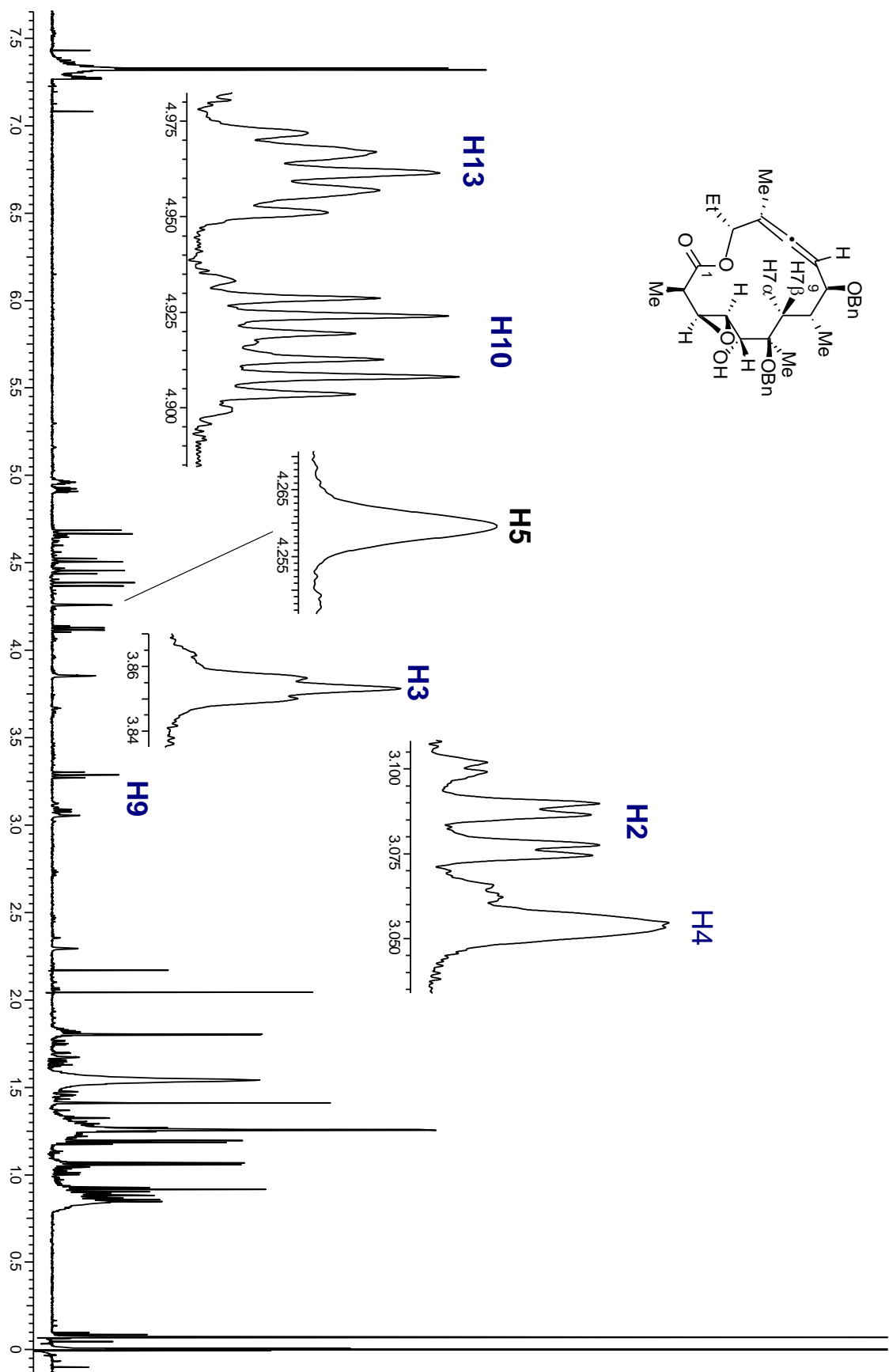
1d TOCSY

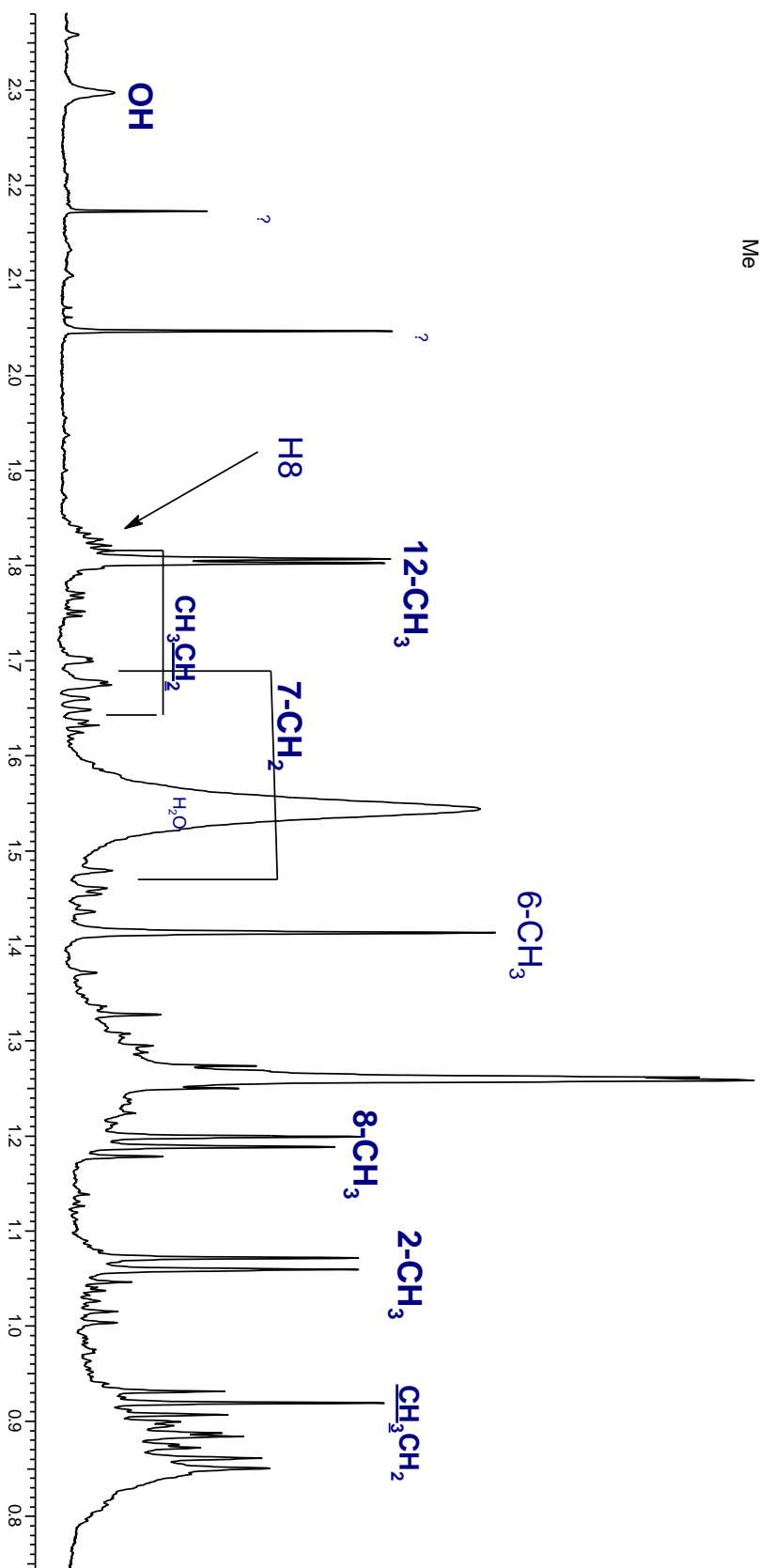
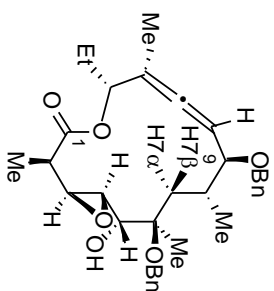


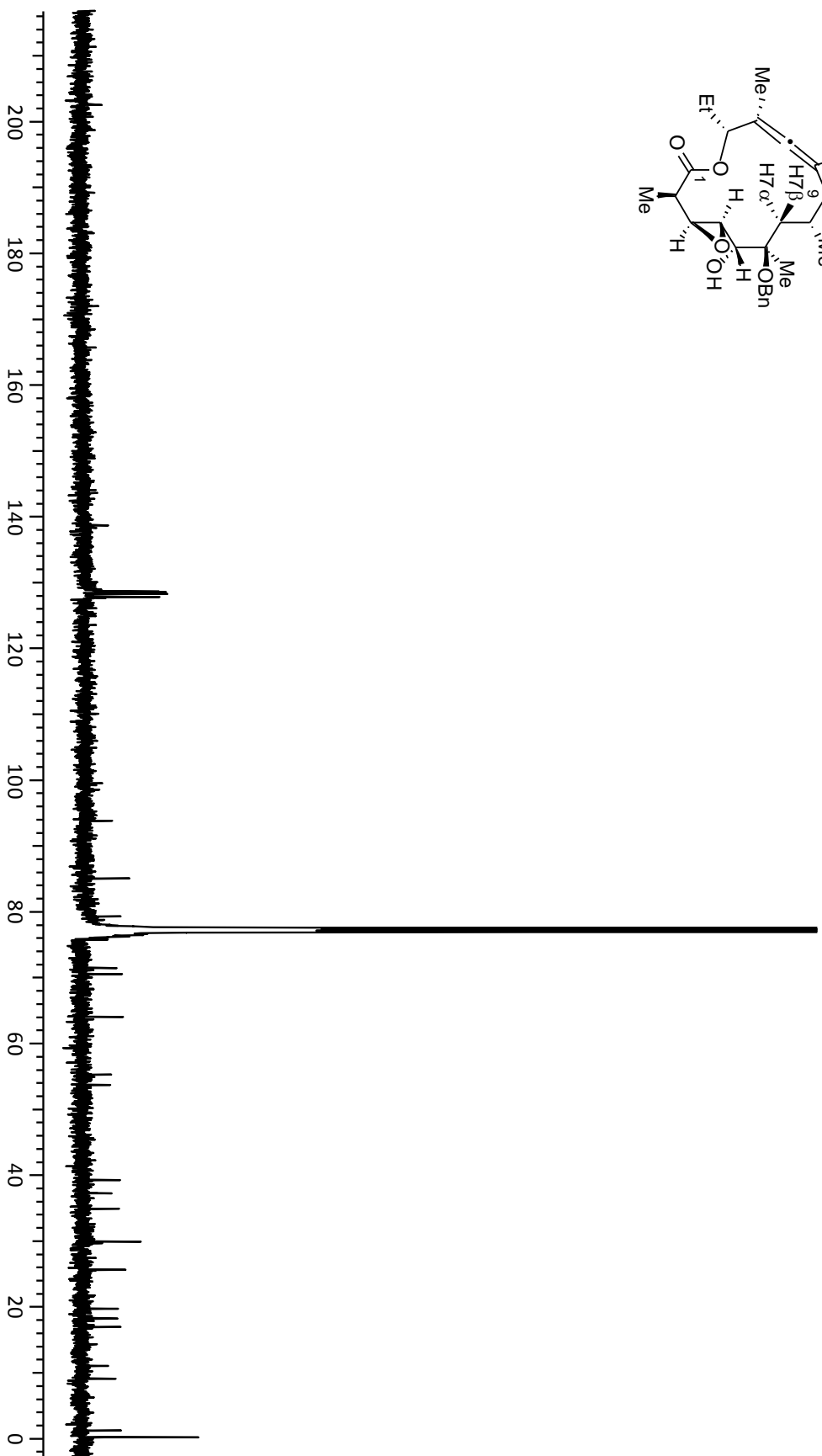
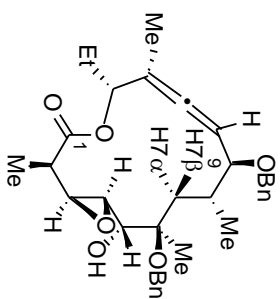
NOESY

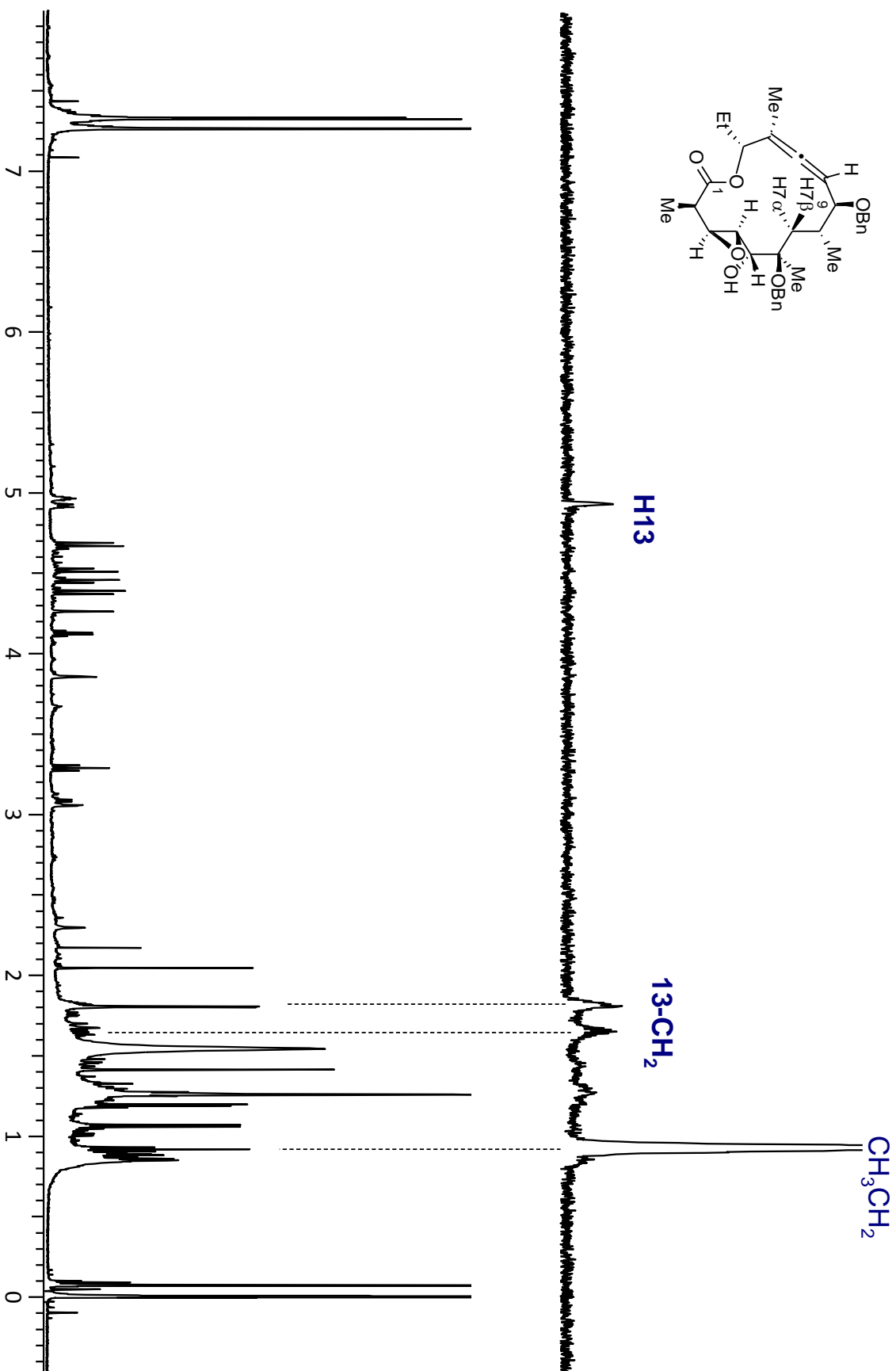
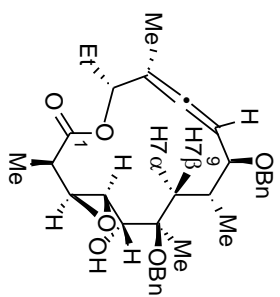


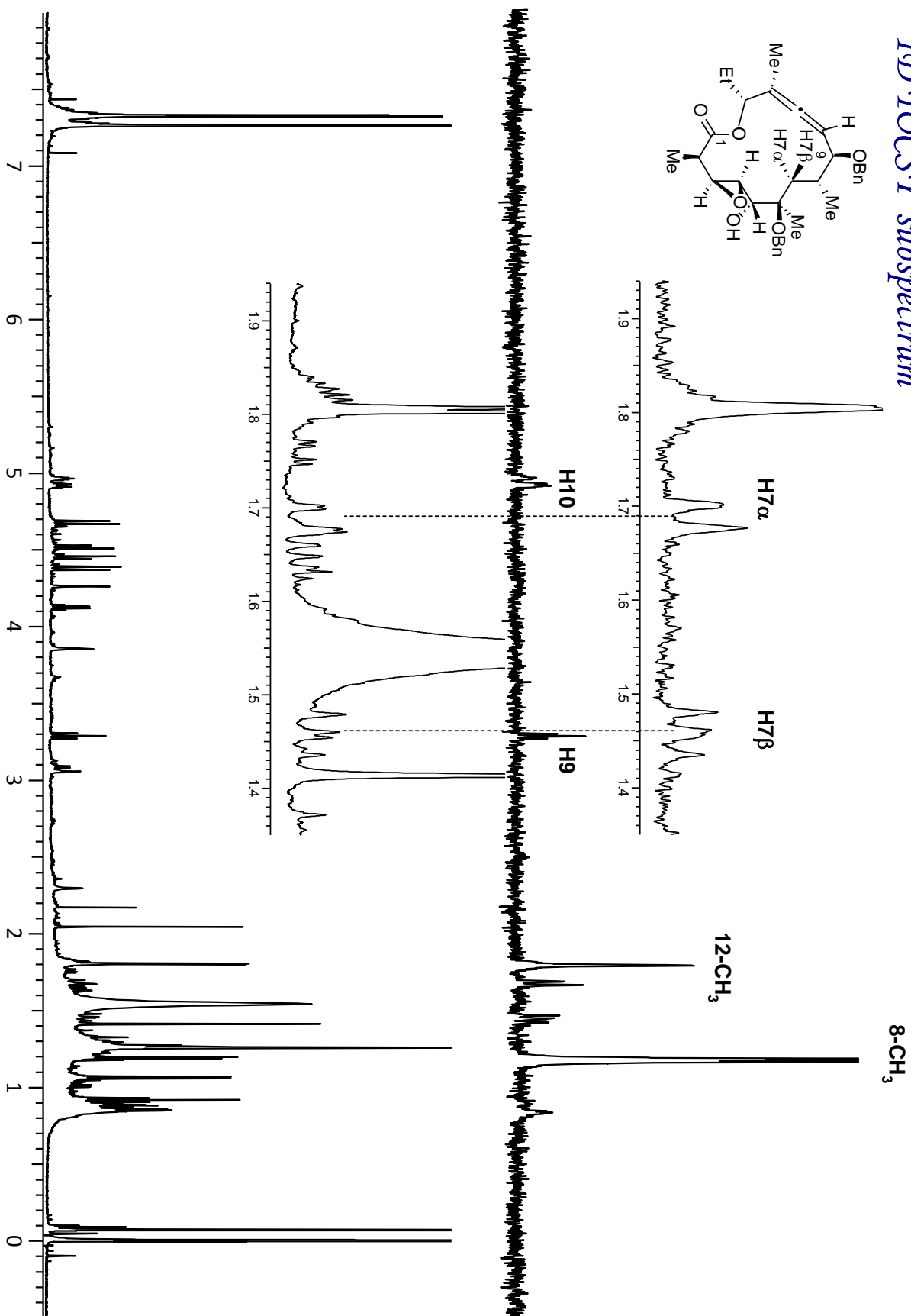


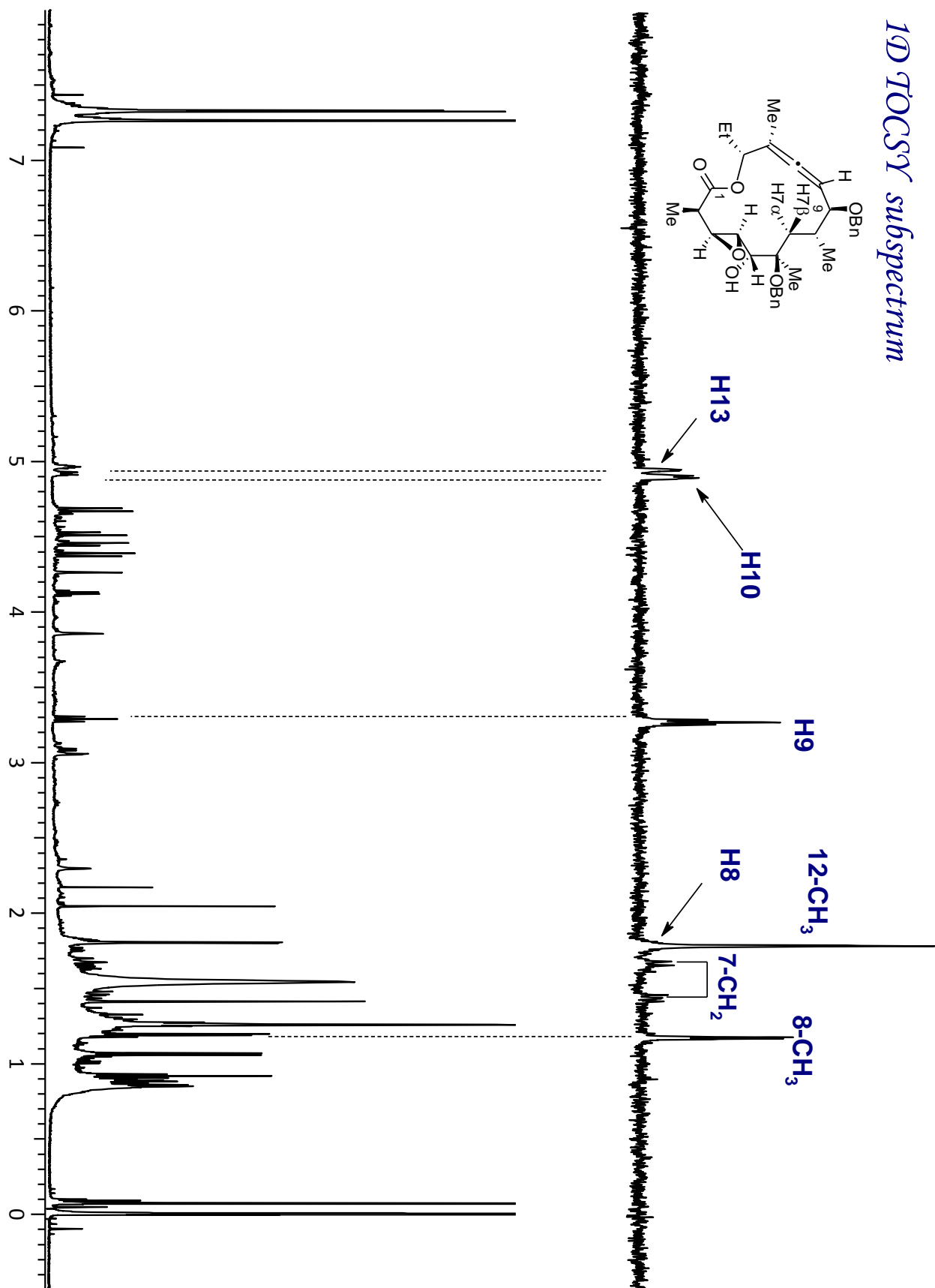


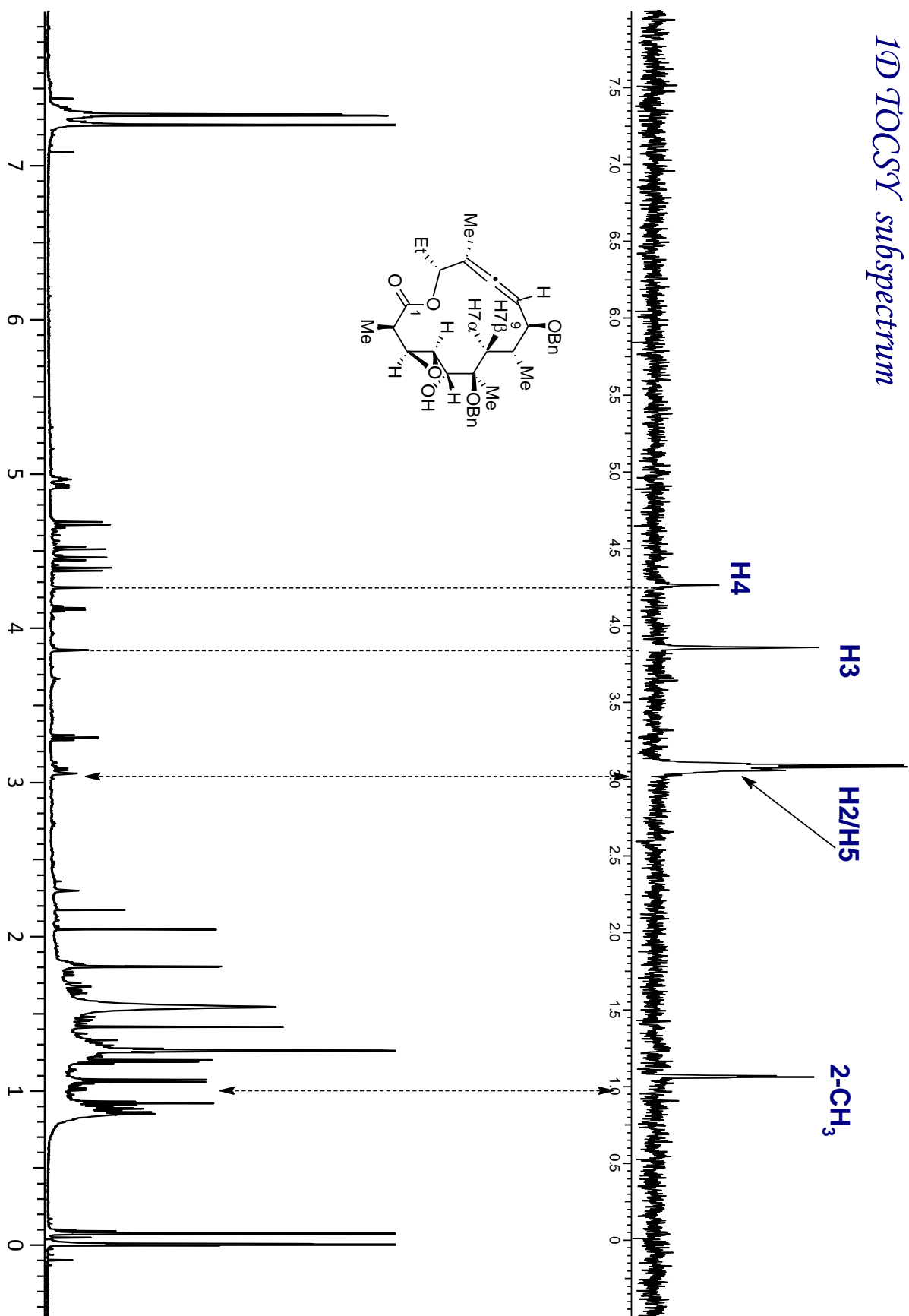
¹H NMR spectrum

^{13}C NMR spectrum

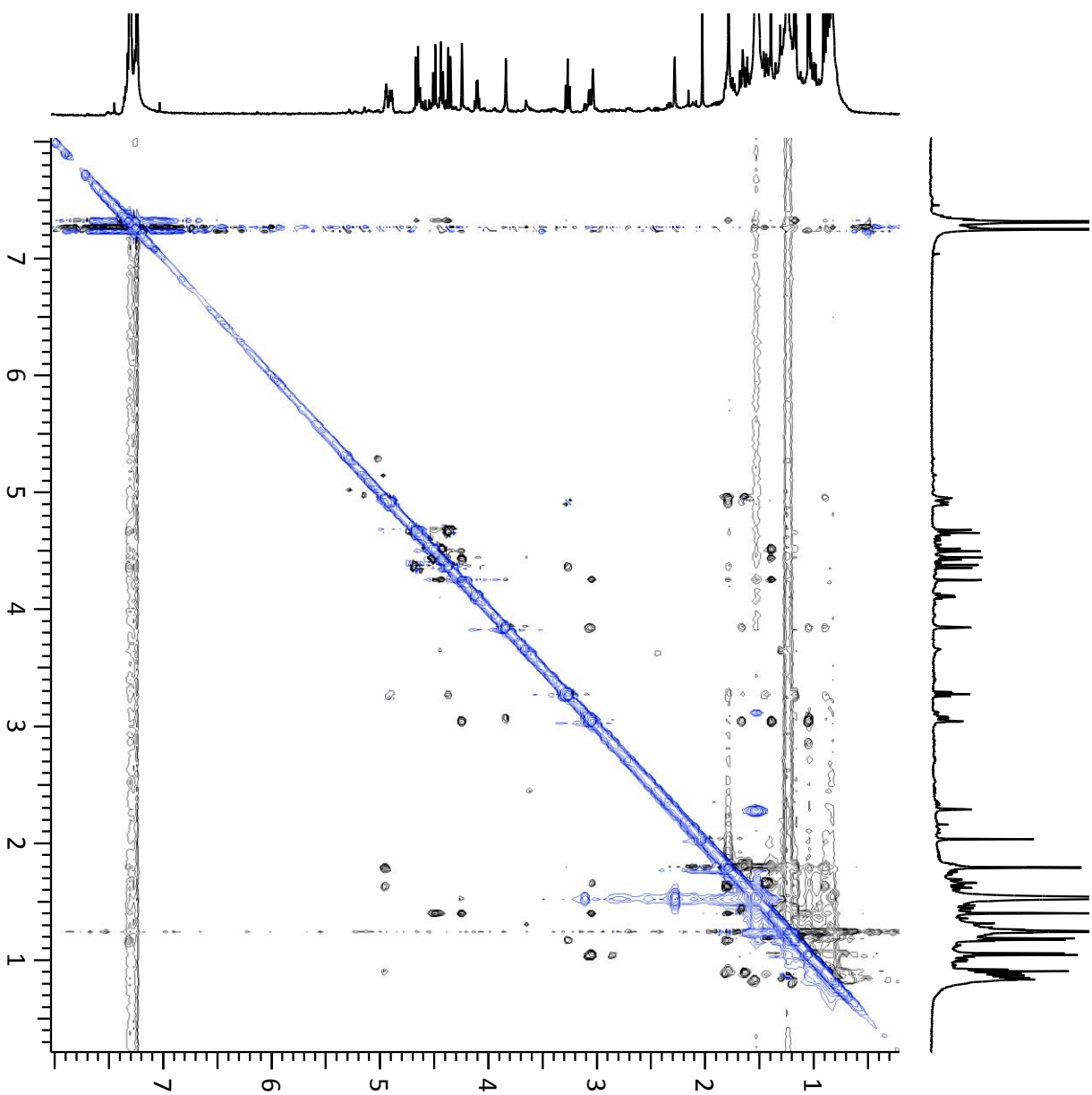
1D TOCSY subspectrum

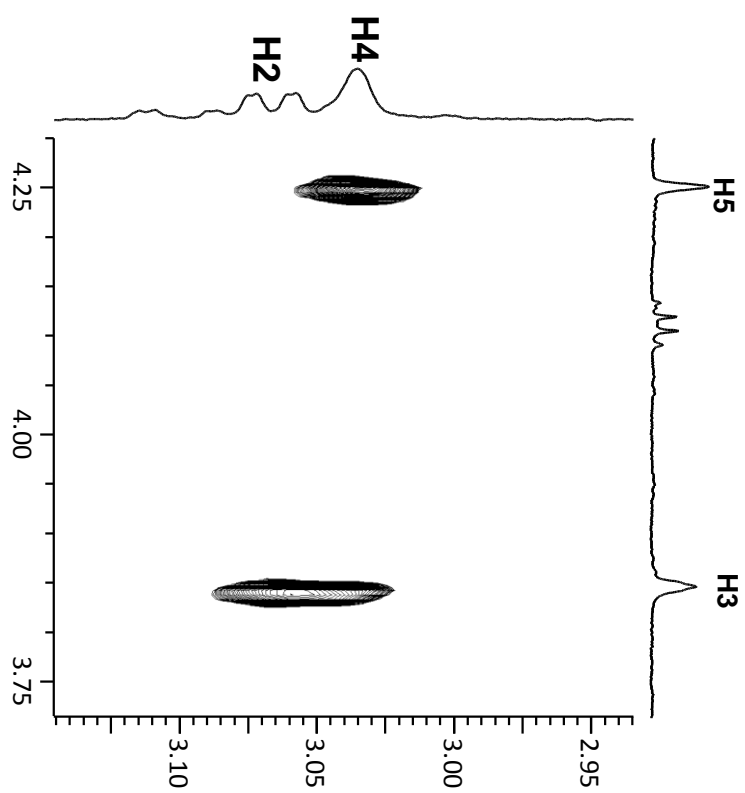
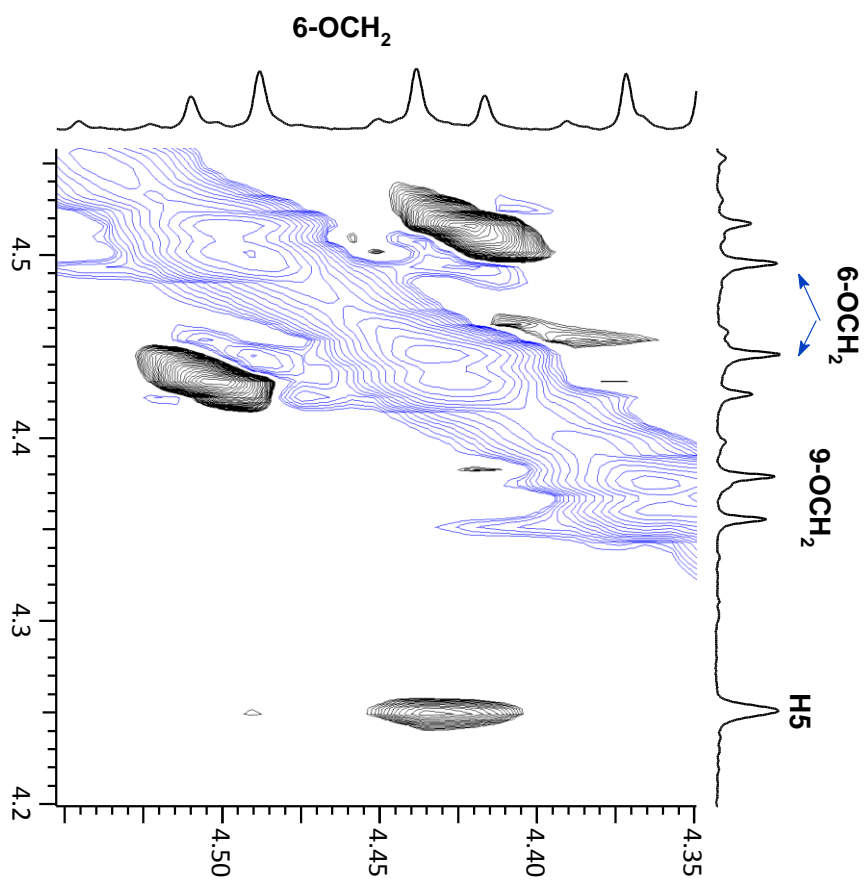
1D TOCSY spectrum

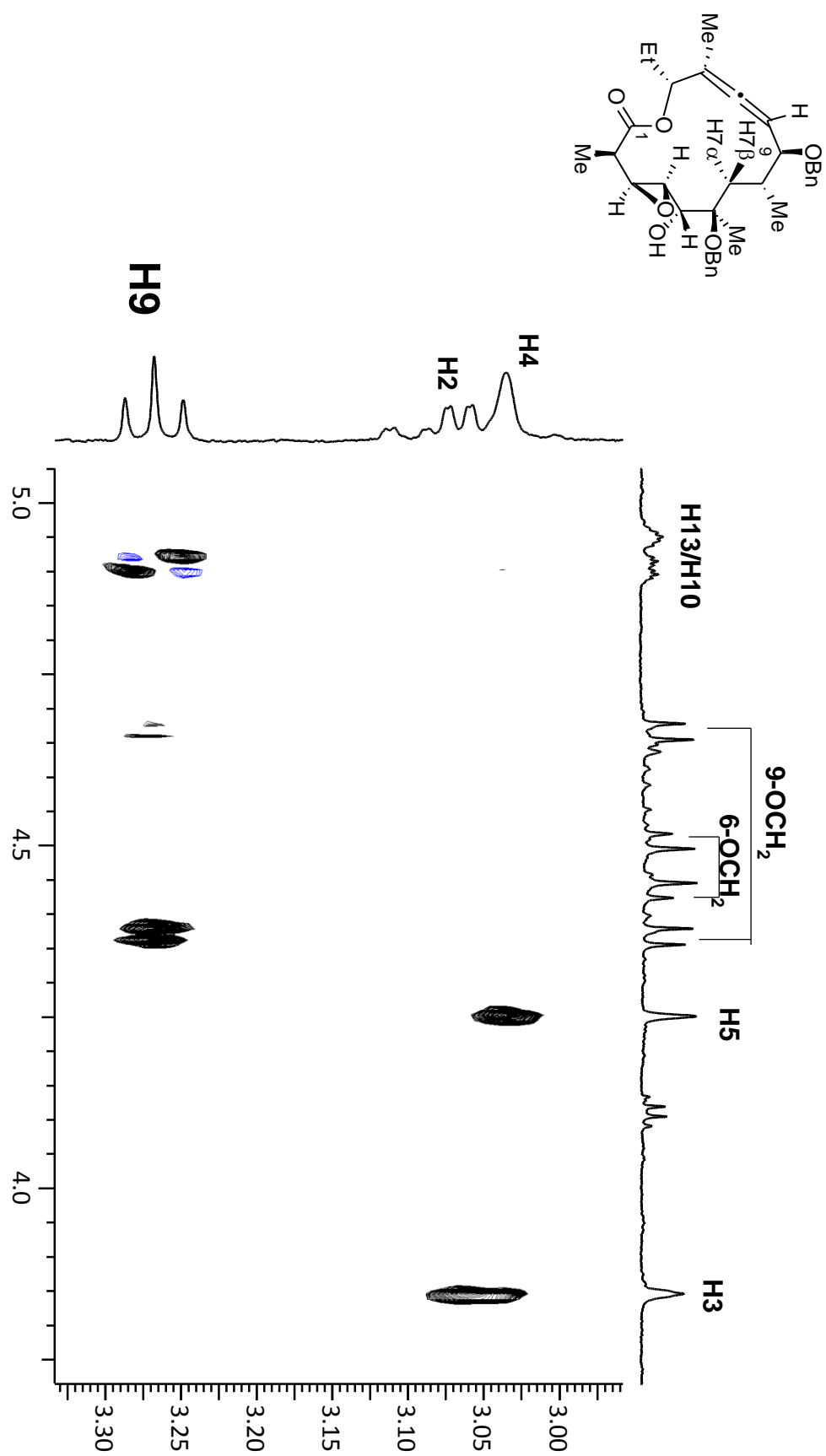
1D TOCSY subspectrum

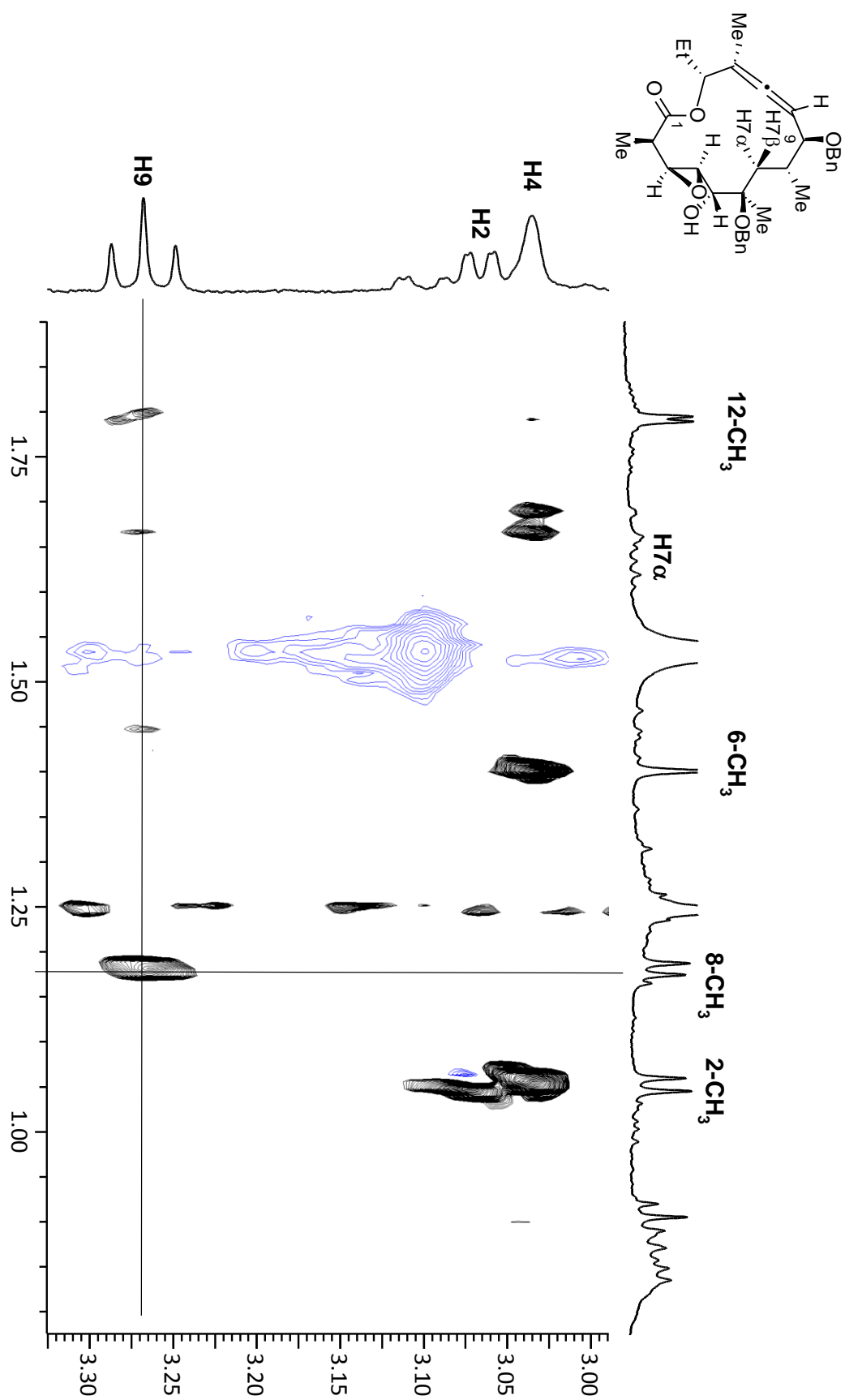
1D TOCSY spectrum

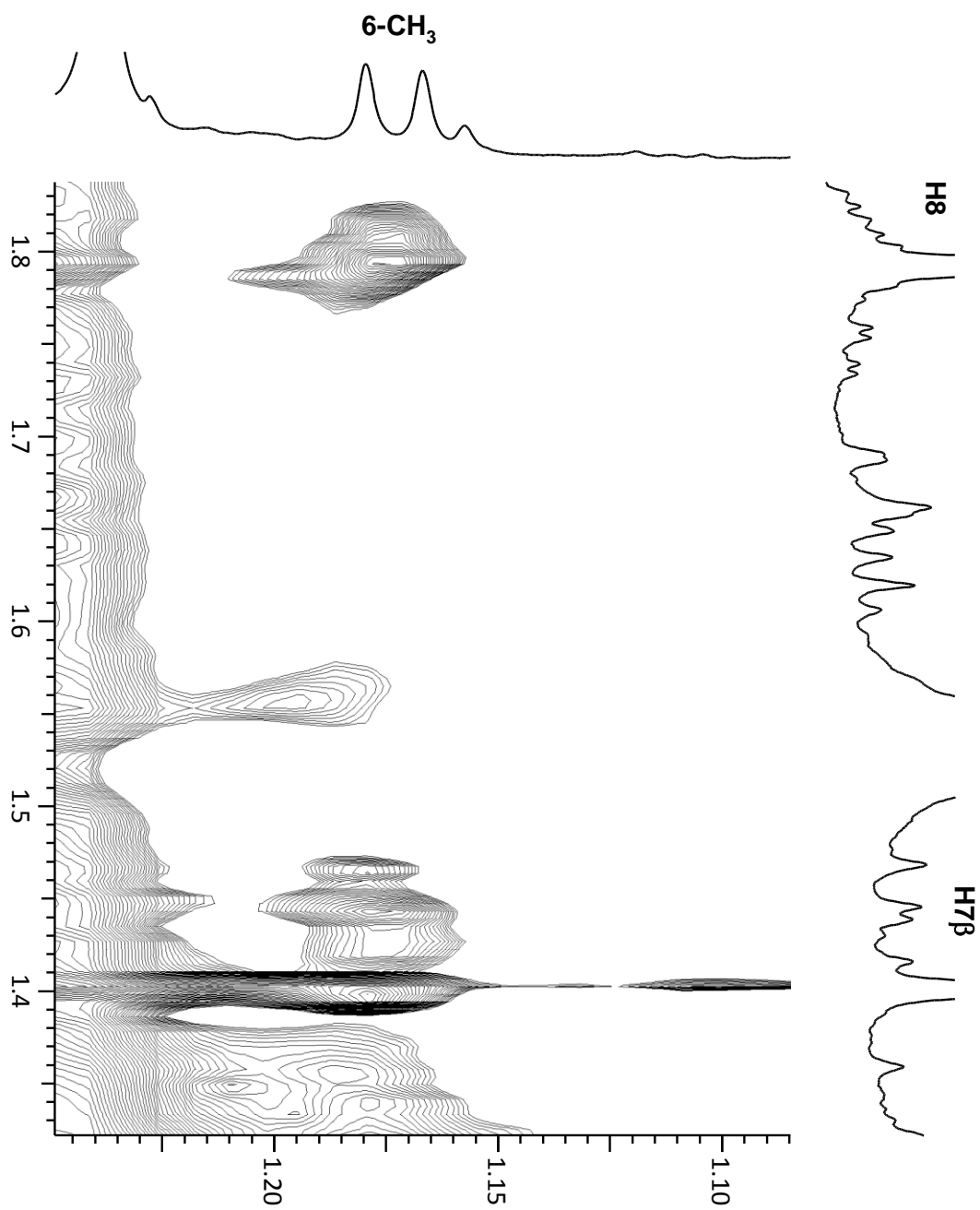
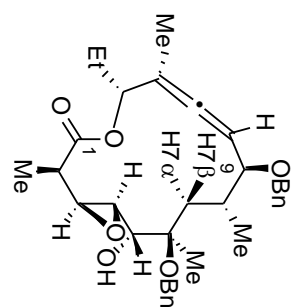
NOESY

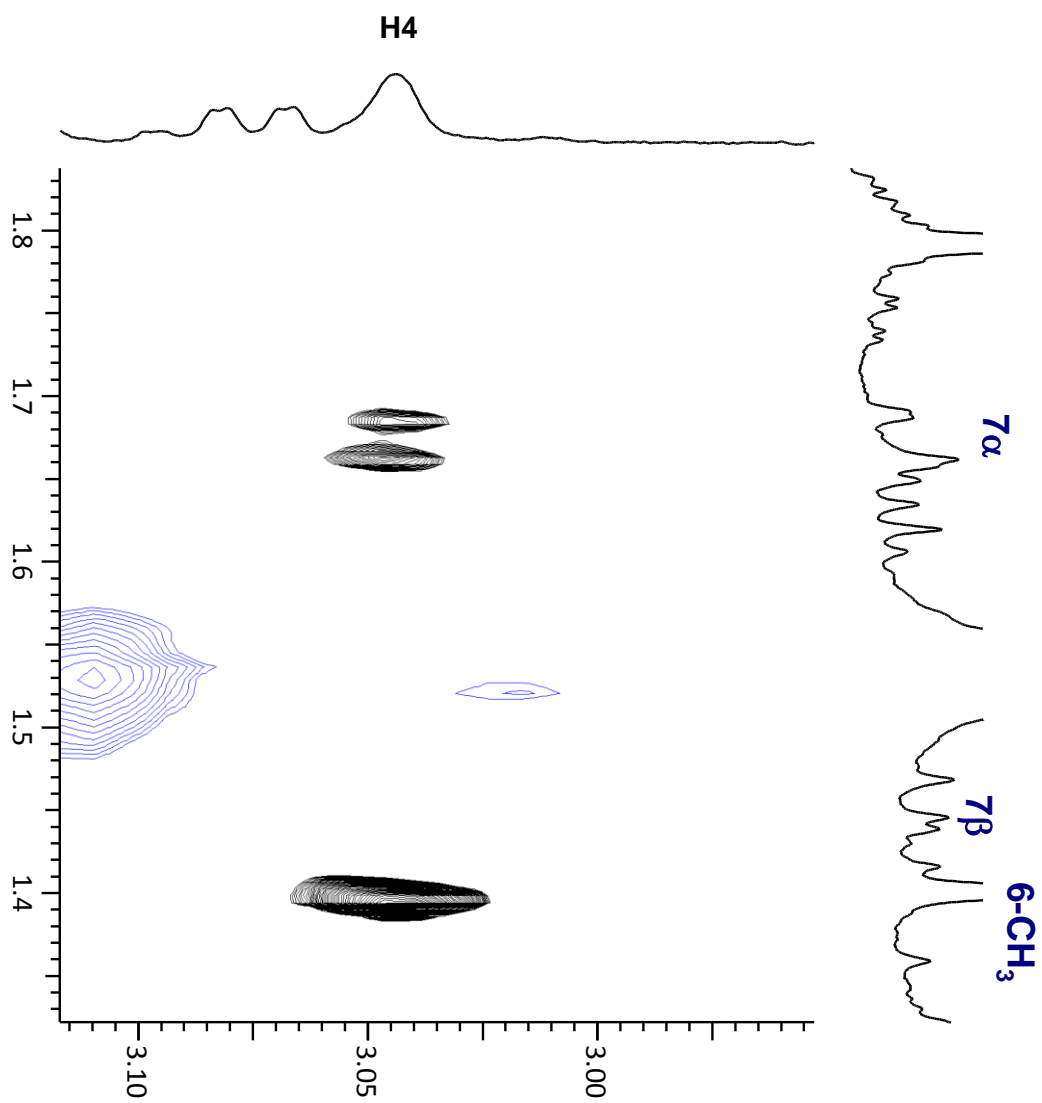
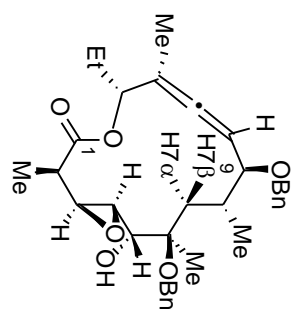


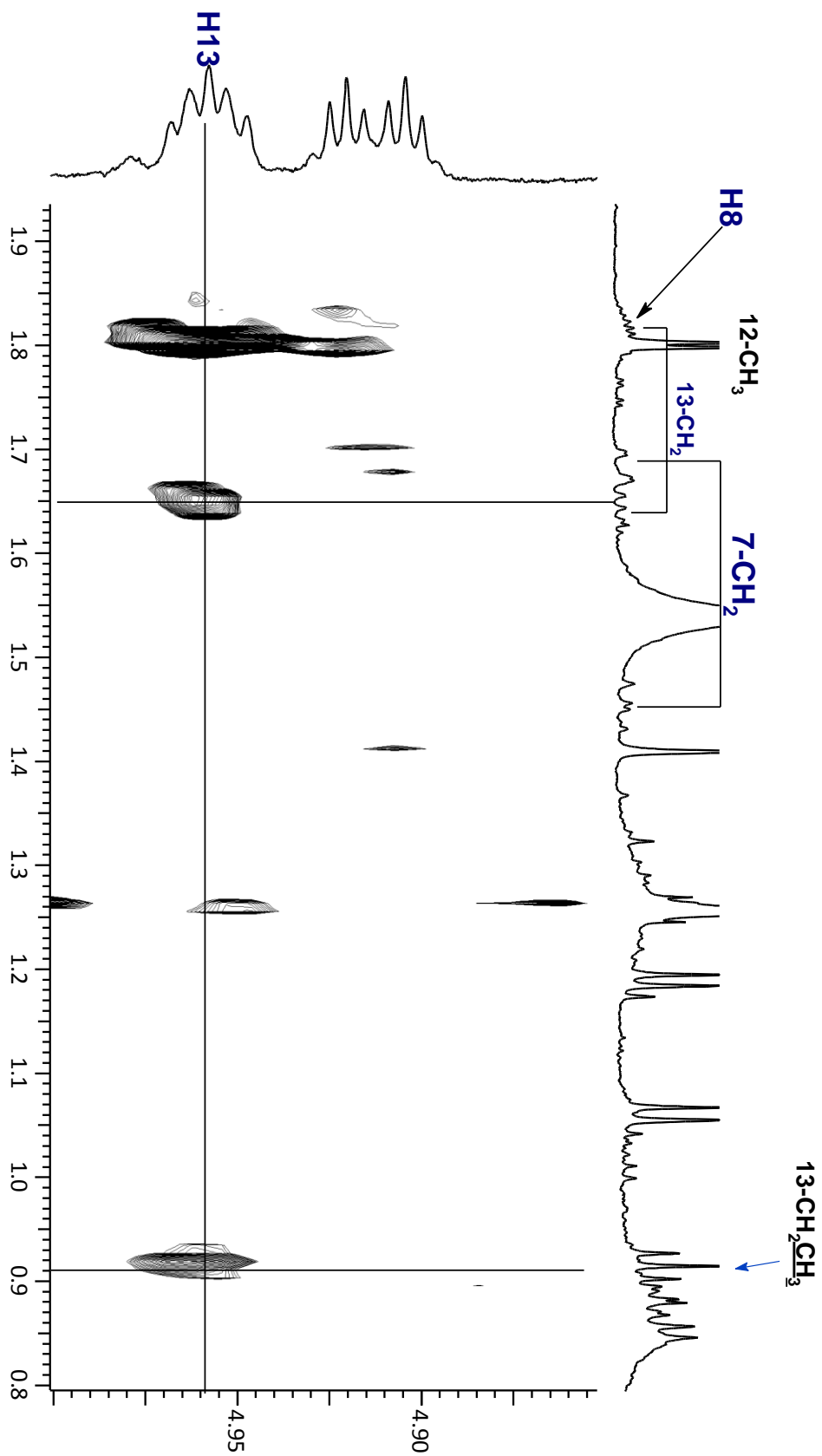


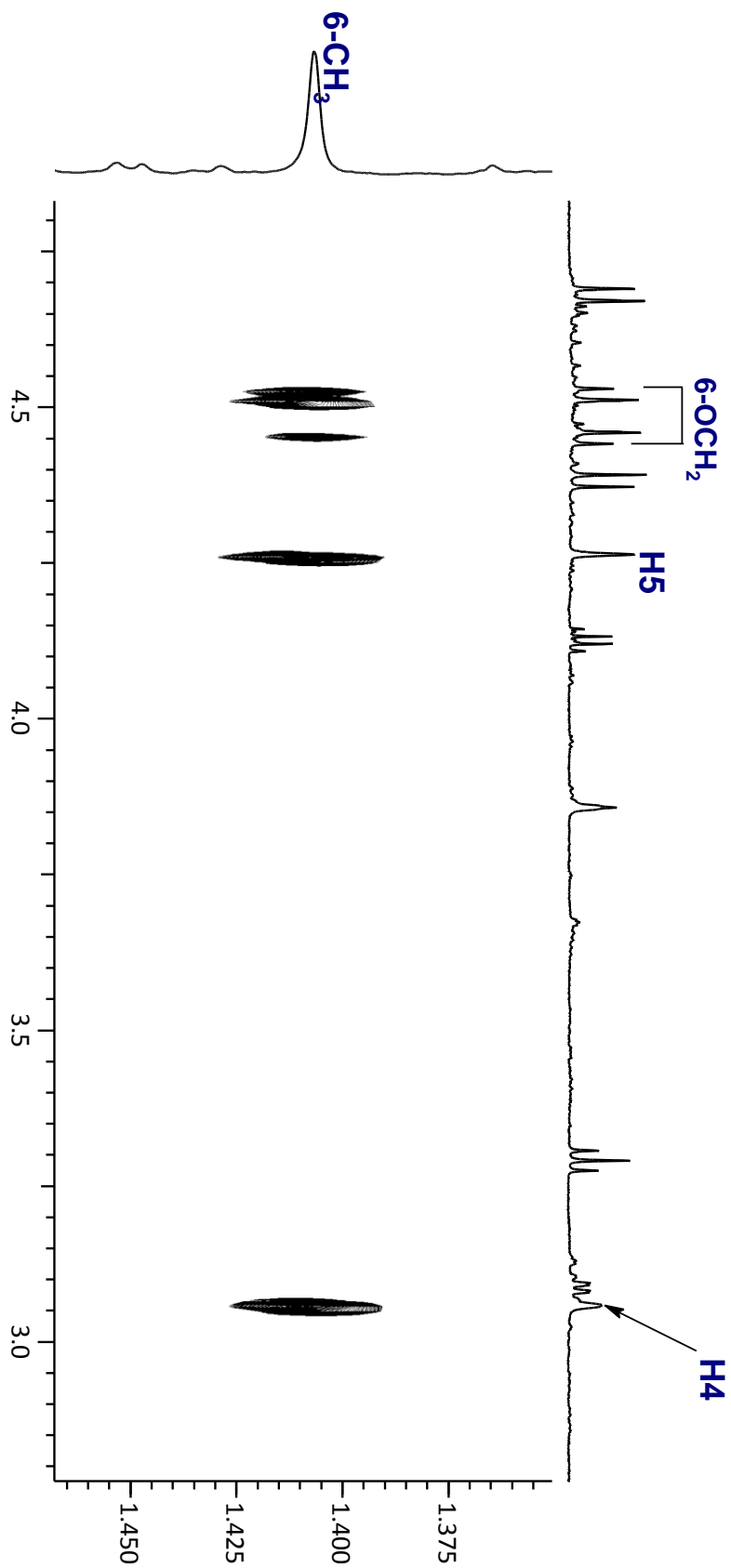
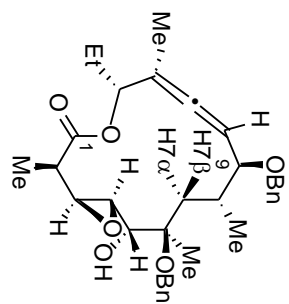


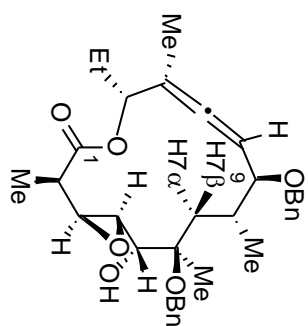


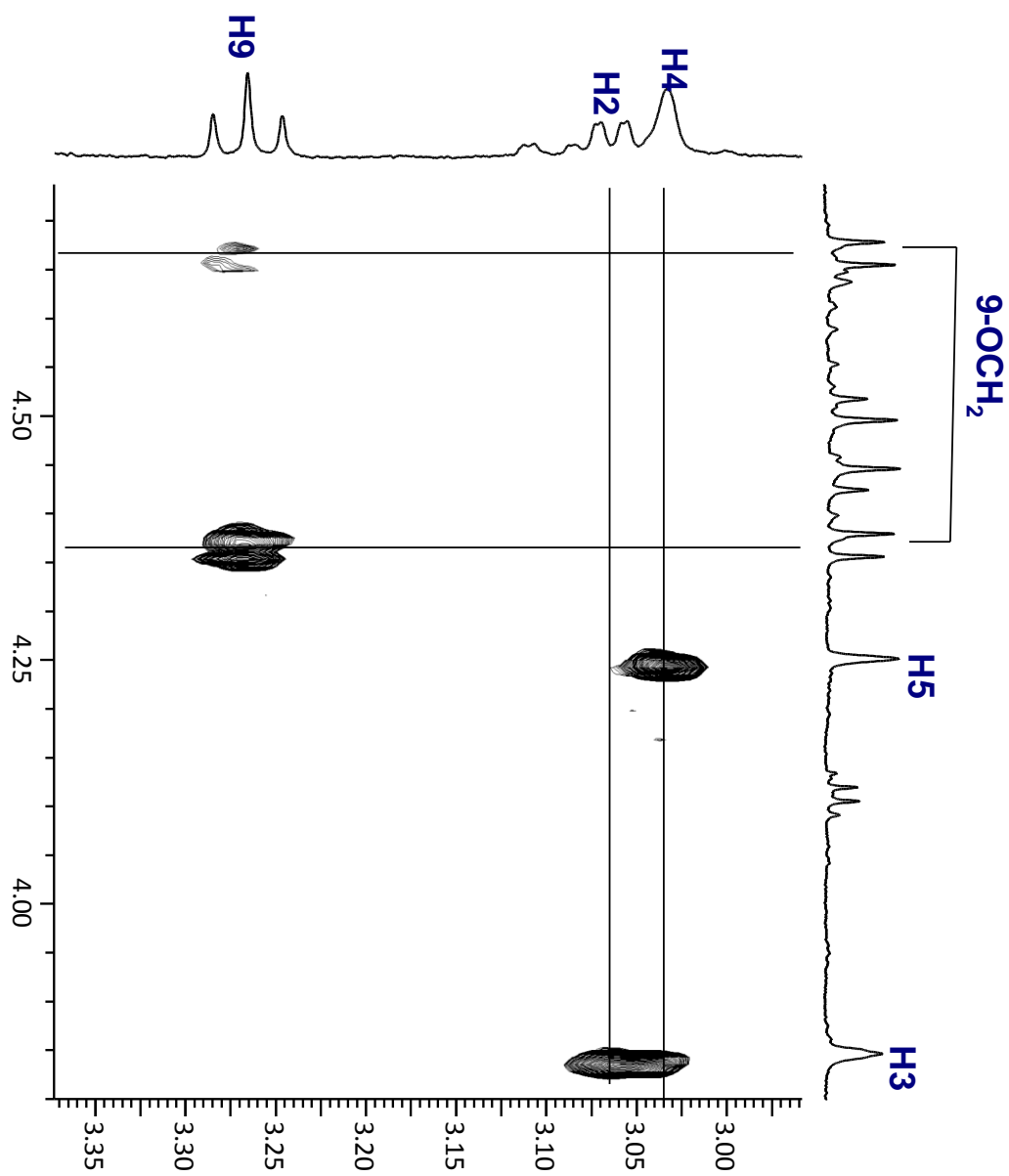
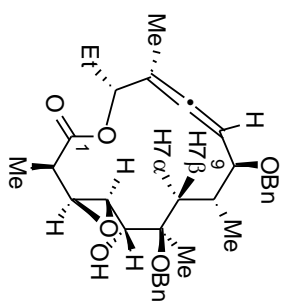


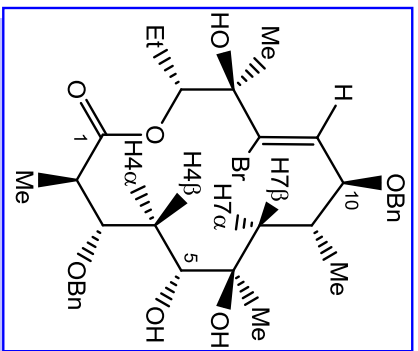












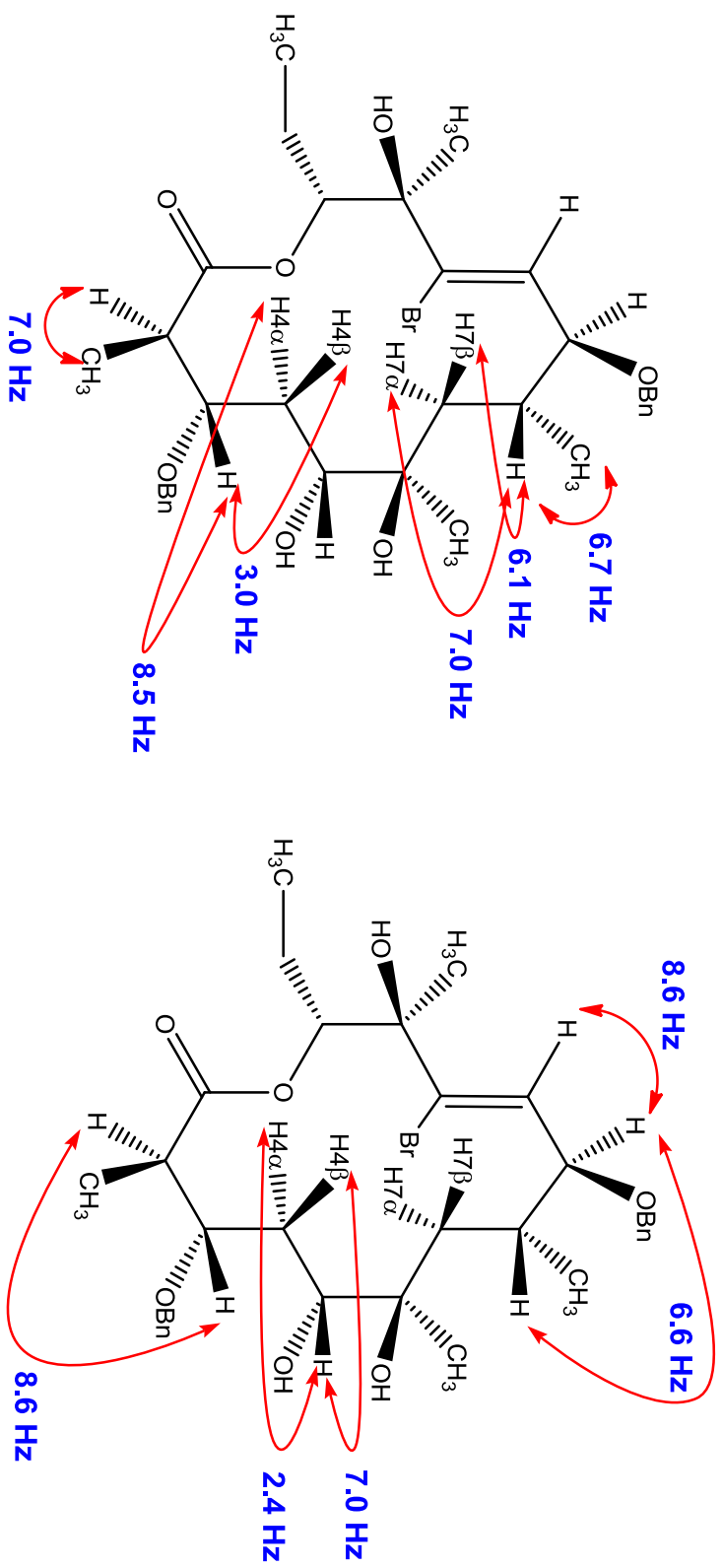
¹H NMR chemical shifts (δ/ppm) & coupling constant (J/Hz)

- 2.65** (qd, $J_{H2, 2-CH3} = 6.9\text{ Hz}$, $J_{H2, H3} = 13.4\text{ Hz}$, **H2**)
1.27 (d, $J_{2-CH3, H2} = 7.0\text{ Hz}$, **2-CH₃**)
4.36 (ddd, $J_{H3, H2} = 8.6\text{ Hz}$, $J_{H3, H4\alpha} = 6.2\text{ Hz}$, $J_{H3, H4\beta} = 2.9\text{ Hz}$, **H3**)
4.58, 4.51 (d, $J_{AB} = 10.7\text{ Hz}$, **C3-OCH₂**)
1.83 (dd, $J_{H4\alpha, H4\beta} = 15.0\text{ Hz}$, $J_{H4\alpha, H3} = 8.5\text{ Hz}$, **H4 α**)
1.77 (dd, $J_{H4\beta, H4\alpha} = 15.0\text{ Hz}$, $J_{H4\beta, H3} = 3.0\text{ Hz}$, **H4 β**)
3.51 (dd, $J_{H5, H4\alpha} = 2.4\text{ Hz}$, $J_{H5, H4\beta} = 7.0\text{ Hz}$, **H5**)
1.28 (s, **6-CH₃**)
1.61 (dd, $J_{H7\beta, H8} = 6.1\text{ Hz}$, $J_{H7\beta, H7\alpha} = 14.7\text{ Hz}$, **H7 β**)
1.17 (dd, $J_{H7\alpha, H8} = 7.0\text{ Hz}$, $J_{H7\alpha, H7\beta} = 14.9\text{ Hz}$, **H7 α**)
2.31 (dt, $J_{H8, 8-CH3} = 6.4\text{ Hz}$, **H8**)
1.12 (d, $J_{8-CH3, H8} = 6.7\text{ Hz}$, **8-CH₃**)
4.11 (dd, $J_{H9, H10} = 8.6\text{ Hz}$, $J_{H9, H8} = 6.6\text{ Hz}$, **H9**)
4.58, 4.47 (d, $J_{AB} = 12.4\text{ Hz}$, **9-OCH₂**)
6.38 (d, $J_{H10, H9} = 8.6\text{ Hz}$, **H10**)
1.50 (s, **12-CH₃**)
4.88 (dd, $J_{H13, H14} = 2.3$, 11.0 Hz , **H13**)
1.73-1.85 (m, **14-CH₂**)
0.89 (t, $J_{14-CH3, H14} = 7.4\text{ Hz}$, **14-CH₃**)

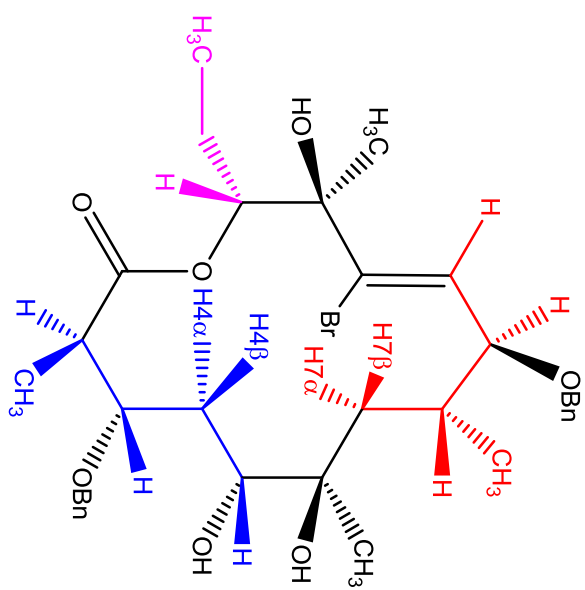
¹³C NMR chemical shift (δ/ppm)

176.8	—	C1
44.8	—	C2
78.2	—	C3
35.9	—	C4
75.2	—	C5
73.7	—	C6
40.8	—	C7
34.6	—	C8
84.7	—	C9
131.4	—	C10
133.0	—	C11
77.6	—	C12
81.3	—	C13
24.7	—	C14
12.4	—	2-CH ₃
27.7	—	6-CH ₃
20.0	—	8-CH ₃
26.0	—	12-CH ₃
11.4	—	14-CH ₃
73.1	—	6-OCH ₃
71.9	—	9-OCH ₃
137.9, 139.0	—	ipsoC (C ₃ , C ₉)
128.1, 128.0	—	orthoC (C ₃ , C ₉)
126.5, 128.3	—	metaC (C ₃ , C ₉)
127.9, 127.6	—	paraC (C ₃ , C ₉)

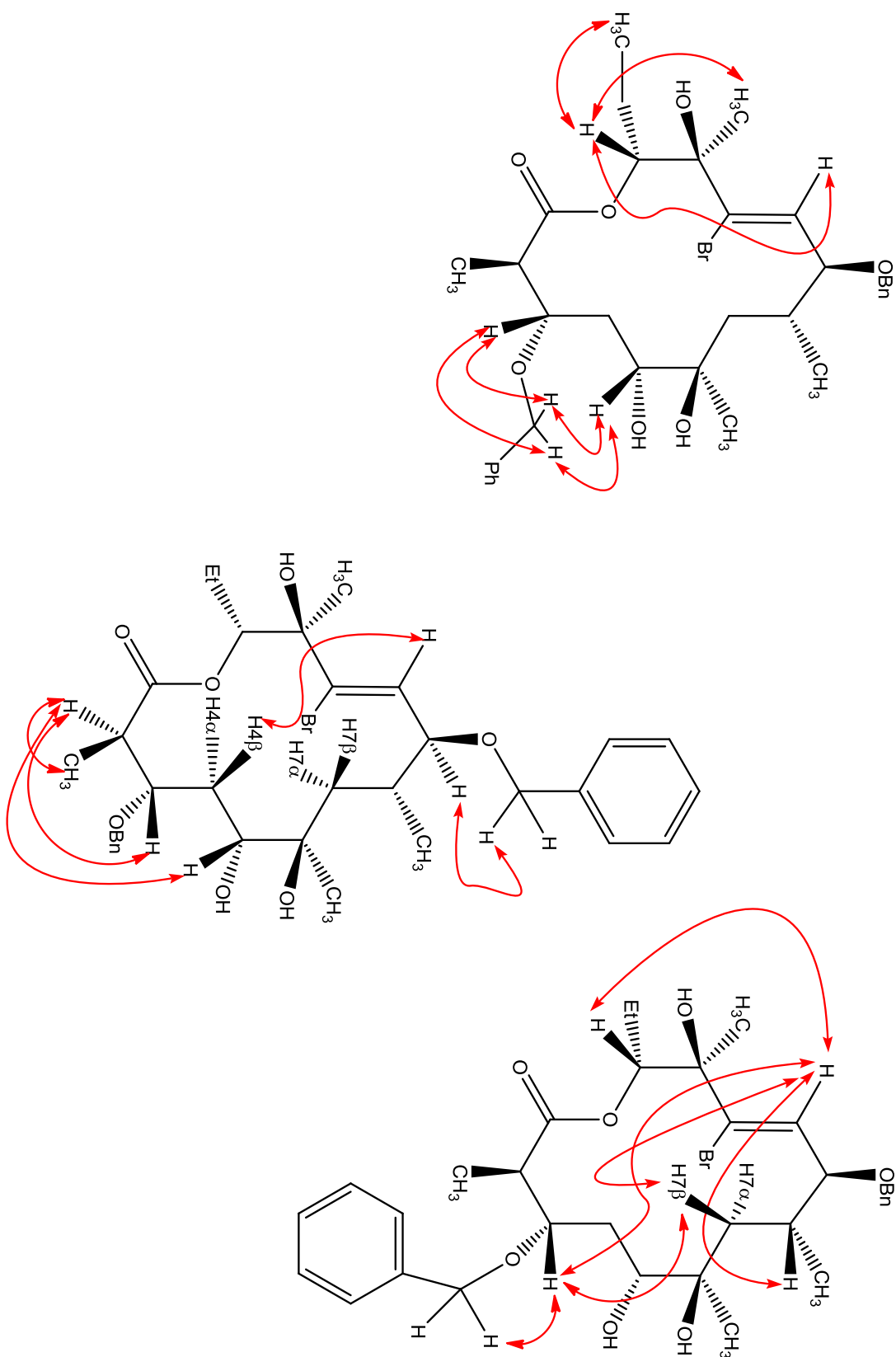
Coupling constant (J_{HH})



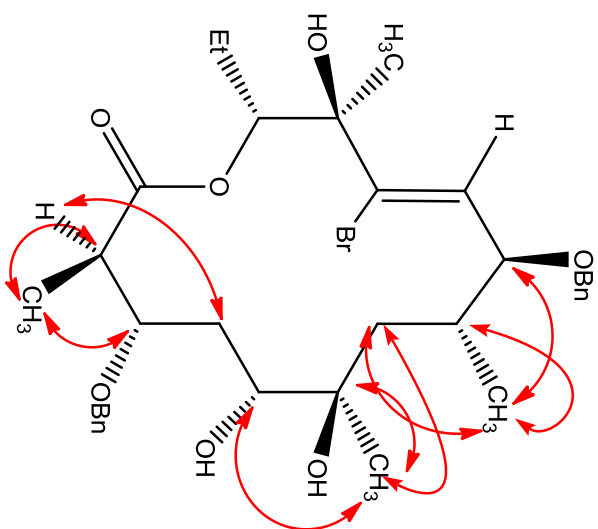
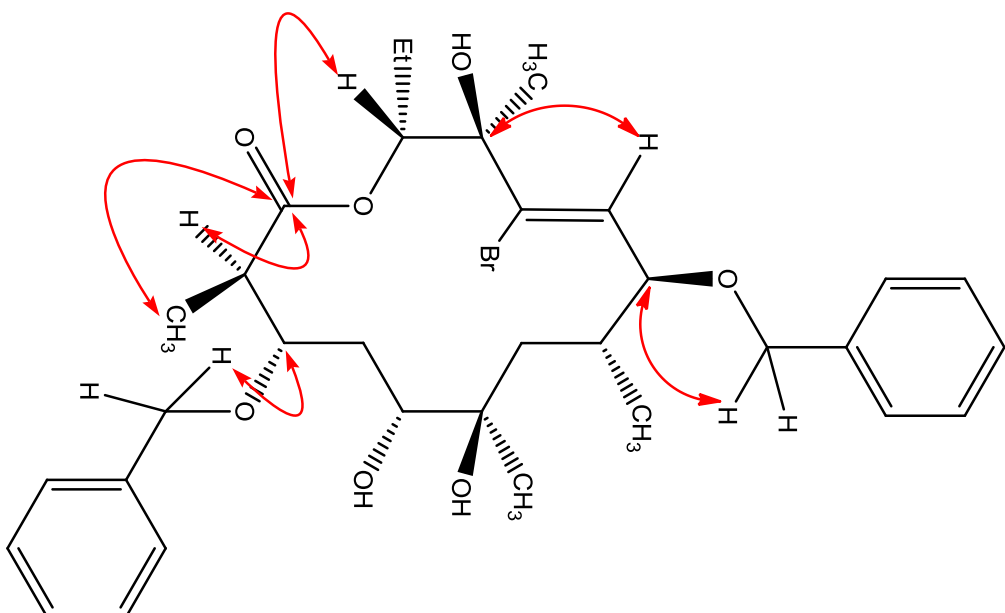
1d TOCSY

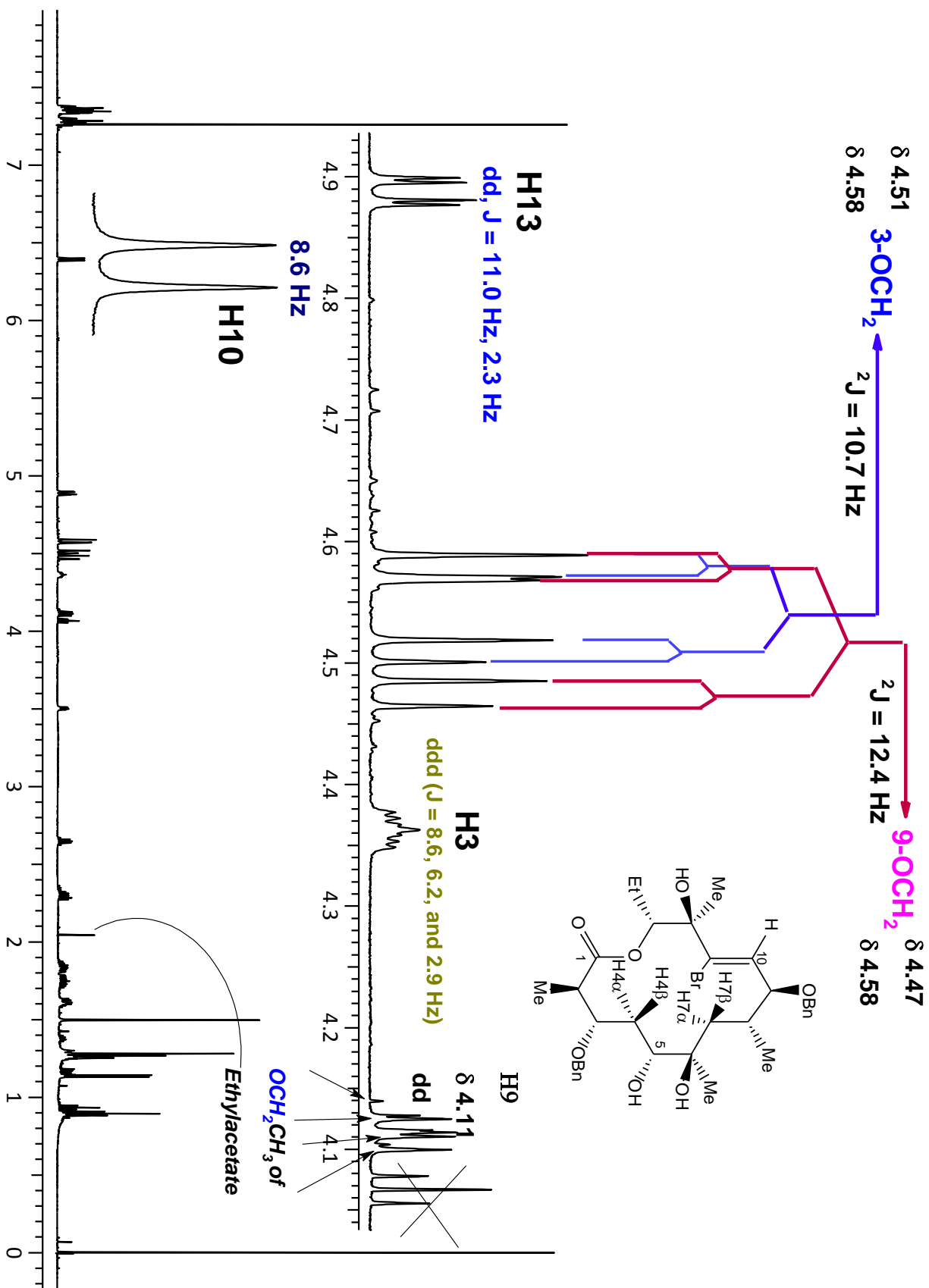


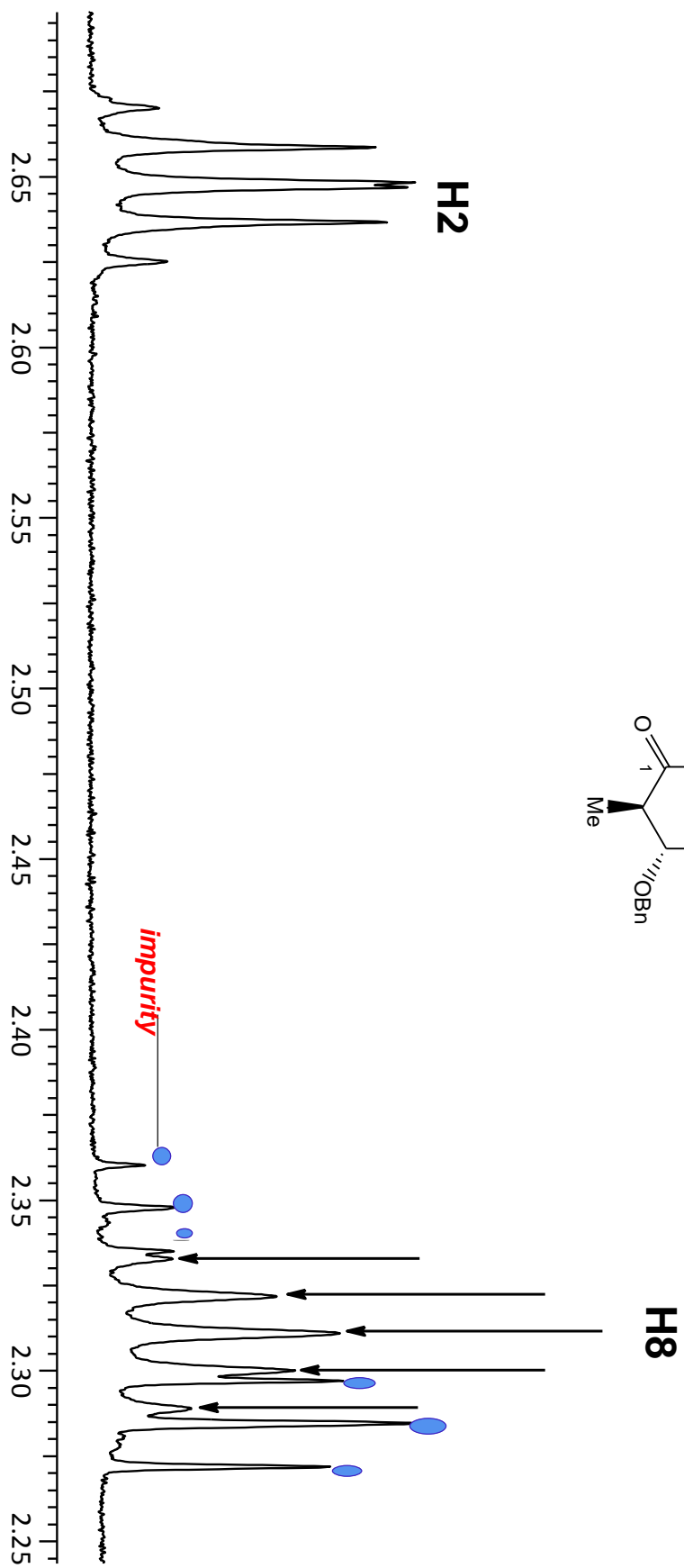
NOE

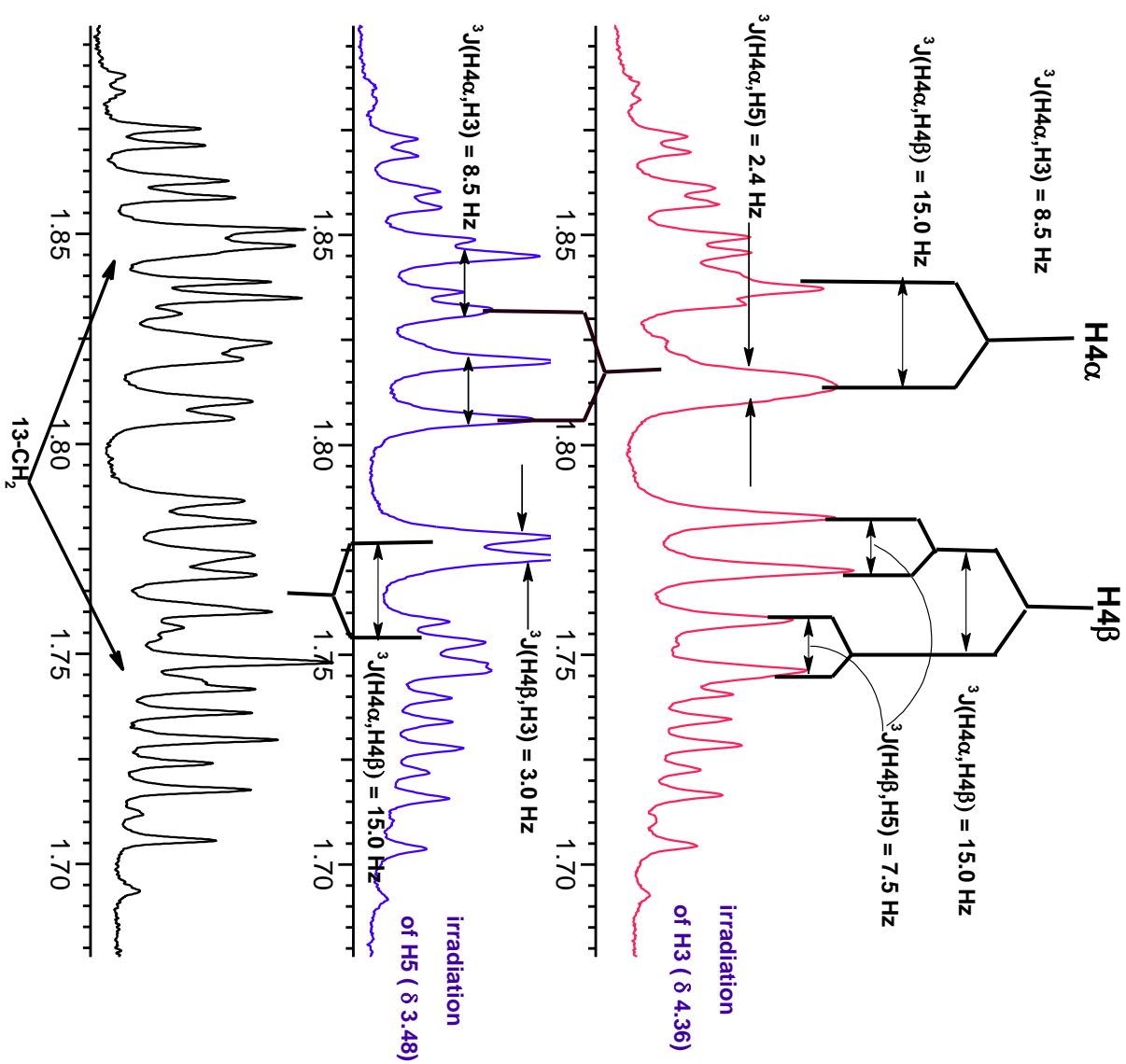
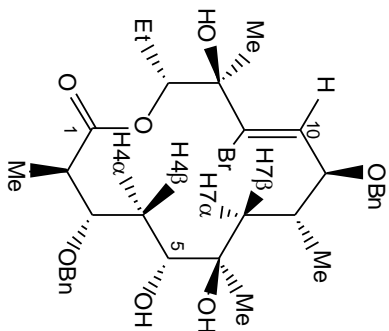


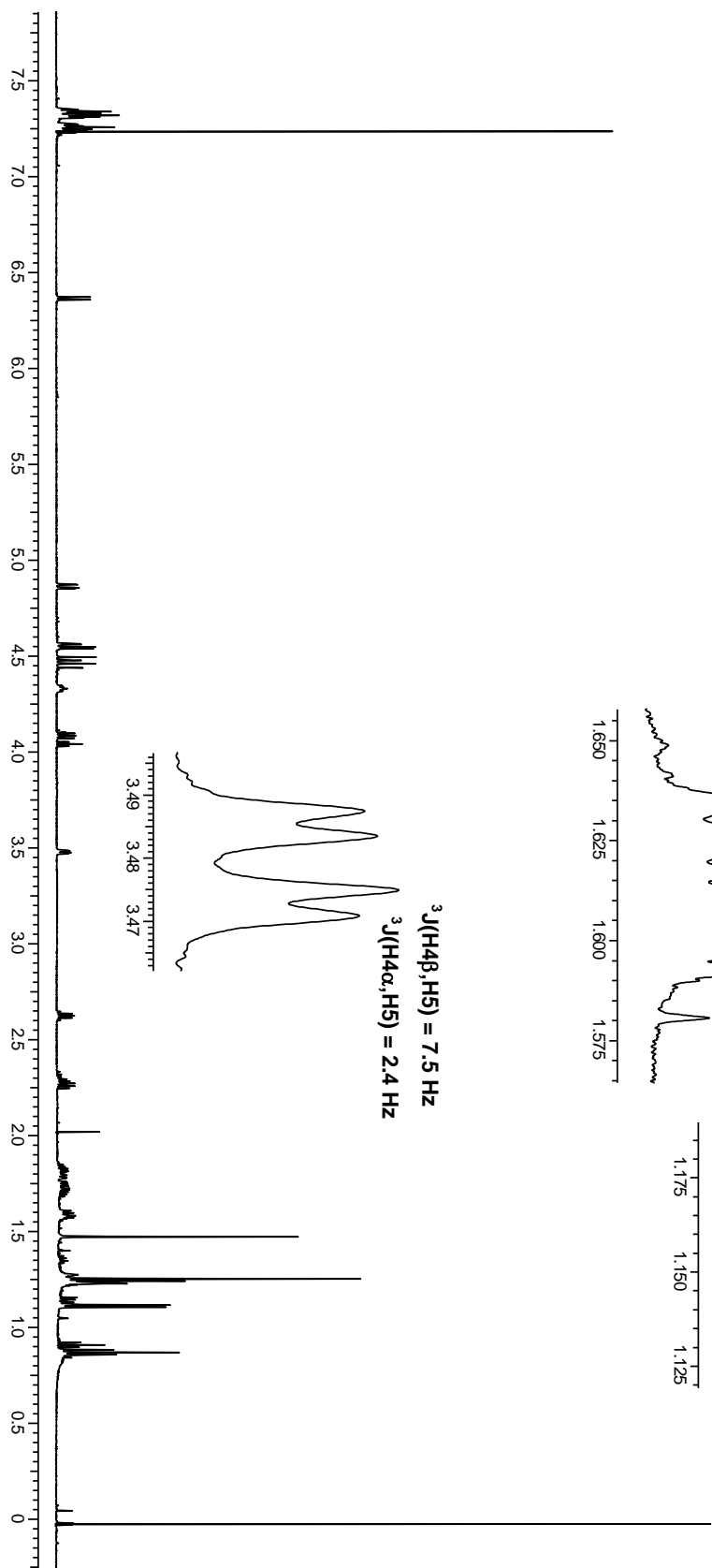
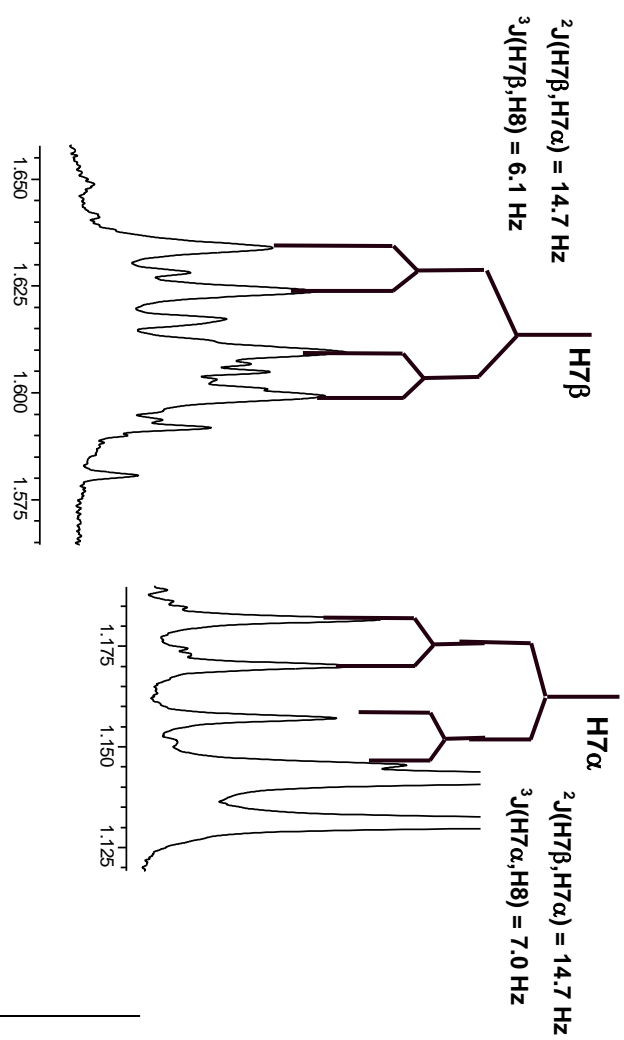
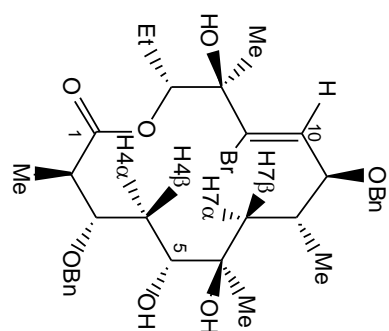
HMBC



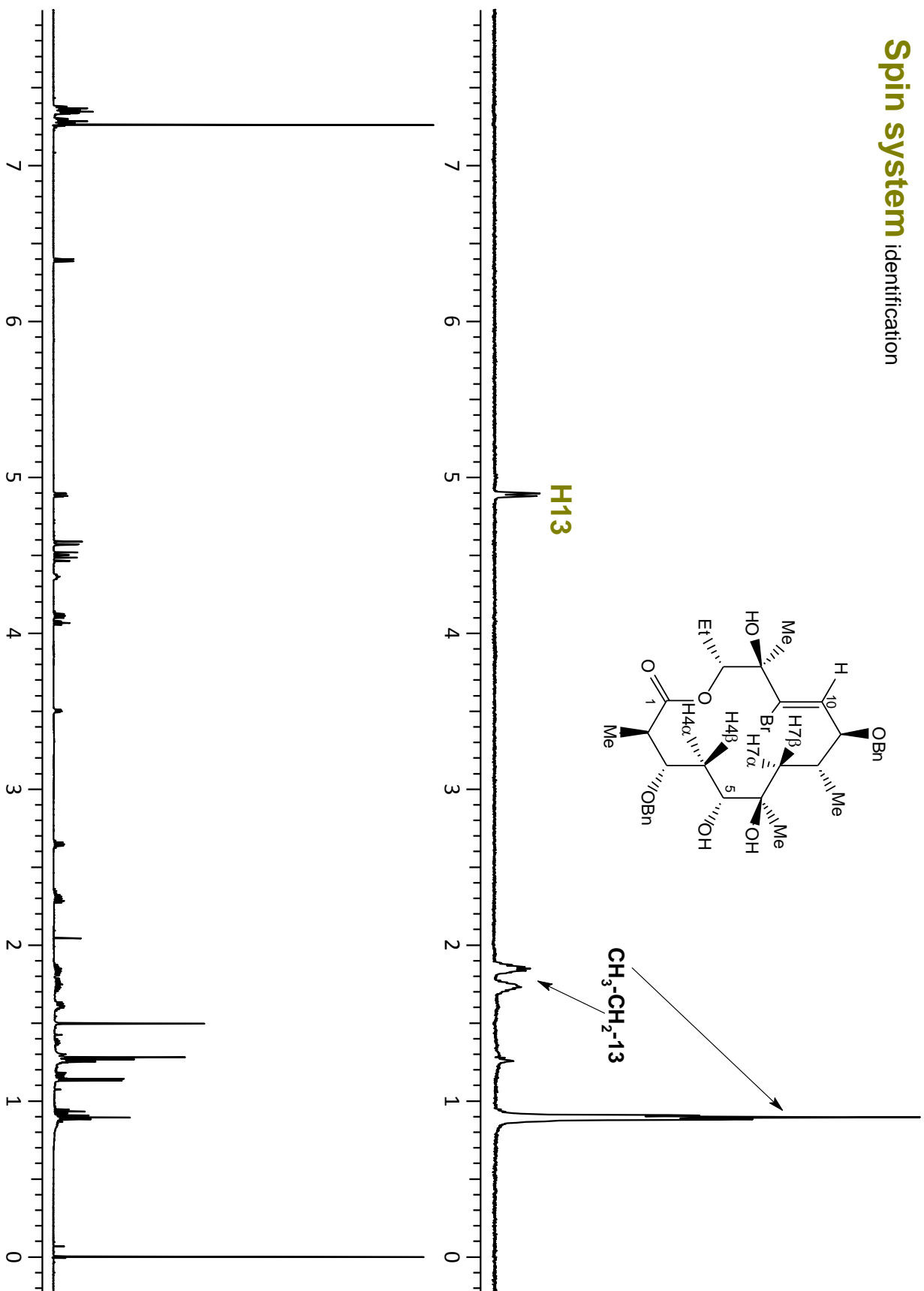




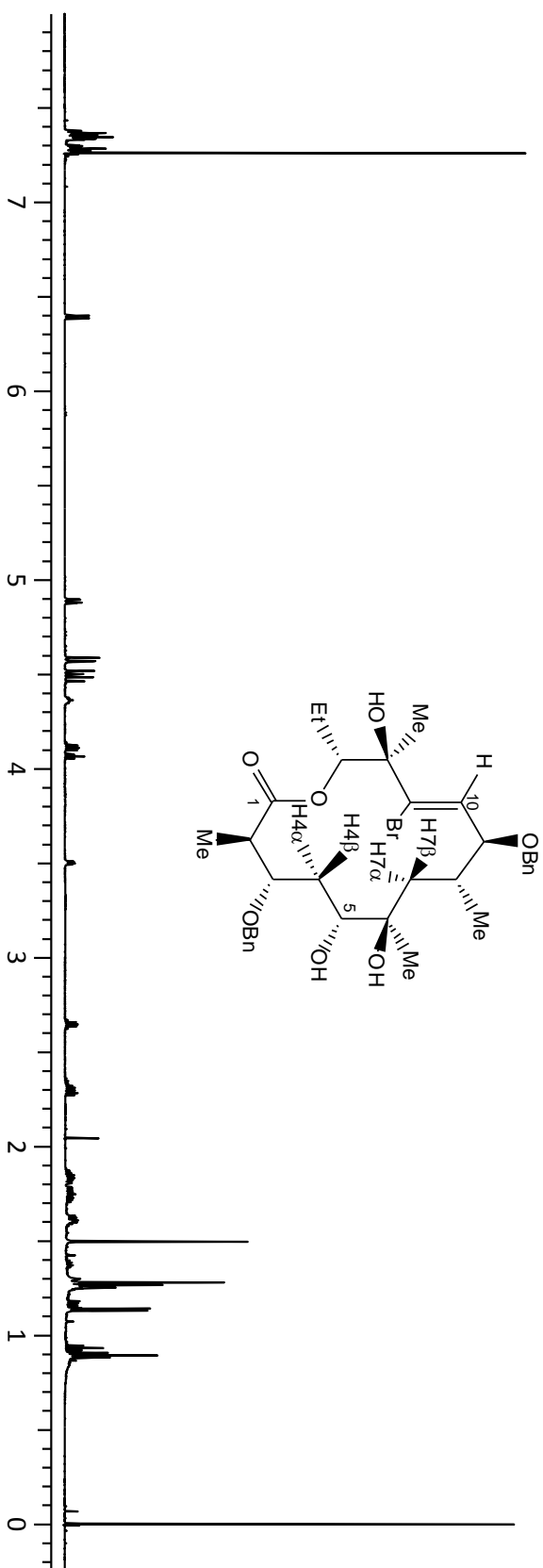
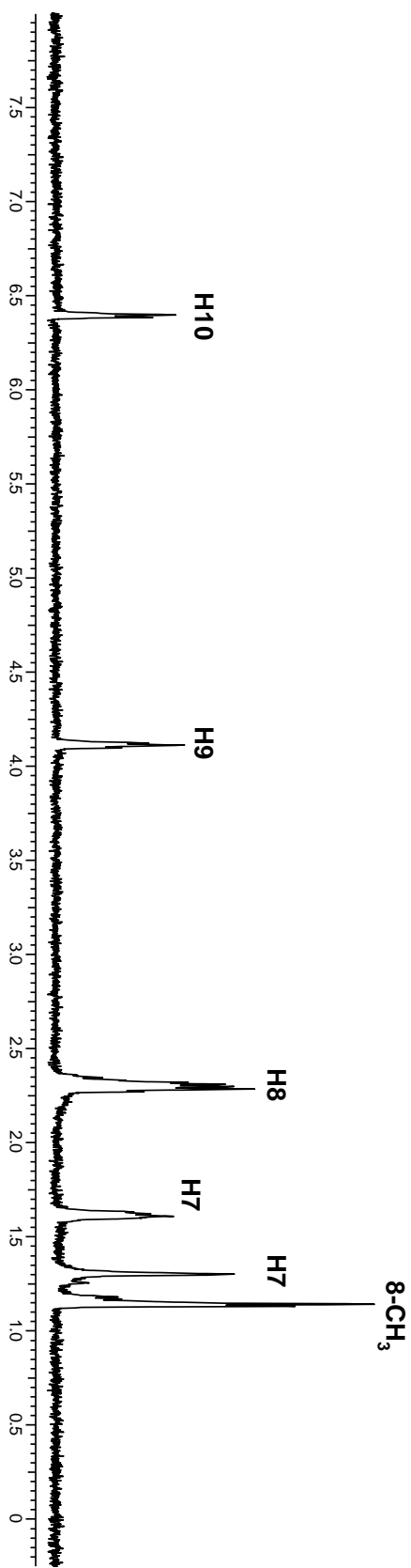




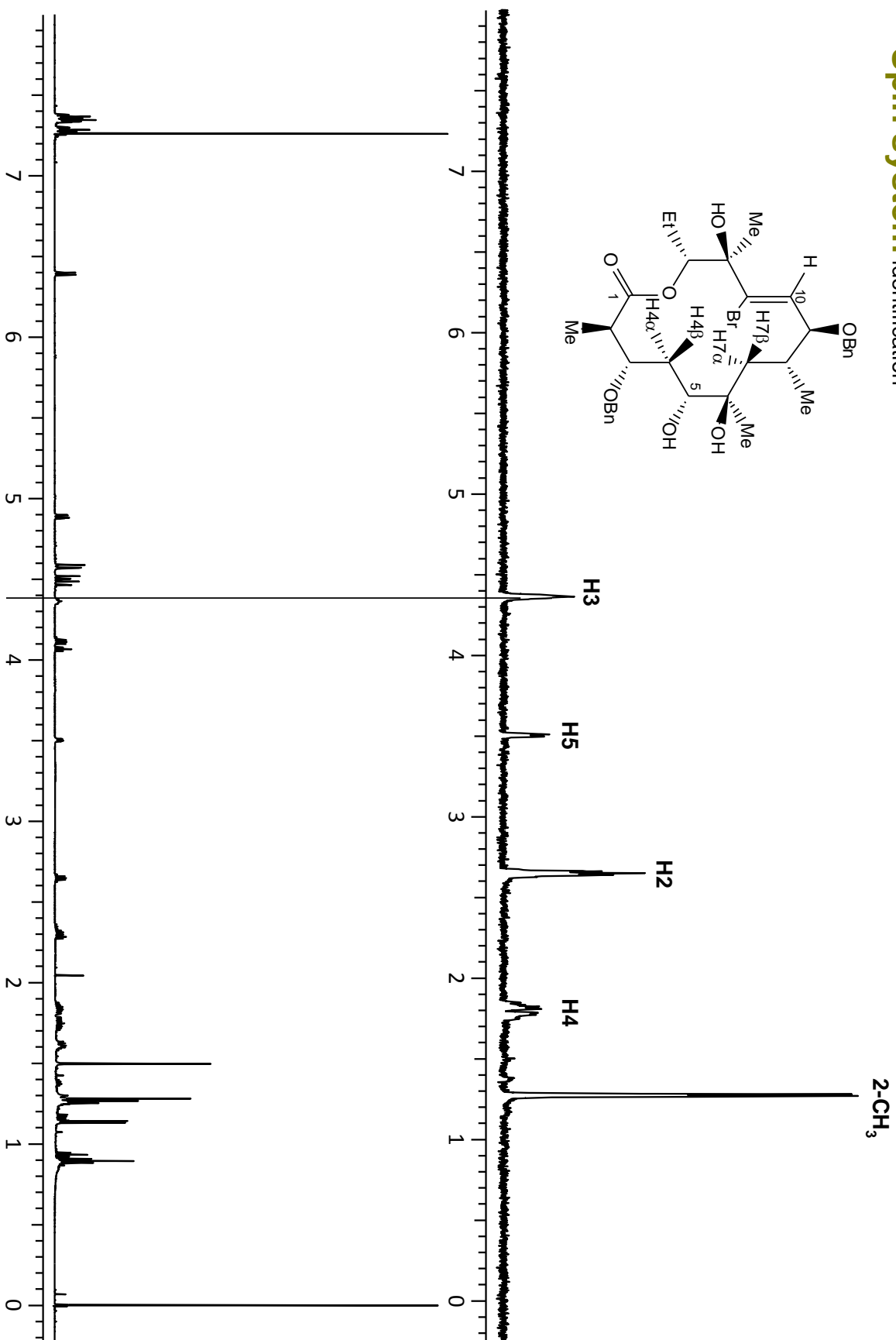
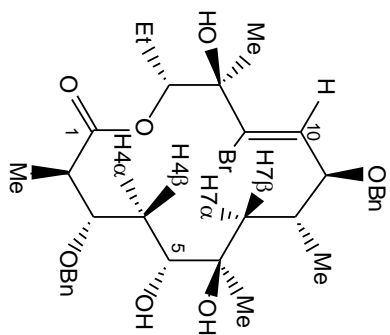
Spin system identification



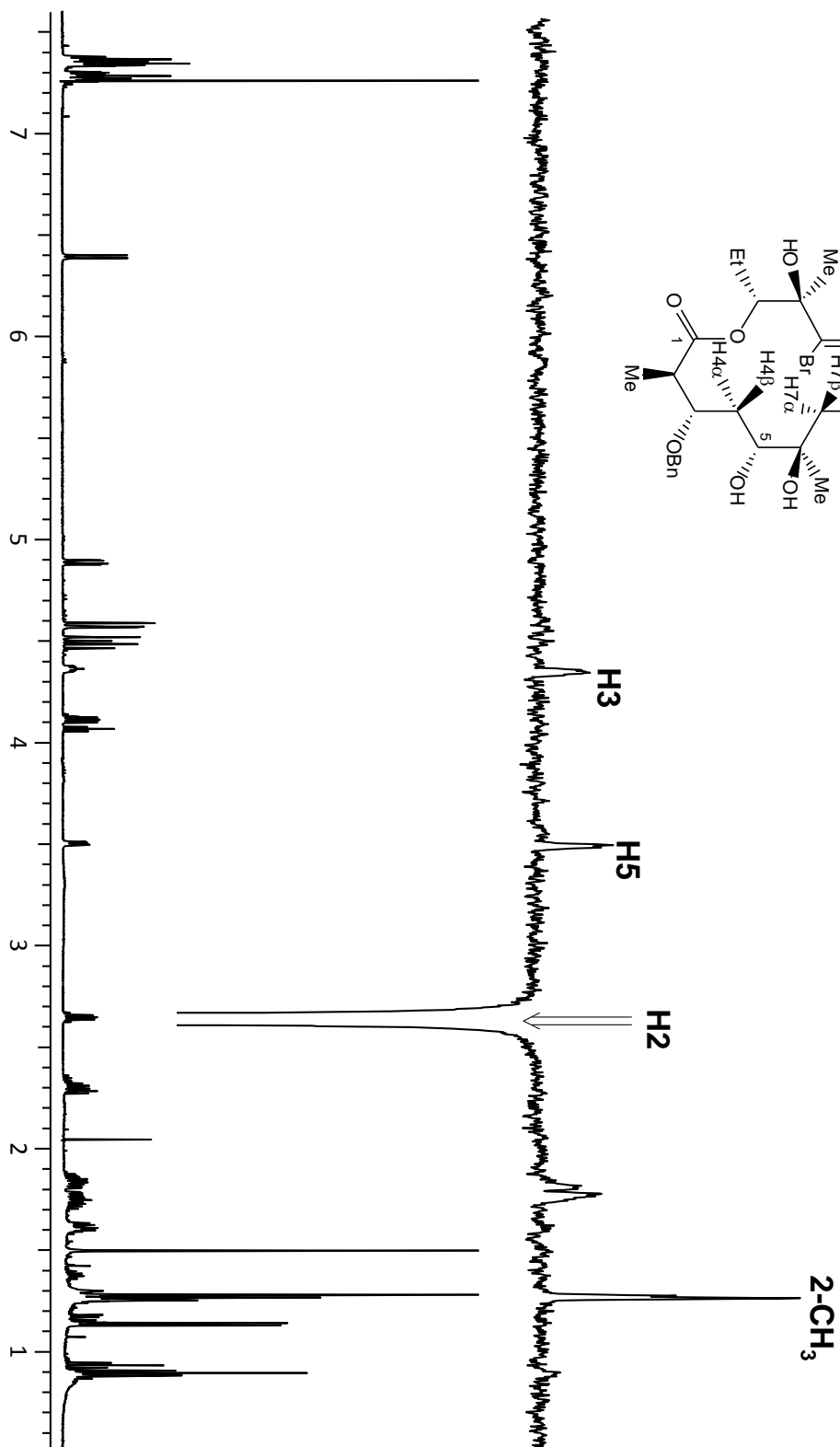
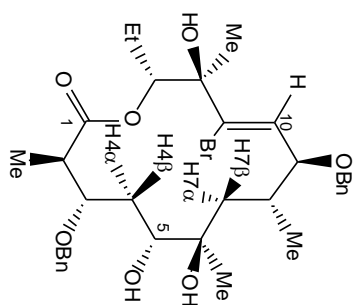
Spin system identification



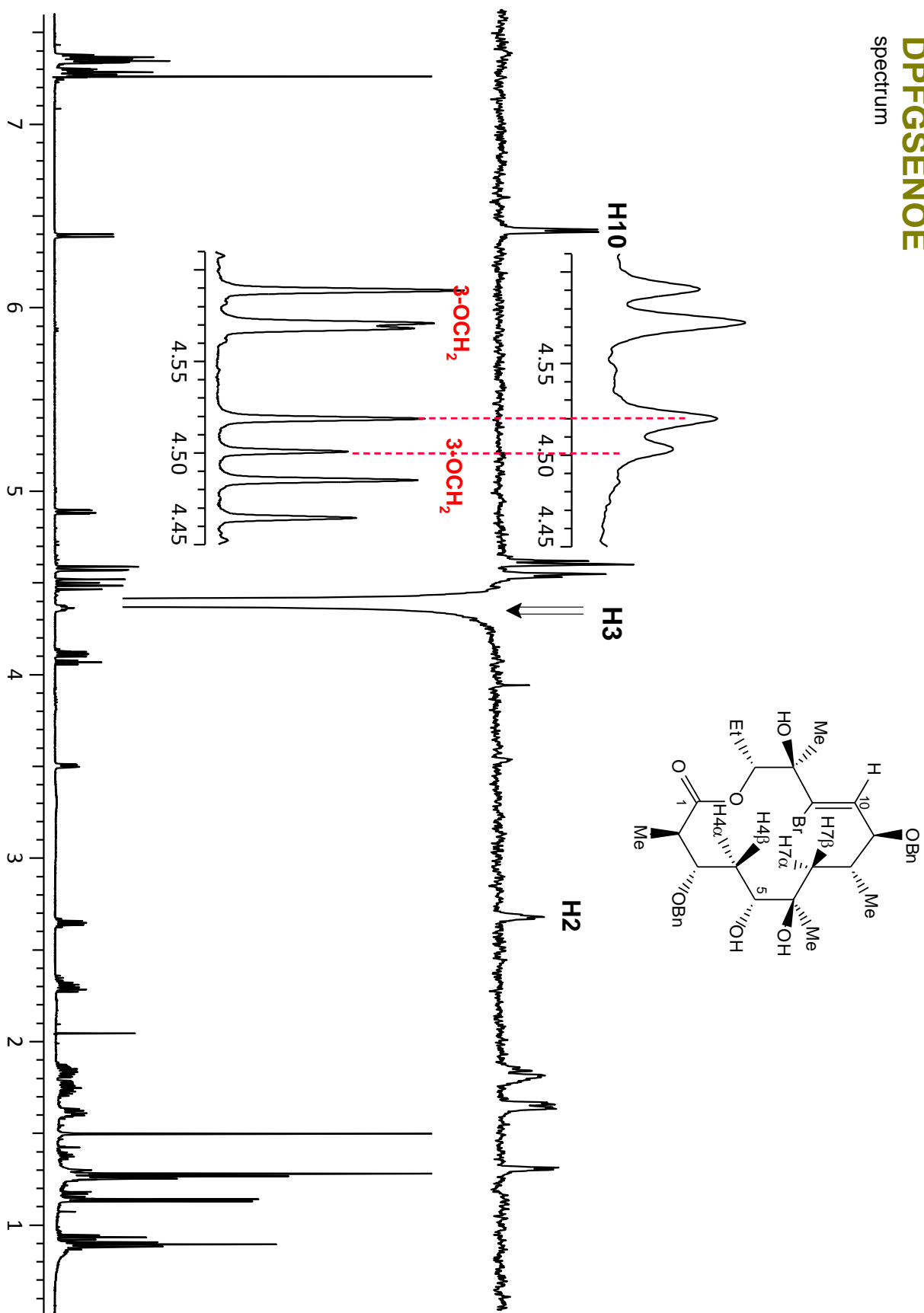
Spin system identification

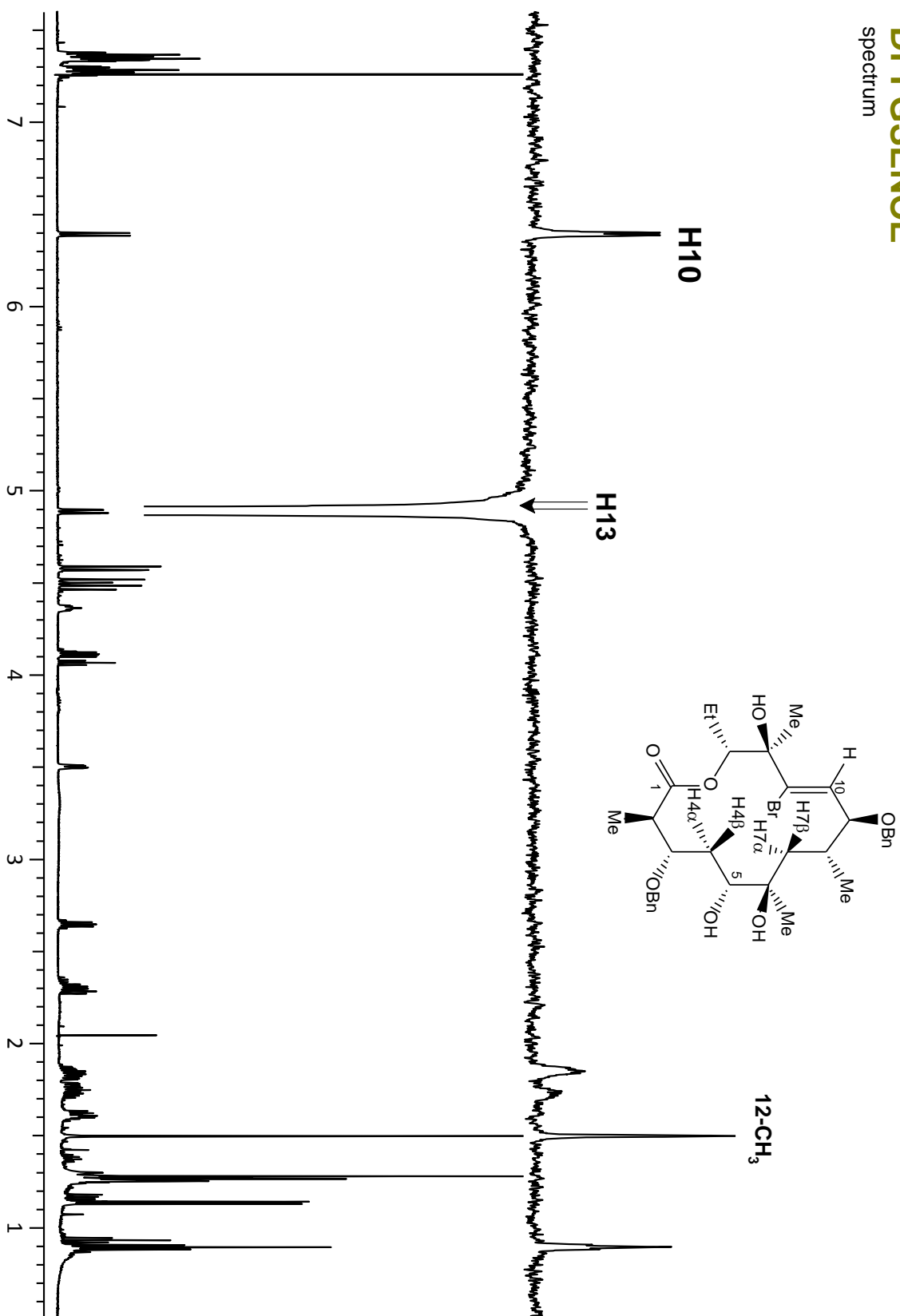


DPFGSENOE spectrum

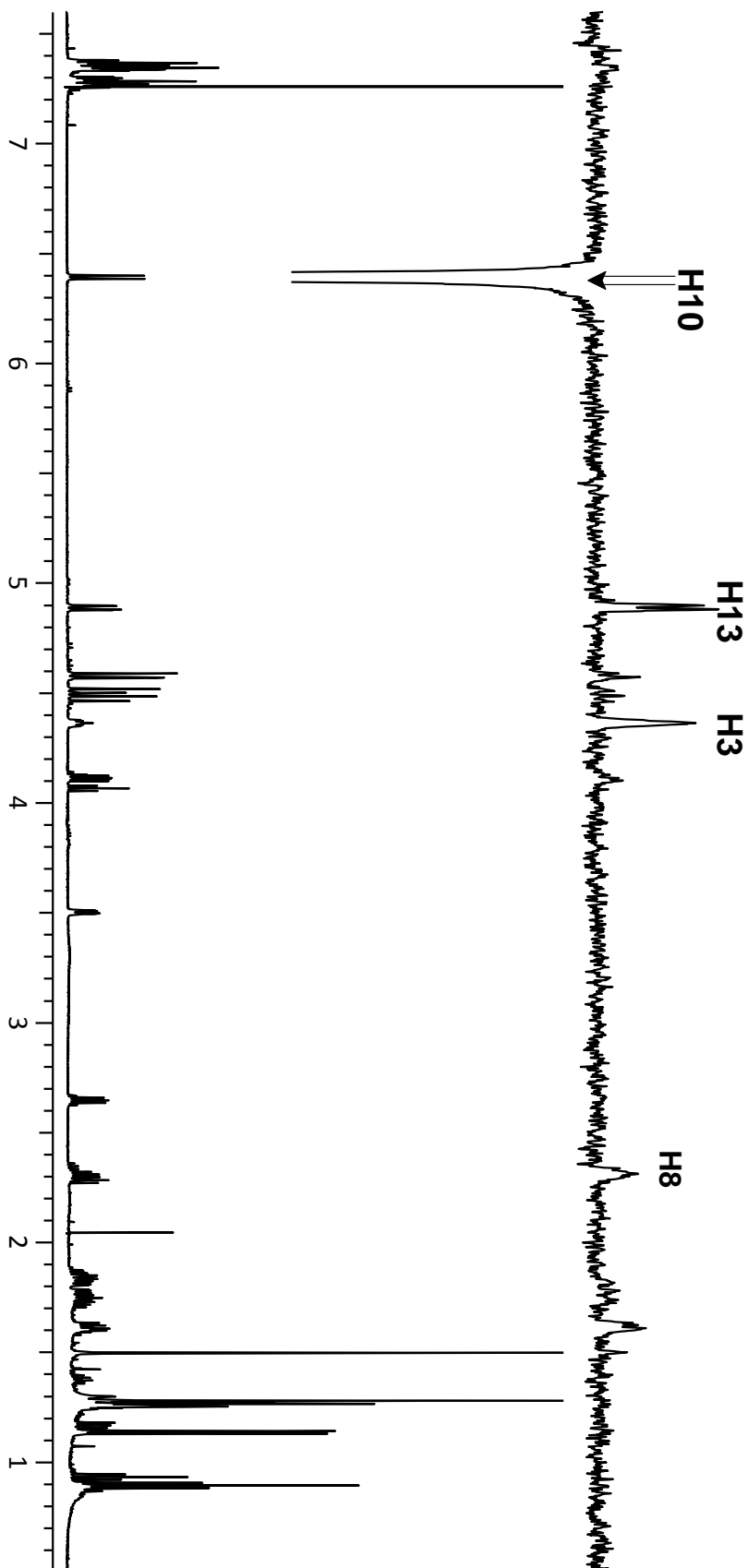
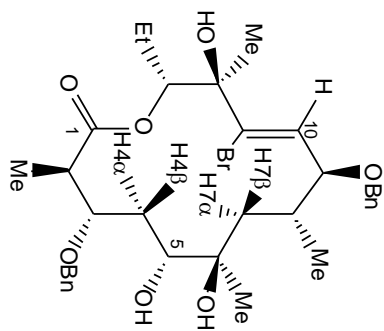


DPFGSENOE spectrum

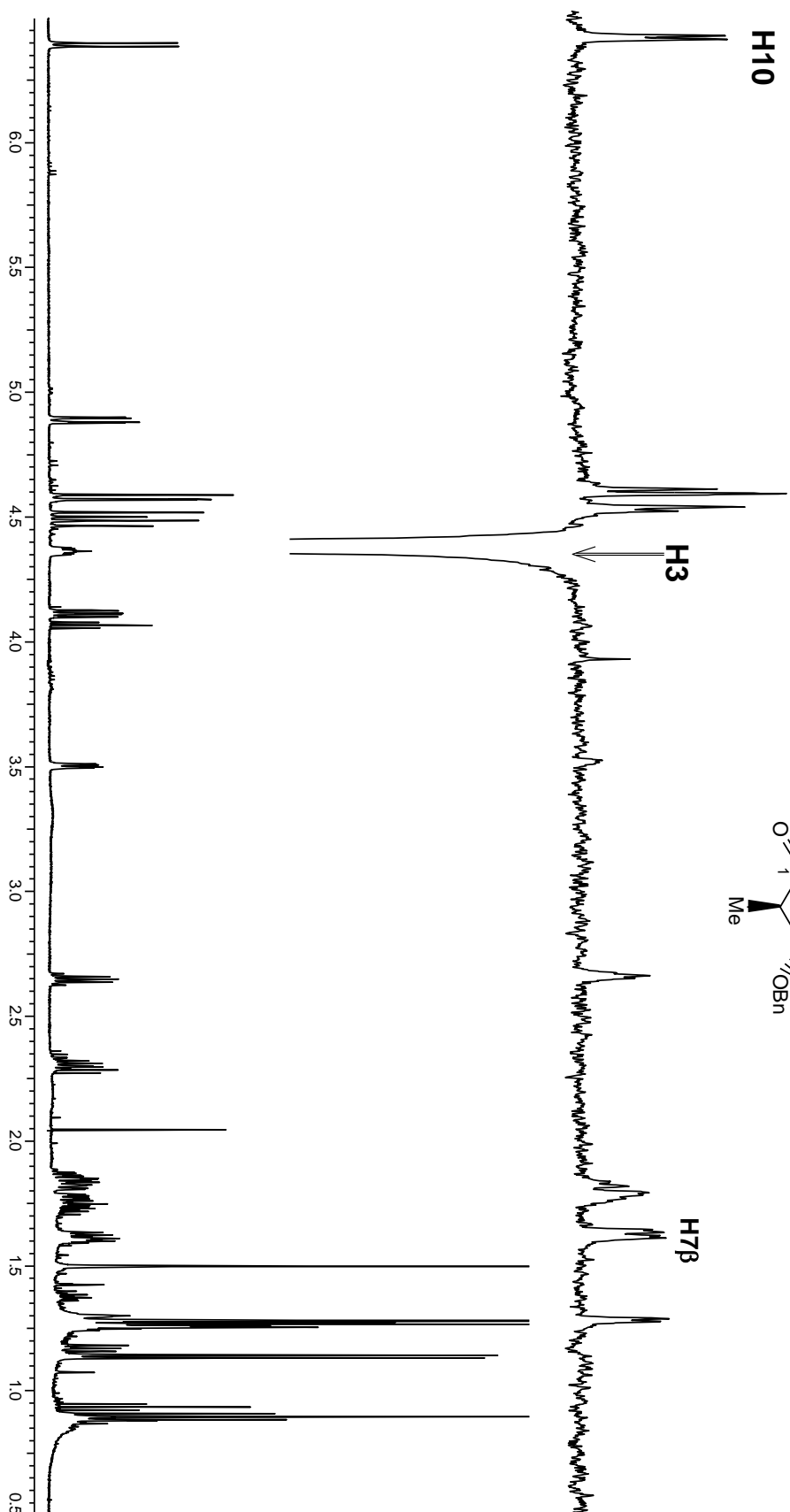


DPFGSENOE
spectrum

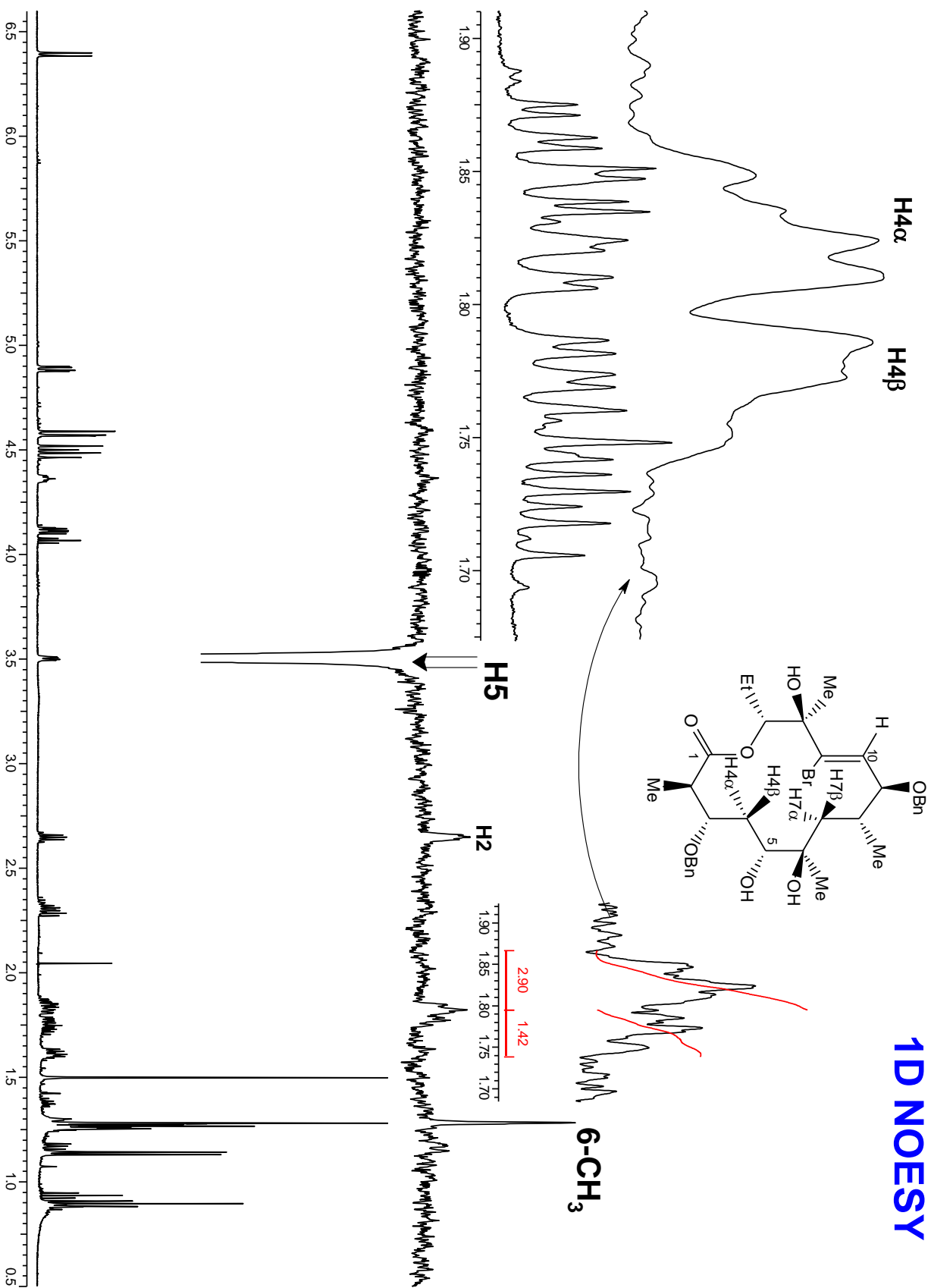
DPFGSENOE spectrum



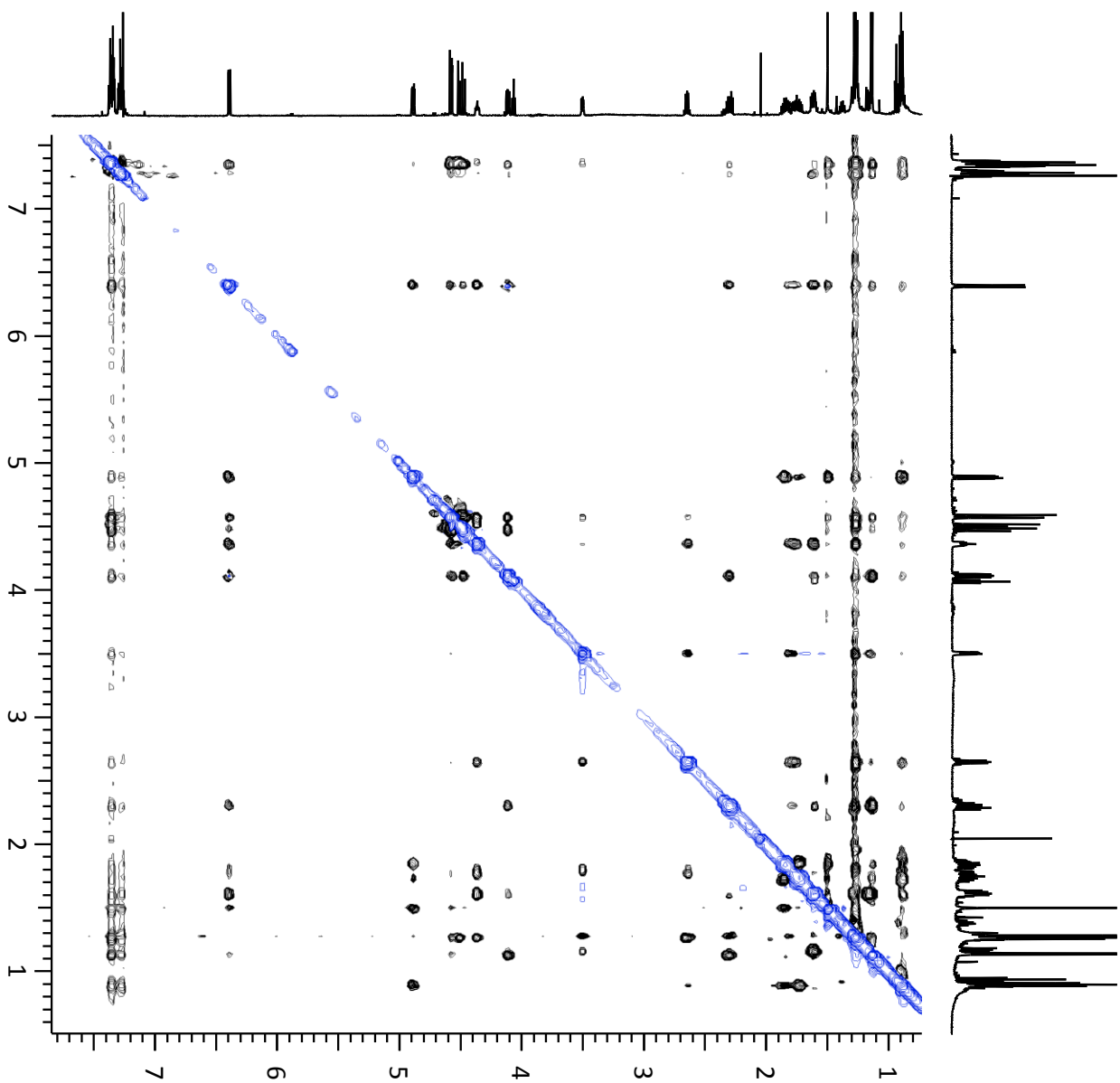
DPFGSENOE spectrum



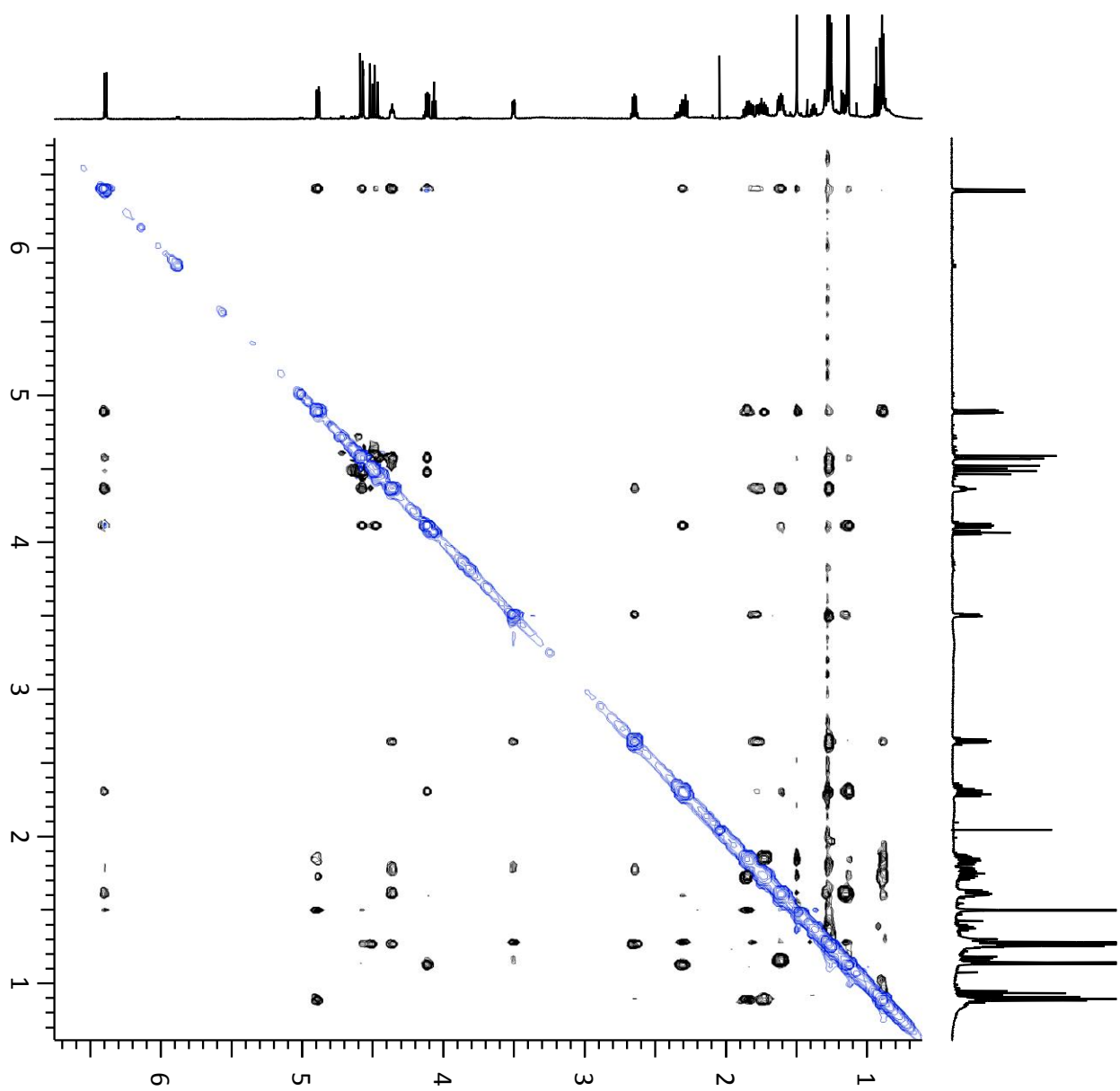
1D NOESY



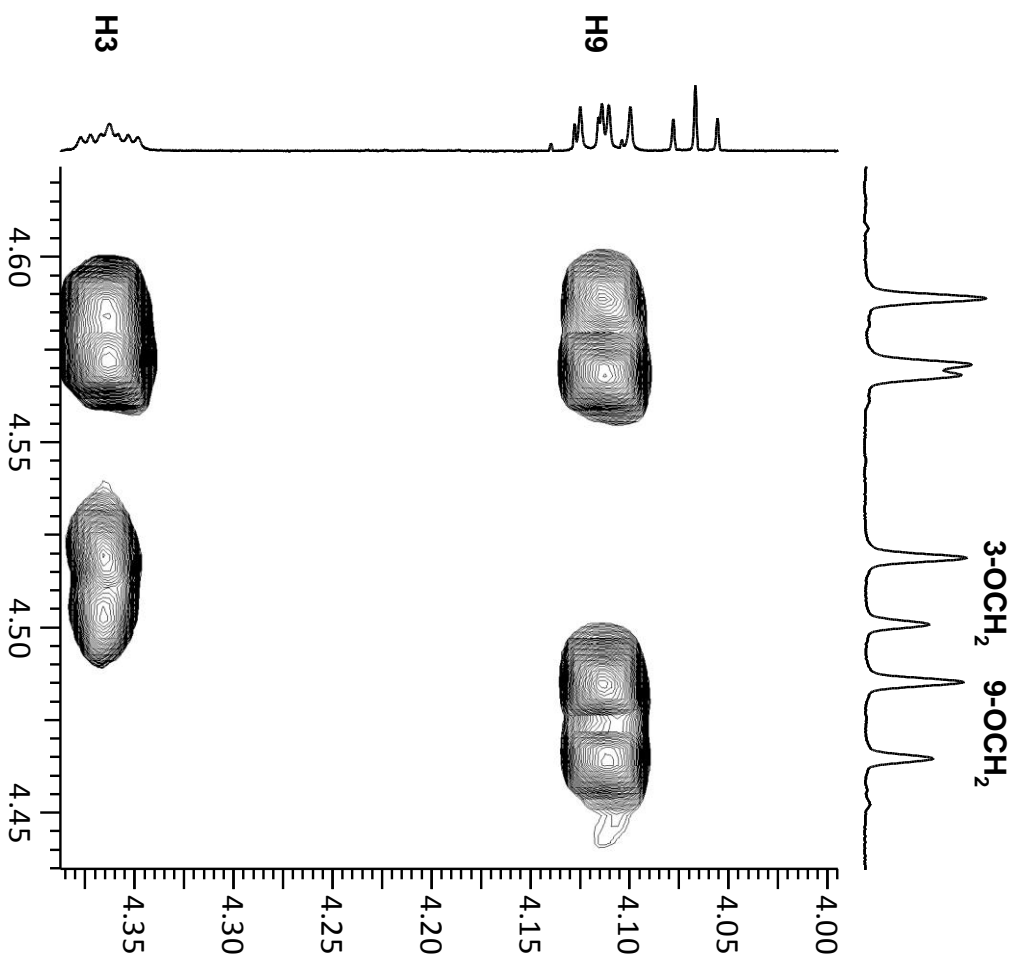
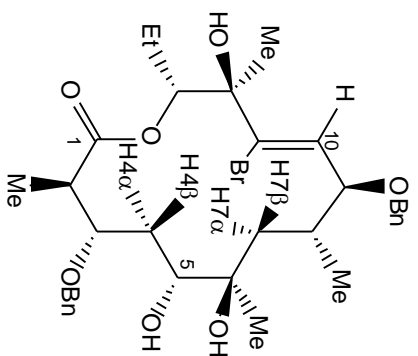
NOESY



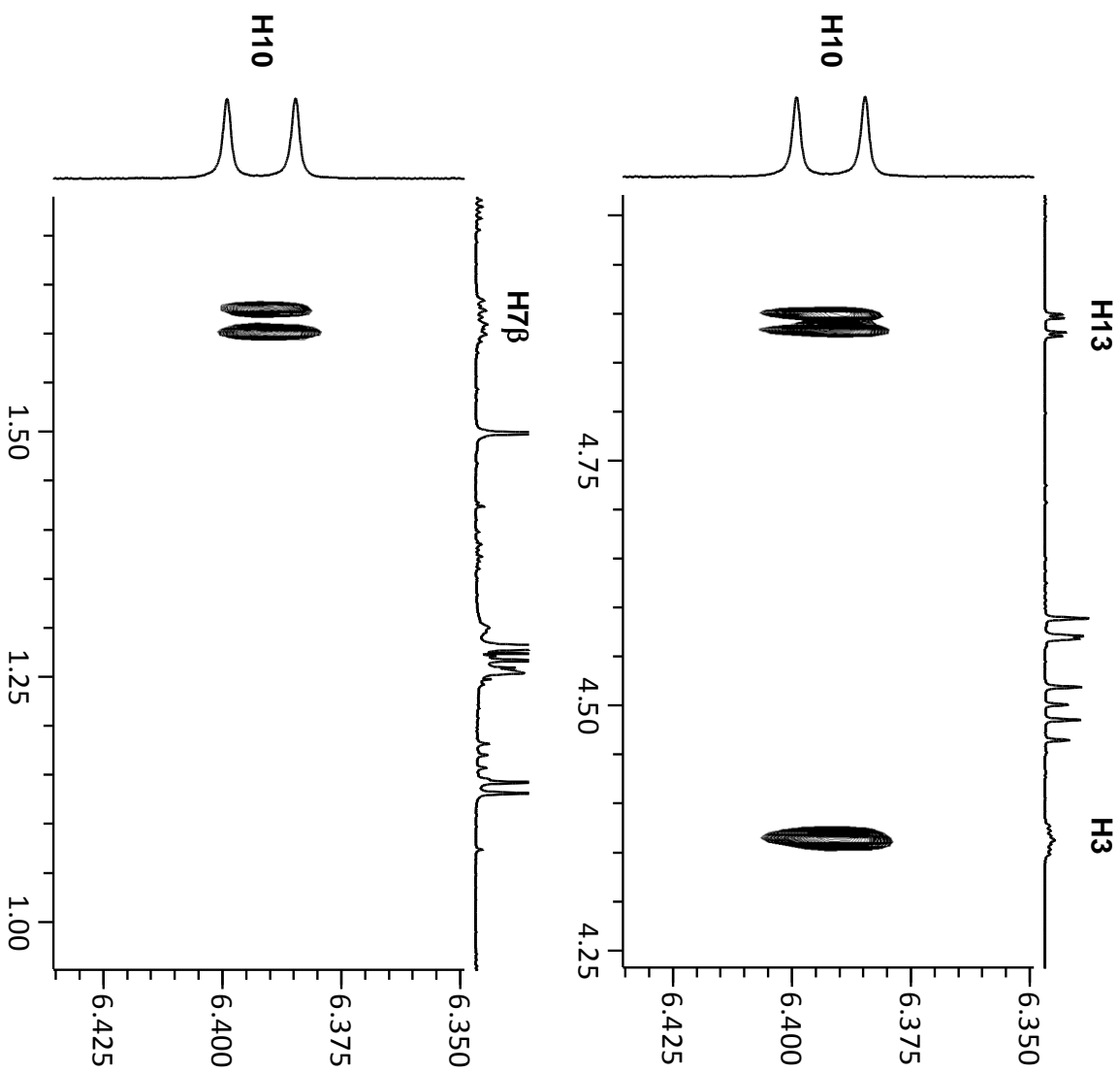
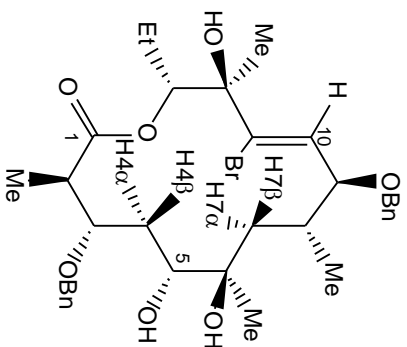
NOESY expansion



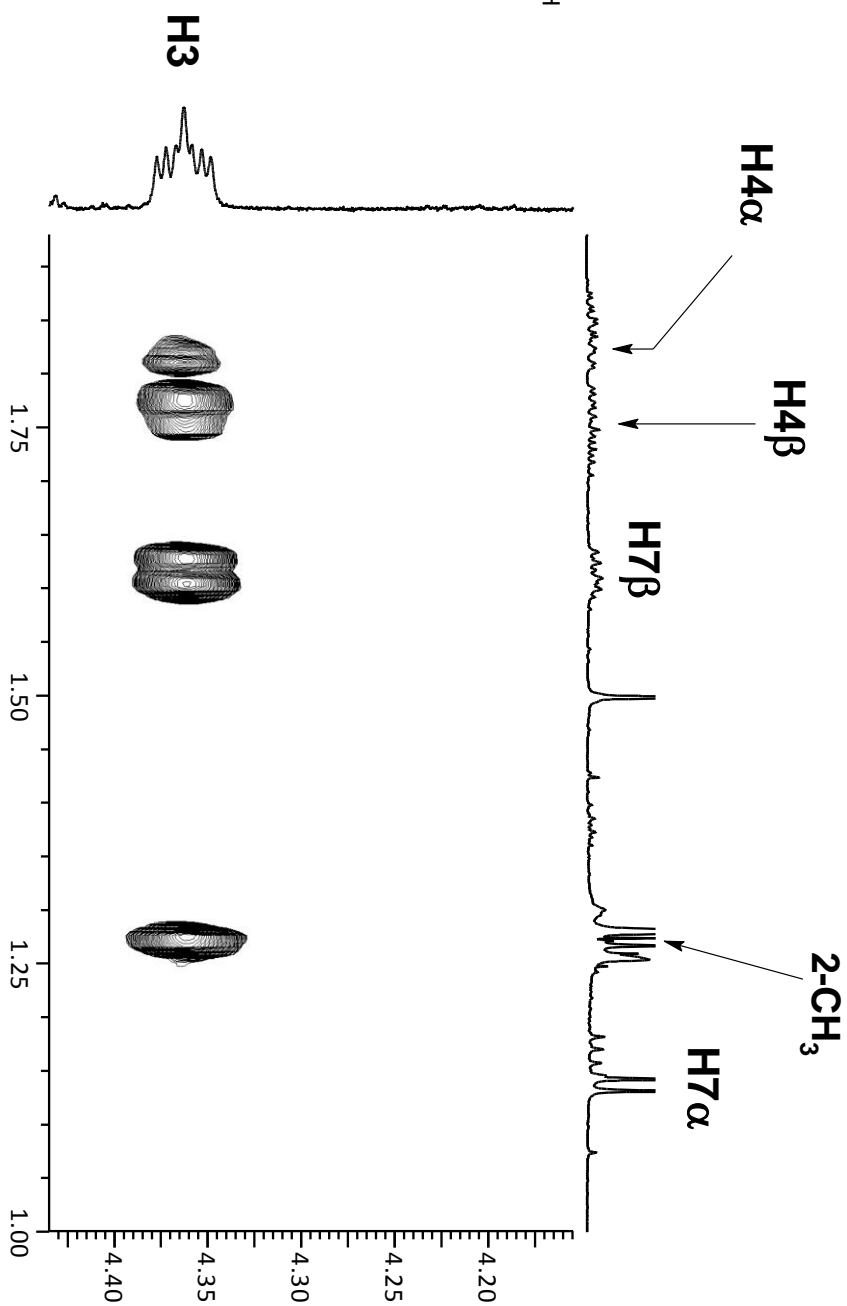
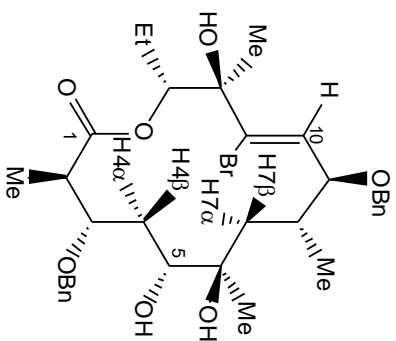
NOESY expansion



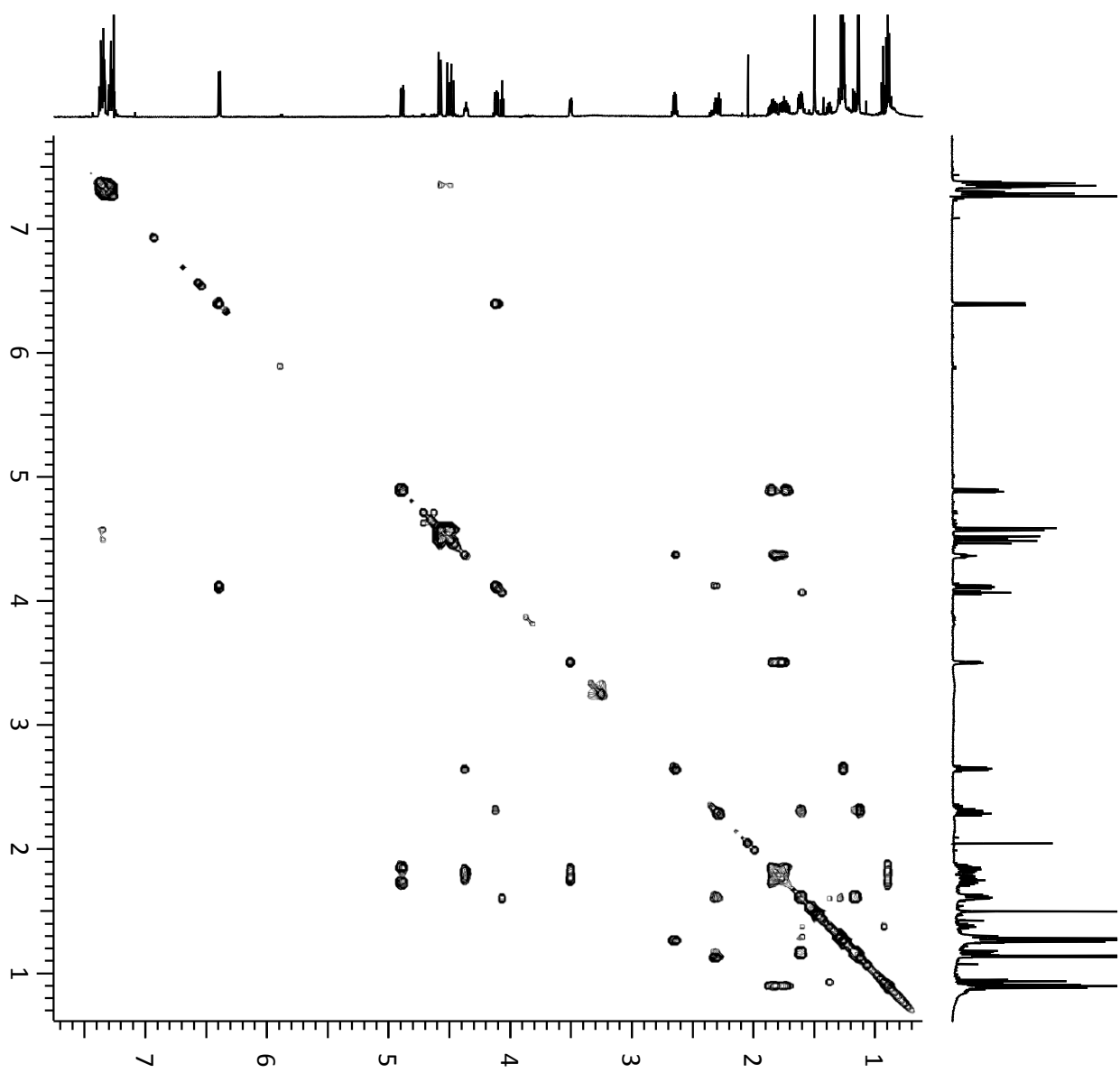
NOESY expansion



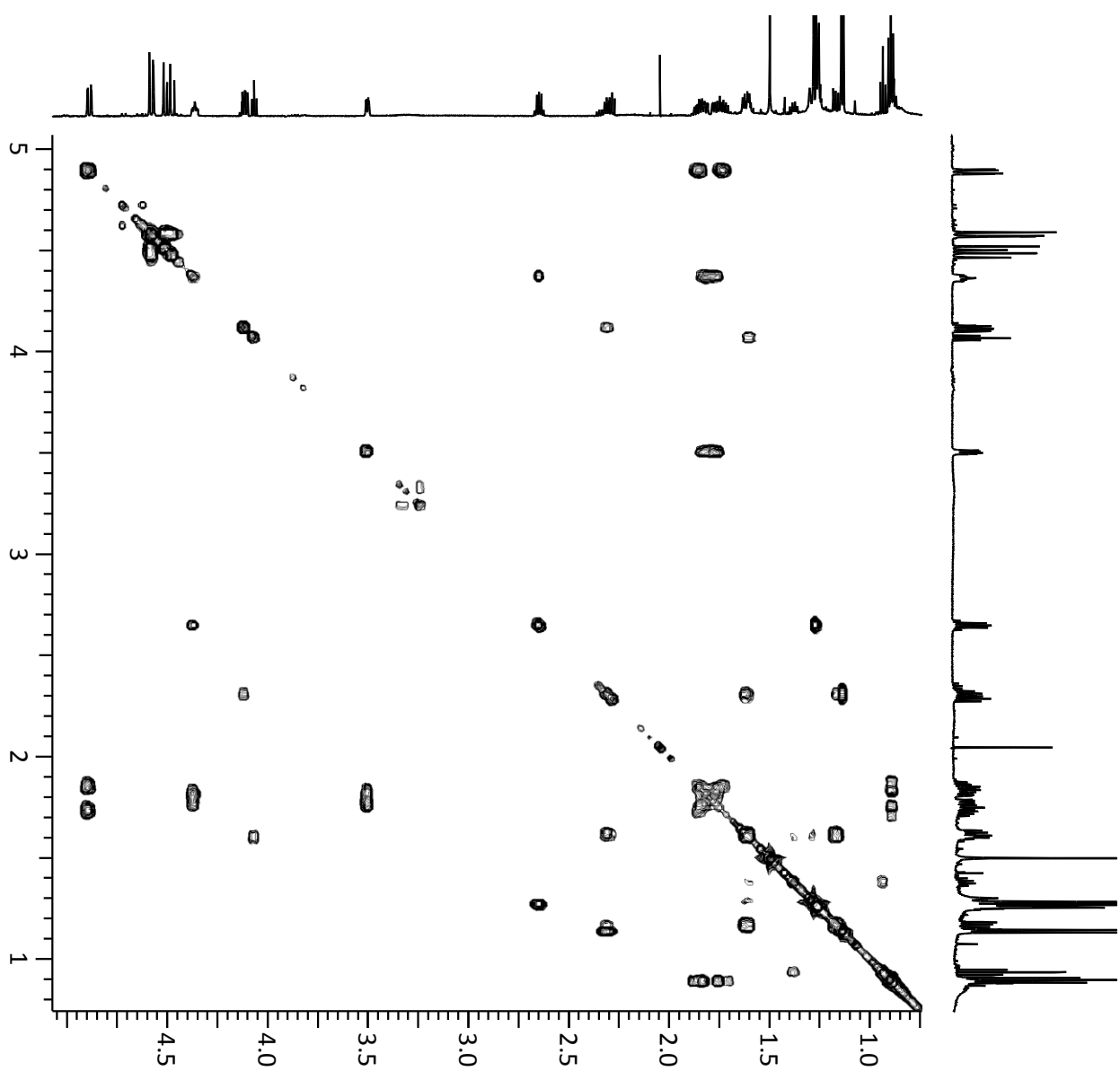
NOESY expansion

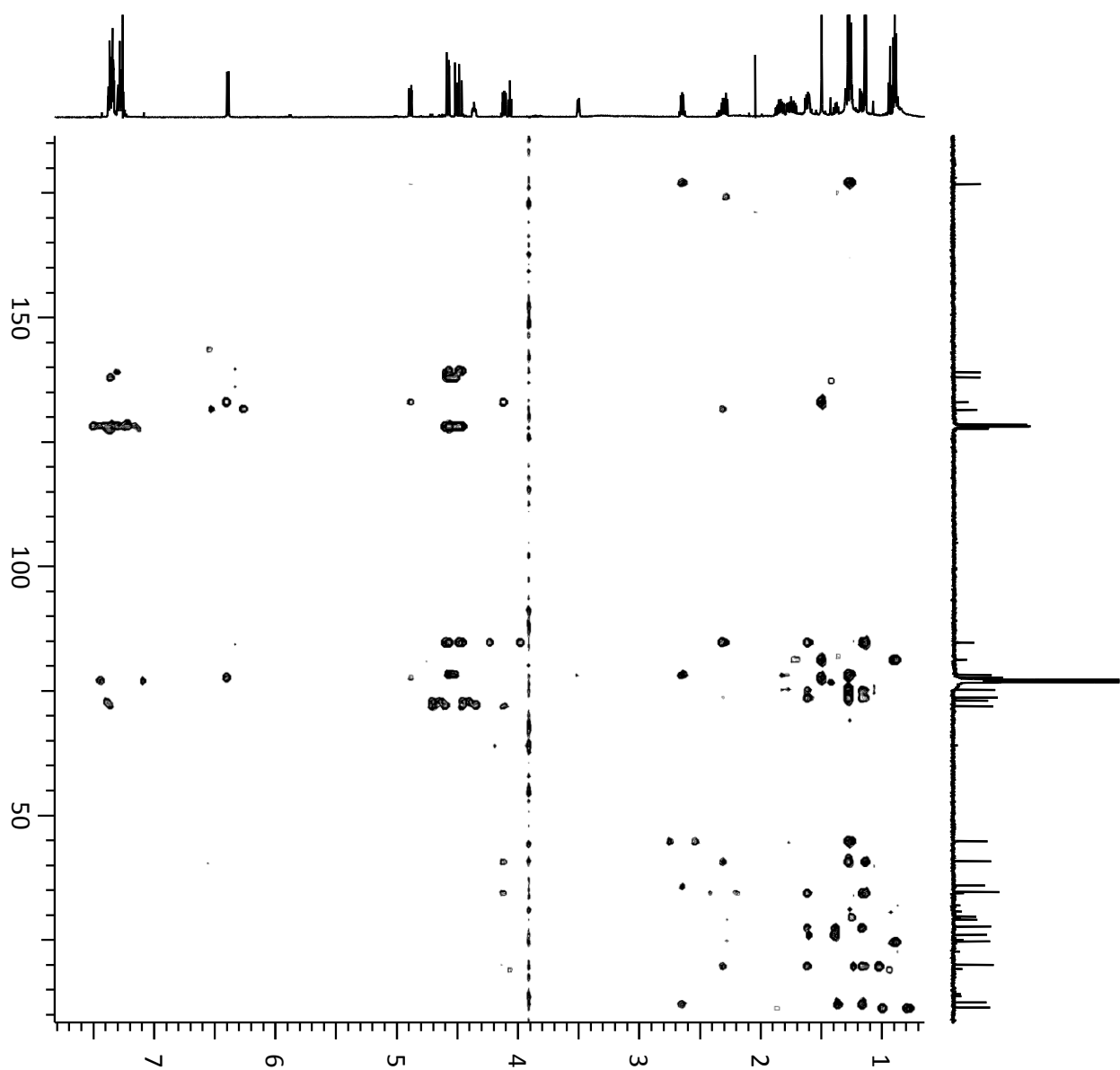


gcosy

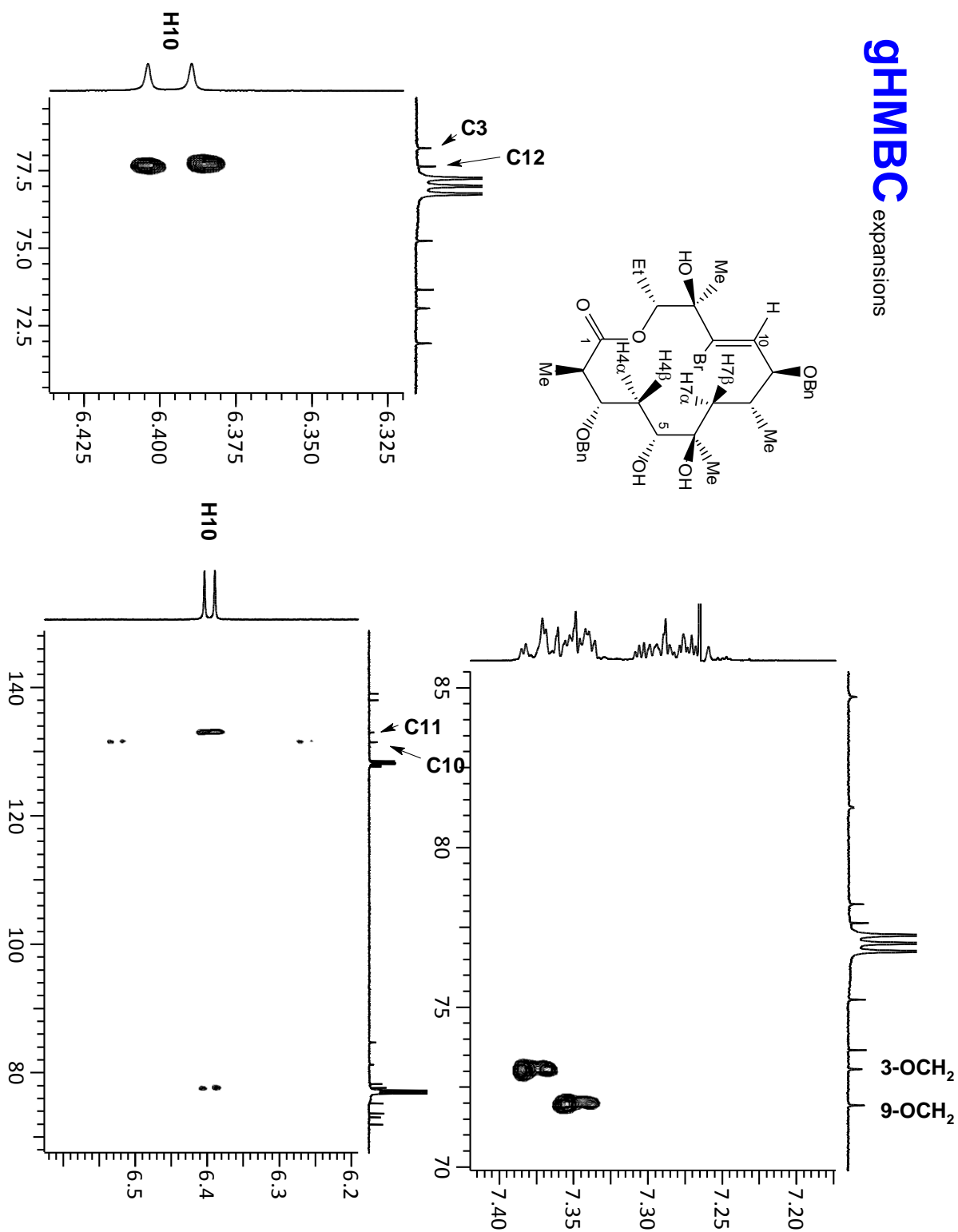


gCOSY expansion

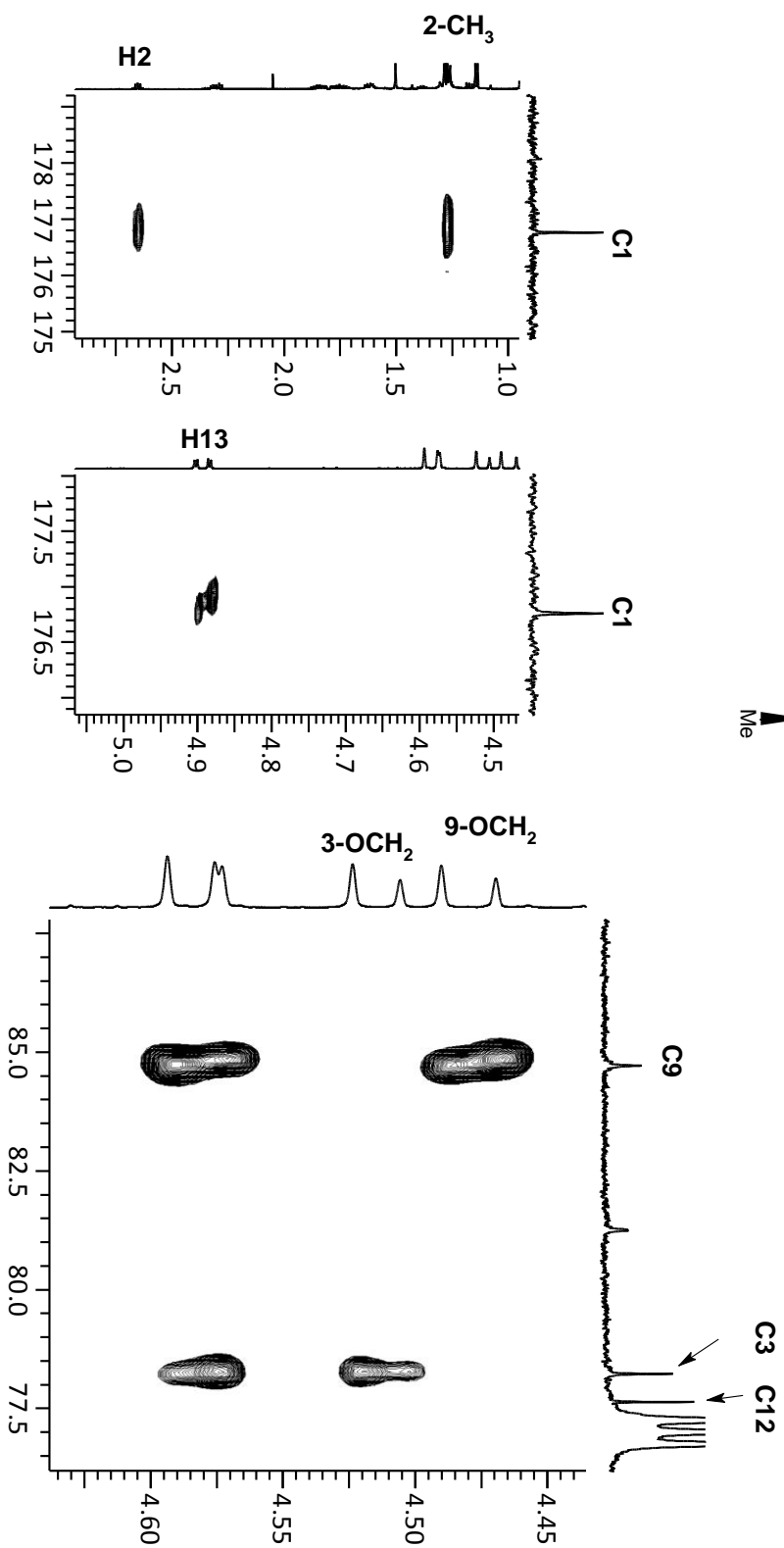
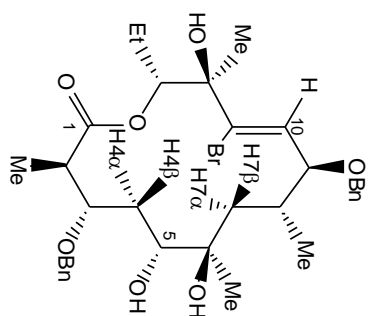


gHMBc

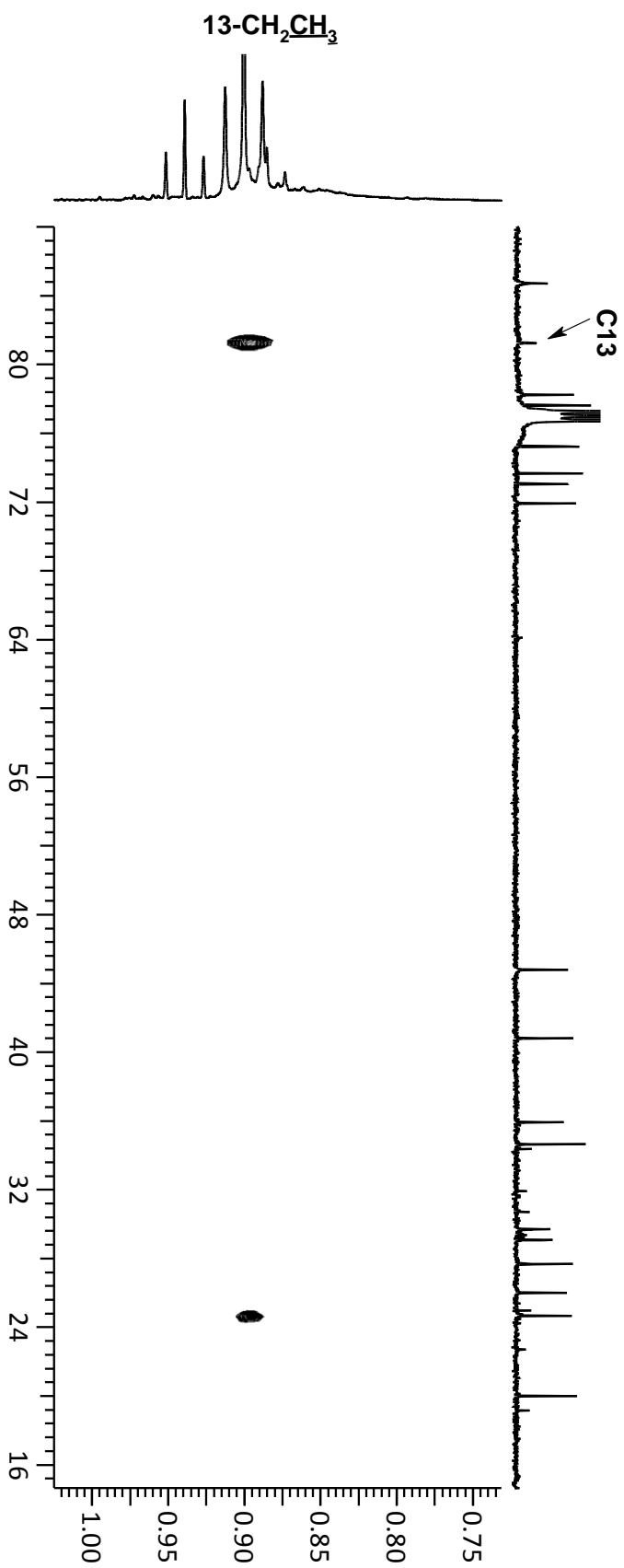
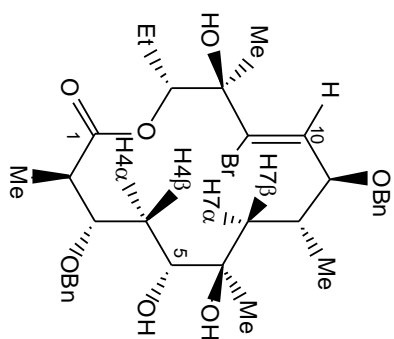
gHMBC expansions



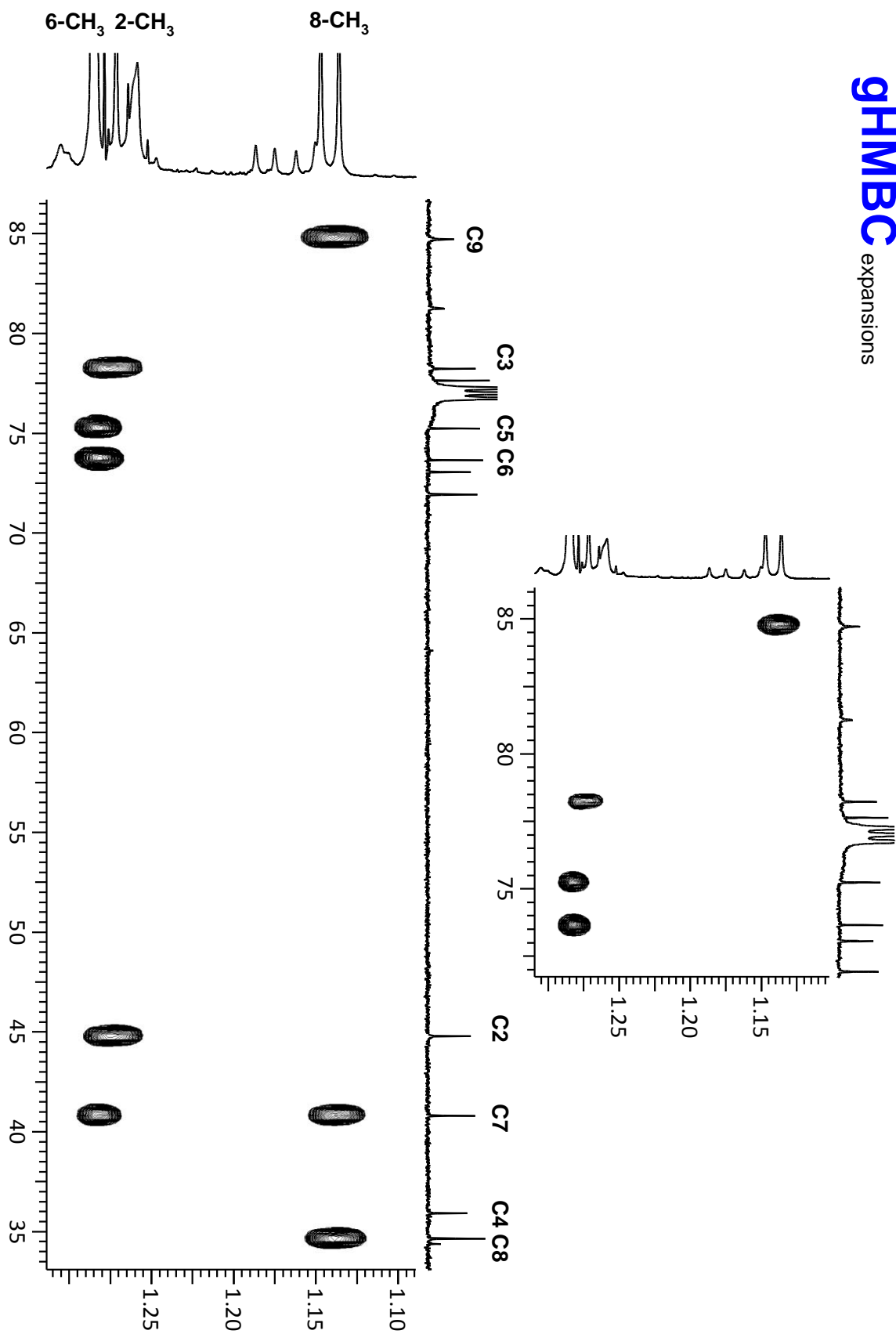
gHMBC expansions



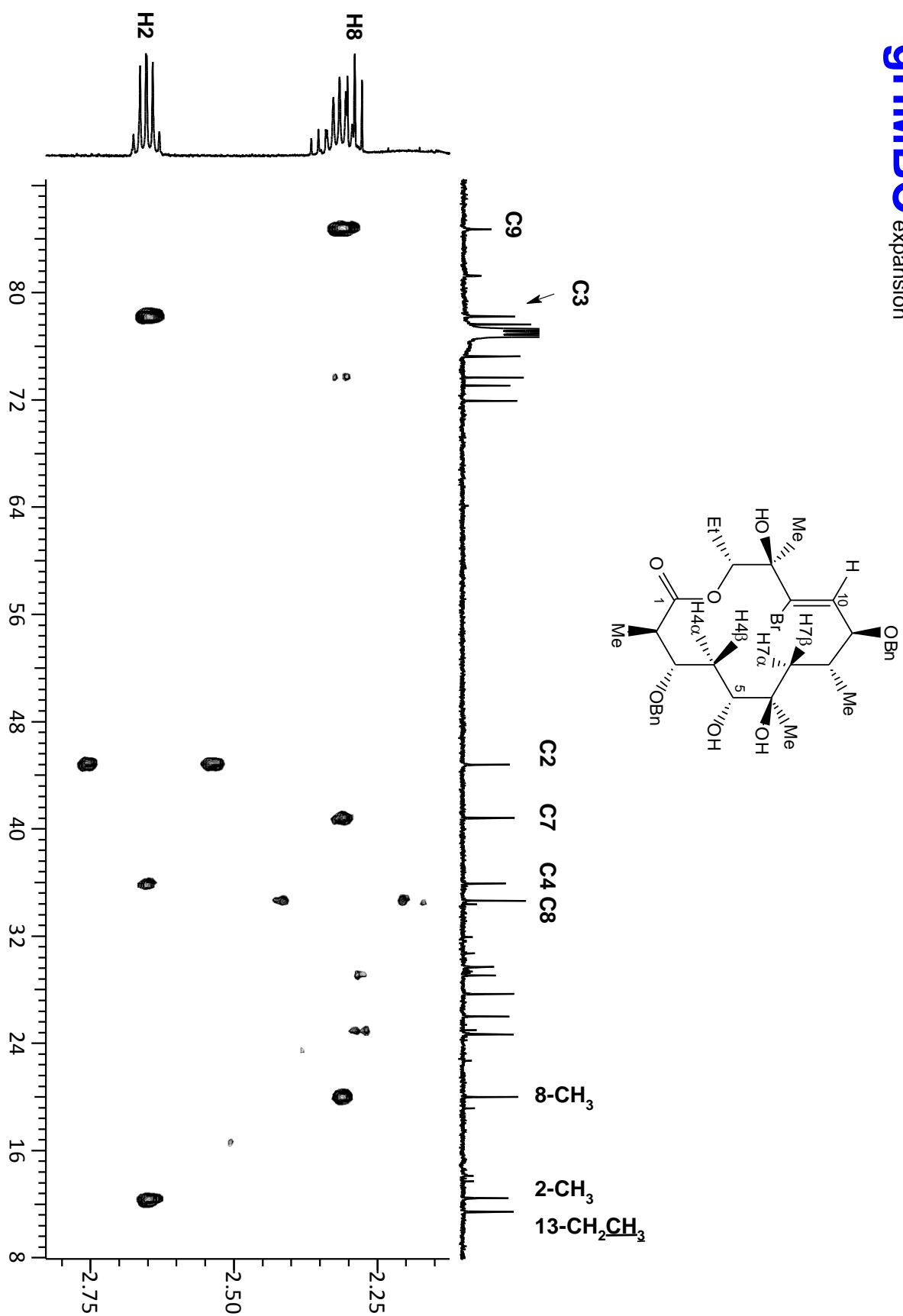
gHMBC expansion

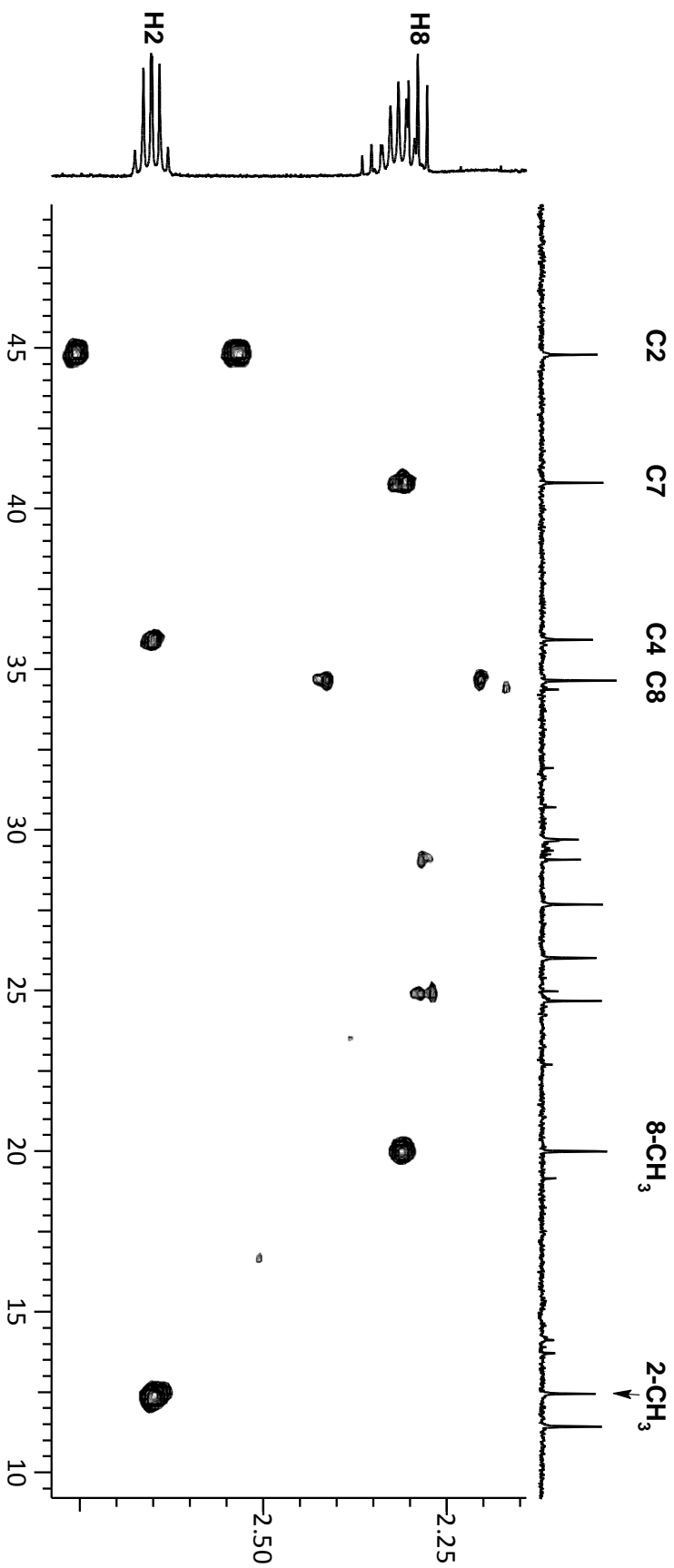


gHMBC expansions

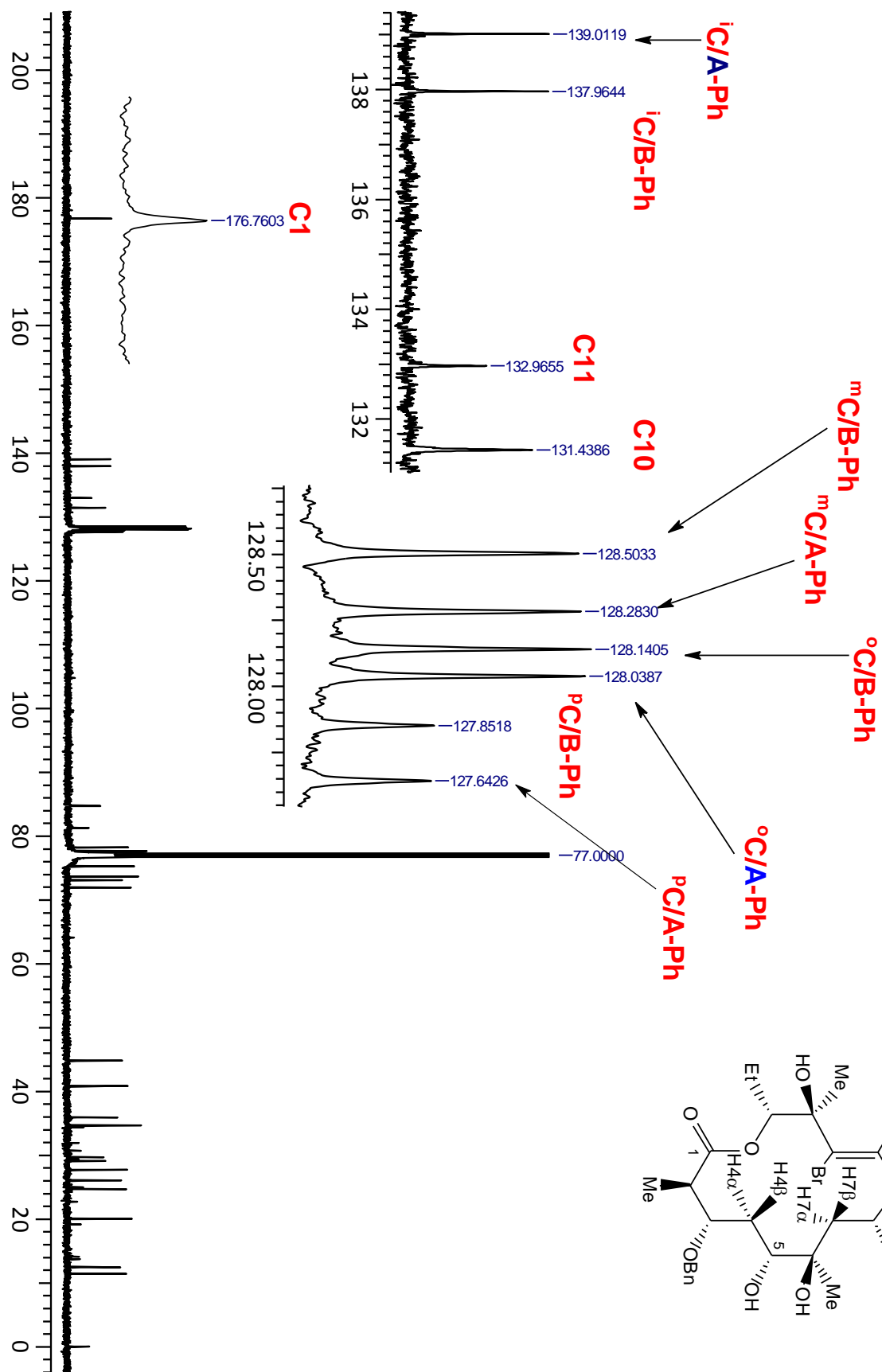


gHMBC expansion

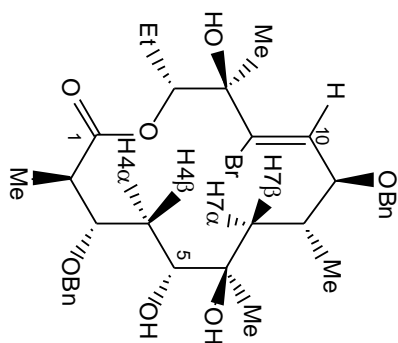
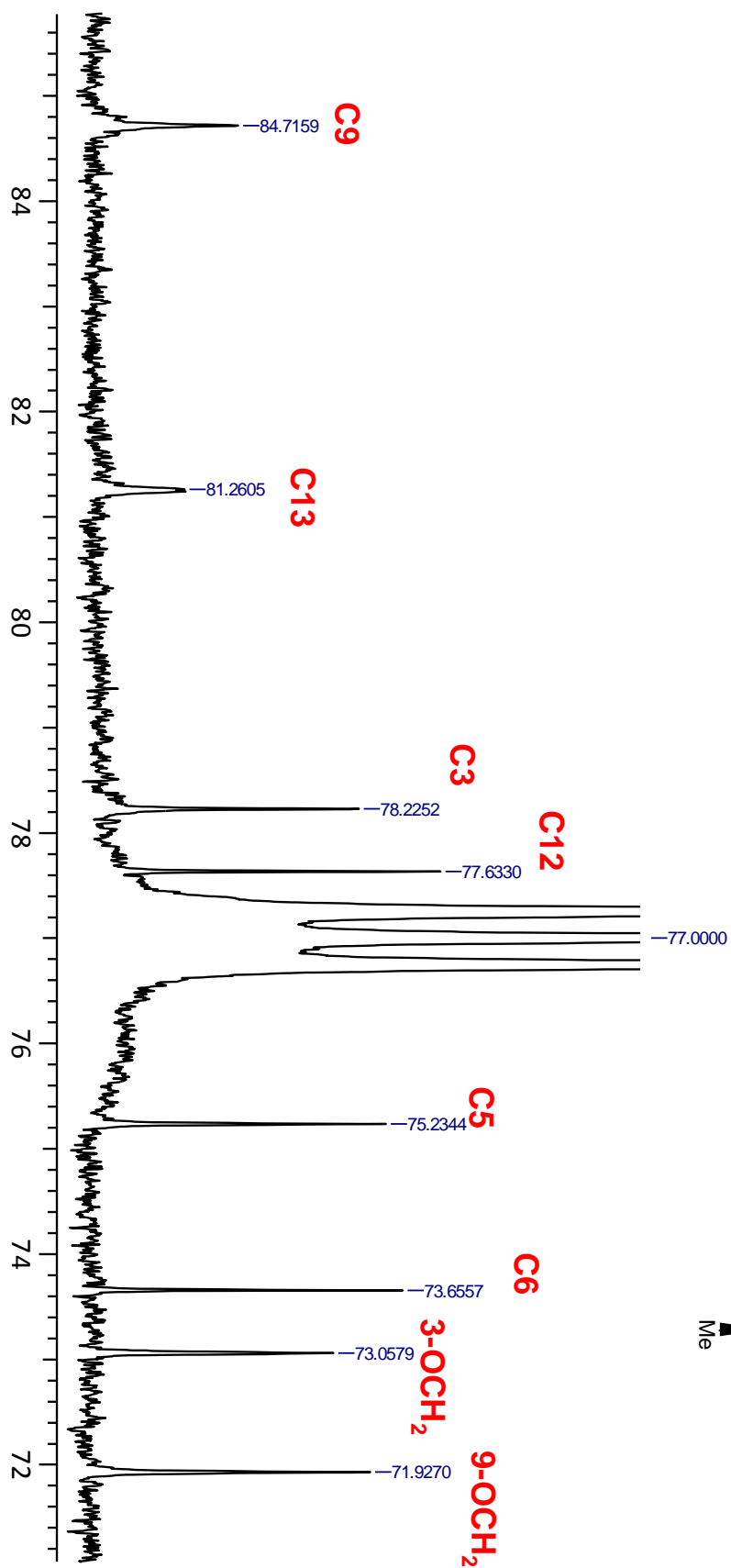




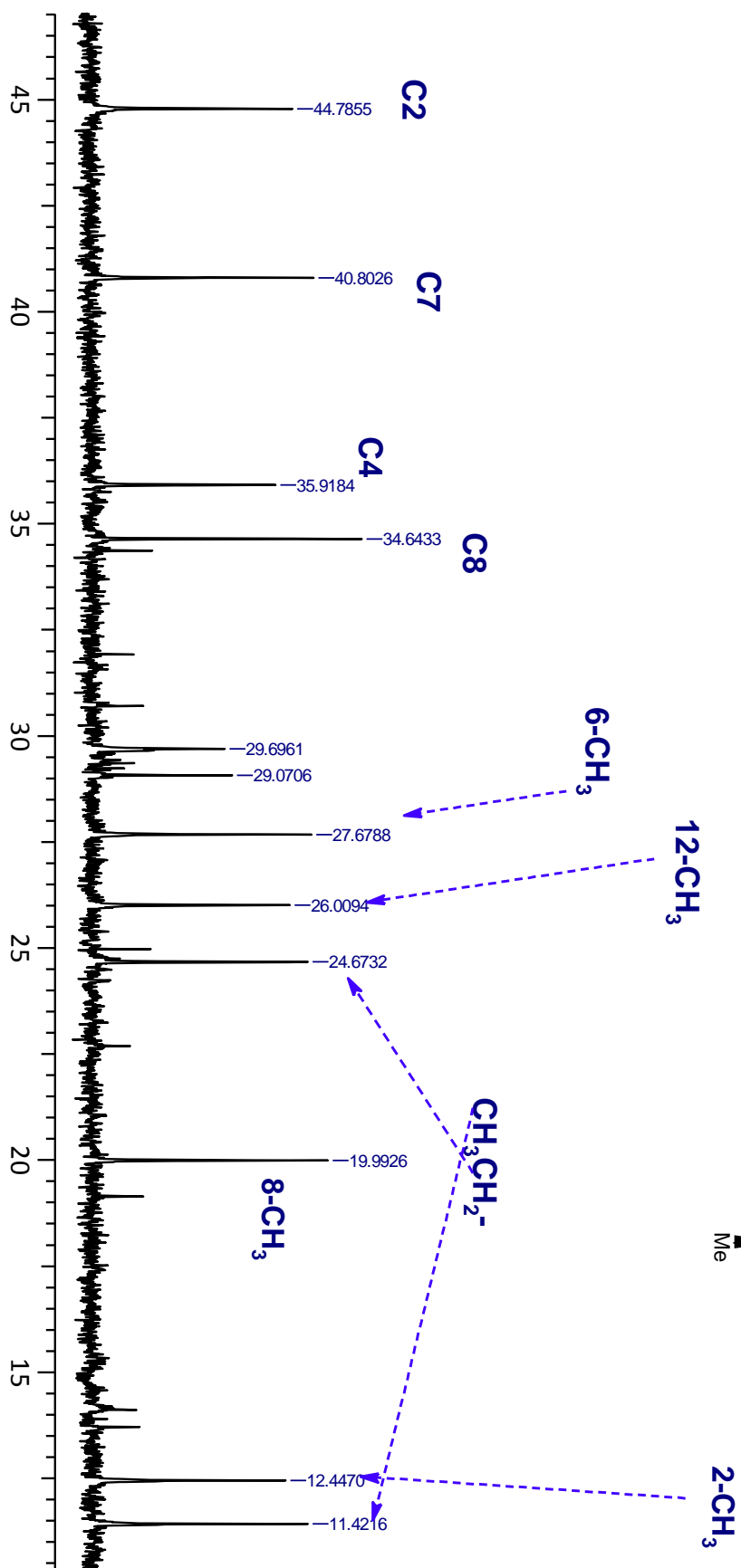
^{13}C NMR spectrum

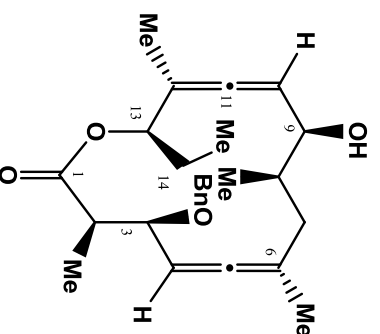


¹³C NMR spectrum



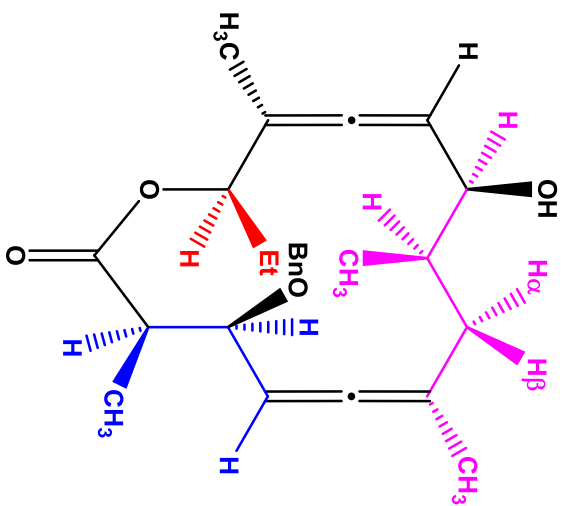
¹³C NMR spectrum



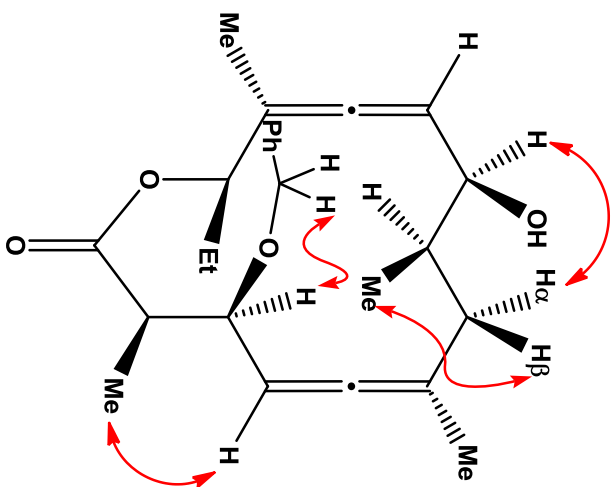


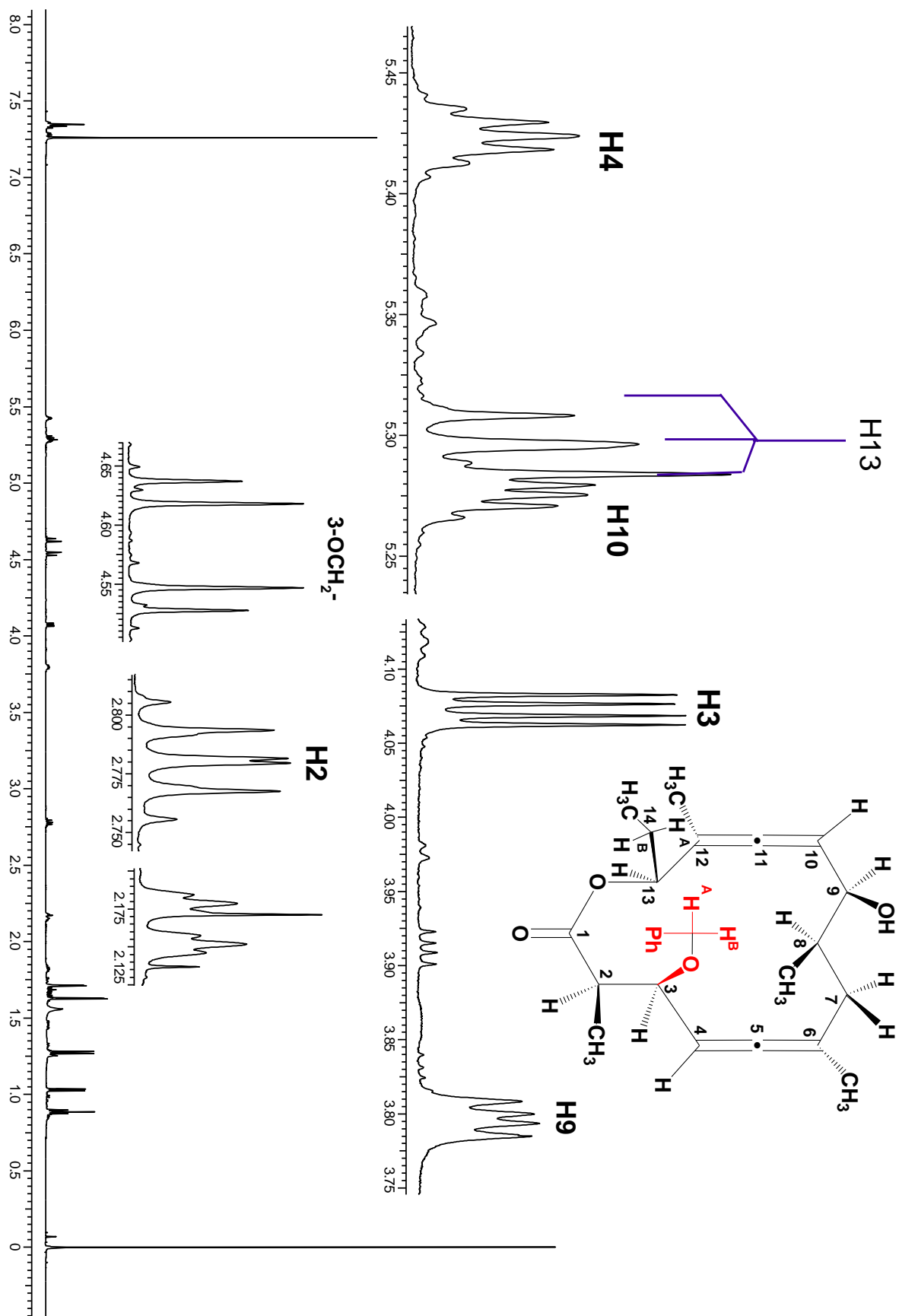
¹ H NMR chemical shifts (δ/ppm) coupling constant (J/Hz)	¹³ C NMR chemical shift (δ/ppm)
2.77 (dq, J _{H2} , H3 = 8.7Hz, J _{H2} , 2-CH3 = 7.1Hz, H2)	173.8 ---- C1
1.27 (d, J _{2-CH3} , H2 = 7.3Hz, 2-CH3)	43.6 ---- C2
4.07 (dd, J _{H3} , H2 = 8.7Hz, J _{H3} , H4 = 3.4Hz, H3)	77.1 ---- C3
5.42 (m, J _{H4} , H3 = 3.4Hz, H4)	91.4 ---- C4
1.72 (d, J _{6-CH3} , H4 = 2.9Hz, 6-CH3)	200.0 ---- C5
1.45 (m, J _{H7β} , H7α = 16.1Hz, H7β)	102.7 ---- C6
2.17 (dt, J _{H7α} , H8 = 6.4Hz, J _{H7α} , H7β = 16.1Hz, H7α)	37.9 ---- C7
1.80 - 1.85 (m, H8)	36.4 ---- C8
1.02 (d, J _{8-CH3} , H8 = 6.6Hz, 8-CH3)	74.2 ---- C9
3.80 (dd, J _{H9} , H8 = 5.1Hz, J _{H9} , H10 = 8.3Hz, H9)	93.7 ---- C10
5.27 (quartet, J _{H10} , H9 = 8.3Hz, J _{H10} , 12-CH3 = 2.7Hz, H10)	202.6 ---- C11
1.62 (d, J _{12-CH3} , H10 = 2.7Hz, 12-CH3)	99.9 ---- C12
5.30 (t, J = 7.3Hz, H13)	75.9 ---- C13
1.60 - 1.70 (m, 14-CH2)	24.7 ---- C14
0.88 (t, J _{14-CH3} , H14 = 7.6Hz, 14-CH3)	15.2 ---- 2-CH ₃
4.55 (d, J=11.5Hz, 3-OCH2Ph)	20.6 ---- 6-CH ₃
4.62 (d, J=11.5Hz, 3-OCH2Ph)	16.9 ---- 8-CH ₃
	12.5 ---- 12-CH ₃
	9.8 ---- 14-CH ₃
	138.5 ---- ipsoC
	128.3 ---- orthoC
	127.8 ---- metaC
	127.5 ---- paraC

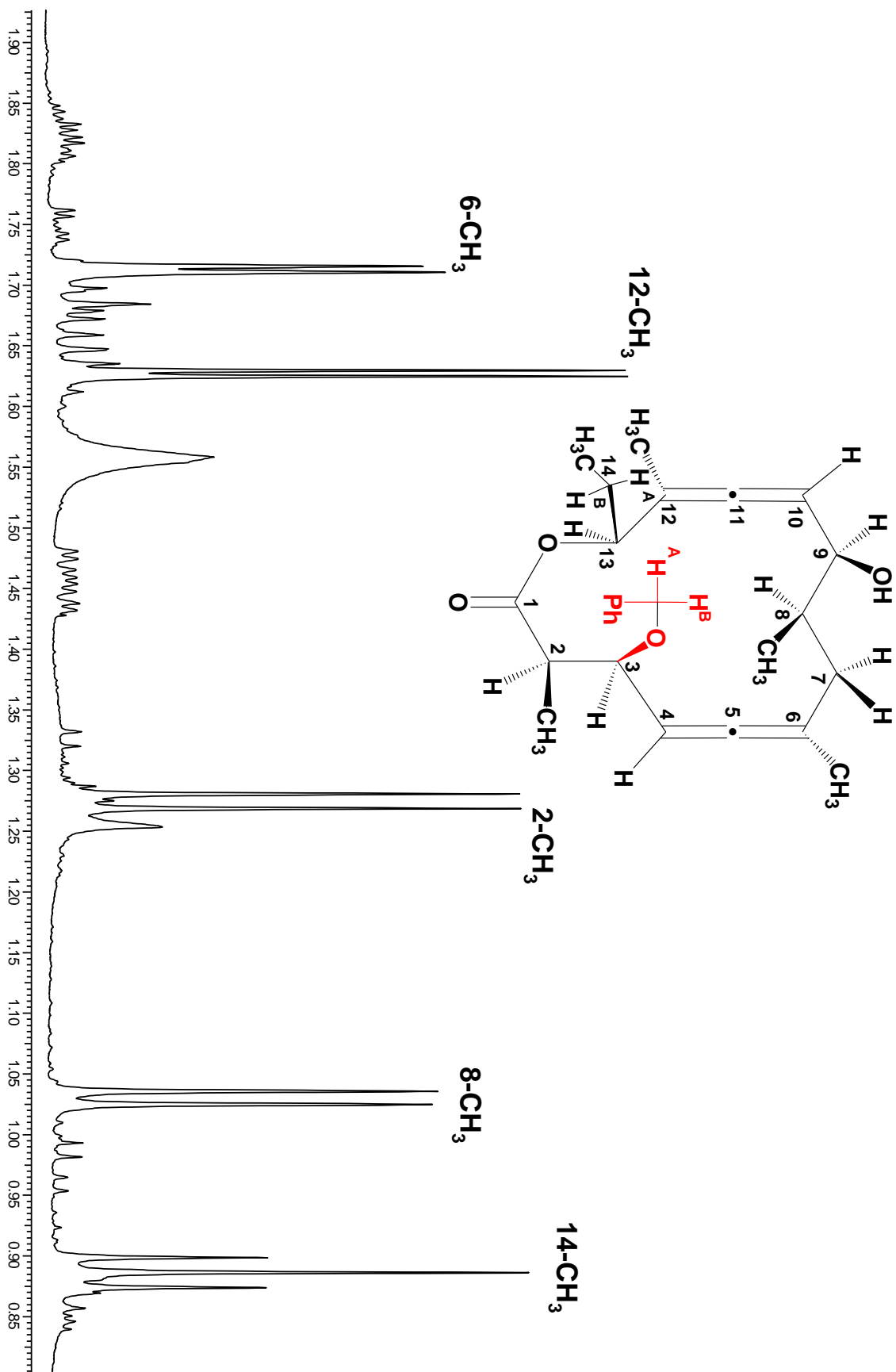
1D TOCSY

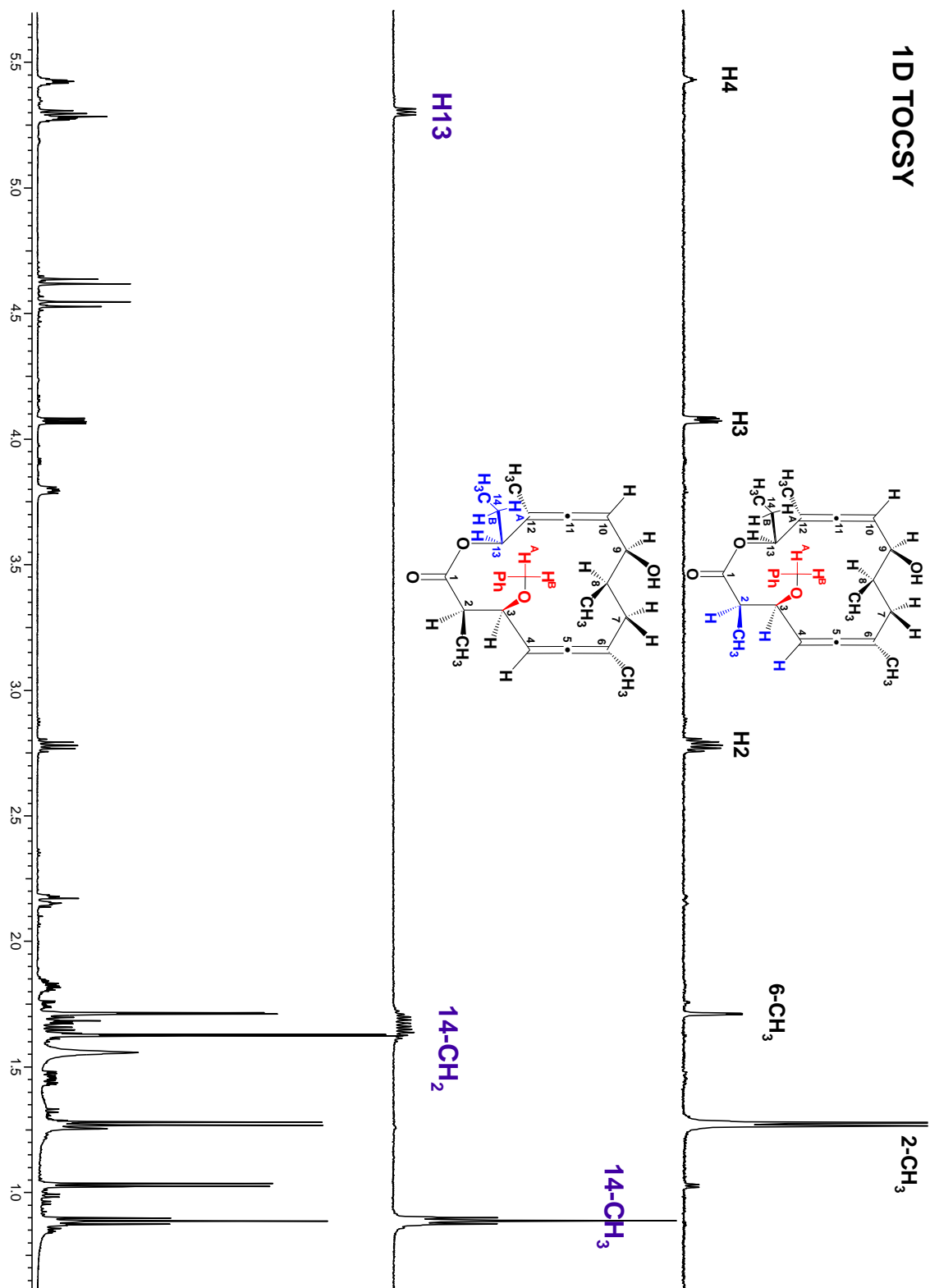


NOESY

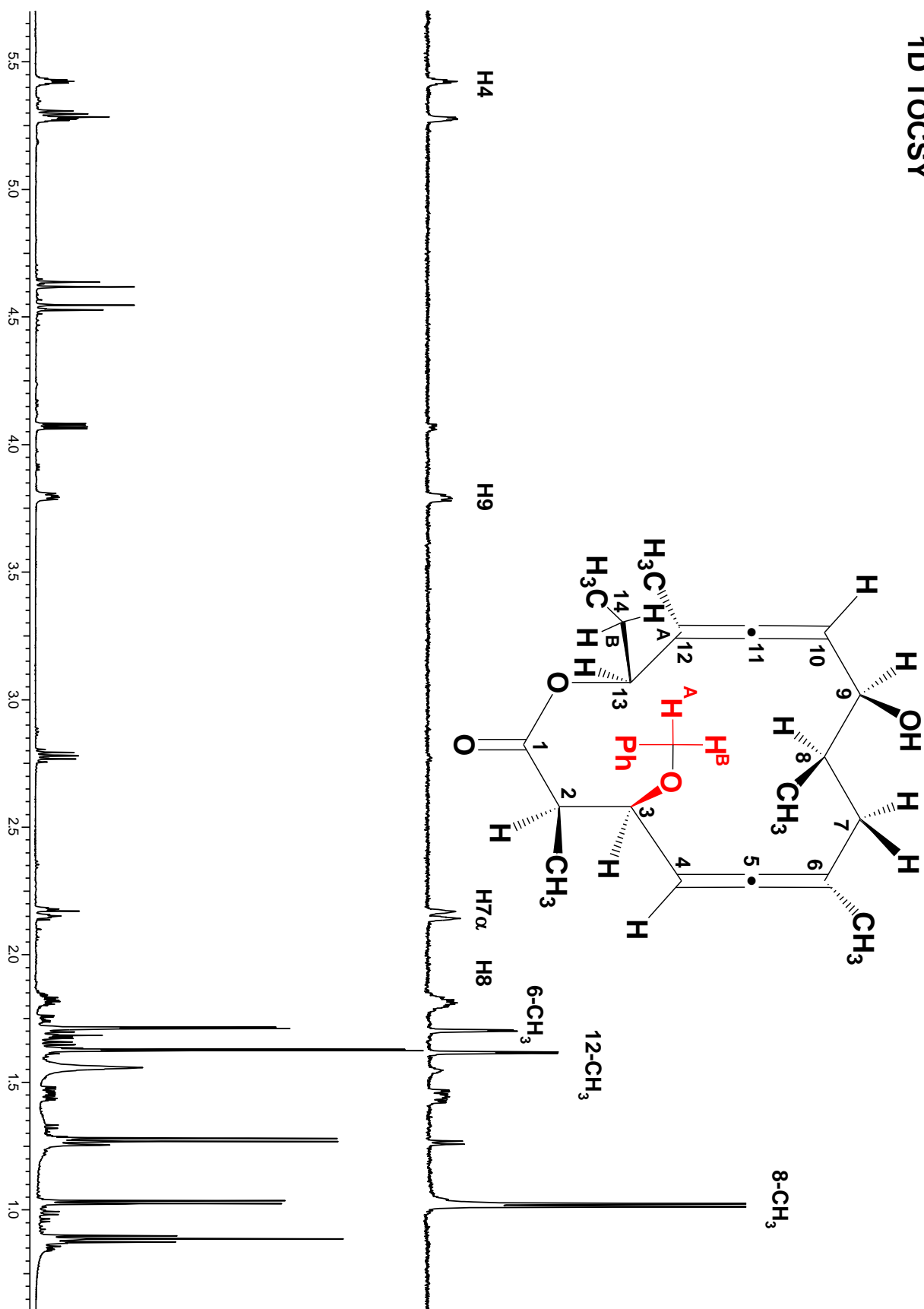


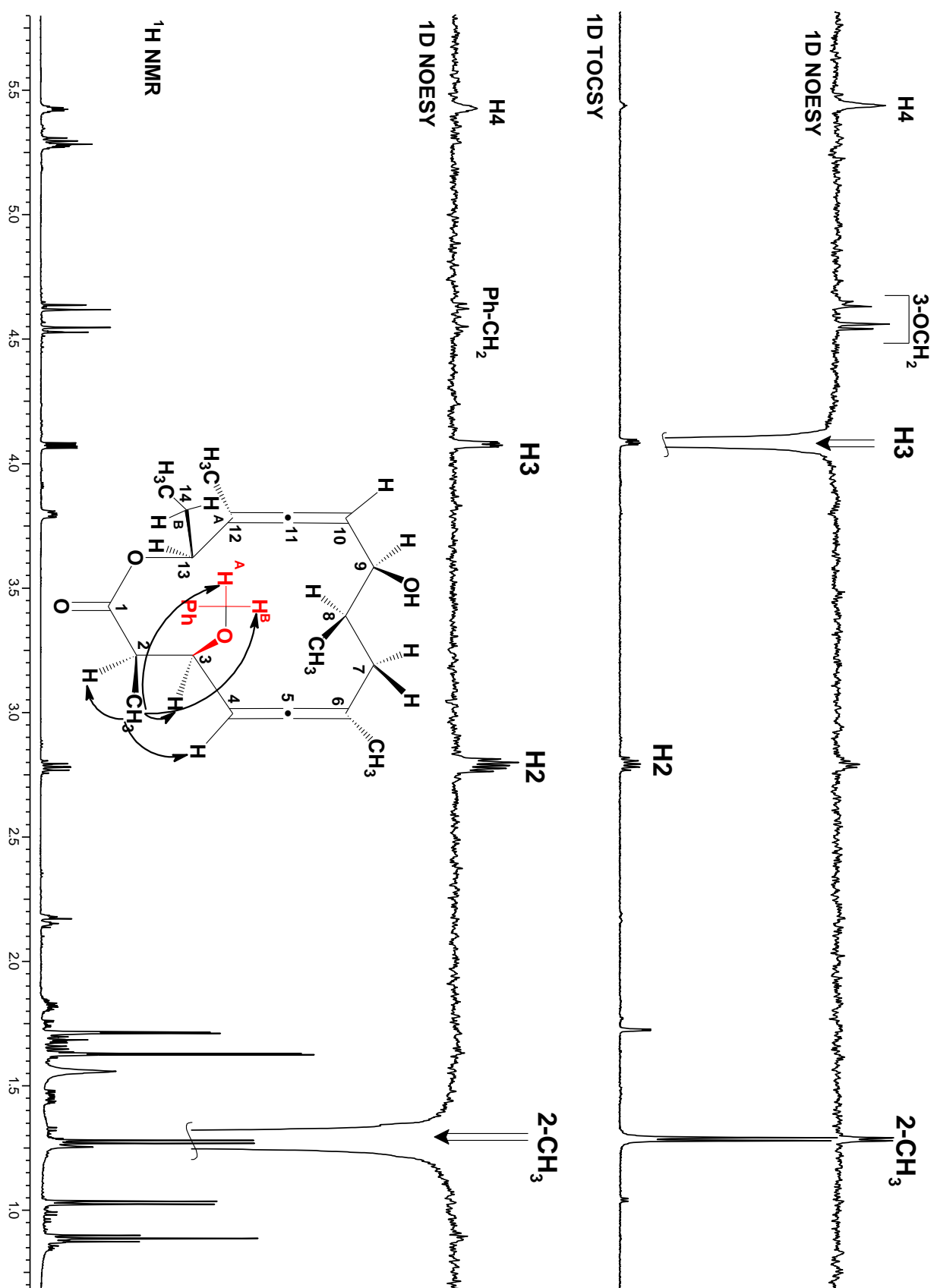


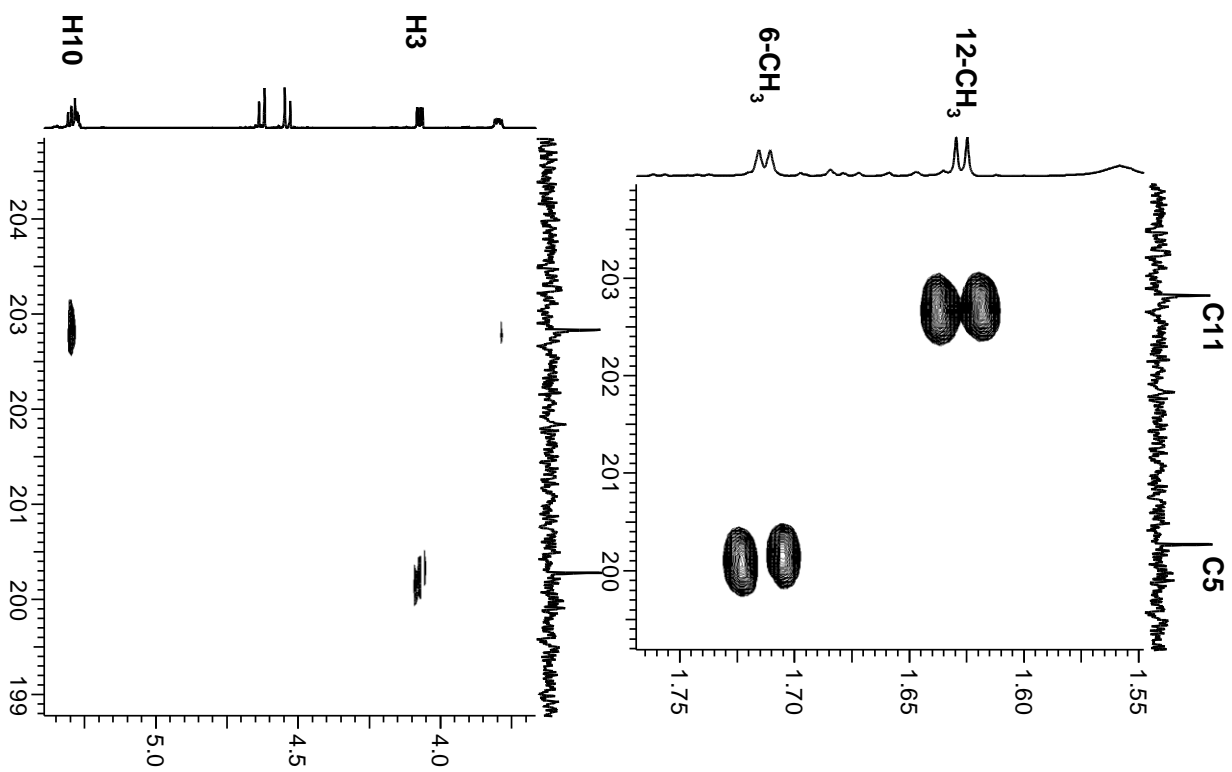
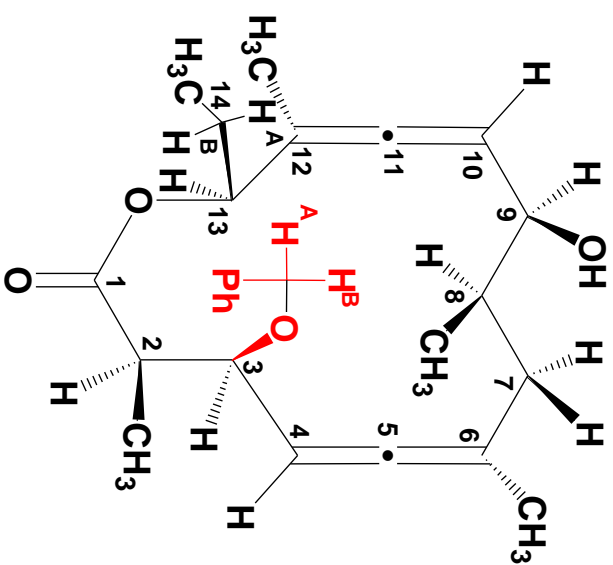


1D TOCSY

1D TOCSY

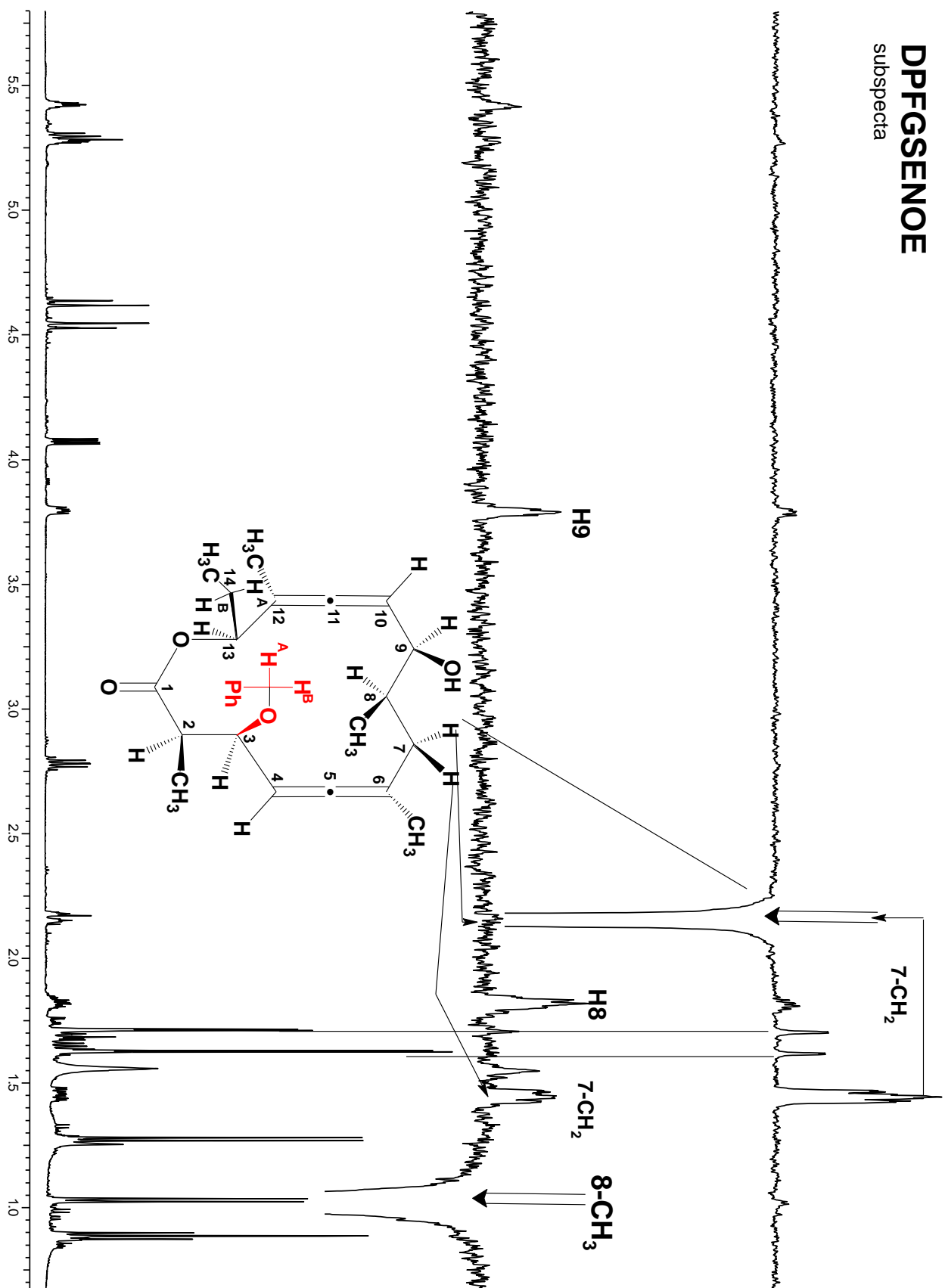


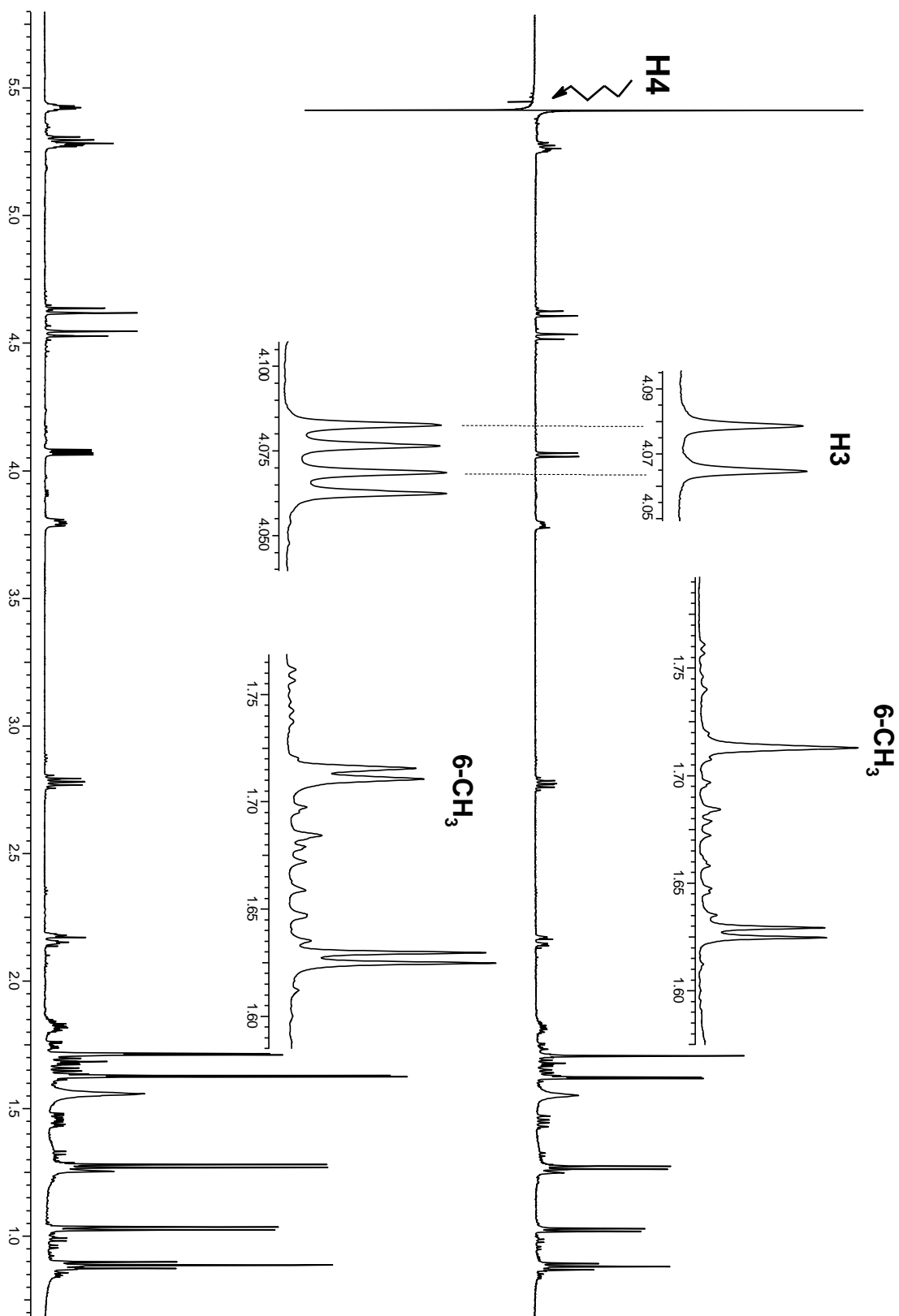


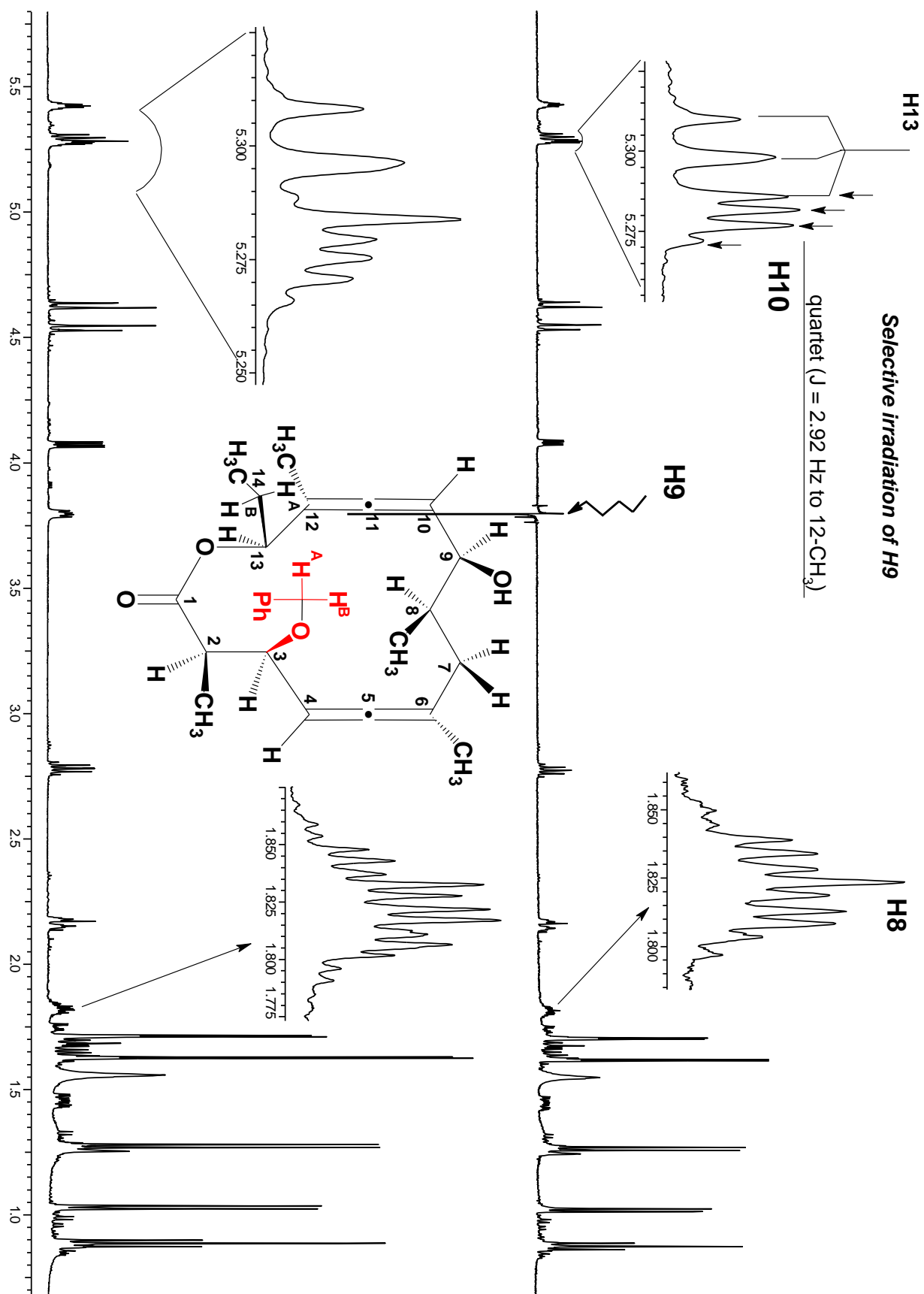
Long-range **gHMBC** correlations

The image displays the chemical structure of a substituted cyclohexane derivative and its corresponding ^1H NMR spectrum. The structure is a cyclohexane ring with various substituents, including a phenyl group (Ph) and a hydroxyl group (OH). The NMR spectrum shows peaks for the protons in the structure, with a specific peak labeled 'C3' corresponding to the proton on the carbon atom bonded to the phenyl group. The spectrum includes a chemical shift scale from 7.0 to 8.0 ppm and an integration curve.

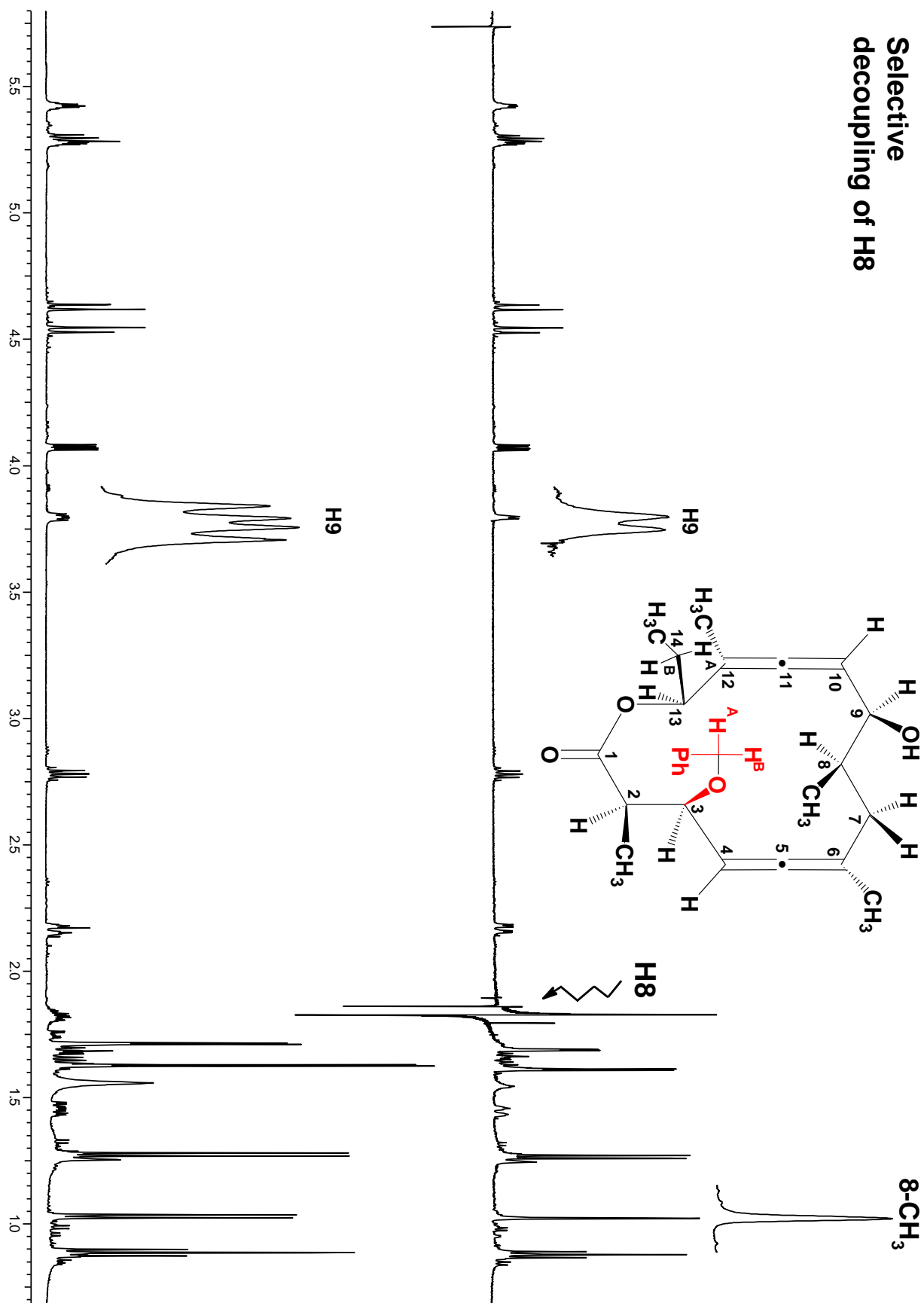
DPFGSENOE subspectra

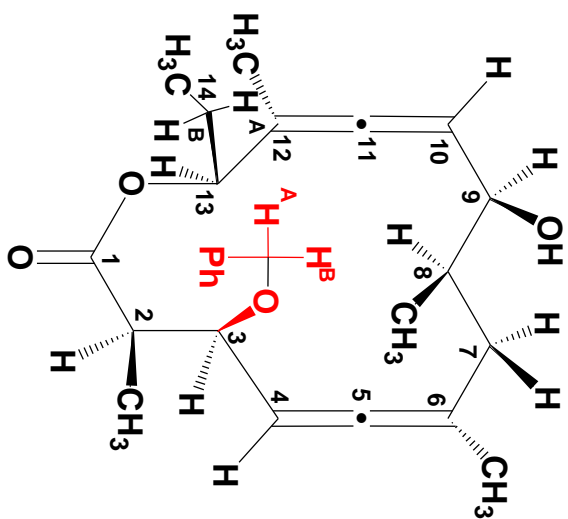
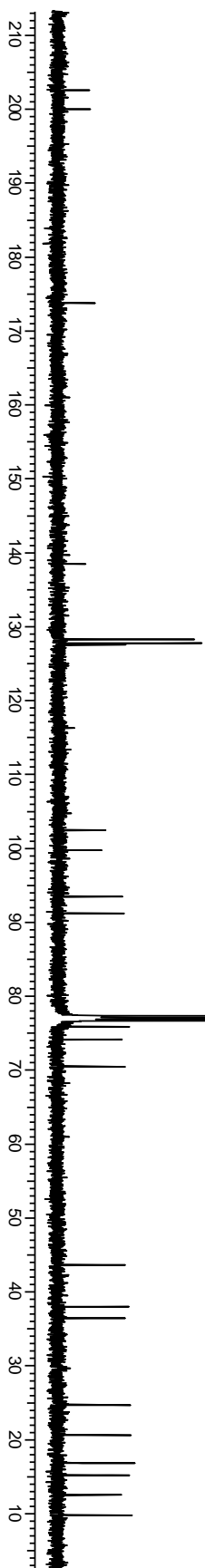
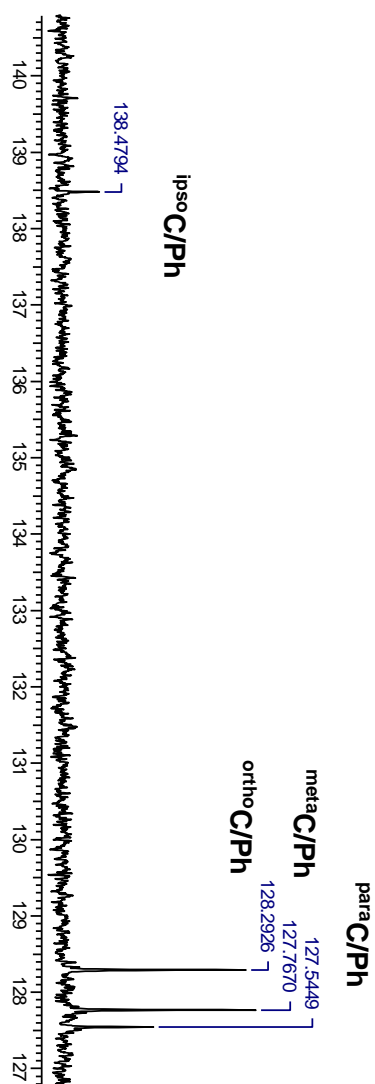
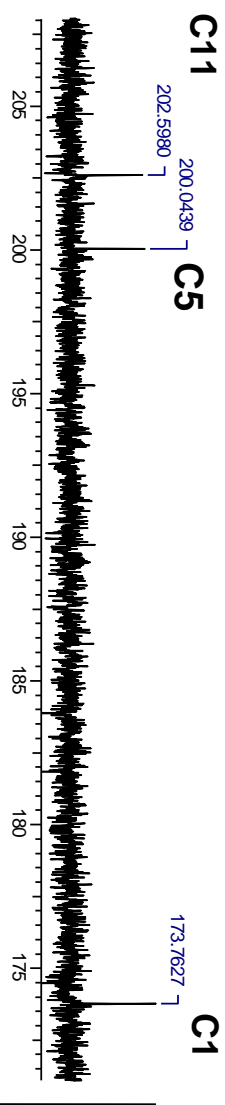
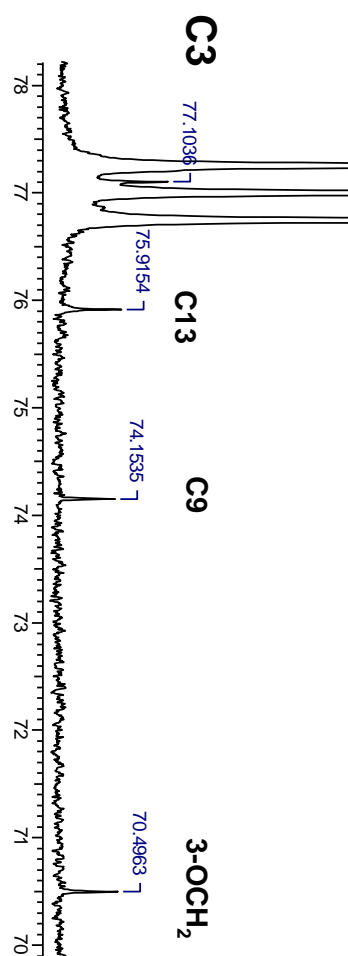


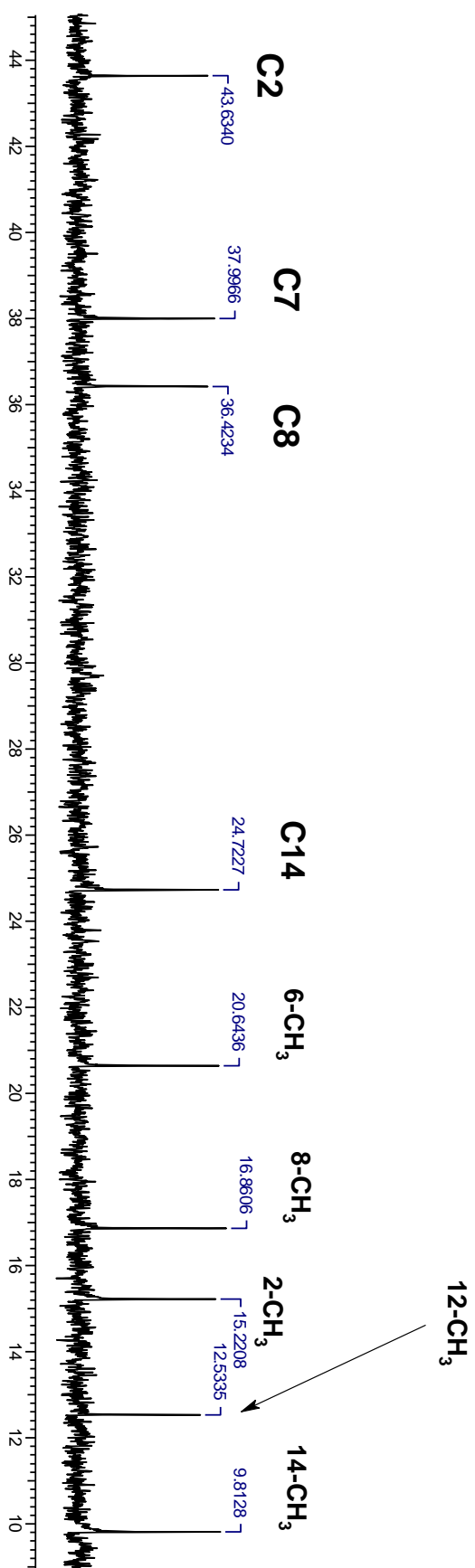
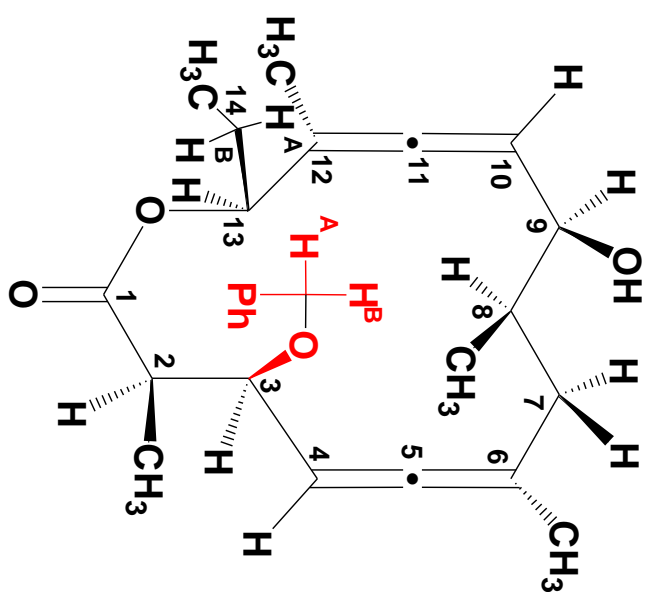
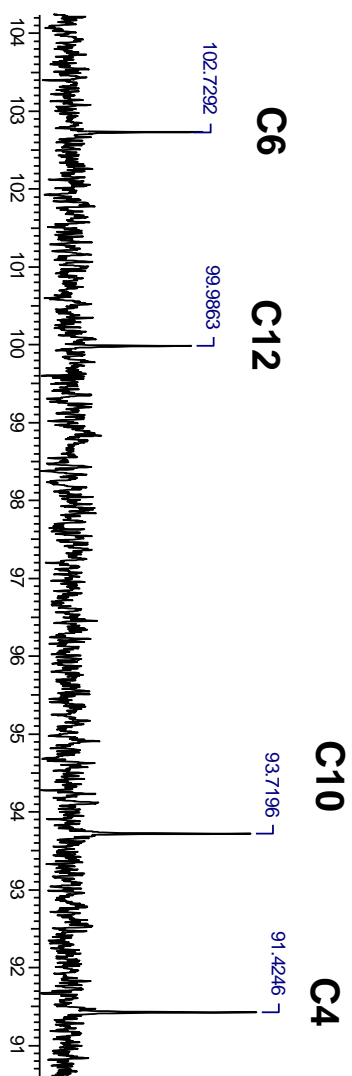
Selective irradiation of H4



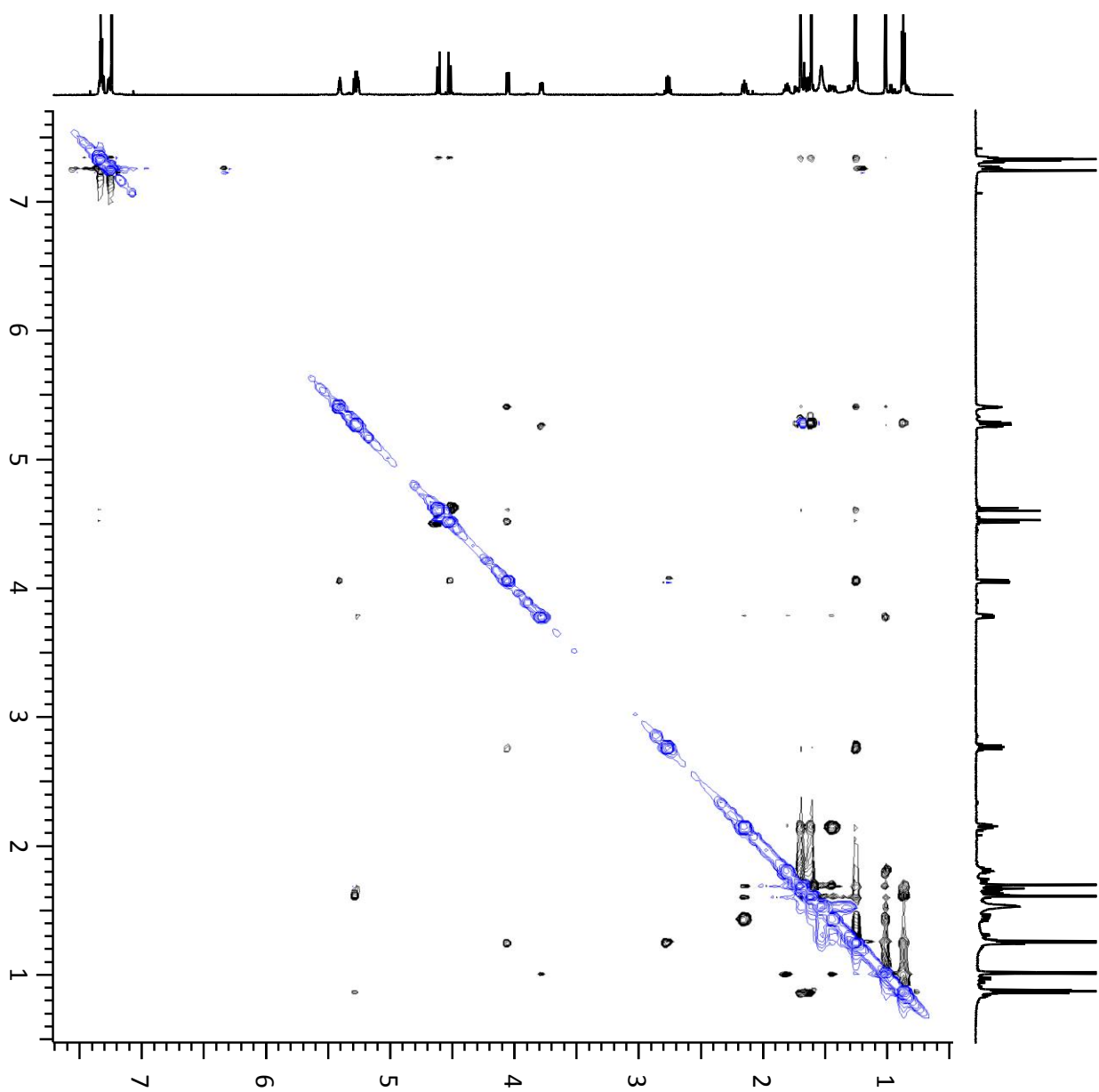
Selective decoupling of H8

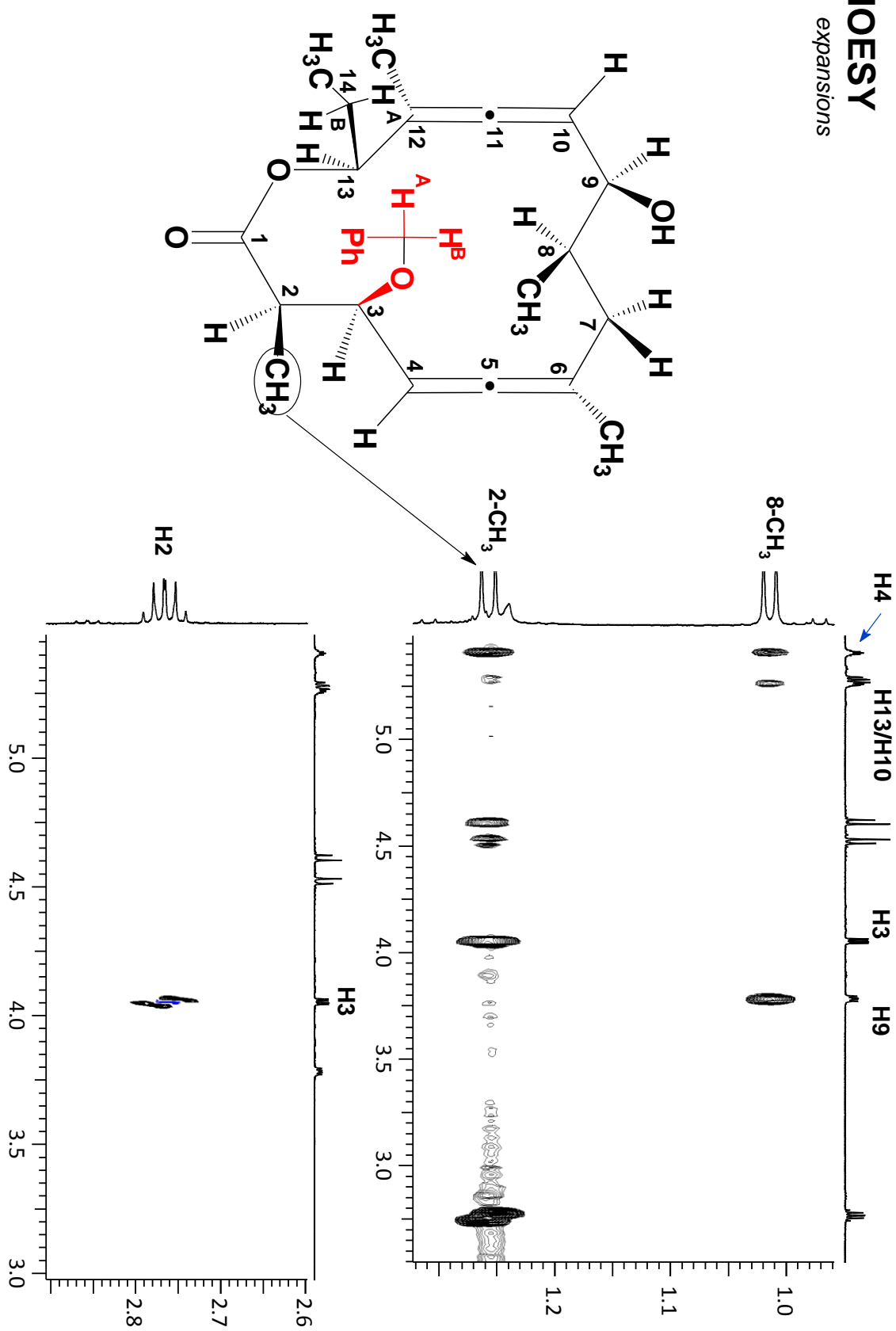




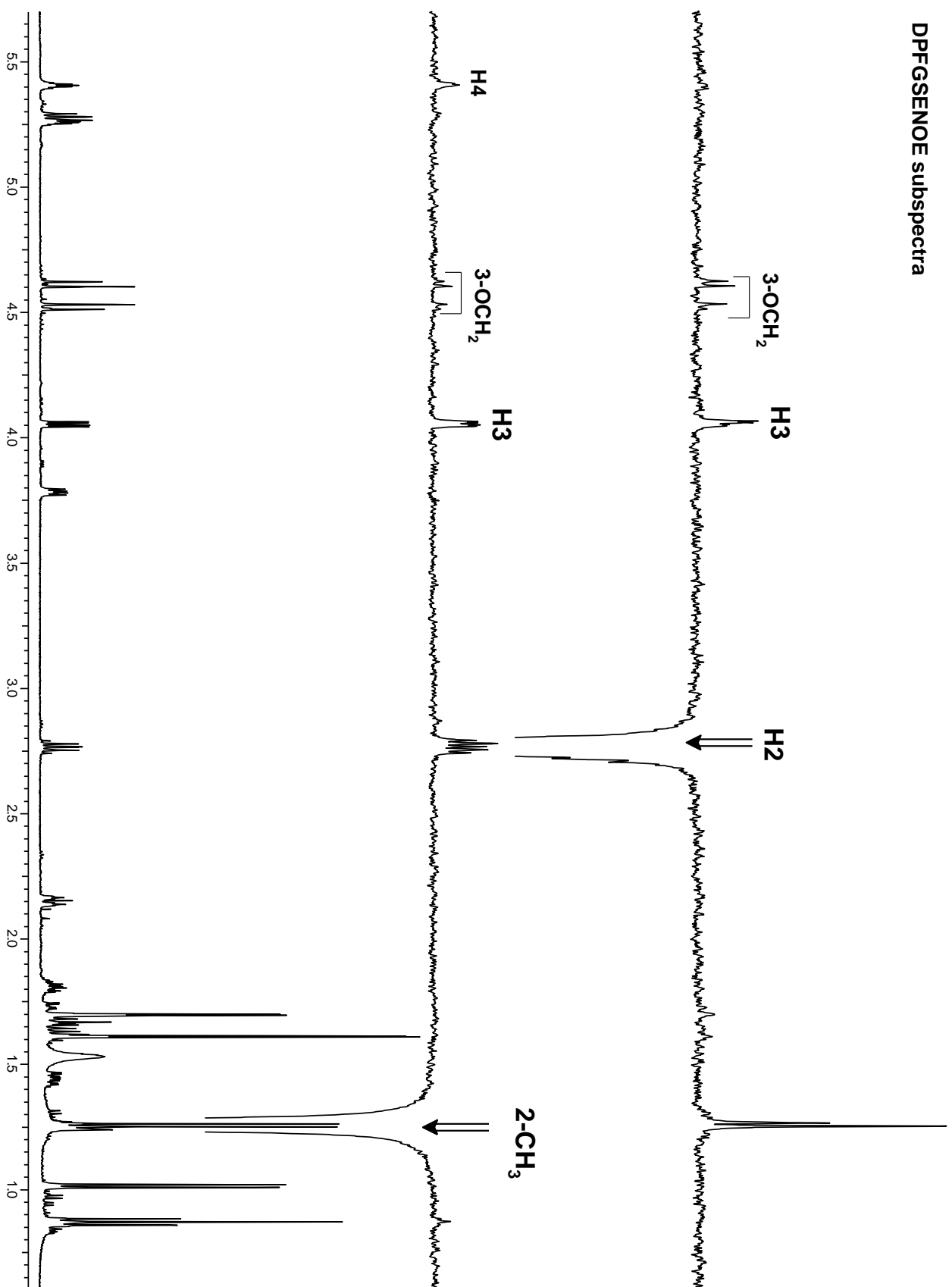
^{13}C NMR spectrum in CDCl_3 

NOESY

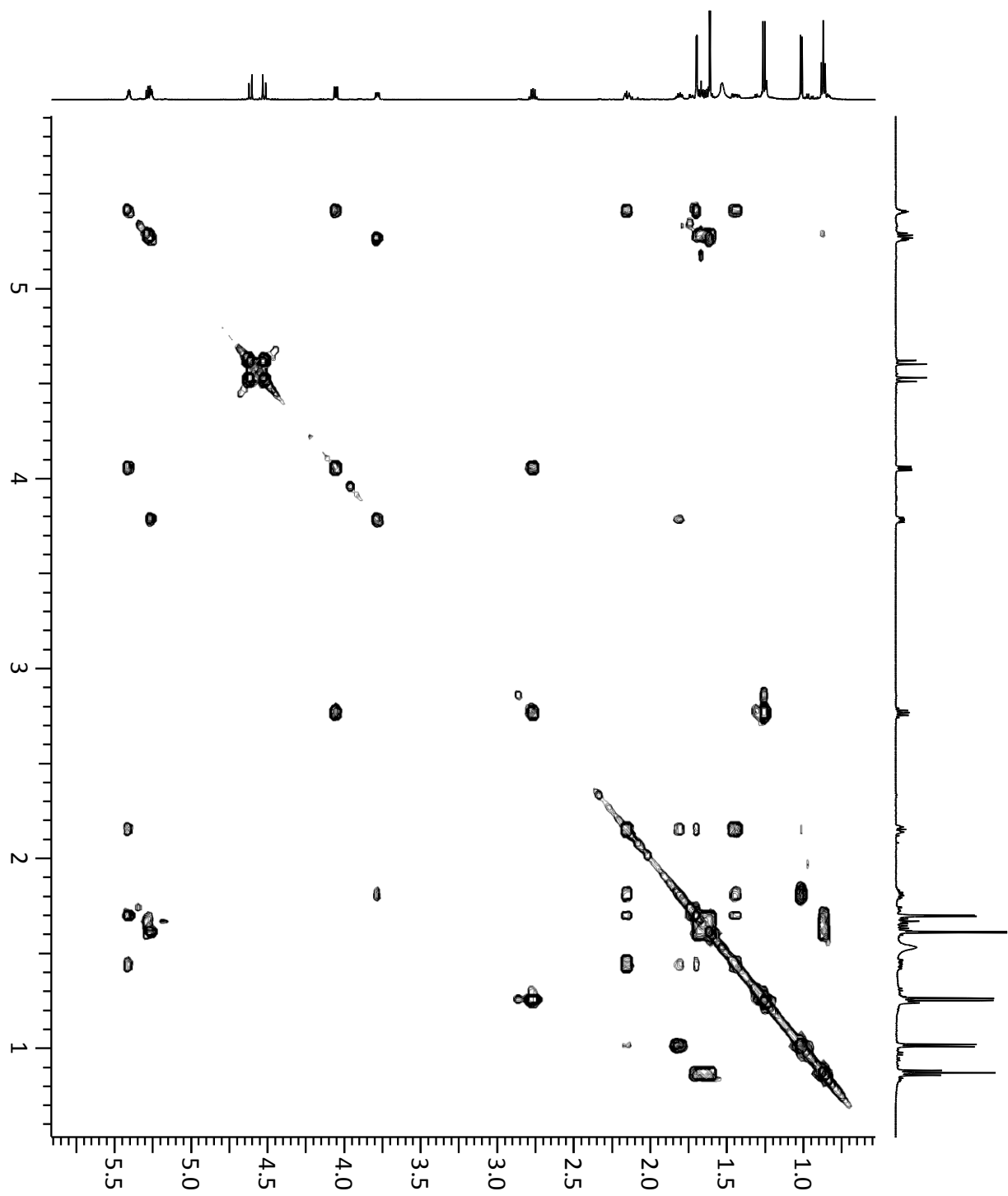




DPFGSENOE subspectra

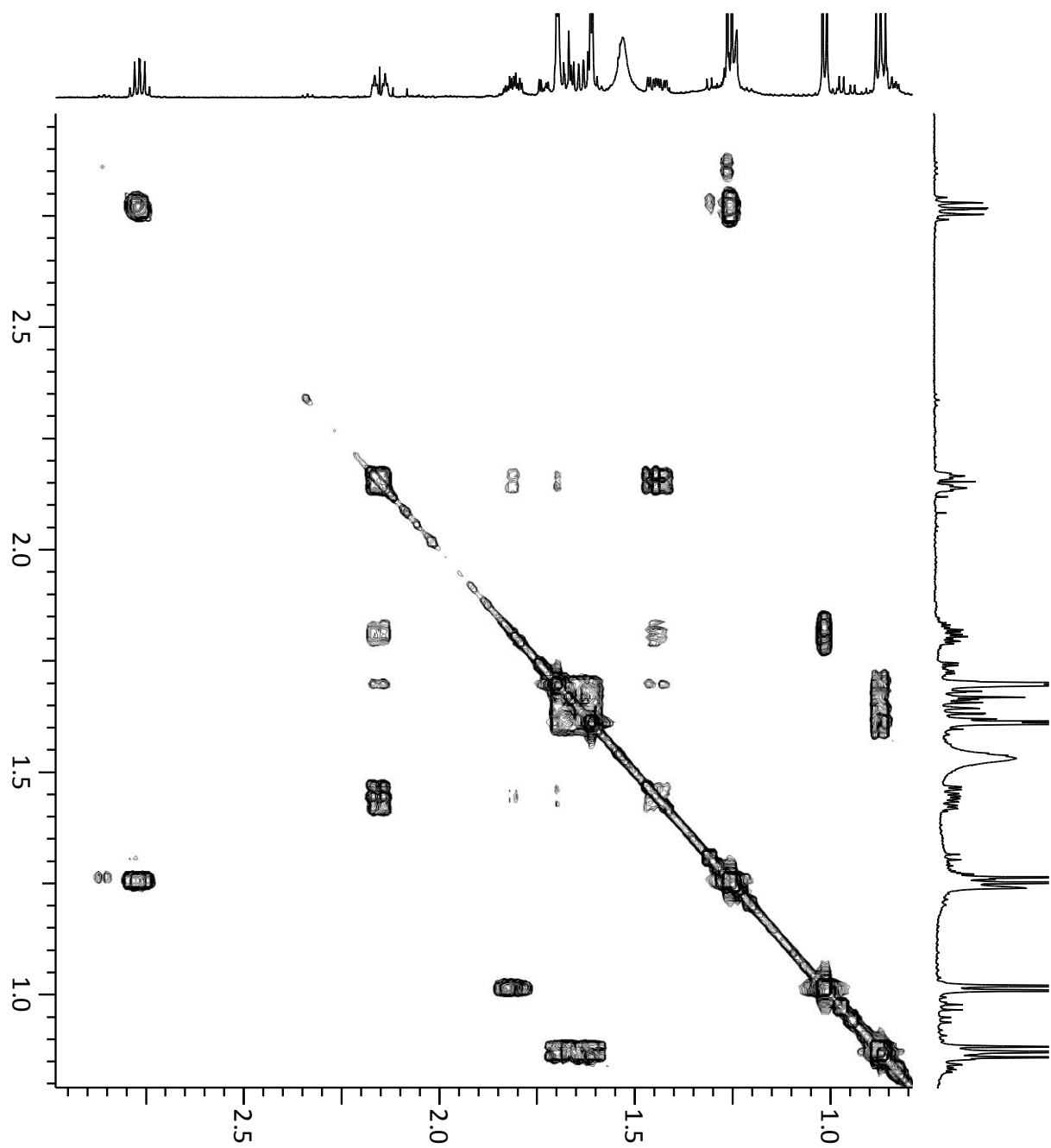


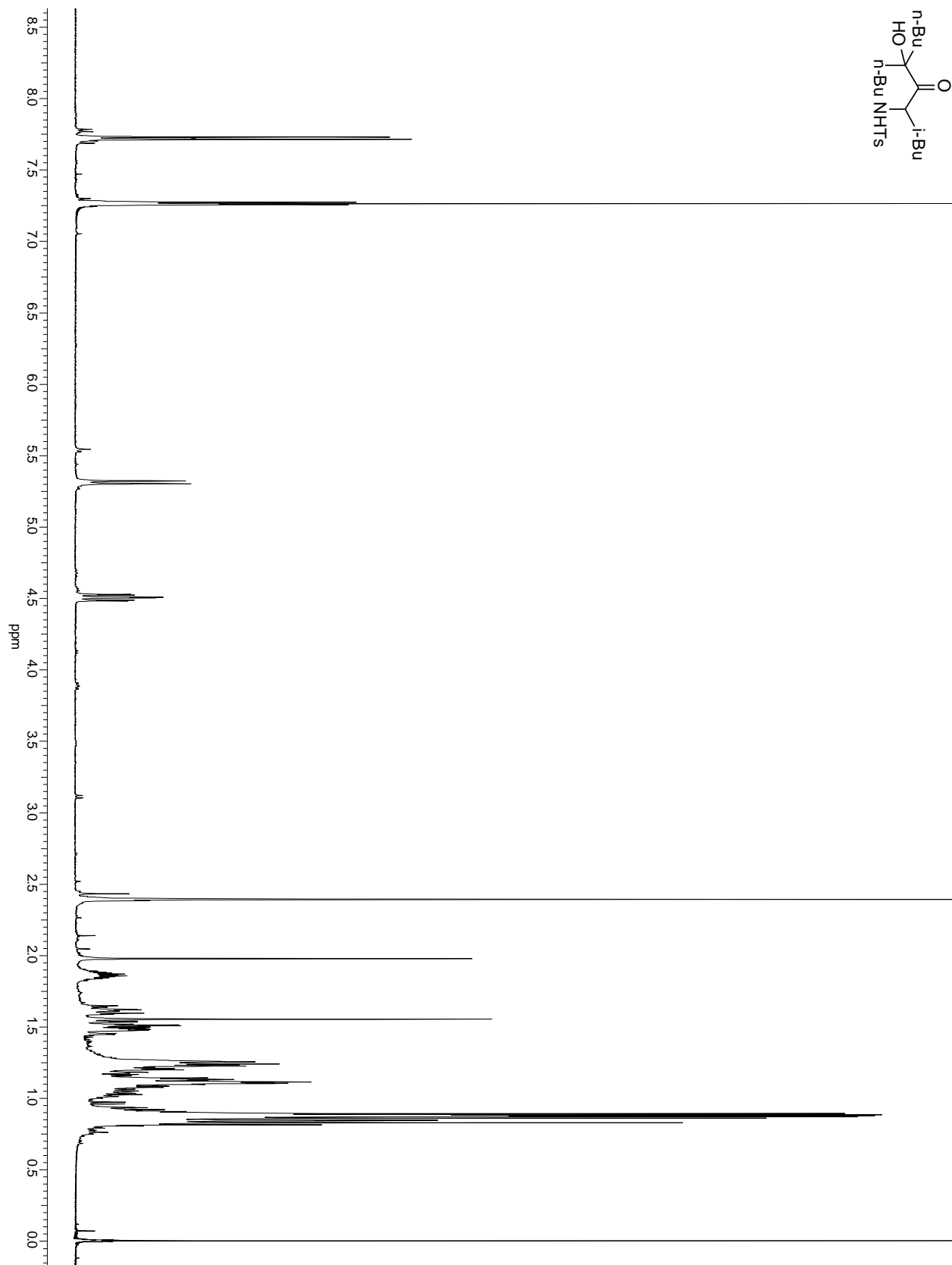
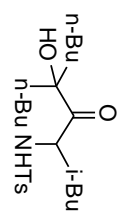
gCOSY

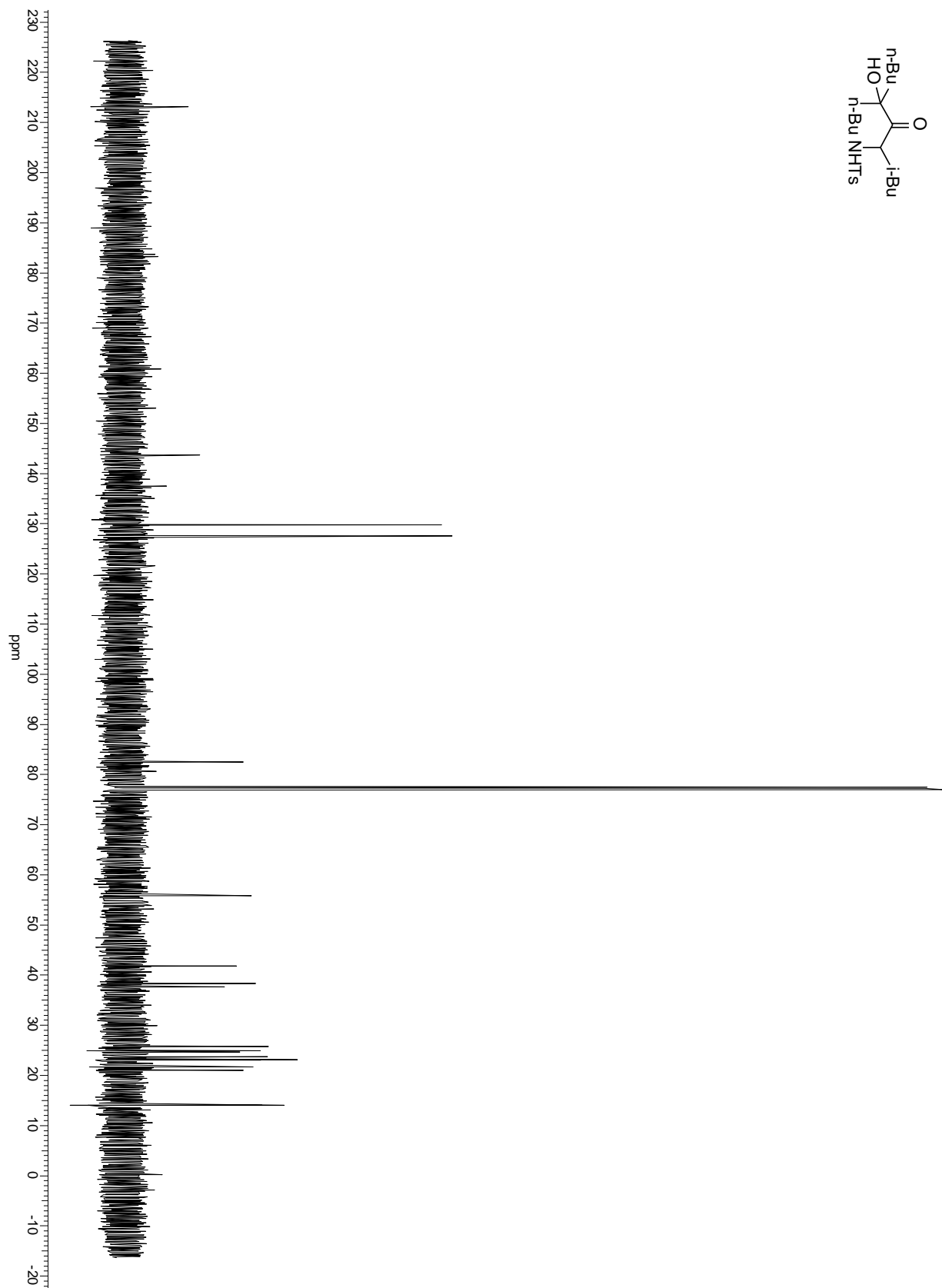
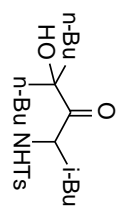


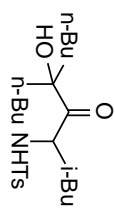
gCOSY

expansion

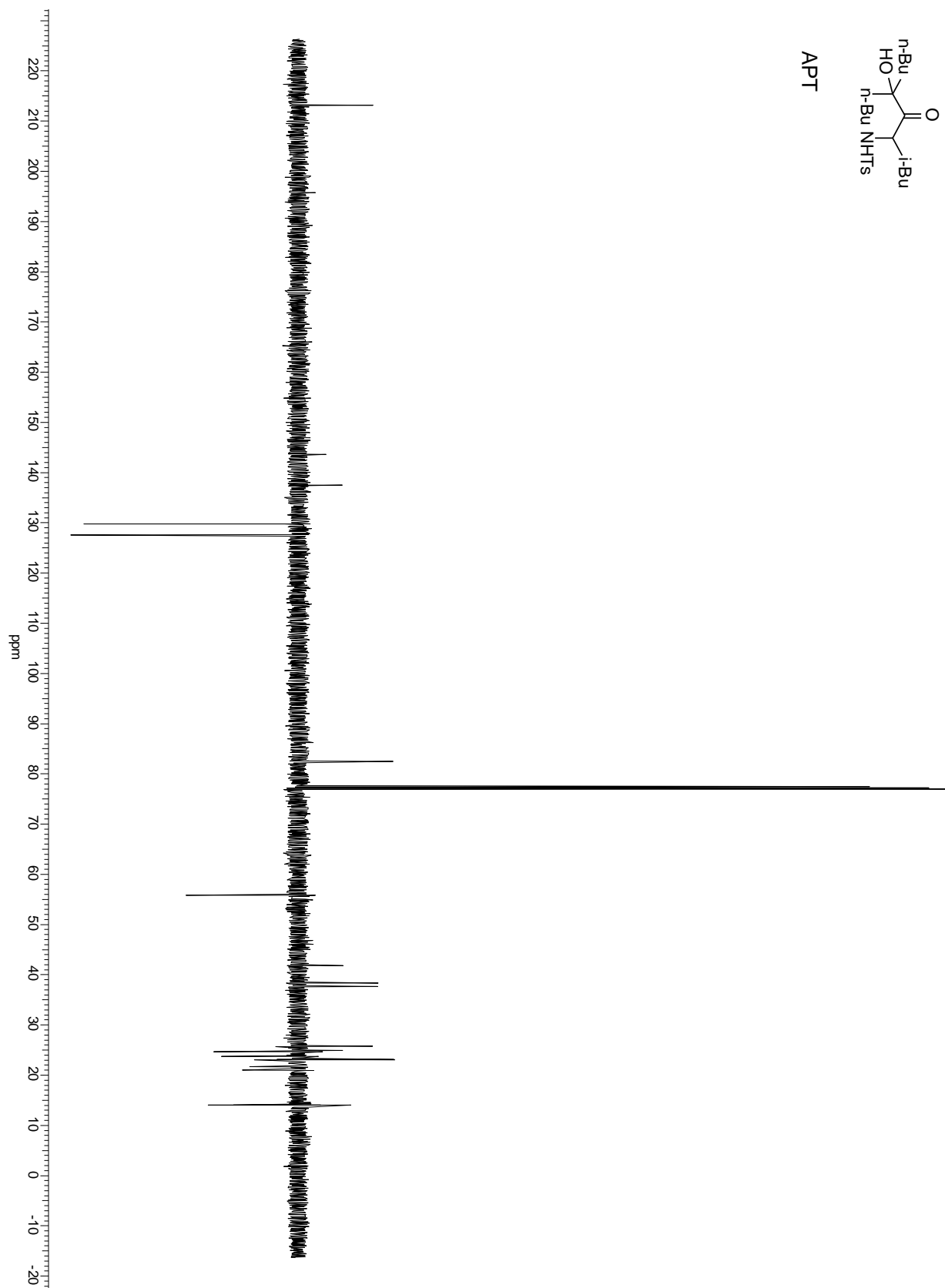


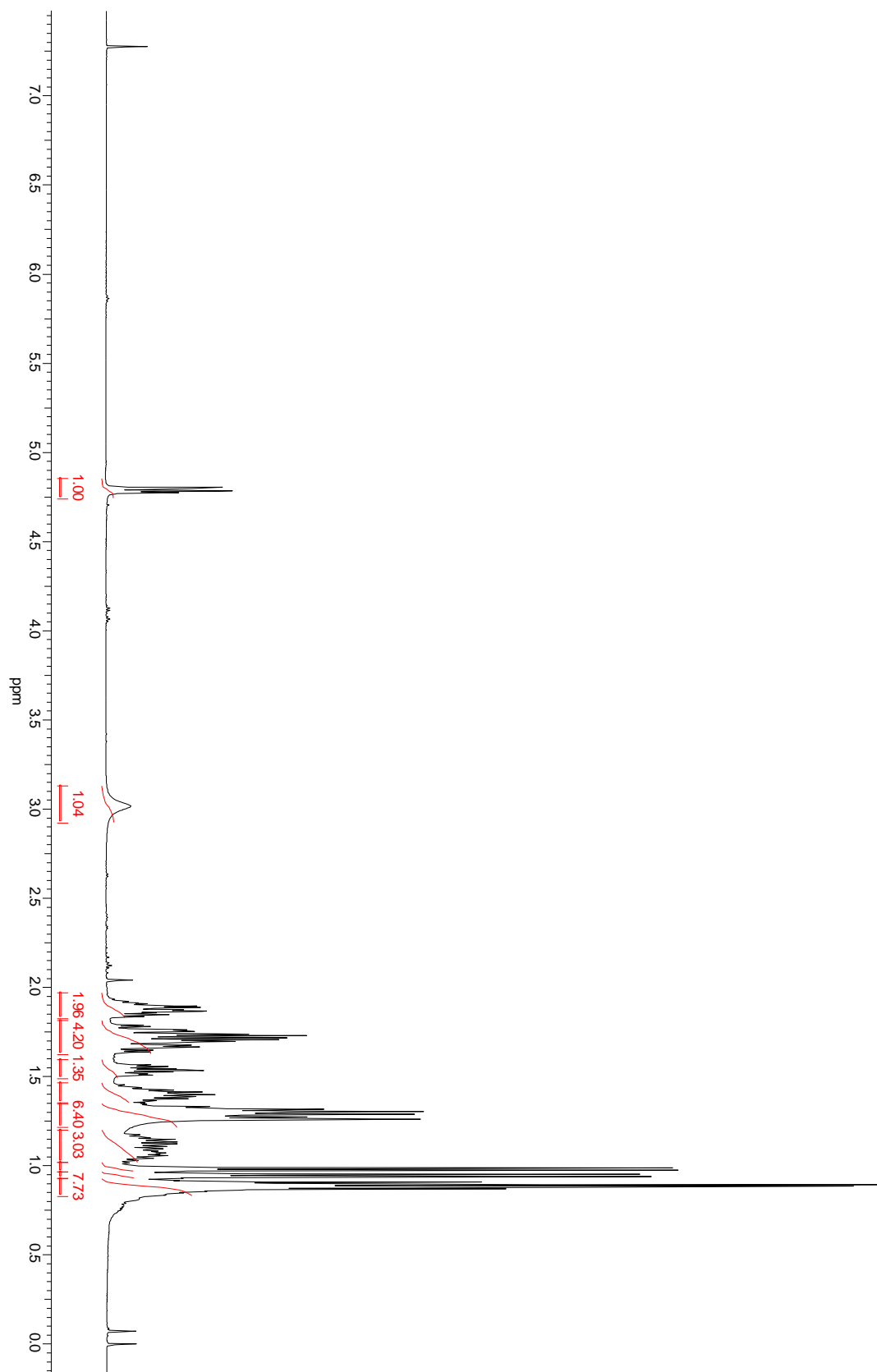
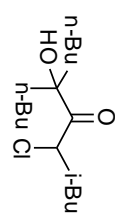


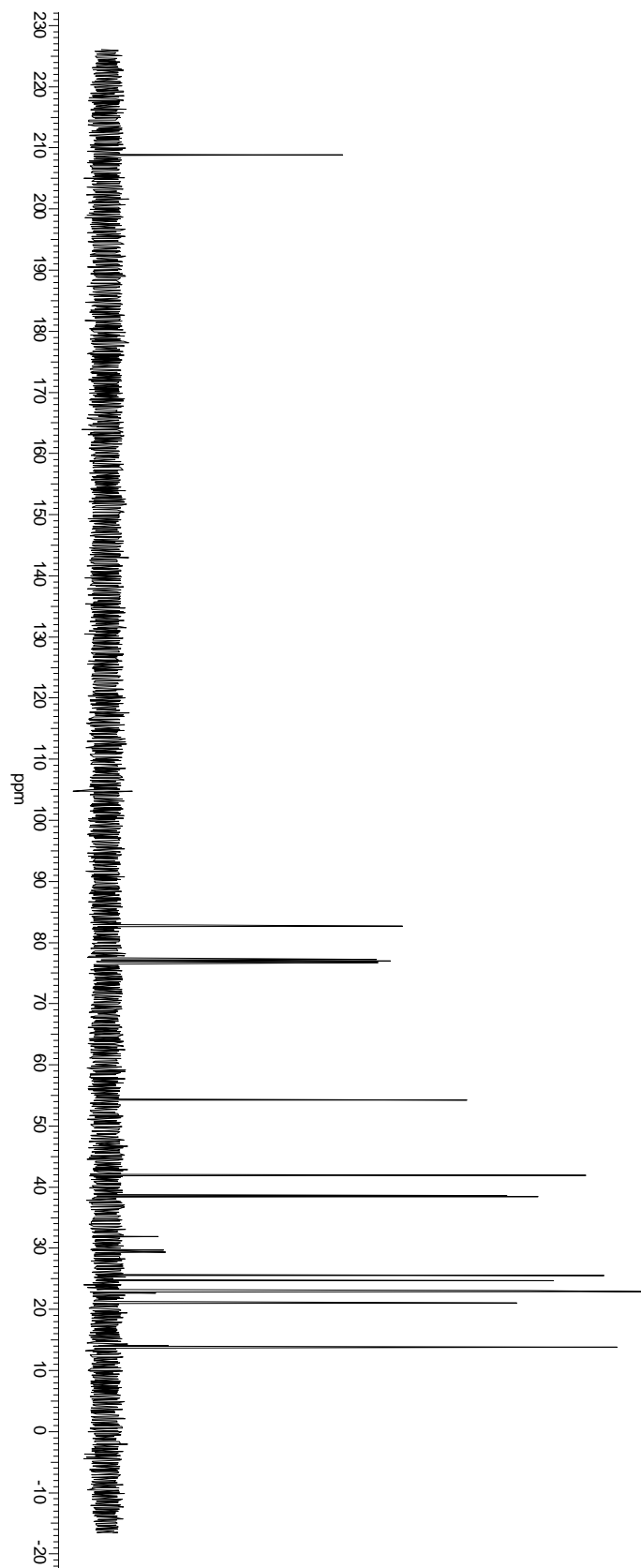
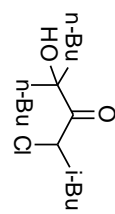


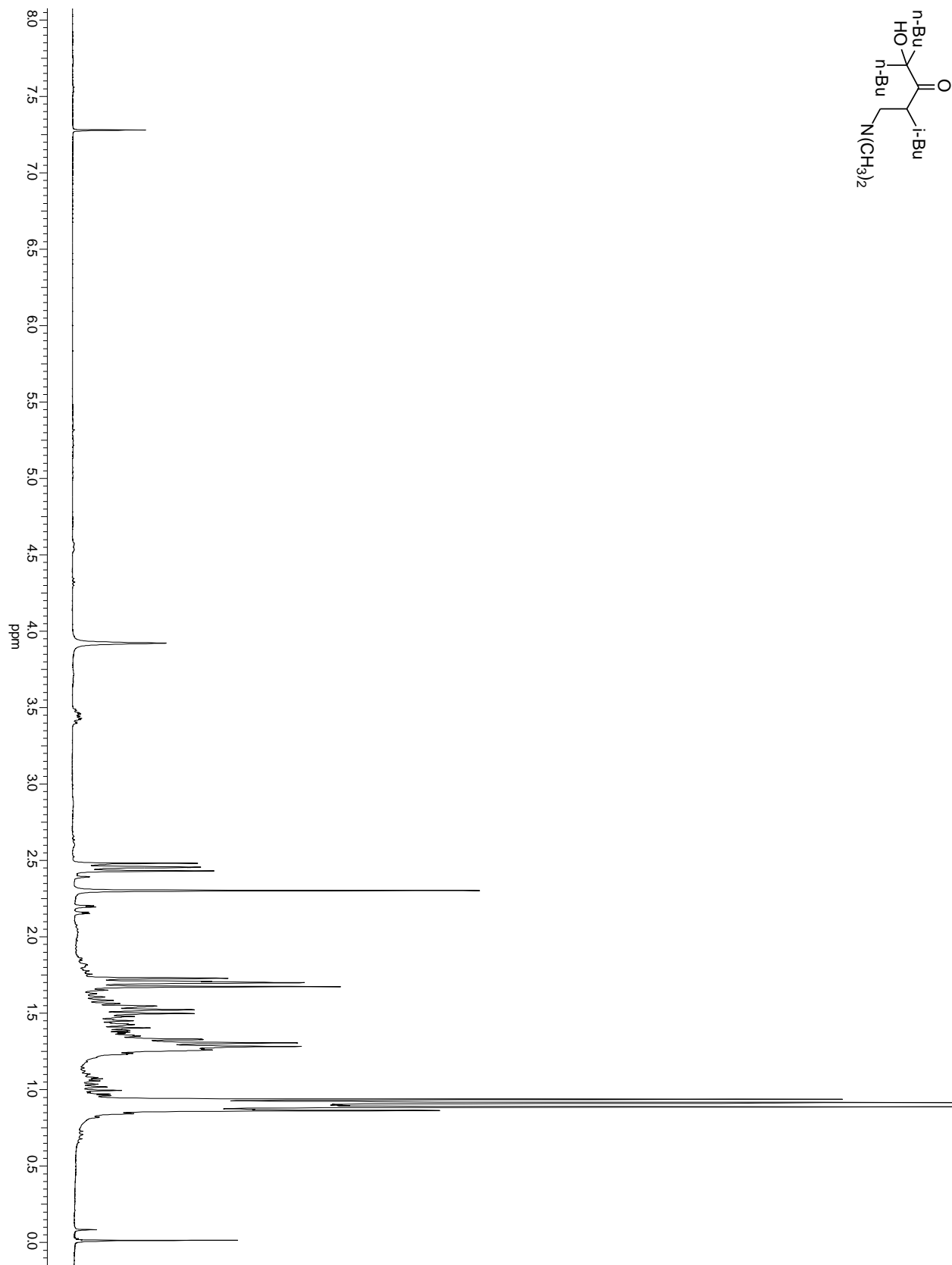
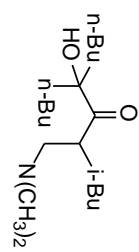


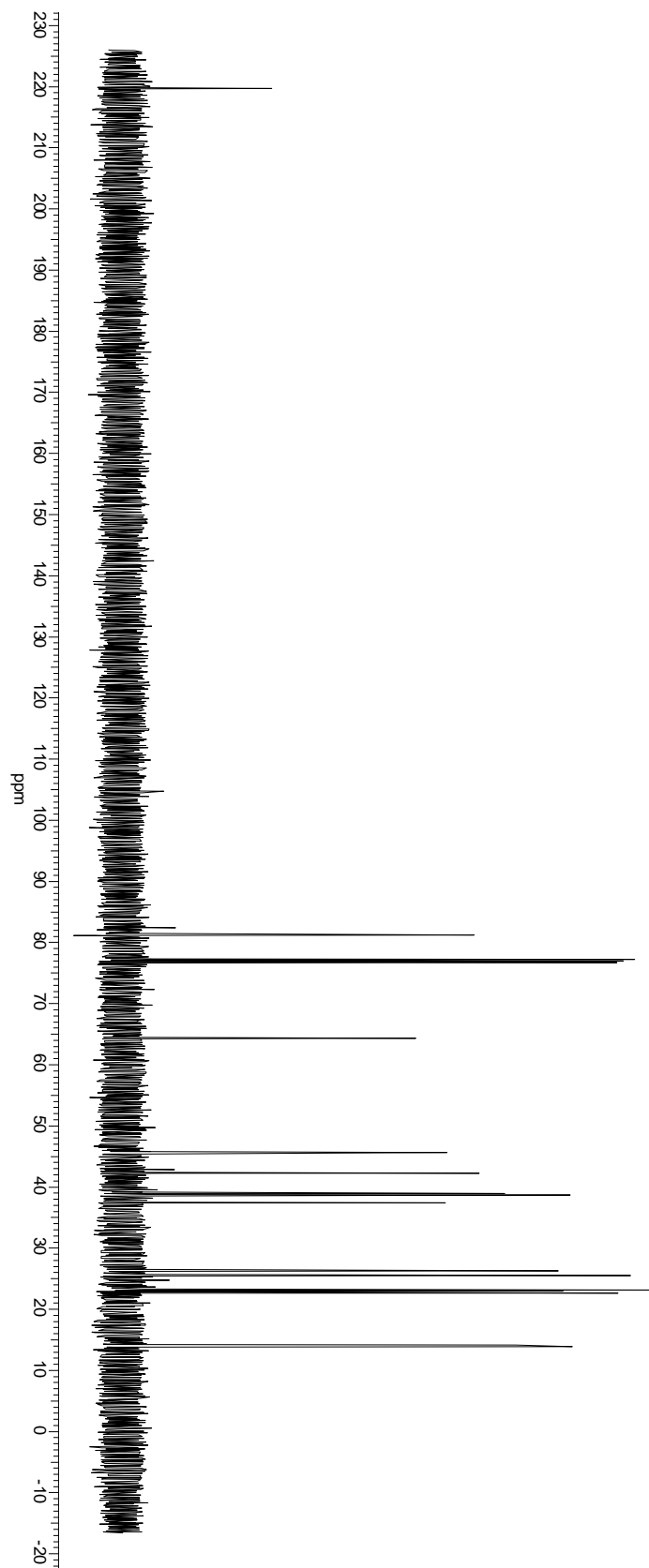
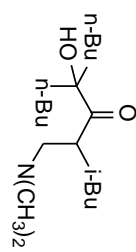
APT

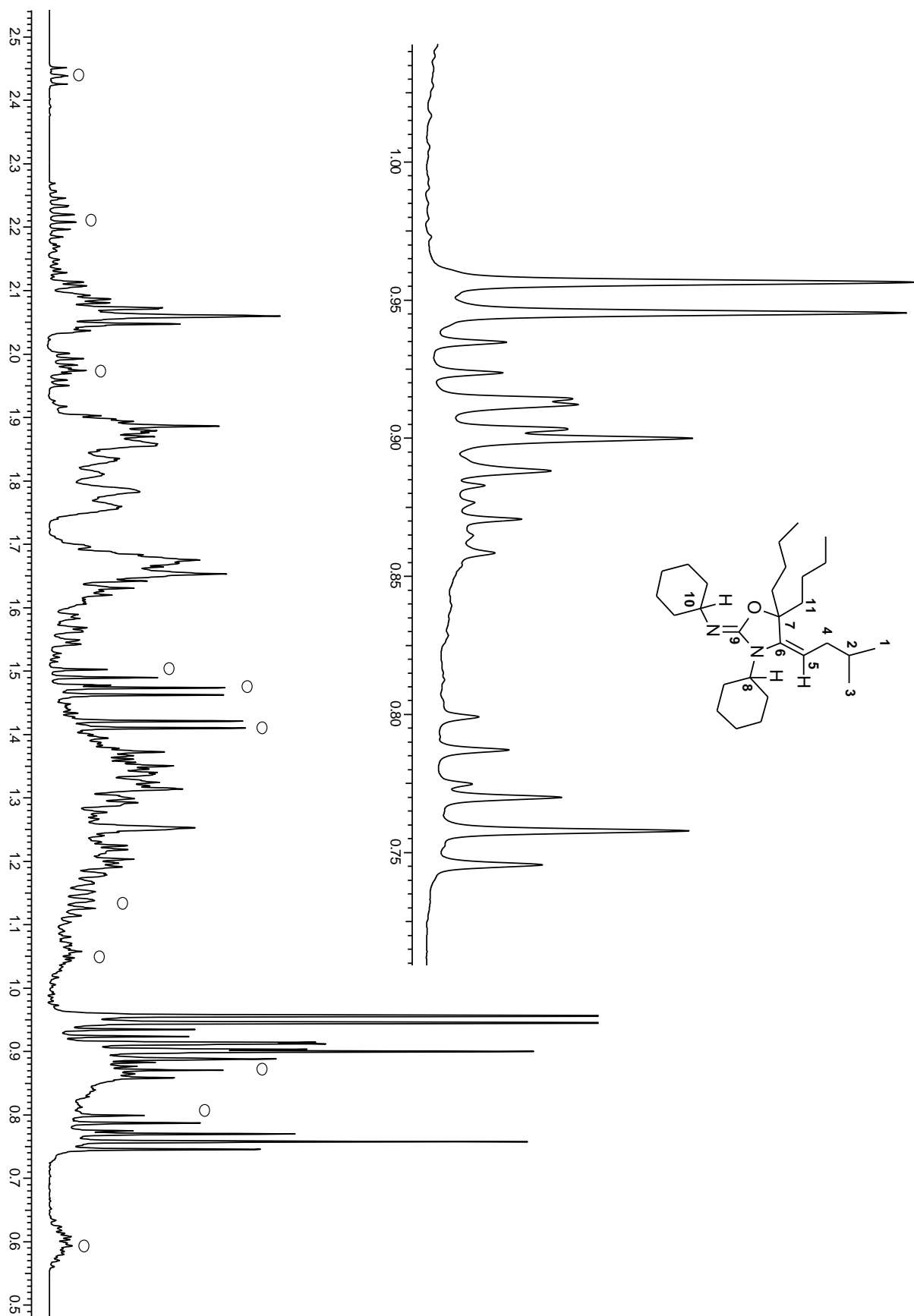




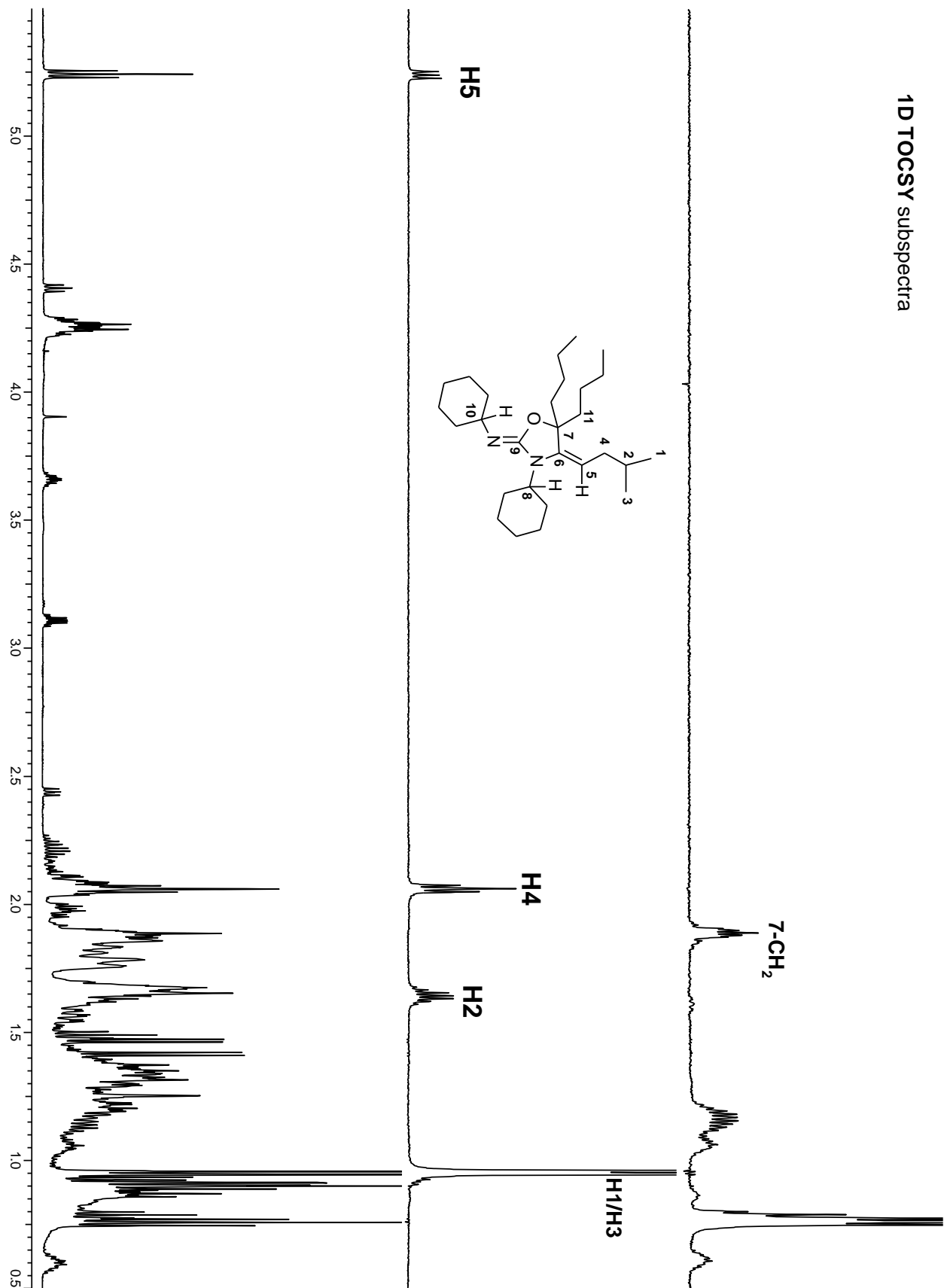


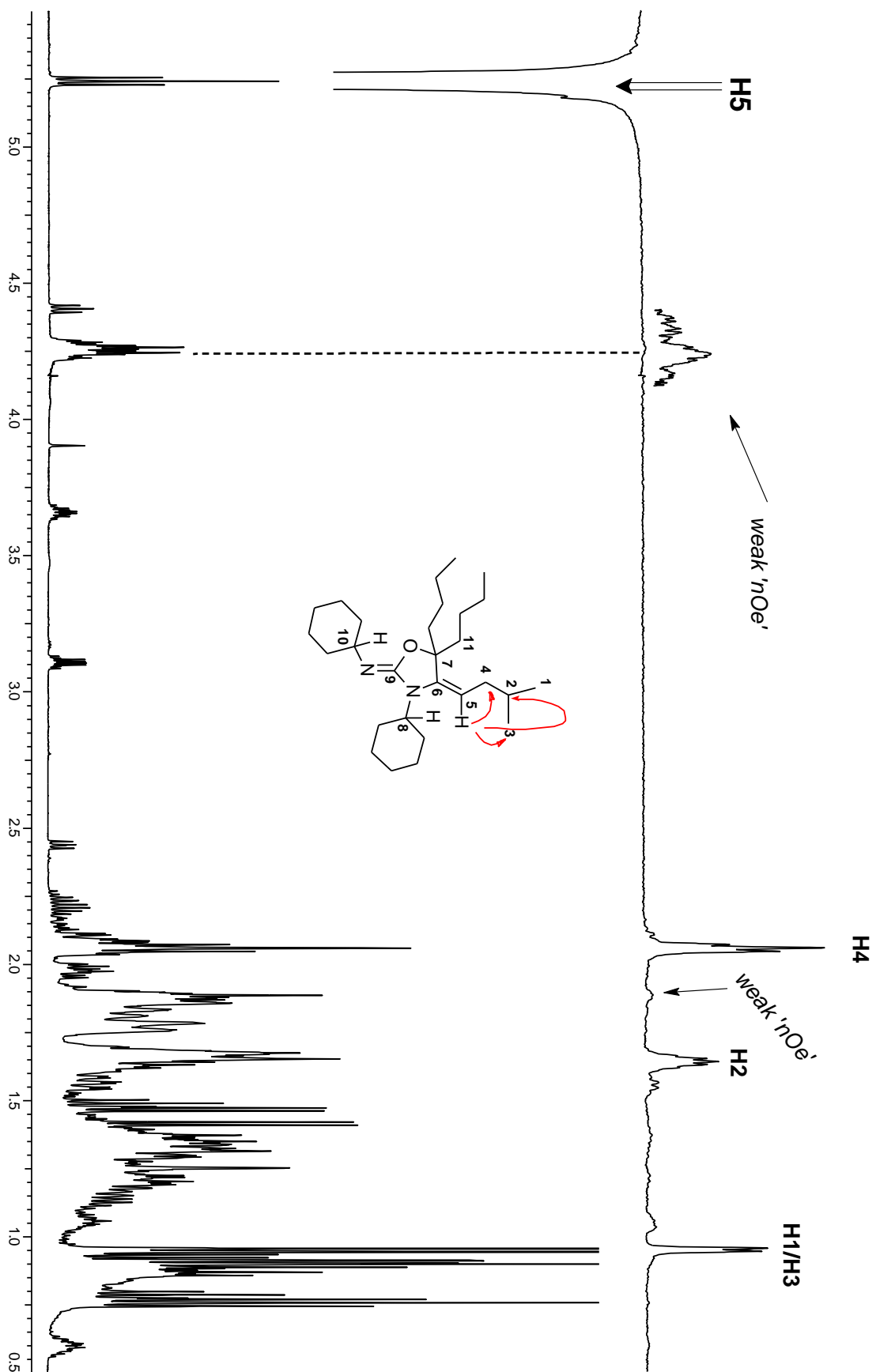


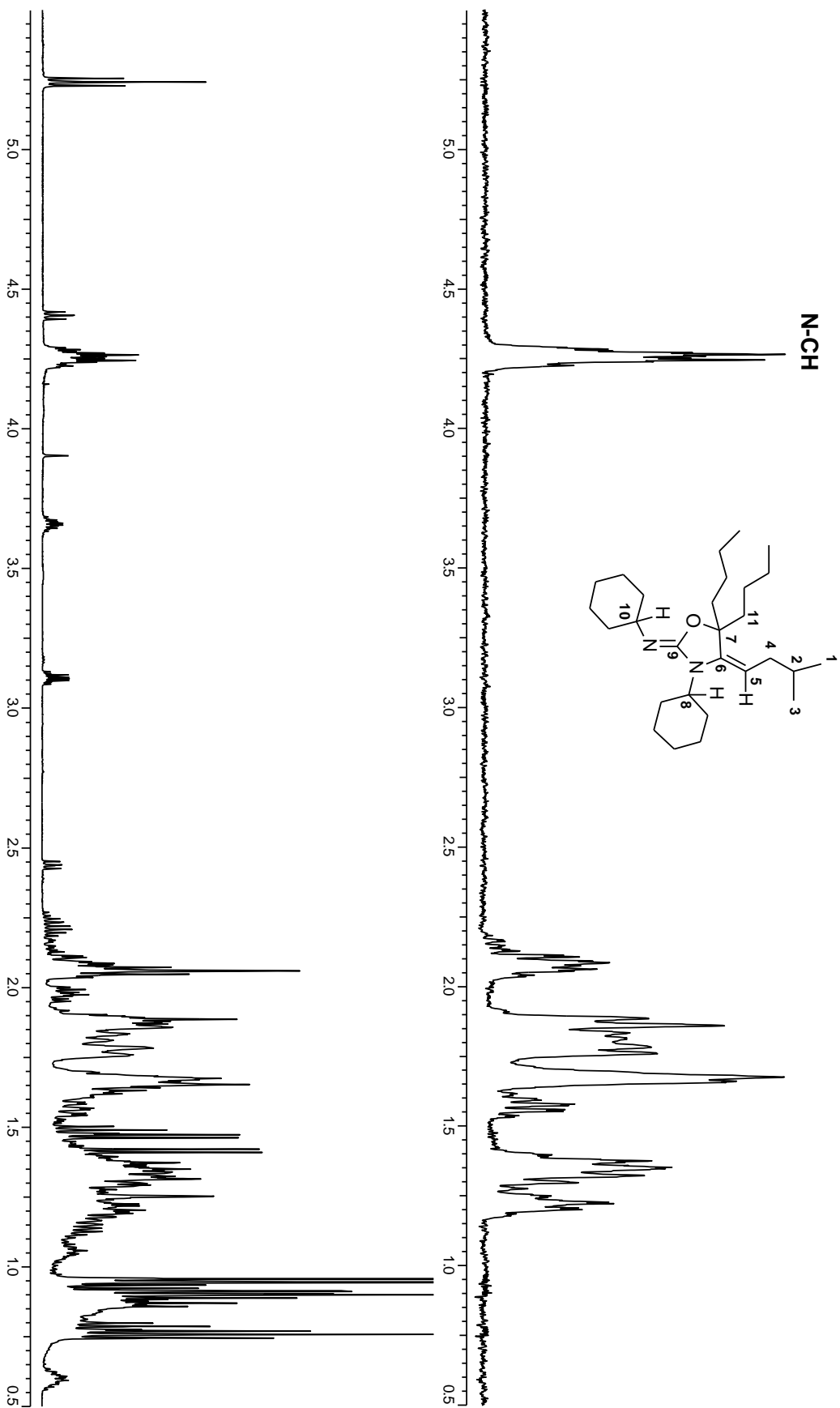




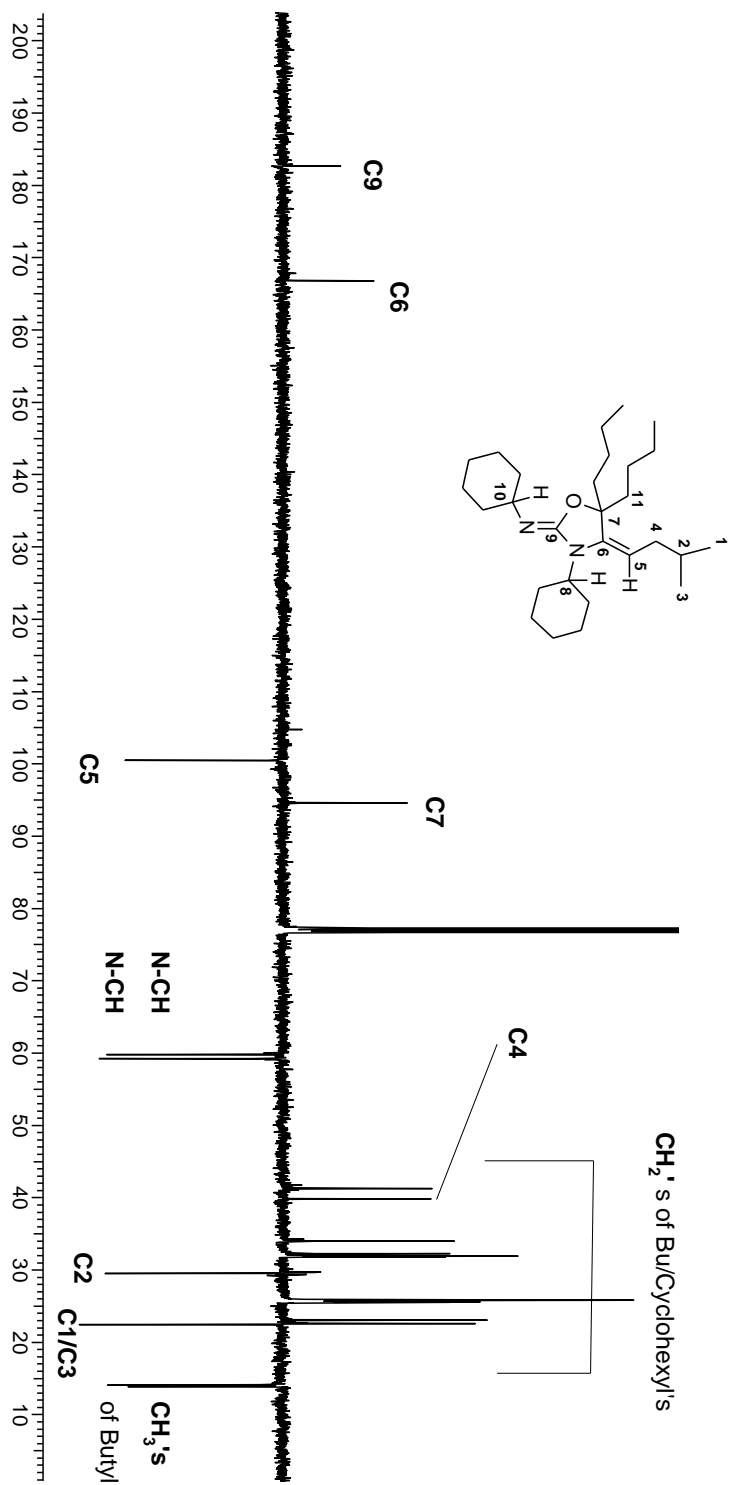
1D TOCSY subspectra



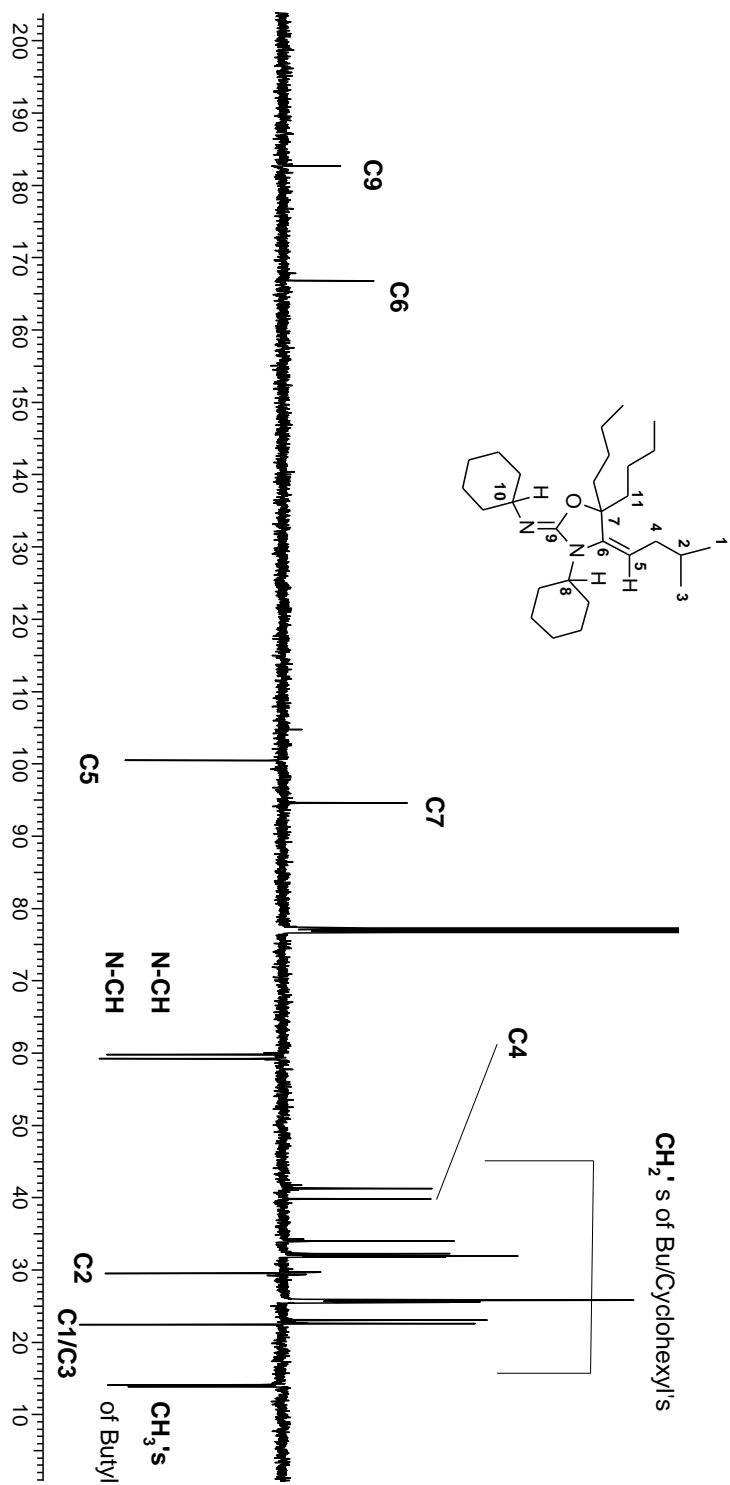
¹D NOESY subspectrum

Cyclohexyl protons identification

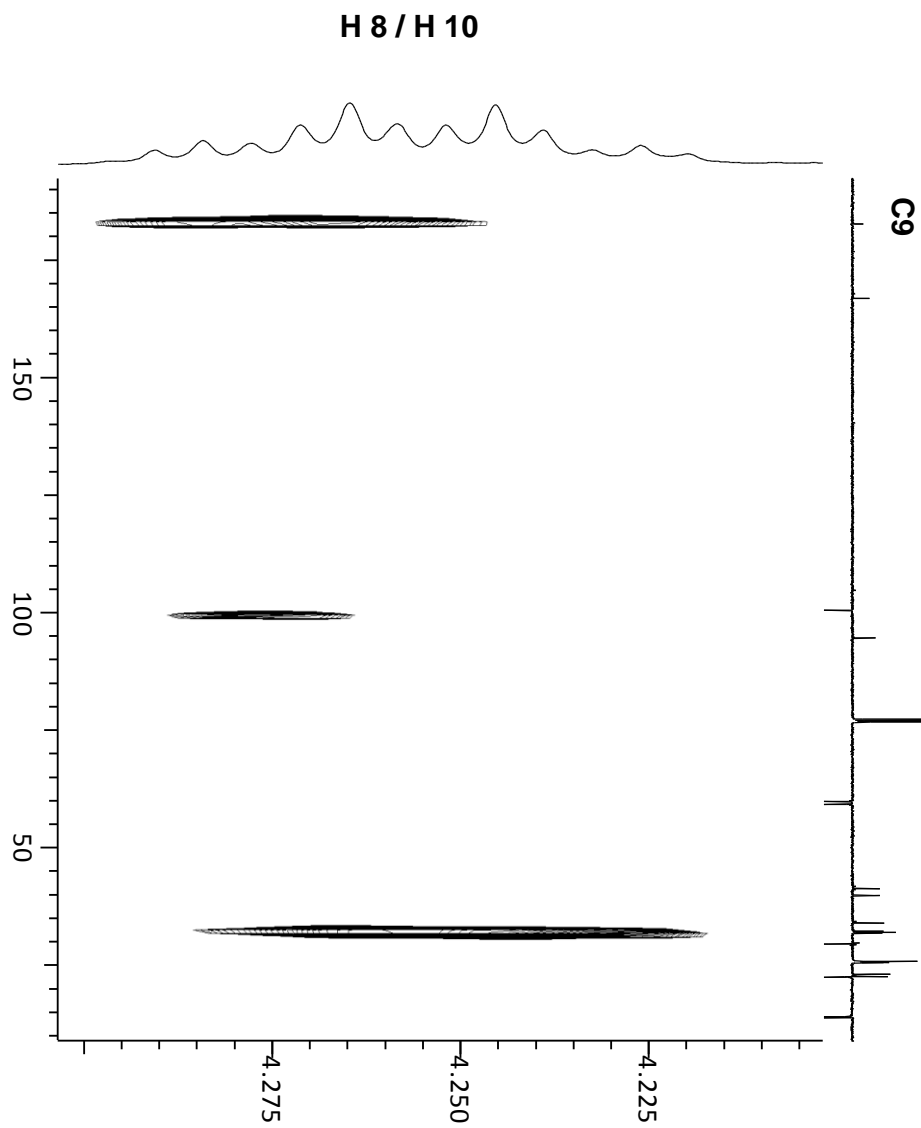
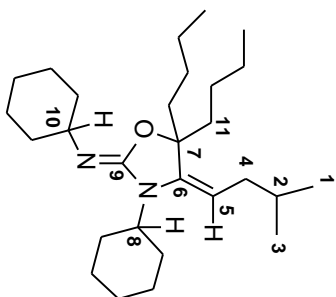
APT

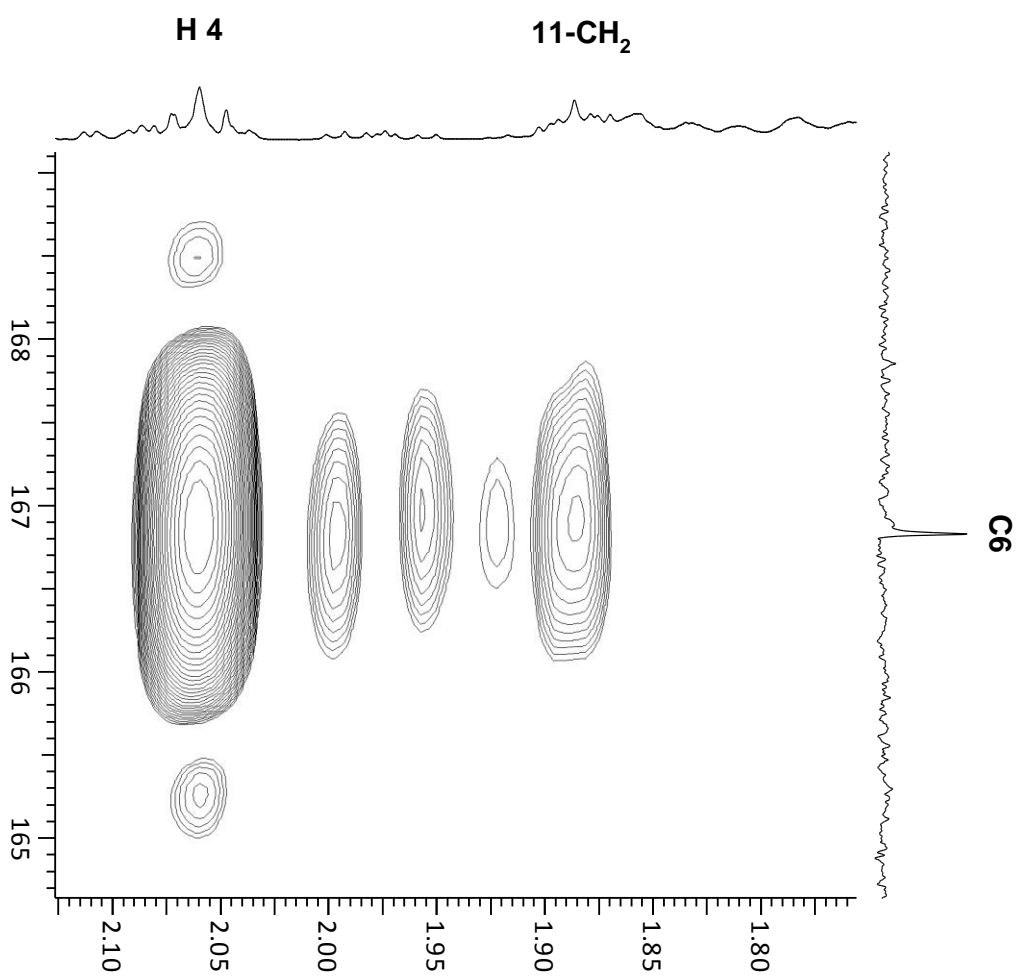
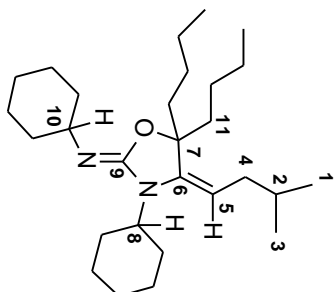


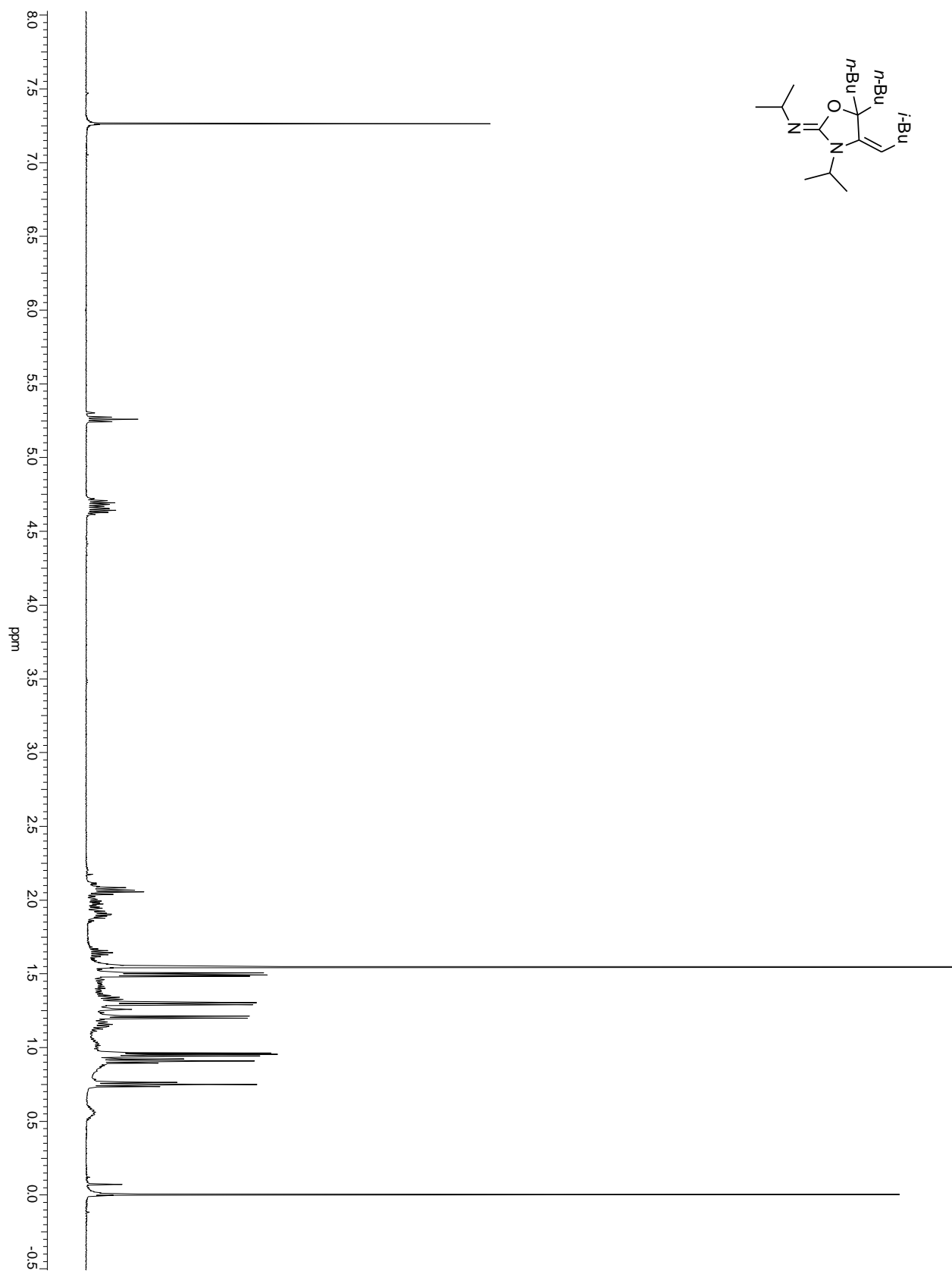
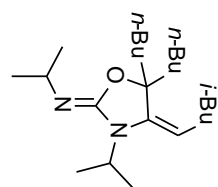
APT

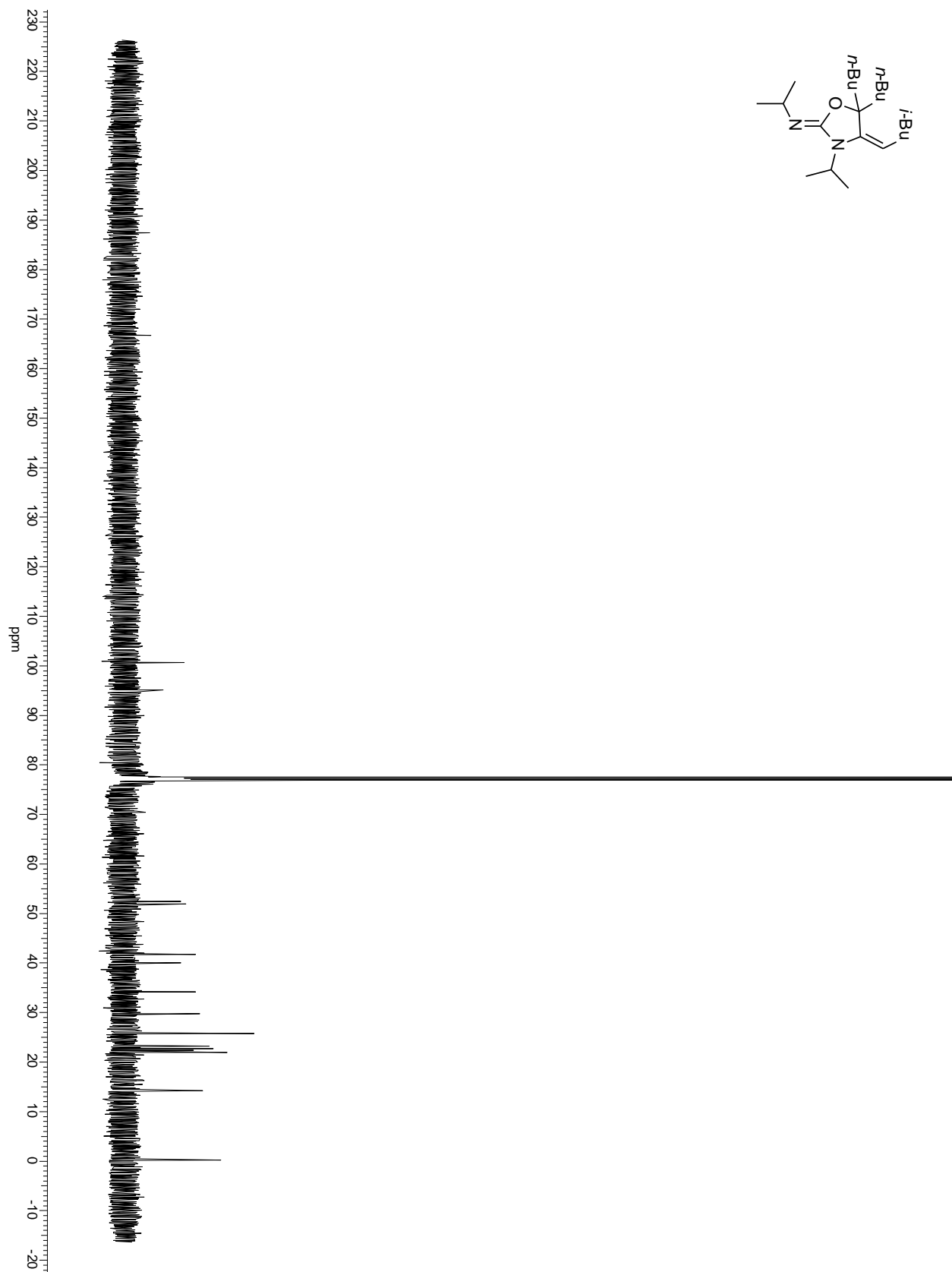
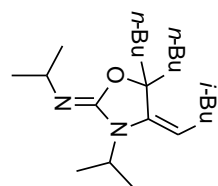


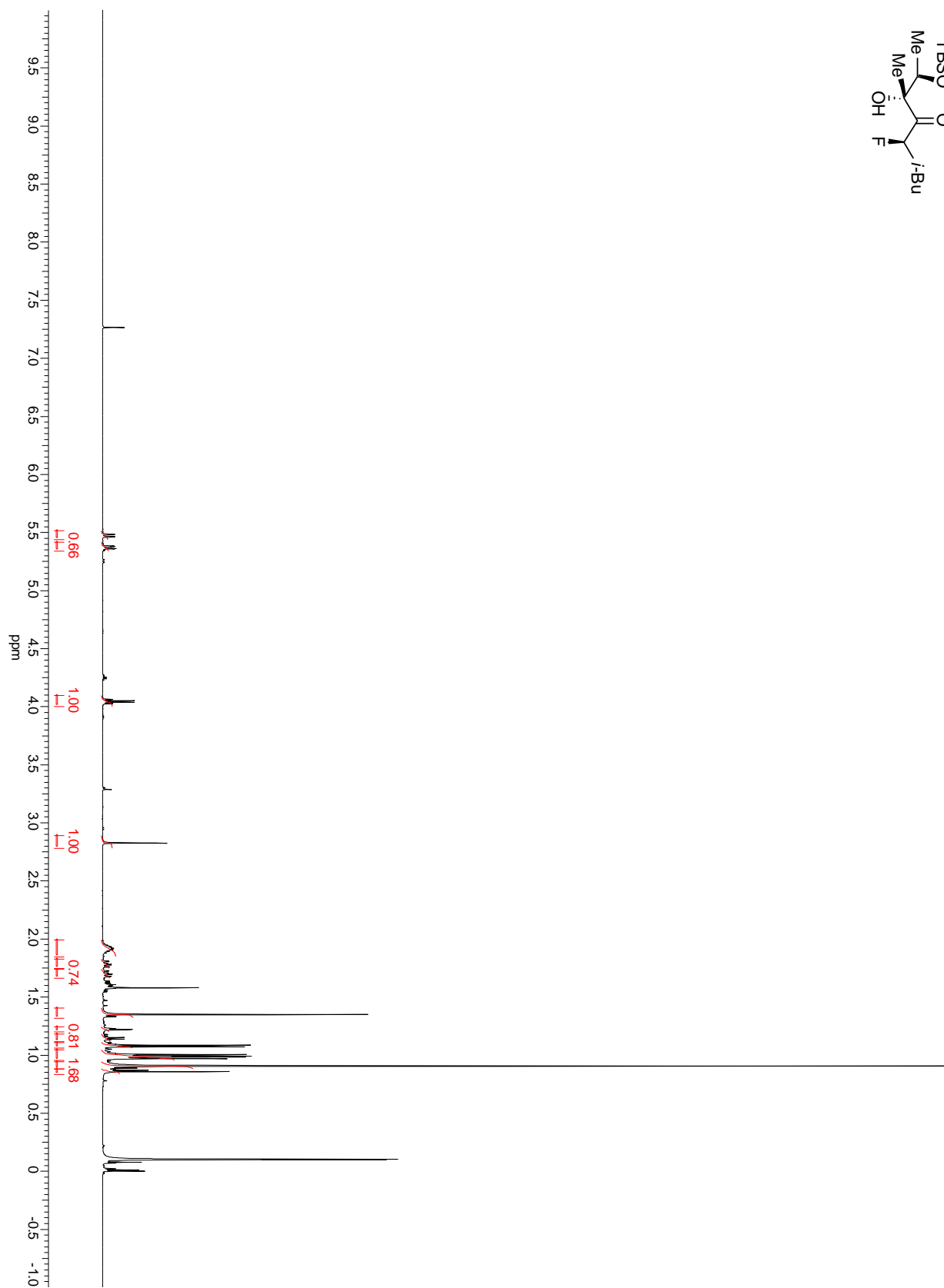
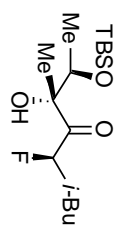
gHMC

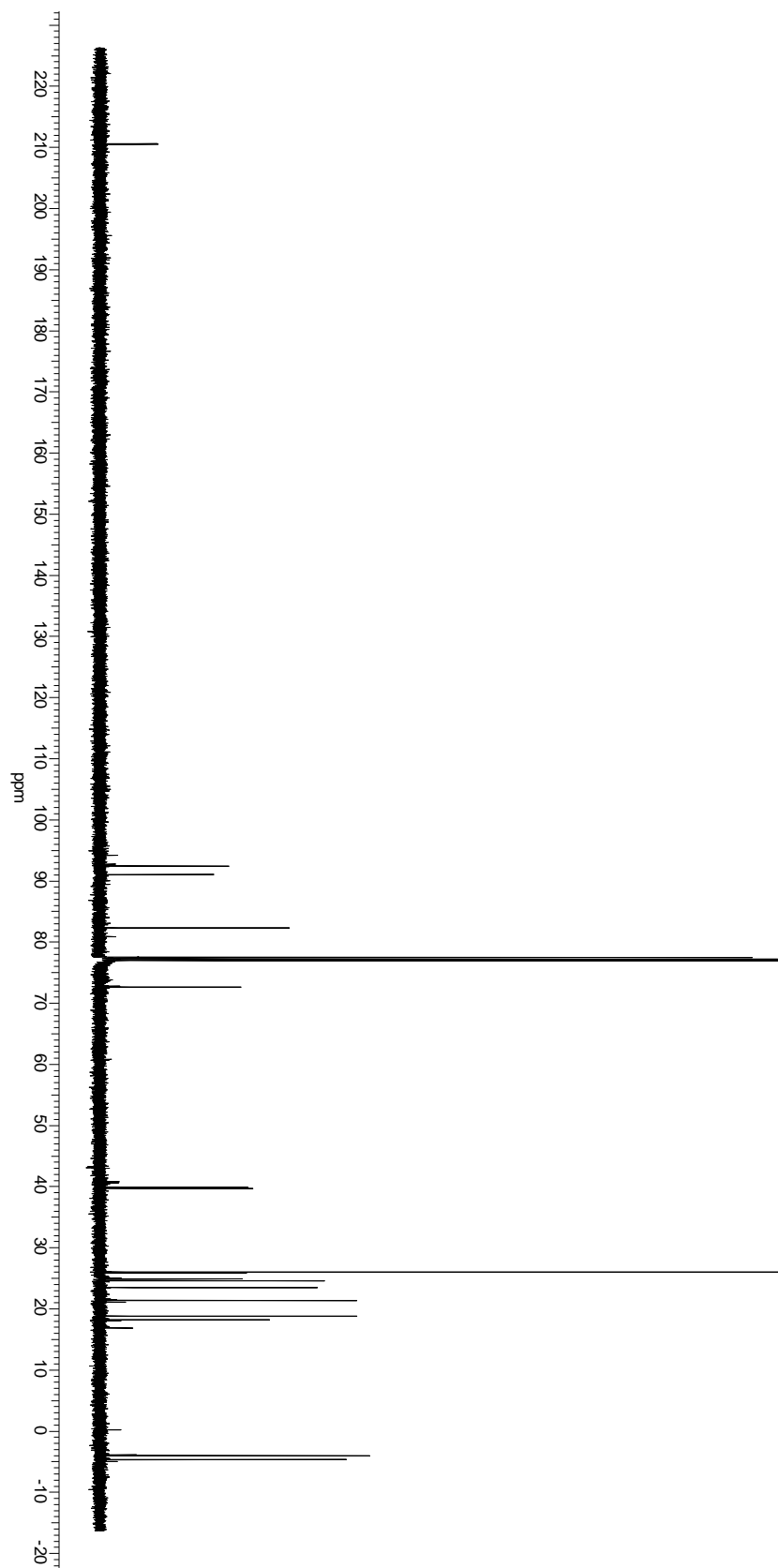
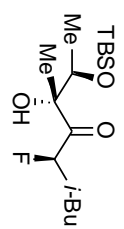


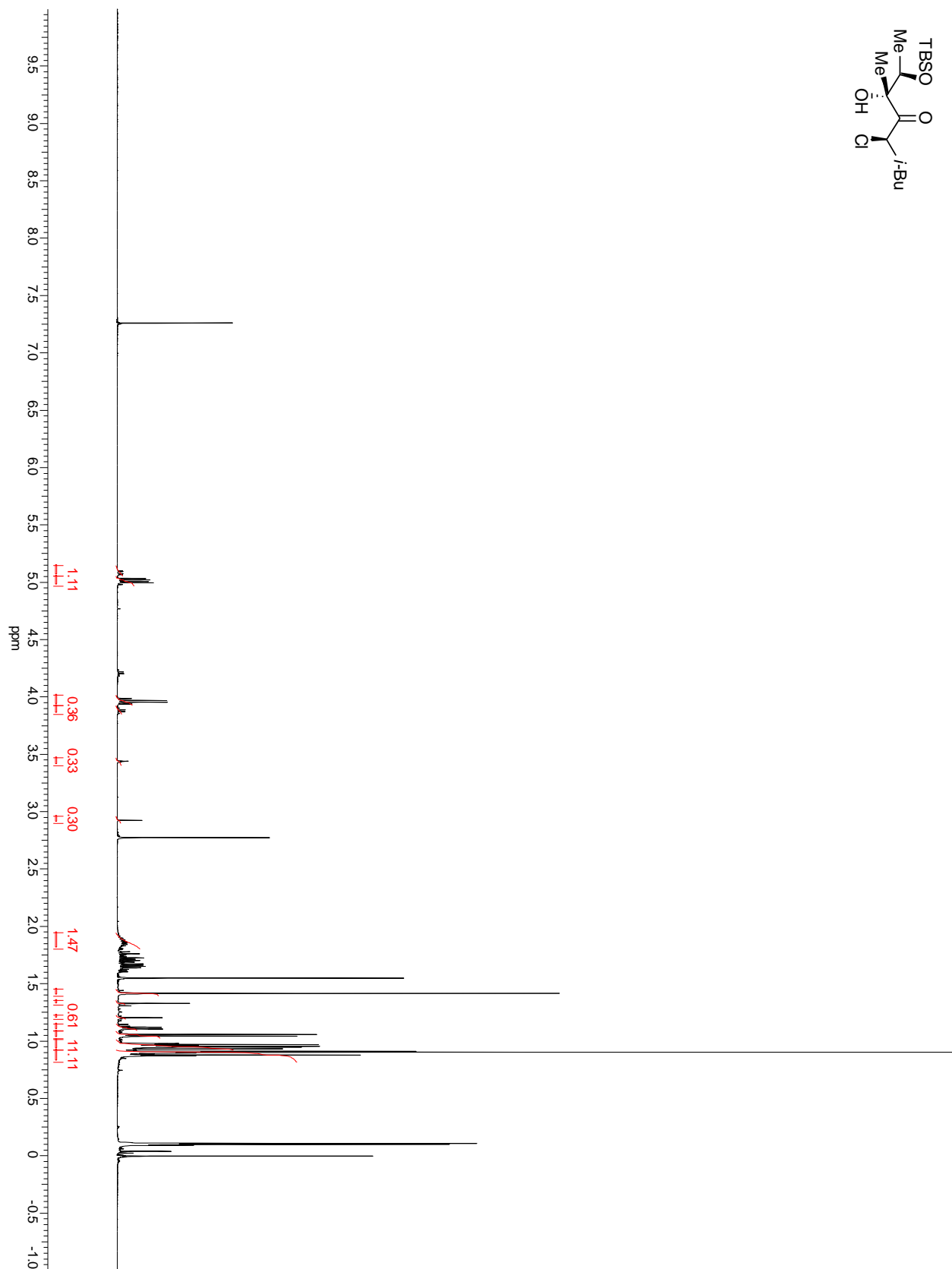
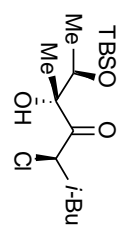
gHMBC

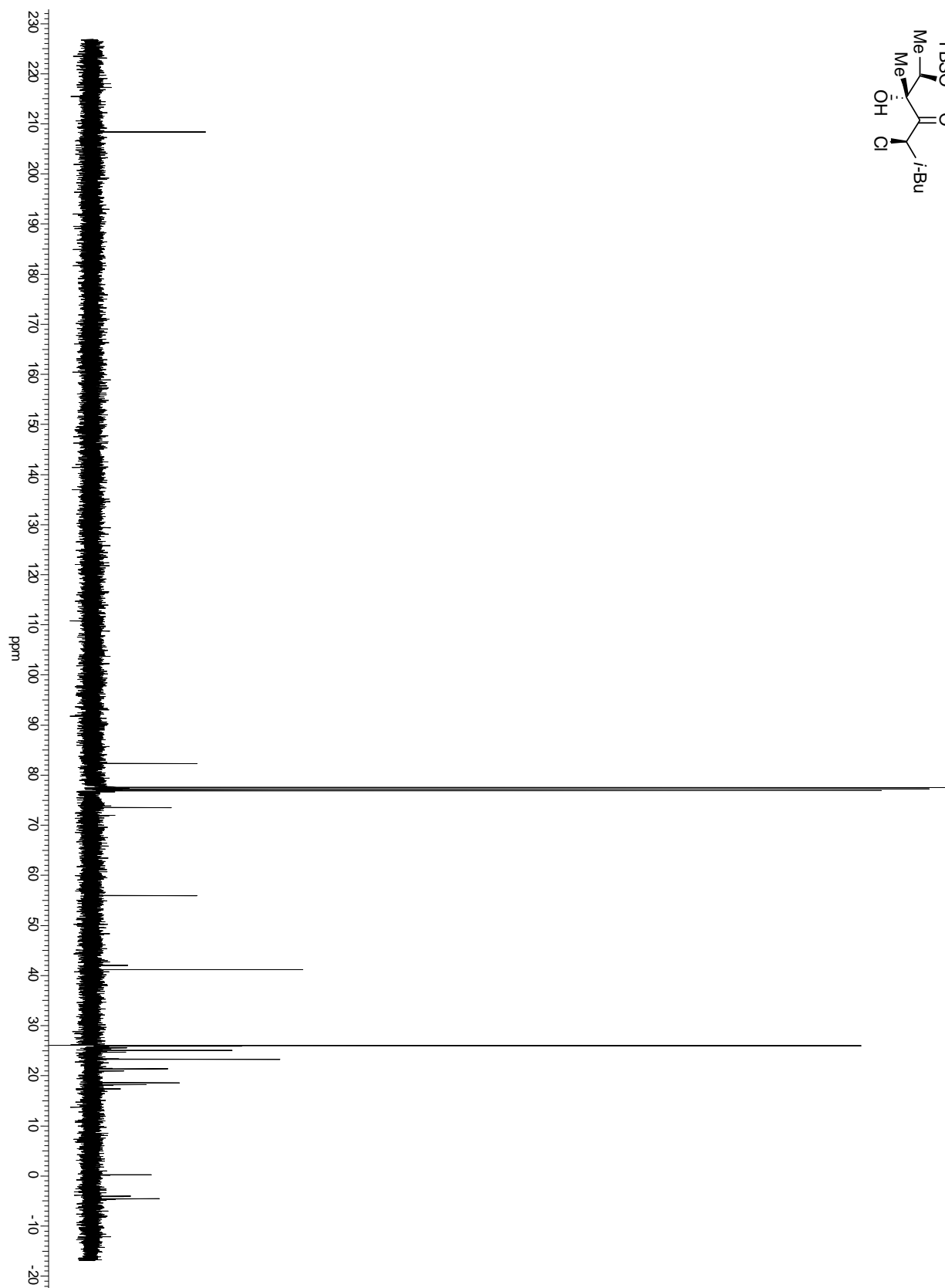
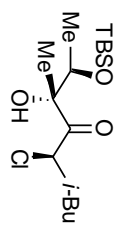


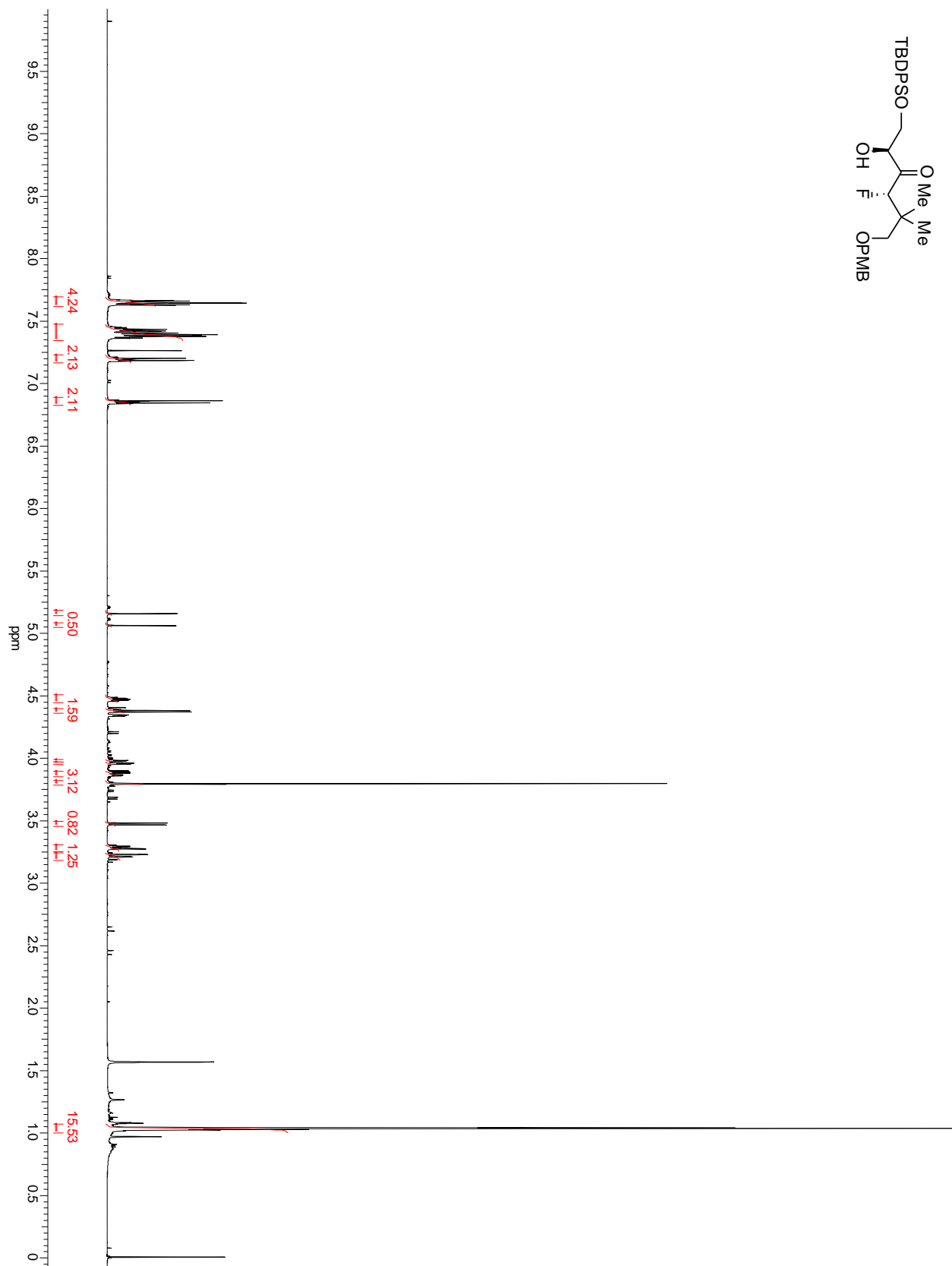
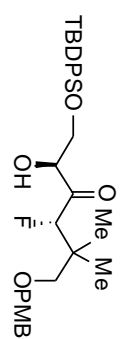


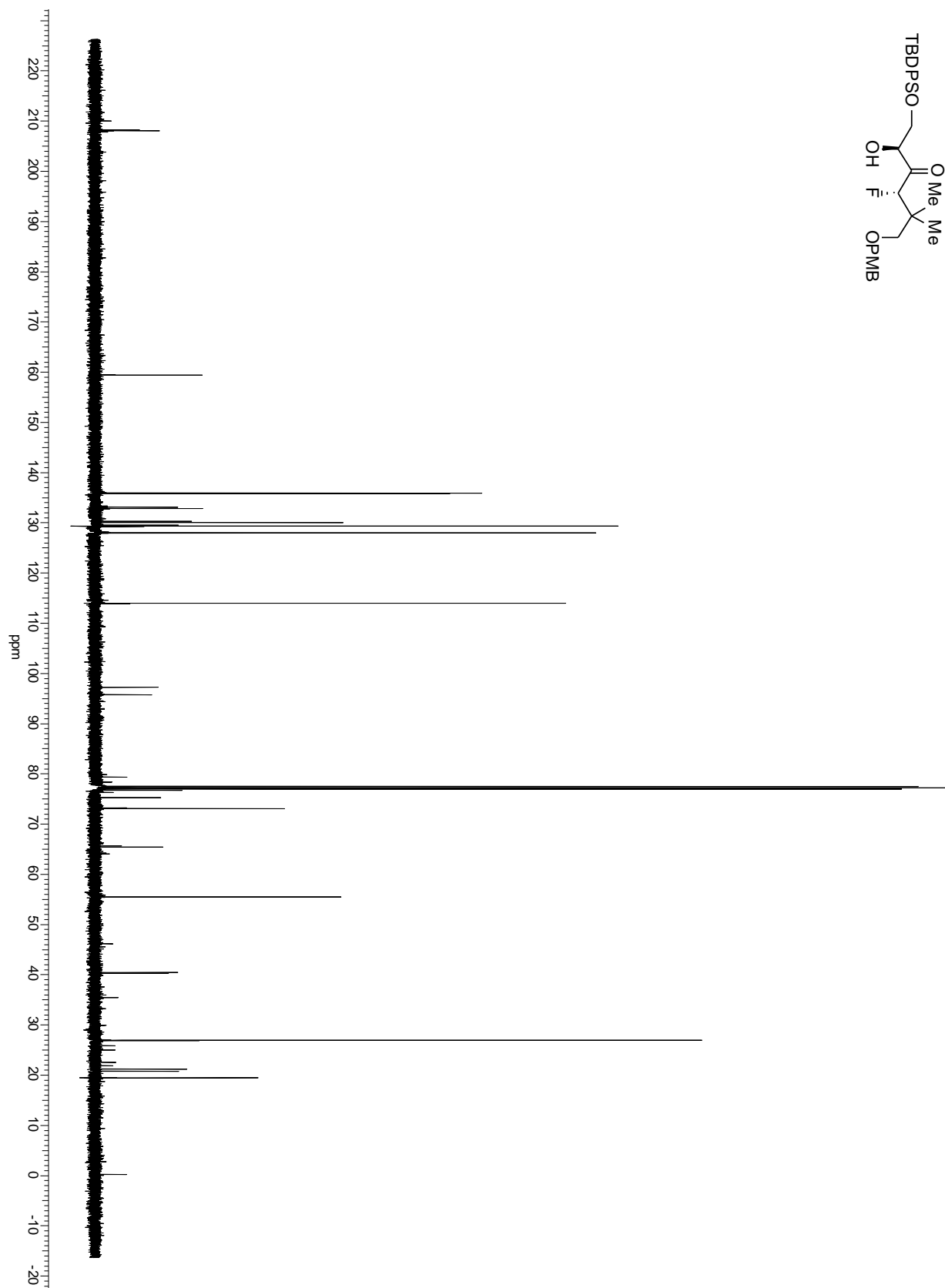
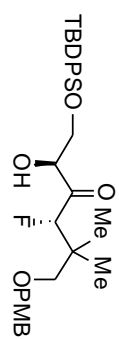


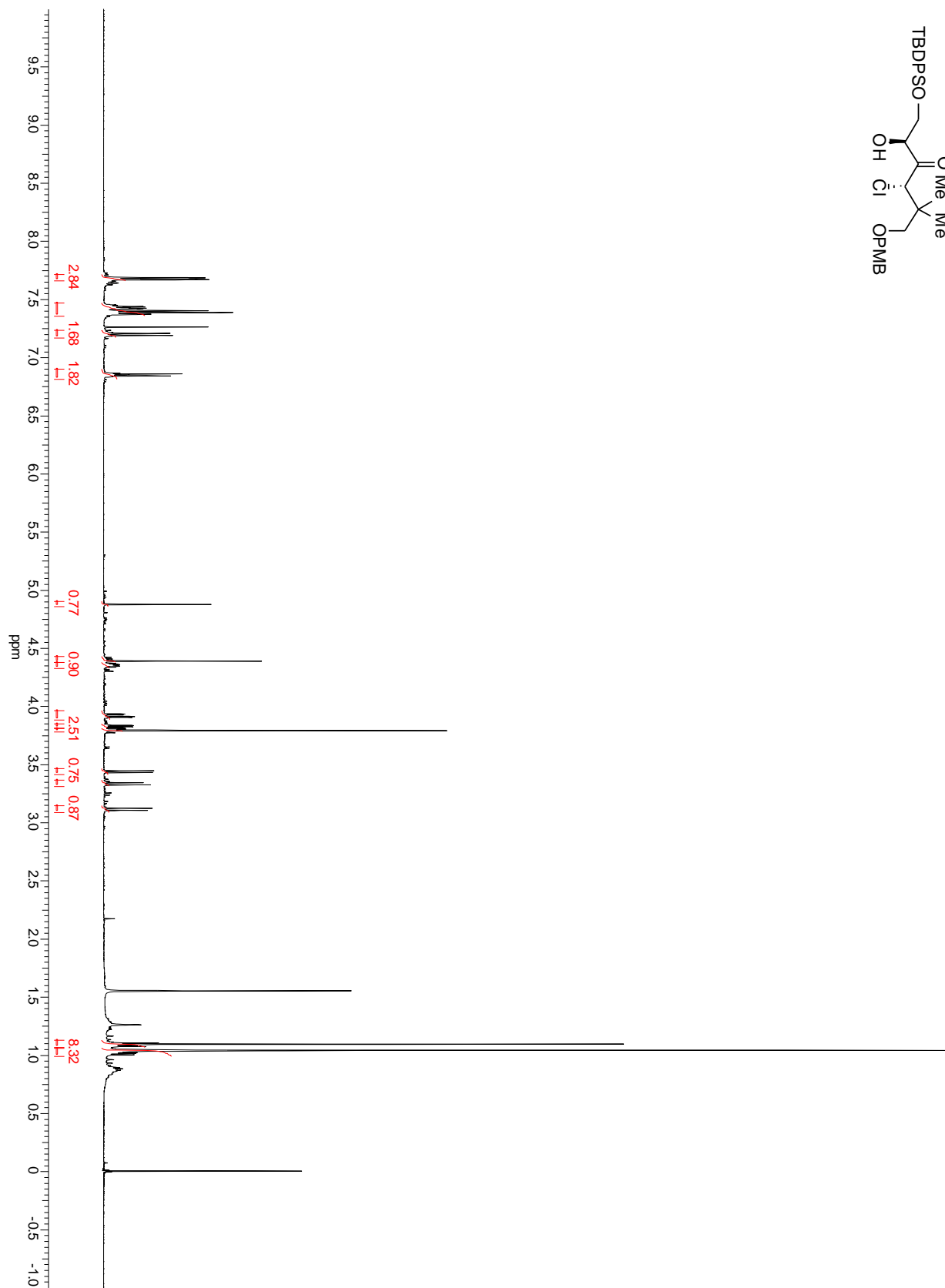
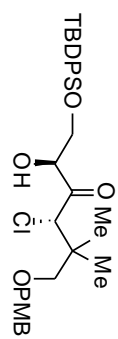


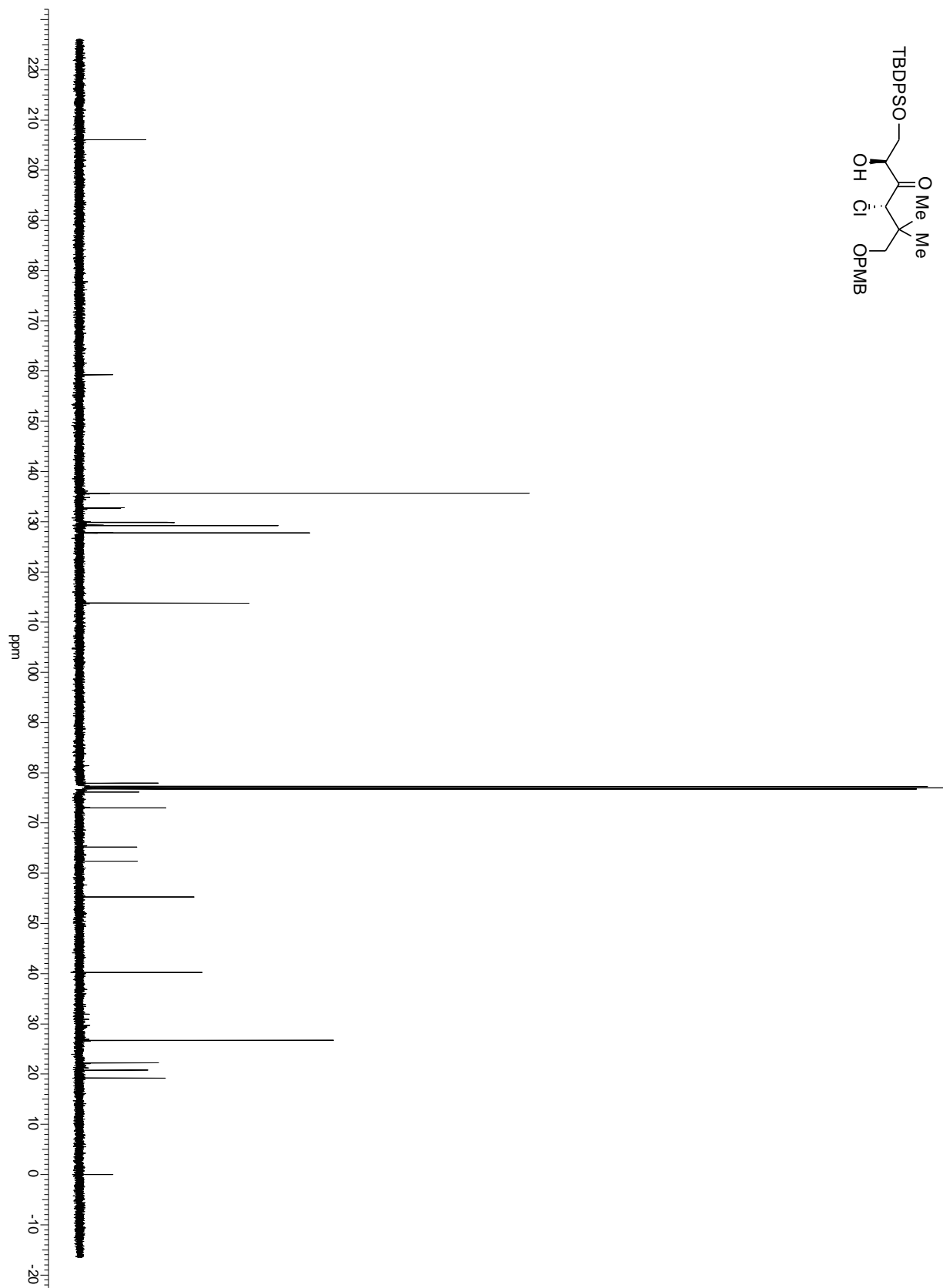
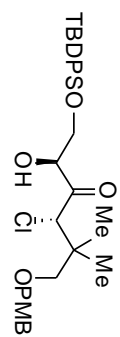


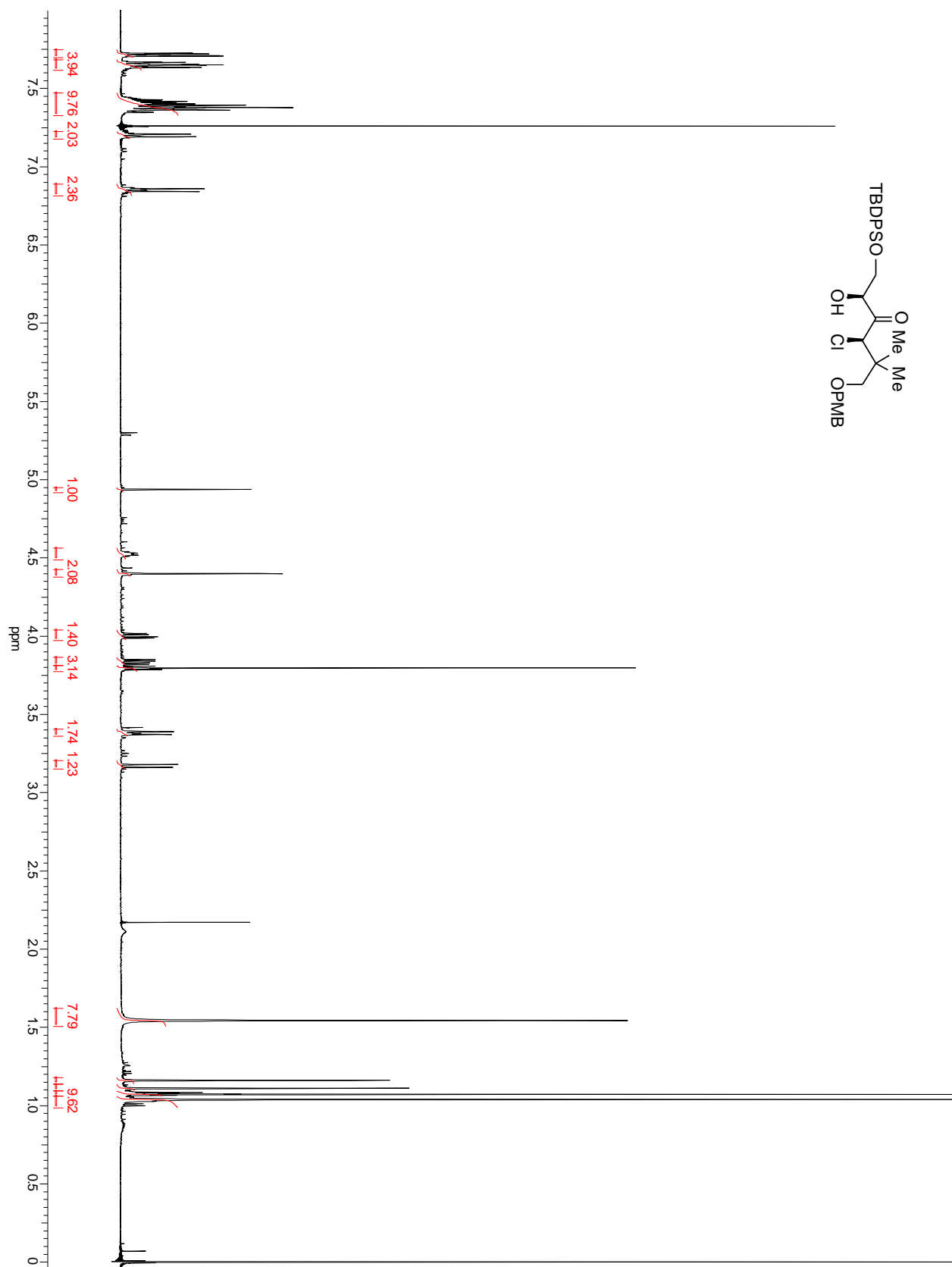
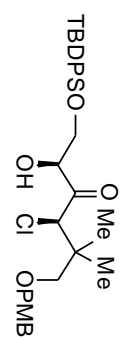


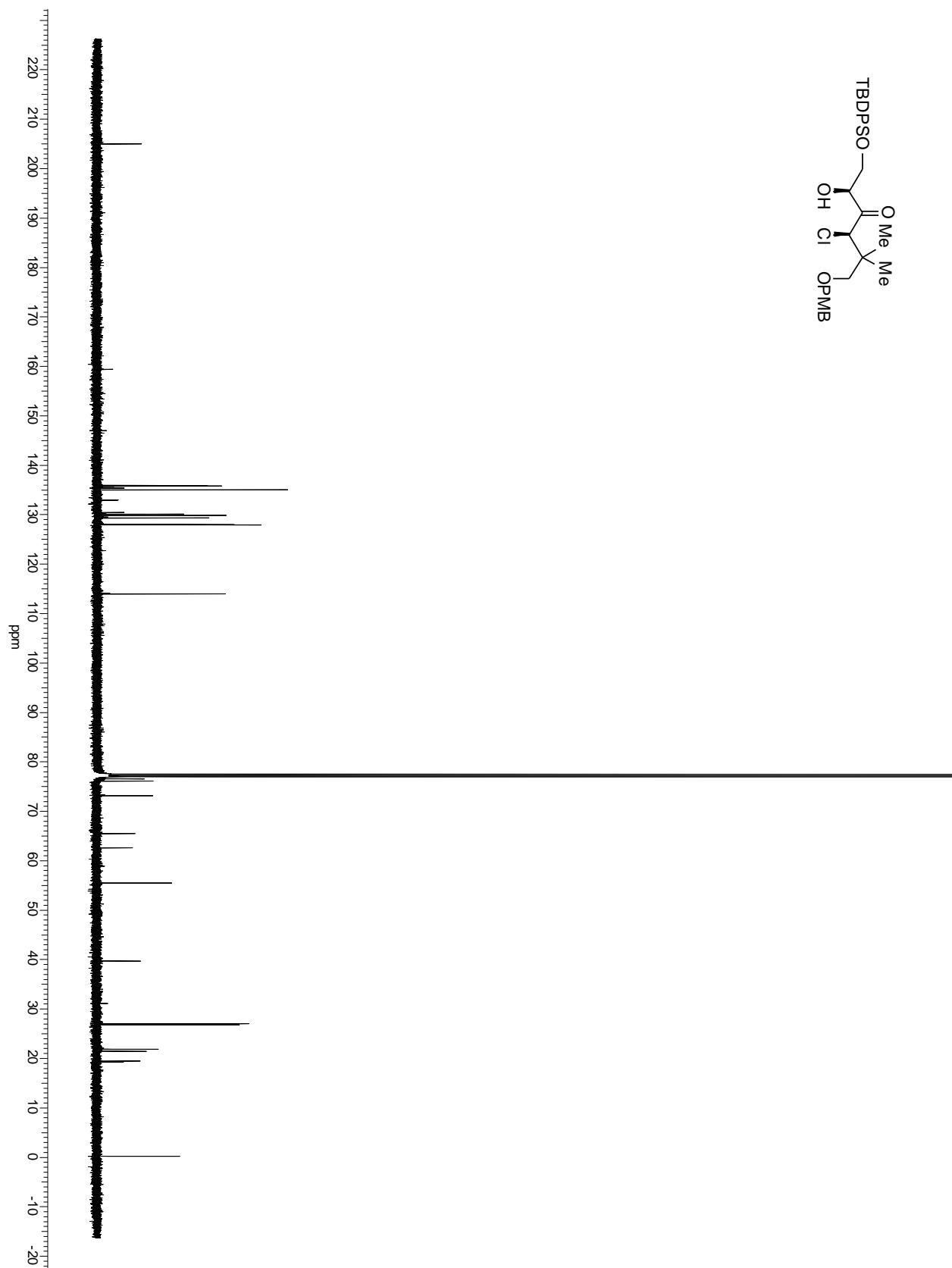
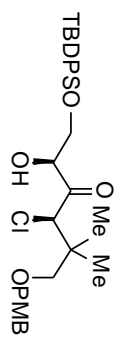


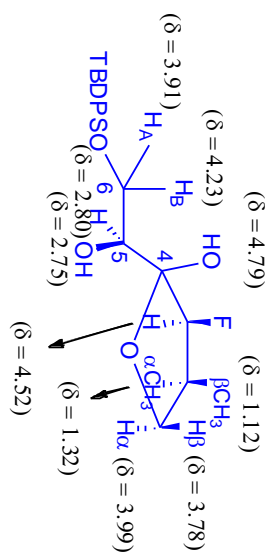




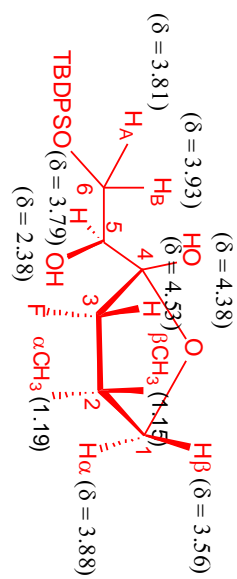




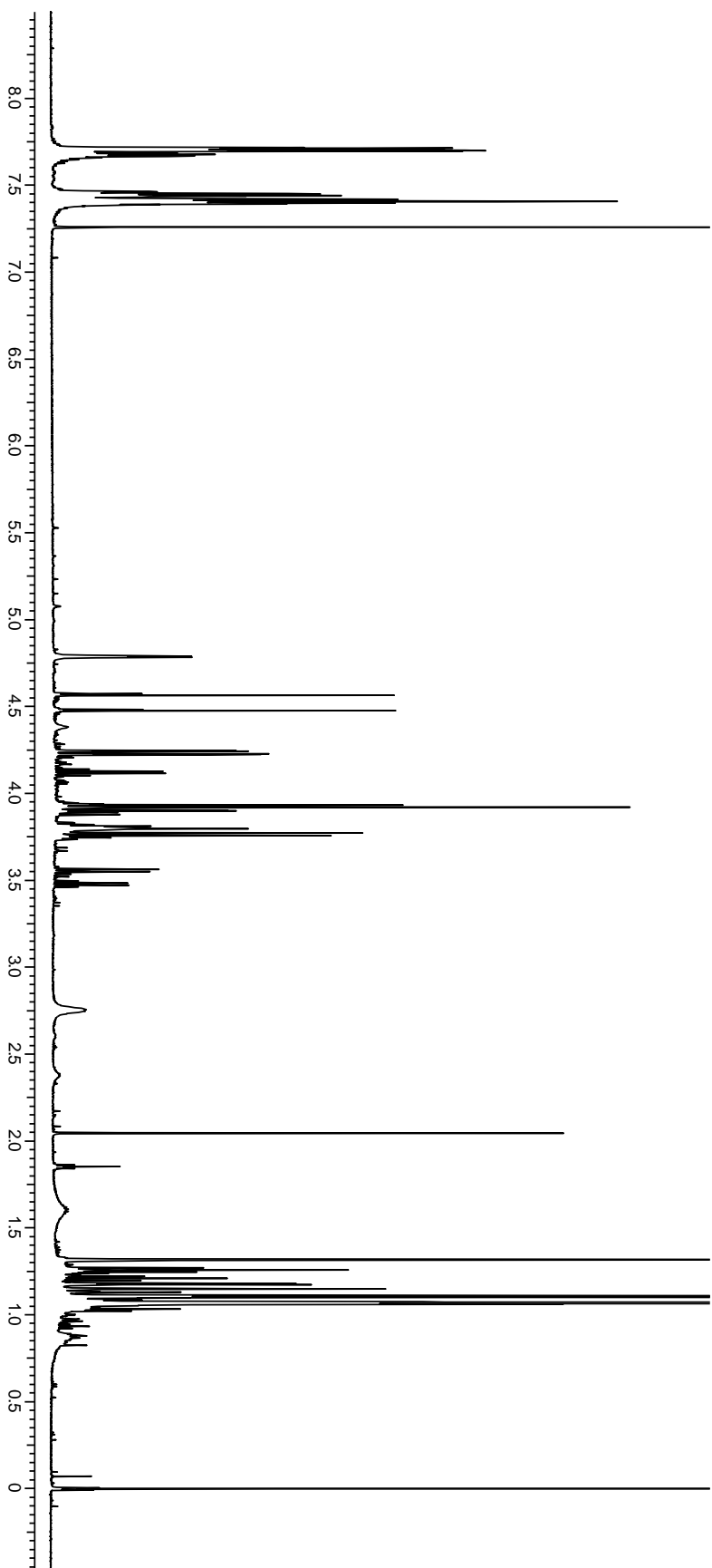


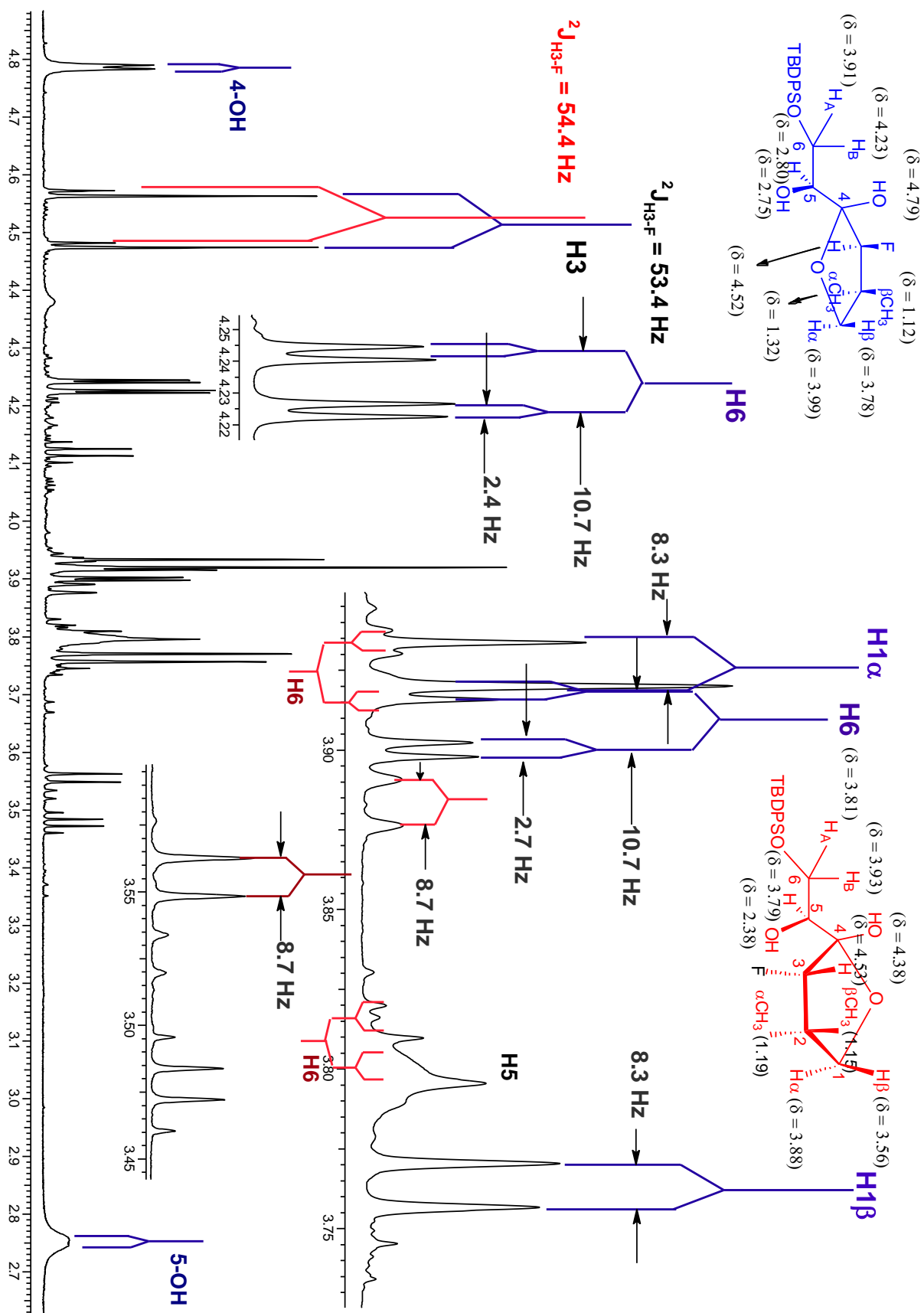


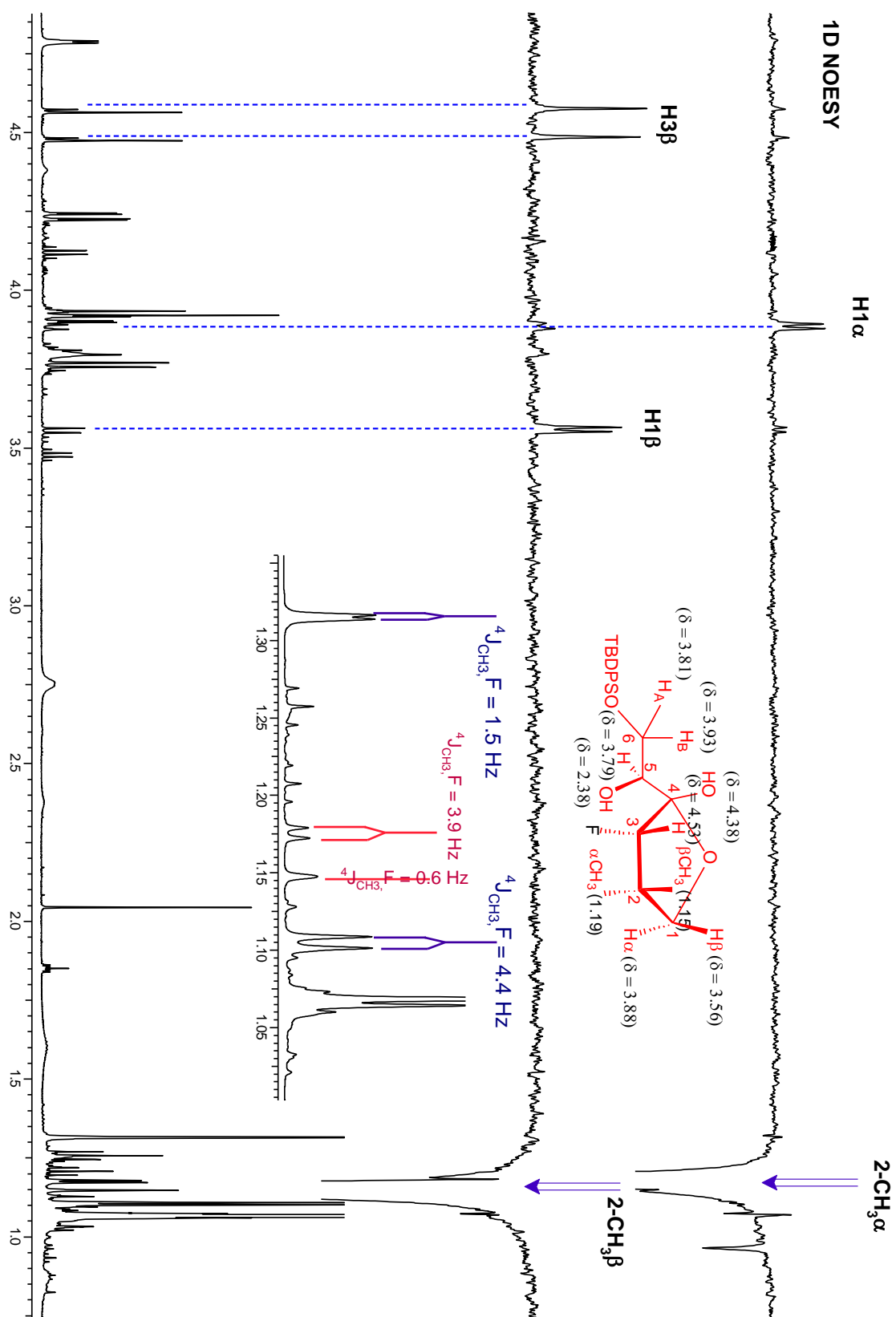
5.46

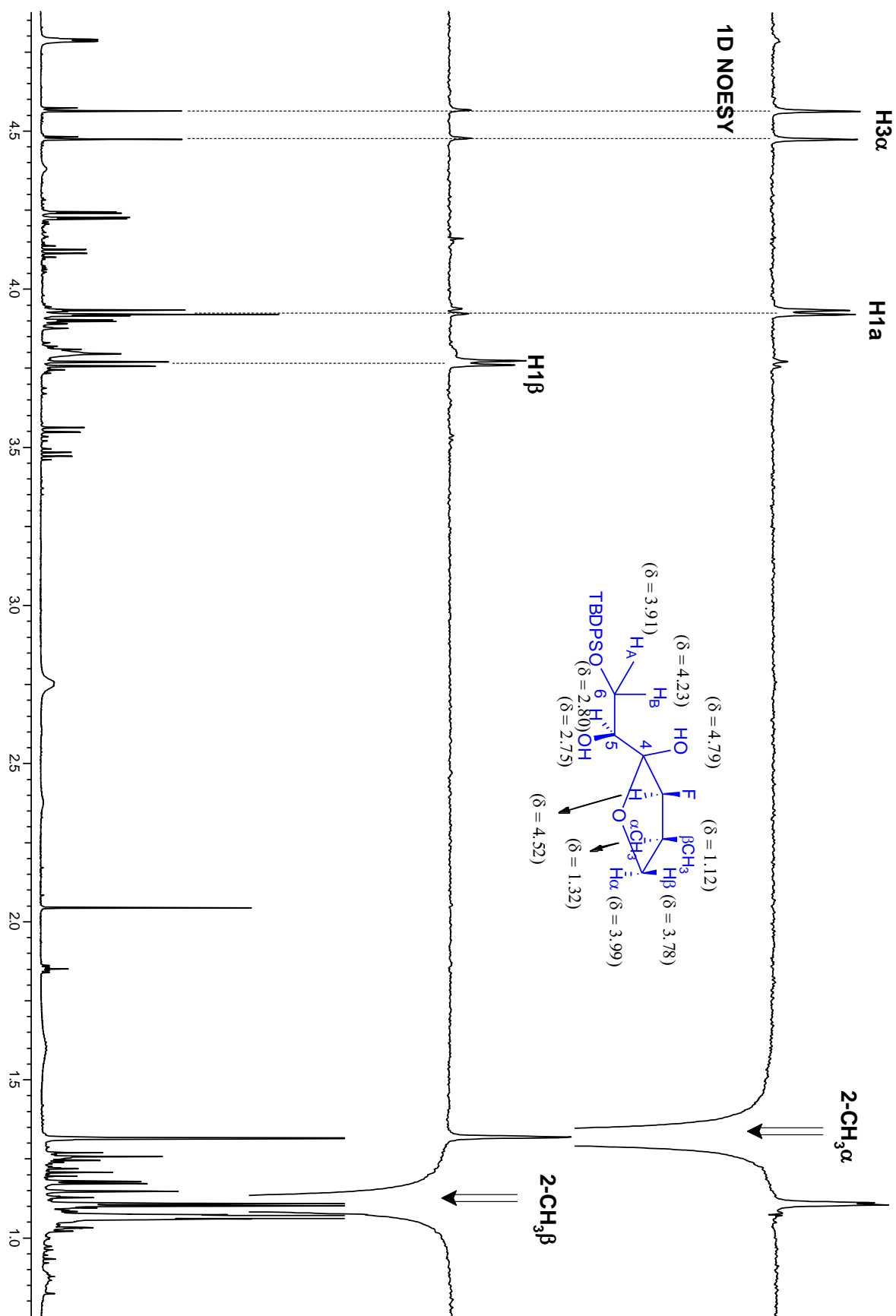


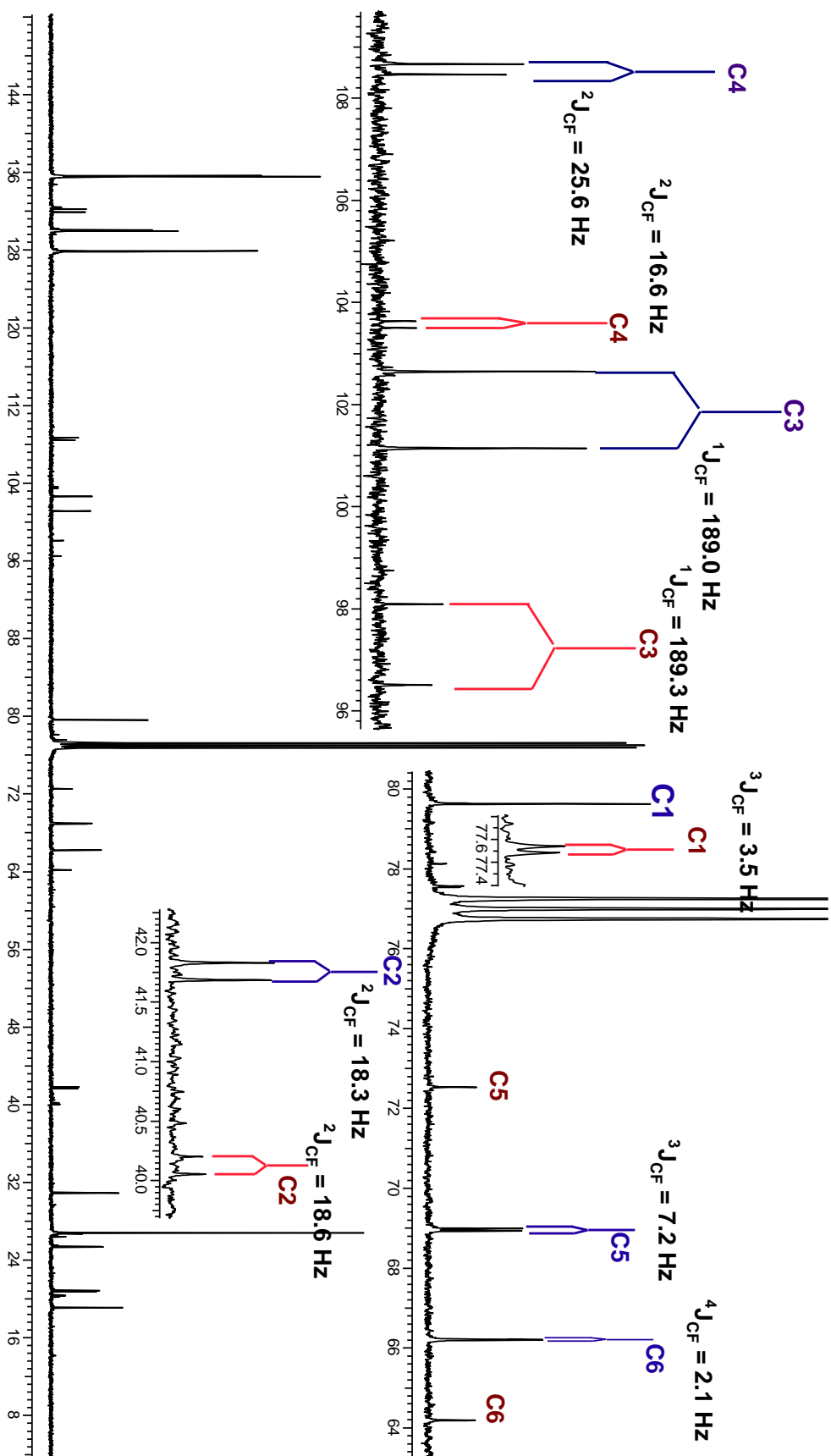
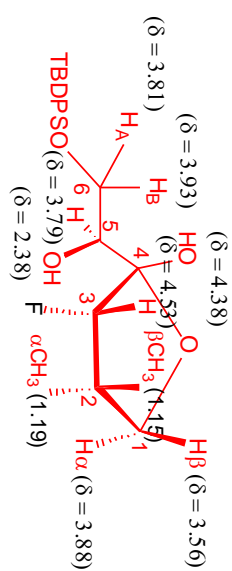
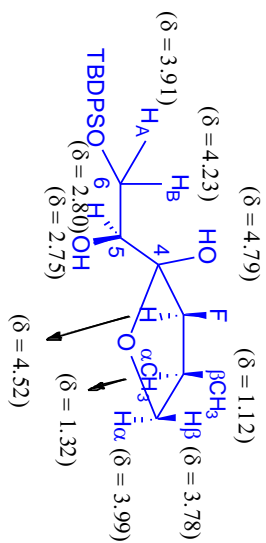
5.45

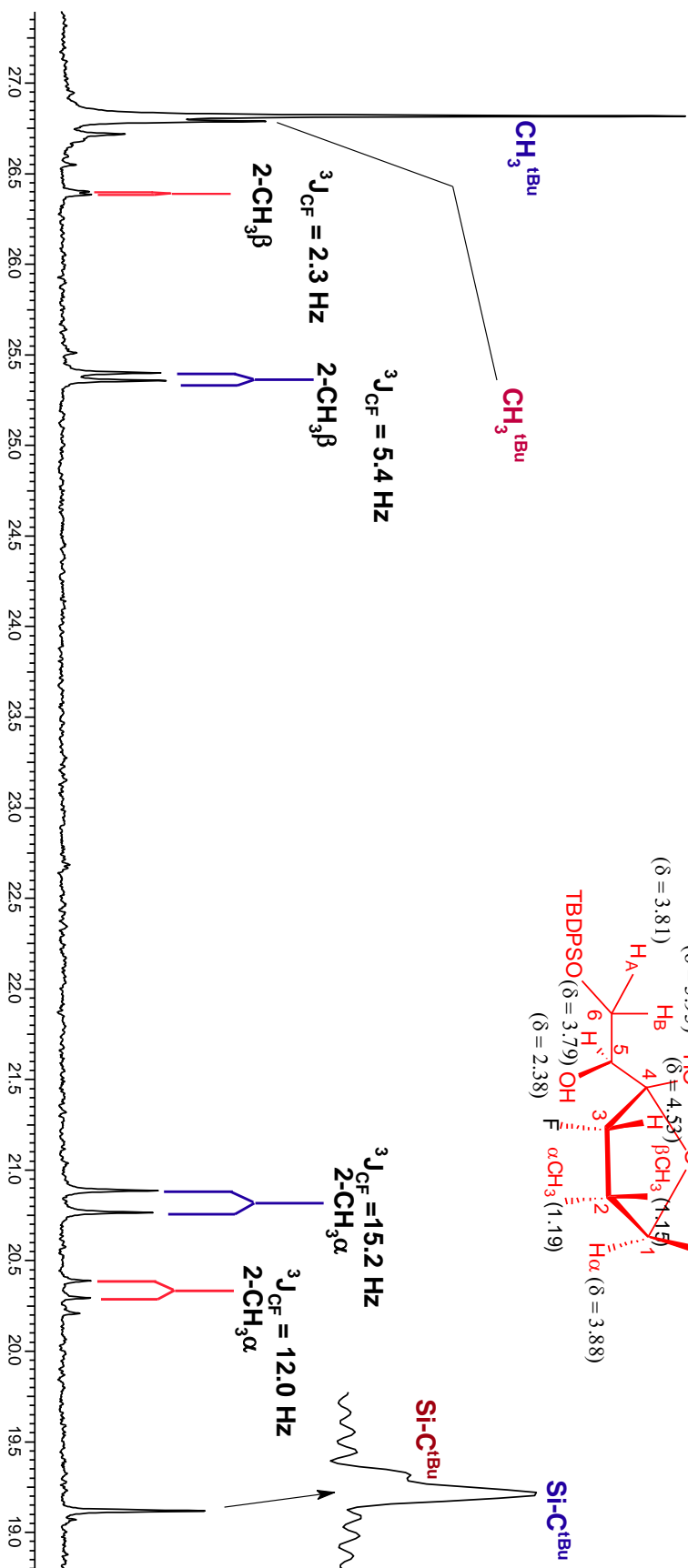
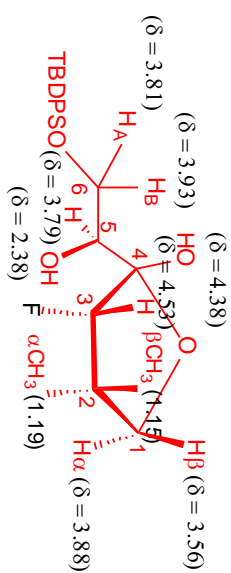
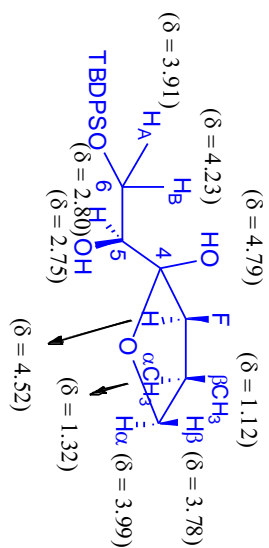


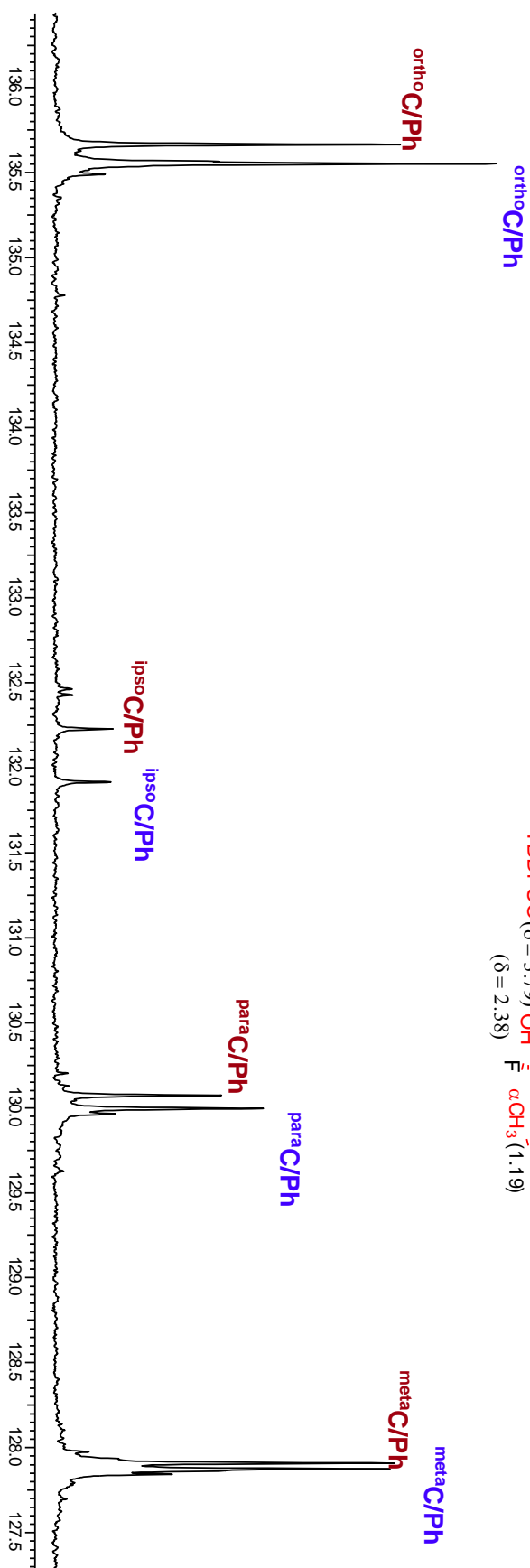
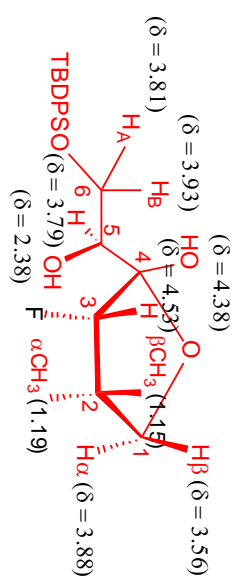
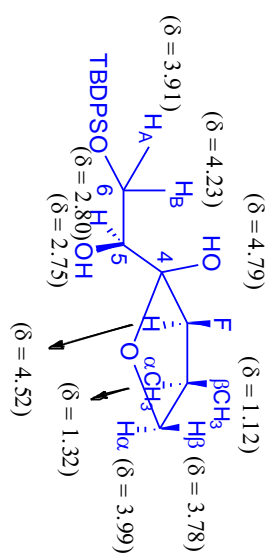


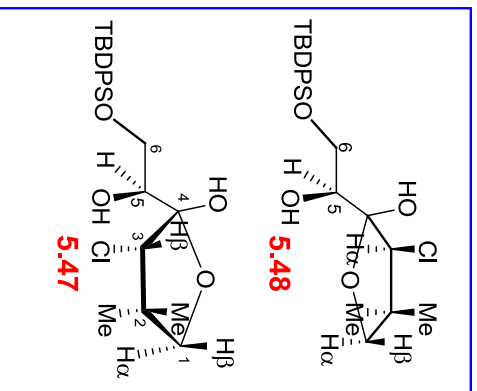






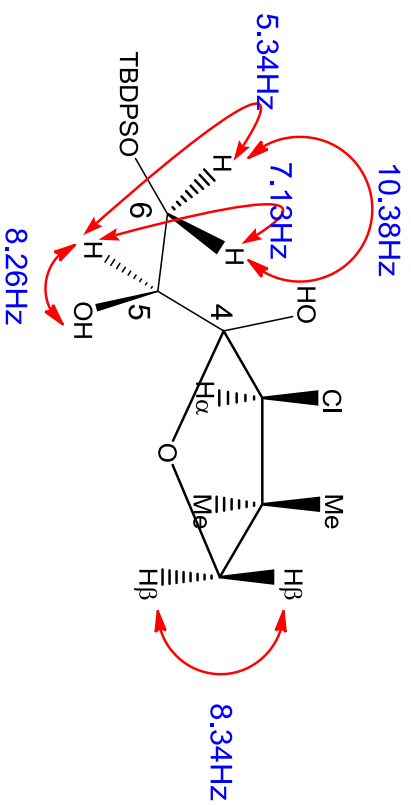




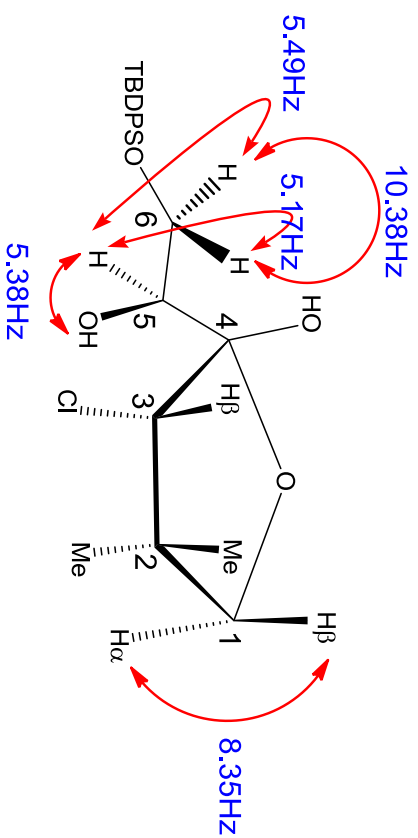


¹ H NMR chemical shifts (δ/ppm) w/ coupling constant (J/Hz)	¹³ C NMR chemical shift (δ/ppm)
3.62 (d, JH1 _α , H1 _β = 8.34 Hz, H1 _α)	C1 --- 78.89 78.55
3.98 (d, H1 _β)	C2 --- 41.82 41.81
1.13 (s, 2-CH3 _α)	C3 --- 67.31 68.20
1.29 (s, 2-CH3 _β)	C4 --- 105.17 104.56
4.01 (d, H3 _α)	C5 --- 70.76 73.95
4.82 (s, 4-OH)	C6 --- 64.31 64.45
3.72 (ddd, JH5, OH = 8.26 Hz, H5)	2CH ₃ ^α --- 22.97 22.78
2.19 (d, 5-OH)	2CH ₃ ^β --- 25.68 25.37
3.83 (dd, H6)	CH ₃ ^{t-Bu} --- 19.10 19.11
3.95 (dd, H6)	CH ₃ ^{t-Bu} --- 26.79 26.79
	ipsoC --- 132.21 132.35
3.94 (d, JH1 _α , H1 _β = 8.35 Hz, H1 _α)	orthoC --- 135.58 135.63
3.59 (d, H1 _β)	metaC --- 127.87 127.67
1.24 (s, 2-CH3 _α)	paraC --- 130.02 130.03
1.11 (s, 2-CH3 _β)	
4.03 (d, H3 _β)	
4.56 (s, 4-OH)	
? (ddd, JH5, OH = 5.38 Hz, H5)	
2.56 (d, 5-OH)	
3.87 (dd, H6)	
3.93 (dd, H6)	
7.66 - 7.70 (m, orthoH/Ph)	
7.42 - 7.36 (m, metaH/Ph)	
7.43 - 7.47 (m, orthoH/Ph)	

Coupling constant (J_{HH})

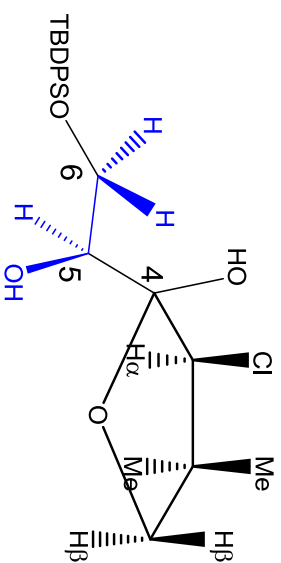


5.48

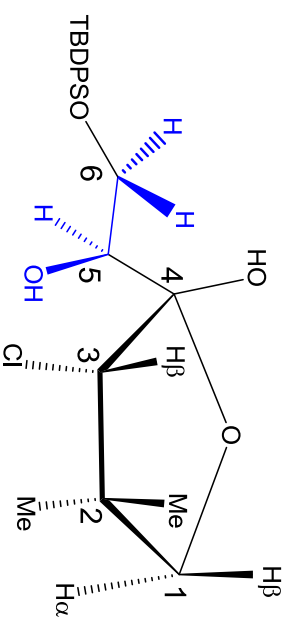


5.47

1d TOCSY

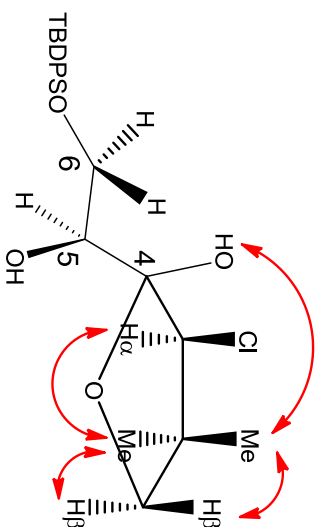


5.48

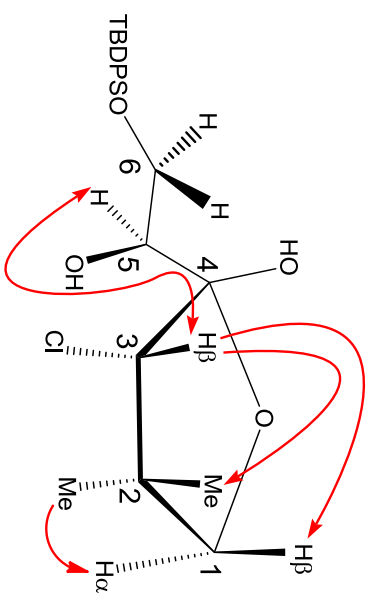


5.47

NOESY

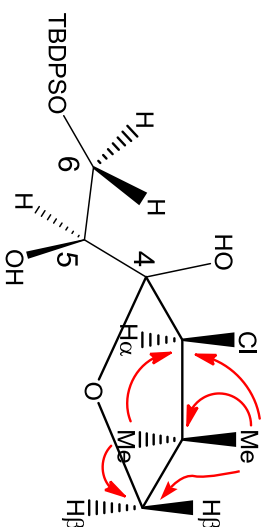


5.48

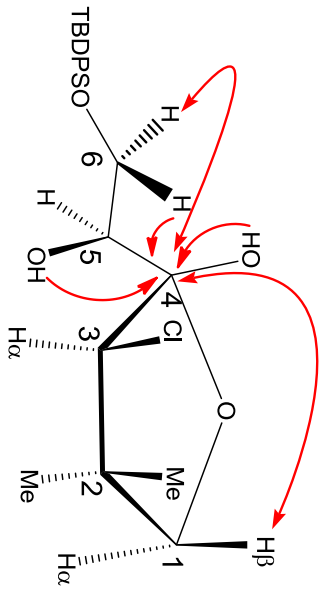


5.47

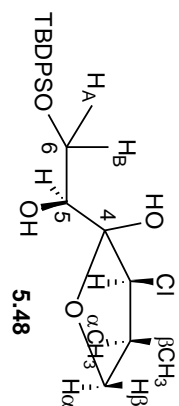
HMBC

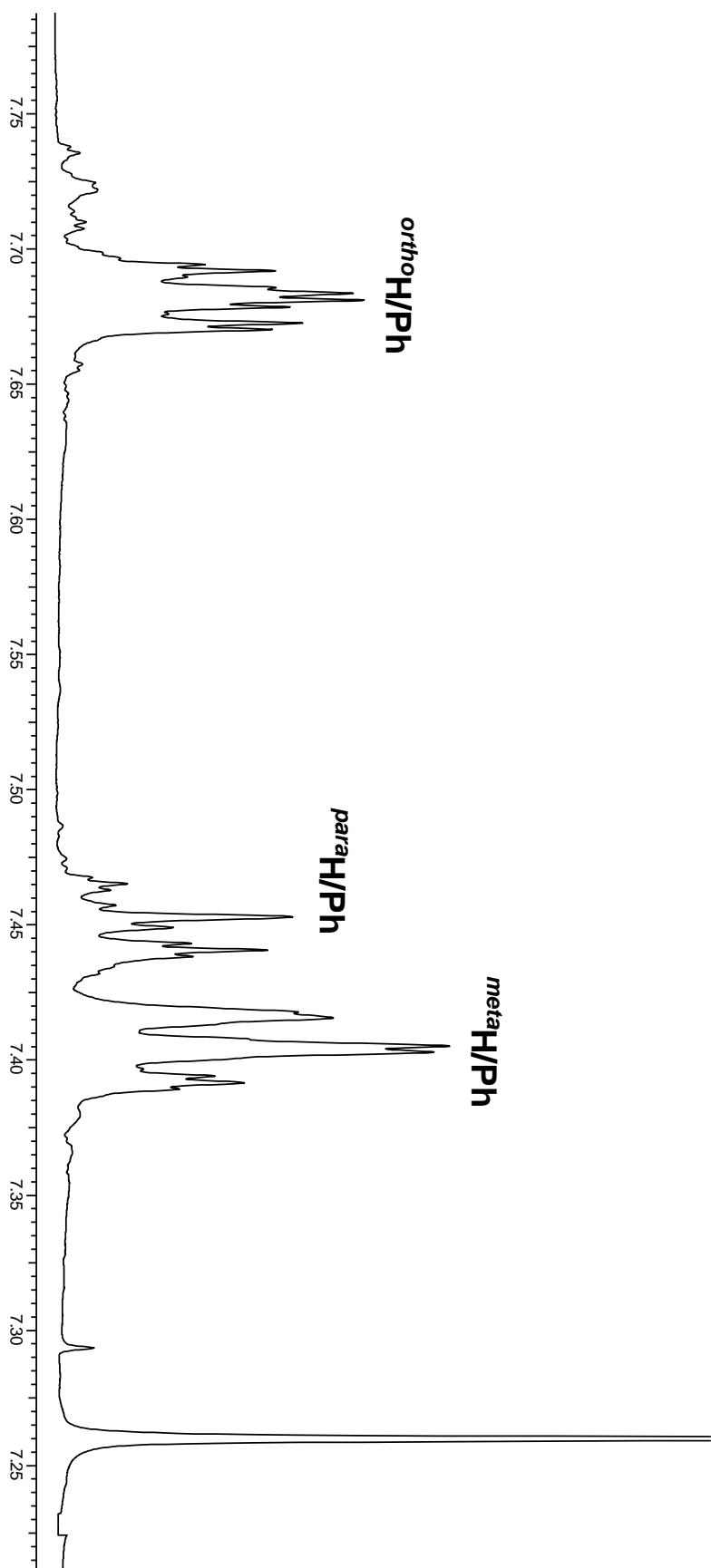


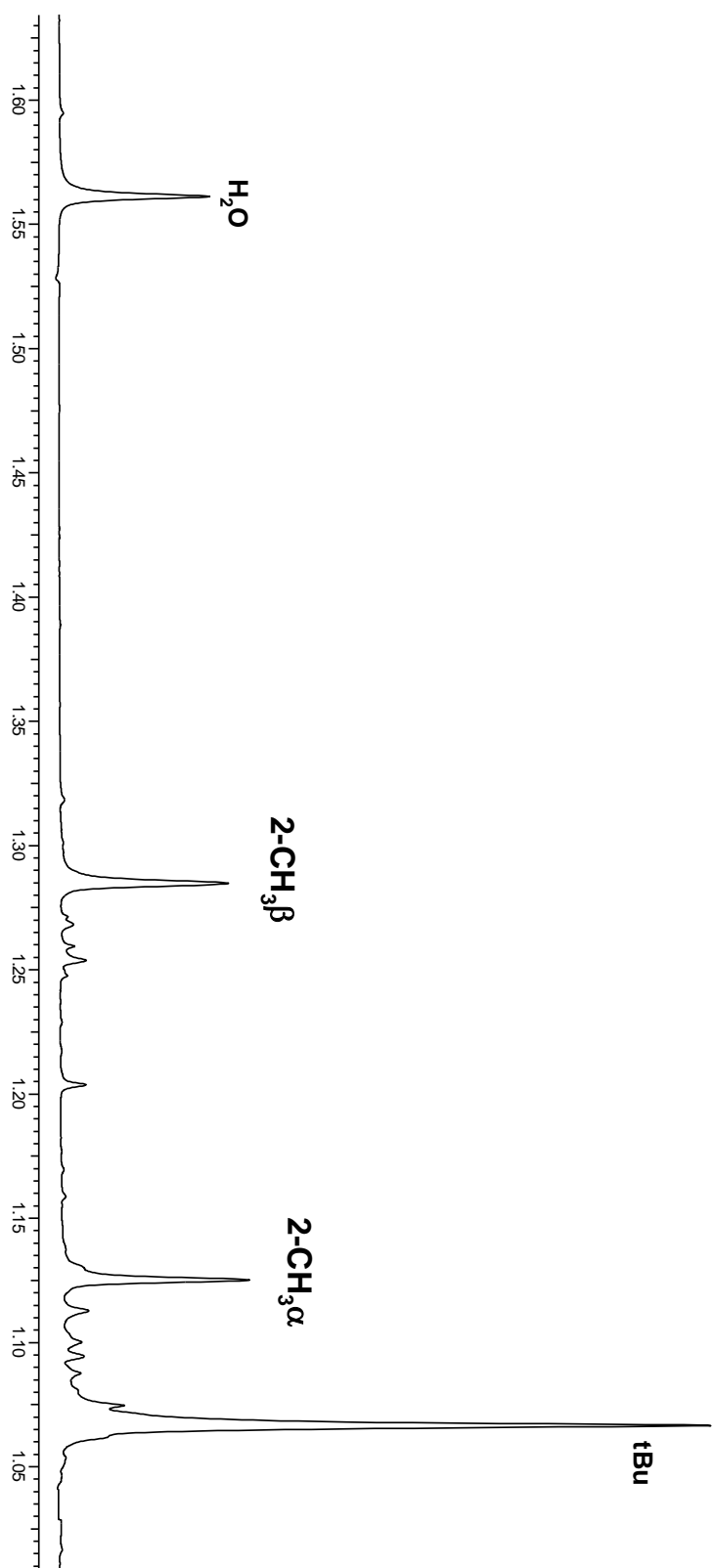
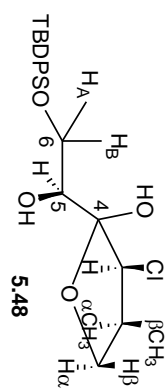
5.48



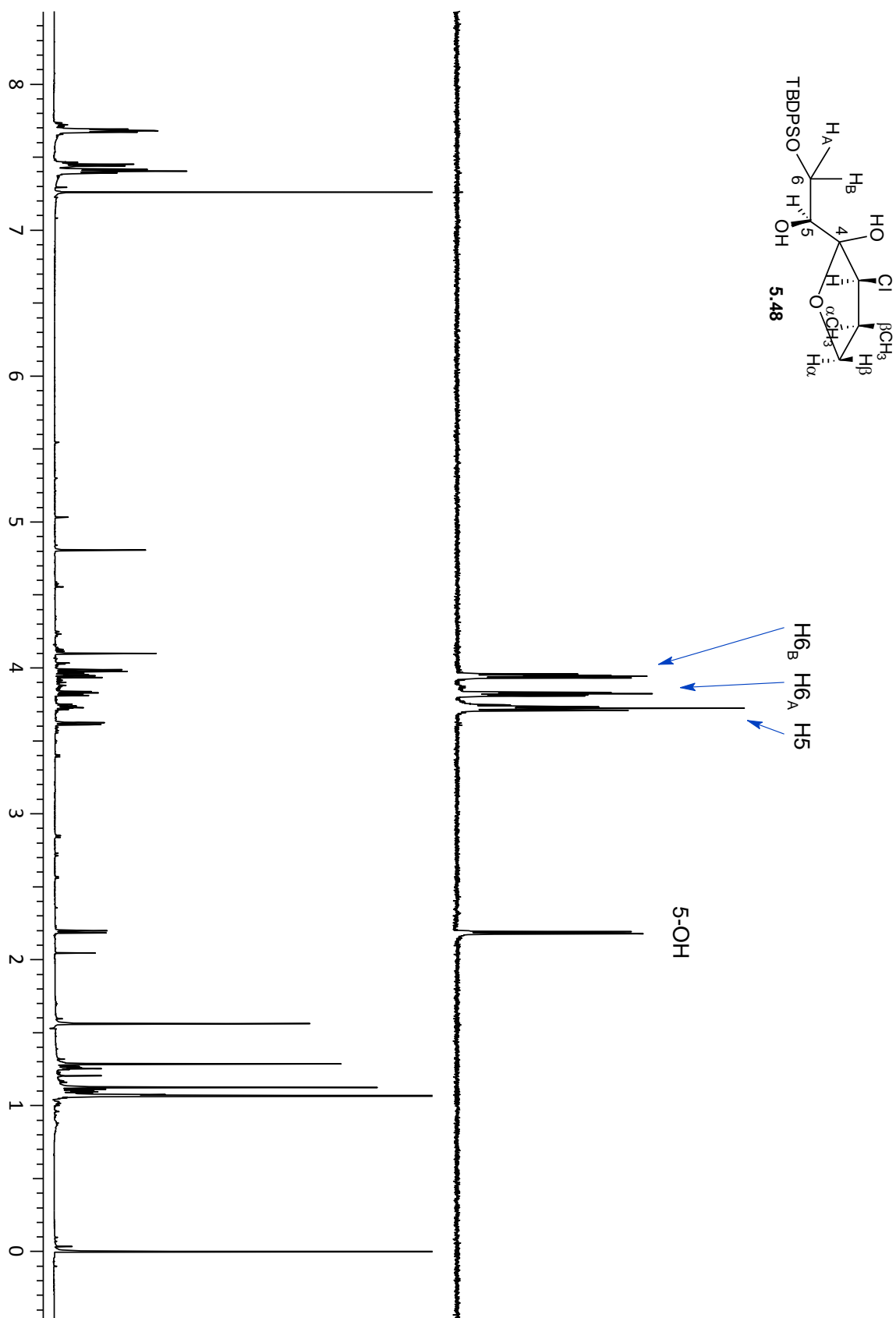
5.47

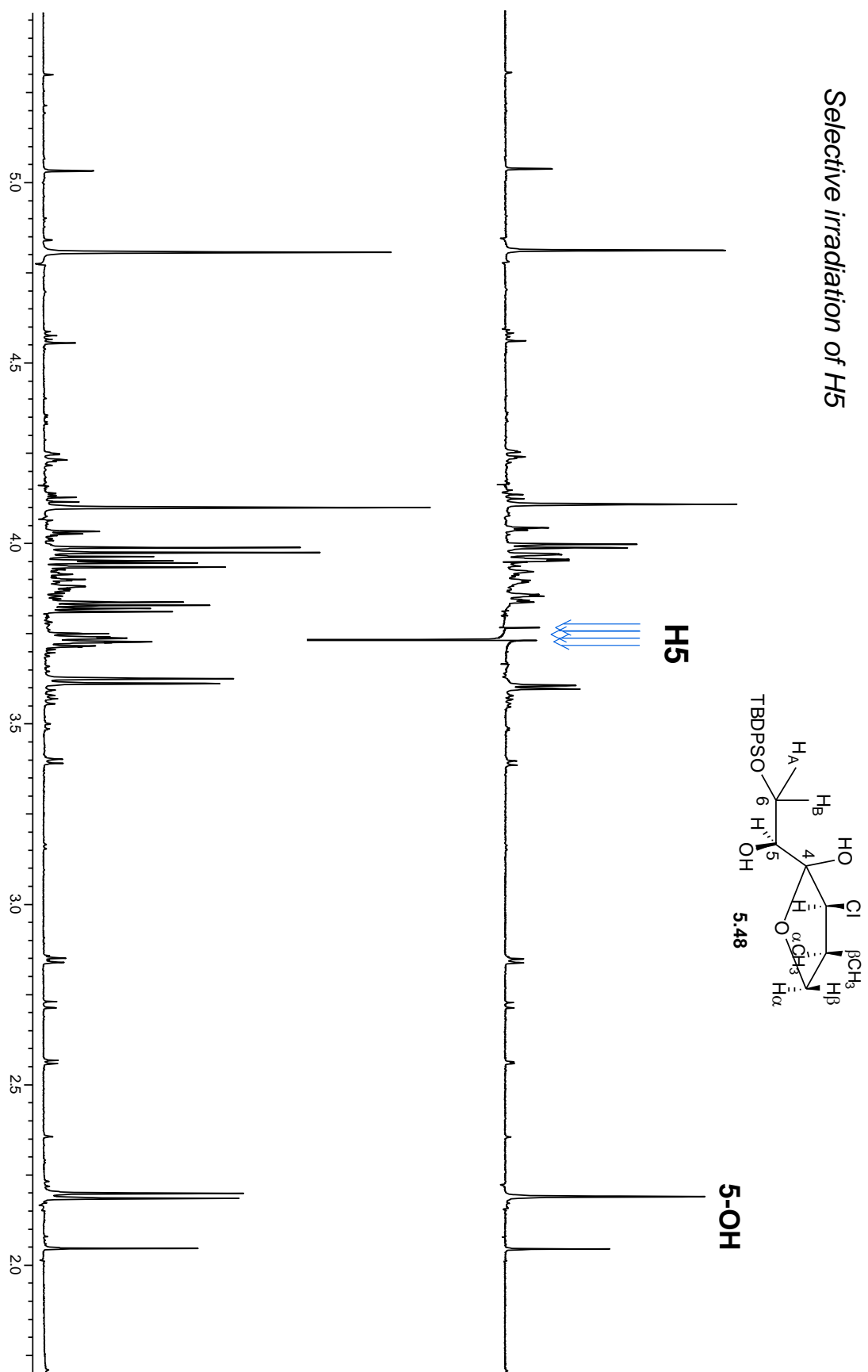




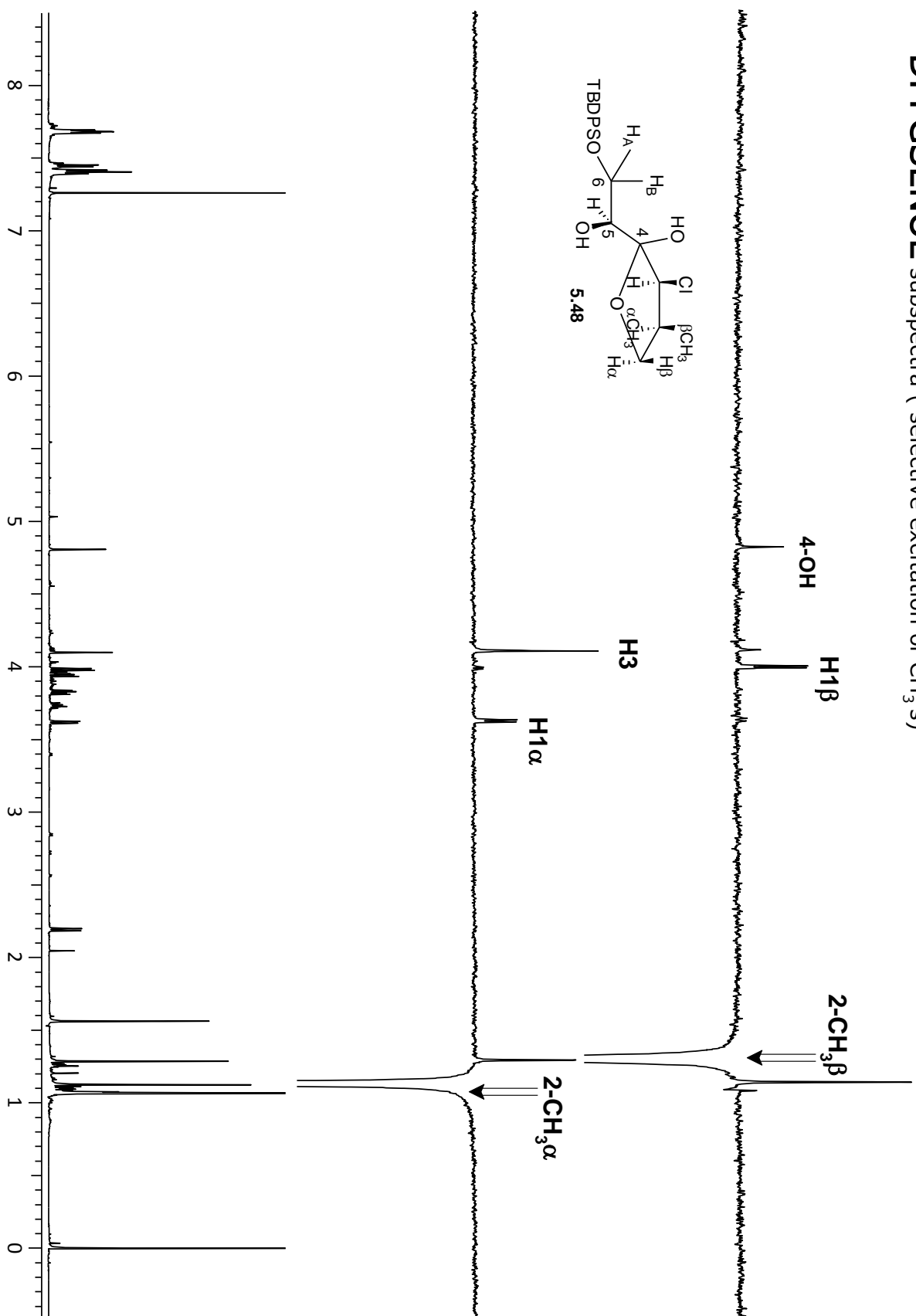


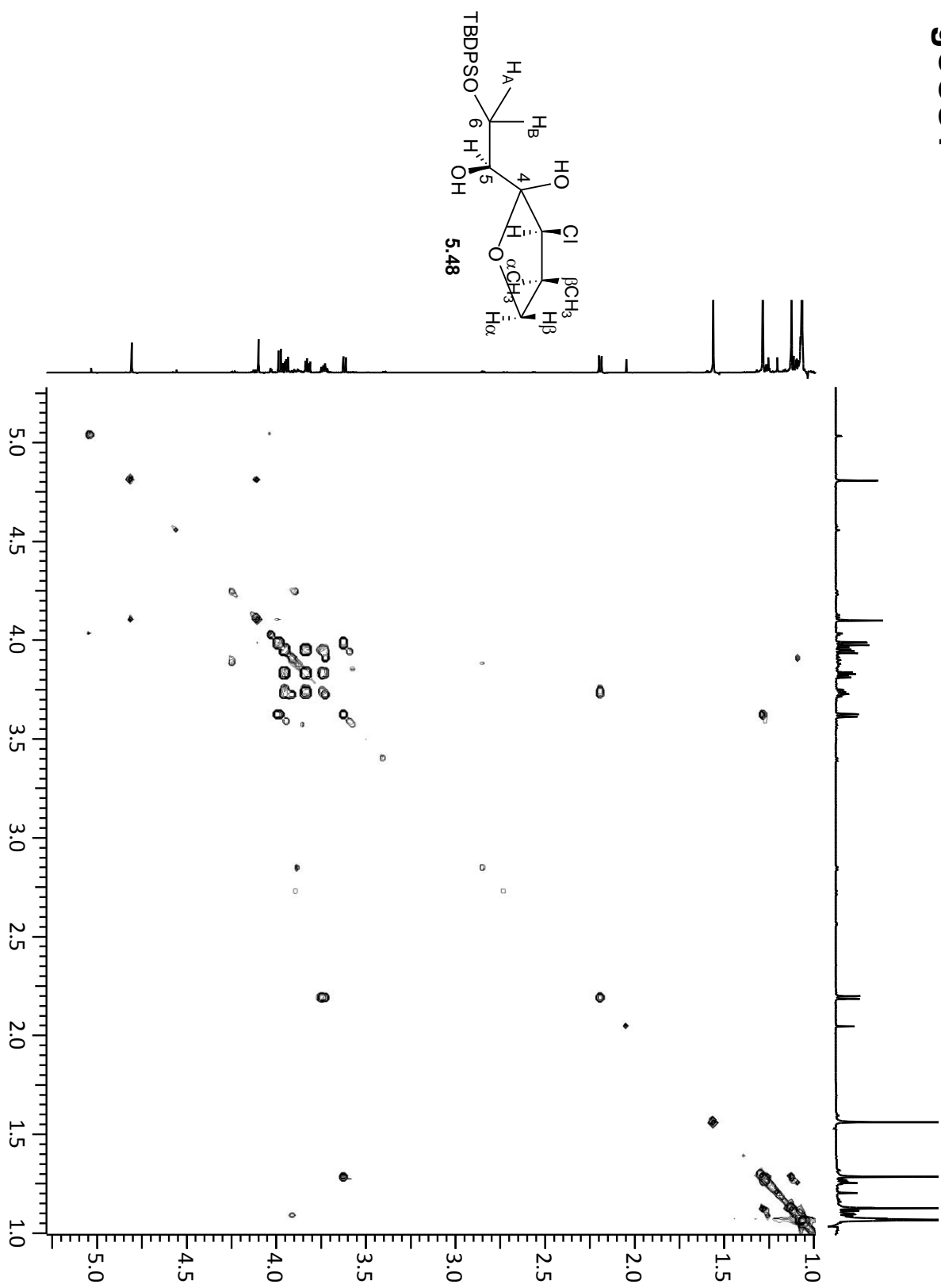
Magnetization transfer pathway (spin system identification)



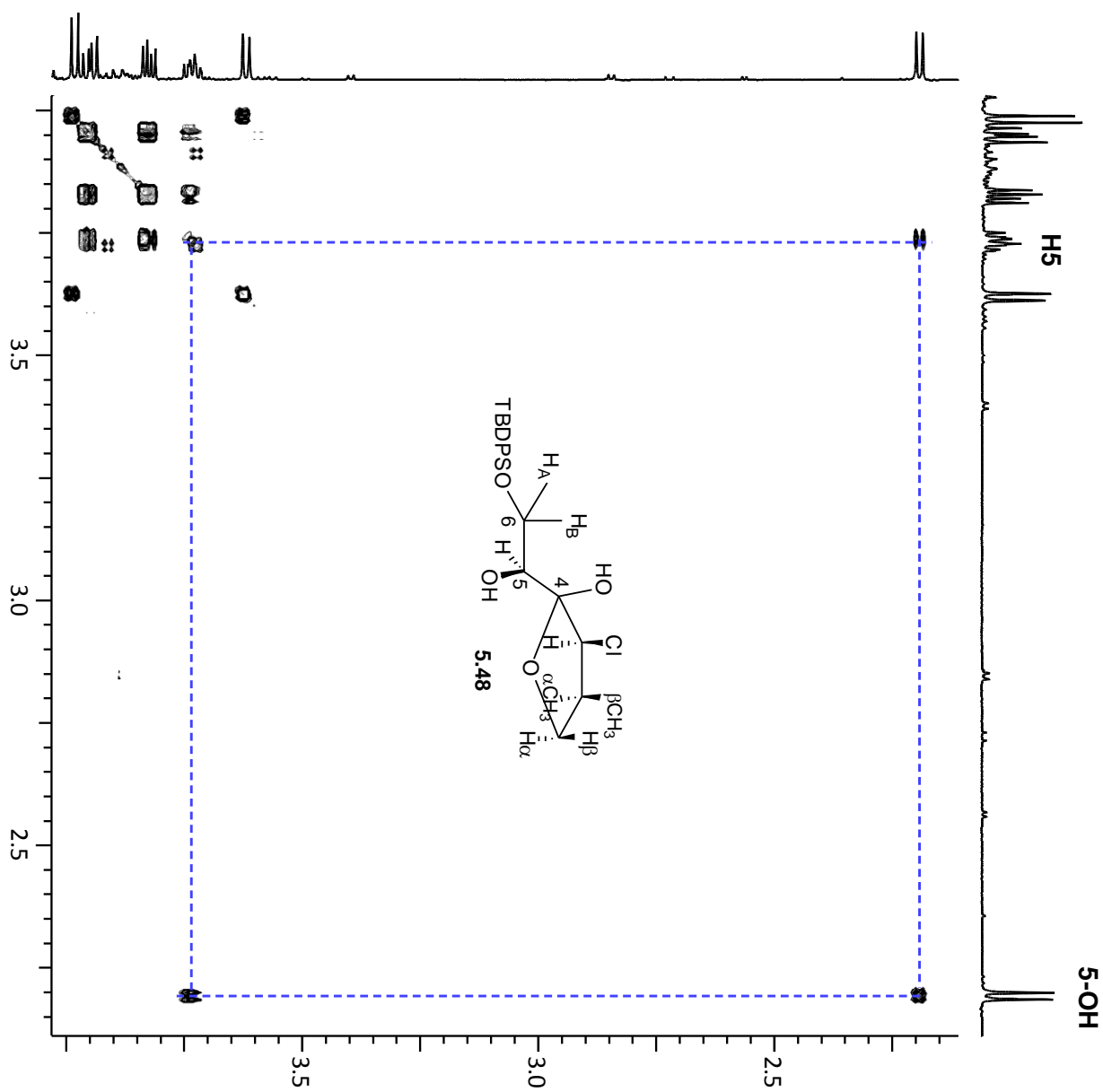


DPFGSENOE subspectra (selective excitation of CH₃'s)

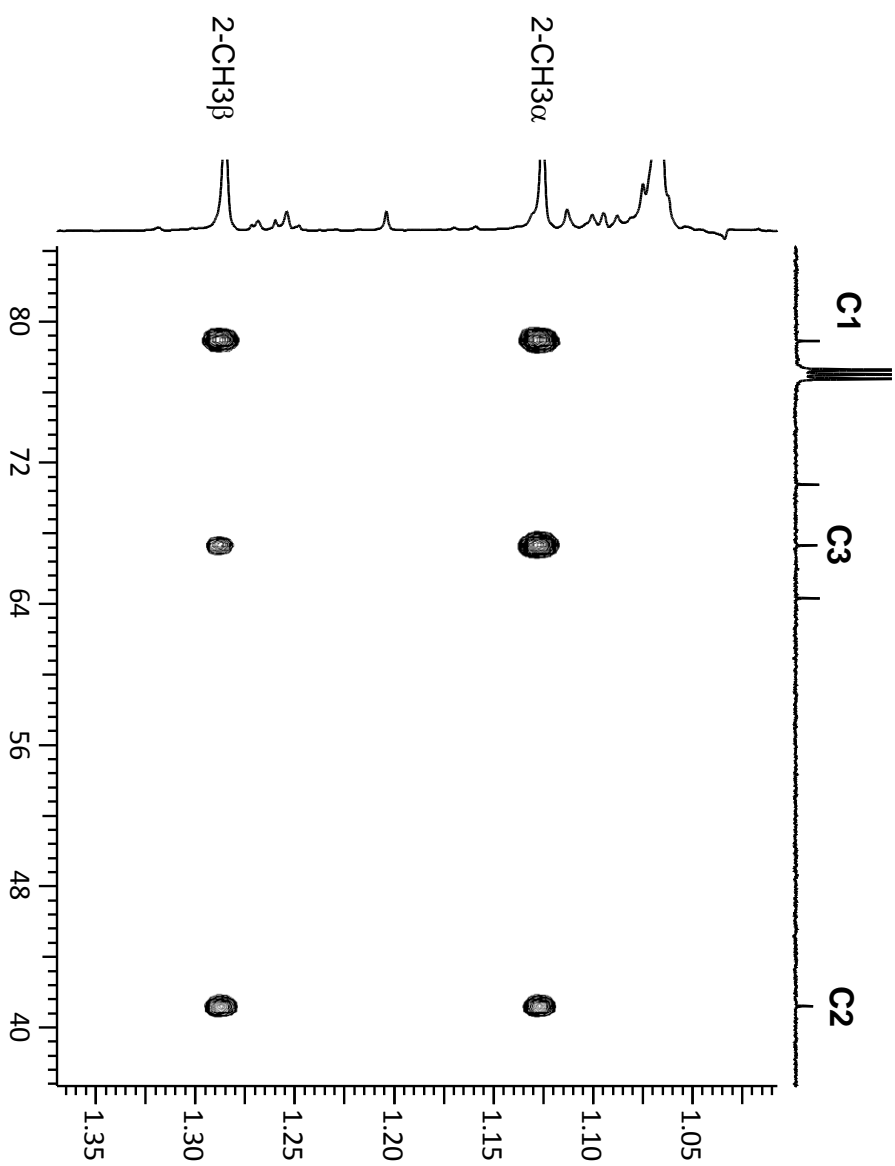
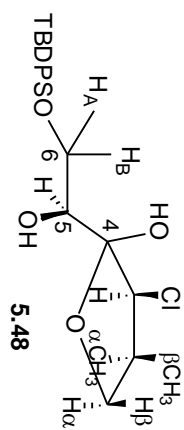




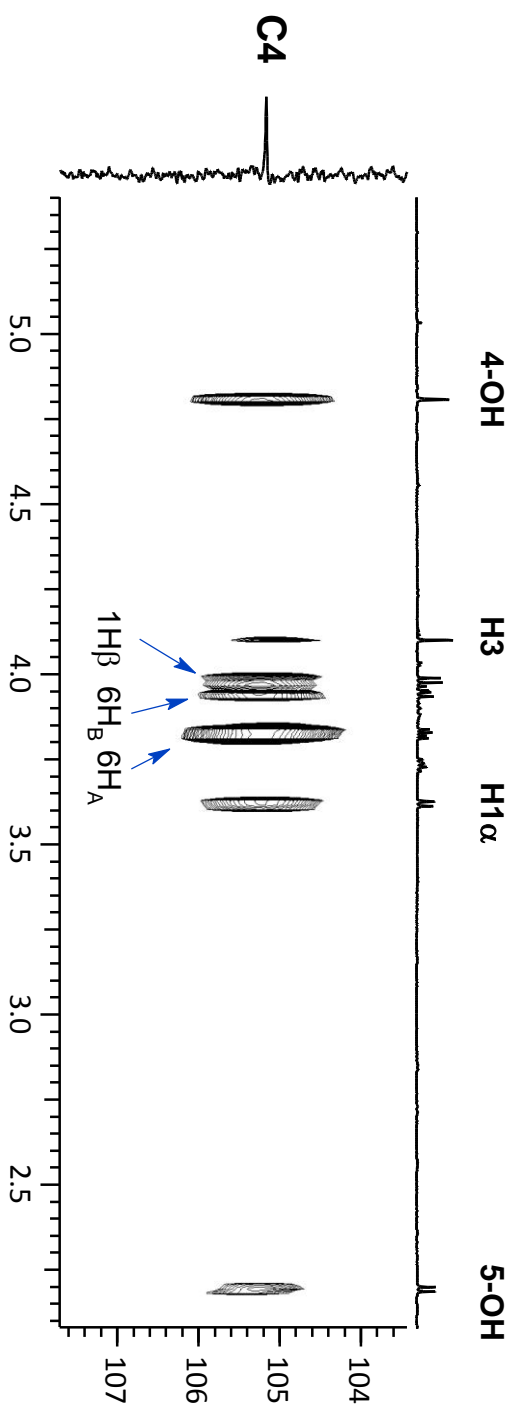
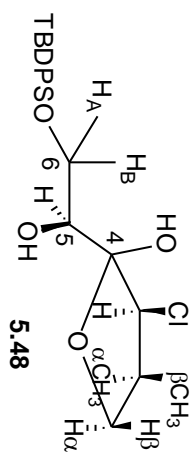
gCOSY

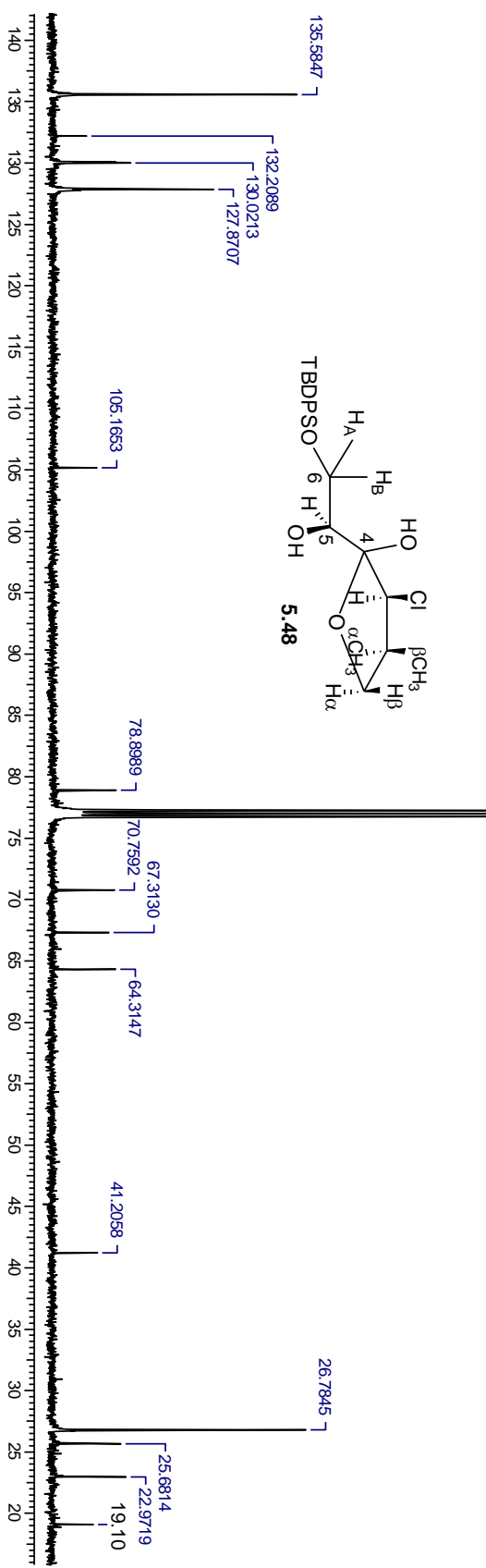
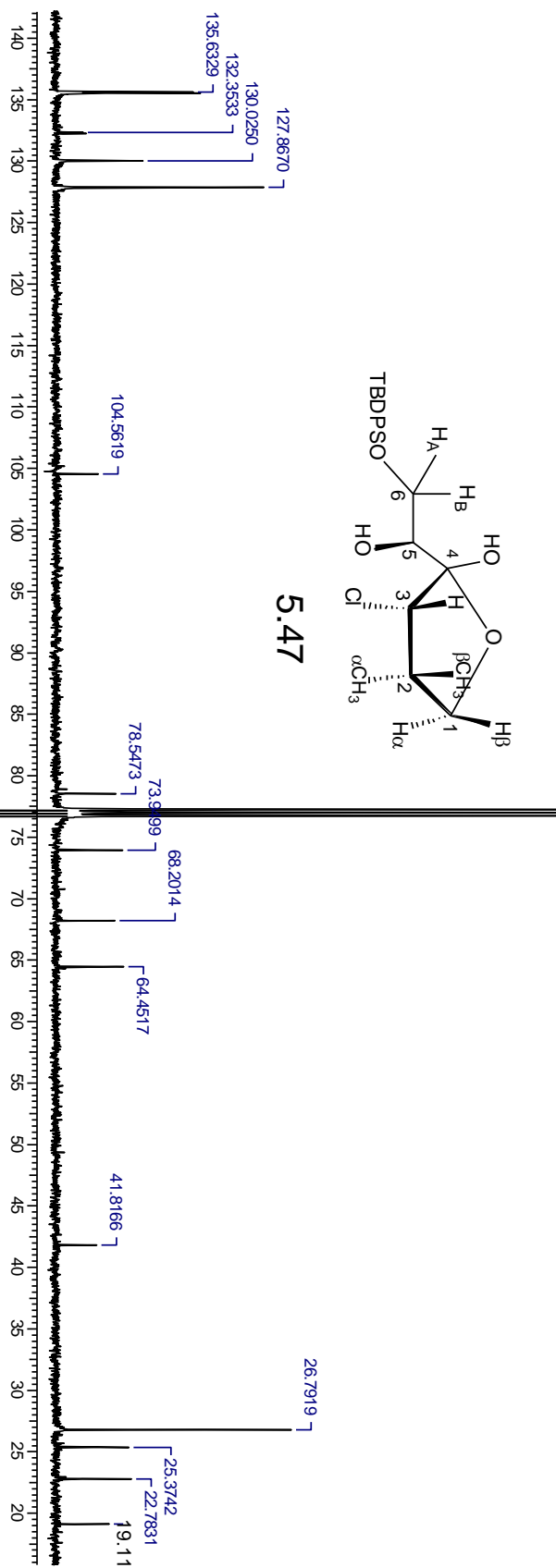


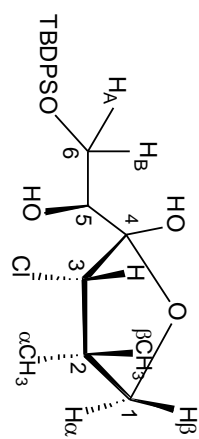
gHMBC



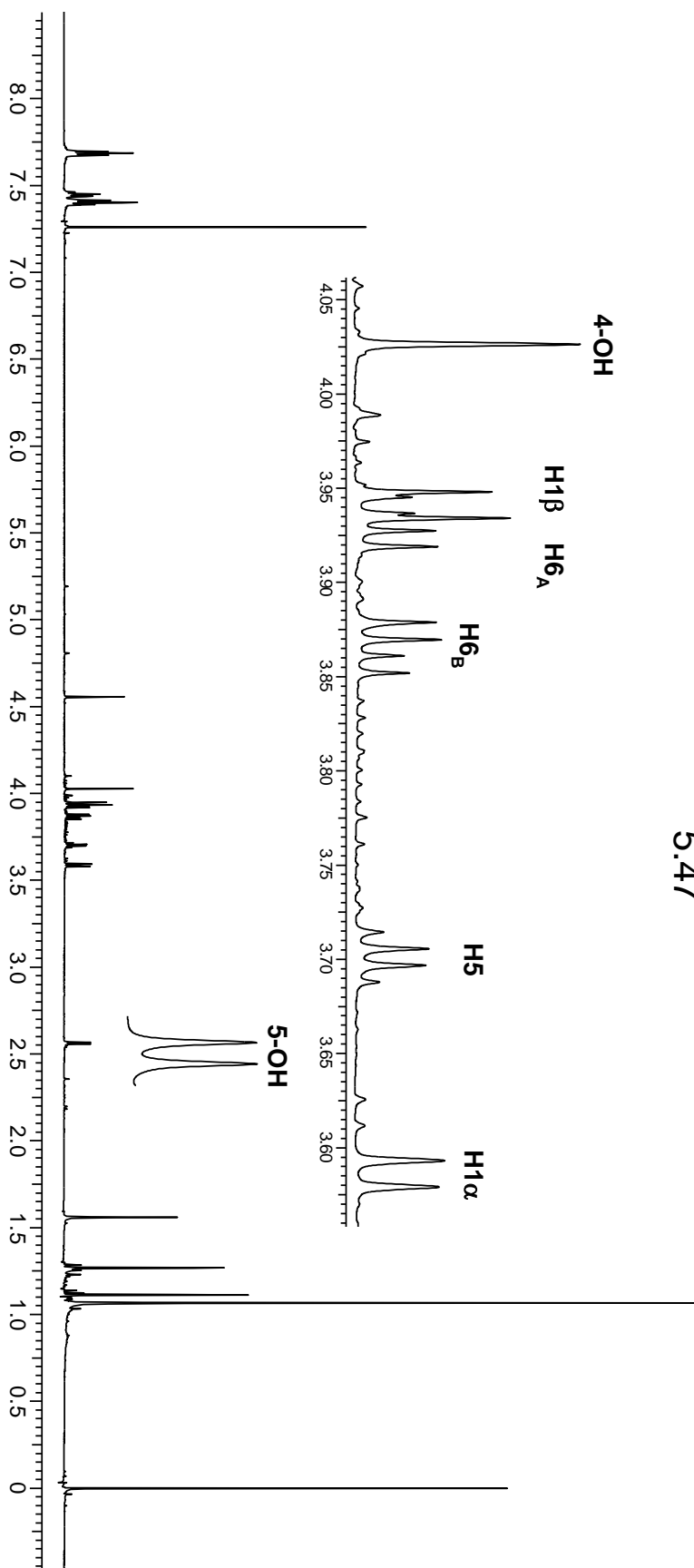
gHMBC

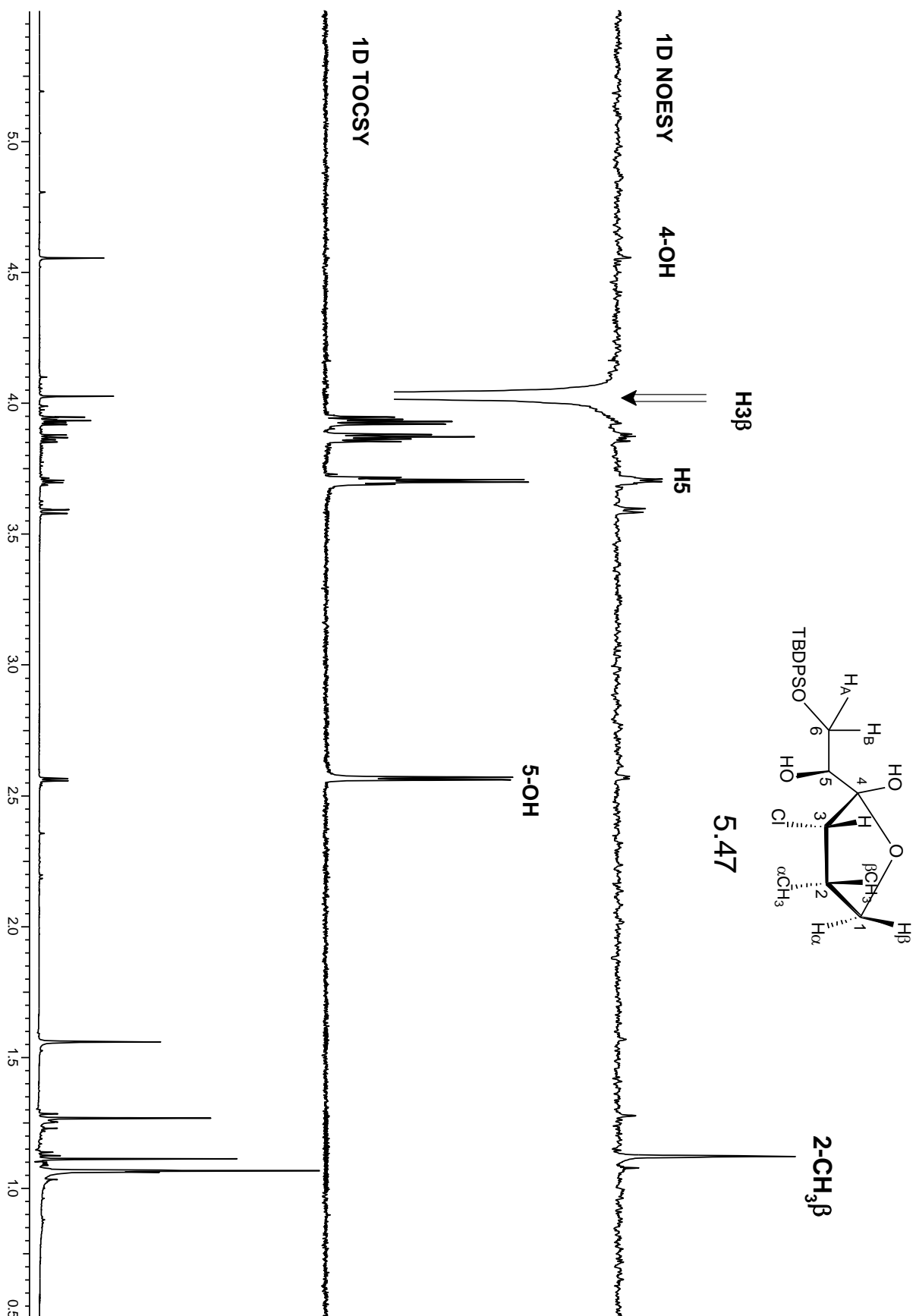


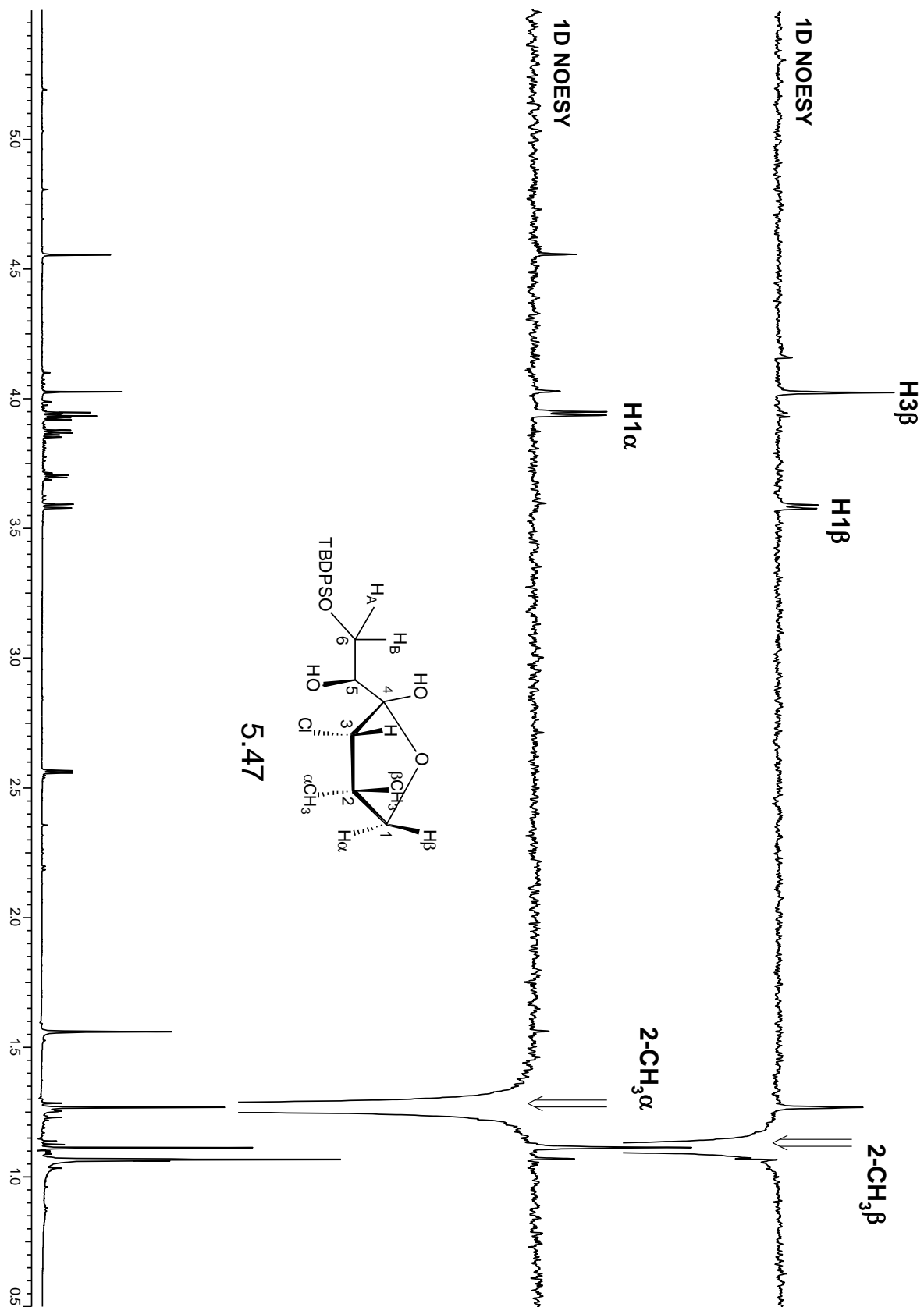
¹³C NMR spectra



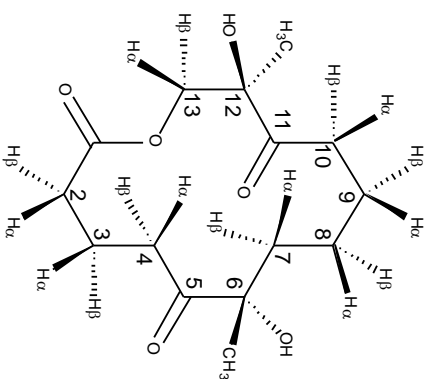
5.47



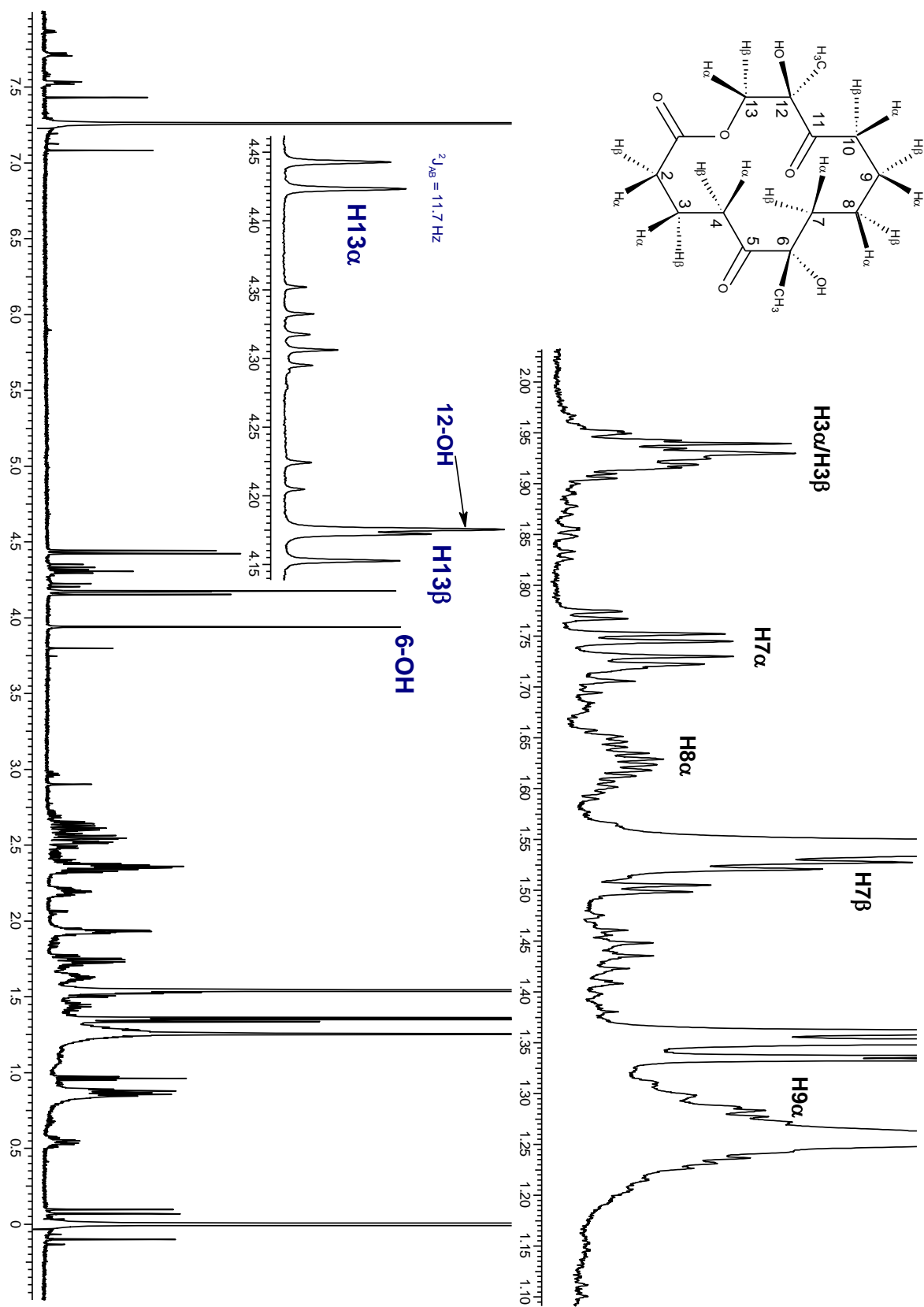


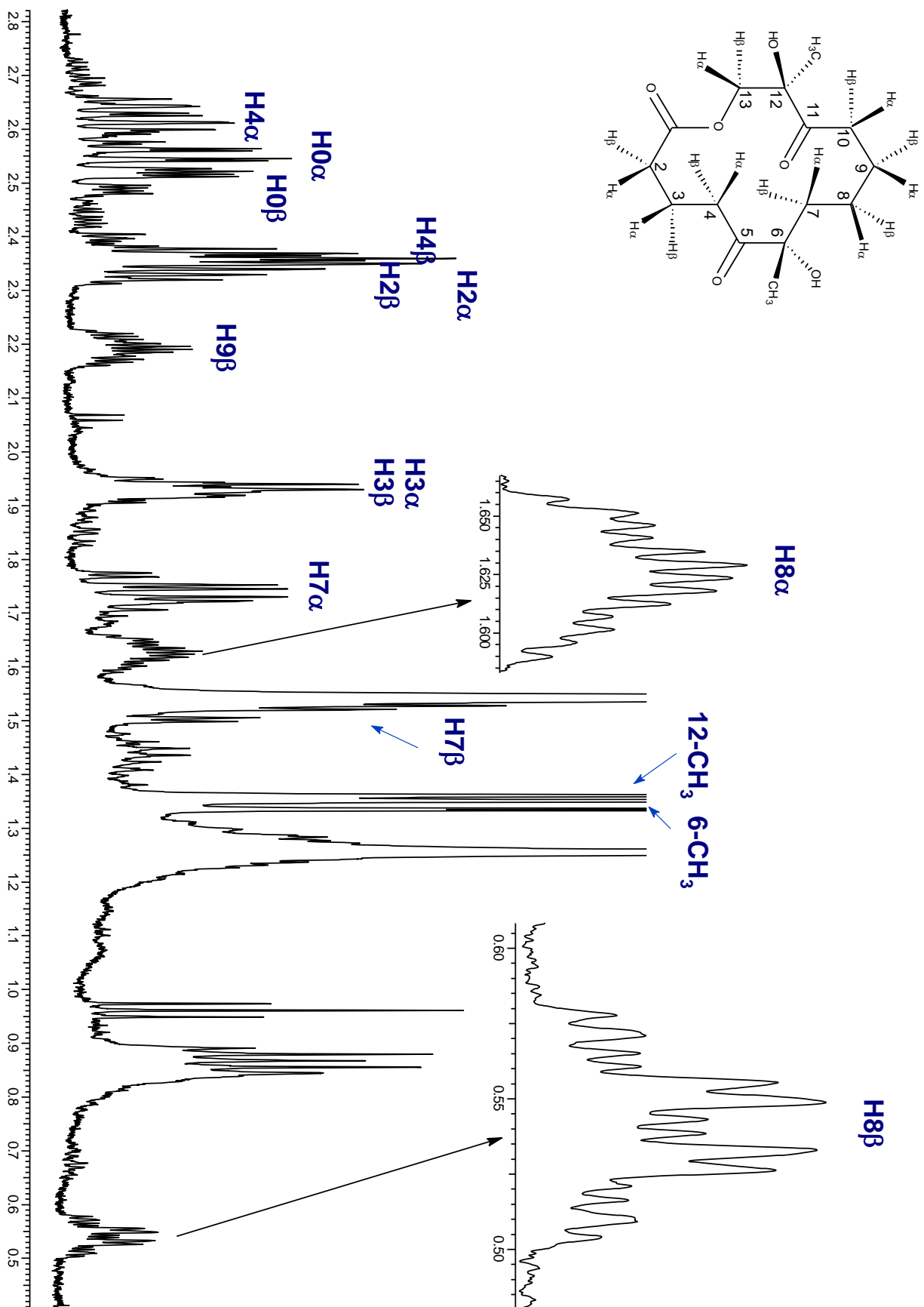


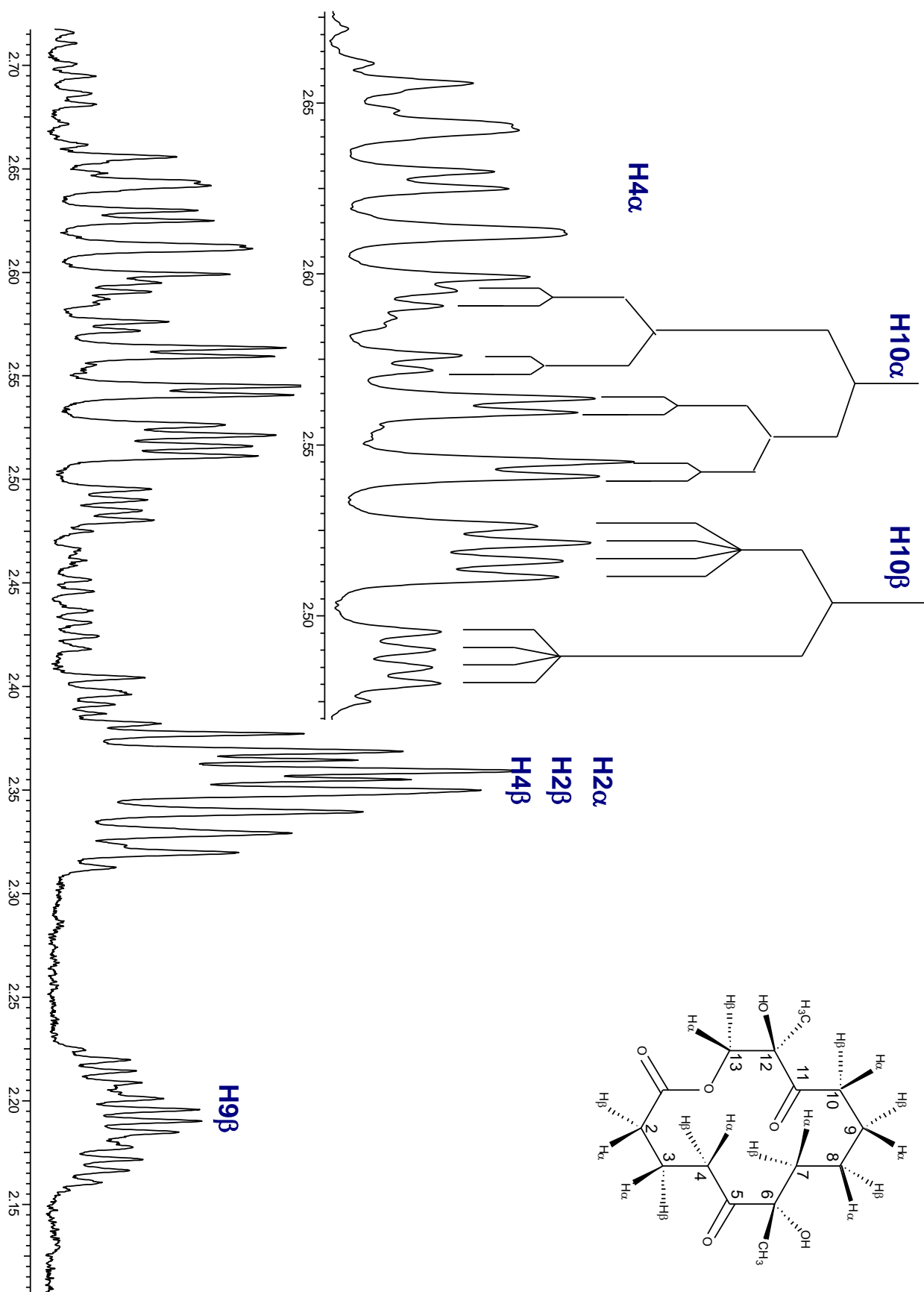
¹H and ¹³C NMR Chemical shifts (δ/ppm) and Coupling constants (J/Hz)



H3α/H3β—1.91–1.95	³ J(H4α–H3α) = 6.22	
H2α/H2βH/4β—2.31–2.40	³ J(H4α–H3β) = 9.41	
H4α—2.62	² J(H4α–H4β) = 18.40	C1-----172.39
6-CH ₃ —1.35	³ J(H3α–H2α) = 5.45	C2-----32.33
6-OH—3.94	² J(H7α–H7β) = 13.91	C3-----18.16
H7α—1.74	² J(H8α–H8β) = 14.02	C4-----33.50
H7β—1.52	³ J(H8α–H7α) = 3.27	C5-----212.98
H8α—1.62	³ J(H8α–H7β) = 12.65	C6-----80.53
H8β—0.54	³ J(H8β–H7α) = 13.12	6-CH ₃ -----25.88
H9α—1.25	³ J(H8β–H7β) = 3.67	C7-----39.72
H9β—2.19	³ J(H9α–H8α) = 3.63	C8-----21.83
H10α—2.56	³ J(H9α–H8β) = 9.78	C9-----21.61
H10β—2.50	³ J(H9β–H8α) = 6.64	C10-----33.59
12-CH ₃ —1.36	³ J(H9β–H8β) = 9.78	C11-----210.01
12-OH—4.18	² J(H13α–H13β) = 11.71	C12-----78.44
H13α—4.43	³ J(H10α–H9α) = 2.27	12-CH ₃ -----21.50
H13β—4.16	³ J(H10α–H9β) = 12.30	C13-----69.66
	² J(H10α–H10β) = 18.65	

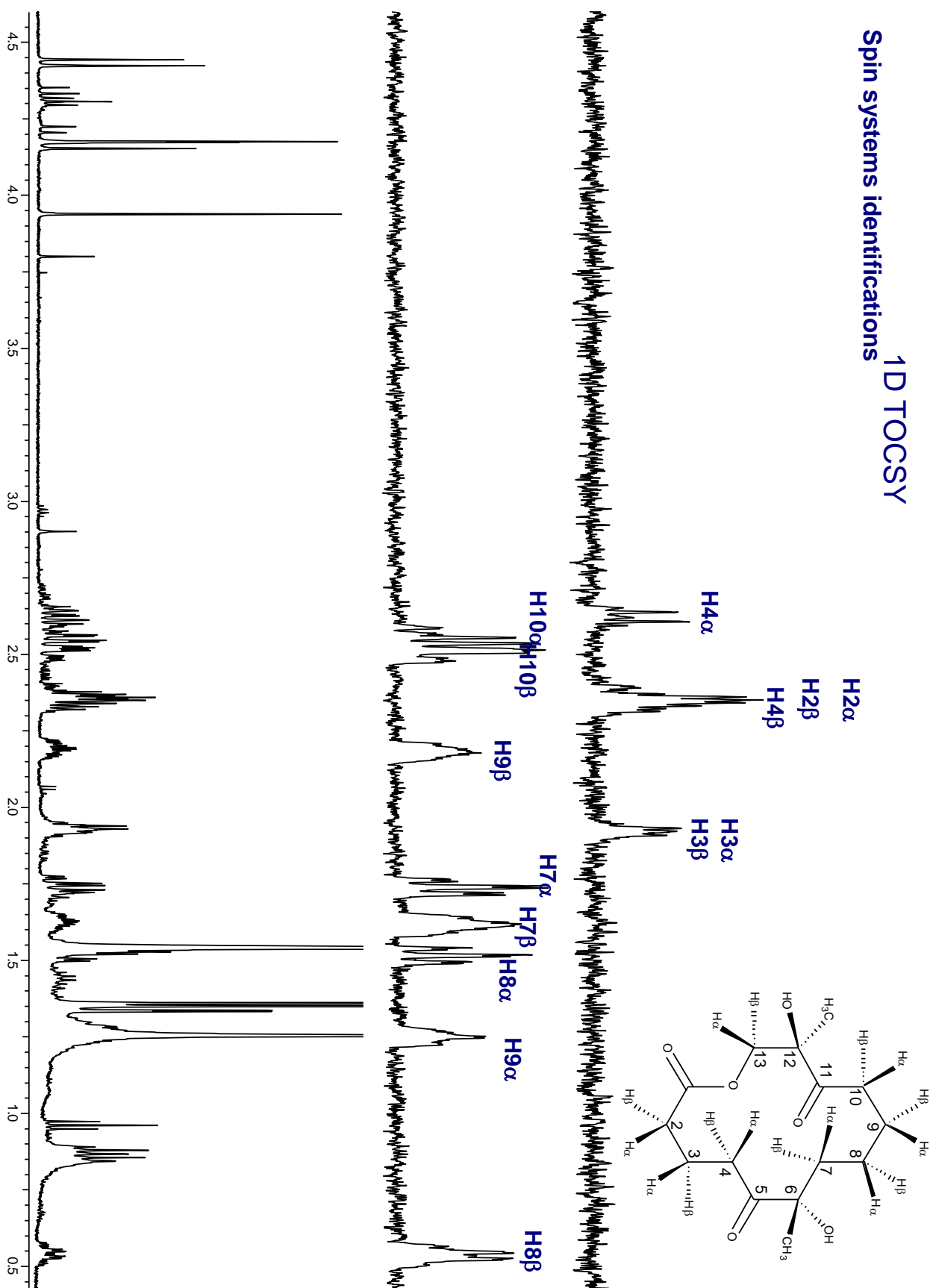


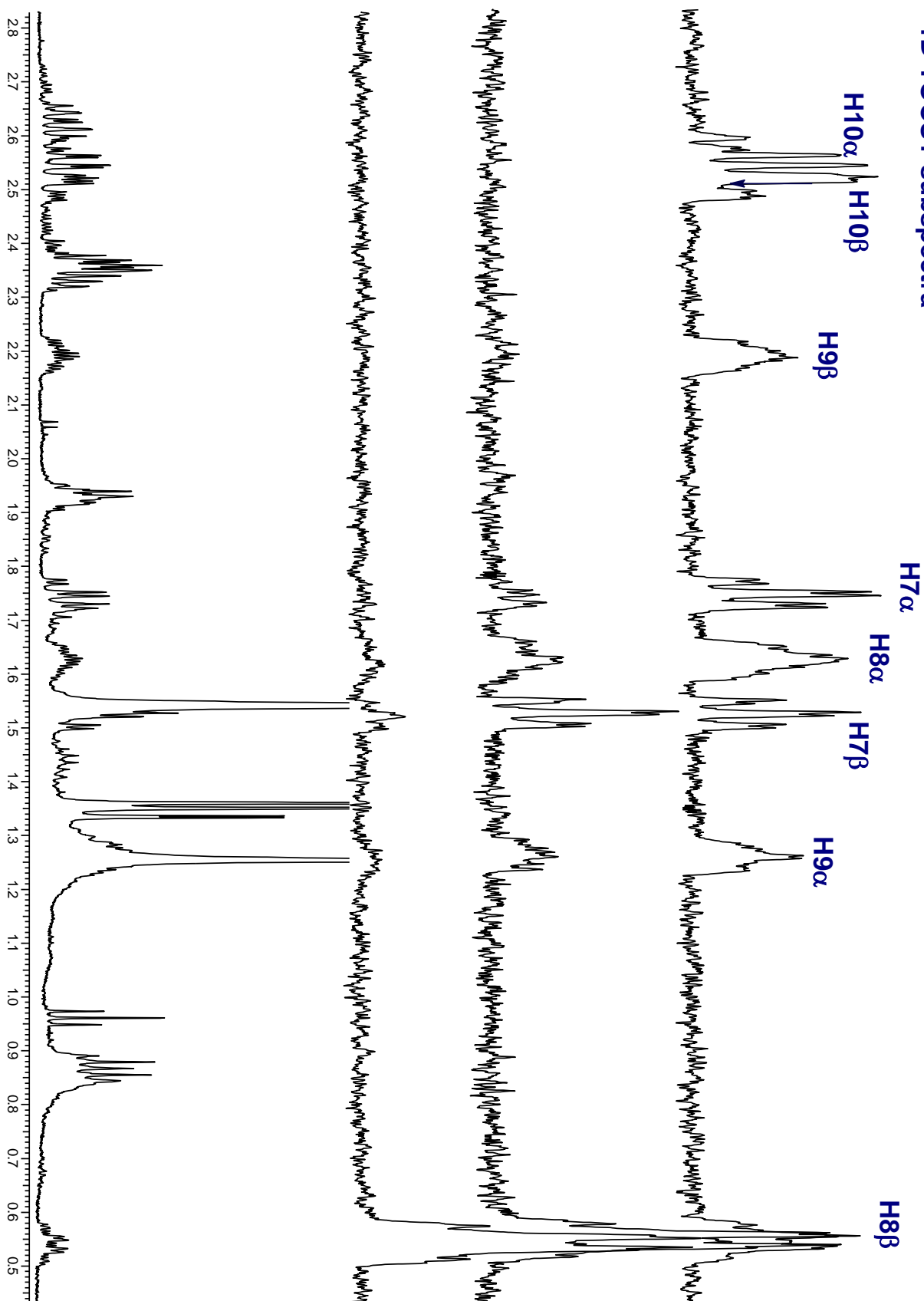


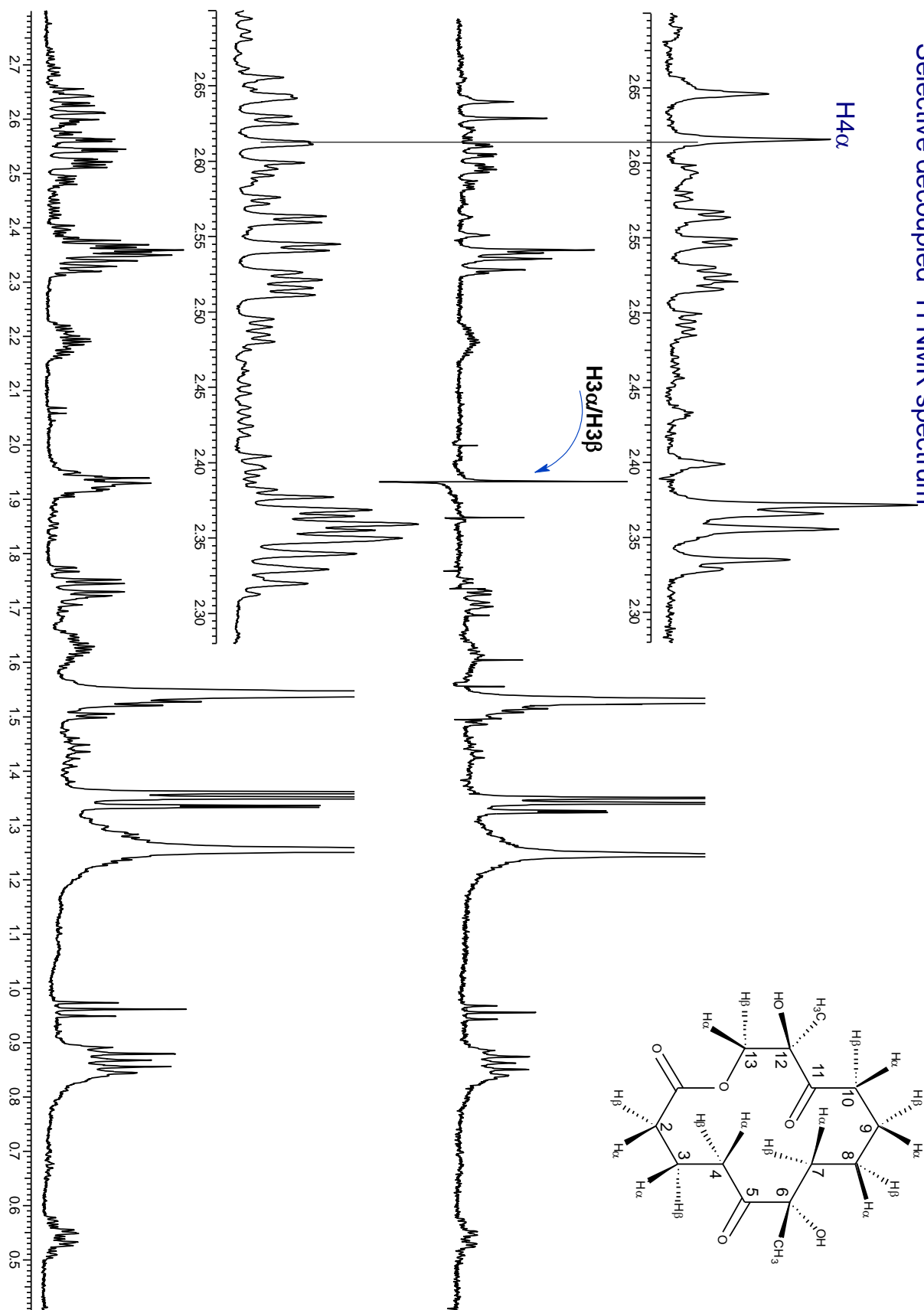


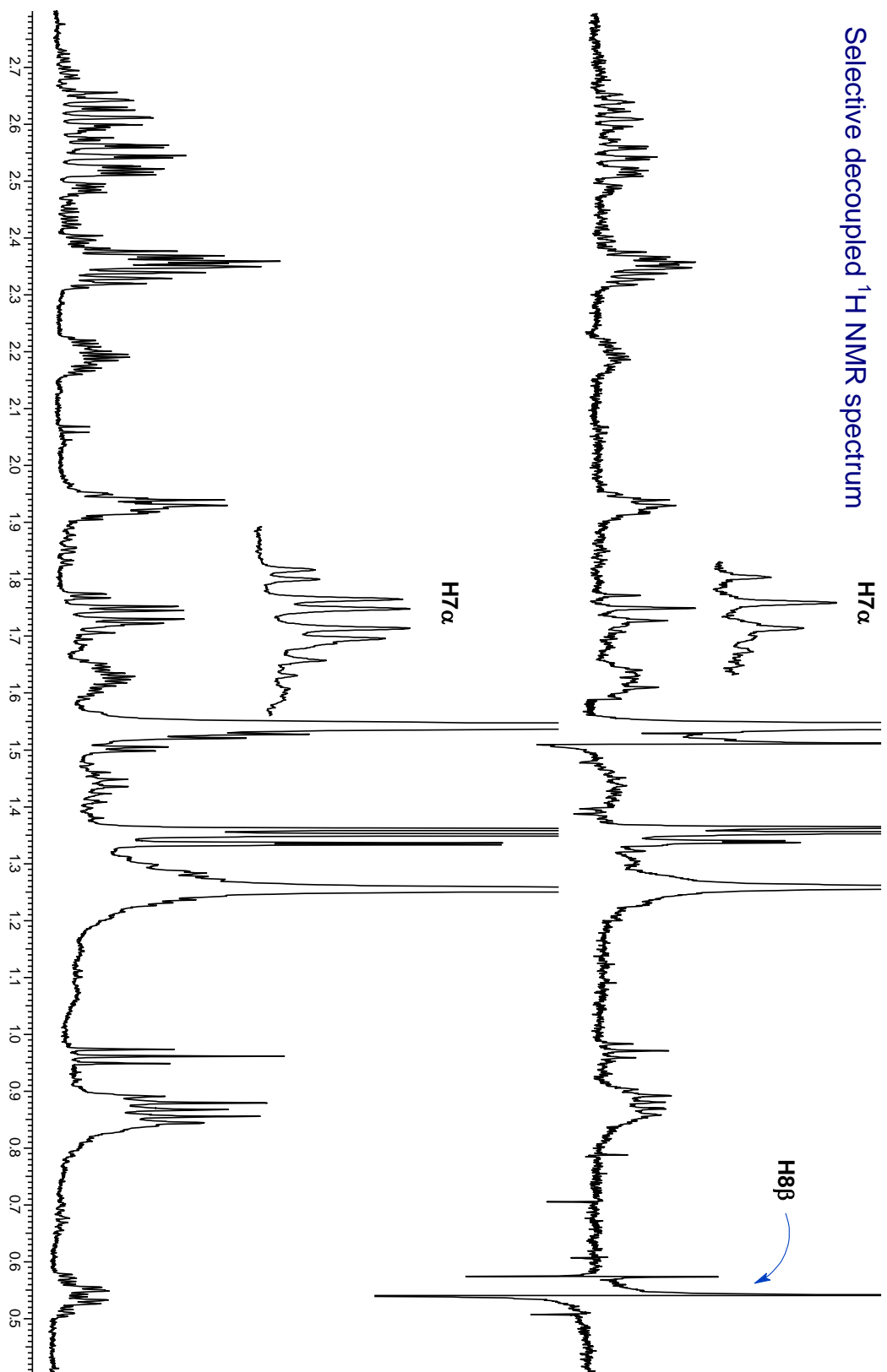
¹D TOCSY

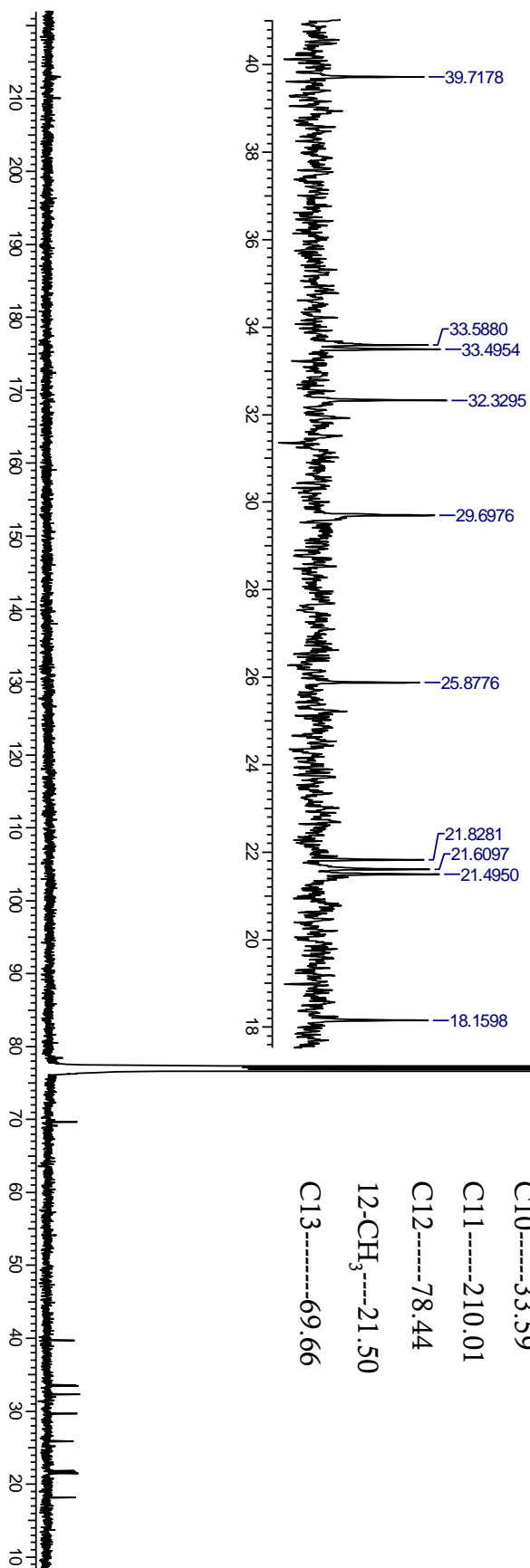
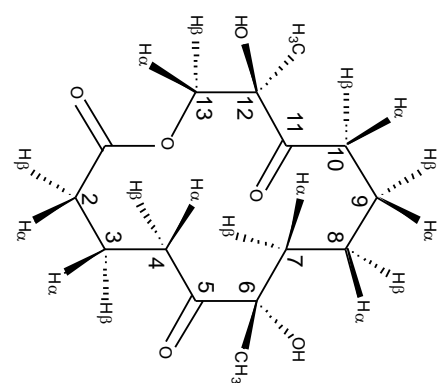
Spin systems identifications



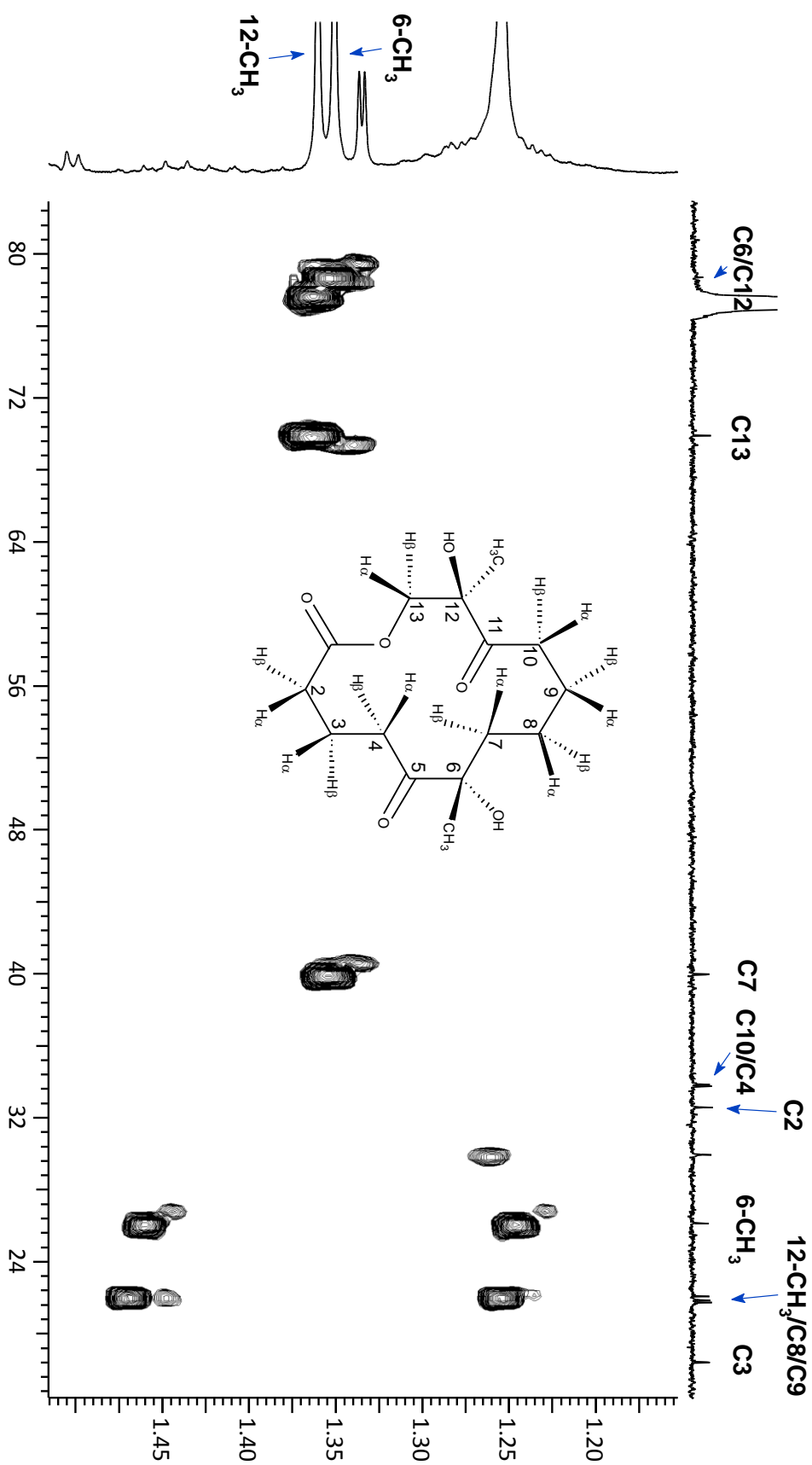
1D TOCSY subspectra selective excitation of **H8 α** at 0.54 ppm

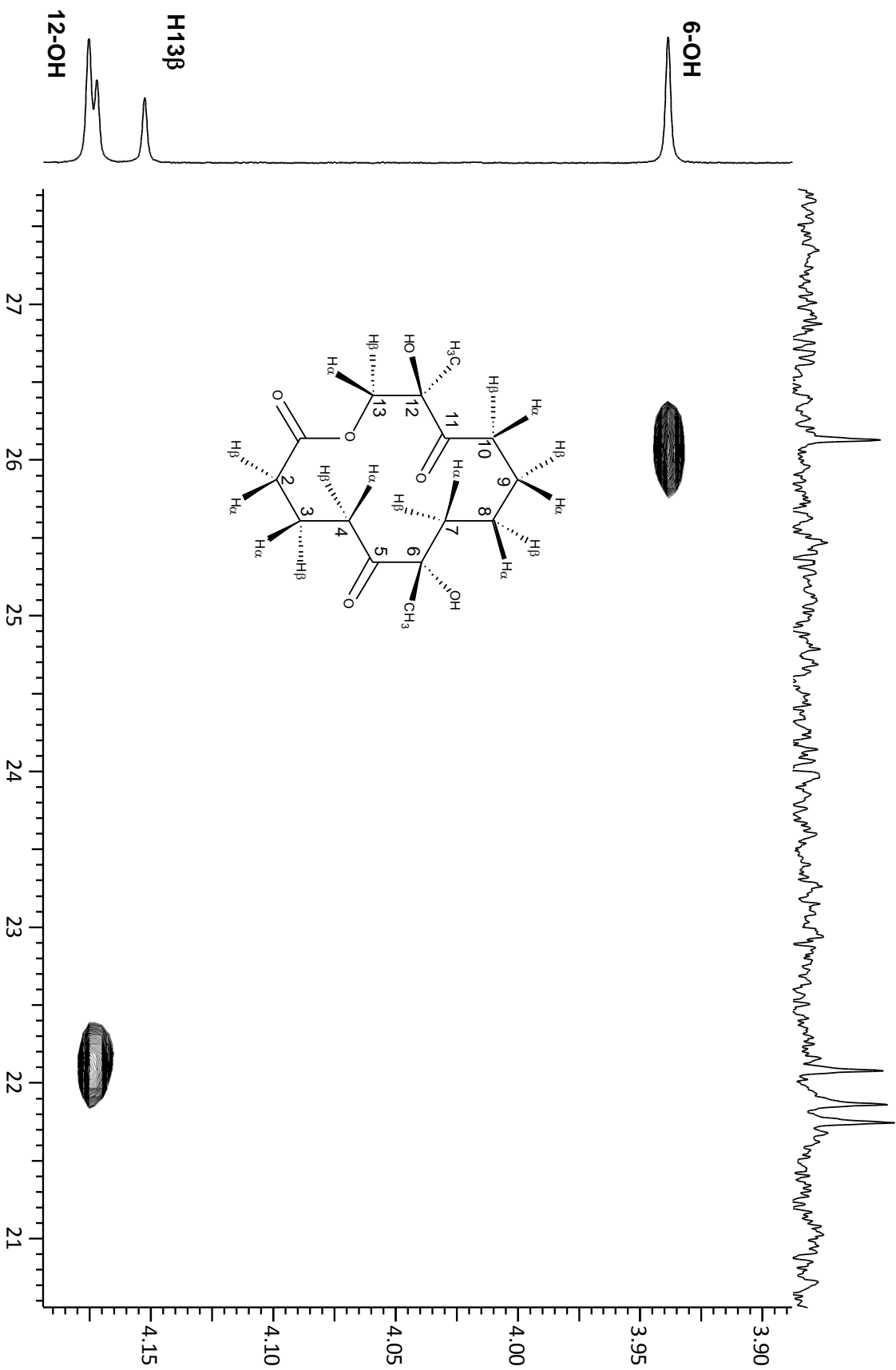
Selective decoupled ^1H NMR spectrum

Selective decoupled ^1H NMR spectrum

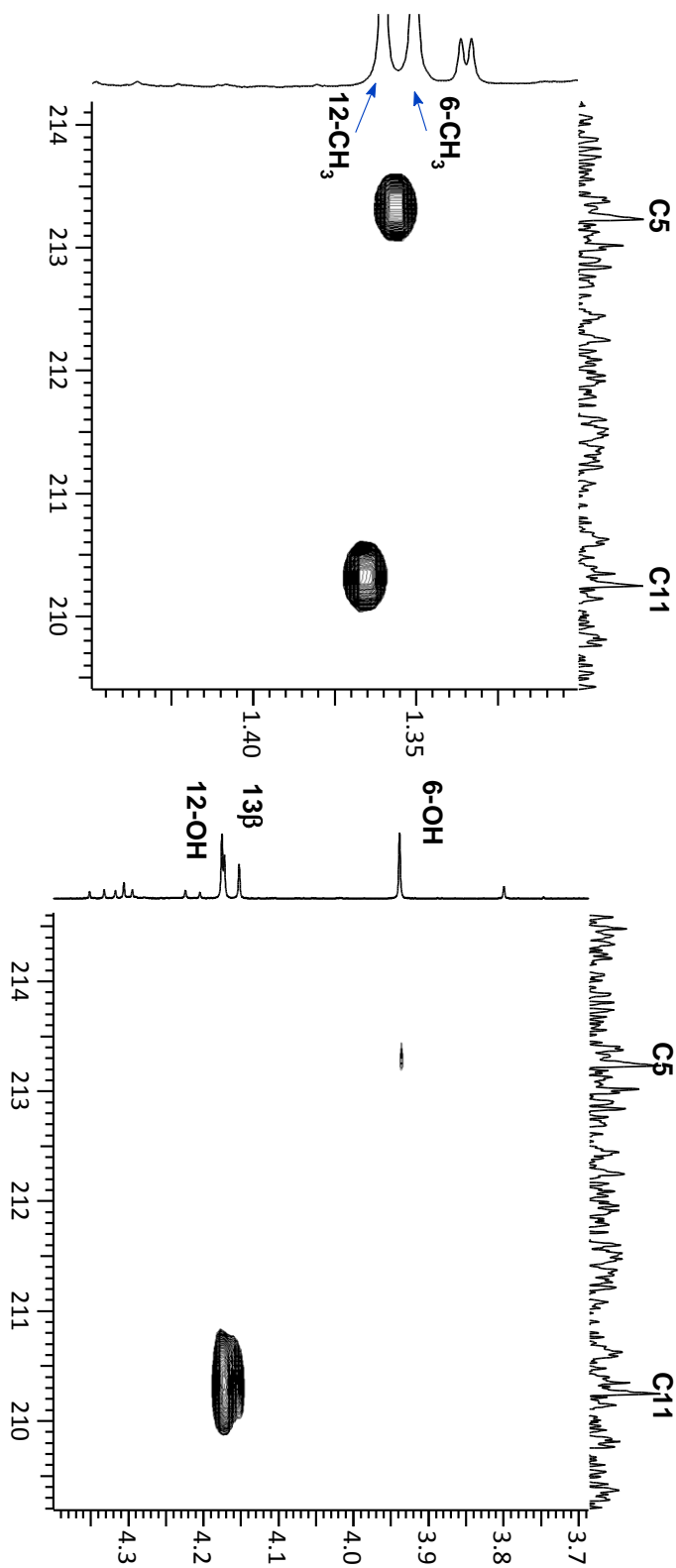
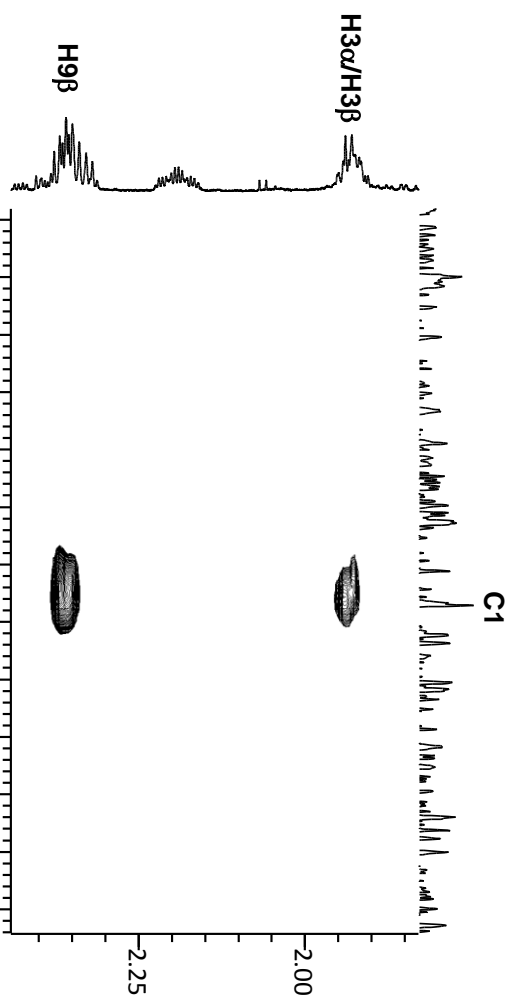
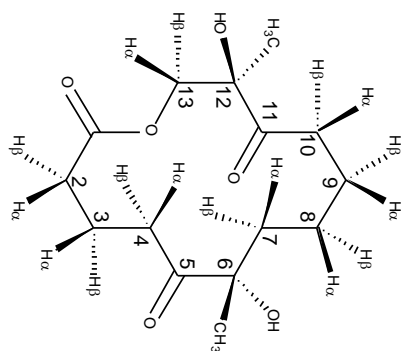


gHMBC



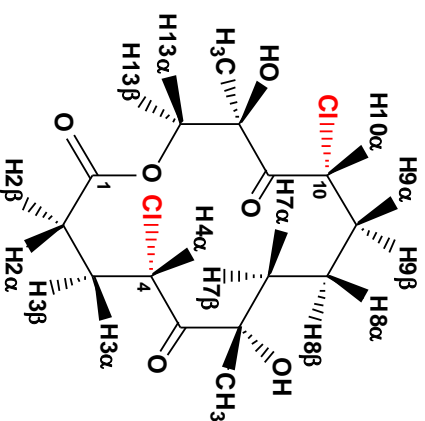
gHMBC**6-CH₃****12-CH₃ C8 C9**

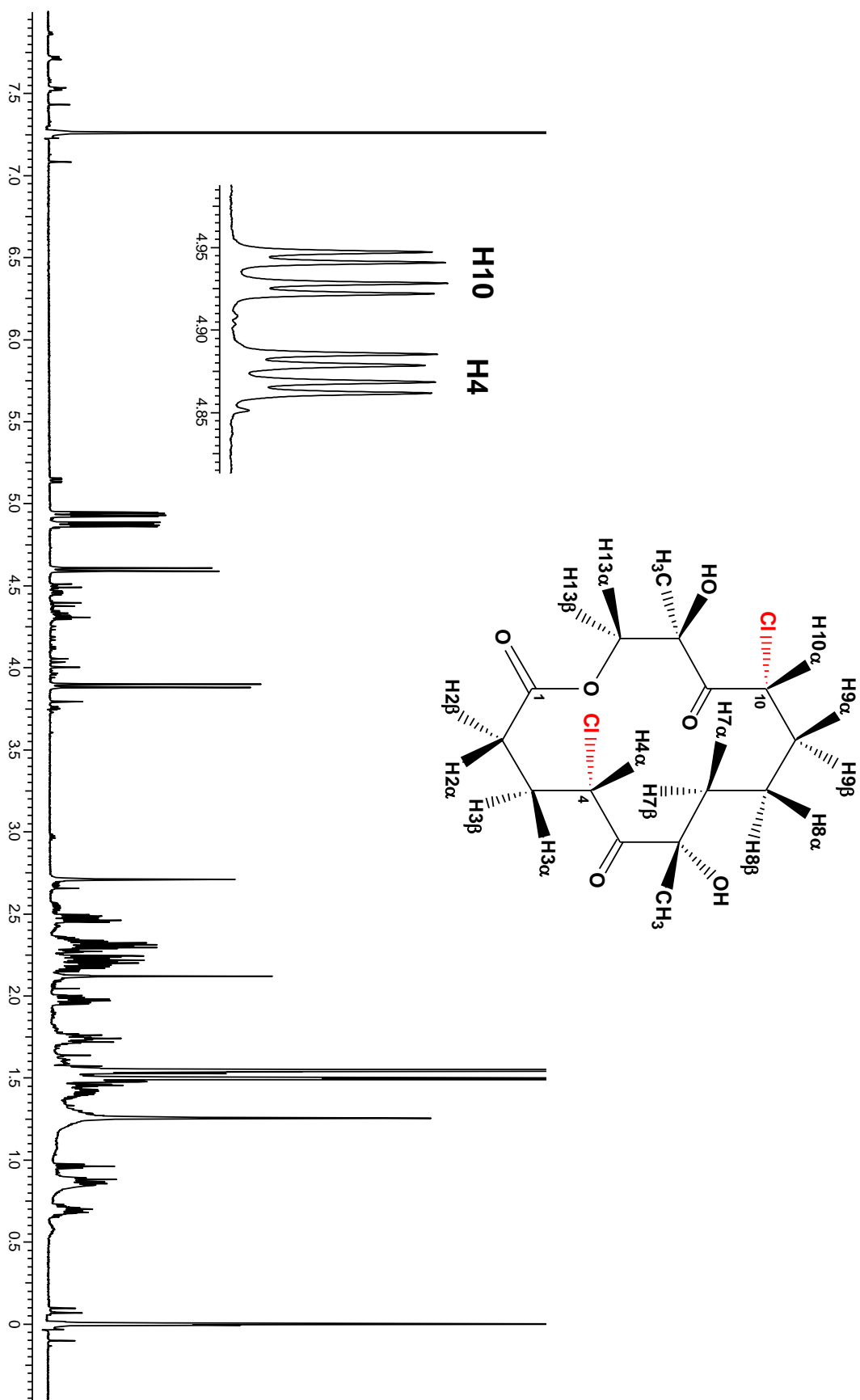
gHMBC

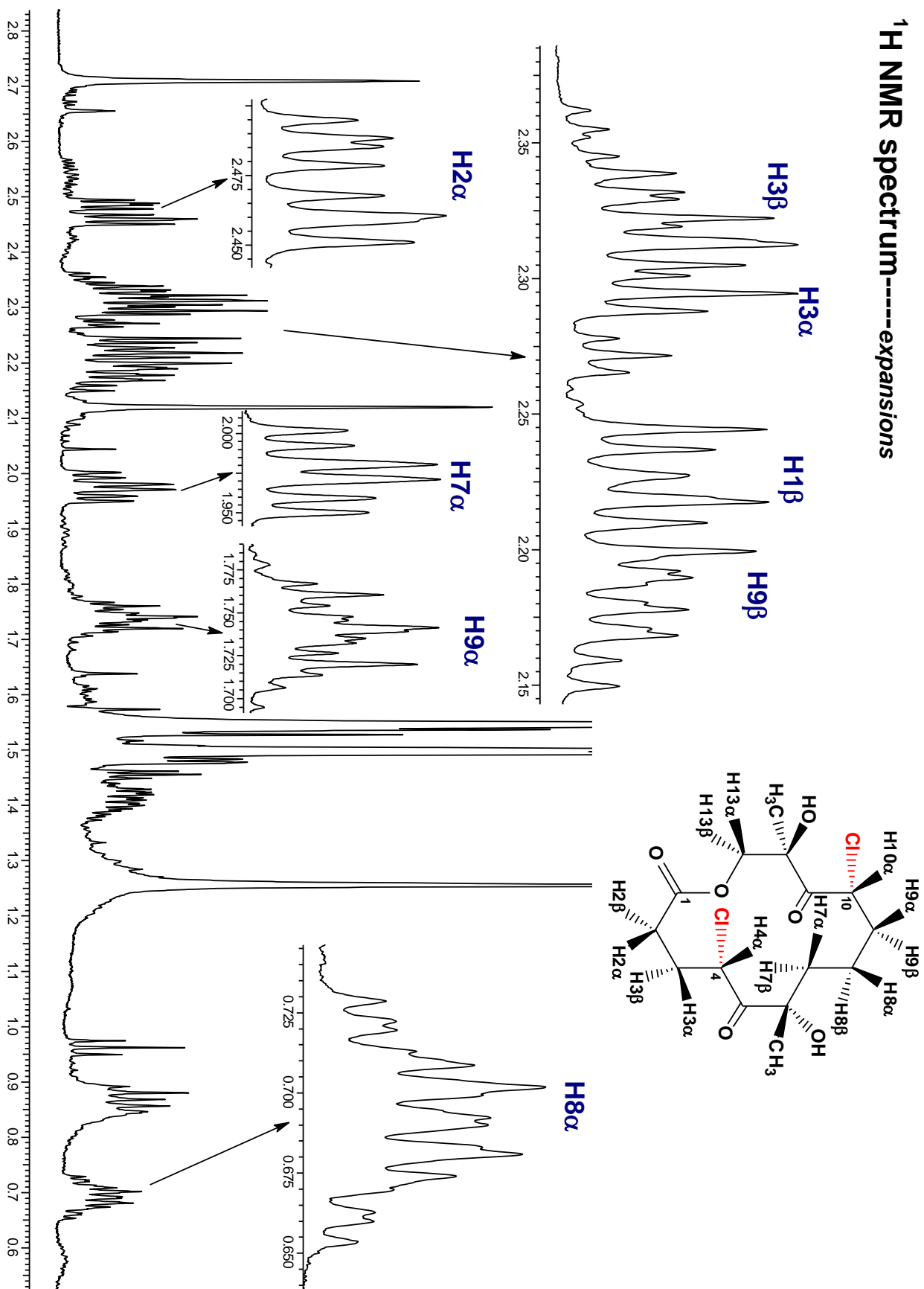


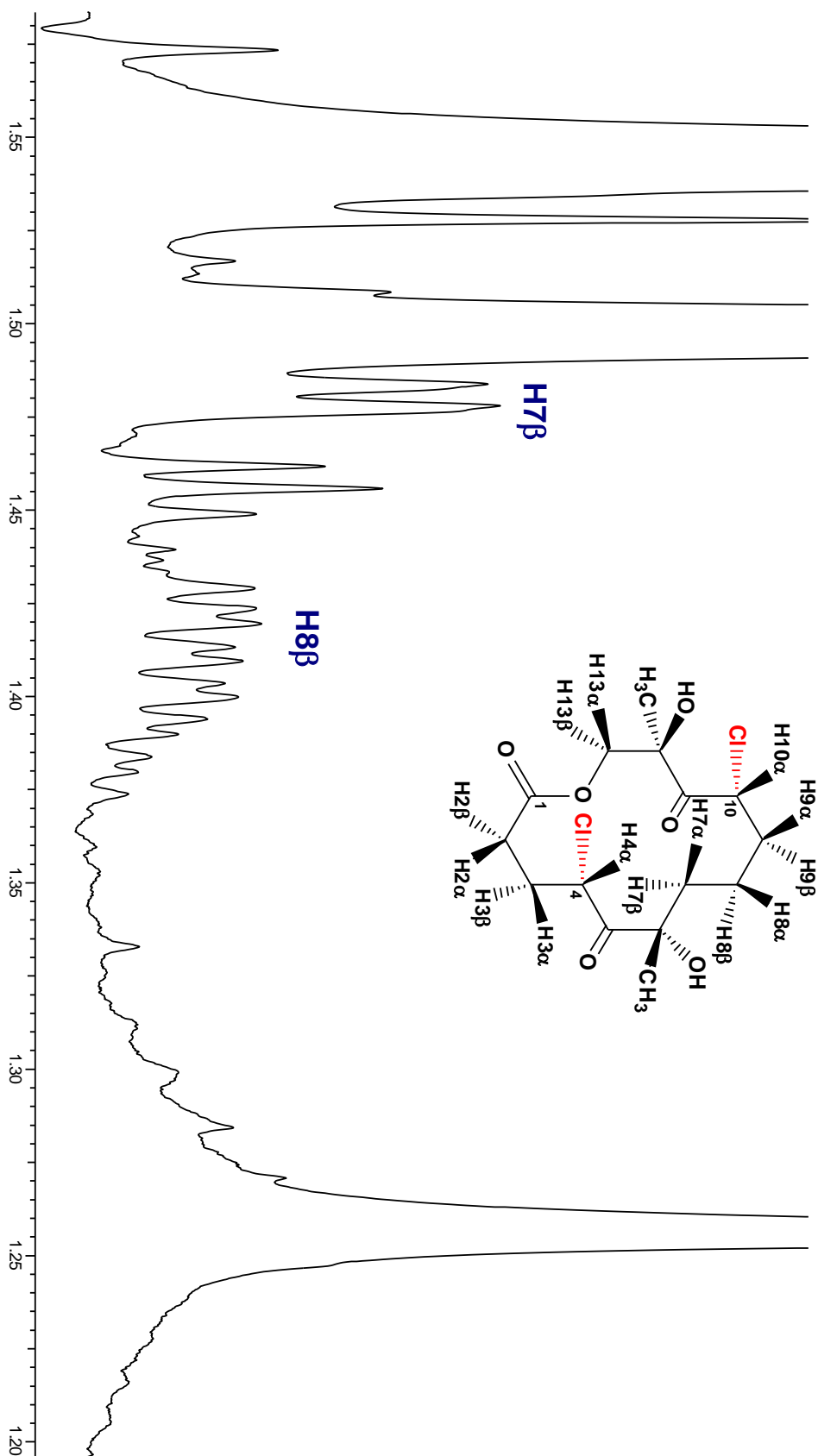
¹H and ¹³C NMR Chemical shifts (δ/ppm) and Coupling constants (J/Hz)

H2α	2.21	C1	171.40	³ J(H4α-H3α) = 3.85	³ J(H9α-H8α) = 3.79
H2β	2.47	C2	30.84	³ J(H4α-H3β) = 10.54	³ J(H9α-H8β) = 3.76
H3α	2.32	C3	27.63	² J(H3α-H3β) = 14.11	³ J(H9β-H8α) = 11.98
H3β	2.29	C4	53.96	³ J(H3α-H2α) = 5.45	³ J(H9β-H8β) = 5.95
H4	4.87	C5	209.80	³ J(H3α-H2β) = 10.92	² J(H8α-H8β) = 11.87
6-CH ₃	1.49	C6	80.48	² J(H2α-H2β) = 16.53	³ J(H8α-H7α) = 5.80
6-OH	2.11	6-CH ₃	29.85	³ J(H2α-H3β) = 4.07	³ J(H8α-H7β) = 12.04
H7α	1.47	C7	41.62	³ J(H2β-H3β) = 3.63	³ J(H8β-H7α) = 12.43
H7β	1.97	C8	21.67	³ J(H10α-H9α) = 3.76	³ J(H8β-H7β) = 3.51
H8α	0.69	C9	33.20	³ J(H10α-H9β) = 11.37	² J(H7α-H7β) = 12.58
H8β	1.41	C10	53.41	² J(H9α-H9β) = 12.11	² J(H13α-H13β) = 11.13
H9α	1.73	C11	207.54		
H9β	2.18	C12	79.10		
H10	4.93	12-CH ₃	24.32		
12-CH ₃	1.49	C13	71.43		
12-OH	2.71				
H13α	3.88				
H13β	4.59				

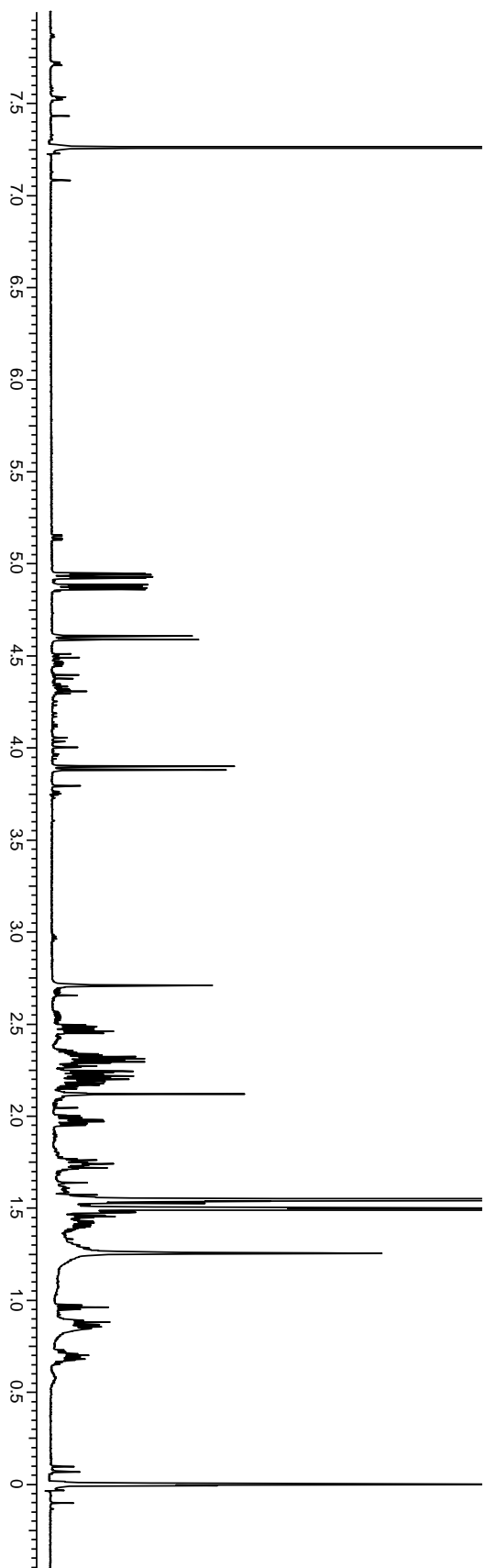
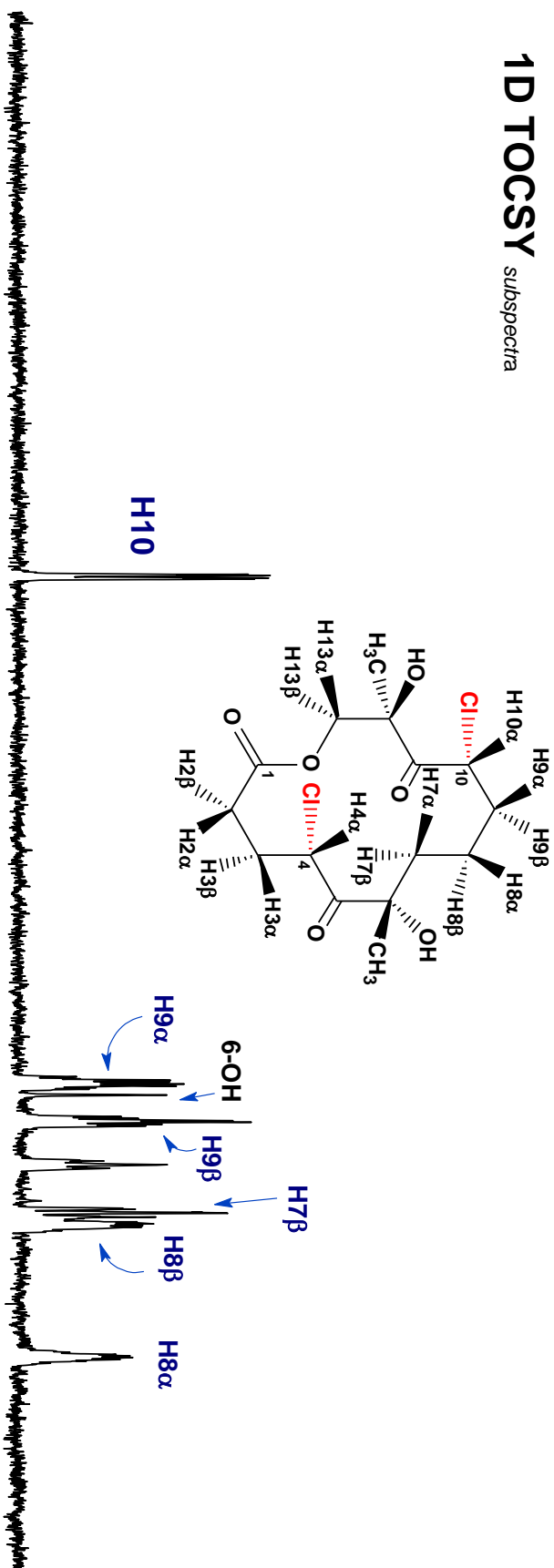


^1H NMR spectrum in CDCl_3 

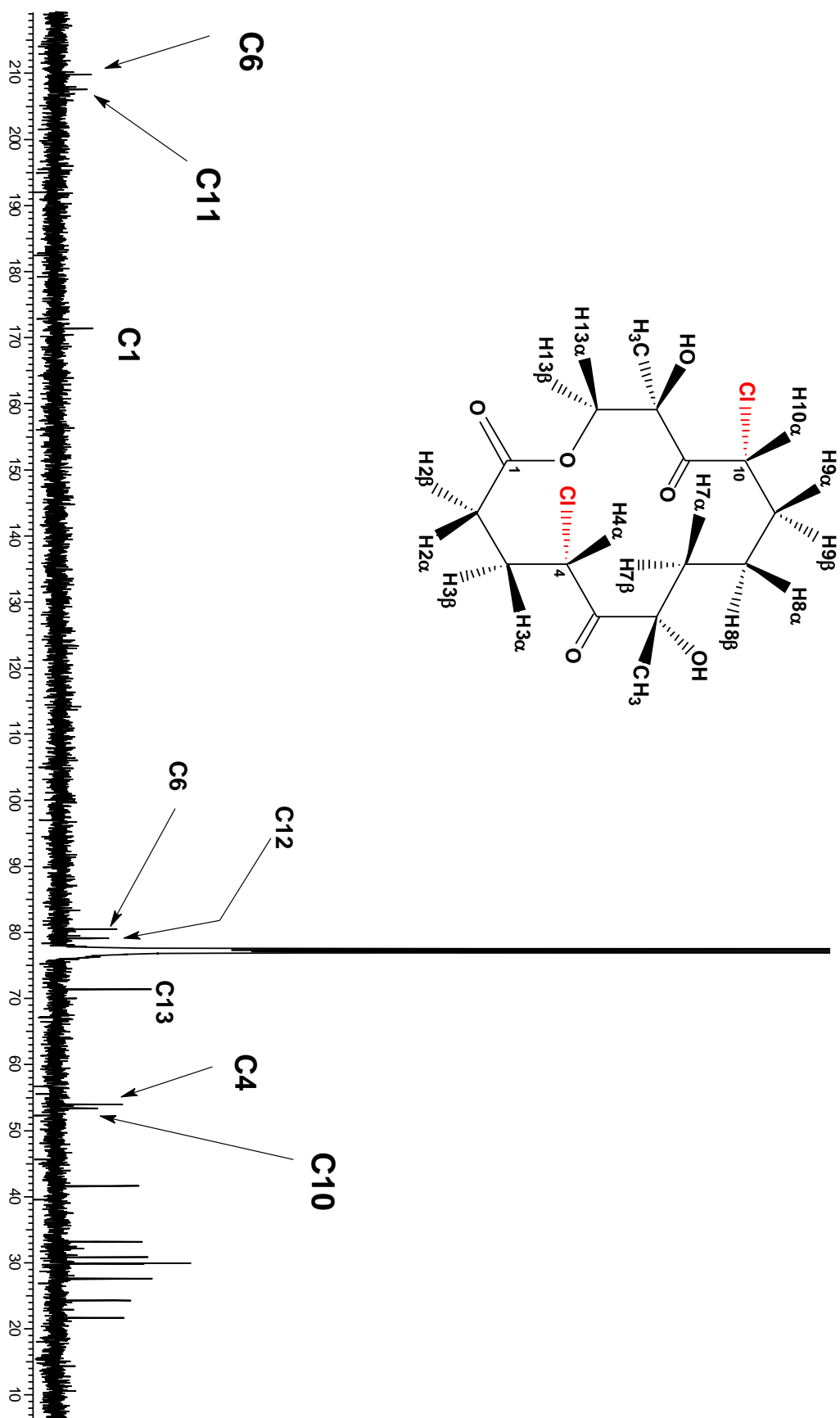
^1H NMR spectrum-----expansions

^1H NMR spectrum-----expansion

1D TOCSY *subspectra*

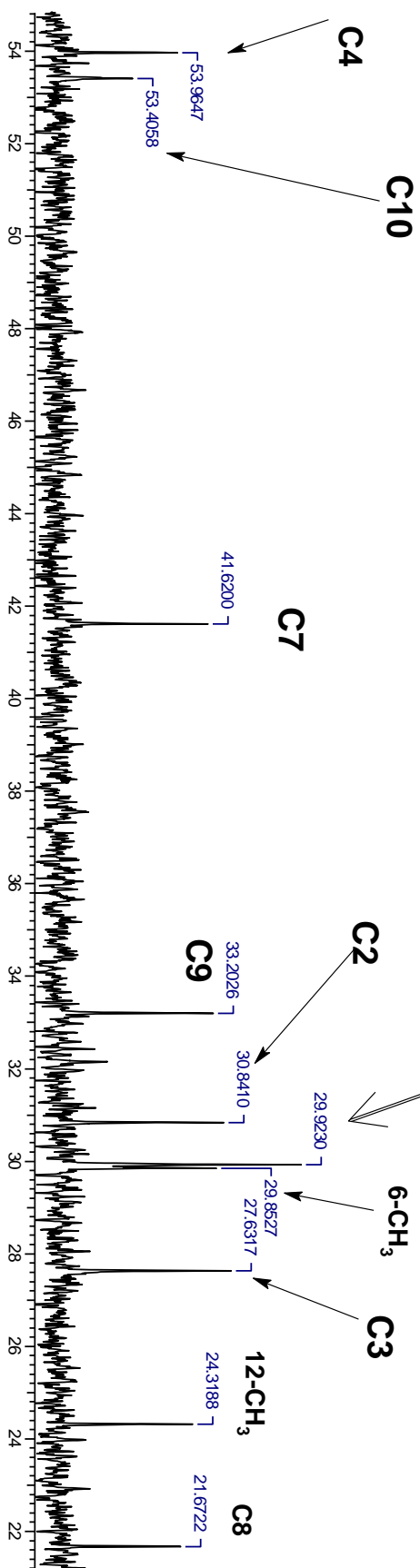
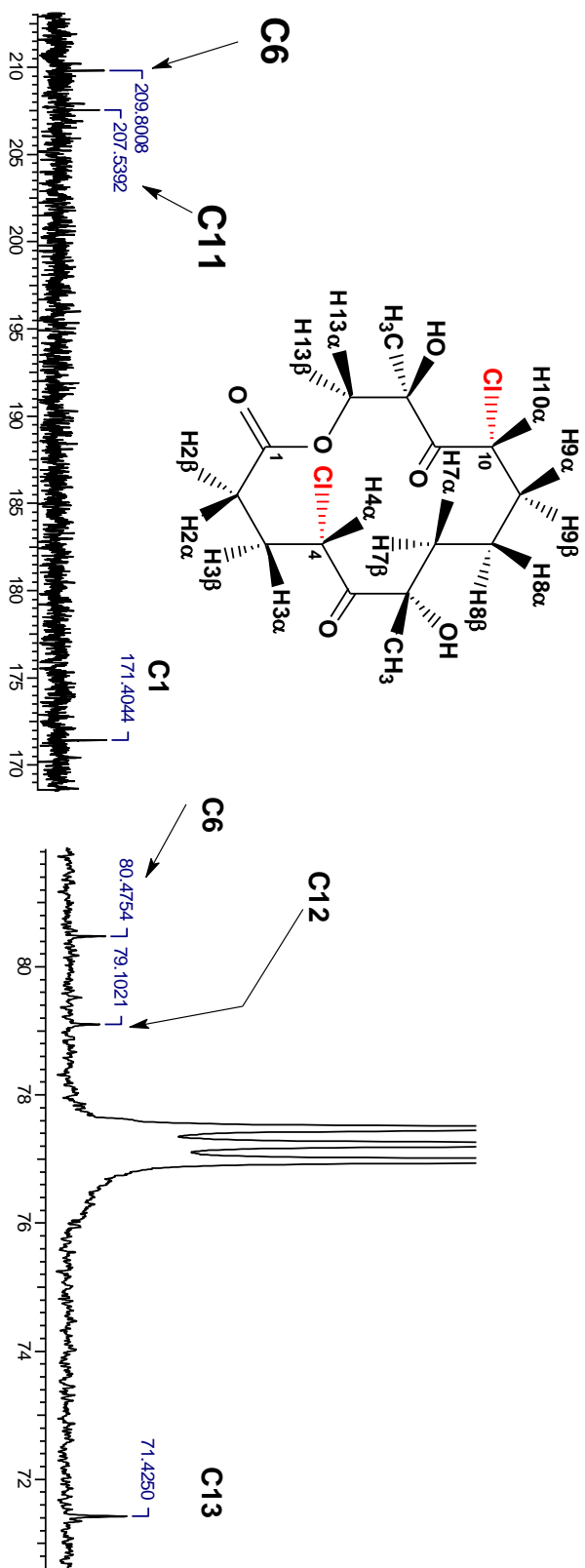


¹³C NMR spectrum in CDCl₃

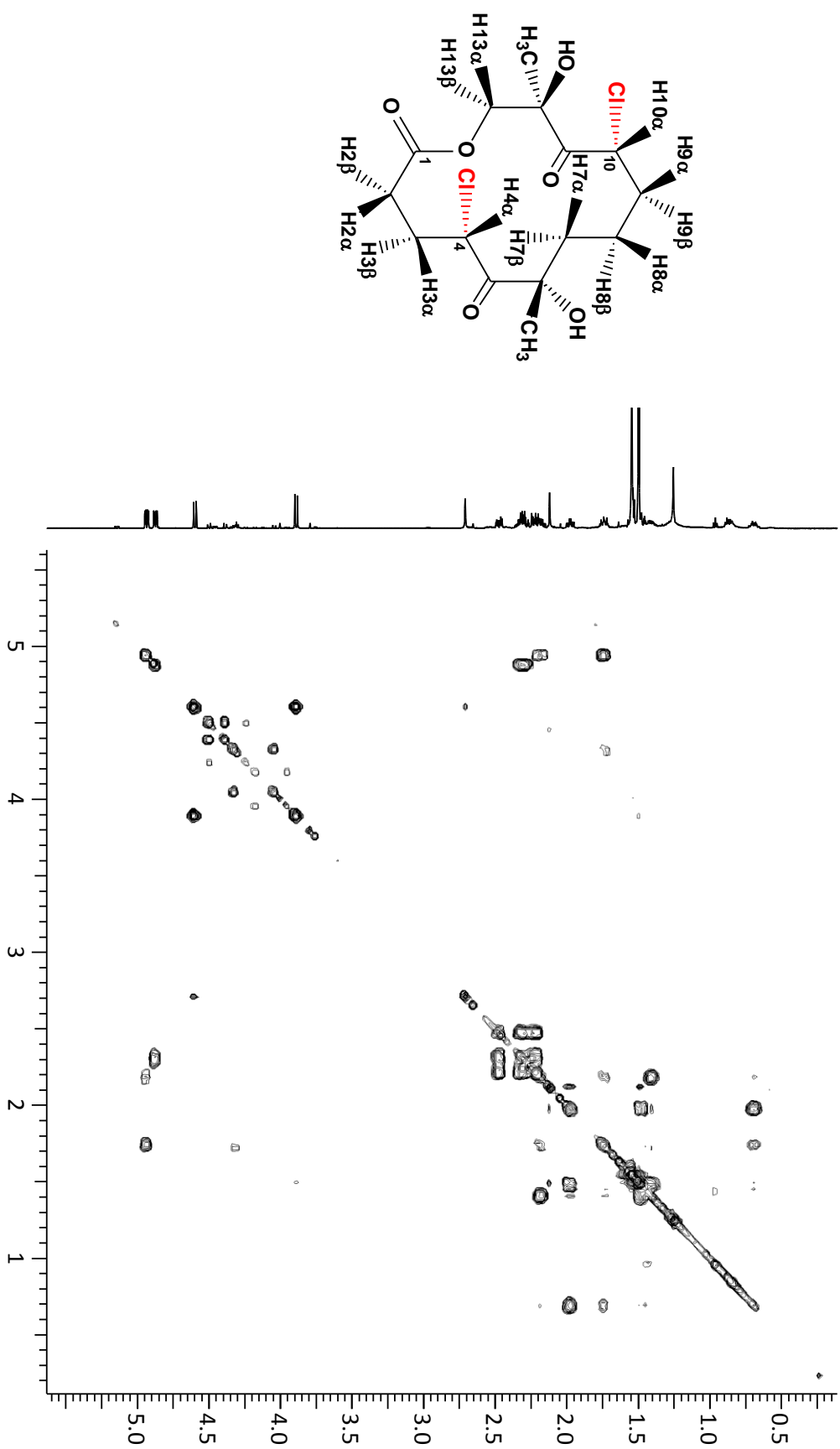


¹³C NMR spectrum in CDCl₃

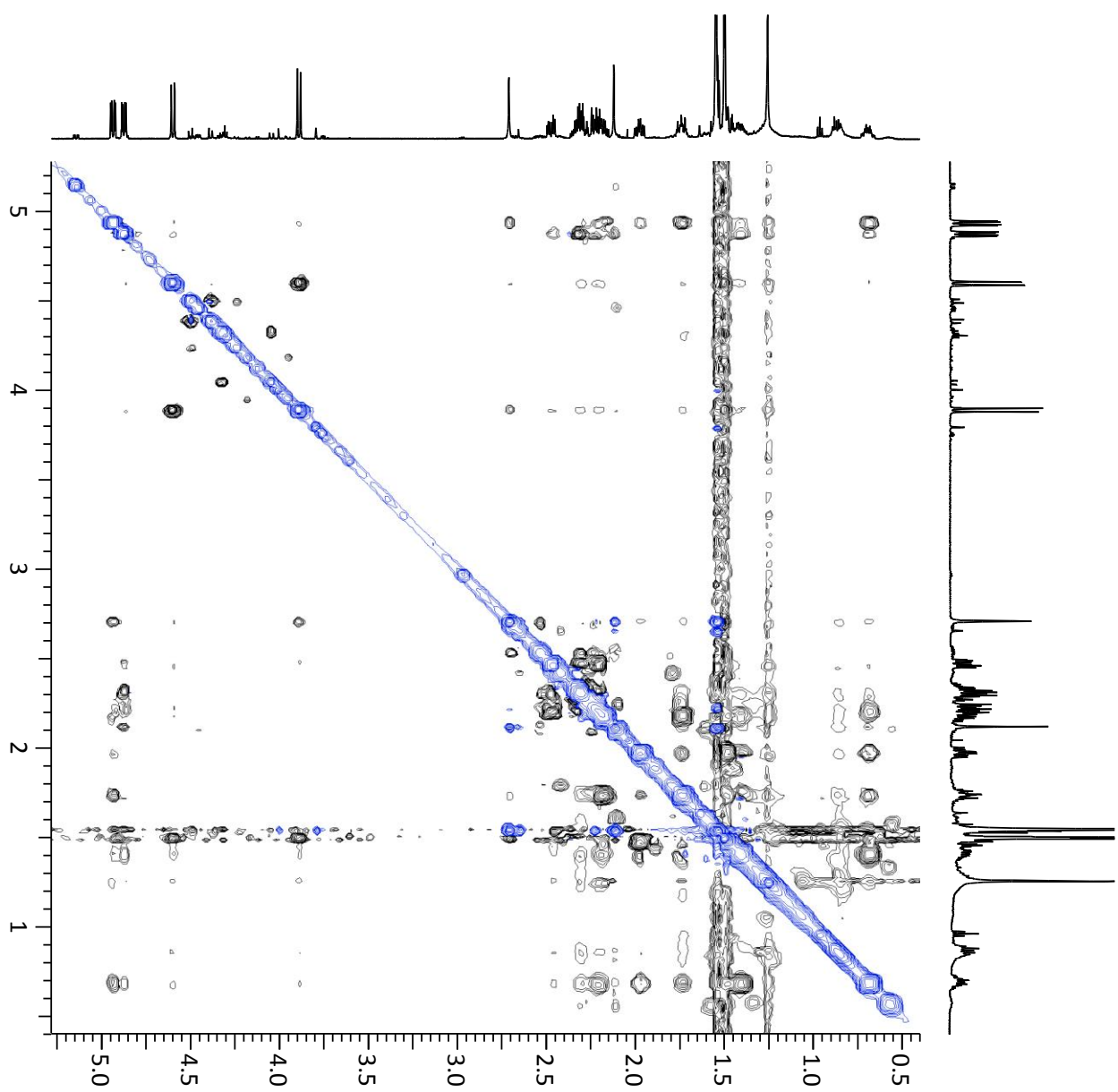
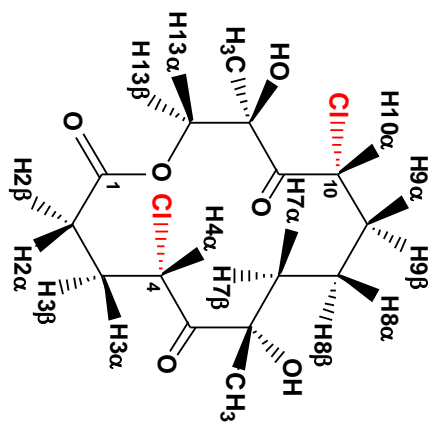
Expansions



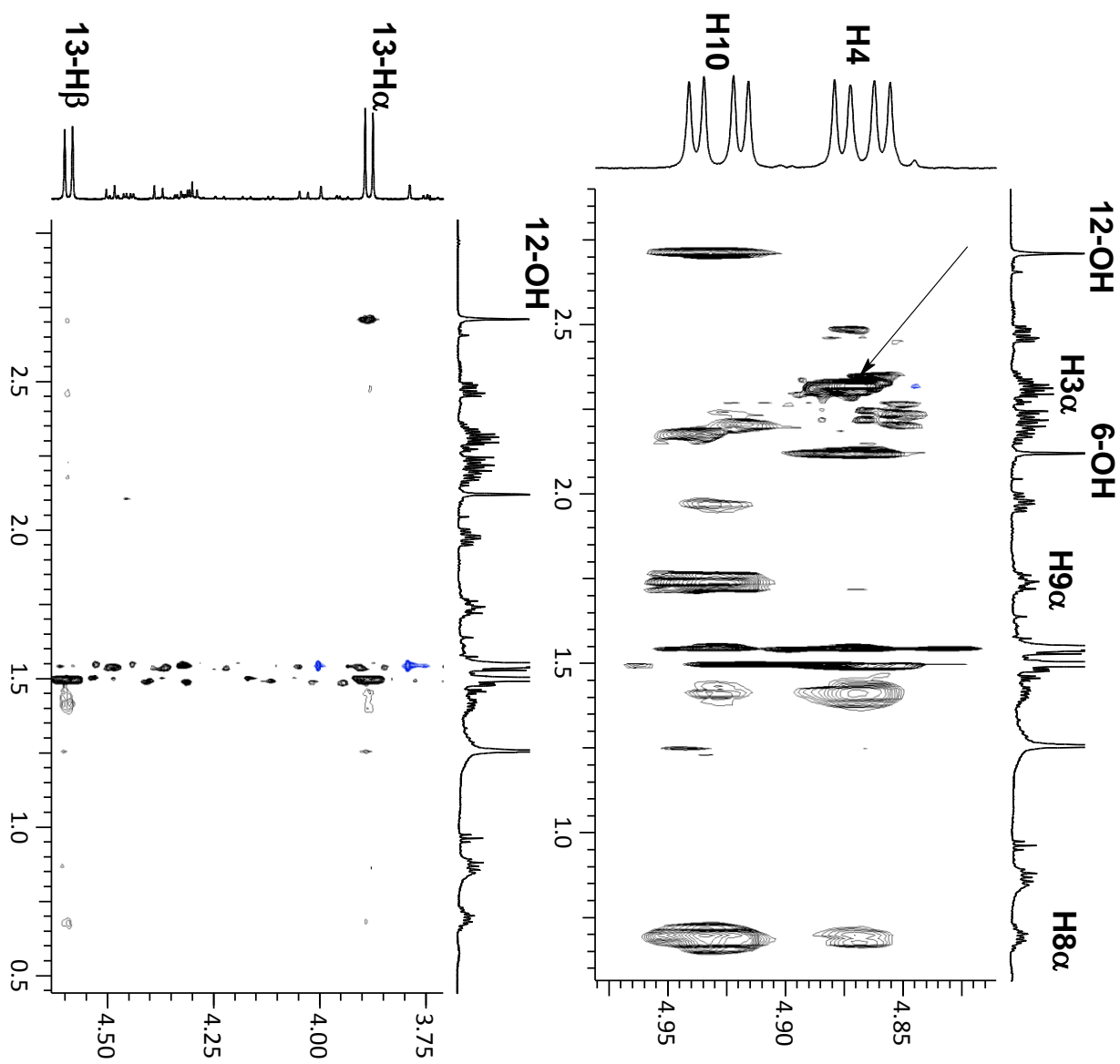
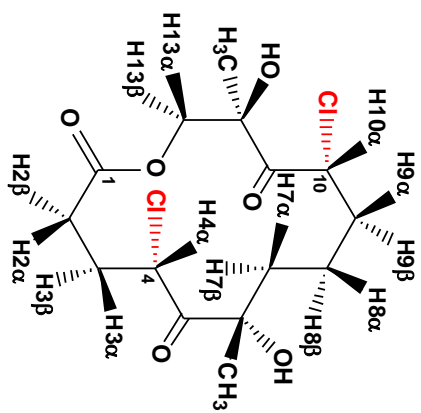
gCOSY



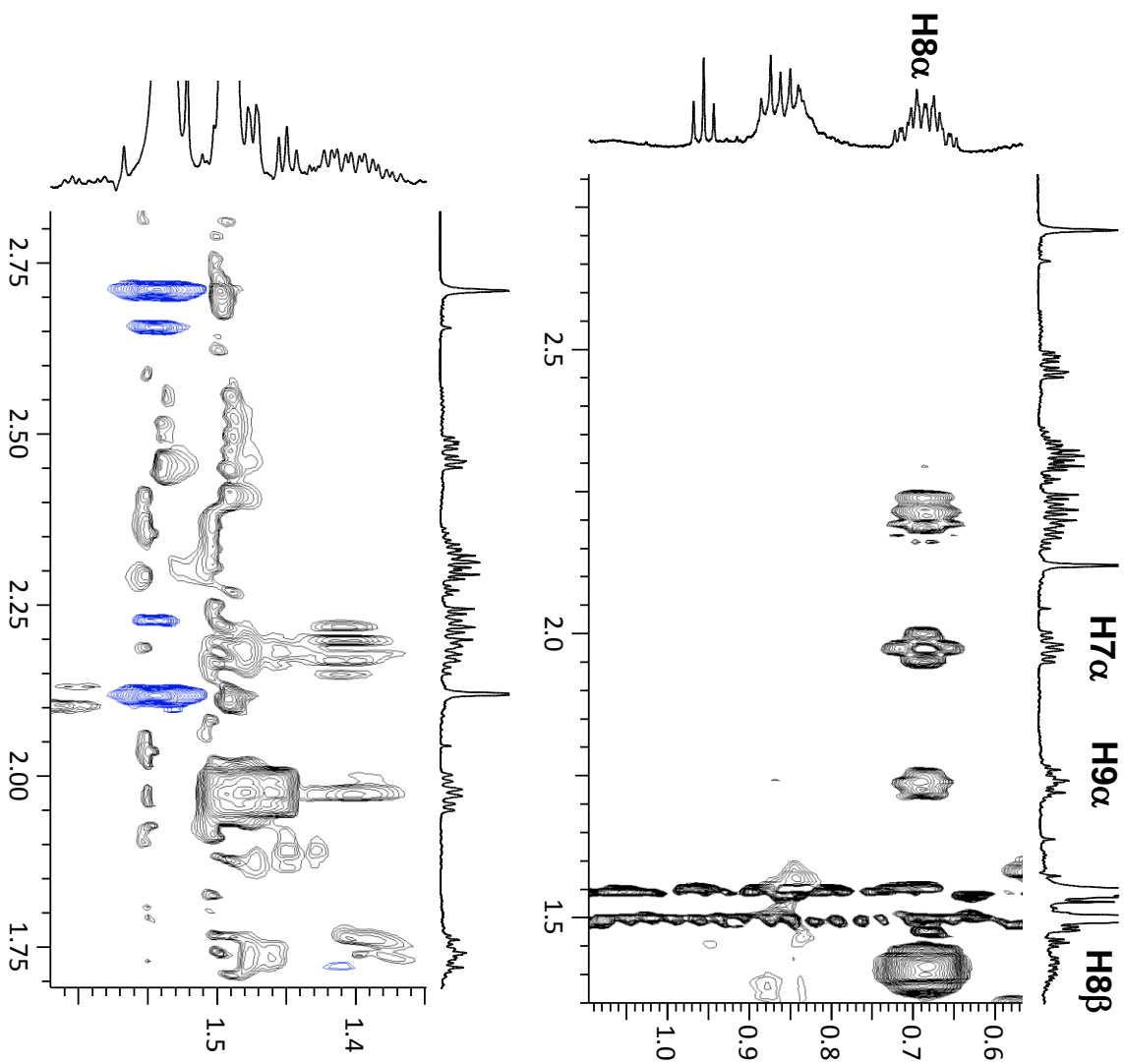
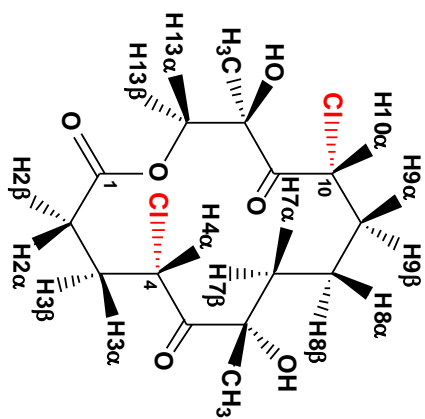
NOESY



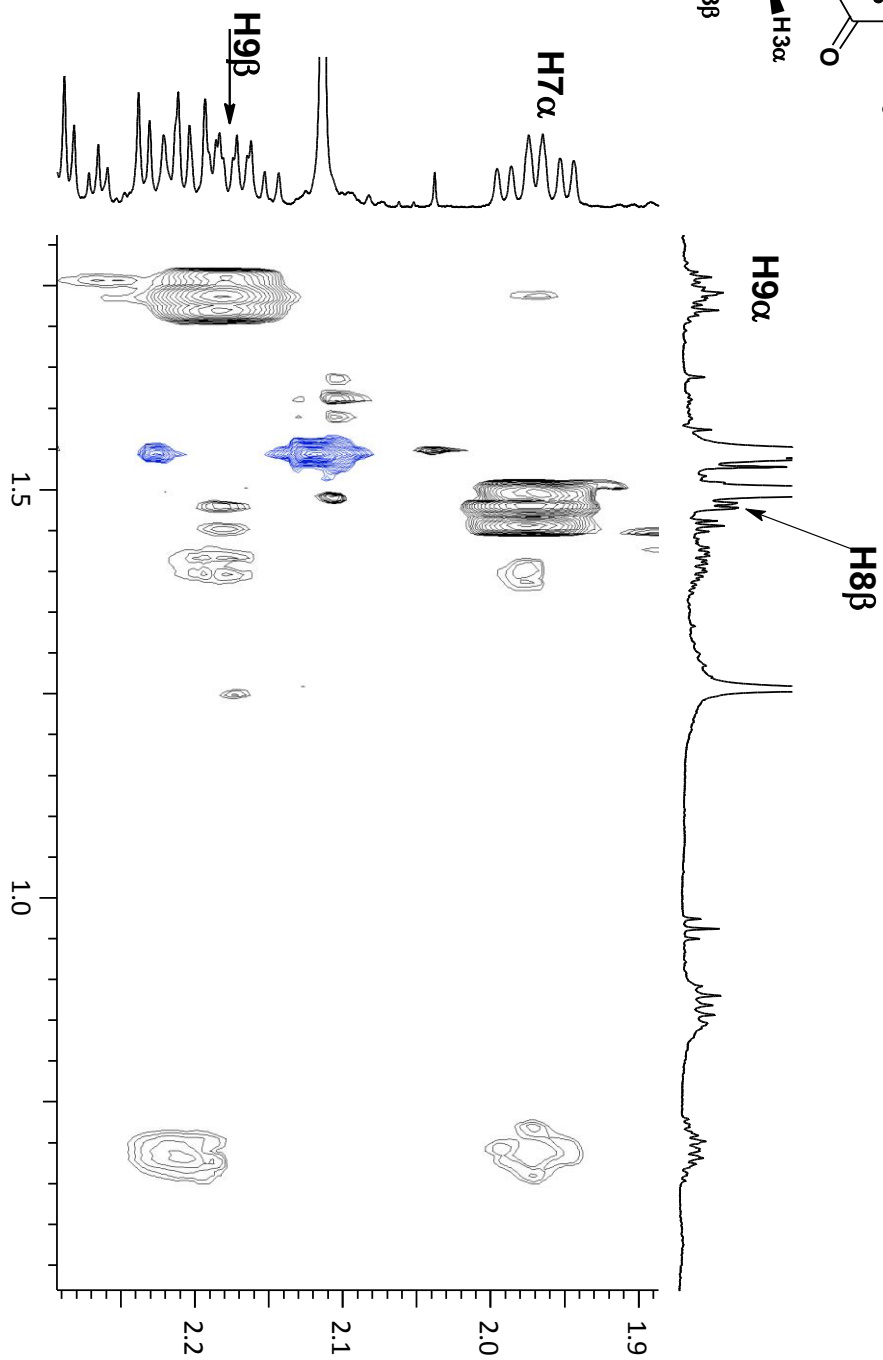
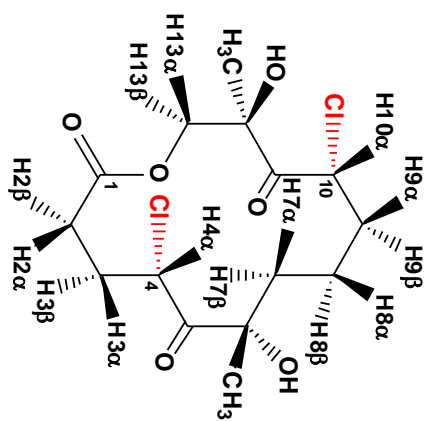
NOESY expansions



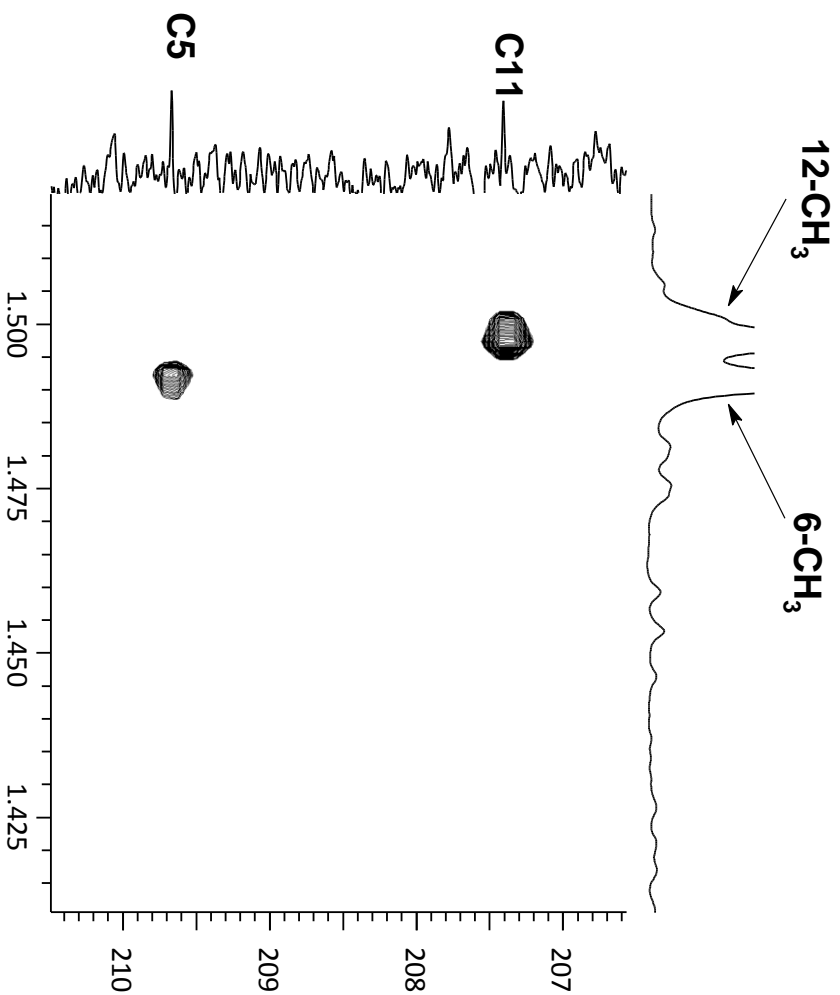
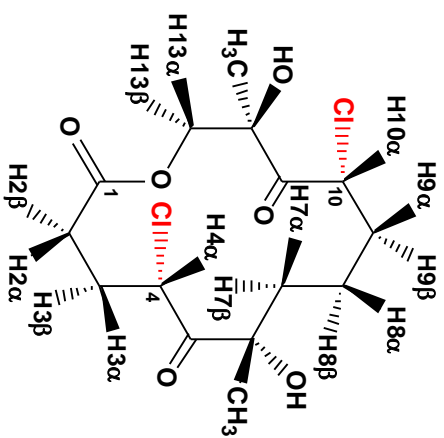
NOESY expansions



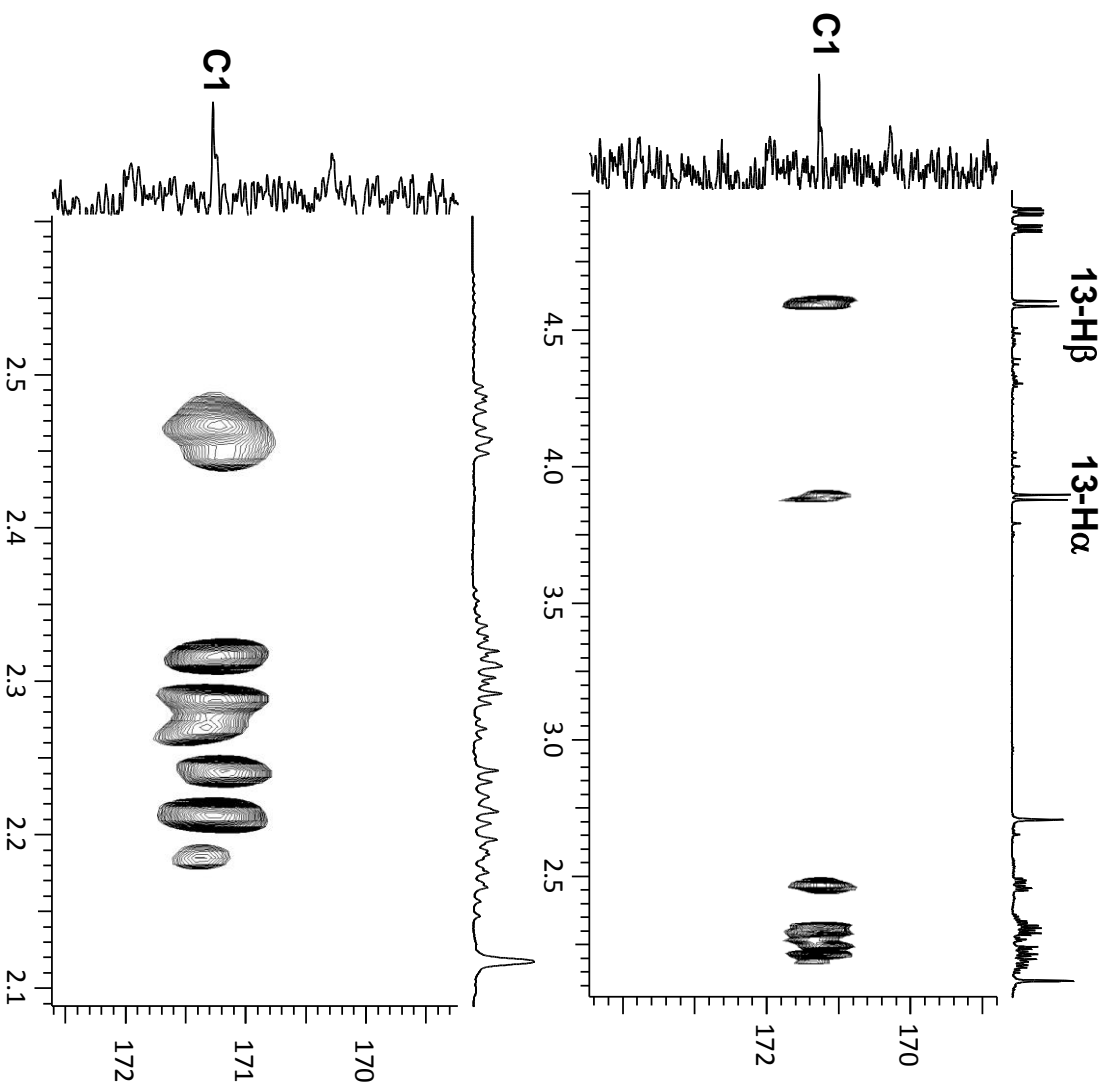
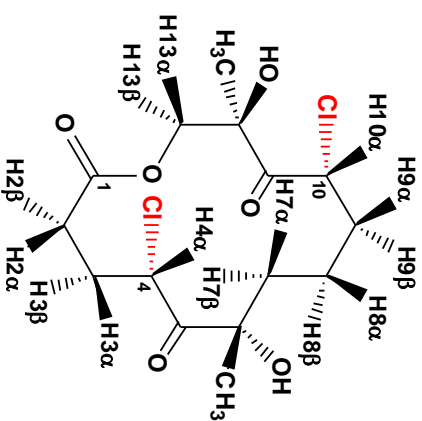
NOESY expansion



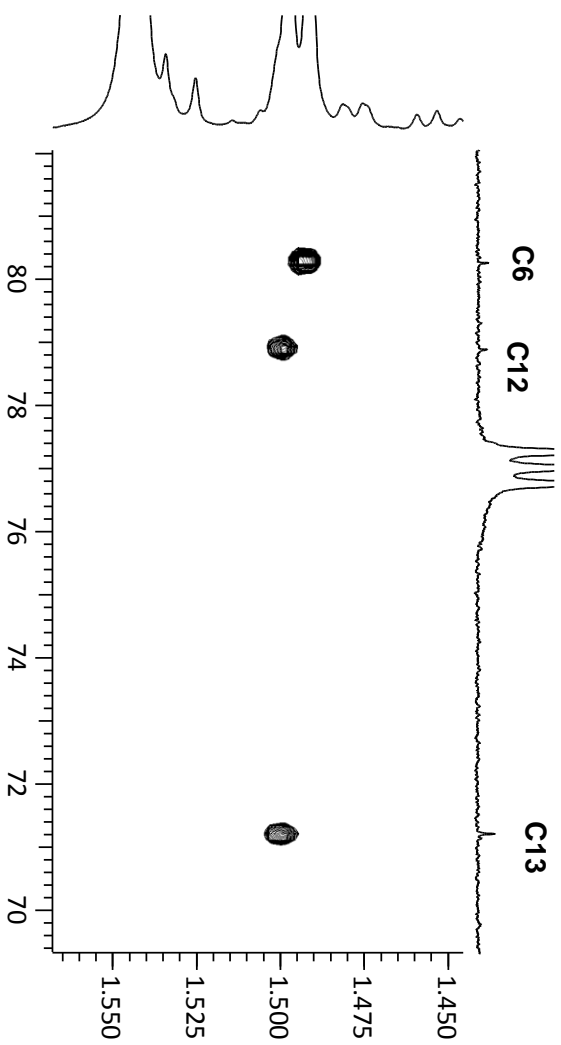
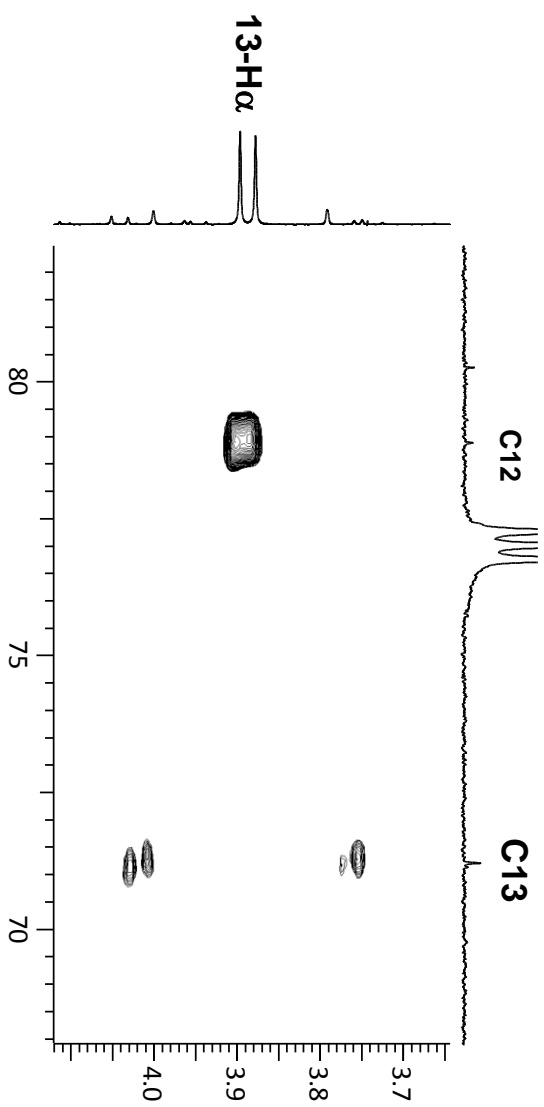
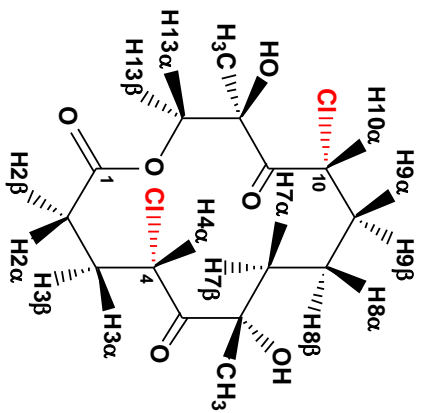
gHMBC long-range correlations

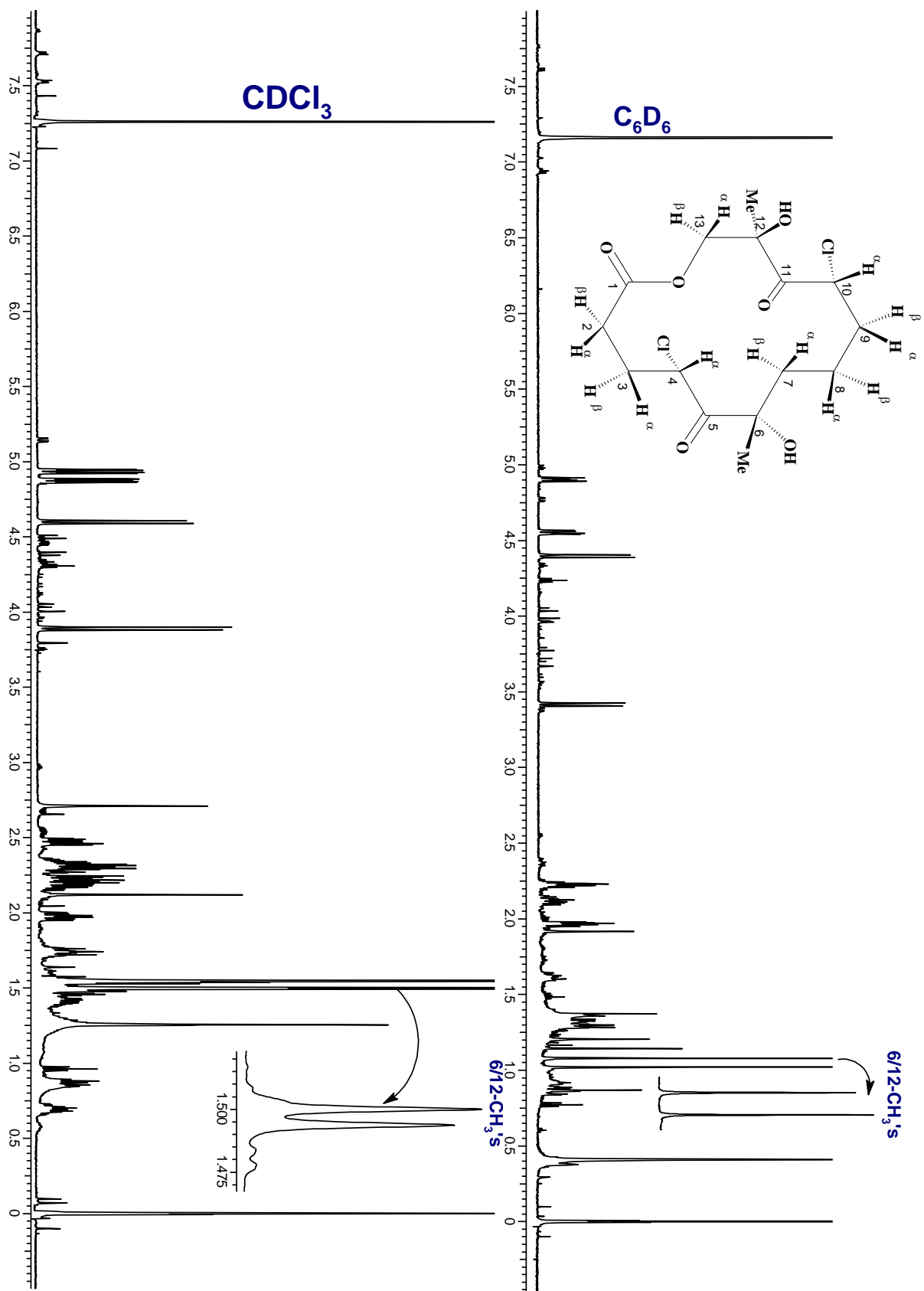


gHMBC long-range correlations

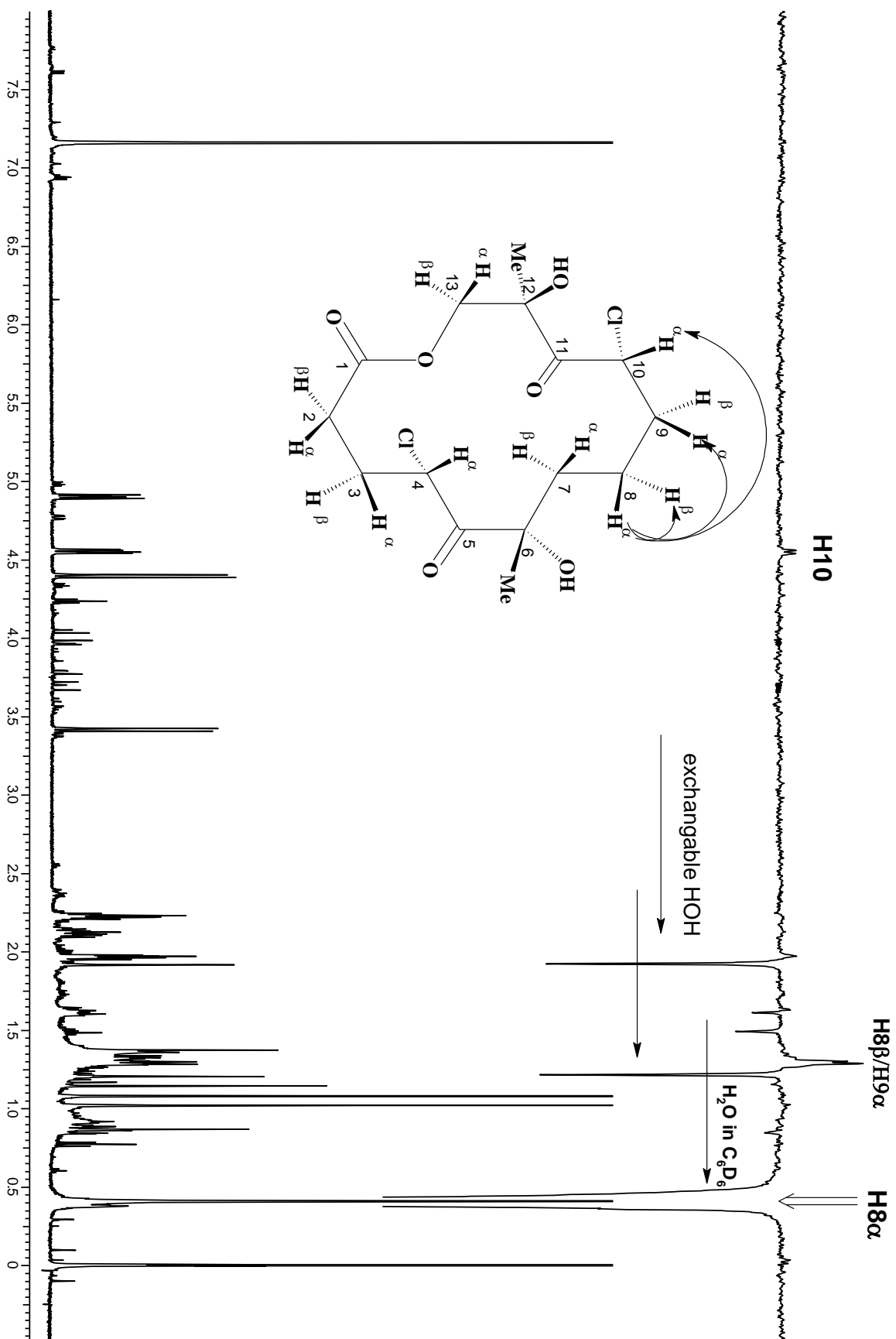


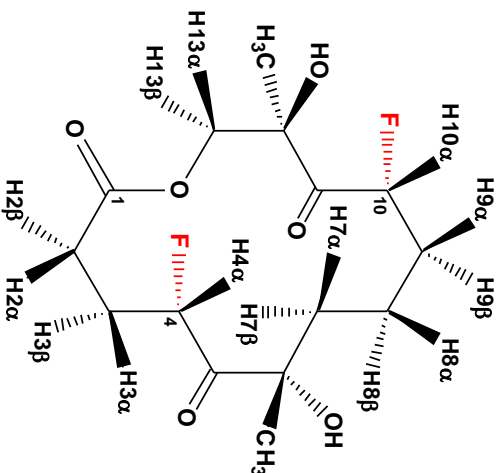
gHMBC long-range correlations





1D NOESY spectrum in Benzene-d₆



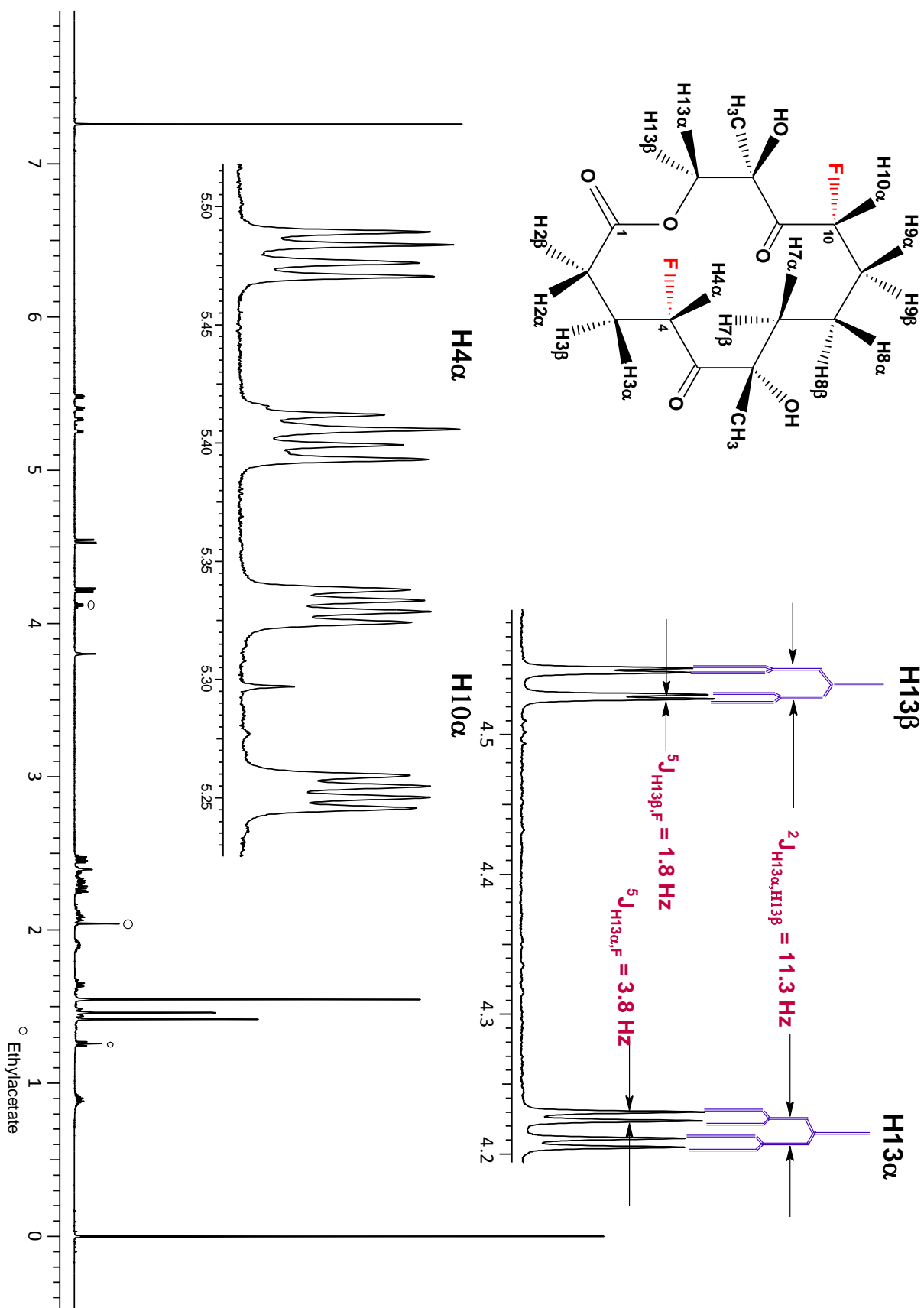


¹H and ¹³C NMR Chemical shifts (δ/ppm) and Coupling constants (J/Hz)

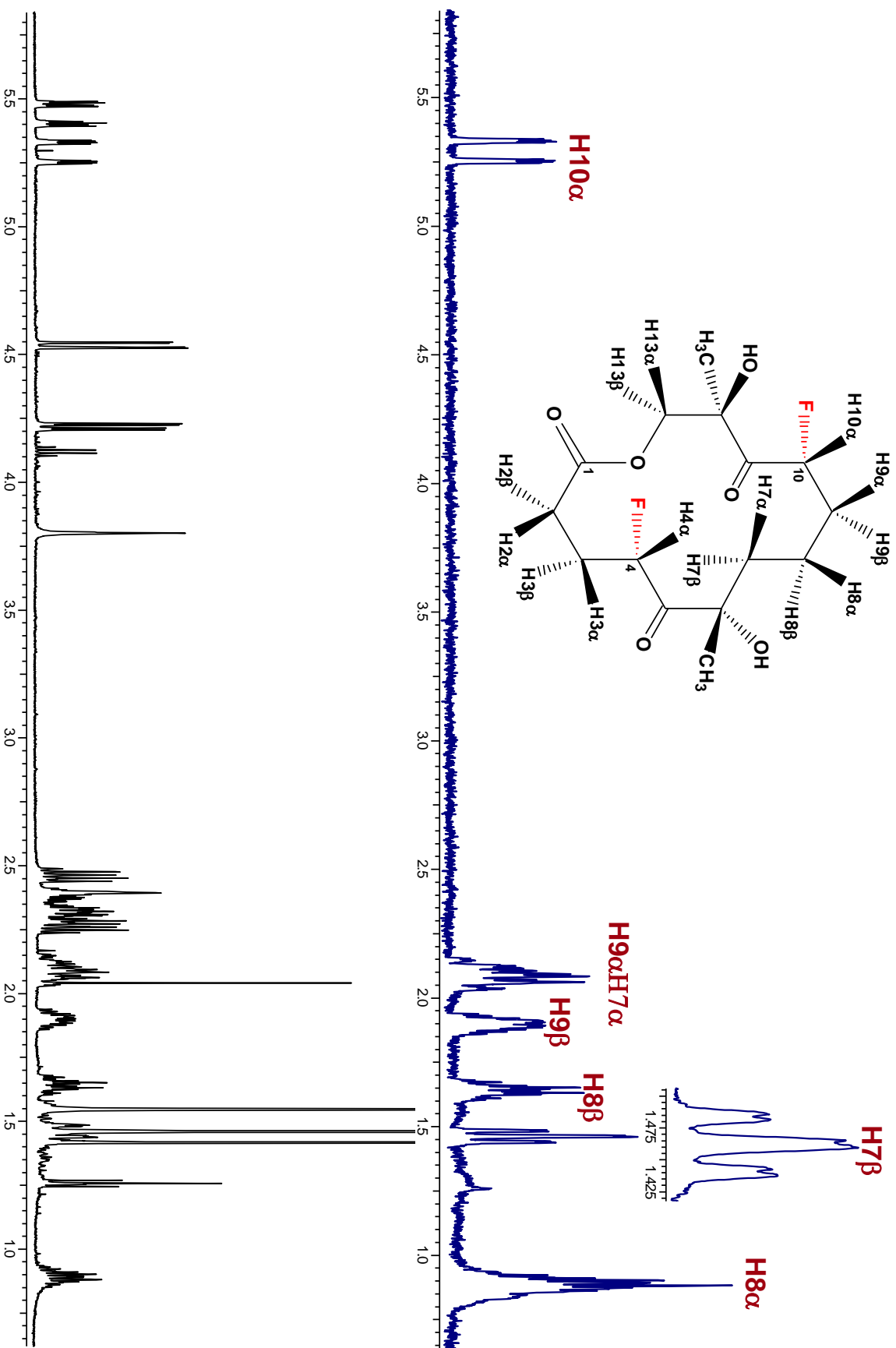
H2α	2.26
H2β	2.46
H3α	2.29
H3β	2.35
H4α	5.43
6-CH ₃	1.46
6-OH	3.80
H7α	2.08
H7β	1.46
H8α	0.89
H8β	1.64
H9α	2.08
H9β	1.89
H10α	5.28
12-CH ₃	1.46
12-OH	3.80
H13α	4.22
H13β	4.54

² J(H2α-H2β) = 15.52
³ J(H2α-H3α) = 5.42
³ J(H2α-H3β) = 7.55
³ J(H2β-H3α) = 7.19
³ J(H2β-H3β) = 6.84
² J(H3α-H3β) = 14.16
³ J(H3α-H4β) = 8.14
³ J(H3α-F) = 8.83
³ J(H3β-H4α) = 3.25
³ J(H3β-F) = 37.82
² J(H4α-F) = 46.39
² J(H7α-H7β) = 13.27
³ J(H7α-H8α) = 4.79
³ J(H7α-H8β) = 12.41
³ J(H7β-H8α) = 12.67
³ J(H7β-H8β) = 3.74
² J(H8α-H8β) = 12.23
³ J(H8α-H9α) = 4.54
³ J(H8α-H9β) = 12.12
³ J(H8β-H9α) = 12.60
³ J(H8β-H9β) = 4.44
² J(H9α-H9β) = 14.49
³ J(H9α-F) = 39.50
³ J(H9α-H10α) = 2.69
³ J(H9β-F) = 10.13
³ J(H9β-H10α) = 5.73
² J(H10α-F) = 47.05

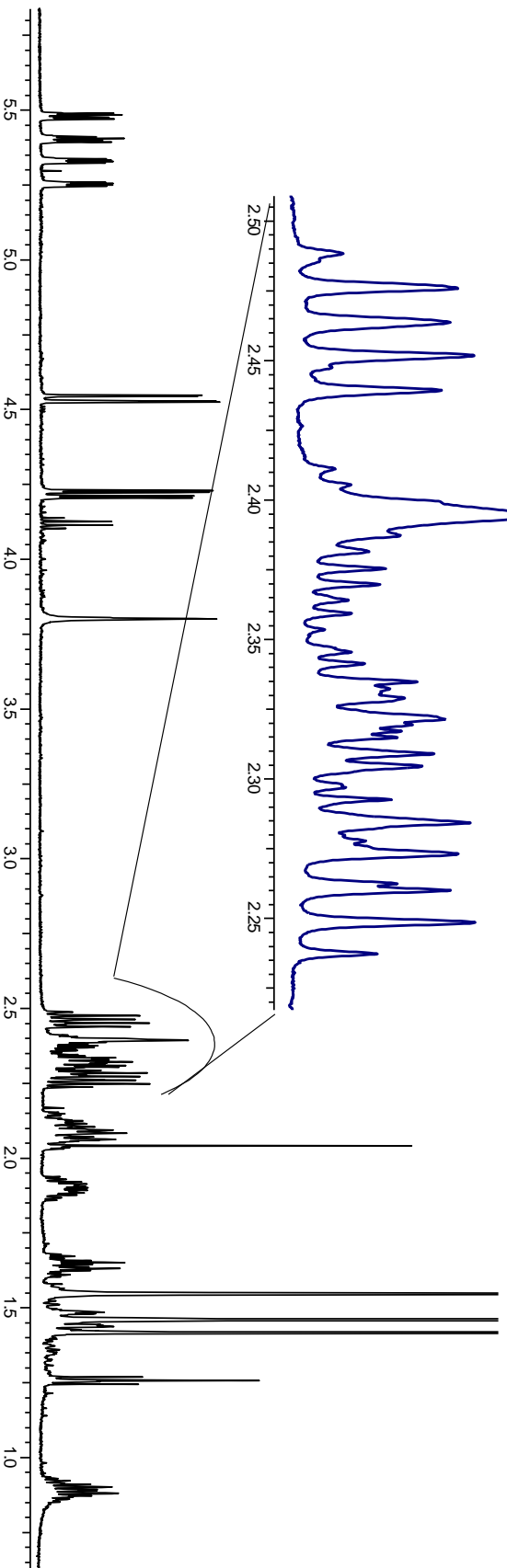
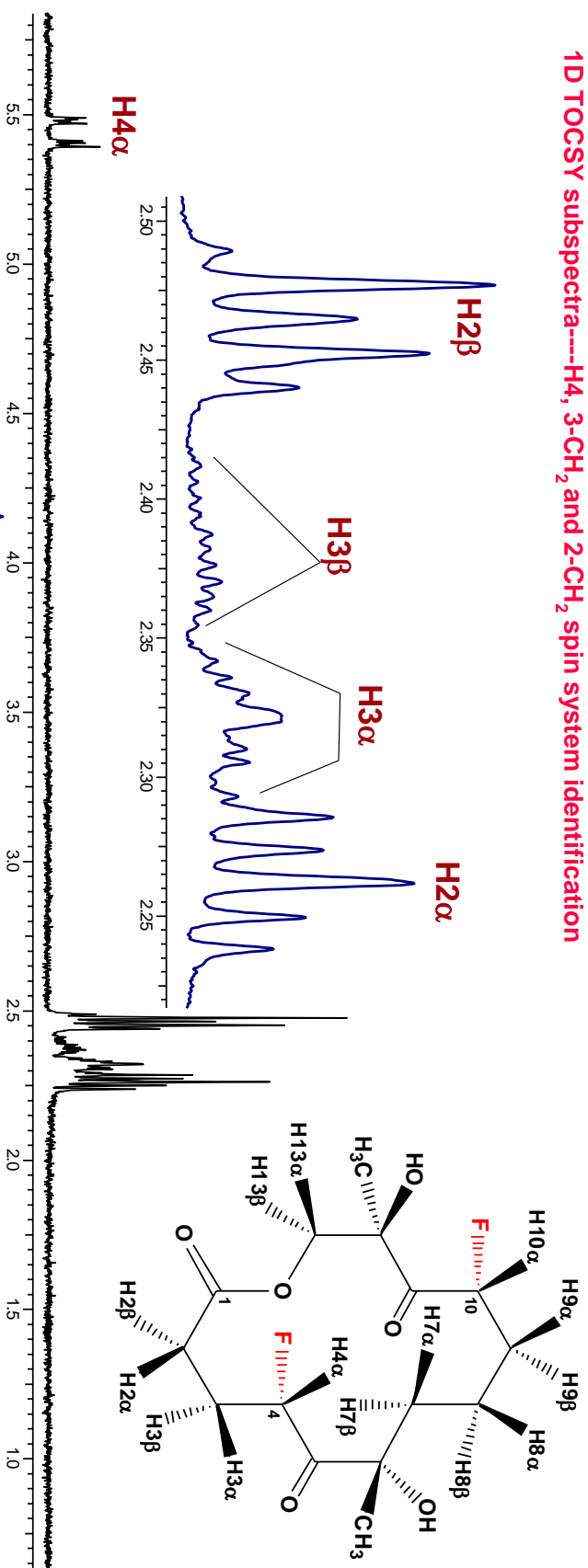
C1	171.74
C2	28.16
C3	24.99
C4	90.91
C5	209.92
C6	80.11
6-CH ₃	27.95
C7	40.43
C8	17.38
C9	31.71
C10	94.93
C11	209.36
C12	78.49
12-CH ₃	21.08
C13	69.15



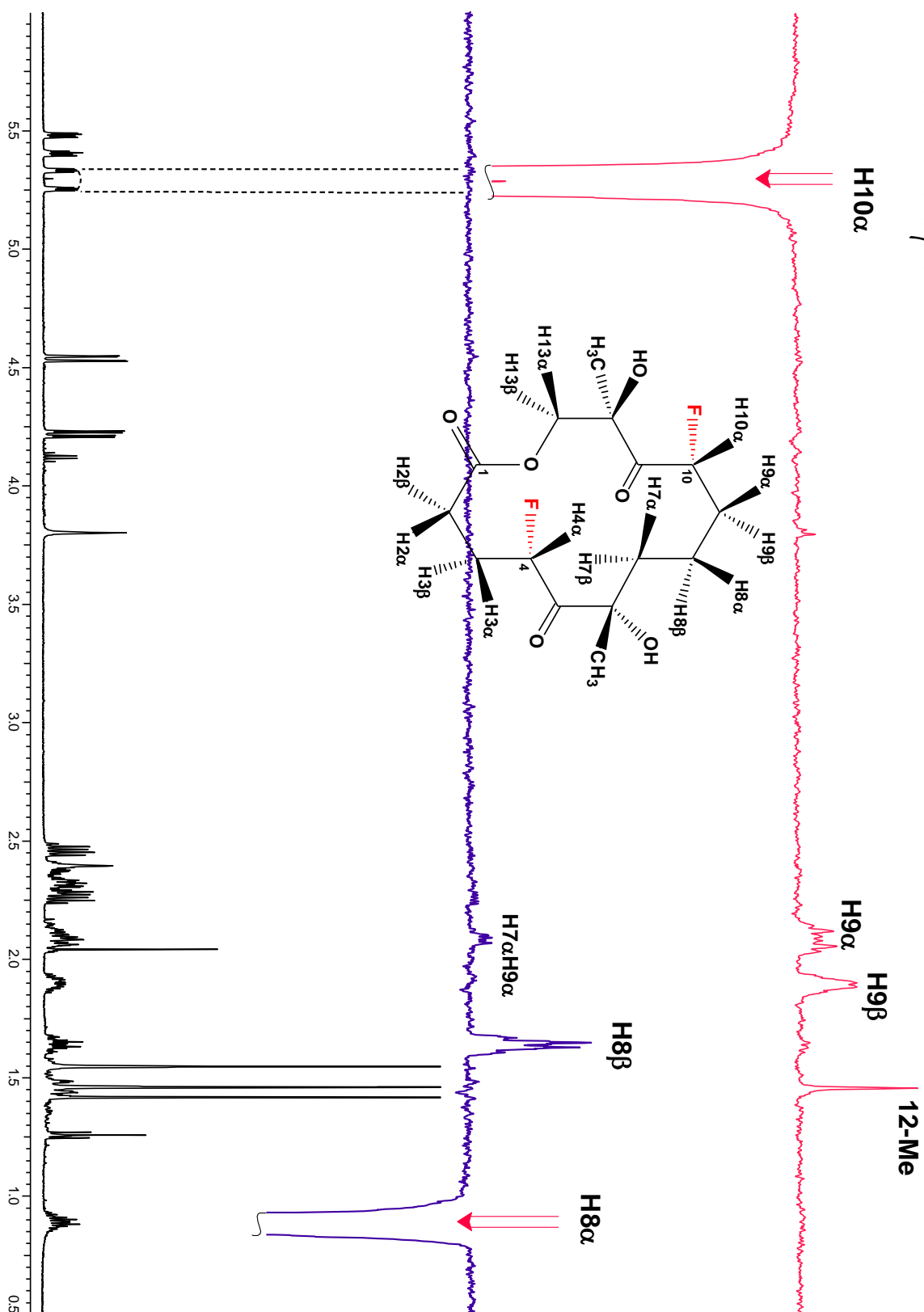
1D TOCSY subspectra-----H10, 9-CH₂, 8-CH₂ and 7-CH₂ spin system identification



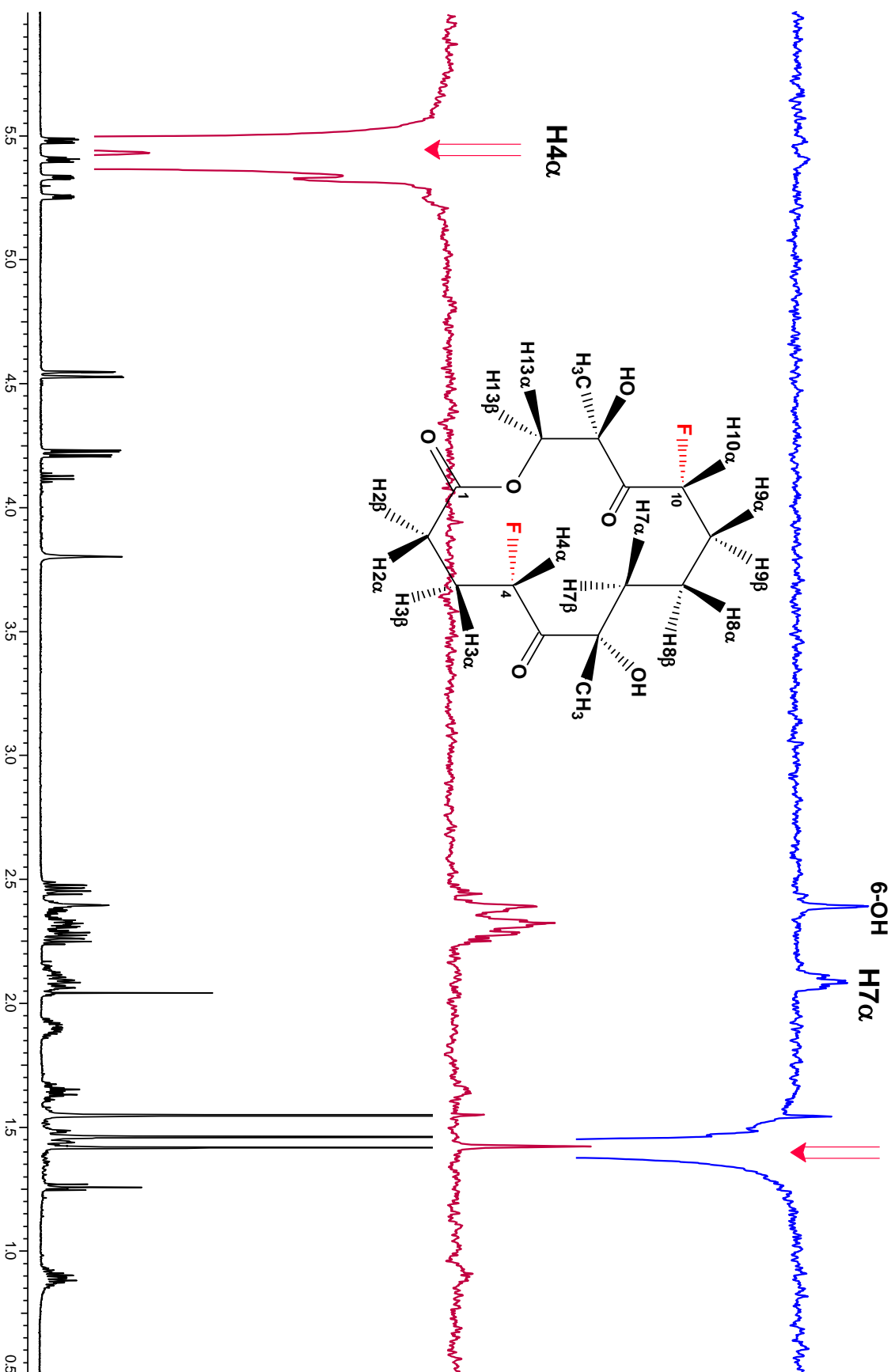
1D TOCSY subspectra-----H4, 3-CH₂ and 2-CH₂ spin system identification



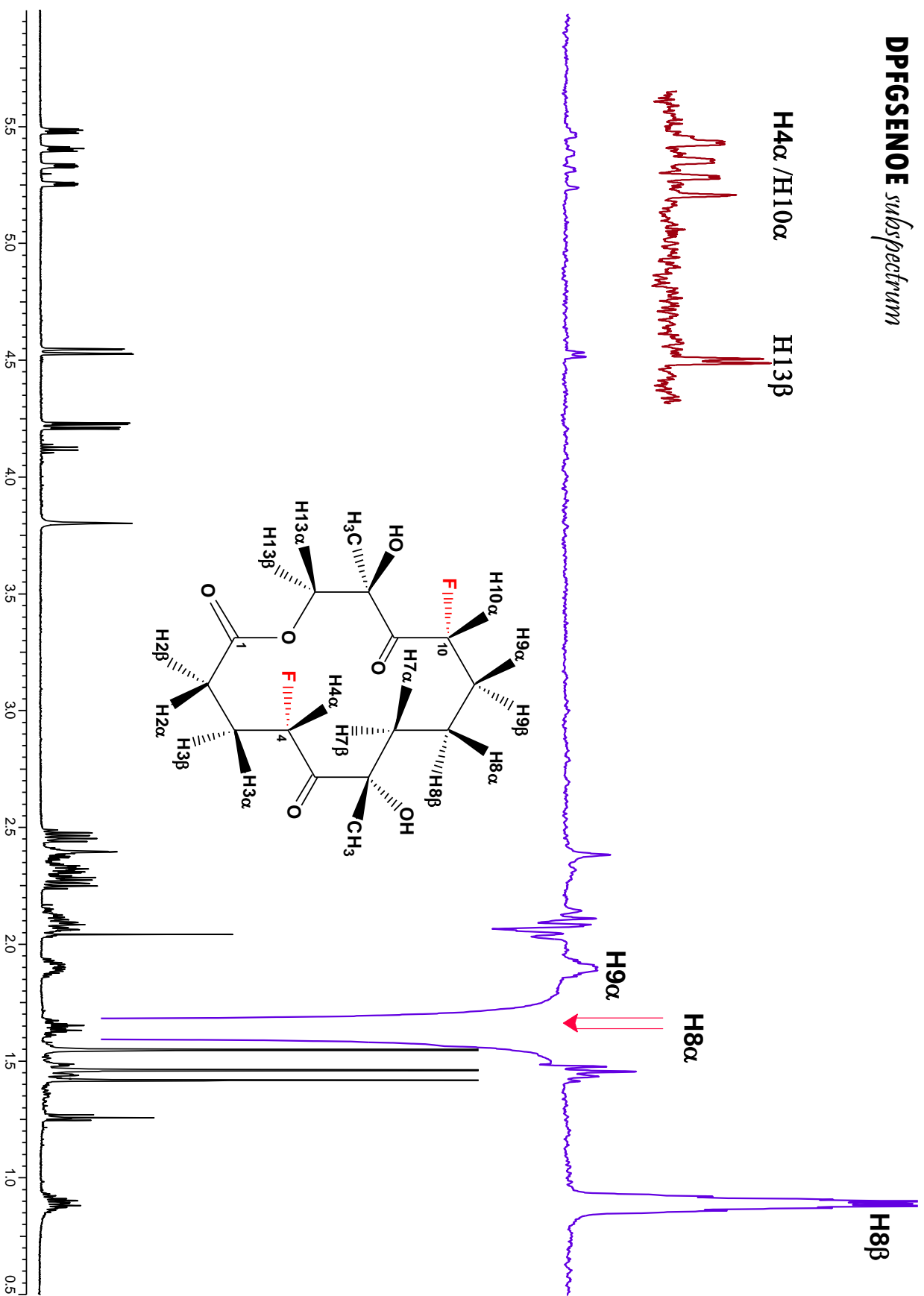
DPFGSENOE subspectra

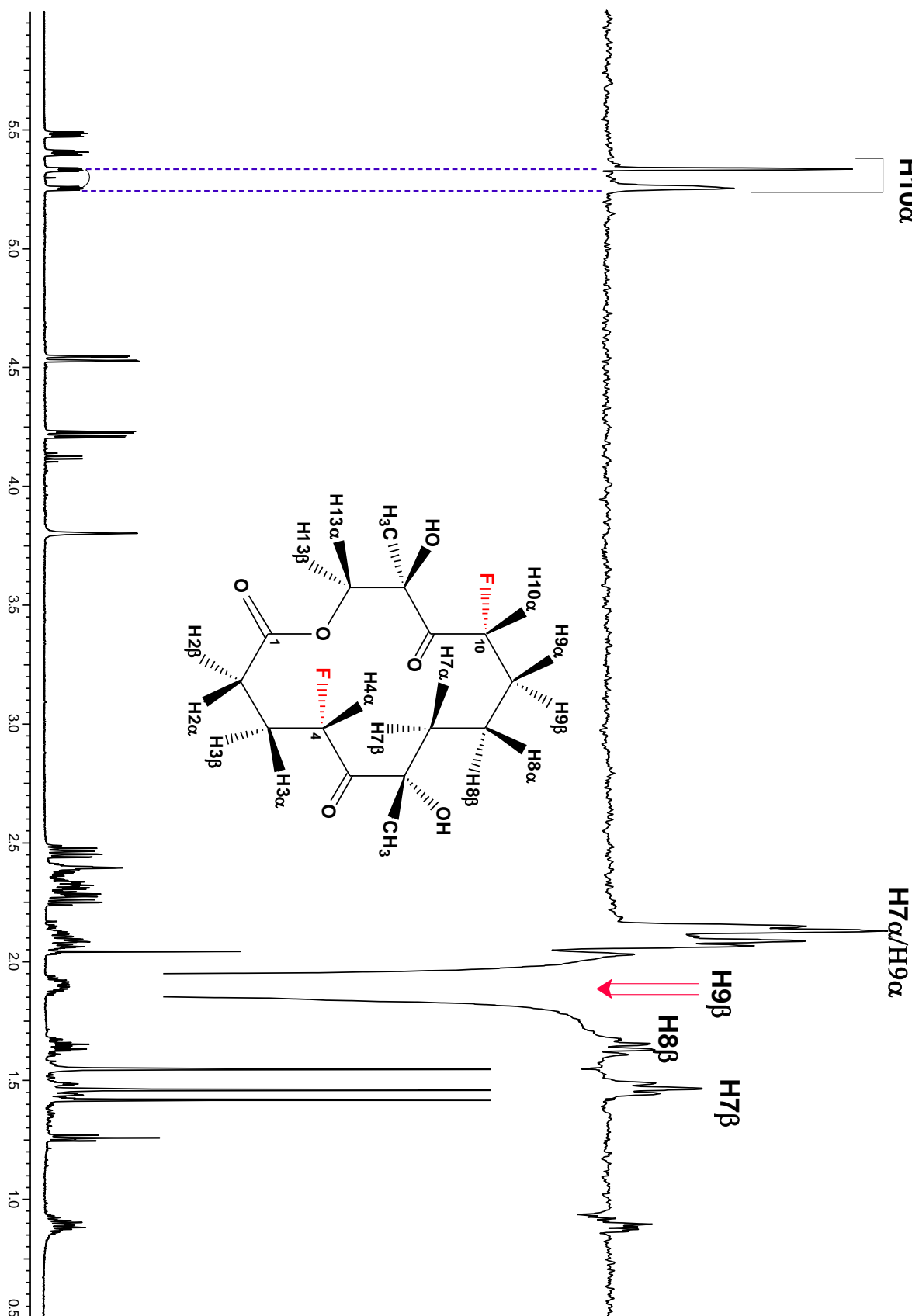


DPFGSENOE subspectra

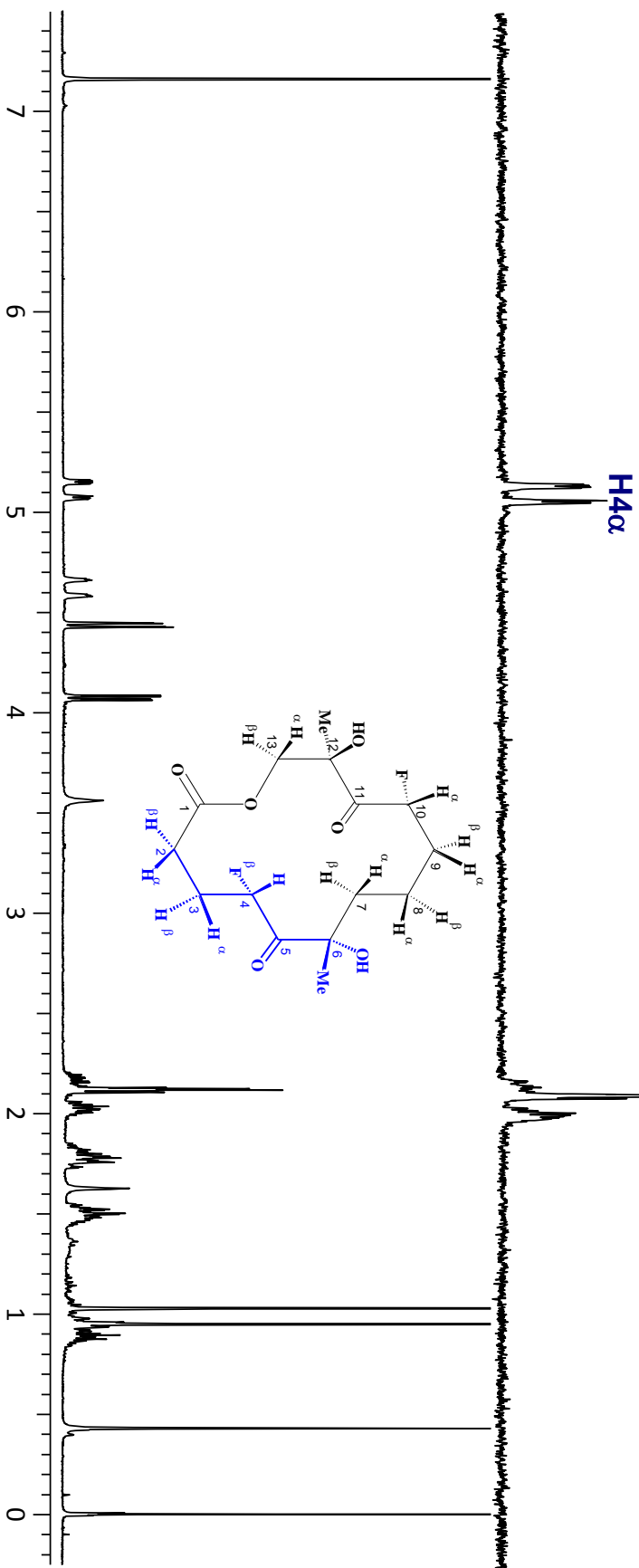
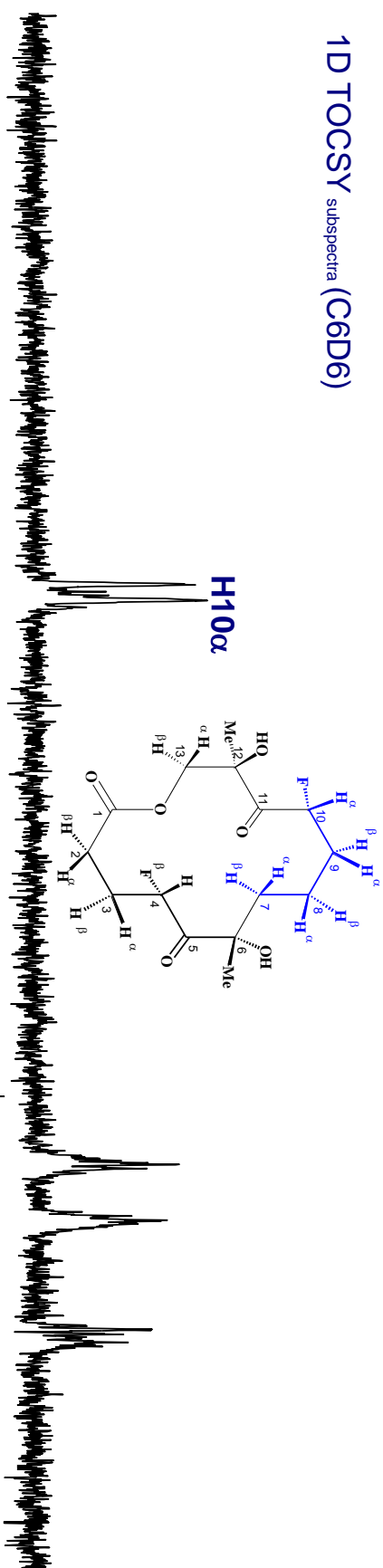


DPFGSENOE *subspectrum*

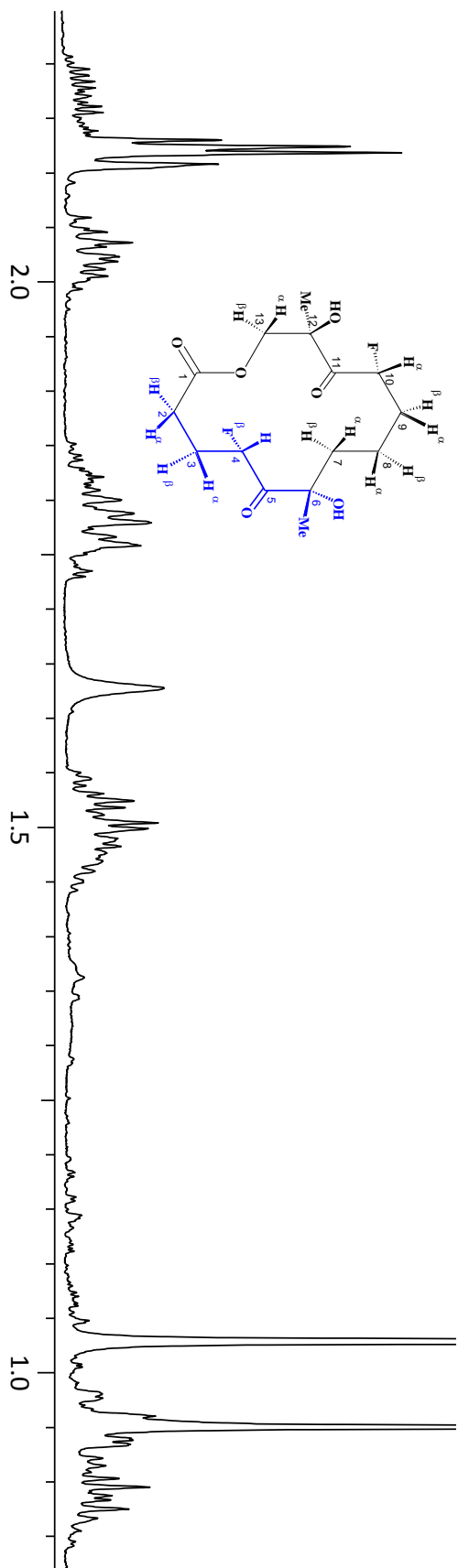
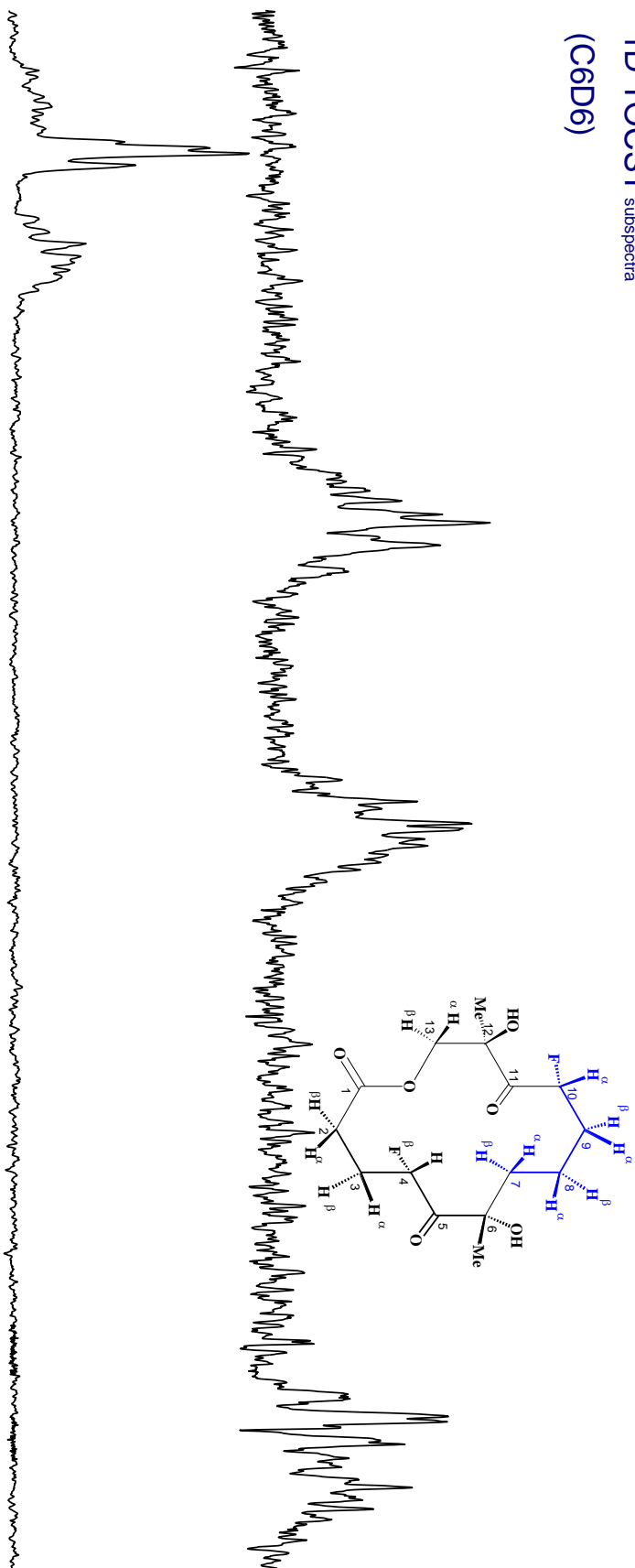


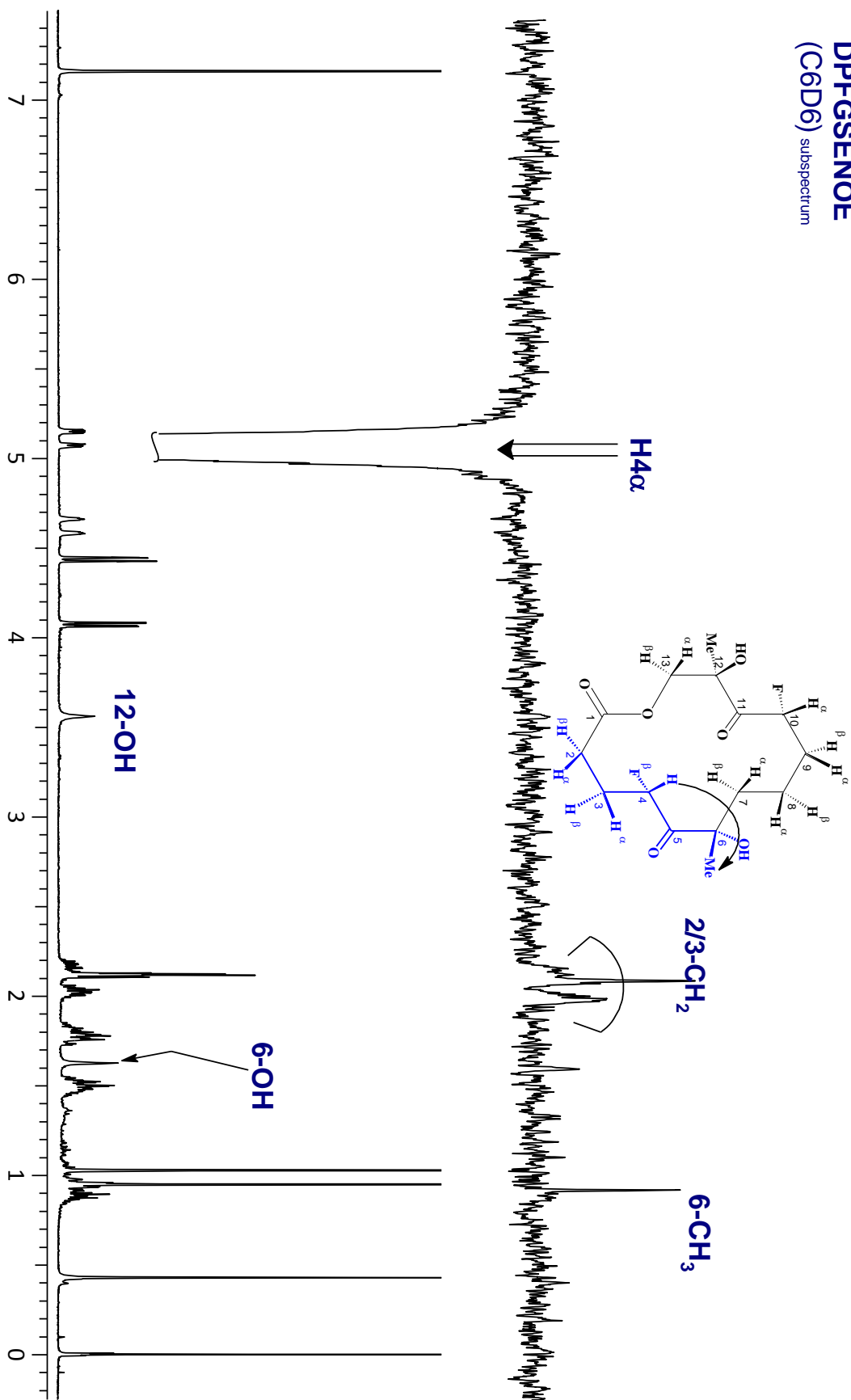
DPFGSENOE *sub spectrum*
H10 α 

1D TOCSY subspectra (C6D6)

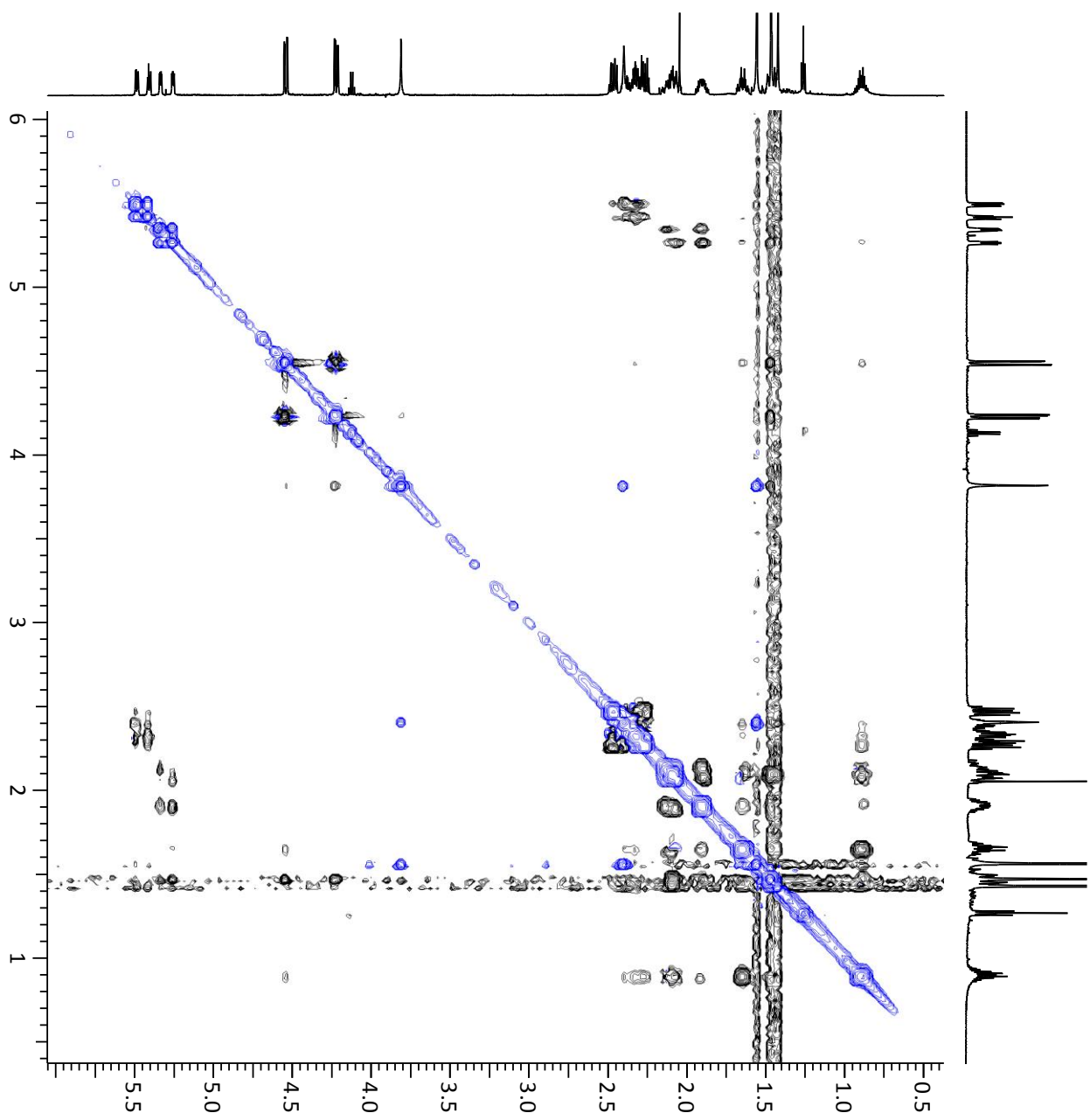


1D TOCSY subspectra
expansions
(C6D6)

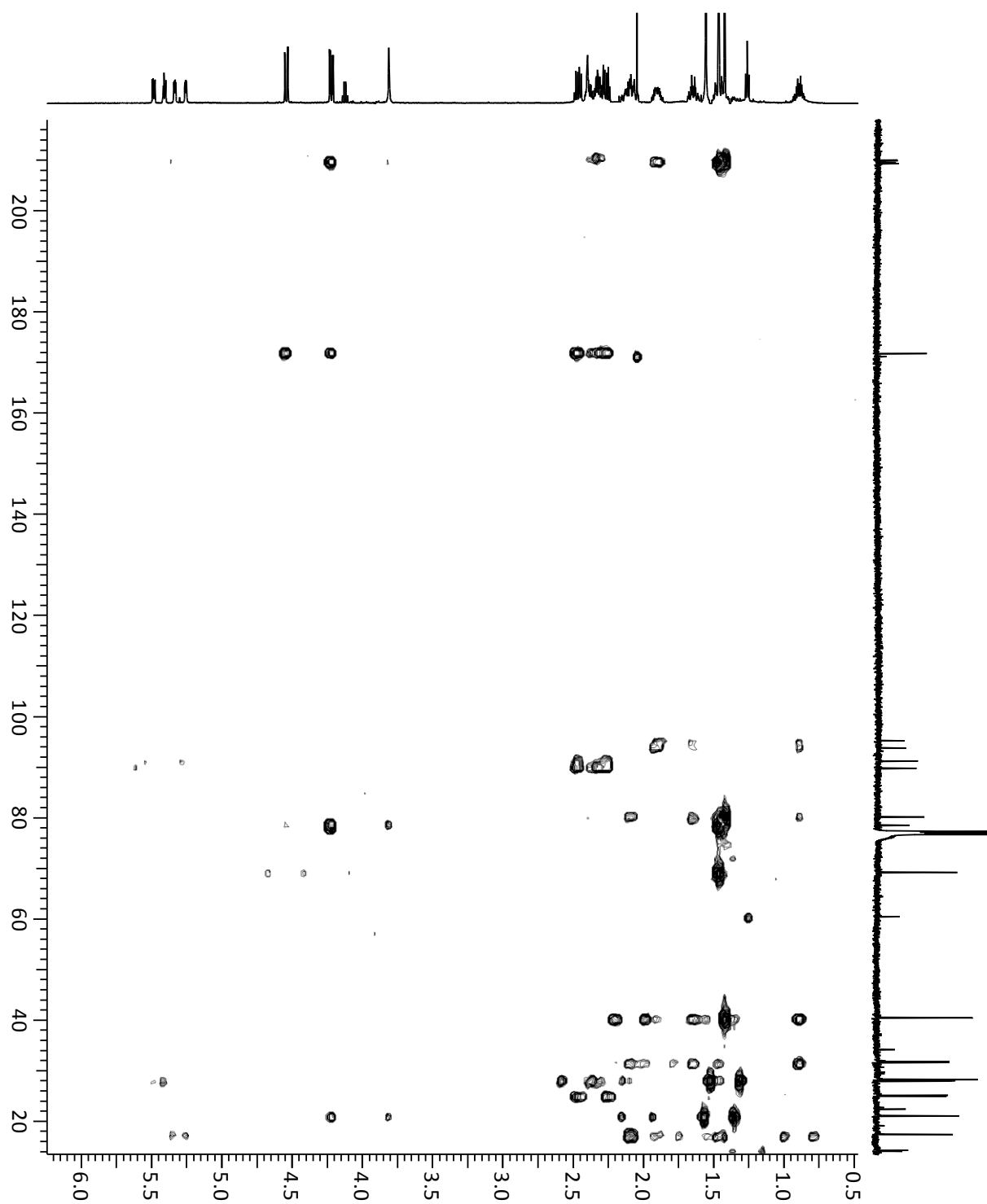


DPFGSENOE
(C6D6) subspectrum

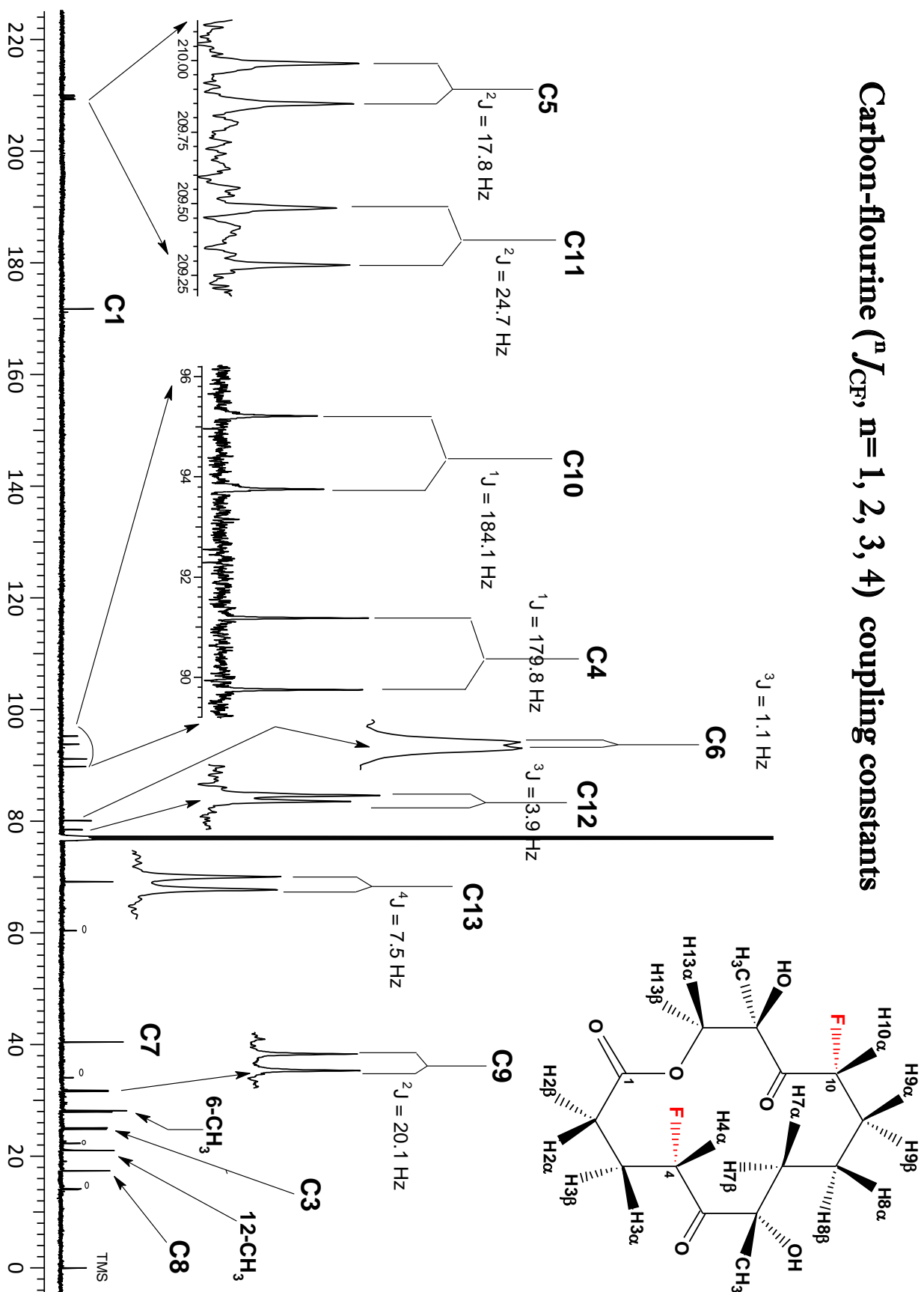
NOESY



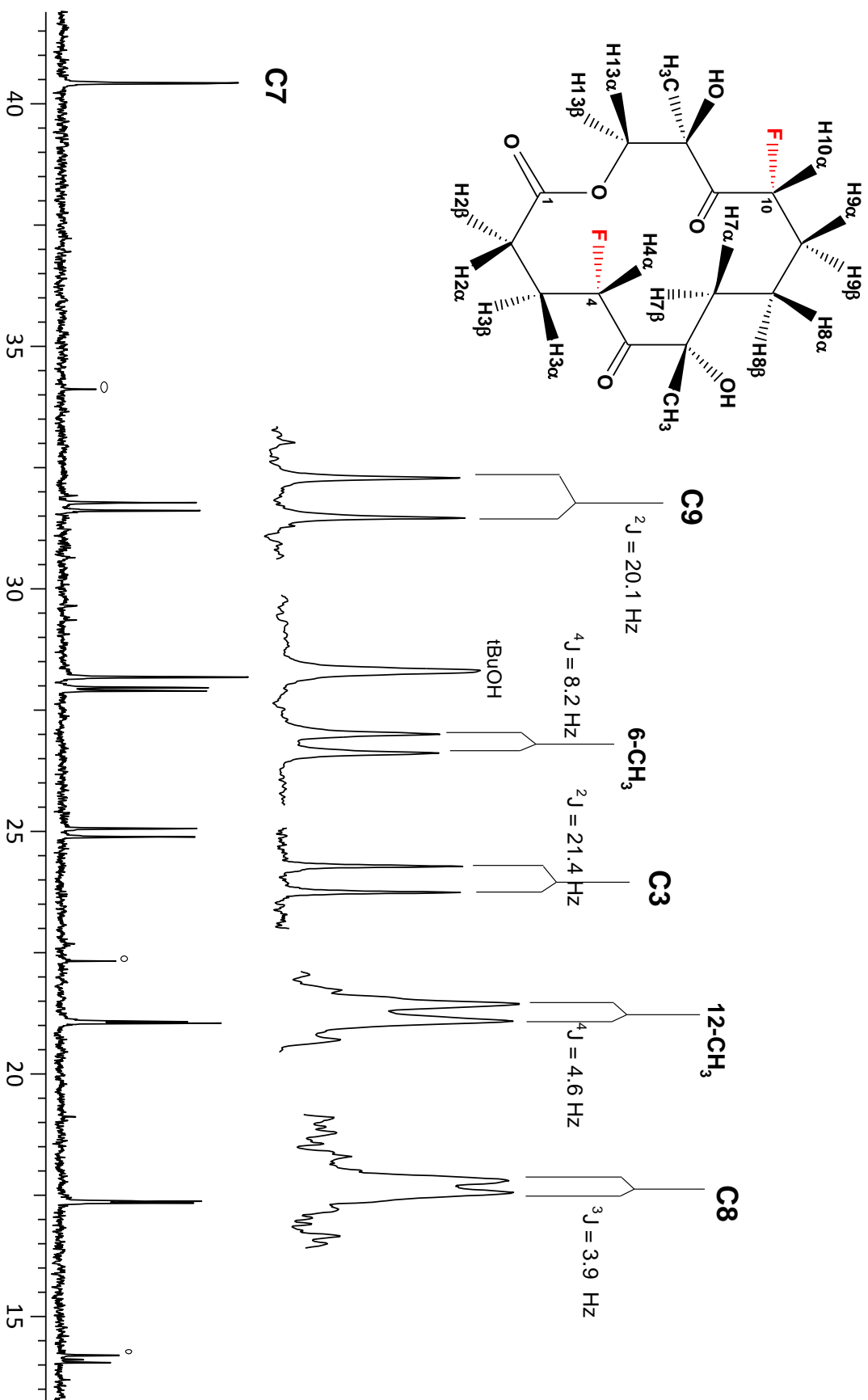
gHMBC

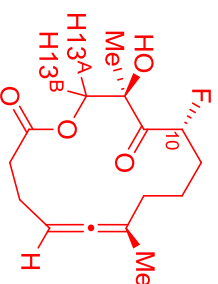
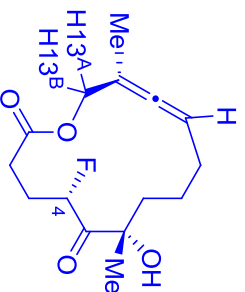


Carbon-fluorine ($^nJ_{CF}$, $n=1, 2, 3, 4$) coupling constants



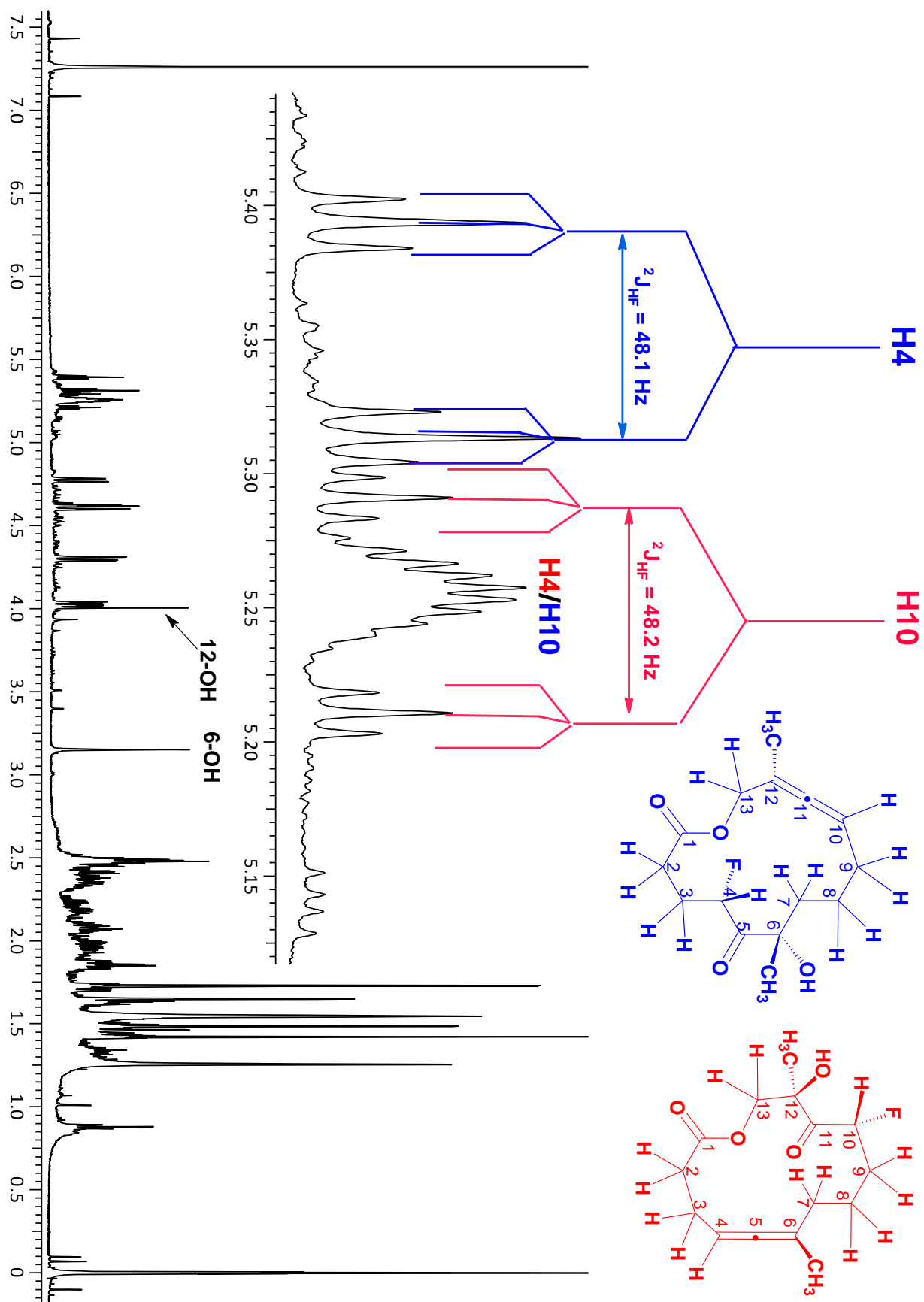
Carbon-flourine ($^nJ_{CF}$, $n=1, 2, 3, 4$) coupling constants

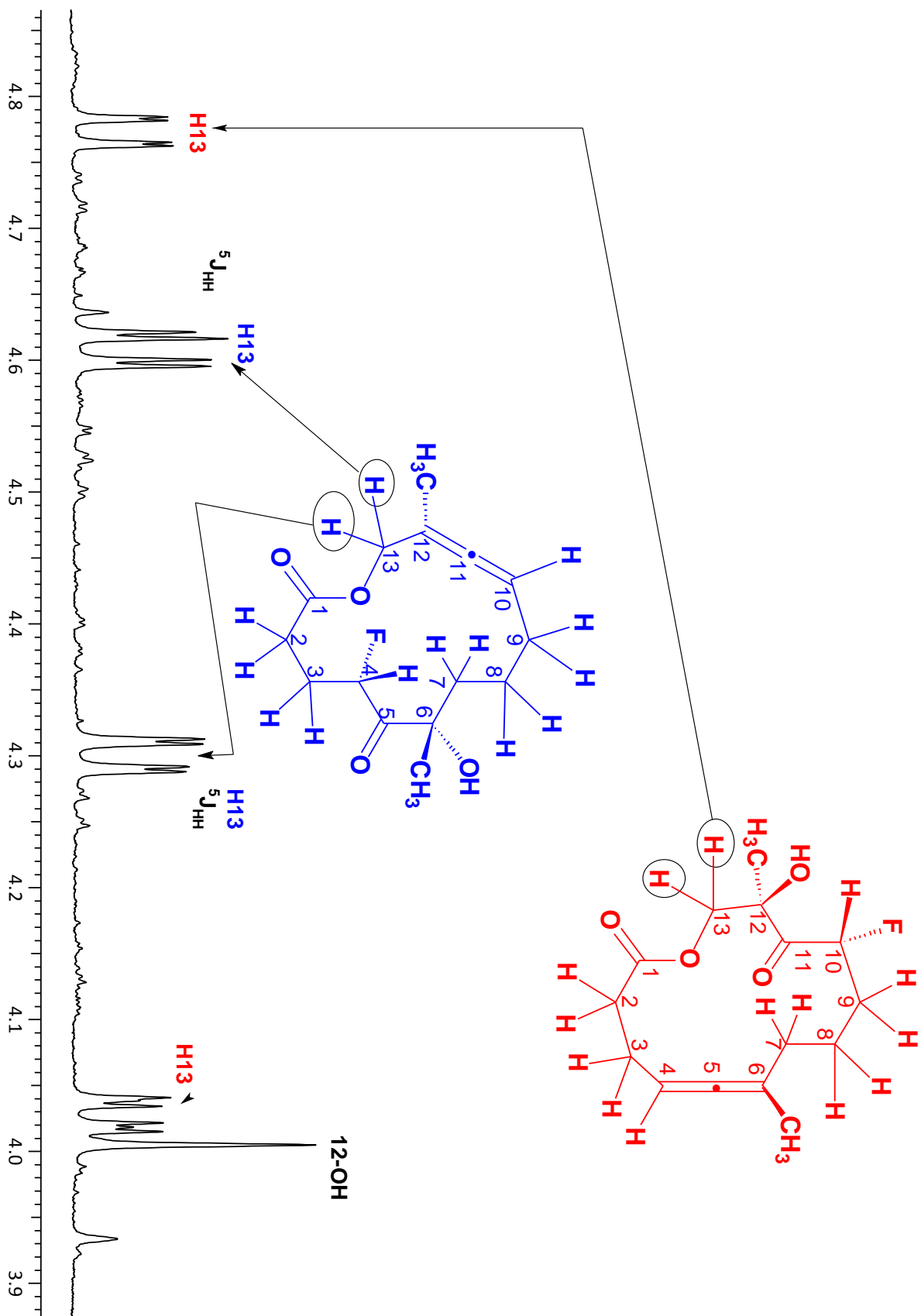


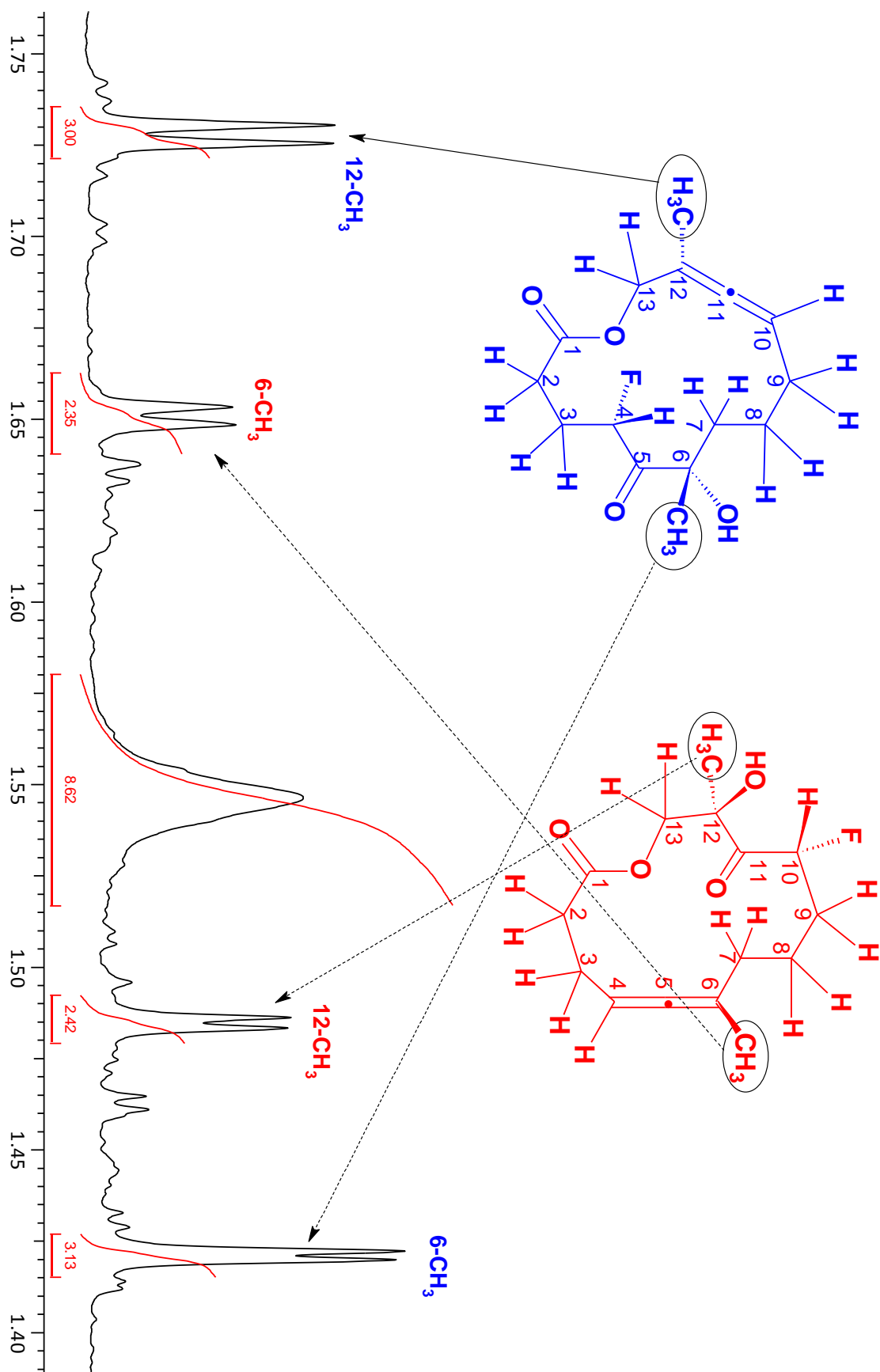


5.52 Observed chemical shifts (δ /ppm, CDCl_3) and coupling constants (Hz) **5.53**

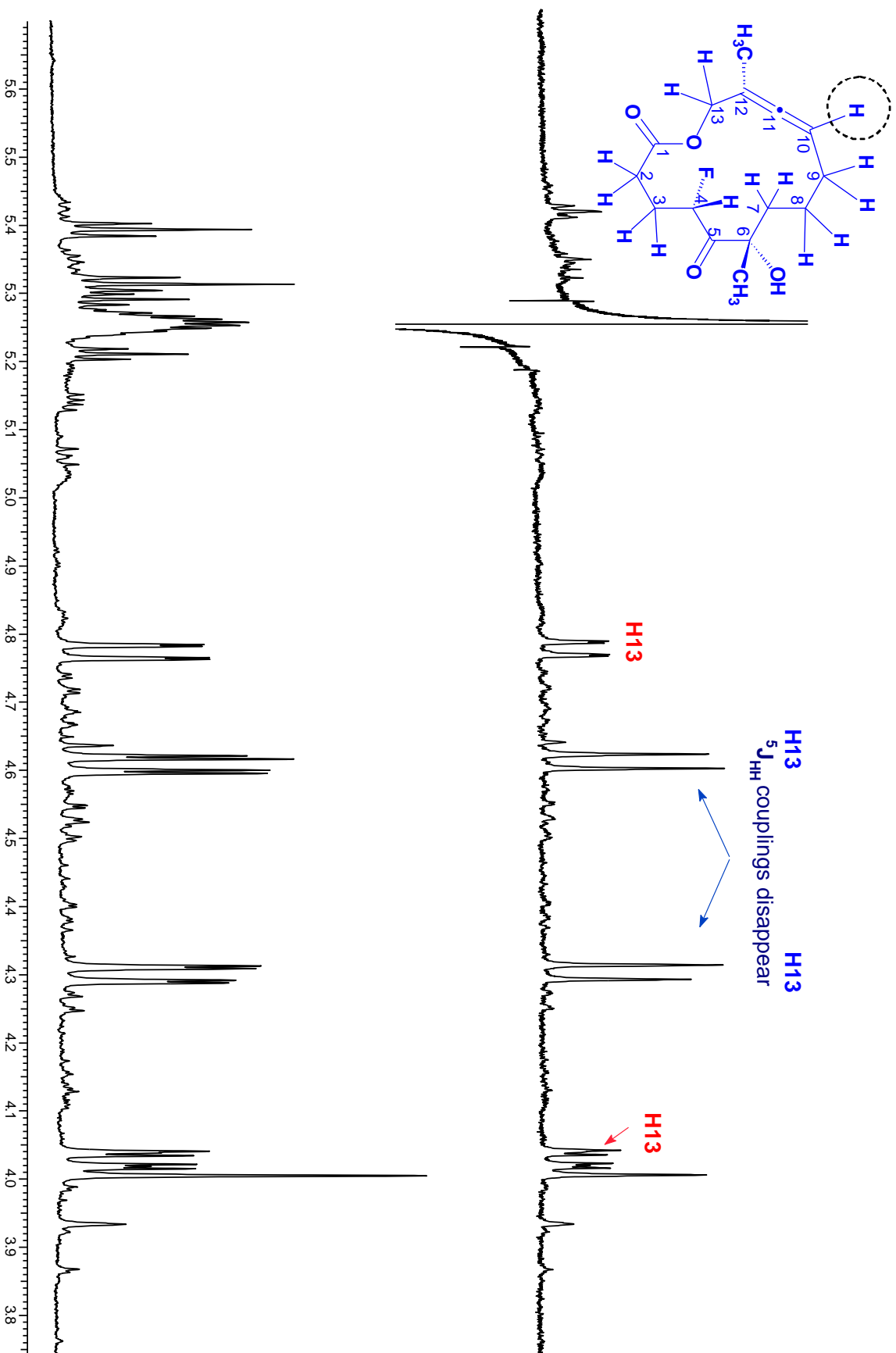
12-CH ₃	1.73 (d, $J_{12\text{-CH}_3, \text{H}10} = 2.97$ Hz, 3H)	12-CH ₃	1.48 (d, $J_{12\text{-CH}_3, 12\text{-OH}} = 1.8$ Hz, 3H)
		12-OH	4.01 (br, 1H)
H4	5.35 (dt, $J_{\text{H}4, \text{F}} = 48.1$ Hz, $J_{\text{H}4, 3\text{-CH}_2} = 5.7$ Hz, 1H)	6-CH ₃	1.65 (d, $J_{6\text{-CH}_3, \text{H}4} = 2.89$ Hz, 3H)
6-CH ₃	1.42 (d, $J = 1.4$ Hz, 3H)	H10	5.35(dt, $J_{\text{H}10, \text{F}} = 48.2$ Hz, $\text{H}10, 9\text{-CH}_2 = 4.6$ Hz, 1H)
6-OH	3.15 (br, s, 1H)		
H13 ^A	4.61 (dd, $J_{\text{H}13\text{A}, \text{H}13\text{B}} = 12.5$ Hz, $J_{\text{H}13\text{A}, \text{H}10} = 2.97$ Hz, 1H)	H13 ^A	4.77 (dd, $J_{\text{H}13\text{A}, \text{H}13\text{B}} = 11.5$ Hz, $J_{\text{H}13\text{A}, ?} = 3.9$ Hz, 1H)
H13 ^B	4.30 (dd, $J_{\text{H}13\text{B}, \text{H}10} = 2.2$ Hz, 1H)	H13 ^B	4.03 (dd, $J_{\text{H}13\text{B}, ?} = 1.6$ Hz, 1H)
7-CH ₂ + 8-CH ₂ + 9-CH ₂ (from 1D TOCSY spectrum, selective excitation of 12-CH ₃ at 1.73 ppm, mix = 360 ms)			
1.30 - 1.37 (1H)			
1.47 - 1.55 (1H)			
1.60 - 1.67 (1H)			
1.82 - 1.88 (1H)			
1.95 - 2.02 (1H)			
2.05 - 2.11 (1H)			
2.30 - 2.48 (2-CH ₂ + 3-CH ₂ , 4H)			



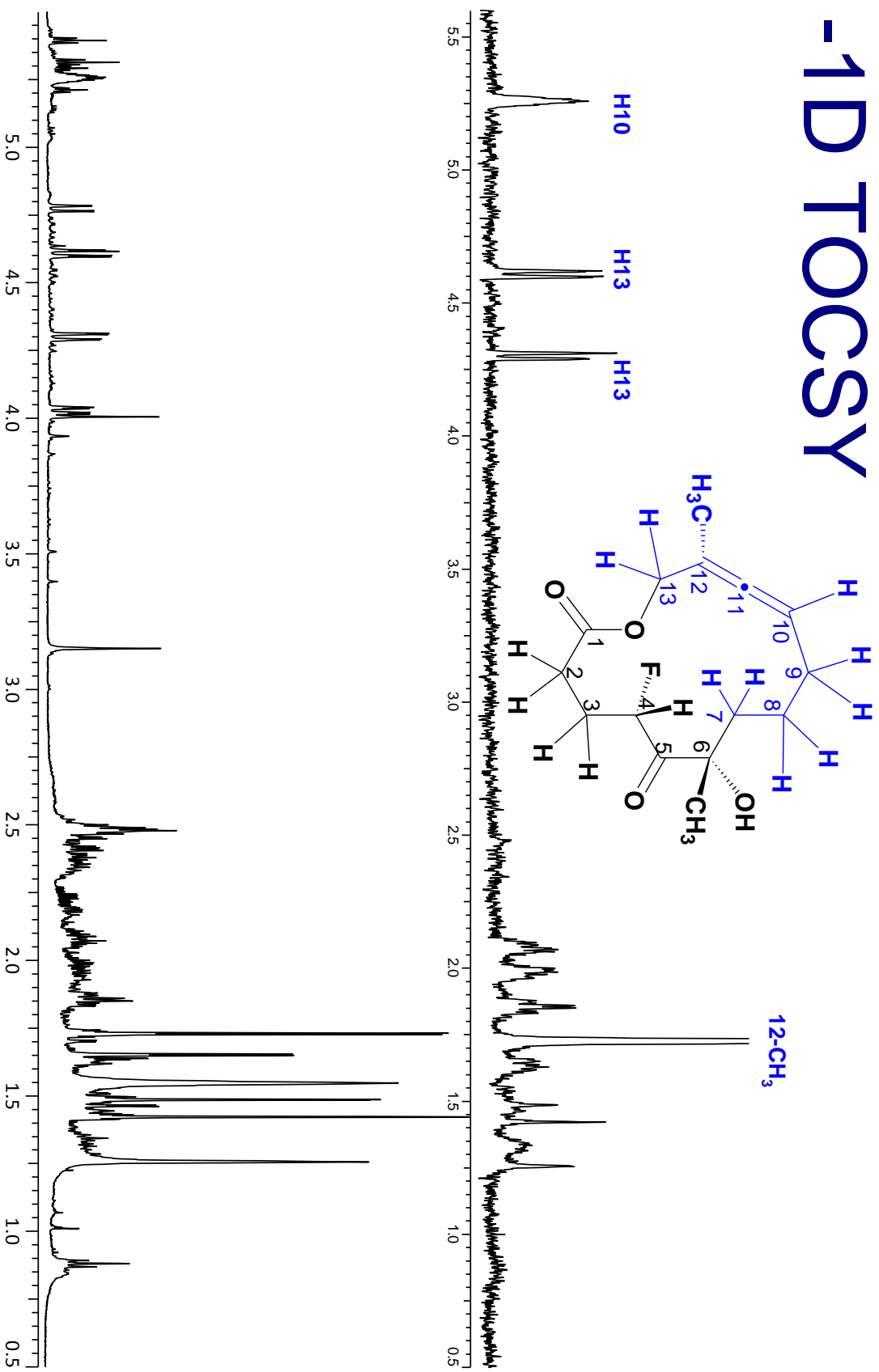




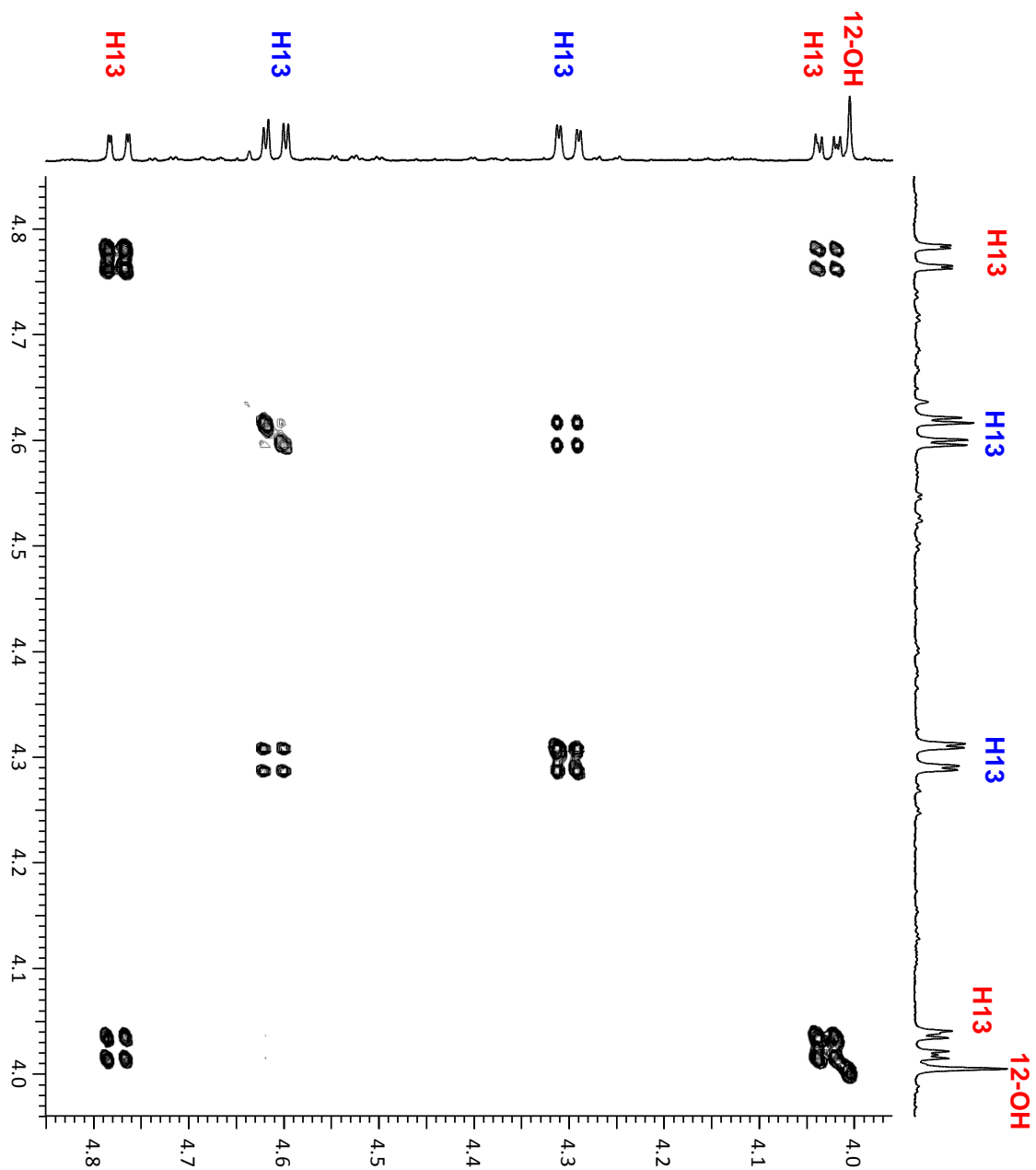
Selective decoupling of H10



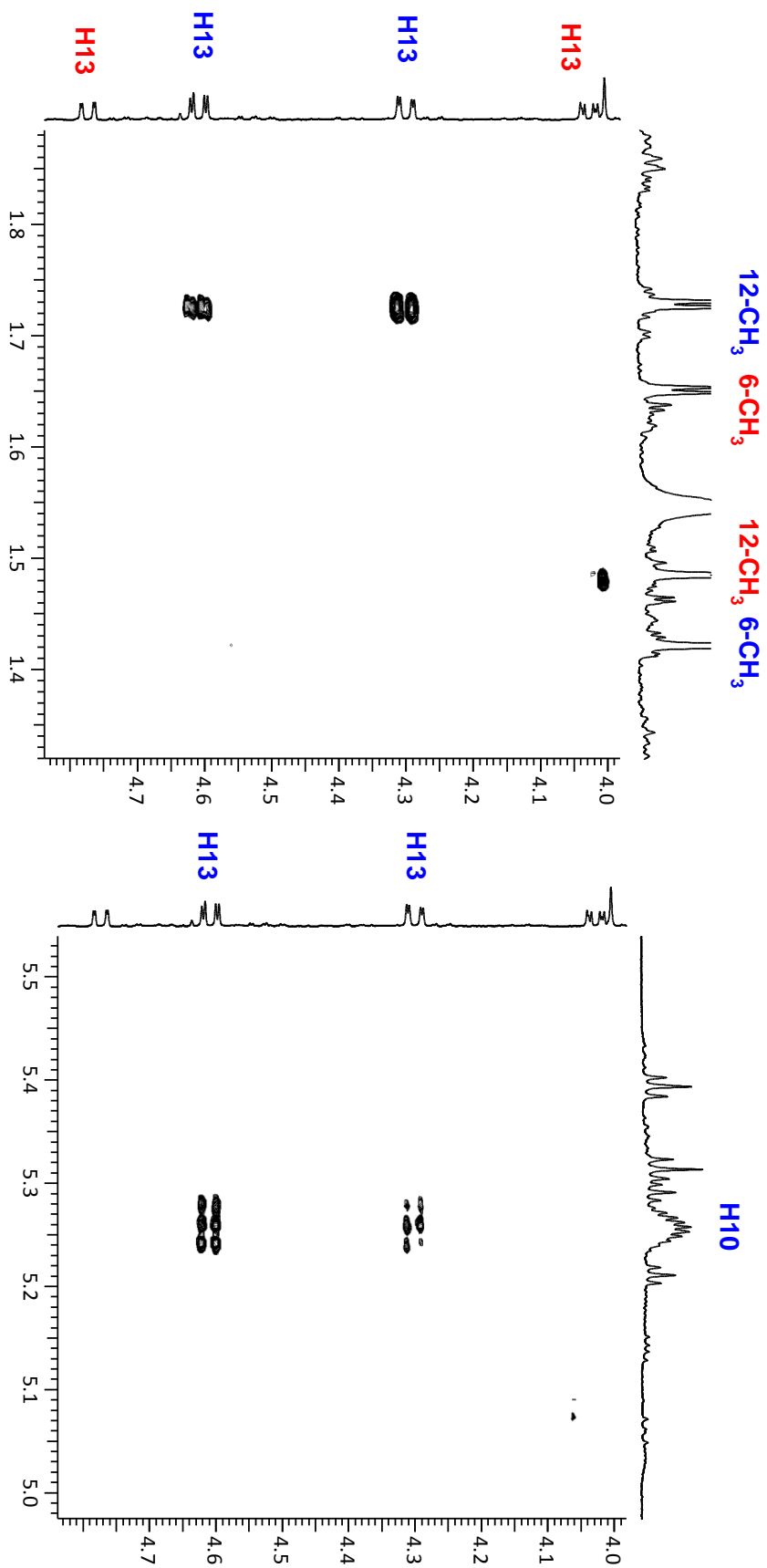
Spin system identification -1D TOCSY



gCOSY

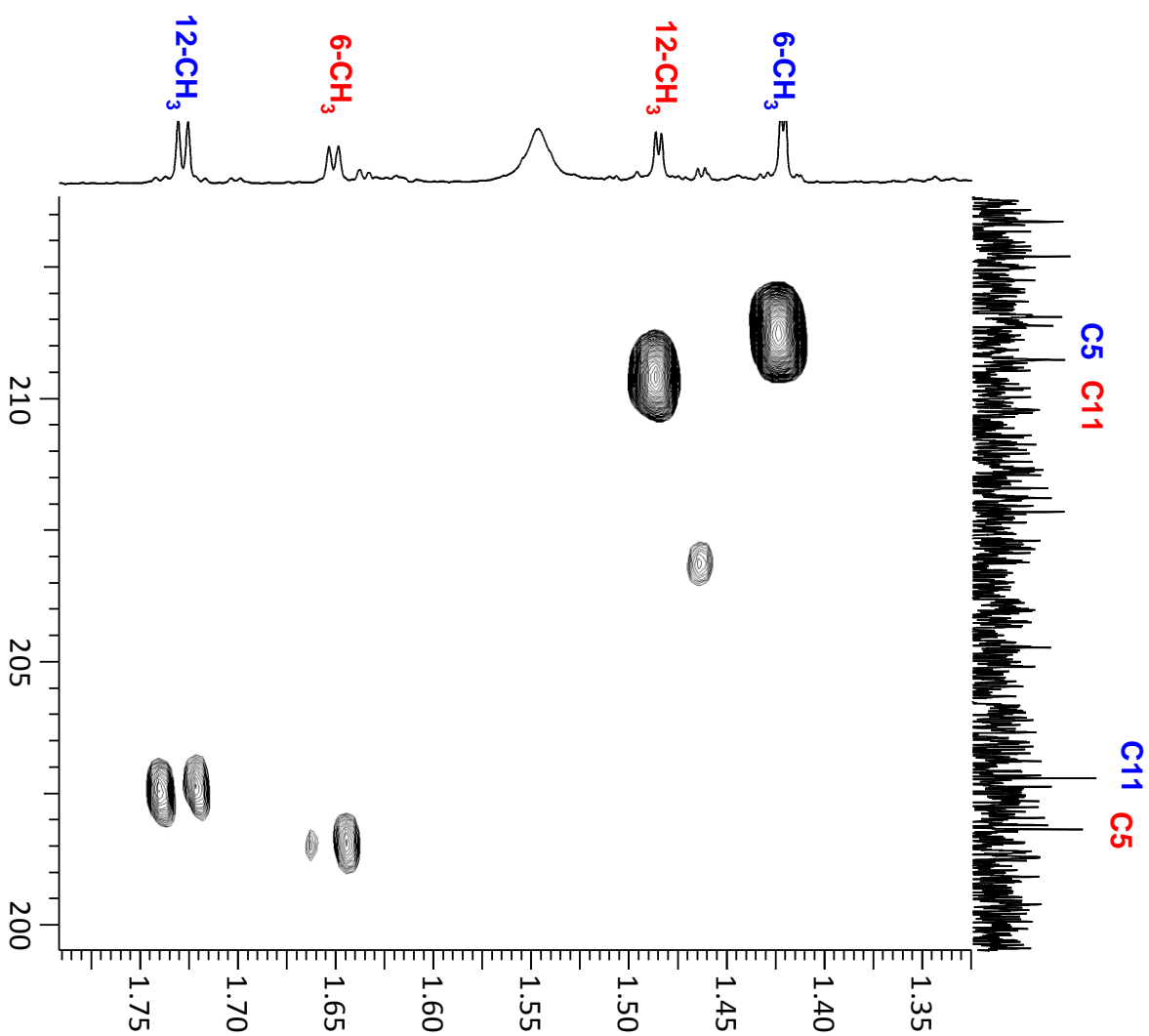
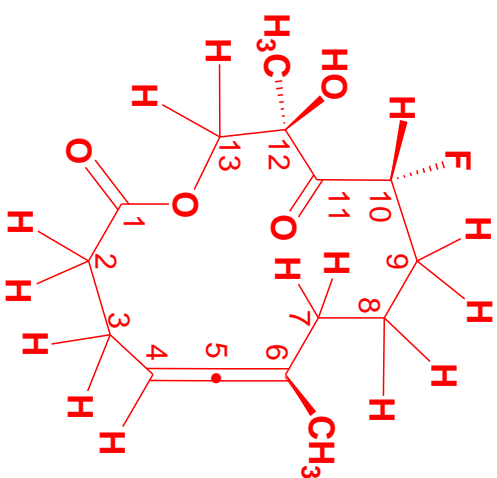
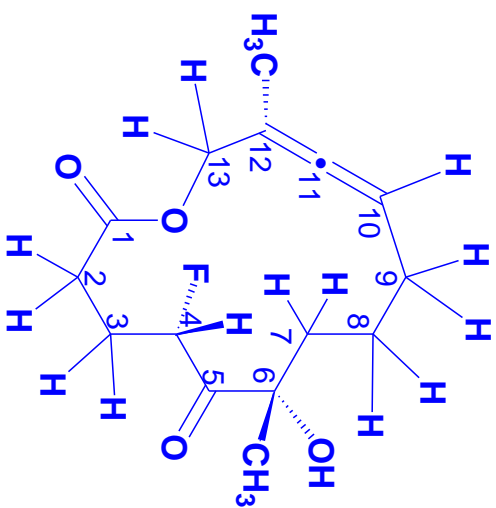


gCOSY



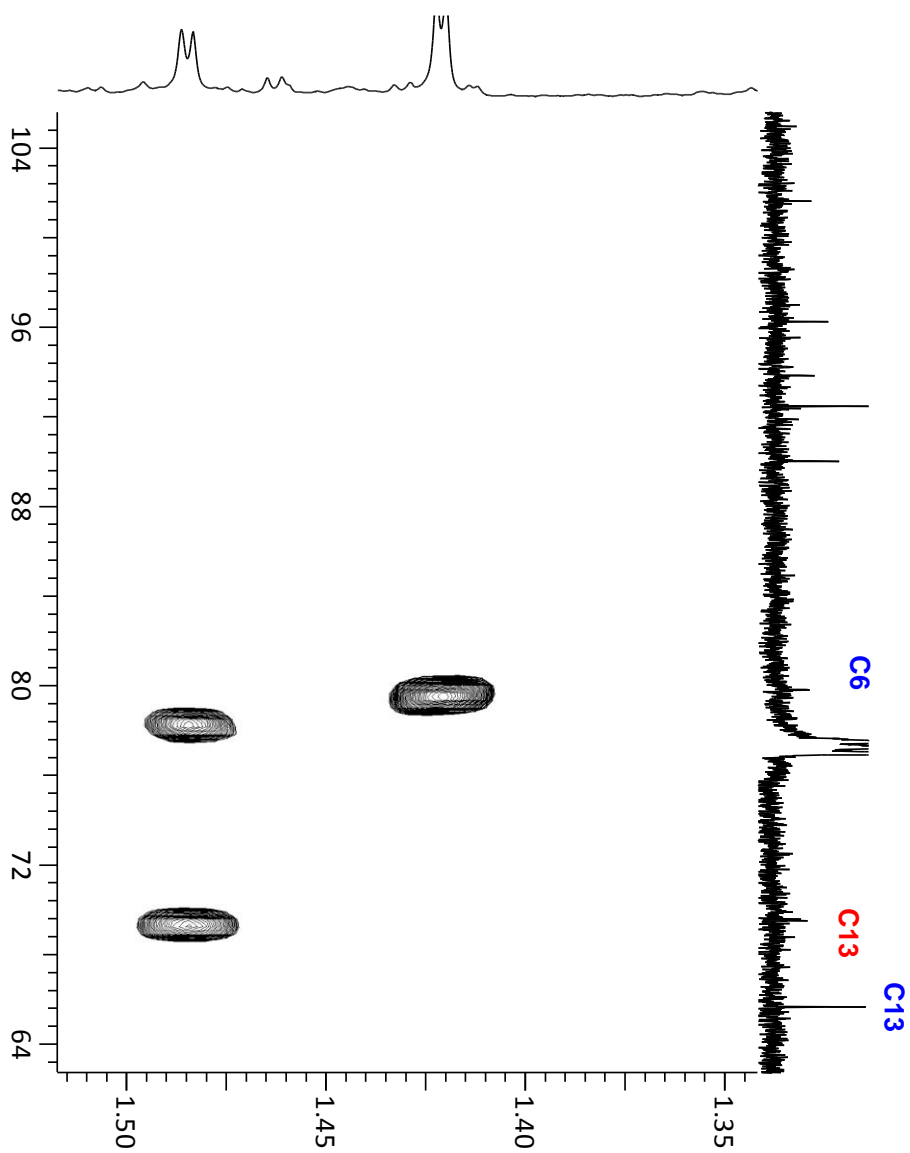
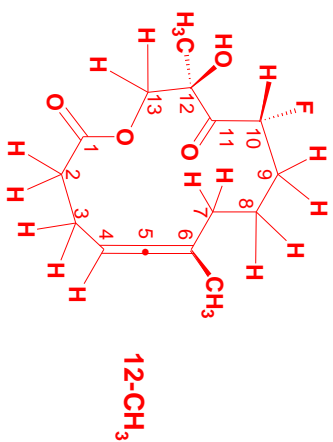
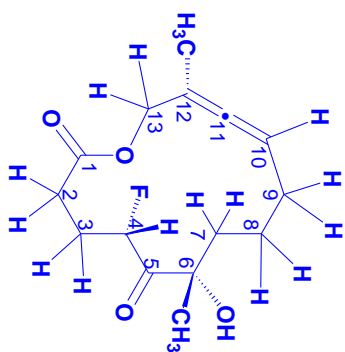
ghMBC

correlations



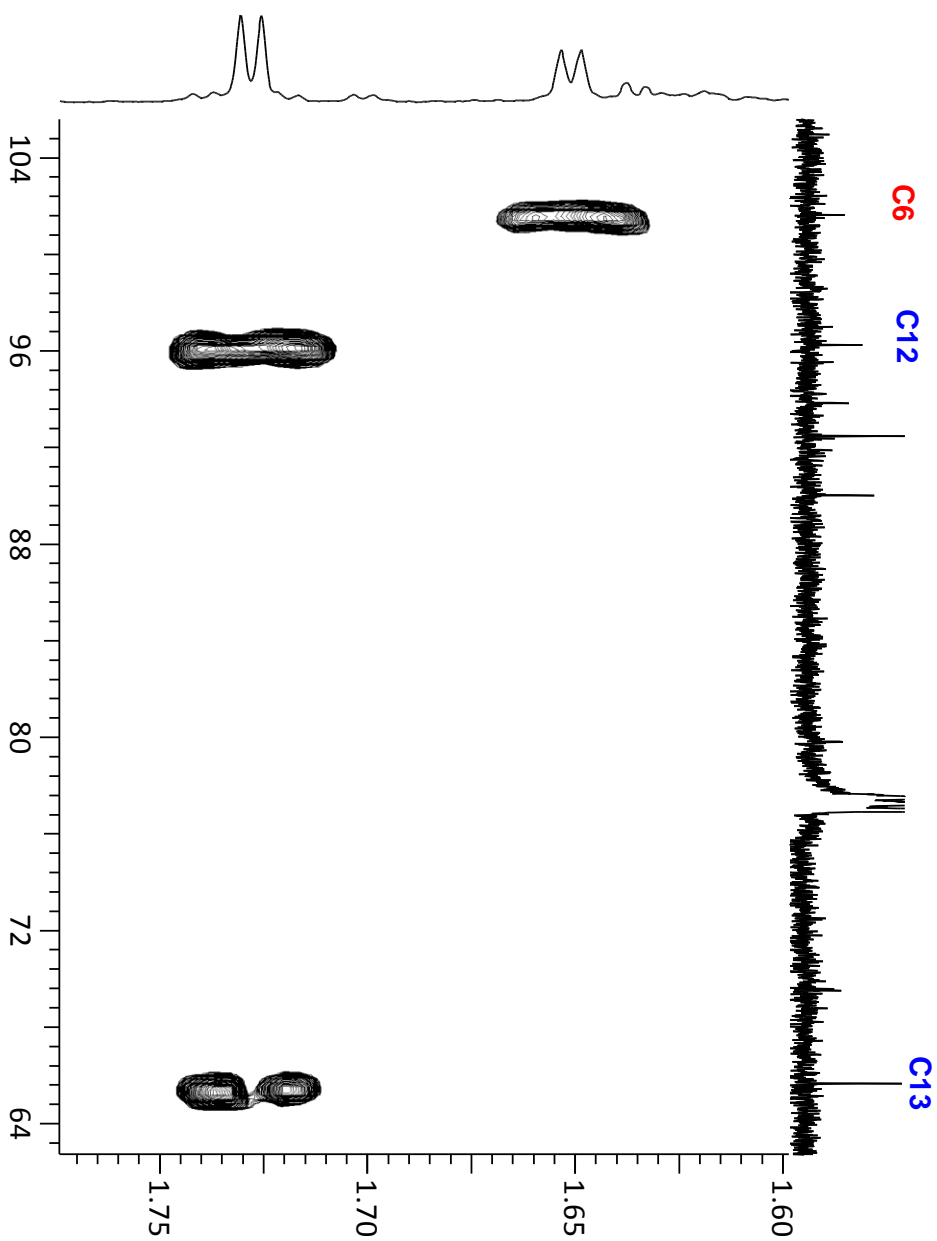
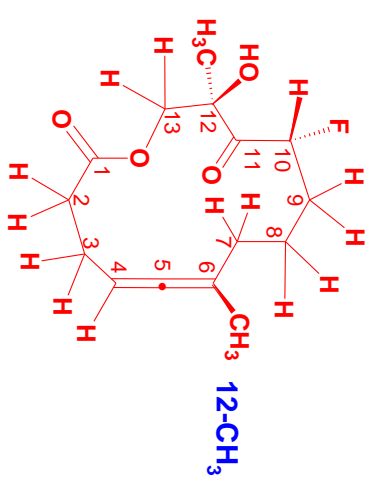
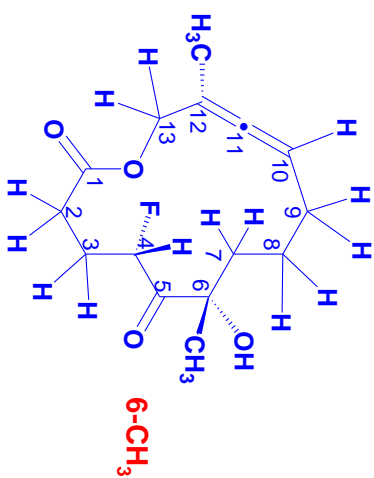
gHMBC

correlations



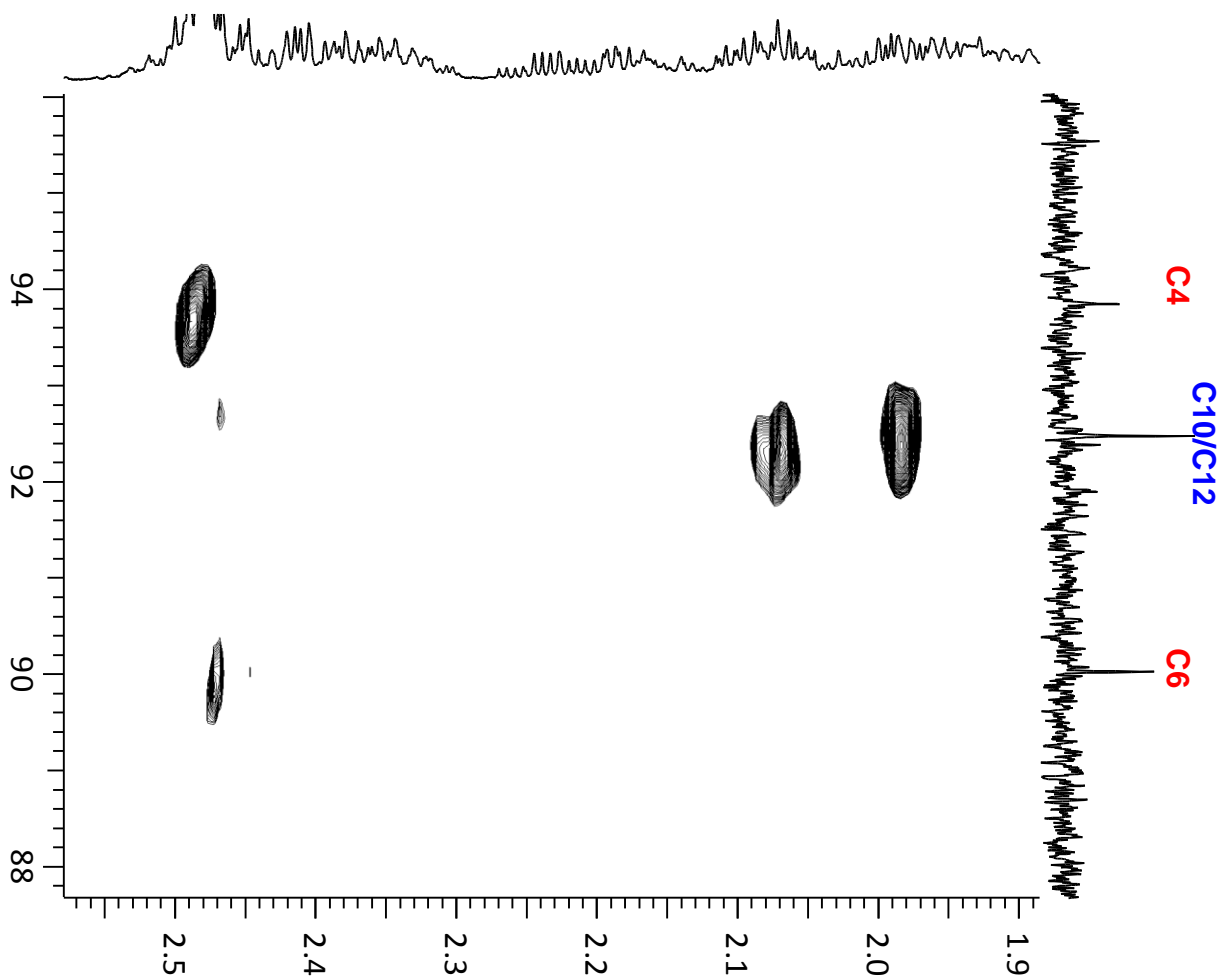
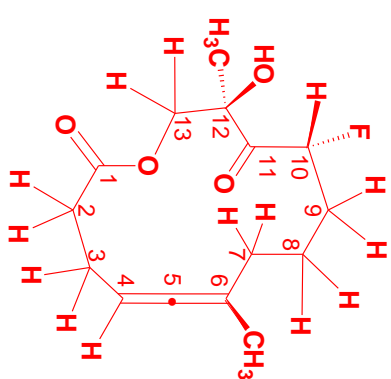
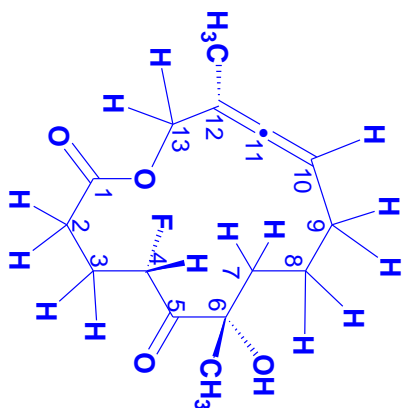
gHMBC

correlations

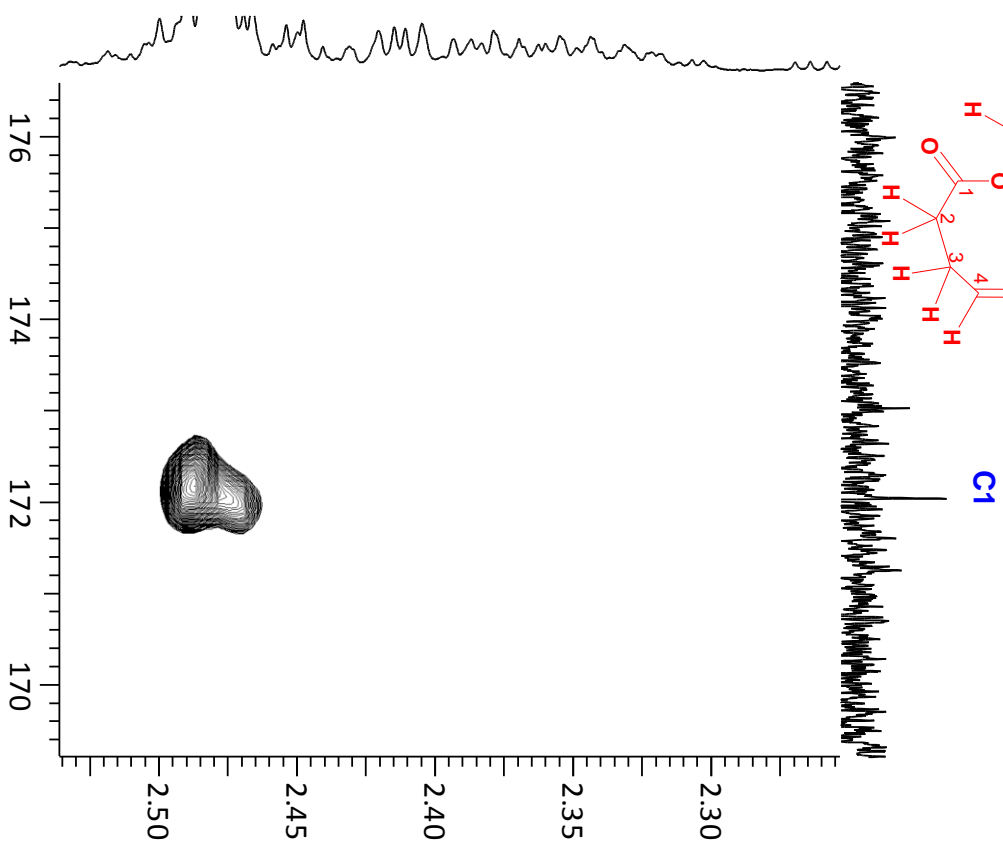
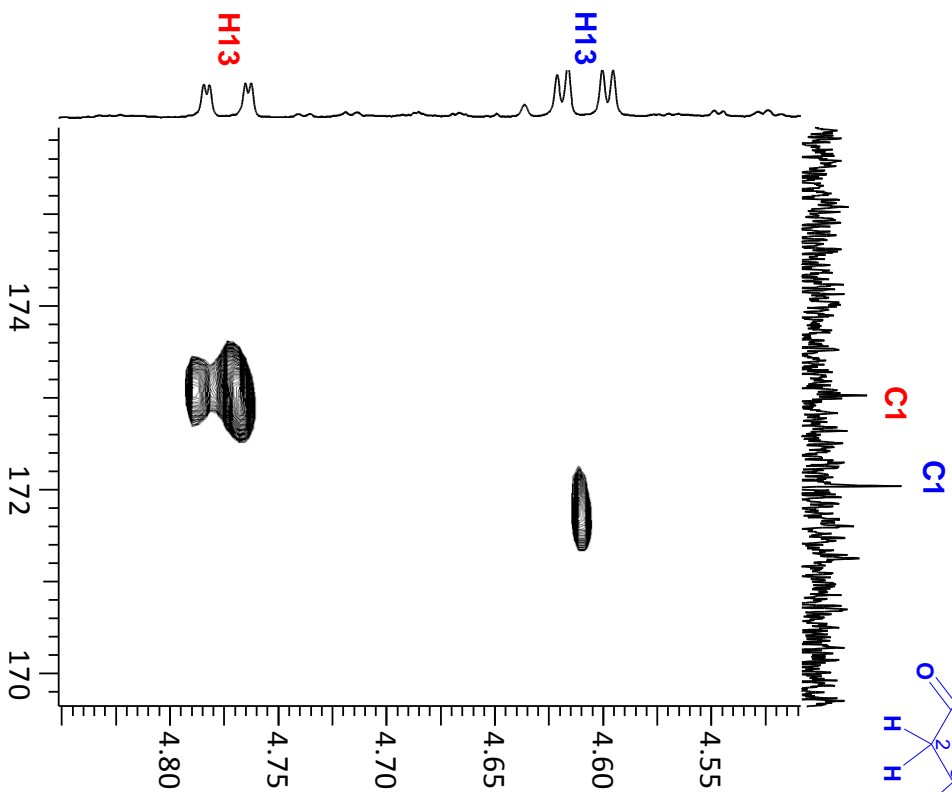
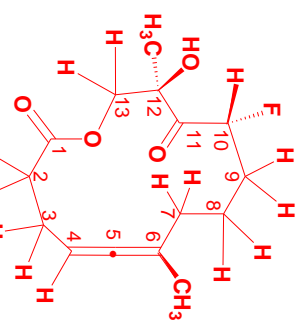
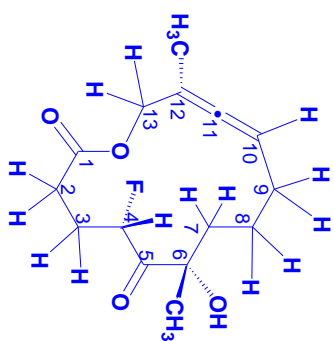


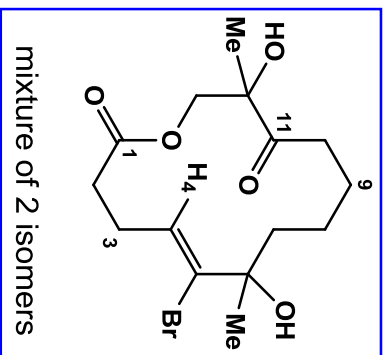
gHMBC

correlations

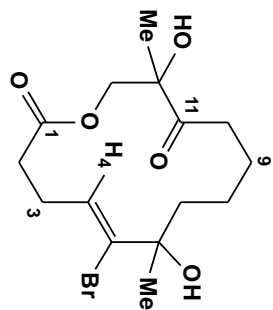


gHMC
correlations

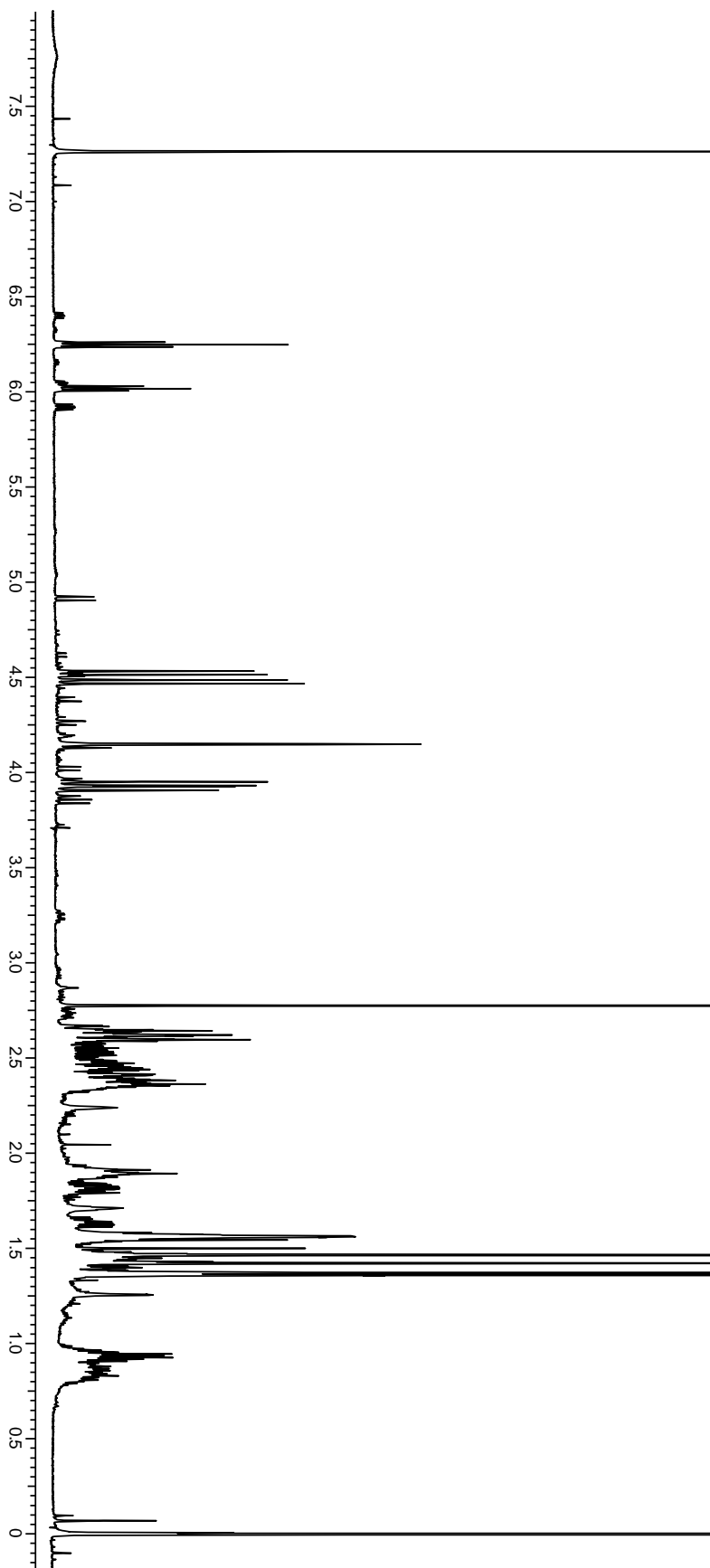


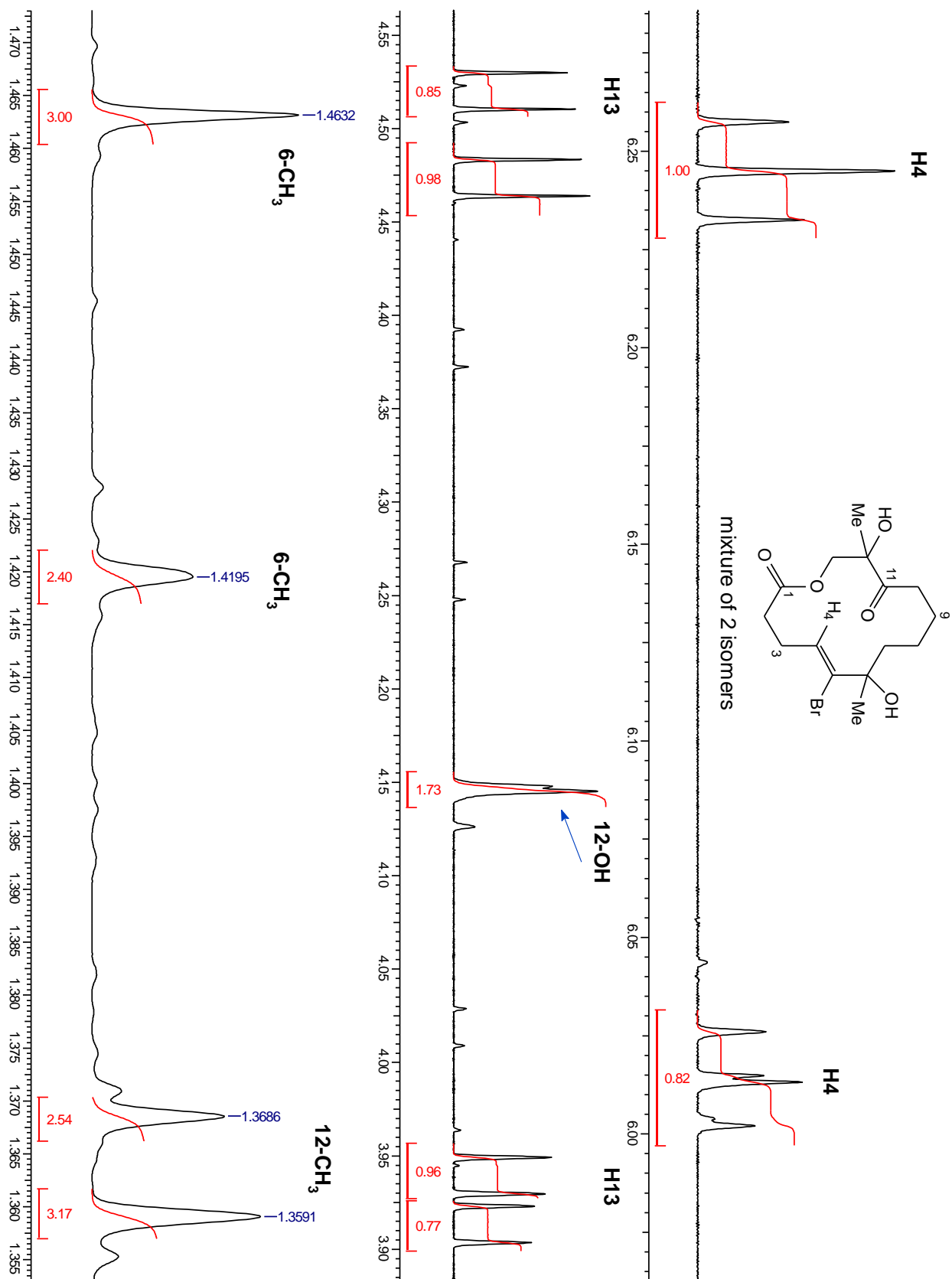


¹H NMR chemical shifts (δ/ppm) with coupling constant (J/Hz)		¹³C NMR chemical shift (δ/ppm)
H2a	2.33 - 2.38	2.45 - 2.48
H2b	2.49 - 2.55	2.60 - 2.65
H3a	2.41 - 2.45	2.32 - 2.36
H3b	2.59 - 2.64	2.52 - 2.58
H4	6.25 (t, J _{H4, 3-CH2} = 7.5 Hz)	6.02 (dd, J _{H4, H3a} = 6.8 Hz) J _{H4, H3b} = 7.6 Hz
6-CH₃	1.47 (s)	1.42 (s)
7-CH₂ + 8-CH₂ + 9-CH₂ + 10-CH₂		
0.88 - 1.00		0.78 - 0.86
1.38 - 1.43		0.89 - 0.97
1.42 - 1.48		1.43 - 1.50
1.78 - 1.84 (2H)		1.54 - 1.58
1.87 - 1.93		1.60 - 1.66
2.35 - 2.40		1.86 - 1.94
2.62 - 2.67		2.37 - 2.42
		2.59 - 2.65
12-CH₃	1.38	1.36
12-OH	4.14	
H13^A	3.94 (² J _{AB} = 11.7 Hz)	3.92 (² J _{AB} = 11.6 Hz)
H13^B	4.48	4.52
		C1 172.71 / 172.69
		C2 36.33 / 36.22
		C3 25.96 / 25.63
		C4 126.47 / 125.68
		C5 137.15 / 135.14
		C6 76.82 / 76.45
		6-CH₃ 26.18 / 29.15
		C7 40.83 / 39.70
		C8 23.77 / 23.45
		C9 25.49 / 24.31
		C10 32.52 / 32.40
		C11 211.66 / 211.58
		C12 77.87
		12-CH₃ 20.78 / 20.74
		C13 68.93

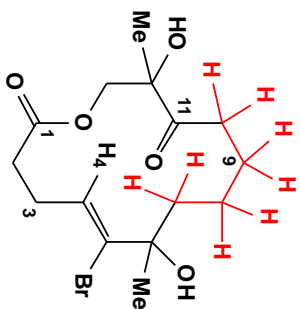


mixture of 2 isomers

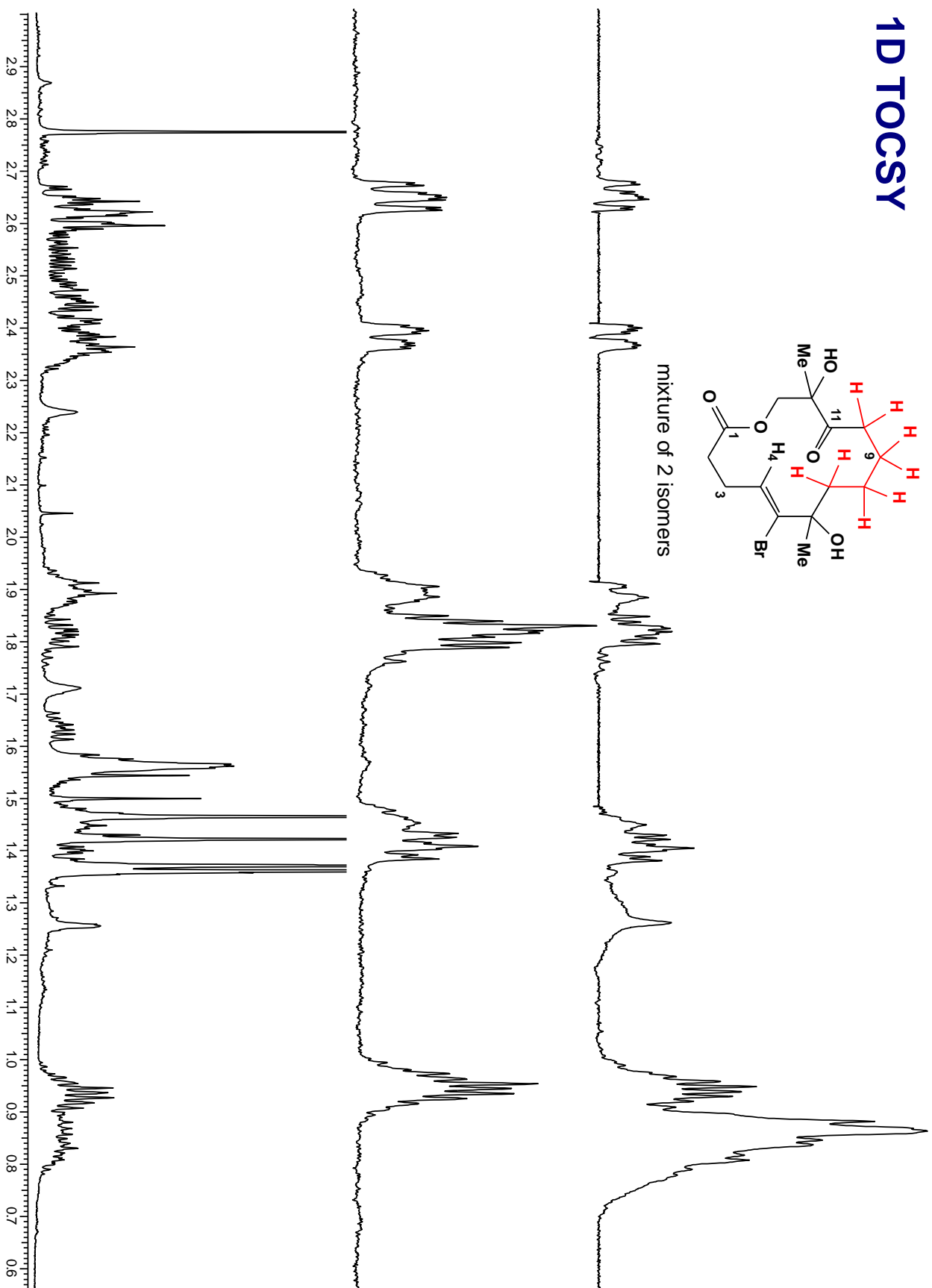




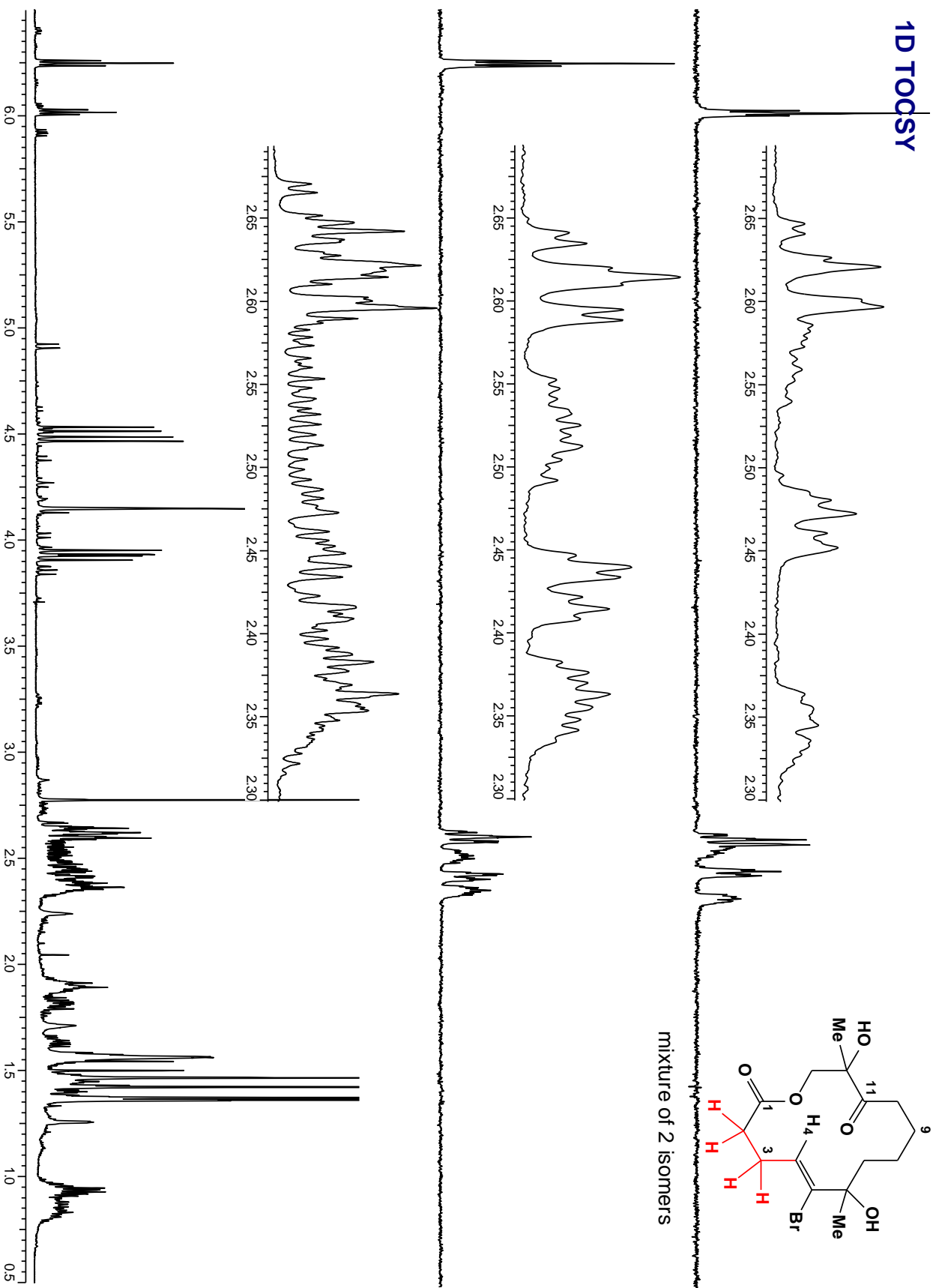
1D TOCSY

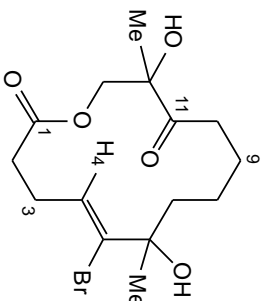
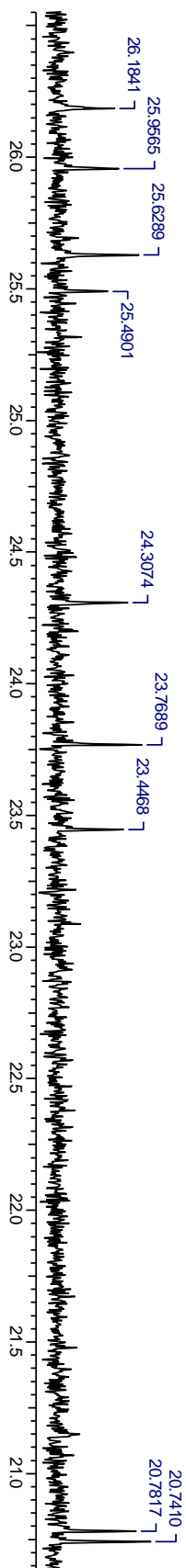
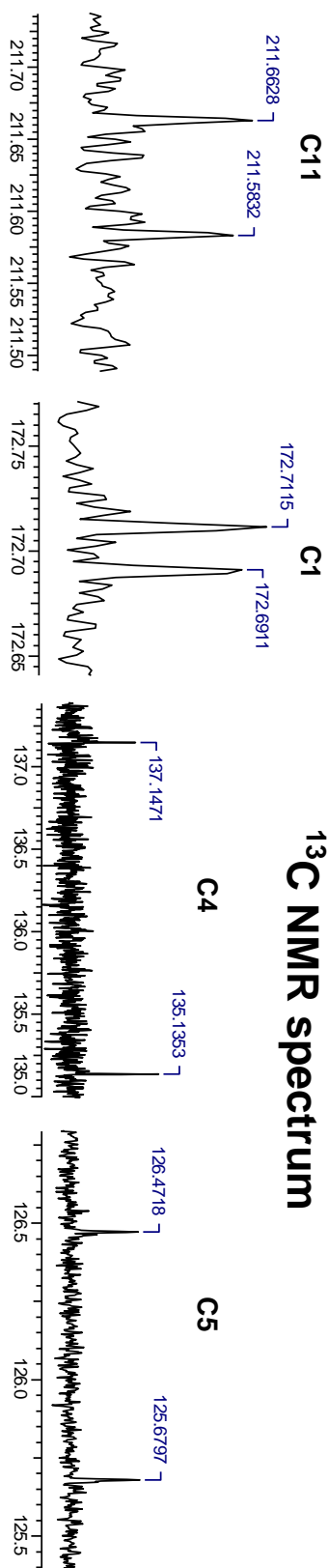


mixture of 2 isomers

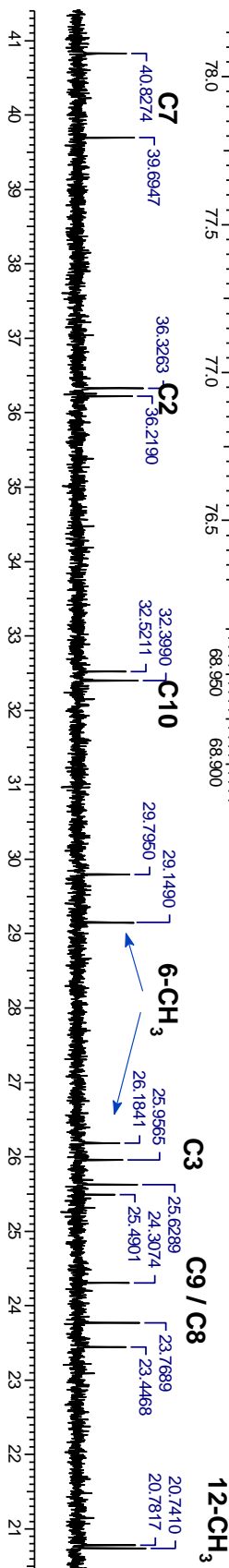


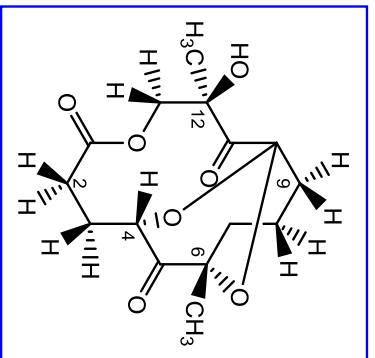
1D TOCSY



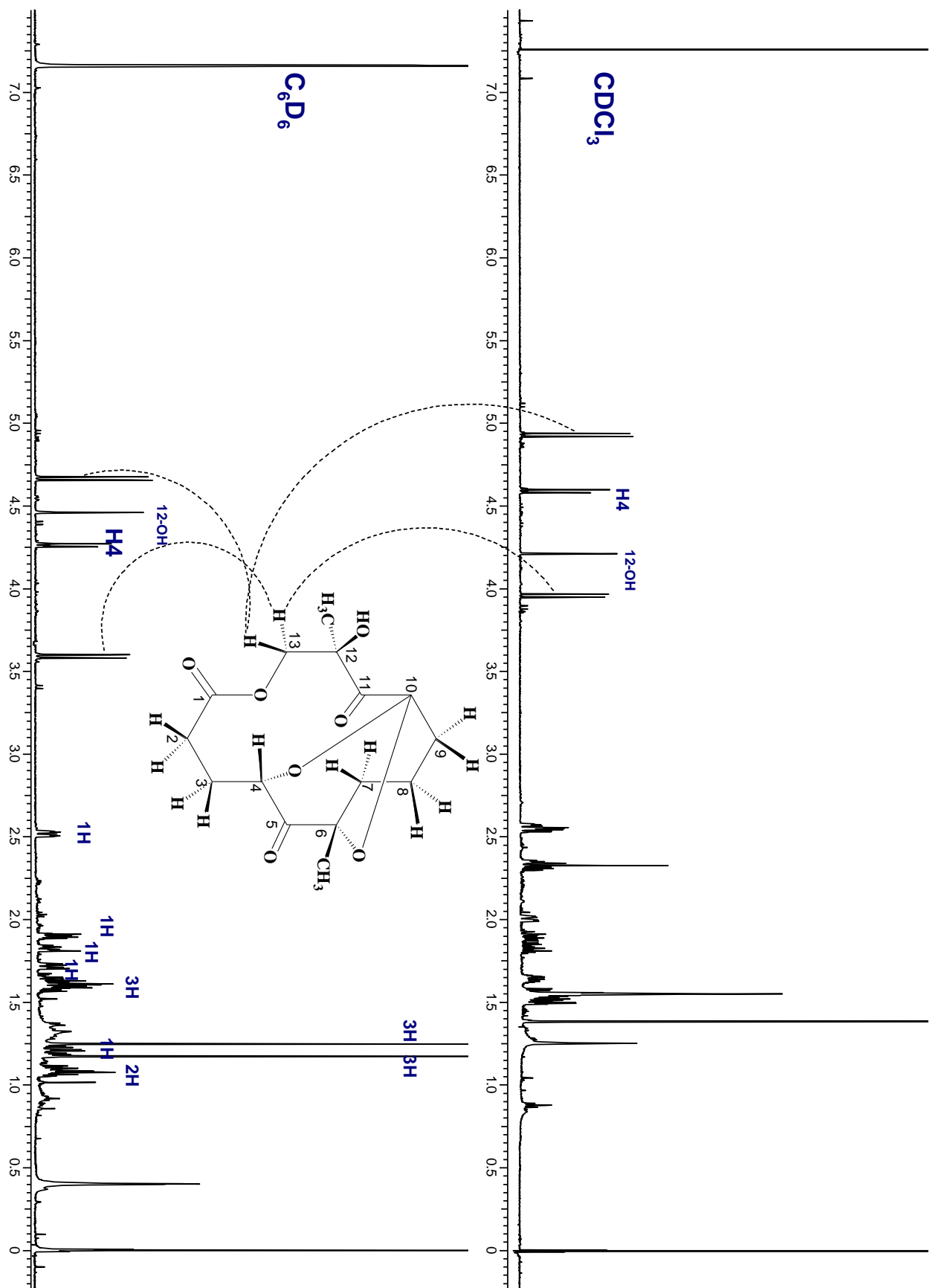
¹³C NMR spectrum

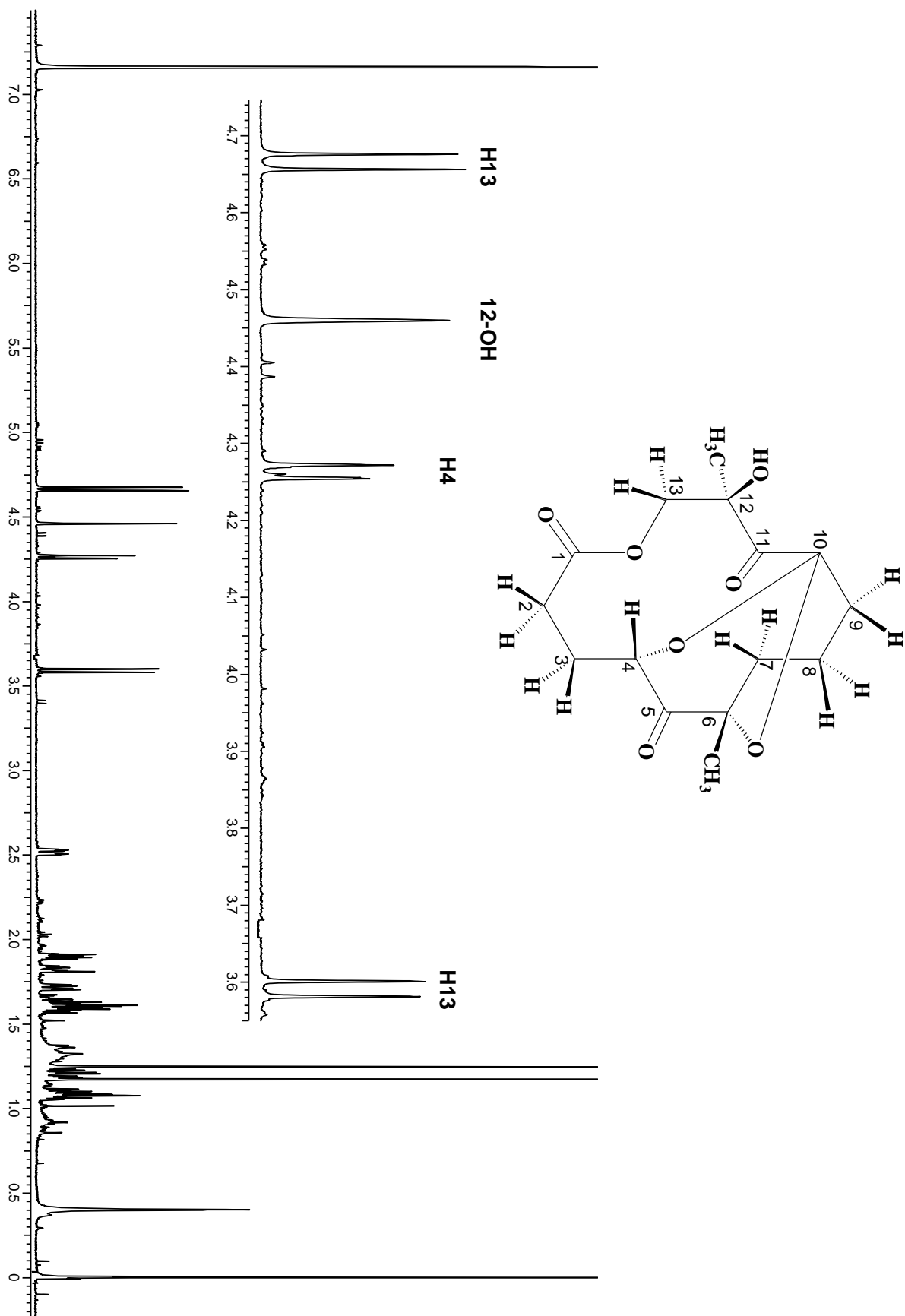
mixture of 2 isomers

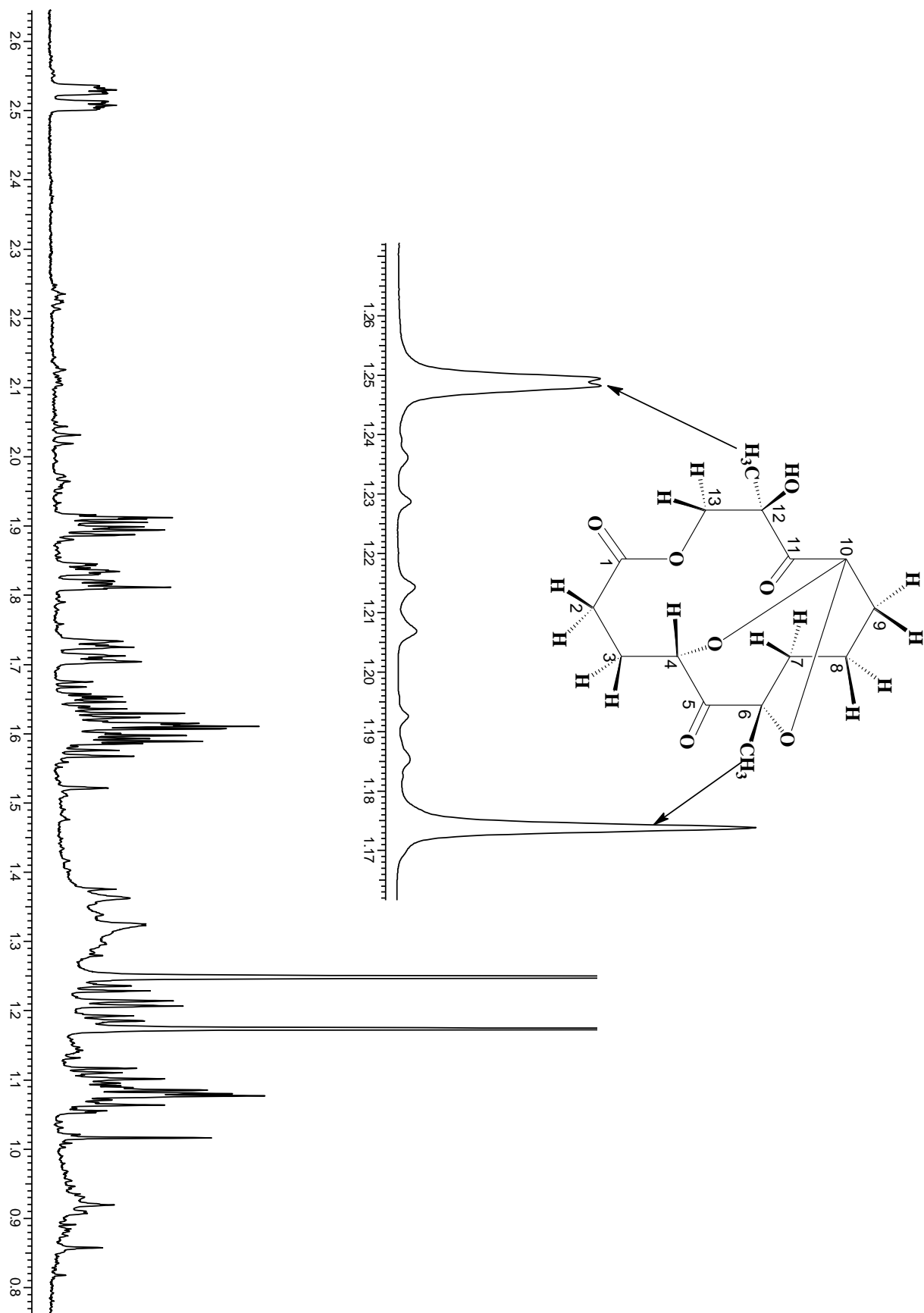


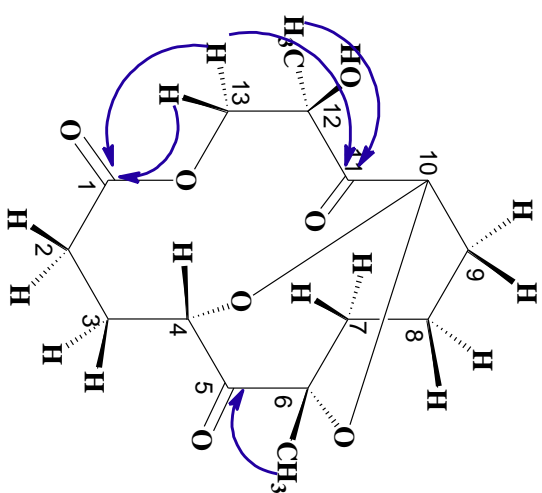
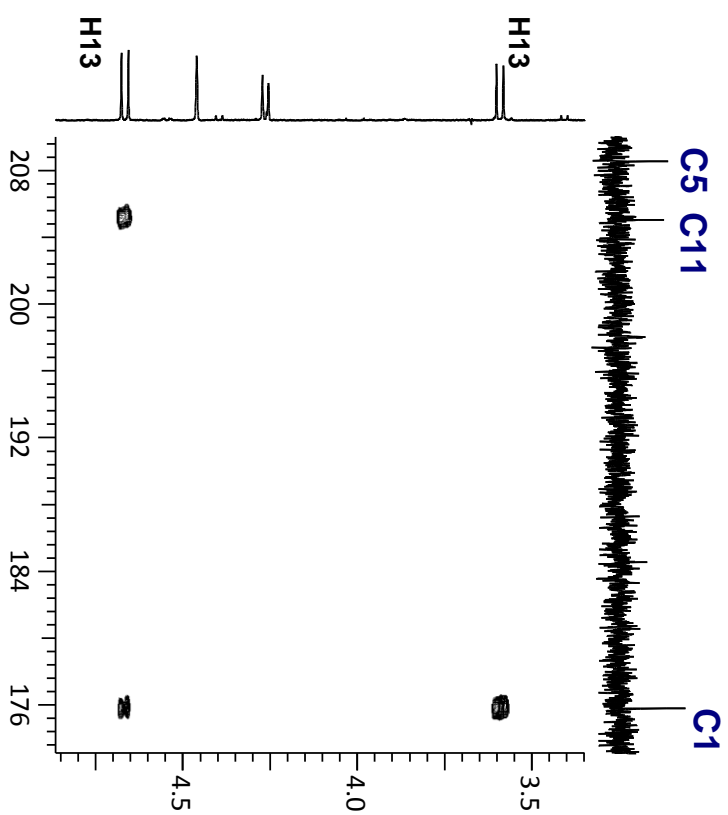


¹H NMR chemical shifts (δ/ppm) with coupling constant (J/Hz), C6D6	¹³C NMR chemical shift (δ/ppm)
4.25 (d, J_{H4, H3} = 9.5Hz, H4)	175.8 — C1
4.46 (s, 12-OH)	32.2 — C2
4.66, 3.60 (2H, d, J = 11.8Hz, H13)	23.3 — C3
2.51 (1H, m, H9)	73.1 — C4
1.92 - 1.88 (1H, m, H2)	208.6 — C5
1.85 - 1.81 (1H, m, H2)	82.3 — C6
1.73 - 1.70 (1H, m, H9)	32.0 — C7
1.66 - 1.57 (3H, m, H7, H3)	16.3 — C8
1.25 (3H,s, 12-CH₃)	29.9 — C9
1.17 (3H,s, 6-CH₃)	100.0 — C10
1.24 - 1.19 (1H, m, H7)	205.0 — C11
1.12 - 1.05 (2H, m, H8)	83.0 — C12
	72.8 — C13
	24.1 — 6-CH ₃
	23.6 — 12-CH ₃

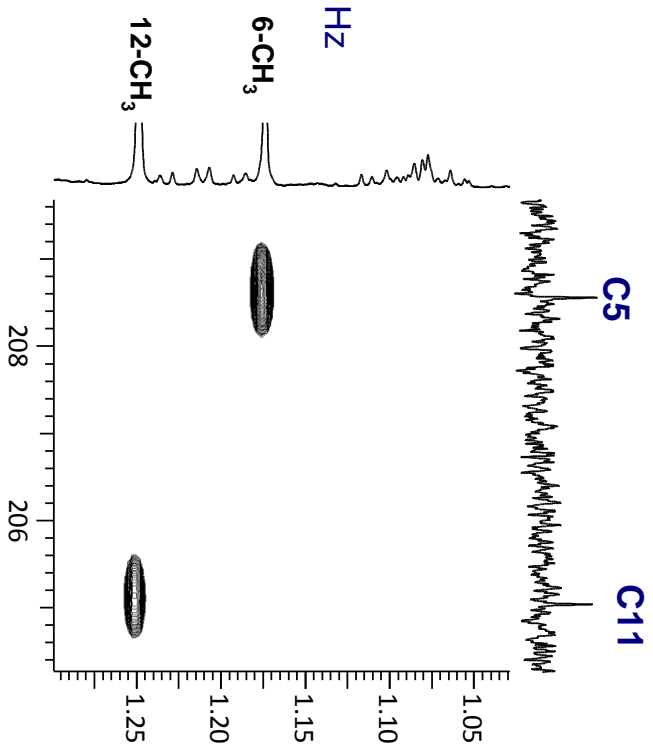




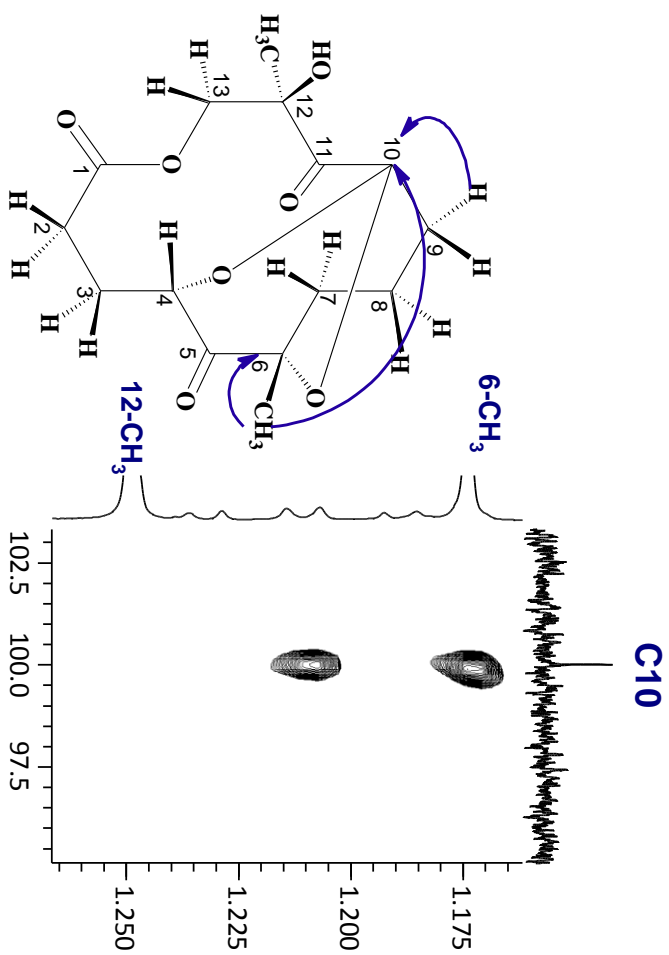
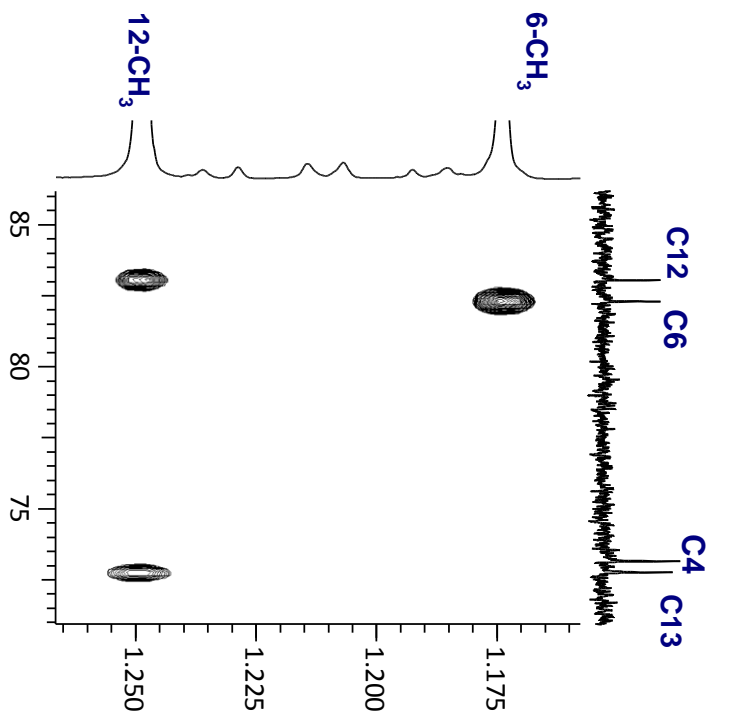




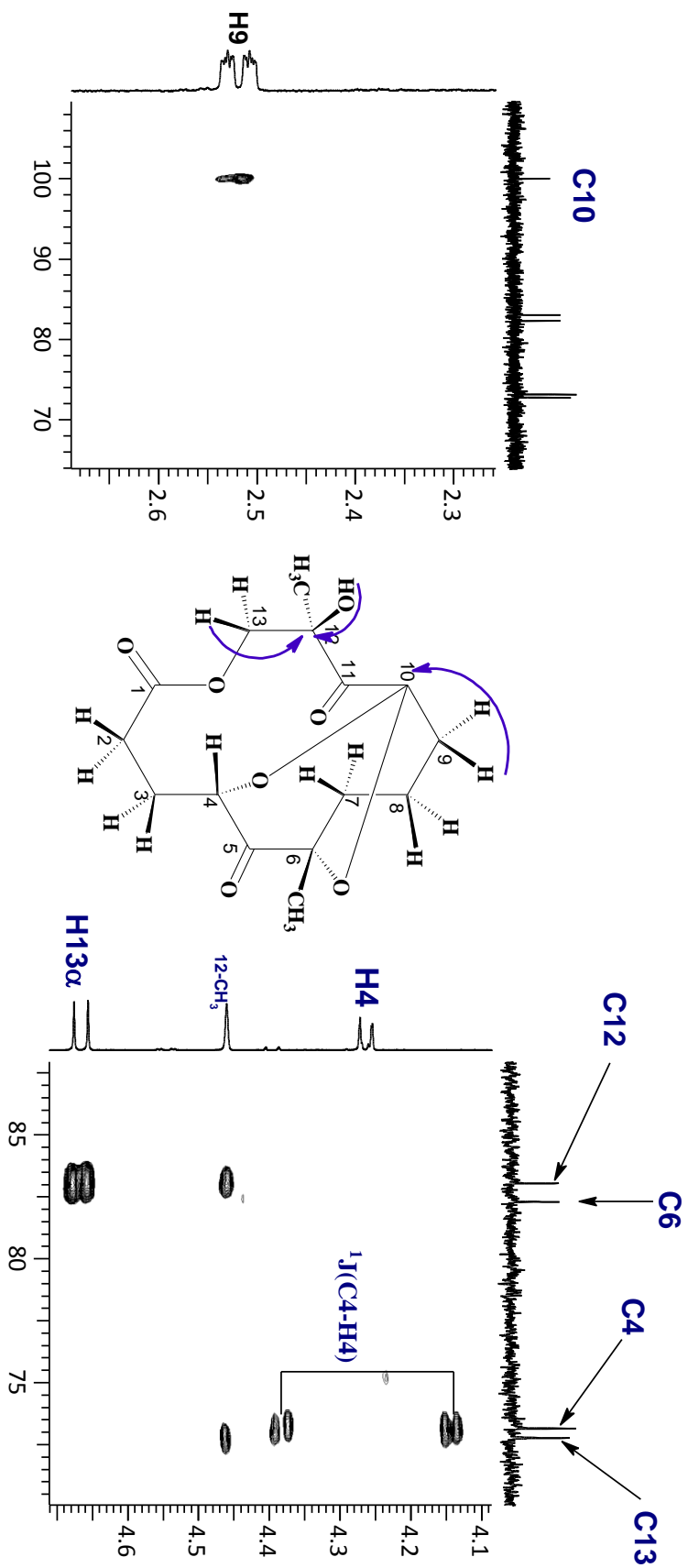
Long-range correlations in C_6D_6 : $^1J_{CH}$ was set to 132 Hz



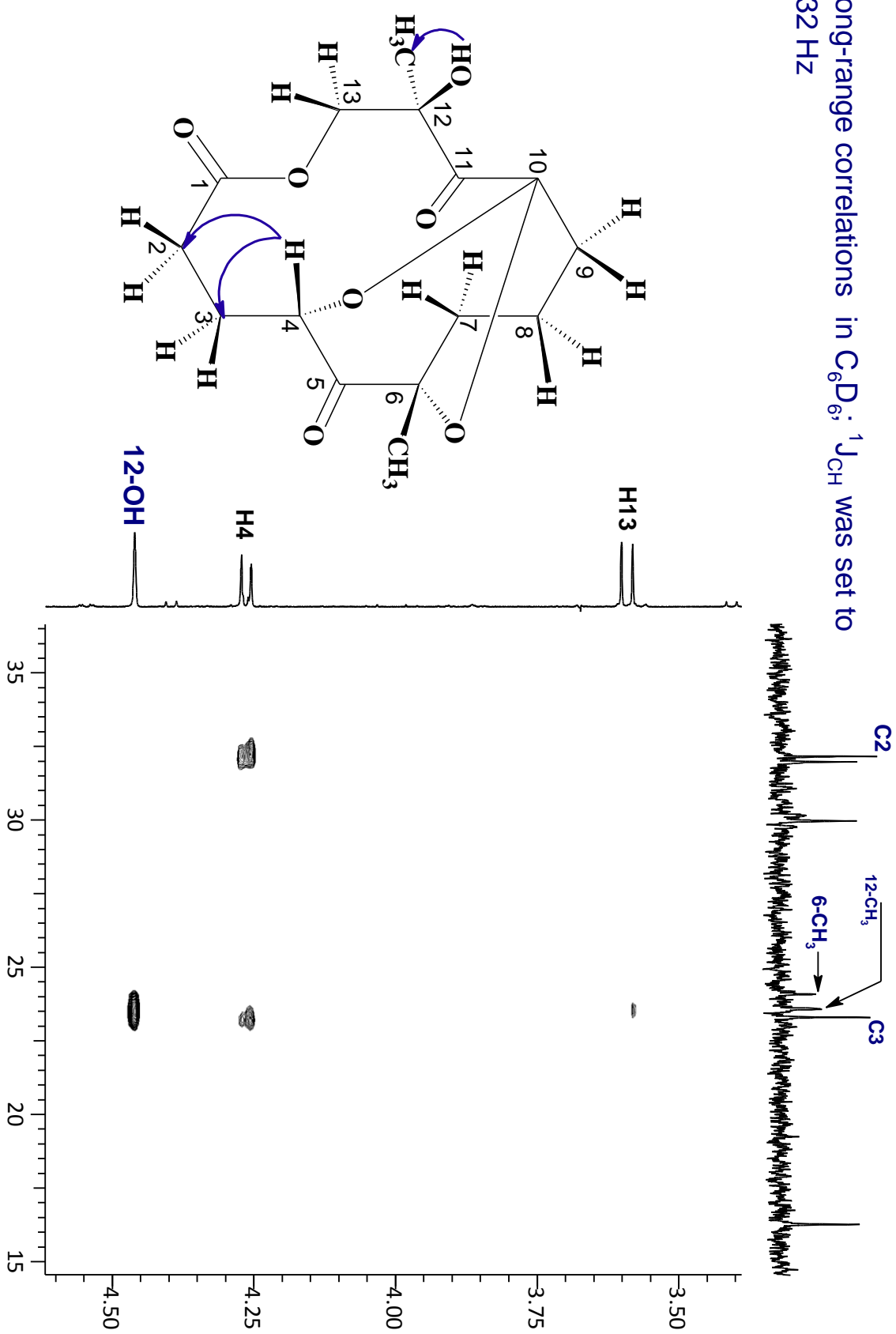
Long-range correlations in C_6D_6 : $^1J_{CH}$ was set to 132 Hz



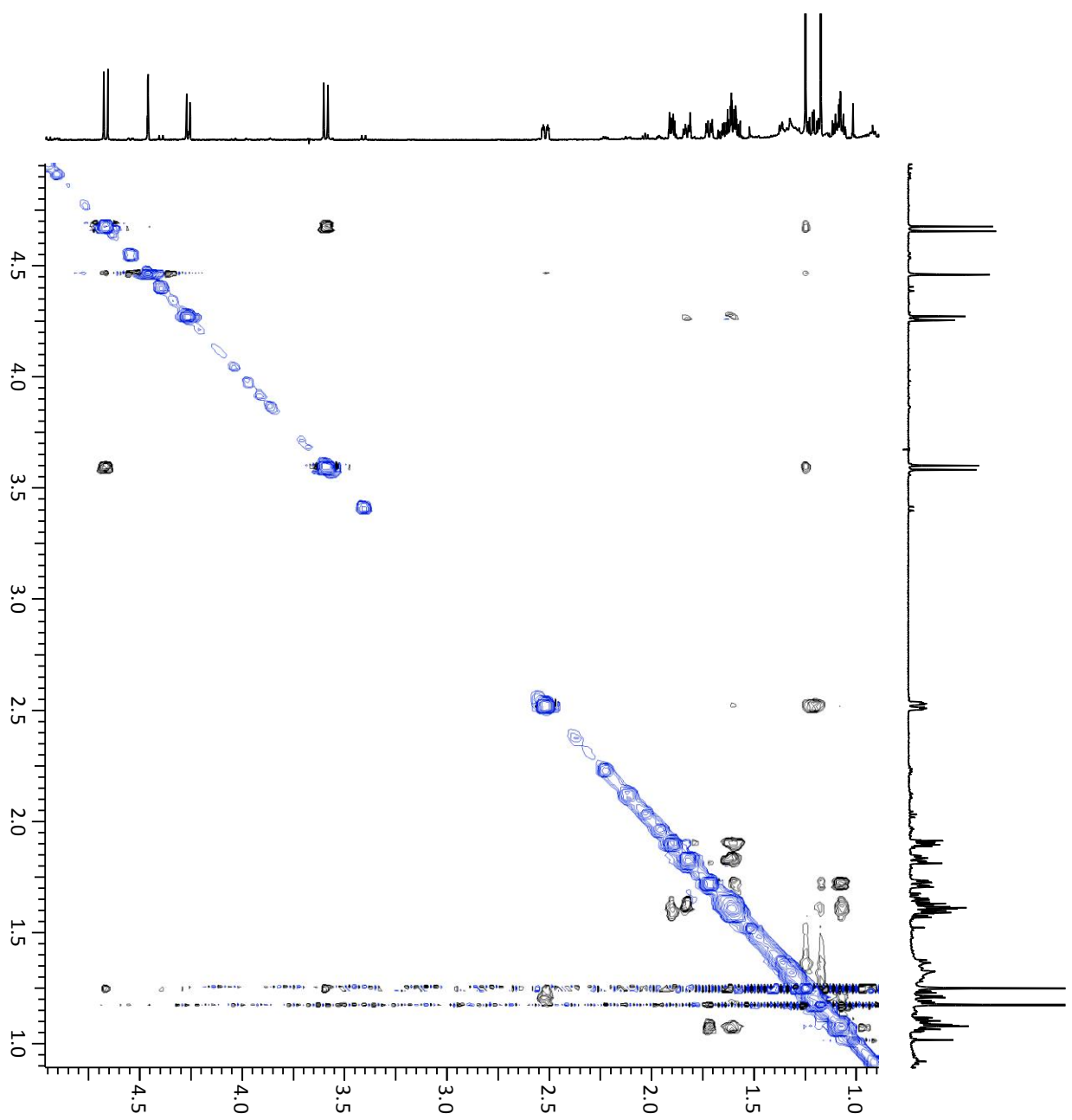
Long-range correlations in C_6D_6 : $^1J_{CH}$ was set to 132 Hz

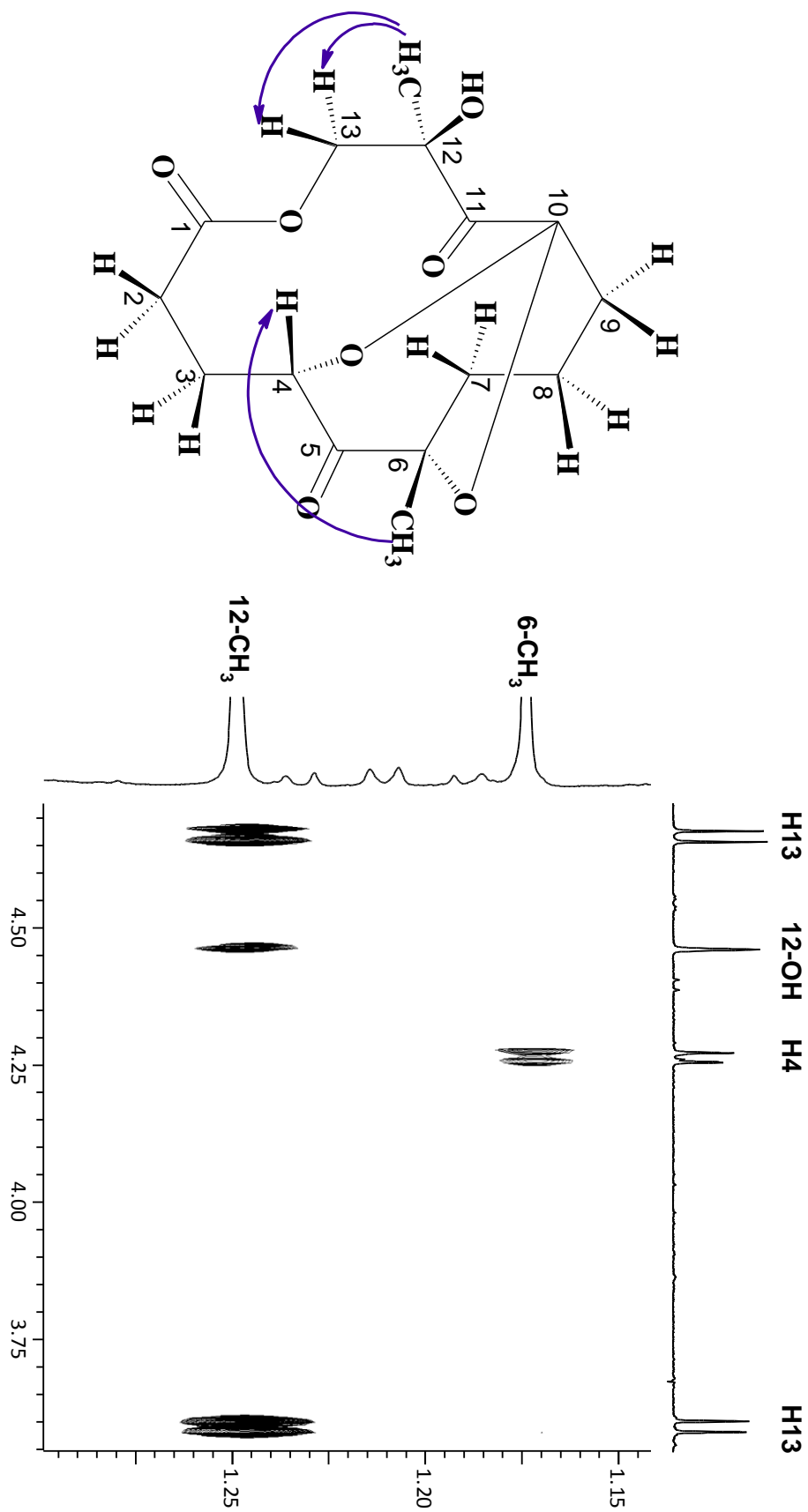


Long-range correlations in C_6D_6 : $^1J_{CH}$ was set to 132 Hz

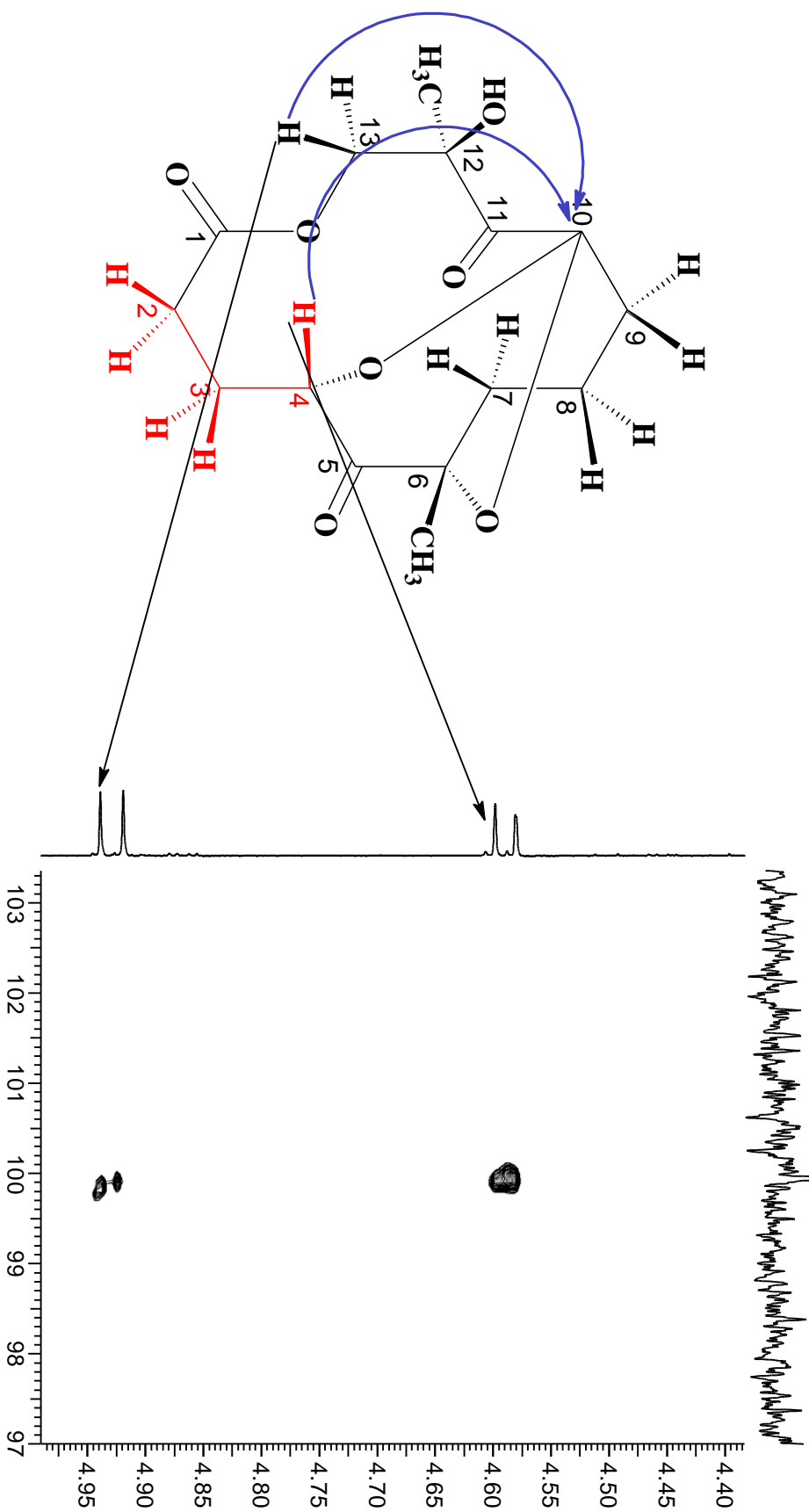


NOESY

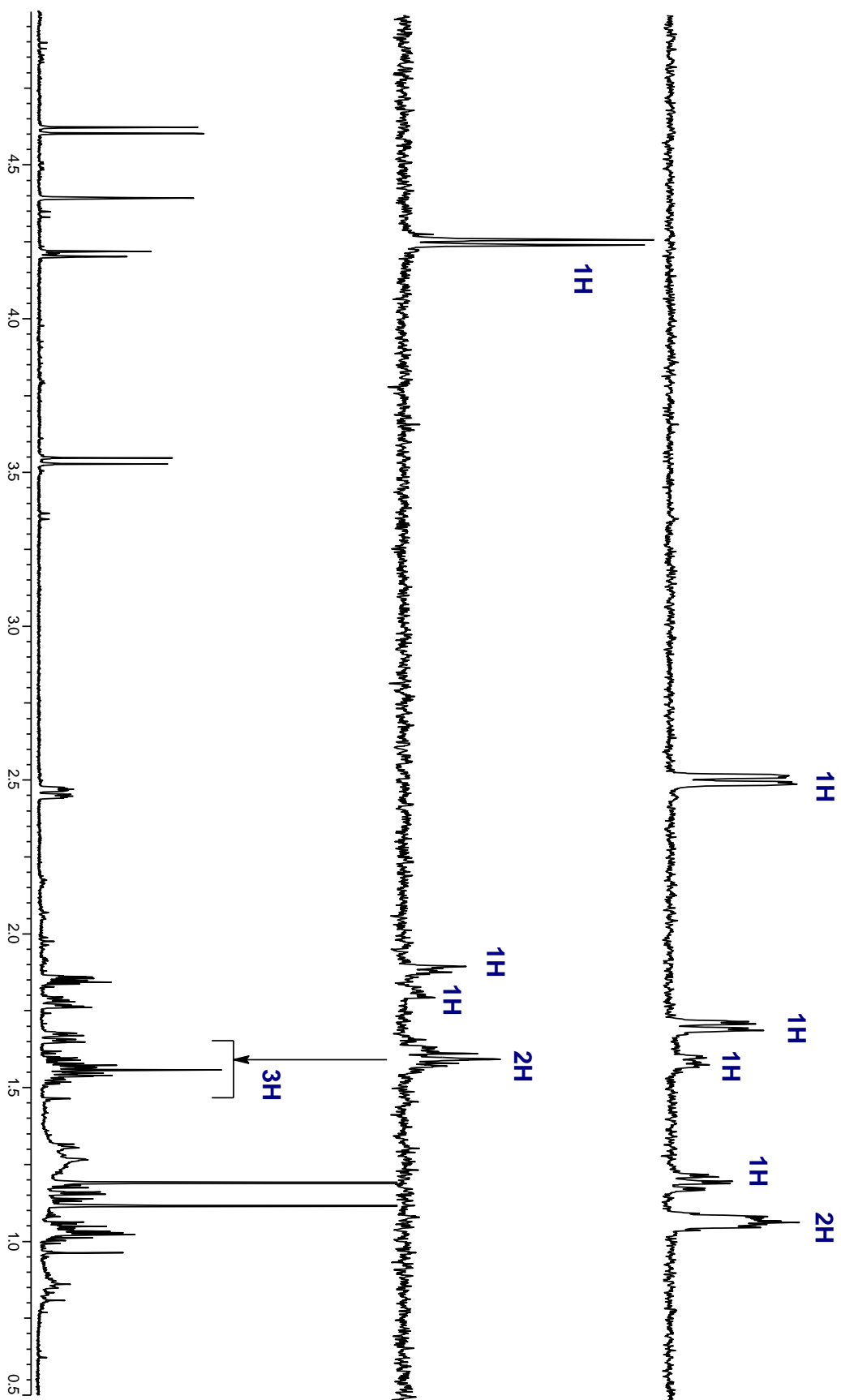


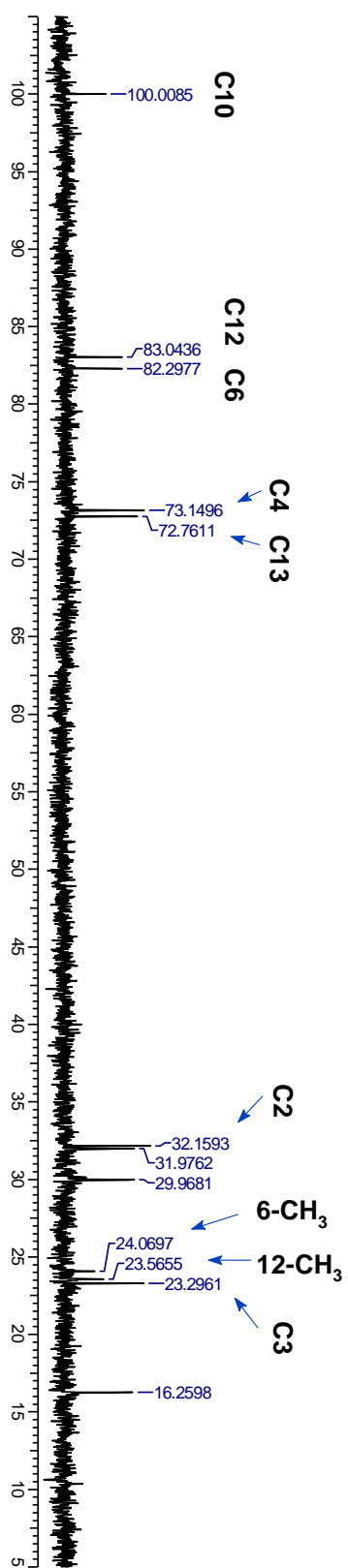
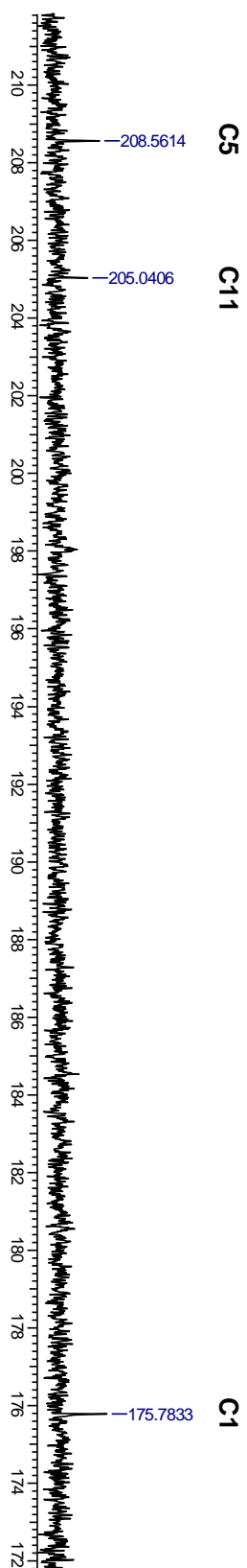
NOESY*expansion*

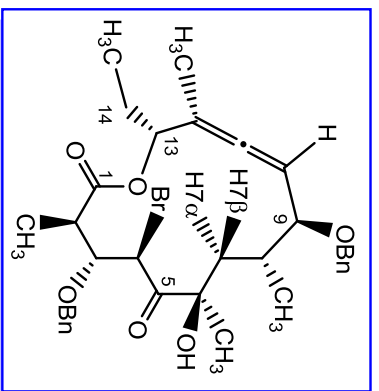
Long-range correlations through oxygen in CDCl_3 ;
 $^1J_{\text{CH}}$ was set to 145 Hz



Spin system isolations

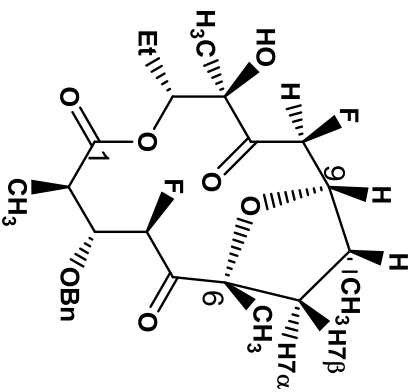


^{13}C NMR spectrum in C_6D_6 



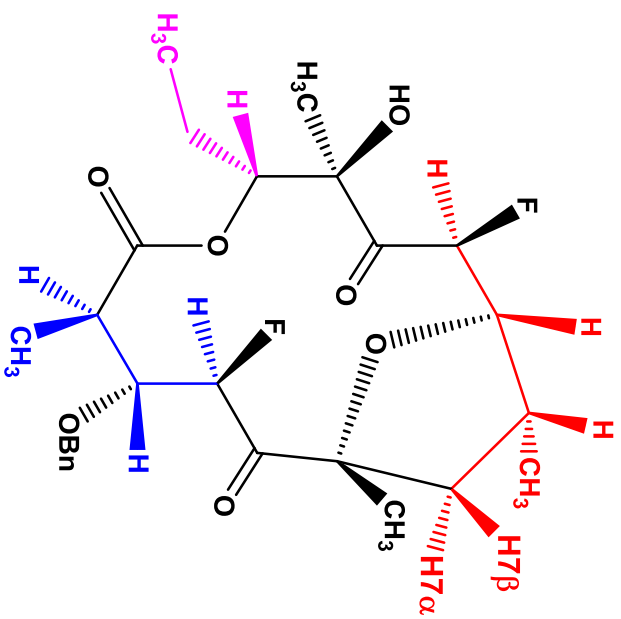
¹H NMR chemical shifts (δ/ppm) & coupling constant (J/Hz)

- 2.76** (quintet, $J_{H2, H3} = 6.6\text{Hz}$, **H2**)
1.25 (d, $J_{2\text{-CH}_3, H2} = 7.3\text{Hz}$, **2-CH₃**)
3.53 (dd, $J_{H3, H4} = 8.6\text{Hz}$, $J_{H3, H2} = 6.6\text{Hz}$, **H3**)
4.98 (d, $J_{H4, H3} = 4.2\text{Hz}$, **H4**)
1.49 (s, **6-CH₃**)
1.32 (dd, $J_{H7\beta, H7\alpha} = 14.2\text{Hz}$, **H7β**)
2.08 (dd, $J_{H7\alpha, H8} = 6.1\text{ Hz}$, $J_{H7\alpha, H7\beta} = 14.4\text{Hz}$, **H7α**)
1.81 - 1.68 (m, **H8**)
1.05 (d, $J_{8\text{-CH}_3, H8} = 6.9\text{Hz}$, **8-CH₃**)
4.38 (m, **H9**)
4.70, 4.58 (d, $J_{AB} = 10.5\text{Hz}$, **9-OCH₂**)
4.76, 4.51 (d, $J_{AB} = 12.0\text{Hz}$, **9-OCH₂**)
5.25 - 5.21 (m, **H10**)
1.83 (d, $J_{12\text{-CH}_3, H10} = 2.9\text{Hz}$, **12-CH₃**)
5.31 (T, $J_{H13, 14\text{-CH}_2} = 7.3\text{Hz}$, **H13**)
2.18 - 2.11 (m, **14-CH₂**)
0.90 (t, $J_{14\text{-CH}_3, 14\text{-CH}_2} = 7.3\text{Hz}$, **14-CH₃**)
7.42 - 7.29 (m, 8H, **Ph**)

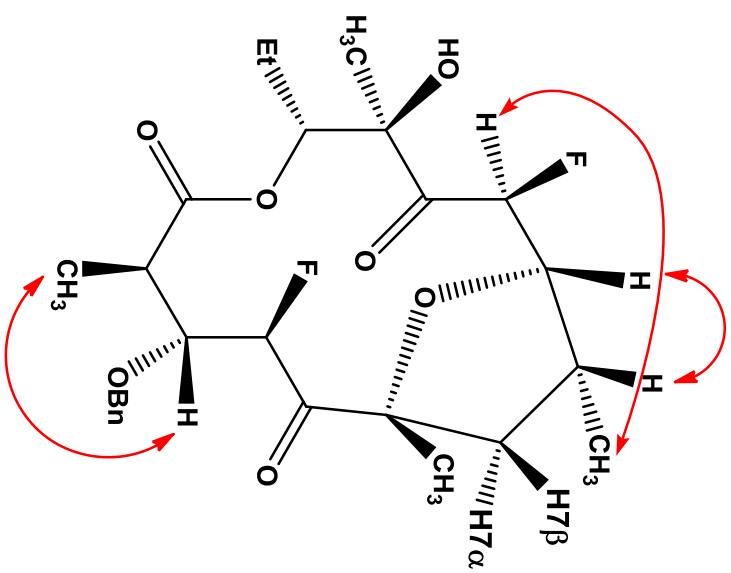


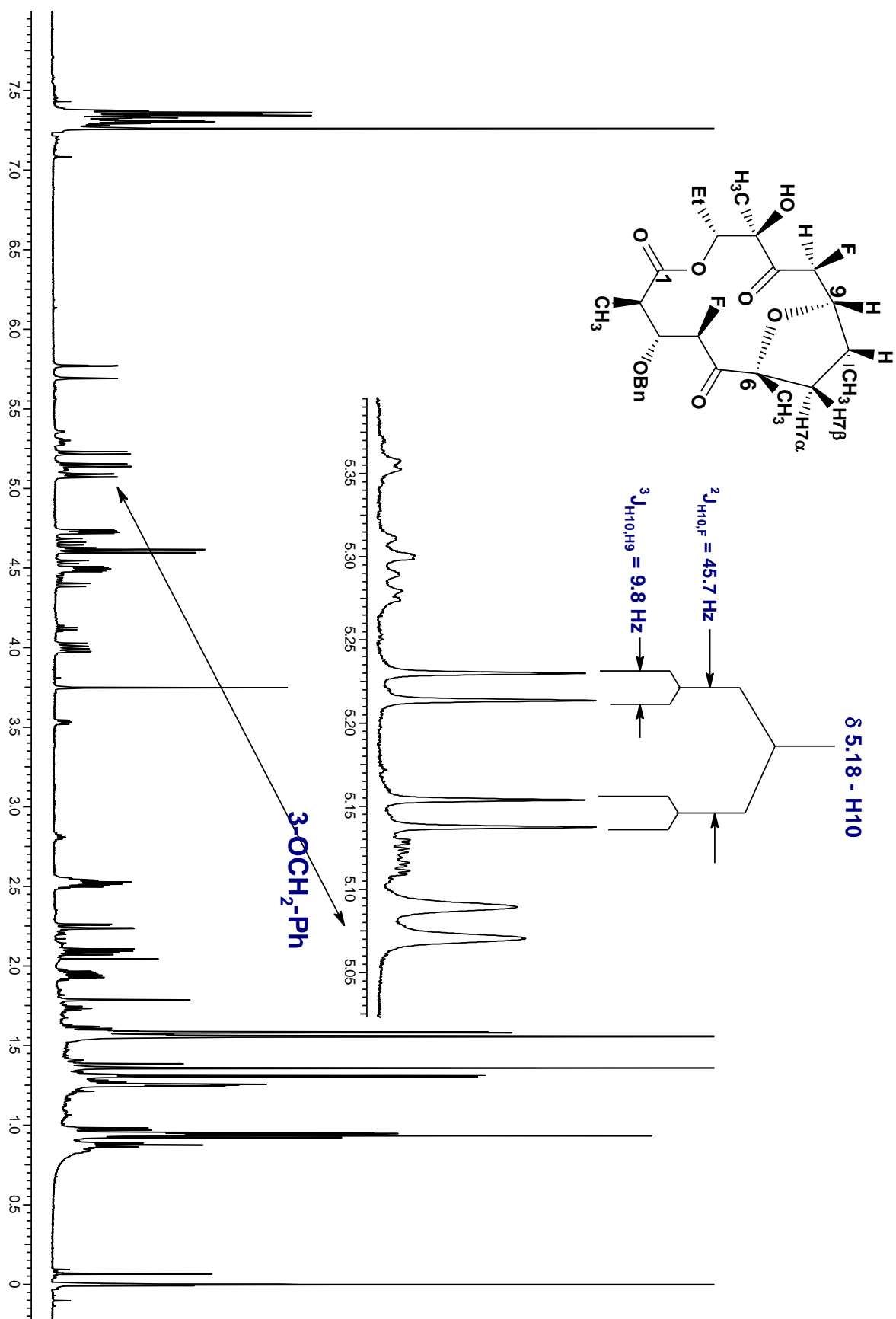
¹ H NMR chemical shifts (δ/ppm) & coupling constant (J/Hz)	¹³ C NMR chemical shift (δ/ppm)
2.51 (dq, J _{H2} , H3 = 10.6Hz, H2)	172.9 — C1
1.31 (d, J _{2-CH3} , H2 = 7.3Hz, 2-CH3)	41.0 — C2, J _{CF} =10.2Hz
4.01 (dd, J _{H3} , F = 20.9Hz, J _{H3} , H2 = 11.2Hz, H3)	79.1 — C3
5.75 (dd, J _{H4} , F = 46.9Hz, J _{H4} , H3 = 1.0Hz, H4)	91.4 — C4, J _{CF} =178.6Hz
1.35 (s, 6-CH3)	202.7 — C5, J _{CF} =14.9Hz
2.25 (dd, J _{H7α} , H8 = 2.5 Hz, J _{H7α} , H7β = 13.6Hz, H7α)	89.2 — C6
2.09 (dd, J _{H7β} , H8 = 8.1Hz, J _{H7β} , H7α = 13.6Hz, H7β)	40.8 — C7
2.53 (dddd, H8)	33.6 — C8
0.95 (d, J _{8-CH3} , H8 = 7.1Hz, 8-CH3)	75.5 — C9, J _{CF} =31.6Hz
4.49 (ddd, J _{H9} , H8 = 5.3Hz, J _{H9} , H10 = 9.8Hz, J _{H9} , F = 2.6Hz, H9)	85.1 — C10, J _{CF} =170.3Hz
4.61 (d, J _{AB} = 11.5Hz, 3-OCH2)	205.7 — C11, J _{CF} =13.5Hz
5.08 (d, J _{AB} = 11.5Hz, 3-OCH2)	78.1 — C12
5.18 (dd, J ₁₀ , F = 45.7, J _{H10} , H9 = 9.8Hz, H10)	79.5 — C13
1.58 (d, J _{12CH3} , 12-OH = 2.5Hz, 12-CH3)	22.9 — C14
3.74 (s, 12-OH)	16.4 — 2-CH3
4.73 (ddd, J _{H13} , H4 = 3.6 Hz, J _{H13} , H8 = 9.1 Hz, H13)	24.8 — 6-CH3
1.91 - 1.98, 1.56 - 1.63 (m, 14-CH2)	15.0 — 8-CH3
0.93 (t, J _{14-CH3} , 13-CH2 = 7.6Hz, 14-CH3)	16.2 — 12-CH3
7.36 (orthoH / Ph)	10.6 — 14-CH3
7.34 (metaH / Ph)	74.5 — 3-OCH ₂ PH
7.30 (paraH / Ph)	137.8 — ipsoC
	128.6 — orthoC
	128.3 — metaC
	127.8 — paraC

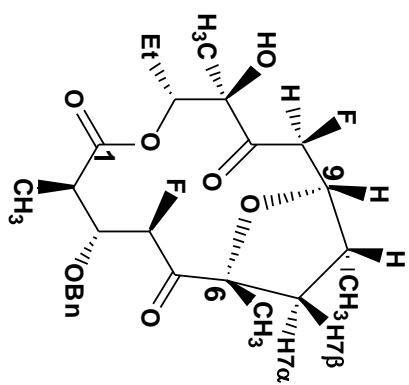
¹d TOCSY



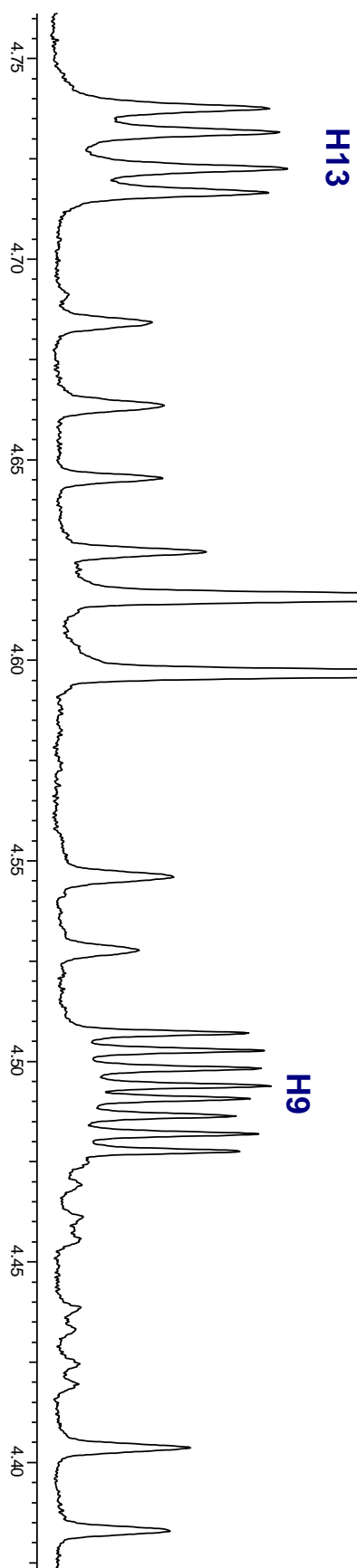
NOESY

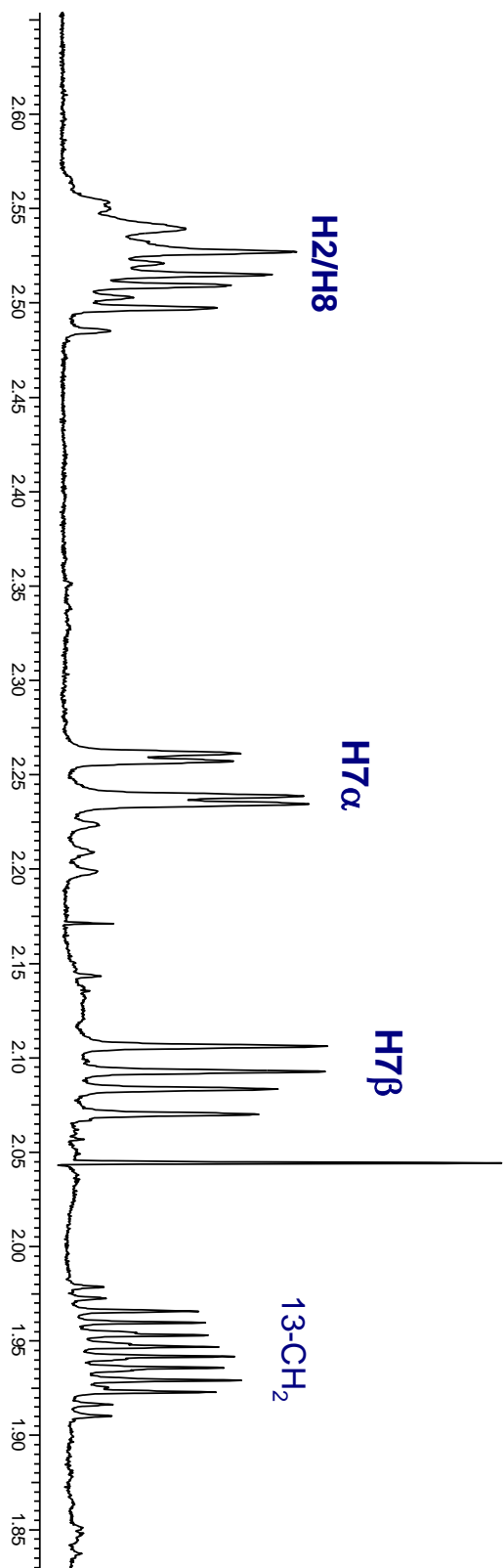
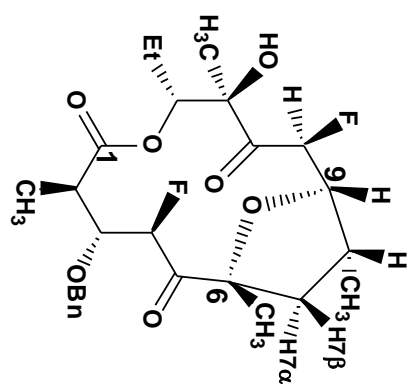


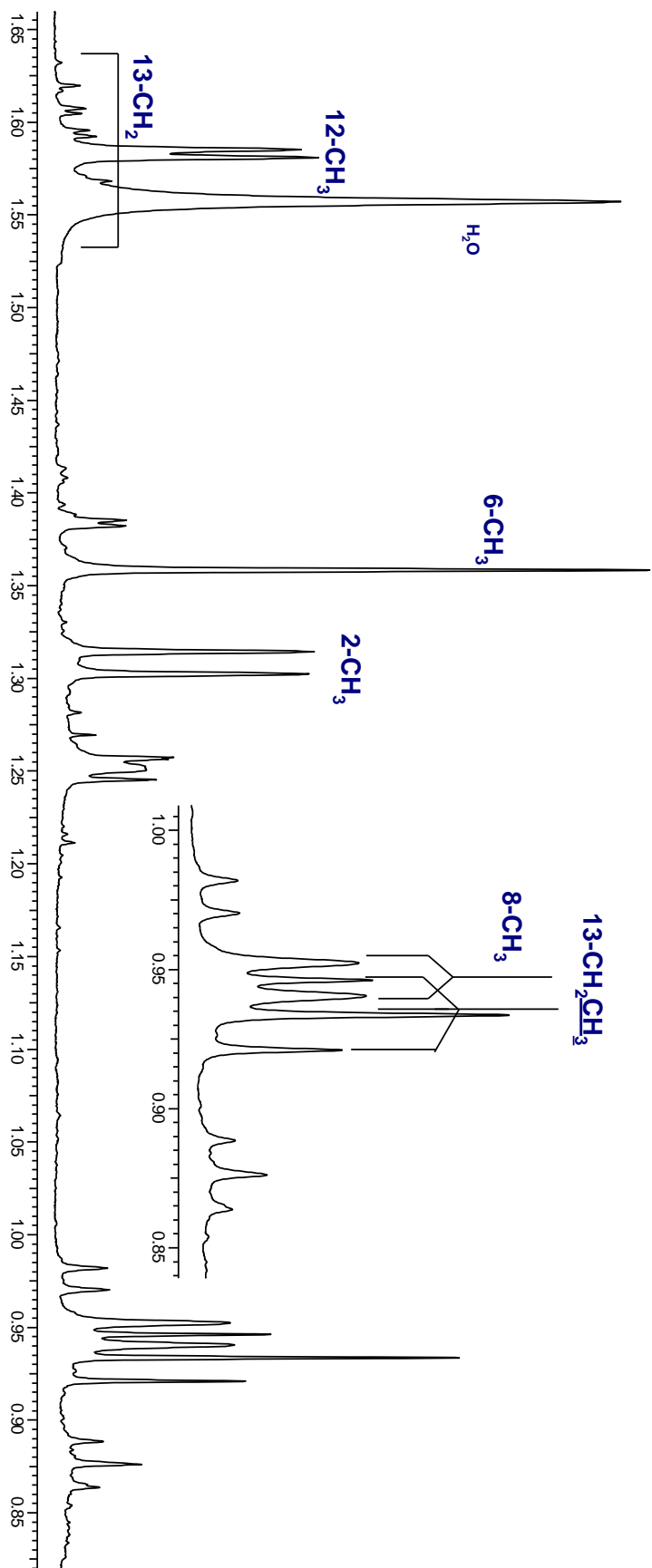
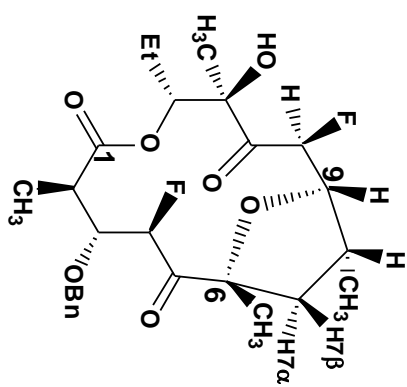




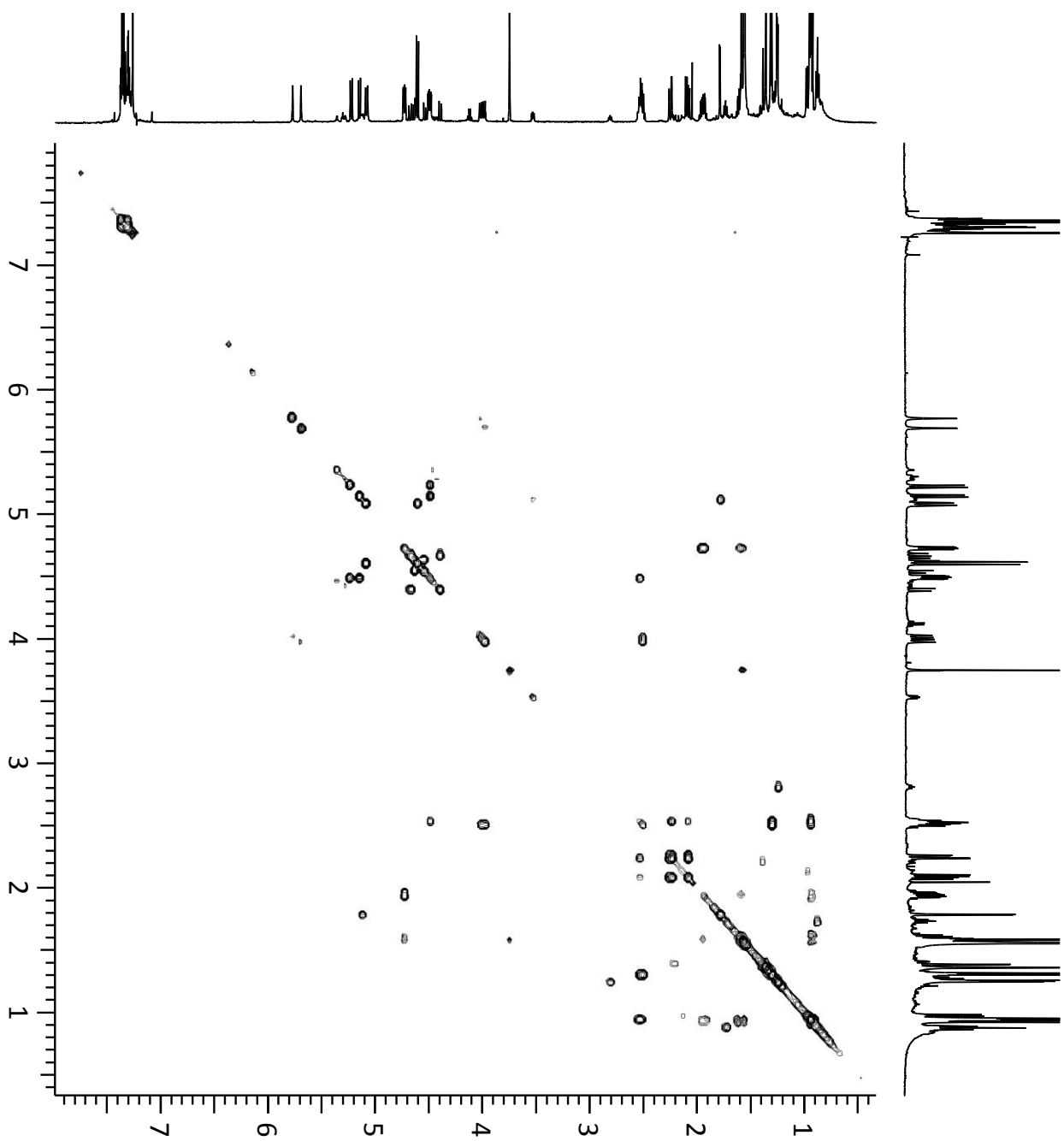
3-OCH₂





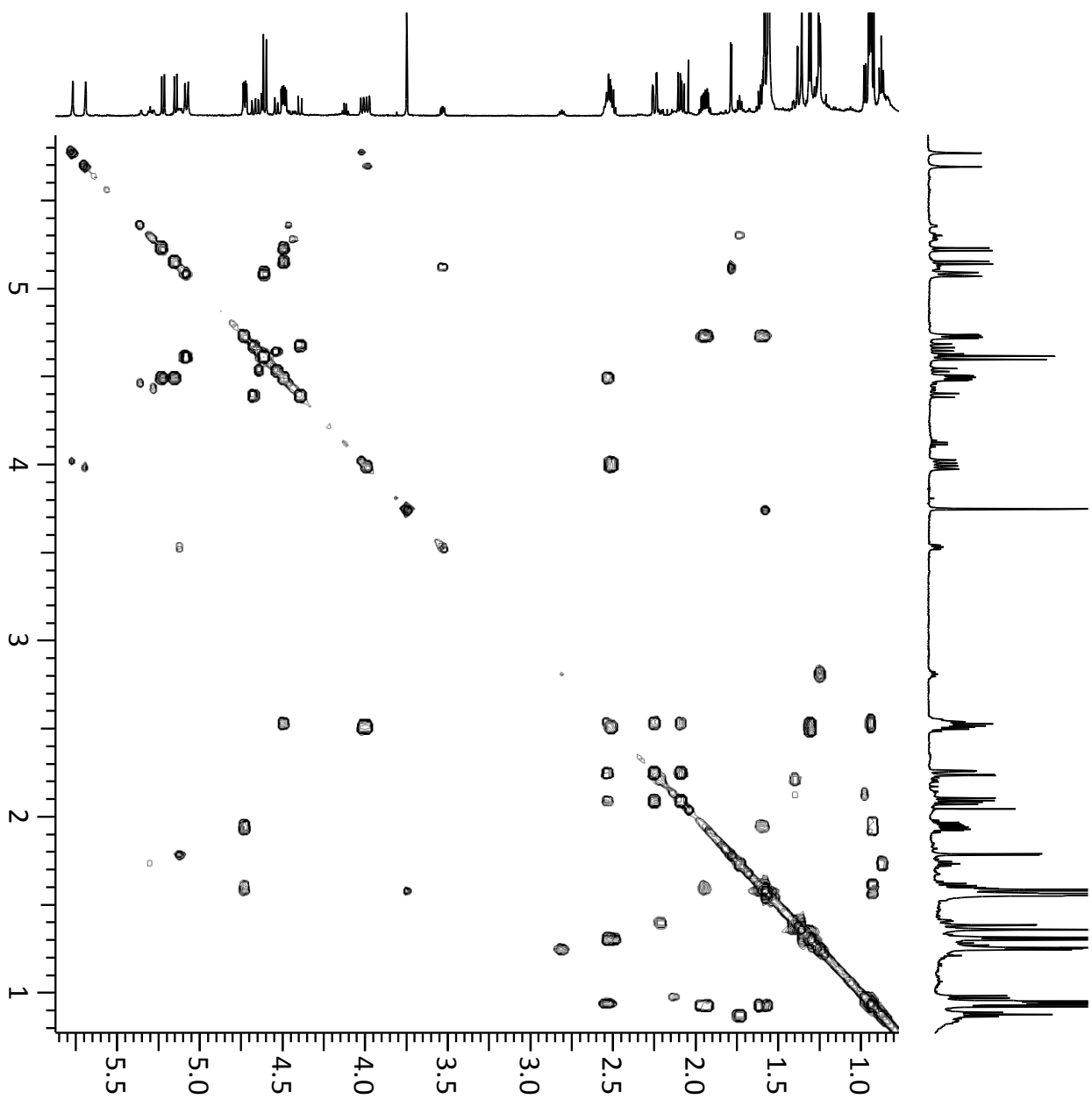


gCOSY

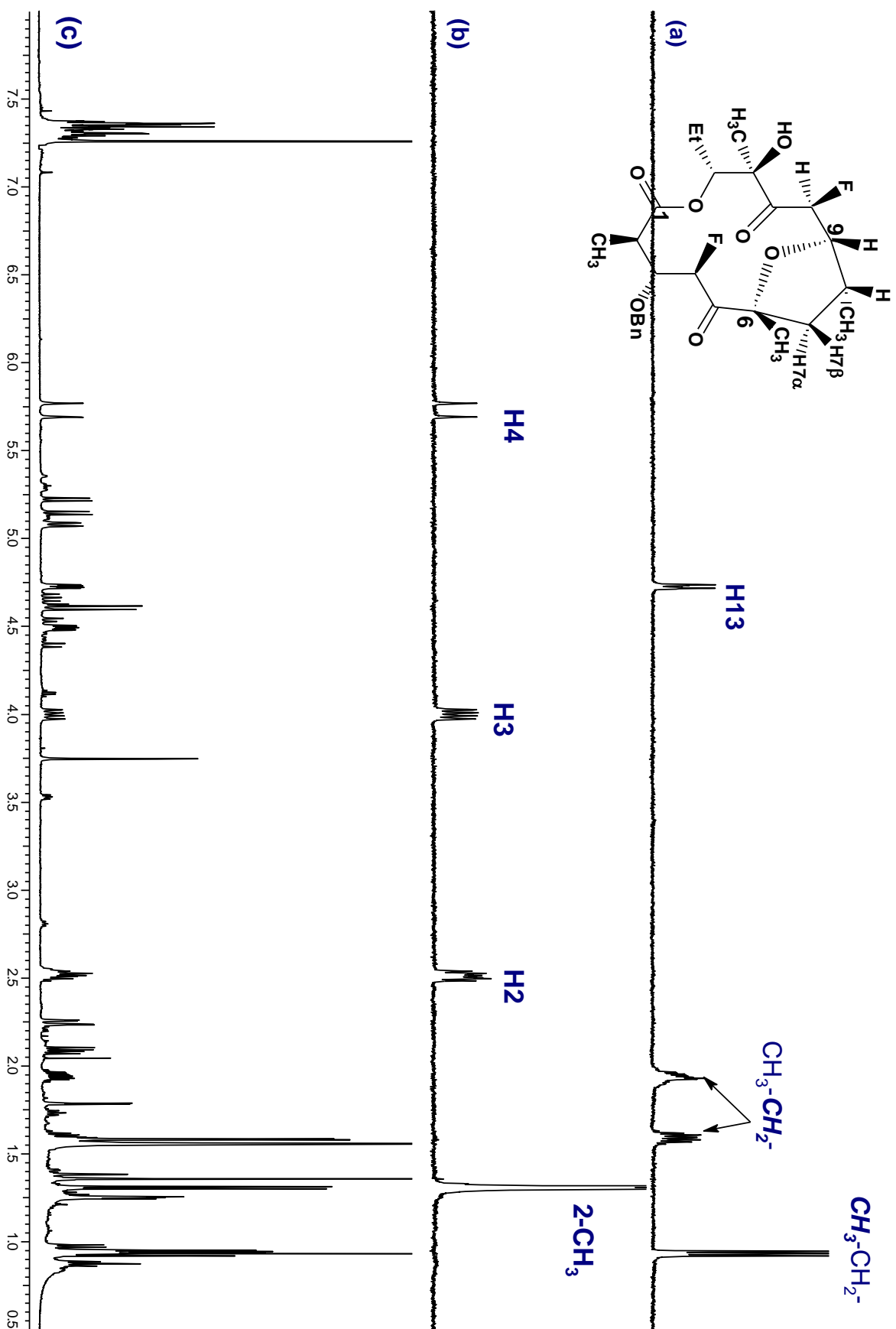


gcosy

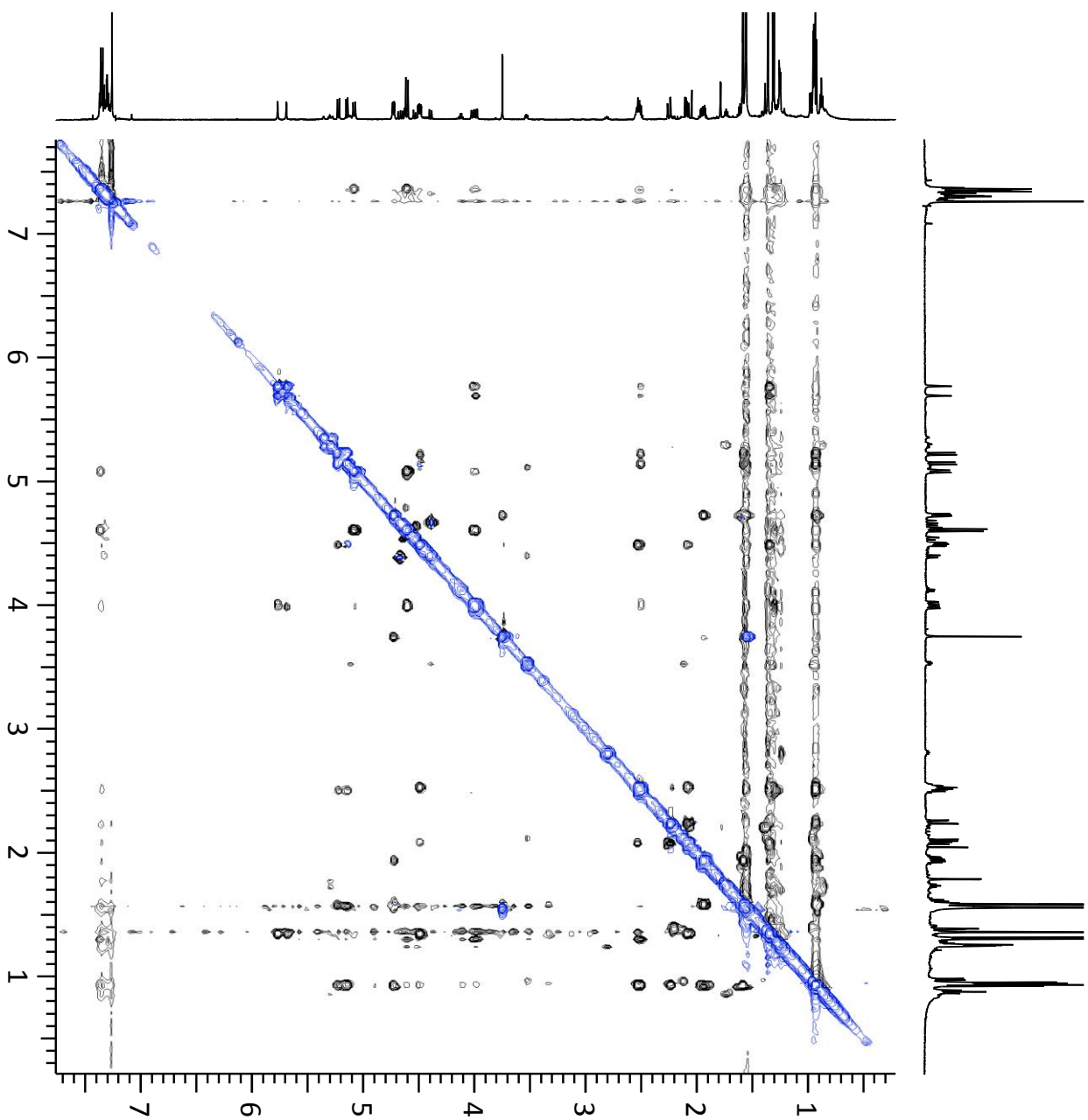
aliphatic region



1D TOCSY experimental subspectra (a-b); c- control ^1H NMR spectrum

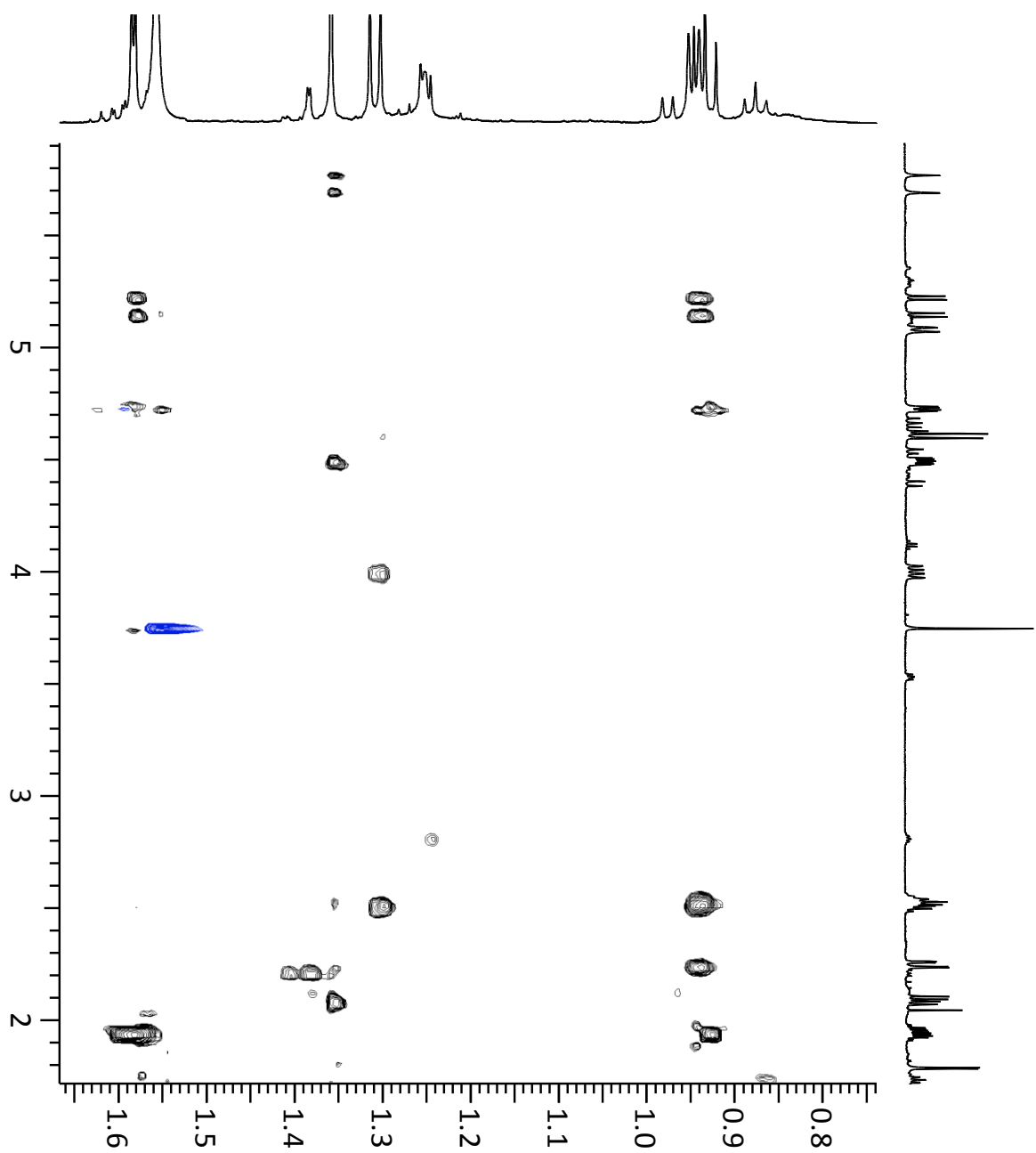


NOESY

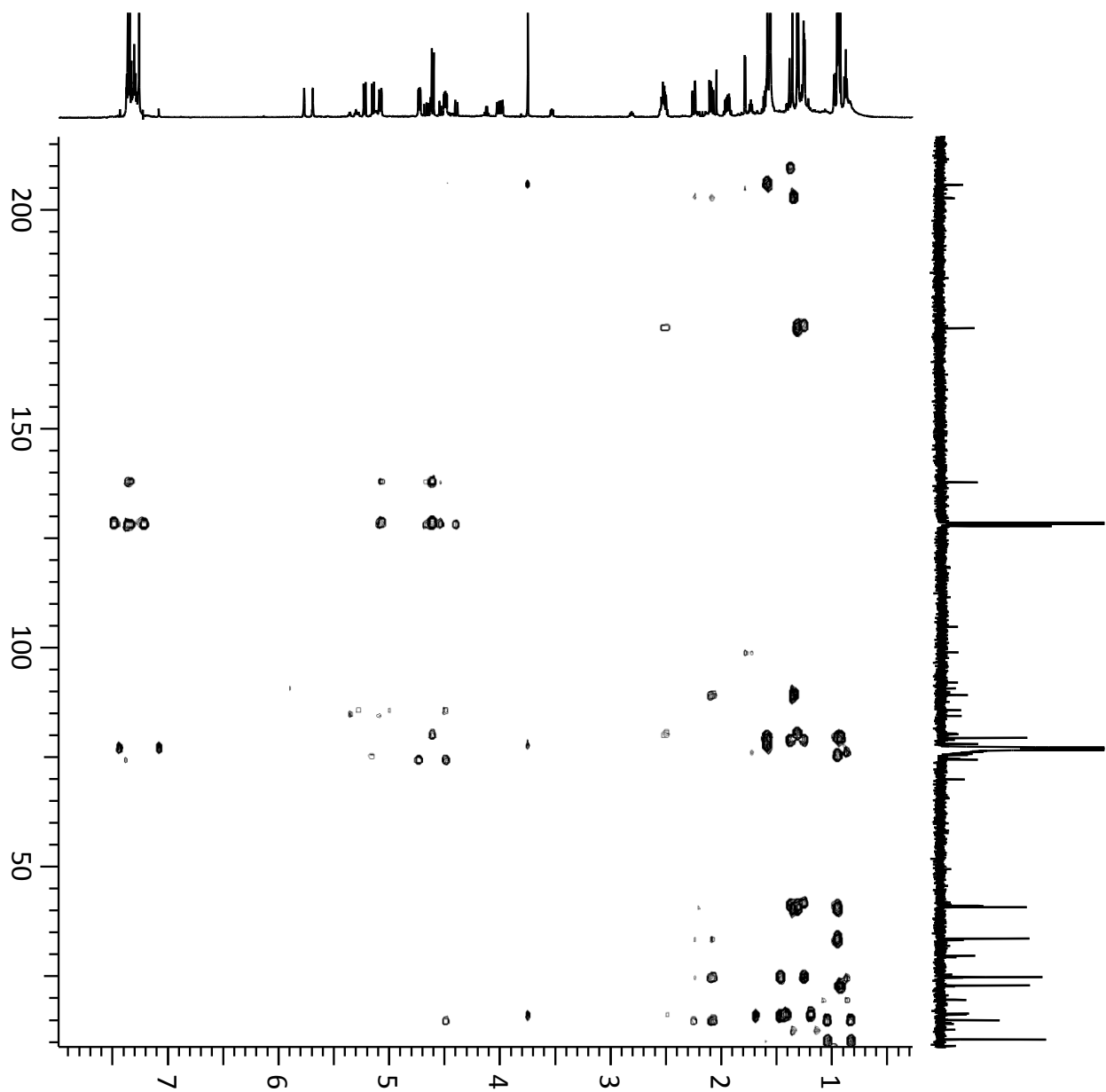


NOESY

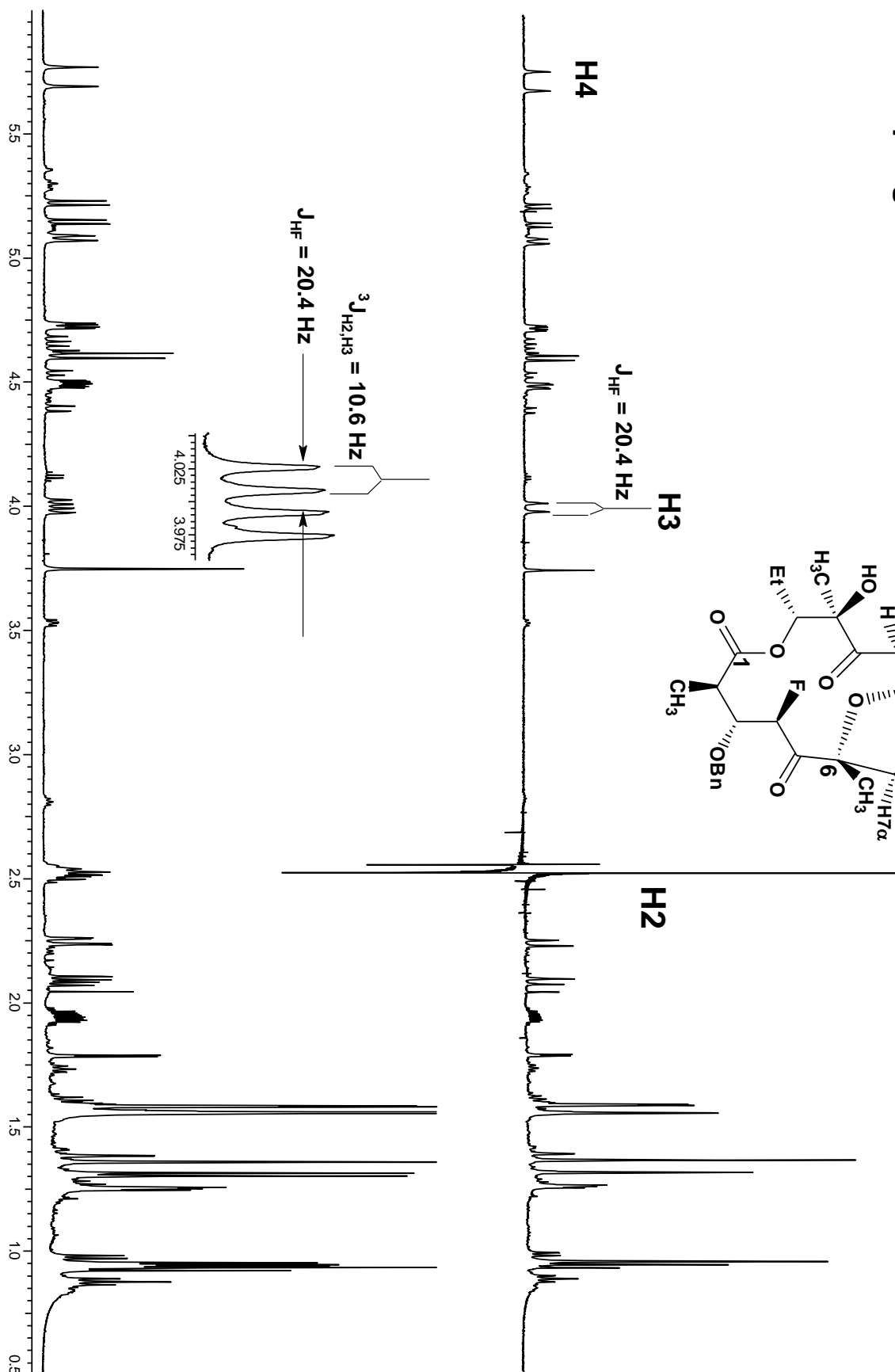
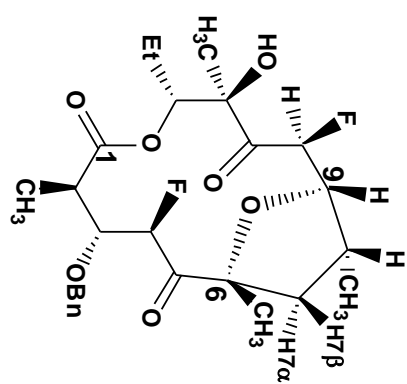
expansion



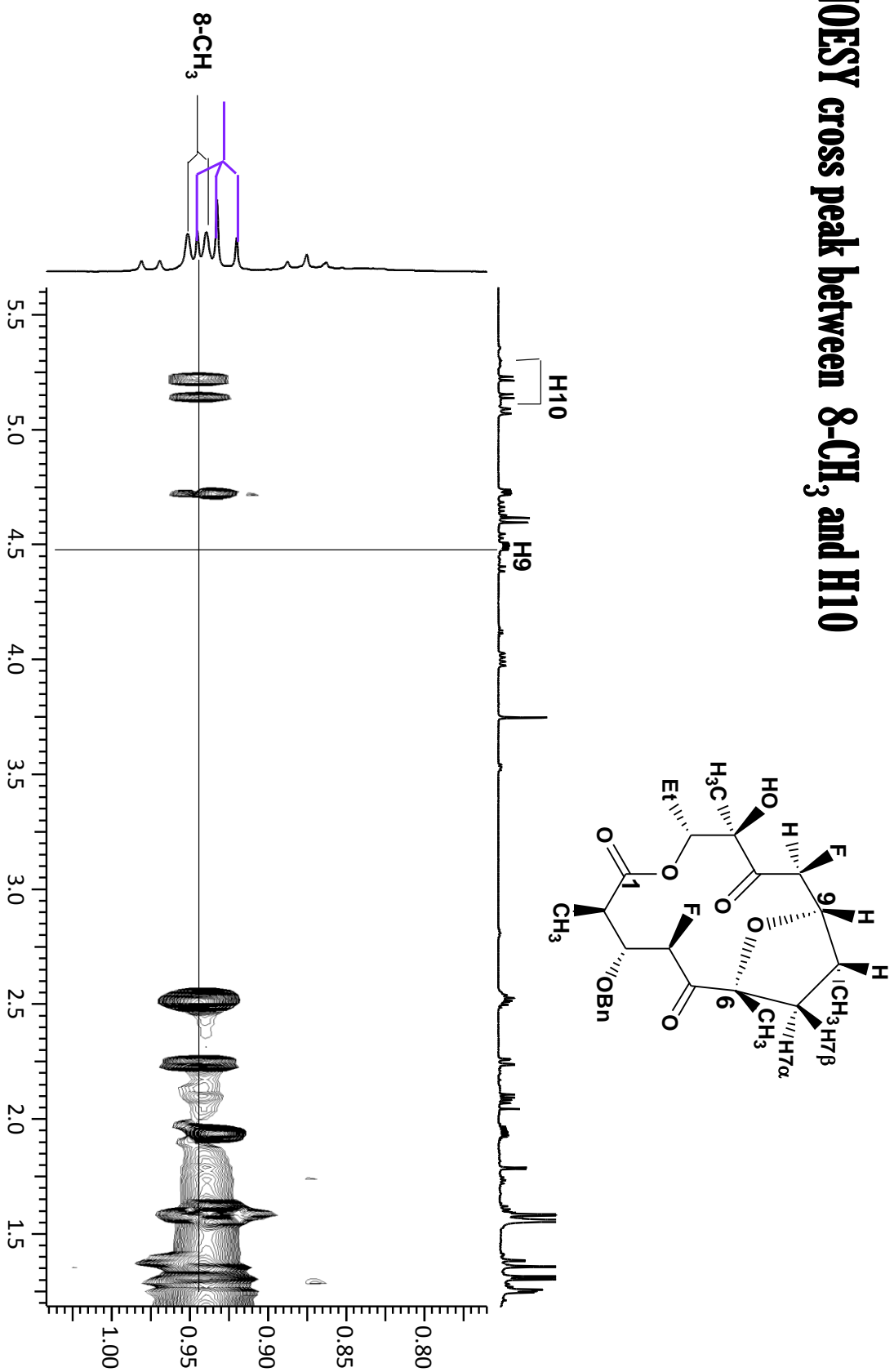
gHMBc



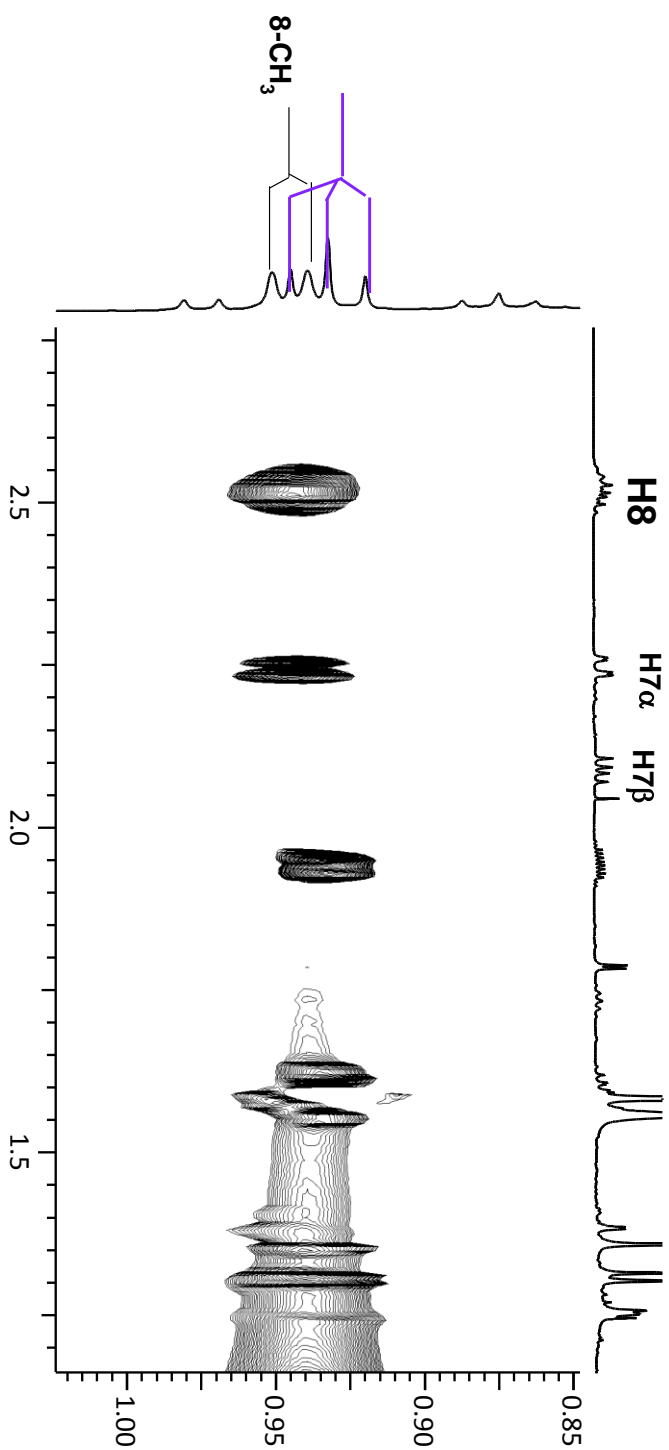
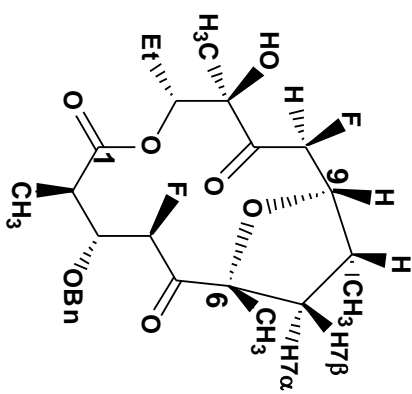
Selective decoupling of H2



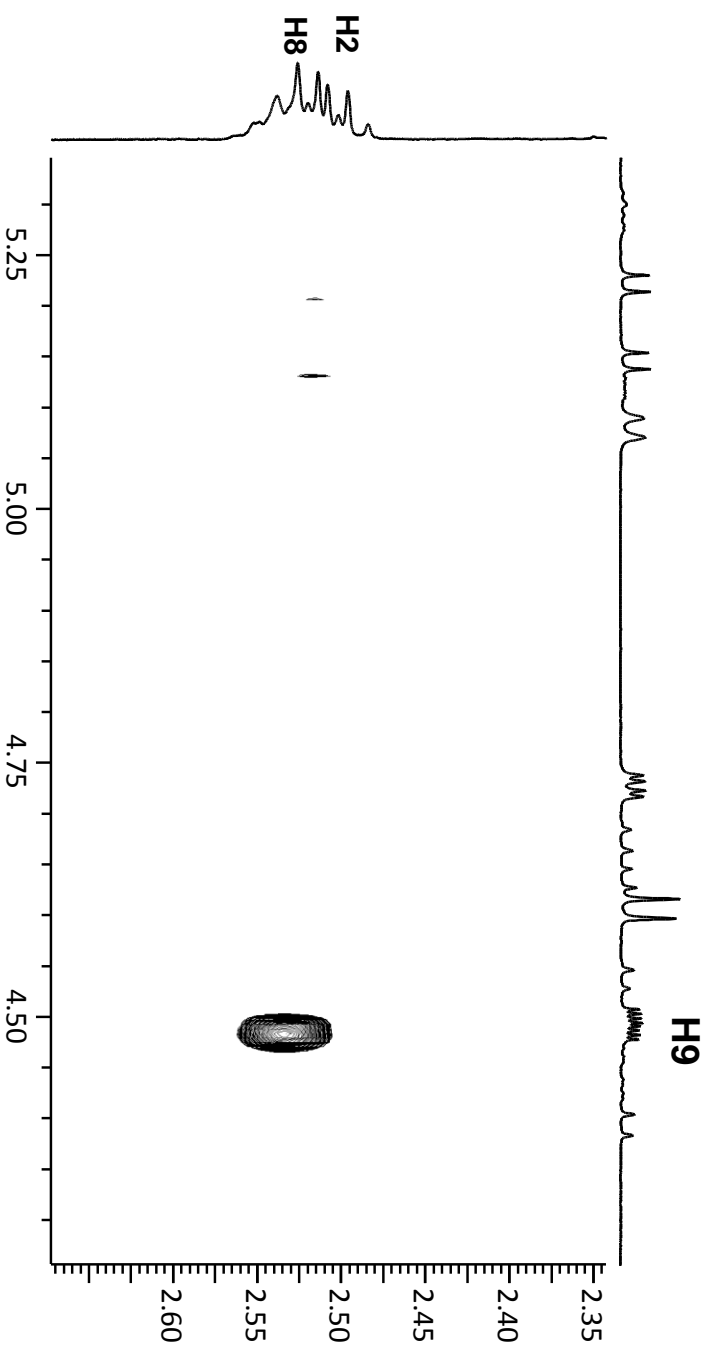
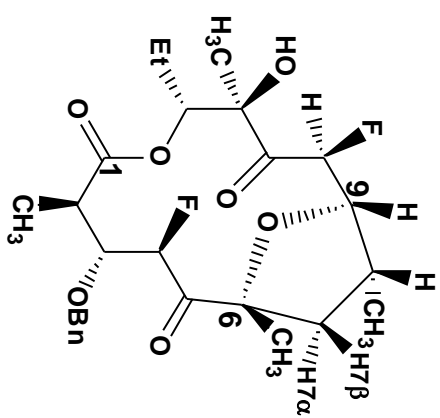
NOESY cross peak between 8-CH₃ and H10



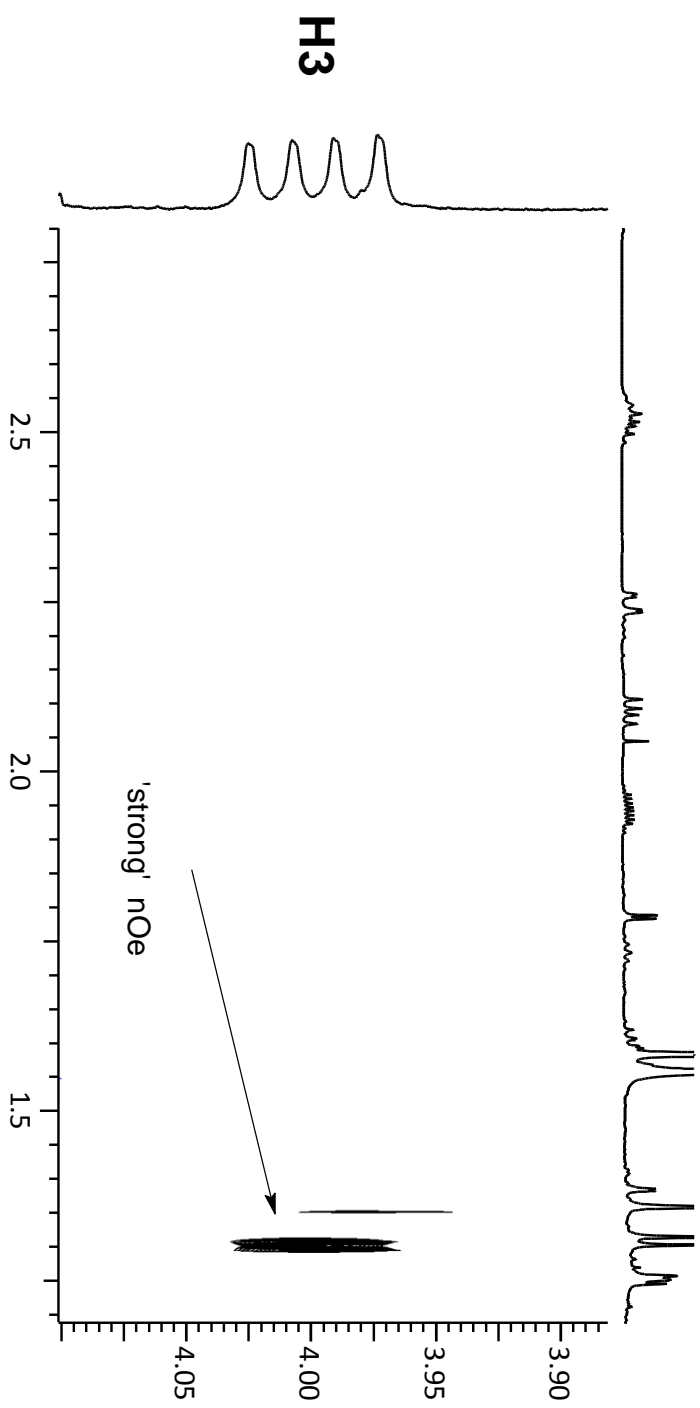
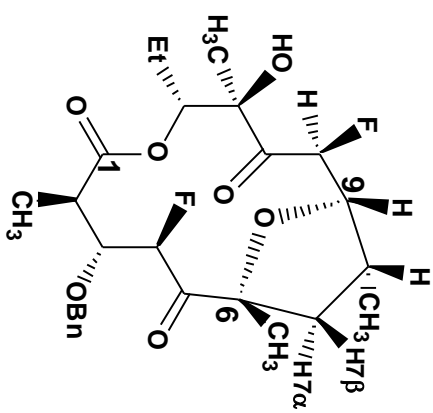
NOESY cross peaks between 8-CH₃ and others

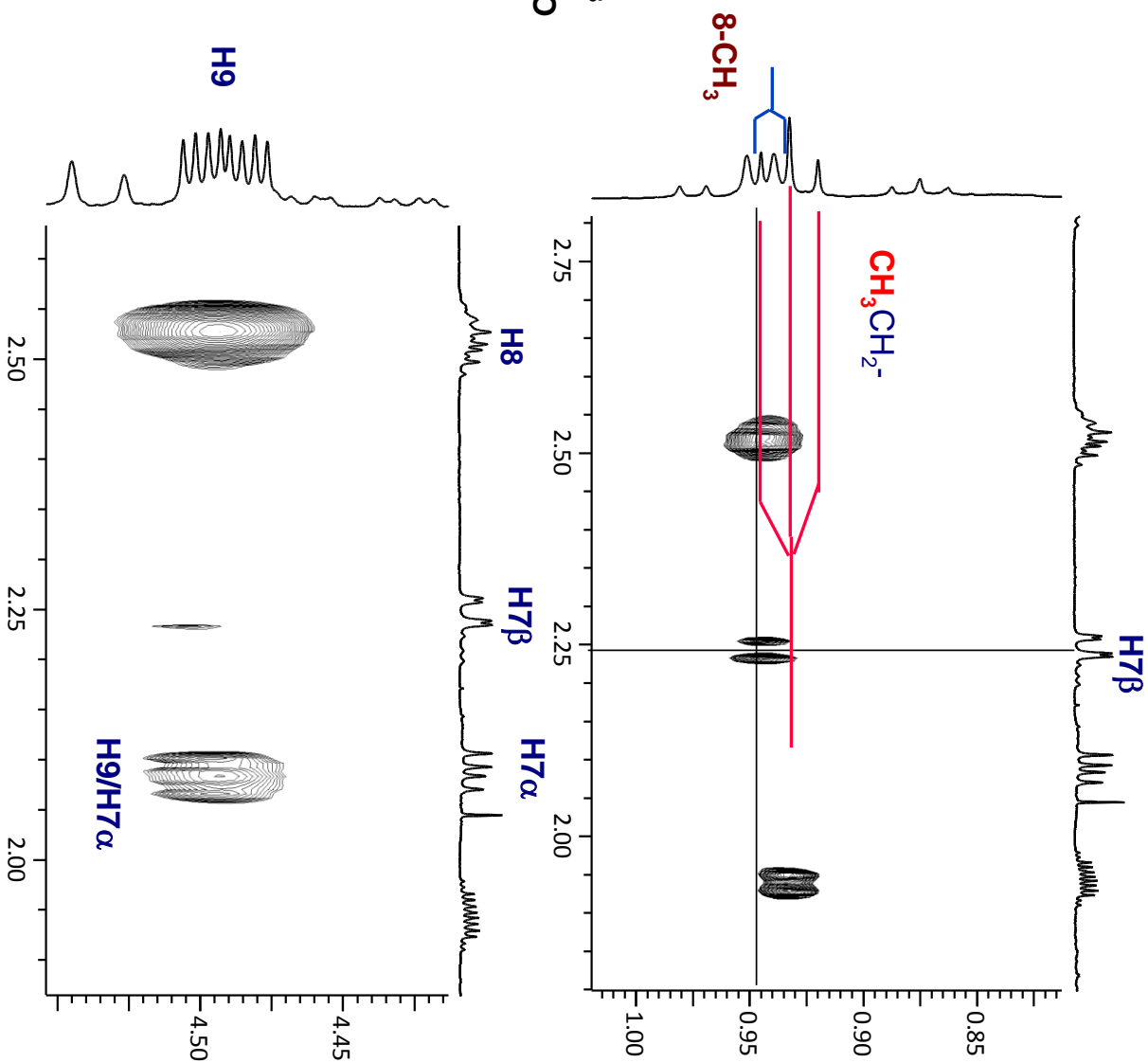
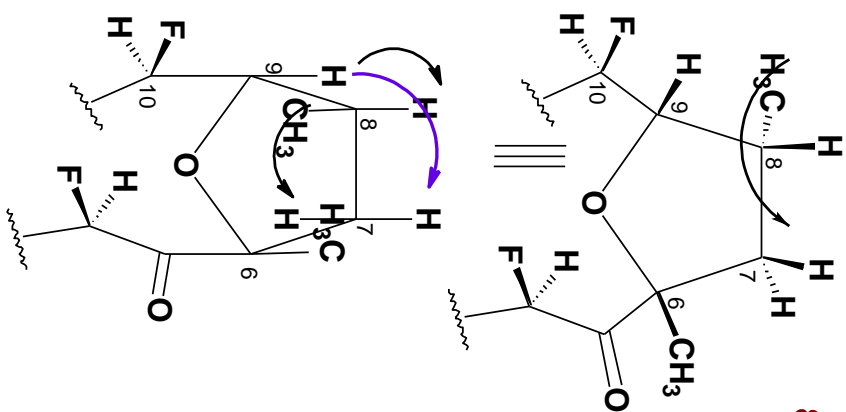
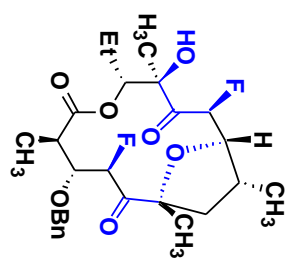


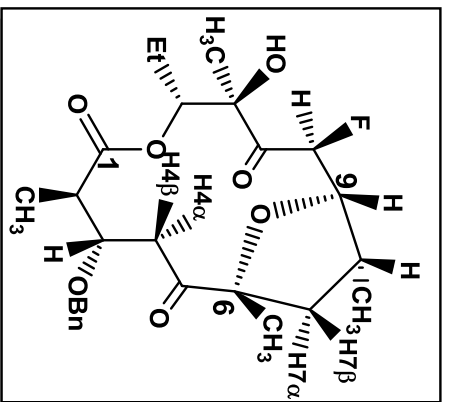
NOESY cross peak between H8 and H9



NOESY cross peak between H3 and 2-CH₃

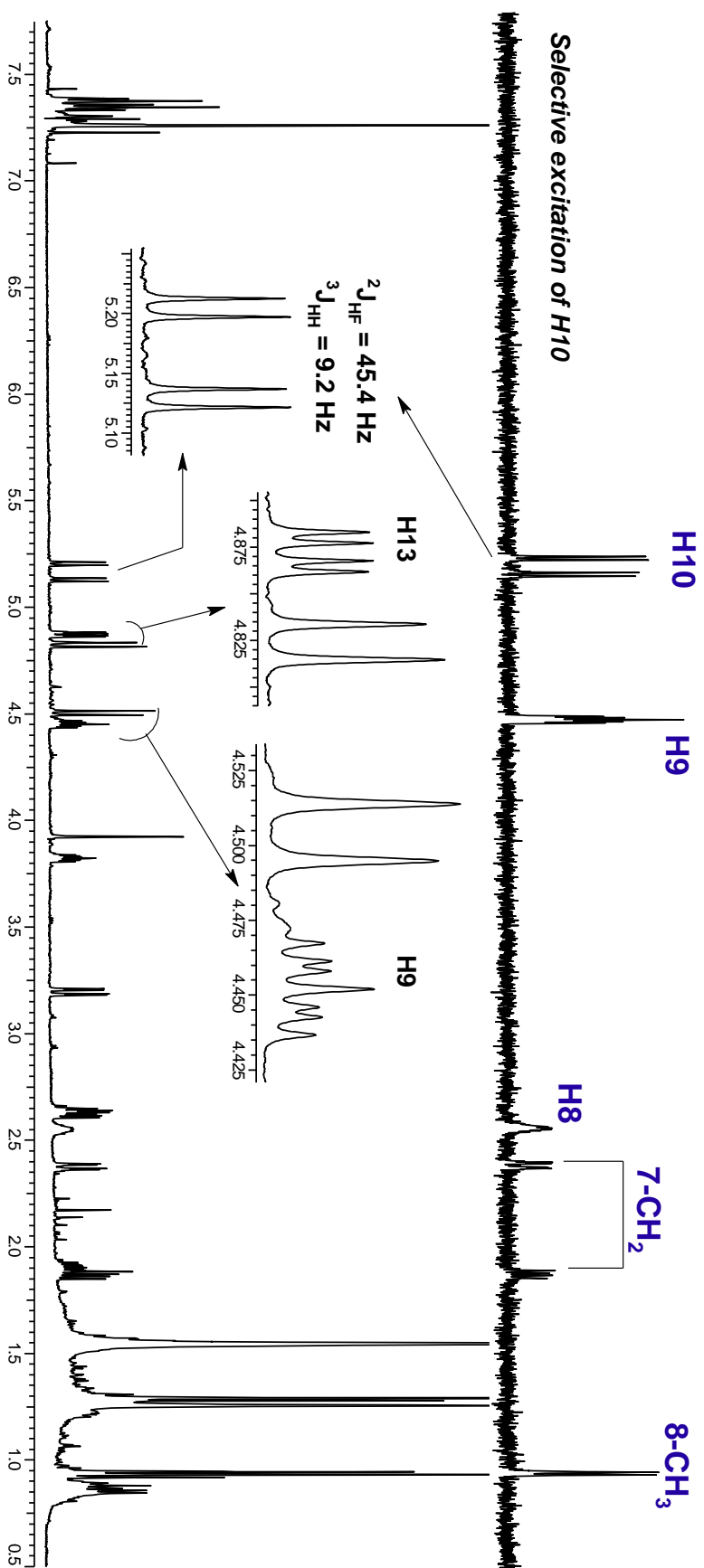
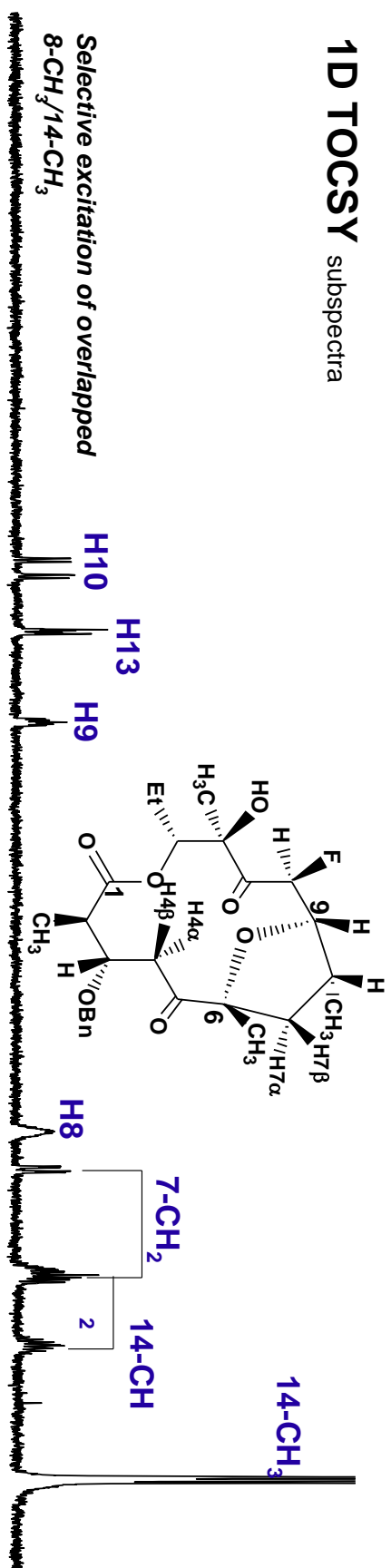




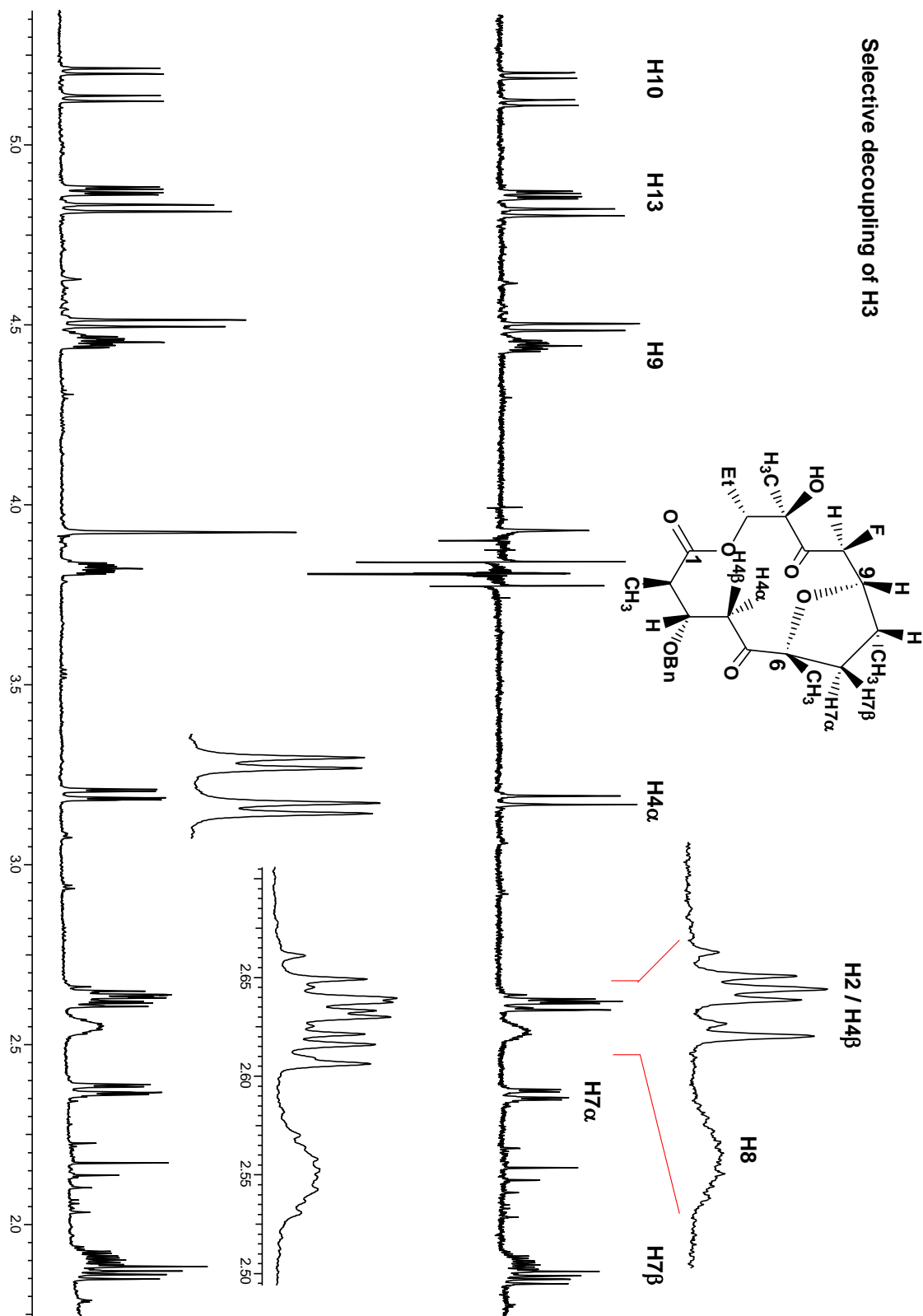


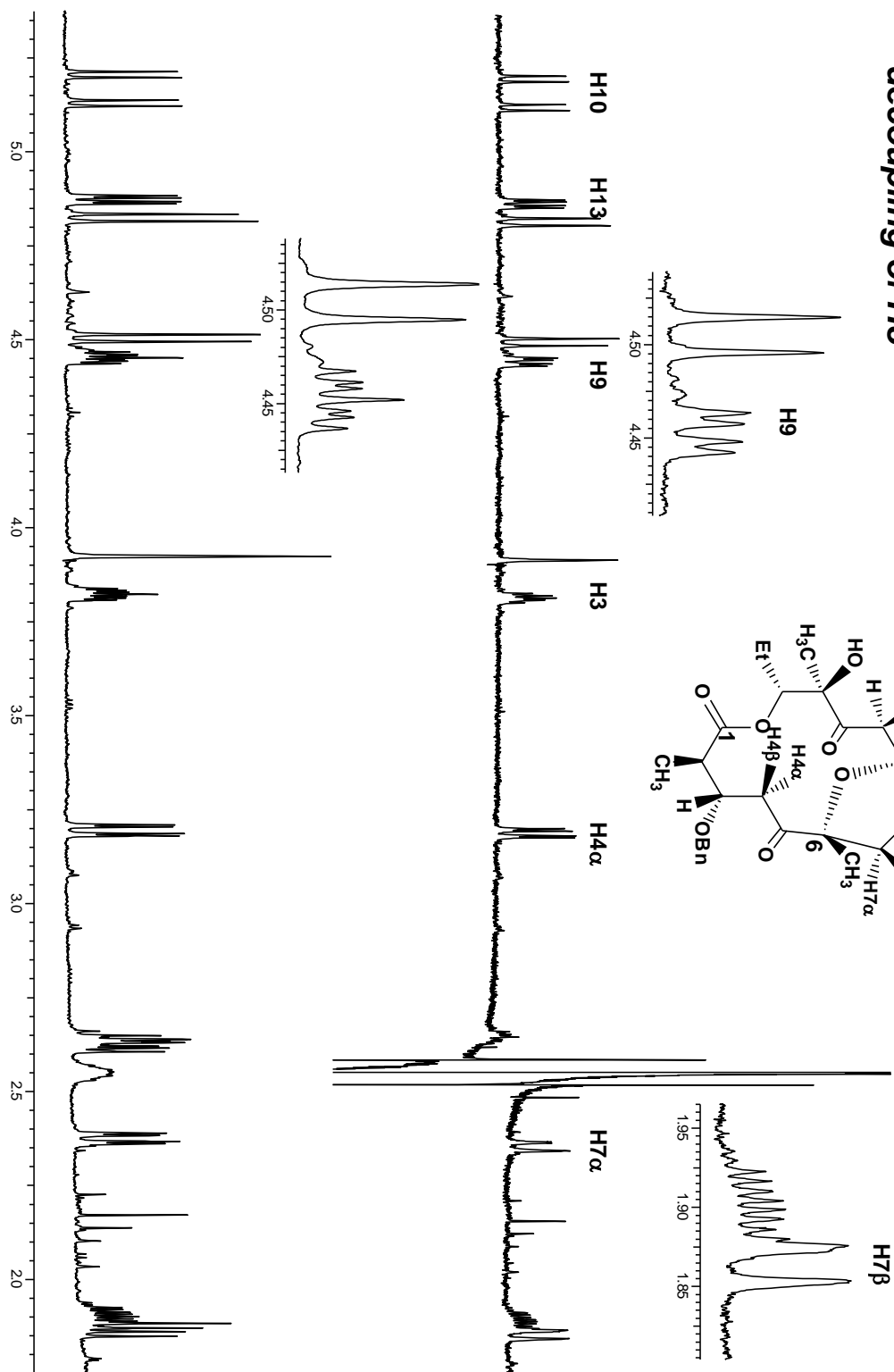
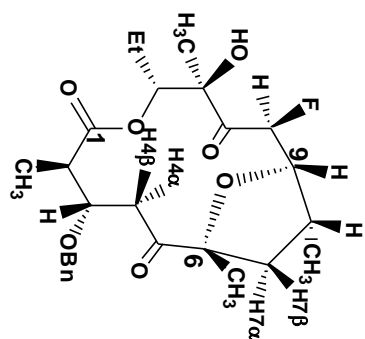
¹ H NMR chemical shifts (δ/ppm) & coupling constant (J/Hz)	¹³ C NMR chemical shift (δ/ppm)
2.61 (q, J _{H2, H3} = 9.4Hz, H2)	173.9 — C1
1.29 (d, J _{2-CH3, H2} = 7.1Hz, 2-CH₃)	44.2 — C2
3.82 (ddd, J _{H3, H2} = 9.4Hz, J _{H3, H4β} = 3.3Hz, J _{H3, H4α} = 5.9Hz H3)	76.9 — C3
4.50 (d, J _{AB} = 11.4Hz, 3-OCH₂)	35.7 — C4
4.82 (d, J _{AB} = 11.4Hz, 3-OCH₂)	207.2 — C5
3.19 (dd, J _{H4α, H4β} = 14.2Hz, J _{H4α, H3} = 5.9Hz, H4α)	90.1 — C6
2.62 (dd, J _{H4α, H3} = 3.3Hz, H4β)	39.9 — C7
1.29 (s, 6-CH₃)	34.9 — C8
1.87 (dd, J _{H7β, H8} = 7.5 Hz, J _{H7β, H7α} = 13.3Hz, H7β)	77.3 — C9
2.38 (dd, J _{H7α, H8} = 3.6Hz, J _{H7α, H7β} = 13.3Hz, H7α)	87.6 — C10, J _{CF} =173.1Hz
2.51 (m, H8)	205.9 — C11, J _{CF} =13.6Hz
0.94 (d, J _{8-CH3, H8} = 7.4Hz, 8-CH₃)	78.8 — C12
4.45 (ddd, J _{H9, H8} = 5.6Hz, J _{H9, H10} = 9.2Hz, J _{H9, F} = 3.6Hz, H9)	79.4 — C13
5.15 (dd, J _{10, F} = 45.7, J _{H10, H9} = 9.8Hz, H10)	23.4 — C14
1.54 (s, 12-CH₃)	24.8 — 2-CH ₃
3.92 (s, 12-OH)	16.1 — 6-CH ₃
4.87 (dd, J _{H13, H4} = 2.6 Hz, J _{H13, H8} = 11.2 Hz, H13)	14.7 — 8-CH ₃
1.91 - 1.98, 1.56 - 1.63 (m, 14-CH₂)	17.1 — 12-CH ₃
0.94 (t, J _{14-CH3, 13-CH2} = 7.4Hz, 14-CH₃)	11.0 — 14-CH ₃
7.39 - 7.28 (m, 5H, Ph)	71.6 — 3-OCH ₂ Ph
	137.8 — ipsoC
	128.4 — orthoC
	128.3 — metaC
	127.8 — paraC

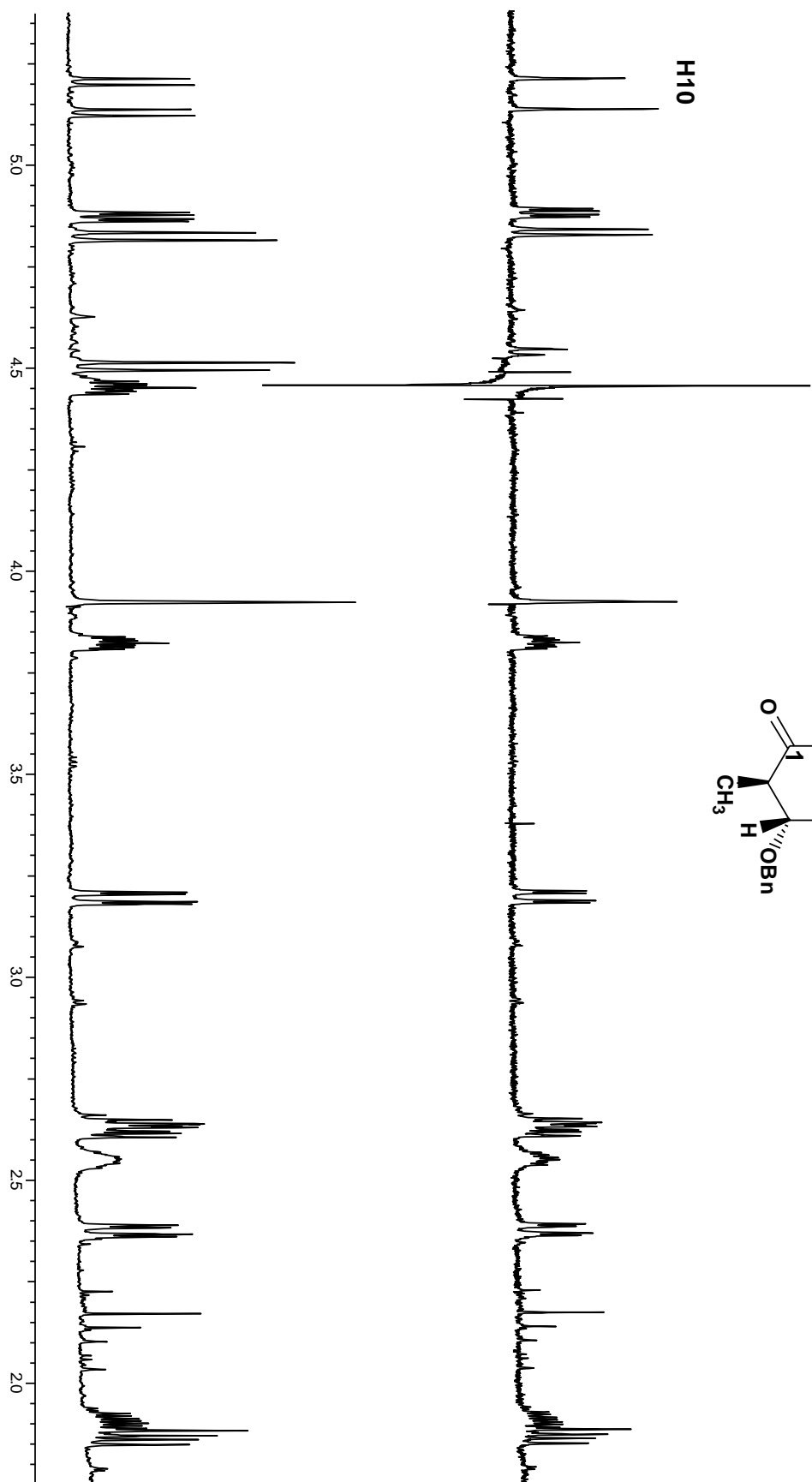
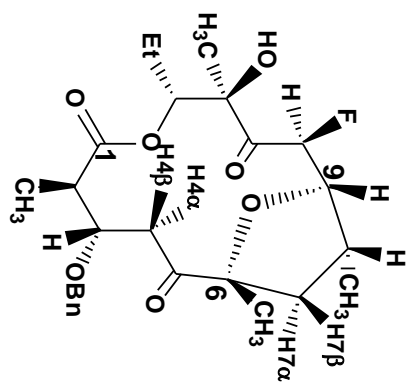
1D TOCSY spectra



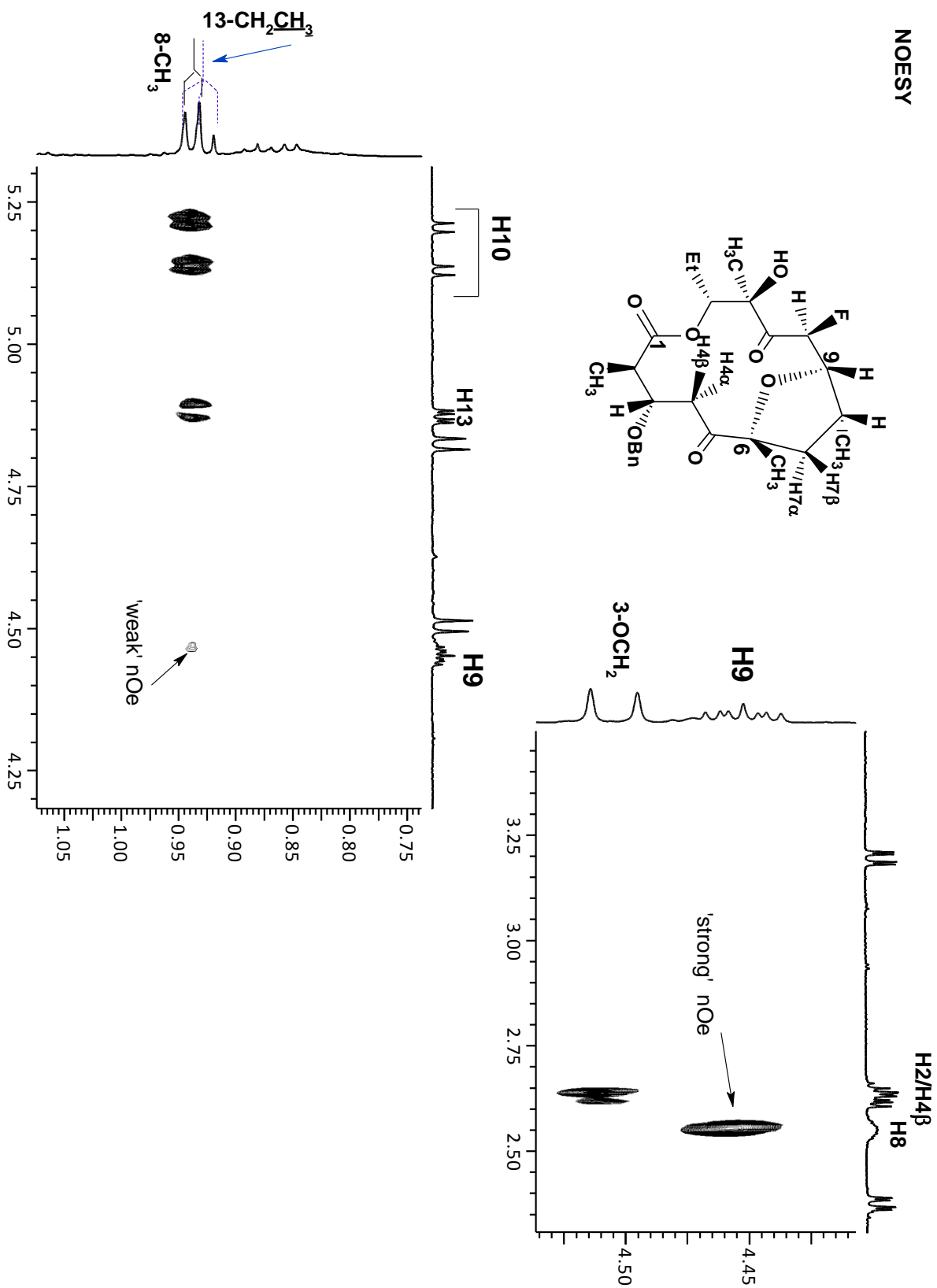
Selective decoupling of H3



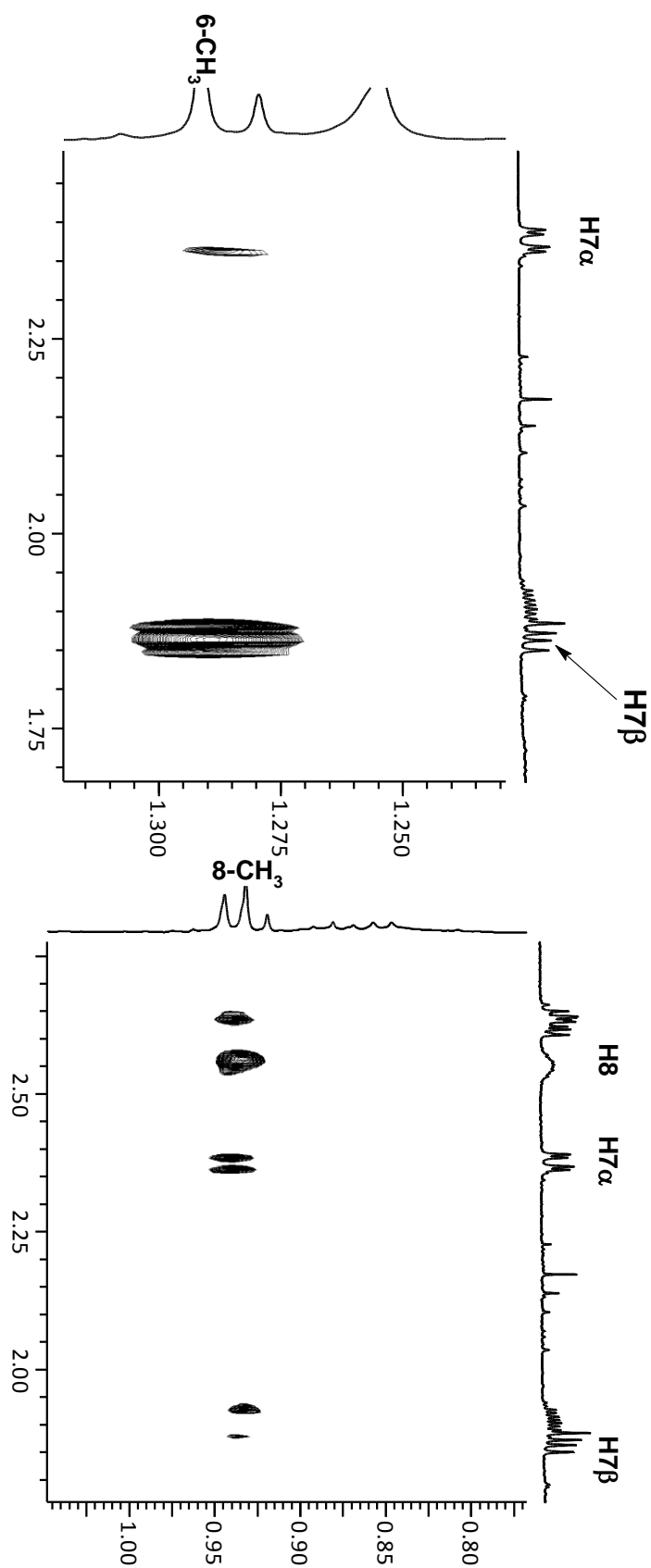
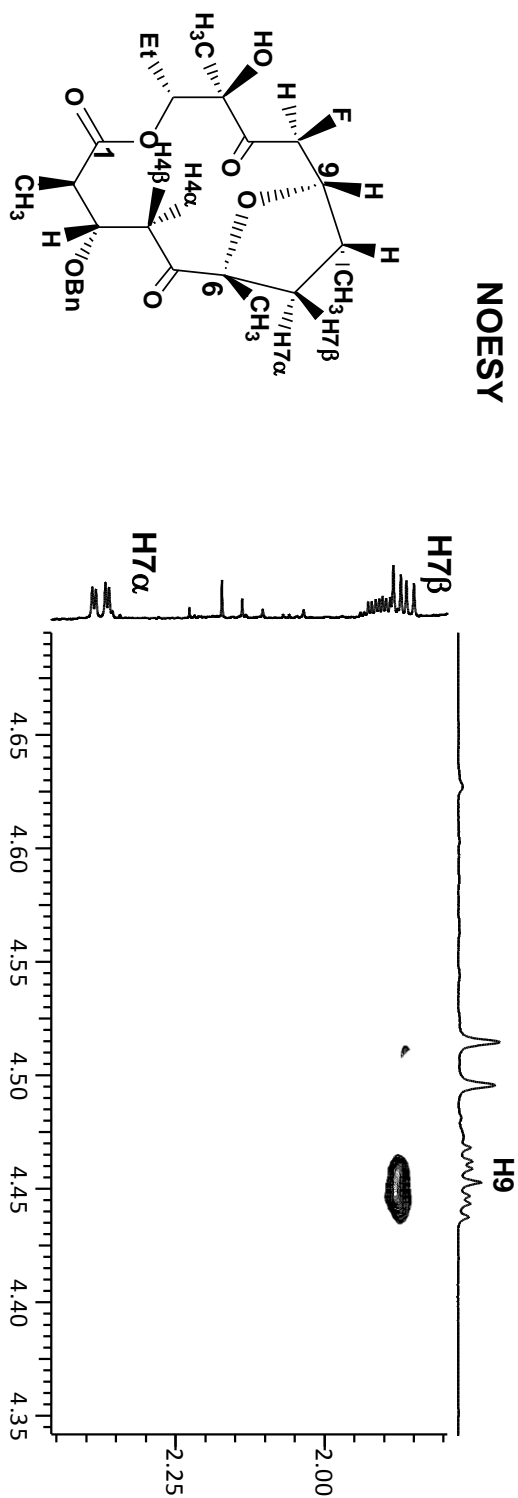


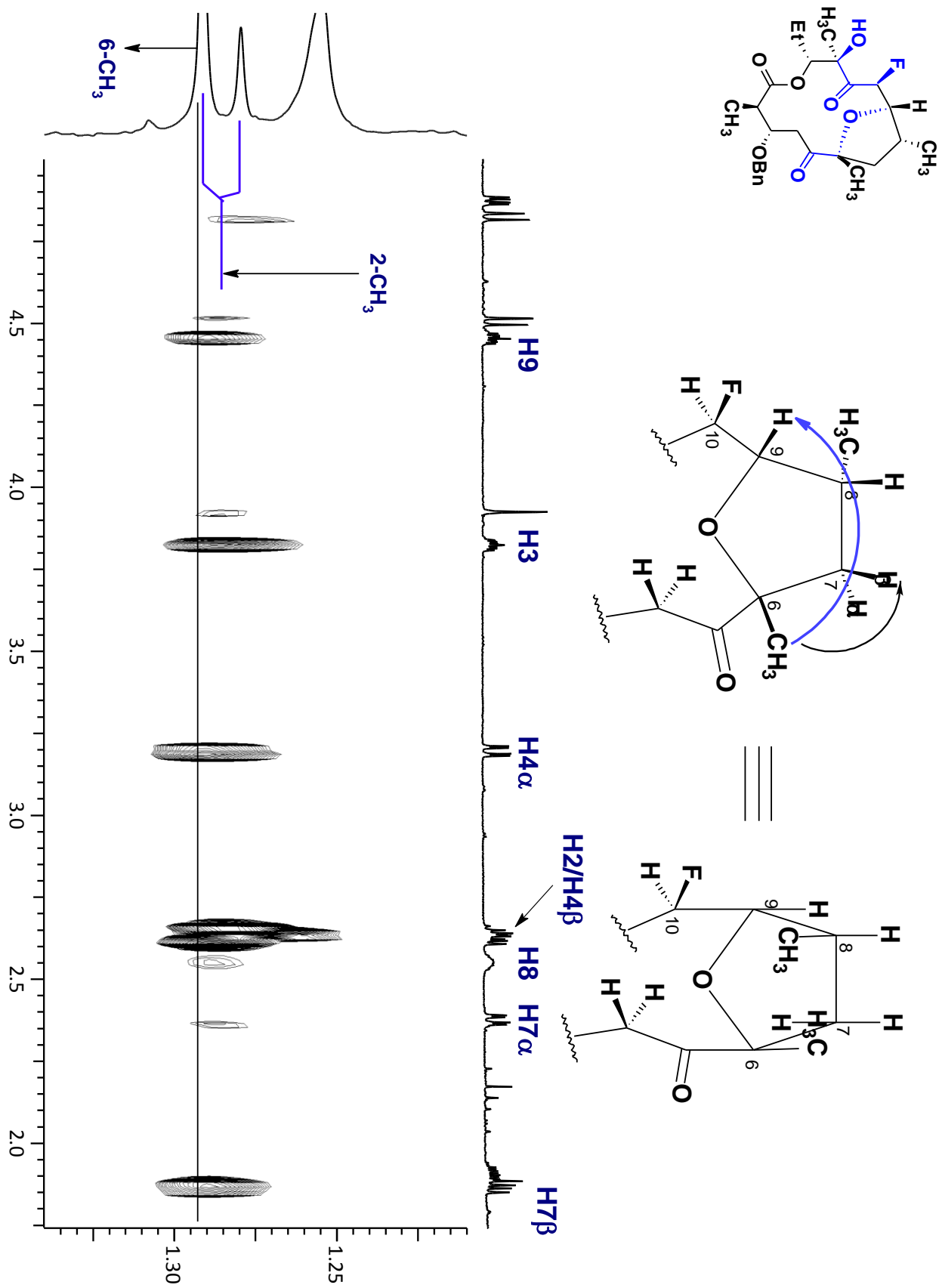


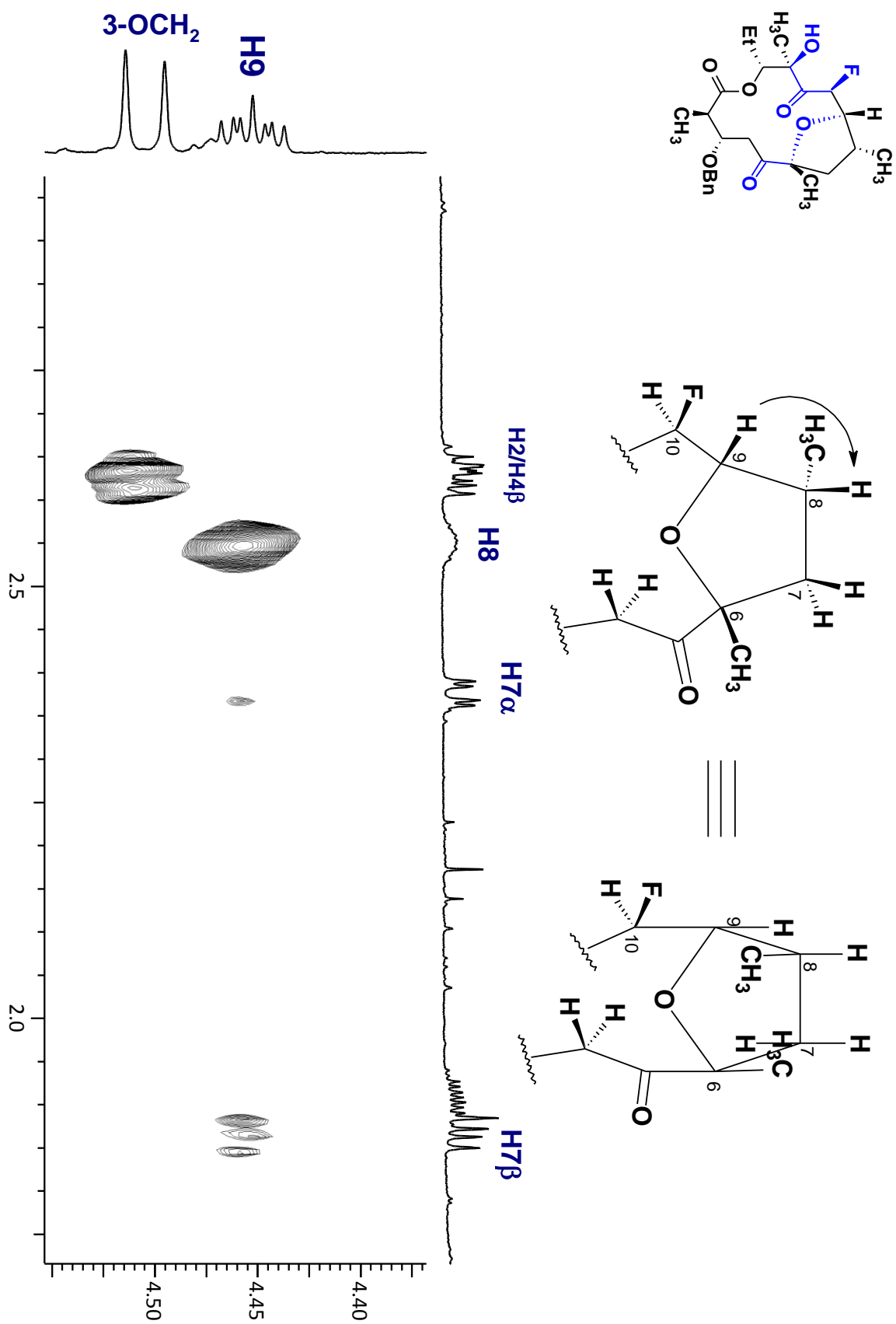
NOESY

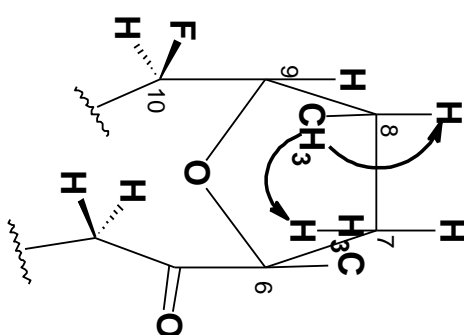
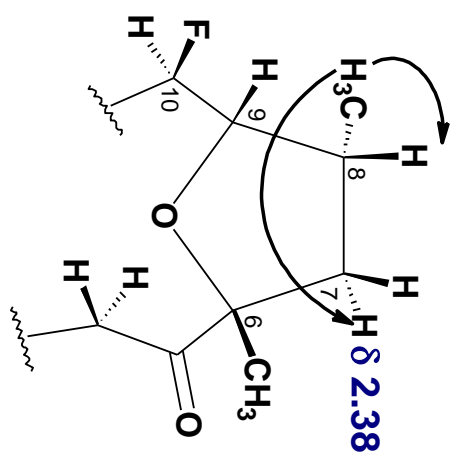
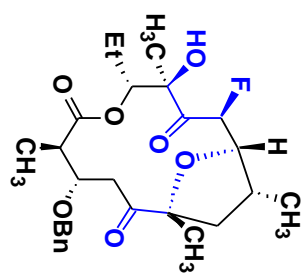


NOESY

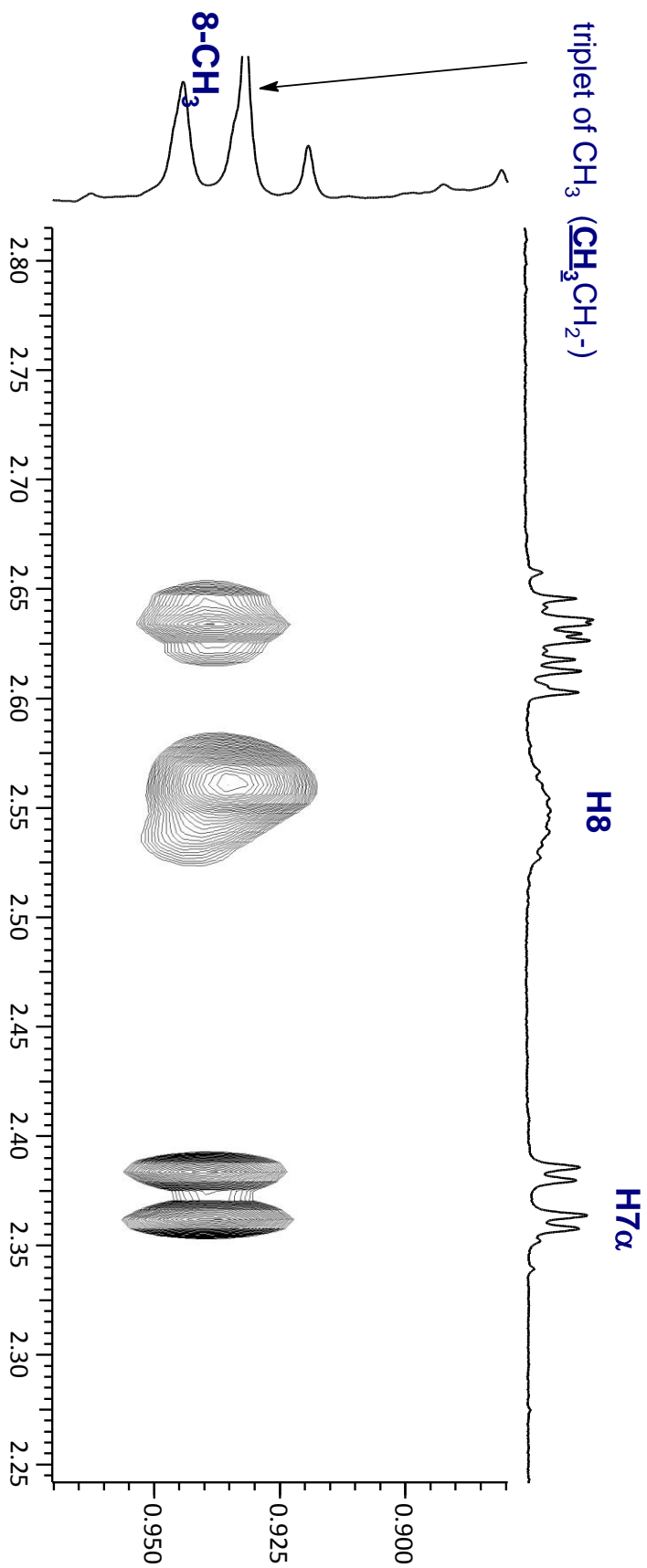


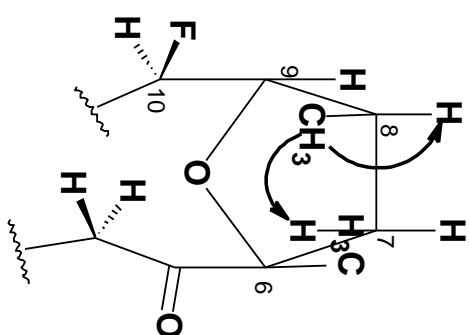
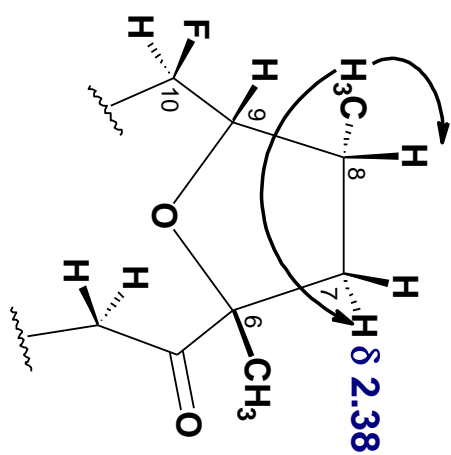
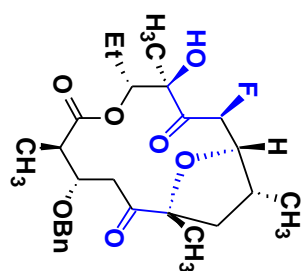




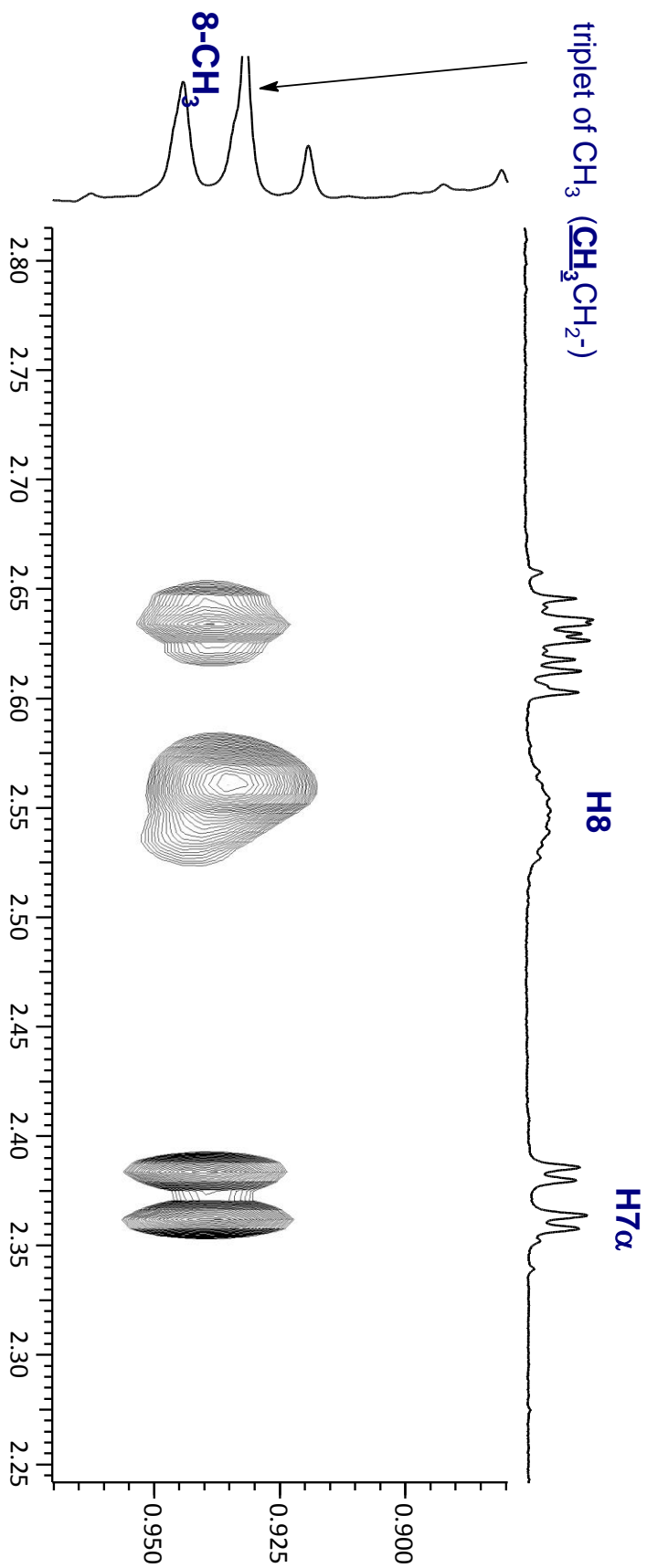


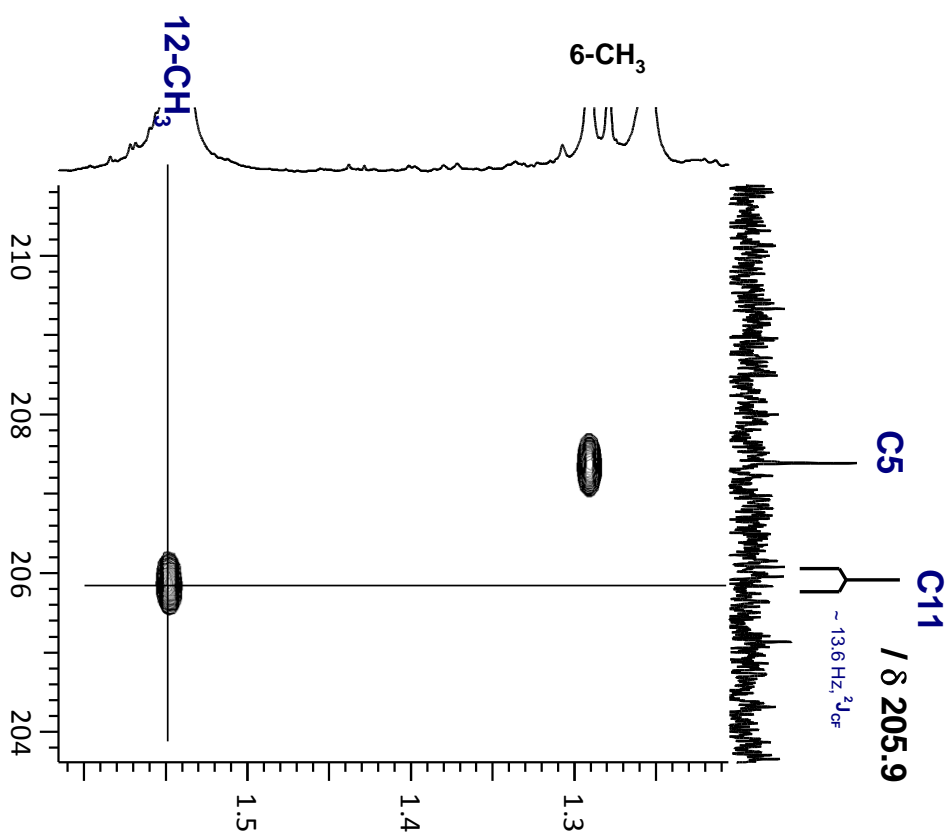
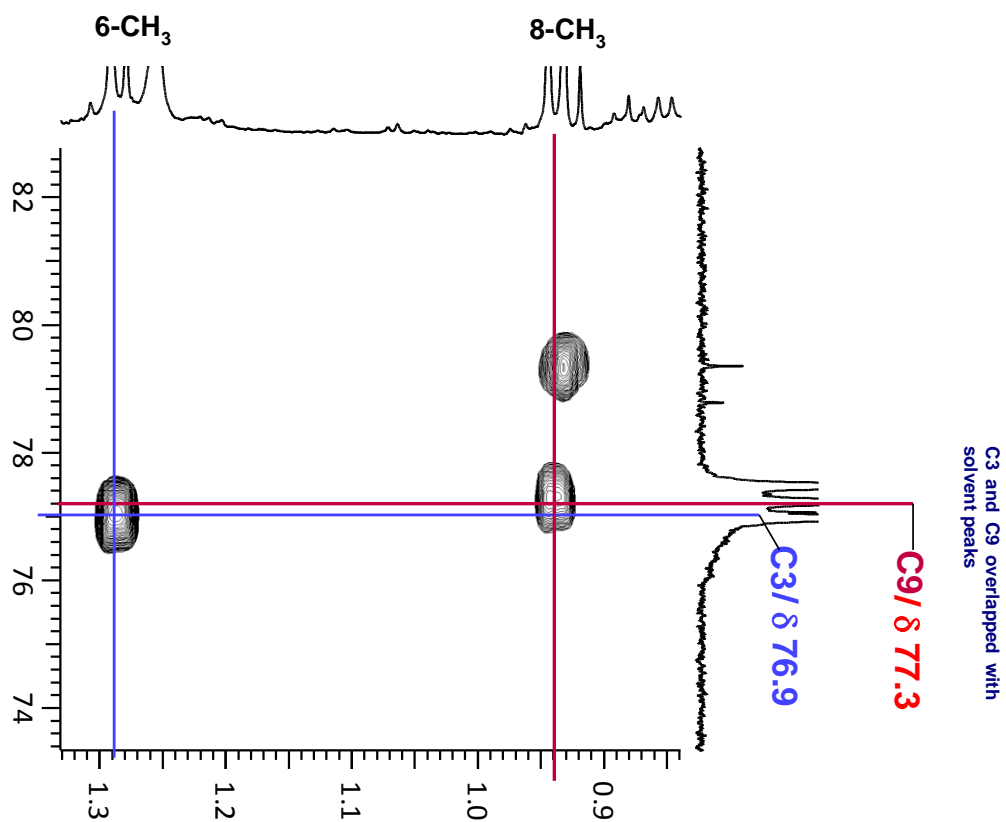
triplet of CH_3 (CH_2CH_2 -)

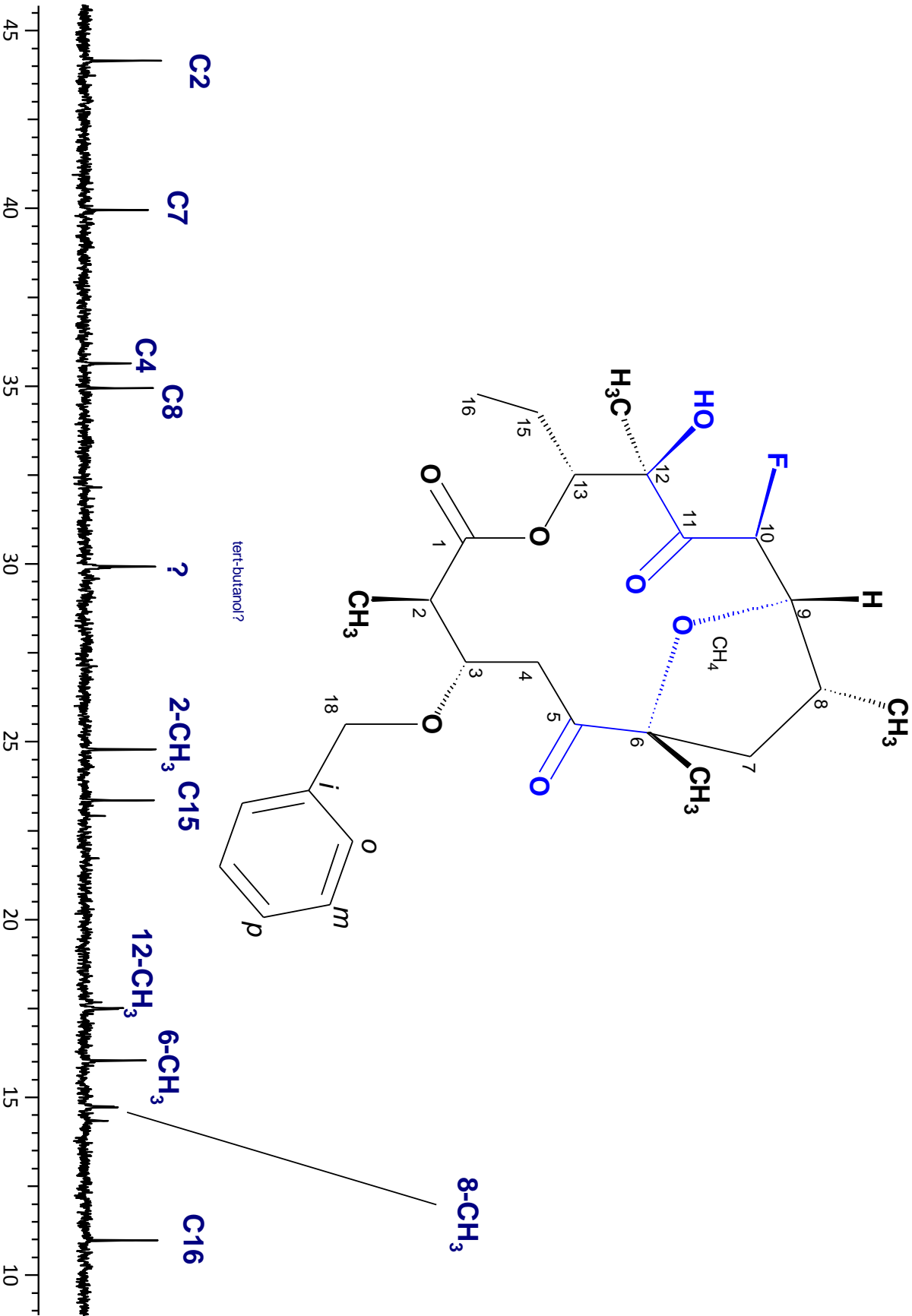




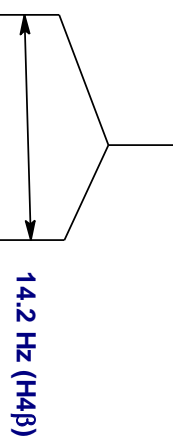
triplet of CH_3 (CH_2CH_2 -)



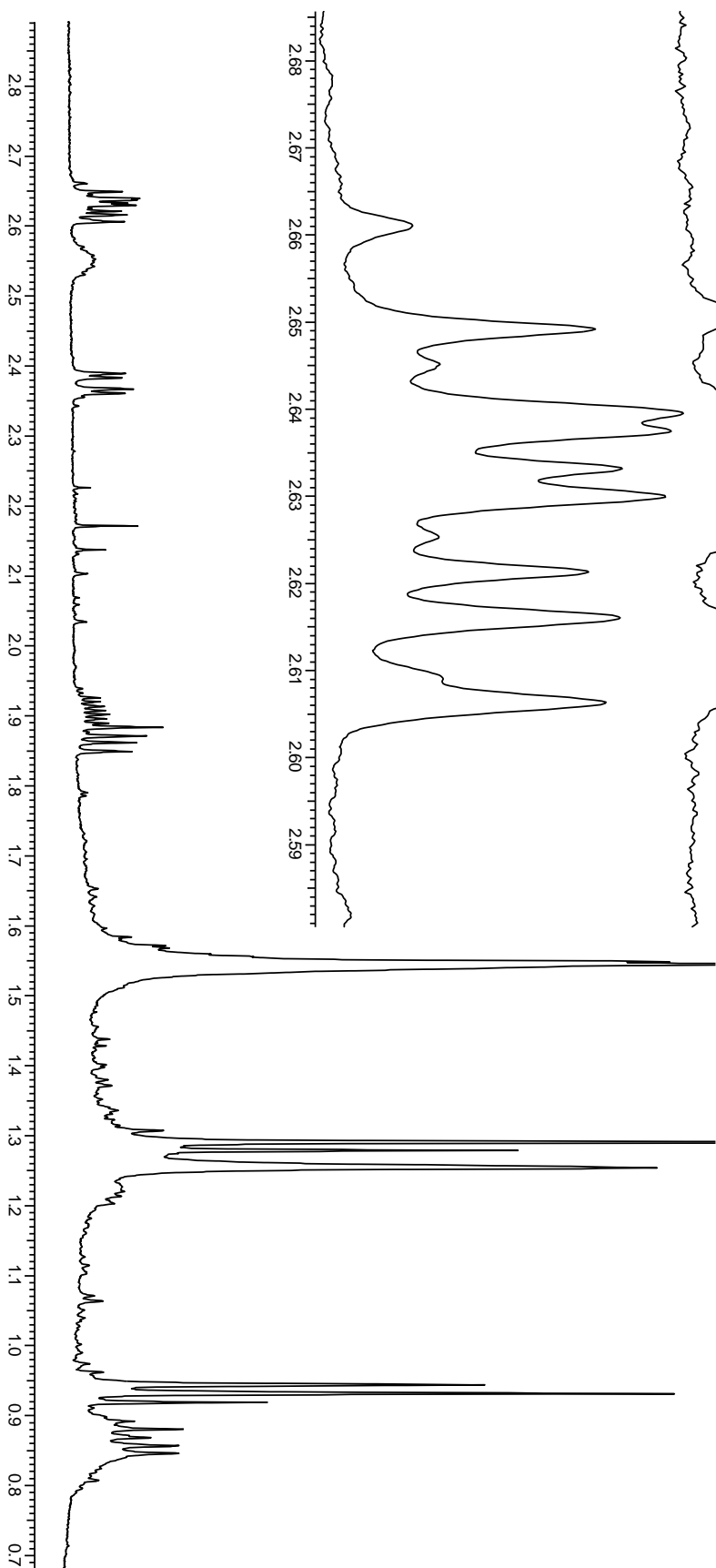




**selective irradiation of H3
at 3.82 ppm**

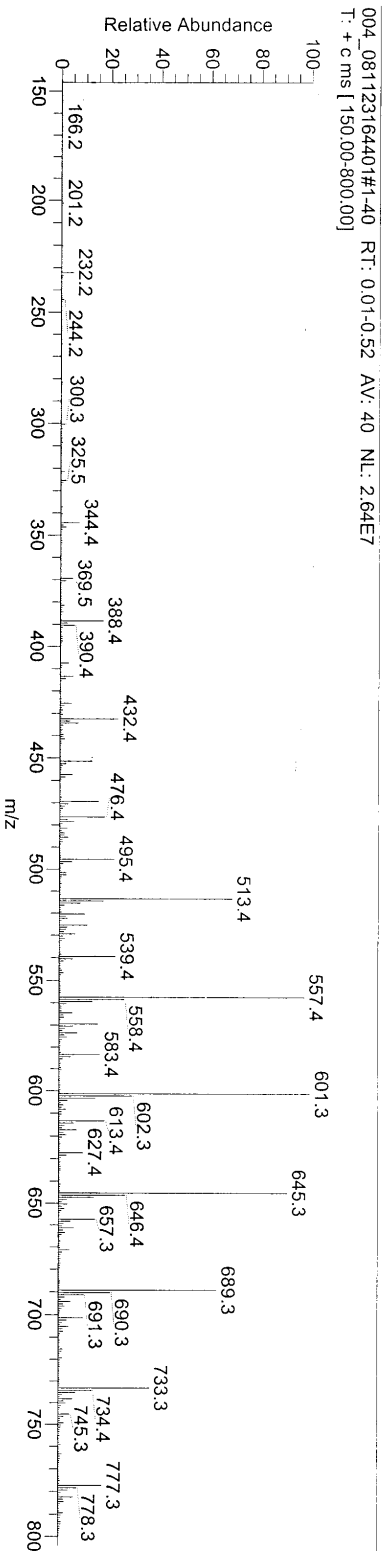
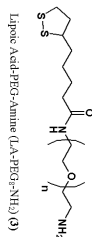
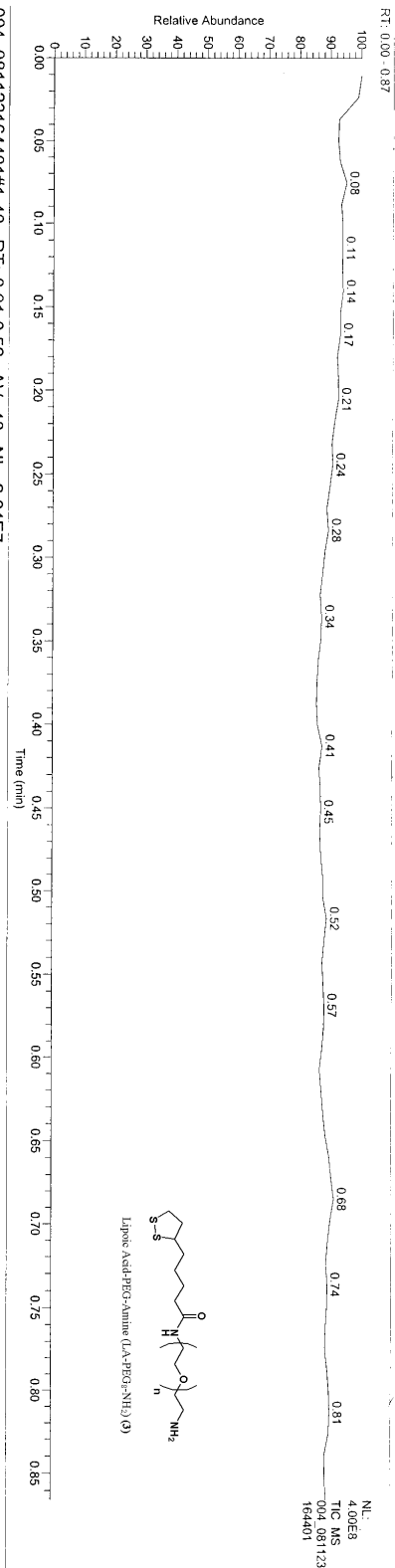


quartet lines of H2



D:\Michael\004_081123164401

11/23/2008 04:44 PM



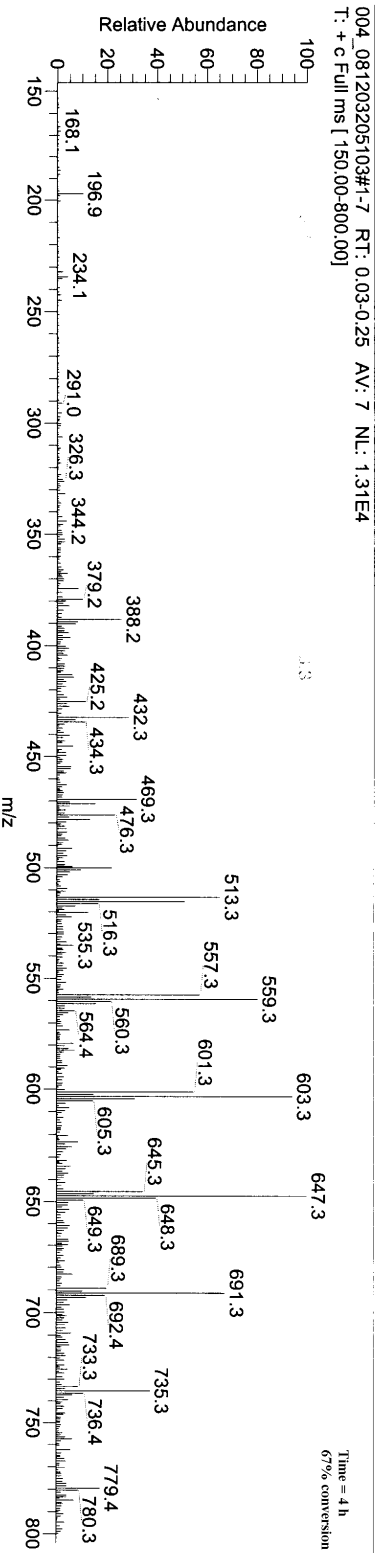
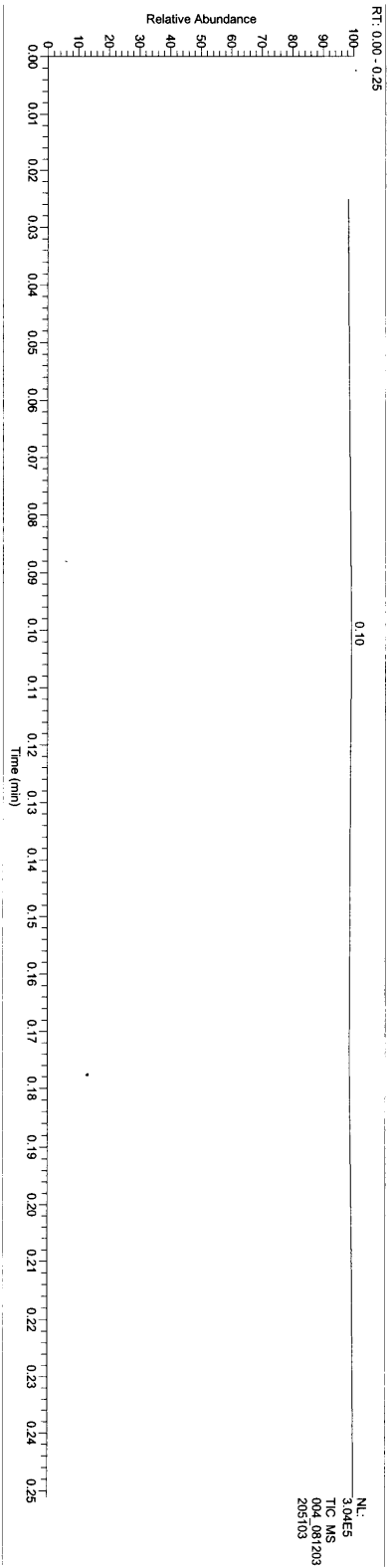
004_081123164401#1-40 RT: 0.01-0.52 AV: 40

T: + c ms [150.00-800.00]

m/z	Intensity	Relative
432.43	6057648.5	100.00
495.44	5682525.7	93.81
476.43	4760604.8	78.59
388.44	4453938.2	73.53
469.41	4070761.0	67.20
451.47	3351374.5	55.32
344.40	1930992.0	31.88
434.42	1909039.1	31.51
478.43	1478813.8	24.41
390.43	1463203.4	24.15

D:\Michael\004_081203205103

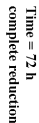
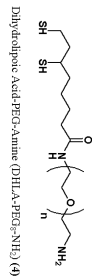
12/03/2008 08:51:03 PM



004_081203205103#1-7 RT: 0.03-0.25 AV: 7

T: + c Full ms [150.00-800.00]

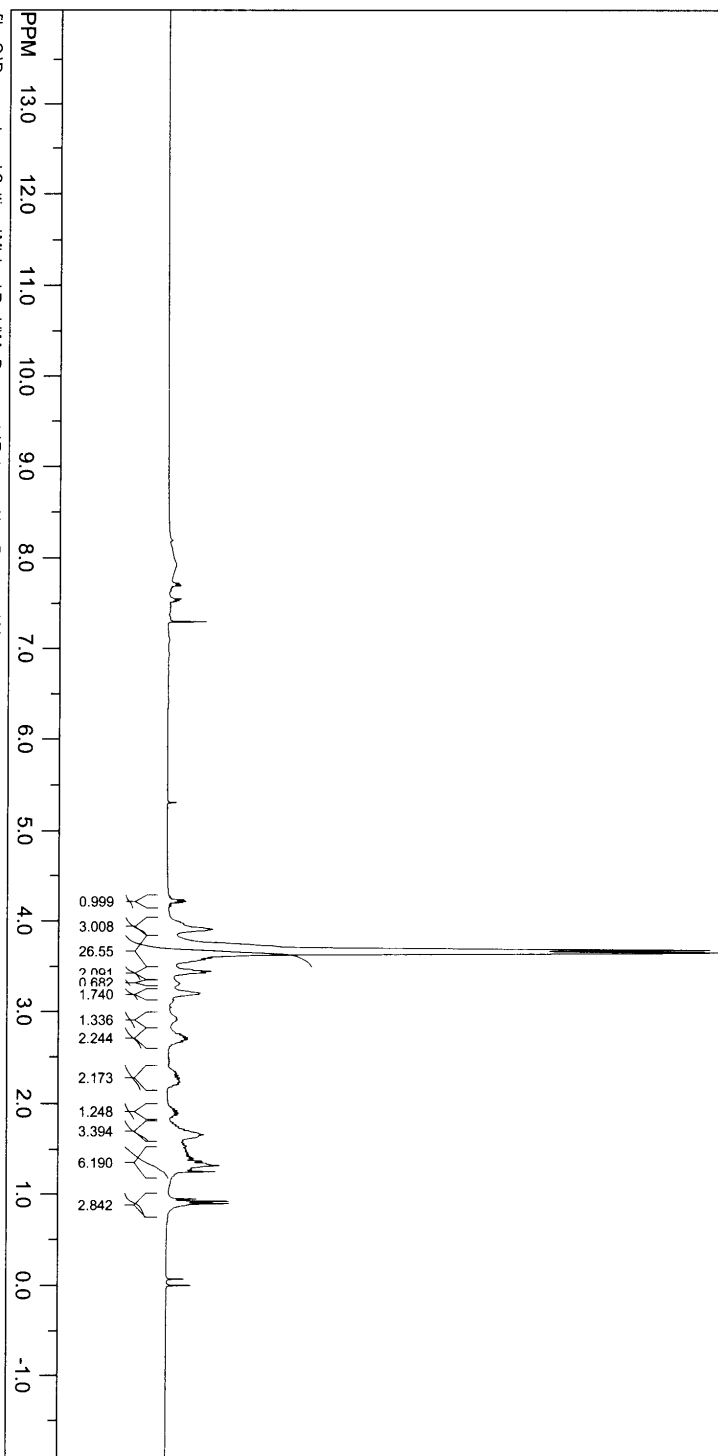
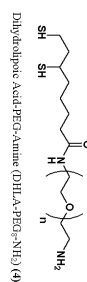
m/z	Intensity	Relative
469.31	4144.3	100.00
432.31	3739.0	90.22
388.20	3356.3	80.99
476.30	3023.9	72.96
499.97	2856.3	68.92
471.21	1985.9	47.92
478.36	1720.6	41.52
425.19	1485.1	35.84
434.31	1437.1	34.68
379.20	1314.6	31.72



m/z= 150.00-500.00

m/z	Intensity	Relative
391.02	4719.2	100.00
478.10	4321.8	91.58
434.04	4056.1	85.95
471.38	3384.5	71.72
499.89	3342.2	70.82
455.98	3235.1	68.55
432.30	2548.7	54.01
344.23	2056.0	43.57
388.34	2013.2	42.66
371.15	1521.3	32.24

SpinWorks 2.5: Std proton



file: C:\Documents and Settings\Michael Drahl\My Documents\Rudgers - New Brunswick\2008 - 2009\Resfreq, of 0 ppm: 299.938377 MHz\20011-5-fid\fid block# 1 exp1 "s2pu"

transmitter freq.: 299.940183 MHz

time domain size: 19698 points

width: 4807.69 Hz = 16.028837 ppm = 0.244070 Hz/pl

number of scans: 8

processed size: 65536 complex points

LB: 0.200 GB: 0.0000

Hz/cm: 192.307 ppm/cm: 0.64115

Std proton

File: Proton

Pulse Sequence: szpu1

Solvent: cdcl3

Temp: 25.0 C / 298.1 K

Operator: Kevin

VMRS-300 "nm/300"

Relax. delay 1.000 sec

Pulse 45.0 degrees

Acq. time 2.012 sec

VH1 400.142 MHz

8 repetitions

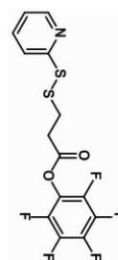
OBSERVE H1, 299.303871 MHz

DATA PROCESSING

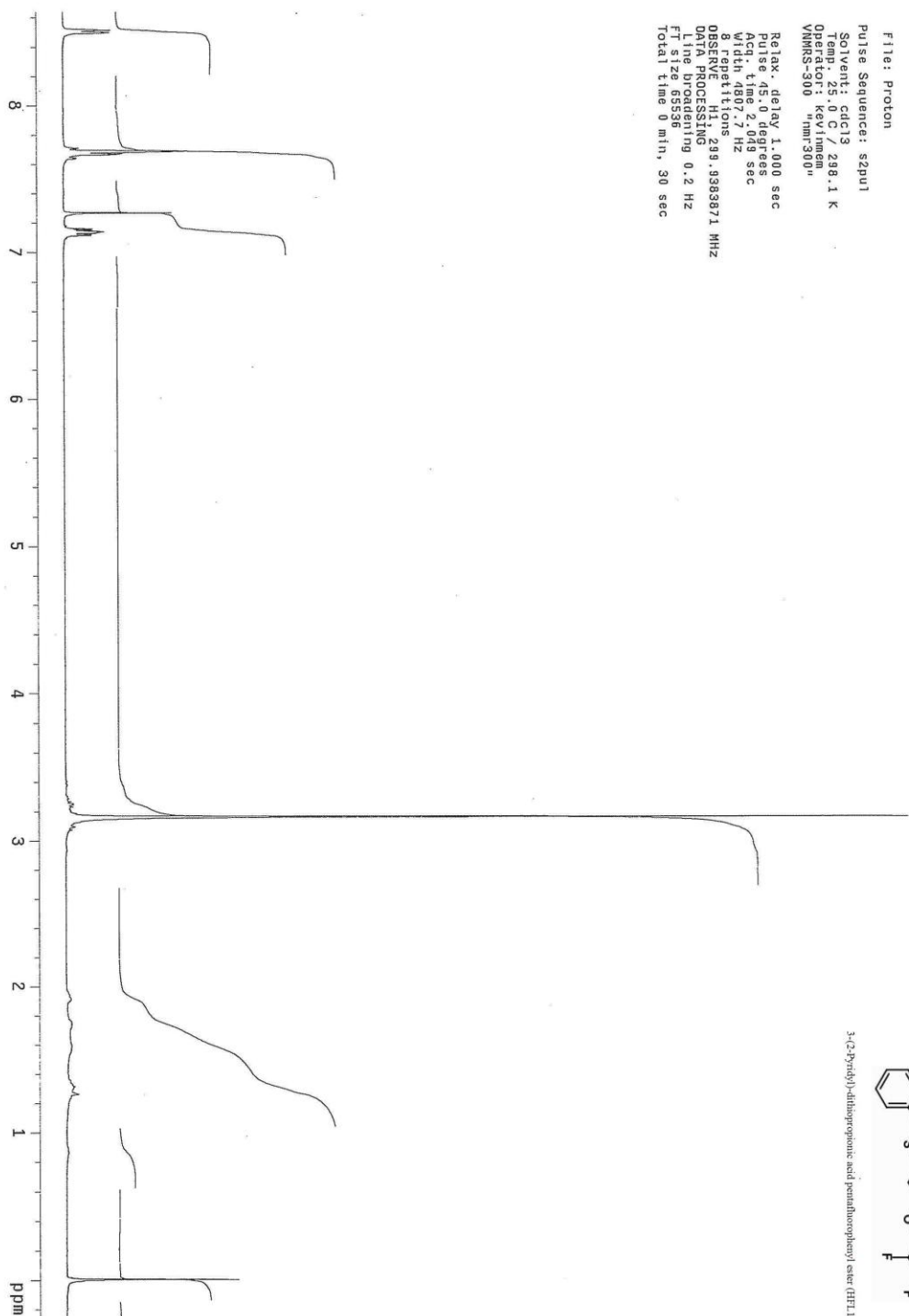
Line broadening 0.2 Hz

FT size 65536

Total time 0 min, 30 sec



3-(2-Pyridyl)-ethanesulfonyl ester (HFL1) (6)



CURRICULUM VITAE

Hiyun Kim

September 1996 – December 2000

Grand Canyon University
Phoenix, AZ
Subject: Chemistry
Degree Earned: B.S.

September 2001 – October 2007

Rutgers, the State University of New Jersey
New Brunswick, NJ
Subject: Chemistry
Degree Earned: M.S.

September 2008 – January 2012

Rutgers, the State University of New Jersey
New Brunswick, NJ
Subject: Chemistry
Degree Earned: Ph.D.

PUBLICATIONS

Kai Liu, Hiyun Kim, Partha Ghosh, Novruz G. Ahkmedov, Lawrence J. Williams, *J. Am. Chem. Soc.*, **2011**, *133*, 14968-14971. "Direct Entry to Erythronolides via a Cyclic Bis[Allene]."

Rojita Sharma, Madhuri Manpadi, Yue Zhang, Hiyun Kim, Novruz G. Ahkmedov, Lawrence J. Williams, *Org. Lett.*, **2011**, *13*, 3352-3355. "Spirodiepoxide-Based Cascades: Direct Access to Diverse Motifs."

Jongjin Jung, Aniruddh Solanki, Kevin A. Memoli, Ken-ichiro Kamei, Hiyun Kim, Michael A. Drahl, Lawrence J. Williams, Hsian-Rong Tseng, KiBum Lee, *Angew. Chem. Inter. Ed.*, **2010**, *49*(1), 103-107. "Selective Inhibition of Human Brain Tumor Cells through Multifunctional Quantum-Dot-Based siRNA Delivery."

Hiyun Kim, Lawrence J. Williams, *Curr. Opin. Drug Discovery Dev.*, **2008**, *11*(6), 870. "Recent Developments in Allene-based Synthetic Methods."

Troy C. Messina, Hiyun Kim, Jason T. Giurleo, David S. Talaga, *J. Phys. Chem. B.*, **2006**, *110*(33), 16366-16376. "Hidden Markov Model Analysis of Multichromophore Photobleaching."